

**Ongoing Face Recognition
Vendor Test (FRVT)**
Part 1: Verification

Patrick Grother
Mei Ngan
Kayee Hanaoka
Joyce C. Yang
Austin Hom

*Information Access Division
Information Technology Laboratory*

This publication is available free of charge from:
<https://www.nist.gov/programs-projects/face-recognition-vendor-test-frvt-ongoing>

2022/08/30



ACKNOWLEDGMENTS

The authors are grateful for the long-standing support and collaboration of the the Department of Homeland Security's Science & Technology Directorate (S&T) and the Office of Biometric Identity Management (OBIM).

Additionally, the authors are grateful to staff in the NIST Biometrics Research Laboratory for infrastructure supporting rapid evaluation of algorithms.

DISCLAIMER

Specific hardware and software products identified in this report were used in order to perform the evaluations described in this document. In no case does identification of any commercial product, trade name, or vendor, imply recommendation or endorsement by the National Institute of Standards and Technology, nor does it imply that the products and equipment identified are necessarily the best available for the purpose.

INSTITUTIONAL REVIEW BOARD

The National Institute of Standards and Technology's Research Protections Office reviewed the protocol for this project and determined it is not human subjects research as defined in Department of Commerce Regulations, 15 CFR 27, also known as the Common Rule for the Protection of Human Subjects (45 CFR 46, Subpart A).

FRVT STATUS

This report is a draft NIST Interagency Report, and is open for comment. It is the thirty sixth edition of the report since the first was published in June 2017. Prior editions of this report are maintained on the FRVT [website](#), and may contain useful information about older algorithms and datasets no longer used in FRVT.

FRVT remains open: All [four tracks](#) of the FRVT are open to new algorithm submissions.

2022-08-30 changes since 2022-07-29:

- ▷ We have added results for first algorithms from two developers: Aximetria, Intellibrain Technological Projects
- ▷ We have added results for new algorithms from twelve returning developers: Alchera Inc, Dermalog, Idemia, Incode Technologies Inc, Intellivision, Kasikorn Labs, Megvii/Face++, Techsign, TuringTech.vip, Universidade de Coimbra, Verijelais, Vixvizon
- ▷ We have retired results for six algorithms per our policy to only list results for two algorithms per developer. Results for retired algorithms appear in prior versions of this report in the [archive](#).

2022-07-29 changes since 2022-06-27:

- ▷ We have added results for first algorithms from seven developers: FRP LLC (Hawaii), IMDS Software, Inspur (Beijing) Electronic Information Industry, Intema - LGL Group, PAPAGO, Qaz Biometric Systems, and VIDA-Digital Identity
- ▷ We have added results for new algorithms from nine returning developers: Cyberextruder, Glory, Maxvision Technology, Rank One Computing, Securif AI, Suprema AI, Suprema ID, Toshiba, and Yuan High-Tech Development.
- ▷ We have retired results for nine algorithms per our policy to only list results for two algorithms per developer. Results for retired algorithms appear in prior versions of this report in the [archive](#).

2022-07-29 changes since 2022-06-27:

- ▷ We have added results for first algorithms from seven developers: FRP LLC (Hawaii), IMDS Software, Inspur (Beijing) Electronic Information Industry, Intema - LGL Group, PAPAGO, Qaz Biometric Systems, and VIDA-Digital Identity
- ▷ We have added results for new algorithms from nine returning developers: Cyberextruder, Glory, Maxvision Technology, Rank One Computing, Securif AI, Suprema AI, Suprema ID, Toshiba, and Yuan High-Tech Development.
- ▷ We have retired results for nine algorithms per our policy to only list results for two algorithms per developer. Results for retired algorithms appear in prior versions of this report in the [archive](#).

2022-06-27 changes since 2022-06-03:

- ▷ We have added results for first algorithms from two developers: Krungthai Bank, and Smartbiometrik.
- ▷ We have added results for new algorithms from thirteen returning developers: Aiseemu, Corsight, Digidata, Griaule, Guangzhou Pixel Solutions, Hangzhuo AI Network Information Technology, Neurrotechnology, Real Networks, Samsung S1, Sensetime Group, Smart Engines, Verihubs Inteligensia, and VinBigData.

- ▷ We have retired results for eight algorithms per our policy to only list results for two algorithms per developer. Results for retired algorithms appear in prior versions of this report in the [archive](#).

2022-06-03 changes since 2022-05-05:

- ▷ We have added results for first algorithms from seven developers: Jaak IT, Metsakuur, Palit Microsystems, Smarvist Teknoloji, and Touchless ID.
- ▷ We have added results for new algorithms from sixteen returning developers: Cyberlink, FaceOnLive, Kakao Enterprise, Line Corporation (Line Clova), Multi-Modality Intelligence, NEO Systems, and Unissey
- ▷ We have retired results for four algorithms per our policy to only list results for two algorithms per developer. Results for retired algorithms appear in prior versions of this report in the [archive](#).
- ▷ We have moved the results for the twenty human-difficult pairs used in the May 2018 paper *Face recognition accuracy of forensic examiners, superrecognizers, and face recognition algorithms* by Phillips et al. [1]. to the algorithm-specific report cards (example: [PDF](#)).
- ▷ Likewise, we have added figures showing impostor distribution shifts across demographics to the report card.

2022-05-05 changes since 2022-03-18:

- ▷ We have added results for first algorithms from seven developers: Accurascan, DICIO, FacePhi, Pangiam, University of Surrey-CVSSP, and Veridium.
- ▷ We have added results for new algorithms from sixteen returning developers: ACI Software, Canon Inc, Cloudwalk - Moontime Smart Technology, Cybercore,

2022-05-05 changes since 2022-03-18:

- ▷ We have added results for first algorithms from seven developers: Accurascan, DICIO, FacePhi, Pangiam, University of Surrey-CVSSP, and Veridium.
- ▷ We have added results for new algorithms from sixteen returning developers: ACI Software, Canon Inc, Cloudwalk - Moontime Smart Technology, Cybercore, Cyberextruder, Gemalto Cogent, HyperVerge Inc, KuKe3D Technology, Megvii/Face++, Mobbeel Solutions, Panasonic R+D Center Singapore, Qnap Security, Samsung-SDS, Vietnam Posts and Telecommunications Group, Viettel Group, and Vision Intelligence Center of Meituan.
- ▷ We have retired results for 12 algorithms per our policy to only list results for two algorithms per developer. Results for retired algorithms appear in prior versions of this report in the [archive](#).

2022-03-18 changes since 2022-02-23:

- ▷ We have added support for the detection of multiple people in a single image (see Section 1.2). Specifically the API allows an algorithm to extract features from one or more faces it detects in an image. NIST scores such cases as a correct match when any detected face matches the reference photo, and as a false positive when either face matches a non-mated reference photo. The expected effect of doing this will be to improve reported false non-match rates, and to minimally elevate false match rates. This technique was only applied to images of type "border" and "kiosk".

- ▷ We have added results for first algorithms from four developers: IntelliVIX, Kasikorn Labs, Lebentech Biometrics, and Wicket.
- ▷ We have added results for new algorithms from 10 returning developers: Chunghwa Telecom, Cloudmatrix, Beijing DeepSense Technologies, FarBar Inc, Imagus Technology Pty, Intellivision, Maxvision Technology, NHN Corp, Seventh Sense Artificial Intelligence, and Verigram.
- ▷ We have retired results for 4 algorithms per our policy to only list results for two algorithms per developer. Results for retired algorithms appear in prior versions of this report in the [archive](#).

2022-02-23 changes since 2022-01-24:

- ▷ We have added results for first algorithms from four developers: AFIS and Biometrics Consulting, Digi-data, Graymatics, Hangzhuo Allu Network Information Technology, KnowUTech LLC, Sukshi Technology Innovation, T4iSB, and TuringTech.vip
- ▷ We have added results for new algorithms from 18 returning developers: Cognitec Systems GmbH, GeoVision Inc, Glory, Herta Security, Intel Research Group, InsightFace AI, Kakao Enterprise, N-Tech Lab, Omnidarde Ltd, Papilon Savunma, Paravision, Reallnetworks Inc, Reveal Media Ltd, Shenzhen Inst Adv Integrated Tech CAS, Suprema AI Inc, Toshiba, Universidade de Coimbra, and Yuan High-Tech Development
- ▷ We have retired results for 14 algorithms per our policy to only list results for two algorithms per developer. Results for retired algorithms appear in prior versions of this report in the [archive](#).

2022-01-24 changes since 2022-01-20:

- ▷ We have added results for new algorithms from one returning developer: Vocord.

2022-01-20 changes since 2021-12-18:

- ▷ We have added results for first algorithms from four developers: Armatura, Beyne.AI, One More Security, and VinBigData
- ▷ We have added results for new algorithms from 19 returning developers: AuthenMetric, BOE Technology Group, Cybercore, Cyberlink, Dahua Technology, FaceTag Co, Innovatrics, Megvii, Mobbeel Solutions, Neurotechnology, Oz Forensics, Rank One Computing, Regula Forensics, Samsung S1, Securif AI, Sensetime Group, TigerIT Americas, Videmo Intelligent Videoanalyse, and YooniK.
- ▷ We have retired results for 14 algorithms per our policy to only list results for two algorithms per developer. Results for retired algorithms appear in prior versions of this report in the [archive](#).

: 2021-12-16 changes since 2021-11-22:

- ▷ We have added results for first algorithms from five developers: Alfabeta, Cloudmatrix, Euronovate SA, FaceOnLive Inc, and Mobicin Technology.
- ▷ We have added results for new algorithms from ten returning developers: ACI Software, ITMO University, NEO Systems, Guangzhou Pixel Solutions, Panasonic R+D Center Singapore, Qnap Security, Scanovate, Tevian, Unissey, and Vietnam Posts and Telecommunications Group.
- ▷ We have retired results for eight algorithms per our policy to only list results for two algorithms per developer. Results for retired algorithms appear in prior versions of this report in the [archive](#).

- ▷ We have revamped the figure showing performance on 20 pairs of open-source images. It now color-codes false negatives and positives against a default threshold value.

2021-11-22 changes since 2021-10-28:

- ▷ We have added results to the [website](#) for kiosk-collected images where the design and geometry configuration mean that many images have considerable downward pitch angle. In some images, the face is partially cropped. Some images have other background faces.
- ▷ We have stopped using child exploitation images in FRVT, as we lost access to the imagery. All results for that set have been removed from the [website](#), and will be removed from future PDF reports.
- ▷ We have added results for first algorithms from seven new developers: CUDO Communication, Daon, KuKe3D Technology, Mantra Softtech India, Maxvision Technology, Multi-Modality Intelligence, and Samsung-SDS.
- ▷ We have added results for new algorithms from seven returning developers: Acer Incorporated, Cloudwalk-Moontime Smart Technology, Gorilla Technology, ID3 Technology, Incode Technologies, NSENSE Corp., and SQIssoft.
- ▷ We have retired results for six algorithms per our policy to only list results for two algorithms per developer. Results for retired algorithms appear in prior versions of this report in the [archive](#).

2021-10-28 changes since 2021-09-08:

- ▷ We have substantially revised the algorithm-specific report cards that are linked from the [FRVT results page](#). (Example: [HTML](#)).
- ▷ We have added results for first algorithms from eight new developers: Beijing Mendaxia Technology, Beijing Hisign Technology, Biocube Matrics, Clearview AI, Reveal Media, Toppan ID Gate, Verigram, and Viettel High Technology.
- ▷ We have added results for new algorithms from thirty returning developers: 20Face, 3divi, Canon Inc Chunghwa Telecom, Corsight, Decatur Industries, Deepglint, Dermalog, FaceTag, Fiberhome Telecommunication Technologies, GeoVision, ICM Airport Technics, Imagus Technology, InsightFace AI, Kakao Enterprise, Kookmin University, Line Corporation, N-Tech Lab, NotionTag Technologies, Realnetworks, Suprema ID, Taiwan-Certificate Authority, Toshiba, Tripleize, Trueface.ai, Veridas Digital Authentication, Visidon, VisionLabs, YooniK, and Yuan High-Tech Development.
- ▷ We have retired results for twenty algorithms per our policy to only list results for two algorithms per developer. Results for retired algorithms appear in prior versions of this report in the [archive](#).

2021-09-08 changes since 2021-08-02:

- ▷ We have added results for first algorithms from seven new developers: Griaule, SQIssoft, Qnap Security, Techsign, Smart Engines, Verihubs, and Wuhan Tianyu Information Industry.
- ▷ We have added results for new algorithms from sixteen returning developers: ADVANCE.AI, AuthenMetric, CloudSmart Consulting, Code Everest Pvt, Cognitec Systems, Thales Gemalto Cogent, Intel Research Group, Omnidarde, Oz Forensics, Rank One Computing, Samsung S1 Corp, Securif AI, Tevian, TigerIT Americas, Universidade de Coimbra, and Vigilant Solutions
- ▷ We have retired results for eleven algorithms per our policy to only list results for two algorithms per developer. Results for retired algorithms appear in prior versions of this report in the [archive](#).

2021-08-02 changes since 2021-06-25:

- ▷ We have added results for first algorithms from eight new developers: Bee the Data, Closeli Inc, Coretech Knowledge Inc, Deepsense (France), ioNetworks Inc, Kakao Pay Corp, Seventh Sense Artificial Intelligence, and SK Telecom.
- ▷ We have added results for new algorithms from fifteen returning developers: Alchera Inc, Adera Global PTE, Aware, Bresee Technology, Cyberlink Corp, Expasoft LLC, Fujitsu Research and Development Center, Gorilla Technology, Idemia, Neurotechnology, NEO Systems, NHN Corp, Paravision, Panasonic R+D Center Singapore, and Shenzhen University-Macau University of Science and Technology.
- ▷ We have retired results for twelve algorithms per our policy to only list results for two algorithms per developer. Results for retired algorithms appear in prior versions of this report in the [archive](#).

2021-06-25 changes since 2021-05-21:

- ▷ We have added results for first algorithms from six new developers: Alice Biometrics, BOE Technology Group, Fincore, Neosecu, Sodec App, and Yuntu Data and Technology.
- ▷ We have added results for new algorithms from seven returning developers: Incode Technologies, HyperVerge, Mobbeel Solutions, Guangzhou Pixel Solutions, Remark Holdings, Sensetime, and Vietnam Posts and Telecommunications Group.
- ▷ We have retired results for four algorithms per our policy to only list results for two algorithms per developer. Results for retired algorithms appear in prior versions of this report in the [archive](#).

2021-05-21 changes since 2021-04-26:

- ▷ We have added results for first algorithms from five new developers: Ekin Smart City Technologies, Suprema ID, Tripleize, Taiwan-Certificate Authority, and Vision Intelligence Center of Meituan.
- ▷ We have added results for new algorithms from eight returning developers: ID3 Technology, Imagus Technology, Momentum Digital, N-Tech Lab, NSENSE, Shanghai Jiao Tong University, Vision-Box, and Yuan High-Tech Development
- ▷ We have retired results for seven algorithms per our policy to only list results for two algorithms per developer. Results for retired algorithms appear in prior versions of this report in the [archive](#).

2021-04-26 changes since 2021-04-16:

- ▷ We have added results for first algorithms from three new developers: Quantasoft, Rendip, and NEO Systems.
- ▷ We have added results for new algorithms from four returning developers: 3Divi, Realnetworks, Veridas Digital Authentication Solutions, and Universidade de Coimbra.
- ▷ We have retired results for three algorithms per our policy to only list results for two algorithms per developer. Results for retired algorithms appear in prior versions of this report in the [archive](#).

2021-04-16 changes since 2021-03-19:

- ▷ We have added results for first algorithms from six new developers: 20Face, Beijing DeepSense Technologies, BitCenter UK, Enface, FaceTag, InsightFace AI, Line Corporation, Lema Labs, Nanjing Kiwi Network Technology, Omnidarde, Regula Forensics, and Suprema.
- ▷ We have added results for new algorithms from ten returning developers: CloudSmart Consulting, Dermalog, GeoVision, Neurotechnology, Panasonic R+D Center Singapore, Samsung S1, Securif AI, Trueface.ai, Vigilant Solutions, and Visidon.
- ▷ We have retired results for ten algorithms per our policy to only list results for two algorithms per developer. Results for retired algorithms appear in prior versions of this report in the [archive](#).

2021-03-19 changes since 2021-03-05:

- ▷ We have added results for first algorithms from six new developers: Ajou University, AuthenMetric, Code Everest, Corsight, Papilon Savunma, and NHN Corp
- ▷ We have added results for new algorithms from seven returning developers: Alchera, Deepglint, Fiber-home Telecommunication Technologies, Kakao Enterprise, Kookmin University, Megvii/Face++, and NotionTag Technologies.
- ▷ We have updated many of the hyperlinked HTML report-cards to include seven figures on demographic dependence. Figures of this kind first appeared, and are documented in, the December 2019 document, [NIST Interagency Report 8280](#) on demographic differentials in face recognition. The figures quantify false negative dependence on demographics using “visa-border” comparisons, and false positive dependence using comparisons of “application” photos that uniformly of quality and similar to visa photos.

2021-03-05 changes since 2021-01-19:

- ▷ We have added results for first algorithms from three new developers: IVA Cognitive, Mobbeel, and MoreDian Technology.
- ▷ We have added results for new algorithms from returning developers: Ability Enterprise - Andro Video, ACI Software, Adera Global, AnyVision, BioID Technologies, China Electronics Import-Export, Cognitec Systems, Fujitsu Research and Development Center, Glory, Guangzhou Pixel Solutions, Hengrui AI Technology, Incode Technologies, Intel Research, iQIYI, Mobai, Oz Forensics, Paravision, VisionLabs, and Xforward AI Technology.
- ▷ We have added a new “resources” tab to the main [webpage](#). It includes sortable columns for data related to speed, model size, storage, and memory consumption.
- ▷ We have retired results for 13 algorithms per our policy to only list results for two algorithms per developer. Results for retired algorithms appear in prior versions of this report in the [archive](#).

2021-01-19 changes since 2020-12-18:

- ▷ This report adds results for first algorithms from four developers: Herta Security, Irex AI, Shenzhen University-Macau University of Science and Technology, and Vietnam Posts and Telecommunications Group. See Table 7 for more information.
- ▷ The report also includes results for thirteen developers who have previously submitted algorithms: Bresee Technology, Canon (previously Canon Information Technology (Beijing)), Cyberlink, CSA IntelliCloud Technology, Dahua Technology, ID3 Technology, Imagus Technology (Vixvizion), Moontime Smart Technology, N-Tech Lab, Thales Cogent, Veridas Digital Authentication Solutions, Vocord, and Yuan High-Tech Development.

- ▷ We have retired results for ten algorithms per our policy to only list results for two algorithms per developer. Results for retired algorithms appear in prior versions of this report in the [archive](#).

2020-12-18 changes since 2020-10-09:

- ▷ This report adds results for first algorithms from ten developers: BitCenter UK, CloudSmart Consulting, Cubox, Institute of Computing Technology, Naver Corp, Minivision, NSENSE Corp, Viettel Group, Visage Technologies, and Xiamen University. See Table 7 for more information.
- ▷ The report also includes results for eighteen developers who have previously submitted algorithms: ADVANCE.AI, Awudit Systems, Chosun University, Dermalog, GeoVision, ICM Airport Technics, Idemia, Institute of Information Technologies, Kakao Enterprise, Neurotechnology, Panasonic R+D Center Singapore, Rank One Computing, SenseTime Group, Shanghai Jiao Tong University, TigerIT Americas LLC, Vigilant Solutions, Winsense, and YooniK
- ▷ We have retired results for twelve algorithms per our policy to only list results for two algorithms per developer. Results for retired algorithms appear in prior versions of this report in the [archive](#).

Changes since September 18, 2020:

- ▷ This report adds results for first algorithms from five developers: Aigen, Cortica, Kookmin University, Securif AI and Vinai.
- ▷ The report also includes results for three developers who have previously submitted algorithms: Fujitsu Laboratories, Hengrui AI, and X-Forward AI.
- ▷ In the per-algorithm report-cards linked from tables and the main webpage, we have added a chart to showing reduction in error rates over the course of FRVT i.e. from 2017 onwards for all algorithms supplied by that developer. Similarly we have added a chart showing error rate reductions for our test of protective face mask verification.
- ▷ We plan to continue evaluating algorithms on various mask datasets. We hold that algorithms should be capable of detecting masks and verifying identity of all combinations of masked and unmasked faces. We have accordingly increased the amount of time allowed to extract those features from 1.0 to 1.5 seconds.

Changes since August 25, 2020:

- ▷ This report adds results for first algorithms from eight new developers. Akurat Satu Indonesia, Cybercore, Decatur Industries, Innef Labs, Satellite Innovation/Eocortex, Expasoft, and Mobai.
- ▷ The report includes results for seven developers who have previously submitted algorithms: 3Divi, BioID Technologies, Incode Technologies, Innovatrics, iSAP Solution, Synology, and Tevian.
- ▷ We have retired results for five algorithms per our policy to only list results for two algorithms per developer. Results for retired algorithms appear in prior versions of this report in the [archive](#).

Changes since July 27, 2020:

- ▷ We have introduced per-algorithm report sheets. These are HTML documents linked from the accuracy tables in this report (i.e. Table 29) and on the FRVT 1:1 [homepage](#). The sheets contain interactive graphics allowing, for example, mouseover exploration of FNMR(T) and FMR(T). Some of their content had previously appeared in this document.
- ▷ This report adds results for algorithms from six new developers. ACI Software, Bresee Technology, Fiberhome Telecommunication Technologies, Imageware Systems, Oz Forensics, and Pensees.
- ▷ The report includes results for thirteen developers who have previously submitted algorithms: Canon Information Technology (Beijing), Cyberlink, Dahua Technology, Gorilla Technology, ID3 Technology, Intel Research Group, iQIYI Inc, Momentum Digital, Netbridge Technology, Tech5 SA, Shenzhen AiMall Tech, Vigilant Solutions, and VisionLabs.
- ▷ We have retired results for nine algorithms per our policy to only list results for two algorithms per developer. Results for retired algorithms appear in prior versions of this report in the [archive](#).

Changes since May 18, 2020:

- ▷ The report is the first FRVT update since the pandemic closed it from March to June 2020.
- ▷ This report includes results for algorithms from nine new developers: GeoVision Inc, Su Zhou NaZhi-TianDi Intelligent Technology, YooniK, AYF Technology, PXL Vision AG, Yuan High-Tech Development, Beihang University-ERCACAT, ICM Airport Technics, and Staqu Technologies
- ▷ This report includes results for algorithms from 15 returning developers Acer Incorporated, Antheus Technologia, Chosun University, Chunghwa Telecom, Idemia, Moontime Smart Technology, Neurotechnology, Guangzhou Pixel Solutions, Panasonic R+D Center Singapore, Rank One Computing, Scanovate, Shanghai Universiy - Shanghai Film Academy, Synesis, Trueface.ai, and Veridas Digital Authentication Solutions
- ▷ We have retired results for ten algorithms per our policy to only list results for two algorithms per developer. Results for retired algorithms appear in prior versions of this report in the [archive](#).
- ▷ We separated timing and other resource consumption from the main participation table. The new Table 18 includes template generation durations for four kinds of images, not just mugshots.
- ▷ We have published a separate report, [NIST Interagency Report 8311](#) on accuracy of pre-pandemic algorithms on subjects wearing face masks. We plan to track improvements in accuracy on masked images going forward. In particular, we invite submission of algorithms that can detect whether a person is wearing a mask, extract features from the full face or the exposed periocular region, and do appropriate comparison. We do not intend to evaluate algorithms that assume 100% of images will be of masked individuals.

Changes since March 25, 2020:

- ▷ The report is a maintenance release - it does not add any new algorithms, and FRVT has been closed to new algorithms since mid March 2020.
- ▷ We modified the primary accuracy summary, Table 29, as follows:
 - ▷▷ For visa images, the column for FNMR at FMR = 0.0001 has been removed. The visa images are so highly controlled that the error rates for the most accurate algorithms are dominated by false rejection of very young children and by the presence of a few noisy greyscale images. For now, two visa columns remain: FNMR at FMR= 10^{-6} and, for matched covariates, FNMR at FMR= 10^{-4} .

- ▷▷ We have inserted a new column labelled “BORDER” giving accuracy for comparison of moderately poor webcam border-crossing photos that exhibit pose variations, poor compression, and low contrast due to strong background illumination. The accuracies are the worst from all cooperative image datasets used in FRVT.
- ▷ Accordingly, we updated the failure-to-template rates in Table 37.
- ▷ We withdrew a figure showing how false matches are concentrated in certain visa images used in cross-comparison, because it didn’t attempt to include demographic information.

Changes since February 27, 2020:

- ▷ The report adds results algorithms from two new developers: Beijing Alleyes Technology, and the Chinese University of Hong Kong. Results for newly submitted algorithms from two other developers will appear in the next report.
- ▷ The report adds results for algorithms from thirteen returning developers: ASUSTek Computer, Aware, Cyberlink Corp, Gorilla Technology, Innovative Technology, Kakao Enterprise, Lomonosov Moscow State University, Panasonic R+D Center Singapore, Shenzhen AiMall Technology, Shenzhen Intellifusion Technologies, Synology, Tech5 SA, and Via Technologies.
- ▷ Per policy to only list results for two algorithms per developer, we have dropped results for algorithms from Aware, Cyberlink, Gorilla Technology, Kakao Enterprise, Lomonosov Moscow State University, Panasonic R+D Center Singapore, and Tech5 SA.

Changes since January 20, 2020:

- ▷ The report adds results for five new developers: Ability Enterprise (Andro Video), Chosun University, Fujitsu Research and Development Center, University of Coimbra, and Xforward AI Technology.
- ▷ The report adds results for algorithms from six returning developers: AlphaSSTG, Incode Technologies, Kneron, Shanghai Jiao Tong University, Vocord, and X-Laboratory.
- ▷ We have corrected template comparison timing numbers for algorithms submitted September 2019 to January 2020. The values reported previously were slower due to a software bug.
- ▷ We have dropped results for algorithms from Vocord and Incode per policy to only list results for two algorithms per developer.
- ▷ The [FRVT 1:1 homepage](#) has been updated with latest accuracy results.
- ▷ The [FRVT 1:N homepage](#) now includes an update to the September 2019 NIST Interagency Report 8271. The new report adds results for one-to-many search algorithms submitted to NIST from June 2019 to January 2020.

Changes since January 6, 2020:

- ▷ Section 2 has been updated to better describe the Visa and Border images. The caption for Table 29 has been updated to better relate the accuracy values to particular image comparisons.
- ▷ The report adds results for five new developers: Acer, Advance.AI, Expasoft, Netbridge Technology, and Videmo Intelligent Videoanalyse.
- ▷ The report adds results for algorithms from 7 returning developers: China Electronics Import-Export Corp, Intel Research Group, ITMO University, Neurotechnology, N-Tech Lab, Rokid, and VisionLabs.

- ▷ We have dropped results from this edition of the report per policy to only list results for two algorithms per developer: N-Tech Lab, Neurotechnology, ITMO, Visionlabs, and CEIEC.
- ▷ The [FRVT homepage](#) has been updated with latest accuracy results.

Changes since November 11, 2019:

- ▷ Table 18 has been updated to include runtime memory usage. This is the first time such a quantity has been reported. The value is the peak size of the resident set size logged during enrollment of single images.
- ▷ We have migrated summary results table to a new platform that supports sortable tables:
<https://pages.nist.gov/frvt/html/frvt11.html>
- ▷ The report adds results for four new developers: Antheus Technologia, BioID Technologies SA, Canon Information Tech. (Beijing), Samsung S1 (listed in the tables as S1), and Taiwan AI Labs.
- ▷ The report adds results for algorithms from 13 returning developers: Anke Investments, Chunghwa Telecom, Deepglint, Institute of Information Technologies, iQIYI, Kneron, Ping An Technology, Paravision, KanKan Ai, Rokid Corporation, Shanghai Universiy - Shanghai Film Academy, Veridas Digital Authentication Solutions, and Videonetics Technology.
- ▷ We have dropped results from this edition of the report per policy to only list results for two algorithms per developer: remarkai-000, veridas-001, senesetime-001, iit-000, anke-003, and everai-002. Results for these are available in prior editions of this report linked from the FRVT page.
- ▷ We issued [NIST Interagency Report 8280: FRVT Part 3: Demographics](#) on 2019-12-19. It includes results for many of the algorithms covered by this report.

Changes since October 16, 2019:

- ▷ The report adds results for ten new developers: Ai-Union Technology, ASUSTek Computer, DiDi ChuXing Technology, Innovative Technology, Luxand, MVision, Pyramid Cyber Security + Forensic, Scanovate, Shenzhen AiMall Tech, and TUPU Technology.
- ▷ The report adds results for 12 returning developers: CTBC Bank Glory Gorilla Technology Guangzhou Pixel Solutions Imagus Technology Incode Technologies Lomonosov Moscow State University Rank One Computing Samtech InfoNet Shanghai Ulucu Electronics Technology Synesis, and Winsense.
- ▷ We have dropped results from this edition of the report per policy to only list results for two algorithms per developer: glory-000, gorilla-002, incode-003, rankone-006, and synesis-004.
- ▷ Results for five recently submitted algorithms will appear in the next report.

Changes since September 11, 2019:

- ▷ The report adds results for five new participants: Awidit Systems (Awiros), Momentum Digital (Sertis), Trueface AI, Shanghai Jiao Tong University, and X-Laboratory.
- ▷ The report adds results for five new algorithms from returning developers: Cyberlink, Hengrui AI Technology, Idemia, Panasonic R+D Singapore, and Tevian. This causes three algorithms to be de-listed from the report per policy to list results for two algorithms per developer.

Changes since July 31 2019:

- ▷ The HTML table on the [FRVT 1:1 homepage](#) has been updated to include a column for cross-domain Visa-Border verification. Results for this new dataset appeared in the July 29 report under the name "CrossEV" - these are now renamed "Visa-Border".
- ▷ The [FRVT 1:1 homepage](#) lists algorithms according to lowest mean rank accuracy:

$$\begin{aligned} \text{Rank(FNMR}_{\text{VISA}} \text{ at FMR = 0.000001}) + \\ \text{Rank(FNMR}_{\text{VISA-BORDER}} \text{ at FMR = 0.000001}) + \\ \text{Rank(FNMR}_{\text{MUGSHOT}} \text{ at FMR = 0.00001 after 14 years}) + \\ \text{Rank(FNMR}_{\text{WILD}} \text{ at FMR = 0.00001}) \end{aligned}$$

This ordering rewards high accuracy across all datasets.
- ▷ The main results in Table 29 is now in landscape format to accomodate extra columns for the Visa-Border set, and mugshot comparisons after at least 12 years.
- ▷ The report adds results for nine new participants: Alpha SSTG, Intel Research, ULSee, Chungwa Telecon, iSAP Solution, Rokid, Shenzhen EI Networks, CSA Intellicloud, Shenzhen Intellifusion Technologies.
- ▷ The reports adds results for six new algorithms from returning developers: Innovatrics, Dahua Technology, Tech5 SA, Intellivision, Nodeflux and Imperial College, London. One algorithm, from Imperial has been retired, per policy to list results for two algorithms per developer.
- ▷ The cross-country false match rate heatmaps have been replotted to reveal more structure by listing countries by region instead of alphabetically.
- ▷ The next version of this report will be posted around October 18, 2019.

Changes since July 3 2019:

- ▷ The HTML table on the [FRVT 1:1 homepage](#) has been updated to list the 20 most accurate developers rather than algorithms, choosing the most accurate algorithm from each developer based on visa and mugshot results. Also, the algorithms are ordered in terms of lowest mean rank across mugshot, visa and wild datasets, rewarding broad accuracy over a good result on one particular dataset.
- ▷ This report includes results for a new dataset - see the column labelled "visa-border" in Table 5. It compares a new set of high quality visa-like portraits with a set webcam border-crossing photos that exhibit moderately poor pose variations and background illumination. The two new sets are described in sections 2.2 and 2.3. The comparisons are "cross-domain" in that the algorithm must compare "visa" and "wild" images. Results for other algorithms will be added in future reports as they become available.
- ▷ This report adds results for algorithms from 9 developers submitted in early July 2019. These are from 3DiVi, Camvi, EverAI-Paravision, Facesoft, Farbar (F8), Institute of Information Technologies, Shanghai U. Film Academy, Via Technologies, and Ulucu Electronics Tech. Six of these are new participants.
- ▷ Several other algorithms have been submitted and are being evaluated. Results will be released in the next report, scheduled for September 5. That report will include results for new datasets.
- ▷ Older algorithms from Everai, Camvi and 3DiVi, have been retired, per the policy to list only two algorithms per developer.

Changes since June 20 2019:

- ▷ This report adds results for algorithms from 18 developers submitted in early June 2019. These are from CTBC Bank, Deep Glint, Thales Cogent, Ever AI Paravision, Gorilla Technology, Imagus, Incode, Kneron, N-Tech Lab, Neurotechnology, Notiontag Technologies, Star Hybrid, Videonetics, Vigilant Solutions, Winsense, Anke Investments, CEIEC, and DSK. Nine of these are new participants.
- ▷ Several other algorithms have been submitted and are being evaluated. Results will be released in the next report, scheduled for August 1.
- ▷ Older algorithms from Everai, Thales Cogent, Gorilla Technology, Incode, Neurotechnology, N-Tech Lab and Vigilant Solutions have been retired, per the policy to list only two algorithms per developer.

Changes since April 2019:

- ▷ This report adds results for nine algorithms from nine developers submitted in early June 2019. These are from Tencent Deepsea, Hengrui, Kedacom, Moontime, Guangzhou Pixel, Rank One Computing, Synesis, Sensetime and Vocord.
- ▷ Another 23 algorithms have been submitted and are being evaluated. Results will be released in the next report, scheduled for July 3.
- ▷ Older algorithms for Rank One, Synesis, and Vocord have been retired, per the policy to list only two algorithms per developer.

Changes since February 2019:

- ▷ This report adds results for 49 algorithms from 42 developers submitted in early March 2019.
- ▷ This report omits results for algorithms that we retired. We retired for three reasons: 1. The developer submitted a new algorithm, and we only list two. 2. The algorithm needs a GPU, and we no longer allow GPU-based algorithms. 3. Inoperable algorithms.
- ▷ Previous results for retired algorithms are available in older editions of this report linked [here](#).
- ▷ The mugshot database used from February 2017 to January 2019 has been replaced with an extract of the mugshot database documented in NIST Interagency Report 8238, November 2018. The new mugshot set is described in section [2.4](#) and is adopted because:
 - ▷▷ It has much better identity label integrity, so that false non-match rates are substantially lower than those reported in FRVT 1:1 reports to date - see Figure [107](#).
 - ▷▷ It includes images collected over a 17 year period such that ageing can be much better characterized - - see Figure [342](#).
- ▷ Using the new mugshot database, Figure [342](#) shows accuracy for four demographic groups identified in the biographic metadata that accompanies the data: black females, black males, white females and white males.
- ▷ The report added a figure (now moved to web) with results for the twenty human-difficult pairs used in the May 2018 paper *Face recognition accuracy of forensic examiners, superrecognizers, and face recognition algorithms* by Phillips et al. [[1](#)].
- ▷ The report uses an update to the wild image database that corrects some ground truth labels.
- ▷ Some results for the child exploitation database are not complete. They are typically updated less frequently than for other image sets.

Contents

| | |
|--|-----------|
| ACKNOWLEDGMENTS | 1 |
| DISCLAIMER | 1 |
| INSTITUTIONAL REVIEW BOARD | 1 |
| 1 METRICS | 54 |
| 1.1 CORE ACCURACY | 54 |
| 1.2 MULTI-TEMPLATE SCORING METHODOLOGY | 54 |
| 2 DATASETS | 55 |
| 2.1 VISA IMAGES | 55 |
| 2.2 APPLICATION IMAGES | 55 |
| 2.3 BORDER CROSSING IMAGES | 55 |
| 2.4 MUGSHOT IMAGES | 56 |
| 2.5 KIOSK IMAGES | 56 |
| 2.6 WILD IMAGES | 56 |
| 3 RESULTS | 57 |
| 3.1 TEST GOALS | 57 |
| 3.2 TEST DESIGN | 57 |
| 3.3 FAILURE TO ENROLL | 60 |
| 3.4 RECOGNITION ACCURACY | 69 |
| 3.5 GENUINE DISTRIBUTION STABILITY | 344 |
| 3.5.1 EFFECT OF BIRTH PLACE ON THE GENUINE DISTRIBUTION | 344 |
| 3.5.2 EFFECT OF AGEING | 382 |
| 3.5.3 EFFECT OF AGE ON GENUINE SUBJECTS | 411 |
| 3.6 IMPOSTOR DISTRIBUTION STABILITY | 450 |
| 3.6.1 EFFECT OF BIRTH PLACE ON THE IMPOSTOR DISTRIBUTION | 450 |
| 3.6.2 EFFECT OF AGE ON IMPOSTORS | 453 |

List of Tables

| | |
|-------------------------------------|----|
| 1 PARTICIPANT INFORMATION | 23 |
| 2 PARTICIPANT INFORMATION | 24 |
| 3 PARTICIPANT INFORMATION | 25 |
| 4 PARTICIPANT INFORMATION | 26 |
| 5 PARTICIPANT INFORMATION | 27 |
| 6 PARTICIPANT INFORMATION | 28 |
| 7 PARTICIPANT INFORMATION | 29 |
| 8 ALGORITHM SUMMARY | 30 |
| 9 ALGORITHM SUMMARY | 31 |
| 10 ALGORITHM SUMMARY | 32 |
| 11 ALGORITHM SUMMARY | 33 |
| 12 ALGORITHM SUMMARY | 34 |
| 13 ALGORITHM SUMMARY | 35 |
| 14 ALGORITHM SUMMARY | 36 |
| 15 ALGORITHM SUMMARY | 37 |
| 16 ALGORITHM SUMMARY | 38 |
| 17 ALGORITHM SUMMARY | 39 |
| 18 ALGORITHM SUMMARY | 40 |
| 19 FALSE NON-MATCH RATE | 41 |

| | | |
|----|------------------------|----|
| 20 | FALSE NON-MATCH RATE | 42 |
| 21 | FALSE NON-MATCH RATE | 43 |
| 22 | FALSE NON-MATCH RATE | 44 |
| 23 | FALSE NON-MATCH RATE | 45 |
| 24 | FALSE NON-MATCH RATE | 46 |
| 25 | FALSE NON-MATCH RATE | 47 |
| 26 | FALSE NON-MATCH RATE | 48 |
| 27 | FALSE NON-MATCH RATE | 49 |
| 28 | FALSE NON-MATCH RATE | 50 |
| 29 | FALSE NON-MATCH RATE | 51 |
| 30 | FAILURE TO ENROL RATES | 61 |
| 31 | FAILURE TO ENROL RATES | 62 |
| 32 | FAILURE TO ENROL RATES | 63 |
| 33 | FAILURE TO ENROL RATES | 64 |
| 34 | FAILURE TO ENROL RATES | 65 |
| 35 | FAILURE TO ENROL RATES | 66 |
| 36 | FAILURE TO ENROL RATES | 67 |
| 37 | FAILURE TO ENROL RATES | 68 |

List of Figures

| | | |
|-----|--|----|
| 1 | PERFORMANCE SUMMARY: FNMR VS. TEMPLATE SIZE TRADEOFF | 52 |
| 2 | PERFORMANCE SUMMARY: FNMR VS. TEMPLATE TIME TRADEOFF | 53 |
| 3 | EXAMPLE IMAGES | 57 |
| (A) | VISA | 57 |
| (B) | MUGSHOT | 57 |
| (C) | WILD | 57 |
| (D) | BORDER | 57 |
| 4 | PERFORMANCE ON 20 HUMAN-DIFFICULT PAIRS | 70 |
| 5 | PERFORMANCE ON 20 HUMAN-DIFFICULT PAIRS | 71 |
| 6 | PERFORMANCE ON 20 HUMAN-DIFFICULT PAIRS | 72 |
| 7 | PERFORMANCE ON 20 HUMAN-DIFFICULT PAIRS | 73 |
| 8 | PERFORMANCE ON 20 HUMAN-DIFFICULT PAIRS | 74 |
| 9 | PERFORMANCE ON 20 HUMAN-DIFFICULT PAIRS | 75 |
| 10 | PERFORMANCE ON 20 HUMAN-DIFFICULT PAIRS | 76 |
| 11 | PERFORMANCE ON 20 HUMAN-DIFFICULT PAIRS | 77 |
| 12 | PERFORMANCE ON 20 HUMAN-DIFFICULT PAIRS | 78 |
| 13 | PERFORMANCE ON 20 HUMAN-DIFFICULT PAIRS | 79 |
| 14 | PERFORMANCE ON 20 HUMAN-DIFFICULT PAIRS | 80 |
| 15 | PERFORMANCE ON 20 HUMAN-DIFFICULT PAIRS | 81 |
| 16 | PERFORMANCE ON 20 HUMAN-DIFFICULT PAIRS | 82 |
| 17 | PERFORMANCE ON 20 HUMAN-DIFFICULT PAIRS | 83 |
| 18 | PERFORMANCE ON 20 HUMAN-DIFFICULT PAIRS | 84 |
| 19 | PERFORMANCE ON 20 HUMAN-DIFFICULT PAIRS | 85 |
| 20 | PERFORMANCE ON 20 HUMAN-DIFFICULT PAIRS | 86 |
| 21 | PERFORMANCE ON 20 HUMAN-DIFFICULT PAIRS | 87 |
| 22 | PERFORMANCE ON 20 HUMAN-DIFFICULT PAIRS | 88 |
| 23 | PERFORMANCE ON 20 HUMAN-DIFFICULT PAIRS | 89 |
| 24 | PERFORMANCE ON 20 HUMAN-DIFFICULT PAIRS | 90 |
| 25 | PERFORMANCE ON 20 HUMAN-DIFFICULT PAIRS | 91 |
| 26 | PERFORMANCE ON 20 HUMAN-DIFFICULT PAIRS | 92 |
| 27 | PERFORMANCE ON 20 HUMAN-DIFFICULT PAIRS | 93 |
| 28 | PERFORMANCE ON 20 HUMAN-DIFFICULT PAIRS | 94 |
| 29 | PERFORMANCE ON 20 HUMAN-DIFFICULT PAIRS | 95 |
| 30 | PERFORMANCE ON 20 HUMAN-DIFFICULT PAIRS | 96 |

| | | |
|----|---|-----|
| 31 | PERFORMANCE ON 20 HUMAN-DIFFICULT PAIRS | 97 |
| 32 | PERFORMANCE ON 20 HUMAN-DIFFICULT PAIRS | 98 |
| 33 | PERFORMANCE ON 20 HUMAN-DIFFICULT PAIRS | 99 |
| 34 | PERFORMANCE ON 20 HUMAN-DIFFICULT PAIRS | 100 |
| 35 | PERFORMANCE ON 20 HUMAN-DIFFICULT PAIRS | 101 |
| 36 | PERFORMANCE ON 20 HUMAN-DIFFICULT PAIRS | 102 |
| 37 | PERFORMANCE ON 20 HUMAN-DIFFICULT PAIRS | 103 |
| 38 | PERFORMANCE ON 20 HUMAN-DIFFICULT PAIRS | 104 |
| 39 | PERFORMANCE ON 20 HUMAN-DIFFICULT PAIRS | 105 |
| 40 | ERROR TRADEOFF CHARACTERISTIC: VISA IMAGES | 106 |
| 41 | ERROR TRADEOFF CHARACTERISTIC: VISA IMAGES | 107 |
| 42 | ERROR TRADEOFF CHARACTERISTIC: VISA IMAGES | 108 |
| 43 | ERROR TRADEOFF CHARACTERISTIC: VISA IMAGES | 109 |
| 44 | ERROR TRADEOFF CHARACTERISTIC: VISA IMAGES | 110 |
| 45 | ERROR TRADEOFF CHARACTERISTIC: VISA IMAGES | 111 |
| 46 | ERROR TRADEOFF CHARACTERISTIC: VISA IMAGES | 112 |
| 47 | ERROR TRADEOFF CHARACTERISTIC: VISA IMAGES | 113 |
| 48 | ERROR TRADEOFF CHARACTERISTIC: VISA IMAGES | 114 |
| 49 | ERROR TRADEOFF CHARACTERISTIC: VISA IMAGES | 115 |
| 50 | ERROR TRADEOFF CHARACTERISTIC: VISA IMAGES | 116 |
| 51 | ERROR TRADEOFF CHARACTERISTIC: VISA IMAGES | 117 |
| 52 | ERROR TRADEOFF CHARACTERISTIC: VISA IMAGES | 118 |
| 53 | ERROR TRADEOFF CHARACTERISTIC: VISA IMAGES | 119 |
| 54 | ERROR TRADEOFF CHARACTERISTIC: VISA IMAGES | 120 |
| 55 | ERROR TRADEOFF CHARACTERISTIC: VISA IMAGES | 121 |
| 56 | ERROR TRADEOFF CHARACTERISTIC: VISA IMAGES | 122 |
| 57 | ERROR TRADEOFF CHARACTERISTIC: VISA IMAGES | 123 |
| 58 | ERROR TRADEOFF CHARACTERISTIC: VISA IMAGES | 124 |
| 59 | ERROR TRADEOFF CHARACTERISTIC: VISA IMAGES | 125 |
| 60 | ERROR TRADEOFF CHARACTERISTIC: VISA IMAGES | 126 |
| 61 | ERROR TRADEOFF CHARACTERISTIC: VISA IMAGES | 127 |
| 62 | ERROR TRADEOFF CHARACTERISTIC: VISA IMAGES | 128 |
| 63 | ERROR TRADEOFF CHARACTERISTIC: VISA IMAGES | 129 |
| 64 | ERROR TRADEOFF CHARACTERISTIC: VISA IMAGES | 130 |
| 65 | ERROR TRADEOFF CHARACTERISTIC: VISA IMAGES | 131 |
| 66 | ERROR TRADEOFF CHARACTERISTIC: VISA IMAGES | 132 |
| 67 | ERROR TRADEOFF CHARACTERISTIC: VISA IMAGES | 133 |
| 68 | ERROR TRADEOFF CHARACTERISTIC: VISA IMAGES | 134 |
| 69 | ERROR TRADEOFF CHARACTERISTIC: VISA IMAGES | 135 |
| 70 | ERROR TRADEOFF CHARACTERISTIC: VISA IMAGES | 136 |
| 71 | ERROR TRADEOFF CHARACTERISTIC: VISA IMAGES | 137 |
| 72 | ERROR TRADEOFF CHARACTERISTIC: VISA IMAGES | 138 |
| 73 | ERROR TRADEOFF CHARACTERISTIC: VISA IMAGES | 139 |
| 74 | ERROR TRADEOFF CHARACTERISTIC: VISA IMAGES | 140 |
| 75 | ERROR TRADEOFF CHARACTERISTIC: VISA IMAGES | 141 |
| 76 | ERROR TRADEOFF CHARACTERISTIC: VISA IMAGES | 142 |
| 77 | ERROR TRADEOFF CHARACTERISTIC: VISA IMAGES | 143 |
| 78 | ERROR TRADEOFF CHARACTERISTIC: VISA IMAGES | 144 |
| 79 | ERROR TRADEOFF CHARACTERISTIC: VISA IMAGES | 145 |
| 80 | ERROR TRADEOFF CHARACTERISTIC: VISA IMAGES | 146 |
| 81 | ERROR TRADEOFF CHARACTERISTIC: VISA IMAGES | 147 |
| 82 | ERROR TRADEOFF CHARACTERISTIC: VISA IMAGES | 148 |
| 83 | ERROR TRADEOFF CHARACTERISTIC: VISA IMAGES | 149 |
| 84 | ERROR TRADEOFF CHARACTERISTIC: VISA IMAGES | 150 |
| 85 | ERROR TRADEOFF CHARACTERISTIC: MUGSHOT IMAGES | 151 |
| 86 | ERROR TRADEOFF CHARACTERISTIC: MUGSHOT IMAGES | 152 |

| | | |
|-----|--|-----|
| 87 | ERROR TRADEOFF CHARACTERISTIC: MUGSHOT IMAGES | 153 |
| 88 | ERROR TRADEOFF CHARACTERISTIC: MUGSHOT IMAGES | 154 |
| 89 | ERROR TRADEOFF CHARACTERISTIC: MUGSHOT IMAGES | 155 |
| 90 | ERROR TRADEOFF CHARACTERISTIC: MUGSHOT IMAGES | 156 |
| 91 | ERROR TRADEOFF CHARACTERISTIC: MUGSHOT IMAGES | 157 |
| 92 | ERROR TRADEOFF CHARACTERISTIC: MUGSHOT IMAGES | 158 |
| 93 | ERROR TRADEOFF CHARACTERISTIC: MUGSHOT IMAGES | 159 |
| 94 | ERROR TRADEOFF CHARACTERISTIC: MUGSHOT IMAGES | 160 |
| 95 | ERROR TRADEOFF CHARACTERISTIC: MUGSHOT IMAGES | 161 |
| 96 | ERROR TRADEOFF CHARACTERISTIC: MUGSHOT IMAGES | 162 |
| 97 | ERROR TRADEOFF CHARACTERISTIC: MUGSHOT IMAGES | 163 |
| 98 | ERROR TRADEOFF CHARACTERISTIC: MUGSHOT IMAGES | 164 |
| 99 | ERROR TRADEOFF CHARACTERISTIC: MUGSHOT IMAGES | 165 |
| 100 | ERROR TRADEOFF CHARACTERISTIC: MUGSHOT IMAGES | 166 |
| 101 | ERROR TRADEOFF CHARACTERISTIC: MUGSHOT IMAGES | 167 |
| 102 | ERROR TRADEOFF CHARACTERISTIC: MUGSHOT IMAGES | 168 |
| 103 | ERROR TRADEOFF CHARACTERISTIC: MUGSHOT IMAGES | 169 |
| 104 | ERROR TRADEOFF CHARACTERISTIC: MUGSHOT IMAGES | 170 |
| 105 | ERROR TRADEOFF CHARACTERISTIC: MUGSHOT IMAGES | 171 |
| 106 | ERROR TRADEOFF CHARACTERISTIC: MUGSHOT IMAGES | 172 |
| 107 | ERROR TRADEOFF CHARACTERISTIC: MUGSHOT IMAGES | 173 |
| 108 | ERROR TRADEOFF CHARACTERISTIC: WILD IMAGES | 174 |
| 109 | ERROR TRADEOFF CHARACTERISTIC: WILD IMAGES | 175 |
| 110 | ERROR TRADEOFF CHARACTERISTIC: WILD IMAGES | 176 |
| 111 | ERROR TRADEOFF CHARACTERISTIC: WILD IMAGES | 177 |
| 112 | ERROR TRADEOFF CHARACTERISTIC: WILD IMAGES | 178 |
| 113 | ERROR TRADEOFF CHARACTERISTIC: WILD IMAGES | 179 |
| 114 | ERROR TRADEOFF CHARACTERISTIC: WILD IMAGES | 180 |
| 115 | ERROR TRADEOFF CHARACTERISTIC: WILD IMAGES | 181 |
| 116 | ERROR TRADEOFF CHARACTERISTIC: WILD IMAGES | 182 |
| 117 | ERROR TRADEOFF CHARACTERISTIC: WILD IMAGES | 183 |
| 118 | ERROR TRADEOFF CHARACTERISTIC: WILD IMAGES | 184 |
| 119 | ERROR TRADEOFF CHARACTERISTIC: WILD IMAGES | 185 |
| 120 | ERROR TRADEOFF CHARACTERISTIC: WILD IMAGES | 186 |
| 121 | ERROR TRADEOFF CHARACTERISTIC: WILD IMAGES | 187 |
| 122 | ERROR TRADEOFF CHARACTERISTIC: WILD IMAGES | 188 |
| 123 | ERROR TRADEOFF CHARACTERISTIC: WILD IMAGES | 189 |
| 124 | ERROR TRADEOFF CHARACTERISTIC: WILD IMAGES | 190 |
| 125 | ERROR TRADEOFF CHARACTERISTIC: WILD IMAGES | 191 |
| 126 | ERROR TRADEOFF CHARACTERISTIC: WILD IMAGES | 192 |
| 127 | FALSE MATCH RATES WITHIN AND ACROSS DEMOGRAPHIC GROUPS | 193 |
| 128 | FALSE MATCH RATES WITHIN AND ACROSS DEMOGRAPHIC GROUPS | 194 |
| 129 | FALSE MATCH RATES WITHIN AND ACROSS DEMOGRAPHIC GROUPS | 195 |
| 130 | FALSE MATCH RATES WITHIN AND ACROSS DEMOGRAPHIC GROUPS | 196 |
| 131 | FALSE MATCH RATES WITHIN AND ACROSS DEMOGRAPHIC GROUPS | 197 |
| 132 | FALSE MATCH RATES WITHIN AND ACROSS DEMOGRAPHIC GROUPS | 198 |
| 133 | FALSE MATCH RATES WITHIN AND ACROSS DEMOGRAPHIC GROUPS | 199 |
| 134 | FALSE MATCH RATES WITHIN AND ACROSS DEMOGRAPHIC GROUPS | 200 |
| 135 | FALSE MATCH RATES WITHIN AND ACROSS DEMOGRAPHIC GROUPS | 201 |
| 136 | FALSE MATCH RATES WITHIN AND ACROSS DEMOGRAPHIC GROUPS | 202 |
| 137 | FALSE MATCH RATES WITHIN AND ACROSS DEMOGRAPHIC GROUPS | 203 |
| 138 | FALSE MATCH RATES WITHIN AND ACROSS DEMOGRAPHIC GROUPS | 204 |
| 139 | FALSE MATCH RATES WITHIN AND ACROSS DEMOGRAPHIC GROUPS | 205 |
| 140 | FALSE MATCH RATES WITHIN AND ACROSS DEMOGRAPHIC GROUPS | 206 |
| 141 | FALSE MATCH RATES WITHIN AND ACROSS DEMOGRAPHIC GROUPS | 207 |
| 142 | FALSE MATCH RATES WITHIN AND ACROSS DEMOGRAPHIC GROUPS | 208 |
| 143 | FALSE MATCH RATES WITHIN AND ACROSS DEMOGRAPHIC GROUPS | 209 |

| | | |
|-----|--|-----|
| 144 | FALSE MATCH RATES WITHIN AND ACROSS DEMOGRAPHIC GROUPS | 210 |
| 145 | FALSE MATCH RATES WITHIN AND ACROSS DEMOGRAPHIC GROUPS | 211 |
| 146 | FALSE MATCH RATES WITHIN AND ACROSS DEMOGRAPHIC GROUPS | 212 |
| 147 | FALSE MATCH RATES WITHIN AND ACROSS DEMOGRAPHIC GROUPS | 213 |
| 148 | FALSE MATCH RATES WITHIN AND ACROSS DEMOGRAPHIC GROUPS | 214 |
| 149 | SEX AND RACE EFFECTS: MUGSHOT IMAGES | 215 |
| 150 | SEX AND RACE EFFECTS: MUGSHOT IMAGES | 216 |
| 151 | SEX AND RACE EFFECTS: MUGSHOT IMAGES | 217 |
| 152 | SEX AND RACE EFFECTS: MUGSHOT IMAGES | 218 |
| 153 | SEX AND RACE EFFECTS: MUGSHOT IMAGES | 219 |
| 154 | SEX AND RACE EFFECTS: MUGSHOT IMAGES | 220 |
| 155 | SEX AND RACE EFFECTS: MUGSHOT IMAGES | 221 |
| 156 | SEX AND RACE EFFECTS: MUGSHOT IMAGES | 222 |
| 157 | SEX AND RACE EFFECTS: MUGSHOT IMAGES | 223 |
| 158 | SEX AND RACE EFFECTS: MUGSHOT IMAGES | 224 |
| 159 | SEX AND RACE EFFECTS: MUGSHOT IMAGES | 225 |
| 160 | SEX AND RACE EFFECTS: MUGSHOT IMAGES | 226 |
| 161 | SEX AND RACE EFFECTS: MUGSHOT IMAGES | 227 |
| 162 | SEX AND RACE EFFECTS: MUGSHOT IMAGES | 228 |
| 163 | SEX AND RACE EFFECTS: MUGSHOT IMAGES | 229 |
| 164 | SEX AND RACE EFFECTS: MUGSHOT IMAGES | 230 |
| 165 | SEX AND RACE EFFECTS: MUGSHOT IMAGES | 231 |
| 166 | SEX AND RACE EFFECTS: MUGSHOT IMAGES | 232 |
| 167 | SEX AND RACE EFFECTS: MUGSHOT IMAGES | 233 |
| 168 | SEX AND RACE EFFECTS: MUGSHOT IMAGES | 234 |
| 169 | SEX AND RACE EFFECTS: MUGSHOT IMAGES | 235 |
| 170 | SEX AND RACE EFFECTS: MUGSHOT IMAGES | 236 |
| 171 | SEX AND RACE EFFECTS: MUGSHOT IMAGES | 237 |
| 172 | SEX EFFECTS: VISA IMAGES | 238 |
| 173 | SEX EFFECTS: VISA IMAGES | 239 |
| 174 | SEX EFFECTS: VISA IMAGES | 240 |
| 175 | SEX EFFECTS: VISA IMAGES | 241 |
| 176 | SEX EFFECTS: VISA IMAGES | 242 |
| 177 | SEX EFFECTS: VISA IMAGES | 243 |
| 178 | SEX EFFECTS: VISA IMAGES | 244 |
| 179 | SEX EFFECTS: VISA IMAGES | 245 |
| 180 | SEX EFFECTS: VISA IMAGES | 246 |
| 181 | SEX EFFECTS: VISA IMAGES | 247 |
| 182 | SEX EFFECTS: VISA IMAGES | 248 |
| 183 | SEX EFFECTS: VISA IMAGES | 249 |
| 184 | SEX EFFECTS: VISA IMAGES | 250 |
| 185 | SEX EFFECTS: VISA IMAGES | 251 |
| 186 | SEX EFFECTS: VISA IMAGES | 252 |
| 187 | SEX EFFECTS: VISA IMAGES | 253 |
| 188 | SEX EFFECTS: VISA IMAGES | 254 |
| 189 | SEX EFFECTS: VISA IMAGES | 255 |
| 190 | SEX EFFECTS: VISA IMAGES | 256 |
| 191 | SEX EFFECTS: VISA IMAGES | 257 |
| 192 | SEX EFFECTS: VISA IMAGES | 258 |
| 193 | SEX EFFECTS: VISA IMAGES | 259 |
| 194 | SEX EFFECTS: VISA IMAGES | 260 |
| 195 | SEX EFFECTS: VISA IMAGES | 261 |
| 196 | SEX EFFECTS: VISA IMAGES | 262 |
| 197 | SEX EFFECTS: VISA IMAGES | 263 |
| 198 | SEX EFFECTS: VISA IMAGES | 264 |
| 199 | SEX EFFECTS: VISA IMAGES | 265 |
| 200 | SEX EFFECTS: VISA IMAGES | 266 |

| | |
|--|-----|
| 201 SEX EFFECTS: VISA IMAGES | 267 |
| 202 SEX EFFECTS: VISA IMAGES | 268 |
| 203 SEX EFFECTS: VISA IMAGES | 269 |
| 204 SEX EFFECTS: VISA IMAGES | 270 |
| 205 SEX EFFECTS: VISA IMAGES | 271 |
| 206 SEX EFFECTS: VISA IMAGES | 272 |
| 207 SEX EFFECTS: VISA IMAGES | 273 |
| 208 SEX EFFECTS: VISA IMAGES | 274 |
| 209 SEX EFFECTS: VISA IMAGES | 275 |
| 210 FALSE MATCH RATE CALIBRATION: MUGSHOT IMAGES | 276 |
| 211 FALSE MATCH RATE CALIBRATION: MUGSHOT IMAGES | 277 |
| 212 FALSE MATCH RATE CALIBRATION: MUGSHOT IMAGES | 278 |
| 213 FALSE MATCH RATE CALIBRATION: MUGSHOT IMAGES | 279 |
| 214 FALSE MATCH RATE CALIBRATION: MUGSHOT IMAGES | 280 |
| 215 FALSE MATCH RATE CALIBRATION: MUGSHOT IMAGES | 281 |
| 216 FALSE MATCH RATE CALIBRATION: MUGSHOT IMAGES | 282 |
| 217 FALSE MATCH RATE CALIBRATION: MUGSHOT IMAGES | 283 |
| 218 FALSE MATCH RATE CALIBRATION: MUGSHOT IMAGES | 284 |
| 219 FALSE MATCH RATE CALIBRATION: MUGSHOT IMAGES | 285 |
| 220 FALSE MATCH RATE CALIBRATION: MUGSHOT IMAGES | 286 |
| 221 FALSE MATCH RATE CALIBRATION: MUGSHOT IMAGES | 287 |
| 222 FALSE MATCH RATE CALIBRATION: MUGSHOT IMAGES | 288 |
| 223 FALSE MATCH RATE CALIBRATION: MUGSHOT IMAGES | 289 |
| 224 FALSE MATCH RATE CALIBRATION: MUGSHOT IMAGES | 290 |
| 225 FALSE MATCH RATE CALIBRATION: MUGSHOT IMAGES | 291 |
| 226 FALSE MATCH RATE CALIBRATION: MUGSHOT IMAGES | 292 |
| 227 FALSE MATCH RATE CALIBRATION: MUGSHOT IMAGES | 293 |
| 228 FALSE MATCH RATE CALIBRATION: MUGSHOT IMAGES | 294 |
| 229 FALSE MATCH RATE CALIBRATION: MUGSHOT IMAGES | 295 |
| 230 FALSE MATCH RATE CALIBRATION: MUGSHOT IMAGES | 296 |
| 231 FALSE MATCH RATE CALIBRATION: MUGSHOT IMAGES | 297 |
| 232 FALSE MATCH RATE CALIBRATION: MUGSHOT IMAGES | 298 |
| 233 FALSE MATCH RATE CALIBRATION: VISA IMAGES | 299 |
| 234 FALSE MATCH RATE CALIBRATION: VISA IMAGES | 300 |
| 235 FALSE MATCH RATE CALIBRATION: VISA IMAGES | 301 |
| 236 FALSE MATCH RATE CALIBRATION: VISA IMAGES | 302 |
| 237 FALSE MATCH RATE CALIBRATION: VISA IMAGES | 303 |
| 238 FALSE MATCH RATE CALIBRATION: VISA IMAGES | 304 |
| 239 FALSE MATCH RATE CALIBRATION: VISA IMAGES | 305 |
| 240 FALSE MATCH RATE CALIBRATION: VISA IMAGES | 306 |
| 241 FALSE MATCH RATE CALIBRATION: VISA IMAGES | 307 |
| 242 FALSE MATCH RATE CALIBRATION: VISA IMAGES | 308 |
| 243 FALSE MATCH RATE CALIBRATION: VISA IMAGES | 309 |
| 244 FALSE MATCH RATE CALIBRATION: VISA IMAGES | 310 |
| 245 FALSE MATCH RATE CALIBRATION: VISA IMAGES | 311 |
| 246 FALSE MATCH RATE CALIBRATION: VISA IMAGES | 312 |
| 247 FALSE MATCH RATE CALIBRATION: VISA IMAGES | 313 |
| 248 FALSE MATCH RATE CALIBRATION: VISA IMAGES | 314 |
| 249 FALSE MATCH RATE CALIBRATION: VISA IMAGES | 315 |
| 250 FALSE MATCH RATE CALIBRATION: VISA IMAGES | 316 |
| 251 FALSE MATCH RATE CALIBRATION: VISA IMAGES | 317 |
| 252 FALSE MATCH RATE CALIBRATION: VISA IMAGES | 318 |
| 253 FALSE MATCH RATE CALIBRATION: VISA IMAGES | 319 |
| 254 FALSE MATCH RATE CALIBRATION: VISA IMAGES | 320 |
| 255 FALSE MATCH RATE CALIBRATION: VISA IMAGES | 321 |
| 256 FALSE MATCH RATE CALIBRATION: VISA IMAGES | 322 |
| 257 FALSE MATCH RATE CALIBRATION: VISA IMAGES | 323 |

| | | |
|-----|---|-----|
| 258 | FALSE MATCH RATE CALIBRATION: VISA IMAGES | 324 |
| 259 | FALSE MATCH RATE CALIBRATION: VISA IMAGES | 325 |
| 260 | FALSE MATCH RATE CALIBRATION: VISA IMAGES | 326 |
| 261 | FALSE MATCH RATE CALIBRATION: VISA IMAGES | 327 |
| 262 | FALSE MATCH RATE CALIBRATION: VISA IMAGES | 328 |
| 263 | FALSE MATCH RATE CALIBRATION: VISA IMAGES | 329 |
| 264 | FALSE MATCH RATE CALIBRATION: VISA IMAGES | 330 |
| 265 | FALSE MATCH RATE CALIBRATION: VISA IMAGES | 331 |
| 266 | FALSE MATCH RATE CALIBRATION: VISA IMAGES | 332 |
| 267 | FALSE MATCH RATE CALIBRATION: VISA IMAGES | 333 |
| 268 | FALSE MATCH RATE CALIBRATION: VISA IMAGES | 334 |
| 269 | FALSE MATCH RATE CALIBRATION: VISA IMAGES | 335 |
| 270 | FALSE MATCH RATE CALIBRATION: VISA IMAGES | 336 |
| 271 | FALSE MATCH RATE CALIBRATION: VISA IMAGES | 337 |
| 272 | FALSE MATCH RATE CALIBRATION: VISA IMAGES | 338 |
| 273 | FALSE MATCH RATE CALIBRATION: VISA IMAGES | 339 |
| 274 | FALSE MATCH RATE CALIBRATION: VISA IMAGES | 340 |
| 275 | FALSE MATCH RATE CALIBRATION: VISA IMAGES | 341 |
| 276 | FALSE MATCH RATE CALIBRATION: VISA IMAGES | 342 |
| 277 | FALSE MATCH RATE CALIBRATION: VISA IMAGES | 343 |
| 278 | EFFECT OF COUNTRY OF BIRTH ON FNMR | 345 |
| 279 | EFFECT OF COUNTRY OF BIRTH ON FNMR | 346 |
| 280 | EFFECT OF COUNTRY OF BIRTH ON FNMR | 347 |
| 281 | EFFECT OF COUNTRY OF BIRTH ON FNMR | 348 |
| 282 | EFFECT OF COUNTRY OF BIRTH ON FNMR | 349 |
| 283 | EFFECT OF COUNTRY OF BIRTH ON FNMR | 350 |
| 284 | EFFECT OF COUNTRY OF BIRTH ON FNMR | 351 |
| 285 | EFFECT OF COUNTRY OF BIRTH ON FNMR | 352 |
| 286 | EFFECT OF COUNTRY OF BIRTH ON FNMR | 353 |
| 287 | EFFECT OF COUNTRY OF BIRTH ON FNMR | 354 |
| 288 | EFFECT OF COUNTRY OF BIRTH ON FNMR | 355 |
| 289 | EFFECT OF COUNTRY OF BIRTH ON FNMR | 356 |
| 290 | EFFECT OF COUNTRY OF BIRTH ON FNMR | 357 |
| 291 | EFFECT OF COUNTRY OF BIRTH ON FNMR | 358 |
| 292 | EFFECT OF COUNTRY OF BIRTH ON FNMR | 359 |
| 293 | EFFECT OF COUNTRY OF BIRTH ON FNMR | 360 |
| 294 | EFFECT OF COUNTRY OF BIRTH ON FNMR | 361 |
| 295 | EFFECT OF COUNTRY OF BIRTH ON FNMR | 362 |
| 296 | EFFECT OF COUNTRY OF BIRTH ON FNMR | 363 |
| 297 | EFFECT OF COUNTRY OF BIRTH ON FNMR | 364 |
| 298 | EFFECT OF COUNTRY OF BIRTH ON FNMR | 365 |
| 299 | EFFECT OF COUNTRY OF BIRTH ON FNMR | 366 |
| 300 | EFFECT OF COUNTRY OF BIRTH ON FNMR | 367 |
| 301 | EFFECT OF COUNTRY OF BIRTH ON FNMR | 368 |
| 302 | EFFECT OF COUNTRY OF BIRTH ON FNMR | 369 |
| 303 | EFFECT OF COUNTRY OF BIRTH ON FNMR | 370 |
| 304 | EFFECT OF COUNTRY OF BIRTH ON FNMR | 371 |
| 305 | EFFECT OF COUNTRY OF BIRTH ON FNMR | 372 |
| 306 | EFFECT OF COUNTRY OF BIRTH ON FNMR | 373 |
| 307 | EFFECT OF COUNTRY OF BIRTH ON FNMR | 374 |
| 308 | EFFECT OF COUNTRY OF BIRTH ON FNMR | 375 |
| 309 | EFFECT OF COUNTRY OF BIRTH ON FNMR | 376 |
| 310 | EFFECT OF COUNTRY OF BIRTH ON FNMR | 377 |
| 311 | EFFECT OF COUNTRY OF BIRTH ON FNMR | 378 |
| 312 | EFFECT OF COUNTRY OF BIRTH ON FNMR | 379 |
| 313 | EFFECT OF COUNTRY OF BIRTH ON FNMR | 380 |
| 314 | EFFECT OF COUNTRY OF BIRTH ON FNMR | 381 |

| | | |
|-----|---|-----|
| 315 | ERROR TRADEOFF CHARACTERISTIC: MUGSHOT IMAGES | 383 |
| 316 | ERROR TRADEOFF CHARACTERISTIC: MUGSHOT IMAGES | 384 |
| 317 | ERROR TRADEOFF CHARACTERISTIC: MUGSHOT IMAGES | 385 |
| 318 | ERROR TRADEOFF CHARACTERISTIC: MUGSHOT IMAGES | 386 |
| 319 | ERROR TRADEOFF CHARACTERISTIC: MUGSHOT IMAGES | 387 |
| 320 | ERROR TRADEOFF CHARACTERISTIC: MUGSHOT IMAGES | 388 |
| 321 | ERROR TRADEOFF CHARACTERISTIC: MUGSHOT IMAGES | 389 |
| 322 | ERROR TRADEOFF CHARACTERISTIC: MUGSHOT IMAGES | 390 |
| 323 | ERROR TRADEOFF CHARACTERISTIC: MUGSHOT IMAGES | 391 |
| 324 | ERROR TRADEOFF CHARACTERISTIC: MUGSHOT IMAGES | 392 |
| 325 | ERROR TRADEOFF CHARACTERISTIC: MUGSHOT IMAGES | 393 |
| 326 | ERROR TRADEOFF CHARACTERISTIC: MUGSHOT IMAGES | 394 |
| 327 | ERROR TRADEOFF CHARACTERISTIC: MUGSHOT IMAGES | 395 |
| 328 | ERROR TRADEOFF CHARACTERISTIC: MUGSHOT IMAGES | 396 |
| 329 | ERROR TRADEOFF CHARACTERISTIC: MUGSHOT IMAGES | 397 |
| 330 | ERROR TRADEOFF CHARACTERISTIC: MUGSHOT IMAGES | 398 |
| 331 | ERROR TRADEOFF CHARACTERISTIC: MUGSHOT IMAGES | 399 |
| 332 | ERROR TRADEOFF CHARACTERISTIC: MUGSHOT IMAGES | 400 |
| 333 | ERROR TRADEOFF CHARACTERISTIC: MUGSHOT IMAGES | 401 |
| 334 | ERROR TRADEOFF CHARACTERISTIC: MUGSHOT IMAGES | 402 |
| 335 | ERROR TRADEOFF CHARACTERISTIC: MUGSHOT IMAGES | 403 |
| 336 | ERROR TRADEOFF CHARACTERISTIC: MUGSHOT IMAGES | 404 |
| 337 | ERROR TRADEOFF CHARACTERISTIC: MUGSHOT IMAGES | 405 |
| 338 | ERROR TRADEOFF CHARACTERISTIC: MUGSHOT IMAGES | 406 |
| 339 | ERROR TRADEOFF CHARACTERISTIC: MUGSHOT IMAGES | 407 |
| 340 | ERROR TRADEOFF CHARACTERISTIC: MUGSHOT IMAGES | 408 |
| 341 | ERROR TRADEOFF CHARACTERISTIC: MUGSHOT IMAGES | 409 |
| 342 | ERROR TRADEOFF CHARACTERISTIC: MUGSHOT IMAGES | 410 |
| 343 | EFFECT OF SUBJECT AGE ON FNMR | 412 |
| 344 | EFFECT OF SUBJECT AGE ON FNMR | 413 |
| 345 | EFFECT OF SUBJECT AGE ON FNMR | 414 |
| 346 | EFFECT OF SUBJECT AGE ON FNMR | 415 |
| 347 | EFFECT OF SUBJECT AGE ON FNMR | 416 |
| 348 | EFFECT OF SUBJECT AGE ON FNMR | 417 |
| 349 | EFFECT OF SUBJECT AGE ON FNMR | 418 |
| 350 | EFFECT OF SUBJECT AGE ON FNMR | 419 |
| 351 | EFFECT OF SUBJECT AGE ON FNMR | 420 |
| 352 | EFFECT OF SUBJECT AGE ON FNMR | 421 |
| 353 | EFFECT OF SUBJECT AGE ON FNMR | 422 |
| 354 | EFFECT OF SUBJECT AGE ON FNMR | 423 |
| 355 | EFFECT OF SUBJECT AGE ON FNMR | 424 |
| 356 | EFFECT OF SUBJECT AGE ON FNMR | 425 |
| 357 | EFFECT OF SUBJECT AGE ON FNMR | 426 |
| 358 | EFFECT OF SUBJECT AGE ON FNMR | 427 |
| 359 | EFFECT OF SUBJECT AGE ON FNMR | 428 |
| 360 | EFFECT OF SUBJECT AGE ON FNMR | 429 |
| 361 | EFFECT OF SUBJECT AGE ON FNMR | 430 |
| 362 | EFFECT OF SUBJECT AGE ON FNMR | 431 |
| 363 | EFFECT OF SUBJECT AGE ON FNMR | 432 |
| 364 | EFFECT OF SUBJECT AGE ON FNMR | 433 |
| 365 | EFFECT OF SUBJECT AGE ON FNMR | 434 |
| 366 | EFFECT OF SUBJECT AGE ON FNMR | 435 |
| 367 | EFFECT OF SUBJECT AGE ON FNMR | 436 |
| 368 | EFFECT OF SUBJECT AGE ON FNMR | 437 |

| | | |
|-----|--|-----|
| 369 | EFFECT OF SUBJECT AGE ON FNMR | 438 |
| 370 | EFFECT OF SUBJECT AGE ON FNMR | 439 |
| 371 | EFFECT OF SUBJECT AGE ON FNMR | 440 |
| 372 | EFFECT OF SUBJECT AGE ON FNMR | 441 |
| 373 | EFFECT OF SUBJECT AGE ON FNMR | 442 |
| 374 | EFFECT OF SUBJECT AGE ON FNMR | 443 |
| 375 | EFFECT OF SUBJECT AGE ON FNMR | 444 |
| 376 | EFFECT OF SUBJECT AGE ON FNMR | 445 |
| 377 | EFFECT OF SUBJECT AGE ON FNMR | 446 |
| 378 | EFFECT OF SUBJECT AGE ON FNMR | 447 |
| 379 | EFFECT OF SUBJECT AGE ON FNMR | 448 |
| 380 | IMPOSTOR COUNTS FOR CROSS COUNTRY FMR CALCULATIONS | 452 |

| | Location | Developer Name | Short Name | Seq. Num. | Validation Date |
|----|----------|----------------------------------|--------------------|-----------|-----------------|
| 1 | NL | 20Face | 20face-000 | 000 | 2021-04-12 |
| 2 | NL | 20Face | 20face-001 | 001 | 2021-09-29 |
| 3 | US | 3DVi | 3divi-006 | 006 | 2021-04-14 |
| 4 | US | 3DVi | 3divi-007 | 007 | 2021-09-27 |
| 5 | TH | ACI Software | acisw-007 | 007 | 2021-11-15 |
| 6 | TH | ACI Software | acisw-008 | 008 | 2022-03-22 |
| 7 | SG | ADVANCE.AI | advance-002 | 002 | 2019-12-19 |
| 8 | SG | ADVANCE.AI | advance-003 | 003 | 2021-08-05 |
| 9 | US | AFIS and Biometrics Consulting | afisbiometrics-000 | 000 | 2022-01-27 |
| 10 | TW | ASUSTek Computer Inc | asusaics-000 | 000 | 2019-10-24 |
| 11 | TW | ASUSTek Computer Inc | asusaics-001 | 001 | 2020-02-25 |
| 12 | CN | AYF Technology | ayftech-001 | 001 | 2020-07-06 |
| 13 | TW | Ability Enterprise - Andro Video | androvideo-000 | 000 | 2021-01-25 |
| 14 | TW | Acer Incorporated | acer-001 | 001 | 2020-06-30 |
| 15 | TW | Acer Incorporated | acer-002 | 002 | 2021-11-10 |
| 16 | SG | Adera Global PTE | adera-002 | 002 | 2021-02-16 |
| 17 | SG | Adera Global PTE | adera-003 | 003 | 2021-07-12 |
| 18 | TH | Ai First | aifirst-001 | 001 | 2019-11-21 |
| 19 | TW | AiUnion Technology | aiunionface-000 | 000 | 2019-10-22 |
| 20 | TH | Aigen | aigen-001 | 001 | 2020-10-06 |
| 21 | TH | Aigen | aigen-002 | 002 | 2021-03-15 |
| 22 | CN | Aiseemu Technology | aiseemu-001 | 001 | 2022-06-16 |
| 23 | KR | Ajou University | ajou-001 | 001 | 2021-03-08 |
| 24 | ID | Akurat Satu Indonesia | ptakuratsatu-000 | 000 | 2020-09-11 |
| 25 | KR | Alchera Inc | alchera-003 | 003 | 2021-07-13 |
| 26 | KR | Alchera Inc | alchera-004 | 004 | 2022-08-12 |
| 27 | ID | Alfabeta | alfabeta-001 | 001 | 2021-12-02 |
| 28 | ES | Alice Biometrics | alice-000 | 000 | 2021-06-15 |
| 29 | RU | Alivia / Innovation Sys | isystems-001 | 001 | 2018-06-12 |
| 30 | RU | Alivia / Innovation Sys | isystems-002 | 002 | 2018-10-18 |
| 31 | IN | AllGoVision | allgovision-000 | 000 | 2019-03-01 |
| 32 | CN | AlphaSSTG | alphaface-001 | 001 | 2019-09-03 |
| 33 | CN | AlphaSSTG | alphaface-002 | 002 | 2020-02-20 |
| 34 | GB | Amplified Group | amplifiedgroup-001 | 001 | 2019-03-01 |
| 35 | CN | Anke Investments | anke-004 | 004 | 2019-06-27 |
| 36 | CN | Anke Investments | anke-005 | 005 | 2019-11-21 |
| 37 | BR | Antheus Technologia | antheus-000 | 000 | 2019-12-05 |
| 38 | BR | Antheus Technologia | antheus-001 | 001 | 2020-06-25 |
| 39 | GB | AnyVision | anyvision-004 | 004 | 2018-06-15 |
| 40 | GB | AnyVision | anyvision-005 | 005 | 2021-02-03 |
| 41 | US | Armatura LLC | armatura-001 | 001 | 2022-01-04 |
| 42 | CN | AuthenMetric | authenmetric-003 | 003 | 2021-08-09 |
| 43 | CN | AuthenMetric | authenmetric-004 | 004 | 2022-01-03 |
| 44 | US | Aware | aware-005 | 005 | 2020-02-27 |
| 45 | US | Aware | aware-006 | 006 | 2021-07-03 |
| 46 | IN | Awidit Systems | awiros-001 | 001 | 2019-09-23 |
| 47 | IN | Awidit Systems | awiros-002 | 002 | 2020-10-28 |
| 48 | CH | Aximetria | aximetria-001 | 001 | 2022-08-10 |
| 49 | JP | Ayonix | ayonix-000 | 000 | 2017-06-22 |
| 50 | CN | BOE Technology Group | boetech-001 | 001 | 2021-06-22 |
| 51 | CN | BOE Technology Group | boetech-002 | 002 | 2021-12-21 |
| 52 | ES | Bee the Data | beethedata-000 | 000 | 2021-07-26 |
| 53 | CN | Beihang University-ERCACAT | ercacat-001 | 001 | 2020-07-06 |
| 54 | CN | Beijing Alleyes Technology | alleyes-000 | 000 | 2020-03-09 |
| 55 | CN | Beijing DeepSense Technologies | deepsense-000 | 000 | 2021-03-19 |
| 56 | CN | Beijing DeepSense Technologies | deepsense-001 | 001 | 2022-03-11 |
| 57 | CN | Beijing Hisign Technology | hisign-001 | 001 | 2021-09-24 |
| 58 | CN | Beijing Mendaxia Technology | mendaxiatech-000 | 000 | 2021-09-15 |
| 59 | CN | Beijing Vion Technology Inc | vion-000 | 000 | 2018-10-19 |
| 60 | KZ | Beyne.AI | beyneai-000 | 000 | 2022-01-03 |
| 61 | CH | BioID Technologies SA | bioidechswiss-001 | 001 | 2020-08-28 |
| 62 | CH | BioID Technologies SA | bioidechswiss-002 | 002 | 2021-02-17 |
| 63 | IN | Biocube Matrics | biocube-001 | 001 | 2021-09-08 |
| 64 | UK | BitCenter UK | farfaces-001 | 001 | 2021-04-09 |
| 65 | CN | Bitmain | bm-001 | 001 | 2018-10-17 |
| 66 | CN | Bresee Technology | bresee-001 | 001 | 2020-12-30 |
| 67 | CN | Bresee Technology | bresee-002 | 002 | 2021-06-30 |
| 68 | CN | CSA IntelliCloud Technology | intellicloudai-001 | 001 | 2019-08-13 |
| 69 | CN | CSA IntelliCloud Technology | intellicloudai-002 | 002 | 2020-12-17 |
| 70 | TW | CTBC Bank | ctcbcbank-000 | 000 | 2019-06-28 |

Table 1: Summary of participant information included in this report.

| | Location | Developer Name | Short Name | Seq. Num. | Validation Date |
|-----|----------|---------------------------------------|-----------------------|-----------|-----------------|
| 71 | TW | CTBC Bank | ctbcbank-001 | 001 | 2019-10-28 |
| 72 | KR | CUDO Communication | cudocommunication-001 | 001 | 2021-10-20 |
| 73 | US | Camvi Technologies | camvi-002 | 002 | 2018-10-19 |
| 74 | US | Camvi Technologies | camvi-004 | 004 | 2019-07-12 |
| 75 | JP | Canon Inc | canon-003 | 003 | 2021-09-15 |
| 76 | JP | Canon Inc | canon-004 | 004 | 2022-04-25 |
| 77 | CN | China Electronics Import-Export Corp | ceiec-003 | 003 | 2020-01-06 |
| 78 | CN | China Electronics Import-Export Corp | ceiec-004 | 004 | 2021-01-18 |
| 79 | CN | China University of Petroleum | upc-001 | 001 | 2019-06-05 |
| 80 | CN | Chinese University of Hong Kong | cuhkee-001 | 001 | 2020-03-18 |
| 81 | KR | Chosun University | chosun-001 | 001 | 2020-07-01 |
| 82 | KR | Chosun University | chosun-002 | 002 | 2020-11-25 |
| 83 | TW | Chunghwa Telecom | chtface-004 | 004 | 2021-10-08 |
| 84 | TW | Chunghwa Telecom | chtface-005 | 005 | 2022-03-09 |
| 85 | US | Clearview AI Inc | clearviewai-000 | 000 | 2021-09-22 |
| 86 | CN | Closeli Inc | closeli-001 | 001 | 2021-07-15 |
| 87 | US | CloudSmart Consulting LLC | csc-002 | 002 | 2021-03-24 |
| 88 | US | CloudSmart Consulting LLC | csc-003 | 003 | 2021-08-26 |
| 89 | TW | Cloudmatrix | cloudmatrix-000 | 000 | 2021-10-22 |
| 90 | TW | Cloudmatrix | cloudmatrix-001 | 001 | 2022-02-16 |
| 91 | CN | Cloudwalk - Hengrui AI Technology | cloudwalk-hr-003 | 003 | 2020-09-25 |
| 92 | CN | Cloudwalk - Hengrui AI Technology | cloudwalk-hr-004 | 004 | 2021-02-10 |
| 93 | CN | Cloudwalk - Moontime Smart Technology | cloudwalk-mt-004 | 004 | 2021-11-09 |
| 94 | CN | Cloudwalk - Moontime Smart Technology | cloudwalk-mt-005 | 005 | 2022-03-29 |
| 95 | IN | Code Everest Pvt | facex-001 | 001 | 2021-03-08 |
| 96 | IN | Code Everest Pvt | facex-002 | 002 | 2021-08-24 |
| 97 | DE | Cognitec Systems GmbH | cognitec-003 | 003 | 2021-07-30 |
| 98 | DE | Cognitec Systems GmbH | cognitec-004 | 004 | 2022-02-10 |
| 99 | TW | Coretech Knowledge Inc | coretech-000 | 000 | 2021-07-12 |
| 100 | IL | Corsight | corsight-002 | 002 | 2021-09-01 |
| 101 | IL | Corsight | corsight-003 | 003 | 2022-06-09 |
| 102 | IL | Cortica | cor-001 | 001 | 2020-09-24 |
| 103 | KR | Cubox | cubox-001 | 001 | 2020-12-07 |
| 104 | KR | Cubox | cubox-002 | 002 | 2021-08-24 |
| 105 | JP | Cybercore | cybercore-001 | 001 | 2021-12-15 |
| 106 | JP | Cybercore | cybercore-002 | 002 | 2022-04-25 |
| 107 | US | Cyberextruder | cyberextruder-003 | 003 | 2022-03-16 |
| 108 | US | Cyberextruder | cyberextruder-004 | 004 | 2022-07-20 |
| 109 | TW | Cyberlink Corp | cyberlink-008 | 008 | 2022-01-07 |
| 110 | TW | Cyberlink Corp | cyberlink-009 | 009 | 2022-05-12 |
| 111 | MX | DICIO | dicio-001 | 001 | 2022-03-22 |
| 112 | CN | DSK | dsk-000 | 000 | 2019-06-28 |
| 113 | CN | Dahua Technology | dahua-006 | 006 | 2020-12-30 |
| 114 | CN | Dahua Technology | dahua-007 | 007 | 2021-12-20 |
| 115 | IE | Daon | daon-000 | 000 | 2021-11-03 |
| 116 | US | Decatur Industries Inc | decatur-000 | 000 | 2020-08-18 |
| 117 | US | Decatur Industries Inc | decatur-001 | 001 | 2021-09-27 |
| 118 | CN | Deepglint | deepglint-003 | 003 | 2021-03-03 |
| 119 | CN | Deepglint | deepglint-004 | 004 | 2021-09-17 |
| 120 | FR | Deepsense | dps-000 | 000 | 2021-07-16 |
| 121 | DE | Dermalog | dermalog-009 | 009 | 2021-10-06 |
| 122 | DE | Dermalog | dermalog-010 | 010 | 2022-07-25 |
| 123 | CN | DiDi ChuXing Technology | didiglobalface-001 | 001 | 2019-10-23 |
| 124 | IN | Digidata | digidata-000 | 000 | 2022-01-27 |
| 125 | IN | Digidata | digidata-001 | 001 | 2022-06-10 |
| 126 | GB | Digital Barriers | digitalbarriers-002 | 002 | 2019-03-01 |
| 127 | TR | Ekin Smart City Technologies | ekin-002 | 002 | 2021-05-04 |
| 128 | RU | Enface | enface-000 | 000 | 2021-04-09 |
| 129 | RU | Enface | enface-001 | 001 | 2021-12-17 |
| 130 | CH | Euronovate SA | euronovate-001 | 001 | 2021-11-15 |
| 131 | RU | Expasoft LLC | expasoft-001 | 001 | 2020-09-03 |
| 132 | RU | Expasoft LLC | expasoft-002 | 002 | 2021-07-26 |
| 133 | US | FRP LLC | frpkauai-001 | 001 | 2022-07-18 |
| 134 | DE | FaceOnLive Inc | faceonlive-001 | 001 | 2021-11-23 |
| 135 | DE | FaceOnLive Inc | faceonlive-002 | 002 | 2022-04-11 |
| 136 | ES | FacePhi | facephi-000 | 000 | 2022-04-06 |
| 137 | GB | FaceSoft | facesoft-000 | 000 | 2019-07-10 |
| 138 | KR | FaceTag Co | facetag-000 | 000 | 2021-03-22 |
| 139 | KR | FaceTag Co | facetag-002 | 002 | 2022-01-06 |
| 140 | TW | FarBar Inc | f8-001 | 001 | 2019-07-11 |

Table 2: Summary of participant information included in this report.

| | Location | Developer Name | Short Name | Seq. Num. | Validation Date |
|-----|----------|---|-----------------------------|-----------|-----------------|
| 141 | TW | FarBar Inc | f8-002 | 002 | 2022-03-02 |
| 142 | CN | Fiberhome Telecommunication Technologies | fiberhome-nanjing-003 | 003 | 2021-03-12 |
| 143 | CN | Fiberhome Telecommunication Technologies | fiberhome-nanjing-004 | 004 | 2021-09-14 |
| 144 | UK | Fincore Ltd | fincore-000 | 000 | 2021-06-07 |
| 145 | CN | Fujitsu Research and Development Center | fujitsulab-002 | 002 | 2021-02-24 |
| 146 | CN | Fujitsu Research and Development Center | fujitsulab-003 | 003 | 2021-07-12 |
| 147 | US | Gemalto Cogent | cogent-006 | 006 | 2021-07-28 |
| 148 | US | Gemalto Cogent | cogent-007 | 007 | 2022-04-11 |
| 149 | TW | GeoVision Inc | geo-002 | 002 | 2021-04-01 |
| 150 | TW | GeoVision Inc | geo-004 | 004 | 2022-02-10 |
| 151 | JP | Glory | glory-004 | 004 | 2022-02-08 |
| 152 | JP | Glory | glory-005 | 005 | 2022-07-08 |
| 153 | TW | Gorilla Technology | gorilla-007 | 007 | 2021-06-28 |
| 154 | TW | Gorilla Technology | gorilla-008 | 008 | 2021-11-08 |
| 155 | US | Graymatics | graymatics-001 | 001 | 2022-01-13 |
| 156 | US | Griaule | griaule-000 | 000 | 2021-08-20 |
| 157 | US | Griaule | griaule-001 | 001 | 2022-05-31 |
| 158 | CN | Guangzhou Pixel Solutions | pixelall-006 | 006 | 2021-06-17 |
| 159 | CN | Guangzhou Pixel Solutions | pixelall-008 | 008 | 2022-06-16 |
| 160 | CN | Hangzhuo Allu Network Information Technology | hzailu-001 | 001 | 2022-01-27 |
| 161 | CN | Hangzhuo Allu Network Information Technology | hzailu-002 | 002 | 2022-06-02 |
| 162 | ES | Herta Security | hertasecurity-000 | 000 | 2021-01-05 |
| 163 | ES | Herta Security | hertasecurity-001 | 001 | 2022-01-18 |
| 164 | CN | Hikvision Research Institute | hik-001 | 001 | 2019-03-01 |
| 165 | IN | HyperVerge Inc | hyperverge-002 | 002 | 2021-05-27 |
| 166 | IN | HyperVerge Inc | hyperverge-003 | 003 | 2022-04-11 |
| 167 | AU | ICM Airport Technics | icm-002 | 002 | 2020-11-13 |
| 168 | AU | ICM Airport Technics | icm-003 | 003 | 2021-09-06 |
| 169 | FR | ID3 Technology | id3-006 | 006 | 2020-12-17 |
| 170 | FR | ID3 Technology | id3-008 | 008 | 2021-11-10 |
| 171 | CA | IMDS Software | imds-software-001 | 001 | 2022-07-06 |
| 172 | RU | ITMO University | itmo-007 | 007 | 2020-01-06 |
| 173 | RU | ITMO University | itmo-008 | 008 | 2021-11-19 |
| 174 | RU | IVA Cognitive | ivacognitive-001 | 001 | 2021-01-29 |
| 175 | FR | Idemia | idemia-008 | 008 | 2021-07-07 |
| 176 | FR | Idemia | idemia-009 | 009 | 2022-07-27 |
| 177 | US | Imageware Systems | iws-000 | 000 | 2020-08-12 |
| 178 | GB | Imperial College London | imperial-000 | 000 | 2019-03-01 |
| 179 | GB | Imperial College London | imperial-002 | 002 | 2019-08-28 |
| 180 | US | Incode Technologies Inc | incode-010 | 010 | 2021-10-22 |
| 181 | US | Incode Technologies Inc | incode-011 | 011 | 2022-08-10 |
| 182 | IN | Innef Labs | innefulabs-000 | 000 | 2020-09-04 |
| 183 | GB | Innovative Technology | innovativetechnologyltd-001 | 001 | 2019-10-22 |
| 184 | GB | Innovative Technology | innovativetechnologyltd-002 | 002 | 2020-02-26 |
| 185 | SK | Innovatrics | innovatrics-007 | 007 | 2020-08-19 |
| 186 | SK | Innovatrics | innovatrics-008 | 008 | 2021-12-15 |
| 187 | CN | InsightFace AI | insightface-001 | 001 | 2021-09-27 |
| 188 | CN | InsightFace AI | insightface-002 | 002 | 2022-01-31 |
| 189 | CN | Inspur (Beijing) Electronic Information Industry Co | inspur-000 | 000 | 2022-07-19 |
| 190 | CN | Institute of Computing Technology | ichttc-000 | 000 | 2020-11-29 |
| 191 | RU | Institute of Information Technologies | iit-002 | 002 | 2019-12-04 |
| 192 | RU | Institute of Information Technologies | iit-003 | 003 | 2020-12-01 |
| 193 | IS | Intel Research Group | intelresearch-004 | 004 | 2021-08-24 |
| 194 | IS | Intel Research Group | intelresearch-005 | 005 | 2022-02-13 |
| 195 | KR | IntelliVIX | intellivix-001 | 001 | 2022-02-25 |
| 196 | KR | IntelliVIX | intellivix-002 | 002 | 2022-07-14 |
| 197 | AE | Intellibrain Technological Projects | g42-intellibrain-001 | 001 | 2022-07-27 |
| 198 | US | Intellivision | intellivision-003 | 003 | 2022-03-07 |
| 199 | US | Intellivision | intellivision-004 | 004 | 2022-07-28 |
| 200 | LU | Intema-LGL Group | intema-000 | 000 | 2022-07-15 |
| 201 | US | IrexAI | irex-000 | 000 | 2020-12-17 |
| 202 | IL | Is It You | isityou-000 | 000 | 2017-06-26 |
| 203 | MX | Jaak IT | jaakit-001 | 001 | 2022-05-20 |
| 204 | KR | Kakao Enterprise | kakao-007 | 007 | 2022-01-12 |
| 205 | KR | Kakao Enterprise | kakao-008 | 008 | 2022-05-12 |
| 206 | KR | Kakao Pay Corp | kakaopay-001 | 001 | 2021-07-06 |
| 207 | TH | Kasikorn Labs | kasikornlabs-000 | 000 | 2022-03-02 |
| 208 | TH | Kasikorn Labs | kasikornlabs-001 | 001 | 2022-07-26 |
| 209 | SG | Kedacom International Pte | kedacom-000 | 000 | 2019-06-03 |
| 210 | US | Kneron Inc | kneron-003 | 003 | 2019-07-01 |

Table 3: Summary of participant information included in this report.

| | Location | Developer Name | Short Name | Seq. Num. | Validation Date |
|-----|----------|--|----------------------|-----------|-----------------|
| 211 | US | Kneron Inc | kneron-005 | 005 | 2020-02-21 |
| 212 | US | KnowUTech LLC | knowutech-000 | 000 | 2022-02-13 |
| 213 | KR | Kookmin University | kookmin-002 | 002 | 2021-03-05 |
| 214 | TH | Krunghai | krunghai-002 | 002 | 2022-06-21 |
| 215 | CN | KuKe3D Technology | kuke3d-001 | 001 | 2021-10-28 |
| 216 | CN | KuKe3D Technology | kuke3d-002 | 002 | 2022-04-14 |
| 217 | MX | Lebentech Biometrics | lebentech-000 | 000 | 2022-02-16 |
| 218 | IN | Lema Labs | lemalabs-001 | 001 | 2021-04-13 |
| 219 | JP | Line Corporation | lineclova-001 | 001 | 2021-09-26 |
| 220 | JP | Line Corporation | lineclova-002 | 002 | 2022-05-18 |
| 221 | RU | Lomonosov Moscow State University | intsysmsu-001 | 001 | 2019-10-22 |
| 222 | RU | Lomonosov Moscow State University | intsysmsu-002 | 002 | 2020-03-12 |
| 223 | IN | Lookman Electroplast Industries | lookman-002 | 002 | 2018-06-13 |
| 224 | IN | Lookman Electroplast Industries | lookman-004 | 004 | 2019-06-03 |
| 225 | US | Luxand Inc | luxand-000 | 000 | 2019-11-07 |
| 226 | RU | MVision | mvision-001 | 001 | 2019-11-12 |
| 227 | IN | Mantra Softtech India | mantra-000 | 000 | 2021-10-28 |
| 228 | CN | Maxvision Technology | maxvision-001 | 001 | 2022-03-03 |
| 229 | CN | Maxvision Technology | maxvision-002 | 002 | 2022-07-12 |
| 230 | CN | Megvii/Face++ | megvii-005 | 005 | 2022-03-28 |
| 231 | CN | Megvii/Face++ | megvii-006 | 006 | 2022-08-08 |
| 232 | KR | Metsakuur | metsakuurcompany-001 | 001 | 2022-05-12 |
| 233 | GB | MicroFocus | microfocus-001 | 001 | 2018-06-13 |
| 234 | GB | MicroFocus | microfocus-002 | 002 | 2018-10-17 |
| 235 | CN | Minivision | minivision-000 | 000 | 2020-10-28 |
| 236 | NO | Mobai | mobai-000 | 000 | 2020-08-26 |
| 237 | NO | Mobai | mobai-001 | 001 | 2021-02-17 |
| 238 | ES | Mobbeel Solutions | mobbl-001 | 001 | 2021-06-16 |
| 239 | ES | Mobbeel Solutions | mobbl-003 | 003 | 2022-04-19 |
| 240 | KR | Mobipin Technology | mobilpintech-000 | 000 | 2021-11-23 |
| 241 | TH | Momentum Digital | sertis-000 | 000 | 2019-10-07 |
| 242 | TH | Momentum Digital | sertis-002 | 002 | 2021-05-13 |
| 243 | CN | MoreDian Technology | moredian-000 | 000 | 2021-02-24 |
| 244 | US | Mukh Technologies | mukh-001 | 001 | 2022-03-22 |
| 245 | CN | Multi-Modality Intelligence | multimodality-000 | 000 | 2021-10-19 |
| 246 | CN | Multi-Modality Intelligence | multimodality-001 | 001 | 2022-05-16 |
| 247 | RU | N-Tech Lab | ntechlab-011 | 011 | 2021-09-13 |
| 248 | RU | N-Tech Lab | ntechlab-012 | 012 | 2022-01-20 |
| 249 | CA | NEO Systems | neosystems-003 | 003 | 2021-11-11 |
| 250 | CA | NEO Systems | neosystems-004 | 004 | 2022-05-02 |
| 251 | KR | NHN Corp | nhn-002 | 002 | 2021-07-15 |
| 252 | KR | NHN Corp | nhn-003 | 003 | 2022-02-22 |
| 253 | KR | NSENSE Corp | nsensecorp-002 | 002 | 2021-05-06 |
| 254 | KR | NSENSE Corp | nsensecorp-003 | 003 | 2021-10-29 |
| 255 | CN | Nanjing Kiwi Network Technology | kiwitech-000 | 000 | 2021-03-19 |
| 256 | KR | Neosecu Co | openface-001 | 001 | 2021-06-15 |
| 257 | TW | Netbridge Technology Incoporation | netbridgegetech-001 | 001 | 2020-01-08 |
| 258 | TW | Netbridge Technology Incoporation | netbridgegetech-002 | 002 | 2020-08-11 |
| 259 | LT | Neurotechnology | neurotechnology-013 | 013 | 2022-01-07 |
| 260 | LT | Neurotechnology | neurotechnology-015 | 015 | 2022-06-07 |
| 261 | ID | Nodeflux | nodeflux-002 | 002 | 2019-08-13 |
| 262 | IN | NotionTag Technologies Private Limited | notiontag-001 | 001 | 2021-03-04 |
| 263 | IN | NotionTag Technologies Private Limited | notiontag-002 | 002 | 2021-09-17 |
| 264 | US | Omnigarde Ltd | omnigarde-001 | 001 | 2021-08-23 |
| 265 | US | Omnigarde Ltd | omnigarde-002 | 002 | 2022-01-19 |
| 266 | KR | One More Security | omface-000 | 000 | 2021-12-15 |
| 267 | RU | Oz Forensics LLC | oz-003 | 003 | 2021-08-09 |
| 268 | RU | Oz Forensics LLC | oz-004 | 004 | 2021-12-13 |
| 269 | TW | PAPAGO Inc | papago-001 | 001 | 2022-07-19 |
| 270 | CH | PXL Vision AG | pxl-001 | 001 | 2020-06-30 |
| 271 | TW | Palit Microsystems | palit-000 | 000 | 2022-05-16 |
| 272 | SG | Panasonic R+D Center Singapore | psl-009 | 009 | 2021-12-08 |
| 273 | SG | Panasonic R+D Center Singapore | psl-010 | 010 | 2022-04-19 |
| 274 | US | Pangiam | pangiam-000 | 000 | 2022-04-04 |
| 275 | TR | Papilon Savunma | papsav1923-001 | 001 | 2021-03-10 |
| 276 | TR | Papilon Savunma | papsav1923-002 | 002 | 2022-01-20 |
| 277 | US | Paravision | paravision-008 | 008 | 2021-06-30 |
| 278 | US | Paravision (EverAI) | paravision-010 | 010 | 2022-02-02 |
| 279 | SG | Pensees Pte | pensees-001 | 001 | 2020-08-17 |
| 280 | IN | Pyramid Cyber Security + Forensic (P) | pyramid-000 | 000 | 2019-11-04 |

Table 4: Summary of participant information included in this report.

| | Location | Developer Name | Short Name | Seq. Num. | Validation Date |
|-----|----------|--|--------------------|-----------|-----------------|
| 281 | KZ | Qaz Biometric Systems | qazbs-000 | 000 | 2022-06-22 |
| 282 | TW | Qnap Security | qnap-001 | 001 | 2021-12-09 |
| 283 | TW | Qnap Security | qnap-002 | 002 | 2022-04-15 |
| 284 | CZ | Quantasoft | quantasoft-003 | 003 | 2021-04-19 |
| 285 | US | Rank One Computing | rankone-012 | 012 | 2021-12-27 |
| 286 | US | Rank One Computing | rankone-013 | 013 | 2022-07-09 |
| 287 | US | Realnetworks Inc | realnetworks-006 | 006 | 2022-02-09 |
| 288 | US | Realnetworks Inc | realnetworks-007 | 007 | 2022-06-14 |
| 289 | US | Regula Forensics | regula-000 | 000 | 2021-04-13 |
| 290 | US | Regula Forensics | regula-001 | 001 | 2021-12-14 |
| 291 | CN | Remark Holdings | remarkai-001 | 001 | 2019-03-01 |
| 292 | CN | Remark Holdings | remarkai-003 | 003 | 2021-06-22 |
| 293 | SG | Rendip | rendip-000 | 000 | 2021-04-19 |
| 294 | UK | Reveal Media Ltd | revealmedia-005 | 005 | 2021-09-24 |
| 295 | UK | Reveal Media Ltd | revealmedia-006 | 006 | 2022-01-26 |
| 296 | CN | Rokid Corporation | rokid-000 | 000 | 2019-08-01 |
| 297 | CN | Rokid Corporation | rokid-001 | 001 | 2019-12-13 |
| 298 | KR | SK Telecom | sktelecom-000 | 000 | 2021-07-09 |
| 299 | KR | SQISoft | sqisoft-001 | 001 | 2021-07-27 |
| 300 | KR | SQISoft | sqisoft-002 | 002 | 2021-11-03 |
| 301 | DE | Saffe | saffe-001 | 001 | 2018-10-19 |
| 302 | DE | Saffe | saffe-002 | 002 | 2019-03-01 |
| 303 | KR | Samsung S1 Corp | s1-004 | 004 | 2022-01-04 |
| 304 | KR | Samsung S1 Corp | s1-005 | 005 | 2022-06-17 |
| 305 | KR | Samsung-SDS | samsungsds-000 | 000 | 2021-10-28 |
| 306 | KR | Samsung-SDS | samsungsds-001 | 001 | 2022-04-18 |
| 307 | IN | Samtech InfoNet Limited | samtech-001 | 001 | 2019-10-15 |
| 308 | RU | Satellite Innovation/Eocortex | eocortex-000 | 000 | 2020-08-26 |
| 309 | IL | Scanovate | scanovate-002 | 002 | 2020-06-26 |
| 310 | IL | Scanovate | scanovate-003 | 003 | 2021-11-15 |
| 311 | RO | Securif AI | securifai-004 | 004 | 2021-12-21 |
| 312 | RO | Securif AI | securifai-005 | 005 | 2022-05-16 |
| 313 | CN | Sensetime Group | sensetime-006 | 006 | 2021-12-28 |
| 314 | CN | Sensetime Group | sensetime-007 | 007 | 2022-06-17 |
| 315 | SG | Seventh Sense Artificial Intelligence | sevensense-000 | 000 | 2021-06-29 |
| 316 | SG | Seventh Sense Artificial Intelligence | sevensense-001 | 001 | 2022-03-04 |
| 317 | US | Shaman Software | shaman-000 | 000 | 2017-12-05 |
| 318 | US | Shaman Software | shaman-001 | 001 | 2018-01-13 |
| 319 | CN | Shanghai Jiao Tong University | sjtu-003 | 003 | 2020-11-02 |
| 320 | CN | Shanghai Jiao Tong University | sjtu-004 | 004 | 2021-05-13 |
| 321 | CN | Shanghai Ulucu Electronics Technology | uluface-002 | 002 | 2019-07-10 |
| 322 | CN | Shanghai Ulucu Electronics Technology | uluface-003 | 003 | 2019-11-12 |
| 323 | CN | Shanghai University - Shanghai Film Academy | shu-002 | 002 | 2019-12-10 |
| 324 | CN | Shanghai University - Shanghai Film Academy | shu-003 | 003 | 2020-06-24 |
| 325 | CN | Shanghai Yitu Technology | yitu-003 | 003 | 2019-03-01 |
| 326 | CN | Shenzhen AiMall Tech | aimall-002 | 002 | 2020-03-12 |
| 327 | CN | Shenzhen AiMall Tech | aimall-003 | 003 | 2020-08-12 |
| 328 | CN | Shenzhen EI Networks | einetworks-000 | 000 | 2019-08-13 |
| 329 | CN | Shenzhen Inst Adv Integrated Tech CAS | siat-002 | 002 | 2018-06-13 |
| 330 | CN | Shenzhen Inst Adv Integrated Tech CAS | siat-005 | 005 | 2022-02-08 |
| 331 | CN | Shenzhen Intellifusion Technologies | intellifusion-001 | 001 | 2019-08-22 |
| 332 | CN | Shenzhen Intellifusion Technologies | intellifusion-002 | 002 | 2020-03-18 |
| 333 | CN | Shenzhen University-Macau University of Science and Technology | sztu-000 | 000 | 2020-12-17 |
| 334 | CN | Shenzhen University-Macau University of Science and Technology | sztu-001 | 001 | 2021-07-13 |
| 335 | RU | Smart Engines | smartengines-000 | 000 | 2021-08-25 |
| 336 | RU | Smart Engines | smartengines-001 | 001 | 2022-05-31 |
| 337 | ES | Smartbiometrik | smartbiometrik-001 | 001 | 2022-05-16 |
| 338 | TR | Smarvist Teknoloji | smarvist-000 | 000 | 2022-05-10 |
| 339 | DE | Smilart | smilart-002 | 002 | 2018-02-06 |
| 340 | DE | Smilart | smilart-003 | 003 | 2019-03-01 |
| 341 | TR | Sodec App Inc | sodec-000 | 000 | 2021-06-02 |
| 342 | IN | Staqu Technologies | st aqu-000 | 000 | 2020-07-15 |
| 343 | CN | Star Hybrid Limited | starhybrid-001 | 001 | 2019-06-19 |
| 344 | CN | Su Zhou NaZhiTianDi intelligent technology | nazhai-000 | 000 | 2020-06-25 |
| 345 | IN | Sukshi Technology Innovation | sukshi-000 | 000 | 2022-02-13 |
| 346 | KR | Suprema AI Inc | suprema-002 | 002 | 2022-02-11 |
| 347 | KR | Suprema AI Inc | suprema-003 | 003 | 2022-07-20 |
| 348 | KR | Suprema ID Inc | supremaid-001 | 001 | 2021-05-04 |
| 349 | KR | Suprema ID Inc | supremaid-002 | 002 | 2022-06-24 |
| 350 | RU | Synesis | synesis-006 | 006 | 2019-10-10 |

Table 5: Summary of participant information included in this report.

| | Location | Developer Name | Short Name | Seq. Num. | Validation Date |
|-----|----------|---|---------------------------|-----------|-----------------|
| 351 | RU | Synesis | synesis-007 | 007 | 2020-06-24 |
| 352 | TW | Synology Inc | synology-000 | 000 | 2019-10-23 |
| 353 | TW | Synology Inc | synology-002 | 002 | 2020-08-20 |
| 354 | BR | T4iSB | t4isb-000 | 000 | 2022-01-28 |
| 355 | CN | TUPU Technology | tuputech-000 | 000 | 2019-10-11 |
| 356 | TW | Taiwan AI Labs | ailabs-001 | 001 | 2019-12-18 |
| 357 | TW | Taiwan-Certificate Authority Incorporation | twface-000 | 000 | 2021-05-14 |
| 358 | TW | Taiwan-Certificate Authority Incorporation | twface-001 | 001 | 2021-09-14 |
| 359 | CH | Tech5 SA | tech5-004 | 004 | 2020-03-09 |
| 360 | CH | Tech5 SA | tech5-005 | 005 | 2020-07-24 |
| 361 | TR | Techsign | techsign-000 | 000 | 2021-08-25 |
| 362 | TR | Techsign | techsign-001 | 001 | 2022-07-01 |
| 363 | CN | Tencent Deepsea Lab | deepsea-001 | 001 | 2019-06-03 |
| 364 | RU | Tevian | tevian-007 | 007 | 2021-08-06 |
| 365 | RU | Tevian | tevian-008 | 008 | 2021-12-06 |
| 366 | US | TigerIT Americas LLC | tiger-005 | 005 | 2021-07-29 |
| 367 | US | TigerIT Americas LLC | tiger-006 | 006 | 2021-12-13 |
| 368 | RU | Tinkoff Bank | tinkoff-001 | 001 | 2021-05-13 |
| 369 | CN | TongYi Transportation Technology | tongyi-005 | 005 | 2019-06-12 |
| 370 | TW | Toppan ID Gate | toppanidgate-000 | 000 | 2021-09-28 |
| 371 | JP | Toshiba | toshiba-004 | 004 | 2021-09-27 |
| 372 | JP | Toshiba | toshiba-006 | 006 | 2022-06-29 |
| 373 | ES | Touchless ID | touchlessid-000 | 000 | 2022-05-02 |
| 374 | JP | Tripleize | aize-001 | 001 | 2021-04-23 |
| 375 | JP | Tripleize | aize-002 | 002 | 2021-10-08 |
| 376 | US | Trueface.ai | trueface-002 | 002 | 2021-03-29 |
| 377 | US | Trueface.ai | trueface-003 | 003 | 2021-09-30 |
| 378 | CN | TuringTech.vip | turingtechvip-001 | 001 | 2022-02-03 |
| 379 | CN | TuringTech.vip | turingtechvip-002 | 002 | 2022-07-27 |
| 380 | CN | ULSee Inc | ulsee-001 | 001 | 2019-07-31 |
| 381 | FR | Unissey | unissey-001 | 001 | 2021-11-29 |
| 382 | FR | Unissey | unissey-002 | 002 | 2022-04-29 |
| 383 | PT | Universidade de Coimbra | visteam-003 | 003 | 2022-01-31 |
| 384 | PT | Universidade de Coimbra | visteam-004 | 004 | 2022-08-01 |
| 385 | UK | University of Surrey-CVSSP | surrey-cvssp-000 | 000 | 2022-03-25 |
| 386 | US | VCognition | vcog-002 | 002 | 2017-06-12 |
| 387 | ES | Veridas Digital Authentication Solutions S.L. | veridas-006 | 006 | 2021-04-15 |
| 388 | ES | Veridas Digital Authentication Solutions S.L. | veridas-007 | 007 | 2021-09-02 |
| 389 | UK | Veridium | veridium-000 | 000 | 2022-03-28 |
| 390 | KZ | Verigram | verigram-000 | 000 | 2021-09-06 |
| 391 | KZ | Verigram | verigram-001 | 001 | 2022-03-09 |
| 392 | ID | Verihubs | verihubs-inteligensia-000 | 000 | 2021-07-27 |
| 393 | ID | Verihubs | verihubs-inteligensia-001 | 001 | 2022-06-16 |
| 394 | | Verijelas | verijelas-000 | 000 | 2022-08-01 |
| 395 | TW | Via Technologies Inc | via-000 | 000 | 2019-07-08 |
| 396 | TW | Via Technologies Inc | via-001 | 001 | 2020-01-08 |
| 397 | DE | Videmo Intelligente Videoanalyse | videmo-000 | 000 | 2019-12-19 |
| 398 | DE | Videmo Intelligente Videoanalyse | videmo-001 | 001 | 2021-12-22 |
| 399 | IN | Videonetics Technology Pvt | videonetics-001 | 001 | 2019-06-19 |
| 400 | IN | Videonetics Technology Pvt | videonetics-002 | 002 | 2019-11-21 |
| 401 | VN | Vietnam Posts and Telecommunications Group | vnpt-003 | 003 | 2021-12-01 |
| 402 | VN | Vietnam Posts and Telecommunications Group | vnpt-004 | 004 | 2022-04-15 |
| 403 | VN | Viettel Group | vts-000 | 000 | 2020-11-04 |
| 404 | VN | Viettel Group | vts-001 | 001 | 2022-04-20 |
| 405 | VN | Viettel High Technology | viettelhightech-000 | 000 | 2021-08-04 |
| 406 | US | Vigilant Solutions | vigilantsolutions-010 | 010 | 2021-04-07 |
| 407 | US | Vigilant Solutions | vigilantsolutions-011 | 011 | 2021-08-07 |
| 408 | VN | VinAI Research VietNam | vinai-000 | 000 | 2020-09-24 |
| 409 | VN | VinBigData | vinbigdata-001 | 001 | 2022-01-06 |
| 410 | VN | VinBigData | vinbigdata-002 | 002 | 2022-06-07 |
| 411 | SE | Visage Technologies | visage-000 | 000 | 2020-12-09 |
| 412 | FI | Visidon | vd-002 | 002 | 2021-04-12 |
| 413 | FI | Visidon | vd-003 | 003 | 2021-10-12 |
| 414 | CN | Vision Intelligence Center of Meituan | meituan-000 | 000 | 2021-05-14 |
| 415 | CN | Vision Intelligence Center of Meituan | meituan-001 | 001 | 2022-03-25 |
| 416 | PT | Vision-Box | visionbox-001 | 001 | 2019-03-01 |
| 417 | PT | Vision-Box | visionbox-002 | 002 | 2021-04-29 |
| 418 | RU | VisionLabs | visionlabs-010 | 010 | 2021-01-25 |
| 419 | RU | VisionLabs | visionlabs-011 | 011 | 2021-10-13 |
| 420 | AU | Vixvizion | vixvizion-005 | 005 | 2022-03-03 |

Table 6: Summary of participant information included in this report.

| | Location | Developer Name | Short Name | Seq. Num. | Validation Date |
|-----|----------|---------------------------------------|------------------|-----------|-----------------|
| 421 | AU | Vixvizon | vixvizon-006 | 006 | 2022-08-11 |
| 422 | RU | Vocord | vocord-009 | 009 | 2020-12-28 |
| 423 | RU | Vocord | vocord-010 | 010 | 2021-12-20 |
| 424 | US | Wicket | wicket-000 | 000 | 2022-02-14 |
| 425 | CN | Winsense | winsense-001 | 001 | 2019-10-16 |
| 426 | CN | Winsense | winsense-002 | 002 | 2020-11-20 |
| 427 | CN | Wuhan Tianyu Information Industry | wuhantianyu-001 | 001 | 2021-08-05 |
| 428 | CN | X-Laboratory | x-laboratory-000 | 000 | 2019-09-03 |
| 429 | CN | X-Laboratory | x-laboratory-001 | 001 | 2020-01-21 |
| 430 | CN | Xforward AI Technology | xforwardai-001 | 001 | 2020-09-25 |
| 431 | CN | Xforward AI Technology | xforwardai-002 | 002 | 2021-02-10 |
| 432 | CN | Xiamen Meiya Pico Information | meiya-001 | 001 | 2019-03-01 |
| 433 | CN | Xiamen University | xm-000 | 000 | 2020-10-19 |
| 434 | PT | Yoonik | yoonik-002 | 002 | 2021-09-06 |
| 435 | PT | Yoonik | yoonik-003 | 003 | 2022-01-06 |
| 436 | TW | Yuan High-Tech Development | yuan-004 | 004 | 2022-01-14 |
| 437 | TW | Yuan High-Tech Development | yuan-005 | 005 | 2022-06-22 |
| 438 | CN | Yuntu Data and Technology | ytu-000 | 000 | 2021-06-16 |
| 439 | CN | Zhuhai Yisheng Electronics Technology | yisheng-004 | 004 | 2018-06-12 |
| 440 | CN | iQIYI Inc | iqface-000 | 000 | 2019-06-04 |
| 441 | CN | iQIYI Inc | iqface-003 | 003 | 2021-02-23 |
| 442 | TW | iSAP Solution Corporation | isap-001 | 001 | 2019-08-07 |
| 443 | TW | iSAP Solution Corporation | isap-002 | 002 | 2020-09-01 |
| 444 | TW | ioNetworks Inc | ionetworks-000 | 000 | 2021-07-20 |

Table 7: Summary of participant information included in this report.

| ALGORITHM | CONFIG | LIBRARY | TEMPLATE | | | | | | | | | COMPARISON ⁴ | | | | | | | | | | | |
|-----------|--------------------|---------|-------------------|-------------------|-------------------|------|---------|----------|----------|-----------------------------------|-----------|-------------------------|----------|------------------------|----------|-----------|----------|--------------|----------|--------------|--------------|-------------|-----------|
| | | | NAME | | DATA | | MEMORY | | SIZE | GENERATION TIME (ms) ⁴ | | | | TIME (ns) ⁵ | | | | | | | | | |
| | | | (KB) ¹ | (KB) ² | (MB) ³ | (B) | MUGSHOT | 480x720 | 960x1440 | 1600x2400 | 3000x4500 | GENUINE | IMPOSTOR | | | | | | | | | | |
| 1 | 20face-000 | | 117155 | 324083 | 208 | 905 | 257 | 2048 ± 0 | 38 | 232 ± 1 | 28 | 223 ± 1 | 21 | 222 ± 1 | 16 | 224 ± 1 | 417 | 44880 ± 134 | 416 | 44462 ± 163 | | | |
| 2 | 20face-001 | | 226824 | 324119 | 351 | 1940 | 404 | 4096 ± 0 | 48 | 279 ± 2 | 32 | 266 ± 1 | 26 | 266 ± 1 | 20 | 267 ± 0 | 323 | 5553 ± 54 | 321 | 5541 ± 65 | | | |
| 3 | 3divi-006 | | 273866 | 52656 | | 83 | 472 | 138 | 2048 ± 0 | 204 | 654 ± 1 | 169 | 651 ± 0 | 150 | 660 ± 1 | 133 | 678 ± 2 | 136 | 759 ± 13 | 110 | 775 ± 19 | | |
| 4 | 3divi-007 | | 483115 | 24723 | 278 | 1285 | 244 | 2048 ± 0 | 184 | 615 ± 1 | 156 | 616 ± 1 | 136 | 623 ± 1 | 121 | 644 ± 1 | 126 | 727 ± 5 | 94 | 707 ± 31 | 96 | 712 ± 25 | |
| 5 | acer-001 | | 36650 | 66086 | | 68 | 417 | 35 | 512 ± 0 | 34 | 199 ± 0 | 29 | 237 ± 28 | 25 | 229 ± 26 | 24 | 242 ± 37 | 19 | 259 ± 21 | 244 | 2453 ± 44 | 245 | 2461 ± 62 |
| 6 | acer-002 | | 43922 | 624858 | | 35 | 187 | 260 | 2048 ± 0 | 31 | 184 ± 0 | 22 | 184 ± 0 | 17 | 185 ± 0 | 14 | 185 ± 0 | 13 | 186 ± 0 | 281 | 3370 ± 47 | 281 | 3350 ± 54 |
| 7 | acisw-007 | | 267619 | 36111 | | 48 | 286 | 154 | 2048 ± 0 | 53 | 283 ± 0 | 42 | 293 ± 3 | 58 | 414 ± 0 | 51 | 404 ± 0 | 53 | 484 ± 1 | 166 | 1316 ± 22 | 166 | 1297 ± 23 |
| 8 | acisw-008 | | 171703 | 39359 | 249 | 1101 | 227 | 2048 ± 0 | 89 | 400 ± 1 | 62 | 362 ± 28 | 47 | 369 ± 9 | 30 | 300 ± 2 | 24 | 336 ± 5 | 167 | 1327 ± 19 | 169 | 1337 ± 32 | |
| 9 | ader-a-002 | | 0 | 749797 | 214921 | 431 | 5120 | ± 0 | 426 | 1394 ± 11 | 385 | 1381 ± 1 | 384 | 1393 ± 1 | 363 | 1403 ± 1 | 314 | 1464 ± 2 | 233 | 2163 ± 32 | 235 | 2158 ± 28 | |
| 10 | ader-a-003 | | 0 | 749778 | 212917 | 430 | 5120 | 0 | 419 | 1381 ± 12 | 387 | 1385 ± 1 | 385 | 1394 ± 1 | 359 | 1401 ± 1 | 315 | 1469 ± 1 | 232 | 2148 ± 34 | 232 | 2130 ± 32 | |
| 11 | advance-002 | | 257173 | 20434 | 51 | 295 | 258 | 2048 ± 0 | 260 | 811 ± 2 | 218 | 803 ± 2 | 167 | 696 ± 2 | 141 | 699 ± 4 | 122 | 718 ± 1 | 129 | 987 ± 10 | 128 | 988 ± 45 | |
| 12 | advance-003 | | 258867 | 78699 | 100 | 518 | 142 | 2048 ± 0 | 170 | 586 ± 0 | 142 | 584 ± 0 | 120 | 583 ± 0 | 103 | 588 ± 0 | 82 | 591 ± 1 | 211 | 1813 ± 17 | 207 | 1788 ± 26 | |
| 13 | afisbiometrics-000 | | 545886 | 32882 | 246 | 1088 | 19 | 512 ± 0 | 382 | 1219 ± 1 | 323 | 1135 ± 1 | 309 | 1137 ± 2 | 275 | 1137 ± 1 | 229 | 1147 ± 1 | 172 | 1400 ± 29 | 170 | 1357 ± 32 | |
| 14 | aifirst-001 | | 224157 | 808777 | 86 | 485 | 206 | 2048 ± 0 | 171 | 587 ± 2 | 134 | 568 ± 2 | 121 | 584 ± 3 | 107 | 601 ± 6 | 134 | 755 ± 5 | 147 | 1099 ± 14 | 149 | 1087 ± 45 | |
| 15 | aigen-001 | | 256958 | 595227 | 256 | 1136 | 225 | 2048 ± 0 | 433 | 1448 ± 9 | 402 | 1451 ± 8 | 407 | 1759 ± 6 | 404 | 2594 ± 4 | 391 | 5691 ± 44 | 295 | 3772 ± 57 | 294 | 3736 ± 56 | |
| 16 | aigen-002 | | 205300 | 1316138 | 202 | 874 | 236 | 2048 ± 0 | 168 | 586 ± 24 | 141 | 582 ± 4 | 236 | 920 ± 4 | 388 | 1758 ± 5 | 390 | 5427 ± 17 | 291 | 3678 ± 44 | 290 | 3646 ± 48 | |
| 17 | ailabs-001 | | 1054663 | 338989 | 270 | 1252 | 232 | 2048 ± 0 | 210 | 664 ± 4 | 209 | 774 ± 50 | 312 | 1145 ± 12 | 393 | 1972 ± 74 | 387 | 5205 ± 272 | 437 | 104034 ± 661 | 103415 ± 722 | | |
| 18 | aimall-002 | | 370156 | 25210 | 315 | 1576 | 222 | 2048 ± 0 | 249 | 776 ± 4 | 268 | 927 ± 27 | 244 | 940 ± 21 | 225 | 955 ± 34 | 196 | 1003 ± 75 | 434 | 72811 ± 7399 | 71216 ± 6286 | | |
| 19 | aimall-003 | | 504324 | 171935 | 347 | 1913 | 77 | 1024 ± 0 | 207 | 662 ± 1 | 198 | 740 ± 51 | 183 | 752 ± 62 | 159 | 741 ± 46 | 146 | 807 ± 47 | 411 | 34565 ± 93 | 412 | 34598 ± 118 | |
| 20 | aiseemu-001 | | 0 | 1005354 | 383 | 2697 | 406 | 4096 ± 0 | 333 | 1001 ± 1 | 294 | 1017 ± 0 | 278 | 1014 ± 5 | 247 | 1022 ± 2 | 212 | 1059 ± 4 | 312 | 4864 ± 25 | 312 | 4855 ± 32 | |
| 21 | aiunionface-000 | | 241642 | 840295 | 65 | 402 | 288 | 2048 ± 0 | 196 | 637 ± 13 | 204 | 754 ± 41 | 280 | 1025 ± 28 | 290 | 1179 ± 29 | 337 | 1639 ± 47 | 141 | 1072 ± 19 | 147 | 1080 ± 47 | |
| 22 | aize-001 | | 268456 | 168970 | 302 | 1436 | 228 | 2048 ± 0 | 107 | 437 ± 10 | 85 | 440 ± 8 | 106 | 542 ± 17 | 162 | 756 ± 27 | 333 | 1583 ± 53 | 222 | 1937 ± 22 | 218 | 1919 ± 23 | |
| 23 | aize-002 | | 257106 | 182517 | 120 | 586 | 220 | 2048 ± 0 | 119 | 467 ± 1 | 97 | 479 ± 1 | 185 | 756 ± 1 | 376 | 1477 ± 1 | 385 | 4617 ± 41 | 60 | 597 ± 16 | 65 | 598 ± 14 | |
| 24 | ajou-001 | | 363257 | 31734 | 76 | 442 | 195 | 2048 ± 0 | 141 | 530 ± 0 | 120 | 536 ± 0 | 102 | 535 ± 0 | 91 | 549 ± 0 | 78 | 577 ± 0 | 59 | 597 ± 19 | 64 | 596 ± 13 | |
| 25 | alchera-003 | | 487718 | 24613 | 290 | 1376 | 119 | 2048 ± 0 | 280 | 854 ± 3 | 238 | 862 ± 2 | 218 | 870 ± 1 | 198 | 882 ± 2 | 175 | 918 ± 1 | 284 | 3426 ± 57 | 282 | 3383 ± 53 | |
| 26 | alchera-004 | | 1001019 | 388616 | 274 | 1270 | 273 | 2048 ± 0 | 323 | 975 ± 0 | 278 | 955 ± 0 | 254 | 960 ± 0 | 235 | 989 ± 0 | 230 | 1152 ± 1 | 287 | 3529 ± 54 | 287 | 3530 ± 63 | |
| 27 | alfabeta-001 | | 128232 | 21780 | 873 | 32 | 512 ± 0 | 43 | 271 ± 0 | 37 | 276 ± 0 | 72 | 459 ± 2 | 201 | 886 ± 2 | 367 | 2547 ± 9 | 42 | 470 ± 25 | 44 | 458 ± 20 | | |
| 28 | alice-000 | | 1741293 | 19355 | 332 | 1732 | 382 | 4096 ± 0 | 316 | 950 ± 2 | 270 | 933 ± 1 | 249 | 949 ± 1 | 246 | 1011 ± 3 | 259 | 1264 ± 8 | 378 | 14975 ± 201 | 378 | 14890 ± 229 | |
| 29 | alleyes-000 | | 507636 | 997090 | 199 | 857 | 207 | 2048 ± 0 | 253 | 784 ± 1 | 280 | 970 ± 61 | 258 | 974 ± 62 | 221 | 943 ± 69 | 210 | 1057 ± 23 | 165 | 1298 ± 34 | 167 | 1303 ± 51 | |
| 30 | allgovision-000 | | 172509 | 155862 | 113 | 561 | 281 | 2048 ± 0 | 87 | 384 ± 8 | 69 | 395 ± 17 | 57 | 413 ± 14 | 68 | 471 ± 14 | 120 | 710 ± 21 | 403 | 29903 ± 406 | 404 | 29735 ± 194 | |
| 31 | alphaface-001 | | 259849 | 81636 | 103 | 527 | 252 | 2048 ± 0 | 180 | 612 ± 1 | 152 | 613 ± 3 | 132 | 612 ± 1 | 111 | 619 ± 1 | 101 | 640 ± 2 | 133 | 1008 ± 10 | 133 | 1002 ± 19 | |
| 32 | alphaface-002 | | 768995 | 70692 | 301 | 1434 | 249 | 2048 ± 0 | 191 | 628 ± 2 | 206 | 746 ± 19 | 182 | 751 ± 18 | 168 | 779 ± 22 | 152 | 828 ± 40 | 124 | 945 ± 25 | 125 | 935 ± 17 | |
| 33 | amplifiedgroup-001 | | 0 | 47053 | 12 | 81 | 63 | 866 ± 2 | 129 | 930 ± 3 | - | - | - | - | - | - | 427 | 57803 ± 4210 | 425 | 56365 ± 1196 | | | |
| 34 | androvideo-000 | | 174847 | 585063 | 66 | 403 | 187 | 2048 ± 0 | 47 | 277 ± 0 | 40 | 285 ± 0 | 34 | 314 ± 0 | 42 | 372 ± 1 | 91 | 620 ± 0 | 262 | 2860 ± 28 | 262 | 2847 ± 22 | |
| 35 | anke-004 | | 349388 | 410776 | 153 | 706 | 350 | 2056 ± 0 | 188 | 625 ± 1 | 159 | 627 ± 2 | 144 | 635 ± 3 | 126 | 653 ± 2 | 191 | 982 ± 8 | 78 | 633 ± 22 | 80 | 632 ± 34 | |
| 36 | anke-005 | | 328553 | 429160 | 254 | 1134 | 338 | 2056 ± 0 | 172 | 590 ± 2 | 148 | 594 ± 5 | 129 | 601 ± 3 | 120 | 638 ± 4 | 150 | 821 ± 24 | 89 | 685 ± 19 | 93 | 687 ± 26 | |
| 37 | antheus-000 | | 119453 | 41994 | 20 | 116 | 50 | 520 ± 0 | 16 | 109 ± 1 | 24 | 187 ± 1 | 19 | 189 ± 1 | 13 | 195 ± 1 | 17 | 236 ± 2 | 339 | 6901 ± 268 | 339 | 6936 ± 103 | |
| 38 | antheus-001 | | 119453 | 41962 | 21 | 118 | 52 | 520 ± 0 | 19 | 120 ± 1 | 31 | 265 ± 13 | 76 | 468 ± 22 | 305 | 1223 ± 27 | 368 | 2660 ± 87 | 335 | 6218 ± 47 | 334 | 6216 ± 45 | |
| 39 | anyvision-004 | | 401001 | 630797 | 250 | 1102 | 66 | 1024 ± 0 | 355 | 51 ± 1 | - | - | - | - | - | - | 218 | 1891 ± 51 | 211 | 1829 ± 85 | 1829 | 1825 ± 85 | |
| 40 | anyvision-005 | | 190979 | 116595 | 221 | 963 | 76 | 1024 ± 0 | 327 | 985 ± 1 | 285 | 997 ± 1 | 274 | 1004 ± 1 | 237 | 995 ± 1 | 193 | 995 ± 1 | 102 | 733 ± 14 | 103 | 733 ± 16 | |
| 41 | armatura-001 | | 0 | 374608 | 258 | 1151 | 250 | 2048 ± 0 | 220 | 688 ± 1 | 183 | 689 ± 1 | 165 | 693 ± 1 | 147 | 708 ± 3 | 135 | 756 ± 13 | 18 | 270 ± 17 | 20 | 268 ± 11 | |
| 42 | asusaics-000 | | 257418 | 245320 | 127 | 605 | 149 | 2048 ± 0 | 128 | 484 ± 13 | 114 | 506 ± 21 | 211 | 850 ± 26 | 389 | 1789 ± 61 | 393 | 6305 ± 188 | 321 | 5455 ± 78 | 320 | 5422 ± 112 | |
| 43 | asusaics-001 | | 257418 | 245330 | 124 | 595 | 385 | 4096 ± 0 | 277 | 842 ± 17 | 292 | 1008 ± 20 | 375 | 1377 ± 22 | 403 | 2423 ± 90 | 398 | 7284 ± 277 | 350 | 8618 ± 42 | 350 | 8638 ± 136 | |
| 44 | authenmetric-003 | | 293599 | 39492 | 225 | 982 | 253 | 2048 ± 0 | 330 | 992 ± 1 | 289 | 1006 ± 1 | 272 | 1003 ± 2 | 242 | 1002 ± 1 | 202 | 1036 ± 1 | 201 | 1757 ± 19 | 201 | 1755 ± 19 | |

Notes

- 1 The configuration size does not capture static data included in libraries.
 - 2 The library size is the combined total of all files provided in the submission lib folder. These libraries e.g. OpenCV may or may not be installed on any end user's platform natively and would not need to be installed with the algorithm. Some developers put neural network models in their libraries.
 - 3 The memory usage is the peak resident set size reported by the ps system call during template generation.
 - 4 The median template creation times are measured on Intel® Xeon® CPU E5-2630 v4 @ 2.20GHz processors.
 - 5 The comparison durations, in nanoseconds, are estimated using std::chrono::high_resolution_clock which on the machine in (2) counts 1ns clock ticks. Precision is somewhat worse than that however. The \pm value is the median absolute deviation times 1.48 for Normal consistency.

| ALGORITHM | CONFIG | LIBRARY | TEMPLATE | | | | | | | | COMPARISON ⁴ | | | | | | | | | | |
|-----------|--------------------|---------|----------|------|------|--------|----------|-----------------------------------|-------------------|-------------------|-------------------------|------------------------|-----------|----------|------------|-----------|--------------|-----------|---------------|-----------|----------------|
| | | | NAME | DATA | DATA | MEMORY | SIZE | GENERATION TIME (ms) ⁴ | | | | TIME (ns) ⁵ | | | | | | | | | |
| | | | | | | | | (KB) ¹ | (KB) ² | (MB) ³ | (B) | MUGSHOT | 480x720 | 960x1440 | 1600x2400 | 3000x4500 | GENUINE | IMPOSTOR | | | |
| 45 | authenmetric-004 | 381165 | 39492 | 264 | 1214 | 124 | 2048 ± 0 | 301 | 910 ± 1 | 262 | 909 ± 1 | 232 | 915 ± 1 | 213 | 921 ± 2 | 184 | 950 ± 1 | 196 | 1724 ± 14 | 194 | 1691 ± 29 |
| 46 | aware-005 | 300017 | 26320 | 272 | 1265 | 97 | 1572 ± 0 | 298 | 886 ± 23 | 303 | 1038 ± 21 | 302 | 1121 ± 22 | 335 | 1337 ± 58 | 352 | 2195 ± 144 | 183 | 1475 ± 63 | 179 | 1427 ± 115 |
| 47 | aware-006 | 298543 | 14124 | 219 | 943 | 15 | 352 ± 0 | 366 | 1148 ± 3 | 329 | 1146 ± 2 | 327 | 1190 ± 2 | 325 | 1306 ± 20 | 345 | 1754 ± 84 | 252 | 2598 ± 42 | 252 | 2559 ± 60 |
| 48 | awiros-001 | 15499 | 87480 | 14 | 88 | 26 | 512 ± 0 | 13 | 97 ± 6 | 11 | 98 ± 4 | 12 | 138 ± 6 | 22 | 225 ± 7 | 74 | 556 ± 8 | 143 | 1079 ± 44 | 142 | 1050 ± 45 |
| 49 | awiros-002 | 289016 | 203723 | 114 | 562 | 196 | 2048 ± 0 | 124 | 479 ± 0 | 110 | 500 ± 0 | 101 | 534 ± 0 | 110 | 618 ± 0 | 182 | 946 ± 1 | 223 | 1966 ± 31 | 224 | 1957 ± 25 |
| 50 | aximetria-001 | 408902 | 487912 | 141 | 674 | 194 | 2048 ± 0 | 337 | 1013 ± 1 | 295 | 1023 ± 21 | 283 | 1029 ± 5 | 239 | 999 ± 2 | 220 | 1091 ± 5 | 305 | 4401 ± 94 | 304 | 4490 ± 80 |
| 51 | ayftech-001 | 195423 | 43580 | 164 | 731 | 23 | 512 ± 0 | 96 | 408 ± 23 | 96 | 476 ± 52 | 198 | 814 ± 108 | 391 | 1827 ± 384 | 389 | 5412 ± 1029 | 70 | 615 ± 16 | 121 | 885 ± 44 |
| 52 | ayonix-000 | 58505 | 5252 | 6 | 69 | 82 | 1036 ± 0 | 2 | 18 ± 2 | - | - | - | - | - | - | - | - | 73 | 621 ± 23 | 76 | 620 ± 26 |
| 53 | beethedata-000 | 227849 | 1087592 | 112 | 555 | 235 | 2048 ± 0 | 117 | 465 ± 0 | 95 | 467 ± 0 | 78 | 468 ± 0 | 67 | 467 ± 0 | 50 | 467 ± 0 | 230 | 2121 ± 34 | 231 | 2110 ± 38 |
| 54 | beyneai-000 | 256958 | 591433 | 252 | 1124 | 189 | 2048 ± 0 | 110 | 451 ± 8 | 88 | 449 ± 1 | 187 | 767 ± 7 | 384 | 1603 ± 25 | 386 | 4669 ± 124 | 293 | 3730 ± 57 | 291 | 3668 ± 54 |
| 55 | biocube-001 | 25030 | 6192987 | 80 | 458 | 412 | 4096 ± 0 | 51 | 282 ± 22 | 41 | 292 ± 24 | 99 | 521 ± 57 | 134 | 684 ± 59 | 265 | 1282 ± 68 | 392 | 21787 ± 96 | 392 | 21812 ± 109 |
| 56 | bioditechswiss-001 | 1178769 | 120811 | 304 | 1455 | 16 | 512 ± 0 | 322 | 966 ± 4 | 360 | 1270 ± 270 | 353 | 1294 ± 96 | 364 | 1409 ± 157 | 347 | 1793 ± 79 | 253 | 2610 ± 25 | 253 | 2624 ± 32 |
| 57 | bioditechswiss-002 | 744786 | 114842 | 229 | 993 | 30 | 512 ± 0 | 305 | 917 ± 2 | 269 | 930 ± 2 | 251 | 952 ± 2 | 223 | 947 ± 3 | 211 | 1058 ± 11 | 235 | 2177 ± 29 | 237 | 2170 ± 31 |
| 58 | bm-001 | 287734 | 38076 | 26 | 148 | 1 | 64 ± 0 | 108 | 444 ± 88 | - | - | - | - | - | - | - | 217 | 1887 ± 31 | 216 | 1877 ± 26 | |
| 59 | boetech-001 | 261376 | 88710 | 293 | 1384 | 130 | 2048 ± 0 | 44 | 271 ± 1 | 33 | 268 ± 1 | 27 | 273 ± 0 | 28 | 286 ± 1 | 22 | 318 ± 1 | 431 | 68519 ± 1921 | 431 | 67648 ± 822 |
| 60 | boetech-002 | 294347 | 88710 | 308 | 1489 | 297 | 2048 ± 0 | 59 | 305 ± 4 | 44 | 296 ± 1 | 30 | 302 ± 1 | 31 | 313 ± 1 | 27 | 348 ± 2 | 432 | 68921 ± 2137 | 432 | 69473 ± 2104 |
| 61 | bresee-001 | 287880 | 23227 | 265 | 1214 | 131 | 2048 ± 0 | 383 | 1223 ± 3 | 345 | 1216 ± 1 | 362 | 1331 ± 1 | 308 | 1227 ± 1 | 284 | 1360 ± 1 | 412 | 37240 ± 655 | 413 | 37167 ± 584 |
| 62 | bresee-002 | 313627 | 30902 | 353 | 1956 | 117 | 2048 ± 0 | 238 | 743 ± 4 | 326 | 1143 ± 2 | 313 | 1146 ± 2 | 278 | 1148 ± 2 | 243 | 1176 ± 2 | 204 | 1778 ± 22 | 204 | 1775 ± 23 |
| 63 | camvi-002 | 236278 | 225285 | 165 | 737 | 69 | 1024 ± 0 | 215 | 677 ± 7 | 196 | 726 ± 36 | 214 | 869 ± 28 | 269 | 1129 ± 43 | 373 | 2785 ± 113 | 69 | 612 ± 26 | 69 | 603 ± 20 |
| 64 | camvi-004 | 280733 | 615819 | 213 | 919 | 155 | 2048 ± 0 | 242 | 759 ± 10 | 237 | 861 ± 17 | 264 | 986 ± 34 | 322 | 1279 ± 51 | 375 | 2891 ± 158 | 125 | 948 ± 40 | 126 | 963 ± 31 |
| 65 | canon-003 | 2550850 | 101378 | 428 | 5472 | 434 | 6180 ± 0 | 393 | 1263 ± 3 | 358 | 1263 ± 1 | 349 | 1283 ± 1 | 333 | 1320 ± 1 | 319 | 1482 ± 2 | 310 | 4783 ± 17 | 307 | 4780 ± 19 |
| 66 | canon-004 | 2399160 | 114188 | 430 | 5956 | 435 | 6200 ± 0 | 314 | 948 ± 4 | 276 | 955 ± 3 | 253 | 959 ± 3 | 229 | 977 ± 3 | 215 | 1064 ± 2 | 345 | 7172 ± 63 | 344 | 7169 ± 51 |
| 67 | ceiec-003 | 260371 | 88707 | 72 | 430 | 259 | 2048 ± 0 | 264 | 817 ± 4 | 252 | 883 ± 57 | 224 | 897 ± 60 | 206 | 899 ± 72 | 180 | 944 ± 72 | 241 | 2256 ± 38 | 241 | 2241 ± 54 |
| 68 | ceiec-004 | 263476 | 67011 | 67 | 408 | 146 | 2048 ± 0 | 341 | 1024 ± 1 | 298 | 1027 ± 1 | 282 | 1027 ± 1 | 249 | 1030 ± 1 | 208 | 1055 ± 1 | 213 | 1844 ± 26 | 212 | 1836 ± 20 |
| 69 | chosun-001 | 765615 | 707 | 90 | 491 | 158 | 2048 ± 0 | 251 | 783 ± 2 | 226 | 826 ± 4 | 406 | 1662 ± 13 | 409 | 3679 ± 67 | 406 | 11694 ± 243 | 130 | 998 ± 25 | 140 | 1035 ± 11 |
| 70 | chosun-002 | 234001 | 31875 | 77 | 450 | 202 | 2048 ± 0 | 39 | 248 ± 3 | 34 | 273 ± 3 | 401 | 1495 ± 14 | 410 | 7920 ± 90 | 407 | 80302 ± 1349 | 74 | 623 ± 17 | 83 | 634 ± 13 |
| 71 | chiface-004 | 409656 | 311027 | 307 | 1487 | 255 | 2048 ± 0 | 68 | 332 ± 0 | 50 | 323 ± 1 | 39 | 329 ± 1 | 36 | 335 ± 1 | 32 | 377 ± 1 | 197 | 1727 ± 17 | 196 | 1720 ± 16 |
| 72 | chiface-005 | 408364 | 311100 | 297 | 1412 | 104 | 2048 ± 0 | 65 | 322 ± 0 | 48 | 316 ± 1 | 36 | 325 ± 2 | 33 | 324 ± 1 | 41 | 411 ± 2 | 219 | 1907 ± 19 | 217 | 1898 ± 23 |
| 73 | clearviewai-000 | 342491 | 211852 | 390 | 2750 | 112 | 2048 ± 0 | 430 | 1402 ± 1 | 396 | 1403 ± 1 | 391 | 1412 ± 1 | 367 | 1420 ± 1 | 304 | 1418 ± 1 | 188 | 1592 ± 37 | 186 | 1561 ± 37 |
| 74 | closeli-001 | 420342 | 9851 | 173 | 773 | 403 | 4096 ± 0 | 276 | 839 ± 1 | 237 | 843 ± 1 | 209 | 841 ± 1 | 188 | 845 ± 1 | 163 | 865 ± 1 | 320 | 5404 ± 17 | 319 | 5400 ± 25 |
| 75 | cloudmatrix-000 | 309939 | 542141 | 160 | 727 | 305 | 2048 ± 0 | 240 | 754 ± 10 | 201 | 750 ± 2 | 184 | 754 ± 4 | 166 | 764 ± 1 | 142 | 793 ± 2 | 420 | 49192 ± 206 | 420 | 49275 ± 176 |
| 76 | cloudmatrix-001 | 10390 | 542121 | 41 | 249 | 162 | 2048 ± 0 | 18 | 114 ± 1 | 13 | 117 ± 0 | 11 | 118 ± 0 | 10 | 123 ± 1 | 12 | 169 ± 1 | 421 | 50263 ± 212 | 421 | 50243 ± 237 |
| 77 | cloudwalk-hr-003 | 383739 | 144263 | 227 | 984 | 359 | 2057 ± 0 | 178 | 606 ± 0 | 144 | 588 ± 0 | 125 | 594 ± 0 | 109 | 612 ± 1 | - | 341 | 6982 ± 80 | 340 | 6972 ± 84 | |
| 78 | cloudwalk-hr-004 | 502916 | 520169 | 296 | 1394 | 315 | 2049 ± 0 | 289 | 873 ± 1 | 248 | 877 ± 1 | 219 | 876 ± 1 | 197 | 879 ± 1 | 171 | 902 ± 3 | 363 | 11652 ± 127 | 363 | 11608 ± 123 |
| 79 | cloudwalk-mt-004 | 1384602 | 512628 | 426 | 5426 | 190 | 2048 ± 0 | 307 | 923 ± 2 | 264 | 919 ± 1 | 234 | 918 ± 0 | 212 | 919 ± 0 | 176 | 927 ± 1 | 364 | 11744 ± 170 | 364 | 11631 ± 126 |
| 80 | cloudwalk-mt-005 | 846026 | 573253 | 397 | 2928 | 248 | 2048 ± 0 | 372 | 1179 ± 3 | 342 | 1200 ± 3 | 332 | 1209 ± 3 | 307 | 1226 ± 5 | 254 | 1229 ± 3 | 371 | 12525 ± 225 | 370 | 12394 ± 152 |
| 81 | cogent-006 | 1078167 | 58108 | 312 | 1547 | 85 | 1602 ± 0 | 246 | 768 ± 0 | 213 | 789 ± 1 | 205 | 831 ± 2 | 215 | 930 ± 1 | 189 | 971 ± 1 | 208 | 1802 ± 17 | 208 | 1797 ± 23 |
| 82 | cogent-007 | 621565 | 72316 | 346 | 1884 | 59 | 550 ± 0 | 411 | 1329 ± 2 | 377 | 1333 ± 5 | 364 | 1337 ± 4 | 340 | 1353 ± 5 | 295 | 1390 ± 4 | 31 | 355 ± 8 | 34 | 367 ± 14 |
| 83 | cognitec-003 | 471458 | 62502 | 187 | 817 | 326 | 2052 ± 0 | 81 | 366 ± 9 | 73 | 403 ± 9 | 55 | 408 ± 9 | 57 | 509 ± 13 | 283 | 3417 ± 51 | 285 | 3433 ± 53 | | |
| 84 | cognitec-004 | 705645 | 62678 | 119 | 585 | 316 | 2052 ± 0 | 114 | 463 ± 9 | 106 | 497 ± 9 | 91 | 504 ± 10 | 82 | 521 ± 10 | 92 | 631 ± 12 | 271 | 3028 ± 197 | 272 | 3059 ± 238 |
| 85 | cor-001 | 1194948 | 11240 | 269 | 1249 | 362 | 2060 ± 0 | 228 | 699 ± 3 | 239 | 863 ± 76 | 212 | 865 ± 80 | 194 | 872 ± 89 | 185 | 952 ± 39 | 440 | 270145 ± 2259 | 440 | 282686 ± 11788 |
| 86 | coretech-000 | 186423 | 43964 | 64 | 393 | 33 | 512 ± 0 | 177 | 602 ± 15 | 170 | 659 ± 12 | 310 | 1139 ± 24 | 280 | 1149 ± 25 | 237 | 1165 ± 23 | 26 | 333 ± 14 | 27 | 321 ± 13 |
| 87 | corsight-002 | 1474921 | 32093 | 359 | 2061 | 364 | 2080 ± 0 | 400 | 1290 ± 1 | 364 | 1287 ± 1 | 350 | 1290 ± 1 | 327 | 1307 ± 2 | 294 | 1388 ± 4 | 398 | 24953 ± 637 | 397 | 24263 ± 578 |
| 88 | corsight-003 | 1413063 | 32198 | 323 | 1637 | 365 | 2080 ± 0 | 379 | 1202 ± 2 | 341 | 1190 ± 5 | 330 | 1199 ± 3 | 309 | 1236 ± 3 | 280 | 1349 ± 7 | 402 | 28754 ± 434 | 403 | 28279 ± 446 |

Notes

1 The configuration size does not capture static data included in libraries.

2 The library size is the combined total of all files provided in the submission lib folder. These libraries e.g. OpenCV may or may not be installed on any end user's platform natively and would not need to be installed with the algorithm. Some developers put neural network models in their libraries.

3 The memory usage is the peak resident set size reported by the ps system call during template generation.

4 The median template creation times are measured on Intel® Xeon® CPU E5-2630 v4 @ 2.20GHz processors.

5 The comparison durations, in nanoseconds, are estimated using std::chrono::high_resolution_clock which on the machine in (2) counts 1ns clock ticks. Precision is somewhat worse than that however. The ± value is the median absolute deviation times 1.48 for Normal consistency.

| | ALGORITHM | CONFIG | LIBRARY | TEMPLATE | | | | | | | | COMPARISON ⁴ | | | | | | | | | | |
|-----|-----------------------|--------|---------|-------------------|-------------------|-------------------|-----|----------|---------|-----------|-----------|-----------------------------------|---------|-----------|---------|------------|-------------|-------------|-------------|-------------|-------------|-------------|
| | | | | NAME | | DATA | | MEMORY | | SIZE | | GENERATION TIME (ms) ⁴ | | | | | | | | | | |
| | | | | (KB) ¹ | (KB) ² | (MB) ³ | (B) | MUGSHOT | 480x720 | 960x1440 | 1600x2400 | 3000x4500 | GENUINE | IMPOSTOR | | | | | | | | |
| 89 | csc-002 | | 0 | 519768 | 291 | 1376 | 56 | 544 ± 0 | 121 | 473 ± 0 | 105 | 494 ± 0 | 80 | 481 ± 1 | 73 | 490 ± 1 | 61 | 514 ± 5 | 34 | 367 ± 11 | 35 | 371 ± 10 |
| 90 | csc-003 | | 0 | 400435 | 321 | 1609 | 55 | 544 ± 0 | 133 | 499 ± 0 | 109 | 500 ± 1 | 89 | 502 ± 0 | 79 | 508 ± 1 | 67 | 535 ± 4 | 37 | 393 ± 8 | 38 | 397 ± 7 |
| 91 | ctcbcbank-000 | | 257208 | 599238 | 117 | 570 | 239 | 2048 ± 0 | 159 | 568 ± 43 | 150 | 606 ± 38 | 164 | 690 ± 53 | 148 | 711 ± 50 | 153 | 831 ± 51 | 288 | 3551 ± 87 | 309 | 4805 ± 209 |
| 92 | ctcbcbank-001 | | 275511 | 599238 | 125 | 603 | 249 | 2048 ± 0 | 201 | 652 ± 35 | 211 | 781 ± 30 | 218 | 875 ± 43 | 205 | 898 ± 51 | 201 | 1030 ± 47 | 296 | 3926 ± 45 | 295 | 3924 ± 56 |
| 93 | cubox-001 | | 369627 | 75427 | 134 | 649 | 168 | 2048 ± 0 | 299 | 907 ± 1 | 260 | 902 ± 1 | 227 | 903 ± 0 | 210 | 917 ± 0 | 177 | 931 ± 0 | 169 | 1379 ± 37 | 176 | 1417 ± 38 |
| 94 | cubox-002 | | 542254 | 90975 | 354 | 1964 | 212 | 2048 ± 0 | 306 | 921 ± 1 | 265 | 921 ± 1 | 238 | 922 ± 1 | 217 | 933 ± 1 | 195 | 1003 ± 1 | 226 | 2008 ± 72 | 226 | 1969 ± 57 |
| 95 | cudocommunication-001 | | 385258 | 341277 | 242 | 1077 | 271 | 2048 ± 0 | 309 | 925 ± 1 | 266 | 923 ± 1 | 243 | 928 ± 1 | 216 | 932 ± 0 | 186 | 964 ± 1 | 248 | 2534 ± 20 | 250 | 2537 ± 20 |
| 96 | cuhkee-001 | | 787853 | 74917 | 375 | 2515 | 327 | 2052 ± 0 | 325 | 977 ± 31 | - | - | - | - | - | - | - | - | 255 | 2719 ± 60 | 259 | 2783 ± 56 |
| 97 | cybercore-001 | | 166096 | 7791 | 379 | 2574 | 246 | 2048 ± 0 | 130 | 487 ± 0 | 101 | 486 ± 0 | 85 | 488 ± 0 | 72 | 487 ± 0 | 56 | 502 ± 0 | 424 | 52119 ± 111 | 424 | 52127 ± 111 |
| 98 | cybercore-002 | | 166096 | 7374 | 378 | 2564 | 234 | 2048 ± 0 | 131 | 489 ± 1 | 105 | 500 ± 4 | 85 | 500 ± 1 | 77 | 499 ± 2 | 65 | 528 ± 1 | 369 | 12389 ± 123 | 369 | 12352 ± 112 |
| 99 | cyberextruder-003 | | 253300 | 12354 | 74 | 437 | 20 | 512 ± 0 | 88 | 390 ± 1 | 68 | 388 ± 1 | 53 | 393 ± 1 | 48 | 399 ± 1 | 43 | 435 ± 1 | 10 | 198 ± 4 | 11 | 189 ± 8 |
| 100 | cyberextruder-004 | | 169301 | 12354 | 58 | 349 | 2 | 128 ± 0 | 36 | 206 ± 0 | 27 | 208 ± 0 | 23 | 209 ± 0 | 23 | 229 ± 0 | 18 | 249 ± 1 | 5 | 145 ± 14 | 6 | 155 ± 14 |
| 101 | cyberlink-008 | | 380047 | 102470 | 336 | 1748 | 436 | 6212 ± 0 | 233 | 729 ± 1 | 195 | 725 ± 0 | 178 | 727 ± 0 | 156 | 732 ± 0 | 137 | 760 ± 0 | 17 | 263 ± 17 | 19 | 255 ± 13 |
| 102 | cyberlink-009 | | 588443 | 102201 | 327 | 1704 | 422 | 4164 ± 0 | 422 | 1384 ± 2 | 394 | 1395 ± 2 | 386 | 1398 ± 2 | 360 | 1401 ± 2 | 312 | 1456 ± 2 | 22 | 299 ± 17 | 29 | 304 ± 16 |
| 103 | dahua-006 | | 831641 | 119261 | 422 | 5068 | 198 | 2048 ± 0 | 428 | 1398 ± 2 | 395 | 1397 ± 1 | 388 | 1404 ± 1 | 361 | 1402 ± 1 | 299 | 1402 ± 1 | 16 | 249 ± 13 | 18 | 250 ± 11 |
| 104 | dahua-007 | | 1578737 | 119418 | 435 | 7237 | 394 | 4096 ± 0 | 425 | 1393 ± 2 | 384 | 1373 ± 1 | 377 | 1378 ± 1 | 350 | 1378 ± 1 | 289 | 1379 ± 2 | 35 | 367 ± 102 | 39 | 434 ± 108 |
| 105 | daon-000 | | 280726 | 2307 | 358 | 2013 | 363 | 2065 ± 0 | 154 | 562 ± 3 | 140 | 581 ± 5 | 190 | 791 ± 9 | 185 | 838 ± 15 | 207 | 1055 ± 32 | 381 | 16052 ± 88 | 381 | 16041 ± 85 |
| 106 | decatur-000 | | 350495 | 171271 | 209 | 907 | 416 | 4100 ± 0 | 339 | 1024 ± 2 | - | - | - | - | - | - | - | 362 | 11439 ± 80 | 362 | 11418 ± 112 | |
| 107 | decatur-001 | | 342866 | 253734 | 309 | 1507 | 318 | 2052 ± 0 | 352 | 1103 ± 2 | 308 | 1064 ± 2 | 294 | 1063 ± 2 | 258 | 1067 ± 2 | 217 | 1084 ± 2 | 68 | 610 ± 19 | 68 | 602 ± 8 |
| 108 | deepglint-003 | | 838065 | 262081 | 370 | 2374 | 433 | 6144 ± 0 | 368 | 1159 ± 1 | 327 | 1145 ± 1 | 314 | 1148 ± 1 | 279 | 1148 ± 1 | 236 | 1163 ± 1 | 383 | 17227 ± 41 | 383 | 17210 ± 51 |
| 109 | deepglint-004 | | 1073382 | 261571 | 399 | 3084 | 262 | 2048 ± 0 | 438 | 1470 ± 1 | 406 | 1474 ± 1 | 400 | 1485 ± 1 | 375 | 1474 ± 1 | 320 | 1492 ± 2 | 331 | 5961 ± 34 | 332 | 5955 ± 29 |
| 110 | deepsea-001 | | 147497 | 336250 | 60 | 358 | 71 | 1024 ± 0 | 192 | 630 ± 7 | 202 | 752 ± 37 | 181 | 746 ± 30 | 153 | 727 ± 32 | 149 | 820 ± 32 | 174 | 1401 ± 37 | 180 | 1467 ± 50 |
| 111 | deeepsense-000 | | 357113 | 936618 | 436 | 7618 | 263 | 2048 ± 0 | 209 | 664 ± 3 | 168 | 645 ± 1 | 151 | 660 ± 2 | 136 | 687 ± 2 | 147 | 808 ± 3 | 43 | 480 ± 22 | 45 | 459 ± 34 |
| 112 | deeepsense-001 | | 73173 | 1288355 | 423 | 5314 | 28 | 512 ± 0 | 362 | 1142 ± 2 | 332 | 1164 ± 3 | 325 | 1183 ± 3 | 300 | 1201 ± 3 | 275 | 1323 ± 2 | 243 | 2356 ± 35 | 243 | 2354 ± 42 |
| 113 | dermalog-009 | | 0 | 319363 | 137 | 664 | 41 | 512 ± 0 | 73 | 349 ± 0 | 55 | 351 ± 0 | 43 | 352 ± 0 | 39 | 357 ± 0 | 36 | 389 ± 0 | 45 | 487 ± 34 | 37 | 385 ± 29 |
| 114 | dermalog-010 | | 0 | 525908 | 232 | 1023 | 42 | 512 ± 0 | 195 | 635 ± 0 | 166 | 640 ± 1 | 145 | 639 ± 4 | 122 | 647 ± 3 | 112 | 691 ± 5 | 39 | 444 ± 13 | 31 | 341 ± 26 |
| 115 | dicio-001 | | 61751 | 119517 | 17 | 77 | 49 | 520 ± 0 | 146 | 538 ± 0 | 133 | 563 ± 10 | 23 | 915 ± 3 | 390 | 1800 ± 7 | 388 | 5286 ± 30 | 259 | 2818 ± 20 | 260 | 2807 ± 31 |
| 116 | didiglobalface-001 | | 259849 | 70680 | 102 | 527 | 307 | 2048 ± 0 | 179 | 612 ± 1 | 163 | 633 ± 3 | 142 | 634 ± 3 | 124 | 650 ± 15 | 107 | 666 ± 4 | 127 | 973 ± 20 | 127 | 988 ± 20 |
| 117 | digidata-000 | | 133370 | 30249 | 44 | 257 | 214 | 2048 ± 0 | 80 | 361 ± 0 | 60 | 360 ± 0 | 45 | 361 ± 0 | 40 | 363 ± 0 | 34 | 380 ± 0 | 229 | 2084 ± 37 | 228 | 2039 ± 42 |
| 118 | digidata-001 | | 254564 | 33036 | 61 | 367 | 178 | 2048 ± 0 | 153 | 559 ± 1 | 131 | 561 ± 1 | 112 | 562 ± 1 | 93 | 564 ± 1 | 86 | 602 ± 1 | 359 | 10308 ± 102 | 359 | 10301 ± 121 |
| 119 | digitalbarriers-002 | | 83002 | 598577 | 349 | 1930 | 343 | 2056 ± 0 | 37 | 209 ± 11 | 30 | 250 ± 19 | 56 | 411 ± 37 | 173 | 808 ± 72 | 354 | 2236 ± 123 | 372 | 13409 ± 228 | 372 | 13267 ± 206 |
| 120 | dps-000 | | 0 | 2211812 | 236 | 1058 | 387 | 4096 ± 0 | 282 | 868 ± 2 | 257 | 893 ± 6 | 396 | 1445 ± 9 | 406 | 2910 ± 38 | 400 | 9345 ± 17 | 182 | 1473 ± 37 | 182 | 1479 ± 37 |
| 121 | dsk-000 | | 11967 | 782905 | 43 | 252 | 25 | 512 ± 0 | 58 | 304 ± 47 | 49 | 317 ± 33 | 271 | 1001 ± 96 | 405 | 2660 ± 170 | 404 | 10451 ± 832 | 344 | 7152 ± 115 | 342 | 7134 ± 111 |
| 122 | einetworks-000 | | 372608 | 219883 | 205 | 880 | 351 | 2056 ± 0 | 199 | 645 ± 3 | - | - | - | - | - | - | - | 313 | 4876 ± 66 | 314 | 5156 ± 77 | |
| 123 | ekin-002 | | 51434 | 278 | 24 | 139 | 373 | 3072 ± 0 | 376 | 1186 ± 13 | 339 | 1180 ± 12 | 323 | 1181 ± 11 | 298 | 1191 ± 11 | 249 | 1207 ± 8 | 303 | 4294 ± 80 | 323 | 5569 ± 112 |
| 124 | enface-000 | | 369598 | 153781 | 136 | 662 | 75 | 1024 ± 0 | 152 | 555 ± 4 | 130 | 558 ± 4 | 155 | 669 ± 6 | 234 | 987 ± 15 | 358 | 2349 ± 54 | 342 | 7059 ± 62 | 341 | 6980 ± 65 |
| 125 | enface-001 | | 370710 | 173609 | 140 | 670 | 73 | 1024 ± 0 | 150 | 550 ± 4 | 129 | 555 ± 3 | 154 | 668 ± 7 | 230 | 981 ± 15 | 363 | 2416 ± 59 | 337 | 6734 ± 68 | 337 | 6766 ± 69 |
| 126 | eocortex-000 | | 255937 | 59432 | 40 | 224 | 219 | 2048 ± 0 | 60 | 305 ± 22 | 56 | 341 ± 25 | 69 | 440 ± 47 | 64 | 464 ± 45 | 58 | 513 ± 44 | 123 | 923 ± 11 | 124 | 918 ± 11 |
| 127 | ercacat-001 | | 811623 | 58012 | 392 | 2816 | 328 | 2052 ± 0 | 348 | 1052 ± 3 | - | - | - | - | - | - | - | 250 | 2551 ± 62 | 247 | 2501 ± 81 | |
| 128 | euronovate-001 | | 0 | 1774966 | 283 | 1308 | 88 | 1177 ± 0 | 344 | 1034 ± 2 | 333 | 1165 ± 3 | 318 | 1160 ± 3 | 289 | 1177 ± 3 | 241 | 1172 ± 2 | 436 | 81294 ± 591 | 436 | 81631 ± 931 |
| 129 | expasoft-001 | | 39057 | 983064 | 25 | 142 | 210 | 2048 ± 0 | 80 | 70 ± 0 | 674 ± 0 | 677 ± 0 | 573 ± 0 | 474 ± 0 | 191 | 1660 ± 35 | 341 | 1660 ± 35 | 192 | 1676 ± 48 | 192 | 1676 ± 48 |
| 130 | expasoft-002 | | 38760 | 59825 | 31 | 168 | 174 | 2048 ± 0 | 53 | 34 ± 0 | 334 ± 0 | 334 ± 0 | 234 ± 0 | 234 ± 0 | 351 | 8870 ± 78 | 351 | 8838 ± 77 | 380 | 15262 ± 139 | 380 | 15277 ± 212 |
| 131 | f8-001 | | 272977 | 19668 | 275 | 1276 | 182 | 2048 ± 0 | 270 | 822 ± 39 | - | - | - | - | - | - | - | 380 | 15262 ± 139 | 380 | 15277 ± 212 | |
| 132 | f8-002 | | 28278 | 215616 | 13 | 83 | 197 | 2048 ± 0 | 639 ± 0 | 441 ± 0 | 575 ± 0 | 18 | 197 ± 1 | 117 | 702 ± 1 | 377 | 14765 ± 131 | 377 | 14790 ± 133 | 377 | 14790 ± 133 | |

Notes

- 1 The configuration size does not capture static data included in libraries.
- 2 The library size is the combined total of all files provided in the submission lib folder. These libraries e.g. OpenCV may or may not be installed on any end user's platform natively and would not need to be installed with the algorithm. Some developers put neural network models in their libraries.
- 3 The memory usage is the peak resident set size reported by the ps system call during template generation.
- 4 The median template creation times are measured on Intel® Xeon® CPU E5-2630 v4 @ 2.20GHz processors.
- 5 The comparison durations, in nanoseconds, are estimated using std::chrono::high_resolution_clock which on the machine in (2) counts 1ns clock ticks. Precision is somewhat worse than that however. The ± value is the median absolute deviation times 1.48 for Normal consistency.

Table 10: Summary of algorithms and properties included in this report. The red superscripts give ranking for the quantity in that column.

| | ALGORITHM | CONFIG | LIBRARY | TEMPLATE | | | | | | | | COMPARISON ⁴ | | | | | | | | | |
|-----|-----------------------|---------|---------|----------|-------|------|----------|------|-----------------------------------|-------------------|-------------------|-------------------------|------------------------|---------|-----------|-----------|------------|-------------|-------------|-------------|-------------|
| | | | | NAME | DATA | DATA | MEMORY | SIZE | GENERATION TIME (ms) ⁴ | | | | TIME (ns) ⁵ | | | | | | | | |
| | | | | | | | | | (KB) ¹ | (KB) ² | (MB) ³ | (B) | MUGSHOT | 480x720 | 960x1440 | 1600x2400 | 3000x4500 | GENUINE | IMPOSTOR | | |
| 133 | faceonline-001 | 0 | 71529 | 53 | 302 | 341 | 2056 ± 0 | 28 | 179 ± 0 | 19 | 179 ± 0 | 21 | 190 ± 0 | 19 | 217 ± 0 | 25 | 343 ± 1 | 140 | 1064 ± 37 | 139 | 1033 ± 35 |
| 134 | faceonline-002 | 155220 | 141019 | 230 | 995 | 139 | 2048 ± 0 | 252 | 783 ± 1 | 217 | 797 ± 2 | 191 | 794 ± 2 | 174 | 809 ± 3 | 170 | 901 ± 2 | 373 | 13798 ± 197 | 373 | 13743 ± 127 |
| 135 | facephi-000 | 148904 | 5219 | 438 | 11481 | 176 | 2048 ± 0 | 285 | 871 ± 2 | 250 | 881 ± 3 | 221 | 880 ± 4 | 202 | 888 ± 4 | 183 | 949 ± 12 | 301 | 4067 ± 53 | 300 | 4047 ± 53 |
| 136 | facesoft-000 | 370120 | 10612 | 177 | 796 | 301 | 2048 ± 0 | 213 | 675 ± 18 | 174 | 669 ± 3 | 161 | 686 ± 3 | 131 | 675 ± 5 | 110 | 687 ± 2 | 240 | 2239 ± 28 | 242 | 2277 ± 96 |
| 137 | facetag-000 | 1232331 | 4022 | 223 | 965 | 62 | 684 ± 0 | 75 | 355 ± 17 | 63 | 369 ± 8 | 266 | 989 ± 33 | 402 | 2408 ± 91 | 399 | 7930 ± 316 | 433 | 72003 ± 625 | 434 | 71912 ± 612 |
| 138 | facetag-002 | 819806 | 4021 | 139 | 726 | 261 | 2048 ± 0 | 147 | 544 ± 1 | 124 | 544 ± 0 | 104 | 542 ± 0 | 90 | 545 ± 0 | 72 | 554 ± 0 | 198 | 1730 ± 25 | 198 | 1733 ± 25 |
| 139 | facex-001 | 305074 | 930372 | 398 | 2931 | 280 | 2048 ± 0 | 100 | 422 ± 4 | 83 | 434 ± 4 | 98 | 520 ± 7 | 158 | 737 ± 13 | 339 | 1670 ± 27 | 214 | 1871 ± 23 | 213 | 1846 ± 29 |
| 140 | facex-002 | 305074 | 928334 | 400 | 3095 | 272 | 2048 ± 0 | 101 | 426 ± 5 | 81 | 429 ± 4 | 96 | 516 ± 8 | 155 | 730 ± 12 | 344 | 1738 ± 36 | 77 | 631 ± 25 | 74 | 614 ± 19 |
| 141 | farfaces-001 | 346494 | 44581 | 45 | 261 | 39 | 512 ± 0 | 371 | 1179 ± 1 | 338 | 1180 ± 1 | 322 | 1180 ± 0 | 295 | 1185 ± 1 | 250 | 1209 ± 2 | 119 | 855 ± 25 | 118 | 860 ± 31 |
| 142 | fiberhome-nanjing-003 | 352895 | 1482309 | 195 | 845 | 291 | 2048 ± 0 | 358 | 1136 ± 7 | 322 | 1134 ± 4 | 308 | 1132 ± 3 | 277 | 1139 ± 3 | 231 | 1154 ± 5 | 146 | 1097 ± 38 | 148 | 1083 ± 42 |
| 143 | fiberhome-nanjing-004 | 443779 | 1482313 | 234 | 1048 | 381 | 4096 ± 0 | 409 | 1321 ± 5 | 368 | 1304 ± 3 | 357 | 1307 ± 2 | 328 | 1308 ± 3 | 277 | 1326 ± 5 | 164 | 1276 ± 40 | 164 | 1265 ± 38 |
| 144 | fincore-000 | 256615 | 19409 | 107 | 535 | 265 | 2048 ± 0 | 137 | 508 ± 3 | 113 | 505 ± 0 | 92 | 508 ± 1 | 81 | 513 ± 2 | 66 | 535 ± 1 | 202 | 1765 ± 31 | 202 | 1763 ± 22 |
| 145 | frpkauai-001 | 507771 | 24807 | 241 | 1076 | 199 | 2048 ± 0 | 222 | 689 ± 1 | 185 | 691 ± 0 | 169 | 697 ± 2 | 151 | 714 ± 6 | 141 | 775 ± 31 | 105 | 752 ± 29 | 108 | 764 ± 23 |
| 146 | fujitsulab-002 | 0 | 1088887 | 322 | 1613 | 419 | 4104 ± 0 | 386 | 1237 ± 2 | 348 | 1222 ± 2 | 335 | 1236 ± 1 | 311 | 1251 ± 2 | 278 | 1327 ± 2 | 260 | 2836 ± 25 | 261 | 2809 ± 44 |
| 147 | fujitsulab-003 | 662263 | 318209 | 434 | 6907 | 421 | 4104 ± 0 | 317 | 951 ± 20 | 272 | 941 ± 19 | 250 | 952 ± 19 | 228 | 971 ± 20 | 204 | 1045 ± 21 | 261 | 2855 ± 16 | 263 | 2849 ± 19 |
| 148 | g42-intelbrain-001 | 1031335 | 235521 | 443 | 25628 | 9 | 269 ± 0 | 324 | 976 ± 6 | 281 | 975 ± 1 | 270 | 997 ± 2 | 260 | 1068 ± 3 | 286 | 1362 ± 8 | 329 | 5878 ± 96 | 331 | 5865 ± 71 |
| 149 | geo-002 | 369903 | 98667 | 231 | 1018 | 304 | 2048 ± 0 | 255 | 791 ± 1 | 215 | 793 ± 0 | 192 | 794 ± 0 | 170 | 795 ± 1 | 144 | 803 ± 1 | 282 | 3407 ± 45 | 284 | 3422 ± 65 |
| 150 | geo-004 | 168980 | 107714 | 277 | 1280 | 130 | 2048 ± 0 | 394 | 1268 ± 1 | 362 | 1279 ± 1 | 346 | 1274 ± 0 | 315 | 1259 ± 1 | 269 | 1296 ± 1 | 136 | 1023 ± 20 | 138 | 1028 ± 22 |
| 151 | glory-004 | 0 | 999639 | 365 | 2181 | 425 | 4182 ± 0 | 221 | 688 ± 0 | 206 | 759 ± 1 | 245 | 941 ± 1 | 396 | 2134 ± 4 | 401 | 9360 ± 47 | 315 | 4982 ± 66 | 313 | 4990 ± 63 |
| 152 | glory-005 | 0 | 999999 | 371 | 2428 | 426 | 4182 ± 0 | 230 | 703 ± 1 | 214 | 789 ± 0 | 256 | 972 ± 1 | 398 | 2200 ± 25 | 402 | 9679 ± 22 | 317 | 5224 ± 93 | 316 | 5176 ± 81 |
| 153 | gorilla-007 | 441058 | 708166 | 325 | 1691 | 437 | 6288 ± 0 | 174 | 592 ± 1 | 146 | 592 ± 1 | 130 | 603 ± 1 | 116 | 625 ± 2 | 125 | 722 ± 9 | 292 | 3686 ± 37 | 293 | 3709 ± 36 |
| 154 | gorilla-008 | 450175 | 707000 | 339 | 1789 | 440 | 8338 ± 0 | 176 | 595 ± 1 | 145 | 590 ± 0 | 128 | 600 ± 1 | 114 | 621 ± 2 | 123 | 720 ± 9 | 307 | 4530 ± 44 | 305 | 4524 ± 38 |
| 155 | graymatics-001 | 13095 | 70406 | 22 | 127 | 409 | 4096 ± 0 | 33 | 191 ± 1 | 25 | 203 ± 1 | 124 | 592 ± 5 | 386 | 1698 ± 9 | 397 | 7150 ± 34 | 414 | 39874 ± 309 | 414 | 39762 ± 295 |
| 156 | griaule-000 | 0 | 598214 | 233 | 1054 | 317 | 2052 ± 0 | 99 | 416 ± 6 | 79 | 425 ± 7 | 188 | 770 ± 14 | 387 | 1749 ± 43 | 395 | 6406 ± 189 | 299 | 3987 ± 42 | 296 | 3938 ± 38 |
| 157 | griaule-001 | 0 | 412061 | 273 | 1269 | 331 | 2052 ± 0 | 369 | 1164 ± 1 | 315 | 1096 ± 5 | 299 | 1099 ± 4 | 274 | 1136 ± 2 | 322 | 1509 ± 2 | 298 | 3948 ± 23 | 298 | 3957 ± 32 |
| 158 | hertasecurity-000 | 0 | 780014 | 99 | 516 | 425 | 256 ± 0 | 14 | 99 ± 0 | 1098 | ± 0 | 10 | 100 ± 0 | 9 | 107 ± 0 | 9 | 139 ± 0 | 95 | 710 ± 31 | 89 | 667 ± 28 |
| 159 | hertasecurity-001 | 0 | 944427 | 262 | 1183 | 40 | 512 ± 0 | 73 | 346 ± 0 | 57 | 345 ± 0 | 42 | 349 ± 0 | 38 | 354 ± 0 | 35 | 388 ± 0 | 203 | 1770 ± 45 | 197 | 1726 ± 48 |
| 160 | hik-001 | 667866 | 9290 | 432 | 6597 | 92 | 1408 ± 0 | 200 | 651 ± 0 | 173 | 667 ± 8 | 158 | 677 ± 16 | 135 | 686 ± 13 | 129 | 737 ± 12 | 46 | 488 ± 19 | 46 | 477 ± 22 |
| 161 | hisign-001 | 732412 | 167488 | 313 | 1553 | 366 | 2080 ± 0 | 403 | 1306 ± 1 | 372 | 1320 ± 1 | 358 | 1315 ± 1 | 331 | 1312 ± 1 | 276 | 1325 ± 1 | 13 | 201 ± 10 | 9 | 185 ± 13 |
| 162 | hyperverge-002 | 2951900 | 198832 | 355 | 1975 | 74 | 1024 ± 0 | 311 | 938 ± 1 | 271 | 939 ± 1 | 247 | 941 ± 1 | 222 | 945 ± 1 | 190 | 975 ± 1 | 333 | 6023 ± 37 | 333 | 5966 ± 40 |
| 163 | hyperverge-003 | 1167779 | 282156 | 389 | 2748 | 68 | 1024 ± 0 | 441 | 1477 ± 2 | 407 | 1503 ± 3 | 403 | 1520 ± 3 | 379 | 1525 ± 4 | 331 | 1565 ± 3 | 54 | 566 ± 11 | 55 | 561 ± 8 |
| 164 | hzailu-001 | 0 | 372018 | 115 | 563 | 356 | 2056 ± 0 | 356 | 1126 ± 1 | 321 | 1128 ± 1 | 306 | 1130 ± 1 | 270 | 1132 ± 1 | 234 | 1159 ± 1 | 121 | 894 ± 19 | 122 | 899 ± 22 |
| 165 | hzailu-002 | 1515880 | 74047 | 421 | 4715 | 353 | 2056 ± 0 | 367 | 1150 ± 5 | 320 | 1127 ± 6 | 304 | 1129 ± 7 | 276 | 1137 ± 7 | 239 | 1172 ± 3 | 144 | 1079 ± 53 | 144 | 1070 ± 31 |
| 166 | icm-002 | 621586 | 903 | 85 | 484 | 109 | 2048 ± 0 | 343 | 1031 ± 7 | - | - | - | - | - | - | - | 396 | 24052 ± 118 | 395 | 24049 ± 124 | |
| 167 | icm-003 | 1513988 | 940 | 92 | 500 | 163 | 2048 ± 0 | 216 | 681 ± 6 | 176 | 672 ± 4 | 175 | 714 ± 11 | 183 | 837 ± 41 | 290 | 1381 ± 131 | 397 | 24351 ± 161 | 396 | 24227 ± 146 |
| 168 | ichttc-000 | 172459 | 1471004 | 340 | 1805 | 278 | 2048 ± 0 | 72 | 338 ± 11 | 55 | 338 ± 9 | 66 | 437 ± 16 | 144 | 705 ± 24 | 343 | 1719 ± 44 | 319 | 5284 ± 63 | 318 | 5290 ± 54 |
| 169 | id3-006 | 210116 | 7706 | 226 | 982 | 51 | 520 ± 0 | 218 | 683 ± 0 | 310 | 1088 ± 1 | 328 | 1192 ± 1 | 303 | 1209 ± 1 | 260 | 1270 ± 1 | 322 | 5547 ± 34 | 322 | 5563 ± 34 |
| 170 | id3-008 | 242416 | 8151 | 239 | 1068 | 8 | 264 ± 0 | 266 | 819 ± 0 | 343 | 1209 ± 2 | 355 | 1297 ± 2 | 334 | 1329 ± 1 | 310 | 1433 ± 1 | 325 | 5658 ± 44 | 326 | 5624 ± 40 |
| 171 | idemia-008 | 374017 | 69922 | 263 | 1194 | 14 | 348 ± 0 | 112 | 457 ± 1 | 92 | 461 ± 0 | 76 | 466 ± 1 | 69 | 476 ± 2 | 59 | 513 ± 10 | 274 | 3080 ± 41 | 270 | 3046 ± 56 |
| 172 | idemia-009 | 1066728 | 70572 | 384 | 2702 | 61 | 636 ± 0 | 380 | 1207 ± 1 | 346 | 1218 ± 1 | 334 | 1222 ± 2 | 304 | 1222 ± 3 | 263 | 1280 ± 10 | 326 | 5664 ± 84 | 325 | 5597 ± 90 |
| 173 | iit-002 | 259579 | 52070 | 162 | 731 | 166 | 2048 ± 0 | 138 | 514 ± 1 | 116 | 531 ± 2 | 109 | 547 ± 1 | 98 | 583 ± 1 | 127 | 733 ± 2 | 137 | 1023 ± 7 | 134 | 1011 ± 66 |
| 174 | iit-003 | 261288 | 53791 | 188 | 817 | 237 | 2048 ± 0 | 126 | 482 ± 0 | 103 | 493 ± 0 | 93 | 509 ± 0 | 88 | 541 ± 0 | 105 | 661 ± 0 | 25 | 324 ± 17 | 28 | 326 ± 8 |
| 175 | imds-software-001 | 373399 | 352623 | 172 | 772 | 284 | 2048 ± 0 | 116 | 465 ± 1 | 277 | 958 ± 6 | 307 | 1131 ± 5 | 272 | 1134 ± 2 | 224 | 1119 ± 10 | 366 | 11885 ± 120 | 365 | 11779 ± 174 |
| 176 | imperial-000 | 370120 | 10623 | 178 | 796 | 308 | 2048 ± 0 | 212 | 669 ± 1 | 178 | 675 ± 3 | 160 | 683 ± 17 | 132 | 676 ± 2 | 111 | 689 ± 2 | 231 | 2130 ± 32 | 229 | 2052 ± 100 |

Notes
 1 The configuration size does not capture static data included in libraries.
 2 The library size is the combined total of all files provided in the submission lib folder. These libraries e.g. OpenCV may or may not be installed on any end user's platform natively and would not need to be installed with the algorithm. Some developers put neural network models in their libraries.
 3 The memory usage is the peak resident set size reported by the ps system call during template generation.
 4 The median template creation times are measured on Intel®Xeon®CPU E5-2630 v4 @ 2.20GHz processors.
 5 The comparison durations, in nanoseconds, are estimated using std::chrono::high_resolution_clock which on the machine in (2) counts 1ns clock ticks. Precision is somewhat worse than that however. The ± value is the median absolute deviation times 1.48 for Normal consistency.

| ALGORITHM | CONFIG | LIBRARY | TEMPLATE | | | | | | | | COMPARISON ⁴ | | |
|-----------|-----------------------------|---------|----------|--------|----------------------|--------------------------|-------------------------|-----------------------------------|--------------------------|--------------------------|---------------------------|-------------------------------|-------------------------------|
| | | | NAME | DATA | DATA | MEMORY | SIZE | GENERATION TIME (ms) ⁴ | | | | TIME (ns) ⁵ | |
| | | | | | | | | (KB) ¹ | (KB) ² | (MB) ³ | (B) | MUGSHOT | 480x720 |
| 177 | imperial-002 | | 472327 | 16134 | ³⁴¹ 1826 | ²⁶⁸ 2048 ± 0 | ¹⁶⁰ 569 ± 1 | ¹³⁹ 581 ± 15 | ¹¹⁷ 575 ± 5 | ⁹⁶ 576 ± 2 | ⁸⁰ 588 ± 3 | ²⁴² 2278 ± 90 | ²³³ 2131 ± 44 |
| 178 | incode-010 | | 627808 | 21014 | ³⁸¹ 2628 | ¹⁸⁸ 2048 ± 0 | ³⁷⁴ 1180 ± 2 | ³³⁶ 1178 ± 1 | ³²⁴ 1182 ± 1 | ²⁹² 1184 ± 1 | ²⁵² 1221 ± 1 | ¹⁵⁶ 1164 ± 32 | ¹⁵⁶ 1144 ± 32 |
| 179 | incode-011 | | 477280 | 21781 | ³²⁹ 1708 | ¹³² 2048 ± 0 | ²⁸⁷ 872 ± 0 | ²⁴⁷ 875 ± 0 | ²²² 881 ± 1 | ²⁰⁴ 892 ± 1 | ¹⁷⁸ 939 ± 0 | ¹⁵⁰ 1117 ± 31 | ¹⁵² 1109 ± 37 |
| 180 | innefulabs-000 | | 370588 | 162172 | ⁷⁸ 439 | ²⁸⁹ 2048 ± 0 | ³³⁴ 1006 ± 3 | ²⁹⁶ 1025 ± 3 | ²⁸⁴ 1030 ± 4 | ²⁵³ 1041 ± 2 | ²²⁷ 1135 ± 3 | ³²⁷ 5782 ± 41 | ³²⁹ 5741 ± 45 |
| 181 | innovativetechnologyltd-001 | | 177232 | 335757 | ⁵⁶ 341 | ¹⁶⁰ 2048 ± 0 | ¹⁰⁵ 433 ± 7 | ⁸⁷ 446 ± 8 | ⁶⁷ 439 ± 4 | ⁶⁰ 452 ± 4 | ⁵⁴ 485 ± 7 | ²¹⁶ 1877 ± 42 | ²²⁰ 1924 ± 97 |
| 182 | innovativetechnologyltd-002 | | 173939 | 372324 | ²¹⁰ 912 | ²⁸² 2048 ± 0 | ²⁰⁵ 661 ± 2 | ¹⁹⁷ 726 ± 4 | ²⁶¹ 981 ± 27 | ²³⁸ 997 ± 40 | ¹³⁹ 766 ± 3 | ²¹² 1841 ± 50 | ²¹⁵ 1857 ± 59 |
| 183 | innovatrics-007 | | 0 | 493269 | ³⁵⁰ 1937 | ⁸⁶ 1064 ± 0 | ⁴⁴³ 1485 ± 7 | ⁴¹⁰ 1785 ± 184 | ⁴⁰⁹ 2078 ± 24 | ³⁹⁵ 2123 ± 15 | ³⁵³ 2210 ± 42 | ³³² 5978 ± 88 | ³²⁸ 5690 ± 102 |
| 184 | innovatrics-008 | | 307323 | 59842 | ²⁹⁹ 1424 | ⁵⁴ 538 ± 0 | ²⁵⁰ 778 ± 6 | ²⁰⁷ 767 ± 3 | ¹⁸⁹ 770 ± 3 | ¹⁷² 803 ± 3 | ¹⁵⁹ 853 ± 10 | ²⁷⁰ 3021 ± 66 | ²⁵⁵ 2673 ± 88 |
| 185 | insightface-001 | | 776777 | 16606 | ⁴⁰⁹ 3852 | ¹⁵¹ 2048 ± 0 | ⁴¹⁴ 1366 ± 2 | ³⁸² 1368 ± 3 | ³⁷³ 1372 ± 3 | ³⁴⁹ 1375 ± 5 | ²⁹³ 1386 ± 4 | ¹⁵¹ 1119 ± 29 | ¹⁵⁰ 1108 ± 34 |
| 186 | insightface-002 | | 800572 | 16606 | ⁴⁰⁸ 3819 | ²⁹⁹ 2048 ± 0 | ⁴²⁷ 1396 ± 2 | ³⁸⁹ 1389 ± 4 | ³⁸⁷ 1403 ± 3 | ³⁶² 1402 ± 2 | ³⁰³ 1413 ± 3 | ¹⁵⁷ 1169 ± 40 | ¹⁵³ 1118 ± 38 |
| 187 | inspur-000 | | 364844 | 91926 | ¹⁸² 808 | ⁴⁰⁷ 4096 ± 0 | ⁴¹⁵ 1367 ± 1 | ³⁷⁶ 1331 ± 2 | ³⁷² 1368 ± 2 | ³⁷⁴ 1465 ± 1 | ³⁴⁹ 1861 ± 3 | ³⁵⁷ 9831 ± 37 | ³⁵⁶ 9860 ± 40 |
| 188 | intellicloudai-001 | | 220831 | 868246 | ¹³⁵ 655 | ¹⁸⁵ 2048 ± 0 | ¹²⁰ 468 ± 2 | ⁹⁰ 456 ± 1 | ⁷⁴ 466 ± 3 | ⁷⁵ 492 ± 1 | ⁹³ 632 ± 2 | ¹³⁹ 1056 ± 4 | ¹⁴³ 1051 ± 72 |
| 189 | intellicloudai-002 | | 259047 | 58559 | ⁴⁰⁵ 3584 | ⁴¹⁴ 4100 ± 0 | ²⁷⁸ 847 ± 1 | ²³³ 847 ± 2 | ²¹⁰ 849 ± 1 | ¹⁹⁰ 853 ± 1 | ¹⁶⁶ 878 ± 4 | ¹¹⁶ 822 ± 28 | ¹¹⁵ 818 ± 23 |
| 190 | intellifusion-001 | | 271872 | 289387 | ¹⁶⁹ 762 | ¹⁰⁶ 2048 ± 0 | ²⁴³ 764 ± 38 | ²¹⁰ 774 ± 39 | ¹⁹³ 797 ± 42 | ¹⁷¹ 803 ± 34 | ¹⁴⁵ 805 ± 33 | ¹⁴⁹ 1112 ± 28 | ¹⁵⁴ 1128 ± 41 |
| 191 | intellifusion-002 | | 762731 | 385841 | ²¹⁸ 941 | ³⁹⁸ 4096 ± 0 | ³¹⁵ 950 ± 2 | ³¹⁴ 1096 ± 42 | ²⁹⁷ 1088 ± 33 | ²⁸⁰ 1168 ± 31 | ²³⁸ 1171 ± 10 | ¹⁹⁵ 1713 ± 57 | ¹⁹⁷ 1665 ± 87 |
| 192 | intellivision-003 | | 64023 | 133748 | ¹⁷⁹ 799 | ³⁵⁵ 2056 ± 0 | ⁹² 407 ± 3 | ⁷⁰ 398 ± 2 | ⁵⁹ 418 ± 2 | ⁵⁹ 450 ± 1 | ⁸¹ 591 ± 4 | ³⁶⁰ 11069 ± 56 | ³⁶⁰ 11066 ± 75 |
| 193 | intellivision-004 | | 117727 | 131310 | ⁹⁸ 515 | ³⁵⁸ 2056 ± 0 | ⁶⁷ 330 ± 0 | ⁵³ 330 ± 0 | ⁴¹ 347 ± 0 | ⁴⁴ 382 ± 0 | ⁶⁰ 514 ± 0 | ³⁶¹ 11197 ± 63 | ³⁶¹ 11165 ± 72 |
| 194 | intellivix-001 | | 256654 | 111858 | ¹⁹³ 842 | ¹⁴⁸ 2048 ± 0 | ⁸³ 378 ± 1 | ⁶⁴ 379 ± 1 | ⁴⁹ 381 ± 1 | ⁴⁶ 384 ± 1 | ⁴² 421 ± 3 | ¹⁴⁸ 1100 ± 16 | ¹⁵¹ 1109 ± 22 |
| 195 | intellivix-002 | | 361566 | 111612 | ²⁶¹ 1172 | ²⁶⁶ 2048 ± 0 | ³¹⁹ 956 ± 0 | ²⁷⁴ 947 ± 6 | ²⁵⁹ 976 ± 0 | ²³² 984 ± 4 | ²¹⁹ 1089 ± 1 | ⁴⁰⁴ 30096 ± 128 | ⁴⁰⁶ 31287 ± 140 |
| 196 | intelresearch-004 | | 646918 | 85290 | ³⁴⁴ 1856 | ²⁴⁰ 2048 ± 0 | ⁴⁰⁷ 1319 ± 2 | ³⁷³ 1322 ± 3 | ³⁶¹ 1330 ± 3 | ³³⁸ 1345 ± 3 | ³⁰² 1411 ± 5 | ³⁰⁸ 4696 ± 63 | ³⁰⁶ 4692 ± 66 |
| 197 | intelresearch-005 | | 398137 | 85290 | ²⁵⁹ 1158 | ²³³ 2048 ± 0 | ⁴¹⁰ 1328 ± 1 | ³⁷⁸ 1334 ± 2 | ³⁶⁶ 1344 ± 2 | ³⁴¹ 1356 ± 2 | ³⁰⁵ 1423 ± 4 | ³⁰⁶ 4524 ± 87 | ³⁰³ 4461 ± 74 |
| 198 | intema-000 | | 1532392 | 19488 | ²⁴⁸ 1097 | ⁴³ 513 ± 0 | ³³⁶ 1010 ± 0 | ²⁸⁶ 1001 ± 4 | ²⁶⁹ 994 ± 0 | ²³⁶ 993 ± 5 | ²⁰⁹ 1056 ± 1 | ¹²² 910 ± 29 | ¹²³ 906 ± 32 |
| 199 | intsysmsu-001 | | 384409 | 172480 | ¹⁷⁶ 789 | ¹⁰¹ 2048 ± 0 | ¹⁸³ 614 ± 2 | ¹⁵⁵ 615 ± 2 | ¹⁴⁸ 642 ± 2 | ¹⁶⁰ 750 ± 3 | ²³⁵ 1159 ± 4 | ⁷² 621 ± 8 | ⁷² 611 ± 31 |
| 200 | intsysmsu-002 | | 765921 | 172298 | ¹⁷⁵ 786 | ⁶⁴ 1024 ± 0 | ¹⁷⁵ 593 ± 1 | ²¹⁶ 793 ± 2 | ²⁰² 827 ± 1 | ¹⁹³ 875 ± 104 | ²⁶⁸ 1293 ± 3 | ⁵⁰ 549 ± 25 | ⁵³ 548 ± 29 |
| 201 | ionetworks-000 | | 287609 | 51236 | ⁵⁹ 351 | ²²⁶ 2048 ± 0 | ¹⁰³ 430 ± 0 | ⁸⁴ 435 ± 0 | ⁶⁵ 433 ± 0 | ⁵⁷ 432 ± 0 | ⁴⁷ 444 ± 0 | ³⁴⁰ 6913 ± 102 | ³⁴³ 7150 ± 160 |
| 202 | iqface-000 | | 268819 | 596337 | ¹⁵² 704 | ⁴²⁸ 4750 ± 32 | ¹⁴⁵ 538 ± 26 | ¹⁰⁴ 494 ± 2 | ¹⁰⁷ 543 ± 3 | ¹⁵⁷ 734 ± 4 | ²⁹⁶ 1393 ± 4 | ⁴⁴³ 636433 ± 38446 | ⁴⁴³ 632654 ± 85615 |
| 203 | iqface-003 | | 370803 | 963398 | ¹⁸⁰ 817 | ⁴²⁹ 4763 ± 37 | ¹⁴⁰ 529 ± 1 | ¹¹⁸ 532 ± 2 | ¹²⁷ 599 ± 8 | ¹⁸⁹ 850 ± 2 | ³⁴⁰ 1694 ± 2 | ⁴⁴² 575924 ± 2601 | ⁴⁴² 576653 ± 2051 |
| 204 | irex-000 | | 741899 | 47419 | ³⁶¹ 2086 | ³⁷⁵ 3080 ± 0 | ²⁷⁹ 852 ± 2 | ²³⁵ 850 ± 1 | ²¹⁷ 874 ± 2 | ²¹⁹ 939 ± 1 | ²⁵⁶ 1249 ± 5 | ¹² 201 ± 11 | ¹³ 208 ± 8 |
| 205 | isap-001 | | 99049 | 204201 | ¹¹⁸ | ³⁸⁸ 4096 ± 0 | ¹⁰ 0 ± 0 | - | - | - | - | ⁴⁰ 459 ± 17 | ⁴² 456 ± 11 |
| 206 | isap-002 | | 256765 | 49931 | ⁵⁰ 288 | ²⁷⁹ 2048 ± 0 | ²⁴⁷ 769 ± 3 | ²⁹⁷ 1027 ± 2 | ²²⁰ 877 ± 2 | ¹⁶⁵ 761 ± 1 | ¹⁷² 912 ± 2 | ²⁷² 3045 ± 94 | ²⁶⁶ 2973 ± 66 |
| 207 | isityou-000 | | 48010 | 36621 | ¹⁷ 110 | ⁴⁴¹ 1920 ± 0 | ¹⁷ 113 ± 5 | - | - | - | - | ⁴³⁹ 237517 ± 1318 | ⁴³⁹ 237374 ± 1279 |
| 208 | isystems-001 | | 274621 | 639268 | ²⁴⁷ 1091 | ¹⁴¹ 2048 ± 0 | ⁵⁴ 291 ± 9 | - | - | - | - | ⁵² 557 ± 16 | ⁵⁶ 564 ± 22 |
| 209 | isystems-002 | | 358984 | 803389 | ³¹⁹ 1595 | ¹⁴⁰ 2048 ± 0 | ²⁷¹ 822 ± 8 | - | - | - | - | ¹⁰⁴ 749 ± 31 | ⁸¹ 632 ± 28 |
| 210 | itmo-007 | | 415979 | 245376 | ³⁶ 2199 | ¹²⁶ 2048 ± 0 | ²³⁷ 741 ± 2 | - | - | - | - | ²⁴⁹ 2551 ± 50 | ²⁴⁹ 2529 ± 80 |
| 211 | itmo-008 | | 726866 | 318238 | ²⁹² 1377 | ⁴⁰⁵ 4096 ± 0 | ³⁴⁹ 1060 ± 1 | ³⁰⁶ 1058 ± 1 | ²⁹³ 1059 ± 1 | ²⁶¹ 1072 ± 4 | ²²¹ 1104 ± 1 | ²⁸⁹ 3578 ± 25 | ²⁸⁹ 3580 ± 28 |
| 212 | ivacognitive-001 | | 256958 | 62791 | ²²⁰ 947 | ¹¹⁴ 2048 ± 0 | ⁴⁰¹ 1292 ± 3 | ³⁶⁵ 1289 ± 4 | ³⁵¹ 1292 ± 4 | ³²⁴ 1321 ± 4 | ²⁷⁴ 1321 ± 4 | ³⁰² 4228 ± 41 | ³⁰¹ 4226 ± 41 |
| 213 | iws-000 | | 30875 | 3063 | ¹⁰ 77 | ³⁴ 512 ± 0 | ⁴⁶ 277 ± 5 | ³⁹ 283 ± 1 | ⁸⁷ 494 ± 3 | ²³³ 984 ± 3 | ³⁷⁶ 2987 ± 39 | ¹³¹ 999 ± 40 | ¹³⁰ 992 ± 22 |
| 214 | jaakit-001 | | 99024 | 24754 | ⁴² 251 | ²⁷ 512 ± 0 | ⁹ 76 ± 0 | ⁷⁷ 77 ± 0 | ⁷⁹ 79 ± 0 | ⁸¹ 81 ± 0 | ⁶⁹ 93 ± 0 | ²⁴⁶ 2466 ± 57 | ²⁴⁶ 2465 ± 66 |
| 215 | kakao-007 | | 526993 | 129545 | ⁴¹⁶ 3953 | ¹¹³ 2048 ± 0 | ³¹⁸ 952 ± 1 | ²⁷⁸ 961 ± 1 | ²⁵² 958 ± 1 | ²²⁷ 962 ± 1 | ¹⁸⁸ 968 ± 1 | ¹³⁸ 1056 ± 16 | ¹⁴¹ 1047 ± 28 |
| 216 | kakao-008 | | 734583 | 104820 | ⁴¹¹ 3876 | ¹¹⁵ 2048 ± 0 | ³⁵⁷ 1135 ± 3 | ³³⁰ 1148 ± 3 | ³¹⁵ 1150 ± 3 | ²⁸² 1156 ± 1 | ²⁴² 1175 ± 1 | ¹⁰³ 736 ± 23 | ¹⁰¹ 727 ± 22 |
| 217 | kakaopay-001 | | 397864 | 179869 | ¹⁴⁴ 684 | ³⁹³ 4096 ± 0 | ¹⁰⁹ 448 ± 0 | ¹²² 542 ± 0 | ¹⁰⁵ 542 ± 0 | ⁸⁹ 542 ± 0 | ⁶⁹ 553 ± 0 | ⁷⁹ 633 ± 22 | ⁷⁸ 630 ± 22 |
| 218 | kasikornlabs-000 | | 256471 | 61000 | ¹⁴⁸ 693 | ¹⁷³ 2048 ± 0 | ³⁰⁰ 908 ± 36 | ²⁴⁹ 878 ± 22 | ²⁵⁵ 969 ± 39 | ²⁹¹ 1184 ± 54 | ³⁶⁰ 2382 ± 145 | ⁴⁰⁶ 31669 ± 188 | ⁴⁰⁷ 31714 ± 182 |
| 219 | kasikornlabs-001 | | 256471 | 61037 | ¹⁴² 681 | ²⁴² 2048 ± 0 | ³⁰³ 912 ± 38 | ²⁴² 868 ± 10 | ²⁷⁵ 1005 ± 50 | ²⁸⁸ 1176 ± 44 | ³⁶¹ 2387 ± 147 | ⁴⁰⁵ 30759 ± 198 | ⁴⁰⁵ 30867 ± 174 |
| 220 | kedacom-000 | | 245292 | 37401 | ⁴⁴² 23574 | ¹² 292 ± 0 | ¹³⁵ 506 ± 3 | ¹²⁷ 547 ± 10 | ¹³⁴ 614 ± 9 | ¹⁰² 588 ± 10 | ¹⁰⁶ 665 ± 24 | ⁸⁷ 684 ± 14 | ⁹¹ 682 ± 16 |

Notes

1 The configuration size does not capture static data included in libraries.

2 The library size is the combined total of all files provided in the submission lib folder. These libraries e.g. OpenCV may or may not be installed on any end user's platform natively and would not need to be installed with the algorithm. Some developers put neural network models in their libraries.

3 The memory usage is the peak resident set size reported by the ps system call during template generation.

4 The median template creation times are measured on Intel® Xeon® CPU E5-2630 v4 @ 2.20GHz processors.

5 The comparison durations, in nanoseconds, are estimated using std::chrono::high_resolution_clock which on the machine in (2) counts 1ns clock ticks. Precision is somewhat worse than that however. The ± value is the median absolute deviation times 1.48 for Normal consistency.

| | ALGORITHM | CONFIG | LIBRARY | TEMPLATE | | | | | | | | COMPARISON ⁴ | | | |
|-----|----------------------|---------|---------|----------------------|-------------------------|--------------------------|--------------------------|--------------------------|--------------------------|----------------------------|----------------------------|-----------------------------------|---------|----------|--|
| | | | | NAME | | DATA | | MEMORY | | SIZE | | GENERATION TIME (ms) ⁴ | | | |
| | | | | (KB) ¹ | (KB) ² | (MB) ³ | (B) | MUGSHOT | 480x720 | 960x1440 | 1600x2400 | 3000x4500 | GENUINE | IMPOSTOR | |
| 221 | kiwitech-000 | 369711 | 21375 | ¹⁸³ 808 | ²⁶⁹ 2048 ± 0 | ¹⁷³ 591 ± 0 | ¹⁴⁷ 594 ± 0 | ¹²⁶ 595 ± 1 | ¹⁰⁶ 596 ± 0 | ⁸⁸ 609 ± 0 | ²⁰⁰ 1755 ± 20 | ²⁰⁰ 1734 ± 16 | | | |
| 222 | kneron-003 | 58366 | 1747 | ³⁶ 188 | ²⁹⁶ 2048 ± 0 | ⁵⁰ 281 ± 3 | ³⁸ 280 ± 1 | ³⁵ 315 ± 13 | ⁴¹ 365 ± 7 | ²⁵³ 1224 ± 30 | ³¹⁸ 5237 ± 63 | ³¹⁷ 5274 ± 99 | | | |
| 223 | kneron-005 | 375374 | 13633 | ⁷⁹ 457 | ¹⁰⁰ 2048 ± 0 | ¹³⁹ 518 ± 2 | ¹¹³ 522 ± 4 | ¹¹¹ 556 ± 5 | ¹⁶³ 757 ± 19 | ³⁴⁶ 1760 ± 25 | ²²⁰ 1922 ± 11 | ²²¹ 1926 ± 20 | | | |
| 224 | knowutech-000 | 808045 | 32886 | ²⁸² 1303 | ⁹³ 1536 ± 0 | ⁴³² 1419 ± 2 | ³⁸³ 1372 ± 1 | ³⁷⁶ 1377 ± 1 | ³⁵¹ 1382 ± 2 | ²⁹² 1386 ± 2 | ²⁹¹ 3743 ± 31 | ²⁹² 3693 ± 38 | | | |
| 225 | kookmin-002 | 371771 | 30734 | ¹⁹⁰ 827 | ¹⁵⁶ 2048 ± 0 | ³⁴⁶ 1038 ± 2 | ³⁰⁵ 1047 ± 1 | ²⁸⁹ 1045 ± 1 | ²⁵⁷ 1061 ± 1 | ²²² 1116 ± 1 | ⁸¹ 638 ± 19 | ⁸⁴ 636 ± 20 | | | |
| 226 | krungthai-002 | 2360957 | 15033 | ²⁶⁰ 1171 | ²⁵⁶ 2048 ± 0 | ⁶¹ 308 ± 0 | ⁴⁷ 314 ± 5 | ³¹ 309 ± 0 | ³² 319 ± 0 | ³¹ 362 ± 0 | ²⁶⁸ 3014 ± 20 | ²⁶⁷ 2980 ± 22 | | | |
| 227 | kuke3d-001 | 403462 | 68786 | ¹⁰⁵ 530 | ³⁸³ 4096 ± 0 | ²⁶² 814 ± 2 | ²²⁰ 811 ± 2 | ¹⁹⁷ 814 ± 2 | ¹⁷⁵ 814 ± 1 | ¹⁵⁷ 834 ± 1 | ³³⁶ 6412 ± 57 | ³³⁶ 6413 ± 51 | | | |
| 228 | kuke3d-002 | 270544 | 1227855 | ¹⁸⁴ 809 | ²²⁴ 2048 ± 0 | ¹³⁴ 504 ± 3 | ¹¹² 504 ± 1 | ⁹⁴ 511 ± 1 | ⁸⁴ 523 ± 2 | ⁷⁹ 585 ± 1 | ²⁶⁵ 2943 ± 22 | ²⁶⁵ 2966 ± 38 | | | |
| 229 | lebentech-000 | 0 | 10360 | ¹⁸ 110 | ²⁰ 512 ± 0 | ³ 22 ± 0 | ¹ 22 ± 0 | ¹ 22 ± 0 | ¹ 23 ± 0 | ¹ 23 ± 0 | ¹¹⁴ 801 ± 42 | ¹¹⁶ 825 ± 51 | | | |
| 230 | lemalabs-001 | 748400 | 198794 | ³⁸⁸ 2738 | ¹⁴⁴ 2048 ± 0 | ²⁵⁹ 810 ± 0 | ²²¹ 812 ± 0 | ¹⁹⁰ 813 ± 0 | ¹⁷⁷ 819 ± 0 | ¹⁵⁸ 844 ± 1 | ³⁶⁷ 11930 ± 35 | ³⁶⁷ 11913 ± 37 | | | |
| 231 | lineclova-001 | 944355 | 407058 | ³⁶⁹ 2373 | ²⁶⁷ 2048 ± 0 | ²⁷⁴ 833 ± 10 | ²²⁹ 830 ± 3 | ²⁰⁴ 828 ± 4 | ¹⁸⁴ 838 ± 8 | ¹⁵⁵ 833 ± 4 | ²⁵⁴ 2696 ± 23 | ²⁵⁶ 2677 ± 35 | | | |
| 232 | lineclova-002 | 475779 | 406756 | ²⁸⁶ 1353 | ²⁸⁶ 2048 ± 0 | ³⁹⁷ 1284 ± 1 | ³⁶¹ 1275 ± 2 | ³⁴⁷ 1275 ± 1 | ³¹⁹ 1273 ± 2 | ²⁶⁴ 1281 ± 2 | ²⁵⁸ 2765 ± 10 | ²⁵⁸ 2767 ± 31 | | | |
| 233 | lookman-002 | 138200 | 25410 | ⁴⁴⁰ 16518 | ⁵⁷ 548 ± 0 | ²⁸ 173 ± 1 | - | - | - | - | ⁶⁷ 610 ± 19 | ⁷³ 612 ± 22 | | | |
| 234 | lookman-004 | 244775 | 37401 | ⁴⁴¹ 23548 | ⁵⁸ 548 ± 0 | ¹³⁶ 507 ± 5 | ¹²⁵ 545 ± 12 | ¹³³ 613 ± 12 | ¹⁰⁵ 590 ± 11 | ¹⁰² 656 ± 16 | ¹²⁰ 871 ± 29 | ¹²⁰ 878 ± 29 | | | |
| 235 | luxand-000 | 0 | 57908 | ²⁸⁹ 1366 | ⁸³ 1040 ± 0 | ⁹³ 407 ± 23 | ⁸² 433 ± 11 | ⁷⁰ 444 ± 14 | ⁶⁵ 464 ± 14 | ⁷⁵ 562 ± 25 | ¹¹⁷ 828 ± 28 | ¹¹⁷ 828 ± 32 | | | |
| 236 | mantra-000 | 471458 | 62566 | ¹⁶⁷ 749 | ³²⁴ 2052 ± 0 | ⁹⁷ 413 ± 18 | ¹⁰² 487 ± 19 | ⁸⁶ 494 ± 18 | ⁸⁰ 511 ± 18 | ⁸⁴ 598 ± 19 | ²⁷⁷ 3151 ± 51 | ²⁷⁶ 3127 ± 63 | | | |
| 237 | maxvision-001 | 256146 | 61793 | ³⁹⁵ 2880 | ¹⁷⁰ 2048 ± 0 | ⁴⁵ 275 ± 3 | ³⁶ 274 ± 2 | ²⁸ 277 ± 4 | ²⁷ 280 ± 4 | ²³ 325 ± 3 | ⁹⁶ 714 ± 13 | ⁹⁸ 717 ± 13 | | | |
| 238 | maxvision-002 | 171894 | 60623 | ³⁴⁵ 1863 | ¹⁰⁸ 2048 ± 0 | ²⁹ 172 ± 0 | ¹⁸ 171 ± 0 | ¹⁶ 172 ± 0 | ¹³ 174 ± 0 | ¹⁵ 221 ± 0 | ⁹⁸ 725 ± 5 | ¹⁰⁰ 725 ± 5 | | | |
| 239 | megvii-005 | 1378009 | 44038 | ⁴¹⁸ 4036 | ³¹⁴ 2049 ± 0 | ⁴⁰⁸ 1319 ± 5 | ³⁵³ 1247 ± 6 | ³³⁶ 1240 ± 2 | ³¹⁰ 1245 ± 2 | ²⁷⁰ 1298 ± 3 | ⁴¹⁰ 32025 ± 121 | ⁴¹¹ 32008 ± 114 | | | |
| 240 | megvii-006 | 1554938 | 44038 | ⁴²⁰ 4354 | ³¹² 2049 ± 0 | ³⁹⁹ 1287 ± 3 | ³⁶³ 1286 ± 0 | ³⁸² 1393 ± 5 | ³³² 1319 ± 1 | ²⁸⁵ 1360 ± 1 | ⁴⁰⁸ 31845 ± 100 | ⁴⁰⁹ 31872 ± 118 | | | |
| 241 | meituan-000 | 259514 | 333178 | ¹¹⁰ 554 | ²⁹⁰ 2048 ± 0 | ¹⁰⁶ 436 ± 4 | ⁸⁶ 441 ± 1 | ¹³⁷ 626 ± 5 | ²⁶⁴ 1098 ± 15 | ³⁷⁸ 3126 ± 53 | ⁸² 638 ± 17 | ⁸² 633 ± 16 | | | |
| 242 | meituan-001 | 615387 | 333249 | ²⁵¹ 1106 | ¹⁰⁷ 2048 ± 0 | ³³⁸ 1017 ± 4 | ²⁹¹ 1008 ± 3 | ²⁷⁷ 1010 ± 2 | ²⁴⁵ 1010 ± 3 | ¹⁹⁷ 1011 ± 4 | ⁸⁴ 654 ± 10 | ⁸⁷ 658 ± 14 | | | |
| 243 | meiya-001 | 280055 | 264913 | ⁹⁴ 507 | ³¹³ 2049 ± 0 | ¹⁸⁷ 622 ± 12 | - | - | - | - | ³⁴⁸ 8356 ± 615 | ³⁴⁸ 8314 ± 97 | | | |
| 244 | mendaxiatech-000 | 1941475 | 45484 | ⁴⁰³ 3195 | ⁴¹³ 4097 ± 0 | ³⁸⁸ 1243 ± 2 | ³⁵⁵ 1255 ± 1 | ³⁷⁴ 1373 ± 2 | ³⁸³ 1598 ± 3 | ³⁶⁹ 2689 ± 8 | ⁴¹⁹ 46906 ± 275 | ⁴¹⁹ 46872 ± 217 | | | |
| 245 | metsakuurcompany-001 | 445177 | 1091558 | ³¹⁴ 1572 | ³³⁹ 2056 ± 0 | ¹⁶³ 578 ± 1 | ¹⁴³ 587 ± 3 | ¹²² 590 ± 1 | ¹²⁷ 659 ± 1 | ¹⁶⁰ 854 ± 1 | ³⁴⁹ 8600 ± 192 | ³⁴⁹ 8155 ± 298 | | | |
| 246 | microfocus-001 | 104524 | 27242 | ³⁷ 190 | ⁵ 256 ± 0 | ⁴² 264 ± 18 | - | - | - | - | ¹⁵ 215 ± 8 | ¹⁵ 217 ± 10 | | | |
| 247 | microfocus-002 | 96288 | 27362 | ³⁴ 176 | ³ 256 ± 0 | ⁴⁰ 259 ± 18 | - | - | - | - | ²⁷ 337 ± 34 | ¹⁶ 230 ± 25 | | | |
| 248 | minivision-000 | 836697 | 16597 | ⁴¹⁷ 4013 | ³⁸⁰ 4096 ± 0 | ³⁴⁵ 1035 ± 1 | ³⁰² 1033 ± 2 | ²⁸⁷ 1035 ± 1 | ²⁵² 1037 ± 1 | ²¹³ 1059 ± 2 | ²⁴⁵ 2466 ± 26 | ²⁴⁴ 2460 ± 25 | | | |
| 249 | mobai-000 | 365451 | 80573 | ¹⁷⁴ 786 | ⁴³² 6144 ± 0 | ²⁴⁸ 766 ± 8 | ²⁴³ 869 ± 6 | ³³¹ 1205 ± 31 | ³⁹² 1867 ± 45 | ³⁸³ 3549 ± 190 | ³⁸² 16458 ± 333 | ³⁸² 16423 ± 1473 | | | |
| 250 | mobai-001 | 265297 | 60164 | ¹⁰⁶ 534 | ¹¹¹ 2048 ± 0 | ¹⁸¹ 612 ± 3 | ¹⁵³ 614 ± 3 | ¹⁶² 687 ± 9 | ²⁰⁰ 886 ± 31 | ³⁴² 1707 ± 103 | ¹⁷⁰ 1386 ± 25 | ¹⁷¹ 1377 ± 26 | | | |
| 251 | mobbl-001 | 231160 | 58706 | ³⁹ 223 | ²⁹³ 2048 ± 0 | ³⁰ 183 ± 32 | ²³ 184 ± 25 | ⁴⁴ 354 ± 76 | ¹⁸⁰ 823 ± 396 | ³⁷² 2781 ± 1166 | ³⁶⁵ 11832 ± 109 | ³⁶⁶ 11851 ± 88 | | | |
| 252 | mobbl-003 | 172248 | 60960 | ⁴⁷ 270 | ²⁰³ 2048 ± 0 | ²¹¹ 664 ± 6 | ¹⁷¹ 661 ± 5 | ¹⁵³ 663 ± 5 | ¹³⁰ 665 ± 6 | ¹¹³ 691 ± 5 | ³⁷⁰ 12506 ± 111 | ³⁷¹ 12509 ± 100 | | | |
| 253 | mobipintech-000 | 370514 | 303291 | ²⁵³ 1130 | ¹⁸³ 2048 ± 0 | ³⁸⁹ 1245 ± 1 | ³⁴⁹ 1234 ± 1 | ³⁴³ 1264 ± 1 | ³⁴⁵ 1360 ± 1 | ³⁴¹ 1707 ± 1 | ³⁷⁶ 14506 ± 214 | ³⁷⁶ 14433 ± 197 | | | |
| 254 | moreedian-000 | 525259 | 21374 | ²¹⁶ 932 | ²¹⁸ 2048 ± 0 | ²²⁶ 694 ± 0 | ¹⁸⁶ 698 ± 0 | ¹⁷⁰ 699 ± 0 | ¹⁴² 700 ± 0 | ¹²¹ 713 ± 1 | ²⁰⁹ 1803 ± 11 | ²⁰⁹ 1779 ± 23 | | | |
| 255 | mukh-001 | 866223 | 451194 | ³²⁴ 1637 | ⁶⁷ 1024 ± 0 | ⁴¹⁷ 1375 ± 17 | ³⁹⁰ 1390 ± 12 | ³⁸⁹ 1406 ± 8 | ³⁵⁶ 1394 ± 10 | ²⁸³ 1360 ± 11 | ³⁸ 433 ± 14 | ⁴⁰ 435 ± 14 | | | |
| 256 | multimodality-000 | 0 | 503924 | ²⁹⁸ 1417 | ²⁰⁹ 2048 ± 0 | ⁹⁸ 416 ± 0 | ⁷⁸ 420 ± 0 | ⁶² 423 ± 0 | ⁵⁶ 427 ± 0 | ⁴⁹ 463 ± 0 | ¹¹⁸ 848 ± 25 | ¹¹³ 800 ± 28 | | | |
| 257 | multimodality-001 | 185719 | 545045 | ²⁹⁴ 1388 | ³⁹¹ 4096 ± 0 | ³⁷⁸ 1190 ± 2 | ³³⁴ 1169 ± 2 | ³¹⁹ 1165 ± 2 | ²⁸⁵ 1167 ± 2 | ²⁴⁴ 1177 ± 2 | ¹⁷⁷ 1424 ± 35 | ¹⁷³ 1384 ± 42 | | | |
| 258 | mvnvision-001 | 227502 | 149531 | ¹⁵⁸ 723 | ³⁶ 512 ± 0 | ²²⁵ 691 ± 21 | ¹⁸⁸ 702 ± 19 | ¹⁶⁸ 697 ± 24 | ¹⁴⁶ 708 ± 29 | ¹¹⁹ 710 ± 27 | ¹⁵² 1123 ± 40 | ¹⁵⁷ 1154 ± 38 | | | |
| 259 | nazhiai-000 | 547484 | 16141 | ³⁸⁵ 2716 | ³⁰⁹ 2048 ± 0 | ²¹⁷ 683 ± 3 | ¹⁸² 687 ± 2 | ²⁰⁷ 835 ± 27 | ¹⁸⁷ 840 ± 31 | ¹⁵⁶ 834 ± 34 | ²³⁹ 2230 ± 34 | ²³⁴ 2133 ± 81 | | | |
| 260 | neosystems-003 | 599442 | 349942 | ²⁶⁶ 1215 | ¹⁵² 2048 ± 0 | ³⁶³ 1143 ± 2 | ⁴¹¹ 1836 ± 7 | ⁴¹⁰ 2260 ± 3 | ⁴⁰¹ 2273 ± 6 | ³⁵⁵ 2273 ± 3 | ³⁸⁷ 19130 ± 223 | ³⁸⁷ 19167 ± 186 | | | |
| 261 | neosystems-004 | 243546 | 352623 | ¹⁰⁴ 529 | ¹³⁷ 2048 ± 0 | ⁶⁶ 324 ± 0 | ¹⁹¹ 711 ± 3 | ²⁰³ 827 ± 7 | ¹⁹¹ 854 ± 2 | ¹⁷³ 916 ± 2 | ³⁷⁵ 14437 ± 176 | ³⁷⁵ 14355 ± 173 | | | |
| 262 | netbridgetech-001 | 133108 | 205875 | ⁹⁵ 508 | ⁴⁰⁸ 4096 ± 0 | ¹¹ 85 ± 1 | ⁹ 83 ± 0 | ⁸ 84 ± 0 | ⁸ 92 ± 0 | ⁸ 113 ± 4 | ³⁵² 9280 ± 74 | ³⁵² 9446 ± 512 | | | |
| 263 | netbridgetech-002 | 257687 | 49931 | ⁵² 299 | ¹²³ 2048 ± 0 | ²⁷⁵ 838 ± 6 | ²³¹ 838 ± 2 | ²⁰⁸ 839 ± 1 | ¹⁸⁶ 839 ± 3 | ¹⁶¹ 859 ± 3 | ²⁶³ 2893 ± 65 | ²⁷¹ 3050 ± 123 | | | |
| 264 | neurotechnology-013 | 474749 | 85552 | ³⁹⁶ 2894 | ⁴⁰ 514 ± 0 | ³³¹ 1000 ± 1 | ²⁹⁰ 1006 ± 2 | ²⁷⁹ 1022 ± 2 | ²⁵⁶ 1053 ± 2 | ²⁴⁵ 1195 ± 8 | ² 109 ± 4 | ¹ 110 ± 4 | | | |

Notes

- 1 The configuration size does not capture static data included in libraries.
- 2 The library size is the combined total of all files provided in the submission lib folder. These libraries e.g. OpenCV may or may not be installed on any end user's platform natively and would not need to be installed with the algorithm. Some developers put neural network models in their libraries.
- 3 The memory usage is the peak resident set size reported by the ps system call during template generation.
- 4 The median template creation times are measured on Intel®Xeon®CPU E5-2630 v4 @ 2.20GHz processors.
- 5 The comparison durations, in nanoseconds, are estimated using std::chrono::high_resolution_clock which on the machine in (2) counts 1ns clock ticks. Precision is somewhat worse than that however. The ± value is the median absolute deviation times 1.48 for Normal consistency.

Table 13: Summary of algorithms and properties included in this report. The red superscripts give ranking for the quantity in that column.

| | ALGORITHM | CONFIG | LIBRARY | TEMPLATE | | | | | | | | COMPARISON ⁴ | | | | | | | | | |
|-----|---------------------|---------|---------|----------|-------|------|----------|------|-----------------------------------|-------------------|-------------------|-------------------------|------------------------|---------|-------------|-----------|------------|-------------|-------------|-------------|-------------|
| | | | | NAME | DATA | DATA | MEMORY | SIZE | GENERATION TIME (ms) ⁴ | | | | TIME (ns) ⁵ | | | | | | | | |
| | | | | | | | | | (KB) ¹ | (KB) ² | (MB) ³ | (B) | MUGSHOT | 480x720 | 960x1440 | 1600x2400 | 3000x4500 | GENUINE | IMPOSTOR | | |
| 265 | neurotechnology-015 | 474782 | 86045 | 377 | 2564 | 47 | 515 ± 0 | 342 | 1028 ± 3 | 301 | 1033 ± 3 | 292 | 1055 ± 4 | 263 | 1097 ± 4 | 271 | 1304 ± 18 | 4 | 130 ± 2 | 4 | 130 ± 4 |
| 266 | nhn-002 | 363471 | 817674 | 139 | 667 | 395 | 4096 ± 0 | 360 | 1141 ± 3 | 324 | 1138 ± 2 | 311 | 1141 ± 2 | 281 | 1151 ± 6 | 247 | 1203 ± 2 | 425 | 56608 ± 579 | 426 | 56549 ± 606 |
| 267 | nhn-003 | 933665 | 432730 | 305 | 1464 | 390 | 4096 ± 0 | 384 | 1229 ± 2 | 357 | 1261 ± 1 | 342 | 1263 ± 3 | 321 | 1279 ± 2 | 288 | 1375 ± 3 | 422 | 50560 ± 105 | 422 | 50592 ± 142 |
| 268 | nodeflux-002 | 774668 | 690213 | 82 | 466 | 298 | 2048 ± 0 | 232 | 708 ± 4 | 190 | 709 ± 4 | 176 | 716 ± 5 | 152 | 716 ± 7 | 128 | 736 ± 3 | 286 | 3475 ± 62 | 283 | 3408 ± 143 |
| 269 | notiontag-001 | 92753 | 427967 | 116 | 566 | 60 | 584 ± 0 | 310 | 929 ± 35 | 311 | 1092 ± 39 | 411 | 3709 ± 81 | 411 | 10233 ± 180 | - | 415 | 43636 ± 286 | 417 | 43724 ± 330 | |
| 270 | notiontag-002 | 271987 | 967207 | 393 | 2840 | 369 | 2120 ± 0 | 111 | 453 ± 2 | 89 | 453 ± 3 | 71 | 453 ± 3 | 61 | 458 ± 2 | 51 | 471 ± 3 | 390 | 20278 ± 194 | 390 | 20195 ± 186 |
| 271 | nsensecorp-002 | 187421 | 122407 | 111 | 554 | 143 | 2048 ± 0 | 71 | 333 ± 0 | 54 | 333 ± 0 | 40 | 337 ± 0 | 37 | 338 ± 0 | 29 | 351 ± 0 | 418 | 45965 ± 213 | 418 | 45988 ± 158 |
| 272 | nsensecorp-003 | 199895 | 117041 | 155 | 710 | 125 | 2048 ± 0 | 206 | 661 ± 0 | 172 | 664 ± 0 | 152 | 662 ± 1 | 128 | 659 ± 1 | 104 | 659 ± 0 | 416 | 44658 ± 51 | 417 | 44654 ± 72 |
| 273 | ntechlab-011 | 786933 | 209458 | 433 | 6867 | 90 | 1280 ± 0 | 365 | 1148 ± 2 | 325 | 1142 ± 1 | 317 | 1159 ± 1 | 294 | 1185 ± 1 | 267 | 1290 ± 3 | 7 | 179 ± 11 | 8 | 173 ± 11 |
| 274 | ntechlab-012 | 570796 | 212350 | 427 | 5451 | 371 | 2560 ± 0 | 405 | 1309 ± 1 | 374 | 1323 ± 1 | 363 | 1331 ± 1 | 346 | 1360 ± 1 | 313 | 1460 ± 3 | 14 | 211 ± 8 | 14 | 211 ± 7 |
| 275 | omface-000 | 45945 | 844976 | 28 | 150 | 65 | 1024 ± 0 | 32 | 185 ± 1 | 20 | 206 ± 2 | 22 | 203 ± 1 | 16 | 195 ± 1 | 14 | 193 ± 1 | 44 | 481 ± 42 | 43 | 456 ± 20 |
| 276 | omnigarde-001 | 200523 | 32882 | 81 | 464 | 18 | 512 ± 0 | 312 | 941 ± 0 | 253 | 883 ± 1 | 223 | 886 ± 1 | 203 | 891 ± 1 | 168 | 898 ± 0 | 175 | 1405 ± 31 | 172 | 1379 ± 26 |
| 277 | omnigarde-002 | 368860 | 32882 | 168 | 757 | 70 | 1024 ± 0 | 402 | 1303 ± 1 | 352 | 1246 ± 1 | 339 | 1249 ± 1 | 313 | 1253 ± 1 | 258 | 1261 ± 1 | 257 | 2727 ± 34 | 257 | 2686 ± 32 |
| 278 | openface-001 | 0 | 40111 | 16 | 100 | 165 | 2048 ± 0 | 22 | 148 ± 1 | 16 | 154 ± 0 | 46 | 365 ± 3 | 53 | 409 ± 9 | 90 | 616 ± 31 | 66 | 608 ± 14 | 70 | 604 ± 13 |
| 279 | oz-003 | 484147 | 519652 | 439 | 11949 | 337 | 2053 ± 0 | 416 | 1375 ± 12 | 388 | 1388 ± 3 | 408 | 1773 ± 16 | 394 | 2039 ± 6 | 380 | 3209 ± 5 | 435 | 73905 ± 456 | 435 | 73892 ± 444 |
| 280 | oz-004 | 373982 | 1075452 | 437 | 8071 | 336 | 2053 ± 0 | 273 | 832 ± 7 | 244 | 871 ± 6 | 226 | 899 ± 10 | 262 | 1078 ± 12 | 335 | 1608 ± 10 | 429 | 61654 ± 418 | 428 | 61749 ± 450 |
| 281 | palit-000 | 428754 | 144958 | 288 | 1355 | 379 | 4096 ± 0 | 162 | 570 ± 1 | 137 | 578 ± 1 | 118 | 576 ± 3 | 99 | 583 ± 1 | 89 | 614 ± 1 | 238 | 2227 ± 16 | 240 | 2226 ± 16 |
| 282 | pangiam-000 | 464252 | 24512 | 415 | 3919 | 213 | 2048 ± 0 | 190 | 627 ± 5 | 157 | 618 ± 4 | 135 | 615 ± 3 | 112 | 620 ± 3 | 99 | 639 ± 3 | 3 | 118 ± 7 | 3 | 113 ± 7 |
| 283 | papago-001 | 669274 | 52817 | 368 | 2341 | 201 | 2048 ± 0 | 395 | 1272 ± 6 | 367 | 1296 ± 7 | 354 | 1295 ± 6 | 323 | 1281 ± 3 | 279 | 1345 ± 3 | 379 | 15236 ± 169 | 379 | 15184 ± 142 |
| 284 | papsav1923-001 | 279210 | 52625 | 84 | 473 | 275 | 2048 ± 0 | 189 | 626 ± 1 | 160 | 628 ± 1 | 139 | 630 ± 1 | 123 | 648 ± 2 | 132 | 744 ± 3 | 100 | 725 ± 25 | 102 | 731 ± 28 |
| 285 | papsav1923-002 | 491185 | 24727 | 255 | 1136 | 330 | 2052 ± 0 | 256 | 792 ± 1 | 282 | 978 ± 1 | 288 | 1042 ± 1 | 283 | 1158 ± 1 | 338 | 1641 ± 19 | 159 | 1209 ± 29 | 161 | 1206 ± 38 |
| 286 | paravision-008 | 542190 | 204440 | 303 | 1448 | 397 | 4096 ± 0 | 229 | 699 ± 0 | 187 | 700 ± 0 | 171 | 701 ± 0 | 143 | 702 ± 1 | 116 | 702 ± 0 | 28 | 337 ± 17 | 30 | 330 ± 13 |
| 287 | paravision-010 | 688291 | 205854 | 363 | 2150 | 417 | 4100 ± 0 | 194 | 634 ± 0 | 165 | 635 ± 0 | 143 | 635 ± 0 | 118 | 635 ± 0 | 97 | 635 ± 1 | 187 | 1577 ± 35 | 187 | 1571 ± 32 |
| 288 | pensees-001 | 1619431 | 408932 | 348 | 1922 | 439 | 8200 ± 0 | 354 | 1108 ± 3 | 401 | 1448 ± 17 | 393 | 1439 ± 10 | 373 | 1464 ± 5 | 330 | 1546 ± 9 | 276 | 3151 ± 34 | 276 | 3143 ± 25 |
| 289 | pixelall-006 | 0 | 746305 | 217 | 934 | 370 | 2560 ± 0 | 340 | 1024 ± 3 | 299 | 1028 ± 2 | 285 | 1033 ± 1 | 250 | 1032 ± 1 | 206 | 1054 ± 2 | 106 | 754 ± 14 | 99 | 722 ± 10 |
| 290 | pixelall-008 | 0 | 992249 | 335 | 1741 | 438 | 8192 ± 0 | 439 | 1471 ± 3 | 397 | 1405 ± 4 | 390 | 1409 ± 4 | 366 | 1413 ± 3 | 307 | 1426 ± 4 | 206 | 1799 ± 50 | 210 | 1807 ± 48 |
| 291 | psl-009 | 411027 | 411504 | 425 | 5369 | 424 | 4168 ± 0 | 420 | 1382 ± 2 | 386 | 1381 ± 1 | 379 | 1383 ± 1 | 352 | 1383 ± 2 | 291 | 1385 ± 1 | 24 | 316 ± 14 | 23 | 289 ± 14 |
| 292 | psl-010 | 411027 | 591157 | 424 | 5361 | 423 | 4168 ± 0 | 431 | 1403 ± 9 | 393 | 1393 ± 3 | 381 | 1392 ± 3 | 357 | 1395 ± 3 | 298 | 1396 ± 3 | 30 | 354 ± 53 | 29 | 329 ± 29 |
| 293 | ptakuratsatu-000 | 0 | 585434 | 285 | 1347 | 53 | 538 ± 0 | 291 | 875 ± 3 | 240 | 863 ± 48 | 242 | 928 ± 9 | 226 | 958 ± 17 | 216 | 1066 ± 26 | 330 | 5900 ± 103 | 327 | 5687 ± 167 |
| 294 | pxl-001 | 110116 | 78231 | 30 | 168 | 31 | 512 ± 0 | 15 | 101 ± 5 | 20 | 104 ± 5 | 52 | 189 ± 12 | 408 | 27 | 316 | 1470 ± 144 | 324 | 5598 ± 45 | 324 | 5590 ± 68 |
| 295 | pyramid-000 | 372608 | 219883 | 180 | 804 | 344 | 2056 ± 0 | 165 | 583 ± 2 | - | - | - | - | - | - | 343 | 7147 ± 59 | 346 | 7586 ± 425 | | |
| 296 | qazbs-000 | 362015 | 805258 | 198 | 856 | 251 | 2048 ± 0 | 404 | 1307 ± 1 | 351 | 1243 ± 0 | 338 | 1248 ± 9 | 312 | 1253 ± 1 | 261 | 1270 ± 0 | 316 | 5181 ± 62 | 315 | 5167 ± 93 |
| 297 | qnap-001 | 196210 | 13399 | 49 | 286 | 205 | 2048 ± 0 | 182 | 614 ± 1 | 154 | 615 ± 1 | 138 | 627 ± 1 | 115 | 623 ± 1 | 94 | 634 ± 2 | 83 | 649 ± 11 | 85 | 648 ± 14 |
| 298 | qnap-002 | 346963 | 33284 | 150 | 700 | 145 | 2048 ± 0 | 268 | 821 ± 1 | 225 | 824 ± 1 | 201 | 824 ± 1 | 182 | 826 ± 1 | 154 | 832 ± 1 | 20 | 293 ± 13 | 21 | 287 ± 17 |
| 299 | quantasoft-003 | 370518 | 211354 | 237 | 1058 | 181 | 2048 ± 0 | 193 | 632 ± 2 | 164 | 634 ± 0 | 140 | 632 ± 0 | 117 | 631 ± 1 | 95 | 634 ± 0 | 11 | 201 ± 7 | 12 | 203 ± 8 |
| 300 | rankone-012 | 0 | 264182 | 23 | 134 | 7 | 261 ± 0 | 155 | 564 ± 3 | 128 | 554 ± 1 | 113 | 564 ± 1 | 100 | 586 ± 1 | 114 | 695 ± 1 | 19 | 273 ± 17 | 17 | 231 ± 14 |
| 301 | rankone-013 | 0 | 228729 | 27 | 149 | 6 | 261 ± 0 | 223 | 690 ± 5 | 175 | 672 ± 1 | 174 | 712 ± 1 | 169 | 780 ± 1 | 223 | 1118 ± 3 | 32 | 356 ± 23 | 24 | 304 ± 23 |
| 302 | realnetworks-006 | 466225 | 56771 | 317 | 1588 | 345 | 2056 ± 0 | 197 | 638 ± 4 | 161 | 630 ± 3 | 156 | 672 ± 5 | 145 | 706 ± 5 | 140 | 774 ± 5 | 41 | 469 ± 19 | 47 | 478 ± 25 |
| 303 | realnetworks-007 | 570797 | 101527 | 401 | 3137 | 346 | 2056 ± 0 | 412 | 1348 ± 2 | 381 | 1358 ± 11 | 371 | 1363 ± 10 | 353 | 1386 ± 9 | 324 | 1517 ± 6 | 53 | 559 ± 31 | 52 | 539 ± 35 |
| 304 | regula-000 | 262444 | 29384 | 129 | 610 | 294 | 2048 ± 0 | 377 | 1187 ± 1 | 319 | 1126 ± 1 | 305 | 1129 ± 0 | 271 | 1132 ± 1 | 233 | 1159 ± 1 | 48 | 491 ± 16 | 49 | 500 ± 22 |
| 305 | regula-001 | 256075 | 25980 | 224 | 976 | 179 | 2048 ± 0 | 398 | 1284 ± 1 | 347 | 1220 ± 1 | 333 | 1222 ± 1 | 306 | 1226 ± 1 | 257 | 1255 ± 1 | 33 | 361 ± 10 | 32 | 342 ± 25 |
| 306 | remarkai-001 | 241857 | 868314 | 161 | 730 | 321 | 2052 ± 0 | 272 | 831 ± 6 | 234 | 849 ± 18 | 291 | 1055 ± 25 | 299 | 1198 ± 34 | 325 | 1519 ± 38 | 162 | 1229 ± 20 | 114 | 805 ± 56 |
| 307 | remarkai-003 | 280516 | 58559 | 413 | 3896 | 418 | 4100 ± 0 | 328 | 986 ± 1 | 284 | 993 ± 1 | 267 | 992 ± 1 | 240 | 999 ± 3 | 198 | 1019 ± 2 | 112 | 787 ± 20 | 111 | 793 ± 22 |
| 308 | rendip-000 | 0 | 437653 | 143 | 682 | 221 | 2048 ± 0 | 115 | 464 ± 2 | 91 | 458 ± 0 | 79 | 473 ± 0 | 70 | 483 ± 1 | 73 | 556 ± 4 | 55 | 576 ± 13 | 57 | 573 ± 11 |

Notes
 1 The configuration size does not capture static data included in libraries.
 2 The library size is the combined total of all files provided in the submission lib folder. These libraries e.g. OpenCV may or may not be installed on any end user's platform natively and would not need to be installed with the algorithm. Some developers put neural network models in their libraries.
 3 The memory usage is the peak resident set size reported by the ps system call during template generation.
 4 The median template creation times are measured on Intel® Xeon® CPU E5-2630 v4 @ 2.20GHz processors.
 5 The comparison durations, in nanoseconds, are estimated using std::chrono::high_resolution_clock which on the machine in (2) counts 1ns clock ticks. Precision is somewhat worse than that however. The ± value is the median absolute deviation times 1.48 for Normal consistency.

| ALGORITHM | | | CONFIG | | LIBRARY | TEMPLATE | | | | | | COMPARISON ⁴ | | | | | | | | | |
|-----------|--------------------|---------|-------------------|-------------------|-------------------|----------|-----------------------------------|----------|-----------|-----------|------------------------|-------------------------|-----------|----------|-----------|------------|-------------|-----------|-----------------|-----------|-----------------|
| NAME | | | DATA | DATA | MEMORY | SIZE | GENERATION TIME (ms) ⁴ | | | | TIME (ns) ⁵ | | | | | | | | | | |
| | | | (KB) ¹ | (KB) ² | (MB) ³ | (B) | MUGSHOT | 480x720 | 960x1440 | 1600x2400 | 3000x4500 | GENUINE | IMPOSTOR | | | | | | | | |
| 309 | revealmedia-005 | 293933 | 202465 | 171 | 763 | 415 | 4100 ± 0 | 102 | 428 ± 0 | 80 | 428 ± 0 | 64 | 430 ± 0 | 58 | 433 ± 0 | 46 | 442 ± 0 | 227 | 2023 ± 38 | 227 | 2009 ± 26 |
| 310 | revealmedia-006 | 293933 | 200912 | 166 | 741 | 322 | 2052 ± 0 | 86 | 381 ± 0 | 66 | 381 ± 0 | 50 | 382 ± 0 | 45 | 384 ± 0 | 38 | 394 ± 0 | 75 | 626 ± 35 | 67 | 600 ± 2 |
| 311 | rokid-000 | 258612 | 396624 | 267 | 1218 | 348 | 2056 ± 0 | 148 | 546 ± 3 | 123 | 542 ± 2 | 108 | 545 ± 1 | 83 | 522 ± 3 | 76 | 563 ± 4 | 285 | 3457 ± 62 | 286 | 3463 ± 77 |
| 312 | rokid-001 | 641223 | 413733 | 240 | 1071 | 361 | 2060 ± 0 | 302 | 911 ± 2 | 259 | 901 ± 5 | 229 | 899 ± 2 | 207 | 900 ± 3 | 169 | 901 ± 3 | 280 | 3345 ± 50 | 280 | 3346 ± 149 |
| 313 | s1-004 | 246514 | 202623 | 151 | 700 | 277 | 2048 ± 0 | 263 | 815 ± 0 | 200 | 818 ± 1 | 179 | 820 ± 1 | 151 | 828 ± 1 | 278 | 3245 ± 100 | 277 | 3161 ± 88 | | |
| 314 | s1-005 | 482369 | 95685 | 257 | 1137 | 374 | 2048 ± 0 | 332 | 1001 ± 0 | 288 | 1002 ± 0 | 273 | 1004 ± 0 | 243 | 1008 ± 0 | 200 | 1029 ± 2 | 76 | 626 ± 74 | 59 | 589 ± 14 |
| 315 | saffe-001 | 85973 | 62488 | 32 | 168 | 91 | 1280 ± 0 | 49 | 281 ± 1 | - | - | - | - | - | - | 163 | 1274 ± 19 | 165 | 1277 ± 26 | | |
| 316 | saffe-002 | 260622 | 28285 | 197 | 855 | 175 | 2048 ± 0 | 265 | 817 ± 11 | 219 | 805 ± 15 | 195 | 809 ± 19 | 176 | 815 ± 29 | 148 | 813 ± 23 | 97 | 717 ± 7 | 97 | 714 ± 29 |
| 317 | samsungsds-000 | 0 | 307431 | 244 | 1083 | 110 | 2048 ± 0 | 63 | 316 ± 0 | 52 | 326 ± 5 | 37 | 328 ± 4 | 26 | 343 ± 0 | 394 | 23722 ± 295 | 394 | 23874 ± 305 | | |
| 318 | samsungsds-001 | 1189592 | 147444 | 412 | 3893 | 400 | 4096 ± 0 | 359 | 1140 ± 3 | 328 | 1145 ± 4 | 365 | 1344 ± 5 | 348 | 1366 ± 5 | 323 | 1514 ± 7 | 423 | 51559 ± 773 | 423 | 51721 ± 1003 |
| 319 | samtech-001 | 288082 | 219883 | 126 | 605 | 354 | 2056 ± 0 | 53 | 294 ± 3 | - | - | - | - | - | - | 347 | 7694 ± 59 | 347 | 7678 ± 91 | | |
| 320 | scanovate-002 | 256986 | 457227 | 196 | 850 | 191 | 2048 ± 0 | 227 | 696 ± 32 | 192 | 713 ± 33 | 180 | 738 ± 28 | 167 | 779 ± 32 | 240 | 1172 ± 53 | 269 | 3021 ± 38 | 274 | 3120 ± 163 |
| 321 | scanovate-003 | 135585 | 89469 | 181 | 808 | 223 | 2048 ± 0 | 167 | 585 ± 1 | 151 | 613 ± 12 | 123 | 591 ± 1 | 108 | 610 ± 2 | 109 | 684 ± 1 | 264 | 2926 ± 22 | 264 | 2925 ± 20 |
| 322 | securifai-004 | 282177 | 12027 | 133 | 636 | 243 | 2048 ± 0 | 283 | 869 ± 1 | 241 | 867 ± 1 | 213 | 867 ± 1 | 193 | 867 ± 1 | 164 | 865 ± 1 | 194 | 1711 ± 19 | 195 | 1705 ± 29 |
| 323 | securifai-005 | 252532 | 81777 | 101 | 525 | 231 | 2048 ± 0 | 418 | 1377 ± 2 | 380 | 1355 ± 1 | 368 | 1353 ± 0 | 343 | 1357 ± 0 | 282 | 1356 ± 0 | 215 | 1873 ± 25 | | |
| 324 | sensetime-006 | 765353 | 37673 | 431 | 5994 | 79 | 1028 ± 0 | 413 | 1352 ± 17 | 370 | 1311 ± 1 | 360 | 1323 ± 1 | 342 | 1357 ± 1 | 326 | 1523 ± 2 | 158 | 1179 ± 28 | 159 | 1157 ± 29 |
| 325 | sensetime-007 | 765353 | 37533 | 429 | 5699 | 78 | 1028 ± 0 | 423 | 1386 ± 41 | 375 | 1323 ± 2 | 367 | 1347 ± 2 | 347 | 1366 ± 2 | 334 | 1593 ± 8 | 179 | 1460 ± 29 | 178 | 1425 ± 26 |
| 326 | sertis-000 | 265572 | 68770 | 70 | 427 | 230 | 2048 ± 0 | 241 | 754 ± 0 | 205 | 759 ± 0 | 180 | 764 ± 0 | 164 | 760 ± 0 | 138 | 763 ± 0 | 184 | 1497 ± 29 | 188 | 1582 ± 38 |
| 327 | sertis-002 | 460790 | 68929 | 295 | 1391 | 241 | 2048 ± 0 | 375 | 1181 ± 1 | 335 | 1178 ± 0 | 326 | 1183 ± 0 | 297 | 1187 ± 0 | 251 | 1221 ± 0 | 145 | 1086 ± 32 | 145 | 1076 ± 31 |
| 328 | seventhSense-000 | 369850 | 1561668 | 189 | 824 | 334 | 2052 ± 0 | 391 | 1250 ± 3 | 356 | 1257 ± 1 | 341 | 1261 ± 1 | 316 | 1259 ± 1 | 262 | 1272 ± 2 | 207 | 1800 ± 35 | 206 | 1787 ± 32 |
| 329 | seventhSense-001 | 369850 | 3183365 | 185 | 811 | 319 | 2052 ± 0 | 392 | 1255 ± 2 | 366 | 1294 ± 15 | 348 | 1277 ± 3 | 320 | 1275 ± 2 | 266 | 1288 ± 3 | 221 | 1936 ± 26 | 223 | 1943 ± 34 |
| 330 | shaman-000 | 0 | 120033 | 93 | 507 | 384 | 4096 ± 0 | 202 | 653 ± 16 | - | - | - | - | - | - | 36 | 380 ± 25 | 36 | 379 ± 31 | | |
| 331 | shaman-001 | 0 | 174446 | 97 | 511 | 396 | 4096 ± 0 | 56 | 294 ± 2 | - | - | - | - | - | - | 80 | 635 ± 19 | 41 | 441 ± 25 | | |
| 332 | shu-002 | 731250 | 148309 | 206 | 890 | 389 | 4096 ± 0 | 239 | 751 ± 2 | 208 | 769 ± 4 | 237 | 922 ± 4 | 370 | 1431 ± 9 | 382 | 3489 ± 47 | 444 | 2930763 ± 47355 | 444 | 2929759 ± 39149 |
| 333 | shu-003 | 428774 | 146940 | 96 | 511 | 295 | 2048 ± 0 | 267 | 820 ± 6 | 228 | 828 ± 3 | 240 | 941 ± 9 | 329 | 1308 ± 15 | 377 | 3045 ± 44 | 247 | 2506 ± 26 | 247 | 2512 ± 38 |
| 334 | siat-002 | 486842 | 7738 | 372 | 2434 | 320 | 2052 ± 0 | 164 | 579 ± 0 | - | - | - | - | - | - | 109 | 769 ± 13 | 106 | 750 ± 13 | | |
| 335 | siat-005 | 380936 | 16935 | 281 | 1298 | 216 | 2048 ± 0 | 91 | 403 ± 0 | 72 | 400 ± 0 | 54 | 401 ± 0 | 50 | 403 ± 1 | 44 | 422 ± 7 | 56 | 577 ± 13 | 58 | 580 ± 17 |
| 336 | sjtu-003 | 480795 | 148243 | 108 | 538 | 120 | 2048 ± 0 | 269 | 821 ± 2 | 223 | 820 ± 2 | 239 | 923 ± 3 | 301 | 1201 ± 3 | 359 | 2373 ± 9 | 186 | 1560 ± 20 | 185 | 1560 ± 14 |
| 337 | sjtu-004 | 1953267 | 241108 | 380 | 2727 | 427 | 4608 ± 0 | 385 | 1236 ± 2 | 344 | 1209 ± 2 | 352 | 1294 ± 4 | 381 | 1554 ± 5 | 371 | 2738 ± 8 | 273 | 3057 ± 14 | 3070 | 20 ± 20 |
| 338 | sktelecom-000 | 527132 | 298496 | 284 | 1311 | 94 | 1536 ± 0 | 355 | 1110 ± 1 | 316 | 1113 ± 1 | 300 | 1114 ± 1 | 266 | 1120 ± 1 | 232 | 1155 ± 1 | 401 | 26583 ± 128 | 400 | 26508 ± 126 |
| 339 | smartbiometrik-001 | 30875 | 92620 | 7 | 71 | 21 | 512 ± 0 | 186 | 620 ± 7 | 158 | 625 ± 7 | 147 | 640 ± 4 | 154 | 728 ± 6 | 205 | 1047 ± 8 | 92 | 703 ± 31 | 95 | 710 ± 40 |
| 340 | smartengines-000 | 1711 | 3025 | 4 | 50 | 10 | 288 ± 0 | 24 | 168 ± 7 | 20 | 180 ± 1 | 18 | 188 ± 3 | 20 | 217 ± 3 | 21 | 275 ± 1 | 9 | 197 ± 5 | 7 | 167 ± 11 |
| 341 | smartengines-001 | 7095 | 4601 | 3 | 46 | 11 | 288 ± 0 | 69 | 333 ± 89 | 74 | 408 ± 1 | 63 | 423 ± 1 | 62 | 460 ± 2 | 70 | 553 ± 5 | 6 | 153 ± 11 | 5 | 143 ± 13 |
| 342 | smartvist-000 | 5959 | 134084 | 29 | 165 | 37 | 512 ± 0 | 759 ± 0 | 56 ± 0 | 456 ± 0 | 458 ± 0 | 50 | 90 ± 1 | 178 | 1435 ± 31 | 177 | 1422 ± 48 | | | | |
| 343 | smilart-002 | 111826 | 87805 | 46 | 263 | 72 | 1024 ± 0 | 27 | 176 ± 16 | - | - | - | - | - | - | 385 | 18784 ± 136 | 386 | 18795 ± 151 | | |
| 344 | smilart-003 | 67339 | 91670 | 38 | 192 | 512 ± 0 | 29 | 180 ± 12 | 21 | 181 ± 10 | 33 | 313 ± 22 | 129 | 665 ± 49 | 356 | 2299 ± 196 | 171 | 1395 ± 74 | 137 | 1027 ± 66 | |
| 345 | sodec-000 | 836592 | 13142 | 402 | 3186 | 386 | 4096 ± 0 | 347 | 1041 ± 2 | 300 | 1032 ± 1 | 251 | 1037 ± 2 | 214 | 1061 ± 2 | 205 | 1794 ± 37 | 203 | 1775 ± 23 | | |
| 346 | sqisoft-001 | 278968 | 386291 | 146 | 688 | 352 | 2056 ± 0 | 122 | 477 ± 5 | 379 | 1348 ± 18 | 369 | 1353 ± 26 | 337 | 1340 ± 14 | 297 | 1393 ± 28 | 113 | 797 ± 22 | 110 | 788 ± 22 |
| 347 | sqisoft-002 | 278039 | 386291 | 138 | 666 | 357 | 2056 ± 0 | 118 | 466 ± 8 | 94 | 466 ± 2 | 77 | 468 ± 11 | 63 | 461 ± 6 | 52 | 472 ± 4 | 107 | 758 ± 11 | 107 | 760 ± 23 |
| 348 | stacu-000 | 879661 | 624676 | 238 | 1064 | 411 | 4096 ± 0 | 261 | 813 ± 25 | - | - | - | - | - | - | 266 | 2979 ± 31 | 269 | 3007 ± 75 | | |
| 349 | starhybrid-001 | 100509 | 289356 | 194 | 845 | 157 | 2048 ± 0 | 78 | 358 ± 82 | 59 | 355 ± 49 | 48 | 379 ± 58 | 49 | 401 ± 79 | 37 | 393 ± 67 | 142 | 1075 ± 51 | 146 | 1078 ± 53 |
| 350 | sukshi-000 | 94035 | 688738 | 62 | 372 | 443 | 32768 ± 0 | 95 | 407 ± 11 | 75 | 413 ± 8 | 90 | 504 ± 8 | 137 | 689 ± 11 | 332 | 1574 ± 28 | 356 | 9817 ± 50 | 355 | 9787 ± 62 |
| 351 | suprema-002 | 373808 | 41473 | 331 | 1731 | 172 | 2048 ± 0 | 254 | 787 ± 3 | 230 | 833 ± 3 | 240 | 924 ± 4 | 293 | 1185 ± 6 | 366 | 2479 ± 3 | 279 | 3255 ± 17 | 279 | 3253 ± 14 |
| 352 | suprema-003 | 498231 | 116054 | 268 | 1239 | 171 | 2048 ± 0 | 436 | 1448 ± 1 | 399 | 1417 ± 4 | 392 | 1418 ± 3 | 368 | 1421 ± 4 | 311 | 1451 ± 5 | 236 | 2201 ± 10 | 238 | 2198 ± 13 |

Notes

- 1 The configuration size does not capture static data included in libraries.
- 2 The library size is the combined total of all files provided in the submission lib folder. These libraries e.g. OpenCV may or may not be installed on any end user's platform natively and would not need to be installed with the algorithm. Some developers put neural network models in their libraries.
- 3 The memory usage is the peak resident set size reported by the ps system call during template generation.
- 4 The median template creation times are measured on Intel® Xeon® CPU E5-2630 v4 @ 2.20GHz processors.
- 5 The comparison durations, in nanoseconds, are estimated using std::chrono::high_resolution_clock which on the machine in (2) counts 1ns clock ticks. Precision is somewhat worse than that however. The ± value is the median absolute deviation times 1.48 for Normal consistency.

Table 15: Summary of algorithms and properties included in this report. The red superscripts give ranking for the quantity in that column.

| | ALGORITHM | CONFIG | LIBRARY | TEMPLATE | | | | | | | | COMPARISON ⁴ | | | | | | | | | |
|-----|-------------------|---------|---------|----------|------|------|--------------|------|-----------------------------------|-------------------|-------------------|-------------------------|------------------------|---------|------------|-----------|-------------|---------------|--------------|---------------|-------------|
| | | | | NAME | DATA | DATA | MEMORY | SIZE | GENERATION TIME (ms) ⁴ | | | | TIME (ns) ⁵ | | | | | | | | |
| | | | | | | | | | (KB) ¹ | (KB) ² | (MB) ³ | (B) | MUGSHOT | 480x720 | 960x1440 | 1600x2400 | 3000x4500 | GENUINE | IMPOSTOR | | |
| 353 | supremaid-001 | 258193 | 23479 | 109 | 541 | 200 | 2048 ± 0 | 123 | 479 ± 1 | 98 | 481 ± 0 | 81 | 481 ± 0 | 74 | 490 ± 0 | 64 | 522 ± 0 | 93 | 704 ± 19 | 86 | 652 ± 19 |
| 354 | supremaid-002 | 256273 | 23899 | 55 | 335 | 270 | 2048 ± 0 | 127 | 483 ± 0 | 111 | 501 ± 0 | 84 | 488 ± 0 | 78 | 503 ± 0 | 77 | 565 ± 0 | 225 | 1990 ± 19 | 219 | 1923 ± 29 |
| 355 | surrey-cvssp-000 | 158030 | 70795 | 204 | 879 | 129 | 2048 ± 0 | 361 | 1141 ± 3 | 331 | 1157 ± 3 | 316 | 1158 ± 4 | 284 | 1163 ± 3 | 255 | 1245 ± 3 | 354 | 9557 ± 143 | 353 | 9602 ± 186 |
| 356 | synesis-006 | 731941 | 21817 | 306 | 1472 | 420 | 4104 ± 0 | 149 | 549 ± 1 | 126 | 546 ± 1 | 110 | 552 ± 1 | 92 | 558 ± 2 | 100 | 639 ± 28 | 91 | 697 ± 32 | 94 | 688 ± 31 |
| 357 | synesis-007 | 1442961 | 24145 | 373 | 2443 | 374 | 3080 ± 0 | 381 | 1215 ± 5 | 359 | 1268 ± 30 | 356 | 1306 ± 67 | 330 | 1311 ± 58 | 306 | 1423 ± 52 | 86 | 684 ± 32 | 92 | 686 ± 25 |
| 358 | synology-000 | 221021 | 25809 | 78 | 453 | 192 | 2048 ± 0 | 94 | 407 ± 14 | 76 | 415 ± 14 | 166 | 694 ± 31 | 358 | 1396 ± 58 | 384 | 4568 ± 211 | 389 | 19720 ± 203 | 388 | 19767 ± 379 |
| 359 | synology-002 | 256713 | 25943 | 88 | 488 | 186 | 2048 ± 0 | 297 | 886 ± 4 | 256 | 892 ± 3 | 235 | 920 ± 2 | 241 | 1000 ± 5 | 272 | 1317 ± 12 | 181 | 1466 ± 32 | 183 | 1496 ± 45 |
| 360 | sztu-000 | 338637 | 15871 | 279 | 1298 | 254 | 2048 ± 0 | 143 | 531 ± 0 | 117 | 532 ± 0 | 100 | 533 ± 0 | 86 | 537 ± 0 | 68 | 548 ± 0 | 57 | 585 ± 11 | 62 | 592 ± 13 |
| 361 | sztu-001 | 338650 | 15871 | 280 | 1298 | 153 | 2048 ± 0 | 144 | 535 ± 0 | 121 | 537 ± 0 | 103 | 538 ± 0 | 87 | 540 ± 0 | 71 | 553 ± 0 | 62 | 599 ± 10 | 66 | 598 ± 10 |
| 362 | t4isb-000 | 234227 | 115237 | 57 | 343 | 105 | 2048 ± 0 | 331 | 1006 ± 5 | 287 | 1001 ± 1 | 276 | 1006 ± 1 | 244 | 1009 ± 1 | 199 | 1022 ± 2 | 290 | 3586 ± 34 | 288 | 3534 ± 34 |
| 363 | tech5-004 | 2410272 | 118858 | 387 | 2733 | 13 | 321 ± 0 | 286 | 872 ± 2 | 317 | 1117 ± 164 | 301 | 1114 ± 182 | 273 | 1134 ± 179 | 194 | 999 ± 44 | 61 | 597 ± 13 | 61 | 592 ± 16 |
| 364 | tech5-005 | 1178769 | 120517 | 300 | 1426 | 17 | 512 ± 0 | 396 | 1272 ± 109 | 304 | 1038 ± 63 | 290 | 1046 ± 39 | 267 | 1124 ± 38 | 281 | 1351 ± 44 | 251 | 2573 ± 37 | 251 | 2545 ± 32 |
| 365 | techsign-000 | 0 | 1101622 | 352 | 1955 | 136 | 2048 ± 0 | 82 | 366 ± 1 | 71 | 398 ± 1 | 320 | 1172 ± 3 | 408 | 3065 ± 18 | 405 | 10460 ± 65 | 309 | 4758 ± 112 | 308 | 4789 ± 93 |
| 366 | techsign-001 | 0 | 586983 | 334 | 1741 | 164 | 2048 ± 0 | 248 | 772 ± 35 | 212 | 788 ± 23 | 194 | 802 ± 42 | 224 | 949 ± 10 | 301 | 1409 ± 26 | 58 | 592 ± 11 | 63 | 592 ± 13 |
| 367 | tevian-007 | 779934 | 19523 | 330 | 1714 | 80 | 1032 ± 0 | 166 | 583 ± 1 | 138 | 579 ± 0 | 119 | 580 ± 0 | 101 | 588 ± 1 | 98 | 636 ± 0 | 314 | 4894 ± 65 | 311 | 4841 ± 83 |
| 368 | tevian-008 | 847177 | 19519 | 404 | 3490 | 81 | 1032 ± 0 | 296 | 884 ± 2 | 261 | 903 ± 1 | 228 | 903 ± 1 | 209 | 911 ± 1 | 181 | 946 ± 1 | 311 | 4828 ± 40 | 310 | 4811 ± 41 |
| 369 | tiger-005 | 342866 | 253734 | 311 | 1531 | 332 | 2052 ± 0 | 350 | 1097 ± 2 | 309 | 1065 ± 2 | 295 | 1066 ± 2 | 259 | 1067 ± 3 | 218 | 1088 ± 3 | 71 | 620 ± 19 | 75 | 615 ± 16 |
| 370 | tiger-006 | 421186 | 394688 | 154 | 707 | 333 | 2052 ± 0 | 424 | 1392 ± 16 | 398 | 1411 ± 10 | 380 | 1531 ± 11 | 348 | 1848 ± 10 | 210 | 1810 ± 20 | 209 | 1801 ± 13 | | |
| 371 | tinkoff-001 | 274660 | 389272 | 123 | 592 | 310 | 2048 ± 0 | 370 | 1176 ± 3 | 337 | 1179 ± 3 | 321 | 1178 ± 3 | 287 | 1169 ± 2 | 246 | 1203 ± 3 | 304 | 4361 ± 74 | 302 | 4364 ± 75 |
| 372 | tongyi-005 | 1140701 | 138919 | 362 | 2121 | 368 | 2089 ± 0 | 23 | 165 ± 1 | - | - | - | - | - | - | - | - | 386 | 18924 ± 65 | 389 | 20158 ± 103 |
| 373 | toppannidgate-000 | 671181 | 711850 | 338 | 1786 | 378 | 4096 ± 0 | 304 | 915 ± 1 | 263 | 916 ± 1 | 233 | 916 ± 1 | 211 | 917 ± 1 | 174 | 917 ± 1 | 399 | 25262 ± 84 | 398 | 25264 ± 97 |
| 374 | toshiba-004 | 599297 | 27880 | 320 | 1595 | 342 | 2056 ± 0 | 434 | 1447 ± 3 | 403 | 1453 ± 2 | 398 | 1457 ± 9 | 371 | 1457 ± 3 | 318 | 1479 ± 4 | 134 | 1020 ± 25 | 131 | 998 ± 32 |
| 375 | toshiba-006 | 599566 | 44078 | 318 | 1588 | 347 | 2056 ± 0 | 442 | 1481 ± 16 | 408 | 1515 ± 7 | 402 | 1506 ± 6 | 378 | 1521 ± 2 | 329 | 1546 ± 30 | 135 | 1022 ± 17 | 136 | 1022 ± 23 |
| 376 | touchlessid-000 | 92561 | 64467 | 157 | 716 | 215 | 2048 ± 0 | 62 | 309 ± 5 | 45 | 305 ± 2 | 32 | 312 ± 5 | 26 | 277 ± 4 | 28 | 349 ± 17 | 409 | 31935 ± 292 | 410 | 31958 ± 243 |
| 377 | trueface-002 | 253947 | 123116 | 87 | 486 | 99 | 2000 ± 0 | 79 | 360 ± 0 | 61 | 361 ± 0 | 61 | 423 ± 0 | 104 | 590 ± 1 | - | 8 | 192 ± 14 | 10 | 186 ± 19 | |
| 378 | trueface-003 | 346530 | 24308 | 414 | 3915 | 177 | 2048 ± 0 | 353 | 1107 ± 22 | 179 | 677 ± 3 | 179 | 732 ± 7 | 208 | 905 ± 5 | - | 1 | 103 ± 11 | 2 | 112 ± 29 | |
| 379 | tuputech-000 | 11476 | 17185 | 23 | 33 | 211 | 2048 ± 0 | 20 | 122 ± 4 | 14 | 120 ± 1 | 13 | 142 ± 2 | 17 | 196 ± 5 | 40 | 411 ± 14 | 395 | 23893 ± 406 | 399 | 25279 ± 406 |
| 380 | turingtechvip-001 | 399874 | 54535 | 131 | 617 | 285 | 2048 ± 0 | 421 | 1384 ± 4 | 391 | 1391 ± 1 | 383 | 1393 ± 1 | 369 | 1411 ± 1 | 317 | 1476 ± 2 | 199 | 1733 ± 19 | 199 | 1734 ± 20 |
| 381 | turingtechvip-002 | 167556 | 140995 | 203 | 876 | 127 | 2048 ± 0 | 444 | 1493 ± 2 | 369 | 1306 ± 1 | 378 | 1382 ± 1 | 336 | 1337 ± 1 | 308 | 1426 ± 3 | 374 | 13819 ± 103 | 374 | 13807 ± 137 |
| 382 | twface-000 | 661735 | 11782 | 380 | 2610 | 229 | 2048 ± 0 | 284 | 871 ± 1 | 245 | 873 ± 1 | 216 | 876 ± 2 | 167 | 898 ± 1 | 185 | 1504 ± 29 | 184 | 1510 ± 34 | | |
| 383 | twface-001 | 671511 | 11782 | 394 | 2855 | 118 | 2048 ± 0 | 308 | 923 ± 1 | 267 | 925 ± 2 | 241 | 926 ± 1 | 214 | 929 ± 2 | 179 | 940 ± 2 | 173 | 1400 ± 32 | 174 | 1402 ± 37 |
| 384 | ulsee-001 | 370519 | 57261 | - | - | 311 | 2048 ± 0 | 203 | 654 ± 2 | - | - | - | - | - | - | - | 334 | 6065 ± 94 | 335 | 6228 ± 77 | |
| 385 | uluface-002 | 0 | 480761 | 249 | 1088 | 102 | 2048 ± 0 | 290 | 873 ± 42 | 236 | 855 ± 9 | 260 | 978 ± 24 | 317 | 1271 ± 40 | 357 | 2333 ± 68 | 388 | 19207 ± 1114 | 385 | 18501 ± 274 |
| 386 | uluface-003 | 97357 | 529422 | 271 | 1264 | 372 | 3072 ± 0 | 321 | 965 ± 11 | 279 | 968 ± 10 | 296 | 1087 ± 20 | 354 | 1387 ± 36 | 365 | 2469 ± 86 | 400 | 26057 ± 195 | 402 | 26865 ± 566 |
| 387 | unissey-001 | 0 | 1956593 | 318 | 1584 | 399 | 4096 ± 0 | 294 | 880 ± 3 | 255 | 892 ± 3 | 397 | 1452 ± 8 | 407 | 3048 ± 12 | 403 | 10017 ± 387 | 180 | 1463 ± 35 | 181 | 1471 ± 34 |
| 388 | unissey-002 | 0 | 1443765 | 170 | 763 | 410 | 4096 ± 0 | 236 | 736 ± 1 | 203 | 752 ± 1 | 268 | 994 ± 1 | 369 | 1426 ± 1 | 381 | 3331 ± 2 | 368 | 12308 ± 91 | 368 | 12302 ± 137 |
| 389 | upc-001 | 0 | 89914 | 243 | 1077 | 84 | 1052 ± 0 | 151 | 551 ± 15 | 189 | 703 ± 56 | 177 | 724 ± 51 | 167 | 751 ± 49 | 162 | 863 ± 33 | 275 | 3114 ± 44 | 278 | 3165 ± 97 |
| 390 | vcog-002 | 3229434 | 118946 | 406 | 3666 | 444 | 61504 ± 5 | 77 | 357 ± 25 | - | - | - | - | - | - | - | 441 | 296154 ± 3077 | 441 | 296436 ± 4183 | |
| 391 | vd-002 | 254498 | 34389 | 147 | 688 | 48 | 516 ± 0 | 219 | 684 ± 5 | 180 | 679 ± 4 | 157 | 676 ± 5 | 139 | 693 ± 5 | 133 | 754 ± 5 | 23 | 300 ± 14 | 26 | 319 ± 32 |
| 392 | vd-003 | 254505 | 44051 | 149 | 696 | 329 | 2052 ± 0 | 224 | 691 ± 5 | 184 | 690 ± 5 | 159 | 683 ± 4 | 138 | 691 ± 5 | 124 | 722 ± 5 | 132 | 1003 ± 11 | 132 | 1001 ± 7 |
| 393 | veridas-006 | 355669 | 896424 | 357 | 1990 | 193 | 2048 ± 0 | 295 | 880 ± 8 | 254 | 885 ± 8 | 345 | 1271 ± 18 | 400 | 2242 ± 38 | 396 | 6414 ± 156 | 426 | 56940 ± 149 | 430 | 66077 ± 194 |
| 394 | veridas-007 | 355105 | 891492 | 376 | 2527 | 116 | 2048 ± 0 | 288 | 872 ± 9 | 246 | 875 ± 8 | 340 | 1261 ± 18 | 399 | 2238 ± 38 | 394 | 6374 ± 147 | 85 | 655 ± 16 | 88 | 660 ± 19 |
| 395 | veridium-000 | 0 | 47198 | 16 | 98 | 442 | 29399 ± 2045 | 10 | 79 ± 0 | 8 | 80 ± 0 | 9 | 89 ± 0 | 7 | 90 ± 0 | 7 | 111 ± 0 | 430 | 64880 ± 171 | 429 | 64697 ± 247 |
| 396 | verigram-000 | 256209 | 7798 | 342 | 1842 | 247 | 2048 ± 0 | 257 | 807 ± 1 | 224 | 821 ± 1 | 257 | 972 ± 2 | 344 | 1358 ± 3 | 374 | 2848 ± 13 | 161 | 1222 ± 17 | 162 | 1219 ± 17 |

Notes

1 The configuration size does not capture static data included in libraries.

2 The library size is the combined total of all files provided in the submission lib folder. These libraries e.g. OpenCV may or may not be installed on any end user's platform natively and would not need to be installed with the algorithm. Some developers put neural network models in their libraries.

3 The memory usage is the peak resident set size reported by the ps system call during template generation.

4 The median template creation times are measured on Intel® Xeon® CPU E5-2630 v4 @ 2.20GHz processors.

5 The comparison durations, in nanoseconds, are estimated using std::chrono::high_resolution_clock which on the machine in (2) counts 1ns clock ticks. Precision is somewhat worse than that however. The ± value is the median absolute deviation times 1.48 for Normal consistency.

| | ALGORITHM | CONFIG | LIBRARY | TEMPLATE | | | | | | | | COMPARISON ⁴ | | | | | | |
|-----|---------------------------|---------|---------|---------------------|-------------------------|-------------------------|--------------------------|--------------------------|-----------------------------------|---------------------------|-----------------------------|-----------------------------|------------------------|---------|----------|-----------|-----------|---------|
| | | | | NAME | DATA | DATA | MEMORY | SIZE | GENERATION TIME (ms) ⁴ | | | | TIME (ns) ⁵ | | | | | |
| | | | | | | | | | (KB) ¹ | (KB) ² | (MB) ³ | (B) | MUGSHOT | 480x720 | 960x1440 | 1600x2400 | 3000x4500 | GENUINE |
| 397 | verigram-001 | 282155 | 11773 | ³⁸² 2638 | ²⁸⁷ 2048 ± 0 | ²⁰⁸ 664 ± 2 | ¹⁷⁷ 675 ± 2 | ²⁰⁶ 833 ± 4 | ³⁰² 1202 ± 7 | ³⁷⁰ 2733 ± 32 | ¹⁹² 1664 ± 60 | ¹⁹⁰ 1648 ± 56 | | | | | | |
| 398 | verihubs-inteligensia-000 | 209562 | 51877 | ⁷¹ 427 | ²⁷⁶ 2048 ± 0 | ¹⁵⁷ 567 ± 0 | ⁴⁰⁹ 1558 ± 8 | ⁴⁰⁵ 1560 ± 8 | ³⁸² 1568 ± 8 | ³³⁶ 1621 ± 8 | ³⁹³ 22351 ± 91 | ³⁹³ 22371 ± 81 | | | | | | |
| 399 | verihubs-inteligensia-001 | 216524 | 51916 | ⁷³ 437 | ¹³³ 2048 ± 0 | ¹⁵⁶ 564 ± 0 | ¹³² 562 ± 0 | ¹¹⁴ 566 ± 1 | ⁹⁴ 566 ± 0 | ⁸⁵ 600 ± 0 | ³⁹¹ 21770 ± 84 | ³⁹¹ 21735 ± 102 | | | | | | |
| 400 | verijelas-000 | 254540 | 10322 | ³³³ 1736 | ³⁰² 2048 ± 0 | ⁶⁴ 321 ± 0 | ⁵¹ 325 ± 1 | ³⁸ 329 ± 0 | ³⁵ 335 ± 5 | ³⁰ 360 ± 0 | ³⁵⁸ 10267 ± 143 | ³⁵⁸ 10218 ± 109 | | | | | | |
| 401 | via-000 | 124422 | 11151 | ²²² 964 | ¹³⁴ 2048 ± 0 | ²³¹ 707 ± 8 | ¹⁹⁹ 740 ± 5 | ²²⁹ 906 ± 41 | ²²⁰ 941 ± 40 | ²⁰³ 1040 ± 5 | ¹²⁰ 966 ± 28 | ¹³⁵ 1021 ± 44 | | | | | | |
| 402 | via-001 | 370255 | 11151 | ³²⁶ 1697 | ¹⁰³ 2048 ± 0 | ³²⁰ 964 ± 3 | ²⁹³ 1011 ± 3 | ²⁸¹ 1026 ± 4 | ²⁵⁴ 1045 ± 3 | ²²⁸ 1137 ± 28 | ¹²⁸ 983 ± 31 | ¹²⁹ 989 ± 40 | | | | | | |
| 403 | videmo-000 | 139643 | 39470 | ⁶³ 390 | ²⁰⁸ 2048 ± 0 | ²¹ 142 ± 5 | ¹⁵ 150 ± 4 | ¹⁴ 150 ± 6 | ¹¹ 151 ± 4 | ¹⁰ 155 ± 8 | ⁴⁹ 513 ± 16 | ⁵⁰ 523 ± 38 | | | | | | |
| 404 | videmo-001 | 212051 | 95063 | ⁵⁴ 304 | ¹⁴⁷ 2048 ± 0 | ³⁵ 199 ± 0 | ¹⁷ 164 ± 0 | ¹⁵ 164 ± 0 | ¹² 164 ± 0 | ¹¹ 165 ± 0 | ²¹ 296 ± 17 | ²² 288 ± 16 | | | | | | |
| 405 | videonetics-001 | 30875 | 5963 | ⁹ 61 | ²⁴ 512 ± 0 | ⁴¹ 262 ± 3 | ³⁵ 273 ± 1 | ⁶⁸ 439 ± 3 | ¹⁷⁸ 820 ± 3 | ³⁶² 2393 ± 43 | ¹⁵³ 1153 ± 38 | ¹⁵⁵ 1142 ± 65 | | | | | | |
| 406 | videonetics-002 | 121981 | 6289 | ¹⁹ 115 | ³²³ 2052 ± 0 | ⁵² 282 ± 5 | ⁴³ 295 ± 1 | ⁹⁵ 513 ± 4 | ²⁴⁸ 1029 ± 3 | ³⁷⁹ 3151 ± 46 | ¹⁶⁰ 1219 ± 57 | ¹⁶³ 1262 ± 56 | | | | | | |
| 407 | viettelhightech-000 | 259471 | 215557 | ⁶⁹ 419 | ¹²² 2048 ± 0 | ¹¹³ 461 ± 1 | ⁹³ 461 ± 2 | ⁷³ 461 ± 1 | ⁶⁶ 467 ± 2 | ⁵⁵ 494 ± 0 | ⁶³ 599 ± 11 | ⁶⁰ 591 ± 13 | | | | | | |
| 408 | vigilantsolutions-010 | 348798 | 49973 | ¹⁹² 840 | ⁹⁶ 1548 ± 0 | ¹⁸⁵ 615 ± 0 | ¹⁶² 631 ± 0 | ¹⁴¹ 632 ± 0 | ¹¹⁹ 636 ± 0 | ¹⁰³ 659 ± 0 | ⁴⁷ 490 ± 13 | ⁴⁸ 488 ± 11 | | | | | | |
| 409 | vigilantsolutions-011 | 255661 | 49973 | ¹²² 591 | ⁹⁵ 1548 ± 0 | ⁹⁰ 402 ± 0 | ⁷⁷ 418 ± 0 | ⁶⁰ 418 ± 0 | ⁵⁴ 422 ± 0 | ⁴⁸ 445 ± 0 | ²⁹ 339 ± 20 | ³³ 366 ± 37 | | | | | | |
| 410 | vinai-000 | 402391 | 866522 | ²³³ 1032 | ¹²⁸ 2048 ± 0 | ³⁵¹ 1099 ± 1 | ³¹³ 1095 ± 1 | ²⁹⁸ 1093 ± 1 | ²⁶⁵ 1099 ± 1 | ²²⁶ 1126 ± 1 | ²⁶⁷ 2996 ± 20 | ²⁶⁸ 2993 ± 26 | | | | | | |
| 411 | vinbigdata-001 | 271405 | 44746 | ¹²¹ 589 | ²⁹² 2048 ± 0 | ⁴²⁹ 1400 ± 5 | ³⁹² 1393 ± 2 | ³⁸⁰ 1391 ± 2 | ³⁵⁵ 1393 ± 1 | ³⁰¹ 1404 ± 1 | ¹⁶⁸ 1351 ± 50 | ¹⁶⁸ 1310 ± 38 | | | | | | |
| 412 | vinbigdata-002 | 256322 | 138864 | ¹²⁸ 606 | ¹³⁵ 2048 ± 0 | ¹⁶¹ 569 ± 2 | ¹³⁶ 572 ± 1 | ¹¹⁵ 571 ± 1 | ⁹⁵ 572 ± 1 | ⁸³ 596 ± 1 | ²³⁴ 2175 ± 44 | ²³⁶ 2160 ± 53 | | | | | | |
| 413 | vion-000 | 228219 | 7533 | ⁹¹ 498 | ³²⁵ 2052 ± 0 | ⁷⁰ 333 ± 1 | - | - | - | - | ⁴¹³ 39839 ± 3561 | ⁴⁰¹ 26830 ± 2241 | | | | | | |
| 414 | visage-000 | 49218 | 70150 | ⁹ 73 | ²² 512 ± 0 | ⁴ 27 ± 0 | ² 27 ± 0 | ² 31 ± 0 | ³ 38 ± 0 | ³ 63 ± 0 | ²³⁷ 2220 ± 14 | ²³⁹ 2218 ± 14 | | | | | | |
| 415 | visionbox-001 | 256869 | 190645 | ¹¹⁸ 579 | ²⁰⁴ 2048 ± 0 | ³²⁶ 983 ± 7 | ³¹² 1093 ± 46 | ³⁷⁰ 1360 ± 68 | ³⁹⁷ 2181 ± 105 | ³⁹² 5955 ± 281 | ¹⁵⁵ 1161 ± 22 | ¹⁵⁸ 1154 ± 20 | | | | | | |
| 416 | visionbox-002 | 259063 | 135281 | ¹³⁰ 612 | ³⁶⁰ 2059 ± 0 | ¹²⁵ 482 ± 1 | ¹⁰⁰ 482 ± 0 | ⁸³ 484 ± 1 | ⁷⁶ 492 ± 1 | ⁶³ 517 ± 3 | ²²⁴ 1969 ± 44 | ²²² 1931 ± 42 | | | | | | |
| 417 | visionlabs-010 | 1067280 | 19357 | ²⁰⁷ 902 | ⁴⁴ 513 ± 0 | ²³⁴ 730 ± 0 | ¹⁹³ 717 ± 1 | ¹⁷² 709 ± 0 | ¹⁴⁹ 713 ± 1 | ¹³⁰ 739 ± 0 | ⁶⁵ 600 ± 41 | ⁷⁷ 626 ± 35 | | | | | | |
| 418 | visionlabs-011 | 1067280 | 19353 | ²⁰⁰ 862 | ⁴⁵ 513 ± 0 | ²³⁵ 731 ± 1 | ¹⁹⁴ 717 ± 1 | ¹⁷³ 710 ± 1 | ¹⁵⁰ 714 ± 1 | ¹³¹ 741 ± 1 | ⁵¹ 556 ± 26 | ⁵⁴ 559 ± 25 | | | | | | |
| 419 | visteam-003 | 215359 | 33730 | ⁸⁹ 489 | ³⁹² 4096 ± 0 | ³⁹⁰ 1249 ± 4 | ³⁵⁴ 1251 ± 4 | ³⁴⁴ 1266 ± 5 | ³¹⁸ 1272 ± 5 | ²⁸⁷ 1370 ± 9 | ³³⁸ 6816 ± 111 | ³³⁸ 6816 ± 105 | | | | | | |
| 420 | visteam-004 | 61594 | 35369 | ³³ 168 | ¹⁶⁹ 2048 ± 0 | ⁵⁷ 303 ± 5 | ⁴⁶ 313 ± 6 | ²⁹ 278 ± 4 | ²⁹ 288 ± 4 | ³³ 377 ± 7 | ²⁹⁷ 3936 ± 72 | ²⁹⁷ 3938 ± 79 | | | | | | |
| 421 | vixvzion-005 | 38886 | 534579 | ¹⁶³ 731 | ³⁰⁶ 2048 ± 0 | ¹⁰⁴ 433 ± 4 | ⁶⁵ 381 ± 3 | ⁵¹ 383 ± 3 | ⁴³ 373 ± 1 | ³⁹ 411 ± 1 | ¹⁰¹ 731 ± 63 | ⁷⁹ 632 ± 32 | | | | | | |
| 422 | vixvzion-006 | 594053 | 396294 | ²¹¹ 914 | ²³⁸ 2048 ± 0 | ²⁹² 876 ± 9 | ²²⁷ 828 ± 3 | ¹⁹⁹ 817 ± 1 | ¹⁸¹ 825 ± 2 | ¹⁶⁵ 871 ± 1 | ⁶⁴ 600 ± 23 | ⁷¹ 611 ± 25 | | | | | | |
| 423 | vnpt-003 | 369956 | 297997 | ¹⁵⁶ 714 | ³⁷⁷ 4096 ± 0 | ⁴⁰⁶ 1315 ± 4 | ³⁷¹ 1315 ± 4 | ³⁵⁹ 1318 ± 2 | ³³⁹ 1350 ± 3 | ³⁰⁹ 1428 ± 3 | ³⁴⁶ 7397 ± 31 | ³⁴⁵ 7384 ± 29 | | | | | | |
| 424 | vnpt-004 | 370110 | 240841 | ²²⁸ 988 | ³⁰³ 2048 ± 0 | ³⁸⁷ 1238 ± 1 | ³⁵⁰ 1241 ± 1 | ³³⁷ 1242 ± 2 | ³²⁶ 1307 ± 2 | ³²¹ 1505 ± 2 | ³⁰⁰ 4047 ± 48 | ²⁹⁹ 4008 ± 108 | | | | | | |
| 425 | vocord-009 | 1380132 | 201560 | ⁴¹⁹ 4162 | ⁹⁸ 1920 ± 0 | ⁴⁴⁰ 1472 ± 2 | ⁴⁰⁵ 1472 ± 1 | ⁴⁰⁴ 1549 ± 1 | ³⁸⁵ 1667 ± 2 | ³⁵¹ 2064 ± 2 | ²²⁸ 2052 ± 50 | ²³⁰ 2056 ± 39 | | | | | | |
| 426 | vocord-010 | 902552 | 206873 | ⁴¹⁰ 3858 | ⁸⁷ 1088 ± 0 | ⁴³⁷ 1459 ± 2 | ⁴⁰⁴ 1459 ± 1 | ³⁹⁹ 1463 ± 2 | ³⁷⁷ 1484 ± 1 | ³²⁷ 1535 ± 3 | ²⁵⁶ 2724 ± 31 | ²⁵⁴ 2653 ± 45 | | | | | | |
| 427 | vts-000 | 256589 | 169760 | ³²⁸ 1704 | ²⁸³ 2048 ± 0 | ¹²⁹ 486 ± 1 | ⁹⁹ 481 ± 0 | ⁸² 484 ± 0 | ⁷¹ 485 ± 1 | ⁶² 517 ± 0 | ⁴³⁸ 124209 ± 352 | ⁴³⁸ 123652 ± 358 | | | | | | |
| 428 | vts-001 | 293000 | 475743 | ¹³² 618 | ³⁰⁰ 2048 ± 0 | ²¹⁴ 676 ± 1 | ¹⁸¹ 683 ± 6 | ¹⁶³ 687 ± 3 | ¹⁴⁰ 695 ± 2 | ¹¹⁸ 709 ± 2 | ³⁵⁵ 9620 ± 44 | ³⁵⁴ 9618 ± 54 | | | | | | |
| 429 | wicket-000 | 826392 | 641802 | ³⁶⁰ 2071 | ¹²¹ 2048 ± 0 | ⁴³³ 1419 ± 2 | ⁴⁰⁰ 1429 ± 3 | ³⁹⁴ 1444 ± 4 | ³⁷² 1460 ± 3 | ³²⁸ 1537 ± 6 | ⁴²⁸ 60976 ± 232 | ⁴²⁷ 61096 ± 323 | | | | | | |
| 430 | winsense-001 | 264428 | 32035 | ²¹⁵ 922 | ⁸⁹ 1280 ± 0 | ²⁴⁴ 766 ± 7 | ³⁰⁷ 1058 ± 47 | ²⁶² 983 ± 97 | ²⁵⁵ 1053 ± 119 | ²⁷³ 1320 ± 84 | ¹⁸⁹ 1631 ± 28 | ²²⁵ 1964 ± 171 | | | | | | |
| 431 | winsense-002 | 281379 | 25780 | ³³⁷ 1781 | ¹⁸⁰ 2048 ± 0 | ¹³² 494 ± 2 | ¹⁰⁷ 498 ± 1 | ⁹⁷ 519 ± 1 | ⁸⁵ 537 ± 1 | ⁹⁶ 634 ± 1 | ¹⁹³ 1683 ± 8 | ¹⁹³ 1685 ± 7 | | | | | | |
| 432 | wuhantianyu-001 | 465118 | 66457 | ²⁰¹ 866 | ²⁶⁴ 2048 ± 0 | ¹⁹⁸ 642 ± 1 | ¹⁶⁷ 642 ± 1 | ¹⁴⁹ 644 ± 0 | ¹²⁵ 652 ± 0 | ¹¹⁵ 697 ± 0 | ³⁵³ 9502 ± 151 | ³⁵⁷ 9920 ± 253 | | | | | | |
| 433 | x-laboratory-000 | 52020 | 197310 | ³¹⁰ 1524 | ³⁴⁰ 2056 ± 0 | ²⁵⁸ 808 ± 7 | ²⁵⁸ 897 ± 113 | ²³⁰ 907 ± 103 | ¹⁹⁸ 886 ± 103 | ¹⁰⁸ 673 ± 39 | ⁹⁹ 725 ± 19 | ¹⁰⁵ 749 ± 34 | | | | | | |
| 434 | x-laboratory-001 | 625140 | 398792 | ³⁴³ 1844 | ³⁴⁹ 2056 ± 0 | ¹⁶⁹ 586 ± 2 | ¹⁴⁹ 596 ± 5 | ¹³¹ 603 ± 6 | ¹¹³ 620 ± 7 | ¹⁴³ 793 ± 14 | ¹¹⁵ 813 ± 28 | ¹¹⁹ 872 ± 32 | | | | | | |
| 435 | xforwardai-001 | 340100 | 51163 | ³⁶⁴ 2173 | ¹⁸⁴ 2048 ± 0 | ³⁷³ 1180 ± 2 | ³⁴⁰ 1182 ± 1 | ³²⁹ 1194 ± 1 | ²⁹⁶ 1186 ± 2 | ²⁴⁸ 1203 ± 1 | ¹¹⁷ 779 ± 17 | ¹¹² 797 ± 13 | | | | | | |
| 436 | xforwardai-002 | 707715 | 51163 | ³⁵⁶ 1989 | ⁴⁰² 4096 ± 0 | ³¹³ 944 ± 1 | ²⁷³ 942 ± 1 | ²⁴⁸ 943 ± 4 | ²¹⁸ 935 ± 1 | ¹⁸⁷ 967 ± 1 | ¹⁷⁶ 1406 ± 8 | ¹⁷⁵ 1405 ± 13 | | | | | | |
| 437 | xm-000 | 578041 | 148920 | ¹⁴⁵ 688 | ³³⁵ 2052 ± 0 | ²⁹³ 878 ± 2 | ²⁵¹ 882 ± 1 | ²⁶⁵ 988 ± 2 | ³¹⁴ 1258 ± 3 | ³⁶⁴ 2434 ± 7 | ¹⁹⁰ 1634 ± 17 | ¹⁸⁹ 1632 ± 20 | | | | | | |
| 438 | yisheng-004 | 486351 | 38653 | ²⁷⁶ 1279 | ³⁷⁶ 3704 ± 0 | ⁸⁴ 378 ± 12 | - | - | - | - | ⁹⁰ 693 ± 137 | ⁵¹ 526 ± 34 | | | | | | |
| 439 | yitu-003 | 1525719 | 138919 | ⁴⁰⁷ 3737 | <sup | | | | | | | | | | | | | |

| | ALGORITHM | CONFIG | LIBRARY | TEMPLATE | | | | | | | | COMPARISON ⁴ | | | | | | |
|-----|-------------|---------|---------|---------------------|-------------------------|------------------------|------------------------|------------------------|-----------------------------------|-------------------------|----------------------------|----------------------------|------------------------|---------|----------|-----------|-----------|---------|
| | | | | NAME | DATA | DATA | MEMORY | SIZE | GENERATION TIME (ms) ⁴ | | | | TIME (ns) ⁵ | | | | | |
| | | | | | | | | | (KB) ¹ | (KB) ² | (MB) ³ | (B) | MUGSHOT | 480x720 | 960x1440 | 1600x2400 | 3000x4500 | GENUINE |
| 441 | yoonyik-003 | 346691 | 265415 | ³⁶⁶ 2196 | ¹⁵⁹ 2048 ± 0 | ³²⁹ 991 ± 3 | ²⁸³ 980 ± 1 | ²⁶³ 984 ± 4 | ²³¹ 982 ± 1 | ¹⁹² 983 ± 1 | ⁸⁸ 684 ± 45 | ⁹⁰ 678 ± 41 | | | | | | |
| 442 | ytu-000 | 1477360 | 44032 | ³⁷⁴ 2484 | ¹⁶¹ 2048 ± 0 | ¹⁴² 530 ± 0 | ¹¹⁹ 533 ± 0 | ¹⁴⁶ 640 ± 0 | ¹⁹² 861 ± 2 | ³⁵⁰ 1949 ± 8 | ⁴⁰⁷ 31797 ± 131 | ⁴⁰⁸ 31794 ± 133 | | | | | | |
| 443 | yuan-004 | 428665 | 50011 | ²⁸⁷ 1353 | ⁴⁰¹ 4096 ± 0 | ¹⁵⁸ 567 ± 0 | ¹³⁵ 569 ± 0 | ¹¹⁶ 573 ± 0 | ⁹⁷ 579 ± 0 | ⁸⁷ 607 ± 0 | ³²⁸ 5816 ± 35 | ³³⁰ 5800 ± 31 | | | | | | |
| 444 | yuan-005 | 258312 | 145564 | ¹⁹¹ 839 | ²¹⁷ 2048 ± 0 | ⁸⁵ 381 ± 0 | ⁶⁷ 386 ± 0 | ⁵² 387 ± 2 | ⁴⁷ 390 ± 4 | ⁴² 421 ± 3 | ¹⁵⁴ 1156 ± 8 | ¹⁶⁰ 1196 ± 26 | | | | | | |

Notes

- The configuration size does not capture static data included in libraries.
- The library size is the combined total of all files provided in the submission lib folder. These libraries e.g. OpenCV may or may not be installed on any end user's platform natively and would not need to be installed with the algorithm. Some developers put neural network models in their libraries.
- The memory usage is the peak resident set size reported by the ps system call during template generation.
- The median template creation times are measured on Intel® Xeon® CPU E5-2630 v4 @ 2.20GHz processors.
- The comparison durations, in nanoseconds, are estimated using std::chrono::high_resolution_clock which on the machine in (2) counts 1ns clock ticks. Precision is somewhat worse than that however. The ± value is the median absolute deviation times 1.48 for Normal consistency.

Table 18: Summary of algorithms and properties included in this report. The red superscripts give ranking for the quantity in that column.

FNMR(T)
FMR(T)
“False non-match rate”
“False match rate”

| | Algorithm | FALSE NON-MATCH RATE (FNMR) | | | | | | | | | | LESS CONSTRAINED, NON-COOP. | | | | | |
|----|--------------------|-----------------------------|--------|--------|---------|---------------|------------|--------|--------|--------|-----|-----------------------------|-----|--------|--------|--------|-----|
| | | CONSTRAINED, COOPERATIVE | | | | | | | | WILD | | | | | | | |
| | | Name | VISAMC | VISA | MUGSHOT | MUGSHOT12+YRS | VISABORDER | BORDER | BORDER | 1E-05 | | | | | | | |
| | FMR | 0.0001 | 1E-06 | 1E-05 | 1E-05 | 1E-06 | 1E-06 | 1E-06 | 1E-05 | 0.0001 | | | | | | | |
| 1 | 20face-000 | 0.1268 | 387 | 0.1828 | 380 | 0.1748 | 387 | 0.2768 | 387 | 0.1765 | 376 | 0.1864 | 299 | 0.0927 | 329 | 0.0405 | 273 |
| 2 | 20face-001 | 0.0521 | 365 | 0.0732 | 364 | 0.1414 | 385 | 0.2549 | 386 | 0.0769 | 355 | 0.1354 | 293 | 0.0419 | 288 | 0.0295 | 166 |
| 3 | 3divi-006 | 0.0064 | 177 | 0.0094 | 176 | 0.0047 | 156 | 0.0066 | 160 | 0.0091 | 168 | 0.0191 | 158 | 0.0113 | 148 | 0.0289 | 143 |
| 4 | 3divi-007 | 0.0024 | 51 | 0.0038 | 56 | 0.0028 | 57 | 0.0034 | 51 | 0.0046 | 79 | 0.0101 | 79 | 0.0082 | 93 | 0.0300 | 181 |
| 5 | acer-001 | 0.0294 | 345 | 0.0504 | 348 | 0.0240 | 338 | 0.0463 | 340 | 0.0436 | 334 | 0.0622 | 261 | 0.0360 | 282 | 0.0307 | 195 |
| 6 | acer-002 | 0.0169 | 313 | 0.0262 | 312 | 0.0103 | 271 | 0.0167 | 281 | 0.0182 | 270 | 0.0281 | 200 | 0.0159 | 202 | 0.0297 | 173 |
| 7 | acisw-007 | 0.4276 | 415 | 0.5493 | 417 | 0.8425 | 429 | 0.9185 | 429 | 0.8424 | 415 | 0.9976 | 410 | 0.9930 | 424 | 0.4963 | 416 |
| 8 | acisw-008 | 0.0100 | 244 | 0.0147 | 237 | 0.0094 | 266 | 0.0126 | 235 | 0.1740 | 375 | 0.6651 | 351 | 0.4545 | 378 | 0.0925 | 349 |
| 9 | ader-a-002 | 0.0052 | 134 | 0.0071 | 131 | 0.0047 | 153 | 0.0064 | 154 | 0.0087 | 158 | 0.0159 | 131 | 0.0136 | 175 | 0.0990 | 352 |
| 10 | ader-a-003 | 0.0043 | 115 | 0.0059 | 114 | 0.0036 | 109 | 0.0043 | 92 | 0.0076 | 137 | 0.0151 | 120 | 0.0128 | 169 | 0.0989 | 351 |
| 11 | advance-002 | 0.0089 | 223 | 0.0137 | 227 | 0.0073 | 224 | 0.0115 | 226 | 0.0400 | 327 | 0.0722 | 268 | 0.0593 | 310 | 0.0498 | 301 |
| 12 | advance-003 | 0.0060 | 170 | 0.0087 | 168 | 0.0052 | 173 | 0.0067 | 161 | 0.0389 | 326 | 0.4914 | 335 | 0.1291 | 334 | 0.0508 | 303 |
| 13 | afisbiometrics-000 | 0.0051 | 133 | 0.0073 | 136 | 0.0030 | 73 | 0.0050 | 113 | 0.0044 | 74 | 0.0077 | 43 | 0.0057 | 35 | 0.0282 | 93 |
| 14 | aifirst-001 | 0.0119 | 267 | 0.0170 | 260 | 0.0084 | 246 | 0.0127 | 242 | 0.0131 | 229 | 0.0212 | 169 | 0.0138 | 178 | 0.0432 | 286 |
| 15 | aigen-001 | 0.0124 | 276 | 0.0219 | 290 | 0.0143 | 308 | 0.0217 | 304 | 0.0236 | 296 | 0.8960 | 378 | 0.3255 | 366 | 0.0681 | 330 |
| 16 | aigen-002 | 0.0192 | 324 | 0.0343 | 328 | 0.0256 | 339 | 0.0402 | 334 | 0.0389 | 325 | 0.9196 | 382 | 0.3876 | 372 | 0.1096 | 358 |
| 17 | ailabs-001 | 0.0158 | 306 | 0.0276 | 318 | 0.0192 | 325 | 0.0317 | 326 | 0.0352 | 320 | 0.0608 | 258 | 0.0434 | 292 | 0.0338 | 235 |
| 18 | aimall-002 | 0.0119 | 268 | 0.0167 | 257 | 0.0224 | 333 | 0.0411 | 336 | 0.0233 | 293 | 0.0373 | 232 | 0.0235 | 252 | 0.0327 | 222 |
| 19 | aimall-003 | 0.0033 | 84 | 0.0041 | 66 | 0.0033 | 96 | 0.0035 | 61 | 0.0056 | 104 | 0.0109 | 87 | 0.0087 | 106 | 0.0312 | 204 |
| 20 | aiseemu-001 | 0.0021 | 39 | 0.0029 | 35 | 0.0027 | 46 | 0.0033 | 48 | 0.0038 | 54 | 0.0339 | 221 | 0.0057 | 36 | 0.0282 | 84 |
| 21 | aiunionface-000 | 0.0104 | 248 | 0.0154 | 246 | 0.0082 | 244 | 0.0122 | 231 | 0.0141 | 236 | 0.0243 | 183 | 0.0169 | 210 | 0.0306 | 193 |
| 22 | aize-001 | 0.0223 | 332 | 0.0344 | 329 | 0.0199 | 326 | 0.0313 | 325 | 0.0367 | 322 | 0.0522 | 252 | 0.0359 | 281 | 0.0446 | 291 |
| 23 | aize-002 | 0.0210 | 330 | 0.0327 | 324 | 0.0280 | 342 | 0.0489 | 343 | 0.0504 | 340 | 0.0692 | 265 | 0.0434 | 291 | 0.0854 | 345 |
| 24 | ajou-001 | 0.0093 | 232 | 0.0147 | 239 | 0.0071 | 221 | 0.0126 | 236 | 0.0173 | 268 | 0.0274 | 195 | 0.0186 | 227 | 0.0348 | 243 |
| 25 | alchera-003 | 0.0044 | 117 | 0.0055 | 106 | 0.0031 | 79 | 0.0039 | 78 | 0.0042 | 69 | 0.0077 | 45 | 0.0065 | 52 | 0.0339 | 237 |
| 26 | alchera-004 | 0.0035 | 93 | 0.0052 | 100 | 0.0028 | 62 | 0.0039 | 79 | 0.0029 | 20 | 0.0075 | 39 | 0.0044 | 11 | 0.0304 | 188 |
| 27 | alfabeta-001 | 0.4867 | 423 | 0.5831 | 421 | 0.6855 | 415 | 0.8156 | 418 | 0.8253 | 414 | 0.7765 | 366 | 0.6416 | 393 | 0.3427 | 404 |
| 28 | alice-000 | 0.0119 | 270 | 0.0192 | 277 | 0.0106 | 278 | 0.0170 | 282 | 0.0167 | 259 | 0.0265 | 191 | 0.0150 | 195 | 0.0288 | 132 |
| 29 | alleyes-000 | 0.0058 | 158 | 0.0090 | 171 | 0.0055 | 183 | 0.0087 | 203 | 0.0068 | 125 | 0.0105 | 85 | 0.0076 | 81 | 0.0282 | 92 |
| 30 | allgovision-000 | 0.0346 | 355 | 0.0527 | 351 | 0.0232 | 335 | 0.0339 | 327 | 0.0372 | 324 | 0.0620 | 260 | 0.0443 | 296 | 0.0607 | 319 |
| 31 | alphaface-001 | 0.0065 | 179 | 0.0097 | 184 | 0.0039 | 122 | 0.0063 | 153 | 0.0083 | 152 | - | - | - | 0.0280 | 73 | |
| 32 | alphaface-002 | 0.0052 | 137 | 0.0075 | 141 | 0.0030 | 68 | 0.0044 | 95 | 1.0000 | 436 | 0.0115 | 95 | 0.0084 | 99 | 0.0279 | 61 |
| 33 | amplifiedgroup-001 | 0.5034 | 425 | 0.5848 | 422 | 0.6973 | 419 | 0.8316 | 419 | 0.7807 | 409 | 0.7724 | 364 | 0.6354 | 390 | 0.4250 | 411 |
| 34 | androvideo-000 | 0.0243 | 335 | 0.0438 | 343 | 0.0239 | 337 | 0.0365 | 331 | 0.0483 | 339 | 0.1870 | 300 | 0.0635 | 313 | 0.1163 | 361 |
| 35 | anke-004 | 0.0080 | 211 | 0.0154 | 247 | 0.0073 | 223 | 0.0112 | 223 | 0.0102 | 195 | 0.0178 | 151 | 0.0118 | 156 | 0.0288 | 134 |
| 36 | anke-005 | 0.0070 | 188 | 0.0109 | 203 | 0.0059 | 194 | 0.0094 | 208 | 0.0105 | 198 | 0.0142 | 111 | 0.0102 | 129 | 0.0289 | 141 |
| 37 | antheus-000 | 0.2564 | 399 | 0.3776 | 402 | 0.7240 | 420 | 0.8699 | 424 | 0.8899 | 422 | 0.9872 | 400 | 0.9483 | 416 | 0.7668 | 426 |
| 38 | antheus-001 | 0.1311 | 388 | 0.2306 | 388 | 0.5113 | 406 | 0.6797 | 408 | 0.8748 | 421 | 0.9908 | 404 | 0.9649 | 420 | 0.7586 | 425 |
| 39 | anyvision-004 | 0.0267 | 340 | 0.0385 | 337 | 0.0258 | 340 | 0.0487 | 342 | 0.0234 | 295 | 0.0301 | 205 | 0.0191 | 231 | 0.0470 | 295 |
| 40 | anyvision-005 | 0.0023 | 50 | 0.0037 | 53 | 0.0027 | 55 | 0.0035 | 57 | 0.0049 | 87 | 0.0084 | 56 | 0.0069 | 64 | 0.0285 | 111 |
| 41 | armatura-001 | 0.0033 | 85 | 0.0042 | 74 | 0.0031 | 77 | 0.0037 | 67 | 0.0056 | 103 | 0.0110 | 88 | 0.0092 | 115 | 0.0815 | 342 |
| 42 | asusaics-000 | 0.0125 | 279 | 0.0209 | 285 | 0.0085 | 247 | 0.0134 | 249 | 0.0143 | 240 | 0.7189 | 356 | 0.285 | 267 | 0.0295 | 165 |
| 43 | asusaics-001 | 0.0125 | 280 | 0.0210 | 286 | 0.0085 | 249 | 0.0134 | 250 | 0.0143 | 241 | 0.7437 | 360 | 0.0289 | 268 | 0.0295 | 164 |
| 44 | authenmetric-003 | 0.0036 | 96 | 0.0053 | 103 | 0.0039 | 128 | 0.0051 | 115 | 0.0095 | 181 | 0.9930 | 405 | 0.5932 | 387 | 0.0290 | 144 |

Table 19: FNMR is the proportion of mated comparisons below a threshold set to achieve the FMR given in the header on the fourth row. FMR is the proportion of impostor comparisons at or above that threshold. The light grey values give rank over all algorithms in that column. The pink columns use only same-sex impostors; others are selected regardless of demographics. The exception, in the green column, uses “matched-covariates” i.e. impostors of the same sex, age group, and country of birth. The second pink column includes effects of extended ageing. Missing entries for border, visa, mugshot and wild images generally mean the algorithm did not run to completion. The VISA columns compare images described in section 2.1. The MUGSHOT columns compare images described in section 2.4. The VISA-BORDER column compare images described in section 2.2 with those of section 2.3. The BORDER column compares images described in section 2.3. The WILD columns compare images described in section 2.6.

| | Algorithm | FALSE NON-MATCH RATE (FNMR) | | | | | | | | | | LESS CONSTRAINED, NON-COOP. | | | | | |
|----|-------------------|-----------------------------|--------|--------|---------|---------------|-------------|--------|--------|--------|--------|-----------------------------|--------|--------|--------|--------|-----|
| | | CONSTRAINED, COOPERATIVE | | | | | | | | WILD | | | | | | | |
| | | Name | VISAMC | VISA | MUGSHOT | MUGSHOT12+YRS | VISA BORDER | BORDER | BORDER | | | | | | | | |
| | FMR | 0.0001 | 1E-06 | 1E-05 | 1E-05 | 1E-06 | 1E-06 | 1E-06 | 1E-05 | | 0.0001 | | | | | | |
| 45 | authenmetric-004 | 0.0027 | 61 | 0.0042 | 73 | 0.0033 | 92 | 0.0036 | 64 | 0.0083 | 155 | 0.9879 | 401 | 0.4058 | 374 | 0.0290 | 149 |
| 46 | aware-005 | 0.0457 | 362 | 0.0643 | 359 | 0.0603 | 369 | 0.1094 | 370 | 0.0613 | 346 | 0.1075 | 285 | 0.0491 | 298 | 0.0314 | 208 |
| 47 | aware-006 | 0.0487 | 363 | 0.0819 | 368 | 0.0529 | 364 | 0.1090 | 369 | 0.1011 | 366 | 0.1058 | 282 | 0.0502 | 301 | 0.0317 | 213 |
| 48 | awiros-001 | 0.4044 | 413 | 0.4622 | 408 | 0.5530 | 408 | 0.6518 | 405 | 0.2008 | 379 | 0.1994 | 303 | 0.1386 | 339 | 0.5584 | 420 |
| 49 | awiros-002 | 0.1990 | 392 | 0.2561 | 390 | 0.3319 | 395 | 0.4411 | 395 | 0.3821 | 393 | 0.9938 | 406 | 0.2634 | 357 | 0.0997 | 353 |
| 50 | aximetria-001 | 0.0111 | 256 | 0.0186 | 272 | 0.0110 | 284 | 0.0148 | 266 | 0.0170 | 263 | 0.3928 | 325 | 0.2090 | 349 | 0.0409 | 276 |
| 51 | ayftech-001 | 0.0946 | 381 | 0.1941 | 382 | 0.2438 | 391 | 0.3625 | 391 | 0.1558 | 372 | 0.1589 | 295 | 0.0936 | 330 | 0.0785 | 338 |
| 52 | ayonix-000 | 0.4351 | 418 | 0.4872 | 410 | 0.6150 | 413 | 0.7510 | 413 | 0.6557 | 403 | 0.6361 | 347 | 0.4981 | 379 | 0.3635 | 406 |
| 53 | beethedata-000 | 0.0127 | 284 | 0.0195 | 278 | 0.0092 | 260 | 0.0157 | 272 | 0.0171 | 265 | 0.0306 | 207 | 0.0204 | 240 | 0.0285 | 114 |
| 54 | beyneai-000 | 0.0071 | 194 | 0.0107 | 200 | 0.0104 | 275 | 0.0131 | 247 | 0.0170 | 264 | 0.9837 | 398 | 0.6171 | 389 | 0.0597 | 318 |
| 55 | biocube-001 | 0.5596 | 431 | 0.6834 | 430 | 0.7700 | 427 | 0.8712 | 425 | 0.8446 | 416 | 0.9661 | 395 | 0.7922 | 405 | 0.2377 | 388 |
| 56 | bioidechswiss-001 | 0.0054 | 144 | 0.0072 | 133 | 0.0069 | 214 | 0.0124 | 234 | 0.0060 | 112 | 0.0094 | 70 | 0.0065 | 56 | 0.0313 | 207 |
| 57 | bioidechswiss-002 | 0.0049 | 126 | 0.0067 | 127 | 0.0064 | 201 | 0.0116 | 227 | 0.0067 | 124 | 0.0117 | 97 | 0.0086 | 103 | 0.0279 | 52 |
| 58 | bm-001 | 0.7431 | 439 | 0.9494 | 440 | 0.9586 | 434 | 0.9843 | 433 | 0.9049 | 424 | 0.9021 | 381 | 0.8395 | 410 | 0.9935 | 435 |
| 59 | boetech-001 | 0.0662 | 373 | 0.0802 | 367 | 0.0493 | 361 | 0.0791 | 360 | 0.0682 | 351 | 0.1074 | 284 | 0.0758 | 320 | 0.1719 | 373 |
| 60 | boetech-002 | 0.0535 | 367 | 0.0565 | 356 | 0.0114 | 292 | 0.0136 | 252 | 0.0403 | 328 | 0.0650 | 262 | 0.0606 | 311 | 0.1697 | 372 |
| 61 | bresee-001 | 0.0085 | 220 | 0.0143 | 234 | 0.0086 | 252 | 0.0153 | 270 | 0.0108 | 202 | 0.0168 | 140 | 0.0115 | 153 | 0.0355 | 256 |
| 62 | bresee-002 | 0.0079 | 210 | 0.0101 | 191 | 0.0065 | 205 | 0.0079 | 187 | 0.0129 | 224 | 0.0263 | 190 | 0.0224 | 249 | 0.0327 | 223 |
| 63 | camvi-002 | 0.0125 | 281 | 0.0221 | 291 | 0.0089 | 257 | 0.0145 | 264 | 0.0142 | 238 | 0.2650 | 314 | 0.0166 | 209 | 0.0288 | 131 |
| 64 | camvi-004 | 0.0171 | 318 | 0.0316 | 323 | 0.0042 | 138 | 0.0049 | 111 | 0.0097 | 187 | 0.6636 | 350 | 0.0141 | 183 | 0.0284 | 102 |
| 65 | canon-003 | 0.0041 | 113 | 0.0059 | 113 | 0.0030 | 67 | 0.0040 | 82 | 0.0040 | 58 | 0.0073 | 36 | 0.0059 | 39 | 0.0274 | 21 |
| 66 | canon-004 | 0.0052 | 136 | 0.0091 | 173 | 0.0033 | 95 | 0.0058 | 137 | 0.0037 | 49 | 0.0770 | 270 | 0.0494 | 299 | 0.0267 | 3 |
| 67 | ceiec-003 | 0.0071 | 195 | 0.0107 | 197 | 0.0061 | 198 | 0.0079 | 189 | 0.0160 | 251 | 0.0316 | 210 | 0.0260 | 260 | 0.0308 | 200 |
| 68 | ceiec-004 | 0.0038 | 104 | 0.0051 | 98 | 0.0045 | 149 | 0.0053 | 119 | 0.0062 | 118 | 0.3939 | 327 | 0.0104 | 135 | 0.0325 | 219 |
| 69 | chosun-001 | 0.0525 | 366 | 0.0936 | 370 | 0.0742 | 373 | 0.1263 | 375 | 0.0978 | 365 | 1.0000 | 431 | 0.9354 | 415 | 0.4446 | 413 |
| 70 | chosun-002 | 0.0390 | 357 | 0.0646 | 360 | 0.0339 | 353 | 0.0576 | 352 | 0.0455 | 338 | 0.6904 | 353 | 0.1746 | 346 | 0.0696 | 332 |
| 71 | chtface-004 | 0.0046 | 121 | 0.0062 | 119 | 0.0052 | 172 | 0.0080 | 190 | 0.0088 | 164 | 0.0152 | 121 | 0.0106 | 138 | 0.0306 | 194 |
| 72 | chtface-005 | 0.0033 | 80 | 0.0049 | 92 | 0.0029 | 64 | 0.0041 | 85 | 0.0044 | 73 | 0.0317 | 211 | 0.0066 | 59 | 0.0306 | 192 |
| 73 | clearviewai-000 | 0.0010 | 6 | 0.0019 | 15 | 0.0024 | 14 | 0.0028 | 26 | 0.0030 | 23 | 0.0058 | 17 | 0.0050 | 17 | 0.0271 | 7 |
| 74 | cloeseli-001 | 0.0136 | 287 | 0.0163 | 252 | 0.0039 | 125 | 0.0054 | 122 | 0.0072 | 131 | 1.0000 | 425 | 0.0094 | 119 | 0.0318 | 214 |
| 75 | cloudmatrix-000 | 0.0192 | 325 | 0.0340 | 327 | 0.0133 | 303 | 0.0220 | 305 | 0.9837 | 430 | 1.0000 | 427 | 0.0281 | 266 | 0.0668 | 326 |
| 76 | cloudmatrix-001 | 0.0668 | 374 | 0.1141 | 373 | 0.0539 | 365 | 0.0905 | 364 | 0.3509 | 390 | 0.9819 | 397 | 0.9010 | 413 | 0.0636 | 322 |
| 77 | cloudwalk-hr-003 | 0.0026 | 58 | 0.0041 | 62 | 0.0040 | 132 | 0.0058 | 136 | 0.0060 | 116 | 0.9992 | 413 | 0.0094 | 117 | 0.7206 | 424 |
| 78 | cloudwalk-hr-004 | 0.0009 | 4 | 0.0018 | 10 | 0.0034 | 99 | 0.0028 | 31 | 0.0052 | 93 | 0.9992 | 414 | 0.0093 | 116 | 0.1625 | 371 |
| 79 | cloudwalk-mt-004 | 0.0009 | 5 | 0.0013 | 3 | 0.0024 | 16 | 0.0021 | 3 | 0.0028 | 18 | 0.0054 | 11 | 0.0050 | 18 | 0.0285 | 116 |
| 80 | cloudwalk-mt-005 | 0.0006 | 1 | 0.0009 | 1 | 0.0025 | 26 | 0.0022 | 5 | 0.0017 | 1 | 0.9286 | 386 | 0.5956 | 388 | 0.0287 | 126 |
| 81 | cogent-006 | 0.0046 | 122 | 0.0059 | 116 | 0.0036 | 105 | 0.0047 | 102 | 0.0058 | 109 | 0.0113 | 92 | 0.0091 | 112 | 0.0343 | 239 |
| 82 | cogent-007 | 0.0022 | 43 | 0.0038 | 55 | 0.0028 | 60 | 0.0031 | 42 | 0.0040 | 60 | 0.0082 | 52 | 0.0067 | 60 | 0.0438 | 289 |
| 83 | cognitec-003 | 0.0038 | 103 | 0.0052 | 99 | 0.0054 | 181 | 0.0057 | 133 | 0.0225 | 289 | 0.0416 | 238 | 0.0388 | 285 | 0.0348 | 244 |
| 84 | cognitec-004 | 0.0036 | 94 | 0.0053 | 102 | 0.0053 | 174 | 0.0056 | 130 | 0.0098 | 188 | 0.0202 | 168 | 0.0154 | 198 | 0.0352 | 254 |
| 85 | cor-001 | 0.0075 | 205 | 0.0113 | 207 | 0.0055 | 185 | 0.0084 | 195 | 0.0091 | 170 | 0.0148 | 116 | 0.0092 | 114 | 0.0277 | 40 |
| 86 | coretech-000 | 0.7699 | 441 | 1.0000 | 444 | 1.0000 | 442 | - | 1.0000 | 441 | 1.0000 | 445 | 1.0000 | 441 | 1.0000 | 442 | |
| 87 | corsight-002 | 0.0053 | 141 | 0.0068 | 129 | 0.0030 | 71 | 0.0041 | 86 | 0.0039 | 56 | 0.0079 | 47 | 0.0054 | 32 | 0.0276 | 36 |
| 88 | corsight-003 | 0.0026 | 57 | 0.0040 | 60 | 0.0028 | 58 | 0.0045 | 97 | 0.0035 | 44 | 0.0059 | 19 | 0.0046 | 12 | 0.0279 | 55 |

Table 20: FNMR is the proportion of mated comparisons below a threshold set to achieve the FMR given in the header on the fourth row. FMR is the proportion of impostor comparisons at or above that threshold. The light grey values give rank over all algorithms in that column. The pink columns use only same-sex impostors; others are selected regardless of demographics. The exception, in the green column, uses “matched-covariates” i.e. impostors of the same sex, age group, and country of birth. The second pink column includes effects of extended ageing. Missing entries for border, visa, mugshot and wild images generally mean the algorithm did not run to completion. The VISA columns compare images described in section 2.1. The MUGSHOT columns compare images described in section 2.4. The VISA-BORDER column compare images described in section 2.2 with those of section 2.3. The BORDER column compares images described in section 2.3. The WILD columns compare images described in section 2.6.

| Algorithm | Name | FALSE NON-MATCH RATE (FNMR) | | | | | | | | | | WILD | | | | | |
|-----------|-----------------------|-----------------------------|-------|---------|---------------|------------|--------|--------|-------|-----------------------------|-----|--------|-----|--------|-----|--------|-----|
| | | CONSTRAINED, COOPERATIVE | | | | | | | | LESS CONSTRAINED, NON-COOP. | | | | | | | |
| | | VISAMC | VISA | MUGSHOT | MUGSHOT12+YRS | VISABORDER | BORDER | BORDER | 1E-05 | | | | | | | | |
| FMR | | 0.0001 | 1E-06 | 1E-05 | 1E-05 | 1E-06 | 1E-06 | 1E-06 | | | | 0.0001 | | | | | |
| 89 | csc-002 | 0.0099 | 242 | 0.0132 | 222 | 0.0077 | 230 | 0.0142 | 261 | 0.0126 | 222 | 0.0195 | 161 | 0.0146 | 189 | 0.1779 | 375 |
| 90 | csc-003 | 0.0053 | 140 | 0.0065 | 124 | 0.0037 | 113 | 0.0047 | 103 | 0.0074 | 133 | 0.0124 | 104 | 0.0112 | 147 | 0.1773 | 374 |
| 91 | ctbcbank-000 | 0.0168 | 311 | 0.0250 | 306 | 0.0146 | 311 | 0.0224 | 307 | 0.0211 | 286 | 0.8964 | 379 | 0.3779 | 371 | 1.0000 | 438 |
| 92 | ctbcbank-001 | 0.0155 | 304 | 0.0235 | 300 | 0.0148 | 316 | 0.0243 | 312 | 0.0207 | 283 | 0.9279 | 385 | 0.3469 | 367 | 1.0000 | 446 |
| 93 | cubox-001 | 0.0064 | 176 | 0.0080 | 153 | 0.0037 | 111 | 0.0055 | 125 | 0.0060 | 113 | 0.0111 | 89 | 0.0077 | 82 | 0.0300 | 179 |
| 94 | cubox-002 | 0.0034 | 92 | 0.0041 | 65 | 0.0025 | 23 | 0.0025 | 17 | 0.0033 | 37 | 0.0064 | 24 | 0.0058 | 38 | 0.0480 | 298 |
| 95 | cudocommunication-001 | 0.4777 | 421 | 1.0000 | 446 | 0.4373 | 401 | 0.5360 | 398 | 1.0000 | 439 | 1.0000 | 438 | 1.0000 | 446 | 1.0000 | 445 |
| 96 | cuhkee-001 | 0.0036 | 97 | 0.0045 | 82 | 0.0031 | 83 | 0.0046 | 100 | 0.0051 | 92 | 0.0095 | 73 | 0.0079 | 85 | 0.1492 | 366 |
| 97 | cybercore-001 | 0.3759 | 411 | 0.5677 | 419 | 0.6928 | 418 | 0.7926 | 415 | 0.8118 | 412 | 0.9291 | 389 | 0.7080 | 398 | 0.3811 | 407 |
| 98 | cybercore-002 | 0.0092 | 230 | 0.0119 | 211 | 0.0049 | 161 | 0.0072 | 168 | 0.9105 | 426 | 1.0000 | 430 | 1.0000 | 433 | 0.5484 | 418 |
| 99 | cyberextruder-003 | 0.0109 | 254 | 0.0169 | 259 | 0.0071 | 219 | 0.0112 | 224 | 0.0165 | 257 | 0.0410 | 237 | 0.0272 | 265 | 0.0302 | 186 |
| 100 | cyberextruder-004 | 0.0118 | 266 | 0.0181 | 268 | 0.0081 | 241 | 0.0133 | 248 | 0.0191 | 278 | 0.0329 | 214 | 0.0268 | 263 | 0.0679 | 329 |
| 101 | cyberlink-008 | 0.0042 | 114 | 0.0056 | 110 | 0.0038 | 119 | 0.0048 | 105 | 0.0053 | 95 | 0.0099 | 76 | 0.0074 | 77 | 0.0274 | 18 |
| 102 | cyberlink-009 | 0.0018 | 31 | 0.0027 | 31 | 0.0047 | 152 | 0.0046 | 98 | 0.0040 | 63 | 0.0086 | 62 | 0.0062 | 49 | 0.0280 | 72 |
| 103 | dahua-006 | 0.0027 | 59 | 0.0039 | 58 | 0.0031 | 81 | 0.0039 | 80 | 0.0039 | 55 | 0.0067 | 29 | 0.0058 | 37 | 0.0280 | 64 |
| 104 | dahua-007 | 0.0017 | 29 | 0.0023 | 21 | 0.0026 | 38 | 0.0032 | 46 | 0.0033 | 34 | 0.0060 | 20 | 0.0054 | 31 | 0.0278 | 45 |
| 105 | daon-000 | 0.0095 | 237 | 0.0117 | 210 | 0.0068 | 209 | 0.0077 | 183 | 0.0092 | 173 | 0.0174 | 147 | 0.0137 | 177 | 0.0331 | 227 |
| 106 | decatur-000 | 0.0714 | 375 | 0.1115 | 372 | 0.0608 | 370 | 0.1106 | 371 | 0.0866 | 359 | 1.0000 | 428 | 0.0714 | 317 | 0.0658 | 325 |
| 107 | decatur-001 | 0.0424 | 359 | 0.0711 | 362 | 0.0237 | 336 | 0.0458 | 339 | 0.0447 | 336 | 1.0000 | 423 | 0.9969 | 428 | 0.0280 | 70 |
| 108 | deepglint-003 | 0.0027 | 60 | 0.0038 | 54 | 0.0030 | 70 | 0.0032 | 45 | 0.0043 | 71 | 0.0082 | 53 | 0.0076 | 80 | 0.0279 | 54 |
| 109 | deepglint-004 | 0.0025 | 56 | 0.0034 | 44 | 0.0039 | 126 | 0.0061 | 149 | 0.0050 | 89 | 0.0091 | 66 | 0.0082 | 92 | 0.0285 | 118 |
| 110 | deepsea-001 | 0.0136 | 289 | 0.0215 | 287 | 0.0142 | 307 | 0.0214 | 303 | 0.0163 | 255 | 0.0250 | 186 | 0.0192 | 232 | 0.0347 | 242 |
| 111 | deepsense-000 | 0.0145 | 296 | 0.0265 | 314 | 0.0113 | 290 | 0.0196 | 296 | 0.0151 | 245 | 0.0215 | 172 | 0.0129 | 170 | 0.0290 | 145 |
| 112 | deepsense-001 | 0.0013 | 18 | 0.0019 | 12 | 0.0024 | 19 | 0.0025 | 15 | 0.0027 | 16 | 0.0115 | 96 | 0.0053 | 26 | 0.0285 | 112 |
| 113 | dermalog-009 | 0.0067 | 182 | 0.0094 | 175 | 0.0051 | 170 | 0.0069 | 163 | 0.0116 | 214 | 0.0312 | 208 | 0.0177 | 218 | 0.0270 | 6 |
| 114 | dermalog-010 | 0.0030 | 70 | 0.0041 | 61 | 0.0034 | 101 | 0.0037 | 69 | 0.0075 | 134 | 0.5181 | 339 | 0.2530 | 353 | 0.0275 | 23 |
| 115 | dicio-001 | 0.5486 | 430 | 0.6442 | 424 | 0.7516 | 423 | 0.8607 | 421 | 0.8678 | 420 | 0.8268 | 373 | 0.7034 | 397 | 0.3605 | 405 |
| 116 | didiglobalface-001 | 0.0055 | 148 | 0.0092 | 174 | 0.0030 | 69 | 0.0045 | 96 | 0.0088 | 162 | 0.0119 | 101 | 0.0085 | 101 | 0.0282 | 90 |
| 117 | digidata-000 | 0.0967 | 382 | 0.1410 | 376 | 0.2596 | 392 | 0.3462 | 390 | 0.0293 | 312 | 0.0363 | 228 | 0.0212 | 244 | 0.0310 | 201 |
| 118 | digidata-001 | 0.0224 | 333 | 0.0352 | 331 | 0.0330 | 351 | 0.0570 | 351 | 0.0109 | 204 | 0.0481 | 247 | 0.0123 | 164 | 0.0288 | 128 |
| 119 | digitalbarriers-002 | 0.3360 | 408 | 0.3690 | 400 | 0.0877 | 376 | 0.1557 | 376 | 0.0971 | 364 | 0.0951 | 278 | 0.0497 | 300 | 0.0436 | 288 |
| 120 | dps-000 | 0.0115 | 261 | 0.0176 | 264 | 0.0149 | 318 | 0.0185 | 291 | 0.0173 | 267 | 0.0275 | 197 | 0.0180 | 221 | 0.1067 | 356 |
| 121 | dsk-000 | 0.1526 | 389 | 0.2169 | 387 | 0.3787 | 397 | 0.5426 | 400 | 0.3115 | 386 | 0.3089 | 319 | 0.1994 | 348 | 0.2201 | 384 |
| 122 | einetworks-000 | 0.0099 | 241 | 0.0180 | 267 | 0.0088 | 256 | 0.0140 | 258 | 0.0130 | 225 | 0.0225 | 178 | 0.0147 | 191 | 0.0293 | 159 |
| 123 | ekin-002 | 0.1168 | 384 | 0.2042 | 384 | 0.1530 | 386 | 0.2524 | 385 | 0.1777 | 377 | 0.2773 | 316 | 0.1347 | 337 | 0.4801 | 415 |
| 124 | enface-000 | 0.0028 | 65 | 0.0049 | 93 | 0.0043 | 140 | 0.0072 | 166 | 0.0058 | 110 | 0.0150 | 118 | 0.0090 | 111 | 0.0290 | 152 |
| 125 | enface-001 | 0.0072 | 201 | 0.0107 | 199 | 0.0071 | 216 | 0.0138 | 254 | 0.0068 | 126 | 0.0515 | 250 | 0.0094 | 120 | 0.0284 | 107 |
| 126 | eocortex-000 | 0.3485 | 409 | 0.6943 | 431 | 0.1122 | 378 | 0.1574 | 377 | 0.2155 | 383 | 0.2257 | 309 | 0.1606 | 345 | 0.2546 | 395 |
| 127 | ercacat-001 | 0.0036 | 99 | 0.0044 | 80 | 0.0033 | 91 | 0.0047 | 104 | 0.0106 | 199 | 0.0202 | 167 | 0.0184 | 225 | 0.0258 | 1 |
| 128 | euronovate-001 | 0.2786 | 402 | 0.3608 | 399 | 0.4489 | 403 | 0.6105 | 404 | 0.5010 | 397 | 0.5392 | 341 | 0.3769 | 370 | 0.4333 | 412 |
| 129 | expasoft-001 | 0.0328 | 352 | 0.0488 | 345 | 0.0211 | 330 | 0.0342 | 329 | 0.0629 | 349 | 0.6483 | 348 | 0.2816 | 360 | 0.0552 | 313 |
| 130 | expasoft-002 | 0.0170 | 314 | 0.0274 | 316 | 0.0787 | 375 | 0.0768 | 359 | 0.1629 | 373 | 0.9996 | 419 | 0.9631 | 419 | 0.0337 | 232 |
| 131 | f8-001 | 0.0249 | 337 | 0.0336 | 325 | 0.0178 | 323 | 0.0232 | 308 | 0.0303 | 315 | 0.0615 | 259 | 0.0408 | 287 | 0.0475 | 297 |
| 132 | f8-002 | 0.0340 | 354 | 0.0591 | 358 | 0.0213 | 332 | 0.0374 | 332 | 0.0452 | 337 | 0.0760 | 269 | 0.0502 | 302 | 0.1601 | 370 |

Table 21: FNMR is the proportion of mated comparisons below a threshold set to achieve the FMR given in the header on the fourth row. FMR is the proportion of impostor comparisons at or above that threshold. The light grey values give rank over all algorithms in that column. The pink columns use only same-sex impostors; others are selected regardless of demographics. The exception, in the green column, uses “matched-covariates” i.e. impostors of the same sex, age group, and country of birth. The second pink column includes effects of extended ageing. Missing entries for border, visa, mugshot and wild images generally mean the algorithm did not run to completion. The VISA columns compare images described in section 2.1. The MUGSHOT columns compare images described in section 2.4. The VISA-BORDER column compare images described in section 2.2 with those of section 2.3. The BORDER column compares images described in section 2.3. The WILD columns compare images described in section 2.6.

| Algorithm | FALSE NON-MATCH RATE (FNMR) | | | | | | | | | | LESS CONSTRAINED, NON-COOP. | | | | | | |
|-----------|-----------------------------|--------|-------|---------|---------------|------------|--------|--------|--------|--------|-----------------------------|--------|--------|--------|--------|--------|-----|
| | CONSTRAINED, COOPERATIVE | | | | | | | | | | | | | | | | |
| | Name | VISAMC | VISA | MUGSHOT | MUGSHOT12+YRS | VISABORDER | BORDER | BORDER | WILD | | | | | | | | |
| FMR | 0.0001 | 1E-06 | 1E-05 | 1E-05 | 1E-06 | 1E-06 | 1E-06 | 1E-05 | 0.0001 | | | | | | | | |
| 133 | faceonline-001 | 0.0269 | 341 | 0.0359 | 333 | 0.0387 | 356 | 0.0721 | 358 | 0.0246 | 304 | 0.0349 | 224 | 0.0220 | 246 | 0.0548 | 311 |
| 134 | faceonline-002 | 0.0121 | 271 | 0.0135 | 226 | 0.0033 | 93 | 0.0041 | 84 | 0.0037 | 51 | 0.9427 | 391 | 0.7927 | 406 | 0.0405 | 274 |
| 135 | facephi-000 | 0.0044 | 118 | 0.0059 | 115 | 0.0047 | 154 | 0.0057 | 134 | 0.0088 | 163 | 1.0000 | 433 | 1.0000 | 435 | 0.0308 | 197 |
| 136 | facesoft-000 | 0.0085 | 219 | 0.0112 | 206 | 0.0064 | 203 | 0.0107 | 219 | 0.0091 | 169 | 0.0171 | 143 | 0.0107 | 139 | 0.0275 | 24 |
| 137 | facetag-000 | 0.2836 | 403 | 0.4081 | 405 | 0.2933 | 394 | 0.4303 | 394 | 0.3448 | 388 | 0.6312 | 346 | 0.3530 | 368 | 0.2087 | 382 |
| 138 | facetag-002 | 0.0098 | 240 | 0.0147 | 238 | 0.0064 | 204 | 0.0110 | 221 | 0.0116 | 213 | 0.0190 | 157 | 0.0119 | 160 | 0.0675 | 328 |
| 139 | facex-001 | 1.0000 | 446 | 1.0000 | 445 | 1.0000 | 439 | - | 1.0000 | 437 | 1.0000 | 435 | 1.0000 | 437 | 1.0000 | 437 | |
| 140 | facex-002 | 0.0803 | 377 | 0.1404 | 375 | 0.1283 | 381 | 0.1979 | 382 | 0.1440 | 371 | 0.1952 | 302 | 0.1299 | 336 | 0.2377 | 387 |
| 141 | farfaces-001 | 0.4890 | 424 | 0.5860 | 423 | 0.5650 | 409 | 0.7268 | 411 | 0.8015 | 411 | 0.7511 | 361 | 0.5892 | 386 | 0.1976 | 380 |
| 142 | fiberhome-nanjing-003 | 0.0090 | 224 | 0.0139 | 231 | 0.0082 | 243 | 0.0144 | 262 | 0.0110 | 205 | 0.0174 | 145 | 0.0107 | 140 | 0.0272 | 13 |
| 143 | fiberhome-nanjing-004 | 0.0037 | 102 | 0.0056 | 111 | 0.0031 | 78 | 0.0043 | 91 | 0.0043 | 72 | 0.0083 | 54 | 0.0061 | 46 | 0.0272 | 11 |
| 144 | fincore-000 | 0.0309 | 350 | 0.0502 | 347 | 0.0281 | 343 | 0.0510 | 346 | 0.0521 | 342 | 0.0815 | 272 | 0.0522 | 303 | 0.0681 | 331 |
| 145 | frpkauai-001 | 0.0023 | 48 | 0.0035 | 49 | 0.0026 | 32 | 0.0030 | 39 | 0.0040 | 62 | 0.0080 | 48 | 0.0072 | 70 | 0.0290 | 151 |
| 146 | fujitsulab-002 | 0.0091 | 229 | 0.0124 | 217 | 0.0105 | 276 | 0.0156 | 271 | 0.0169 | 262 | 0.0345 | 223 | 0.0146 | 190 | 0.0282 | 86 |
| 147 | fujitsulab-003 | 0.0045 | 119 | 0.0065 | 125 | 0.0057 | 190 | 0.0083 | 193 | 0.0080 | 144 | 0.0154 | 126 | 0.0101 | 126 | 0.0280 | 63 |
| 148 | g42-intelbrain-001 | 0.0006 | 2 | 0.0009 | 2 | 0.0037 | 112 | 0.0044 | 93 | 0.0030 | 28 | 0.0059 | 18 | 0.0053 | 29 | 0.0292 | 157 |
| 149 | geo-002 | 0.0171 | 317 | 0.0187 | 273 | 0.0035 | 104 | 0.0051 | 117 | 0.0064 | 120 | 0.0117 | 98 | 0.0083 | 97 | 0.0302 | 185 |
| 150 | geo-004 | 0.0030 | 69 | 0.0041 | 63 | 0.0025 | 29 | 0.0030 | 36 | 0.0035 | 43 | 0.0065 | 26 | 0.0053 | 28 | 0.0286 | 120 |
| 151 | glory-004 | 0.0077 | 208 | 0.0123 | 214 | 0.0074 | 227 | 0.0098 | 214 | 0.0122 | 219 | 0.0193 | 159 | 0.0134 | 173 | 0.0743 | 336 |
| 152 | glory-005 | 0.0056 | 150 | 0.0076 | 142 | 0.0054 | 182 | 0.0072 | 169 | 0.0075 | 135 | 0.9237 | 384 | 0.7853 | 403 | 0.0727 | 334 |
| 153 | gorilla-007 | 0.0074 | 204 | 0.0111 | 205 | 0.0065 | 206 | 0.0126 | 237 | 0.0100 | 193 | 0.0151 | 119 | 0.0102 | 128 | 0.0278 | 41 |
| 154 | gorilla-008 | 0.0058 | 157 | 0.0091 | 172 | 0.0049 | 160 | 0.0079 | 188 | 0.0079 | 143 | 0.0126 | 107 | 0.0091 | 113 | 0.0278 | 49 |
| 155 | graymetrics-001 | 0.1039 | 383 | 0.1620 | 379 | 0.1344 | 383 | 0.1917 | 380 | 0.1648 | 374 | 0.5160 | 338 | 0.2689 | 358 | 0.3057 | 401 |
| 156 | griaule-000 | 0.0071 | 197 | 0.0099 | 188 | 0.0050 | 164 | 0.0072 | 165 | 0.0160 | 249 | 0.0304 | 206 | 0.0267 | 262 | 0.0338 | 233 |
| 157 | griaule-001 | 0.0057 | 152 | 0.0078 | 148 | 0.0045 | 148 | 0.0065 | 157 | 0.0070 | 127 | 0.7515 | 362 | 0.5106 | 380 | 0.0277 | 39 |
| 158 | hertasecurity-000 | 0.0630 | 372 | 0.0780 | 366 | 0.0503 | 363 | 0.0898 | 363 | 0.0738 | 352 | 0.0693 | 267 | 0.0420 | 289 | 0.0575 | 316 |
| 159 | hertasecurity-001 | 0.0249 | 336 | 0.0309 | 322 | 0.0105 | 277 | 0.0161 | 274 | 0.0245 | 302 | 0.0447 | 241 | 0.0359 | 280 | 0.0486 | 300 |
| 160 | hik-001 | 0.0096 | 238 | 0.0125 | 218 | 0.0093 | 265 | 0.0164 | 279 | 0.0108 | 203 | 0.0937 | 275 | 0.0127 | 167 | 0.0271 | 8 |
| 161 | hisign-001 | 0.0036 | 98 | 0.0050 | 95 | 0.0034 | 97 | 0.0046 | 99 | 0.0079 | 142 | 0.0153 | 125 | 0.0133 | 171 | 0.0286 | 123 |
| 162 | hyperverge-002 | 0.0050 | 127 | 0.0066 | 126 | 0.0035 | 103 | 0.0051 | 114 | 0.0062 | 117 | 0.0107 | 86 | 0.0074 | 78 | 0.0276 | 35 |
| 163 | hyperverge-003 | 0.0019 | 36 | 0.0030 | 36 | 0.0025 | 24 | 0.0029 | 34 | 0.0027 | 13 | 0.0049 | 6 | 0.0042 | 9 | 0.0280 | 71 |
| 164 | hzailu-001 | 0.0122 | 272 | 0.0164 | 254 | 0.0095 | 268 | 0.0196 | 295 | 0.0079 | 140 | 0.0118 | 99 | 0.0090 | 110 | 0.0392 | 269 |
| 165 | hzailu-002 | 0.0051 | 131 | 0.0072 | 132 | 0.0038 | 121 | 0.0055 | 127 | 0.0040 | 59 | 0.0077 | 41 | 0.0062 | 50 | 0.0391 | 268 |
| 166 | icm-002 | 0.0143 | 294 | 0.0249 | 305 | 0.0144 | 309 | 0.0256 | 313 | 0.0236 | 298 | 0.0386 | 234 | 0.0263 | 261 | 0.0339 | 236 |
| 167 | icm-003 | 0.0138 | 291 | 0.0222 | 292 | 0.0149 | 317 | 0.0282 | 320 | 0.0227 | 290 | 0.0384 | 233 | 0.0257 | 258 | 0.0333 | 229 |
| 168 | icthtc-000 | 0.0260 | 339 | 0.0396 | 338 | 0.0207 | 329 | 0.0339 | 328 | 0.0291 | 311 | 0.0474 | 246 | 0.0346 | 276 | 0.0459 | 294 |
| 169 | id3-006 | 0.0072 | 200 | 0.0103 | 193 | 0.0049 | 162 | 0.0074 | 175 | 0.0095 | 179 | 0.0165 | 138 | 0.0119 | 159 | 0.9938 | 436 |
| 170 | id3-008 | 0.0039 | 106 | 0.0055 | 108 | 0.0032 | 88 | 0.0042 | 88 | 0.0081 | 149 | 0.0155 | 127 | 0.0134 | 172 | 0.8856 | 430 |
| 171 | idemia-008 | 0.0023 | 49 | 0.0032 | 39 | 0.0023 | 10 | 0.0028 | 25 | 0.0034 | 40 | 0.0067 | 28 | 0.0056 | 33 | 0.0290 | 148 |
| 172 | idemia-009 | 0.0022 | 44 | 0.0030 | 37 | 0.0022 | 4 | 0.0023 | 9 | 0.0023 | 7 | 0.0046 | 4 | 0.0039 | 5 | 0.0285 | 110 |
| 173 | iit-002 | 0.0111 | 258 | 0.0177 | 266 | 0.0085 | 248 | 0.0140 | 257 | 0.0193 | 279 | 0.0332 | 217 | 0.0260 | 259 | 0.1373 | 363 |
| 174 | iit-003 | 0.0082 | 216 | 0.0151 | 244 | 0.0053 | 176 | 0.0084 | 196 | 0.0122 | 218 | 0.0199 | 165 | 0.0137 | 176 | 0.0407 | 275 |
| 175 | imds-software-001 | 0.0126 | 282 | 0.0228 | 294 | 0.0130 | 301 | 0.0221 | 306 | 0.0231 | 291 | 0.0469 | 245 | 0.0199 | 239 | 0.0365 | 261 |
| 176 | imperial-000 | 0.0067 | 183 | 0.0108 | 202 | 0.0080 | 238 | 0.0134 | 251 | 0.0087 | 159 | 0.0581 | 254 | 0.0102 | 130 | 0.0281 | 78 |

Table 22: FNMR is the proportion of mated comparisons below a threshold set to achieve the FMR given in the header on the fourth row. FMR is the proportion of impostor comparisons at or above that threshold. The light grey values give rank over all algorithms in that column. The pink columns use only same-sex impostors; others are selected regardless of demographics. The exception, in the green column, uses “matched-covariates” i.e. impostors of the same sex, age group, and country of birth. The second pink column includes effects of extended ageing. Missing entries for border, visa, mugshot and wild images generally mean the algorithm did not run to completion. The VISA columns compare images described in section 2.1. The MUGSHOT columns compare images described in section 2.4. The VISA-BORDER column compare images described in section 2.2 with those of section 2.3. The BORDER column compares images described in section 2.3. The WILD columns compare images described in section 2.6.

| | Algorithm | FALSE NON-MATCH RATE (FNMR) | | | | | | | | | | LESS CONSTRAINED, NON-COOP. | | | | | |
|-----|-----------------------------|-----------------------------|--------|--------|---------|---------------|------------|--------|--------|--------|--------|-----------------------------|-----|--------|-----|--------|-----|
| | | CONSTRAINED, COOPERATIVE | | | | | | | | WILD | | | | | | | |
| | | Name | VISAMC | VISA | MUGSHOT | MUGSHOT12+YRS | VISABORDER | BORDER | BORDER | 1E-06 | 1E-05 | | | | | | |
| | FMR | 0.0001 | 1E-06 | 1E-05 | 1E-05 | 1E-05 | 1E-06 | 1E-06 | 1E-05 | 0.0001 | 0.0001 | | | | | | |
| 177 | imperial-002 | 0.0058 | 159 | 0.0081 | 156 | 0.0055 | 184 | 0.0085 | 199 | 0.0083 | 153 | 0.0157 | 128 | 0.0103 | 131 | 0.0273 | 15 |
| 178 | incode-010 | 0.0041 | 112 | 0.0063 | 122 | 0.0028 | 61 | 0.0043 | 90 | 0.0047 | 83 | 0.0077 | 44 | 0.0061 | 45 | 0.0296 | 172 |
| 179 | incode-011 | 0.0032 | 76 | 0.0044 | 78 | 0.0026 | 40 | 0.0034 | 55 | 0.0032 | 32 | 0.0359 | 226 | 0.0140 | 181 | 0.0295 | 167 |
| 180 | innefulabs-000 | 0.0122 | 274 | 0.0199 | 280 | 0.0112 | 289 | 0.0197 | 297 | 0.0222 | 288 | 0.0372 | 231 | 0.0271 | 264 | 0.0348 | 245 |
| 181 | innovativetechnologyltd-001 | 0.0578 | 370 | 0.0938 | 371 | 0.0501 | 362 | 0.0981 | 365 | 0.0592 | 345 | 0.0779 | 271 | 0.0422 | 290 | 0.0449 | 293 |
| 182 | innovativetechnologyltd-002 | 0.0451 | 361 | 0.0716 | 363 | 0.0541 | 366 | 0.1009 | 367 | 0.0506 | 341 | 0.0682 | 263 | 0.0371 | 283 | 0.0804 | 341 |
| 183 | innovatrics-007 | 0.0040 | 108 | 0.0054 | 104 | 0.0057 | 189 | 0.0078 | 184 | 0.0079 | 141 | 0.0123 | 102 | 0.0088 | 107 | 0.0282 | 91 |
| 184 | innovatrics-008 | 0.0047 | 124 | 0.0064 | 123 | 0.0038 | 118 | 0.0052 | 118 | 0.0053 | 96 | 0.0088 | 63 | 0.0069 | 65 | 0.0287 | 124 |
| 185 | insightface-001 | 0.0009 | 3 | 0.0014 | 4 | 0.0027 | 45 | 0.0024 | 10 | 0.0035 | 42 | 0.0070 | 32 | 0.0065 | 54 | 0.0279 | 59 |
| 186 | insightface-002 | 0.0011 | 11 | 0.0019 | 13 | 0.0027 | 51 | 0.0026 | 19 | 0.0036 | 48 | 0.0069 | 31 | 0.0065 | 53 | 0.0280 | 62 |
| 187 | inspur-000 | 0.0060 | 169 | 0.0078 | 146 | 0.7415 | 422 | 0.9093 | 428 | 0.2838 | 385 | 0.9996 | 417 | 0.9976 | 429 | 0.0283 | 97 |
| 188 | intellicloudai-001 | 0.0142 | 293 | 0.0234 | 298 | 0.0092 | 262 | 0.0145 | 263 | 0.0162 | 253 | 0.0371 | 230 | 0.0171 | 213 | 0.0409 | 277 |
| 189 | intellicloudai-002 | 0.0059 | 165 | 0.0085 | 161 | 0.0060 | 196 | 0.0069 | 164 | 0.0108 | 201 | 0.2477 | 313 | 0.0171 | 212 | 0.0303 | 187 |
| 190 | intellifusion-001 | 0.0072 | 198 | 0.0094 | 178 | 0.0056 | 188 | 0.0085 | 200 | 0.0111 | 208 | 0.0212 | 170 | 0.0143 | 186 | 0.0289 | 139 |
| 191 | intellifusion-002 | 0.0059 | 164 | 0.0077 | 145 | 0.0040 | 131 | 0.0074 | 174 | 0.0085 | 157 | 0.5352 | 340 | 0.0104 | 136 | 0.0305 | 191 |
| 192 | intellivision-003 | 0.1177 | 385 | 0.2006 | 383 | 0.0760 | 374 | 0.1244 | 374 | 0.1069 | 367 | 0.1431 | 294 | 0.0839 | 323 | 0.0829 | 344 |
| 193 | intellivision-004 | 0.0271 | 342 | 0.0559 | 355 | 0.0294 | 348 | 0.0503 | 345 | 0.0327 | 319 | 0.0461 | 243 | 0.0293 | 271 | 0.0645 | 324 |
| 194 | intellivix-001 | 0.0064 | 178 | 0.0087 | 165 | 0.0046 | 150 | 0.0063 | 152 | 0.0072 | 130 | 0.9233 | 383 | 0.7856 | 404 | 0.0340 | 238 |
| 195 | intellivix-002 | 0.0062 | 172 | 0.0085 | 162 | 0.0039 | 124 | 0.0056 | 129 | 0.0060 | 115 | 0.3464 | 322 | 0.0857 | 326 | 0.0289 | 140 |
| 196 | intelresearch-004 | 0.0025 | 55 | 0.0035 | 46 | 0.0032 | 86 | 0.0038 | 73 | 0.0049 | 88 | 0.0094 | 69 | 0.0072 | 68 | 0.0290 | 150 |
| 197 | intelresearch-005 | 0.0016 | 26 | 0.0023 | 20 | 0.0028 | 56 | 0.0034 | 53 | 0.0042 | 70 | 0.0084 | 55 | 0.0066 | 58 | 0.0290 | 147 |
| 198 | intema-000 | 0.0012 | 12 | 0.0017 | 8 | 0.0023 | 5 | 0.0022 | 6 | 0.0022 | 6 | 0.0172 | 144 | 0.0061 | 44 | 0.0279 | 58 |
| 199 | intsysmsu-001 | 0.9543 | 444 | 0.9888 | 442 | 0.9923 | 435 | - | - | 0.9977 | 431 | 0.9955 | 407 | 0.9892 | 422 | 0.7871 | 428 |
| 200 | intsysmsu-002 | 0.0130 | 285 | 0.0254 | 308 | 0.0137 | 305 | 0.0267 | 318 | 0.0160 | 250 | 0.0267 | 193 | 0.0145 | 188 | 0.0289 | 142 |
| 201 | ionetworks-000 | 0.0060 | 168 | 0.0087 | 163 | 0.0044 | 142 | 0.0058 | 139 | 0.0080 | 148 | 0.0144 | 114 | 0.0112 | 145 | 0.0319 | 215 |
| 202 | iqface-000 | 0.0091 | 228 | 0.0143 | 233 | 0.0075 | 228 | 0.0110 | 222 | 0.0171 | 266 | 0.2234 | 307 | 0.0359 | 279 | 0.0381 | 265 |
| 203 | iqface-003 | 0.0058 | 160 | 0.0079 | 152 | 0.0051 | 169 | 0.0058 | 140 | 0.0104 | 197 | 0.0200 | 166 | 0.0193 | 233 | 0.0402 | 271 |
| 204 | irex-000 | 0.0052 | 135 | 0.0099 | 187 | 0.0056 | 187 | 0.0083 | 194 | 0.0137 | 234 | 0.0163 | 136 | 0.0078 | 83 | 0.0285 | 113 |
| 205 | isap-001 | 0.5092 | 426 | 0.6588 | 427 | 0.6899 | 417 | 0.7978 | 416 | 0.7200 | 405 | 0.7253 | 357 | 0.5373 | 382 | 0.1931 | 379 |
| 206 | isap-002 | 0.0114 | 260 | 0.0186 | 271 | 0.0087 | 254 | 0.0151 | 269 | 0.0156 | 248 | 0.5134 | 337 | 0.0333 | 272 | 0.0354 | 255 |
| 207 | isityou-000 | 0.5682 | 432 | 0.7033 | 433 | 1.0000 | 441 | - | - | 1.0000 | 442 | 1.0000 | 446 | 1.0000 | 440 | 1.0000 | 441 |
| 208 | isystems-001 | 0.0149 | 301 | 0.0245 | 303 | 0.0138 | 306 | 0.0210 | 301 | 0.0209 | 285 | 0.0332 | 216 | 0.0223 | 248 | 0.0524 | 308 |
| 209 | isystems-002 | 0.0118 | 264 | 0.0182 | 269 | 0.0111 | 286 | 0.0162 | 277 | 0.0166 | 258 | 0.0284 | 202 | 0.0195 | 235 | 0.0516 | 304 |
| 210 | itmo-007 | 0.0080 | 212 | 0.0125 | 219 | 0.0107 | 279 | 0.0185 | 289 | 0.0167 | 260 | 0.0222 | 176 | 0.0144 | 187 | 0.0300 | 180 |
| 211 | itmo-008 | 0.0090 | 225 | 0.0150 | 242 | 0.0058 | 192 | 0.0059 | 144 | 0.0187 | 274 | 0.0355 | 225 | 0.0339 | 273 | 0.1498 | 367 |
| 212 | ivacognitive-001 | 0.0189 | 322 | 0.0351 | 330 | 0.0123 | 297 | 0.0235 | 309 | 0.0198 | 281 | 0.0274 | 196 | 0.0155 | 199 | 0.0296 | 169 |
| 213 | iws-000 | 0.4824 | 422 | 0.5801 | 420 | 0.6859 | 416 | 0.8155 | 417 | 0.8251 | 413 | 0.7756 | 365 | 0.6400 | 392 | 0.3251 | 403 |
| 214 | jaakit-001 | 0.5830 | 433 | 0.7146 | 434 | 0.8173 | 428 | 0.8893 | 427 | 0.8950 | 423 | 0.8387 | 376 | 0.7091 | 399 | 0.5849 | 421 |
| 215 | kakao-007 | 0.0019 | 34 | 0.0028 | 32 | 0.0024 | 13 | 0.0026 | 20 | 0.0033 | 36 | 0.0061 | 21 | 0.0053 | 27 | 0.0427 | 283 |
| 216 | kakao-008 | 0.0011 | 9 | 0.0018 | 11 | 0.0023 | 6 | 0.0023 | 7 | 0.0021 | 5 | 0.0041 | 3 | 0.0035 | 2 | 0.0427 | 284 |
| 217 | kakaoipay-001 | 0.0152 | 303 | 0.0252 | 307 | 0.0145 | 310 | 0.0270 | 319 | 0.0232 | 292 | 0.0344 | 222 | 0.0194 | 234 | 0.0416 | 280 |
| 218 | kasikornlabs-000 | 0.0112 | 259 | 0.0184 | 270 | 0.0086 | 250 | 0.0137 | 253 | 0.0130 | 227 | 0.0225 | 177 | 0.0148 | 193 | 0.0674 | 327 |
| 219 | kasikornlabs-001 | 0.0138 | 290 | 0.0206 | 282 | 0.0087 | 253 | 0.0139 | 256 | 0.0142 | 237 | 0.0236 | 181 | 0.0171 | 211 | 0.0729 | 335 |
| 220 | kedacom-000 | 0.0055 | 147 | 0.0081 | 157 | 0.0111 | 288 | 0.0120 | 229 | 0.0415 | 330 | 0.0966 | 280 | 0.0686 | 314 | 0.2511 | 392 |

Table 23: FNMR is the proportion of mated comparisons below a threshold set to achieve the FMR given in the header on the fourth row. FMR is the proportion of impostor comparisons at or above that threshold. The light grey values give rank over all algorithms in that column. The pink columns use only same-sex impostors; others are selected regardless of demographics. The exception, in the green column, uses “matched-covariates” i.e. impostors of the same sex, age group, and country of birth. The second pink column includes effects of extended ageing. Missing entries for border, visa, mugshot and wild images generally mean the algorithm did not run to completion. The VISA columns compare images described in section 2.1. The MUGSHOT columns compare images described in section 2.4. The VISA-BORDER column compare images described in section 2.2 with those of section 2.3. The BORDER column compares images described in section 2.3. The WILD columns compare images described in section 2.6.

| | Algorithm | FALSE NON-MATCH RATE (FNMR) | | | | | | | | | | WILD | | | | | | |
|-----|----------------------|-----------------------------|--------|-------|---------|---------------|------------|--------|-----------------------------|-----|--------|------|--------|-----|--------|-----|--------|-----|
| | | CONSTRAINED, COOPERATIVE | | | | | | | LESS CONSTRAINED, NON-COOP. | | | | | | | | | |
| | | Name | VISAMC | VISA | MUGSHOT | MUGSHOT12+YRS | VISABORDER | BORDER | BORDER | | | | | | | | | |
| | FMR | | 0.0001 | 1E-06 | 1E-05 | 1E-05 | 1E-06 | 1E-06 | 1E-05 | | 0.0001 | | | | | | | |
| 221 | kiwitech-000 | | 0.0076 | 206 | 0.0105 | 195 | 0.0081 | 242 | 0.0128 | 244 | 0.0096 | 182 | 0.0163 | 135 | 0.0101 | 127 | 0.0279 | 60 |
| 222 | kneron-003 | | 0.0542 | 369 | 0.0902 | 369 | 0.0346 | 354 | 0.0562 | 349 | 0.0919 | 361 | 0.1251 | 290 | 0.0973 | 331 | 0.3053 | 400 |
| 223 | kneron-005 | | 0.0157 | 305 | 0.0259 | 310 | 0.0126 | 300 | 0.0212 | 302 | 0.0406 | 329 | 0.0693 | 266 | 0.0542 | 306 | 0.0471 | 296 |
| 224 | knowutech-000 | | 0.0039 | 107 | 0.0055 | 107 | 0.0028 | 63 | 0.0042 | 87 | 0.0042 | 67 | 0.0077 | 42 | 0.0059 | 41 | 0.0271 | 9 |
| 225 | kookmin-002 | | 0.0054 | 146 | 0.0077 | 143 | 0.0043 | 139 | 0.0065 | 156 | 0.0123 | 220 | 0.7591 | 363 | 0.0198 | 238 | 0.0285 | 115 |
| 226 | krungthai-002 | | 0.0105 | 251 | 0.0161 | 249 | 0.0091 | 259 | 0.0141 | 259 | 0.7350 | 407 | 0.9889 | 402 | 0.9605 | 418 | 0.0620 | 320 |
| 227 | kuke3d-001 | | 0.0058 | 156 | 0.0104 | 194 | 0.0083 | 245 | 0.0093 | 207 | 0.0270 | 307 | 0.9901 | 403 | 0.8341 | 409 | 0.0404 | 272 |
| 228 | kuke3d-002 | | 0.0077 | 207 | 0.0135 | 225 | 0.0069 | 213 | 0.0098 | 213 | 0.0111 | 207 | 1.0000 | 432 | 1.0000 | 436 | 0.0316 | 211 |
| 229 | lebentech-000 | | 0.5940 | 434 | 0.7032 | 432 | 0.8854 | 431 | 0.9511 | 430 | 0.9089 | 425 | 0.9970 | 409 | 0.9861 | 421 | 0.6250 | 422 |
| 230 | lemalabs-001 | | 0.0111 | 257 | 0.0175 | 263 | 0.0088 | 255 | 0.0142 | 260 | 0.0143 | 239 | 0.0228 | 179 | 0.0140 | 180 | 0.0281 | 74 |
| 231 | lineclova-001 | | 0.0025 | 54 | 0.0040 | 59 | 0.0026 | 44 | 0.0034 | 56 | 0.0045 | 77 | 0.4127 | 329 | 0.0080 | 89 | 0.0283 | 99 |
| 232 | lineclova-002 | | 0.0021 | 40 | 0.0035 | 48 | 0.0025 | 22 | 0.0027 | 23 | 0.0041 | 64 | 0.0086 | 59 | 0.0072 | 69 | 0.0279 | 50 |
| 233 | lookman-002 | | 0.0297 | 347 | 0.0547 | 354 | 0.0339 | 352 | 0.0562 | 348 | 0.0614 | 347 | 0.0960 | 279 | 0.0790 | 321 | 0.2640 | 397 |
| 234 | lookman-004 | | 0.0074 | 203 | 0.0099 | 186 | 0.0124 | 299 | 0.0149 | 267 | 0.0430 | 333 | 0.0866 | 273 | 0.0694 | 315 | 0.2516 | 393 |
| 235 | luxand-000 | | 0.2056 | 393 | 0.2814 | 392 | 0.4053 | 399 | 0.5365 | 399 | 0.3497 | 389 | 0.3743 | 324 | 0.2605 | 355 | 0.2222 | 386 |
| 236 | mantra-000 | | 0.0037 | 100 | 0.0052 | 101 | 0.0054 | 179 | 0.0056 | 131 | 0.0097 | 186 | 0.0181 | 153 | 0.0151 | 196 | 0.0350 | 248 |
| 237 | maxvision-001 | | 0.0305 | 349 | 0.0528 | 352 | 0.1028 | 377 | 0.1921 | 381 | 0.0650 | 350 | 0.3001 | 318 | 0.1553 | 343 | 0.0539 | 309 |
| 238 | maxvision-002 | | 0.0070 | 192 | 0.0107 | 198 | 0.0061 | 197 | 0.0093 | 206 | 0.0080 | 145 | 0.5726 | 343 | 0.2943 | 362 | 0.0372 | 262 |
| 239 | megvii-005 | | 0.0010 | 7 | 0.0015 | 5 | 0.0026 | 37 | 0.0031 | 44 | 0.0019 | 3 | 0.0500 | 249 | 0.0057 | 34 | 0.0292 | 156 |
| 240 | megvii-006 | | 0.0011 | 8 | 0.0016 | 6 | 0.0026 | 41 | 0.0033 | 50 | 0.0025 | 9 | 0.0050 | 7 | 0.0048 | 15 | 0.0296 | 170 |
| 241 | meituan-000 | | 0.0197 | 326 | 0.0424 | 342 | 0.0078 | 232 | 0.0074 | 173 | 0.0103 | 196 | 0.0193 | 160 | 0.0164 | 206 | 0.1063 | 355 |
| 242 | meituan-001 | | 0.0164 | 310 | 0.1886 | 381 | 0.0025 | 25 | 0.0026 | 18 | 0.0030 | 26 | 0.0074 | 37 | 0.0051 | 20 | 0.1157 | 360 |
| 243 | meiya-001 | | 0.0171 | 316 | 0.0275 | 317 | 0.0159 | 320 | 0.0261 | 317 | 0.0311 | 316 | 0.2250 | 308 | 0.0245 | 256 | 0.0363 | 260 |
| 244 | mendaxiatech-000 | | 0.0027 | 62 | 0.0036 | 50 | 0.0029 | 65 | 0.0036 | 65 | 0.0031 | 31 | 0.0057 | 16 | 0.0051 | 21 | 0.0275 | 27 |
| 245 | metsakuurcompany-001 | | 0.0068 | 186 | 0.0087 | 166 | 0.0068 | 211 | 0.0078 | 185 | 0.0095 | 180 | 0.8972 | 380 | 0.5635 | 384 | 0.0351 | 250 |
| 246 | microfocus-001 | | 0.4482 | 419 | 0.5524 | 418 | 0.7256 | 421 | 0.8416 | 420 | 0.7301 | 406 | 0.6926 | 354 | 0.5180 | 381 | 0.2567 | 396 |
| 247 | microfocus-002 | | 0.3605 | 410 | 0.5057 | 412 | 0.5783 | 411 | 0.7223 | 410 | 0.5909 | 399 | 0.5963 | 345 | 0.4160 | 375 | 0.1582 | 369 |
| 248 | minivision-000 | | 0.0033 | 82 | 0.0048 | 90 | 0.0038 | 117 | 0.0049 | 108 | 0.0055 | 100 | 0.0094 | 72 | 0.0079 | 87 | 0.0273 | 14 |
| 249 | mobai-000 | | 0.0360 | 356 | 0.0439 | 344 | 0.0372 | 355 | 0.0700 | 356 | 0.0367 | 323 | 0.0939 | 276 | 0.0795 | 322 | 0.2640 | 398 |
| 250 | mobai-001 | | 0.0199 | 328 | 0.0219 | 289 | 0.0047 | 155 | 0.0061 | 146 | 0.0093 | 177 | 0.0174 | 146 | 0.0138 | 179 | 0.1045 | 354 |
| 251 | mobbl-001 | | 0.3208 | 404 | 0.4375 | 406 | 0.5680 | 410 | 0.7193 | 409 | 0.6282 | 401 | 0.5783 | 344 | 0.3984 | 373 | 0.1866 | 377 |
| 252 | mobbl-003 | | 0.0087 | 221 | 0.0134 | 224 | 0.0062 | 199 | 0.0087 | 202 | 0.0099 | 189 | 0.0197 | 162 | 0.0122 | 163 | 0.0312 | 205 |
| 253 | mobilpintech-000 | | 0.0090 | 226 | 0.0149 | 240 | 0.0039 | 130 | 0.0057 | 132 | 0.0115 | 212 | 0.0465 | 244 | 0.0182 | 223 | 0.0315 | 210 |
| 254 | moredian-000 | | 0.3874 | 412 | 0.4912 | 411 | 0.9988 | 437 | - | - | 0.9990 | 433 | 0.9999 | 421 | 0.9998 | 431 | 0.4788 | 414 |
| 255 | mukh-001 | | 0.0170 | 315 | 0.0285 | 319 | 0.0225 | 334 | 0.0405 | 335 | 0.0272 | 308 | 0.0950 | 277 | 0.0291 | 270 | 0.0301 | 182 |
| 256 | multimodality-000 | | 0.0034 | 90 | 0.0047 | 87 | 0.0036 | 110 | 0.0044 | 94 | 0.0077 | 138 | 0.9976 | 411 | 0.4456 | 377 | 0.0287 | 125 |
| 257 | multimodality-001 | | 0.0029 | 67 | 0.0042 | 71 | 0.0031 | 76 | 0.0035 | 58 | 0.0038 | 52 | 0.0071 | 34 | 0.0059 | 40 | 0.0281 | 77 |
| 258 | mvision-001 | | 0.0191 | 323 | 0.0233 | 296 | 0.0204 | 328 | 0.0356 | 330 | 0.0198 | 282 | 0.0337 | 219 | 0.0242 | 255 | 0.0431 | 285 |
| 259 | nazhiai-000 | | 0.0040 | 111 | 0.0059 | 117 | 0.0036 | 106 | 0.0048 | 106 | 0.0057 | 106 | 0.0125 | 105 | 0.0083 | 96 | 0.0275 | 28 |
| 260 | neosystems-003 | | 0.2429 | 395 | 0.3349 | 395 | 0.1844 | 388 | 0.2999 | 388 | 0.5942 | 400 | 0.3936 | 326 | 0.2292 | 350 | 0.1404 | 364 |
| 261 | neosystems-004 | | 0.0279 | 344 | 0.0495 | 346 | 0.0289 | 345 | 0.0585 | 353 | 0.0439 | 335 | 0.9621 | 393 | 0.1296 | 335 | 0.0333 | 230 |
| 262 | netbridgetech-001 | | 0.4749 | 420 | 0.6599 | 428 | 0.4438 | 402 | 0.5676 | 401 | 0.4491 | 395 | 1.0000 | 424 | 0.9541 | 417 | 0.1098 | 359 |
| 263 | netbridgetech-002 | | 0.0101 | 245 | 0.0166 | 256 | 0.0077 | 231 | 0.0127 | 241 | 0.0133 | 230 | 0.8215 | 371 | 0.0523 | 304 | 0.0351 | 251 |
| 264 | neurotechnology-013 | | 0.0032 | 79 | 0.0045 | 83 | 0.0026 | 43 | 0.0036 | 62 | 0.0037 | 50 | 0.0068 | 30 | 0.0052 | 25 | 0.0278 | 46 |

Table 24: FNMR is the proportion of mated comparisons below a threshold set to achieve the FMR given in the header on the fourth row. FMR is the proportion of impostor comparisons at or above that threshold. The light grey values give rank over all algorithms in that column. The pink columns use only same-sex impostors; others are selected regardless of demographics. The exception, in the green column, uses “matched-covariates” i.e. impostors of the same sex, age group, and country of birth. The second pink column includes effects of extended ageing. Missing entries for border, visa, mugshot and wild images generally mean the algorithm did not run to completion. The VISA columns compare images described in section 2.1. The MUGSHOT columns compare images described in section 2.4. The VISA-BORDER column compare images described in section 2.2 with those of section 2.3. The BORDER column compares images described in section 2.3. The WILD columns compare images described in section 2.6.

| Algorithm | FALSE NON-MATCH RATE (FNMR) | | | | | | | | | | WILD | | | | | | |
|-----------|-----------------------------|--------|-------|---------|---------------|------------|--------|--------|-----------------------------|--------|------|--------|-----|--------|-----|--------|-----|
| | CONSTRAINED, COOPERATIVE | | | | | | | | LESS CONSTRAINED, NON-COOP. | | | | | | | | |
| | Name | VISAMC | VISA | MUGSHOT | MUGSHOT12+YRS | VISABORDER | BORDER | BORDER | 1E-05 | WILD | | | | | | | |
| FMR | 0.0001 | 1E-06 | 1E-05 | 1E-05 | 1E-06 | 1E-06 | 1E-06 | 1E-05 | 0.0001 | | | | | | | | |
| 265 | neurotechnology-015 | 0.0022 | 45 | 0.0036 | 51 | 0.0024 | 12 | 0.0028 | 28 | 0.0030 | 24 | 0.0052 | 9 | 0.0041 | 8 | 0.0276 | 33 |
| 266 | nhn-002 | 0.0068 | 187 | 0.0096 | 182 | 0.0057 | 191 | 0.0087 | 204 | 0.0136 | 233 | 0.0253 | 188 | 0.0186 | 229 | 0.0302 | 184 |
| 267 | nhn-003 | 0.0033 | 81 | 0.0048 | 91 | 0.0027 | 49 | 0.0038 | 72 | 0.0036 | 46 | 0.0198 | 163 | 0.0071 | 67 | 0.0285 | 119 |
| 268 | nodeflux-002 | 0.0186 | 321 | 0.0340 | 326 | 0.0261 | 341 | 0.0451 | 338 | 0.0548 | 343 | 1.0000 | 429 | 1.0000 | 434 | 0.0299 | 176 |
| 269 | notiontag-001 | 0.6846 | 437 | 0.8006 | 437 | 0.3955 | 398 | 0.5247 | 397 | 0.8669 | 418 | 0.8313 | 375 | 0.6362 | 391 | 0.2221 | 385 |
| 270 | notiontag-002 | 0.0066 | 181 | 0.0089 | 169 | 0.0045 | 147 | 0.0061 | 147 | 0.0077 | 139 | 0.0137 | 110 | 0.0104 | 134 | 0.0299 | 175 |
| 271 | nsensemcorp-002 | 0.4277 | 416 | 0.5375 | 416 | 0.6734 | 414 | 0.7924 | 414 | 0.7194 | 404 | 0.6937 | 355 | 0.5617 | 383 | 0.5530 | 419 |
| 272 | nsensemcorp-003 | 0.0251 | 338 | 0.0295 | 321 | 0.0212 | 331 | 0.0305 | 323 | 0.0131 | 228 | 0.2139 | 306 | 0.0141 | 184 | 0.0872 | 347 |
| 273 | ntechlab-011 | 0.0012 | 17 | 0.0019 | 14 | 0.0024 | 17 | 0.0028 | 32 | 0.0029 | 22 | 0.0055 | 12 | 0.0047 | 14 | 0.0288 | 133 |
| 274 | ntechlab-012 | 0.0011 | 10 | 0.0016 | 7 | 0.0023 | 11 | 0.0030 | 37 | 0.0026 | 11 | 0.0050 | 8 | 0.0043 | 10 | 0.0280 | 69 |
| 275 | omface-000 | 0.2573 | 400 | 0.3835 | 403 | 0.3590 | 396 | 0.4903 | 396 | 0.3956 | 394 | 0.5003 | 336 | 0.2595 | 354 | 0.2400 | 389 |
| 276 | omnigarde-001 | 0.0168 | 312 | 0.0260 | 311 | 0.0203 | 327 | 0.0402 | 333 | 0.0243 | 300 | 0.0327 | 213 | 0.0177 | 216 | 0.0288 | 130 |
| 277 | omnigarde-002 | 0.0033 | 86 | 0.0046 | 84 | 0.0027 | 54 | 0.0039 | 75 | 0.0041 | 65 | 0.0076 | 40 | 0.0059 | 43 | 0.0278 | 48 |
| 278 | openface-001 | 0.1804 | 390 | 0.2921 | 393 | 0.2878 | 393 | 0.3906 | 393 | 0.2054 | 381 | 0.2338 | 311 | 0.1549 | 342 | 0.2445 | 390 |
| 279 | oz-003 | 0.0095 | 236 | 0.0143 | 232 | 0.0054 | 180 | 0.0077 | 182 | 0.0096 | 184 | 0.0175 | 149 | 0.0118 | 157 | 0.0288 | 135 |
| 280 | oz-004 | 0.0033 | 88 | 0.0049 | 94 | 0.0038 | 120 | 0.0055 | 124 | 0.0081 | 150 | 0.0163 | 137 | 0.0142 | 185 | 0.0329 | 225 |
| 281 | palit-000 | 0.0062 | 173 | 0.0084 | 160 | 0.0039 | 123 | 0.0055 | 123 | 0.0055 | 101 | 0.4610 | 333 | 0.2468 | 352 | 0.0280 | 68 |
| 282 | pangiam-000 | 0.0031 | 74 | 0.0043 | 76 | 0.0026 | 33 | 0.0030 | 41 | 0.0038 | 53 | 0.0071 | 35 | 0.0061 | 48 | 0.0424 | 282 |
| 283 | papago-001 | 0.0067 | 184 | 0.0096 | 183 | 0.0051 | 171 | 0.0077 | 181 | 0.0071 | 128 | 0.0126 | 106 | 0.0086 | 104 | 0.0816 | 343 |
| 284 | papsav1923-001 | 0.0078 | 209 | 0.0130 | 221 | 0.0068 | 210 | 0.0105 | 218 | 0.0119 | 215 | 0.0221 | 175 | 0.0136 | 174 | 0.0293 | 158 |
| 285 | papsav1923-002 | 0.0021 | 42 | 0.0034 | 42 | 0.0026 | 34 | 0.0030 | 40 | 0.0048 | 84 | 0.0093 | 68 | 0.0086 | 102 | 0.0312 | 206 |
| 286 | paravision-008 | 0.0018 | 32 | 0.0025 | 26 | 0.0024 | 15 | 0.0025 | 14 | 0.0036 | 45 | 0.0070 | 33 | 0.0063 | 51 | 0.0279 | 57 |
| 287 | paravision-010 | 0.0012 | 14 | 0.0021 | 16 | 0.0022 | 3 | 0.0021 | 4 | 0.0027 | 15 | 0.0055 | 13 | 0.0050 | 19 | 0.0288 | 136 |
| 288 | pensees-001 | 0.0087 | 222 | 0.0133 | 223 | 0.0071 | 218 | 0.0122 | 233 | 0.0145 | 242 | 0.0252 | 187 | 0.0195 | 236 | 0.0283 | 96 |
| 289 | pixelall-006 | 0.0032 | 77 | 0.0042 | 70 | 0.0032 | 85 | 0.0039 | 77 | 0.0063 | 119 | 0.9960 | 408 | 0.0723 | 318 | 0.0283 | 95 |
| 290 | pixelall-008 | 0.0015 | 21 | 0.0023 | 22 | 0.0034 | 102 | 0.0049 | 107 | 0.0031 | 30 | 0.0057 | 15 | 0.0052 | 22 | 0.0278 | 43 |
| 291 | psl-009 | 0.0161 | 308 | 0.0294 | 320 | 0.0023 | 8 | 0.0025 | 12 | 0.0036 | 47 | 0.0065 | 27 | 0.0048 | 16 | 0.0482 | 299 |
| 292 | psl-010 | 0.0017 | 30 | 0.0035 | 45 | 0.0023 | 7 | 0.0025 | 11 | 0.0035 | 41 | 0.0104 | 81 | 0.0052 | 24 | 0.0282 | 82 |
| 293 | ptakuratsatu-000 | 0.0060 | 167 | 0.0089 | 170 | 0.0070 | 215 | 0.0104 | 217 | 0.0096 | 185 | 0.0152 | 123 | 0.0100 | 124 | 0.0284 | 103 |
| 294 | pxl-001 | 0.0488 | 364 | 0.0752 | 365 | 0.0586 | 368 | 0.1087 | 368 | 0.0946 | 362 | 0.1065 | 283 | 0.0625 | 312 | 0.1088 | 357 |
| 295 | pyramid-000 | 0.0136 | 288 | 0.0233 | 297 | 0.0117 | 295 | 0.0192 | 293 | 0.0185 | 273 | 0.0322 | 212 | 0.0206 | 242 | 0.0304 | 190 |
| 296 | qazbs-000 | 0.0058 | 154 | 0.0083 | 159 | 0.0046 | 151 | 0.0072 | 167 | 0.0130 | 226 | 0.0244 | 184 | 0.0196 | 237 | 0.0297 | 174 |
| 297 | qnap-001 | 0.0148 | 298 | 0.0215 | 288 | 0.0103 | 272 | 0.0162 | 276 | 0.0183 | 272 | 0.0301 | 204 | 0.0186 | 228 | 0.0360 | 259 |
| 298 | qnap-002 | 0.0122 | 273 | 0.0191 | 275 | 0.0075 | 229 | 0.0095 | 211 | 0.0146 | 243 | 0.0281 | 201 | 0.0184 | 224 | 0.0352 | 253 |
| 299 | quantasoft-003 | 0.0081 | 215 | 0.0113 | 208 | 0.0056 | 186 | 0.0076 | 178 | 0.0091 | 171 | 0.0161 | 133 | 0.0107 | 141 | 0.0414 | 279 |
| 300 | rankone-012 | 0.0043 | 116 | 0.0058 | 112 | 0.0031 | 84 | 0.0038 | 71 | 0.0047 | 81 | 0.0081 | 50 | 0.0065 | 55 | 0.0358 | 257 |
| 301 | rankone-013 | 0.0028 | 64 | 0.0041 | 64 | 0.0026 | 35 | 0.0033 | 49 | 0.0028 | 19 | 0.0055 | 14 | 0.0040 | 6 | 0.0291 | 154 |
| 302 | realnetworks-006 | 0.0040 | 109 | 0.0056 | 109 | 0.8657 | 430 | - | | 0.0059 | 111 | 0.0112 | 90 | 0.0085 | 100 | 0.1790 | 376 |
| 303 | realnetworks-007 | 0.0031 | 73 | 0.0051 | 96 | 0.0028 | 59 | 0.0035 | 59 | 0.0048 | 85 | 0.0091 | 65 | 0.0074 | 76 | 0.0279 | 51 |
| 304 | regula-000 | 0.0184 | 320 | 0.0376 | 336 | 0.0103 | 273 | 0.0185 | 288 | 0.0120 | 216 | 0.9983 | 412 | 0.0231 | 250 | 0.0273 | 16 |
| 305 | regula-001 | 0.0072 | 199 | 0.0107 | 201 | 0.0102 | 270 | 0.0179 | 286 | 0.0123 | 221 | 0.0333 | 218 | 0.0174 | 214 | 0.0295 | 162 |
| 306 | remarkai-001 | 0.0144 | 295 | 0.0256 | 309 | 0.0102 | 269 | 0.0159 | 273 | 0.0162 | 254 | 0.0582 | 255 | 0.0185 | 226 | 0.0308 | 199 |
| 307 | remarkai-003 | 0.0047 | 123 | 0.0063 | 121 | 0.0033 | 94 | 0.0049 | 109 | 0.0054 | 97 | 0.0100 | 78 | 0.0072 | 71 | 0.0275 | 30 |
| 308 | rendip-000 | 0.0055 | 149 | 0.0077 | 144 | 0.0048 | 158 | 0.0060 | 145 | 0.0080 | 146 | 0.0142 | 113 | 0.0110 | 144 | 0.0433 | 287 |

Table 25: FNMR is the proportion of mated comparisons below a threshold set to achieve the FMR given in the header on the fourth row. FMR is the proportion of impostor comparisons at or above that threshold. The light grey values give rank over all algorithms in that column. The pink columns use only same-sex impostors; others are selected regardless of demographics. The exception, in the green column, uses “matched-covariates” i.e. impostors of the same sex, age group, and country of birth. The second pink column includes effects of extended ageing. Missing entries for border, visa, mugshot and wild images generally mean the algorithm did not run to completion. The VISA columns compare images described in section 2.1. The MUGSHOT columns compare images described in section 2.4. The VISA-BORDER column compare images described in section 2.2 with those of section 2.3. The BORDER column compares images described in section 2.3. The WILD columns compare images described in section 2.6.

| Algorithm | Name | FALSE NON-MATCH RATE (FNMR) | | | | | | | | | | LESS CONSTRAINED, NON-COOP. | | | | | |
|-----------|--------------------|-----------------------------|-------|---------|---------------|------------|--------|--------|--------|--------|-----|-----------------------------|-----|--------|-----|--------|-----|
| | | CONSTRAINED, COOPERATIVE | | | | | | | | | | | | | | | |
| | | VISAMC | VISA | MUGSHOT | MUGSHOT12+YRS | VISABORDER | BORDER | BORDER | WILD | | | | | | | | |
| FMR | 0.0001 | 1E-06 | 1E-05 | 1E-05 | 1E-05 | 1E-06 | 1E-06 | 1E-05 | 0.0001 | | | | | | | | |
| 309 | revealmedia-005 | 0.0050 | 130 | 0.0074 | 140 | 0.0050 | 165 | 0.0068 | 162 | 0.0075 | 136 | 0.0124 | 103 | 0.0104 | 137 | 0.3960 | 409 |
| 310 | revealmedia-006 | 0.0040 | 110 | 0.0067 | 128 | 0.0041 | 136 | 0.0056 | 128 | 0.0056 | 102 | 0.0085 | 58 | 0.0068 | 62 | 0.0278 | 47 |
| 311 | rokid-000 | 0.0093 | 233 | 0.0145 | 235 | 0.0073 | 225 | 0.0102 | 216 | 0.0164 | 256 | 0.0280 | 199 | 0.0214 | 245 | 0.0857 | 346 |
| 312 | rokid-001 | 0.0105 | 250 | 0.0162 | 250 | 0.0094 | 267 | 0.0163 | 278 | 0.0181 | 269 | 0.0276 | 198 | 0.0165 | 208 | 0.0325 | 220 |
| 313 | s1-004 | 0.0053 | 139 | 0.0080 | 154 | 0.0038 | 115 | 0.0059 | 143 | 0.0057 | 105 | 0.0103 | 80 | 0.0073 | 74 | 0.0281 | 76 |
| 314 | s1-005 | 0.0024 | 52 | 0.0036 | 52 | 0.0025 | 31 | 0.0029 | 35 | 0.0026 | 12 | 0.0048 | 5 | 0.0038 | 4 | 0.0359 | 258 |
| 315 | saffe-001 | 0.4339 | 417 | 0.5261 | 414 | 0.7539 | 425 | 0.8736 | 426 | 0.7977 | 410 | 0.9810 | 396 | 0.7435 | 402 | 0.3887 | 408 |
| 316 | saffe-002 | 0.0119 | 269 | 0.0206 | 281 | 0.0107 | 282 | 0.0177 | 284 | 0.0244 | 301 | 0.9998 | 420 | 0.2785 | 359 | 0.0308 | 198 |
| 317 | samsungsds-000 | 0.0046 | 120 | 0.0069 | 130 | 0.0132 | 302 | 0.0081 | 191 | 0.0099 | 190 | 0.0179 | 152 | 0.0162 | 204 | 0.1874 | 378 |
| 318 | samsungsds-001 | 0.0015 | 24 | 0.0026 | 29 | 0.0023 | 9 | 0.0023 | 8 | 0.0024 | 8 | 0.1660 | 296 | 0.0536 | 305 | 0.0282 | 81 |
| 319 | samtech-001 | 0.0197 | 327 | 0.0365 | 334 | 0.0146 | 314 | 0.0241 | 311 | 0.0238 | 299 | 0.0394 | 235 | 0.0251 | 257 | 0.0337 | 231 |
| 320 | scanovate-002 | 0.0175 | 319 | 0.0355 | 332 | 0.0146 | 312 | 0.0286 | 321 | 0.0269 | 306 | 0.0301 | 203 | 0.0178 | 219 | 0.0301 | 183 |
| 321 | scanovate-003 | 0.0054 | 143 | 0.0080 | 155 | 0.0054 | 177 | 0.0072 | 171 | 0.0312 | 317 | 0.0599 | 256 | 0.0568 | 307 | 0.0283 | 94 |
| 322 | securifai-004 | 0.0136 | 286 | 0.0192 | 276 | 0.0064 | 202 | 0.0099 | 215 | 0.0115 | 211 | 0.0272 | 194 | 0.0127 | 168 | 0.0347 | 241 |
| 323 | securifai-005 | 0.0125 | 278 | 0.0190 | 274 | 0.0080 | 239 | 0.0126 | 238 | 0.0134 | 231 | 0.9861 | 399 | 0.9205 | 414 | 0.0329 | 224 |
| 324 | sensetime-006 | 0.0014 | 19 | 0.0024 | 23 | 0.0021 | 1 | 0.0020 | 1 | 0.0021 | 4 | 0.0040 | 2 | 0.0036 | 3 | 0.0272 | 12 |
| 325 | sensetime-007 | 0.0012 | 15 | 0.0022 | 17 | 0.0021 | 2 | 0.0020 | 2 | 0.0018 | 2 | 0.0034 | 1 | 0.0029 | 1 | 0.0280 | 65 |
| 326 | sertis-000 | 0.0118 | 265 | 0.0208 | 283 | 0.0080 | 236 | 0.0127 | 240 | 0.0110 | 206 | 0.0176 | 150 | 0.0114 | 150 | 0.0285 | 117 |
| 327 | sertis-002 | 0.0049 | 125 | 0.0061 | 118 | 0.0039 | 129 | 0.0061 | 150 | 0.0055 | 99 | 0.0099 | 77 | 0.0070 | 66 | 0.0281 | 75 |
| 328 | seventhsense-000 | 0.0067 | 185 | 0.0099 | 190 | 0.0045 | 145 | 0.0065 | 158 | 0.0093 | 174 | 0.0169 | 142 | 0.0124 | 165 | 0.0275 | 29 |
| 329 | seventhsense-001 | 0.0034 | 91 | 0.0047 | 88 | 0.0025 | 30 | 0.0031 | 43 | 0.0029 | 21 | 0.0338 | 220 | 0.0109 | 143 | 0.0279 | 53 |
| 330 | shaman-000 | 0.9297 | 443 | 0.9774 | 441 | 0.9990 | 438 | - | - | 0.9999 | 434 | 1.0000 | 426 | 0.9999 | 432 | 0.9575 | 433 |
| 331 | shaman-001 | 0.3346 | 407 | 0.4616 | 407 | 0.2368 | 390 | 0.3723 | 392 | 0.3574 | 391 | 0.3527 | 323 | 0.2304 | 351 | 0.1498 | 368 |
| 332 | shu-002 | - | - | 0.0079 | 151 | 0.0146 | 313 | 0.0308 | 324 | 1.0000 | 435 | 0.0183 | 154 | 0.0115 | 152 | 0.0284 | 104 |
| 333 | shu-003 | 0.0028 | 63 | 0.0041 | 67 | 0.0050 | 163 | 0.0088 | 205 | 0.0081 | 151 | 0.0133 | 109 | 0.0094 | 118 | 0.0283 | 100 |
| 334 | siat-002 | 0.0091 | 227 | 0.0126 | 220 | 0.0109 | 283 | 0.0190 | 292 | 0.0276 | 309 | 0.0516 | 251 | 0.0464 | 297 | 0.0520 | 306 |
| 335 | siat-005 | 0.0021 | 41 | 0.0038 | 57 | 0.0059 | 193 | 0.0049 | 110 | 0.0742 | 353 | 0.9623 | 394 | 0.6801 | 394 | 0.0279 | 56 |
| 336 | sjtu-003 | 0.0017 | 28 | 0.0033 | 40 | 0.0030 | 72 | 0.0037 | 68 | 0.0058 | 107 | 0.0104 | 82 | 0.0081 | 91 | 0.0284 | 109 |
| 337 | sjtu-004 | 0.0014 | 20 | 0.0025 | 25 | 0.0027 | 47 | 0.0028 | 33 | 0.0046 | 78 | 0.0086 | 61 | 0.0073 | 73 | 0.0272 | 10 |
| 338 | sktelecom-000 | 0.0038 | 105 | 0.0054 | 105 | 0.0031 | 74 | 0.0051 | 116 | 0.0042 | 66 | 0.3418 | 321 | 0.0061 | 47 | 0.0293 | 160 |
| 339 | smartbiometrik-001 | 0.5485 | 429 | 0.6442 | 425 | 0.7550 | 426 | 0.8611 | 423 | 0.8677 | 419 | 0.8270 | 374 | 0.7030 | 396 | 0.3144 | 402 |
| 340 | smartengines-000 | 0.6240 | 435 | 0.7562 | 435 | 0.9552 | 433 | 0.9784 | 432 | 0.9515 | 429 | 0.9288 | 388 | 0.8200 | 408 | 0.8037 | 429 |
| 341 | smartengines-001 | 0.6434 | 436 | 0.7666 | 436 | 0.9446 | 432 | 0.9750 | 431 | 0.9387 | 428 | 0.9556 | 392 | 0.8647 | 412 | 0.7748 | 427 |
| 342 | smartvist-000 | 0.0912 | 379 | 0.1587 | 378 | 0.1163 | 380 | 0.1841 | 378 | 0.1397 | 369 | 0.9372 | 390 | 0.7107 | 400 | 0.0779 | 337 |
| 343 | smilart-002 | 0.2440 | 396 | 0.3532 | 398 | - | - | - | - | 0.3785 | 392 | 0.4145 | 330 | 0.2611 | 356 | - | - |
| 344 | smilart-003 | 0.6944 | 438 | 0.8836 | 438 | 0.0695 | 372 | 0.1193 | 372 | 0.0894 | 360 | 0.1221 | 289 | 0.0737 | 319 | 0.1190 | 362 |
| 345 | sodec-000 | 0.0033 | 87 | 0.0044 | 81 | 0.0040 | 133 | 0.0053 | 121 | 0.0054 | 98 | 0.0096 | 74 | 0.0080 | 88 | 0.0274 | 19 |
| 346 | sqisoft-001 | 0.1220 | 386 | 0.2088 | 385 | 0.1978 | 389 | 0.3386 | 389 | 0.2111 | 382 | 0.2798 | 317 | 0.1474 | 341 | 0.0519 | 305 |
| 347 | sqisoft-002 | 0.0082 | 218 | 0.0124 | 215 | 0.0051 | 168 | 0.0086 | 201 | 0.0102 | 194 | 0.0183 | 155 | 0.0122 | 162 | 0.0287 | 127 |
| 348 | stagu-000 | 0.0139 | 292 | 0.0208 | 284 | 0.0104 | 274 | 0.0145 | 265 | 0.0156 | 247 | 0.8063 | 369 | 0.1408 | 340 | 0.0332 | 228 |
| 349 | starhybrid-001 | 0.0108 | 252 | 0.0138 | 228 | 0.0081 | 240 | 0.0113 | 225 | 0.0152 | 246 | 0.0265 | 192 | 0.0189 | 230 | 0.0350 | 249 |
| 350 | sukshi-000 | 0.5409 | 427 | 0.6612 | 429 | 0.4556 | 404 | 0.6567 | 406 | 0.9296 | 427 | 0.8898 | 377 | 0.7384 | 401 | 0.6892 | 423 |
| 351 | suprema-002 | 0.0030 | 71 | 0.0041 | 68 | 0.0034 | 100 | 0.0040 | 81 | 0.0045 | 75 | 0.0085 | 57 | 0.0072 | 72 | 0.0295 | 163 |
| 352 | suprema-003 | 0.0028 | 66 | 0.0041 | 69 | 0.0034 | 98 | 0.0039 | 76 | 0.0030 | 27 | 0.3095 | 320 | 0.0580 | 309 | 0.0284 | 105 |

Table 26: FNMR is the proportion of mated comparisons below a threshold set to achieve the FMR given in the header on the fourth row. FMR is the proportion of impostor comparisons at or above that threshold. The light grey values give rank over all algorithms in that column. The pink columns use only same-sex impostors; others are selected regardless of demographics. The exception, in the green column, uses “matched-covariates” i.e. impostors of the same sex, age group, and country of birth. The second pink column includes effects of extended ageing. Missing entries for border, visa, mugshot and wild images generally mean the algorithm did not run to completion. The VISA columns compare images described in section 2.1. The MUGSHOT columns compare images described in section 2.4. The VISA-BORDER column compare images described in section 2.2 with those of section 2.3. The BORDER column compares images described in section 2.3. The WILD columns compare images described in section 2.6.

| Algorithm | FALSE NON-MATCH RATE (FNMR) | | | | | | | | | | | | | | | | |
|-----------|-----------------------------|--------|-------|---------|---------------|------------|--------|--------|--------|--------|--------|--------|--------|--------|--------|--------|-----|
| | CONSTRAINED, COOPERATIVE | | | | | | | | | | | | | | | | |
| | Name | VISAMC | VISA | MUGSHOT | MUGSHOT12+YRS | VISABORDER | BORDER | BORDER | WILD | | | | | | | | |
| FMR | 0.0001 | 1E-06 | 1E-05 | 1E-05 | 1E-05 | 1E-06 | 1E-06 | 1E-05 | 0.0001 | 0.0001 | 0.0001 | 0.0001 | | | | | |
| 353 | supremaid-001 | 0.0053 | 142 | 0.0073 | 137 | 0.0045 | 146 | 0.0066 | 159 | 0.0099 | 192 | 0.0186 | 156 | 0.0148 | 192 | 0.0352 | 252 |
| 354 | supremaid-002 | 0.0063 | 175 | 0.0094 | 179 | 0.0044 | 141 | 0.0062 | 151 | 0.0072 | 132 | 0.0229 | 180 | 0.0095 | 121 | 0.0345 | 240 |
| 355 | surrey-cvssp-000 | 0.9084 | 442 | 0.9909 | 443 | 0.9923 | 436 | 0.9950 | 434 | 0.9981 | 432 | 0.9994 | 415 | 0.9979 | 430 | 0.9389 | 431 |
| 356 | synesis-006 | 0.0070 | 190 | 0.0096 | 181 | 0.0107 | 280 | 0.0166 | 280 | - | 0.0128 | 108 | 0.0089 | 108 | 0.0292 | 155 | |
| 357 | synesis-007 | 0.0050 | 128 | 0.0073 | 139 | 0.0062 | 200 | 0.0076 | 177 | - | 0.0105 | 83 | 0.0080 | 90 | 0.0288 | 129 | |
| 358 | synology-000 | 0.0149 | 300 | 0.0238 | 301 | 0.0148 | 315 | 0.0261 | 315 | 0.0221 | 287 | 0.0331 | 215 | 0.0209 | 243 | 0.0330 | 226 |
| 359 | synology-002 | 0.0104 | 249 | 0.0153 | 245 | 0.0107 | 281 | 0.0184 | 287 | 0.0189 | 276 | 0.2032 | 304 | 0.0180 | 220 | 0.0312 | 203 |
| 360 | sztu-000 | 0.0092 | 231 | 0.0139 | 230 | 0.0091 | 258 | 0.0201 | 299 | 0.0136 | 232 | 0.0685 | 264 | 0.0118 | 158 | 0.0270 | 5 |
| 361 | sztu-001 | 0.0031 | 72 | 0.0043 | 77 | 0.0025 | 28 | 0.0028 | 30 | 0.0051 | 90 | 0.0113 | 93 | 0.0089 | 109 | 0.0275 | 22 |
| 362 | t4isb-000 | 0.0058 | 155 | 0.0087 | 167 | 0.0041 | 137 | 0.0064 | 155 | 0.0083 | 154 | 0.0157 | 129 | 0.0103 | 132 | 0.0282 | 87 |
| 363 | tech5-004 | 0.0123 | 275 | 0.0234 | 299 | 0.0086 | 251 | 0.0162 | 275 | 0.0065 | 123 | 0.0112 | 91 | 0.0082 | 94 | 0.0281 | 80 |
| 364 | tech5-005 | 0.0054 | 145 | 0.0072 | 134 | 0.0069 | 212 | 0.0122 | 232 | 0.0060 | 114 | 0.0094 | 71 | 0.0066 | 57 | 0.0349 | 247 |
| 365 | techsign-000 | 0.0325 | 351 | 0.0511 | 349 | 0.0435 | 359 | 0.0710 | 357 | 0.0746 | 354 | 0.1104 | 286 | 0.0841 | 324 | 0.0639 | 323 |
| 366 | techsign-001 | 0.0110 | 255 | 0.0196 | 279 | 0.0067 | 208 | 0.0120 | 230 | 0.0087 | 161 | 0.2475 | 312 | 0.0883 | 328 | 0.0299 | 177 |
| 367 | tevian-007 | 0.0019 | 35 | 0.0027 | 30 | 0.0032 | 89 | 0.0041 | 83 | 0.0045 | 76 | 0.0086 | 60 | 0.0078 | 84 | 0.0310 | 202 |
| 368 | tevian-008 | 0.0012 | 16 | 0.0017 | 9 | 0.0033 | 90 | 0.0042 | 89 | 0.0042 | 68 | 0.0081 | 49 | 0.0068 | 63 | 0.0290 | 146 |
| 369 | tiger-005 | 0.0624 | 371 | 0.2450 | 389 | 0.0292 | 347 | 0.0556 | 347 | 0.0430 | 332 | 1.0000 | 422 | 0.9964 | 426 | 0.0278 | 44 |
| 370 | tiger-006 | 0.0066 | 180 | 0.0101 | 192 | 0.0050 | 167 | 0.0075 | 176 | 0.0089 | 166 | 0.0158 | 130 | 0.0117 | 155 | 0.0290 | 153 |
| 371 | tinkoff-001 | 0.0145 | 297 | 0.0244 | 302 | 0.0318 | 350 | 0.0636 | 355 | 0.0236 | 297 | 1.0000 | 442 | 0.0339 | 274 | 0.0563 | 315 |
| 372 | tongyi-005 | 0.0073 | 202 | 0.0146 | 236 | 0.0187 | 324 | 0.0421 | 337 | 0.0161 | 252 | 0.0215 | 171 | 0.0149 | 194 | 0.0399 | 270 |
| 373 | toppanidgate-000 | 0.0021 | 37 | 0.0033 | 41 | 0.0026 | 36 | 0.0028 | 27 | 0.0039 | 57 | 0.0075 | 38 | 0.0068 | 61 | 0.0376 | 264 |
| 374 | toshiba-004 | 0.0030 | 68 | 0.0042 | 72 | 0.0025 | 27 | 0.0027 | 24 | 0.0034 | 39 | 0.0063 | 23 | 0.0053 | 30 | 0.0278 | 42 |
| 375 | toshiba-006 | 0.0022 | 47 | 0.0035 | 47 | 0.0024 | 20 | 0.0025 | 16 | 0.0027 | 14 | 0.7425 | 359 | 0.3070 | 364 | 0.0275 | 25 |
| 376 | touchlessid-000 | 0.3296 | 406 | 0.4804 | 409 | 0.4111 | 400 | 0.6026 | 403 | 0.5324 | 398 | 0.9996 | 418 | 0.9964 | 427 | 0.2521 | 394 |
| 377 | trueface-002 | 0.0060 | 166 | 0.0096 | 180 | 0.0048 | 157 | 0.0061 | 148 | 0.0112 | 209 | 0.0198 | 164 | 0.0155 | 200 | 0.0793 | 340 |
| 378 | trueface-003 | 0.0070 | 191 | 0.0094 | 177 | 0.0053 | 175 | 0.0081 | 192 | 0.0122 | 217 | 0.0217 | 174 | 0.0159 | 203 | 0.0785 | 339 |
| 379 | tuputech-000 | 0.3218 | 405 | 0.3696 | 401 | - | - | - | 0.3237 | 387 | 0.4304 | 331 | 0.2973 | 363 | 0.9415 | 432 | |
| 380 | turingtechvip-001 | 0.0330 | 353 | 0.0540 | 353 | 0.0458 | 360 | 0.1007 | 366 | 0.4715 | 396 | 0.9286 | 387 | 0.8448 | 411 | 0.4035 | 410 |
| 381 | turingtechvip-002 | 0.0126 | 283 | 0.0163 | 251 | 0.0092 | 263 | 0.0118 | 228 | 0.2264 | 384 | 1.0000 | 443 | 0.9925 | 423 | 0.2144 | 383 |
| 382 | twface-000 | 0.0051 | 132 | 0.0072 | 135 | 0.0041 | 135 | 0.0058 | 135 | 0.0071 | 129 | 0.0153 | 124 | 0.0100 | 123 | 0.0276 | 32 |
| 383 | twface-001 | 0.0036 | 95 | 0.0051 | 97 | 0.0031 | 82 | 0.0038 | 70 | 0.0049 | 86 | 0.0091 | 67 | 0.0075 | 79 | 0.0277 | 37 |
| 384 | ulsee-001 | 0.0151 | 302 | 0.0246 | 304 | 0.0113 | 291 | 0.0185 | 290 | 0.0187 | 275 | 0.6766 | 352 | 0.0181 | 222 | 0.0316 | 212 |
| 385 | ultinous-000 | 0.2343 | 394 | 0.3484 | 397 | - | - | - | - | - | - | - | - | - | - | - | |
| 386 | ultinous-001 | 0.2485 | 397 | 0.4003 | 404 | - | - | - | - | - | - | - | - | - | - | - | |
| 387 | uluface-002 | 0.0081 | 214 | 0.0123 | 213 | 0.0071 | 217 | 0.0095 | 212 | 0.0107 | 200 | 1.0000 | 439 | 0.0140 | 182 | 0.0444 | 290 |
| 388 | uluface-003 | 0.0100 | 243 | 0.0150 | 241 | 0.0079 | 233 | 0.0128 | 243 | - | - | - | - | - | 0.0635 | 321 | |
| 389 | unissey-001 | 0.0095 | 235 | 0.0160 | 248 | 0.0134 | 304 | 0.0150 | 268 | 0.0147 | 244 | 0.0253 | 189 | 0.0163 | 205 | 0.0946 | 350 |
| 390 | unissey-002 | 0.0094 | 234 | 0.0151 | 243 | 0.0079 | 234 | 0.0110 | 220 | 0.0114 | 210 | 0.4424 | 332 | 0.1914 | 347 | 0.0420 | 281 |
| 391 | upc-001 | 0.0234 | 334 | 0.0519 | 350 | 0.0291 | 346 | 0.0490 | 344 | 0.0294 | 313 | 0.2316 | 310 | 0.0389 | 286 | 0.0314 | 209 |
| 392 | vcog-002 | 0.7522 | 440 | 0.9033 | 439 | - | - | - | - | - | - | - | - | - | - | - | |
| 393 | vd-002 | 0.0429 | 360 | 0.0704 | 361 | 0.0569 | 367 | 0.0844 | 362 | 0.0801 | 356 | 0.0937 | 274 | 0.0577 | 308 | 0.0556 | 314 |
| 394 | vd-003 | 0.0199 | 329 | 0.0222 | 293 | 0.0115 | 294 | 0.0130 | 246 | 0.0138 | 235 | 0.0239 | 182 | 0.0177 | 217 | 0.0389 | 266 |
| 395 | veridas-006 | 0.0098 | 239 | 0.0167 | 258 | 0.0079 | 235 | 0.0127 | 239 | 0.0127 | 223 | 0.0217 | 173 | 0.0151 | 197 | 0.0286 | 122 |
| 396 | veridas-007 | 0.0063 | 174 | 0.0083 | 158 | 0.0044 | 143 | 0.0058 | 138 | 0.0080 | 147 | 0.0152 | 122 | 0.0120 | 161 | 0.0284 | 106 |

Table 27: FNMR is the proportion of mated comparisons below a threshold set to achieve the FMR given in the header on the fourth row. FMR is the proportion of impostor comparisons at or above that threshold. The light grey values give rank over all algorithms in that column. The pink columns use only same-sex impostors; others are selected regardless of demographics. The exception, in the green column, uses “matched-covariates” i.e. impostors of the same sex, age group, and country of birth. The second pink column includes effects of extended ageing. Missing entries for border, visa, mugshot and wild images generally mean the algorithm did not run to completion. The VISA columns compare images described in section 2.1. The MUGSHOT columns compare images described in section 2.4. The VISA-BORDER column compare images described in section 2.2 with those of section 2.3. The BORDER column compares images described in section 2.3. The WILD columns compare images described in section 2.6.

| Algorithm | Name | FALSE NON-MATCH RATE (FNMR) | | | | | | | | | | LESS CONSTRAINED, NON-COOP. | | | | | |
|-----------|---------------------------|-----------------------------|-------|---------|---------------|------------|--------|--------|-------|--------|-----|-----------------------------|-----|--------|-----|--------|-----|
| | | CONSTRAINED, COOPERATIVE | | | | | | | | WILD | | | | | | | |
| | | VISAMC | VISA | MUGSHOT | MUGSHOT12+YRS | VISABORDER | BORDER | BORDER | 1E-05 | 0.0001 | | | | | | | |
| FMR | | 0.0001 | 1E-06 | 1E-05 | 1E-05 | 1E-06 | 1E-06 | 1E-05 | | | | | | | | | |
| 397 | veridium-000 | 0.0726 | 376 | 0.1248 | 374 | 0.5226 | 407 | 0.6652 | 407 | 0.6425 | 402 | 0.8150 | 370 | 0.7989 | 407 | 0.4988 | 417 |
| 398 | verigram-000 | 0.0032 | 75 | 0.0043 | 75 | 0.0031 | 75 | 0.0034 | 52 | 0.0093 | 176 | 0.0175 | 148 | 0.0164 | 207 | 0.0276 | 31 |
| 399 | verigram-001 | 0.0032 | 78 | 0.0044 | 79 | 0.0027 | 48 | 0.0032 | 47 | 0.0030 | 25 | 0.9995 | 416 | 0.9953 | 425 | 0.0276 | 34 |
| 400 | verihubs-inteligensia-000 | 0.0070 | 189 | 0.0098 | 185 | 0.0048 | 159 | 0.0076 | 180 | 0.0092 | 172 | 0.0160 | 132 | 0.0117 | 154 | 0.0283 | 98 |
| 401 | verihubs-inteligensia-001 | 0.0071 | 193 | 0.0114 | 209 | 0.0050 | 166 | 0.0076 | 179 | 0.0096 | 183 | 0.0165 | 139 | 0.0114 | 151 | 0.0282 | 85 |
| 402 | verijelas-000 | 0.2488 | 398 | 0.3431 | 396 | 0.4861 | 405 | 0.6004 | 402 | 0.0811 | 357 | 0.1148 | 287 | 0.0440 | 293 | 0.0524 | 307 |
| 403 | via-000 | 0.0216 | 331 | 0.0365 | 335 | 0.0177 | 322 | 0.0287 | 322 | 0.0296 | 314 | 0.0572 | 253 | 0.0290 | 269 | 0.0349 | 246 |
| 404 | via-001 | 0.0149 | 299 | 0.0229 | 295 | 0.0114 | 293 | 0.0177 | 285 | 0.0183 | 271 | 0.4056 | 328 | 0.0176 | 215 | 0.0373 | 263 |
| 405 | videmo-000 | 0.0298 | 348 | 0.0423 | 341 | 0.0155 | 319 | 0.0260 | 314 | 0.0246 | 303 | 0.0397 | 236 | 0.0239 | 254 | 0.0541 | 310 |
| 406 | videmo-001 | 0.0295 | 346 | 0.0417 | 339 | 0.0164 | 321 | 0.0261 | 316 | 0.0355 | 321 | 0.0603 | 257 | 0.0442 | 295 | 0.1473 | 365 |
| 407 | videonetics-001 | 0.5483 | 428 | 0.6446 | 426 | 0.7517 | 424 | 0.8607 | 422 | 0.8664 | 417 | 0.8255 | 372 | 0.6956 | 395 | 0.2986 | 399 |
| 408 | videonetics-002 | 0.4274 | 414 | 0.5329 | 415 | 0.6081 | 412 | 0.7438 | 412 | 0.7775 | 408 | 0.7297 | 358 | 0.5756 | 385 | 0.1976 | 381 |
| 409 | viettelhightech-000 | 0.0117 | 263 | 0.0166 | 255 | 0.0110 | 285 | 0.0198 | 298 | 0.0167 | 261 | 0.0249 | 185 | 0.0158 | 201 | 0.0409 | 278 |
| 410 | vigilantsolutions-010 | 0.0109 | 253 | 0.0164 | 253 | 0.0074 | 226 | 0.0095 | 210 | 0.0209 | 284 | 0.0365 | 229 | 0.0233 | 251 | 0.0277 | 38 |
| 411 | vigilantsolutions-011 | 0.0124 | 277 | 0.0176 | 265 | 0.0073 | 222 | 0.0095 | 209 | 0.0196 | 280 | 0.0360 | 227 | 0.0221 | 247 | 0.0274 | 17 |
| 412 | vinai-000 | 0.0081 | 213 | 0.0124 | 216 | 0.0045 | 144 | 0.0072 | 170 | 0.0089 | 165 | 0.1814 | 298 | 0.0112 | 146 | 0.0274 | 20 |
| 413 | vinbigdata-001 | 0.2576 | 401 | 0.2763 | 391 | 0.1404 | 384 | 0.1988 | 383 | 0.1407 | 370 | 0.1150 | 288 | 0.0703 | 316 | 0.9767 | 434 |
| 414 | vinbigdata-002 | 0.0102 | 246 | 0.0175 | 262 | 0.0071 | 220 | 0.0084 | 197 | 0.0090 | 167 | 0.8017 | 368 | 0.3134 | 365 | 0.0304 | 189 |
| 415 | vion-000 | 0.0419 | 358 | 0.0590 | 357 | 0.0422 | 358 | 0.0478 | 341 | 0.0581 | 344 | 0.0968 | 281 | 0.0847 | 325 | 0.2479 | 391 |
| 416 | visage-000 | 0.0933 | 380 | 0.1441 | 377 | 0.1316 | 382 | 0.2416 | 384 | 0.1395 | 368 | 0.1920 | 301 | 0.1001 | 332 | 0.0500 | 302 |
| 417 | visionbox-001 | 0.0159 | 307 | 0.0270 | 315 | 0.0111 | 287 | 0.0173 | 283 | 0.0190 | 277 | 0.0315 | 209 | 0.0205 | 241 | 0.0389 | 267 |
| 418 | visionbox-002 | 0.0058 | 153 | 0.0079 | 150 | 0.0060 | 195 | 0.0074 | 172 | 0.0084 | 156 | 0.0149 | 117 | 0.0113 | 149 | 0.0447 | 292 |
| 419 | visionlabs-010 | 0.0017 | 27 | 0.0024 | 24 | 0.0026 | 39 | 0.0030 | 38 | 0.0033 | 38 | 0.0061 | 22 | 0.0052 | 23 | 0.0282 | 89 |
| 420 | visionlabs-011 | 0.0012 | 13 | 0.0022 | 18 | 0.0024 | 21 | 0.0026 | 21 | 0.0028 | 17 | 0.0053 | 10 | 0.0046 | 13 | 0.0280 | 67 |
| 421 | visteam-003 | 0.0804 | 378 | 0.2166 | 386 | 0.0613 | 371 | 0.1204 | 373 | 0.0963 | 363 | 0.1269 | 291 | 0.0441 | 294 | 0.0296 | 171 |
| 422 | visteam-004 | 0.0541 | 368 | 0.5202 | 413 | 0.0406 | 357 | 0.0827 | 361 | 0.1879 | 378 | 0.1795 | 297 | 0.0347 | 277 | 0.0289 | 138 |
| 423 | vixvzion-005 | 0.0276 | 343 | 0.0420 | 340 | 0.0302 | 349 | 0.0629 | 354 | 0.0288 | 310 | 0.0447 | 240 | 0.0235 | 253 | 0.0265 | 2 |
| 424 | vixvzion-006 | 0.0082 | 217 | 0.0122 | 212 | 0.0093 | 264 | 0.0194 | 294 | 0.0099 | 191 | 0.0169 | 141 | 0.0108 | 142 | 0.0268 | 4 |
| 425 | vnpt-003 | 0.0117 | 262 | 0.0138 | 229 | 0.0040 | 134 | 0.0058 | 141 | 0.0087 | 160 | 0.0161 | 134 | 0.0126 | 166 | 0.0284 | 101 |
| 426 | vnpt-004 | 0.0058 | 161 | 0.0078 | 149 | 0.0037 | 114 | 0.0053 | 120 | 0.0051 | 91 | 0.4640 | 334 | 0.1384 | 338 | 0.0275 | 26 |
| 427 | vocord-009 | 0.0022 | 46 | 0.0029 | 34 | 0.0036 | 107 | 0.0046 | 101 | 0.0052 | 94 | 0.0098 | 75 | 0.0086 | 105 | 0.0284 | 108 |
| 428 | vocord-010 | 0.0024 | 53 | 0.0031 | 38 | 0.0036 | 108 | 0.0049 | 112 | 0.0025 | 10 | 0.0065 | 25 | 0.0040 | 7 | 0.0280 | 66 |
| 429 | vts-000 | 0.0103 | 247 | 0.0174 | 261 | 0.0080 | 237 | 0.0129 | 245 | 0.0250 | 305 | 0.0450 | 242 | 0.0372 | 284 | 0.0596 | 317 |
| 430 | vts-001 | 0.0033 | 83 | 0.0048 | 89 | 0.0027 | 50 | 0.0036 | 63 | 0.0032 | 33 | 0.6519 | 349 | 0.3563 | 369 | 0.0338 | 234 |
| 431 | wicket-000 | 0.0018 | 33 | 0.0028 | 33 | 0.0024 | 18 | 0.0027 | 22 | 0.0031 | 29 | 0.7968 | 367 | 0.4340 | 376 | 0.0323 | 217 |
| 432 | winsense-001 | 0.0062 | 171 | 0.0099 | 189 | 0.0092 | 261 | 0.0210 | 300 | 0.0093 | 175 | 0.0144 | 115 | 0.0098 | 122 | 0.0320 | 216 |
| 433 | winsense-002 | 0.0050 | 129 | 0.0073 | 138 | 0.0038 | 116 | 0.0059 | 142 | 0.0064 | 121 | 0.0118 | 100 | 0.0084 | 98 | 0.0307 | 196 |
| 434 | wuhantianyu-001 | 0.0163 | 309 | 0.0262 | 313 | 0.0281 | 344 | 0.0569 | 350 | 0.0316 | 318 | 0.0486 | 248 | 0.0344 | 275 | 0.0324 | 218 |
| 435 | x-laboratory-000 | 0.0071 | 196 | 0.0106 | 196 | 0.0123 | 298 | 0.0138 | 255 | 0.0419 | 331 | 0.5629 | 342 | 0.2852 | 361 | 0.0295 | 168 |
| 436 | x-laboratory-001 | 0.0059 | 163 | 0.0110 | 204 | 0.0054 | 178 | 0.0078 | 186 | 0.0094 | 178 | 0.0142 | 112 | 0.0100 | 125 | 0.0294 | 161 |
| 437 | xforwardai-001 | 0.0021 | 38 | 0.0034 | 43 | 0.0027 | 52 | 0.0028 | 29 | 0.0046 | 80 | 0.0088 | 64 | 0.0079 | 86 | 0.0281 | 79 |
| 438 | xforwardai-002 | 0.0016 | 25 | 0.0023 | 19 | 0.0026 | 42 | 0.0025 | 13 | 0.0040 | 61 | 0.0081 | 51 | 0.0074 | 75 | 0.0282 | 83 |
| 439 | xm-000 | 0.0015 | 22 | 0.0026 | 28 | 0.0031 | 80 | 0.0038 | 74 | 0.0058 | 108 | 0.0105 | 84 | 0.0082 | 95 | 0.0282 | 88 |
| 440 | yisheng-004 | 0.1988 | 391 | 0.3329 | 394 | 0.1147 | 379 | 0.1849 | 379 | 0.2044 | 380 | - | - | 0.0908 | | 348 | |

Table 28: FNMR is the proportion of mated comparisons below a threshold set to achieve the FMR given in the header on the fourth row. FMR is the proportion of impostor comparisons at or above that threshold. The light grey values give rank over all algorithms in that column. The pink columns use only same-sex impostors; others are selected regardless of demographics. The exception, in the green column, uses “matched-covariates” i.e. impostors of the same sex, age group, and country of birth. The second pink column includes effects of extended ageing. Missing entries for border, visa, mugshot and wild images generally mean the algorithm did not run to completion. The VISA columns compare images described in section 2.1. The MUGSHOT columns compare images described in section 2.4. The VISA-BORDER column compare images described in section 2.2 with those of section 2.3. The BORDER column compares images described in section 2.3. The WILD columns compare images described in section 2.6.

| Algorithm | FALSE NON-MATCH RATE (FNMR) | | | | | | | | | |
|-----------|-----------------------------|--------|-------|---------|---------------|-------------|--------|-----------------------------|--------|--------|
| | CONSTRAINED, COOPERATIVE | | | | | | | LESS CONSTRAINED, NON-COOP. | | |
| | Name | VISAMC | VISA | MUGSHOT | MUGSHOT12+YRS | VISA BORDER | BORDER | BORDER | WILD | |
| FMR | 0.0001 | 1E-06 | 1E-05 | 1E-05 | 1E-06 | 1E-06 | 1E-06 | 1E-05 | 0.0001 | |
| 441 | ytu-003 | 0.0015 | 23 | 0.0026 | 27 | 0.0066 | 207 | 0.0085 | 198 | 0.0064 |
| 442 | yoonik-002 | 0.0052 | 138 | 0.0062 | 120 | 0.0029 | 66 | 0.0034 | 54 | 0.0615 |
| 443 | yoonik-003 | 0.0034 | 89 | 0.0047 | 86 | 0.0032 | 87 | 0.0037 | 66 | 0.0816 |
| 444 | ytu-000 | 0.0057 | 151 | 0.0087 | 164 | 0.0121 | 296 | 0.0238 | 310 | 0.0047 |
| 445 | yuan-004 | 0.0058 | 162 | 0.0078 | 147 | 0.0039 | 127 | 0.0055 | 126 | 0.0234 |
| 446 | yuan-005 | 0.0037 | 101 | 0.0046 | 85 | 0.0027 | 53 | 0.0035 | 60 | 0.0033 |
| | | | | | | | | | | 0.2706 |
| | | | | | | | | | | 315 |
| | | | | | | | | | | 0.0876 |
| | | | | | | | | | | 327 |
| | | | | | | | | | | 0.0288 |
| | | | | | | | | | | 137 |

Table 29: FNMR is the proportion of mated comparisons below a threshold set to achieve the FMR given in the header on the fourth row. FMR is the proportion of impostor comparisons at or above that threshold. The light grey values give rank over all algorithms in that column. The pink columns use only same-sex impostors; others are selected regardless of demographics. The exception, in the green column, uses “matched-covariates” i.e. impostors of the same sex, age group, and country of birth. The second pink column includes effects of extended ageing. Missing entries for border, visa, mugshot and wild images generally mean the algorithm did not run to completion. The VISA columns compare images described in section 2.1. The MUGSHOT columns compare images described in section 2.4. The VISA-BORDER column compare images described in section 2.2 with those of section 2.3. The BORDER column compares images described in section 2.3. The WILD columns compare images described in section 2.6.

FNMR(T)
FMR(T)
“False non-match rate”
“False match rate”

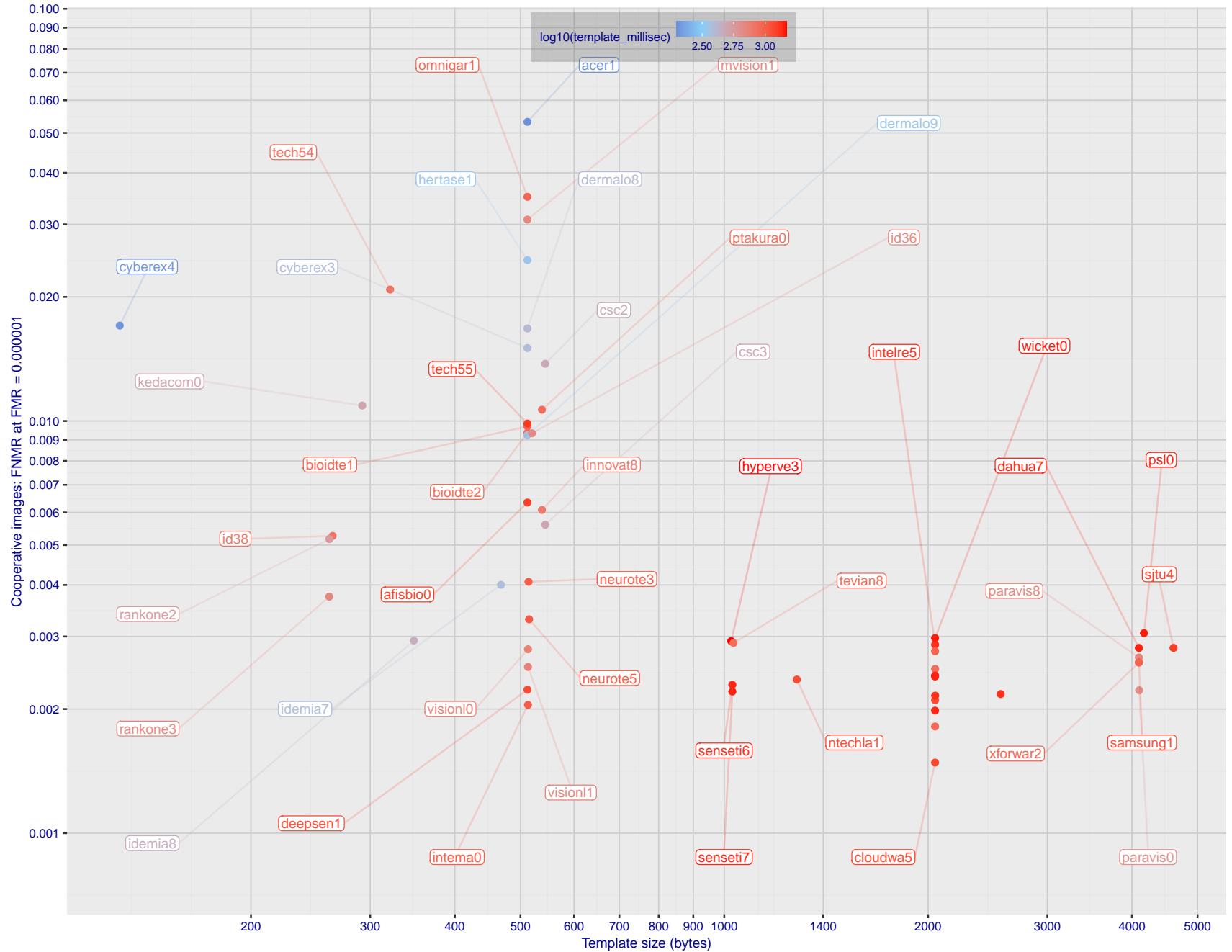


Figure 1: The points show false non-match rates (FNMR) versus the size of the encoded template. FNMR is the geometric mean of FNMR values for visa and mugshot images (from Figs. 84 and 107) at the false match rate (FMR) given in the y-axis label. The color of the points encodes template generation time - which spans at least one order of magnitude. Durations are measured on a single core of a c. 2016 Intel Xeon CPU E5-2630 v4 running at 2.20GHz. Algorithms with poor FNMR are omitted.

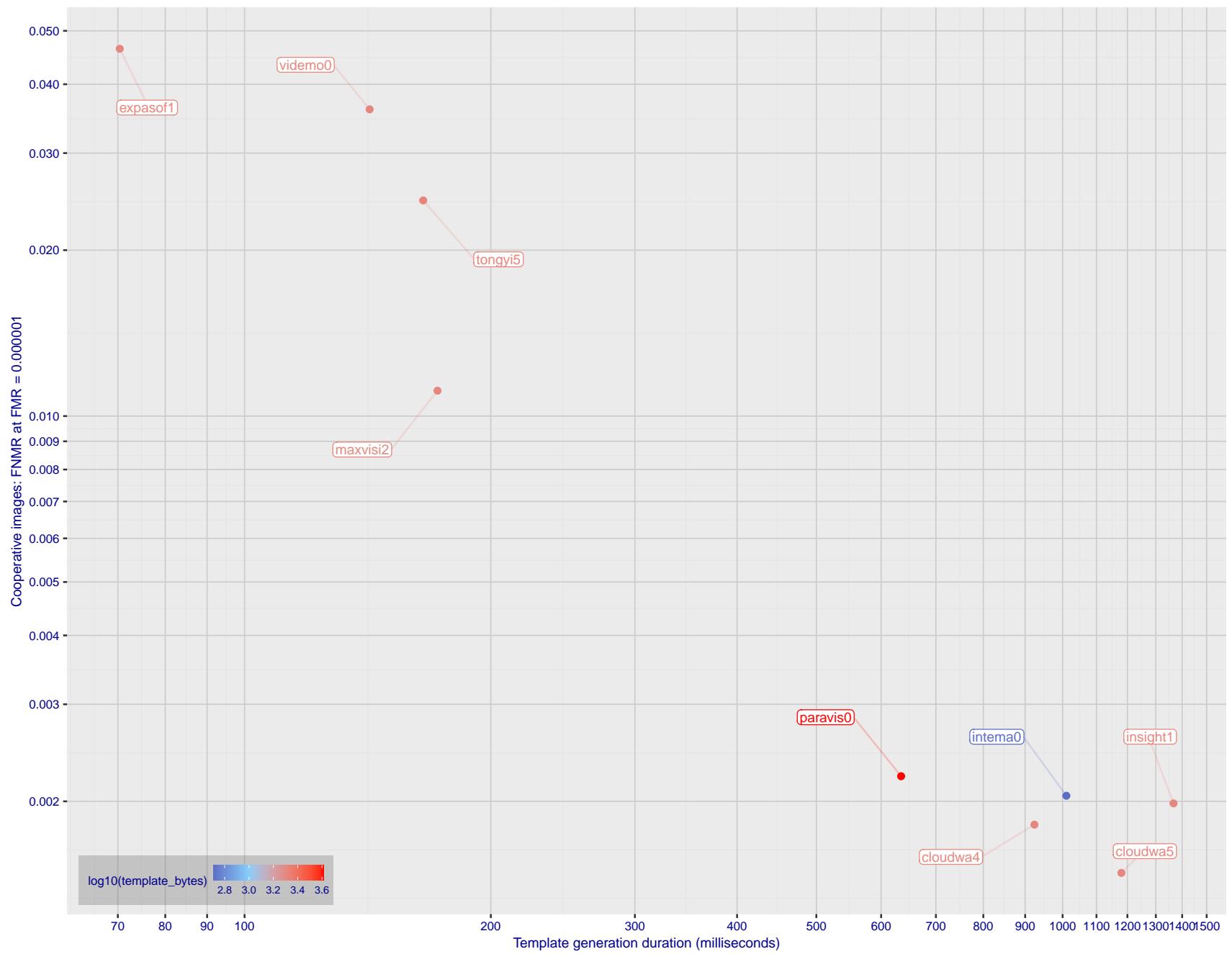


Figure 2: The points show false non-match rates (FNMR) versus the duration of the template generation operation. FNMR is the geometric mean of FNMR values for visa and mugshot images (from Figs. 84 and 107) at a false match rate (FMR) given in the y-axis label. Template generation time is a median estimated over 640 x 480 pixel portraits. It is measured on a single core of a c. 2016 Intel Xeon CPU E5-2630 v4 running at 2.20GHz. The color of the points encodes template size - which span two orders of magnitude. Algorithms with poor FNMR are omitted.

1 Metrics

1.1 Core accuracy

Given a vector of N genuine scores, u , the false non-match rate (FNMR) is computed as the proportion below some threshold, T:

$$\text{FNMR}(T) = 1 - \frac{1}{N} \sum_{i=1}^N H(u_i - T) \quad (1)$$

where $H(x)$ is the unit step function, and $H(0)$ taken to be 1.

Similarly, given a vector of N impostor scores, v , the false match rate (FMR) is computed as the proportion above T:

$$\text{FMR}(T) = \frac{1}{N} \sum_{i=1}^N H(v_i - T) \quad (2)$$

The threshold, T, can take on any value. We typically generate a set of thresholds from quantiles of the observed impostor scores, v , as follows. Given some interesting false match rate range, $[\text{FMR}_L, \text{FMR}_U]$, we form a vector of K thresholds corresponding to FMR measurements evenly spaced on a logarithmic scale

$$T_k = Q_v(1 - \text{FMR}_k) \quad (3)$$

where Q is the quantile function, and FMR_k comes from

$$\log_{10} \text{FMR}_k = \log_{10} \text{FMR}_L + \frac{k}{K} [\log_{10} \text{FMR}_U - \log_{10} \text{FMR}_L] \quad (4)$$

Error tradeoff characteristics are plots of FNMR(T) vs. FMR(T). These are plotted with $\text{FMR}_U \rightarrow 1$ and FMR_L as low as is sustained by the number of impostor comparisons, N. This is somewhat higher than the “rule of three” limit $3/N$ because samples are not independent, due to re-use of images.

1.2 Multi-template scoring methodology

There are some scenarios when one or more people exist and are detected in an image, and some of the proposed test images include $K > 1$ persons for some images and situations where the subject of interest may or may not be the foreground face (largest face in the image). The NIST FRVT 1:1 API supports this by allowing generation of multiple templates representing each person detected in an image. When this occurs, NIST will match all templates generated from the enrollment image with all templates generated from the verification image and use the **maximum** similarity score across all template comparisons. This scoring approach will be used in our calculation of FMR and FNMR (this applies to both genuine and imposter comparisons).

2 Datasets

2.1 Visa images

- ▷ The number of images is on the order of 10^5 .
- ▷ The number of subjects is on the order of 10^5 .
- ▷ The number of subjects with two images is on the order of 10^4 .
- ▷ The images have geometry in reasonable conformance with the ISO/IEC 19794-5 Full Frontal image type. Pose is generally excellent.
- ▷ The images are of size 252x300 pixels. The mean interocular distance (IOD) is 69 pixels.
- ▷ The images are of subjects from greater than 100 countries, with significant imbalance due to visa issuance patterns.
- ▷ The images are of subjects of all ages, including children, again with imbalance due to visa issuance demand.
- ▷ Many of the images are live capture. A substantial number of the images are photographs of paper photographs.
- ▷ When these images are input to the algorithm, they are labelled as being of type "ISO" - see Table 4 of the FRVT API.

2.2 Application images

- ▷ The number of images is on the order of 10^6 .
- ▷ The number of subjects is on the order of 10^6 .
- ▷ The number of subjects with two images is on the order of 10^6 .
- ▷ The images have geometry in good conformance with the ISO/IEC 19794-5 Full Frontal image type. Pose is generally excellent.
- ▷ The images are of size 300x300 pixels. The mean interocular distance (IOD) is 61 pixels.
- ▷ The images are of subjects from greater than 100 countries, with significant imbalance due to population and immigration patterns.
- ▷ The images are of subjects of adults with imbalance due to population and immigration patterns and demand.
- ▷ All of the images are live capture.
- ▷ When these images are input to the algorithm, they are labelled as being of type "ISO" - see Table 4 of the FRVT API.

2.3 Border crossing images

- ▷ The number of images is on the order of 10^6 .
- ▷ The number of subjects is on the order of 10^6 .
- ▷ The number of subjects with two images is on the order of 10^6 .
- ▷ The images are taken with a camera oriented by an attendant toward a cooperating subject. This is done under time constraints so there are roll, pitch and yaw angle variations. Also background illumination is sometimes strong, so the face is under-exposed. There is some perspective distortion due to close range images. Some faces are partially cropped.
- ▷ The images have mean IOD of 38 pixels.
- ▷ The images are of subjects of adults and children aged 12 or above.

- ▷ The images are of subjects from greater than 100 countries, with significant imbalance due to population and immigration patterns.
- ▷ The images are all live capture.
- ▷ When these images are input to the algorithm, they are labelled as being of type "WILD" - see Table 4 of the FRVT API.

2.4 Mugshot images

- ▷ The number of images is on the order of 10^6 .
- ▷ The number of subjects is on the order of 10^6 .
- ▷ The number of subjects with two images is on the order of 10^6 .
- ▷ The images have geometry in reasonable conformance with the ISO/IEC 19794-5 Full Frontal image type.
- ▷ The images are of variable sizes. The median IOD is 105 pixels. The mean IOD is 113 pixels. The 1-st, 5-th, 10-th, 25-th, 75-th, 90-th and 99-th percentiles are 34, 58, 70, 87, 121, 161 and 297 pixels.
- ▷ The images are of subjects from the United States.
- ▷ The images are of adults.
- ▷ The images are all live capture.
- ▷ When these images are input to the algorithm, they are labelled as being of type "mugshot" - see Table 4 of the FRVT API.

2.5 Kiosk images

- ▷ The number of images is on the order of 10^6 .
- ▷ The number of subjects is on the order of 10^5 .
- ▷ The number of subjects with multiple images is the order of 10^5 .
- ▷ The images are taken at kiosk equipped with a camera intended to capture a centered face. However the images have specific quality defects arising from the camera triggering before the subject looks at it. These are downward pitch of the face relative to the optical axis; cropping of the forehead; and cropping of left or right part of the face. Partial cropping affects perhaps 10% of the images. Resolution does not vary widely.
- ▷ The images are of adults.
- ▷ The images have mean IOD of 44 pixels, with maximum below 75, and minimum when both eyes are present above 25 pixels.
- ▷ All of the images are live capture, none are scanned.
- ▷ When these images are input to the algorithm, they are labelled as being of type "WILD" - see Table 4 of the FRVT API.

2.6 Wild images

- ▷ The number of images is on the order of 10^5 .
- ▷ The number of subjects is on the order of 10^4 .
- ▷ The number of subjects with two images on the order of 10^4 .
- ▷ The images include many photojournalism-style images. Images are given to the algorithm using a variable but generally tight crop of the head. Resolution varies very widely. The images are very unconstrained, with wide yaw and pitch pose variation. Faces can be occluded, including hair and hands.

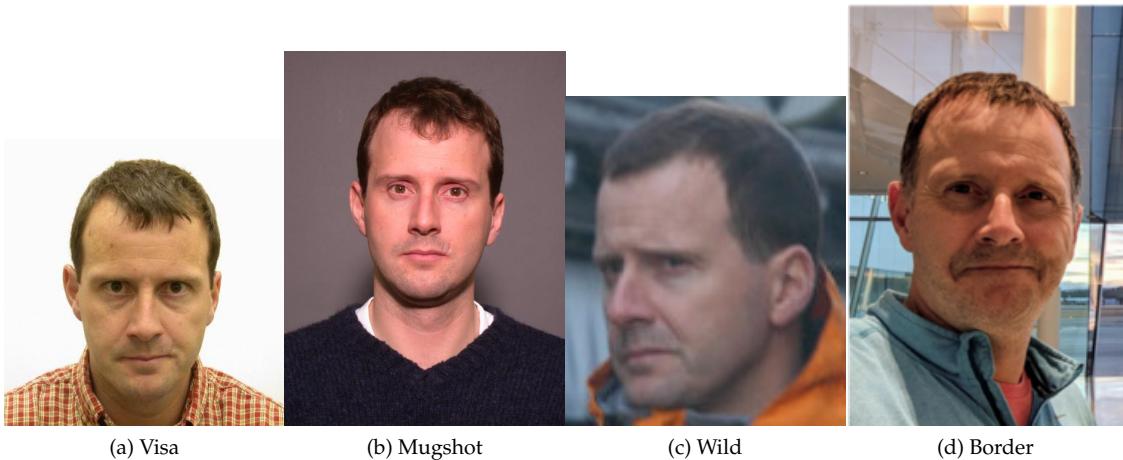


Figure 3: The figure gives simulated samples of image types used in this report.

- ▷ The images are of adults.
 - ▷ All of the images are live capture, none are scanned.
 - ▷ When these images are input to the algorithm, they are labelled as being of type "WILD" - see Table 4 of the FRVT API.

3 Results

3.1 Test goals

- ▷ To state absolute accuracy for different kinds of images, including those with and without subject cooperation.
 - ▷ To state comparative accuracy, across algorithms.

3.2 Test design

Method: For visa images:

- ▷ The comparisons are of visa photos against visa photos.
 - ▷ The number of genuine comparisons is on the order of 10^4 .
 - ▷ The number of impostor comparisons is on the order of 10^{10} .
 - ▷ The comparisons are fully zero-effort, meaning impostors are paired without attention to sex, age or other covariates. However, later analysis is conducted on subsets.
 - ▷ The number of persons is on the order of 10^5 .
 - ▷ The number of images used to make 1 template is 1.
 - ▷ The number of templates used to make each comparison score is two corresponding to simple one-to-one verification.

Method: For mugshot images:

- ▷ The comparisons are of mugshot photos against mugshot photos.

- ▷ The number of genuine comparisons is on the order of 10^6 .
- ▷ The number of impostor comparisons is on the order of 10^8 .
- ▷ The impostors are paired by sex, but not by age or other covariates.
- ▷ The number of persons is on the order of 10^6 .
- ▷ The number of images used to make 1 template is 1.
- ▷ The number of templates used to make each comparison score is two corresponding to simple one-to-one verification.

Method: For visa-border comparisons:

- ▷ The comparisons are of visa-like frontals against border crossing webcam photos.
- ▷ The number of genuine comparisons is on the order of 10^6 .
- ▷ The number of impostor comparisons is on the order of 10^8 .
- ▷ The impostors are paired by sex, but not by age or other covariates.
- ▷ The number of persons is on the order of 10^6 .
- ▷ The number of images used to make 1 template is 1.
- ▷ The number of templates used to make each comparison score is two corresponding to simple one-to-one verification.

Method: For kiosk-border comparisons:

- ▷ The comparisons are of visa-like frontals against kiosk-style photos.
- ▷ The number of genuine comparisons is on the order of 10^6 .
- ▷ The number of impostor comparisons is on the order of 10^8 .
- ▷ The impostors are paired by sex, but not by age or other covariates.
- ▷ The number of persons is on the order of 10^5 .
- ▷ The number of images used to make 1 template is 1.
- ▷ The number of templates used to make each comparison score is two corresponding to simple one-to-one verification.

Method: For border-border comparisons:

- ▷ The comparisons are of border crossing webcam photos.
- ▷ The number of genuine comparisons is on the order of 10^6 .
- ▷ The number of impostor comparisons is on the order of 10^8 .
- ▷ The impostors are paired by sex, but not by age or other covariates.
- ▷ The number of persons is on the order of 10^6 .
- ▷ The number of images used to make 1 template is 1.
- ▷ The number of templates used to make each comparison score is two corresponding to simple one-to-one verification.

Method: For wild images:

- ▷ The comparisons are of wild photos against wild photos.

- ▷ The number of genuine comparisons is on the order of 10^6 .
- ▷ The number of impostor comparisons is on the order of 10^8 .
- ▷ The comparisons are fully zero-effort, meaning impostors are paired without attention to sex, age or other covariates.
- ▷ The number of persons is on the order of 10^4 .
- ▷ The number of images used to make 1 template is 1.
- ▷ The number of templates used to make each comparison score is two corresponding to simple one-to-one verification.

Method: For child exploitation images:

- ▷ The comparisons are of unconstrained child exploitation photos against others of the same type.
- ▷ The number of genuine comparisons is on the order of 10^4 .
- ▷ The number of impostor comparisons is on the order of 10^7 .
- ▷ The comparisons are fully zero-effort, meaning impostors are paired without attention to sex, age or other covariates.
- ▷ The number of persons is on the order of 10^3 .
- ▷ The number of images used to make 1 template is 1.
- ▷ The number of templates used to make each comparison score is two corresponding to simple one-to-one verification.
- ▷ We produce two performance statements. First, is a DET as used for visa and mugshot images. The second is a cumulative match characteristic (CMC) summarizing a simulated one-to-many search process. This is done as follows.
 - We regard M enrollment templates as items in a gallery.
 - These M templates come from $M > N$ individuals, because multiple images of a subject are present in the gallery under separate identifiers.
 - We regard the verification templates as search templates.
 - For each search we compute the rank of the highest scoring mate.
 - This process should properly be conducted with a 1:N algorithm, such as those tested in NIST IR 8009. We use the 1:1 algorithms in a simulated 1:N mode here to a) better reflect what a child exploitation analyst does, and b) to show algorithm efficacy is better than that revealed in the verification DETs.

3.3 Failure to enroll

| | Algorithm | Failure to Enrol Rate ¹ | | | | | | | | | |
|------|---------------------|------------------------------------|----------|----------|----------|----------|-----|---------|-----|--------|-----|
| | | APPLICATION | | BORDER | | KIOSK | | MUGSHOT | | VISA | |
| Name | SEC. 2.2 | SEC. 2.3 | SEC. 2.5 | SEC. 2.4 | SEC. 2.1 | SEC. 2.6 | | | | | |
| 1 | 20face-000 | 0.0000 | 211 | 0.0008 | 226 | 0.0217 | 157 | 0.0000 | 129 | 0.0004 | 249 |
| 2 | 20face-001 | 0.0000 | 240 | 0.0008 | 227 | 0.0000 | 16 | 0.0000 | 128 | 0.0004 | 250 |
| 3 | 3divi-006 | 0.0000 | 298 | 0.0007 | 198 | 0.0214 | 154 | 0.0001 | 236 | 0.0002 | 135 |
| 4 | 3divi-007 | 0.0000 | 280 | 0.0007 | 197 | 0.0214 | 155 | 0.0001 | 238 | 0.0002 | 136 |
| 5 | acer-001 | 0.0000 | 253 | 0.0011 | 284 | - | 387 | 0.0001 | 210 | 0.0004 | 266 |
| 6 | acer-002 | 0.0000 | 367 | 0.0008 | 219 | 0.0191 | 136 | 0.0003 | 323 | 0.0004 | 274 |
| 7 | acisw-007 | 0.0000 | 61 | 0.0000 | 26 | 0.0000 | 21 | 0.0000 | 15 | 0.0000 | 104 |
| 8 | acisw-008 | 0.0000 | 262 | 0.0009 | 250 | 0.0173 | 122 | 0.0004 | 350 | 0.0004 | 189 |
| 9 | adera-002 | 0.0000 | 350 | 0.0034 | 367 | - | 416 | 0.0003 | 330 | 0.0005 | 363 |
| 10 | adera-003 | 0.0000 | 349 | 0.0034 | 368 | 0.0403 | 219 | 0.0003 | 331 | 0.0005 | 364 |
| 11 | advance-002 | 0.0000 | 269 | 0.0013 | 307 | - | 373 | 0.0000 | 192 | 0.0004 | 265 |
| 12 | advance-003 | 0.0000 | 336 | 0.0012 | 293 | 0.0247 | 172 | 0.0001 | 259 | 0.0004 | 317 |
| 13 | afisbiometrics-000 | 0.0000 | 239 | 0.0008 | 209 | 0.0213 | 152 | 0.0000 | 127 | 0.0004 | 273 |
| 14 | aifirst-001 | 0.0000 | 19 | 0.0000 | 2 | - | 299 | 0.0000 | 46 | 0.0000 | 80 |
| 15 | aigen-001 | 0.0000 | 95 | 0.0000 | 65 | - | 376 | 0.0000 | 109 | 0.0000 | 28 |
| 16 | aigen-002 | 0.0000 | 88 | 0.0000 | 39 | 0.0000 | 18 | 0.0000 | 3 | 0.0000 | 90 |
| 17 | ailabs-001 | 0.0000 | 229 | 0.0090 | 406 | - | 343 | 0.0007 | 385 | 0.0005 | 339 |
| 18 | aimall-002 | 0.0000 | 354 | 0.0043 | 382 | - | 349 | 0.0012 | 400 | 0.0005 | 358 |
| 19 | aimall-003 | 0.0000 | 330 | 0.0012 | 300 | - | 359 | 0.0004 | 345 | 0.0005 | 332 |
| 20 | aiseemu-001 | 0.0000 | 129 | 0.0000 | 76 | 0.0000 | 27 | 0.0000 | 93 | 0.0000 | 14 |
| 21 | aiunionface-000 | 0.0000 | 66 | 0.0000 | 25 | - | 351 | 0.0000 | 17 | 0.0000 | 105 |
| 22 | aize-001 | 0.0001 | 396 | 0.0040 | 377 | 0.0652 | 236 | 0.0026 | 420 | 0.0022 | 424 |
| 23 | aize-002 | 0.0000 | 177 | 0.0014 | 310 | 0.0230 | 166 | 0.0005 | 370 | 0.0004 | 246 |
| 24 | ajou-001 | 0.0000 | 203 | 0.0020 | 331 | - | 301 | 0.0001 | 239 | 0.0004 | 321 |
| 25 | alchera-003 | 0.0001 | 408 | 0.0013 | 304 | 0.0317 | 196 | 0.0002 | 302 | 0.0004 | 281 |
| 26 | alchera-004 | 0.0000 | 241 | 0.0009 | 248 | 0.0228 | 164 | 0.0001 | 267 | 0.0004 | 215 |
| 27 | alfabeta-001 | 0.0005 | 419 | 0.0650 | 438 | 0.2142 | 260 | 0.0024 | 415 | 0.0018 | 419 |
| 28 | alice-000 | 0.0000 | 136 | 0.0006 | 171 | 0.0133 | 101 | 0.0000 | 151 | 0.0004 | 203 |
| 29 | alleyes-000 | 0.0000 | 204 | 0.0010 | 265 | - | 302 | 0.0002 | 277 | 0.0004 | 296 |
| 30 | allgovision-000 | 0.0007 | 424 | 0.0062 | 399 | - | 400 | 0.0026 | 419 | 0.0052 | 436 |
| 31 | alphaface-001 | 0.0000 | 258 | 0.0012 | 290 | - | 397 | 0.0000 | 197 | 0.0004 | 292 |
| 32 | alphaface-002 | 0.0000 | 218 | 0.0012 | 289 | - | 281 | 0.0000 | 193 | 0.0004 | 294 |
| 33 | amplifiedgroup-001 | 0.0114 | 439 | 0.1023 | 441 | - | 361 | 0.0189 | 440 | 0.0279 | 445 |
| 34 | androvideo-000 | 0.0000 | 6 | 0.0000 | 12 | - | 286 | 0.0000 | 49 | 0.0000 | 84 |
| 35 | anke-004 | 0.0000 | 290 | 0.0011 | 280 | - | 411 | 0.0001 | 250 | 0.0004 | 301 |
| 36 | anke-005 | 0.0000 | 259 | 0.0012 | 291 | - | 354 | 0.0001 | 263 | 0.0004 | 311 |
| 37 | antheus-000 | 0.0000 | 118 | 0.0000 | 50 | - | 398 | 0.0000 | 105 | 0.0000 | 26 |
| 38 | antheus-001 | 0.0000 | 167 | 0.0000 | 85 | - | 442 | 0.0000 | 73 | 0.0000 | 53 |
| 39 | anyvision-004 | 0.0000 | 339 | 0.0017 | 324 | - | 365 | 0.0001 | 262 | 0.0004 | 253 |
| 40 | anyvision-005 | 0.0000 | 246 | 0.0013 | 301 | - | 324 | 0.0000 | 164 | 0.0004 | 205 |
| 41 | armatura-001 | 0.0000 | 358 | 0.0021 | 338 | 0.0257 | 181 | 0.0005 | 366 | 0.0005 | 344 |
| 42 | asusaics-000 | 0.0000 | 89 | 0.0000 | 38 | - | 325 | 0.0000 | 4 | 0.0000 | 92 |
| 43 | asusaics-001 | 0.0000 | 156 | 0.0000 | 91 | - | 429 | 0.0000 | 81 | 0.0000 | 62 |
| 44 | authenmetric-003 | 0.0000 | 30 | 0.0000 | 23 | 0.0000 | 1 | 0.0000 | 35 | 0.0000 | 69 |
| 45 | authenmetric-004 | 0.0000 | 147 | 0.0000 | 96 | 0.0000 | 48 | 0.0000 | 76 | 0.0000 | 57 |
| 46 | aware-005 | 0.0000 | 309 | 0.0020 | 330 | - | 350 | 0.0001 | 275 | 0.0004 | 304 |
| 47 | aware-006 | 0.0000 | 216 | 0.0009 | 245 | 0.0249 | 174 | 0.0000 | 168 | 0.0004 | 262 |
| 48 | awirots-001 | 0.0039 | 428 | 0.0369 | 431 | - | 377 | 0.0386 | 441 | 0.0872 | 446 |
| 49 | awirots-002 | 0.0000 | 370 | 0.0038 | 375 | - | 406 | 0.0007 | 384 | 0.0012 | 411 |
| 50 | aximetria-001 | 0.0000 | 320 | 0.0010 | 277 | 0.0217 | 158 | 0.0001 | 276 | 0.0004 | 247 |
| 51 | ayftech-001 | 0.0002 | 411 | 0.0046 | 386 | - | 311 | 0.0043 | 430 | 0.0011 | 399 |
| 52 | ayonix-000 | 0.0053 | 432 | 0.0341 | 428 | - | 388 | 0.0113 | 438 | 0.0137 | 441 |
| 53 | beethedata-000 | 0.0005 | 418 | 0.0042 | 381 | 0.0366 | 210 | 0.0002 | 289 | 0.0010 | 393 |
| 54 | beyneai-000 | 0.0000 | 32 | 0.0000 | 21 | 0.0000 | 3 | 0.0000 | 37 | 0.0000 | 72 |
| 55 | biocube-001 | 0.0006 | 422 | 0.0391 | 432 | 0.1207 | 252 | 0.0015 | 405 | 0.0020 | 422 |
| 56 | biodittechswiss-001 | 0.0000 | 288 | 0.0007 | 192 | - | 404 | 0.0000 | 154 | 0.0004 | 283 |
| 57 | biodittechswiss-002 | 0.0000 | 277 | 0.0007 | 195 | - | 430 | 0.0000 | 159 | 0.0004 | 276 |
| 58 | bm-001 | 0.0000 | 78 | 0.0000 | 45 | - | 312 | 0.0000 | 117 | 0.0000 | 101 |

Table 30: FTE is the proportion of failed template generation attempts. Failures can occur because the software throws an exception, or because the software electively refuses to process the input image. This would typically occur if a face is not detected. FTE is measured as the number of function calls that give EITHER a non-zero error code OR that give a “small” template. This is defined as one whose size is less than 0.3 times the median template size for that algorithm. This second rule is needed because some algorithms incorrectly fail to return a non-zero error code when template generation fails.

A hyphen “-” indicates the dataset was not produced.¹ The effects of FTE are included in the accuracy results of this report by regarding any template comparison involving a failed template to produce a low similarity score. Thus higher FTE results in higher FNMR and lower FMR.

| | Algorithm | Failure to Enrol Rate ¹ | | | | | | | | |
|-----|-----------------------|------------------------------------|----------|----------|----------|----------|----------|--------|-----|--------|
| | Name | APPLICATION | BORDER | KIOSK | MUGSHOT | VISA | WILD | | | |
| | Name | SEC. 2.2 | SEC. 2.3 | SEC. 2.5 | SEC. 2.4 | SEC. 2.1 | SEC. 2.6 | | | |
| 59 | boetech-001 | 0.0087 | 437 | 0.0272 | 423 | 0.2117 | 258 | 0.0032 | 425 | 0.0160 |
| 60 | boetech-002 | 0.0087 | 436 | 0.0272 | 422 | 0.2117 | 257 | 0.0032 | 426 | 0.0160 |
| 61 | bressee-001 | 0.0000 | 209 | 0.0010 | 272 | - | 268 | 0.0002 | 288 | 0.0003 |
| 62 | bressee-002 | 0.0000 | 341 | 0.0020 | 336 | 0.0219 | 160 | 0.0008 | 386 | 0.0004 |
| 63 | camvi-002 | 0.0000 | 183 | 0.0000 | 102 | - | 410 | 0.0000 | 55 | 0.0000 |
| 64 | camvi-004 | 0.0000 | 119 | 0.0000 | 114 | - | 399 | 0.0000 | 106 | 0.0000 |
| 65 | canon-003 | 0.0000 | 271 | 0.0008 | 211 | 0.0234 | 169 | 0.0000 | 189 | 0.0004 |
| 66 | canon-004 | 0.0000 | 275 | 0.0008 | 210 | 0.0234 | 170 | 0.0000 | 190 | 0.0004 |
| 67 | ceiec-003 | 0.0000 | 42 | 0.0013 | 308 | - | 279 | 0.0001 | 219 | 0.0004 |
| 68 | ceiec-004 | 0.0000 | 127 | 0.0008 | 224 | - | 357 | 0.0000 | 163 | 0.0004 |
| 69 | chosun-001 | 0.0000 | 60 | 0.0000 | 28 | - | 344 | 0.0000 | 28 | 0.0000 |
| 70 | chosun-002 | 0.0000 | 85 | 0.0000 | 41 | - | 318 | 0.0000 | 1 | 0.0000 |
| 71 | chtface-004 | 0.0000 | 27 | 0.0017 | 320 | 0.0320 | 197 | 0.0000 | 175 | 0.0004 |
| 72 | chtface-005 | 0.0000 | 133 | 0.0017 | 321 | 0.0320 | 198 | 0.0000 | 177 | 0.0004 |
| 73 | clearviewai-000 | 0.0000 | 230 | 0.0003 | 134 | 0.0081 | 82 | 0.0000 | 179 | 0.0003 |
| 74 | closeli-001 | 0.0000 | 103 | 0.0000 | 58 | 0.0000 | 35 | 0.0000 | 97 | 0.0000 |
| 75 | cloudmatrix-000 | 0.0000 | 299 | 0.0012 | 295 | - | 284 | 0.0001 | 215 | 0.0004 |
| 76 | cloudmatrix-001 | 0.0000 | 318 | 0.0028 | 349 | 0.0225 | 162 | 0.0001 | 216 | 0.0004 |
| 77 | cloudwalk-hr-003 | 0.0000 | 244 | 0.0008 | 228 | - | 322 | 0.0001 | 224 | 0.0004 |
| 78 | cloudwalk-hr-004 | 0.0000 | 281 | 0.0011 | 287 | - | 439 | 0.0004 | 347 | 0.0003 |
| 79 | cloudwalk-mt-004 | 0.0000 | 214 | 0.0009 | 234 | 0.0191 | 135 | 0.0002 | 303 | 0.0004 |
| 80 | cloudwalk-mt-005 | 0.0000 | 255 | 0.0005 | 159 | 0.0130 | 100 | 0.0003 | 319 | 0.0004 |
| 81 | cogent-006 | 0.0000 | 124 | 0.0000 | 80 | 0.0000 | 24 | 0.0000 | 91 | 0.0000 |
| 82 | cogent-007 | 0.0000 | 343 | 0.0000 | 112 | 0.0000 | 56 | 0.0000 | 165 | 0.0000 |
| 83 | cognitec-003 | 0.0001 | 389 | 0.0194 | 418 | 0.0820 | 247 | 0.0003 | 337 | 0.0005 |
| 84 | cognitec-004 | 0.0001 | 390 | 0.0037 | 374 | 0.0580 | 229 | 0.0003 | 338 | 0.0005 |
| 85 | cor-001 | 0.0000 | 266 | 0.0006 | 176 | - | 371 | 0.0002 | 314 | 0.0004 |
| 86 | coretech-000 | 0.0000 | 116 | 0.0000 | 51 | 0.0000 | 40 | 0.0000 | 104 | 0.0000 |
| 87 | corsight-002 | 0.0000 | 234 | 0.0005 | 169 | 0.0152 | 112 | 0.0001 | 251 | 0.0004 |
| 88 | corsight-003 | 0.0000 | 220 | 0.0006 | 181 | 0.0175 | 123 | 0.0001 | 244 | 0.0004 |
| 89 | csc-002 | 0.0015 | 427 | 0.0033 | 364 | - | 362 | 0.0006 | 378 | 0.0006 |
| 90 | csc-003 | 0.0015 | 426 | 0.0033 | 363 | 0.0445 | 223 | 0.0006 | 377 | 0.0006 |
| 91 | ctcbcbank-000 | 0.0001 | 392 | 0.0051 | 392 | - | 402 | 0.0011 | 399 | 0.0019 |
| 92 | ctcbcbank-001 | 0.0000 | 369 | 0.0036 | 373 | - | 274 | 0.0005 | 367 | 0.0010 |
| 93 | cubox-001 | 0.0000 | 165 | 0.0000 | 87 | - | 440 | 0.0000 | 71 | 0.0000 |
| 94 | cubox-002 | 0.0000 | 324 | 0.0006 | 179 | 0.0159 | 116 | 0.0002 | 313 | 0.0005 |
| 95 | cudocommunication-001 | 0.0000 | 179 | 0.0000 | 105 | 0.0000 | 44 | 0.0000 | 66 | 0.0000 |
| 96 | cuhkee-001 | 0.0000 | 195 | 0.0011 | 286 | - | 288 | 0.0000 | 131 | 0.0004 |
| 97 | cybercore-001 | 0.0000 | 355 | 0.0001 | 124 | 0.0014 | 64 | 0.0002 | 282 | 0.0002 |
| 98 | cybercore-002 | 0.0000 | 357 | 0.0001 | 125 | 0.0014 | 65 | 0.0002 | 283 | 0.0002 |
| 99 | cyberextruder-003 | 0.0000 | 353 | 0.0077 | 404 | 0.0887 | 250 | 0.0001 | 271 | 0.0006 |
| 100 | cyberextruder-004 | 0.0000 | 348 | 0.0097 | 407 | 0.1025 | 251 | 0.0001 | 265 | 0.0007 |
| 101 | cyberlink-008 | 0.0000 | 139 | 0.0004 | 152 | 0.0106 | 93 | 0.0000 | 126 | 0.0003 |
| 102 | cyberlink-009 | 0.0000 | 34 | 0.0004 | 151 | 0.0106 | 92 | 0.0000 | 123 | 0.0003 |
| 103 | dahua-006 | 0.0000 | 158 | 0.0000 | 111 | - | 434 | 0.0000 | 186 | 0.0003 |
| 104 | dahua-007 | 0.0000 | 1 | 0.0000 | 110 | 0.0000 | 57 | 0.0000 | 182 | 0.0003 |
| 105 | daon-000 | 0.0000 | 376 | 0.0028 | 352 | 0.0577 | 228 | 0.0014 | 404 | 0.0015 |
| 106 | deacatur-000 | 0.0000 | 313 | 0.0020 | 329 | - | 378 | 0.0004 | 354 | 0.0005 |
| 107 | deacatur-001 | 0.0000 | 250 | 0.0009 | 253 | 0.0194 | 137 | 0.0001 | 228 | 0.0004 |
| 108 | deepglint-003 | 0.0000 | 272 | 0.0004 | 153 | - | 423 | 0.0002 | 304 | 0.0004 |
| 109 | deepglint-004 | 0.0000 | 198 | 0.0005 | 156 | 0.0130 | 99 | 0.0002 | 311 | 0.0004 |
| 110 | deepsea-001 | 0.0000 | 134 | 0.0000 | 73 | - | 366 | 0.0000 | 82 | 0.0000 |
| 111 | depsense-000 | 0.0000 | 140 | 0.0006 | 182 | - | 368 | 0.0000 | 145 | 0.0004 |
| 112 | depsense-001 | 0.0000 | 188 | 0.0006 | 185 | 0.0191 | 134 | 0.0000 | 150 | 0.0004 |
| 113 | dermalog-009 | 0.0000 | 365 | 0.0031 | 359 | 0.0148 | 110 | 0.0006 | 374 | 0.0003 |
| 114 | dermalog-010 | 0.0000 | 366 | 0.0031 | 360 | 0.0148 | 109 | 0.0006 | 373 | 0.0003 |
| 115 | dicio-001 | 0.0005 | 421 | 0.0649 | 436 | 0.2136 | 259 | 0.0024 | 413 | 0.0012 |
| 116 | didiglobalface-001 | 0.0000 | 197 | 0.0012 | 288 | - | 291 | 0.0000 | 195 | 0.0004 |
| | | | | | | | | | | |

Table 31: FTE is the proportion of failed template generation attempts. Failures can occur because the software throws an exception, or because the software electively refuses to process the input image. This would typically occur if a face is not detected. FTE is measured as the number of function calls that give EITHER a non-zero error code OR that give a “small” template. This is defined as one whose size is less than 0.3 times the median template size for that algorithm. This second rule is needed because some algorithms incorrectly fail to return a non-zero error code when template generation fails.

A hyphen “-” indicates the dataset was not produced.¹ The effects of FTE are included in the accuracy results of this report by regarding any template comparison involving a failed template to produce a low similarity score. Thus higher FTE results in higher FNMR and lower FMR.

| | Algorithm | Failure to Enrol Rate ¹ | | | | | | | |
|-----|-----------------------|------------------------------------|----------|----------|----------|----------|----------|--------|-----|
| | | APPLICATION | BORDER | KIOSK | MUGSHOT | VISA | WILD | | |
| | Name | SEC. 2.2 | SEC. 2.3 | SEC. 2.5 | SEC. 2.4 | SEC. 2.1 | SEC. 2.6 | | |
| 117 | digidata-000 | 0.0000 | 224 | 0.0023 | 341 | 0.0375 | 214 | 0.0004 | 358 |
| 118 | digidata-001 | 0.0000 | 261 | 0.0023 | 342 | 0.0375 | 215 | 0.0004 | 360 |
| 119 | digitalbarriers-002 | 0.0001 | 399 | 0.0045 | 384 | - | 348 | 0.0028 | 422 |
| 120 | dps-000 | 0.0000 | 168 | 0.0000 | 86 | 0.0000 | 53 | 0.0000 | 72 |
| 121 | dsk-000 | 0.0000 | 54 | 0.0000 | 33 | - | 337 | 0.0000 | 22 |
| 122 | einetworks-000 | 0.0000 | 371 | 0.0017 | 322 | - | 408 | 0.0002 | 300 |
| 123 | ekin-002 | 0.0000 | 166 | 0.0000 | 115 | 0.0004 | 62 | 0.0000 | 125 |
| 124 | enface-000 | 0.0000 | 65 | 0.0012 | 299 | 0.0305 | 194 | 0.0000 | 172 |
| 125 | enface-001 | 0.0000 | 93 | 0.0012 | 297 | 0.0304 | 193 | 0.0000 | 156 |
| 126 | eocortex-000 | 0.0095 | 438 | 0.0602 | 435 | - | 319 | 0.0094 | 437 |
| 127 | ercacat-001 | 0.0000 | 50 | 0.0005 | 162 | - | 332 | 0.0000 | 173 |
| 128 | euronovate-001 | 0.0255 | 443 | 0.0102 | 409 | 0.0517 | 226 | 0.0021 | 410 |
| 129 | expasoft-001 | 0.0000 | 161 | 0.0000 | 88 | - | 436 | 0.0000 | 70 |
| 130 | expasoft-002 | 0.0000 | 105 | 0.0000 | 57 | 0.0000 | 36 | 0.0000 | 98 |
| 131 | f8-001 | 0.0003 | 412 | 0.0059 | 398 | - | 389 | 0.0035 | 427 |
| 132 | f8-002 | 0.0000 | 387 | 0.0150 | 416 | 0.0685 | 243 | 0.0005 | 361 |
| 133 | faceonlive-001 | 0.0000 | 381 | 0.0029 | 356 | 0.0481 | 225 | 0.0013 | 402 |
| 134 | faceonlive-002 | 0.0002 | 409 | 0.0009 | 256 | 0.0075 | 77 | 0.0008 | 388 |
| 135 | facephi-000 | 0.0000 | 23 | 0.0004 | 139 | 0.0090 | 84 | 0.0001 | 252 |
| 136 | facesoft-000 | 0.0000 | 107 | 0.0000 | 56 | - | 391 | 0.0000 | 99 |
| 137 | facetag-000 | 0.0000 | 31 | 0.0000 | 22 | 0.0000 | 2 | 0.0000 | 36 |
| 138 | facetag-002 | 0.0000 | 151 | 0.0000 | 95 | 0.0000 | 49 | 0.0000 | 77 |
| 139 | facex-001 | 0.0001 | 407 | 0.0360 | 429 | - | 345 | 0.0047 | 432 |
| 140 | facex-002 | 0.0001 | 406 | 0.0360 | 430 | 0.2663 | 262 | 0.0047 | 433 |
| 141 | farfaces-001 | 0.0000 | 368 | 0.0007 | 194 | 0.0061 | 74 | 0.0003 | 334 |
| 142 | fiberhome-nanjing-003 | 0.0000 | 13 | 0.0004 | 146 | - | 296 | 0.0000 | 40 |
| 143 | fiberhome-nanjing-004 | 0.0000 | 71 | 0.0004 | 147 | - | 308 | 0.0000 | 8 |
| 144 | fincore-000 | 0.0000 | 205 | 0.0008 | 229 | 0.0185 | 130 | 0.0001 | 203 |
| 145 | frpkauai-001 | 0.0000 | 328 | 0.0024 | 344 | 0.0360 | 208 | 0.0001 | 213 |
| 146 | fujitsulab-002 | 0.0000 | 163 | 0.0009 | 241 | - | 437 | 0.0001 | 261 |
| 147 | fujitsulab-003 | 0.0000 | 51 | 0.0008 | 217 | 0.0166 | 120 | 0.0001 | 248 |
| 148 | g42-intellibrain-001 | 0.0000 | 132 | 0.0000 | 74 | 0.0000 | 29 | 0.0000 | 96 |
| 149 | geo-002 | 0.0000 | 200 | 0.0015 | 311 | 0.0332 | 202 | 0.0001 | 201 |
| 150 | geo-004 | 0.0000 | 284 | 0.0005 | 168 | 0.0138 | 104 | 0.0001 | 237 |
| 151 | glory-004 | 0.0000 | 300 | 0.0020 | 334 | 0.0345 | 204 | 0.0001 | 257 |
| 152 | glory-005 | 0.0000 | 311 | 0.0020 | 335 | 0.0345 | 205 | 0.0001 | 254 |
| 153 | gorilla-007 | 0.0000 | 263 | 0.0009 | 259 | 0.0252 | 177 | 0.0001 | 227 |
| 154 | gorilla-008 | 0.0000 | 291 | 0.0009 | 260 | 0.0259 | 182 | 0.0001 | 225 |
| 155 | graymatics-001 | 0.0000 | 53 | 0.0010 | 261 | 0.0210 | 147 | 0.0001 | 270 |
| 156 | griaule-000 | 0.0000 | 377 | 0.0026 | 348 | 0.0531 | 227 | 0.0004 | 357 |
| 157 | griaule-001 | 0.0000 | 36 | 0.0012 | 298 | 0.0366 | 211 | 0.0000 | 144 |
| 158 | hertasecurity-000 | 0.0133 | 440 | 0.0077 | 405 | - | 396 | 0.0025 | 418 |
| 159 | hertasecurity-001 | 0.0000 | 142 | 0.0000 | 116 | 0.0000 | 58 | 0.0000 | 138 |
| 160 | hik-001 | 0.0000 | 63 | 0.0000 | 118 | - | 347 | 0.0000 | 16 |
| 161 | hisign-001 | 0.0000 | 99 | 0.0000 | 60 | 0.0000 | 34 | 0.0000 | 114 |
| 162 | hyperverge-002 | 0.0000 | 3 | 0.0008 | 216 | 0.0210 | 149 | 0.0002 | 315 |
| 163 | hyperverge-003 | 0.0000 | 148 | 0.0008 | 214 | 0.0210 | 148 | 0.0002 | 316 |
| 164 | hzailu-001 | 0.0000 | 360 | 0.0016 | 316 | 0.0449 | 224 | 0.0003 | 339 |
| 165 | hzailu-002 | 0.0000 | 359 | 0.0015 | 313 | 0.0424 | 220 | 0.0003 | 340 |
| 166 | icm-002 | 0.0000 | 192 | 0.0001 | 122 | - | 419 | 0.0000 | 61 |
| 167 | icm-003 | 0.0000 | 18 | 0.0001 | 121 | 0.0023 | 66 | 0.0000 | 43 |
| 168 | icthtc-000 | 0.0001 | 405 | 0.0047 | 389 | - | 289 | 0.0028 | 423 |
| 169 | id3-006 | 0.0000 | 335 | 0.0009 | 258 | - | 412 | 0.0004 | 349 |
| 170 | id3-008 | 0.0000 | 184 | 0.0006 | 180 | 0.0184 | 127 | 0.0001 | 269 |
| 171 | idemia-008 | 0.0000 | 180 | 0.0004 | 154 | 0.0078 | 81 | 0.0000 | 135 |
| 172 | idemia-009 | 0.0000 | 164 | 0.0004 | 149 | 0.0077 | 78 | 0.0000 | 136 |
| 173 | iit-002 | 0.0000 | 374 | 0.0021 | 337 | - | 305 | 0.0009 | 395 |
| 174 | iit-003 | 0.0000 | 265 | 0.0008 | 230 | - | 370 | 0.0000 | 162 |

Table 32: FTE is the proportion of failed template generation attempts. Failures can occur because the software throws an exception, or because the software electively refuses to process the input image. This would typically occur if a face is not detected. FTE is measured as the number of function calls that give EITHER a non-zero error code OR that give a “small” template. This is defined as one whose size is less than 0.3 times the median template size for that algorithm. This second rule is needed because some algorithms incorrectly fail to return a non-zero error code when template generation fails.

A hyphen “-” indicates the dataset was not produced.¹ The effects of FTE are included in the accuracy results of this report by regarding any template comparison involving a failed template to produce a low similarity score. Thus higher FTE results in higher FNMR and lower FMR.

| | Algorithm | Failure to Enrol Rate ¹ | | | | | | | | | | | |
|-----|-----------------------------|------------------------------------|--------|--------|---------|--------|------|----------|----------|----------|----------|----------|----------|
| | | APPLICATION | BORDER | KIOSK | MUGSHOT | VISA | WILD | SEC. 2.2 | SEC. 2.3 | SEC. 2.5 | SEC. 2.4 | SEC. 2.1 | SEC. 2.6 |
| 175 | imds-software-001 | 0.0000 | 153 | 0.0000 | 93 | 0.0000 | 50 | 0.0000 | 79 | 0.0000 | 60 | 0.0000 | 97 |
| 176 | imperial-000 | 0.0000 | 97 | 0.0000 | 62 | - | 380 | 0.0000 | 112 | 0.0000 | 32 | 0.0000 | 69 |
| 177 | imperial-002 | 0.0000 | 52 | 0.0000 | 34 | - | 335 | 0.0000 | 21 | 0.0000 | 109 | 0.0000 | 43 |
| 178 | incode-010 | 0.0000 | 305 | 0.0009 | 247 | 0.0255 | 180 | 0.0002 | 291 | 0.0004 | 227 | 0.0007 | 279 |
| 179 | incode-011 | 0.0000 | 302 | 0.0009 | 246 | 0.0255 | 179 | 0.0002 | 292 | 0.0004 | 226 | 0.0007 | 278 |
| 180 | innefulabs-000 | 0.0000 | 206 | 0.0024 | 343 | - | 304 | 0.0003 | 333 | 0.0005 | 348 | 0.0004 | 212 |
| 181 | innovativetechnologyltd-001 | 0.0001 | 403 | 0.0050 | 391 | - | 342 | 0.0024 | 416 | 0.0025 | 427 | 0.0055 | 341 |
| 182 | innovativetechnologyltd-002 | 0.0000 | 331 | 0.0046 | 385 | - | 441 | 0.0057 | 436 | 0.0005 | 349 | 0.0247 | 396 |
| 183 | innovatrics-007 | 0.0000 | 231 | 0.0007 | 205 | - | 346 | 0.0001 | 199 | 0.0003 | 161 | 0.0003 | 151 |
| 184 | innovatrics-008 | 0.0000 | 285 | 0.0009 | 252 | 0.0204 | 141 | 0.0000 | 170 | 0.0004 | 185 | 0.0003 | 183 |
| 185 | insightface-001 | 0.0000 | 174 | 0.0000 | 109 | 0.0000 | 41 | 0.0000 | 62 | 0.0000 | 44 | 0.0000 | 86 |
| 186 | insightface-002 | 0.0000 | 106 | 0.0000 | 55 | 0.0000 | 37 | 0.0000 | 100 | 0.0000 | 21 | 0.0000 | 67 |
| 187 | inspur-000 | 0.0000 | 39 | 0.0000 | 19 | 0.0000 | 5 | 0.0000 | 29 | 0.0000 | 63 | 0.0000 | 5 |
| 188 | intellicloudai-001 | 0.0000 | 72 | 0.0000 | 48 | - | 309 | 0.0000 | 7 | 0.0000 | 95 | 0.0001 | 116 |
| 189 | intellicloudai-002 | 0.0000 | 33 | 0.0008 | 220 | - | 269 | 0.0000 | 161 | 0.0004 | 194 | 0.0012 | 302 |
| 190 | intellifusion-001 | 0.0000 | 228 | 0.0005 | 165 | - | 341 | 0.0001 | 223 | 0.0003 | 175 | 0.0005 | 251 |
| 191 | intellifusion-002 | 0.0000 | 25 | 0.0000 | 113 | - | 303 | 0.0000 | 120 | 0.0000 | 81 | 0.0001 | 115 |
| 192 | intellivision-003 | 0.0000 | 273 | 0.0012 | 294 | 0.0308 | 195 | 0.0003 | 327 | 0.0004 | 329 | 0.0185 | 386 |
| 193 | intellivision-004 | 0.0000 | 295 | 0.0011 | 281 | 0.0266 | 186 | 0.0002 | 317 | 0.0004 | 324 | 0.0179 | 384 |
| 194 | intellivix-001 | 0.0000 | 59 | 0.0000 | 29 | 0.0000 | 20 | 0.0000 | 27 | 0.0000 | 114 | 0.0000 | 36 |
| 195 | intellivix-002 | 0.0000 | 43 | 0.0009 | 257 | 0.0184 | 128 | 0.0000 | 31 | 0.0000 | 65 | 0.0000 | 3 |
| 196 | intelresearch-004 | 0.0000 | 237 | 0.0006 | 175 | - | 306 | 0.0000 | 147 | 0.0004 | 214 | 0.0003 | 160 |
| 197 | intelresearch-005 | 0.0000 | 232 | 0.0006 | 174 | 0.0144 | 107 | 0.0000 | 148 | 0.0004 | 216 | 0.0003 | 161 |
| 198 | intema-000 | 0.0000 | 9 | 0.0005 | 157 | 0.0126 | 97 | 0.0000 | 184 | 0.0004 | 200 | 0.0003 | 148 |
| 199 | intsysmsu-001 | 0.0000 | 110 | 0.0010 | 268 | - | 394 | 0.0001 | 242 | 0.0004 | 257 | 0.0004 | 223 |
| 200 | intsysmsu-002 | 0.0000 | 104 | 0.0010 | 269 | - | 390 | 0.0001 | 241 | 0.0004 | 256 | 0.0004 | 224 |
| 201 | ionetworks-000 | 0.0000 | 122 | 0.0016 | 318 | 0.0387 | 216 | 0.0004 | 343 | 0.0005 | 338 | 0.0004 | 230 |
| 202 | iqface-000 | 0.0000 | 138 | 0.0000 | 71 | - | 367 | 0.0000 | 84 | 0.0000 | 3 | 0.0000 | 50 |
| 203 | iqface-003 | 0.0000 | 372 | 0.0076 | 403 | - | 403 | 0.0006 | 372 | 0.0005 | 367 | 0.0069 | 347 |
| 204 | irex-000 | 0.0000 | 340 | 0.0009 | 255 | - | 424 | 0.0000 | 180 | 0.0005 | 334 | 0.0003 | 175 |
| 205 | isap-001 | 0.0000 | 48 | 0.0000 | 36 | - | 328 | 0.0000 | 19 | 0.0000 | 107 | 0.0000 | 44 |
| 206 | isap-002 | 0.0000 | 144 | 0.0000 | 68 | - | 372 | 0.0000 | 87 | 0.0000 | 7 | 0.0000 | 46 |
| 207 | isityou-000 | 0.0068 | 435 | 0.0316 | 426 | - | 271 | 0.0023 | 412 | 0.0010 | 395 | 0.0663 | 412 |
| 208 | isystems-001 | 0.0000 | 380 | 0.0035 | 371 | - | 364 | 0.0010 | 396 | 0.0007 | 382 | 0.0128 | 368 |
| 209 | isystems-002 | 0.0000 | 379 | 0.0035 | 370 | - | 382 | 0.0010 | 397 | 0.0007 | 383 | 0.0128 | 369 |
| 210 | itm0-007 | 0.0000 | 44 | 0.0009 | 239 | - | 280 | 0.0003 | 341 | 0.0000 | 66 | 0.0004 | 199 |
| 211 | itm0-008 | 0.0000 | 135 | 0.0135 | 414 | 0.1239 | 253 | 0.0024 | 417 | 0.0000 | 1 | 0.0836 | 414 |
| 212 | ivacognitive-001 | 0.0000 | 303 | 0.0011 | 283 | - | 278 | 0.0001 | 214 | 0.0004 | 312 | 0.0011 | 294 |
| 213 | iws-000 | 0.0005 | 420 | 0.0650 | 439 | - | 426 | 0.0024 | 414 | 0.0012 | 406 | 0.0936 | 422 |
| 214 | jaakit-001 | 0.0008 | 425 | 0.0858 | 440 | 0.2713 | 263 | 0.0042 | 429 | 0.0021 | 423 | 0.1062 | 427 |
| 215 | kakao-007 | 0.0000 | 67 | 0.0007 | 186 | 0.0165 | 119 | 0.0001 | 232 | 0.0004 | 217 | 0.0097 | 363 |
| 216 | kakao-008 | 0.0000 | 117 | 0.0009 | 243 | 0.0209 | 146 | 0.0001 | 234 | 0.0004 | 210 | 0.0097 | 364 |
| 217 | kakaopay-001 | 0.0000 | 316 | 0.0013 | 305 | 0.0322 | 199 | 0.0001 | 221 | 0.0004 | 314 | 0.0078 | 354 |
| 218 | kasikornlabs-000 | 0.0000 | 384 | 0.0035 | 369 | 0.0713 | 244 | 0.0004 | 355 | 0.0012 | 410 | 0.0270 | 398 |
| 219 | kasikornlabs-001 | 0.0001 | 404 | 0.0050 | 390 | 0.0885 | 249 | 0.0006 | 379 | 0.0035 | 435 | 0.0305 | 399 |
| 220 | kedacom-000 | 0.0000 | 157 | 0.0000 | 90 | - | 432 | 0.0000 | 68 | 0.0000 | 49 | 0.0000 | 93 |
| 221 | kiwitech-000 | 0.0000 | 293 | 0.0009 | 238 | - | 415 | 0.0004 | 353 | 0.0005 | 336 | 0.0004 | 235 |
| 222 | kneron-003 | 0.0239 | 441 | 0.0306 | 424 | - | 331 | 0.0044 | 431 | 0.0016 | 418 | 0.1823 | 438 |
| 223 | kneron-005 | 0.0000 | 383 | 0.0226 | 419 | - | 385 | 0.0006 | 371 | 0.0005 | 345 | 0.0097 | 362 |
| 224 | knowutech-000 | 0.0000 | 287 | 0.0008 | 212 | 0.0215 | 156 | 0.0000 | 167 | 0.0004 | 267 | 0.0003 | 182 |
| 225 | koookmin-002 | 0.0000 | 175 | 0.0000 | 108 | - | 401 | 0.0000 | 63 | 0.0000 | 43 | 0.0000 | 85 |
| 226 | krungthai-002 | 0.0000 | 233 | 0.0005 | 160 | 0.0111 | 95 | 0.0002 | 298 | 0.0003 | 181 | 0.0005 | 241 |
| 227 | kuke3d-001 | 0.0000 | 121 | 0.0000 | 82 | 0.0000 | 23 | 0.0000 | 89 | 0.0000 | 9 | 0.0000 | 60 |
| 228 | kuke3d-002 | 0.0000 | 130 | 0.0000 | 77 | 0.0000 | 28 | 0.0000 | 94 | 0.0000 | 15 | 0.0000 | 58 |
| 229 | lebentech-000 | 0.0042 | 429 | 0.0029 | 358 | 0.0252 | 176 | 0.0051 | 435 | 0.0066 | 438 | 0.0154 | 375 |
| 230 | lemalabs-001 | 0.0000 | 80 | 0.0005 | 167 | 0.0141 | 105 | 0.0002 | 297 | 0.0004 | 201 | 0.0004 | 196 |
| 231 | lineclova-001 | 0.0000 | 91 | 0.0000 | 66 | 0.0000 | 32 | 0.0000 | 108 | 0.0000 | 31 | 0.0001 | 117 |
| 232 | lineclova-002 | 0.0000 | 181 | 0.0007 | 187 | 0.0181 | 124 | 0.0000 | 67 | 0.0000 | 48 | 0.0000 | 102 |

Table 33: FTE is the proportion of failed template generation attempts. Failures can occur because the software throws an exception, or because the software electively refuses to process the input image. This would typically occur if a face is not detected. FTE is measured as the number of function calls that give EITHER a non-zero error code OR that give a “small” template. This is defined as one whose size is less than 0.3 times the median template size for that algorithm. This second rule is needed because some algorithms incorrectly fail to return a non-zero error code when template generation fails.

A hyphen “-” indicates the dataset was not produced.¹ The effects of FTE are included in the accuracy results of this report by regarding any template comparison involving a failed template to produce a low similarity score. Thus higher FTE results in higher FNMR and lower FMR.

| | Algorithm | Failure to Enrol Rate ¹ | | | | | | | | | | | |
|-----|----------------------|------------------------------------|--------|--------|---------|--------|------|----------|----------|----------|----------|----------|----------|
| | | APPLICATION | BORDER | KIOSK | MUGSHOT | VISA | WILD | SEC. 2.2 | SEC. 2.3 | SEC. 2.5 | SEC. 2.4 | SEC. 2.1 | SEC. 2.6 |
| 233 | lookman-002 | 0.0000 | 46 | 0.0000 | 16 | - | 282 | 0.0000 | 33 | 0.0000 | 67 | 0.0000 | 1 |
| 234 | lookman-004 | 0.0000 | 77 | 0.0000 | 44 | - | 313 | 0.0000 | 11 | 0.0000 | 100 | 0.0000 | 30 |
| 235 | luxand-000 | 0.0000 | 189 | 0.0000 | 98 | - | 418 | 0.0000 | 59 | 0.0000 | 41 | 0.0000 | 76 |
| 236 | mantra-000 | 0.0001 | 391 | 0.0041 | 380 | 0.0680 | 242 | 0.0003 | 332 | 0.0004 | 326 | 0.0037 | 331 |
| 237 | maxvision-001 | 0.0000 | 62 | 0.0000 | 27 | 0.0000 | 22 | 0.0000 | 14 | 0.0000 | 103 | 0.0000 | 34 |
| 238 | maxvision-002 | 0.0000 | 235 | 0.0009 | 235 | 0.0229 | 165 | 0.0002 | 279 | 0.0004 | 244 | 0.0004 | 239 |
| 239 | megvii-005 | 0.0000 | 251 | 0.0010 | 263 | 0.0206 | 144 | 0.0002 | 309 | 0.0004 | 293 | 0.0011 | 296 |
| 240 | megvii-006 | 0.0000 | 267 | 0.0010 | 264 | 0.0206 | 143 | 0.0002 | 308 | 0.0004 | 291 | 0.0011 | 295 |
| 241 | meituan-000 | 0.0000 | 128 | 0.0001 | 123 | 0.0013 | 63 | 0.0000 | 139 | 0.0002 | 133 | 0.0001 | 118 |
| 242 | meituan-001 | 0.0000 | 196 | 0.0014 | 309 | 0.0295 | 192 | 0.0001 | 245 | 0.0004 | 279 | 0.0013 | 307 |
| 243 | meiya-001 | 0.0000 | 378 | 0.0028 | 353 | - | 358 | 0.0004 | 356 | 0.0010 | 396 | 0.0025 | 323 |
| 244 | mendaxiatech-000 | 0.0000 | 212 | 0.0010 | 262 | 0.0206 | 142 | 0.0002 | 310 | 0.0004 | 295 | 0.0011 | 297 |
| 245 | metsakuurcompany-001 | 0.0000 | 145 | 0.0011 | 279 | 0.0208 | 145 | 0.0002 | 307 | 0.0004 | 208 | 0.0003 | 170 |
| 246 | microfocus-001 | 0.0001 | 401 | 0.0053 | 395 | - | 363 | 0.0008 | 390 | 0.0016 | 416 | 0.0220 | 391 |
| 247 | microfocus-002 | 0.0001 | 400 | 0.0053 | 394 | - | 333 | 0.0008 | 389 | 0.0016 | 417 | 0.0220 | 390 |
| 248 | minivision-000 | 0.0000 | 92 | 0.0000 | 67 | - | 375 | 0.0000 | 107 | 0.0000 | 30 | 0.0000 | 75 |
| 249 | mobai-000 | 0.0000 | 345 | 0.0114 | 411 | - | 321 | 0.0003 | 336 | 0.0012 | 408 | 0.1242 | 433 |
| 250 | mobai-001 | 0.0000 | 319 | 0.0040 | 376 | - | 433 | 0.0001 | 253 | 0.0012 | 407 | 0.0523 | 410 |
| 251 | mobbbl-001 | 0.0000 | 373 | 0.0052 | 393 | 0.0678 | 241 | 0.0002 | 285 | 0.0005 | 355 | 0.0181 | 385 |
| 252 | mobbbl-003 | 0.0000 | 382 | 0.0029 | 357 | 0.0633 | 234 | 0.0002 | 301 | 0.0009 | 390 | 0.0026 | 325 |
| 253 | mobipintech-000 | 0.0000 | 45 | 0.0000 | 17 | 0.0000 | 6 | 0.0000 | 32 | 0.0000 | 68 | 0.0000 | 2 |
| 254 | moredian-000 | 0.0000 | 243 | 0.0009 | 236 | - | 320 | 0.0004 | 351 | 0.0005 | 337 | 0.0004 | 234 |
| 255 | mukh-001 | 0.0000 | 173 | 0.0010 | 271 | 0.0154 | 113 | 0.0001 | 249 | 0.0003 | 140 | 0.0010 | 290 |
| 256 | multimodality-000 | 0.0000 | 137 | 0.0000 | 72 | 0.0000 | 30 | 0.0000 | 83 | 0.0000 | 4 | 0.0000 | 49 |
| 257 | multimodality-001 | 0.0000 | 57 | 0.0009 | 233 | 0.0259 | 183 | 0.0000 | 23 | 0.0000 | 111 | 0.0000 | 40 |
| 258 | mvision-001 | 0.0000 | 115 | 0.0000 | 52 | - | 395 | 0.0000 | 103 | 0.0000 | 24 | 0.0000 | 65 |
| 259 | nazhiai-000 | 0.0000 | 55 | 0.0000 | 31 | - | 339 | 0.0000 | 24 | 0.0000 | 113 | 0.0000 | 41 |
| 260 | neosystems-003 | 0.0000 | 70 | 0.0000 | 49 | 0.0000 | 15 | 0.0000 | 6 | 0.0000 | 94 | 0.0000 | 31 |
| 261 | neosystems-004 | 0.0000 | 154 | 0.0000 | 94 | 0.0000 | 51 | 0.0000 | 78 | 0.0000 | 59 | 0.0000 | 96 |
| 262 | netbridge-tech-001 | 0.0000 | 170 | 0.0000 | 84 | - | 444 | 0.0000 | 74 | 0.0000 | 55 | 0.0000 | 87 |
| 263 | netbridge-tech-002 | 0.0000 | 187 | 0.0000 | 100 | - | 413 | 0.0000 | 57 | 0.0000 | 38 | 0.0000 | 80 |
| 264 | neurotechnology-y013 | 0.0000 | 24 | 0.0008 | 231 | 0.0185 | 129 | 0.0000 | 130 | 0.0001 | 123 | 0.0004 | 211 |
| 265 | neurotechnology-y015 | 0.0000 | 101 | 0.0004 | 141 | 0.0082 | 83 | 0.0000 | 116 | 0.0000 | 119 | 0.0003 | 138 |
| 266 | nhm-002 | 0.0000 | 114 | 0.0004 | 155 | 0.0091 | 85 | 0.0000 | 160 | 0.0003 | 151 | 0.0003 | 140 |
| 267 | nhn-003 | 0.0000 | 326 | 0.0000 | 11 | 0.0000 | 8 | 0.0001 | 274 | 0.0004 | 278 | 0.0010 | 291 |
| 268 | nodeflux-002 | 0.0000 | 225 | 0.0261 | 421 | - | 336 | 0.0008 | 387 | 0.0005 | 350 | 0.0008 | 285 |
| 269 | notiontag-001 | 0.0000 | 125 | 0.0000 | 78 | - | 355 | 0.0027 | 421 | 0.0000 | 11 | 0.0132 | 372 |
| 270 | notiontag-002 | 0.0000 | 143 | 0.0000 | 69 | 0.0000 | 31 | 0.0000 | 86 | 0.0000 | 6 | 0.0000 | 48 |
| 271 | nsensecorp-002 | 0.0000 | 208 | 0.0009 | 240 | 0.0219 | 159 | 0.0003 | 324 | 0.0011 | 397 | 0.0178 | 383 |
| 272 | nsensecorp-003 | 0.0000 | 69 | 0.0000 | 119 | 0.0002 | 59 | 0.0000 | 146 | 0.0007 | 385 | 0.0150 | 373 |
| 273 | ntechlab-011 | 0.0000 | 4 | 0.0003 | 129 | 0.0057 | 71 | 0.0000 | 183 | 0.0004 | 186 | 0.0003 | 163 |
| 274 | ntechlab-012 | 0.0000 | 76 | 0.0003 | 130 | 0.0057 | 72 | 0.0000 | 181 | 0.0004 | 187 | 0.0003 | 164 |
| 275 | omiface-000 | 0.0000 | 176 | 0.0000 | 107 | 0.0000 | 42 | 0.0000 | 64 | 0.0000 | 45 | 0.1160 | 431 |
| 276 | omnigarde-001 | 0.0000 | 249 | 0.0008 | 207 | 0.0213 | 150 | 0.0000 | 152 | 0.0004 | 264 | 0.0003 | 178 |
| 277 | omnigarde-002 | 0.0000 | 264 | 0.0008 | 208 | 0.0213 | 151 | 0.0000 | 155 | 0.0004 | 255 | 0.0003 | 180 |
| 278 | openface-001 | 0.0000 | 356 | 0.0104 | 410 | 0.0668 | 237 | 0.0004 | 348 | 0.0006 | 378 | 0.0856 | 417 |
| 279 | oz-003 | 0.0000 | 16 | 0.0002 | 127 | 0.0042 | 68 | 0.0000 | 124 | 0.0003 | 139 | 0.0002 | 125 |
| 280 | oz-004 | 0.0000 | 362 | 0.0003 | 132 | 0.0041 | 67 | 0.0000 | 132 | 0.0002 | 128 | 0.0006 | 258 |
| 281 | palit-000 | 0.0000 | 215 | 0.0005 | 161 | 0.0134 | 102 | 0.0002 | 293 | 0.0004 | 212 | 0.0004 | 222 |
| 282 | pangiam-000 | 0.0000 | 172 | 0.0021 | 339 | 0.0364 | 209 | 0.0001 | 202 | 0.0005 | 335 | 0.0095 | 361 |
| 283 | papago-001 | 0.0000 | 315 | 0.0008 | 215 | 0.0159 | 117 | 0.0002 | 318 | 0.0004 | 237 | 0.0190 | 387 |
| 284 | papsav1923-001 | 0.0000 | 201 | 0.0007 | 196 | - | 294 | 0.0001 | 235 | 0.0002 | 137 | 0.0005 | 243 |
| 285 | papsav1923-002 | 0.0000 | 207 | 0.0018 | 326 | 0.0268 | 187 | 0.0000 | 174 | 0.0004 | 271 | 0.0004 | 210 |
| 286 | paravision-008 | 0.0000 | 193 | 0.0010 | 267 | 0.0201 | 139 | 0.0001 | 230 | 0.0004 | 192 | 0.0003 | 181 |
| 287 | paravision-010 | 0.0000 | 159 | 0.0010 | 266 | 0.0201 | 140 | 0.0001 | 231 | 0.0004 | 193 | 0.0003 | 184 |
| 288 | pensees-001 | 0.0000 | 297 | 0.0000 | 97 | - | 417 | 0.0000 | 60 | 0.0000 | 42 | 0.0000 | 77 |
| 289 | pixelall-006 | 0.0000 | 160 | 0.0000 | 89 | 0.0000 | 52 | 0.0000 | 69 | 0.0000 | 50 | 0.0000 | 94 |
| 290 | pixelall-008 | 0.0000 | 146 | 0.0008 | 223 | 0.0247 | 173 | 0.0000 | 88 | 0.0000 | 8 | 0.0000 | 47 |

Table 34: FTE is the proportion of failed template generation attempts. Failures can occur because the software throws an exception, or because the software electively refuses to process the input image. This would typically occur if a face is not detected. FTE is measured as the number of function calls that give EITHER a non-zero error code OR that give a “small” template. This is defined as one whose size is less than 0.3 times the median template size for that algorithm. This second rule is needed because some algorithms incorrectly fail to return a non-zero error code when template generation fails.

A hyphen “-” indicates the dataset was not produced.¹ The effects of FTE are included in the accuracy results of this report by regarding any template comparison involving a failed template to produce a low similarity score. Thus higher FTE results in higher FNMR and lower FMR.

| | Algorithm | Failure to Enrol Rate ¹ | | | | | | | |
|------|--------------------|------------------------------------|----------|----------|----------|----------|----------|----------|----------|
| | | APPLICATION | BORDER | KIOSK | MUGSHOT | VISA | WILD | SEC. 2.1 | SEC. 2.6 |
| Name | SEC. 2.2 | SEC. 2.3 | SEC. 2.5 | SEC. 2.4 | SEC. 2.1 | SEC. 2.6 | SEC. 2.1 | SEC. 2.6 | SEC. 2.1 |
| 291 | psl-009 | 0.0000 | 227 | 0.0004 | 144 | 0.0095 | 86 | 0.0000 | 119 |
| 292 | psl-010 | 0.0000 | 270 | 0.0004 | 145 | 0.0095 | 87 | 0.0000 | 121 |
| 293 | ptakuratsatu-000 | 0.0000 | 194 | 0.0007 | 204 | - | 283 | 0.0001 | 200 |
| 294 | pxl-001 | 0.0000 | 388 | 0.0044 | 383 | - | 420 | 0.0005 | 365 |
| 295 | pyramid-000 | 0.0001 | 398 | 0.0041 | 379 | - | 386 | 0.0005 | 364 |
| 296 | qazbs-000 | 0.0000 | 75 | 0.0009 | 244 | 0.0265 | 185 | 0.0000 | 143 |
| 297 | qnap-001 | 0.0000 | 296 | 0.0000 | 117 | 0.0002 | 60 | 0.0000 | 176 |
| 298 | qnap-002 | 0.0000 | 375 | 0.0033 | 362 | 0.0761 | 246 | 0.0004 | 346 |
| 299 | quantasoft-003 | 0.0000 | 346 | 0.0015 | 314 | 0.0355 | 206 | 0.0005 | 363 |
| 300 | rankone-012 | 0.0000 | 94 | 0.0000 | 64 | 0.0000 | 33 | 0.0000 | 110 |
| 301 | rankone-013 | 0.0000 | 190 | 0.0005 | 158 | 0.0126 | 98 | 0.0000 | 140 |
| 302 | realnetworks-006 | 0.0000 | 226 | 0.0002 | 128 | 0.0045 | 69 | 0.0000 | 118 |
| 303 | realnetworks-007 | 0.0000 | 248 | 0.0013 | 306 | 0.0425 | 221 | 0.0000 | 122 |
| 304 | regula-000 | 0.0000 | 17 | 0.0000 | 5 | 0.0000 | 12 | 0.0000 | 42 |
| 305 | regula-001 | 0.0000 | 126 | 0.0000 | 79 | 0.0000 | 26 | 0.0000 | 92 |
| 306 | remarkai-001 | 0.0000 | 84 | 0.0000 | 43 | - | 317 | 0.0000 | 12 |
| 307 | remarkai-003 | 0.0000 | 257 | 0.0007 | 193 | 0.0187 | 131 | 0.0000 | 178 |
| 308 | rendip-000 | 0.0000 | 329 | 0.0016 | 317 | 0.0293 | 191 | 0.0002 | 290 |
| 309 | revealmedia-005 | 0.0000 | 337 | 0.0007 | 200 | 0.0189 | 132 | 0.0009 | 394 |
| 310 | revealmedia-006 | 0.0000 | 74 | 0.0009 | 251 | 0.0238 | 171 | 0.0001 | 246 |
| 311 | rokid-000 | 0.0000 | 15 | 0.0072 | 401 | - | 297 | 0.0001 | 233 |
| 312 | rokid-001 | 0.0000 | 29 | 0.0013 | 303 | - | 266 | 0.0000 | 34 |
| 313 | s1-004 | 0.0000 | 109 | 0.0000 | 120 | 0.0003 | 61 | 0.0000 | 196 |
| 314 | s1-005 | 0.0000 | 73 | 0.0004 | 148 | 0.0120 | 96 | 0.0001 | 211 |
| 315 | saffe-001 | 0.0000 | 68 | 0.0000 | 24 | - | 352 | 0.0000 | 18 |
| 316 | saffe-002 | 0.0000 | 141 | 0.0000 | 70 | - | 369 | 0.0000 | 85 |
| 317 | samsungsds-000 | 0.0000 | 334 | 0.0055 | 397 | 0.0646 | 235 | 0.0038 | 428 |
| 318 | samsungsds-001 | 0.0000 | 86 | 0.0005 | 164 | 0.0146 | 108 | 0.0001 | 229 |
| 319 | samtech-001 | 0.0001 | 397 | 0.0032 | 361 | - | 329 | 0.0004 | 352 |
| 320 | scanovate-002 | 0.0000 | 301 | 0.0018 | 325 | - | 267 | 0.0000 | 194 |
| 321 | scanovate-003 | 0.0000 | 306 | 0.0233 | 420 | 0.3371 | 265 | 0.0006 | 375 |
| 322 | securifai-004 | 0.0000 | 14 | 0.0000 | 6 | 0.0000 | 11 | 0.0000 | 41 |
| 323 | securifai-005 | 0.0000 | 171 | 0.0000 | 83 | 0.0000 | 54 | 0.0000 | 75 |
| 324 | sensetime-006 | 0.0000 | 49 | 0.0004 | 142 | 0.0106 | 91 | 0.0000 | 158 |
| 325 | sensetime-007 | 0.0000 | 82 | 0.0004 | 143 | 0.0106 | 90 | 0.0000 | 157 |
| 326 | sertis-000 | 0.0000 | 40 | 0.0007 | 199 | - | 275 | 0.0000 | 198 |
| 327 | sertis-002 | 0.0000 | 162 | 0.0007 | 190 | 0.0152 | 111 | 0.0000 | 191 |
| 328 | seventhsense-000 | 0.0000 | 254 | 0.0006 | 183 | 0.0184 | 125 | 0.0001 | 206 |
| 329 | seventhsense-001 | 0.0000 | 286 | 0.0006 | 184 | 0.0184 | 126 | 0.0001 | 205 |
| 330 | shaman-000 | 0.0000 | 8 | 0.0000 | 10 | - | 290 | 0.0000 | 51 |
| 331 | shaman-001 | 0.0000 | 83 | 0.0000 | 42 | - | 316 | 0.0000 | 13 |
| 332 | shu-002 | 0.0000 | 314 | 0.0010 | 273 | - | 392 | 0.0005 | 362 |
| 333 | shu-003 | 0.0000 | 152 | 0.0007 | 188 | - | 425 | 0.0001 | 209 |
| 334 | siat-002 | 0.0000 | 289 | 0.0012 | 296 | - | 405 | 0.0000 | 171 |
| 335 | siat-005 | 0.0000 | 58 | 0.0000 | 30 | 0.0000 | 55 | 0.0000 | 26 |
| 336 | sjtu-003 | 0.0000 | 150 | 0.0005 | 170 | - | 421 | 0.0000 | 187 |
| 337 | sjtu-004 | 0.0000 | 182 | 0.0000 | 104 | 0.0000 | 45 | 0.0000 | 54 |
| 338 | sktelecom-000 | 0.0000 | 199 | 0.0008 | 222 | 0.0190 | 133 | 0.0000 | 185 |
| 339 | smartbiometrik-001 | 0.0005 | 417 | 0.0649 | 437 | 0.2147 | 261 | 0.0017 | 407 |
| 340 | smartengines-000 | 0.0066 | 434 | 0.0150 | 415 | 0.1656 | 254 | 0.0022 | 411 |
| 341 | smartengines-001 | 0.0003 | 413 | 0.0073 | 402 | 0.0714 | 245 | 0.0007 | 382 |
| 342 | smartvist-000 | 0.0000 | 38 | 0.0026 | 347 | 0.0357 | 207 | 0.0002 | 278 |
| 343 | smilart-002 | 0.0000 | 385 | 0.0036 | 372 | - | 445 | - | 445 |
| 344 | smilart-003 | 0.0003 | 414 | 0.0100 | 408 | - | 428 | 0.0014 | 403 |
| 345 | sodec-000 | 0.0000 | 186 | 0.0000 | 101 | 0.0000 | 47 | 0.0000 | 56 |
| 346 | sqisoft-001 | 0.0000 | 26 | 0.0003 | 137 | 0.0078 | 79 | 0.0000 | 134 |
| 347 | sqisoft-002 | 0.0000 | 108 | 0.0003 | 135 | 0.0078 | 80 | 0.0000 | 141 |
| 348 | stachu-000 | 0.0000 | 131 | 0.0000 | 75 | - | 360 | 0.0000 | 95 |
| | | | | | | | | 0.0000 | 16 |
| | | | | | | | | 0.0000 | 54 |

Table 35: FTE is the proportion of failed template generation attempts. Failures can occur because the software throws an exception, or because the software electively refuses to process the input image. This would typically occur if a face is not detected. FTE is measured as the number of function calls that give EITHER a non-zero error code OR that give a “small” template. This is defined as one whose size is less than 0.3 times the median template size for that algorithm. This second rule is needed because some algorithms incorrectly fail to return a non-zero error code when template generation fails.

A hyphen “-” indicates the dataset was not produced.¹ The effects of FTE are included in the accuracy results of this report by regarding any template comparison involving a failed template to produce a low similarity score. Thus higher FTE results in higher FNMR and lower FMR.

| | Algorithm | Failure to Enrol Rate ¹ | | | | | | | | | | | |
|-----|---------------------------|------------------------------------|----------|----------|----------|----------|----------|----------|----------|----------|----------|--------|-----|
| | | APPLICATION | BORDER | KIOSK | MUGSHOT | VISA | WILD | SEC. 2.2 | SEC. 2.3 | SEC. 2.5 | SEC. 2.4 | | |
| | Name | SEC. 2.2 | SEC. 2.3 | SEC. 2.5 | SEC. 2.4 | SEC. 2.1 | SEC. 2.6 | | | | | | |
| 349 | starhybrid-001 | 0.0001 | 402 | 0.0033 | 366 | - | 438 | 0.0009 | 393 | 0.0023 | 426 | 0.0044 | 333 |
| 350 | sukshi-000 | 0.0000 | 178 | 0.0000 | 106 | 0.0000 | 43 | 0.0000 | 65 | 0.0000 | 46 | 0.0000 | 84 |
| 351 | suprema-002 | 0.0000 | 322 | 0.0010 | 276 | 0.0271 | 189 | 0.0002 | 287 | 0.0004 | 220 | 0.0005 | 249 |
| 352 | suprema-003 | 0.0000 | 276 | 0.0008 | 225 | 0.0231 | 167 | 0.0000 | 137 | 0.0004 | 224 | 0.0003 | 172 |
| 353 | supremaid-001 | 0.0000 | 268 | 0.0020 | 333 | 0.0330 | 200 | 0.0001 | 240 | 0.0004 | 318 | 0.0045 | 335 |
| 354 | supremaid-002 | 0.0000 | 252 | 0.0020 | 332 | 0.0330 | 201 | 0.0001 | 243 | 0.0004 | 319 | 0.0045 | 336 |
| 355 | surrey-cvssp-000 | 0.0000 | 47 | 0.0000 | 35 | 0.0000 | 19 | 0.0000 | 20 | 0.0000 | 108 | 0.0000 | 45 |
| 356 | synesis-006 | 0.0000 | 120 | 0.0003 | 138 | - | 353 | 0.0000 | 188 | 0.0003 | 142 | 0.0002 | 128 |
| 357 | synesis-007 | 0.0000 | 292 | 0.0013 | 302 | - | 414 | 0.0002 | 306 | 0.0004 | 240 | 0.0005 | 242 |
| 358 | synology-000 | 0.0000 | 41 | 0.0000 | 18 | - | 277 | 0.0000 | 30 | 0.0000 | 64 | 0.0000 | 4 |
| 359 | synology-002 | 0.0000 | 98 | 0.0000 | 61 | - | 381 | 0.0000 | 113 | 0.0000 | 35 | 0.0000 | 72 |
| 360 | sztu-000 | 0.0000 | 22 | 0.0000 | 1 | - | 300 | 0.0000 | 47 | 0.0000 | 77 | 0.0000 | 10 |
| 361 | sztu-001 | 0.0000 | 11 | 0.0000 | 9 | 0.0000 | 9 | 0.0000 | 52 | 0.0000 | 87 | 0.0000 | 16 |
| 362 | t4isb-000 | 0.0000 | 113 | 0.0000 | 53 | 0.0000 | 39 | 0.0000 | 102 | 0.0000 | 22 | 0.0000 | 63 |
| 363 | tech5-004 | 0.0000 | 238 | 0.0008 | 213 | - | 307 | 0.0003 | 326 | 0.0004 | 316 | 0.0006 | 260 |
| 364 | tech5-005 | 0.0000 | 202 | 0.0007 | 206 | - | 298 | 0.0000 | 153 | 0.0004 | 286 | 0.0049 | 339 |
| 365 | techsign-000 | 0.0007 | 423 | 0.0334 | 427 | 0.2093 | 256 | 0.0020 | 409 | 0.0011 | 400 | 0.0170 | 381 |
| 366 | techsign-001 | 0.0000 | 236 | 0.0008 | 232 | 0.0253 | 178 | 0.0002 | 295 | 0.0004 | 252 | 0.0004 | 217 |
| 367 | tevian-007 | 0.0000 | 217 | 0.0015 | 315 | 0.0429 | 222 | 0.0002 | 299 | 0.0004 | 270 | 0.0008 | 281 |
| 368 | tevian-008 | 0.0000 | 210 | 0.0006 | 172 | 0.0109 | 94 | 0.0000 | 149 | 0.0003 | 157 | 0.0004 | 220 |
| 369 | tiger-005 | 0.0000 | 282 | 0.0009 | 254 | 0.0194 | 138 | 0.0001 | 226 | 0.0004 | 229 | 0.0004 | 232 |
| 370 | tiger-006 | 0.0000 | 321 | 0.0011 | 285 | 0.0396 | 217 | 0.0001 | 268 | 0.0004 | 328 | 0.0009 | 286 |
| 371 | tinkoff-001 | 0.0000 | 304 | 0.0008 | 221 | 0.0171 | 121 | 0.0001 | 260 | 0.0004 | 231 | 0.0014 | 309 |
| 372 | tongyi-005 | 0.0000 | 56 | 0.0000 | 32 | - | 338 | 0.0000 | 25 | 0.0000 | 112 | 0.0000 | 42 |
| 373 | toppanidgate-000 | 0.0000 | 247 | 0.0008 | 218 | 0.0232 | 168 | 0.0004 | 344 | 0.0004 | 263 | 0.0005 | 254 |
| 374 | toshiba-004 | 0.0000 | 185 | 0.0000 | 99 | 0.0000 | 46 | 0.0000 | 58 | 0.0000 | 39 | 0.0000 | 81 |
| 375 | toshiba-006 | 0.0000 | 256 | 0.0004 | 150 | 0.0050 | 70 | 0.0001 | 264 | 0.0003 | 154 | 0.0003 | 142 |
| 376 | touchlessid-000 | 0.0042 | 430 | 0.0133 | 413 | 0.2009 | 255 | 0.0018 | 408 | 0.0032 | 434 | 0.0457 | 407 |
| 377 | trueface-002 | 0.0000 | 312 | 0.0046 | 387 | - | 327 | 0.0003 | 320 | 0.0005 | 360 | 0.0330 | 402 |
| 378 | trueface-003 | 0.0000 | 310 | 0.0046 | 388 | 0.0397 | 218 | 0.0003 | 321 | 0.0005 | 361 | 0.0330 | 403 |
| 379 | tuputech-000 | 0.0003 | 415 | 0.0116 | 412 | - | 340 | - | 443 | 0.0081 | 440 | 0.6383 | 442 |
| 380 | turingtechvip-001 | 0.0001 | 393 | 0.0007 | 201 | 0.0061 | 75 | 0.0007 | 380 | 0.0006 | 370 | 0.0057 | 342 |
| 381 | turingtechvip-002 | 0.0001 | 394 | 0.0017 | 323 | 0.0097 | 88 | 0.0007 | 381 | 0.0006 | 369 | 0.0057 | 343 |
| 382 | twface-000 | 0.0000 | 37 | 0.0000 | 20 | 0.0000 | 4 | 0.0000 | 38 | 0.0000 | 73 | 0.0000 | 6 |
| 383 | twface-001 | 0.0000 | 21 | 0.0000 | 3 | 0.0000 | 13 | 0.0000 | 45 | 0.0000 | 78 | 0.0000 | 11 |
| 384 | ulsee-001 | 0.0000 | 155 | 0.0000 | 92 | - | 427 | 0.0000 | 80 | 0.0000 | 61 | 0.0001 | 111 |
| 385 | ultinious-000 | - | 445 | - | 445 | - | 330 | - | 442 | 0.0003 | 164 | - | 444 |
| 386 | ultinious-001 | - | 444 | - | 444 | - | 270 | - | 444 | 0.0003 | 163 | - | 443 |
| 387 | uluface-002 | 0.0000 | 79 | 0.0000 | 46 | - | 314 | 0.0000 | 9 | 0.0000 | 98 | 0.0000 | 27 |
| 388 | uluface-003 | 0.0000 | 169 | 0.0001 | 126 | - | 443 | 0.0002 | 281 | 0.0002 | 132 | 0.0244 | 395 |
| 389 | unissey-001 | 0.0000 | 5 | 0.0000 | 14 | 0.0000 | 7 | 0.0000 | 48 | 0.0000 | 85 | 0.0000 | 20 |
| 390 | unissey-002 | 0.0000 | 123 | 0.0000 | 81 | 0.0000 | 25 | 0.0000 | 90 | 0.0000 | 12 | 0.0000 | 56 |
| 391 | upc-001 | 0.0000 | 361 | 0.0003 | 133 | - | 435 | 0.0003 | 325 | 0.0003 | 170 | 0.0011 | 292 |
| 392 | vcog-002 | - | 446 | - | 446 | - | 374 | - | 446 | 0.0019 | 421 | - | 445 |
| 393 | vd-002 | 0.0000 | 10 | 0.0000 | 8 | 1.0000 | 292 | 0.0000 | 53 | 0.0000 | 88 | 0.0000 | 17 |
| 394 | vd-003 | 0.0001 | 395 | 0.0041 | 378 | 0.0676 | 240 | 0.0030 | 424 | 0.0029 | 432 | 0.0060 | 345 |
| 395 | veridas-006 | 0.0000 | 351 | 0.0026 | 345 | 0.0595 | 230 | 0.0001 | 256 | 0.0005 | 342 | 0.0006 | 265 |
| 396 | veridas-007 | 0.0000 | 352 | 0.0026 | 346 | 0.0595 | 231 | 0.0001 | 255 | 0.0005 | 343 | 0.0006 | 266 |
| 397 | veridium-000 | 0.0061 | 433 | 0.5956 | 442 | 0.2889 | 264 | 0.0050 | 434 | 0.0009 | 389 | 0.3133 | 440 |
| 398 | verigram-000 | 0.0000 | 333 | 0.0068 | 400 | 0.0822 | 248 | 0.0003 | 342 | 0.0005 | 354 | 0.0004 | 207 |
| 399 | verigram-001 | 0.0000 | 325 | 0.0003 | 136 | 0.0060 | 73 | 0.0002 | 305 | 0.0003 | 172 | 0.0004 | 206 |
| 400 | verihubs-inteligensia-000 | 0.0000 | 221 | 0.0029 | 354 | 0.0669 | 238 | 0.0001 | 212 | 0.0004 | 289 | 0.0003 | 158 |
| 401 | verihubs-inteligensia-001 | 0.0000 | 274 | 0.0029 | 355 | 0.0669 | 239 | 0.0001 | 217 | 0.0004 | 284 | 0.0003 | 154 |
| 402 | verijelias-000 | 0.0000 | 219 | 0.0023 | 340 | 0.0375 | 213 | 0.0004 | 359 | 0.0006 | 373 | 0.0006 | 259 |
| 403 | via-000 | 0.0000 | 90 | 0.0000 | 37 | - | 326 | 0.0000 | 5 | 0.0000 | 93 | 0.0001 | 112 |
| 404 | via-001 | 0.0000 | 102 | 0.0000 | 59 | - | 383 | 0.0000 | 115 | 0.0000 | 36 | 0.0001 | 113 |
| 405 | videmo-000 | 0.0000 | 323 | 0.0019 | 327 | - | 407 | 0.0003 | 335 | 0.0012 | 409 | 0.0158 | 376 |
| 406 | videmo-001 | 0.0000 | 342 | 0.0170 | 417 | 0.0332 | 203 | 0.0010 | 398 | 0.0011 | 404 | 0.0847 | 416 |

Table 36: FTE is the proportion of failed template generation attempts. Failures can occur because the software throws an exception, or because the software electively refuses to process the input image. This would typically occur if a face is not detected. FTE is measured as the number of function calls that give EITHER a non-zero error code OR that give a “small” template. This is defined as one whose size is less than 0.3 times the median template size for that algorithm. This second rule is needed because some algorithms incorrectly fail to return a non-zero error code when template generation fails.

A hyphen “-” indicates the dataset was not produced.¹ The effects of FTE are included in the accuracy results of this report by regarding any template comparison involving a failed template to produce a low similarity score. Thus higher FTE results in higher FNMR and lower FMR.

| | Algorithm | Failure to Enrol Rate ¹ | | | | | | | | | | | |
|-----|-----------------------|------------------------------------|--------|--------|---------|--------|------|----------|----------|----------|----------|----------|----------|
| | | APPLICATION | BORDER | KIOSK | MUGSHOT | VISA | WILD | SEC. 2.2 | SEC. 2.3 | SEC. 2.5 | SEC. 2.4 | SEC. 2.1 | SEC. 2.6 |
| 407 | videonetics-001 | 0.0004 | 416 | 0.0309 | 425 | - | 273 | 0.0015 | 406 | 0.0010 | 394 | 0.0112 | 365 |
| 408 | videonetics-002 | 0.0000 | 332 | 0.0459 | 434 | - | 446 | 0.0006 | 376 | 0.0005 | 365 | 0.0013 | 304 |
| 409 | viettelhightech-000 | 0.0000 | 363 | 0.0019 | 328 | 0.0368 | 212 | 0.0007 | 383 | 0.0005 | 362 | 0.0024 | 321 |
| 410 | vigilantsolutions-010 | 0.0000 | 344 | 0.0028 | 350 | 0.0609 | 232 | 0.0001 | 218 | 0.0004 | 202 | 0.0005 | 246 |
| 411 | vigilantsolutions-011 | 0.0000 | 347 | 0.0028 | 351 | 0.0609 | 233 | 0.0001 | 220 | 0.0004 | 196 | 0.0005 | 247 |
| 412 | vinai-000 | 0.0000 | 7 | 0.0000 | 13 | - | 287 | 0.0000 | 50 | 0.0000 | 83 | 0.0000 | 19 |
| 413 | vinbigdata-001 | 0.0000 | 12 | 0.0000 | 7 | 0.0000 | 10 | 0.0000 | 39 | 0.0000 | 74 | 0.0000 | 14 |
| 414 | vinbigdata-002 | 0.0000 | 28 | 0.0015 | 312 | 0.0250 | 175 | 0.0000 | 166 | 0.0004 | 303 | 0.0012 | 301 |
| 415 | vion-000 | 0.0050 | 431 | 0.0392 | 433 | - | 393 | 0.0130 | 439 | 0.0078 | 439 | 0.1389 | 435 |
| 416 | visage-000 | 0.0000 | 364 | 0.0054 | 396 | - | 310 | 0.0009 | 391 | 0.0006 | 371 | 0.0064 | 346 |
| 417 | visionbox-001 | 0.0000 | 386 | 0.0033 | 365 | - | 295 | 0.0005 | 369 | 0.0011 | 403 | 0.0028 | 326 |
| 418 | visionbox-002 | 0.0000 | 191 | 0.0017 | 319 | 0.0270 | 188 | 0.0000 | 169 | 0.0004 | 325 | 0.0046 | 337 |
| 419 | visionlabs-010 | 0.0000 | 338 | 0.0009 | 242 | - | 384 | 0.0001 | 266 | 0.0004 | 259 | 0.0006 | 268 |
| 420 | visionlabs-011 | 0.0000 | 64 | 0.0006 | 178 | 0.0156 | 114 | 0.0001 | 222 | 0.0004 | 207 | 0.0004 | 190 |
| 421 | visteam-003 | 0.0000 | 283 | 0.0010 | 274 | 0.0225 | 163 | 0.0001 | 207 | 0.0004 | 222 | 0.0005 | 252 |
| 422 | visteam-004 | 0.0000 | 294 | 0.0010 | 275 | 0.0225 | 161 | 0.0001 | 247 | 0.0004 | 218 | 0.0006 | 256 |
| 423 | vixvization-005 | 0.0000 | 111 | 0.0000 | 54 | 0.0000 | 38 | 0.0000 | 101 | 0.0000 | 23 | 0.0000 | 64 |
| 424 | vixvization-006 | 0.0000 | 20 | 0.0000 | 4 | 0.0000 | 14 | 0.0000 | 44 | 0.0000 | 79 | 0.0000 | 12 |
| 425 | vnpt-003 | 0.0000 | 112 | 0.0004 | 140 | 0.0105 | 89 | 0.0002 | 280 | 0.0004 | 184 | 0.0001 | 119 |
| 426 | vnpt-004 | 0.0000 | 222 | 0.0006 | 173 | 0.0160 | 118 | 0.0002 | 286 | 0.0004 | 235 | 0.0003 | 165 |
| 427 | vocord-009 | 0.0000 | 213 | 0.0006 | 177 | - | 276 | 0.0001 | 272 | 0.0003 | 146 | 0.0003 | 141 |
| 428 | vocord-010 | 0.0000 | 307 | 0.0005 | 166 | 0.0141 | 106 | 0.0002 | 296 | 0.0003 | 176 | 0.0004 | 209 |
| 429 | vts-000 | 0.0000 | 327 | 0.0011 | 282 | - | 293 | 0.0001 | 273 | 0.0004 | 322 | 0.0013 | 303 |
| 430 | vts-001 | 0.0000 | 35 | 0.0003 | 131 | 0.0073 | 76 | 0.0000 | 133 | 0.0003 | 141 | 0.0002 | 126 |
| 431 | wicket-000 | 0.0000 | 242 | 0.0009 | 237 | 0.0260 | 184 | 0.0000 | 142 | 0.0004 | 233 | 0.0004 | 195 |
| 432 | winsense-001 | 0.0000 | 81 | 0.0000 | 47 | - | 315 | 0.0000 | 10 | 0.0000 | 99 | 0.0000 | 28 |
| 433 | winsense-002 | 0.0000 | 96 | 0.0000 | 63 | - | 379 | 0.0000 | 111 | 0.0000 | 33 | 0.0000 | 70 |
| 434 | wuhantianyu-001 | 0.0000 | 100 | 0.0007 | 191 | 0.0159 | 115 | 0.0001 | 204 | 0.0004 | 258 | 0.0002 | 129 |
| 435 | x-laboratory-000 | 0.0247 | 442 | 0.0000 | 103 | - | 409 | 0.0005 | 368 | 0.0002 | 134 | 0.0000 | 83 |
| 436 | x-laboratory-001 | 0.0000 | 245 | 0.0012 | 292 | - | 323 | 0.0001 | 258 | 0.0004 | 309 | 0.0007 | 271 |
| 437 | xforwardai-001 | 0.0000 | 223 | 0.0007 | 202 | - | 334 | 0.0003 | 328 | 0.0004 | 305 | 0.0004 | 191 |
| 438 | xforwardai-002 | 0.0000 | 278 | 0.0007 | 203 | - | 431 | 0.0003 | 329 | 0.0004 | 302 | 0.0004 | 192 |
| 439 | xm-000 | 0.0000 | 149 | 0.0007 | 189 | - | 422 | 0.0001 | 208 | 0.0003 | 155 | 0.0004 | 237 |
| 440 | yisheng-004 | 0.0002 | 410 | - | 443 | - | 272 | 0.0013 | 401 | 0.0006 | 377 | 0.0321 | 400 |
| 441 | yitu-003 | 0.0000 | 2 | 0.0000 | 15 | - | 285 | 0.0009 | 392 | 0.0000 | 82 | 0.0000 | 21 |
| 442 | yoonik-002 | 0.0000 | 317 | 0.0010 | 270 | 0.0284 | 190 | 0.0003 | 322 | 0.0006 | 368 | 0.0005 | 250 |
| 443 | yoonik-003 | 0.0000 | 308 | 0.0009 | 249 | 0.0214 | 153 | 0.0002 | 284 | 0.0004 | 280 | 0.0008 | 280 |
| 444 | yitu-000 | 0.0000 | 260 | 0.0010 | 278 | - | 356 | 0.0002 | 312 | 0.0004 | 299 | 0.0011 | 300 |
| 445 | yuan-004 | 0.0000 | 87 | 0.0000 | 40 | 0.0000 | 17 | 0.0000 | 2 | 0.0000 | 91 | 0.0000 | 25 |
| 446 | yuan-005 | 0.0000 | 279 | 0.0005 | 163 | 0.0134 | 103 | 0.0002 | 294 | 0.0004 | 211 | 0.0004 | 225 |

Table 37: FTE is the proportion of failed template generation attempts. Failures can occur because the software throws an exception, or because the software electively refuses to process the input image. This would typically occur if a face is not detected. FTE is measured as the number of function calls that give EITHER a non-zero error code OR that give a “small” template. This is defined as one whose size is less than 0.3 times the median template size for that algorithm. This second rule is needed because some algorithms incorrectly fail to return a non-zero error code when template generation fails.

A hyphen “-” indicates the dataset was not produced. ¹The effects of FTE are included in the accuracy results of this report by regarding any template comparison involving a failed template to produce a low similarity score. Thus higher FTE results in higher FNMR and lower FMR.

3.4 Recognition accuracy

Core algorithm accuracy is stated via:

▷ **Cooperative subjects**

- The summary table of Figure 29;
- The visa image DETs of Figure 84;
- The mugshot DETs of Figure 107;
- The mugshot ageing profiles of Figure 342;
- The human-difficult pairs of Figure 39

▷ **Non-cooperative subjects**

- The photojournalism DET of Figure 126

Figure 277 shows dependence of false match rate on algorithm score threshold. This allows a deployer to set a threshold to target a particular false match rate appropriate to the security objectives of the application.

Figure 232 likewise shows FMR(T) but for mugshots, and specially four subsets of the population.

Note that in both the mugshot and visa sets false match rates vary with the ethnicity, age, and sex, of the enrollee and impostor. For example figure 148 summarizes FMR for impostors paired from four groups black females, black males, white females, white males.

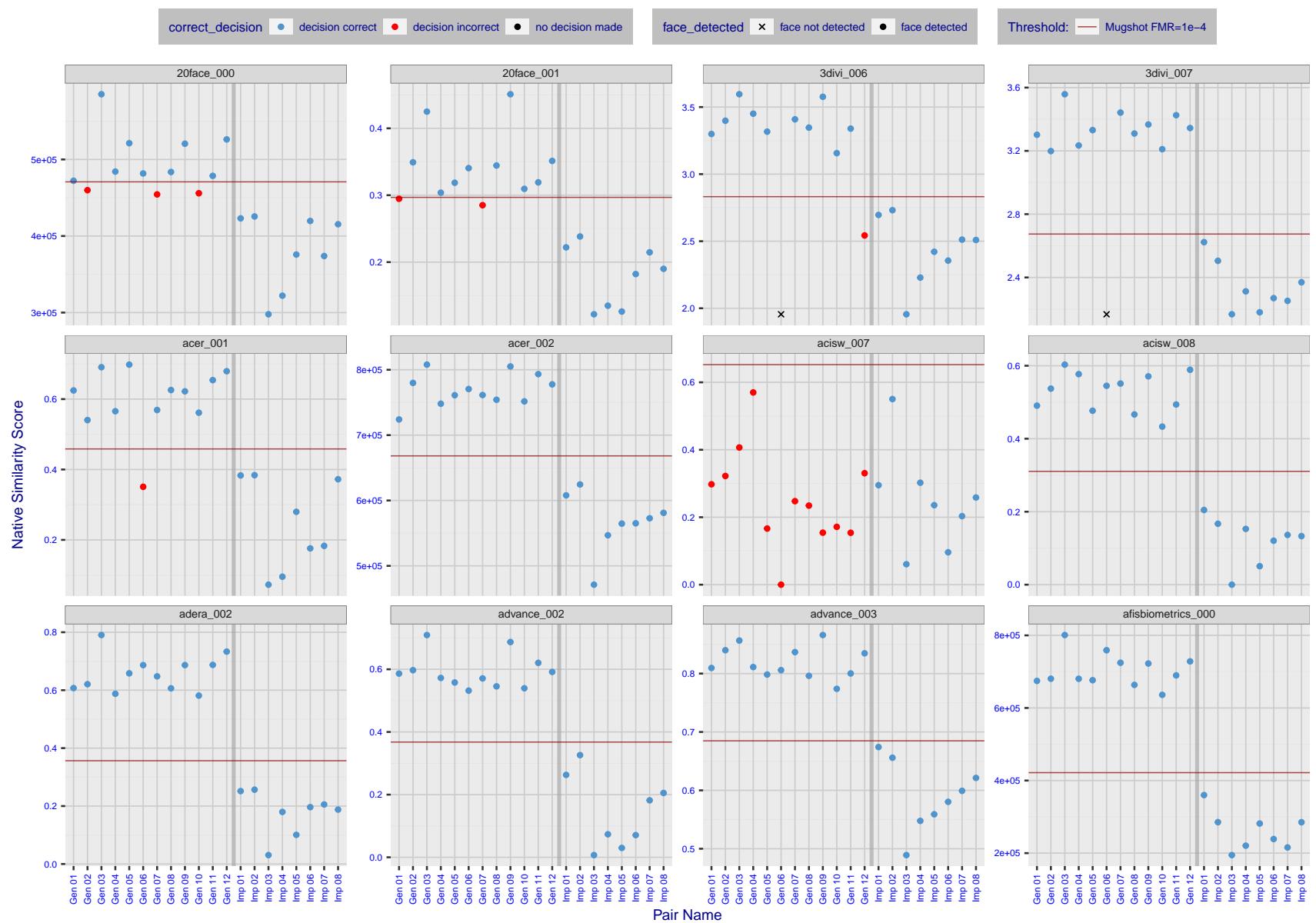


Figure 4: The figure shows algorithms' similarity scores for 12 genuine and 8 impostor image pairs used in a May 2018 paper by Phillips et al. ([1]). The threshold (red horizontal line) is a value calibrated to give $FMR = 0.0001$ on mugshot images. Points above the threshold correspond to pairs determined to be genuine, and points below the threshold correspond to pairs determined to be impostors. If the determined class (genuine or impostor) matches the real class, points will be blue; if not, red. An X represents face detection failure in either of the images in the pair. Note that the sample size ($n=20$) is small, and the figure may change substantially if larger or different sets are used. The images can be viewed on p. 13 of the Appendix, where Gen 01 corresponds to Same-Identity Pair 1, Gen 02 corresponds to Same-Identity Pair 2, and so on.

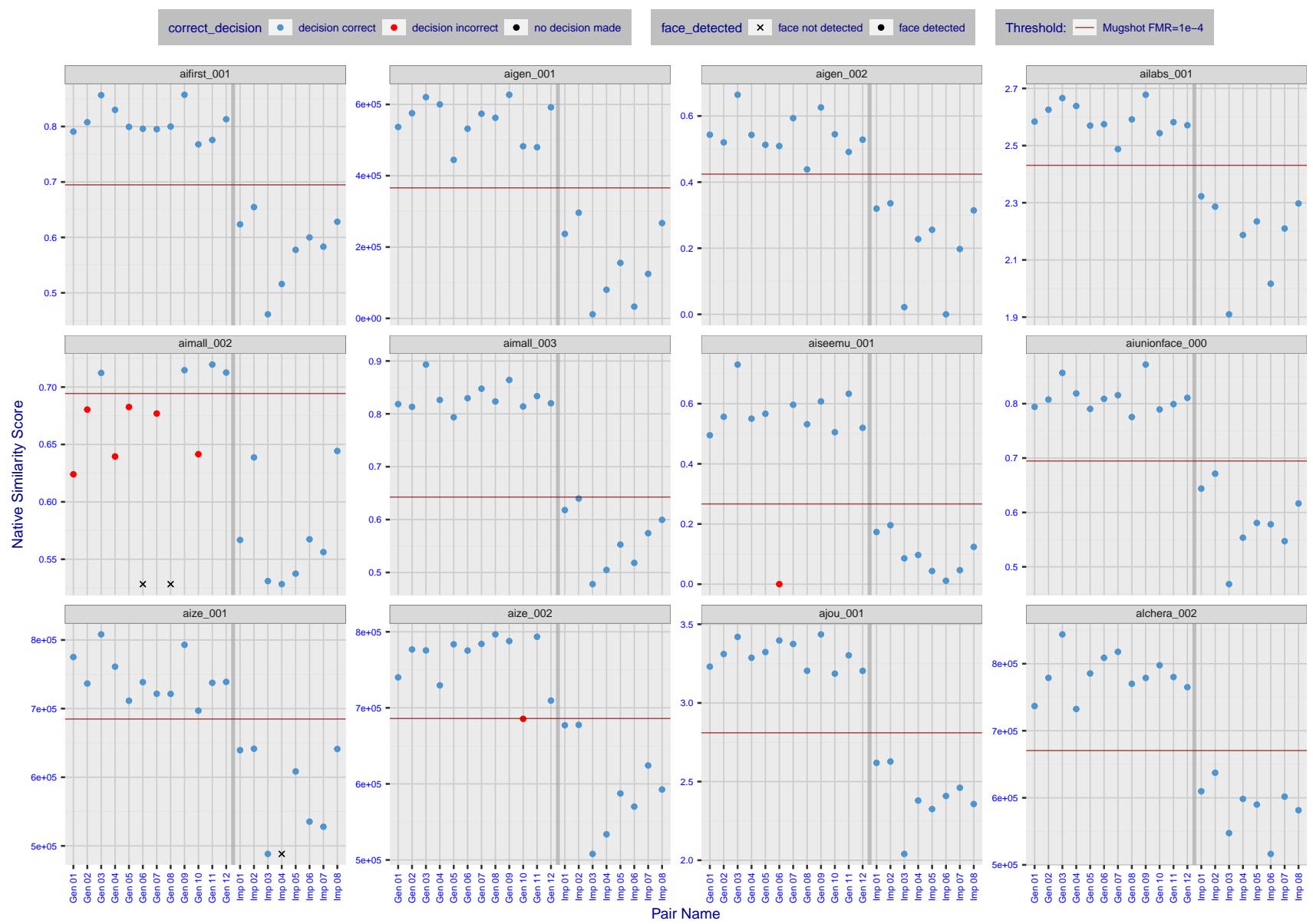


Figure 5: The figure shows algorithms' similarity scores for 12 genuine and 8 impostor image pairs used in a May 2018 paper by Phillips et al. ([1]). The threshold (red horizontal line) is a value calibrated to give $FMR = 0.0001$ on mugshot images. Points above the threshold correspond to pairs determined to be genuine, and points below the threshold correspond to pairs determined to be impostors. If the determined class (genuine or impostor) matches the real class, points will be blue; if not, red. An X represents face detection failure in either of the images in the pair. Note that the sample size ($n=20$) is small, and the figure may change substantially if larger or different sets are used. The images can be viewed on p. 13 of the Appendix, where Gen 01 corresponds to Same-Identity Pair 1, Gen 02 corresponds to Same-Identity Pair 2, and so on.

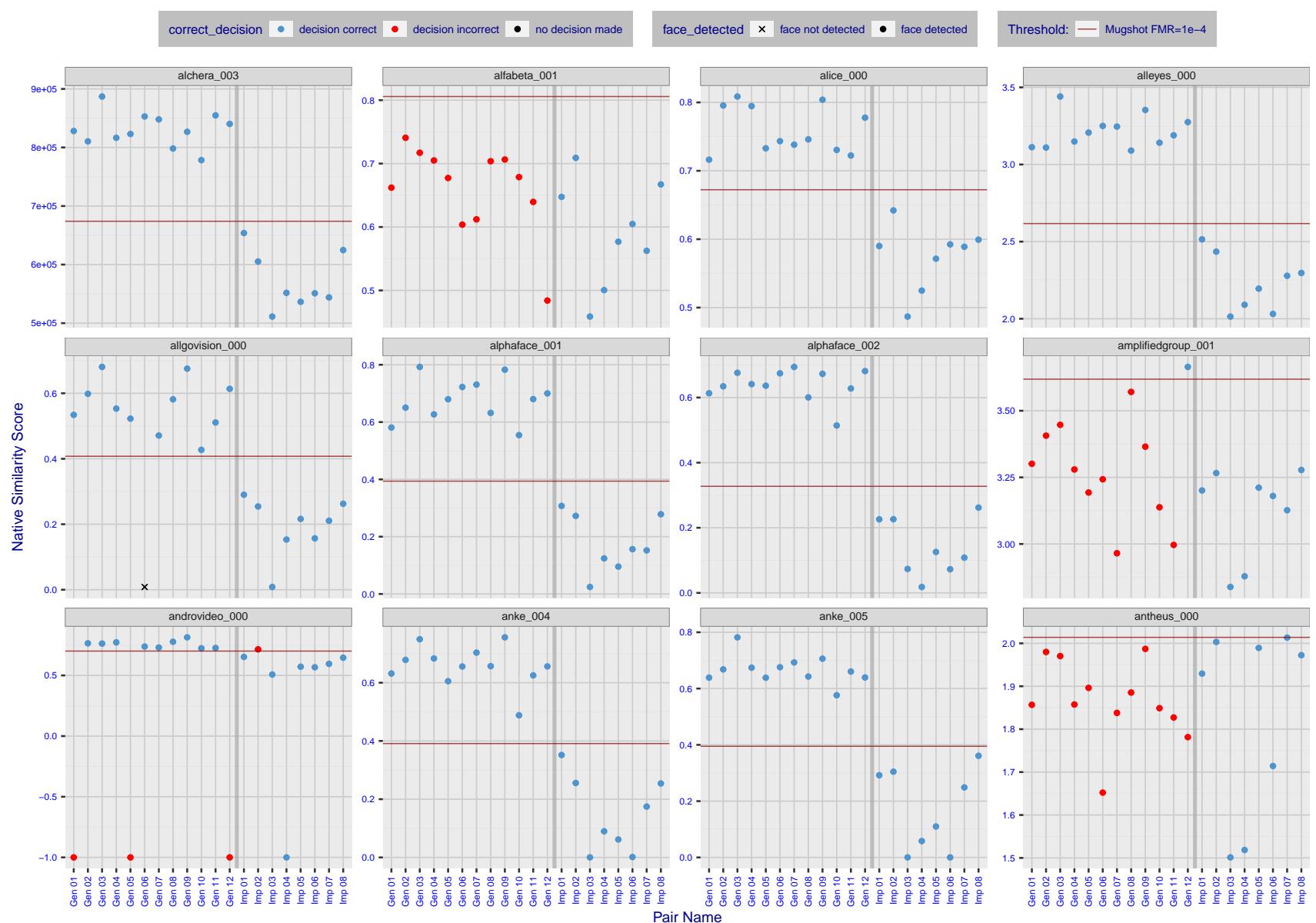


Figure 6: The figure shows algorithms' similarity scores for 12 genuine and 8 impostor image pairs used in a May 2018 paper by Phillips et al. ([1]). The threshold (red horizontal line) is a value calibrated to give $FMR = 0.0001$ on mugshot images. Points above the threshold correspond to pairs determined to be genuine, and points below the threshold correspond to pairs determined to be impostors. If the determined class (genuine or impostor) matches the real class, points will be blue; if not, red. An X represents face detection failure in either of the images in the pair. Note that the sample size ($n=20$) is small, and the figure may change substantially if larger or different sets are used. The images can be viewed on p. 13 of the Appendix, where Gen 01 corresponds to Same-Identity Pair 1, Gen 02 corresponds to Same-Identity Pair 2, and so on.

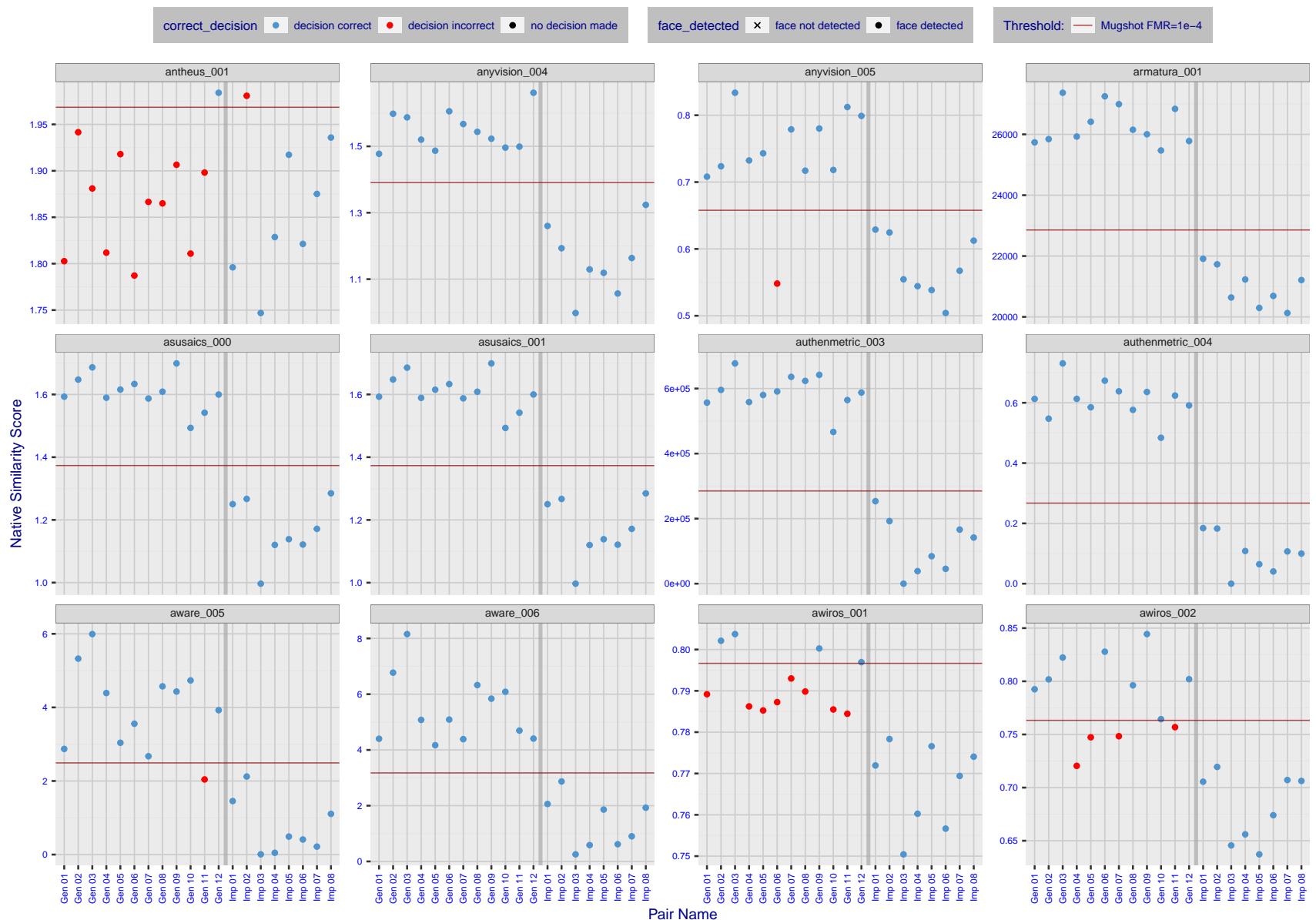


Figure 7: The figure shows algorithms' similarity scores for 12 genuine and 8 impostor image pairs used in a May 2018 paper by Phillips et al. ([1]). The threshold (red horizontal line) is a value calibrated to give $FMR = 0.0001$ on mugshot images. Points above the threshold correspond to pairs determined to be genuine, and points below the threshold correspond to pairs determined to be impostors. If the determined class (genuine or impostor) matches the real class, points will be blue; if not, red. An X represents face detection failure in either of the images in the pair. Note that the sample size ($n=20$) is small, and the figure may change substantially if larger or different sets are used. The images can be viewed on p. 13 of the Appendix, where Gen 01 corresponds to Same-Identity Pair 1, Gen 02 corresponds to Same-Identity Pair 2, and so on.

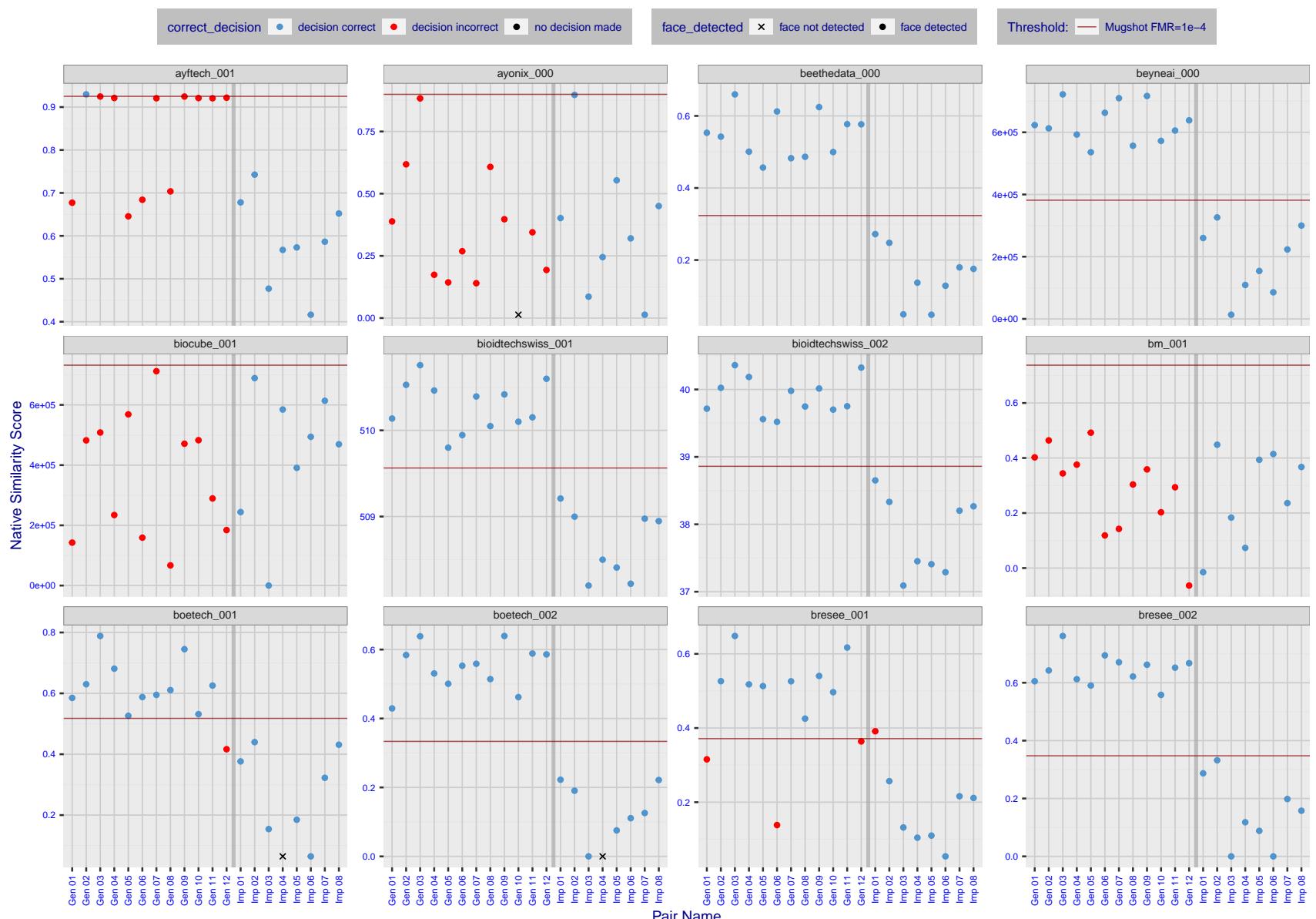


Figure 8: The figure shows algorithms' similarity scores for 12 genuine and 8 impostor image pairs used in a May 2018 paper by Phillips et al. ([1]). The threshold (red horizontal line) is a value calibrated to give $FMR = 0.0001$ on mugshot images. Points above the threshold correspond to pairs determined to be genuine, and points below the threshold correspond to pairs determined to be impostors. If the determined class (genuine or impostor) matches the real class, points will be blue; if not, red. An X represents face detection failure in either of the images in the pair. Note that the sample size ($n=20$) is small, and the figure may change substantially if larger or different sets are used. The images can be viewed on p. 13 of the Appendix, where Gen 01 corresponds to Same-Identity Pair 1, Gen 02 corresponds to Same-Identity Pair 2, and so on.

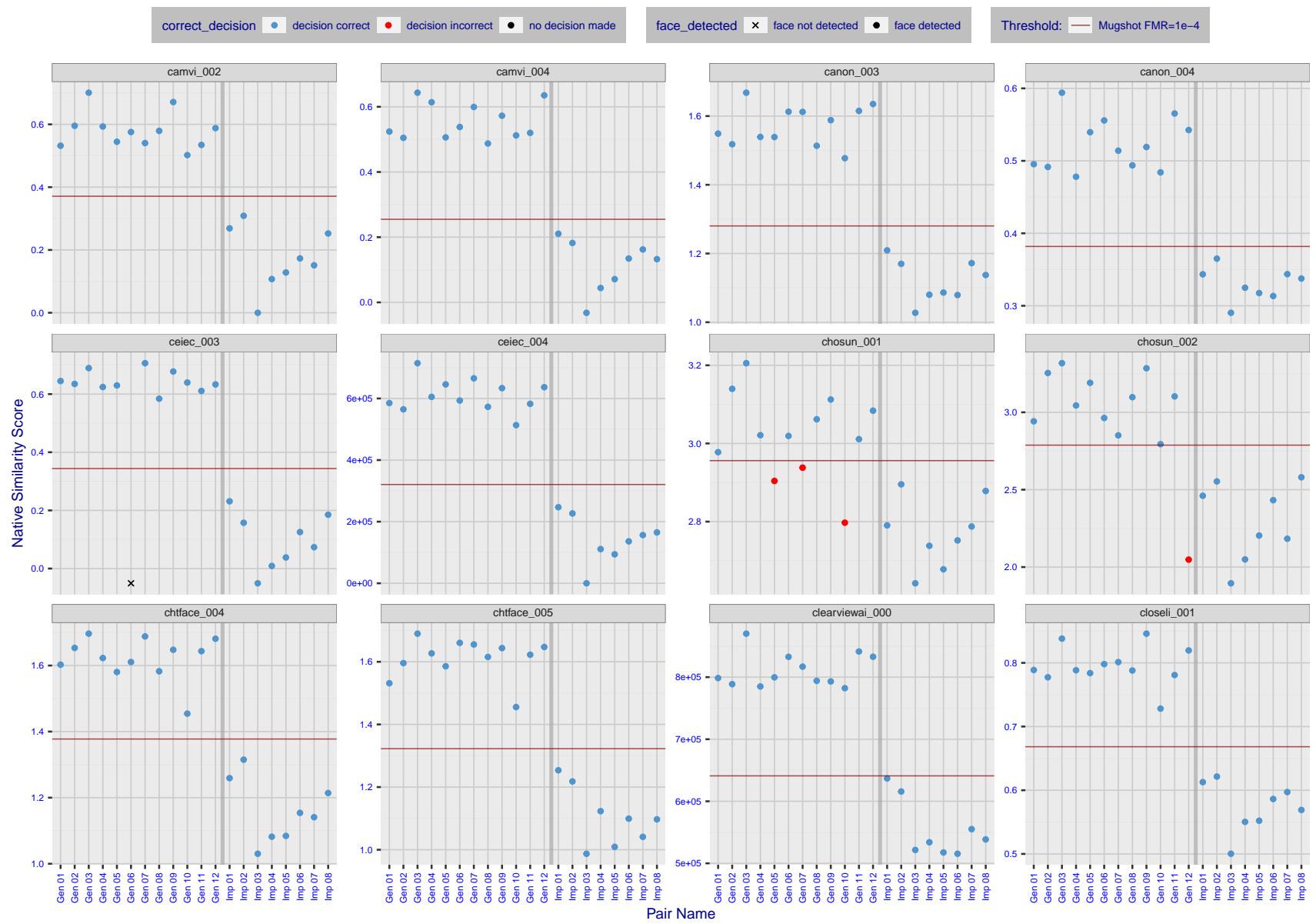


Figure 9: The figure shows algorithms' similarity scores for 12 genuine and 8 impostor image pairs used in a May 2018 paper by Phillips et al. ([1]). The threshold (red horizontal line) is a value calibrated to give $FMR = 0.0001$ on mugshot images. Points above the threshold correspond to pairs determined to be genuine, and points below the threshold correspond to pairs determined to be impostors. If the determined class (genuine or impostor) matches the real class, points will be blue; if not, red. An X represents face detection failure in either of the images in the pair. Note that the sample size ($n=20$) is small, and the figure may change substantially if larger or different sets are used. The images can be viewed on p. 13 of the Appendix, where Gen 01 corresponds to Same-Identity Pair 1, Gen 02 corresponds to Same-Identity Pair 2, and so on.

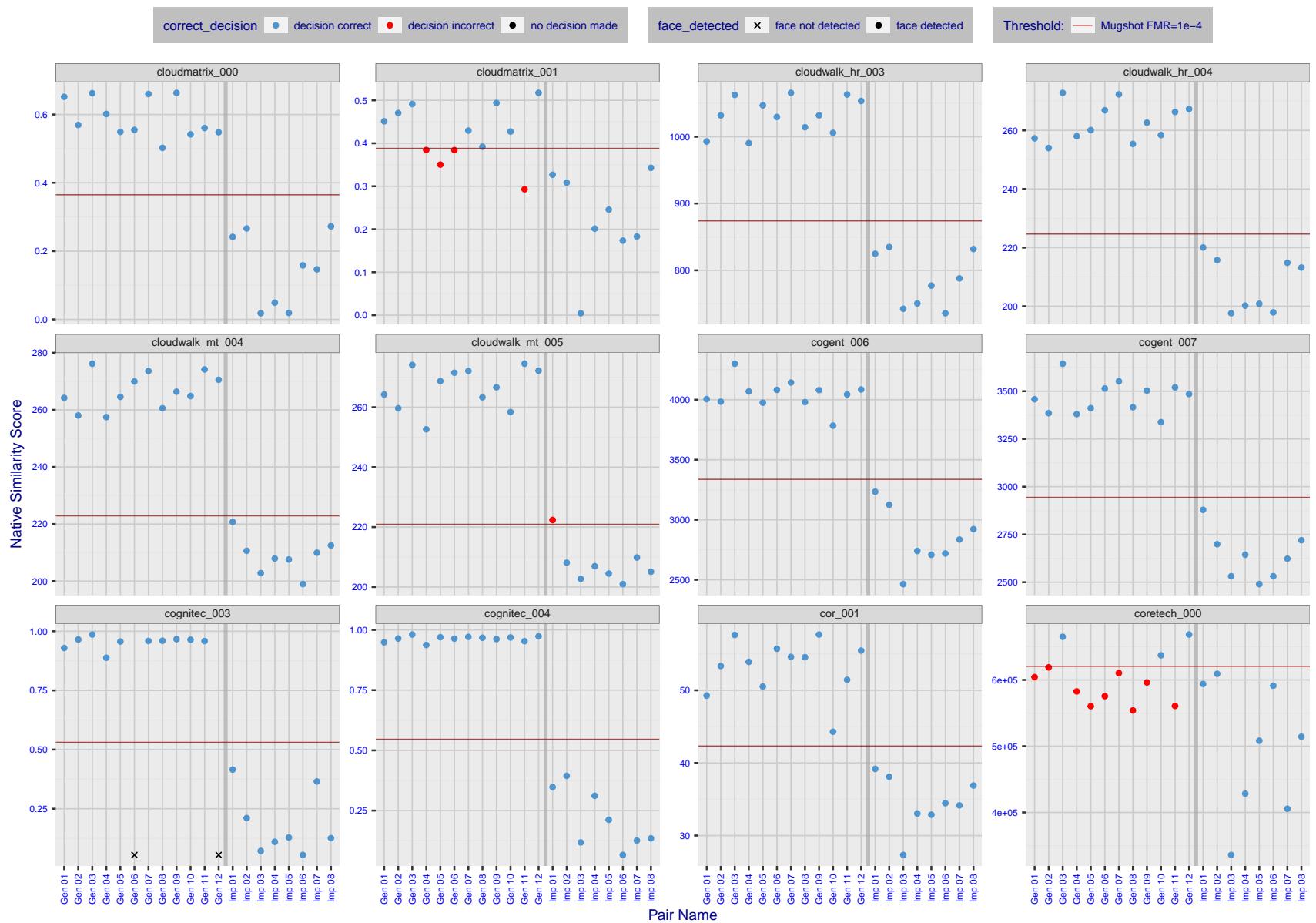


Figure 10: The figure shows algorithms' similarity scores for 12 genuine and 8 impostor image pairs used in a May 2018 paper by Phillips et al. ([1]). The threshold (red horizontal line) is a value calibrated to give $FMR = 0.0001$ on mugshot images. Points above the threshold correspond to pairs determined to be genuine, and points below the threshold correspond to pairs determined to be impostors. If the determined class (genuine or impostor) matches the real class, points will be blue; if not, red. An X represents face detection failure in either of the images in the pair. Note that the sample size ($n=20$) is small, and the figure may change substantially if larger or different sets are used. The images can be viewed on p. 13 of the Appendix, where Gen 01 corresponds to Same-Identity Pair 1, Gen 02 corresponds to Same-Identity Pair 2, and so on.

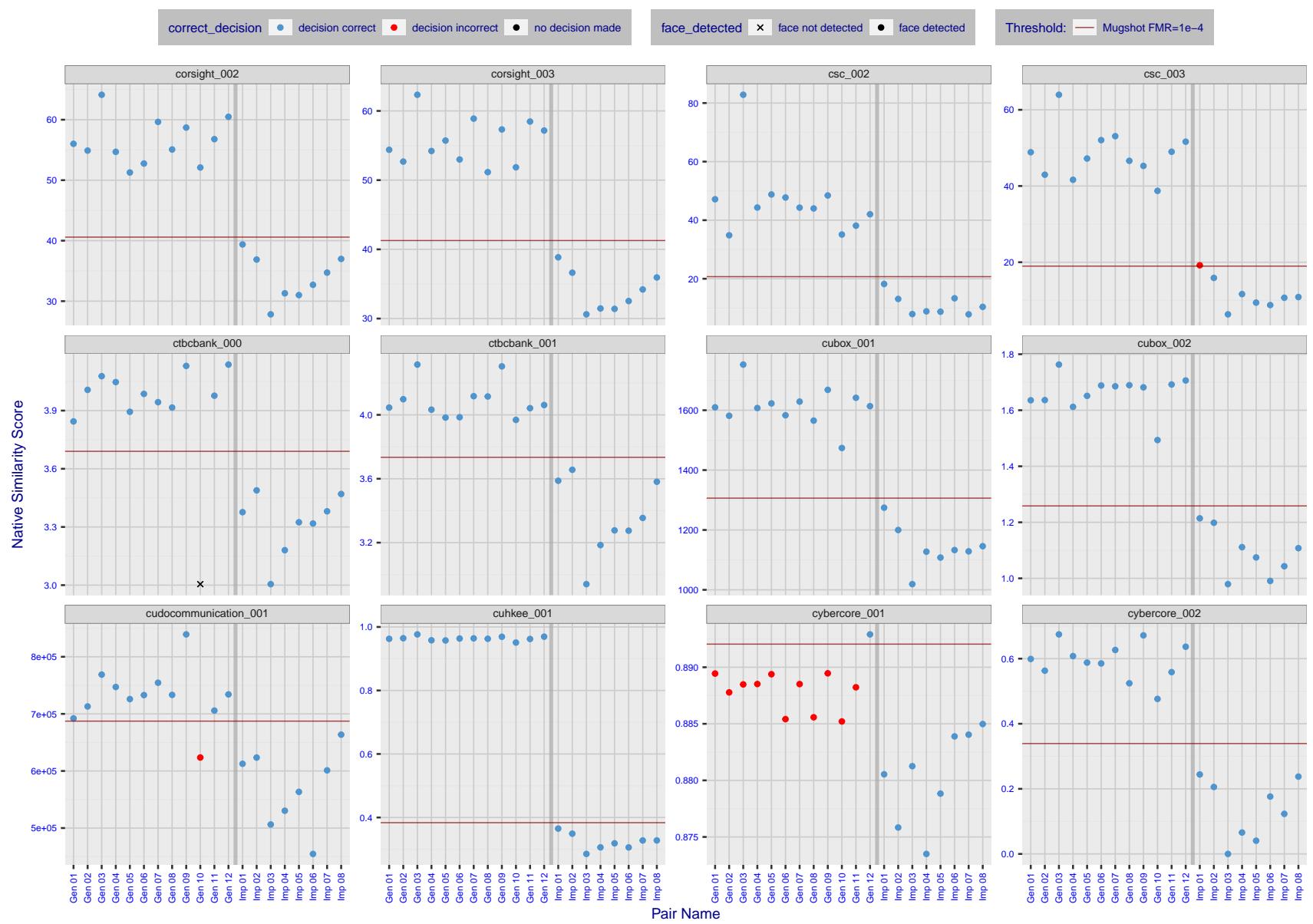


Figure 11: The figure shows algorithms' similarity scores for 12 genuine and 8 impostor image pairs used in a May 2018 paper by Phillips et al. ([1]). The threshold (red horizontal line) is a value calibrated to give $FMR = 0.0001$ on mugshot images. Points above the threshold correspond to pairs determined to be genuine, and points below the threshold correspond to pairs determined to be impostors. If the determined class (genuine or impostor) matches the real class, points will be blue; if not, red. An X represents face detection failure in either of the images in the pair. Note that the sample size ($n=20$) is small, and the figure may change substantially if larger or different sets are used. The images can be viewed on p. 13 of the Appendix, where Gen 01 corresponds to Same-Identity Pair 1, Gen 02 corresponds to Same-Identity Pair 2, and so on.

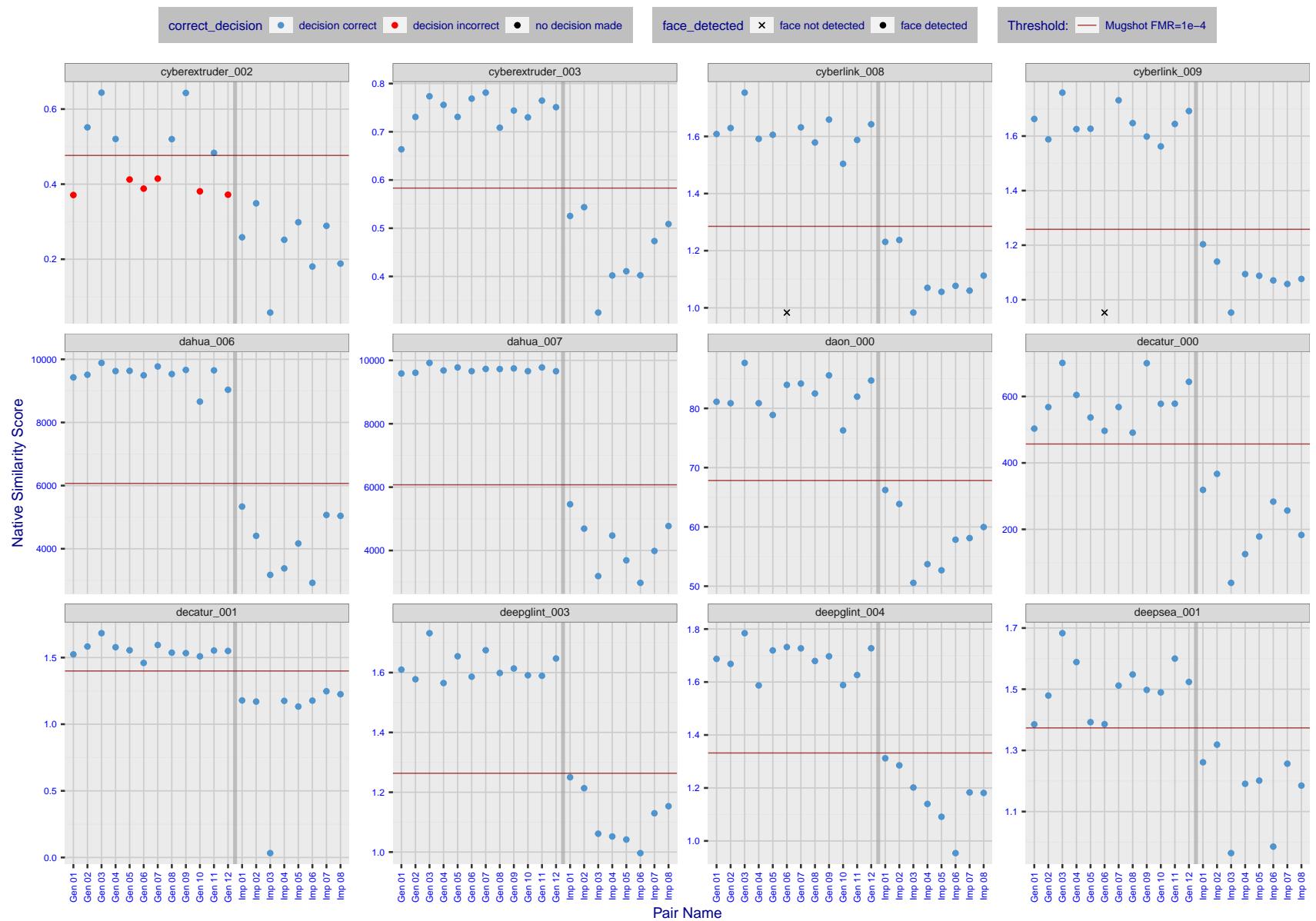


Figure 12: The figure shows algorithms' similarity scores for 12 genuine and 8 impostor image pairs used in a May 2018 paper by Phillips et al. ([1]). The threshold (red horizontal line) is a value calibrated to give $FMR = 0.0001$ on mugshot images. Points above the threshold correspond to pairs determined to be genuine, and points below the threshold correspond to pairs determined to be impostors. If the determined class (genuine or impostor) matches the real class, points will be blue; if not, red. An X represents face detection failure in either of the images in the pair. Note that the sample size ($n=20$) is small, and the figure may change substantially if larger or different sets are used. The images can be viewed on p. 13 of the Appendix, where Gen 01 corresponds to Same-Identity Pair 1, Gen 02 corresponds to Same-Identity Pair 2, and so on.

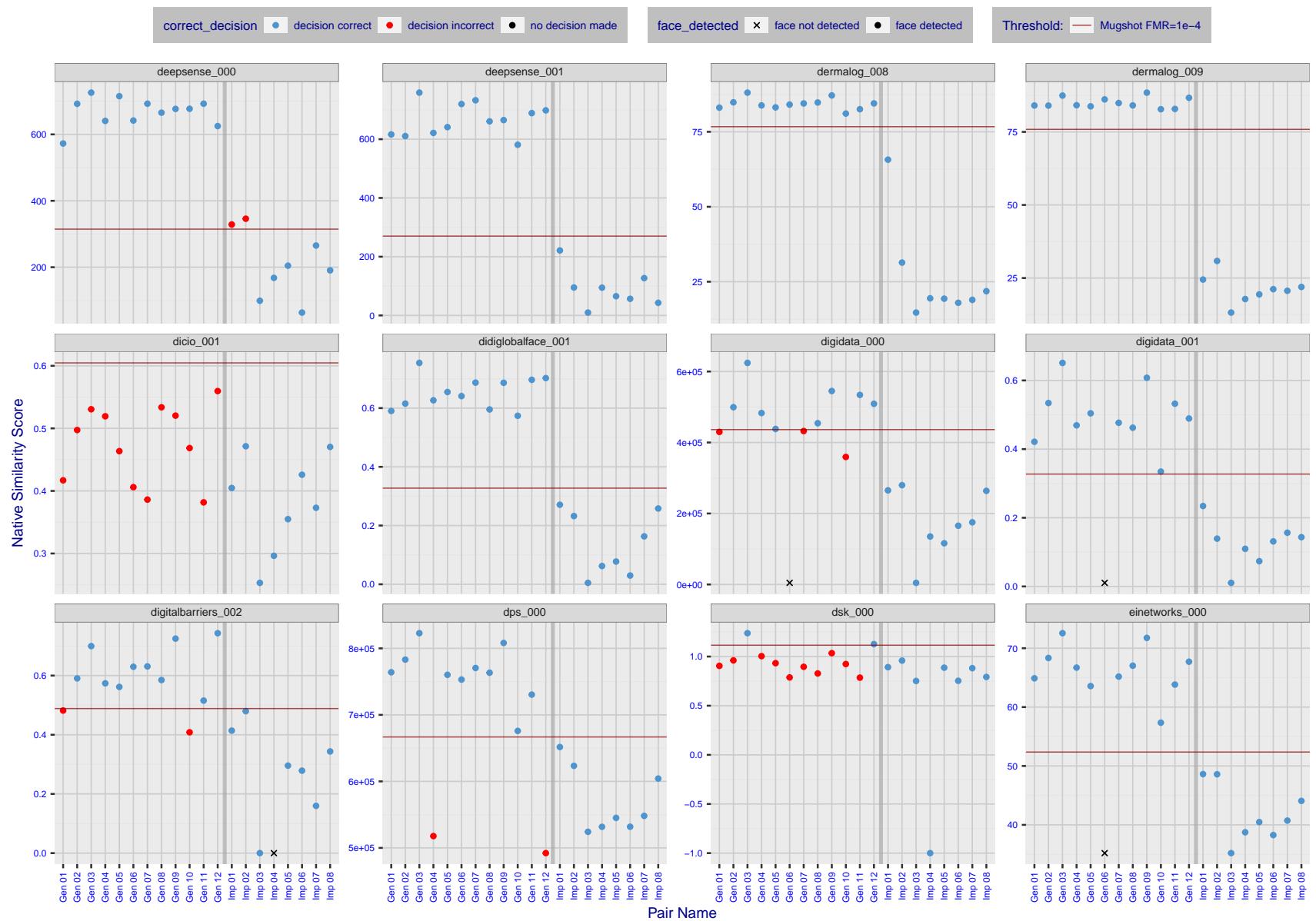


Figure 13: The figure shows algorithms' similarity scores for 12 genuine and 8 impostor image pairs used in a May 2018 paper by Phillips et al. ([1]). The threshold (red horizontal line) is a value calibrated to give $FMR = 0.0001$ on mugshot images. Points above the threshold correspond to pairs determined to be genuine, and points below the threshold correspond to pairs determined to be impostors. If the determined class (genuine or impostor) matches the real class, points will be blue; if not, red. An X represents face detection failure in either of the images in the pair. Note that the sample size ($n=20$) is small, and the figure may change substantially if larger or different sets are used. The images can be viewed on p. 13 of the Appendix, where Gen 01 corresponds to Same-Identity Pair 1, Gen 02 corresponds to Same-Identity Pair 2, and so on.

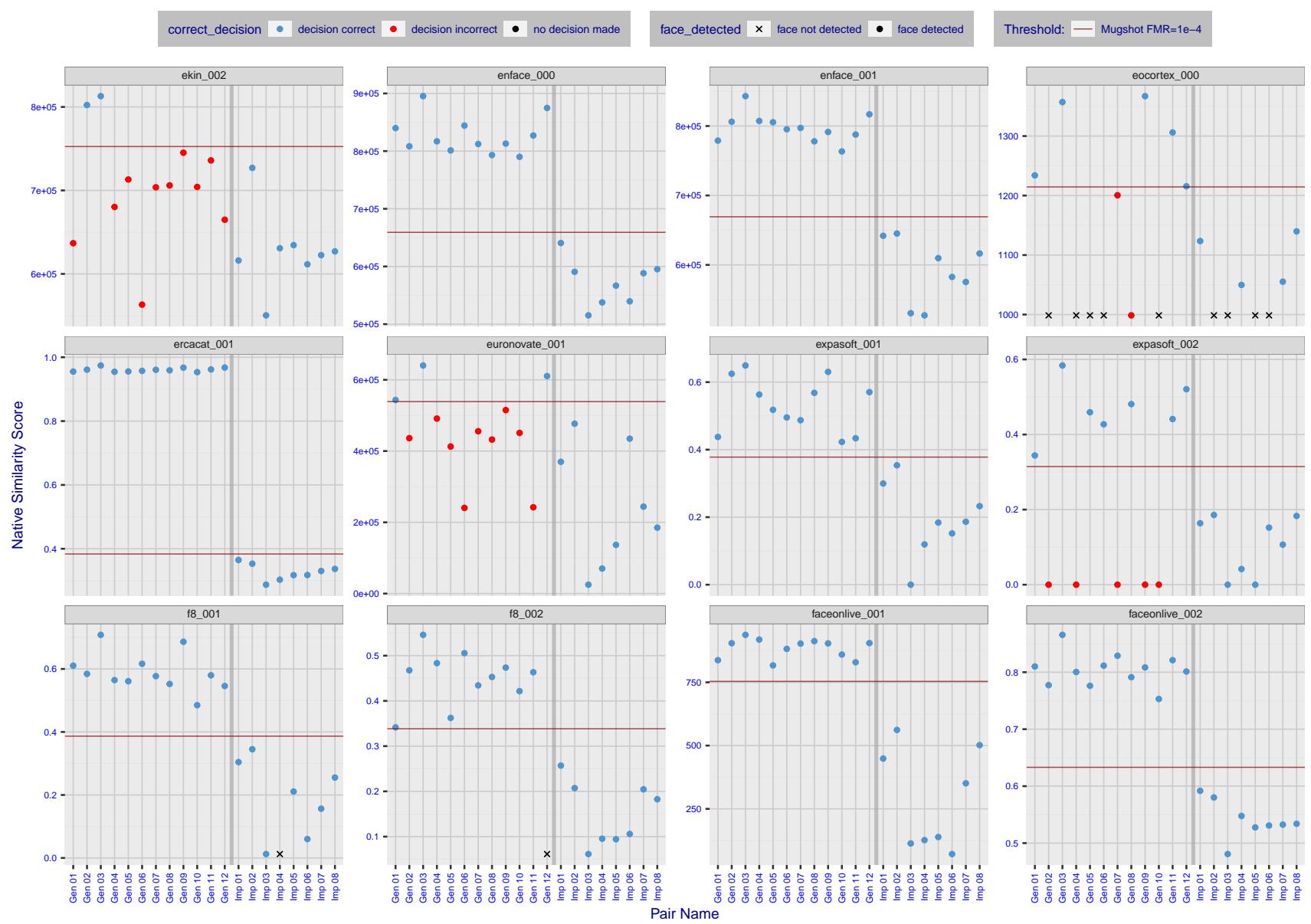


Figure 14: The figure shows algorithms' similarity scores for 12 genuine and 8 impostor image pairs used in a May 2018 paper by Phillips et al. ([1]). The threshold (red horizontal line) is a value calibrated to give $FMR = 0.0001$ on mugshot images. Points above the threshold correspond to pairs determined to be genuine, and points below the threshold correspond to pairs determined to be impostors. If the determined class (genuine or impostor) matches the real class, points will be blue; if not, red. An X represents face detection failure in either of the images in the pair. Note that the sample size ($n=20$) is small, and the figure may change substantially if larger or different sets are used. The images can be viewed on p. 13 of the Appendix, where Gen 01 corresponds to Same-Identity Pair 1, Gen 02 corresponds to Same-Identity Pair 2, and so on.

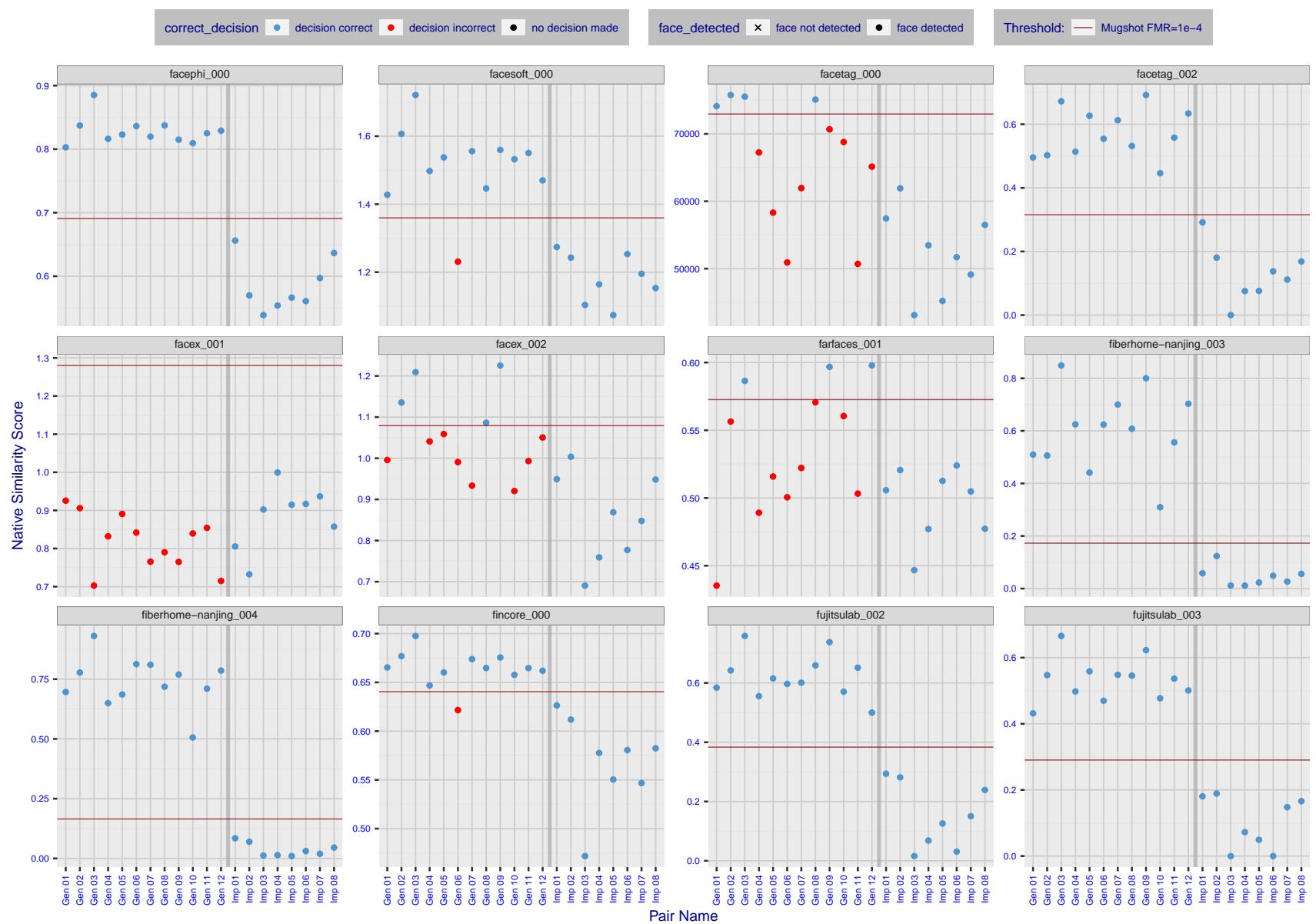


Figure 15: The figure shows algorithms' similarity scores for 12 genuine and 8 impostor image pairs used in a May 2018 paper by Phillips et al. ([1]). The threshold (red horizontal line) is a value calibrated to give $FMR = 0.0001$ on mugshot images. Points above the threshold correspond to pairs determined to be genuine, and points below the threshold correspond to pairs determined to be impostors. If the determined class (genuine or impostor) matches the real class, points will be blue; if not, red. An X represents face detection failure in either of the images in the pair. Note that the sample size ($n=20$) is small, and the figure may change substantially if larger or different sets are used. The images can be viewed on p. 13 of the Appendix, where Gen 01 corresponds to Same-Identity Pair 1, Gen 02 corresponds to Same-Identity Pair 2, and so on.

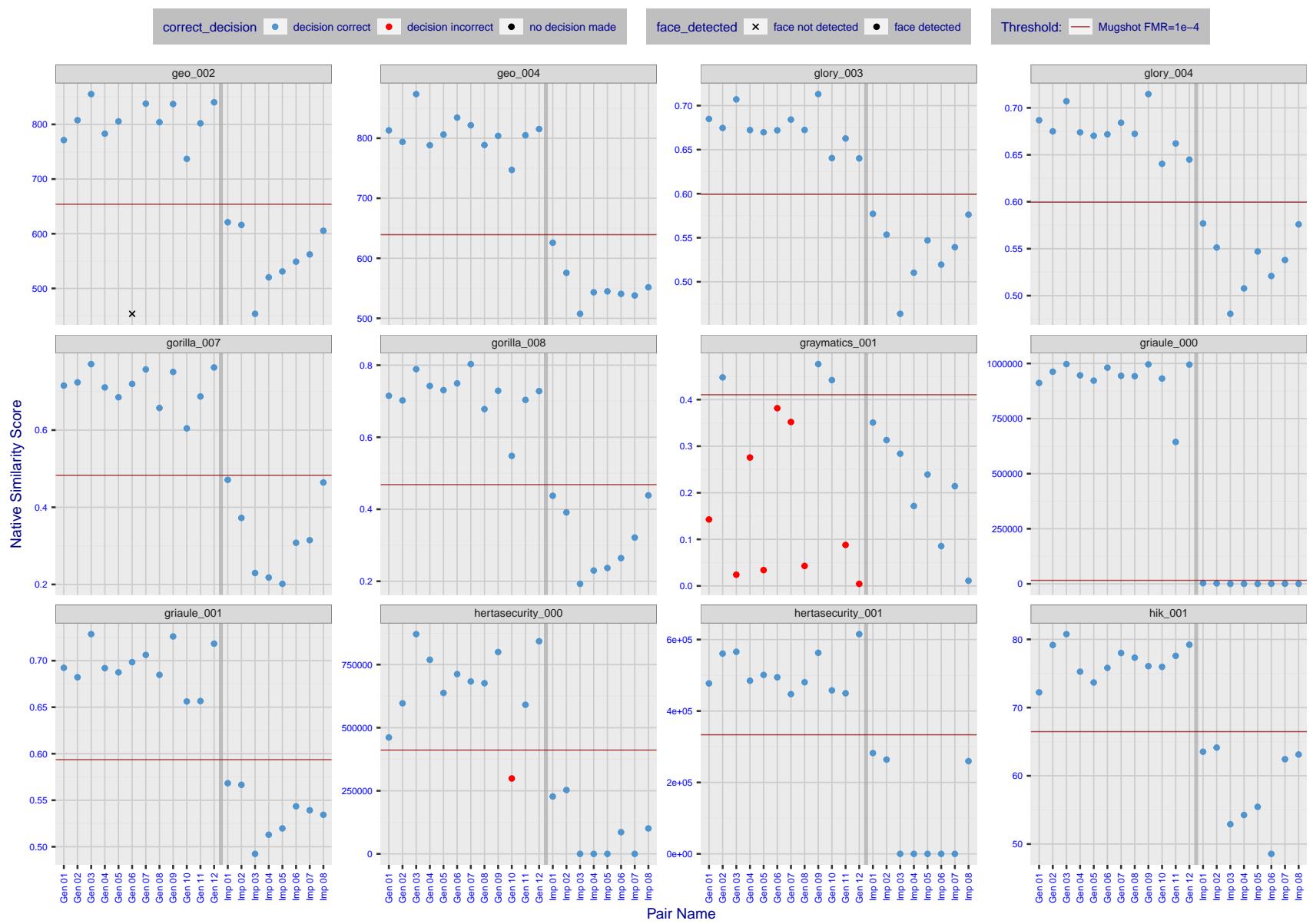


Figure 16: The figure shows algorithms' similarity scores for 12 genuine and 8 impostor image pairs used in a May 2018 paper by Phillips et al. ([1]). The threshold (red horizontal line) is a value calibrated to give $FMR = 0.0001$ on mugshot images. Points above the threshold correspond to pairs determined to be genuine, and points below the threshold correspond to pairs determined to be impostors. If the determined class (genuine or impostor) matches the real class, points will be blue; if not, red. An X represents face detection failure in either of the images in the pair. Note that the sample size ($n=20$) is small, and the figure may change substantially if larger or different sets are used. The images can be viewed on p. 13 of the Appendix, where Gen 01 corresponds to Same-Identity Pair 1, Gen 02 corresponds to Same-Identity Pair 2, and so on.

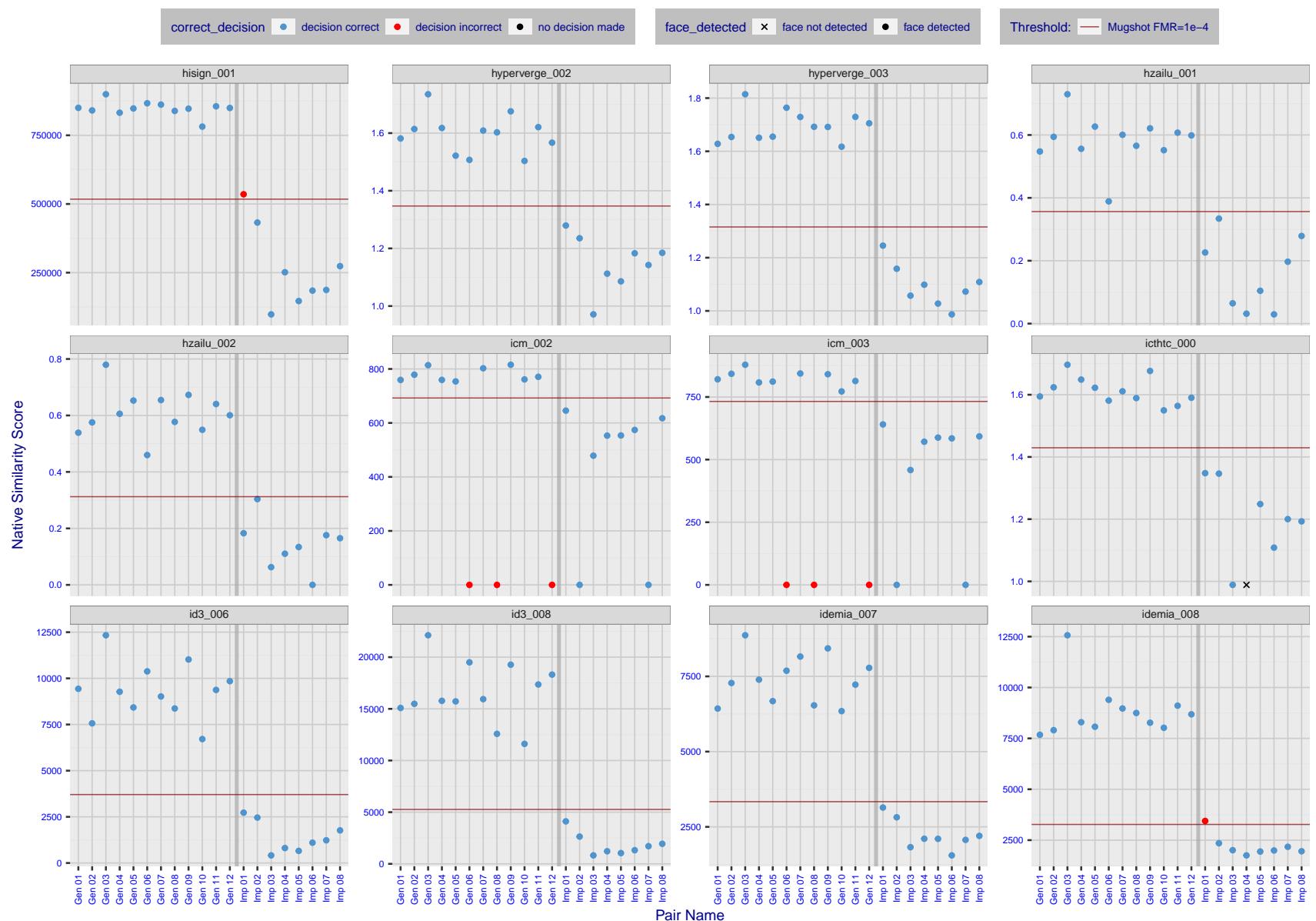


Figure 17: The figure shows algorithms' similarity scores for 12 genuine and 8 impostor image pairs used in a May 2018 paper by Phillips et al. ([1]). The threshold (red horizontal line) is a value calibrated to give $FMR = 0.0001$ on mugshot images. Points above the threshold correspond to pairs determined to be genuine, and points below the threshold correspond to pairs determined to be impostors. If the determined class (genuine or impostor) matches the real class, points will be blue; if not, red. An X represents face detection failure in either of the images in the pair. Note that the sample size ($n=20$) is small, and the figure may change substantially if larger or different sets are used. The images can be viewed on p. 13 of the Appendix, where Gen 01 corresponds to Same-Identity Pair 1, Gen 02 corresponds to Same-Identity Pair 2, and so on.

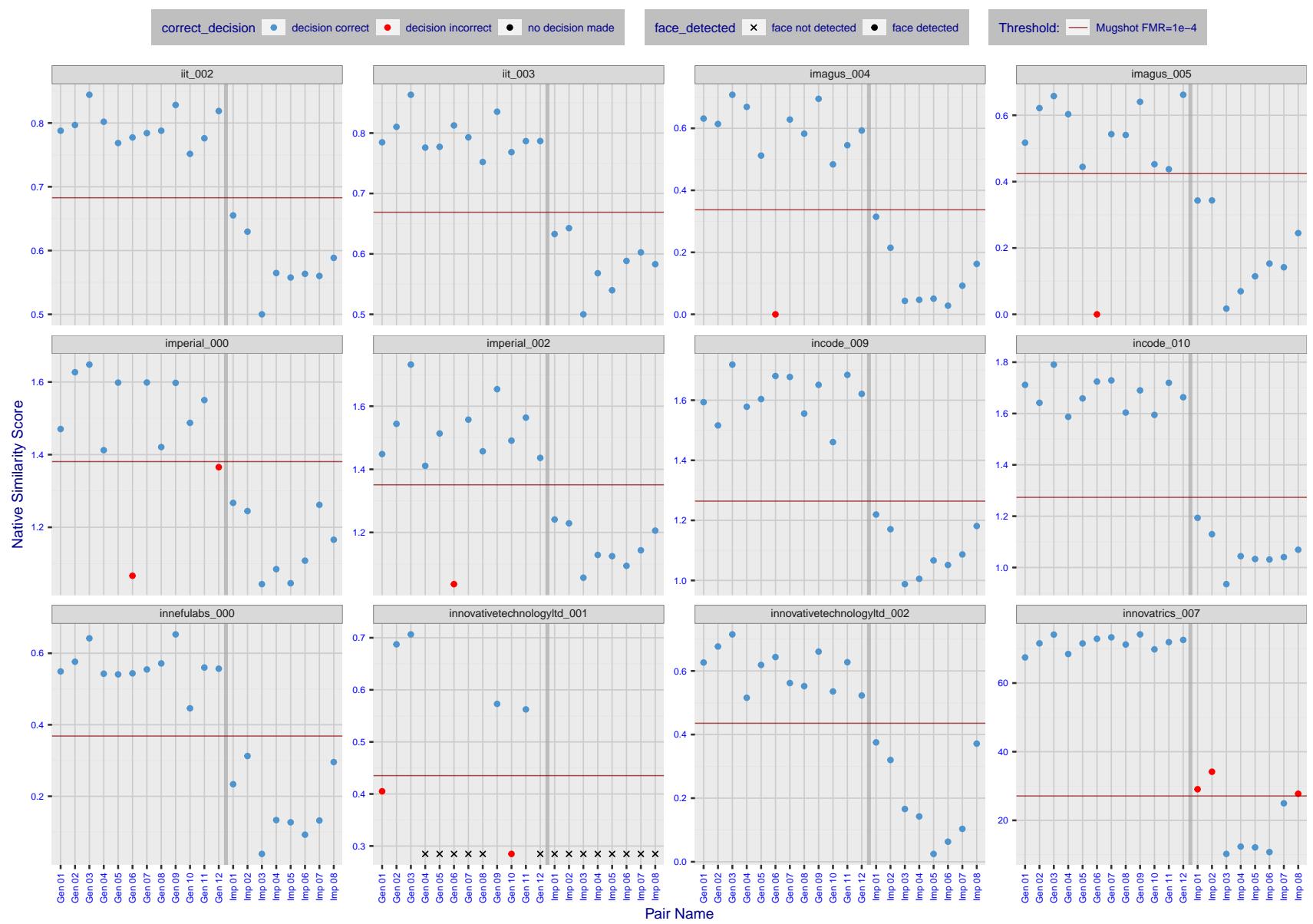


Figure 18: The figure shows algorithms' similarity scores for 12 genuine and 8 impostor image pairs used in a May 2018 paper by Phillips et al. ([1]). The threshold (red horizontal line) is a value calibrated to give $FMR = 0.0001$ on mugshot images. Points above the threshold correspond to pairs determined to be genuine, and points below the threshold correspond to pairs determined to be impostors. If the determined class (genuine or impostor) matches the real class, points will be blue; if not, red. An X represents face detection failure in either of the images in the pair. Note that the sample size ($n=20$) is small, and the figure may change substantially if larger or different sets are used. The images can be viewed on p. 13 of the Appendix, where Gen 01 corresponds to Same-Identity Pair 1, Gen 02 corresponds to Same-Identity Pair 2, and so on.

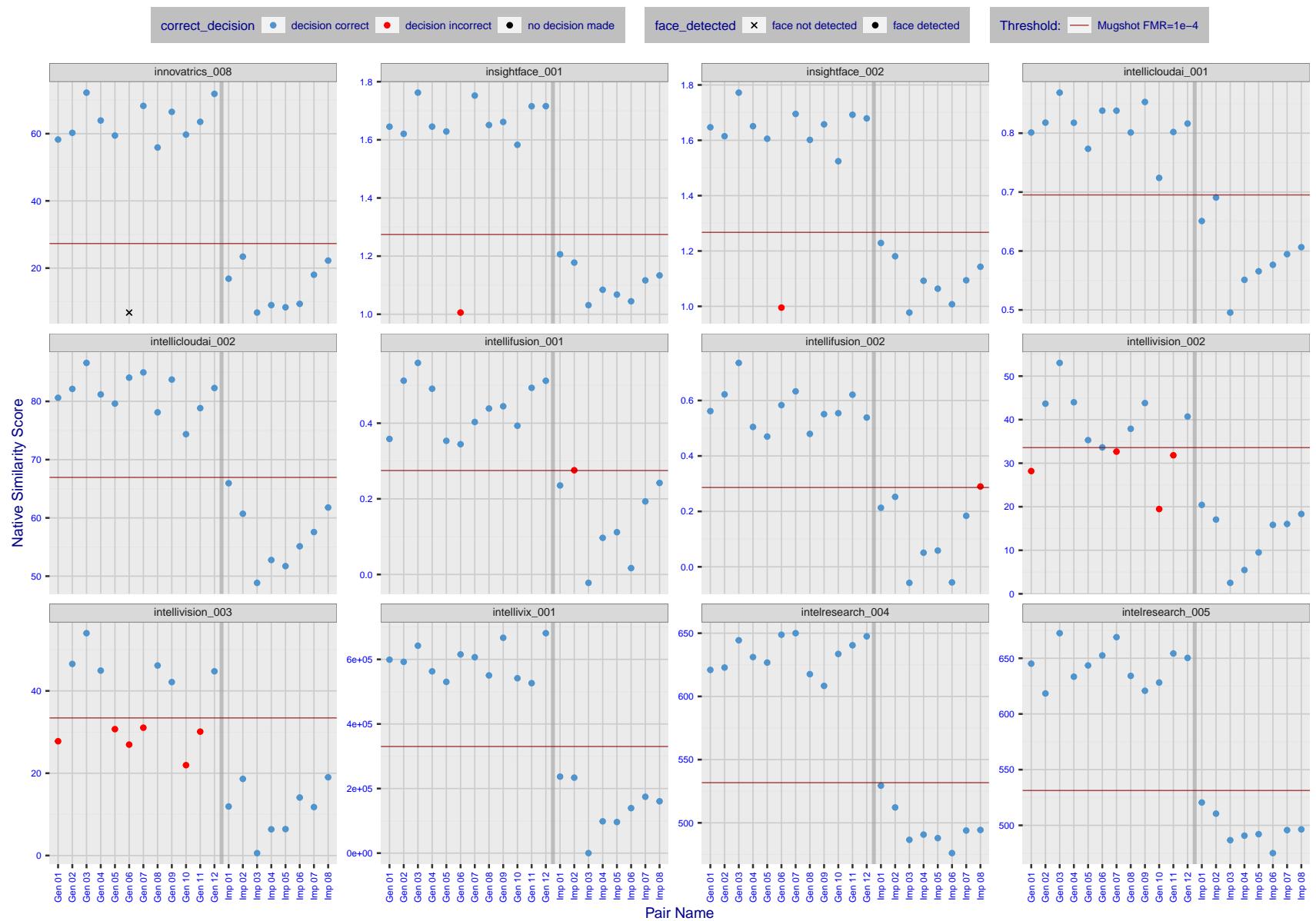


Figure 19: The figure shows algorithms' similarity scores for 12 genuine and 8 impostor image pairs used in a May 2018 paper by Phillips et al. ([1]). The threshold (red horizontal line) is a value calibrated to give $FMR = 0.0001$ on mugshot images. Points above the threshold correspond to pairs determined to be genuine, and points below the threshold correspond to pairs determined to be impostors. If the determined class (genuine or impostor) matches the real class, points will be blue; if not, red. An X represents face detection failure in either of the images in the pair. Note that the sample size ($n=20$) is small, and the figure may change substantially if larger or different sets are used. The images can be viewed on p. 13 of the Appendix, where Gen 01 corresponds to Same-Identity Pair 1, Gen 02 corresponds to Same-Identity Pair 2, and so on.

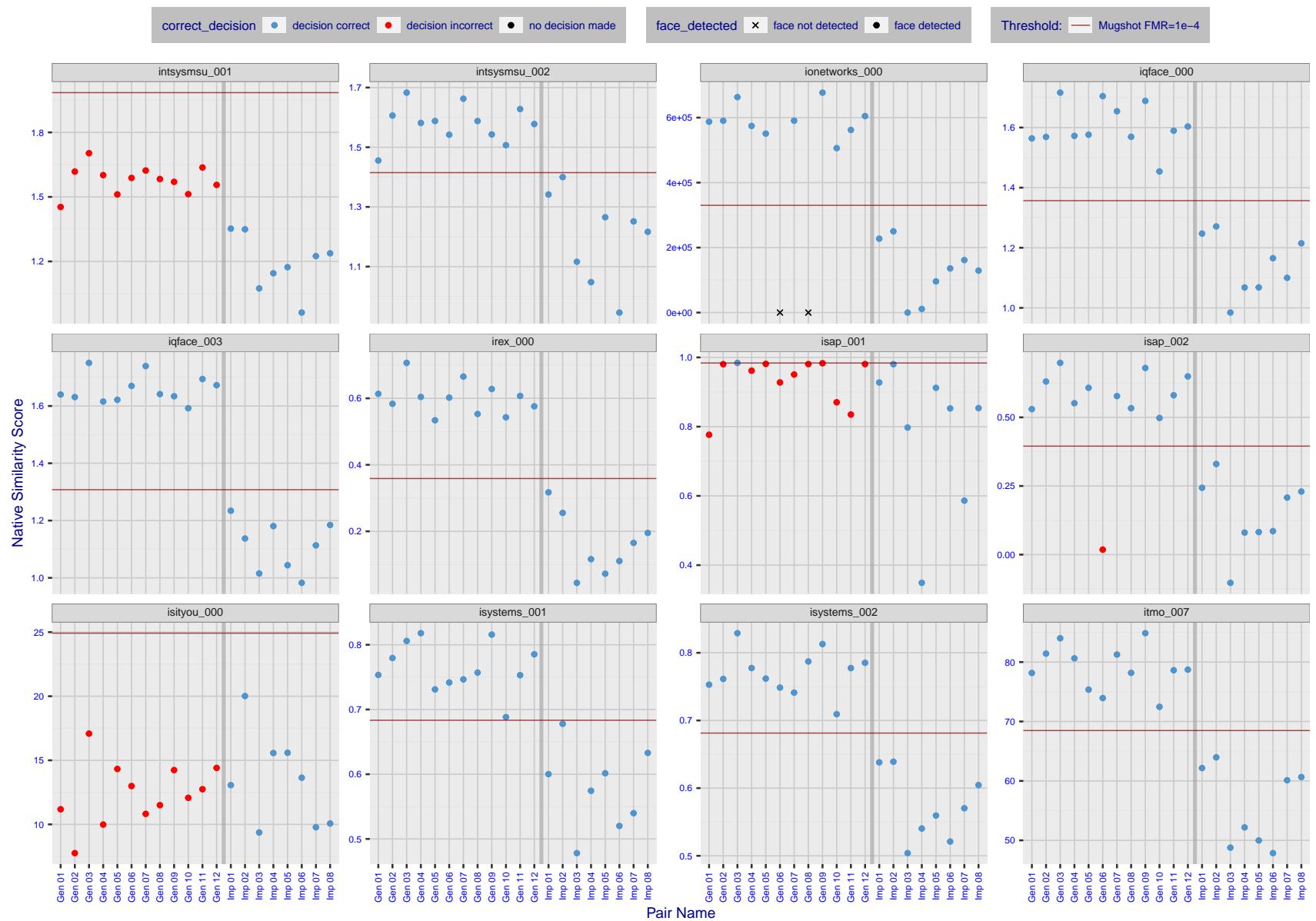


Figure 20: The figure shows algorithms' similarity scores for 12 genuine and 8 impostor image pairs used in a May 2018 paper by Phillips et al. ([1]). The threshold (red horizontal line) is a value calibrated to give $FMR = 0.0001$ on mugshot images. Points above the threshold correspond to pairs determined to be genuine, and points below the threshold correspond to pairs determined to be impostors. If the determined class (genuine or impostor) matches the real class, points will be blue; if not, red. An X represents face detection failure in either of the images in the pair. Note that the sample size ($n=20$) is small, and the figure may change substantially if larger or different sets are used. The images can be viewed on p. 13 of the Appendix, where Gen 01 corresponds to Same-Identity Pair 1, Gen 02 corresponds to Same-Identity Pair 2, and so on.

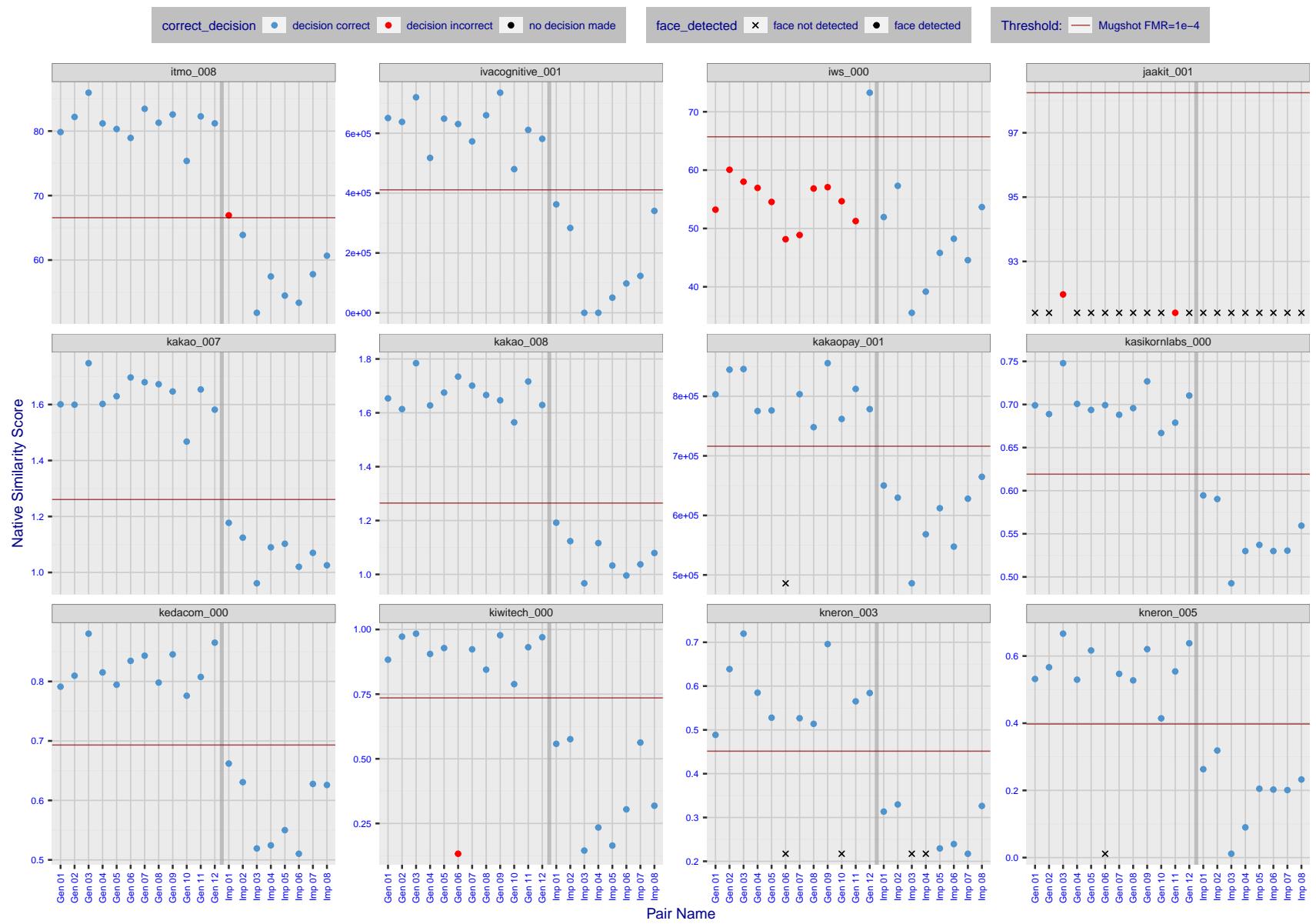


Figure 21: The figure shows algorithms' similarity scores for 12 genuine and 8 impostor image pairs used in a May 2018 paper by Phillips et al. ([1]). The threshold (red horizontal line) is a value calibrated to give $FMR = 0.0001$ on mugshot images. Points above the threshold correspond to pairs determined to be genuine, and points below the threshold correspond to pairs determined to be impostors. If the determined class (genuine or impostor) matches the real class, points will be blue; if not, red. An X represents face detection failure in either of the images in the pair. Note that the sample size ($n=20$) is small, and the figure may change substantially if larger or different sets are used. The images can be viewed on p. 13 of the Appendix, where Gen 01 corresponds to Same-Identity Pair 1, Gen 02 corresponds to Same-Identity Pair 2, and so on.

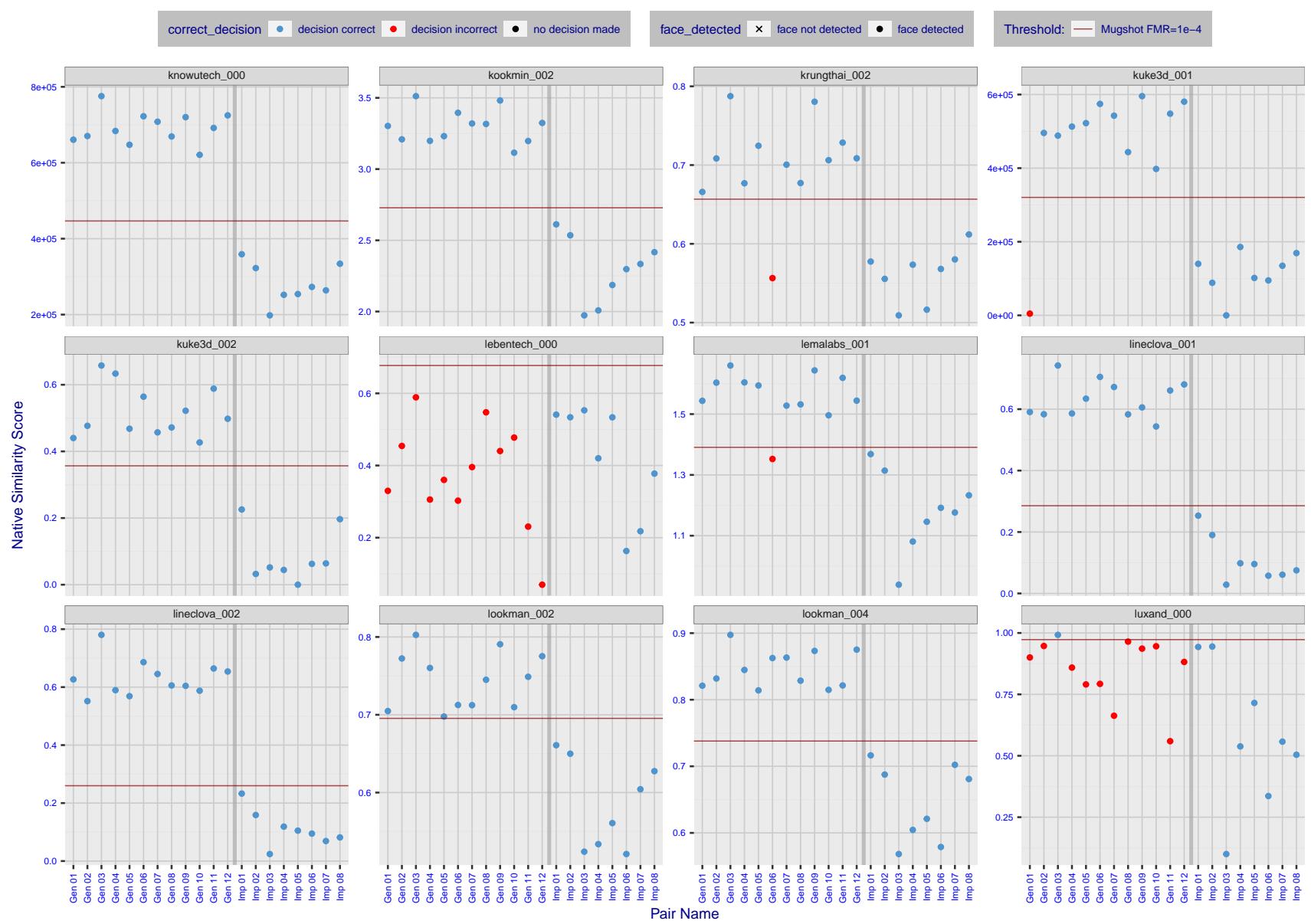


Figure 22: The figure shows algorithms' similarity scores for 12 genuine and 8 impostor image pairs used in a May 2018 paper by Phillips et al. ([1]). The threshold (red horizontal line) is a value calibrated to give $FMR = 0.0001$ on mugshot images. Points above the threshold correspond to pairs determined to be genuine, and points below the threshold correspond to pairs determined to be impostors. If the determined class (genuine or impostor) matches the real class, points will be blue; if not, red. An X represents face detection failure in either of the images in the pair. Note that the sample size ($n=20$) is small, and the figure may change substantially if larger or different sets are used. The images can be viewed on p. 13 of the Appendix, where Gen 01 corresponds to Same-Identity Pair 1, Gen 02 corresponds to Same-Identity Pair 2, and so on.

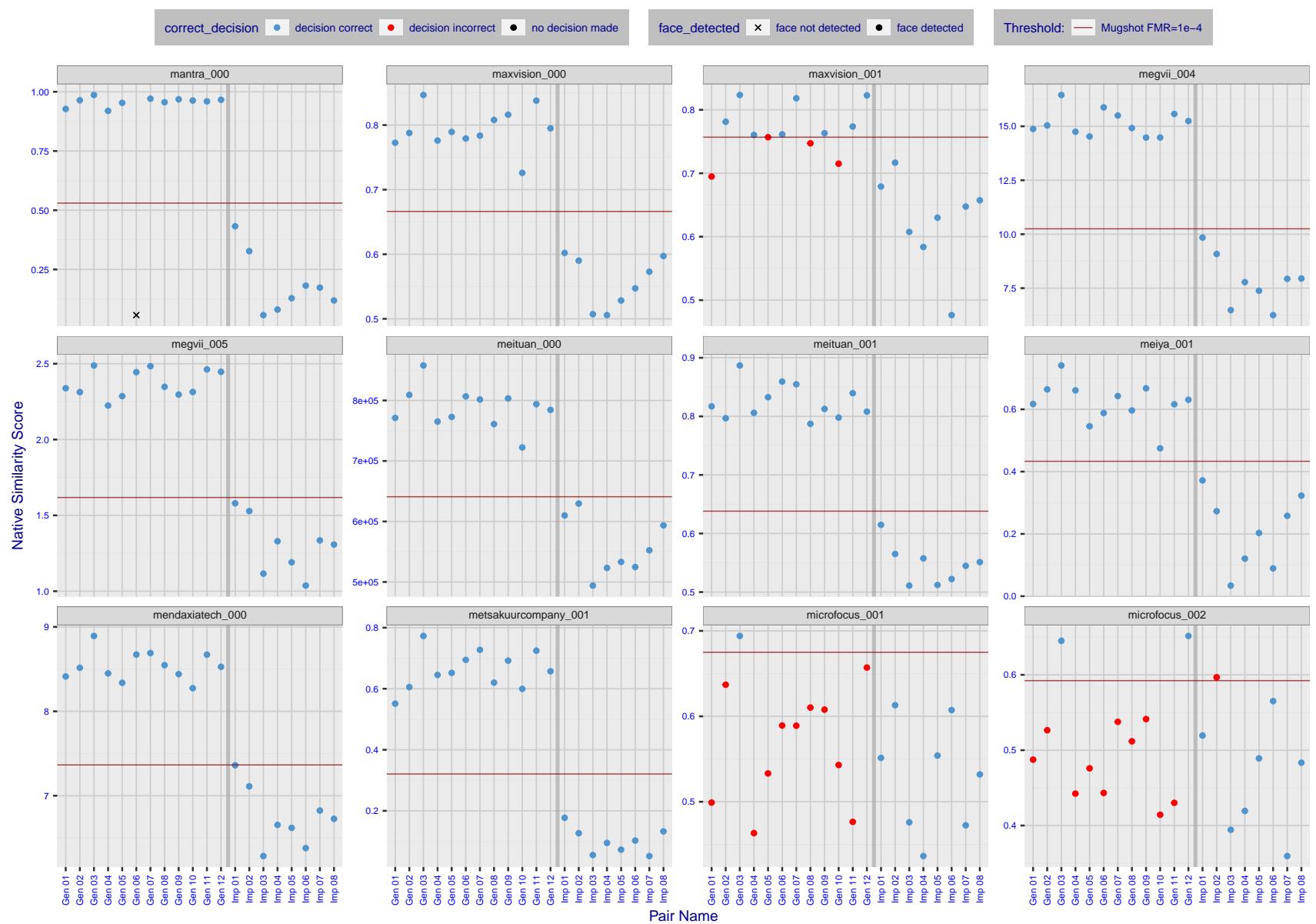


Figure 23: The figure shows algorithms' similarity scores for 12 genuine and 8 impostor image pairs used in a May 2018 paper by Phillips et al. ([1]). The threshold (red horizontal line) is a value calibrated to give $FMR = 0.0001$ on mugshot images. Points above the threshold correspond to pairs determined to be genuine, and points below the threshold correspond to pairs determined to be impostors. If the determined class (genuine or impostor) matches the real class, points will be blue; if not, red. An X represents face detection failure in either of the images in the pair. Note that the sample size ($n=20$) is small, and the figure may change substantially if larger or different sets are used. The images can be viewed on p. 13 of the Appendix, where Gen 01 corresponds to Same-Identity Pair 1, Gen 02 corresponds to Same-Identity Pair 2, and so on.

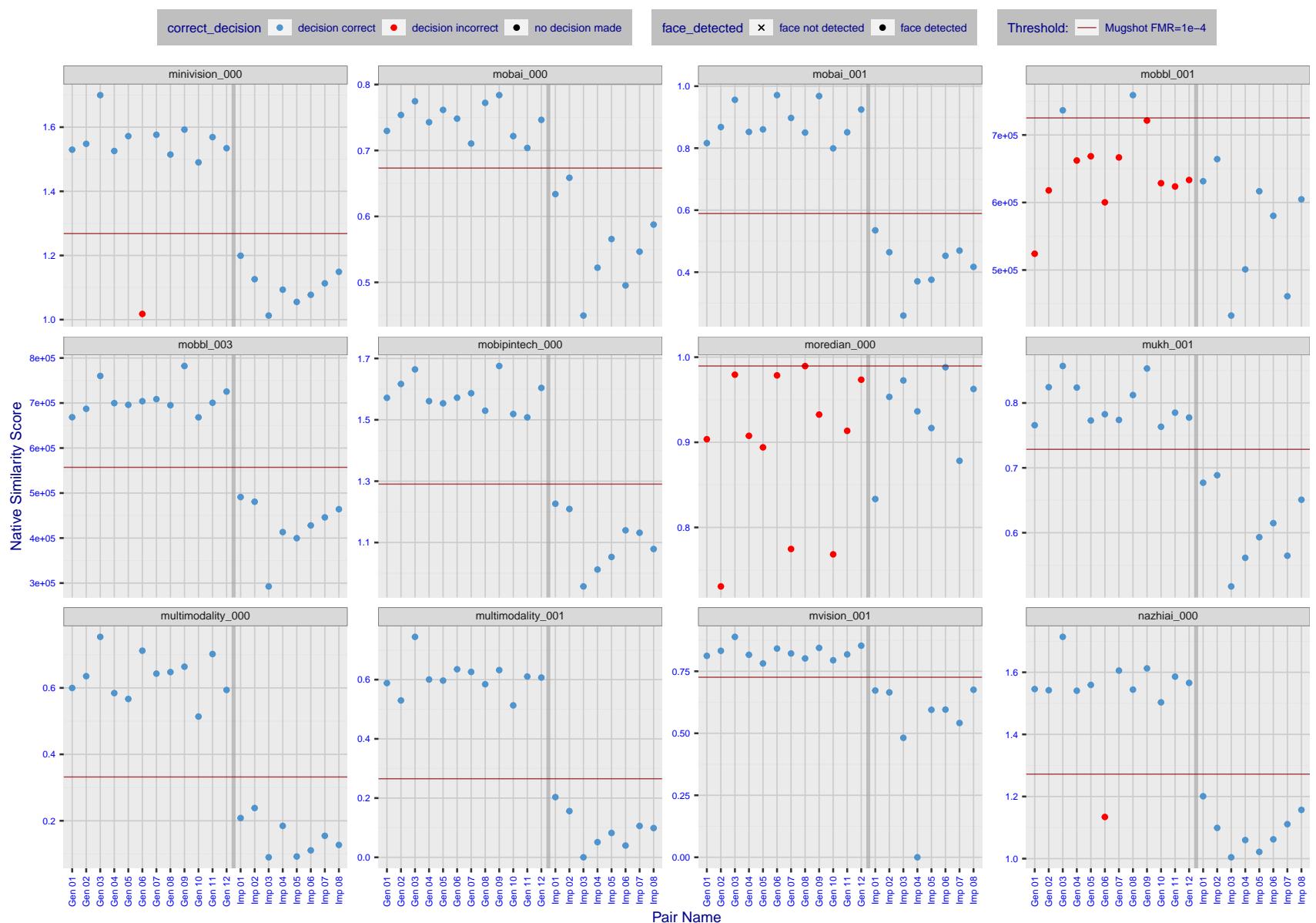


Figure 24: The figure shows algorithms' similarity scores for 12 genuine and 8 impostor image pairs used in a May 2018 paper by Phillips et al. ([1]). The threshold (red horizontal line) is a value calibrated to give $FMR = 0.0001$ on mugshot images. Points above the threshold correspond to pairs determined to be genuine, and points below the threshold correspond to pairs determined to be impostors. If the determined class (genuine or impostor) matches the real class, points will be blue; if not, red. An X represents face detection failure in either of the images in the pair. Note that the sample size ($n=20$) is small, and the figure may change substantially if larger or different sets are used. The images can be viewed on p. 13 of the Appendix, where Gen 01 corresponds to Same-Identity Pair 1, Gen 02 corresponds to Same-Identity Pair 2, and so on.

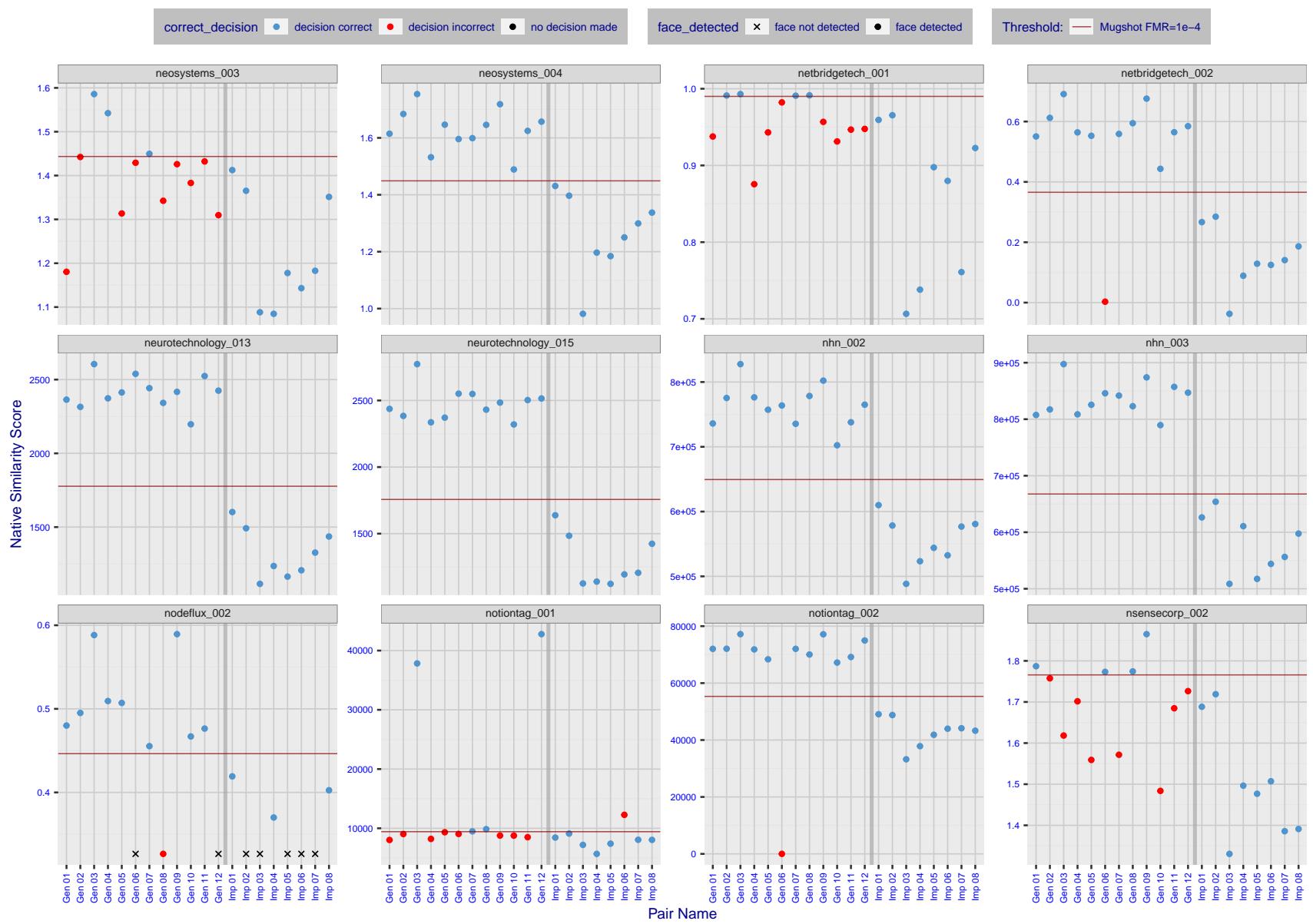


Figure 25: The figure shows algorithms' similarity scores for 12 genuine and 8 impostor image pairs used in a May 2018 paper by Phillips et al. ([1]). The threshold (red horizontal line) is a value calibrated to give $FMR = 0.0001$ on mugshot images. Points above the threshold correspond to pairs determined to be genuine, and points below the threshold correspond to pairs determined to be impostors. If the determined class (genuine or impostor) matches the real class, points will be blue; if not, red. An X represents face detection failure in either of the images in the pair. Note that the sample size ($n=20$) is small, and the figure may change substantially if larger or different sets are used. The images can be viewed on p. 13 of the Appendix, where Gen 01 corresponds to Same-Identity Pair 1, Gen 02 corresponds to Same-Identity Pair 2, and so on.

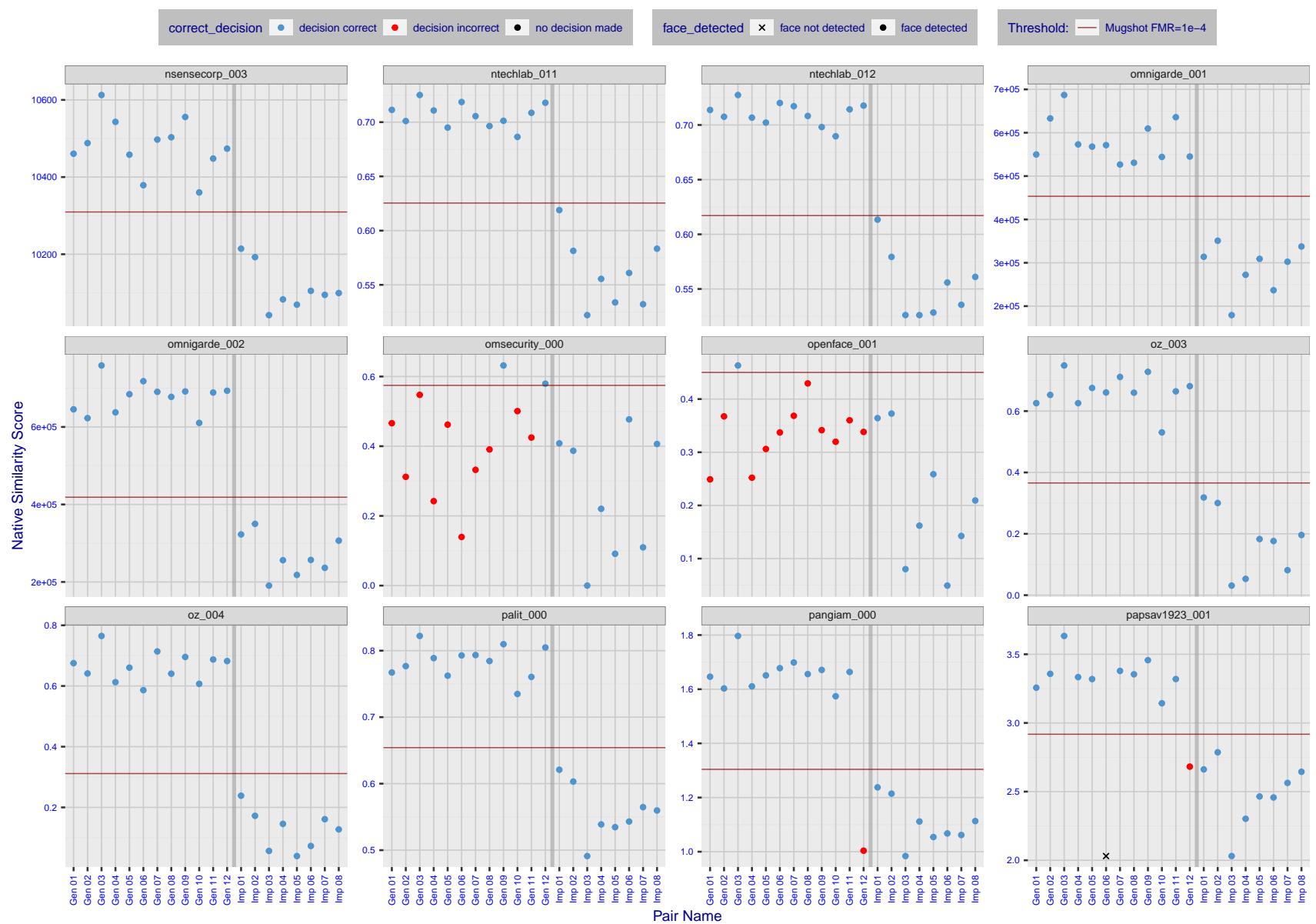


Figure 26: The figure shows algorithms' similarity scores for 12 genuine and 8 impostor image pairs used in a May 2018 paper by Phillips et al. ([1]). The threshold (red horizontal line) is a value calibrated to give $FMR = 0.0001$ on mugshot images. Points above the threshold correspond to pairs determined to be genuine, and points below the threshold correspond to pairs determined to be impostors. If the determined class (genuine or impostor) matches the real class, points will be blue; if not, red. An X represents face detection failure in either of the images in the pair. Note that the sample size ($n=20$) is small, and the figure may change substantially if larger or different sets are used. The images can be viewed on p. 13 of the Appendix, where Gen 01 corresponds to Same-Identity Pair 1, Gen 02 corresponds to Same-Identity Pair 2, and so on.

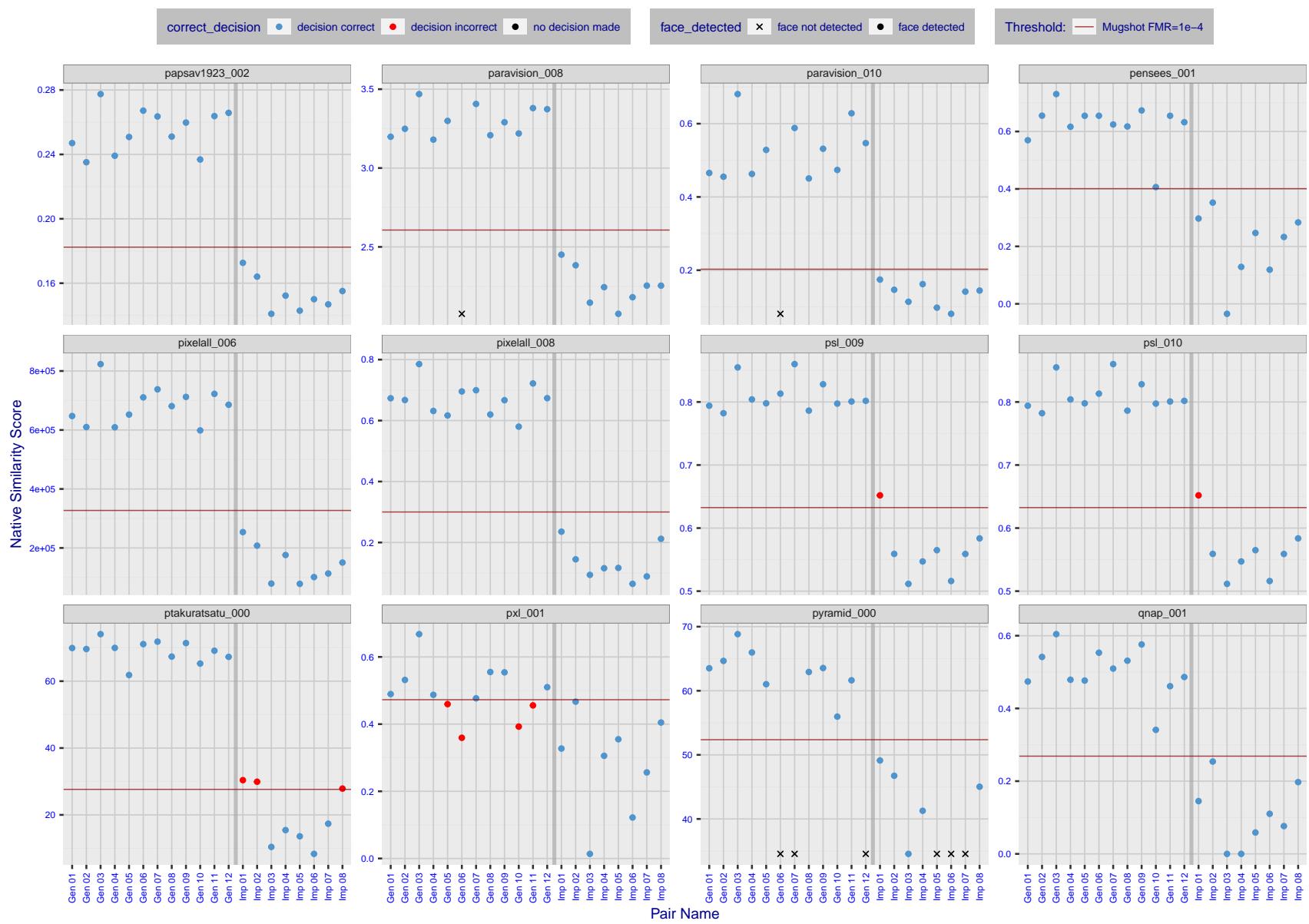


Figure 27: The figure shows algorithms' similarity scores for 12 genuine and 8 impostor image pairs used in a May 2018 paper by Phillips et al. ([1]). The threshold (red horizontal line) is a value calibrated to give $FMR = 0.0001$ on mugshot images. Points above the threshold correspond to pairs determined to be genuine, and points below the threshold correspond to pairs determined to be impostors. If the determined class (genuine or impostor) matches the real class, points will be blue; if not, red. An X represents face detection failure in either of the images in the pair. Note that the sample size ($n=20$) is small, and the figure may change substantially if larger or different sets are used. The images can be viewed on p. 13 of the Appendix, where Gen 01 corresponds to Same-Identity Pair 1, Gen 02 corresponds to Same-Identity Pair 2, and so on.

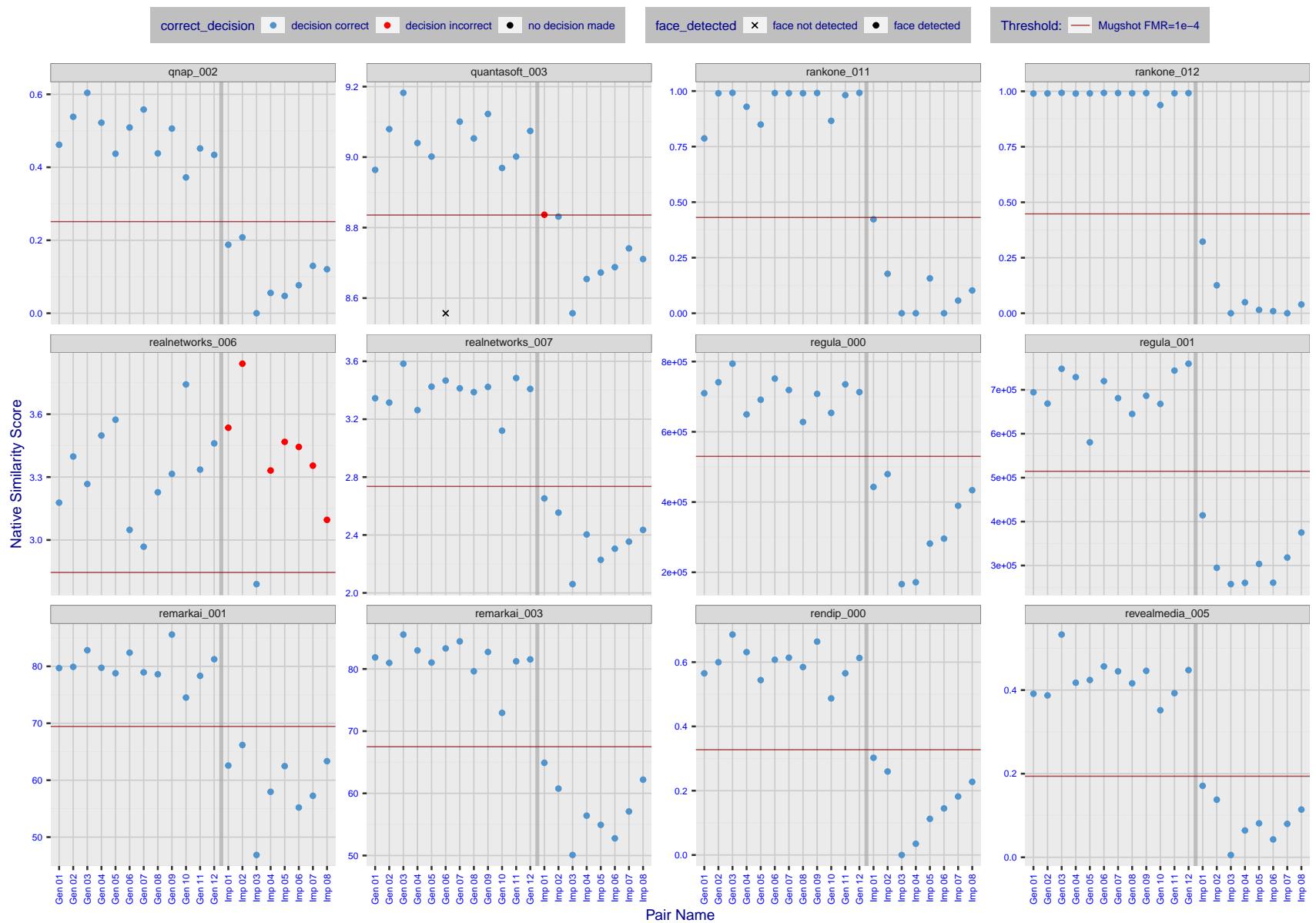


Figure 28: The figure shows algorithms' similarity scores for 12 genuine and 8 impostor image pairs used in a May 2018 paper by Phillips et al. ([1]). The threshold (red horizontal line) is a value calibrated to give $FMR = 0.0001$ on mugshot images. Points above the threshold correspond to pairs determined to be genuine, and points below the threshold correspond to pairs determined to be impostors. If the determined class (genuine or impostor) matches the real class, points will be blue; if not, red. An X represents face detection failure in either of the images in the pair. Note that the sample size ($n=20$) is small, and the figure may change substantially if larger or different sets are used. The images can be viewed on p. 13 of the Appendix, where Gen 01 corresponds to Same-Identity Pair 1, Gen 02 corresponds to Same-Identity Pair 2, and so on.

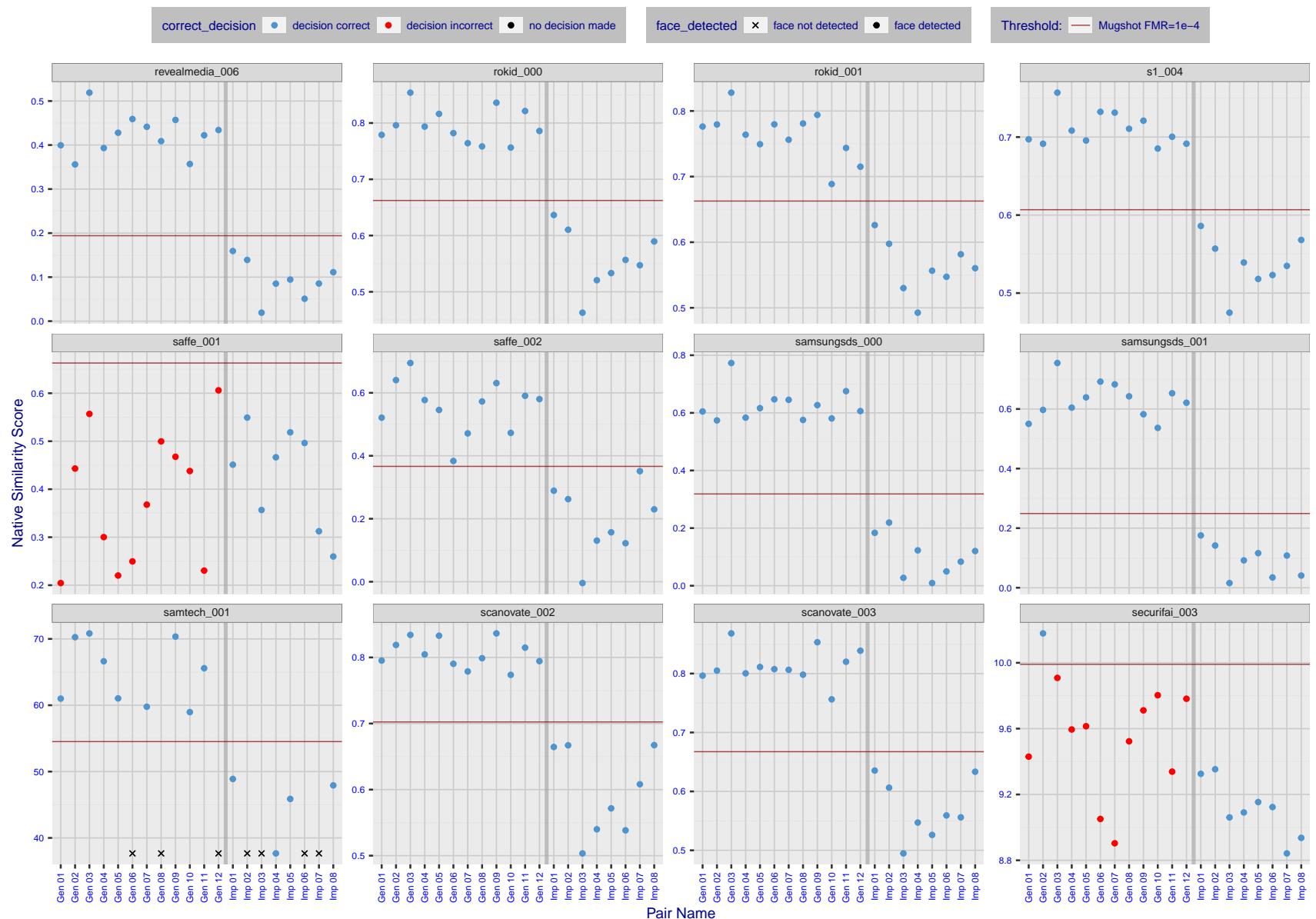


Figure 29: The figure shows algorithms' similarity scores for 12 genuine and 8 impostor image pairs used in a May 2018 paper by Phillips et al. ([1]). The threshold (red horizontal line) is a value calibrated to give $FMR = 0.0001$ on mugshot images. Points above the threshold correspond to pairs determined to be genuine, and points below the threshold correspond to pairs determined to be impostors. If the determined class (genuine or impostor) matches the real class, points will be blue; if not, red. An X represents face detection failure in either of the images in the pair. Note that the sample size ($n=20$) is small, and the figure may change substantially if larger or different sets are used. The images can be viewed on p. 13 of the Appendix, where Gen 01 corresponds to Same-Identity Pair 1, Gen 02 corresponds to Same-Identity Pair 2, and so on.

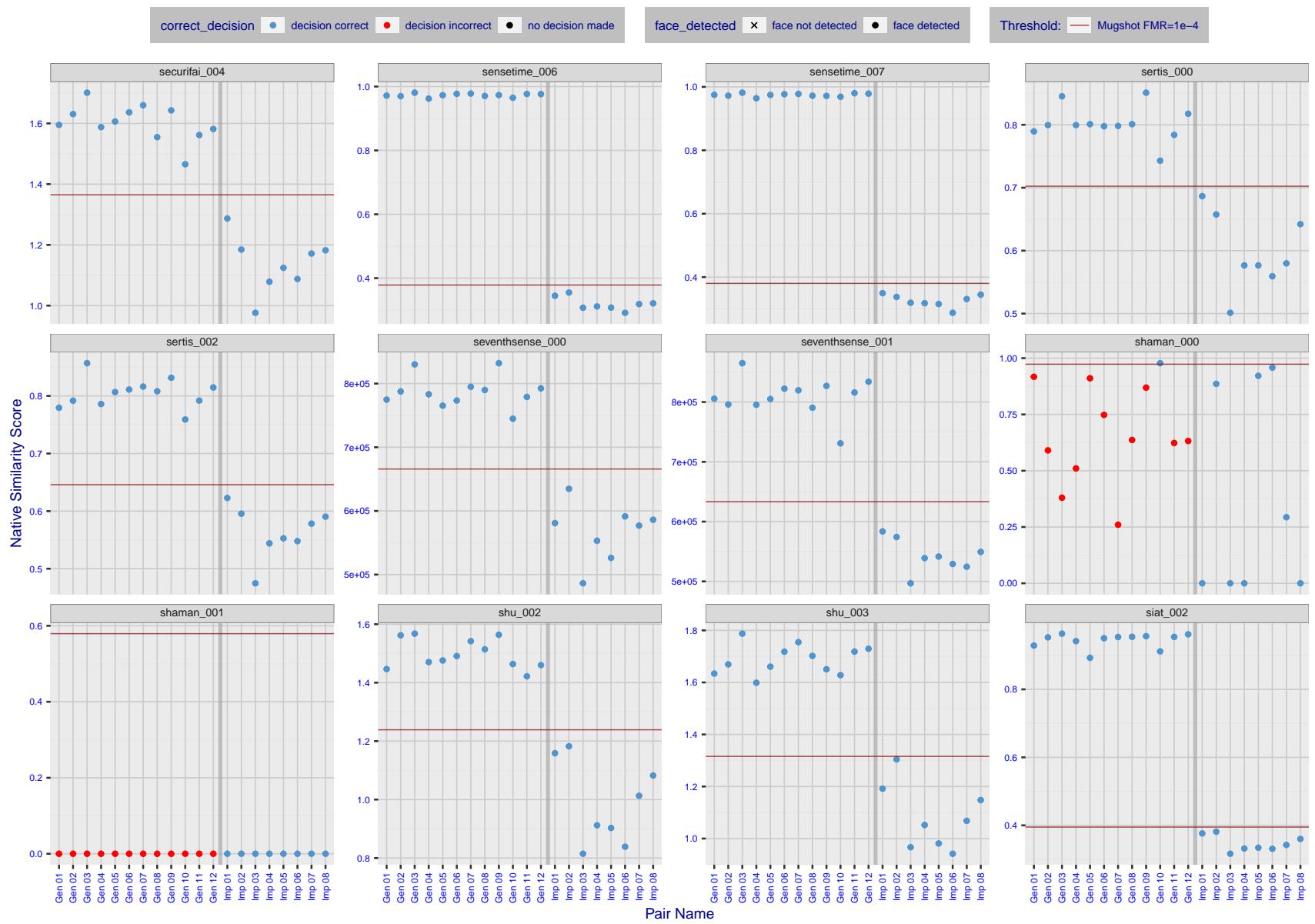


Figure 30: The figure shows algorithms' similarity scores for 12 genuine and 8 impostor image pairs used in a May 2018 paper by Phillips et al. ([1]). The threshold (red horizontal line) is a value calibrated to give $FMR = 0.0001$ on mugshot images. Points above the threshold correspond to pairs determined to be genuine, and points below the threshold correspond to pairs determined to be impostors. If the determined class (genuine or impostor) matches the real class, points will be blue; if not, red. An X represents face detection failure in either of the images in the pair. Note that the sample size ($n=20$) is small, and the figure may change substantially if larger or different sets are used. The images can be viewed on p. 13 of the Appendix, where Gen 01 corresponds to Same-Identity Pair 1, Gen 02 corresponds to Same-Identity Pair 2, and so on.

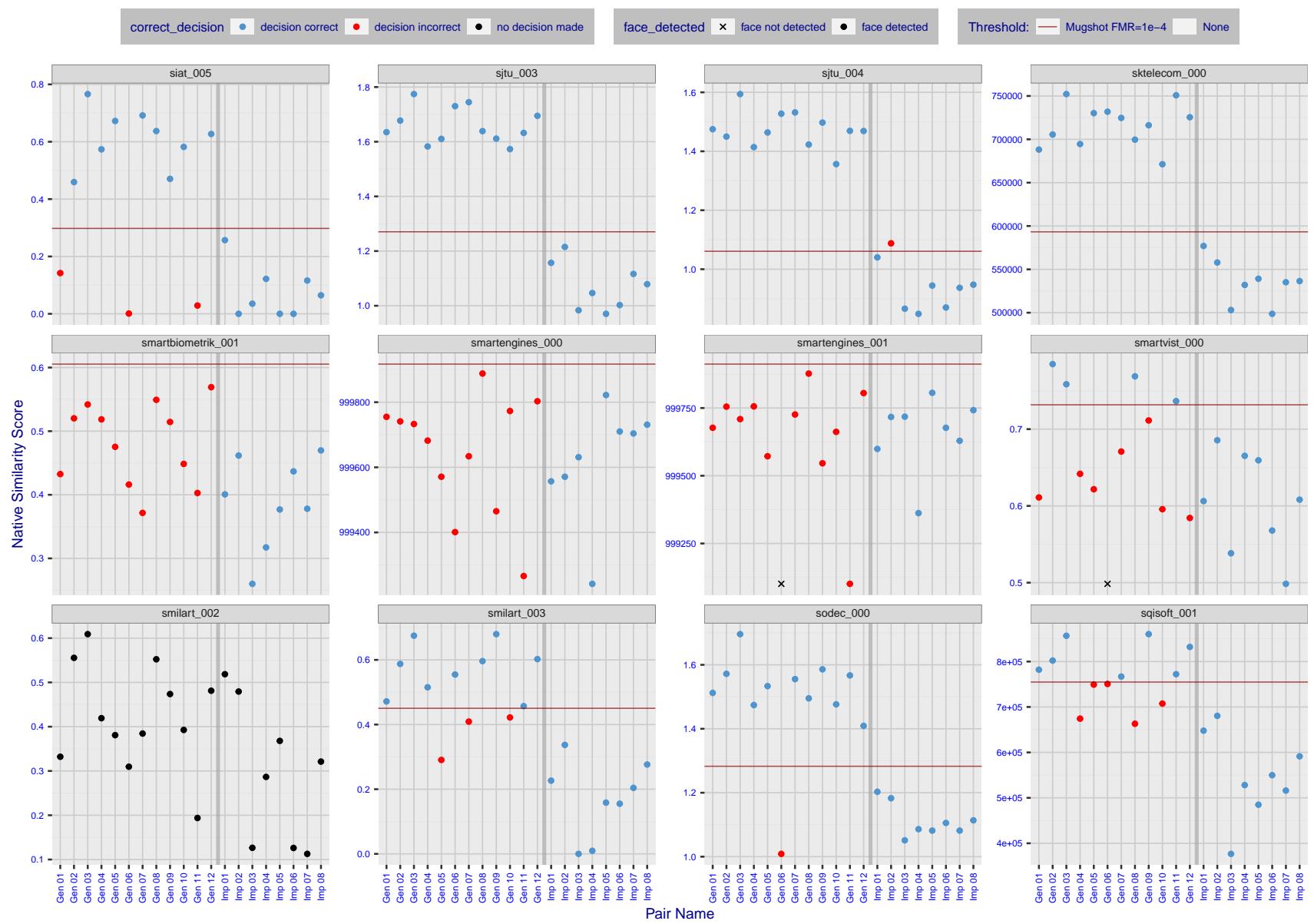


Figure 31: The figure shows algorithms' similarity scores for 12 genuine and 8 impostor image pairs used in a May 2018 paper by Phillips et al. ([1]). The threshold (red horizontal line) is a value calibrated to give $FMR = 0.0001$ on mugshot images. Points above the threshold correspond to pairs determined to be genuine, and points below the threshold correspond to pairs determined to be impostors. If the determined class (genuine or impostor) matches the real class, points will be blue; if not, red. An X represents face detection failure in either of the images in the pair. Note that the sample size ($n=20$) is small, and the figure may change substantially if larger or different sets are used. The images can be viewed on p. 13 of the Appendix, where Gen 01 corresponds to Same-Identity Pair 1, Gen 02 corresponds to Same-Identity Pair 2, and so on.

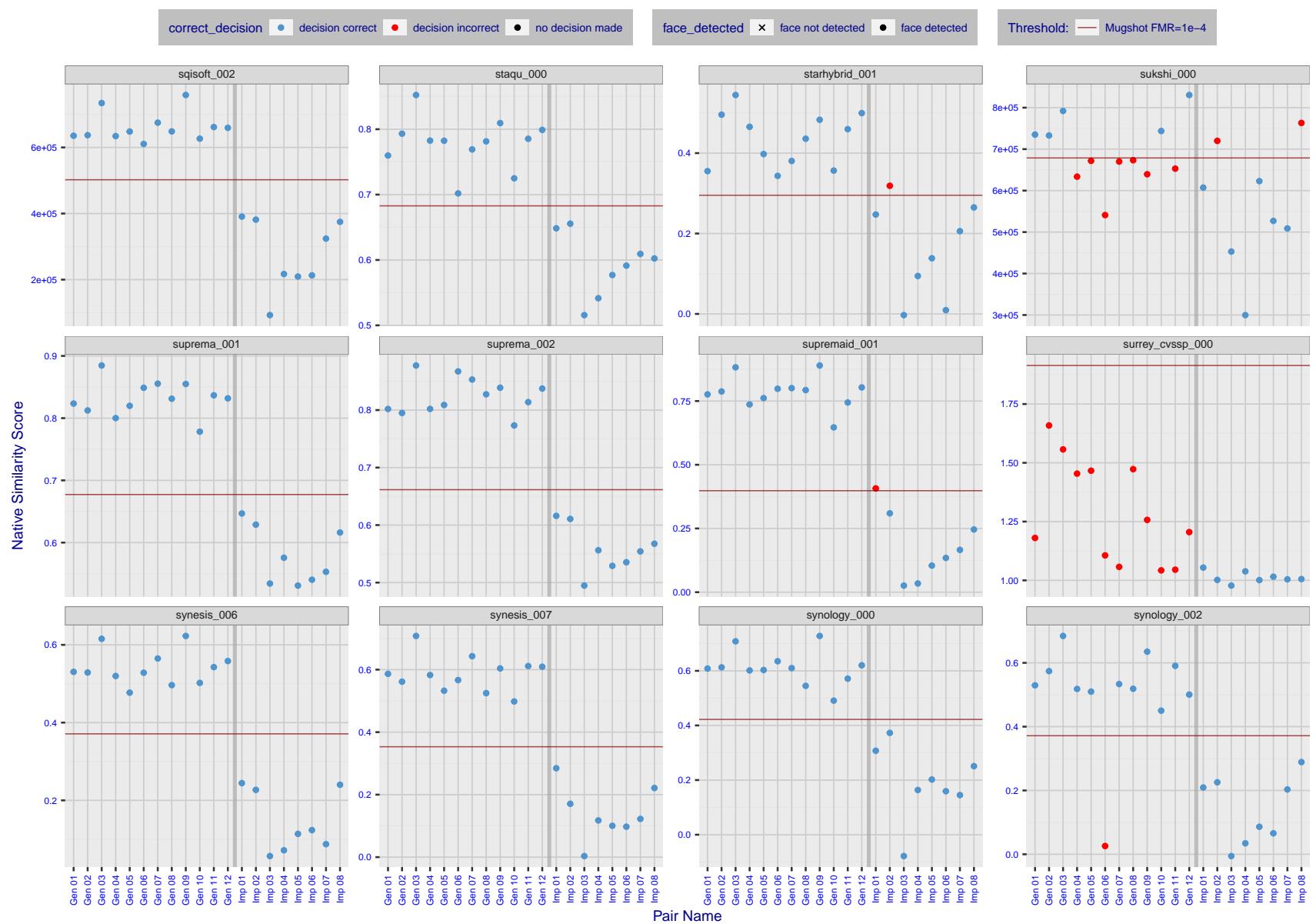


Figure 32: The figure shows algorithms' similarity scores for 12 genuine and 8 impostor image pairs used in a May 2018 paper by Phillips et al. ([1]). The threshold (red horizontal line) is a value calibrated to give $FMR = 0.0001$ on mugshot images. Points above the threshold correspond to pairs determined to be genuine, and points below the threshold correspond to pairs determined to be impostors. If the determined class (genuine or impostor) matches the real class, points will be blue; if not, red. An X represents face detection failure in either of the images in the pair. Note that the sample size ($n=20$) is small, and the figure may change substantially if larger or different sets are used. The images can be viewed on p. 13 of the Appendix, where Gen 01 corresponds to Same-Identity Pair 1, Gen 02 corresponds to Same-Identity Pair 2, and so on.

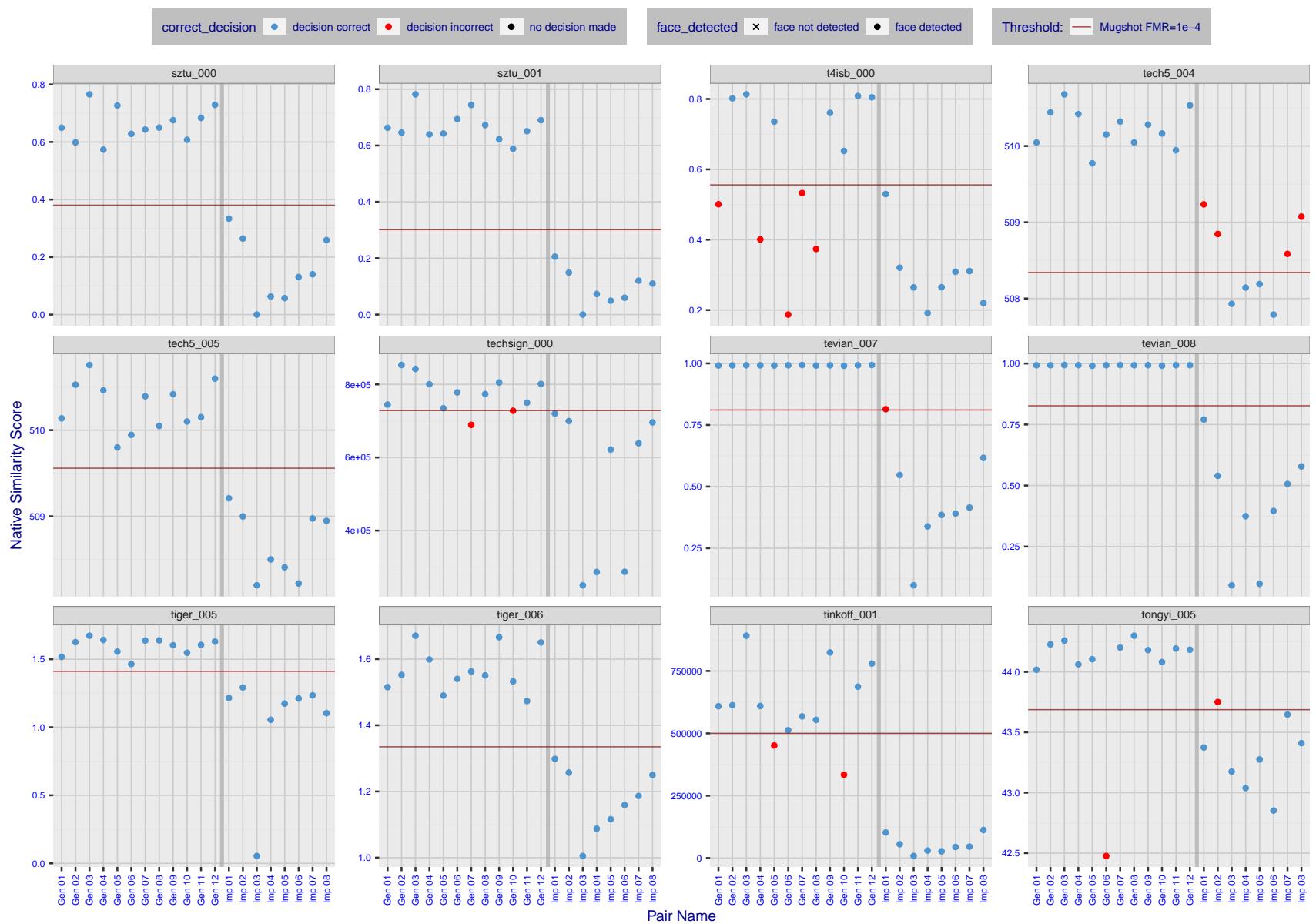


Figure 33: The figure shows algorithms' similarity scores for 12 genuine and 8 impostor image pairs used in a May 2018 paper by Phillips et al. ([1]). The threshold (red horizontal line) is a value calibrated to give $FMR = 0.0001$ on mugshot images. Points above the threshold correspond to pairs determined to be genuine, and points below the threshold correspond to pairs determined to be impostors. If the determined class (genuine or impostor) matches the real class, points will be blue; if not, red. An X represents face detection failure in either of the images in the pair. Note that the sample size ($n=20$) is small, and the figure may change substantially if larger or different sets are used. The images can be viewed on p. 13 of the Appendix, where Gen 01 corresponds to Same-Identity Pair 1, Gen 02 corresponds to Same-Identity Pair 2, and so on.

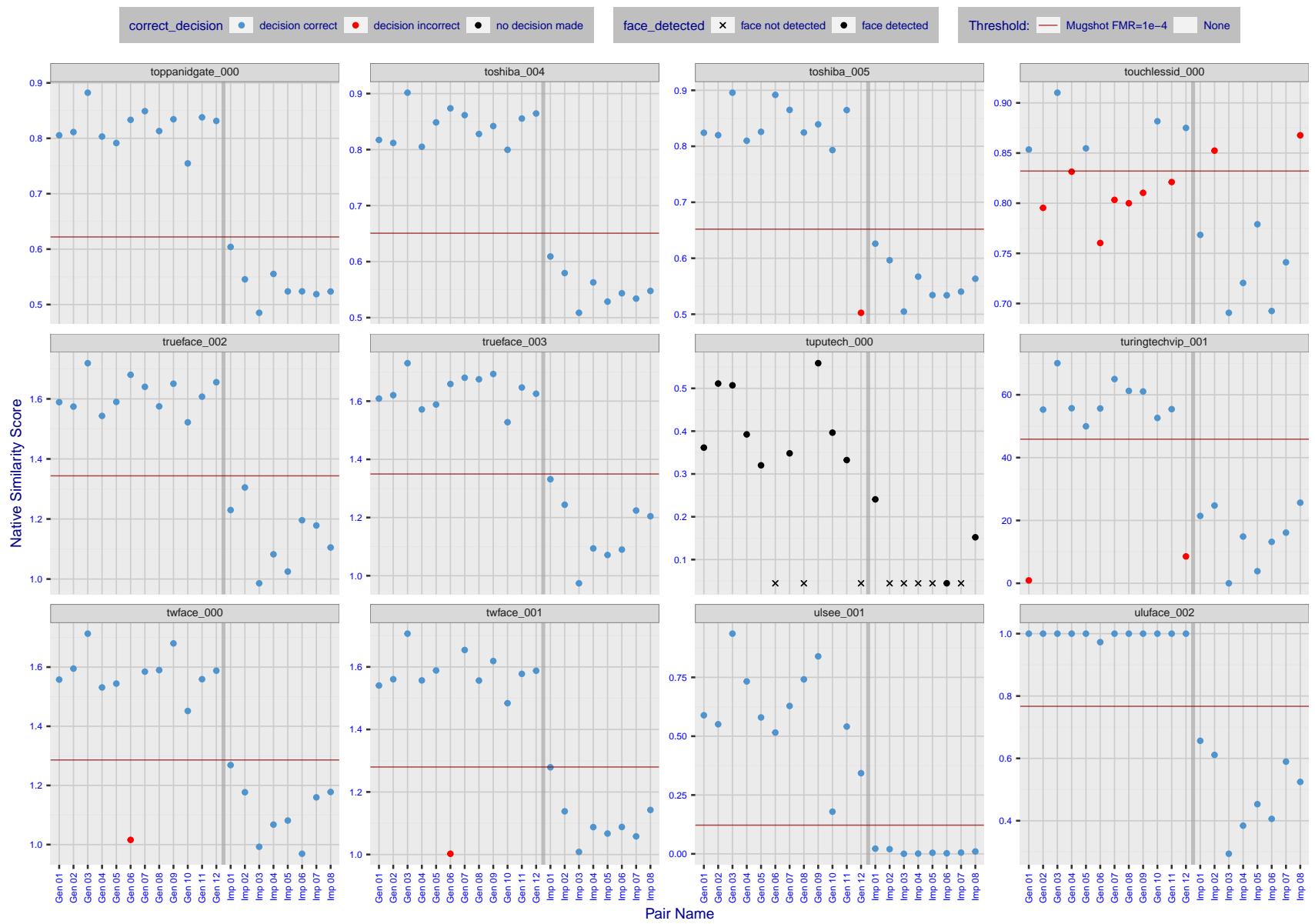


Figure 34: The figure shows algorithms' similarity scores for 12 genuine and 8 impostor image pairs used in a May 2018 paper by Phillips et al. ([1]). The threshold (red horizontal line) is a value calibrated to give $FMR = 0.0001$ on mugshot images. Points above the threshold correspond to pairs determined to be genuine, and points below the threshold correspond to pairs determined to be impostors. If the determined class (genuine or impostor) matches the real class, points will be blue; if not, red. An X represents face detection failure in either of the images in the pair. Note that the sample size ($n=20$) is small, and the figure may change substantially if larger or different sets are used. The images can be viewed on p. 13 of the Appendix, where Gen 01 corresponds to Same-Identity Pair 1, Gen 02 corresponds to Same-Identity Pair 2, and so on.

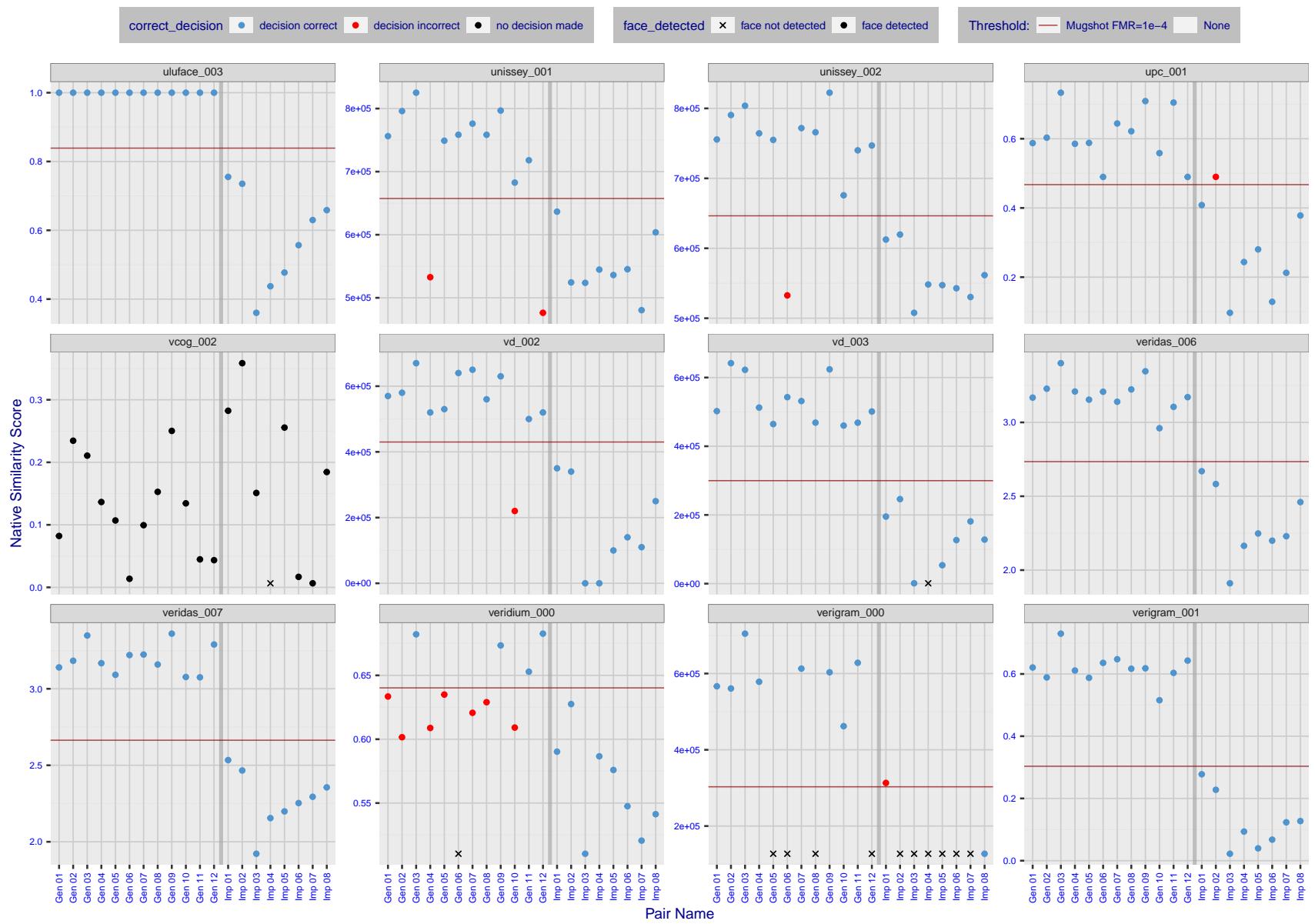


Figure 35: The figure shows algorithms' similarity scores for 12 genuine and 8 impostor image pairs used in a May 2018 paper by Phillips et al. ([1]). The threshold (red horizontal line) is a value calibrated to give $FMR = 0.0001$ on mugshot images. Points above the threshold correspond to pairs determined to be genuine, and points below the threshold correspond to pairs determined to be impostors. If the determined class (genuine or impostor) matches the real class, points will be blue; if not, red. An X represents face detection failure in either of the images in the pair. Note that the sample size ($n=20$) is small, and the figure may change substantially if larger or different sets are used. The images can be viewed on p. 13 of the Appendix, where Gen 01 corresponds to Same-Identity Pair 1, Gen 02 corresponds to Same-Identity Pair 2, and so on.

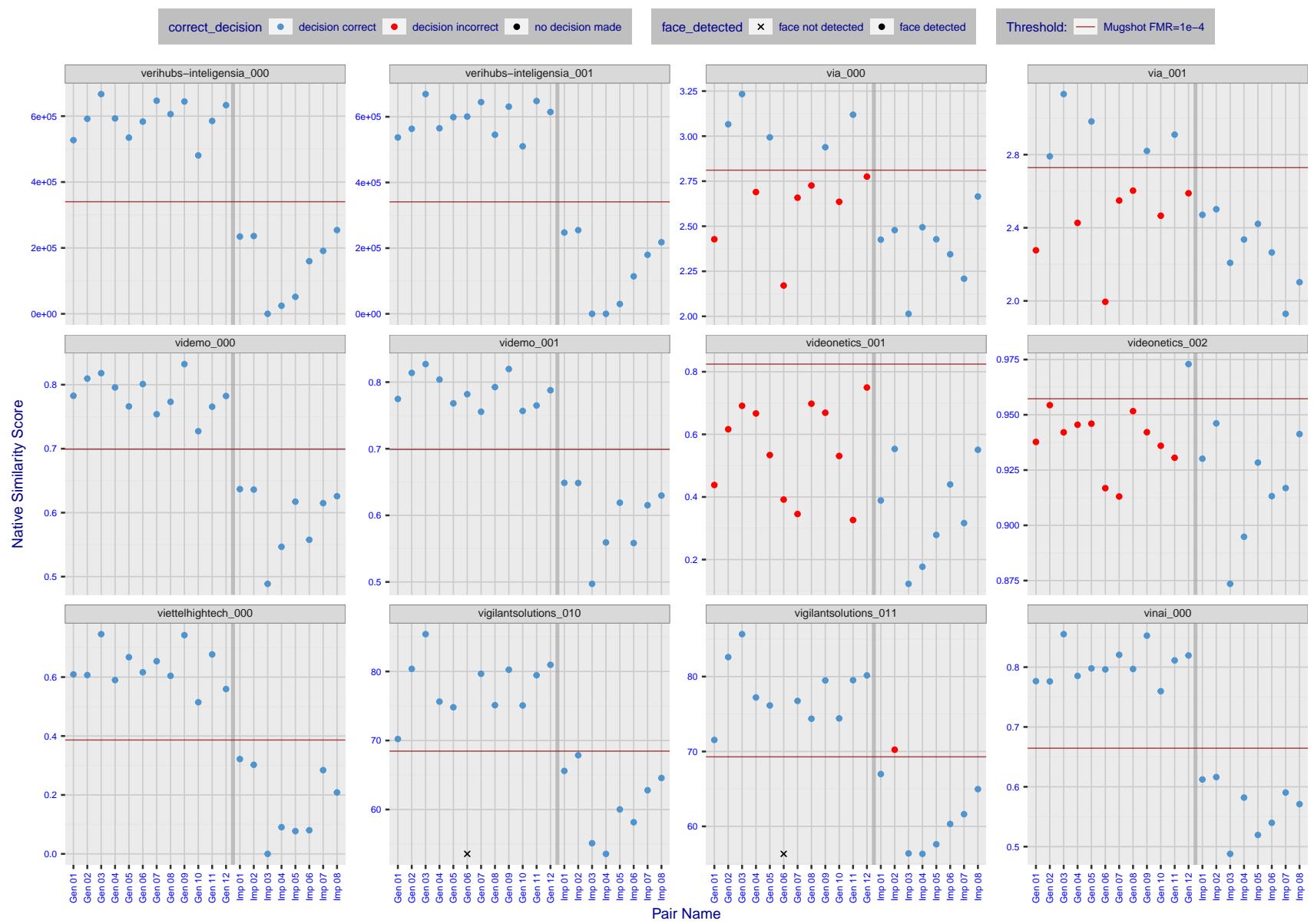


Figure 36: The figure shows algorithms' similarity scores for 12 genuine and 8 impostor image pairs used in a May 2018 paper by Phillips et al. ([1]). The threshold (red horizontal line) is a value calibrated to give $FMR = 0.0001$ on mugshot images. Points above the threshold correspond to pairs determined to be genuine, and points below the threshold correspond to pairs determined to be impostors. If the determined class (genuine or impostor) matches the real class, points will be blue; if not, red. An X represents face detection failure in either of the images in the pair. Note that the sample size ($n=20$) is small, and the figure may change substantially if larger or different sets are used. The images can be viewed on p. 13 of the Appendix, where Gen 01 corresponds to Same-Identity Pair 1, Gen 02 corresponds to Same-Identity Pair 2, and so on.

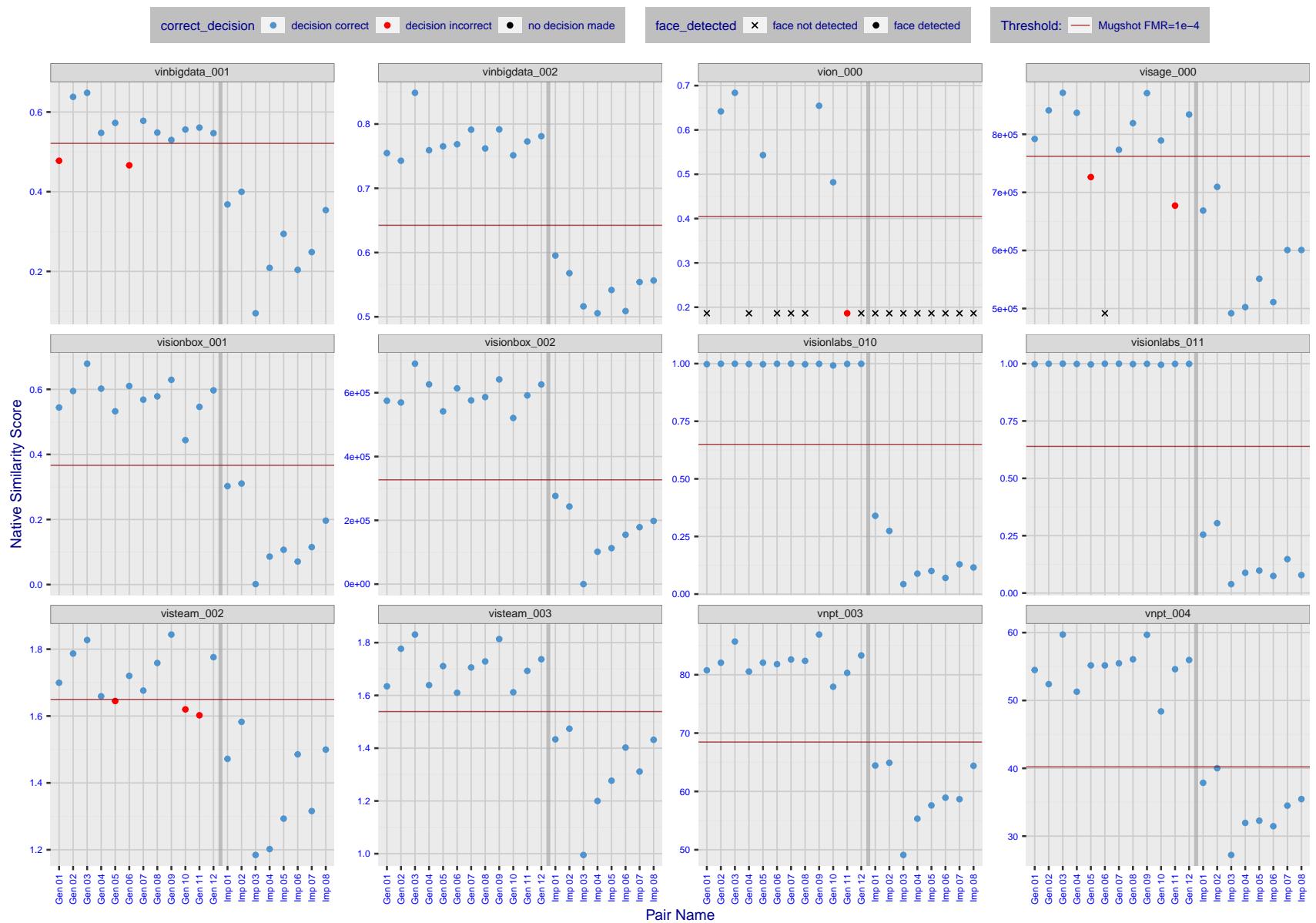


Figure 37: The figure shows algorithms' similarity scores for 12 genuine and 8 impostor image pairs used in a May 2018 paper by Phillips et al. ([1]). The threshold (red horizontal line) is a value calibrated to give $FMR = 0.0001$ on mugshot images. Points above the threshold correspond to pairs determined to be genuine, and points below the threshold correspond to pairs determined to be impostors. If the determined class (genuine or impostor) matches the real class, points will be blue; if not, red. An X represents face detection failure in either of the images in the pair. Note that the sample size ($n=20$) is small, and the figure may change substantially if larger or different sets are used. The images can be viewed on p. 13 of the Appendix, where Gen 01 corresponds to Same-Identity Pair 1, Gen 02 corresponds to Same-Identity Pair 2, and so on.

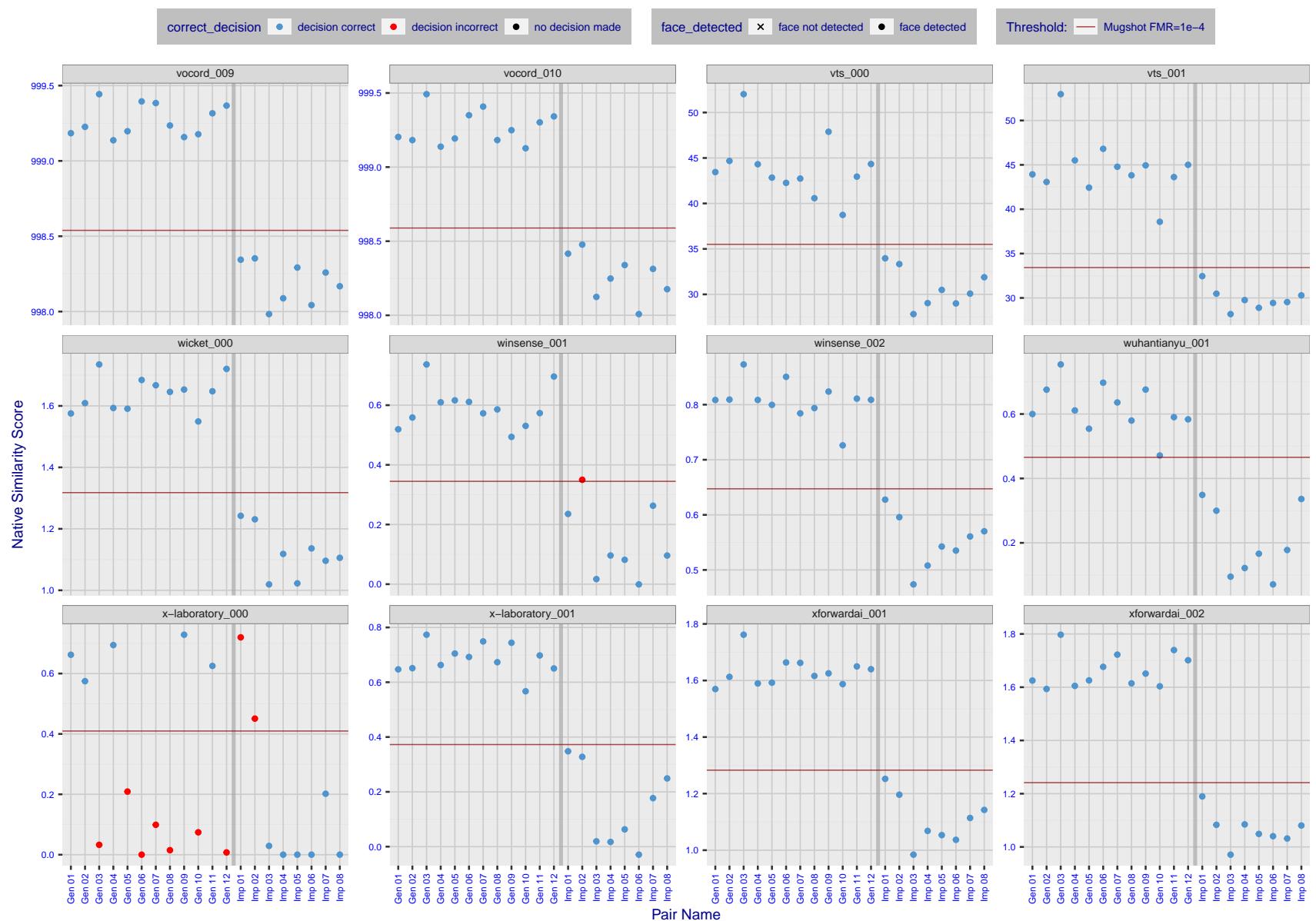


Figure 38: The figure shows algorithms' similarity scores for 12 genuine and 8 impostor image pairs used in a May 2018 paper by Phillips et al. ([1]). The threshold (red horizontal line) is a value calibrated to give $FMR = 0.0001$ on mugshot images. Points above the threshold correspond to pairs determined to be genuine, and points below the threshold correspond to pairs determined to be impostors. If the determined class (genuine or impostor) matches the real class, points will be blue; if not, red. An X represents face detection failure in either of the images in the pair. Note that the sample size ($n=20$) is small, and the figure may change substantially if larger or different sets are used. The images can be viewed on p. 13 of the Appendix, where Gen 01 corresponds to Same-Identity Pair 1, Gen 02 corresponds to Same-Identity Pair 2, and so on.

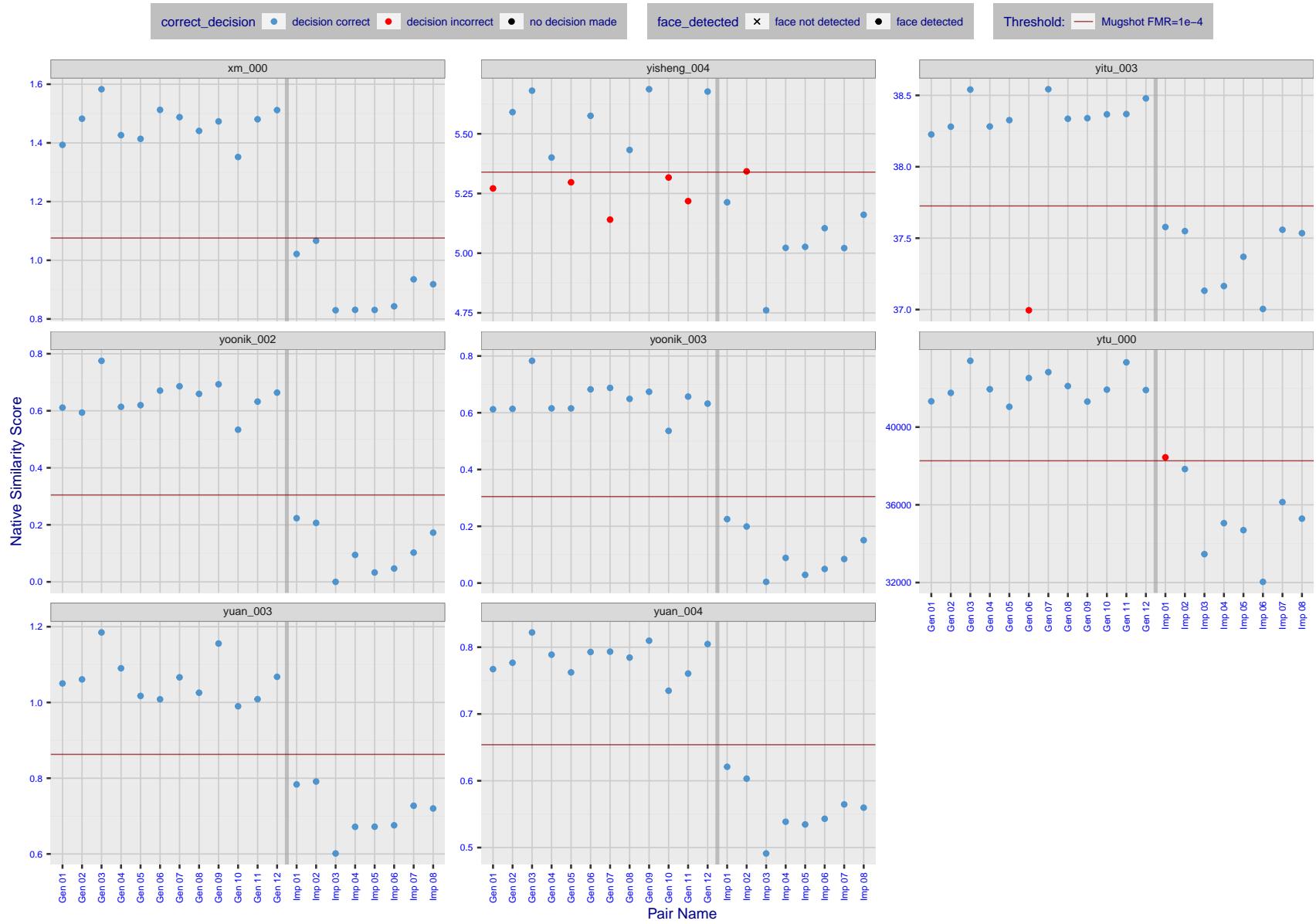


Figure 39: The figure shows algorithms' similarity scores for 12 genuine and 8 impostor image pairs used in a May 2018 paper by Phillips et al. ([1]). The threshold (red horizontal line) is a value calibrated to give $FMR = 0.0001$ on mugshot images. Points above the threshold correspond to pairs determined to be genuine, and points below the threshold correspond to pairs determined to be impostors. If the determined class (genuine or impostor) matches the real class, points will be blue; if not, red. An X represents face detection failure in either of the images in the pair. Note that the sample size ($n=20$) is small, and the figure may change substantially if larger or different sets are used. The images can be viewed on p. 13 of the Appendix, where Gen 01 corresponds to Same-Identity Pair 1, Gen 02 corresponds to Same-Identity Pair 2, and so on.

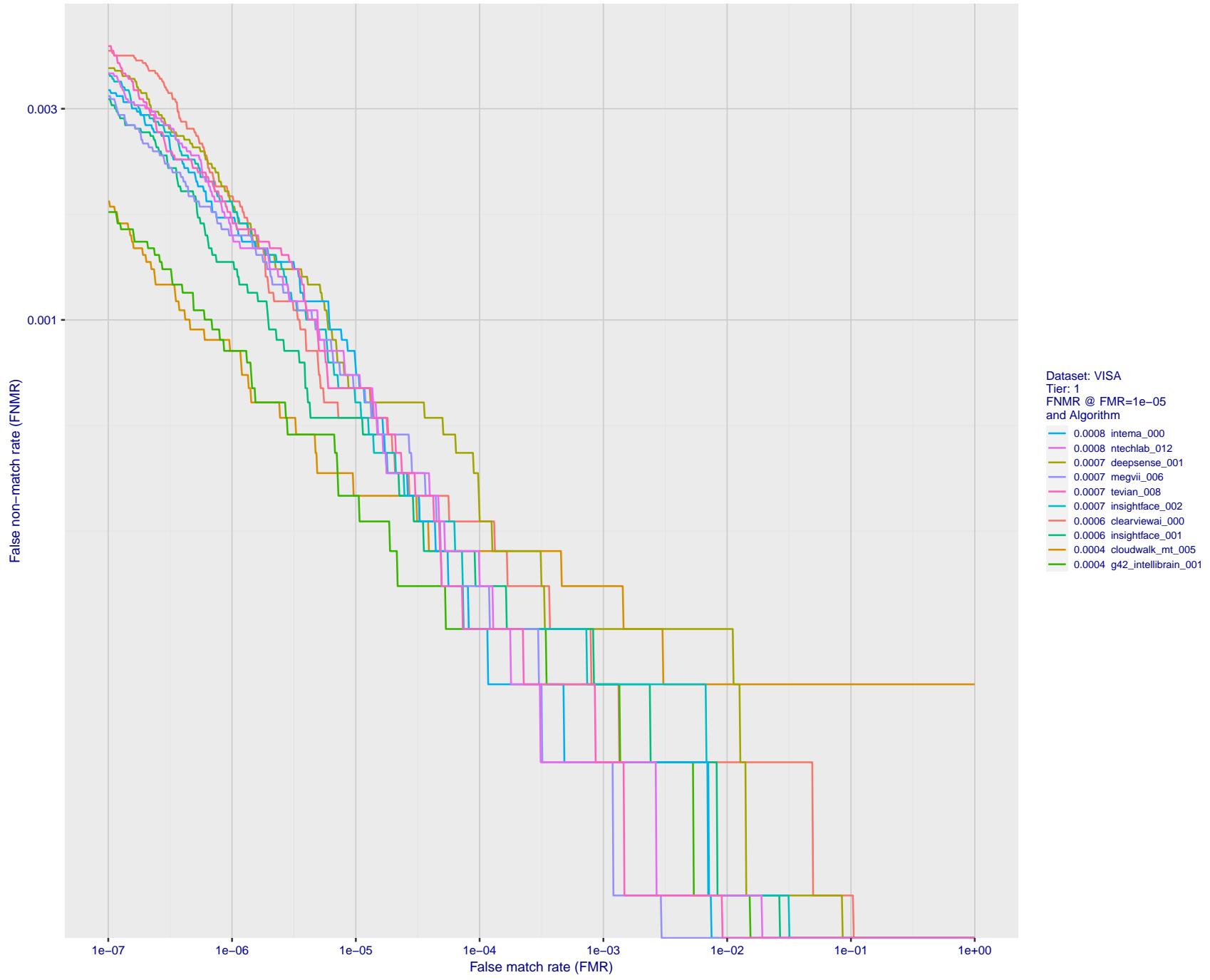


Figure 40: For the visa images, detection error tradeoff (DET) characteristics showing false non-match rate vs. false match rate plotted parametrically on threshold, T . The scales are logarithmic in order to show many decades of FMR.

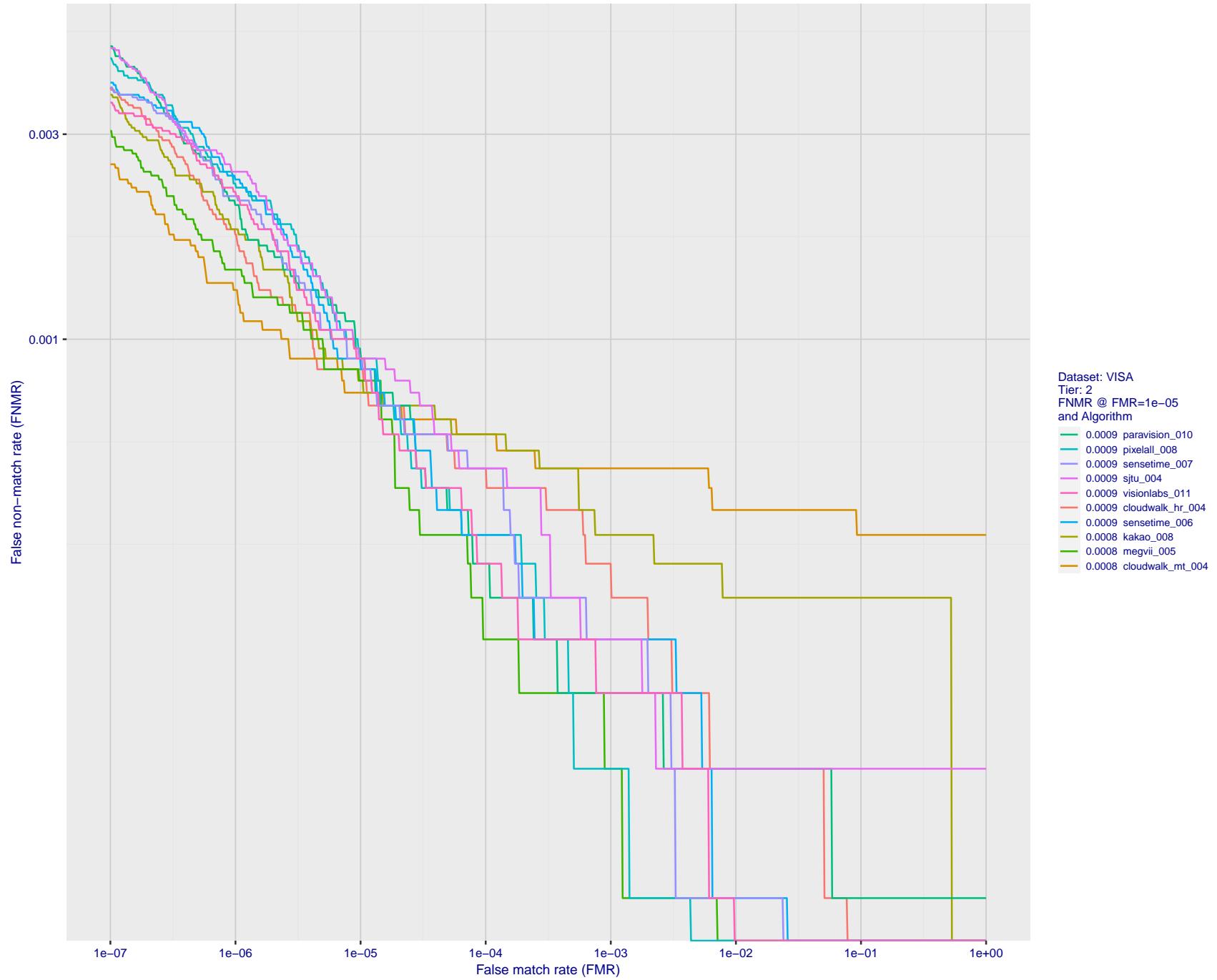


Figure 41: For the visa images, detection error tradeoff (DET) characteristics showing false non-match rate vs. false match rate plotted parametrically on threshold, T . The scales are logarithmic in order to show many decades of FMR.

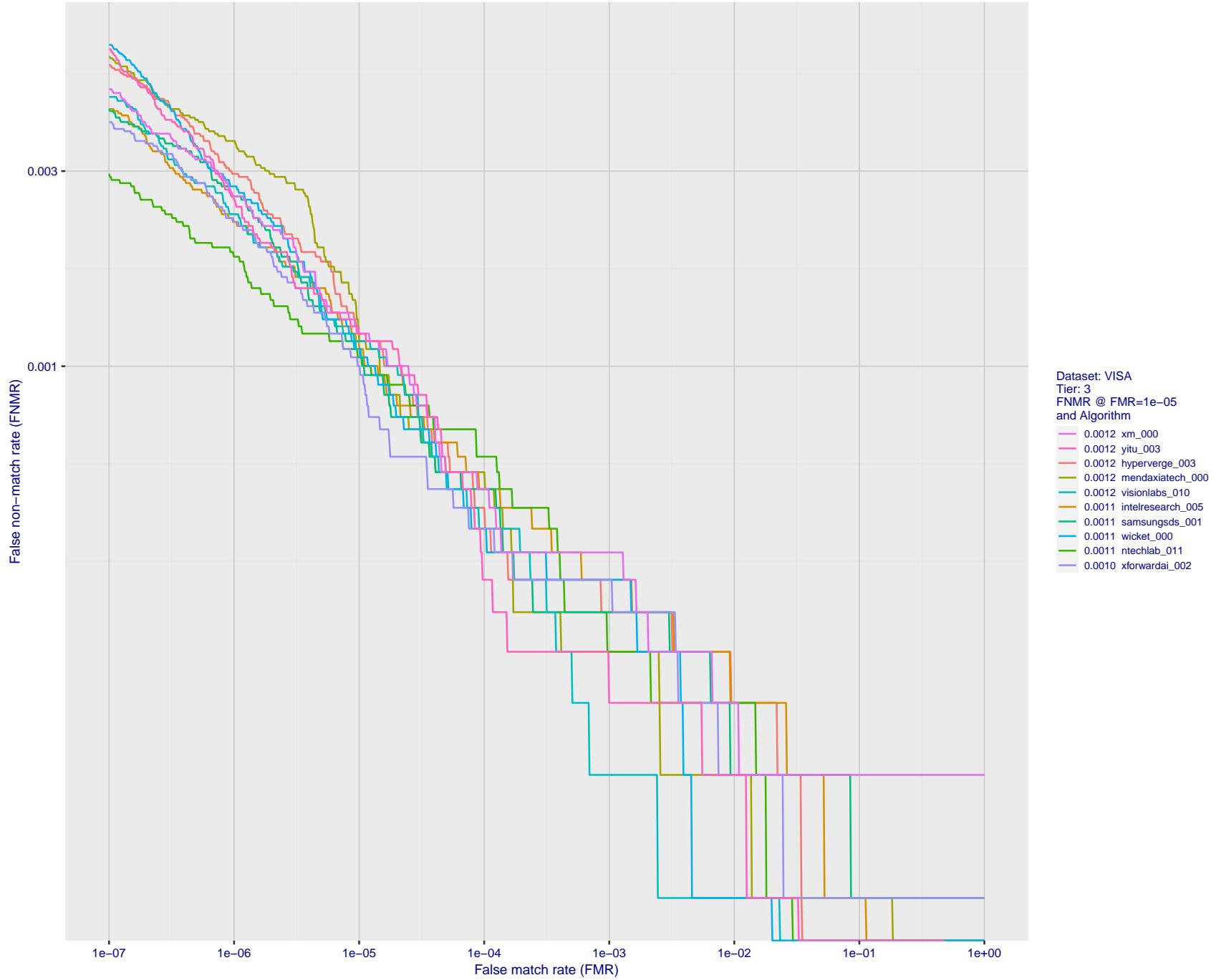


Figure 42: For the visa images, detection error tradeoff (DET) characteristics showing false non-match rate vs. false match rate plotted parametrically on threshold, T . The scales are logarithmic in order to show many decades of FMR.

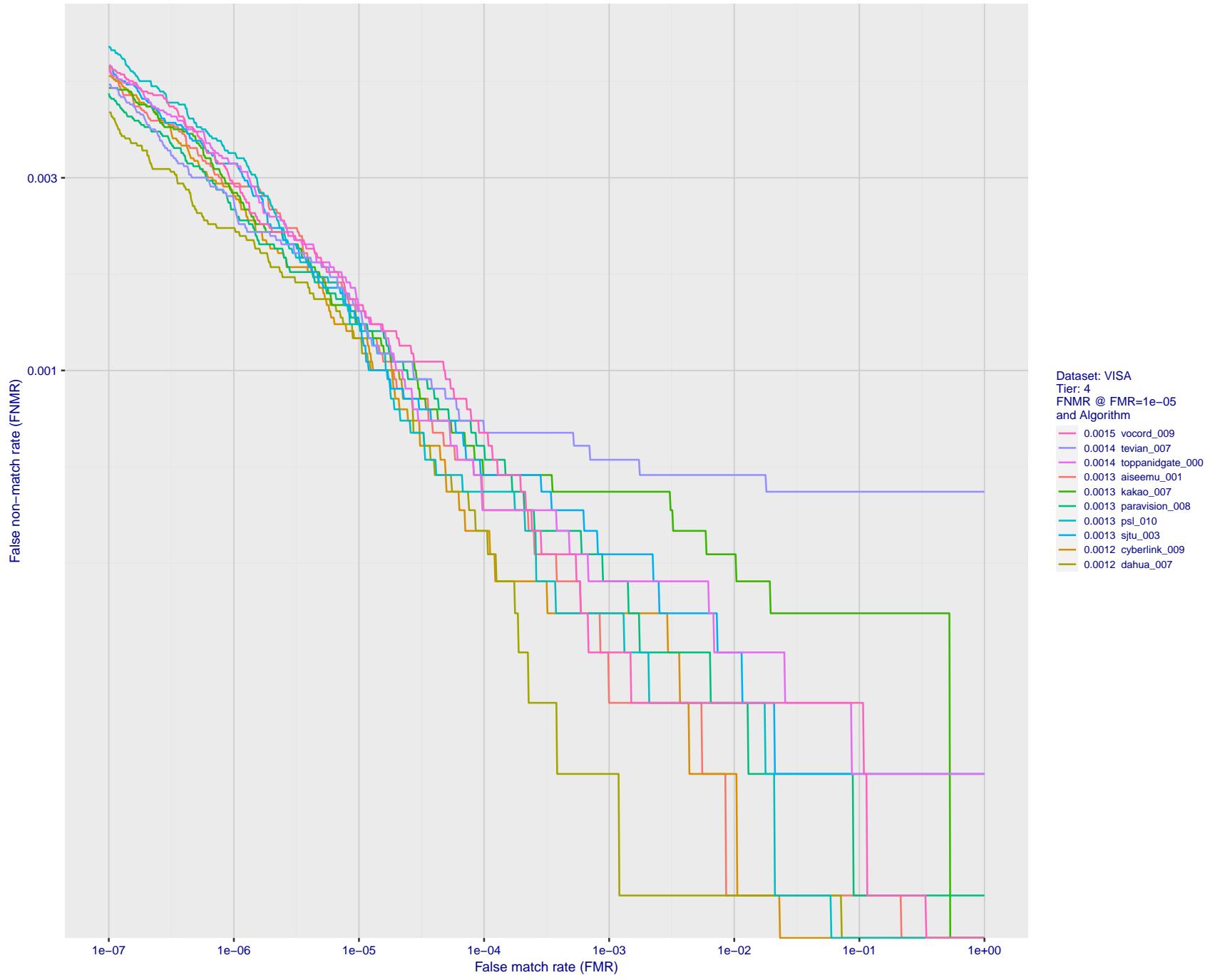


Figure 43: For the visa images, detection error tradeoff (DET) characteristics showing false non-match rate vs. false match rate plotted parametrically on threshold, T . The scales are logarithmic in order to show many decades of FMR.

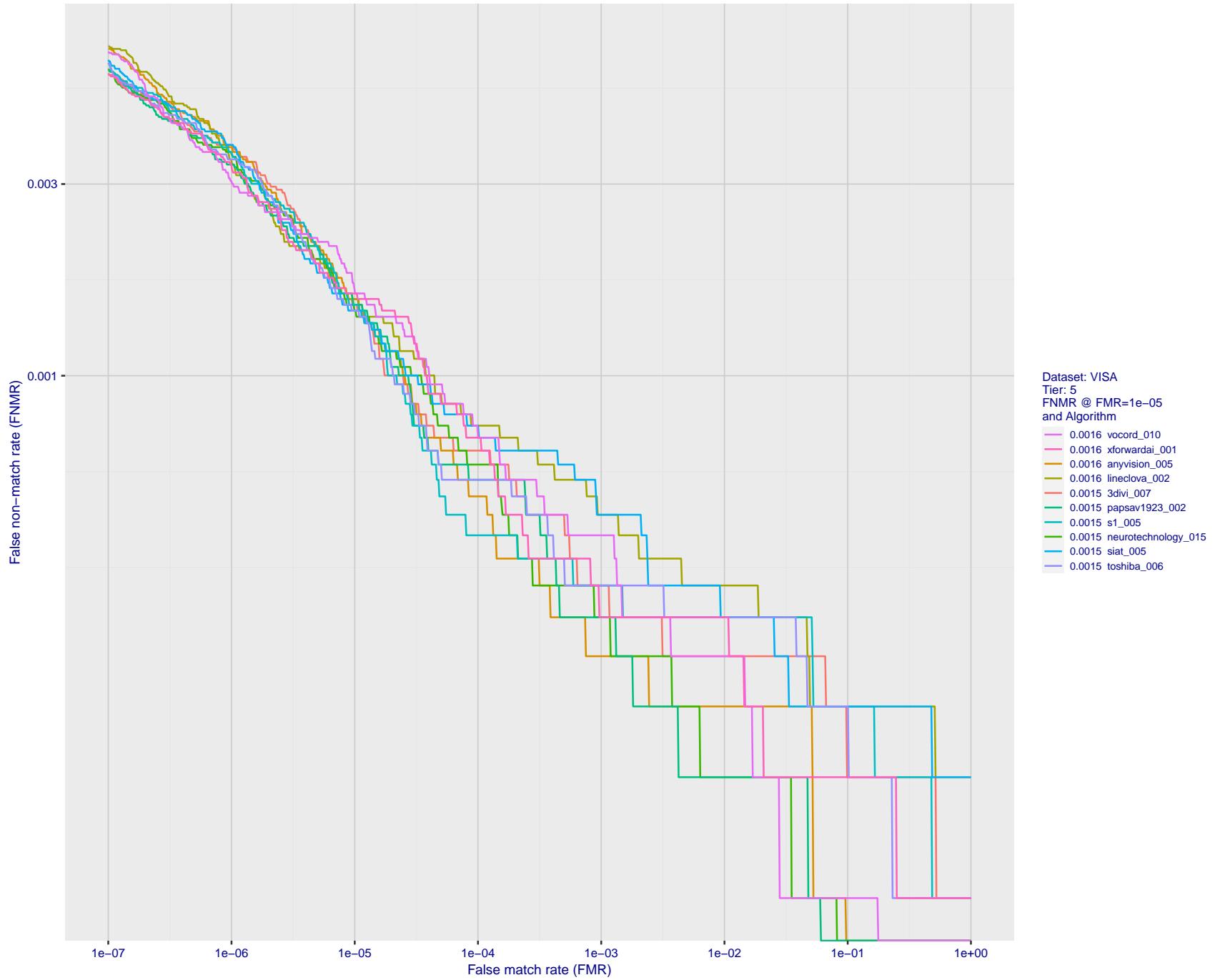


Figure 44: For the visa images, detection error tradeoff (DET) characteristics showing false non-match rate vs. false match rate plotted parametrically on threshold, T . The scales are logarithmic in order to show many decades of FMR.

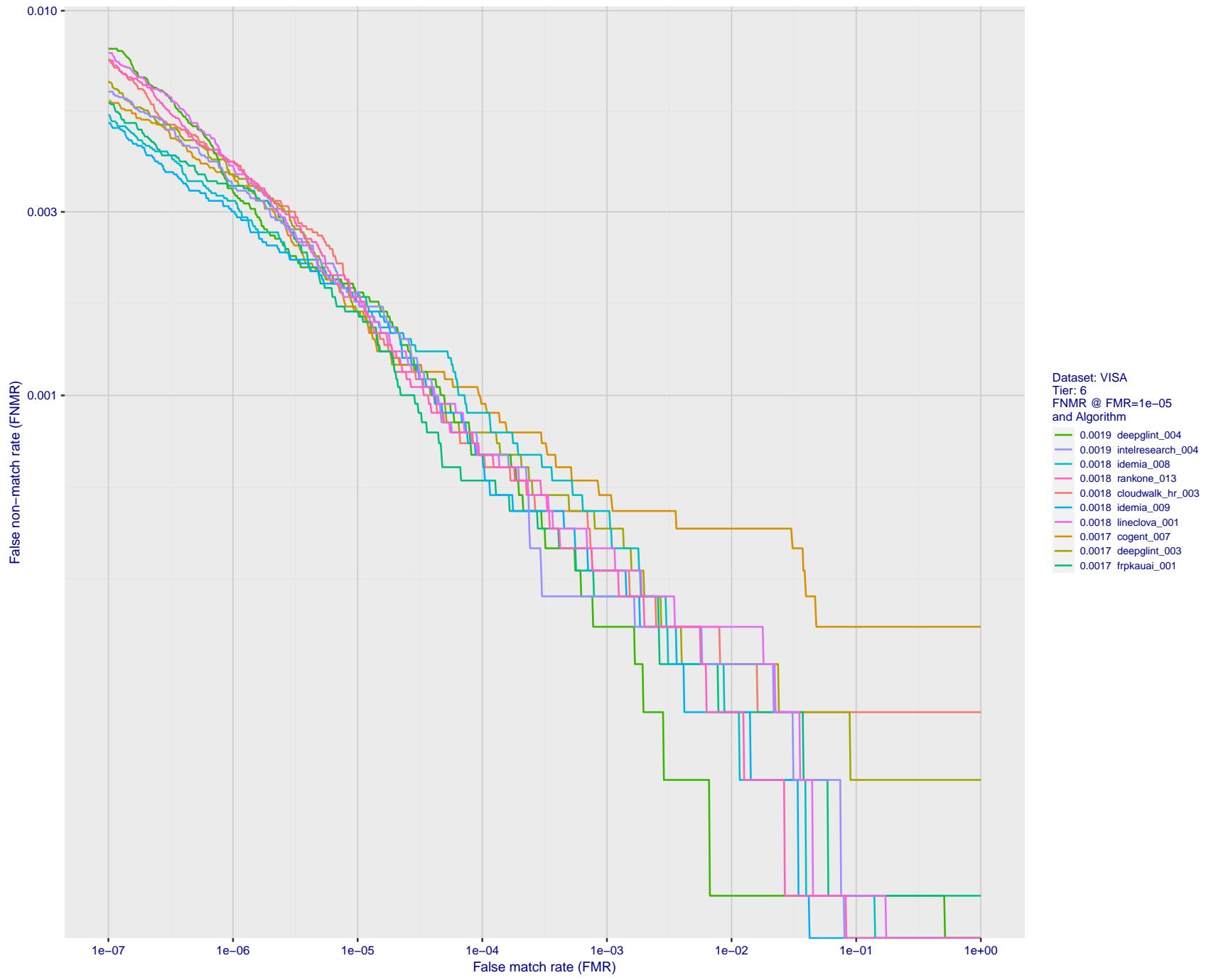


Figure 45: For the visa images, detection error tradeoff (DET) characteristics showing false non-match rate vs. false match rate plotted parametrically on threshold, T . The scales are logarithmic in order to show many decades of FMR.

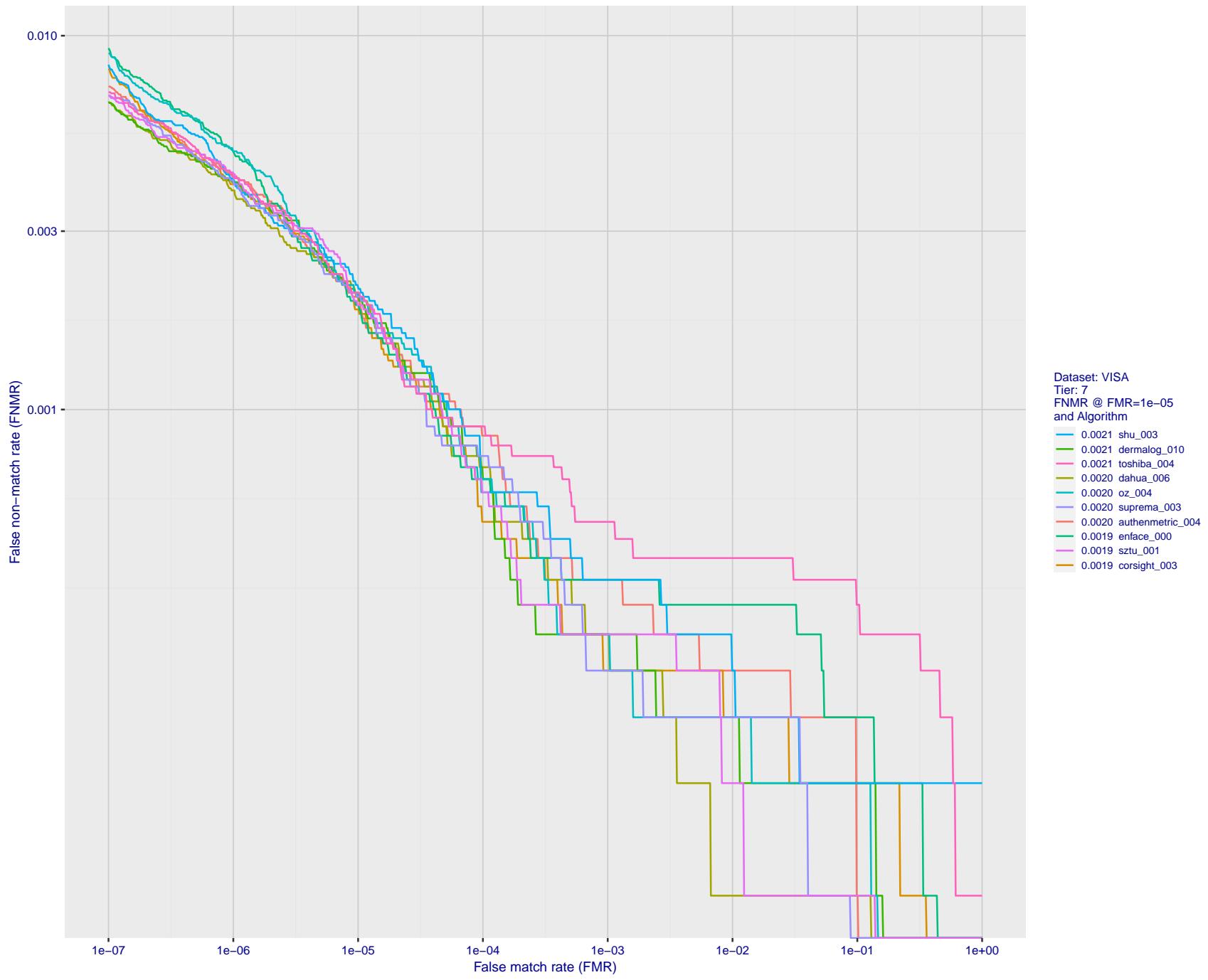


Figure 46: For the visa images, detection error tradeoff (DET) characteristics showing false non-match rate vs. false match rate plotted parametrically on threshold, T . The scales are logarithmic in order to show many decades of FMR.

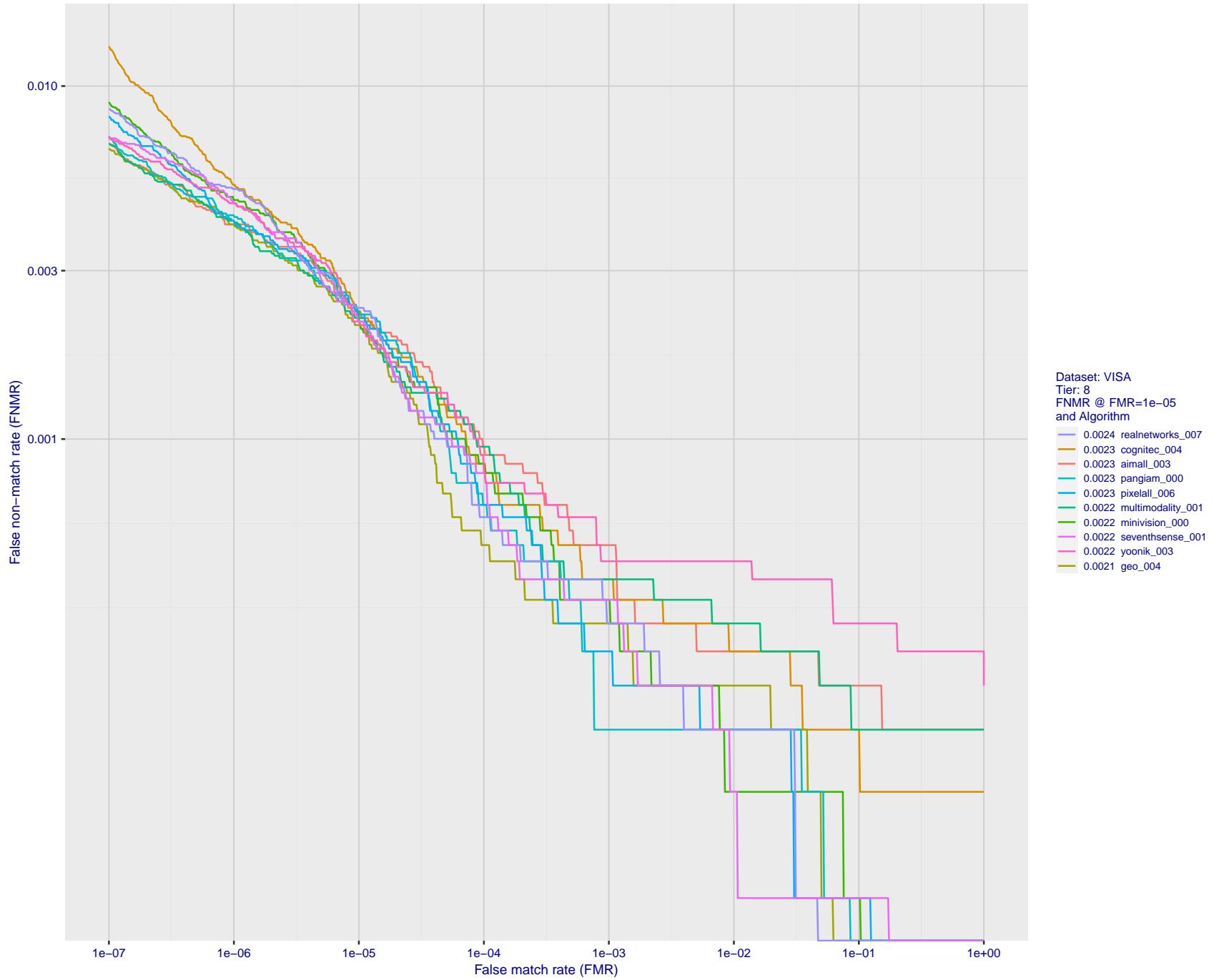


Figure 47: For the visa images, detection error tradeoff (DET) characteristics showing false non-match rate vs. false match rate plotted parametrically on threshold, T . The scales are logarithmic in order to show many decades of FMR.

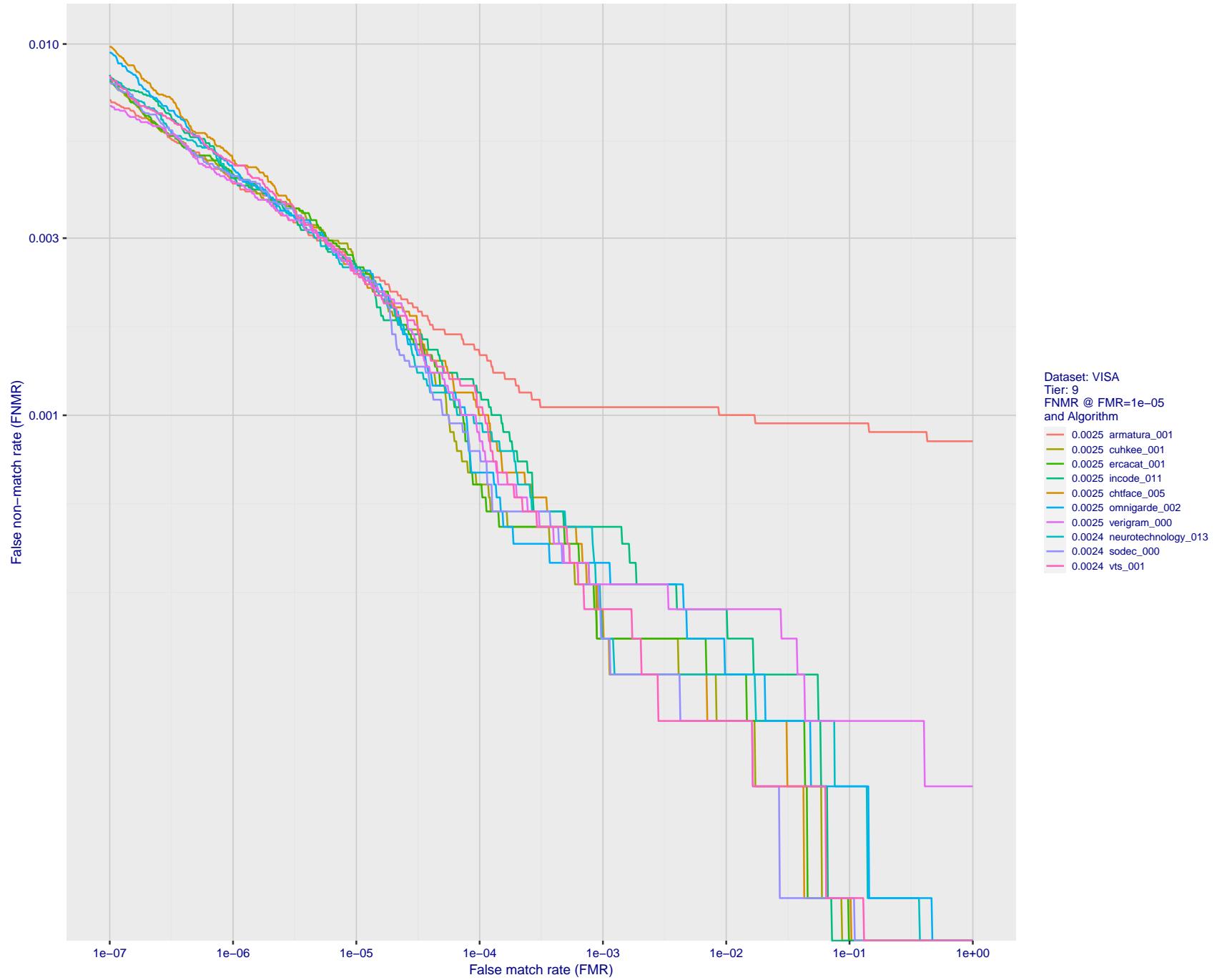


Figure 48: For the visa images, detection error tradeoff (DET) characteristics showing false non-match rate vs. false match rate plotted parametrically on threshold, T . The scales are logarithmic in order to show many decades of FMR.

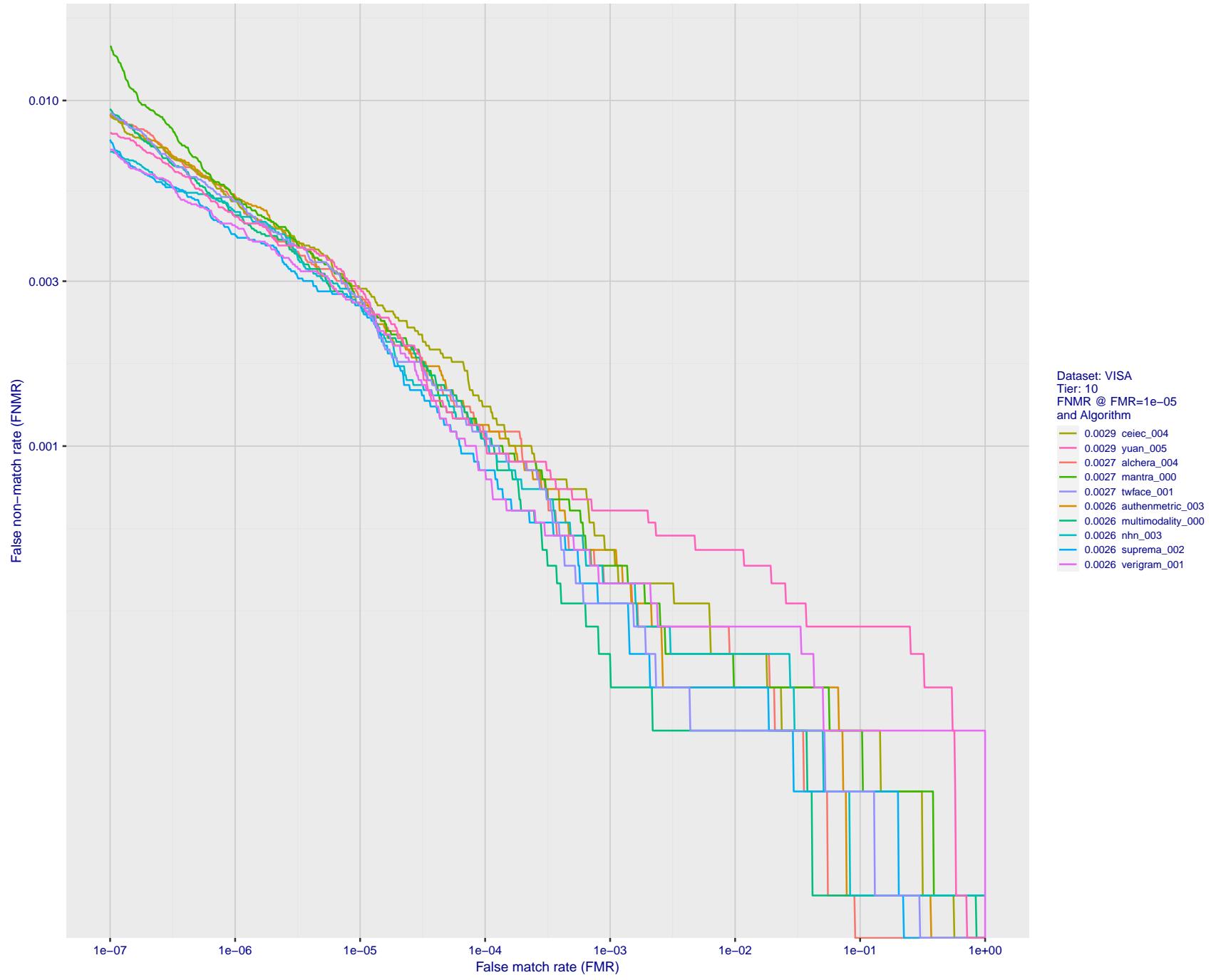


Figure 49: For the visa images, detection error tradeoff (DET) characteristics showing false non-match rate vs. false match rate plotted parametrically on threshold, T . The scales are logarithmic in order to show many decades of FMR.

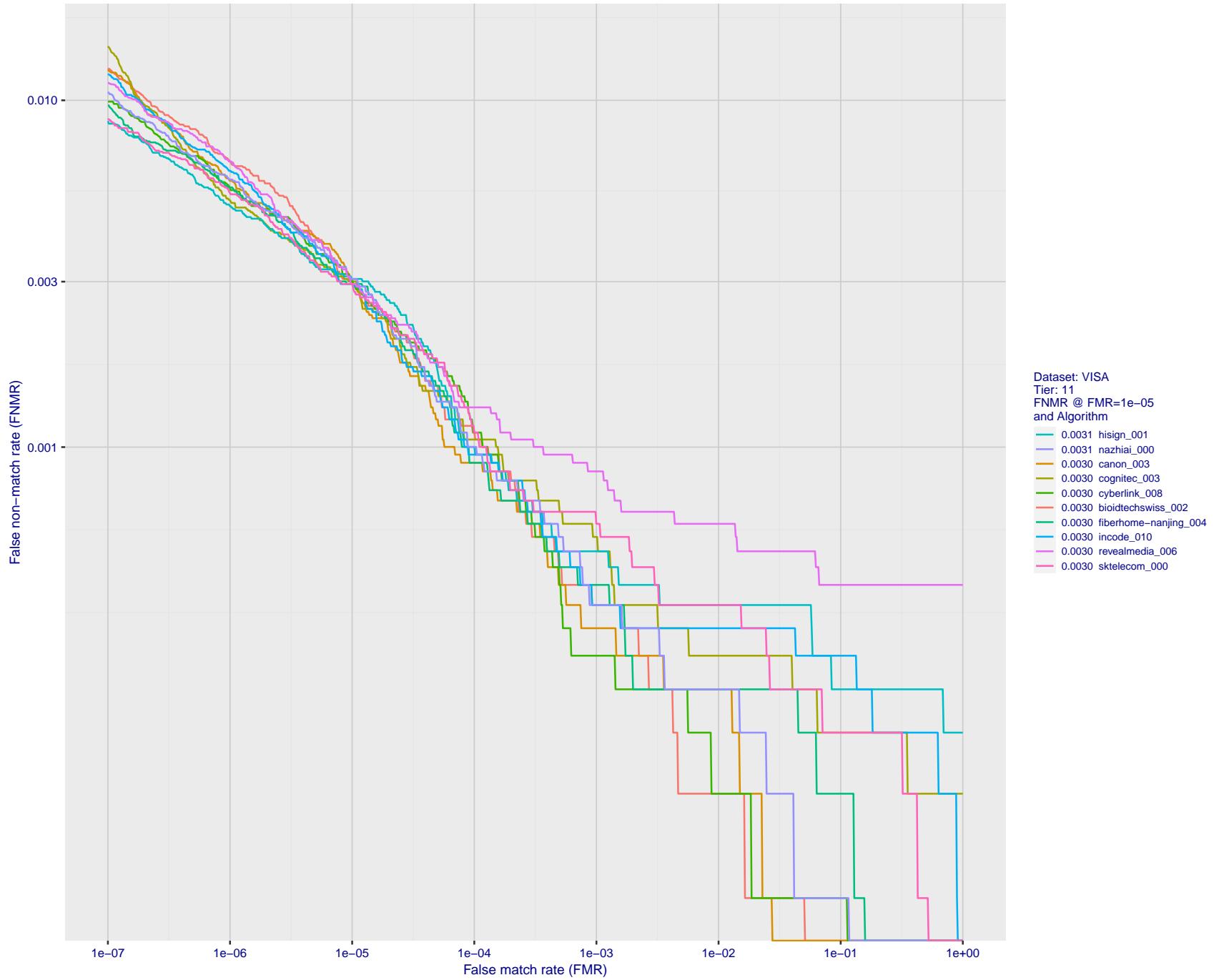


Figure 50: For the visa images, detection error tradeoff (DET) characteristics showing false non-match rate vs. false match rate plotted parametrically on threshold, T . The scales are logarithmic in order to show many decades of FMR.

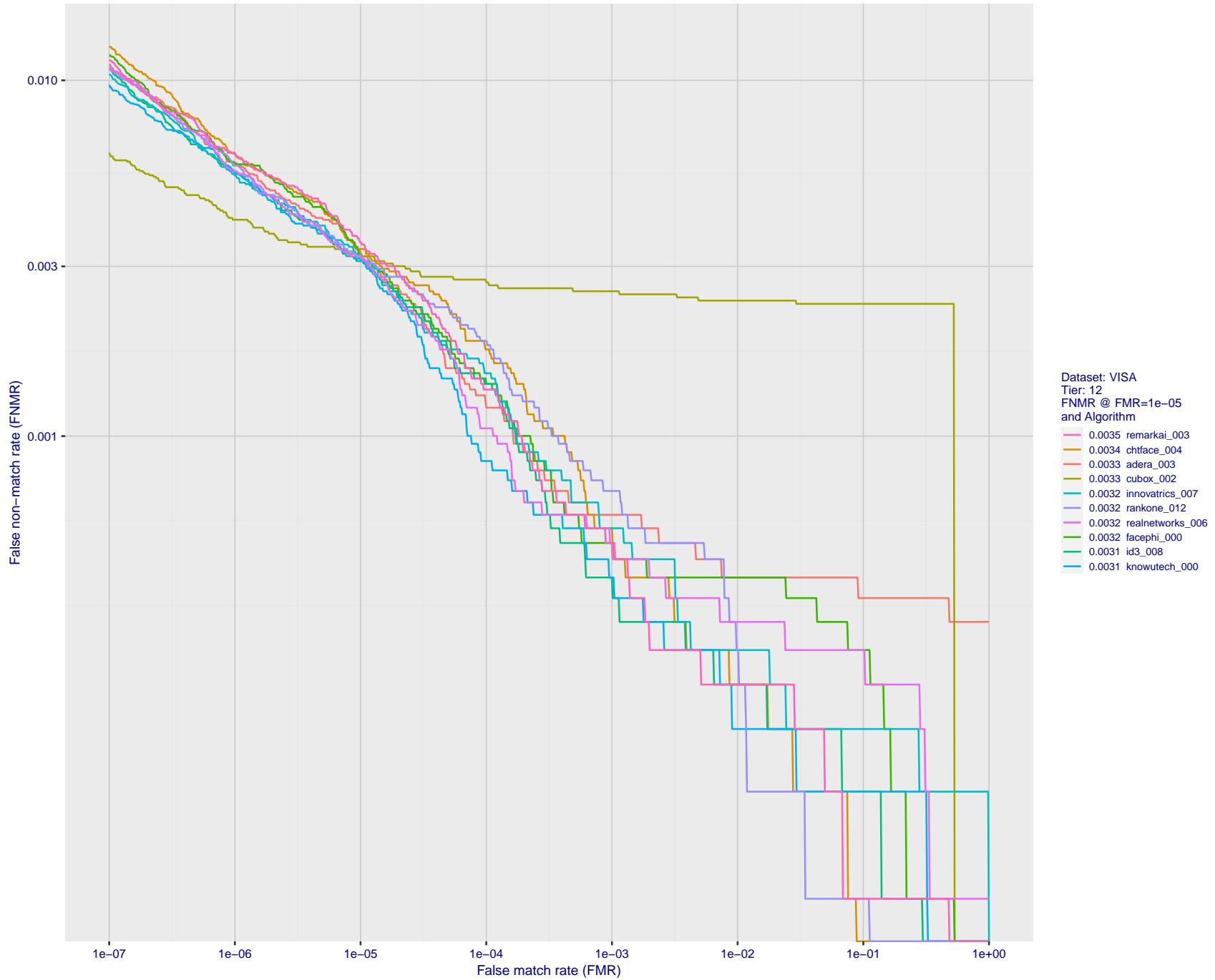


Figure 51: For the visa images, detection error tradeoff (DET) characteristics showing false non-match rate vs. false match rate plotted parametrically on threshold, T . The scales are logarithmic in order to show many decades of FMR.

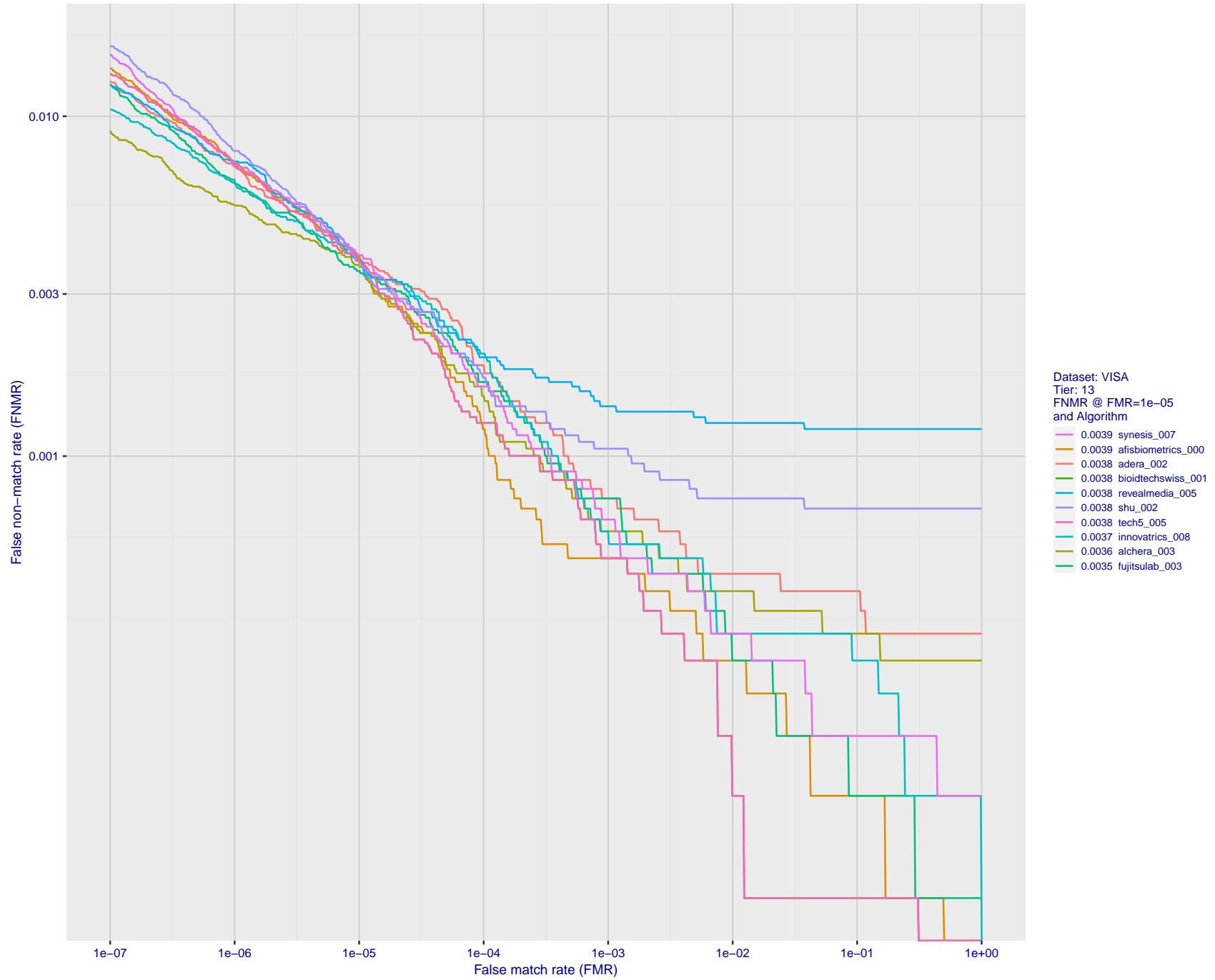


Figure 52: For the visa images, detection error tradeoff (DET) characteristics showing false non-match rate vs. false match rate plotted parametrically on threshold, T . The scales are logarithmic in order to show many decades of FMR.

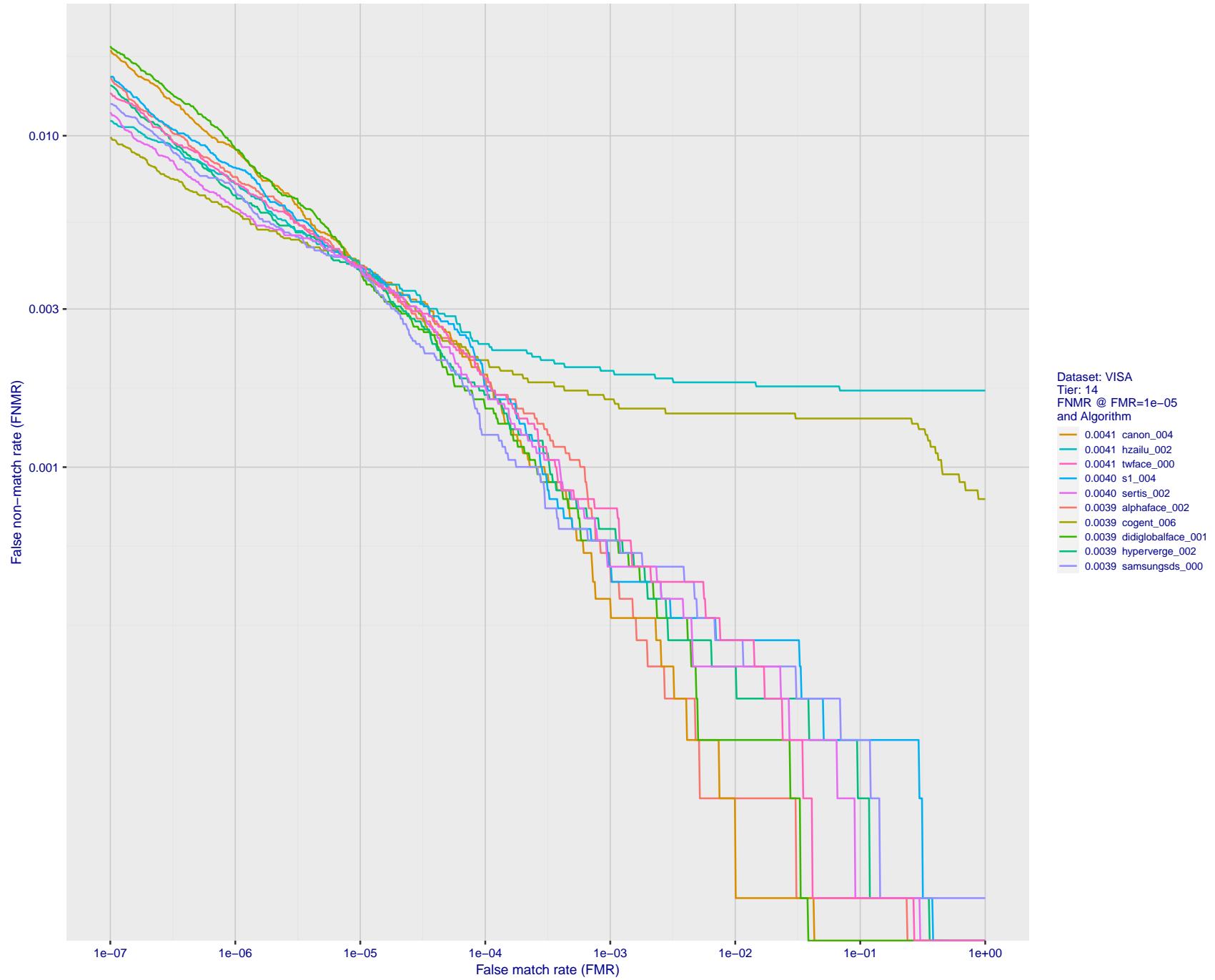


Figure 53: For the visa images, detection error tradeoff (DET) characteristics showing false non-match rate vs. false match rate plotted parametrically on threshold, T . The scales are logarithmic in order to show many decades of FMR.

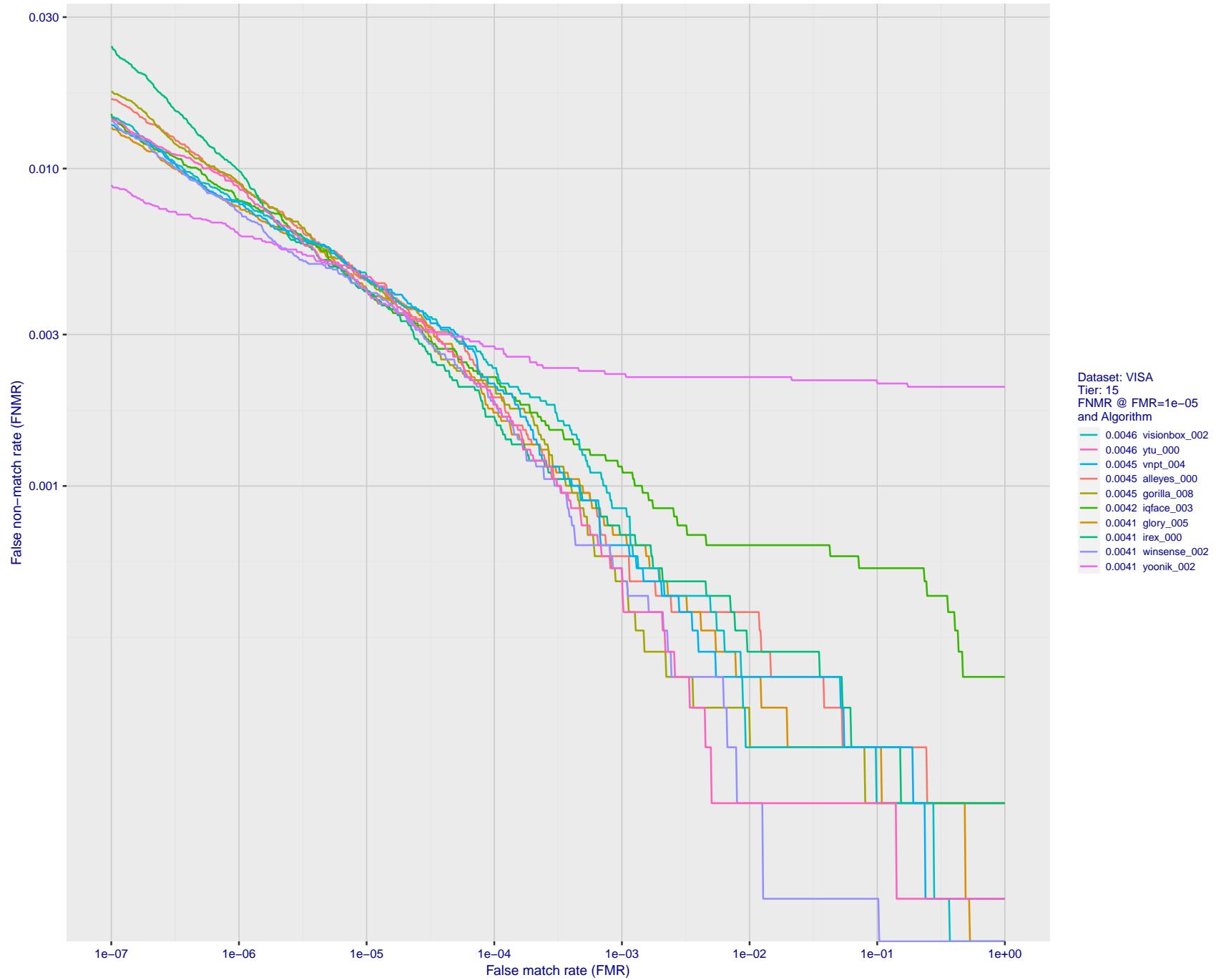


Figure 54: For the visa images, detection error tradeoff (DET) characteristics showing false non-match rate vs. false match rate plotted parametrically on threshold, T . The scales are logarithmic in order to show many decades of FMR.

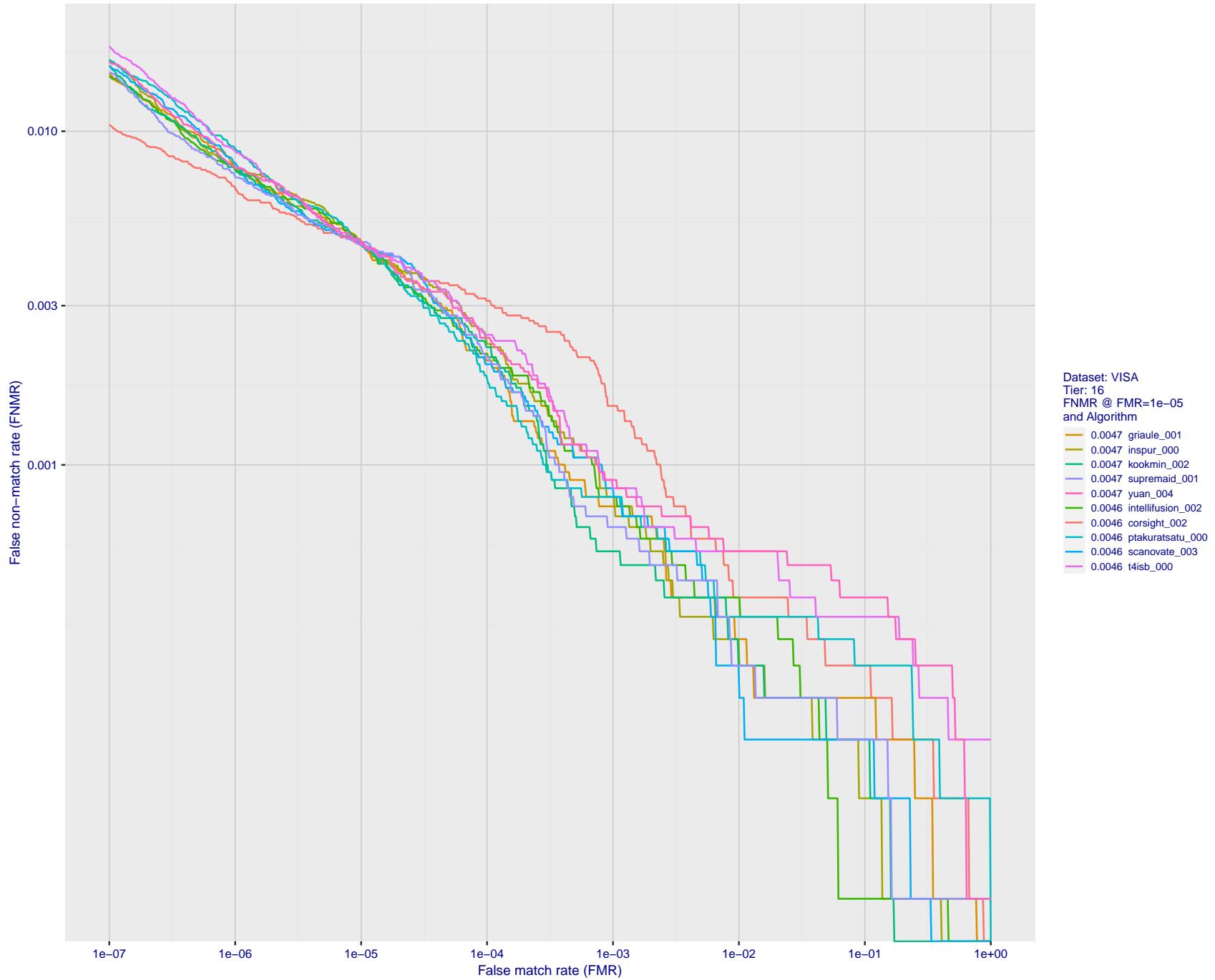


Figure 55: For the visa images, detection error tradeoff (DET) characteristics showing false non-match rate vs. false match rate plotted parametrically on threshold, T . The scales are logarithmic in order to show many decades of FMR.

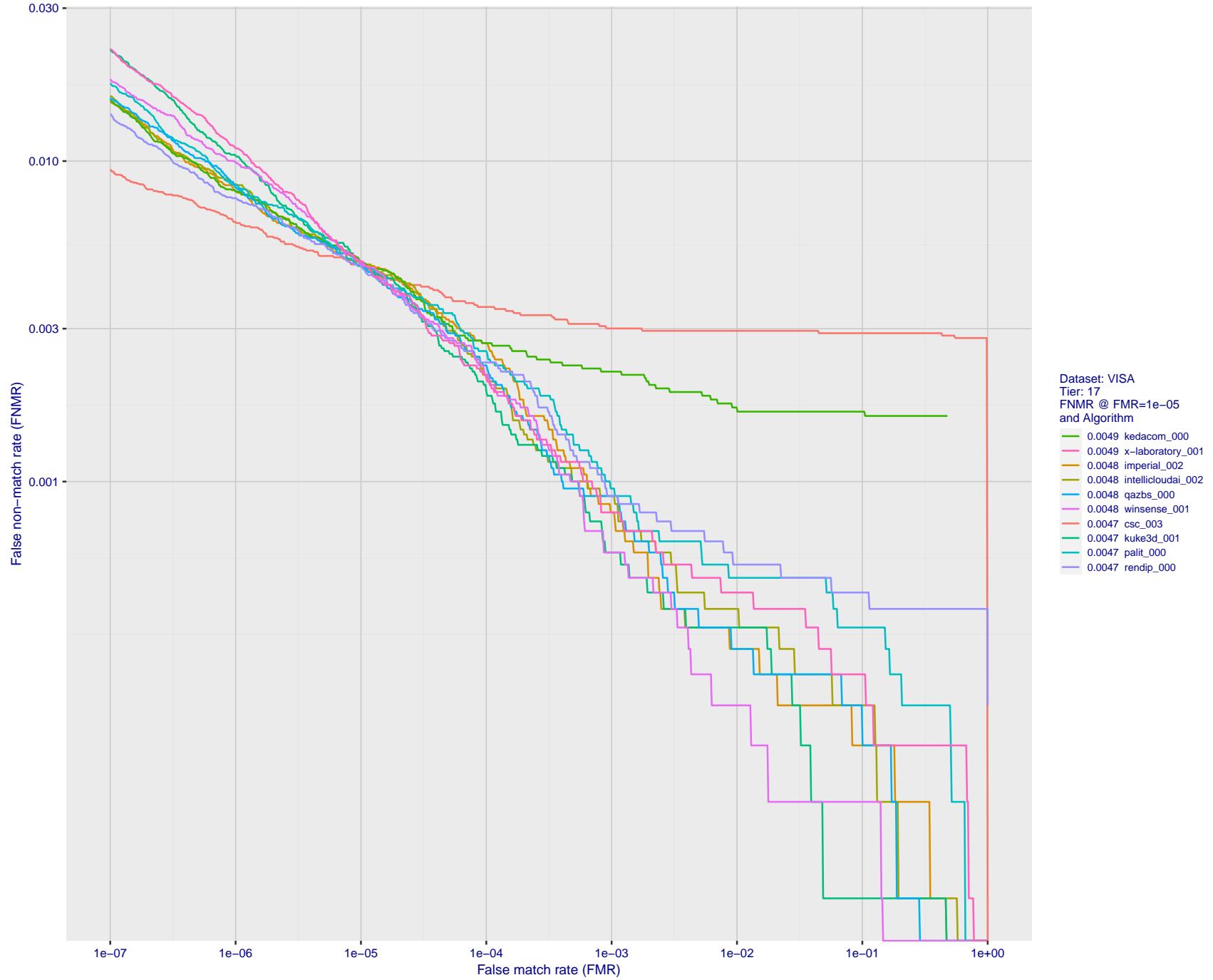


Figure 56: For the visa images, detection error tradeoff (DET) characteristics showing false non-match rate vs. false match rate plotted parametrically on threshold, T . The scales are logarithmic in order to show many decades of FMR.

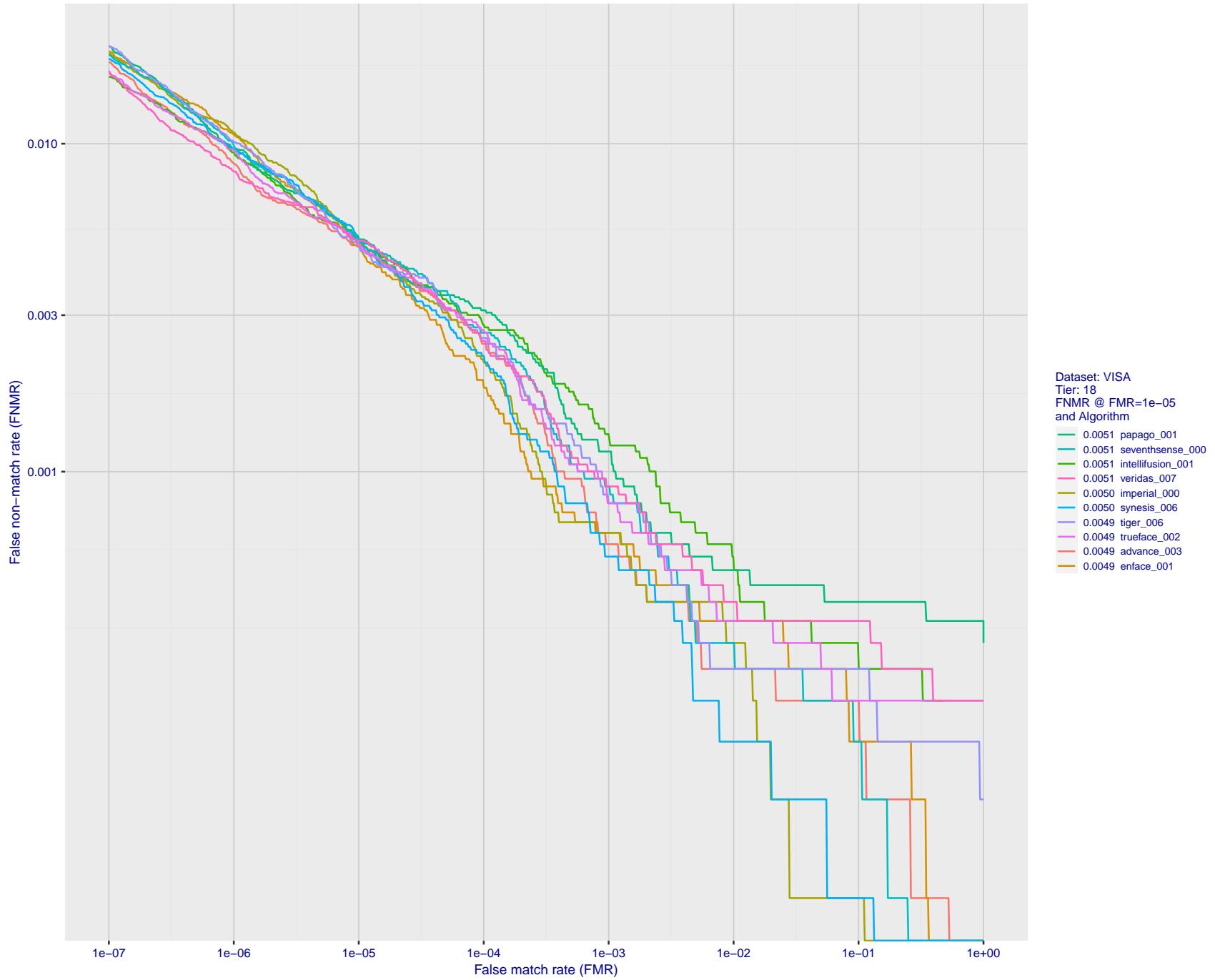


Figure 57: For the visa images, detection error tradeoff (DET) characteristics showing false non-match rate vs. false match rate plotted parametrically on threshold, T . The scales are logarithmic in order to show many decades of FMR.

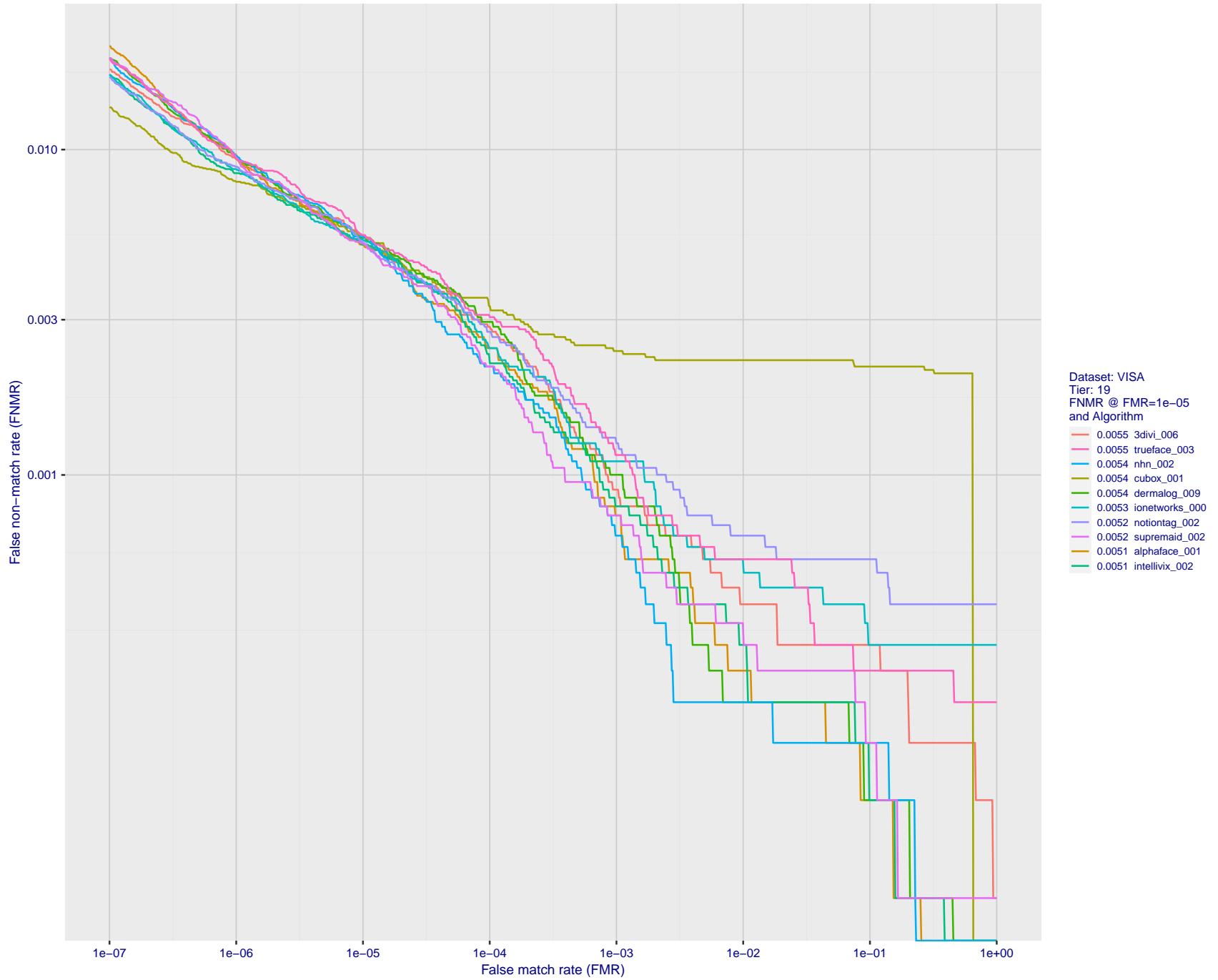


Figure 58: For the visa images, detection error tradeoff (DET) characteristics showing false non-match rate vs. false match rate plotted parametrically on threshold, T . The scales are logarithmic in order to show many decades of FMR.

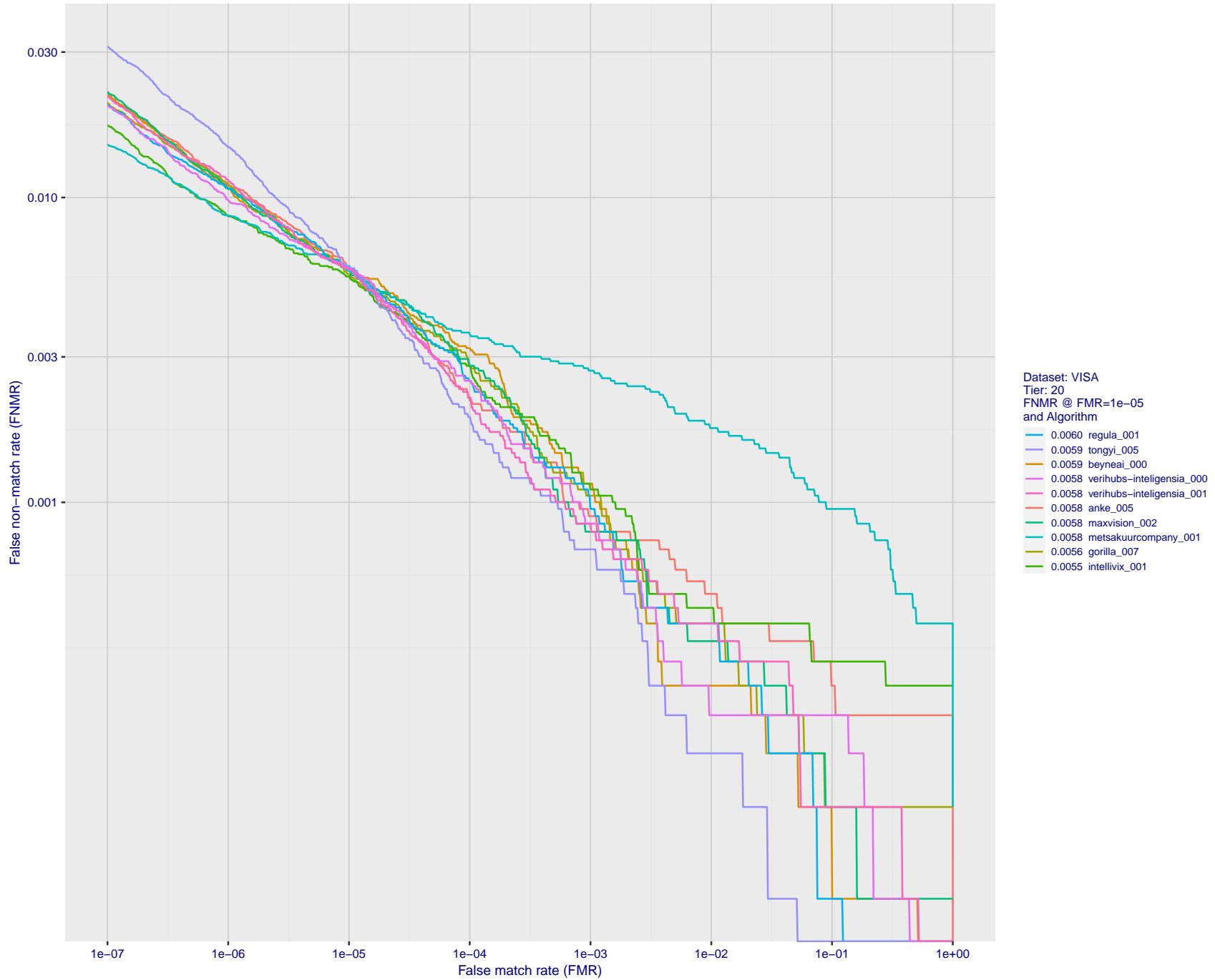


Figure 59: For the visa images, detection error tradeoff (DET) characteristics showing false non-match rate vs. false match rate plotted parametrically on threshold, T . The scales are logarithmic in order to show many decades of FMR.

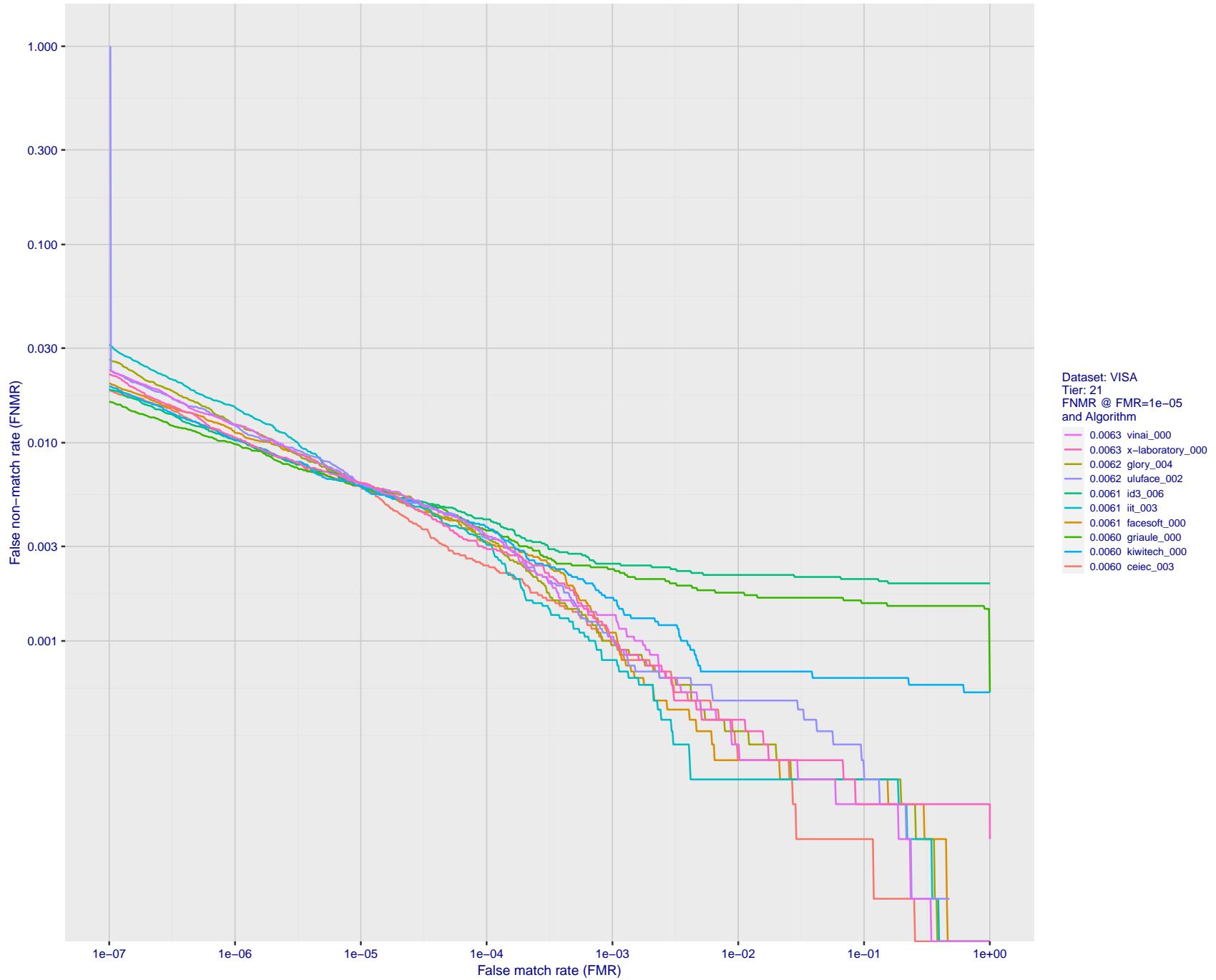


Figure 60: For the visa images, detection error tradeoff (DET) characteristics showing false non-match rate vs. false match rate plotted parametrically on threshold, T . The scales are logarithmic in order to show many decades of FMR.

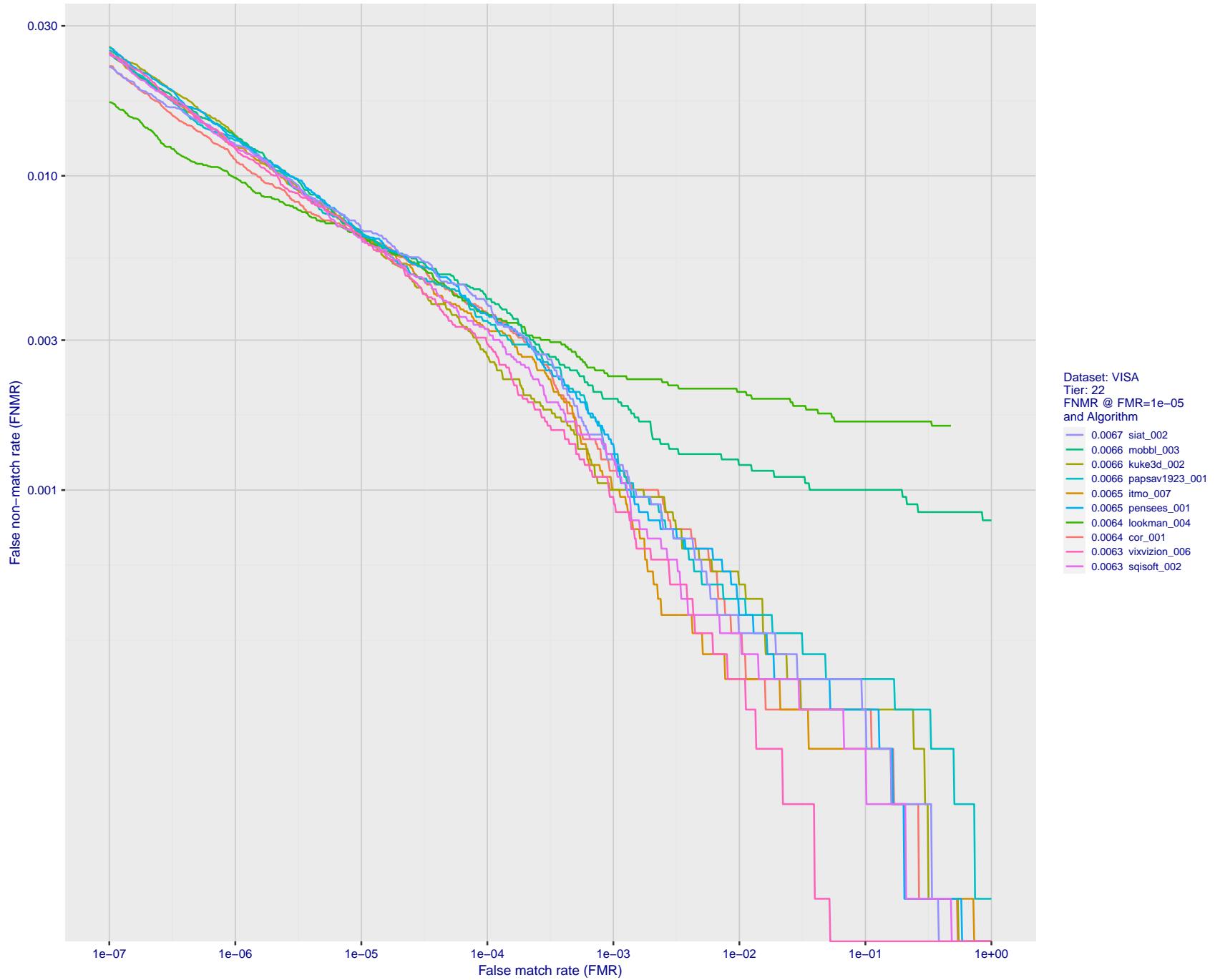


Figure 61: For the visa images, detection error tradeoff (DET) characteristics showing false non-match rate vs. false match rate plotted parametrically on threshold, T . The scales are logarithmic in order to show many decades of FMR.

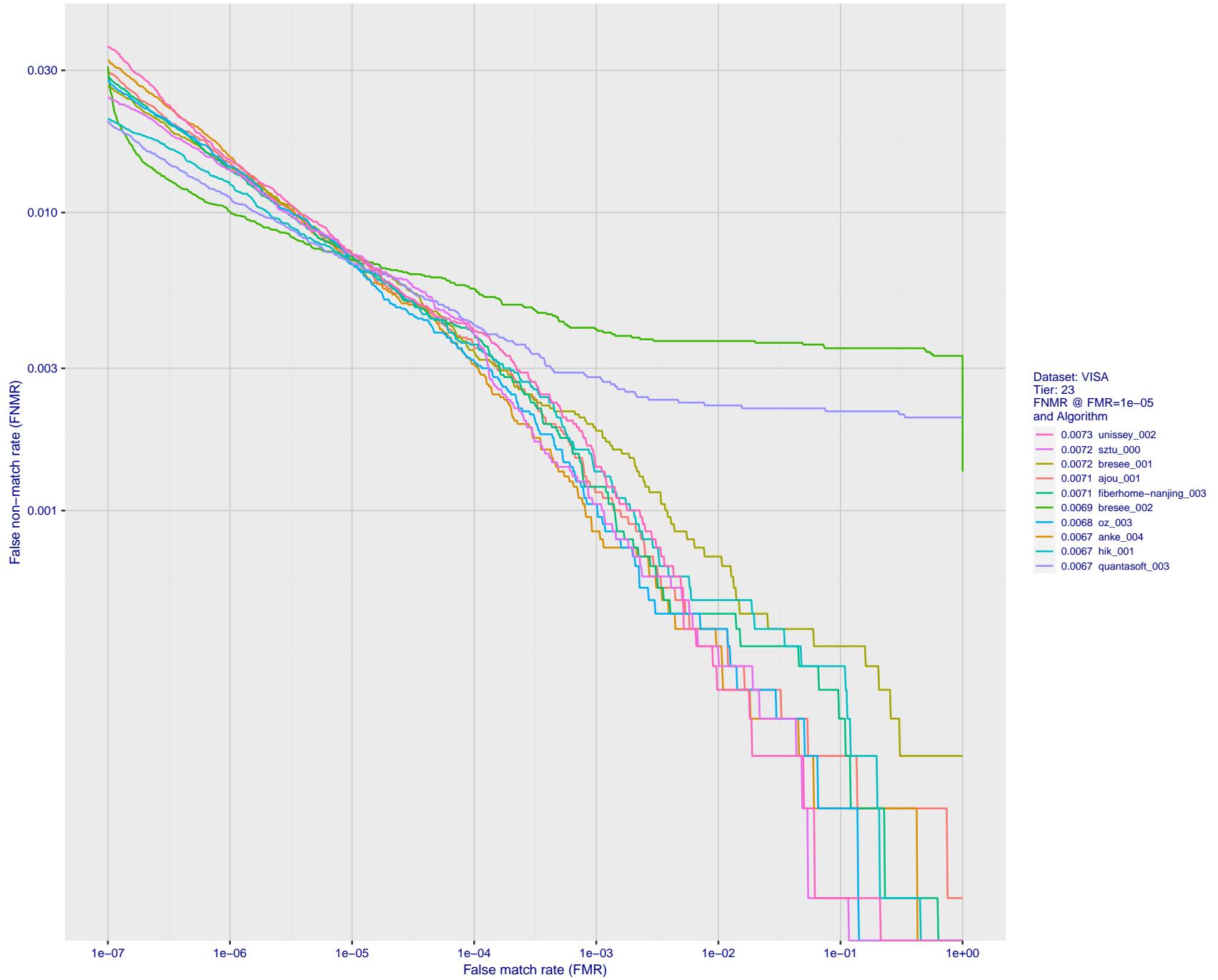


Figure 62: For the visa images, detection error tradeoff (DET) characteristics showing false non-match rate vs. false match rate plotted parametrically on threshold, T . The scales are logarithmic in order to show many decades of FMR.

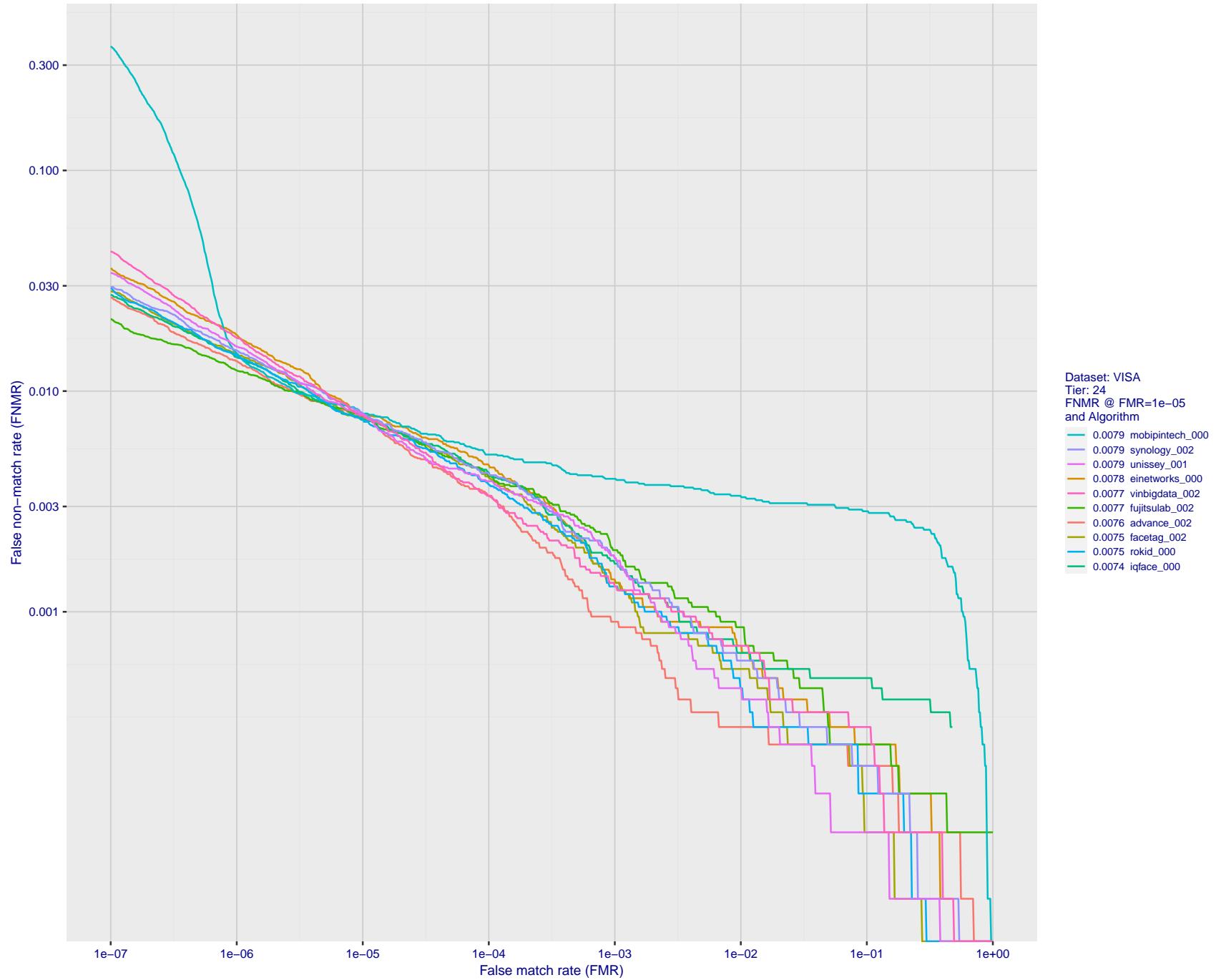


Figure 63: For the visa images, detection error tradeoff (DET) characteristics showing false non-match rate vs. false match rate plotted parametrically on threshold, T . The scales are logarithmic in order to show many decades of FMR.

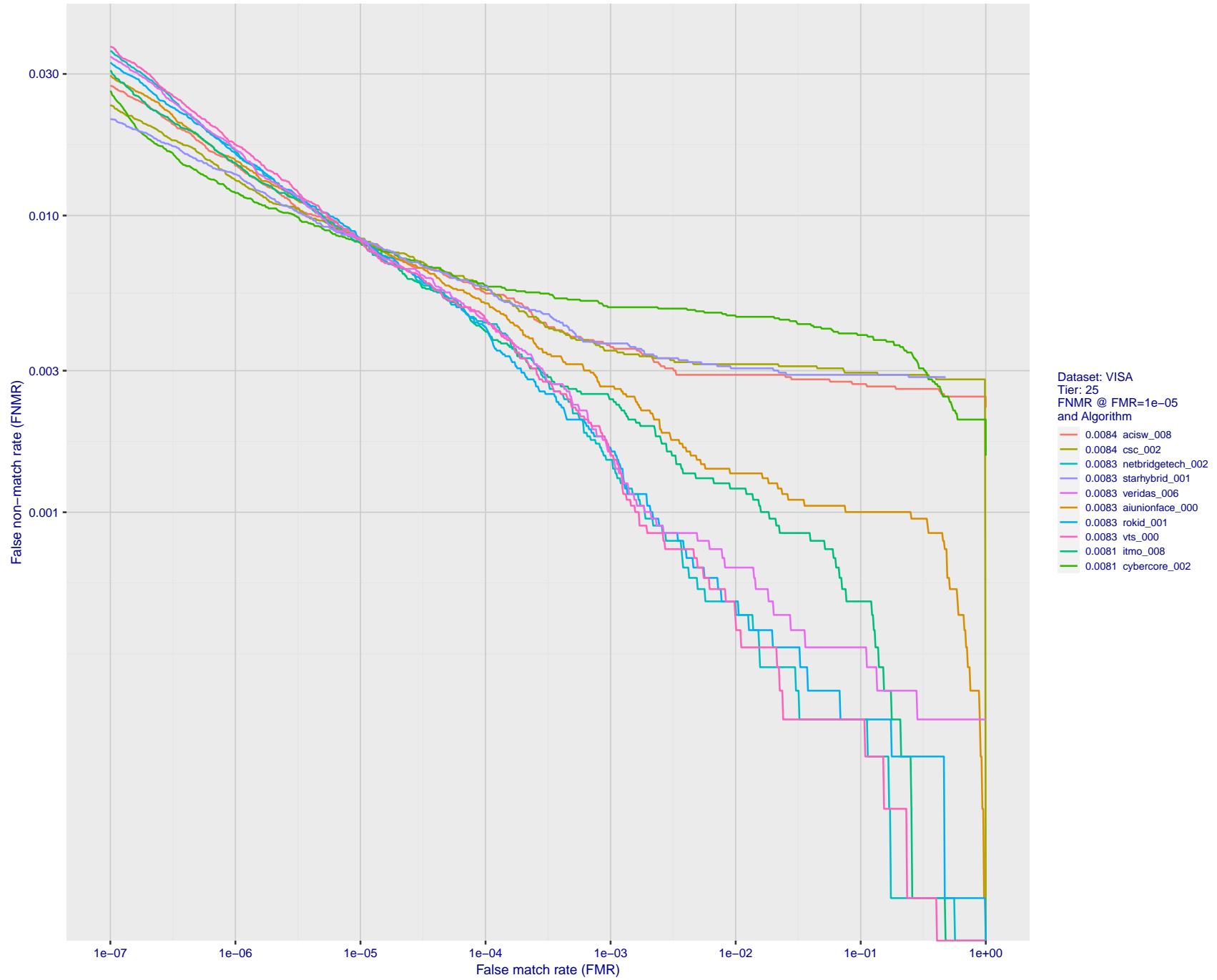


Figure 64: For the visa images, detection error tradeoff (DET) characteristics showing false non-match rate vs. false match rate plotted parametrically on threshold, T . The scales are logarithmic in order to show many decades of FMR.

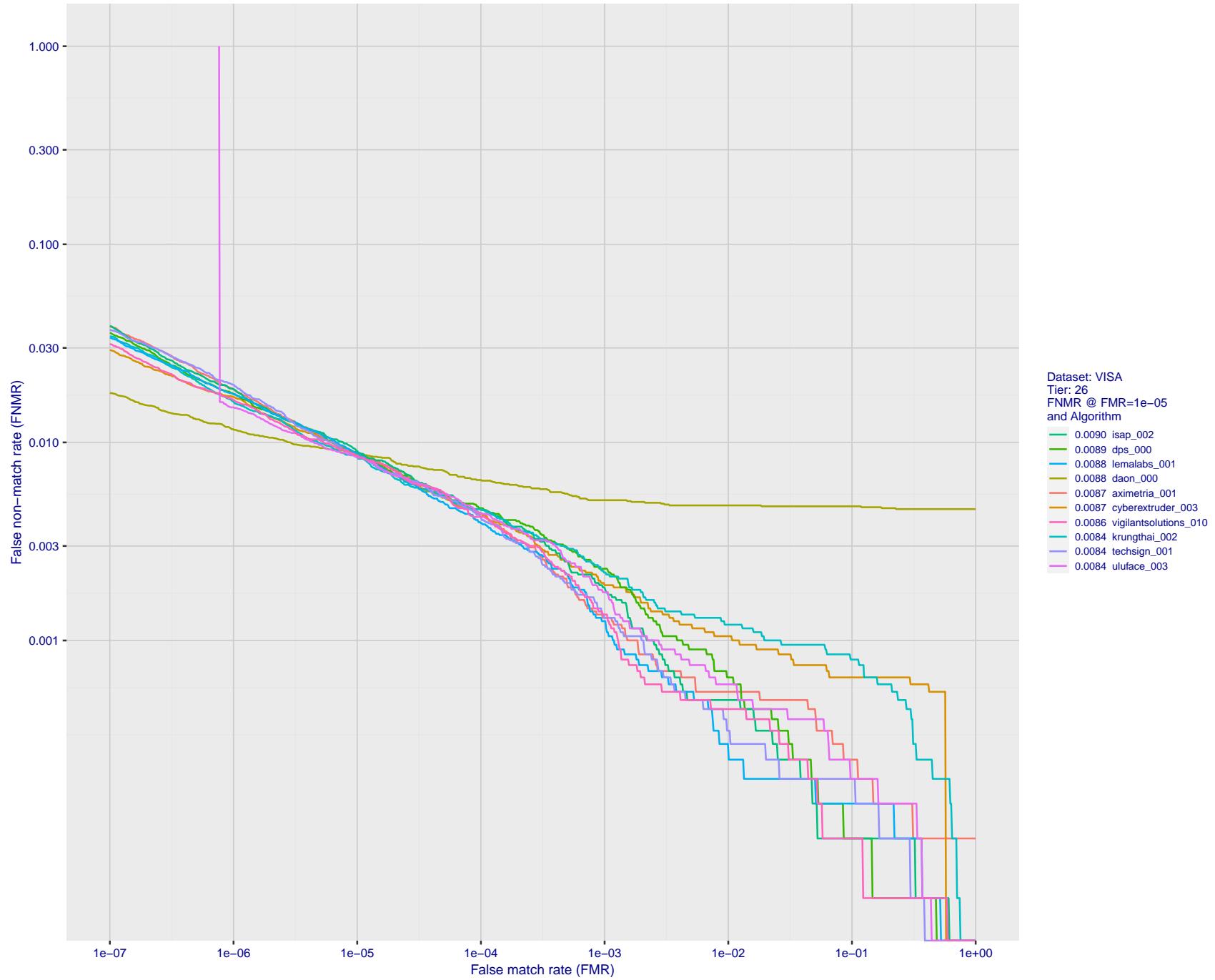


Figure 65: For the visa images, detection error tradeoff (DET) characteristics showing false non-match rate vs. false match rate plotted parametrically on threshold, T . The scales are logarithmic in order to show many decades of FMR.

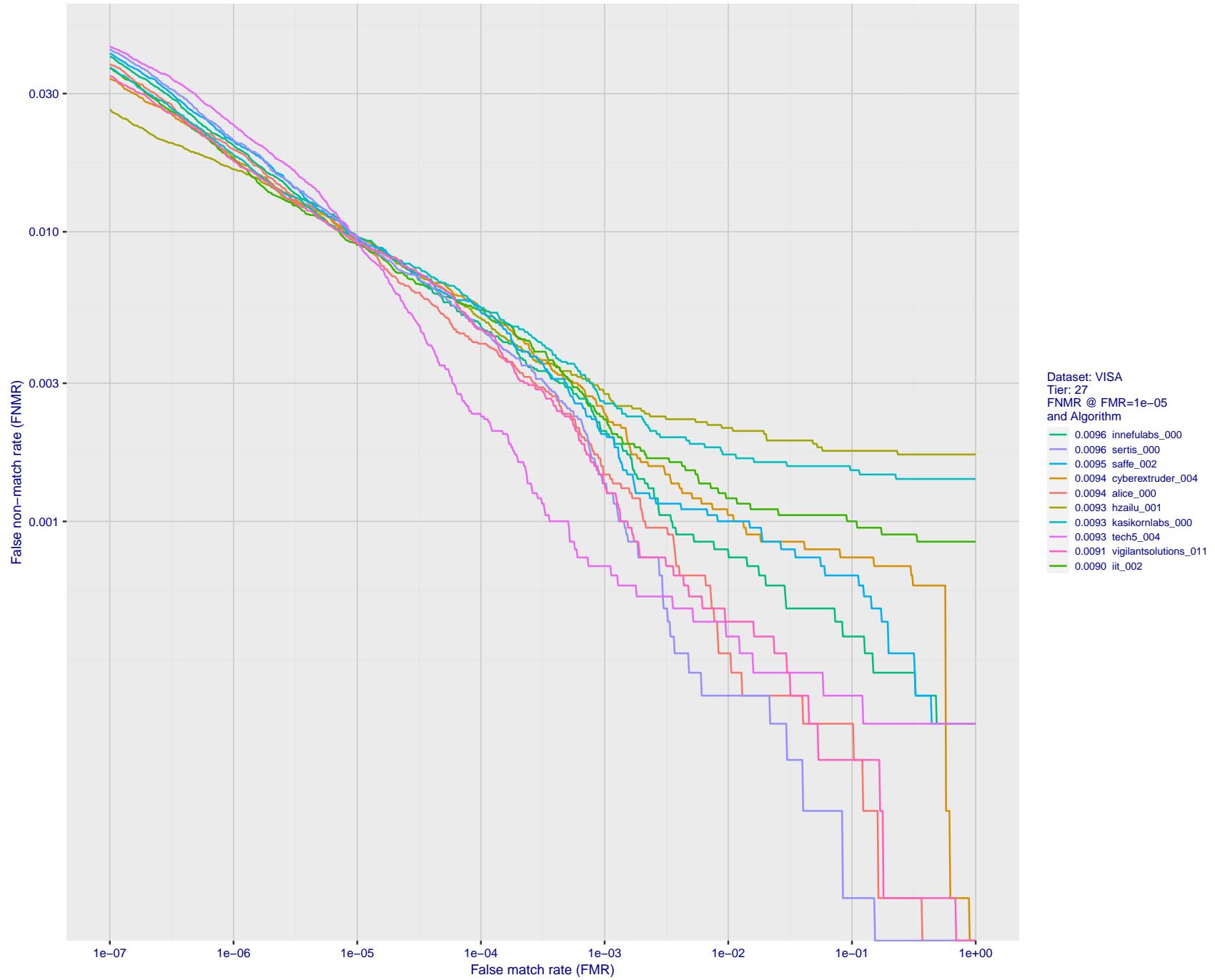


Figure 66: For the visa images, detection error tradeoff (DET) characteristics showing false non-match rate vs. false match rate plotted parametrically on threshold, T . The scales are logarithmic in order to show many decades of FMR.

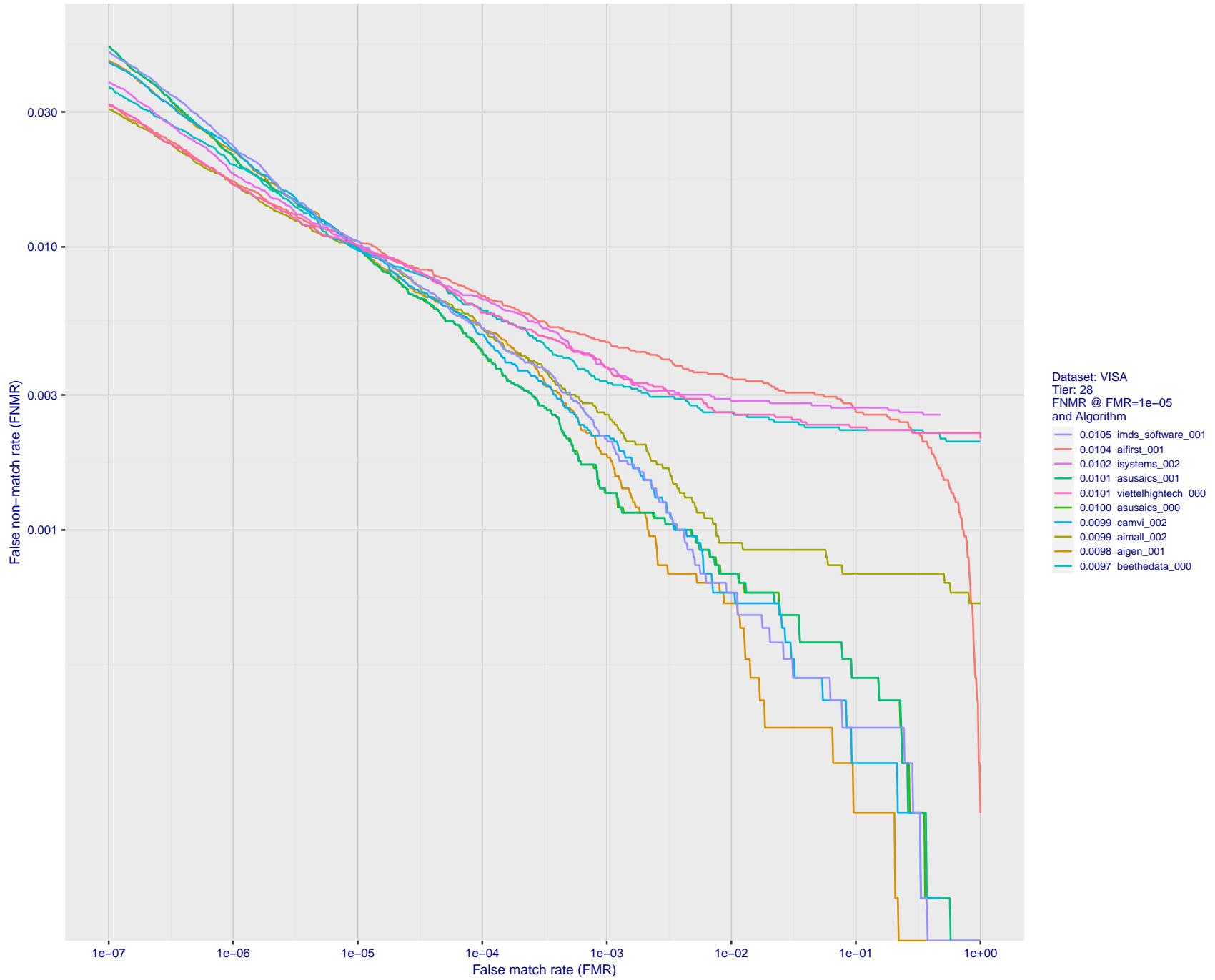


Figure 67: For the visa images, detection error tradeoff (DET) characteristics showing false non-match rate vs. false match rate plotted parametrically on threshold, T . The scales are logarithmic in order to show many decades of FMR.

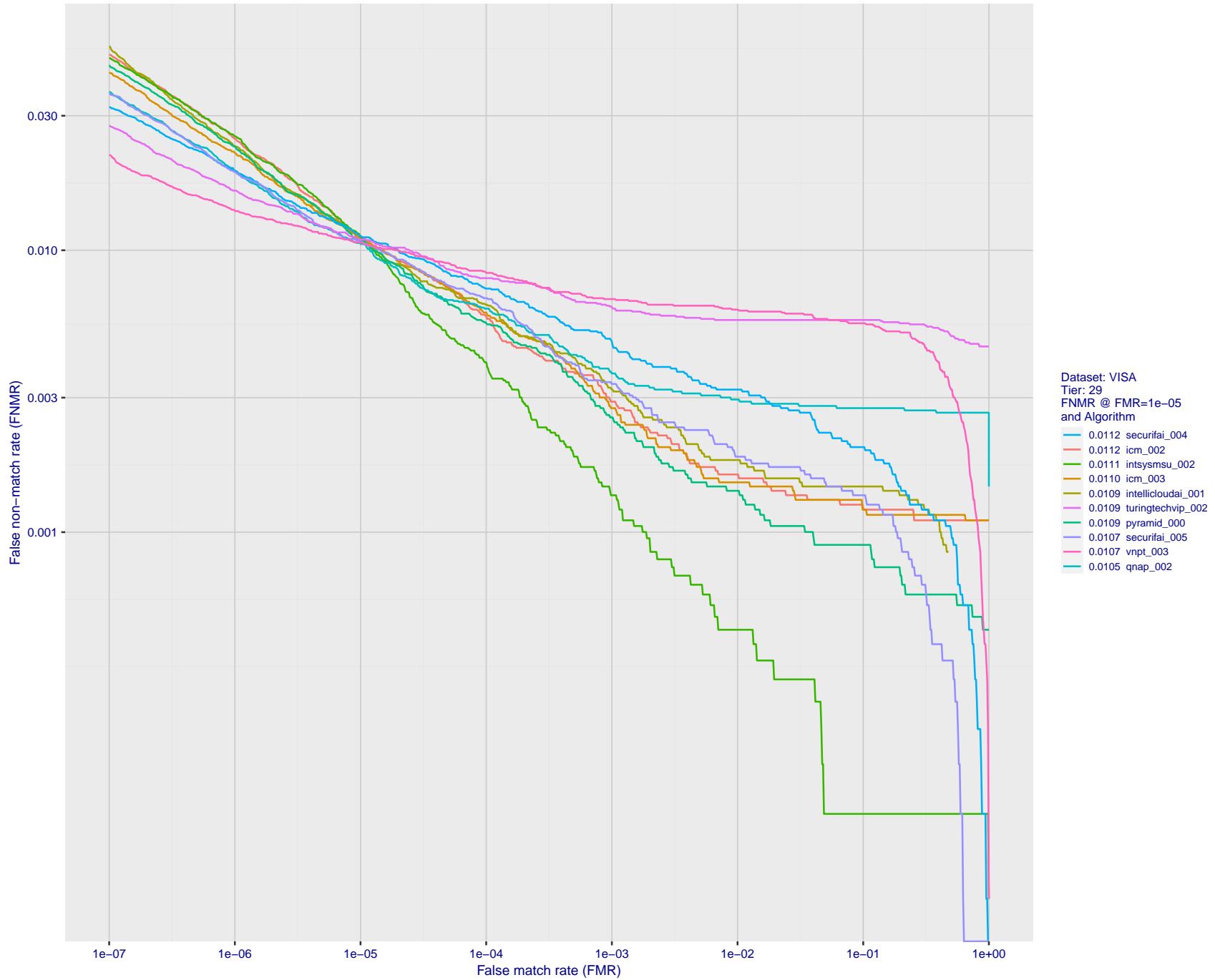


Figure 68: For the visa images, detection error tradeoff (DET) characteristics showing false non-match rate vs. false match rate plotted parametrically on threshold, T . The scales are logarithmic in order to show many decades of FMR.

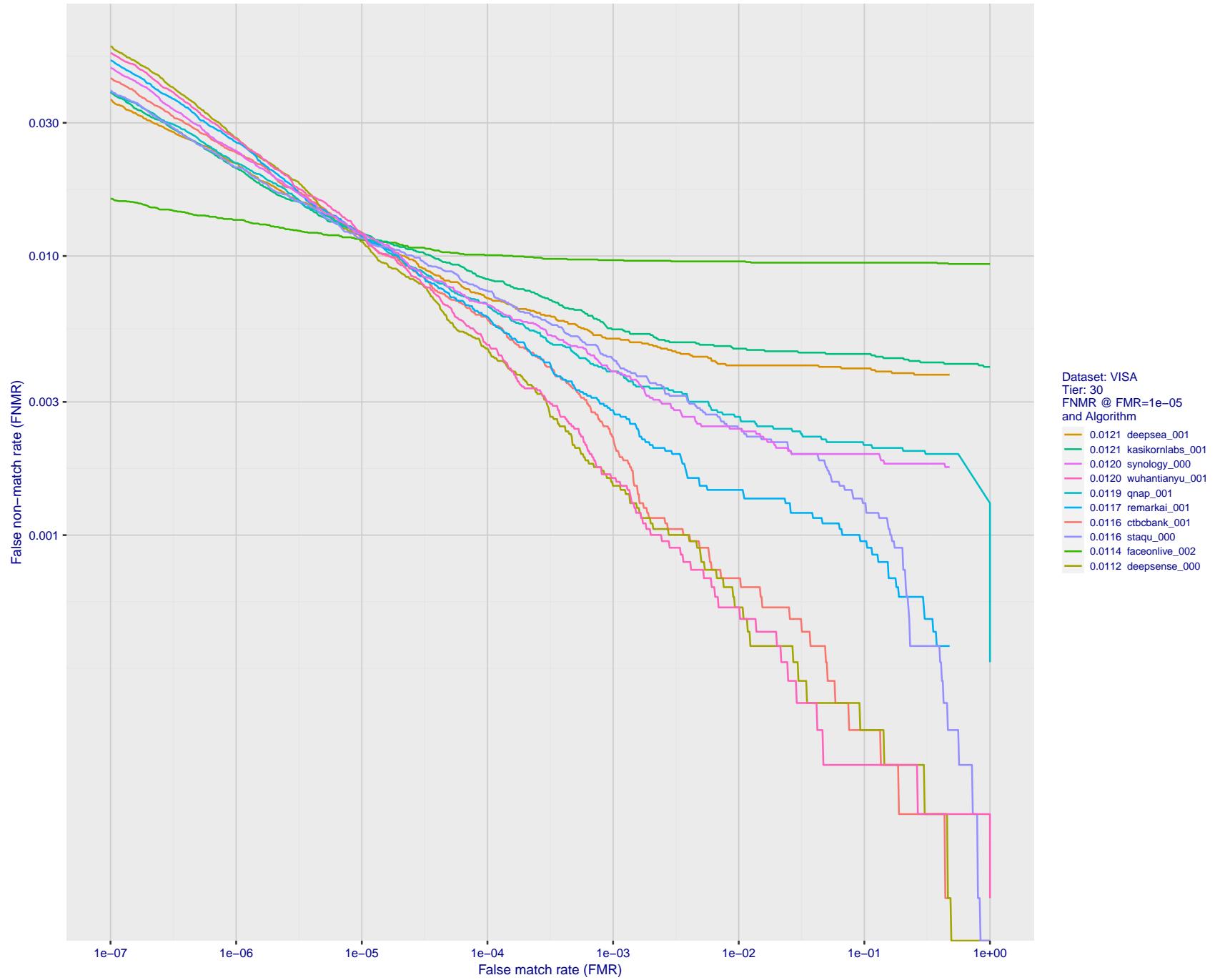


Figure 69: For the visa images, detection error tradeoff (DET) characteristics showing false non-match rate vs. false match rate plotted parametrically on threshold, T . The scales are logarithmic in order to show many decades of FMR.

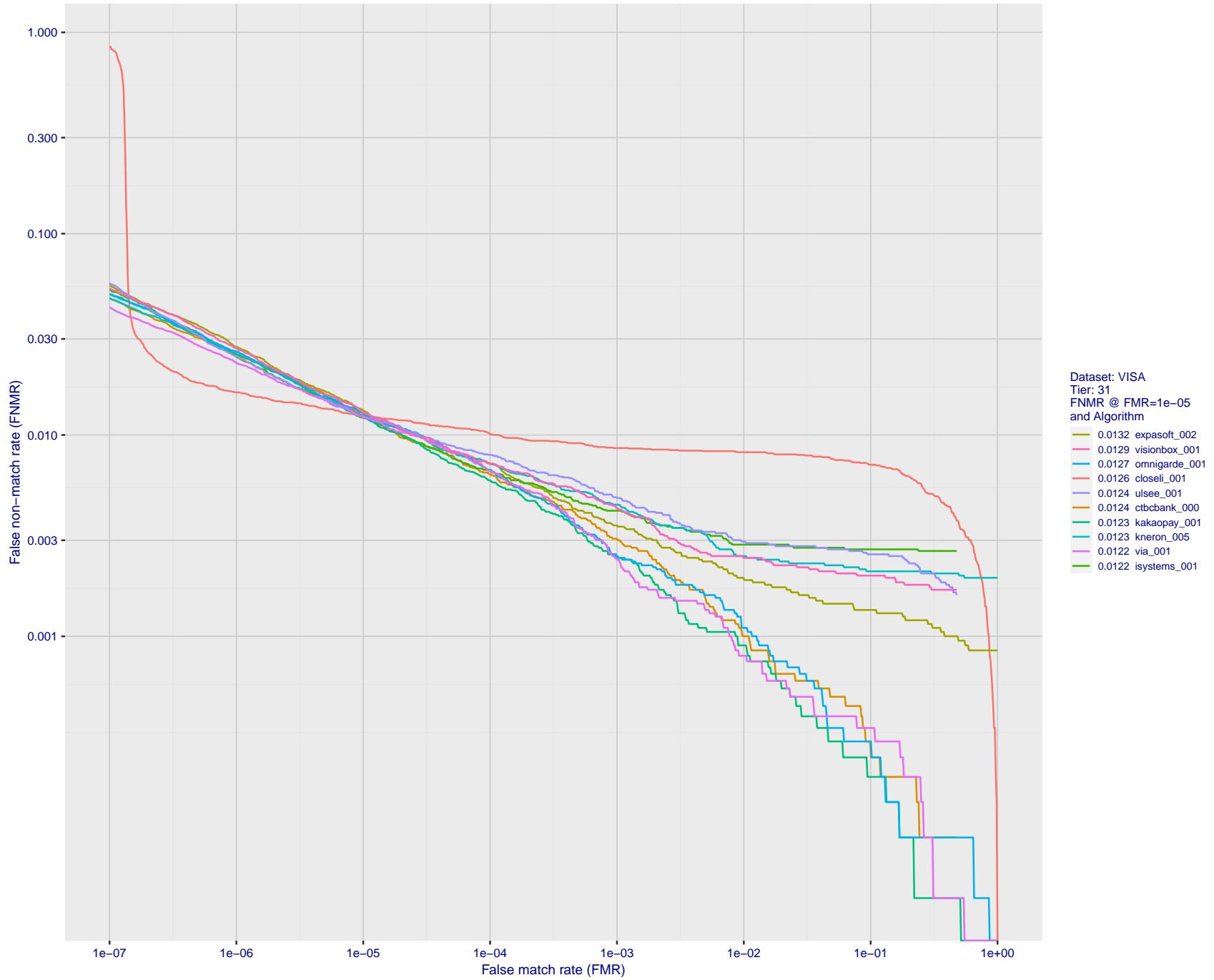


Figure 70: For the visa images, detection error tradeoff (DET) characteristics showing false non-match rate vs. false match rate plotted parametrically on threshold, T . The scales are logarithmic in order to show many decades of FMR.

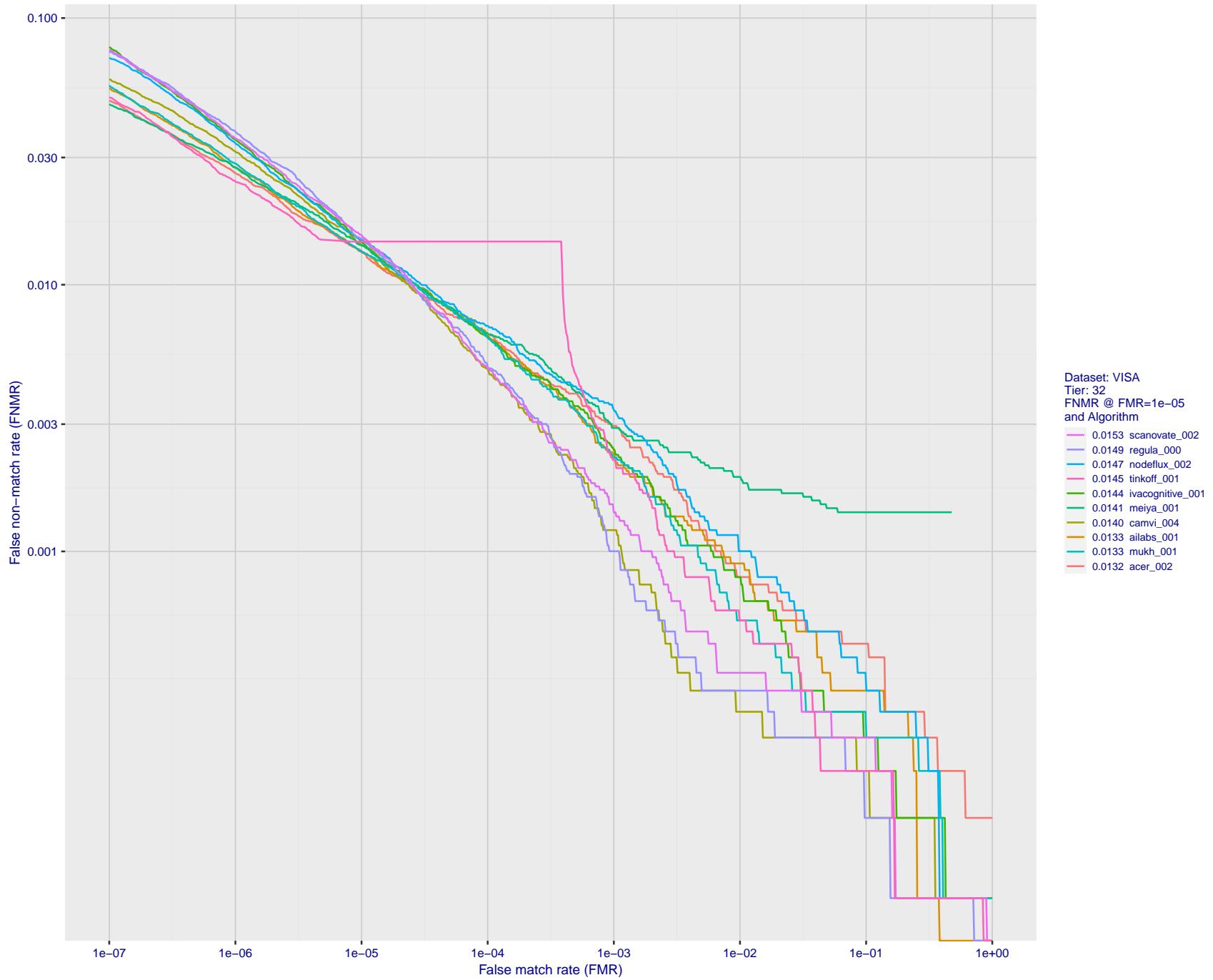


Figure 71: For the visa images, detection error tradeoff (DET) characteristics showing false non-match rate vs. false match rate plotted parametrically on threshold, T . The scales are logarithmic in order to show many decades of FMR.

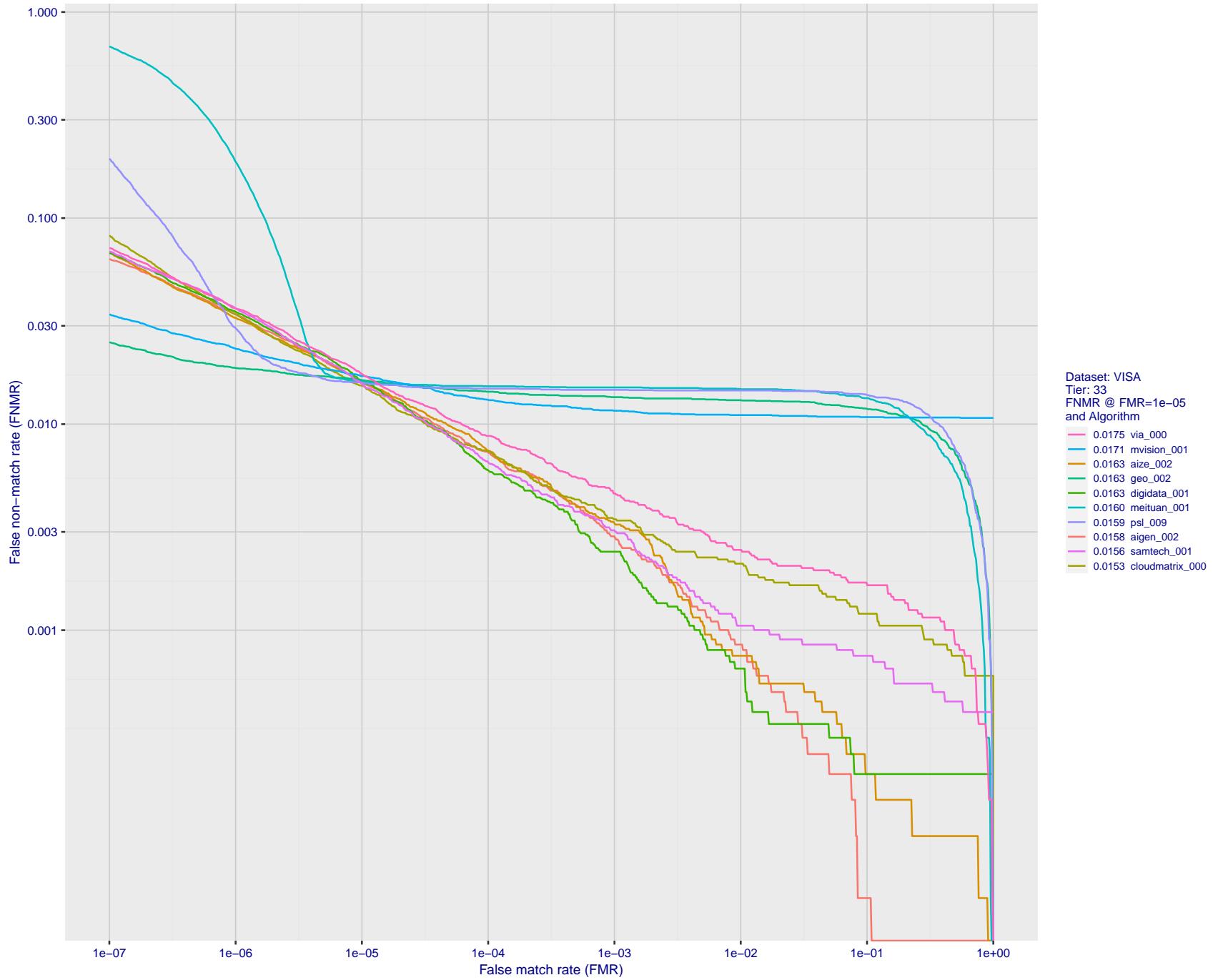


Figure 72: For the visa images, detection error tradeoff (DET) characteristics showing false non-match rate vs. false match rate plotted parametrically on threshold, T . The scales are logarithmic in order to show many decades of FMR.

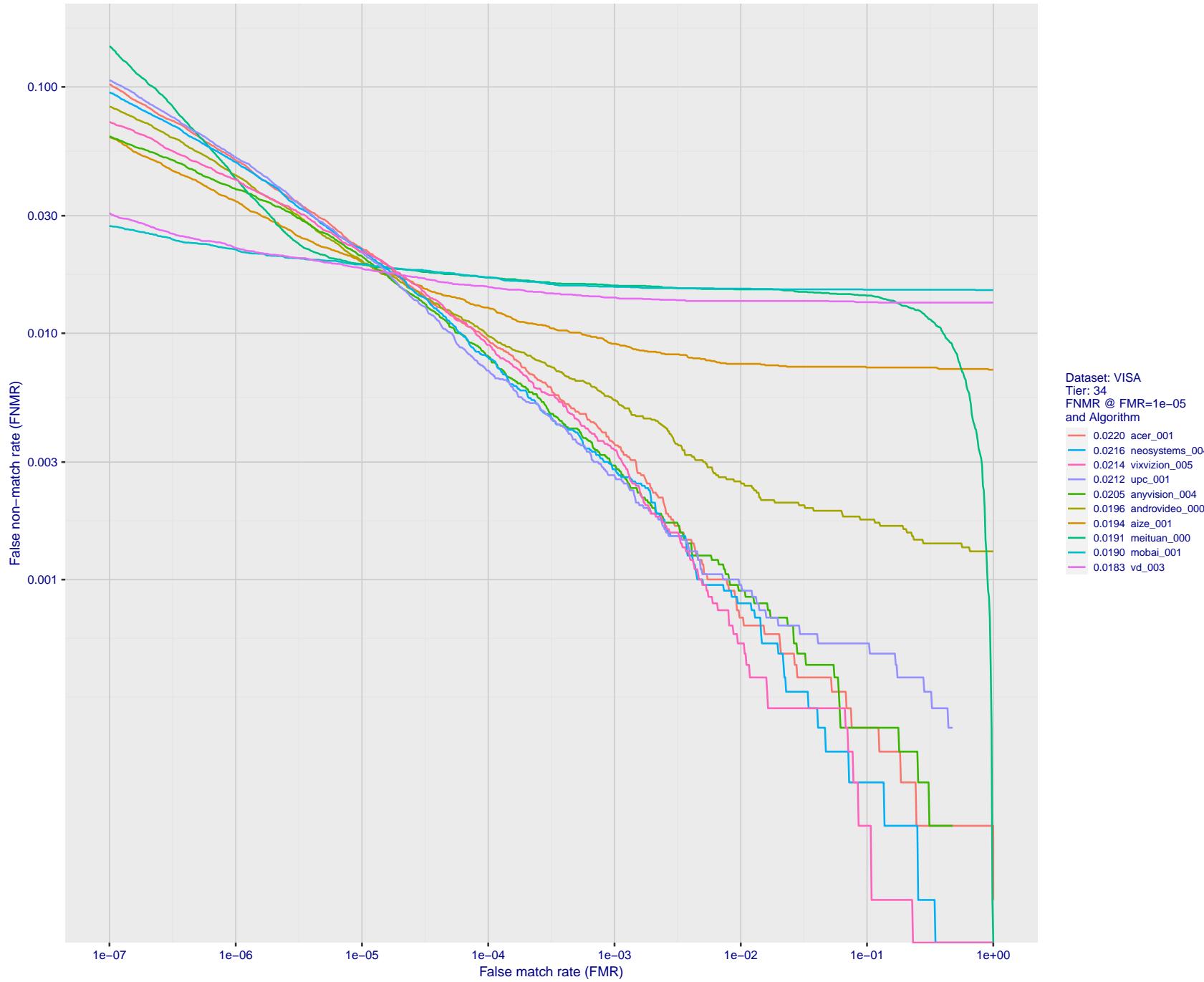


Figure 73: For the visa images, detection error tradeoff (DET) characteristics showing false non-match rate vs. false match rate plotted parametrically on threshold, T . The scales are logarithmic in order to show many decades of FMR.

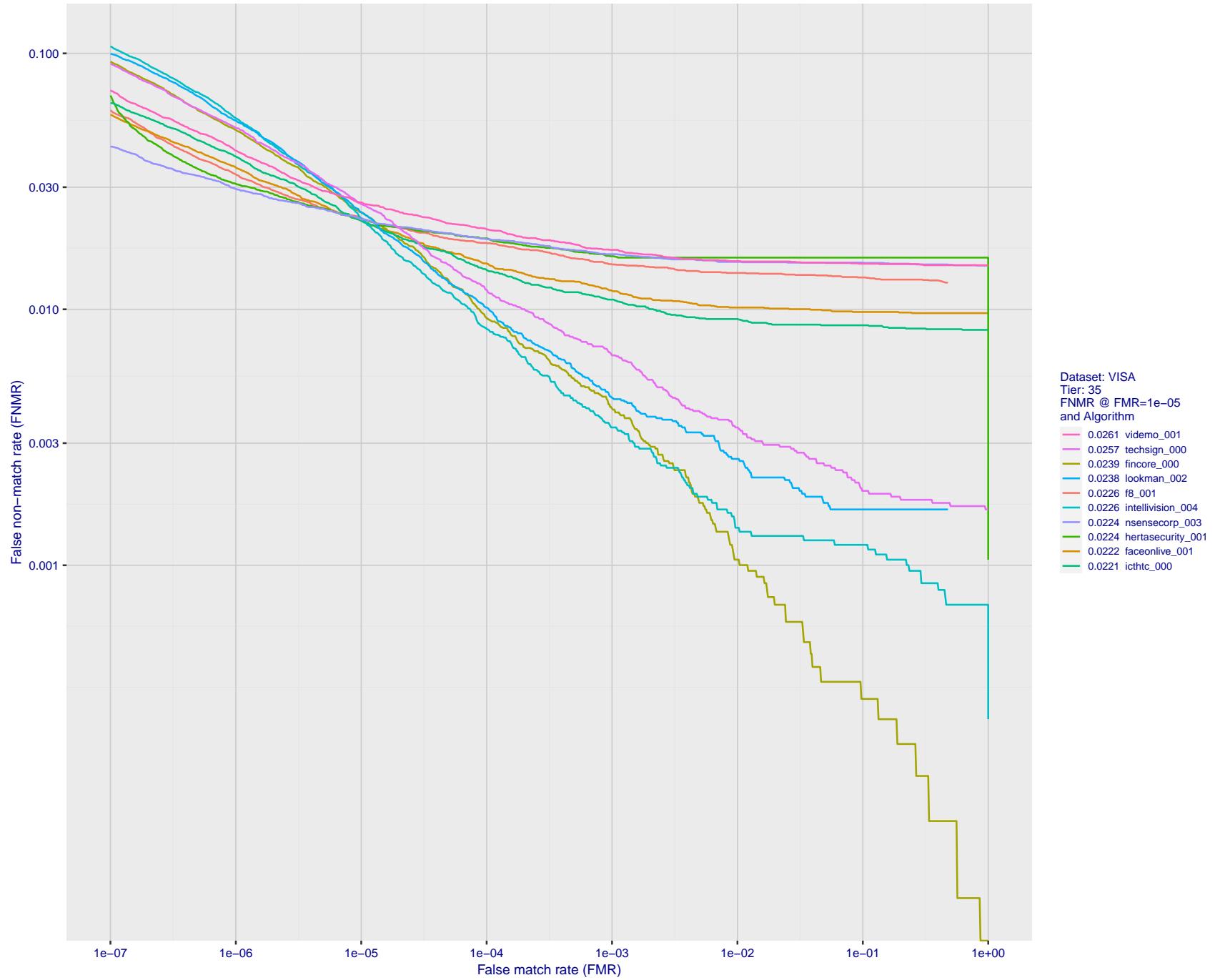


Figure 74: For the visa images, detection error tradeoff (DET) characteristics showing false non-match rate vs. false match rate plotted parametrically on threshold, T . The scales are logarithmic in order to show many decades of FMR.

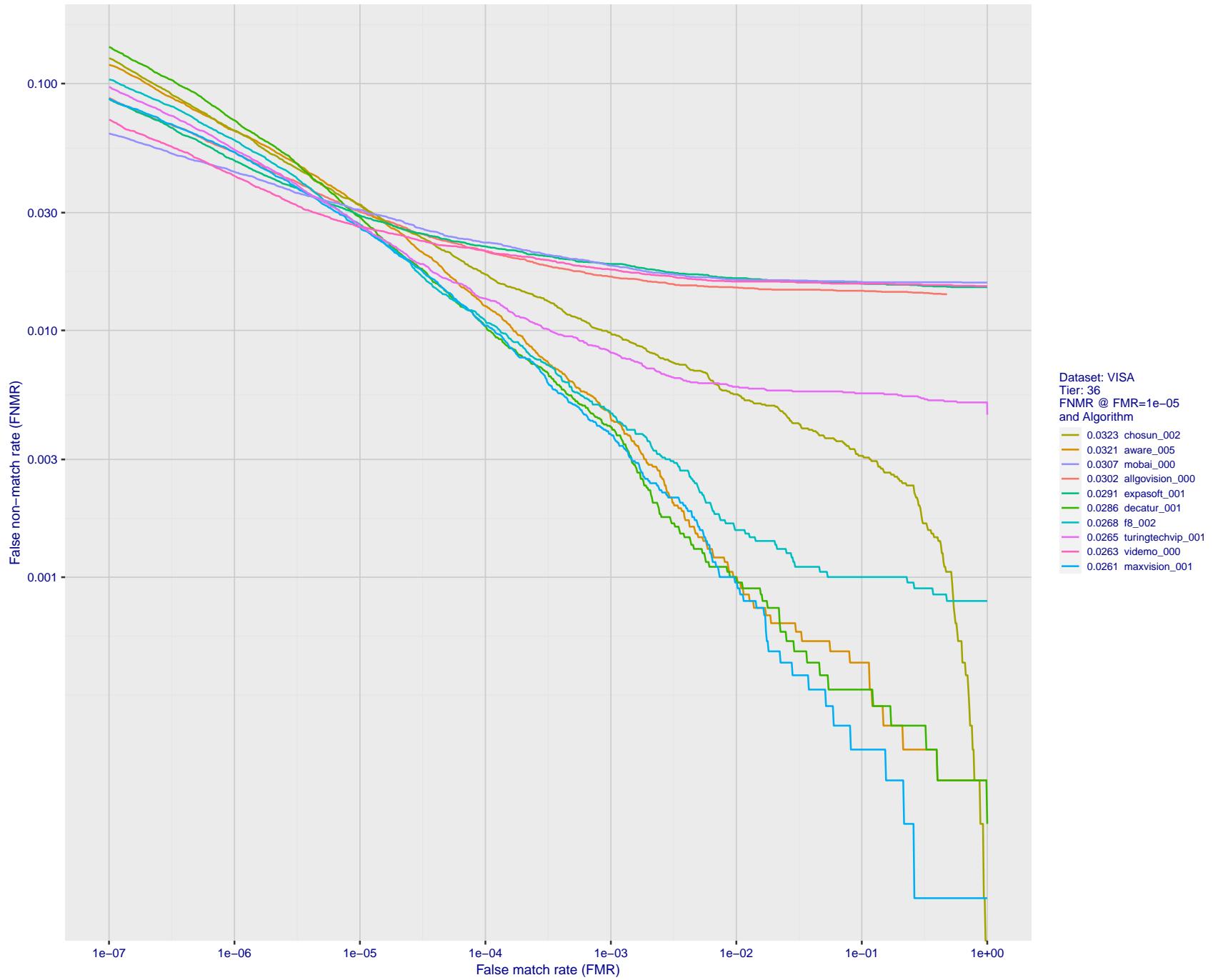


Figure 75: For the visa images, detection error tradeoff (DET) characteristics showing false non-match rate vs. false match rate plotted parametrically on threshold, T . The scales are logarithmic in order to show many decades of FMR.

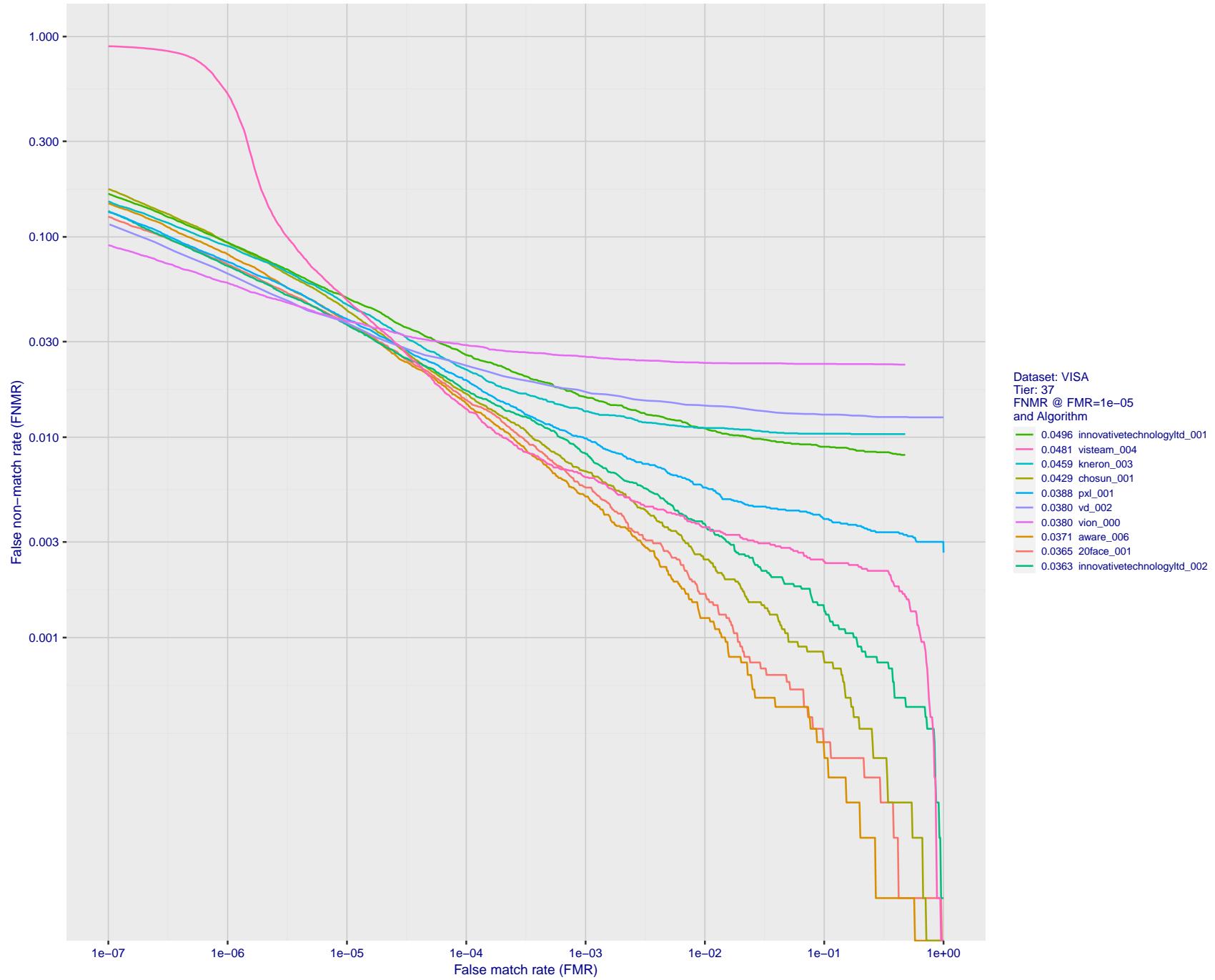


Figure 76: For the visa images, detection error tradeoff (DET) characteristics showing false non-match rate vs. false match rate plotted parametrically on threshold, T . The scales are logarithmic in order to show many decades of FMR.

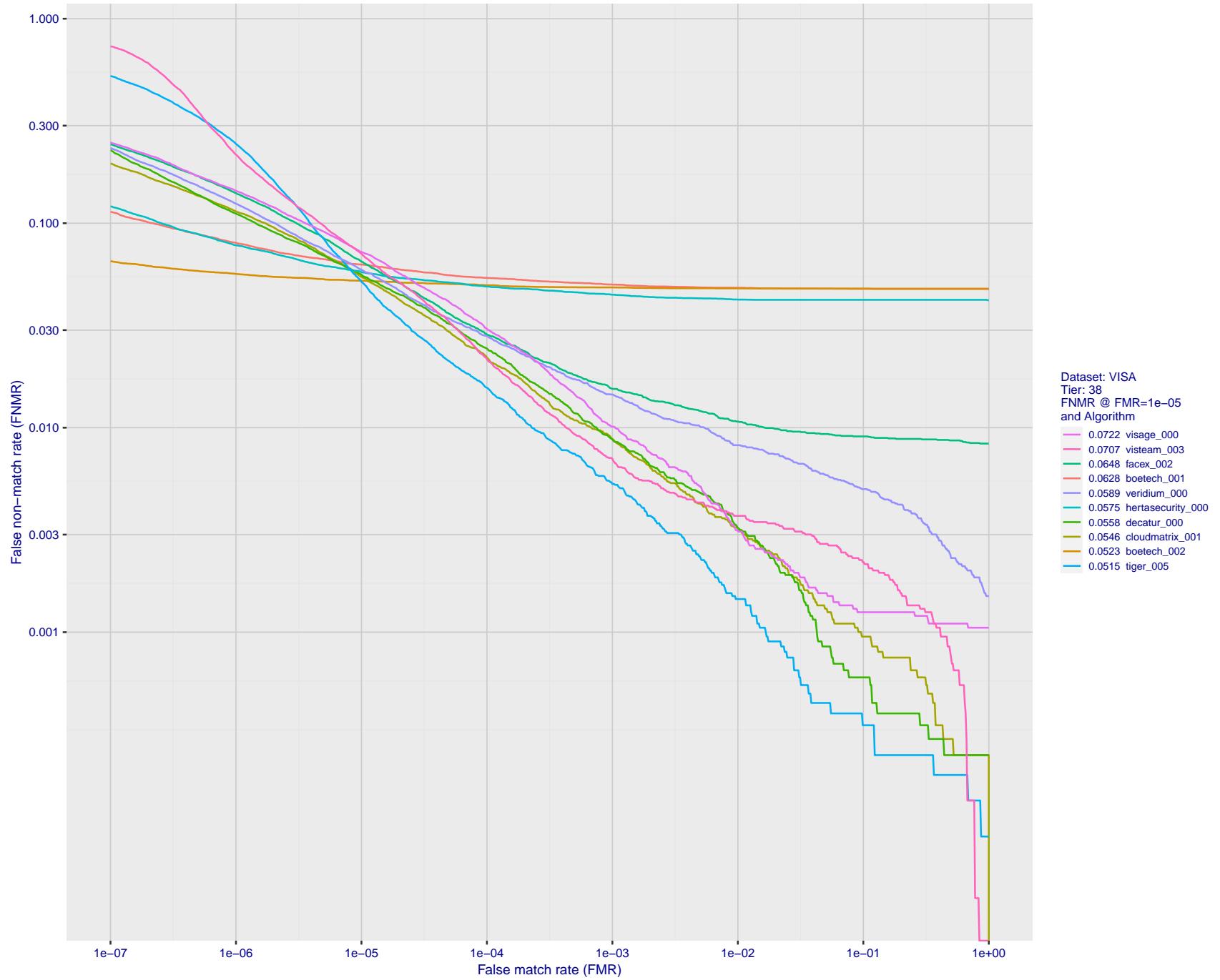


Figure 77: For the visa images, detection error tradeoff (DET) characteristics showing false non-match rate vs. false match rate plotted parametrically on threshold, T . The scales are logarithmic in order to show many decades of FMR.

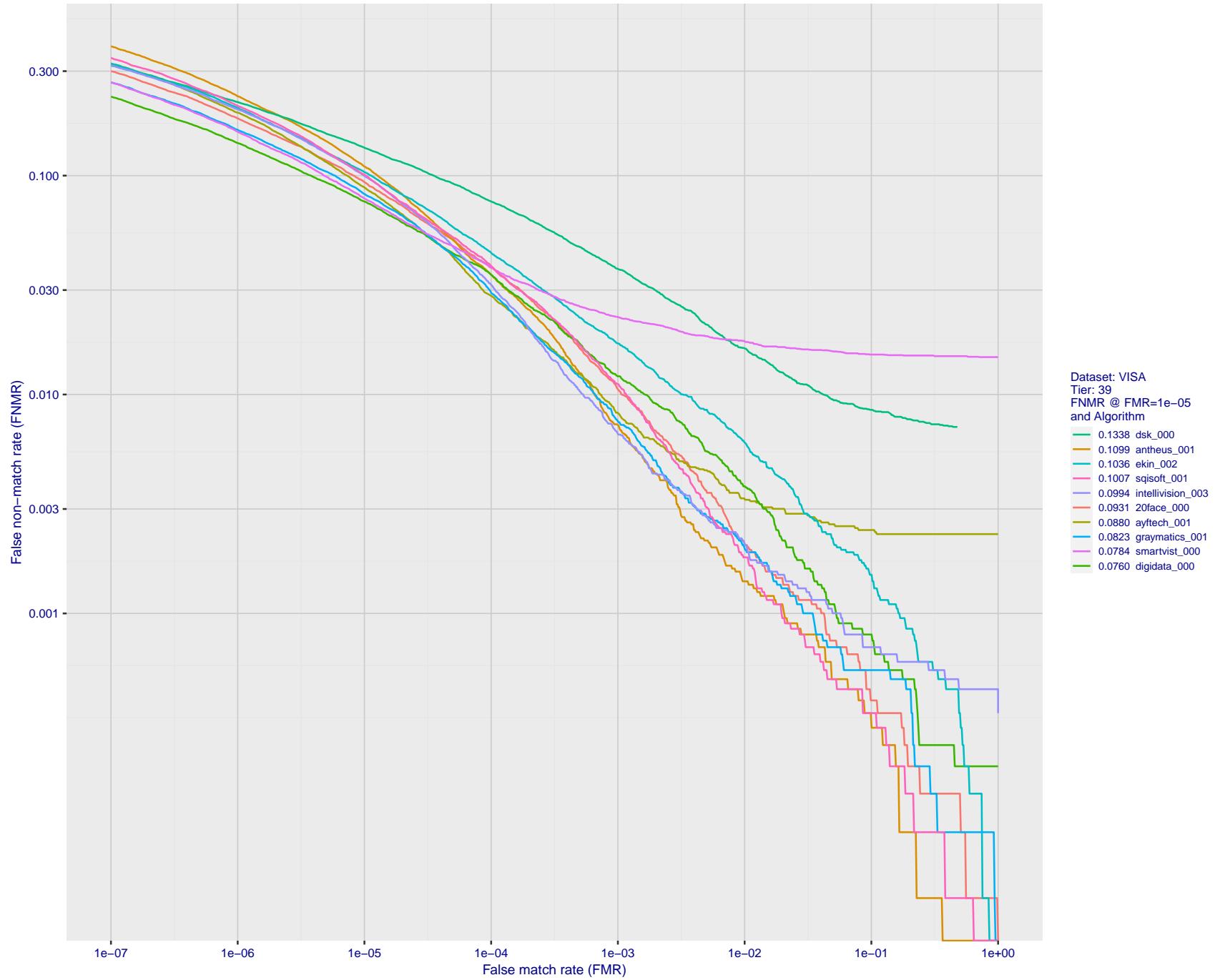


Figure 78: For the visa images, detection error tradeoff (DET) characteristics showing false non-match rate vs. false match rate plotted parametrically on threshold, T . The scales are logarithmic in order to show many decades of FMR.

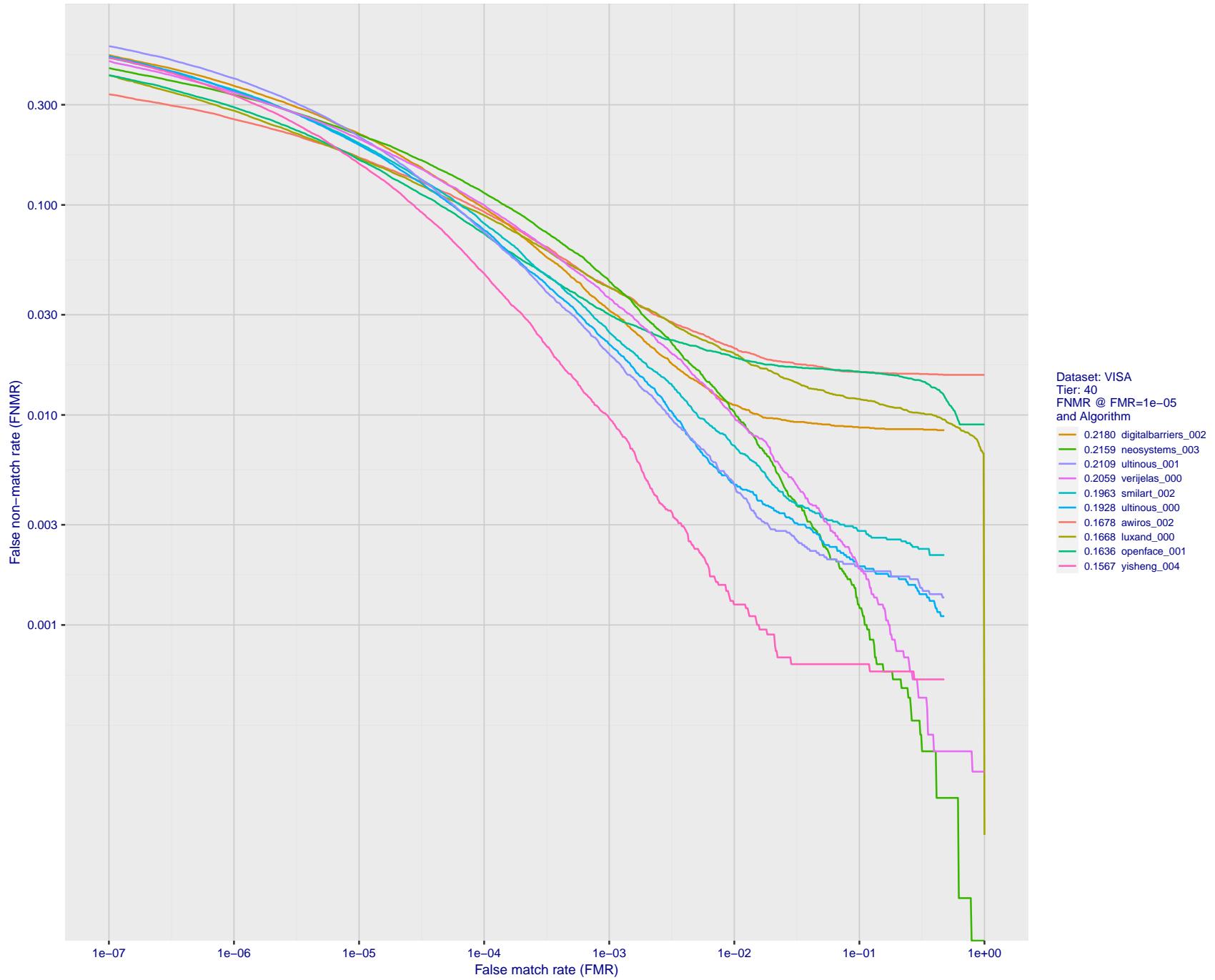


Figure 79: For the visa images, detection error tradeoff (DET) characteristics showing false non-match rate vs. false match rate plotted parametrically on threshold, T . The scales are logarithmic in order to show many decades of FMR.

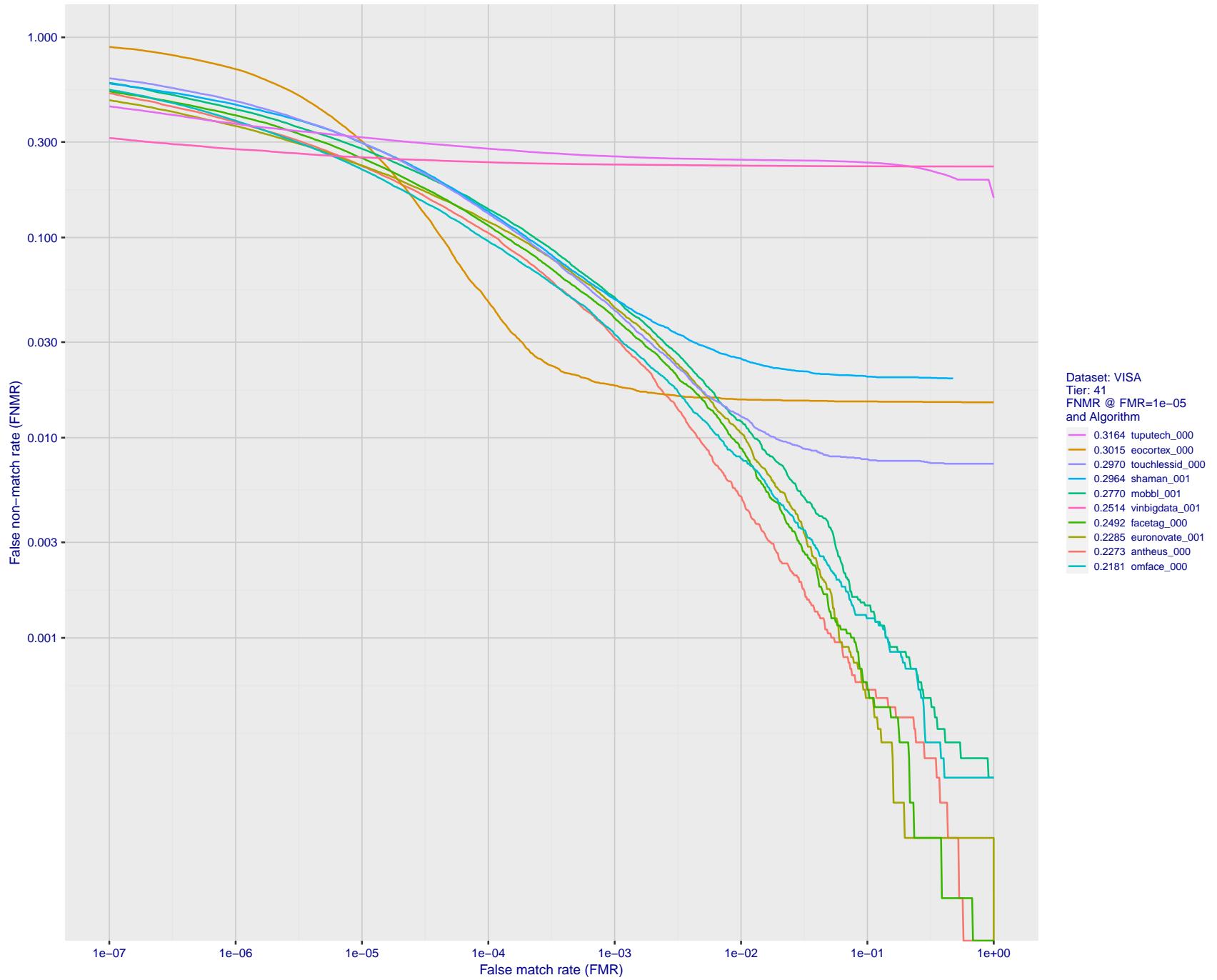
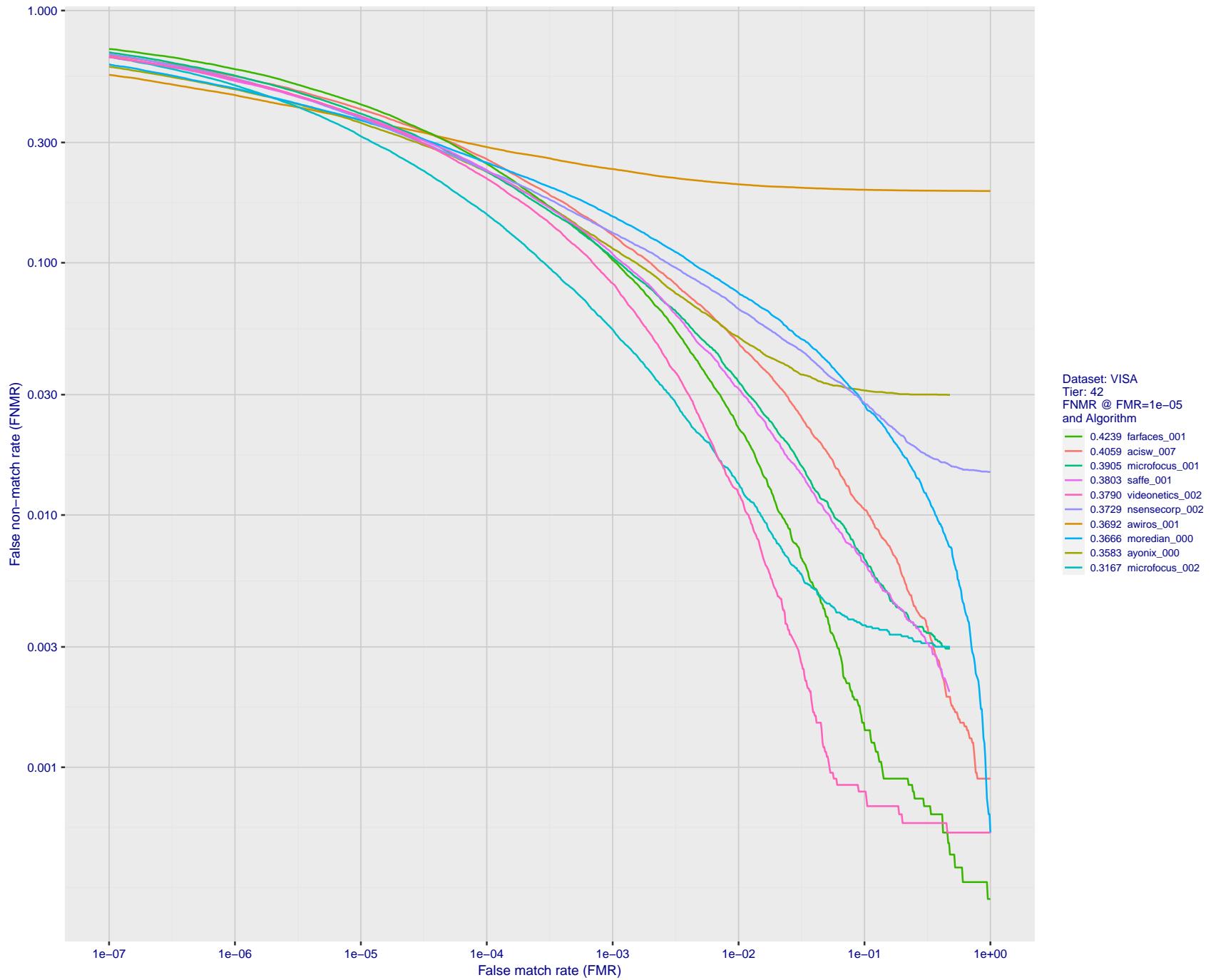


Figure 80: For the visa images, detection error tradeoff (DET) characteristics showing false non-match rate vs. false match rate plotted parametrically on threshold, T . The scales are logarithmic in order to show many decades of FMR.



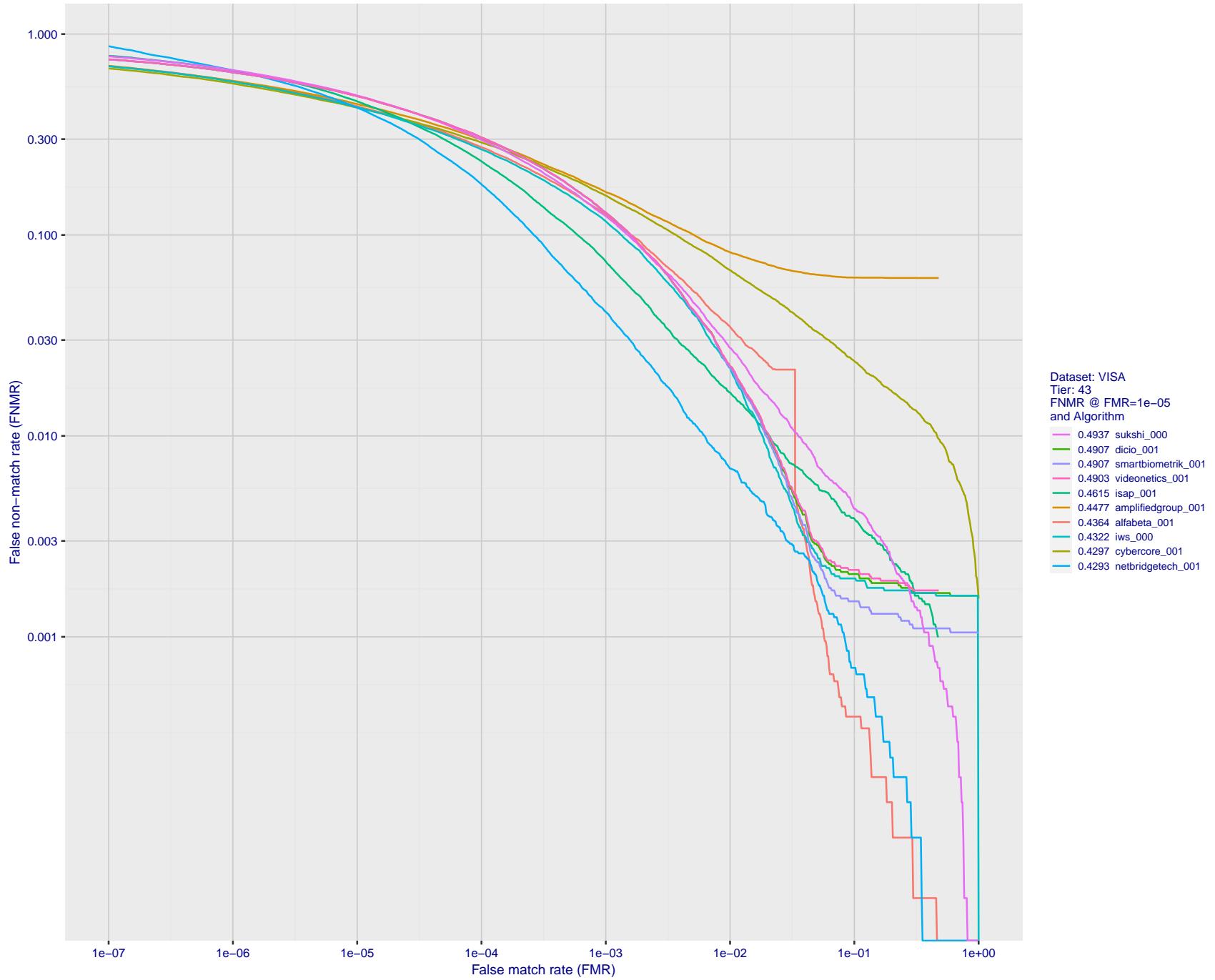


Figure 82: For the visa images, detection error tradeoff (DET) characteristics showing false non-match rate vs. false match rate plotted parametrically on threshold, T . The scales are logarithmic in order to show many decades of FMR.

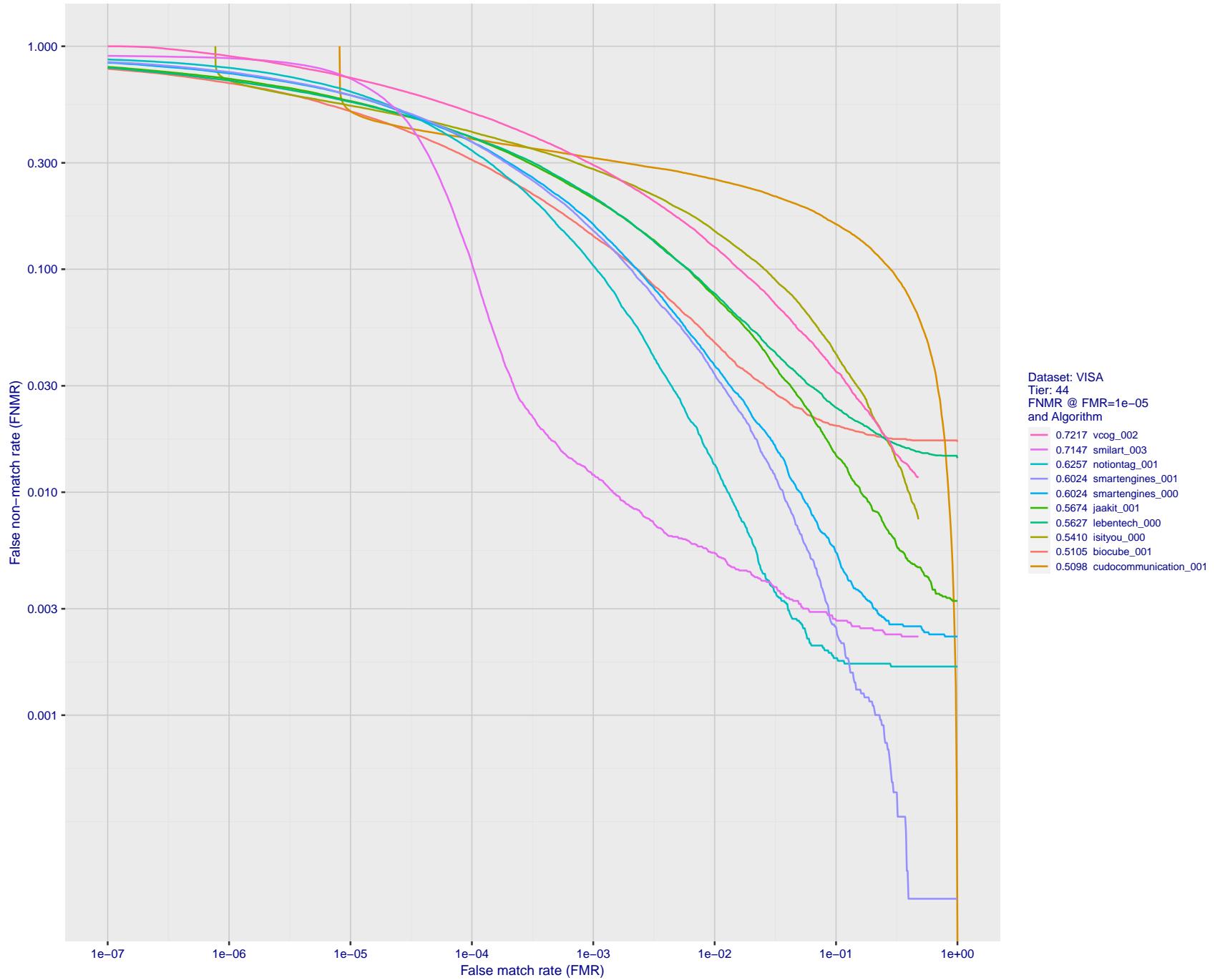


Figure 83: For the visa images, detection error tradeoff (DET) characteristics showing false non-match rate vs. false match rate plotted parametrically on threshold, T . The scales are logarithmic in order to show many decades of FMR.

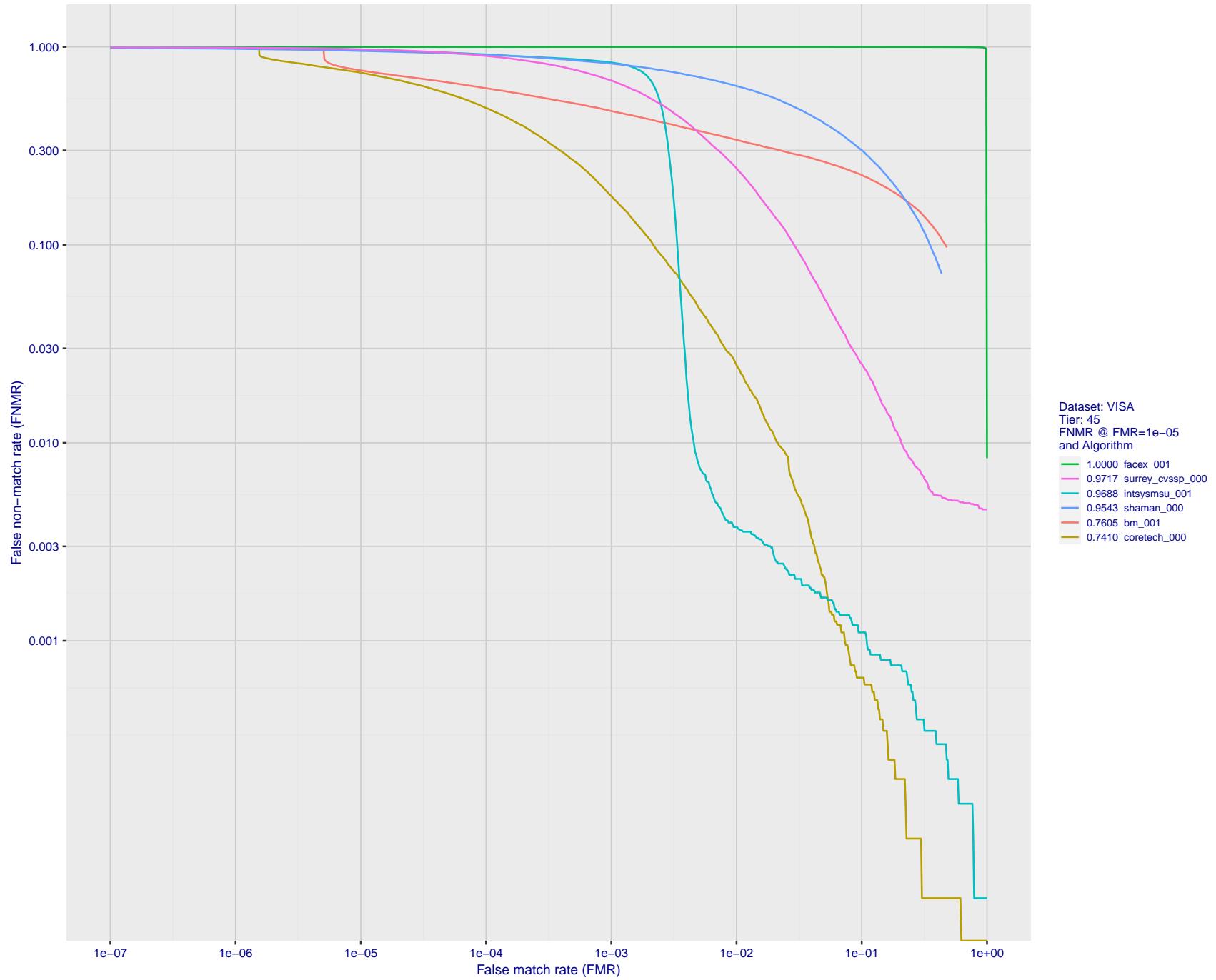
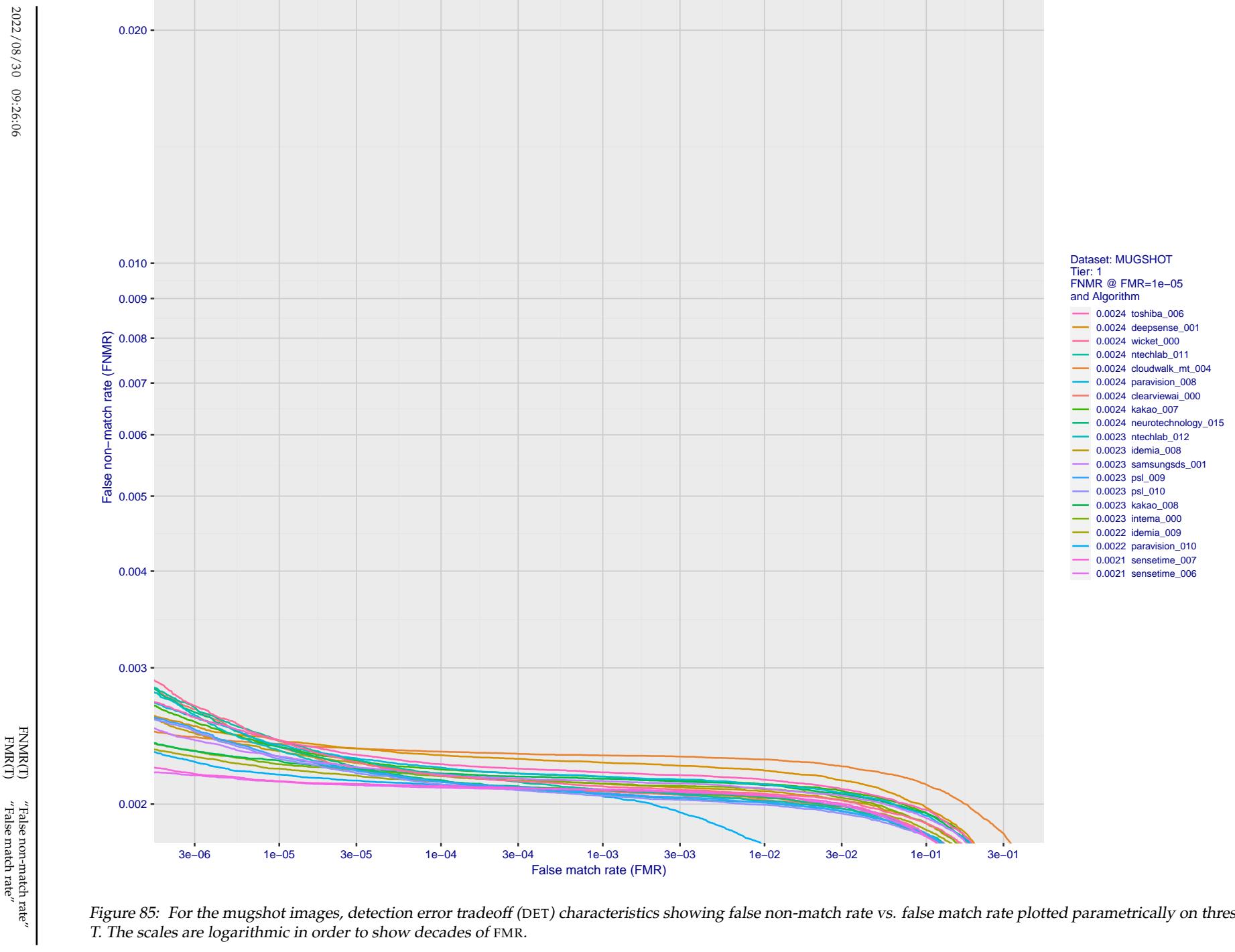


Figure 84: For the visa images, detection error tradeoff (DET) characteristics showing false non-match rate vs. false match rate plotted parametrically on threshold, T . The scales are logarithmic in order to show many decades of FMR.



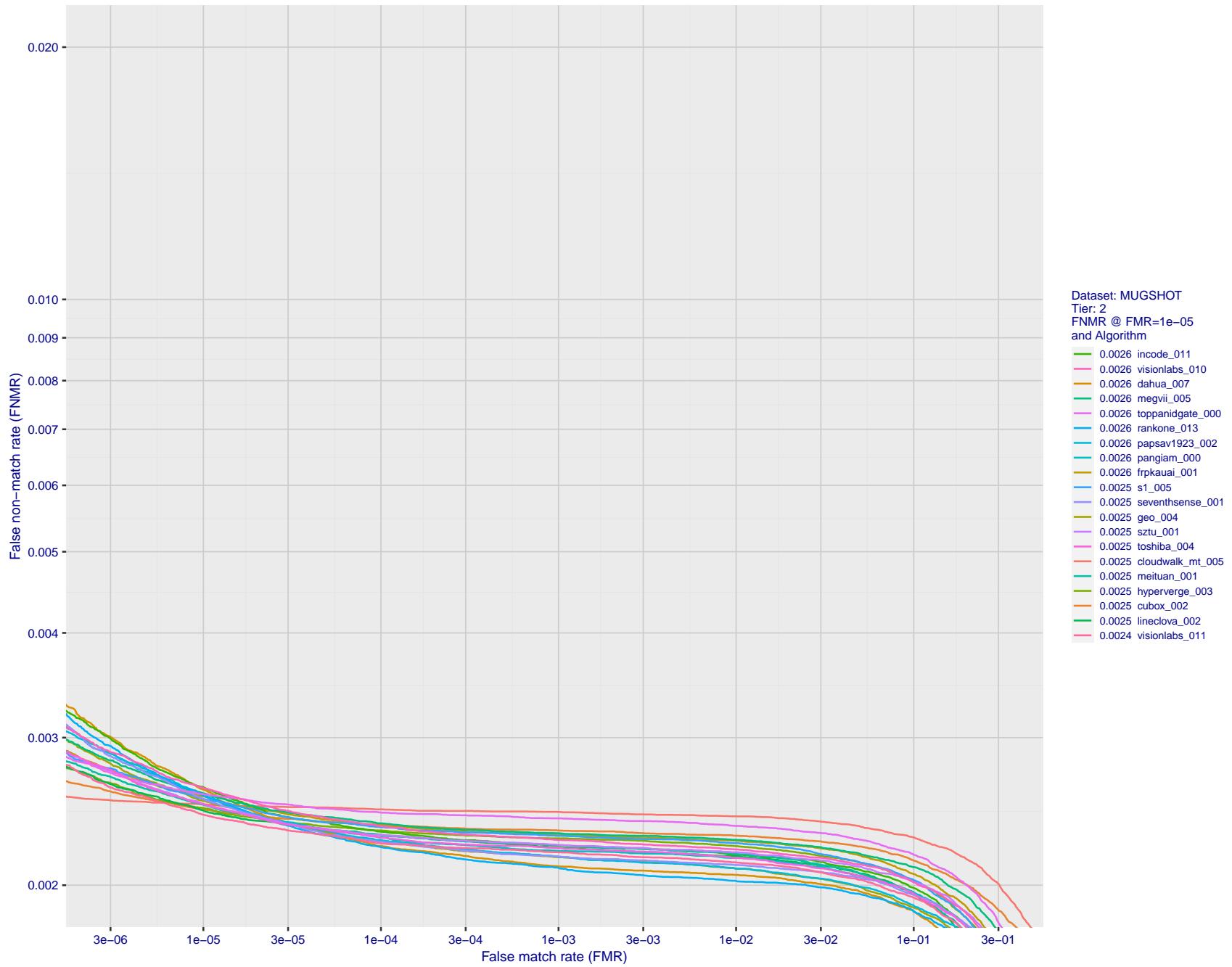


Figure 86: For the mugshot images, detection error tradeoff (DET) characteristics showing false non-match rate vs. false match rate plotted parametrically on threshold, T . The scales are logarithmic in order to show decades of FMR.

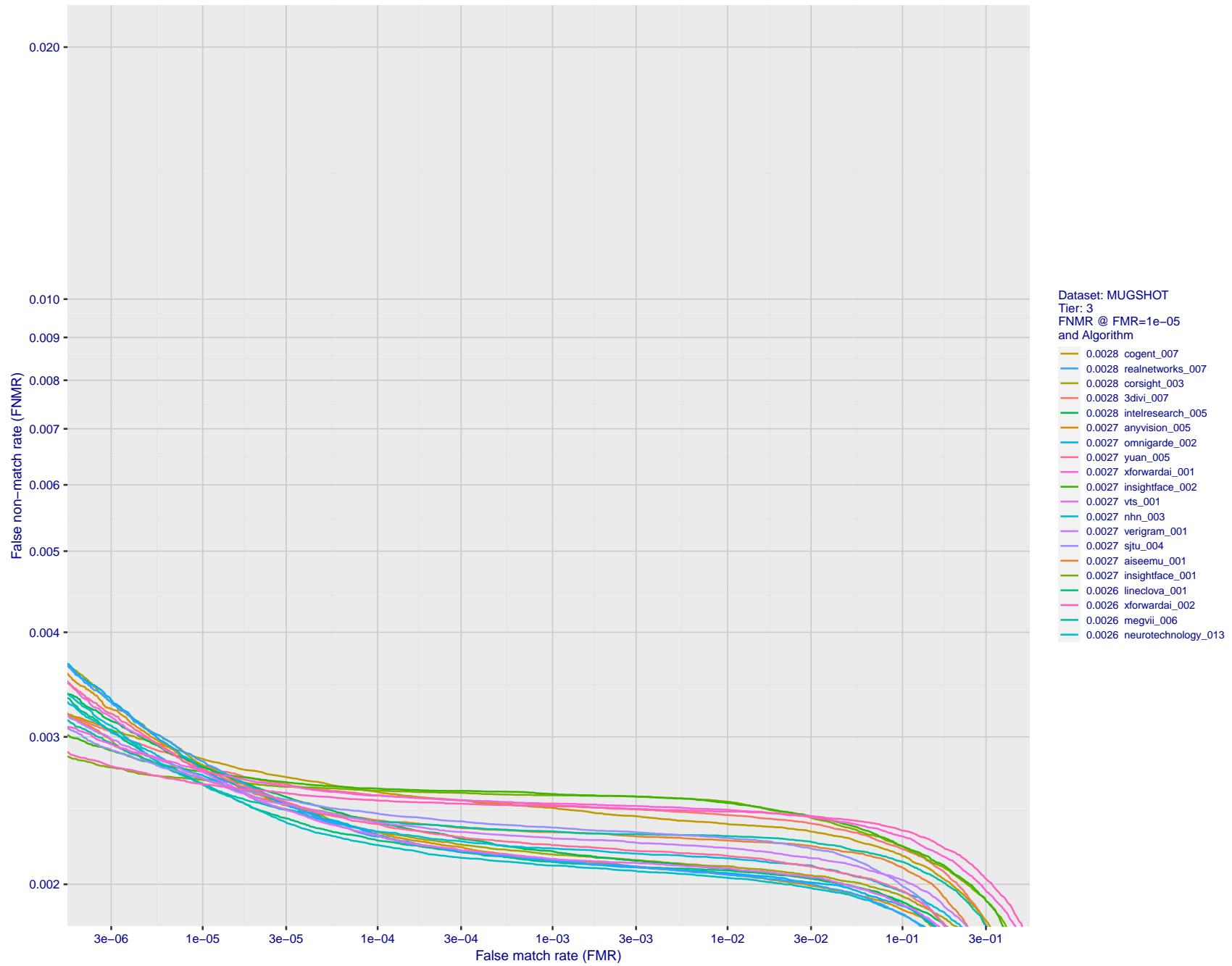


Figure 87: For the mugshot images, detection error tradeoff (DET) characteristics showing false non-match rate vs. false match rate plotted parametrically on threshold, T . The scales are logarithmic in order to show decades of FMR.

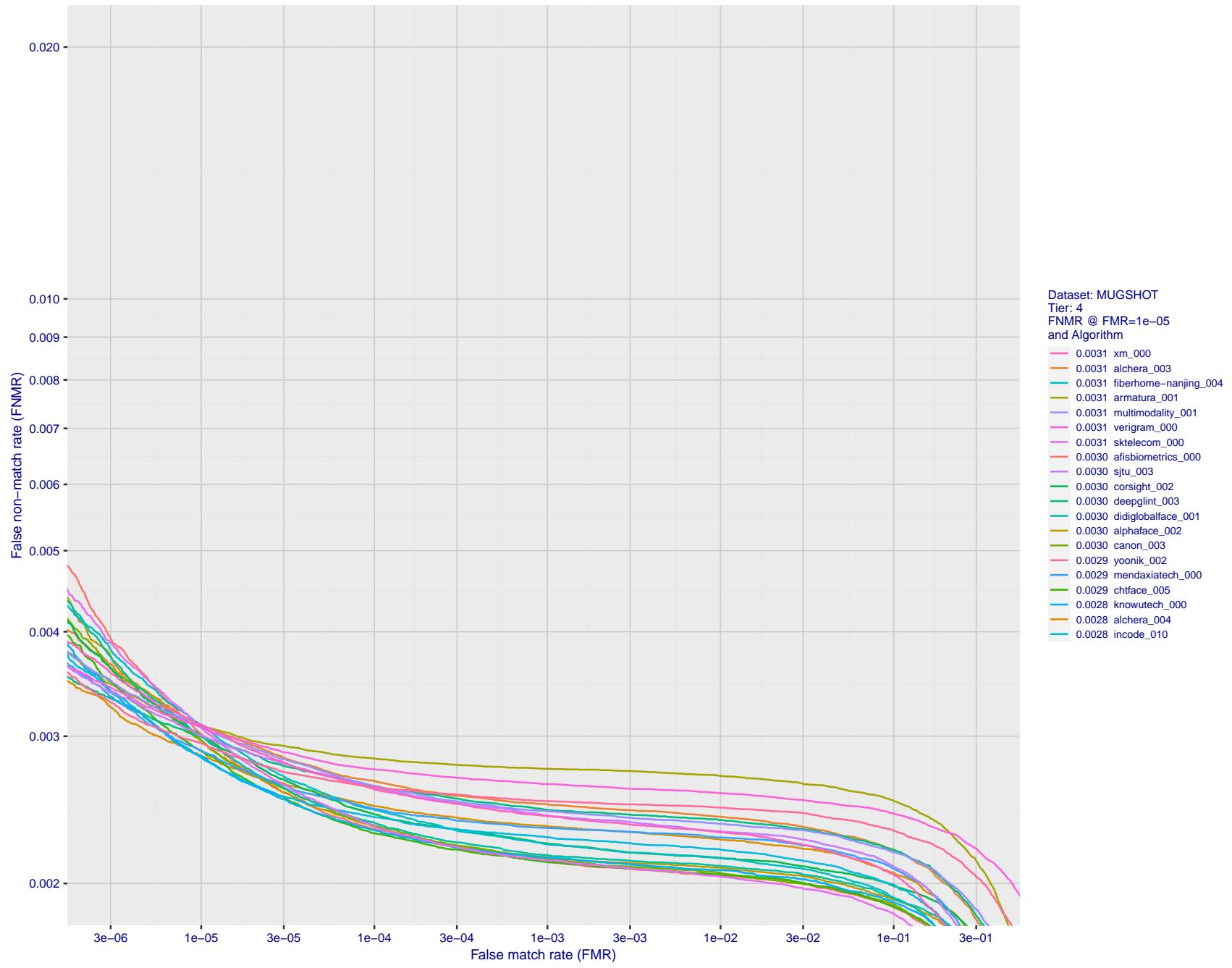


Figure 88: For the mugshot images, detection error tradeoff (DET) characteristics showing false non-match rate vs. false match rate plotted parametrically on threshold, T . The scales are logarithmic in order to show decades of FMR.

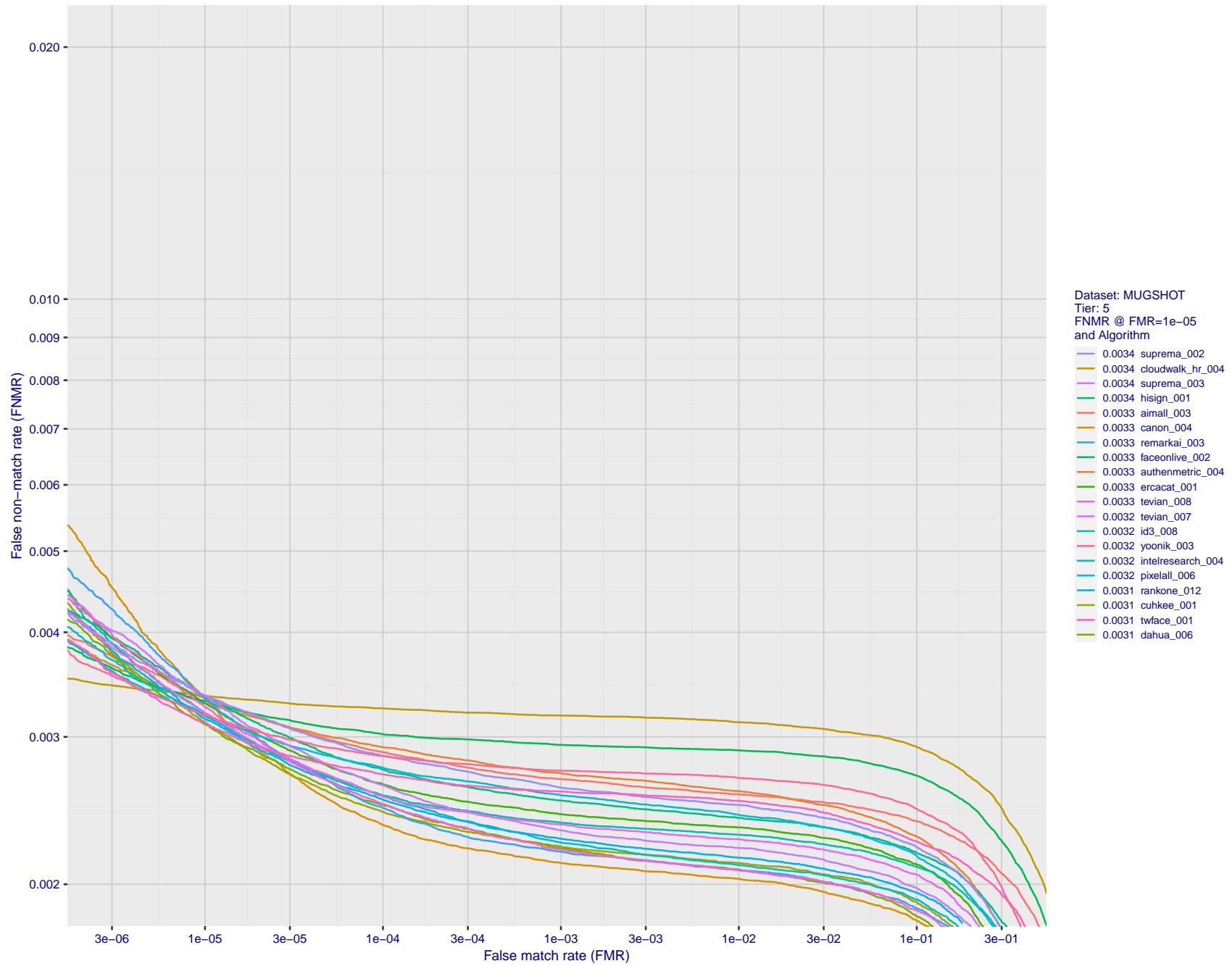


Figure 89: For the mugshot images, detection error tradeoff (DET) characteristics showing false non-match rate vs. false match rate plotted parametrically on threshold, T . The scales are logarithmic in order to show decades of FMR.

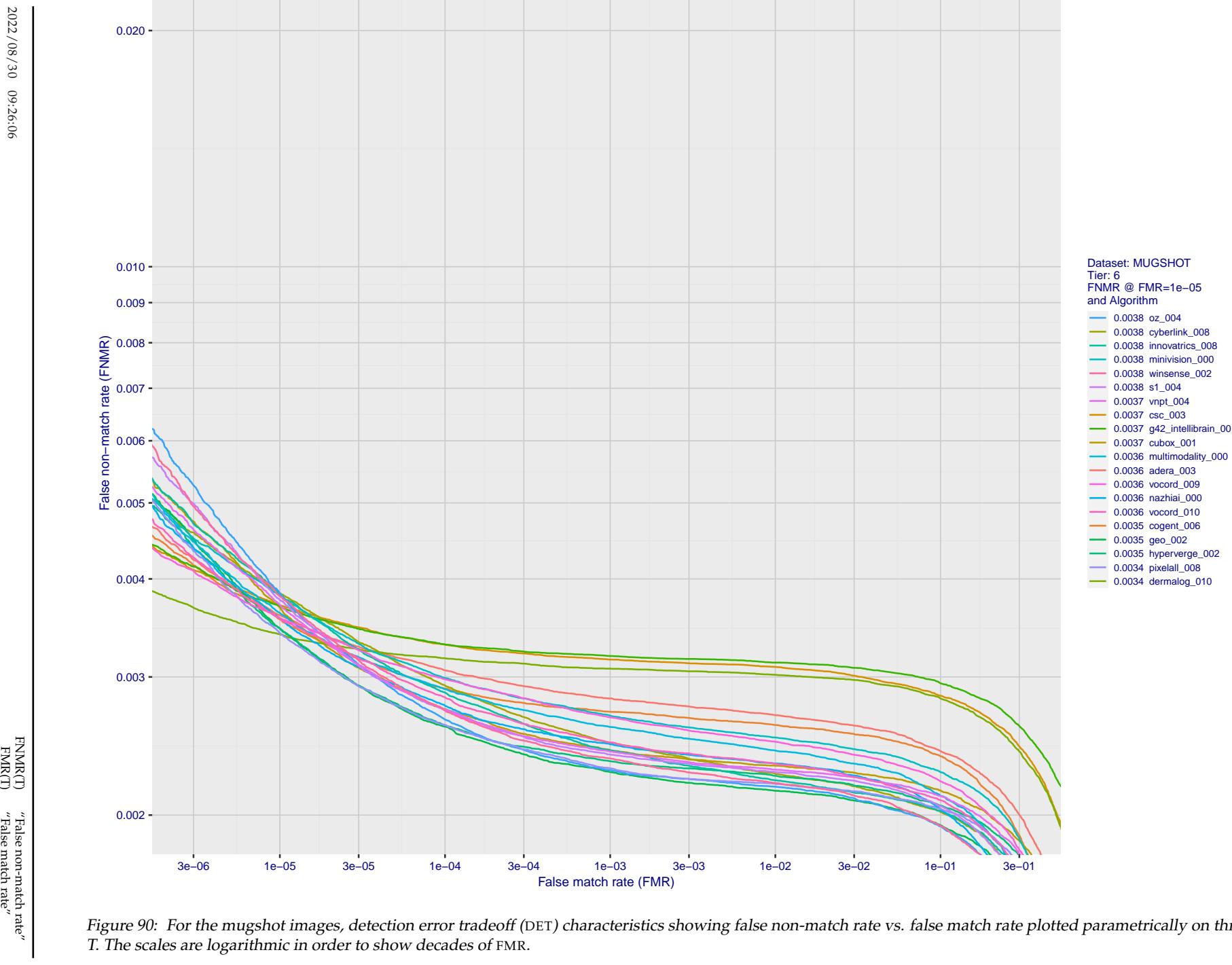


Figure 90: For the mugshot images, detection error tradeoff (DET) characteristics showing false non-match rate vs. false match rate plotted parametrically on threshold, T. The scales are logarithmic in order to show decades of FMR.

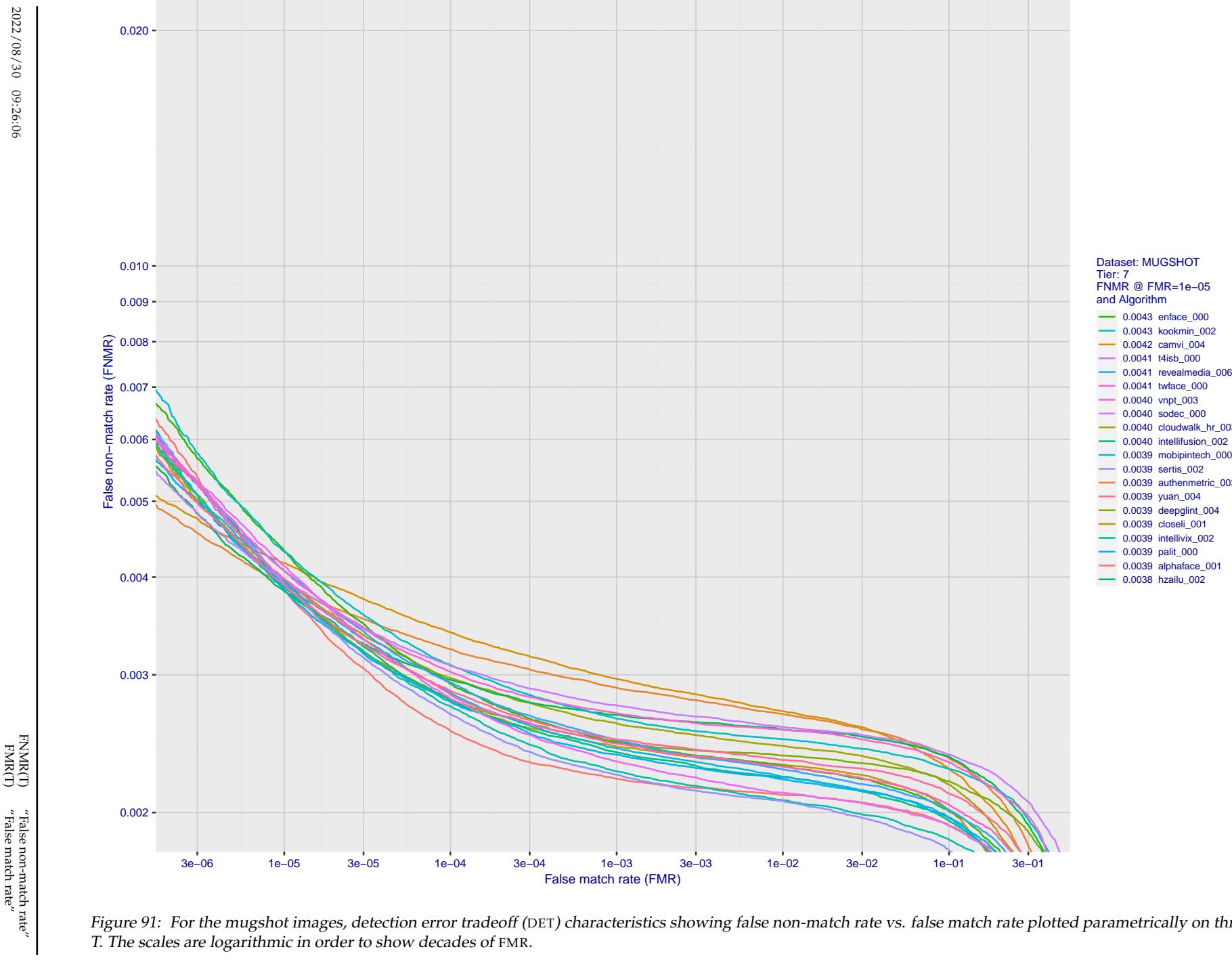


Figure 91: For the mugshot images, detection error tradeoff (DET) characteristics showing false non-match rate vs. false match rate plotted parametrically on threshold, T. The scales are logarithmic in order to show decades of FMR.

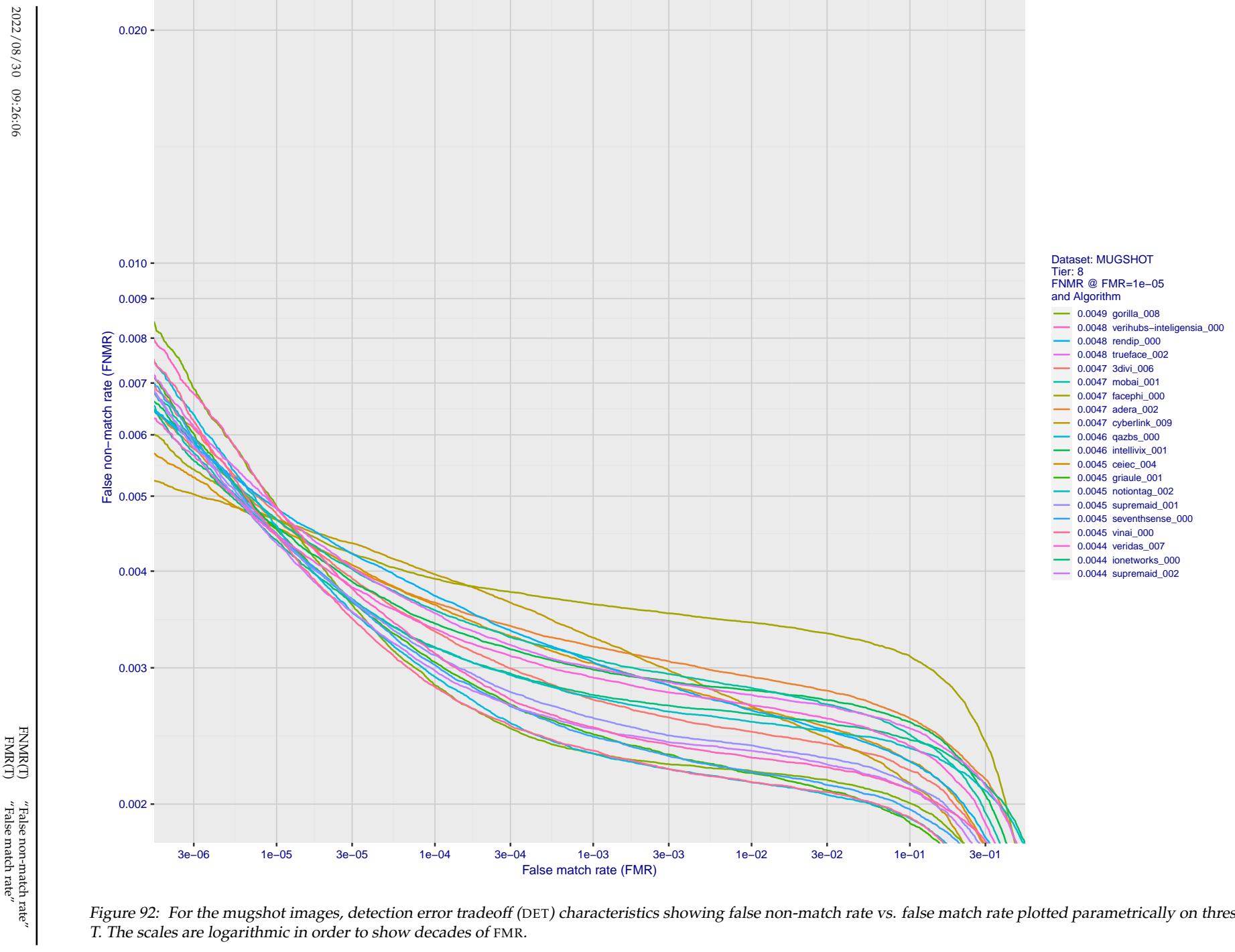


Figure 92: For the mugshot images, detection error tradeoff (DET) characteristics showing false non-match rate vs. false match rate plotted parametrically on threshold, T . The scales are logarithmic in order to show decades of FMR.

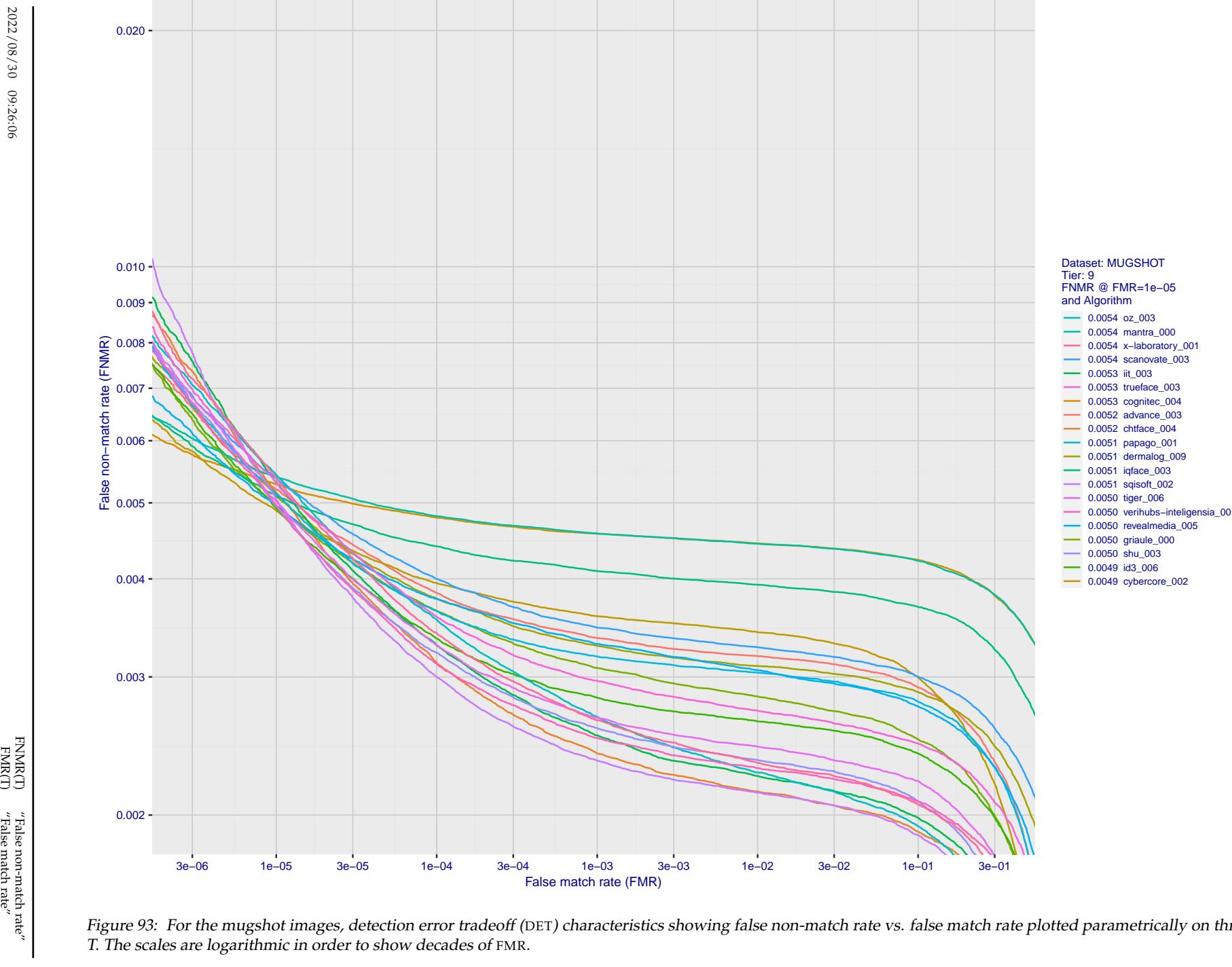


Figure 93: For the mugshot images, detection error tradeoff (DET) characteristics showing false non-match rate vs. false match rate plotted parametrically on threshold, T . The scales are logarithmic in order to show decades of FMR.

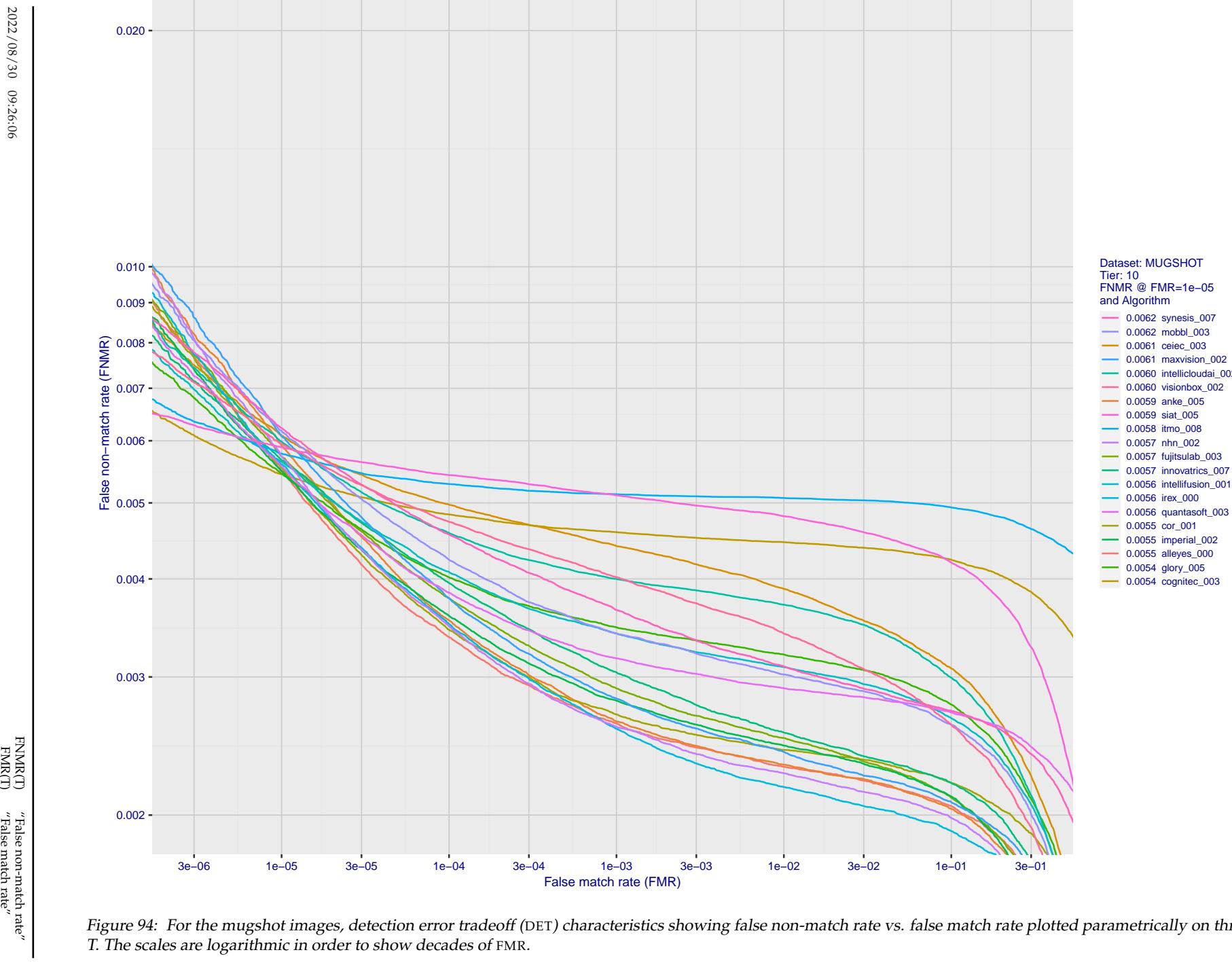
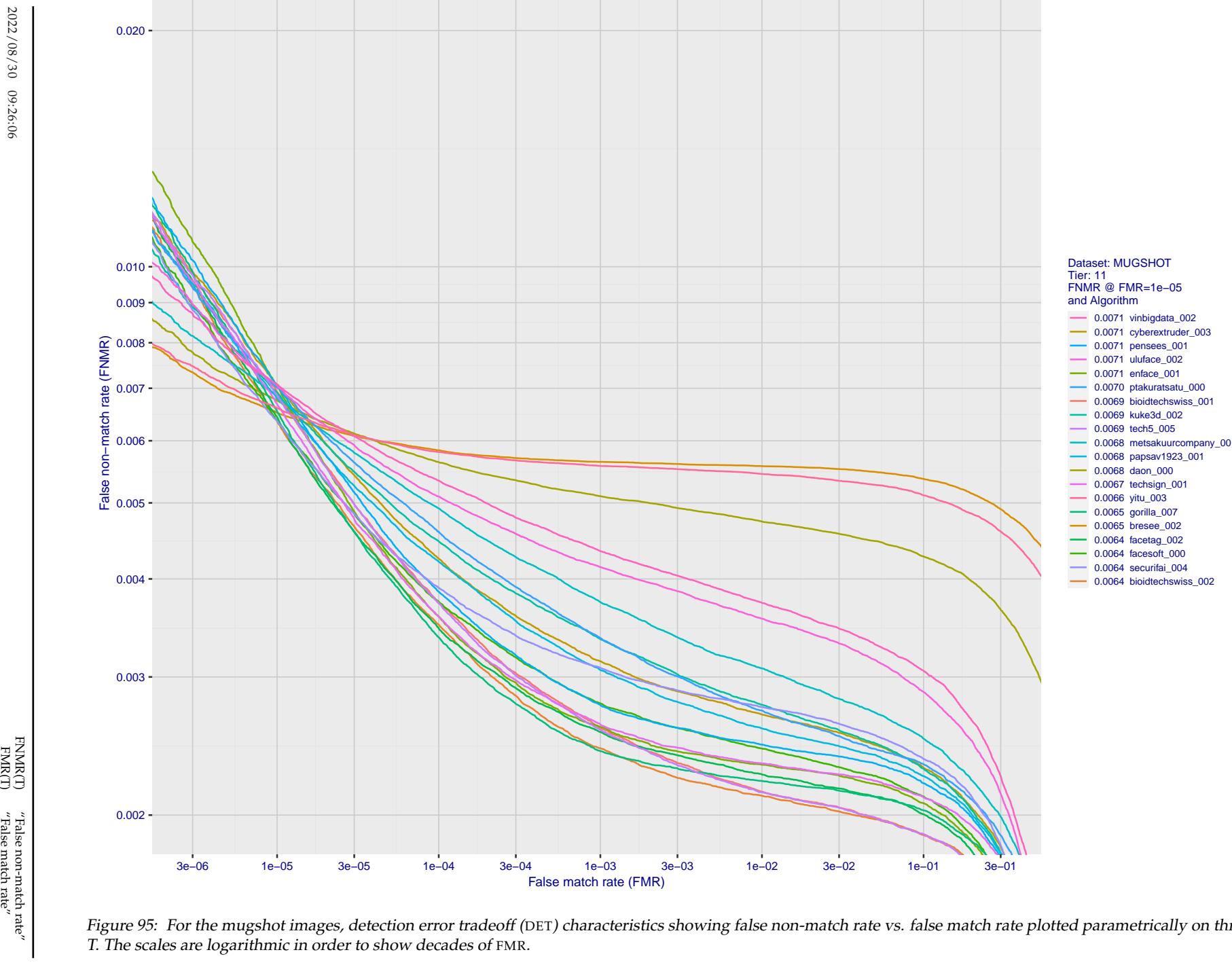


Figure 94: For the mugshot images, detection error tradeoff (DET) characteristics showing false non-match rate vs. false match rate plotted parametrically on threshold, T . The scales are logarithmic in order to show decades of FMR.



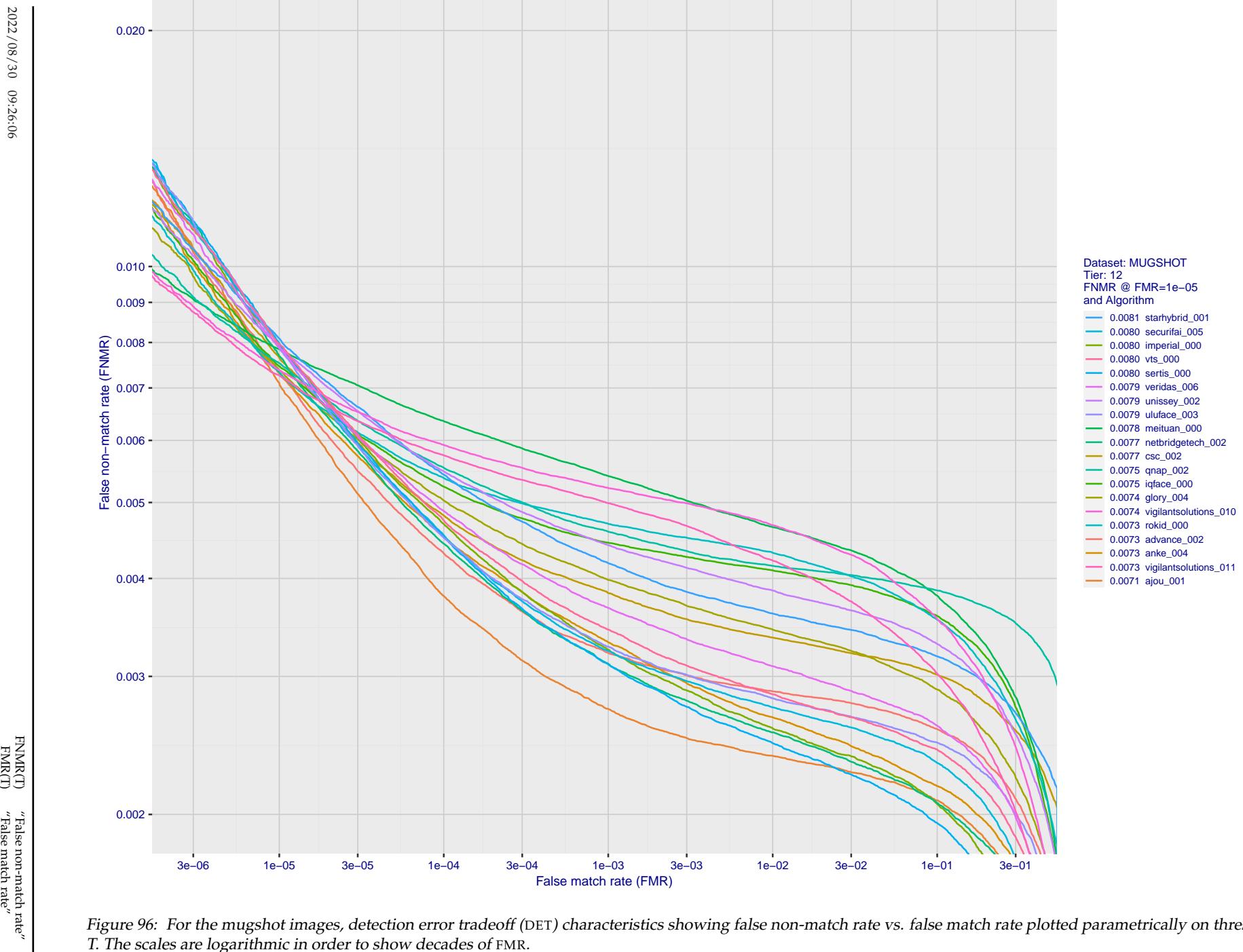


Figure 96: For the mugshot images, detection error tradeoff (DET) characteristics showing false non-match rate vs. false match rate plotted parametrically on threshold, T . The scales are logarithmic in order to show decades of FMR.

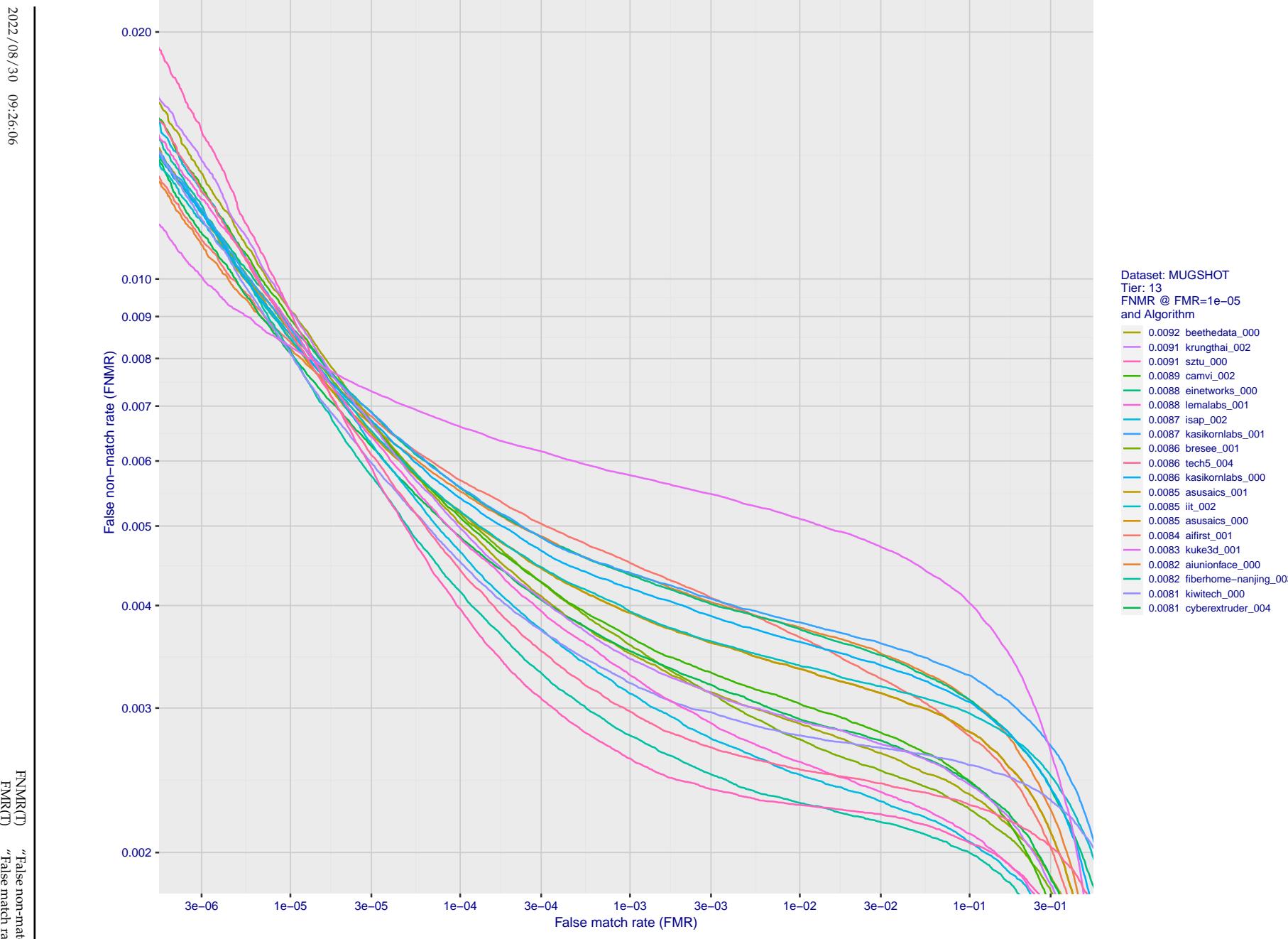


Figure 97: For the mugshot images, detection error tradeoff (DET) characteristics showing false non-match rate vs. false match rate plotted parametrically on threshold, T . The scales are logarithmic in order to show decades of FMR.

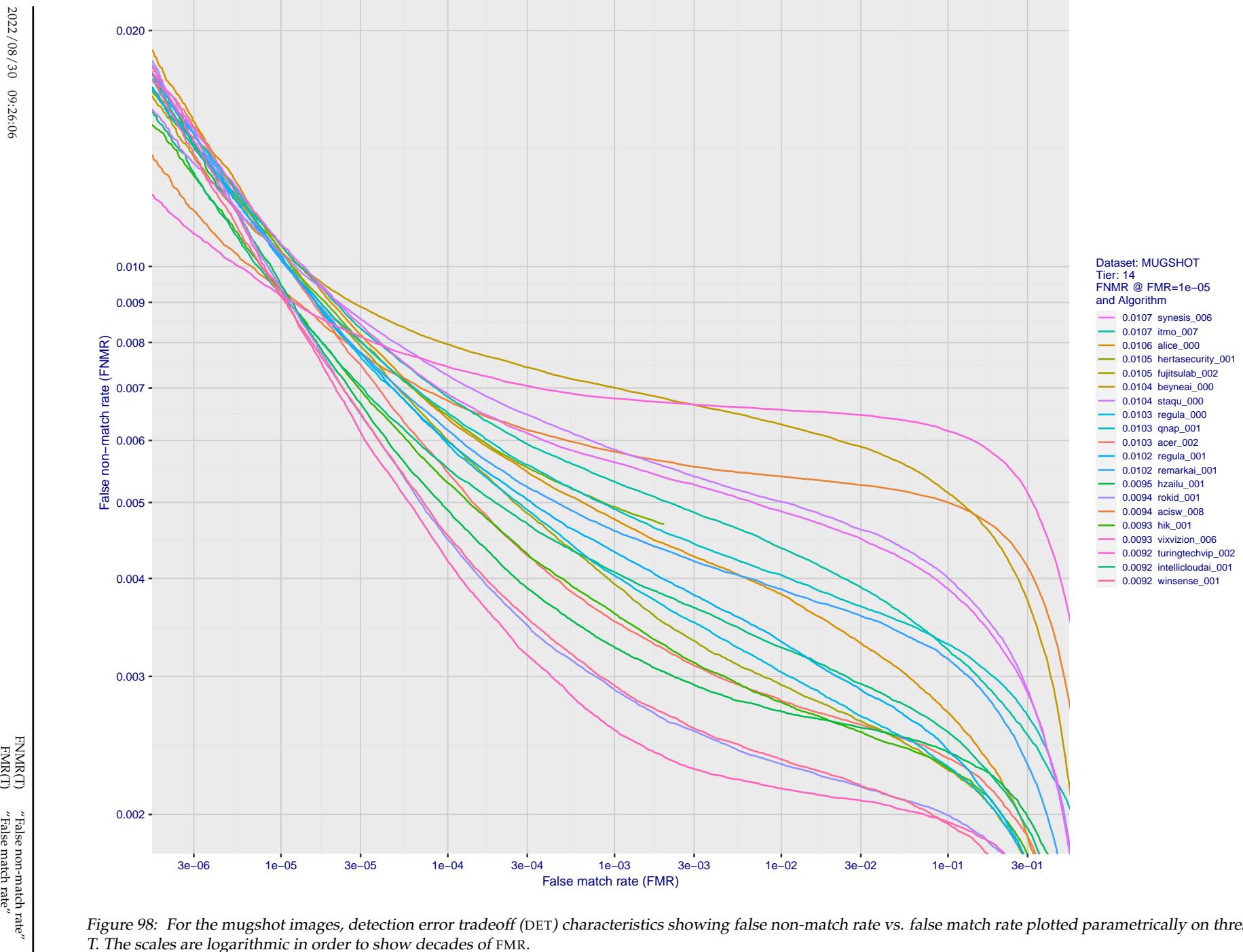


Figure 98: For the mugshot images, detection error tradeoff (DET) characteristics showing false non-match rate vs. false match rate plotted parametrically on threshold, T . The scales are logarithmic in order to show decades of FMR.

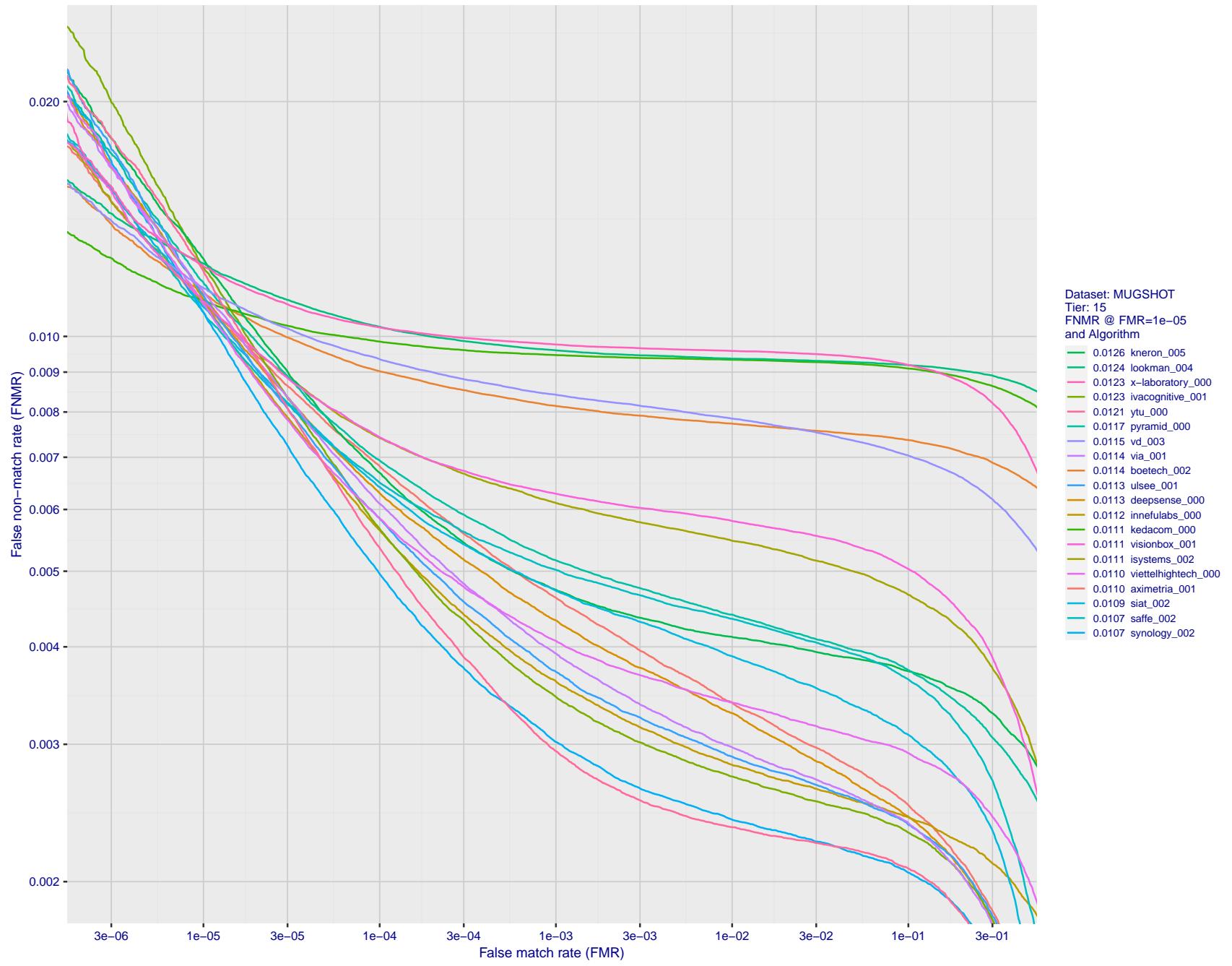


Figure 99: For the mugshot images, detection error tradeoff (DET) characteristics showing false non-match rate vs. false match rate plotted parametrically on threshold, T. The scales are logarithmic in order to show decades of FMR.

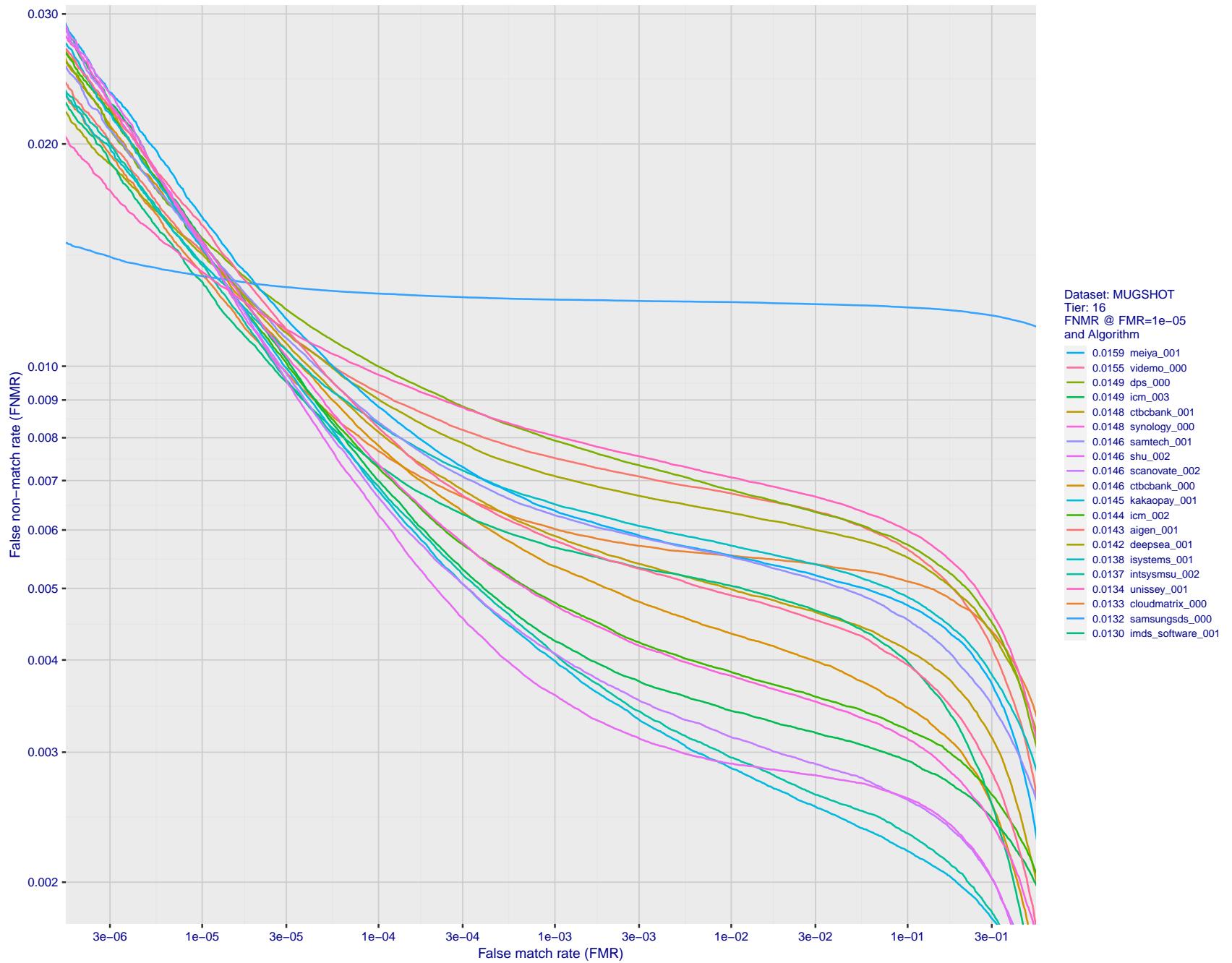


Figure 100: For the mugshot images, detection error tradeoff (DET) characteristics showing false non-match rate vs. false match rate plotted parametrically on threshold, T . The scales are logarithmic in order to show decades of FMR.

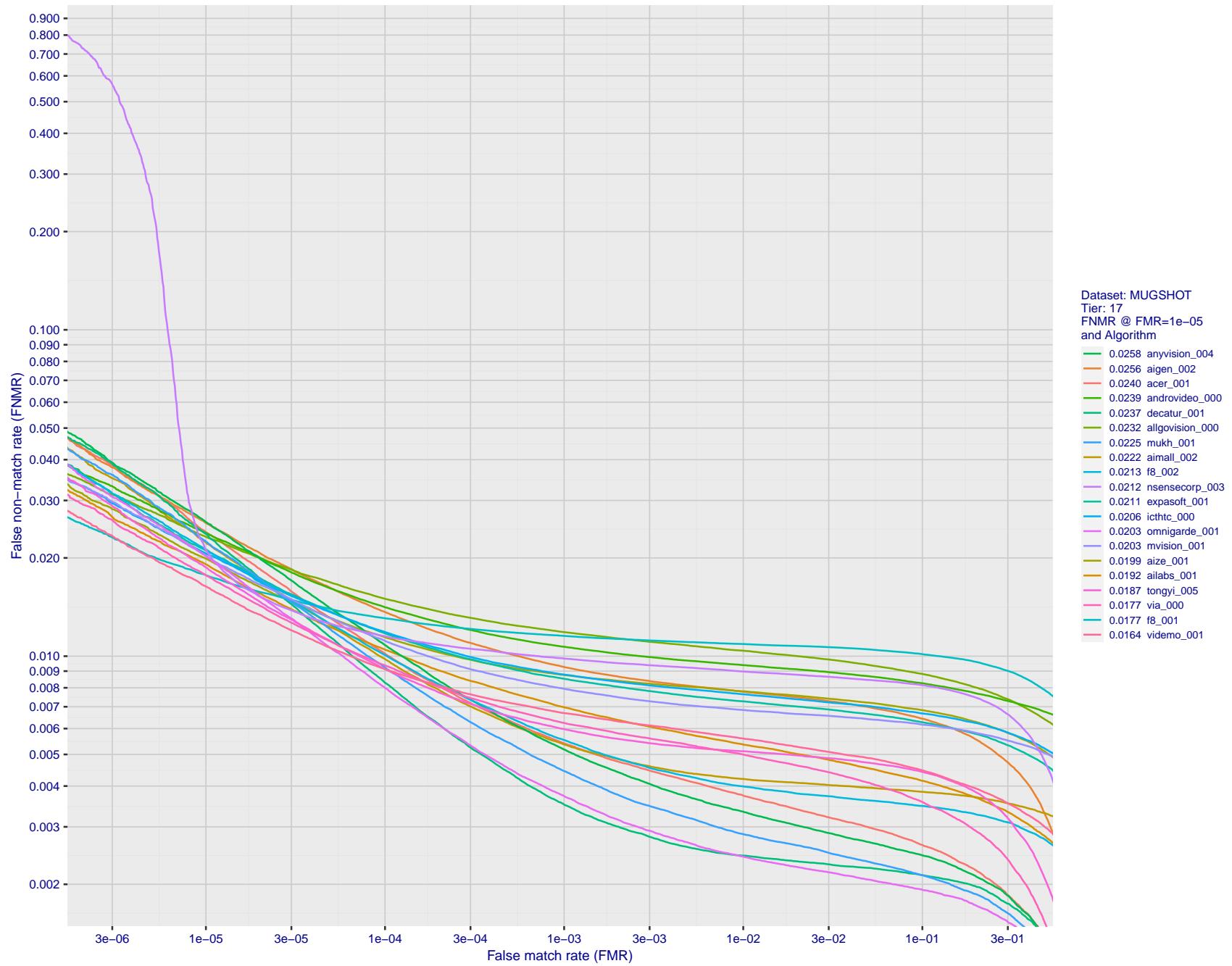


Figure 101: For the mugshot images, detection error tradeoff (DET) characteristics showing false non-match rate vs. false match rate plotted parametrically on threshold, T . The scales are logarithmic in order to show decades of FMR.

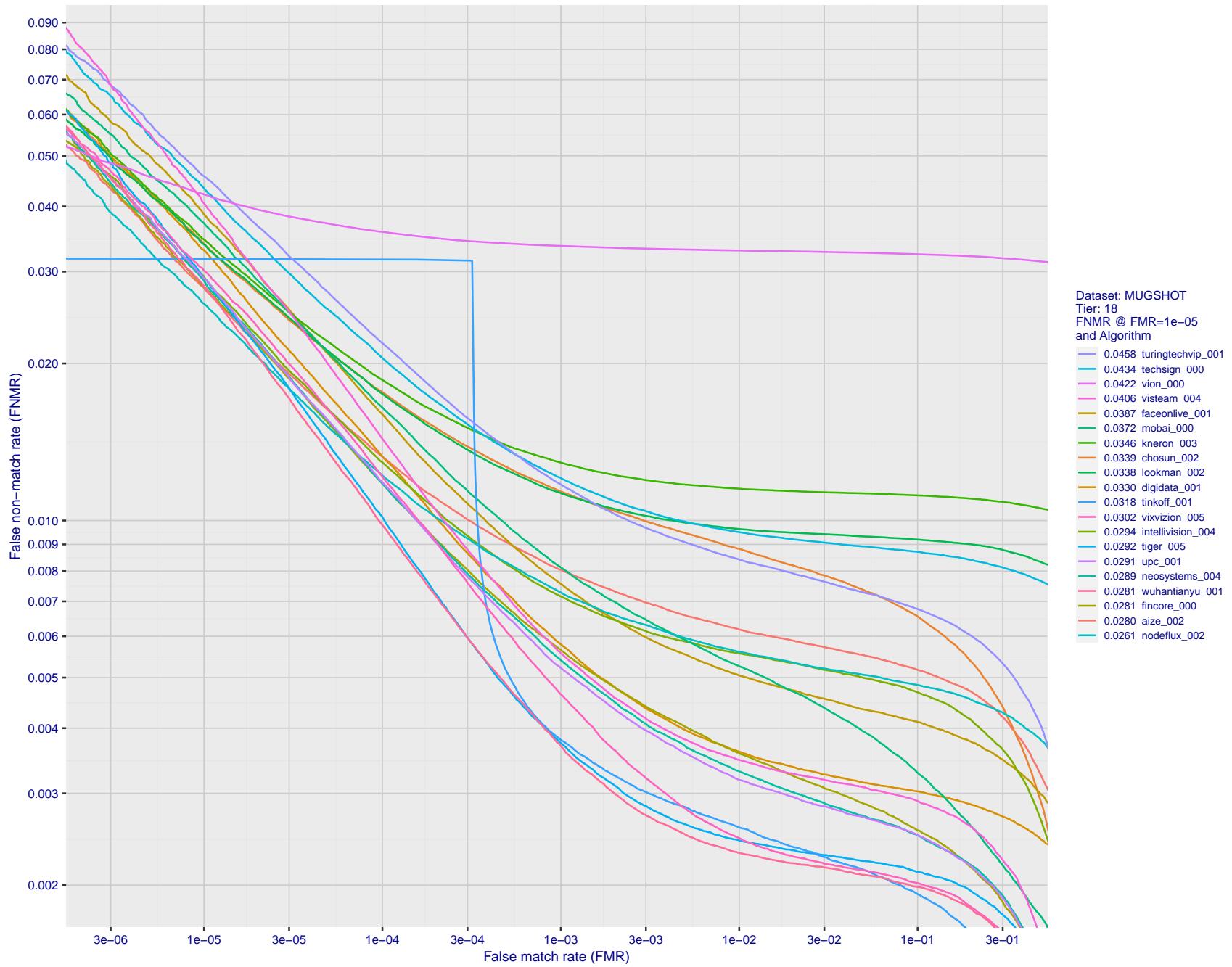


Figure 102: For the mugshot images, detection error tradeoff (DET) characteristics showing false non-match rate vs. false match rate plotted parametrically on threshold, T . The scales are logarithmic in order to show decades of FMR.

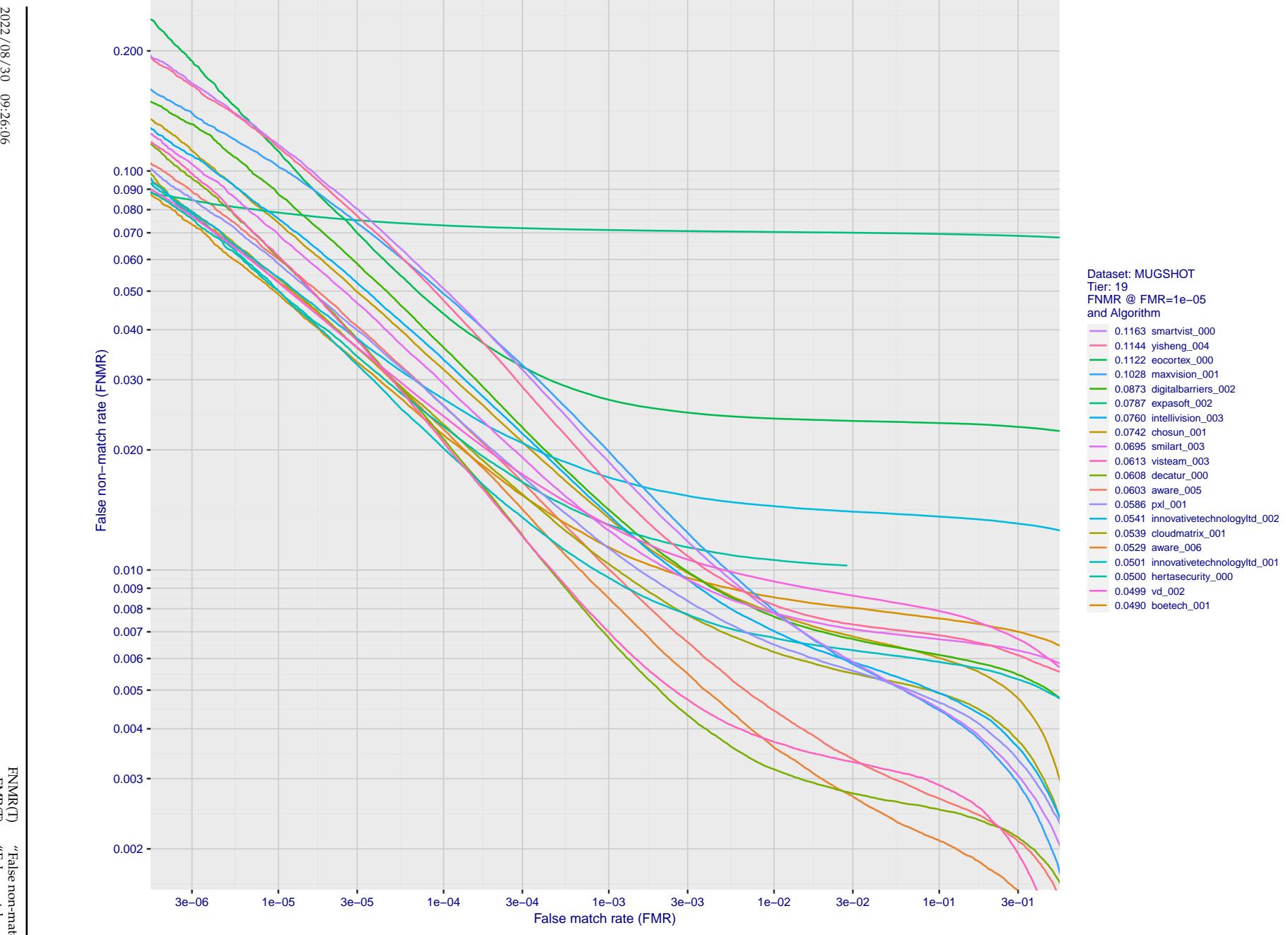


Figure 103: For the mugshot images, detection error tradeoff (DET) characteristics showing false non-match rate vs. false match rate plotted parametrically on threshold, T. The scales are logarithmic in order to show decades of FMR.

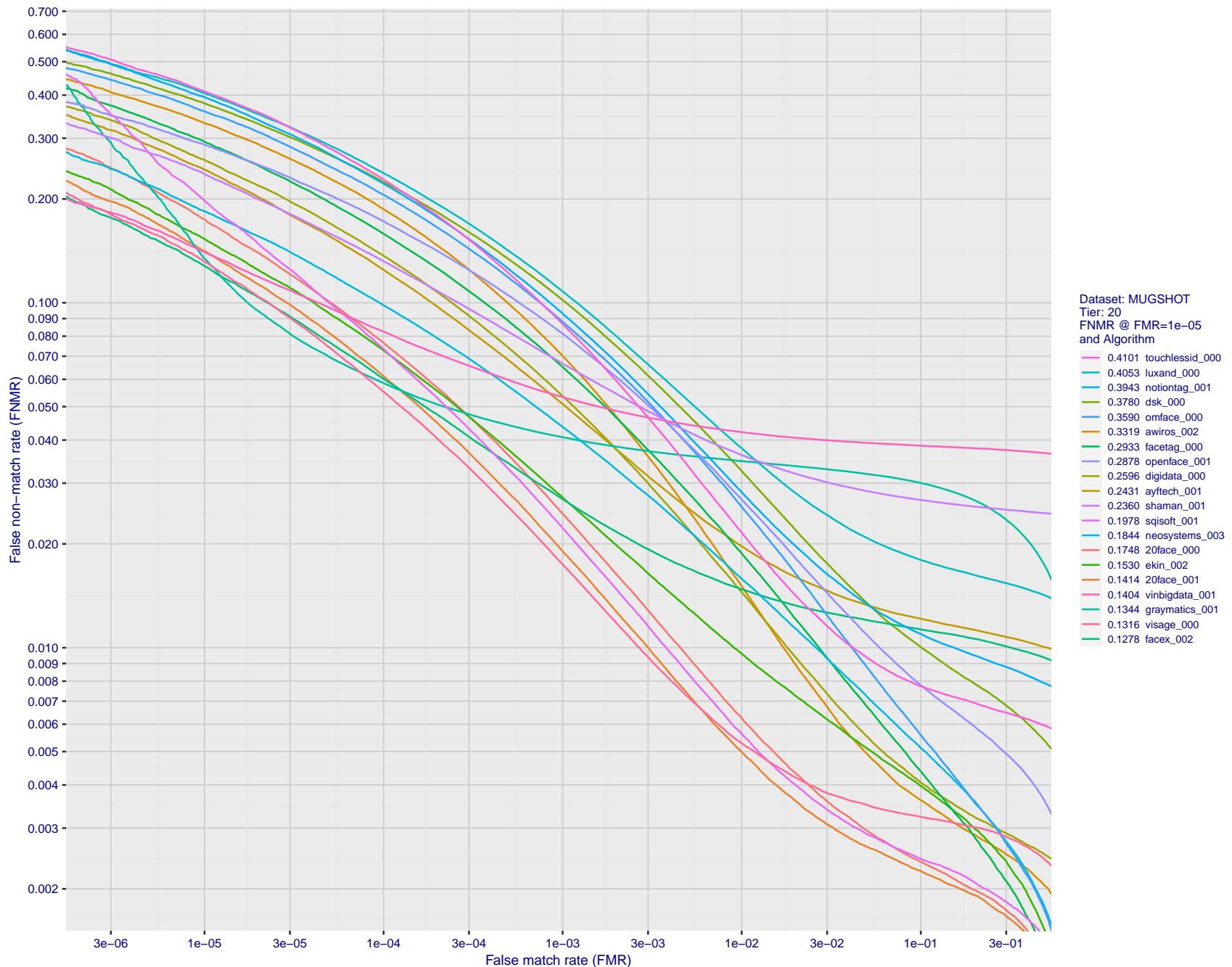


Figure 104: For the mugshot images, detection error tradeoff (DET) characteristics showing false non-match rate vs. false match rate plotted parametrically on threshold, T . The scales are logarithmic in order to show decades of FMR.

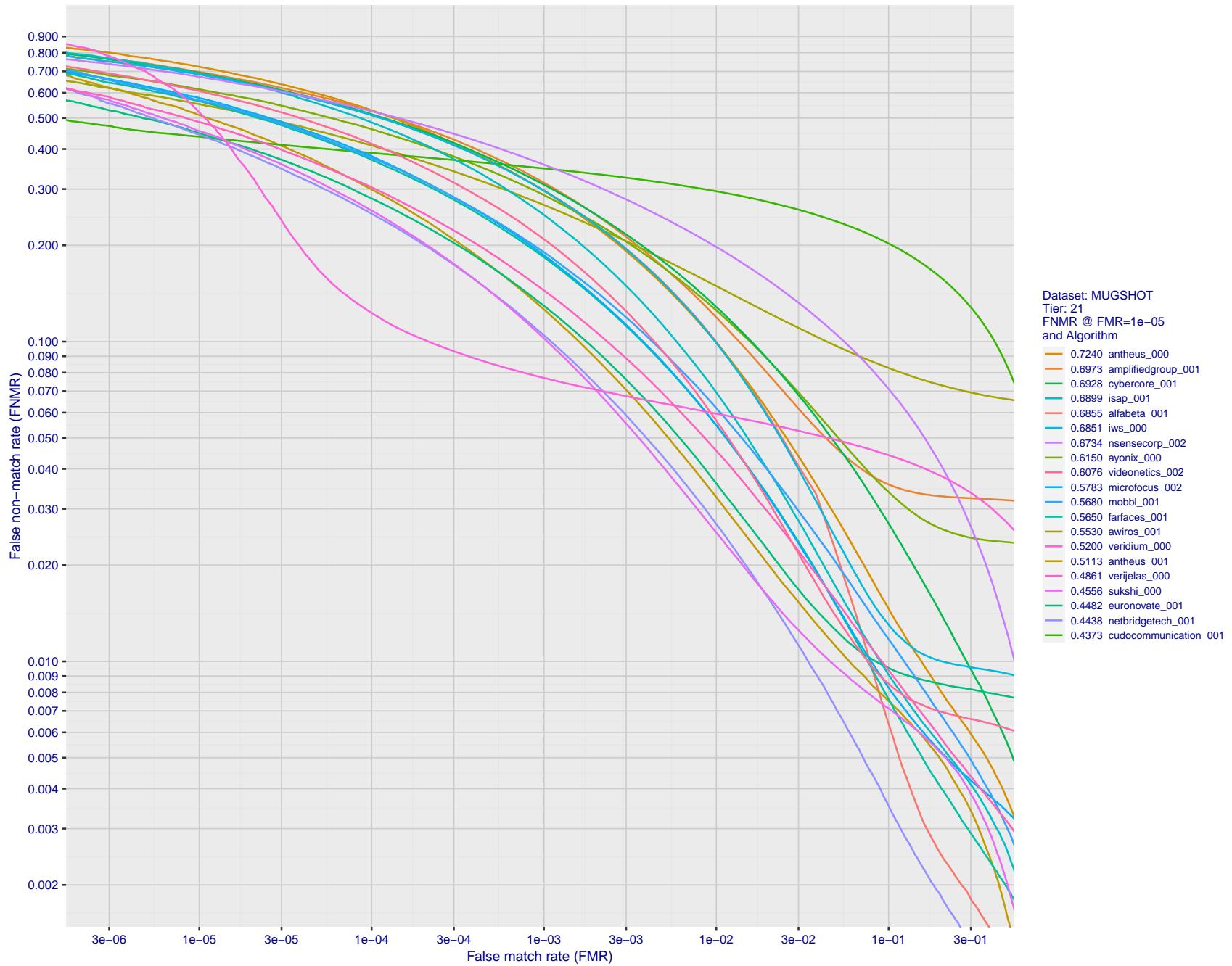


Figure 105: For the mugshot images, detection error tradeoff (DET) characteristics showing false non-match rate vs. false match rate plotted parametrically on threshold, T. The scales are logarithmic in order to show decades of FMR.

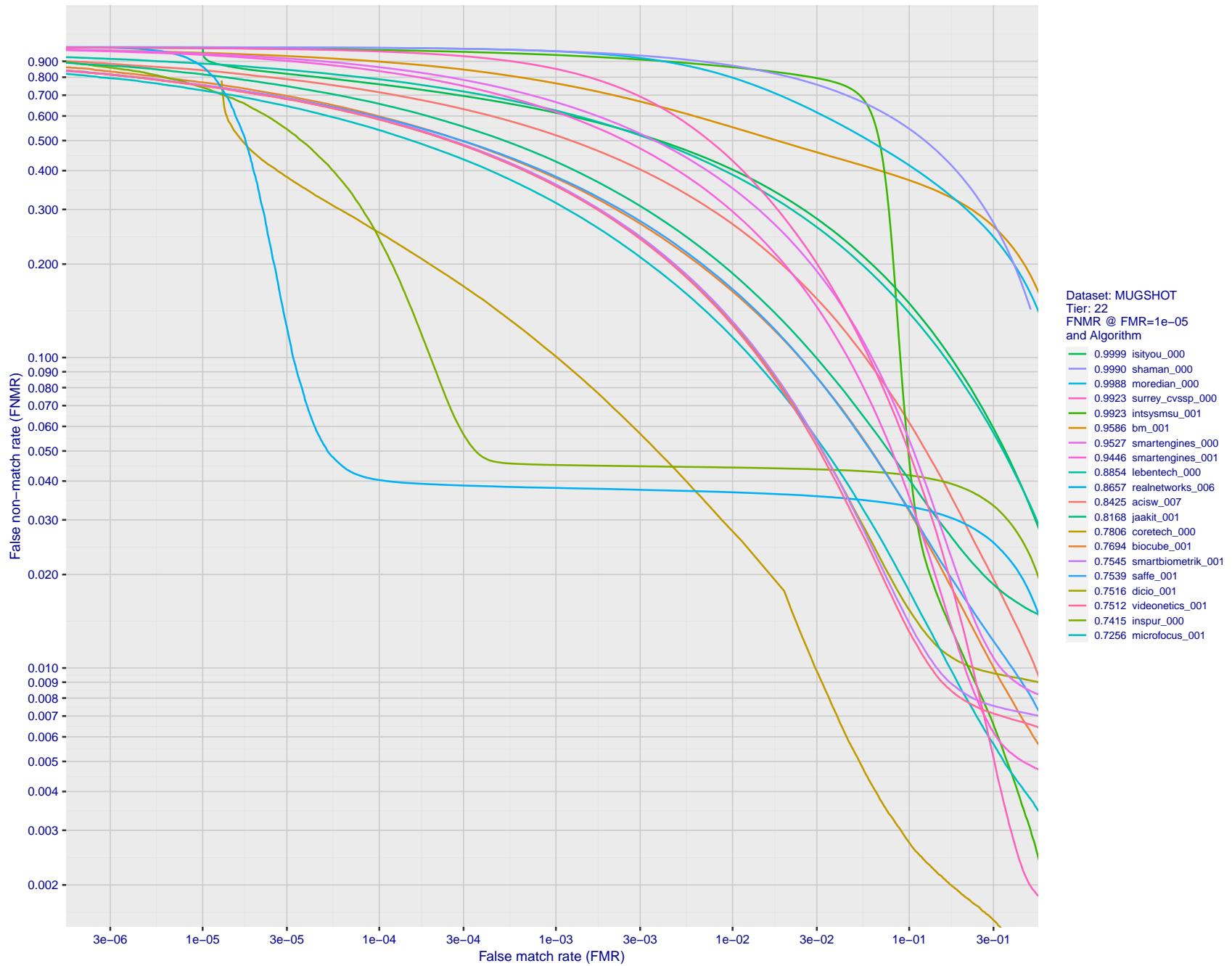


Figure 106: For the mugshot images, detection error tradeoff (DET) characteristics showing false non-match rate vs. false match rate plotted parametrically on threshold, T . The scales are logarithmic in order to show decades of FMR.

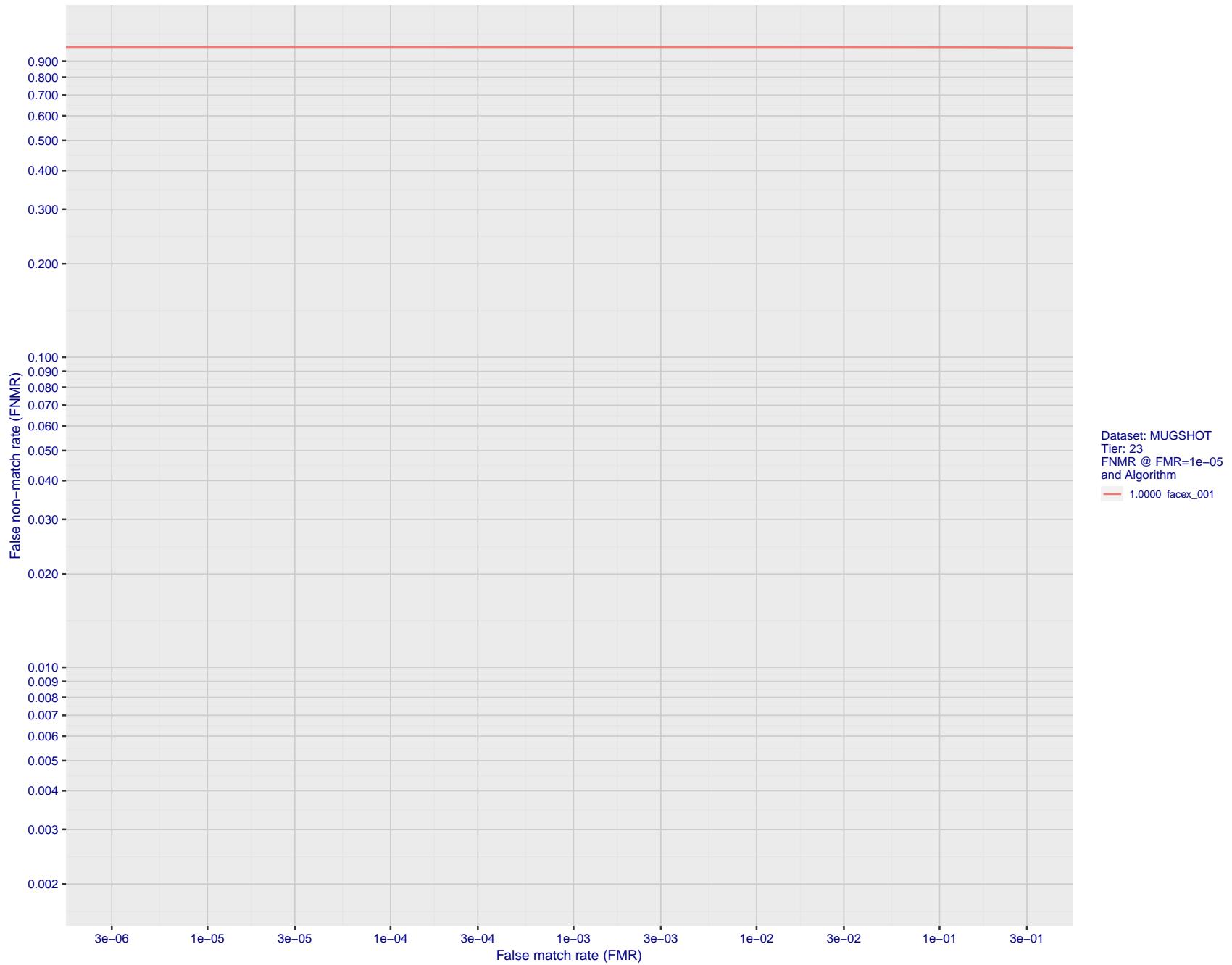


Figure 107: For the mugshot images, detection error tradeoff (DET) characteristics showing false non-match rate vs. false match rate plotted parametrically on threshold, T . The scales are logarithmic in order to show decades of FMR.

2022/08/30 09:26:06

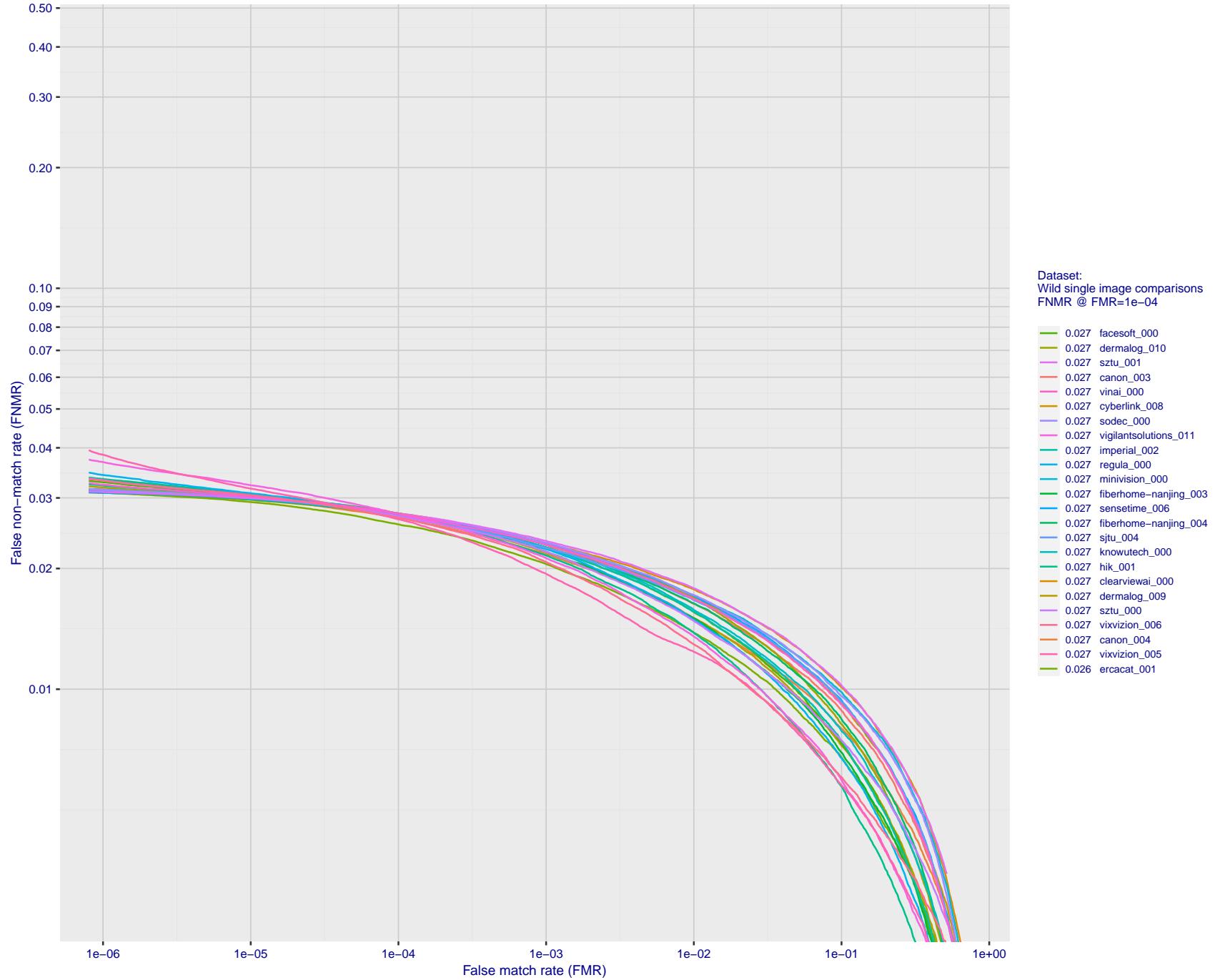


Figure 108: For the 2018 wild image comparisons, detection error tradeoff (DET) characteristics showing false non-match rate vs. false match rate plotted parametrically on threshold, T. The scales are logarithmic in order to show several decades of FMR.

2022/08/30 09:26:06

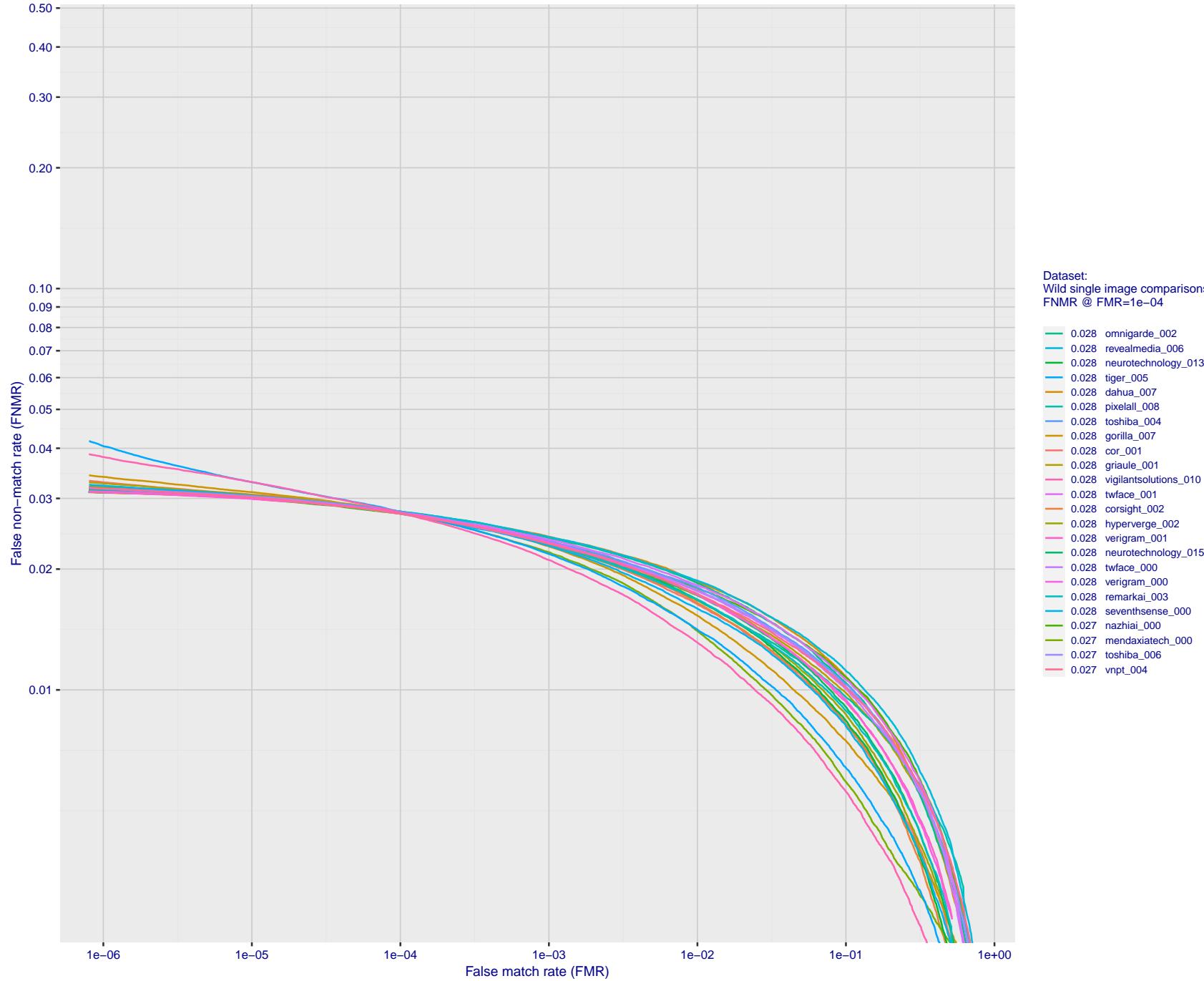


Figure 109: For the 2018 wild image comparisons, detection error tradeoff (DET) characteristics showing false non-match rate vs. false match rate plotted parametrically on threshold, T . The scales are logarithmic in order to show several decades of FMR.

2022/08/30 09:26:06

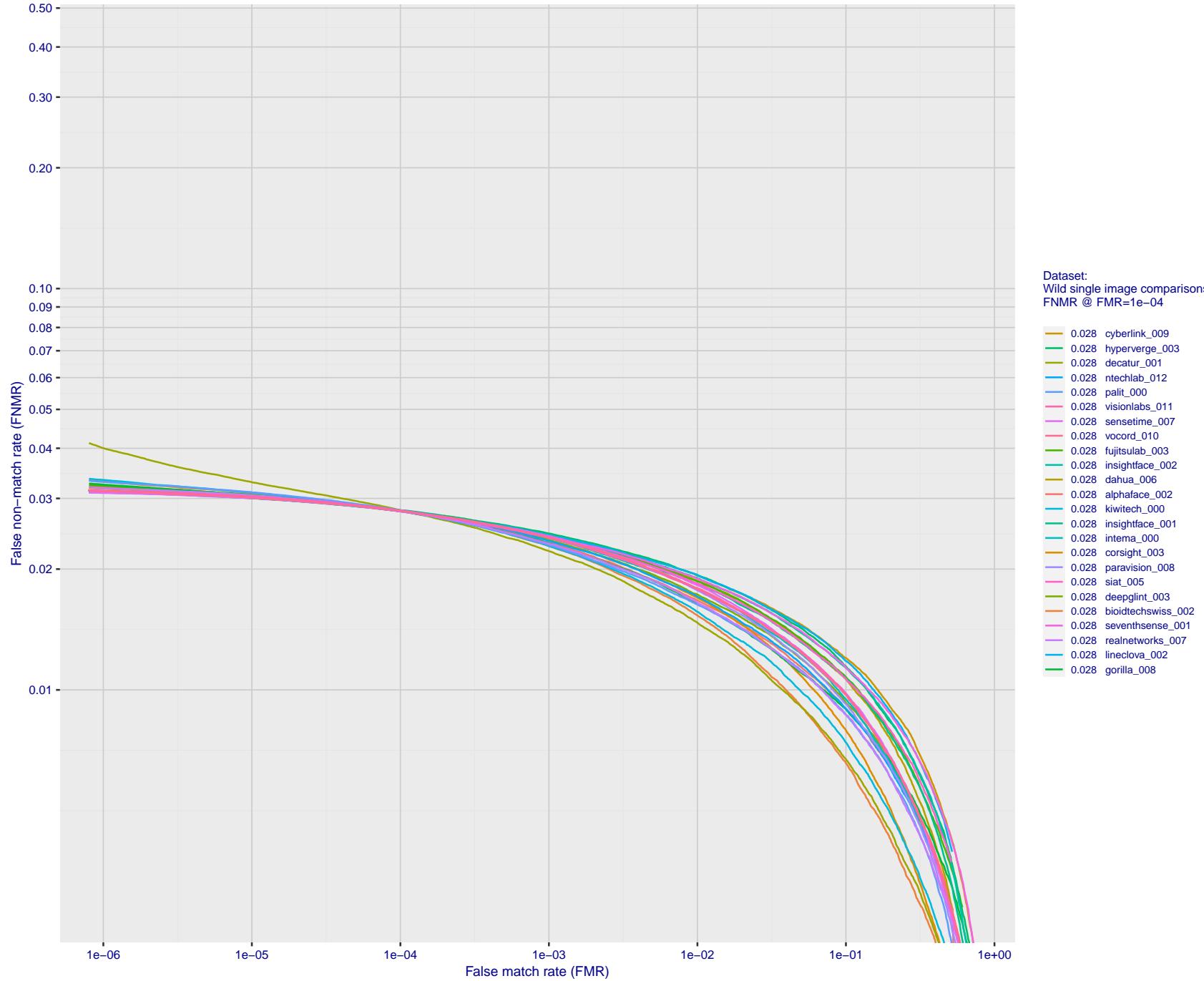


Figure 110: For the 2018 wild image comparisons, detection error tradeoff (DET) characteristics showing false non-match rate vs. false match rate plotted parametrically on threshold, T . The scales are logarithmic in order to show several decades of FMR.

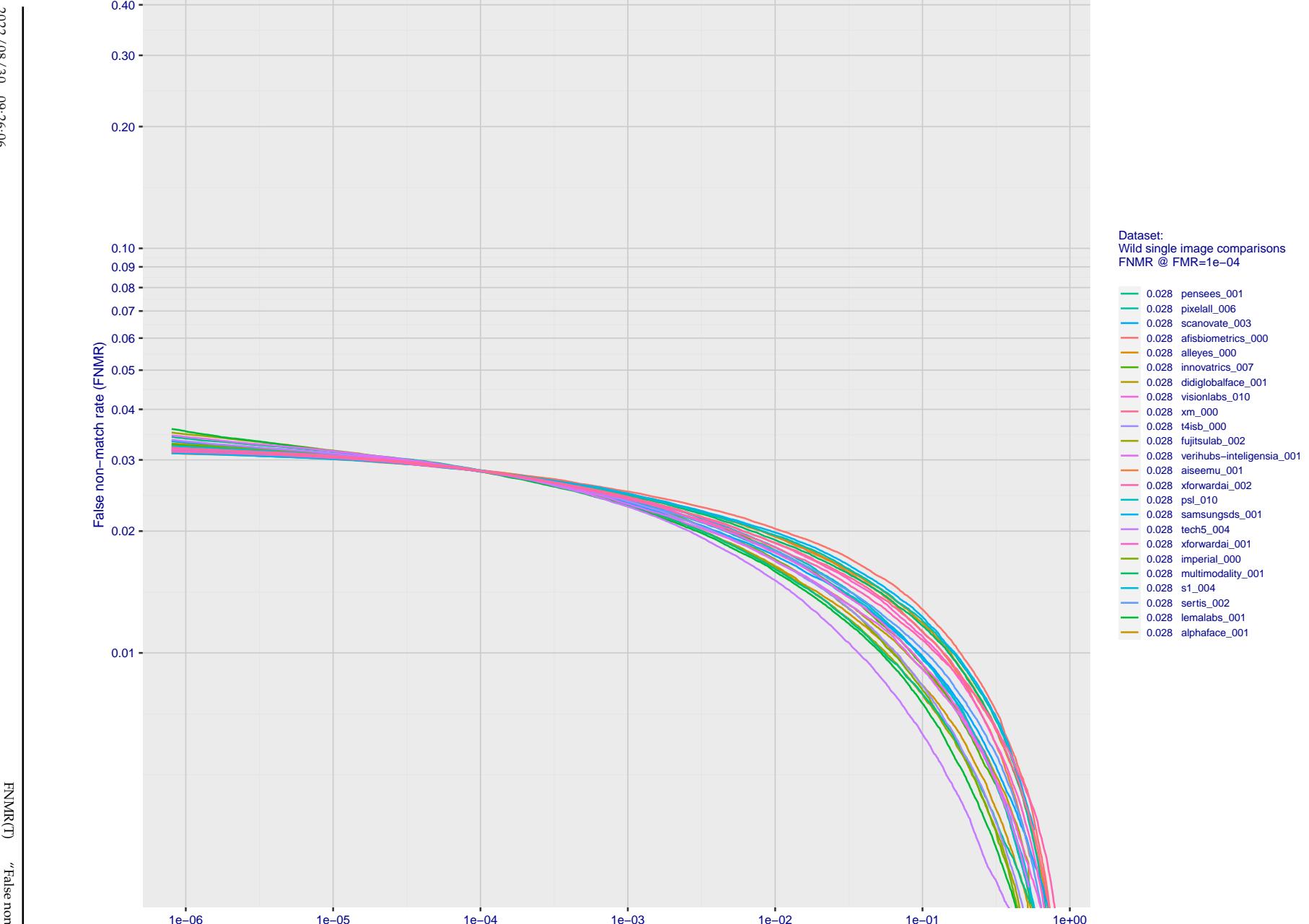


Figure 111: For the 2018 wild image comparisons, detection error tradeoff (DET) characteristics showing false non-match rate vs. false match rate plotted parametrically on threshold, T. The scales are logarithmic in order to show several decades of FMR.

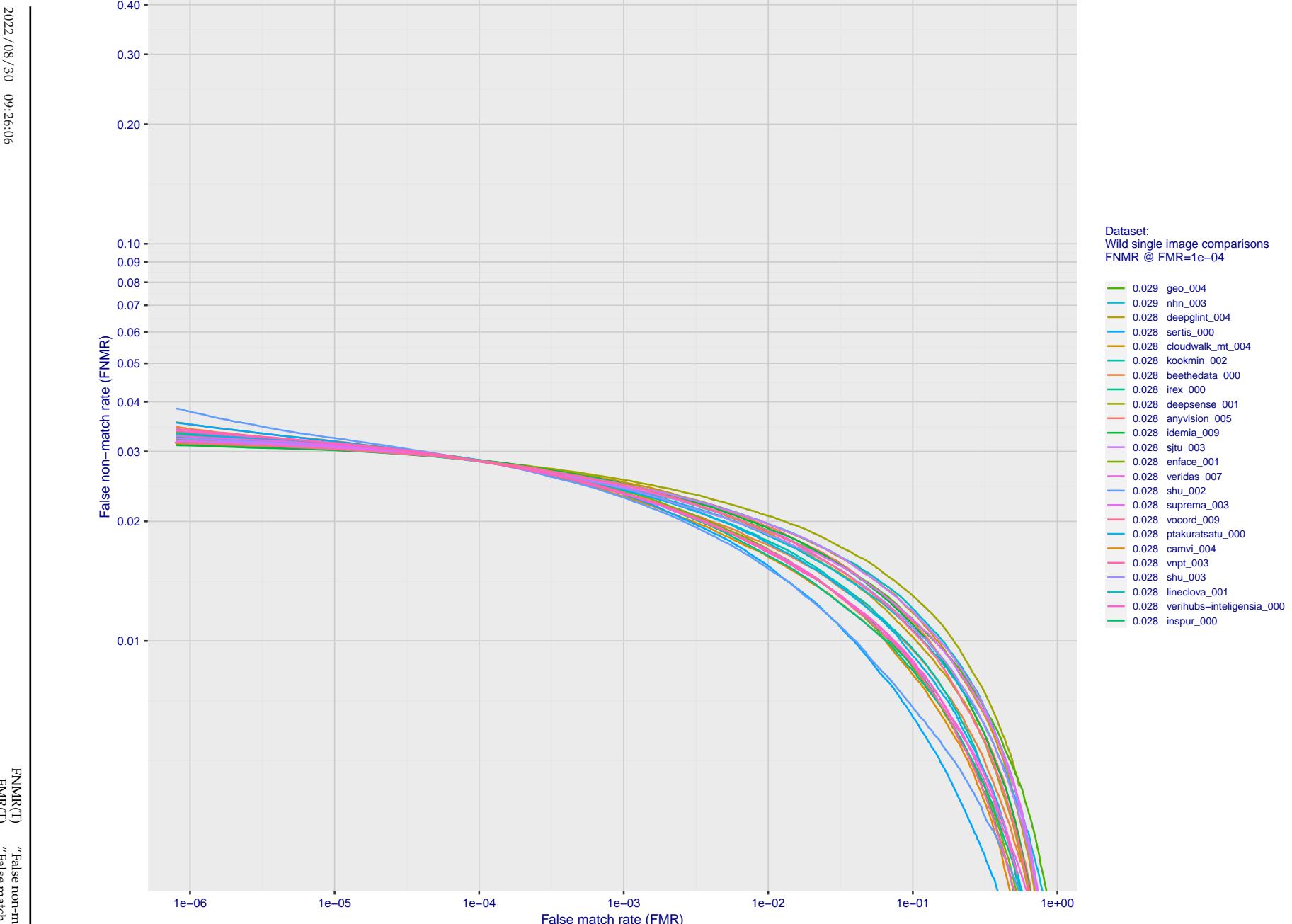


Figure 112: For the 2018 wild image comparisons, detection error tradeoff (DET) characteristics showing false non-match rate vs. false match rate plotted parametrically on threshold, T . The scales are logarithmic in order to show several decades of FMR.

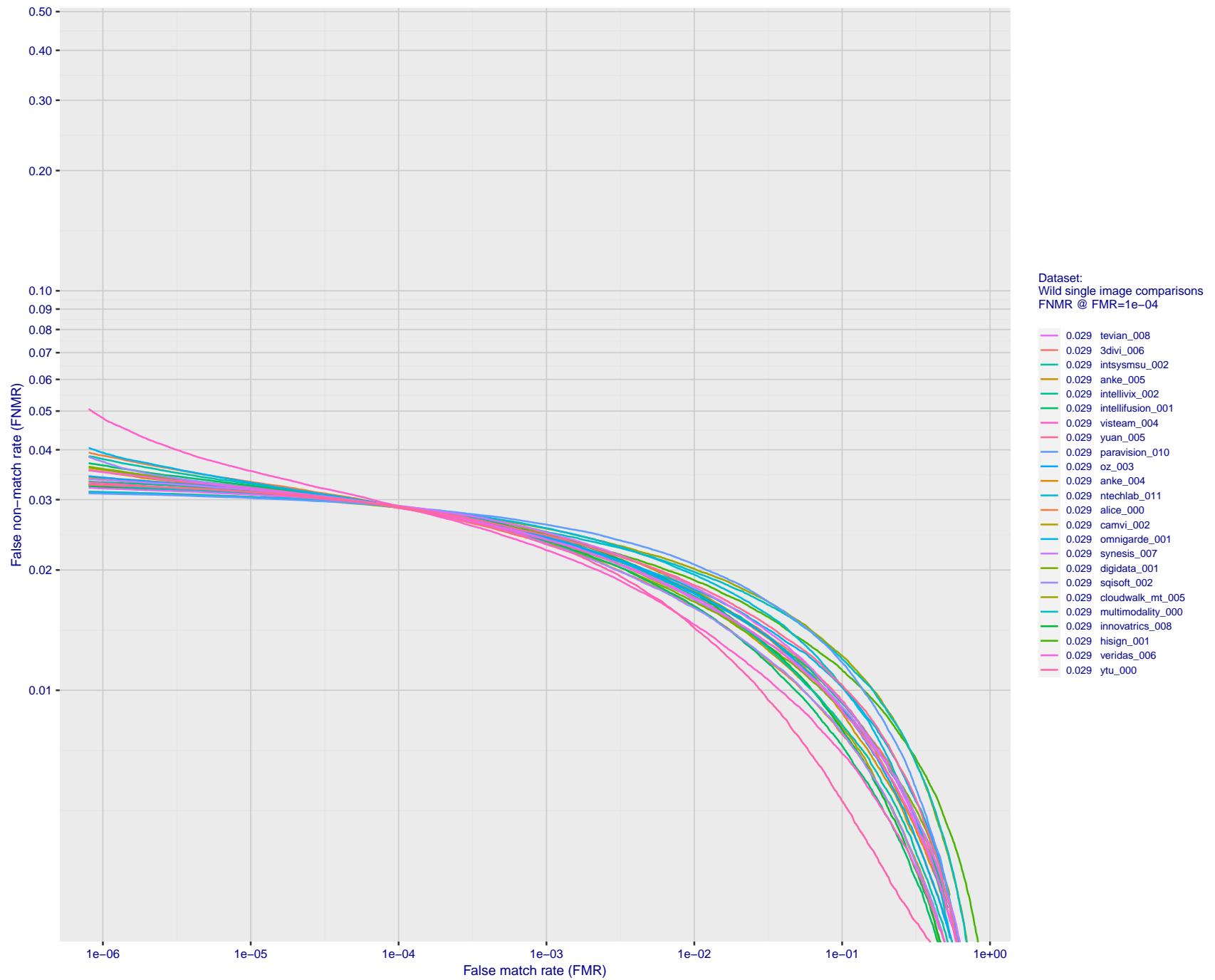


Figure 113: For the 2018 wild image comparisons, detection error tradeoff (DET) characteristics showing false non-match rate vs. false match rate plotted parametrically on threshold, T . The scales are logarithmic in order to show several decades of FMR.

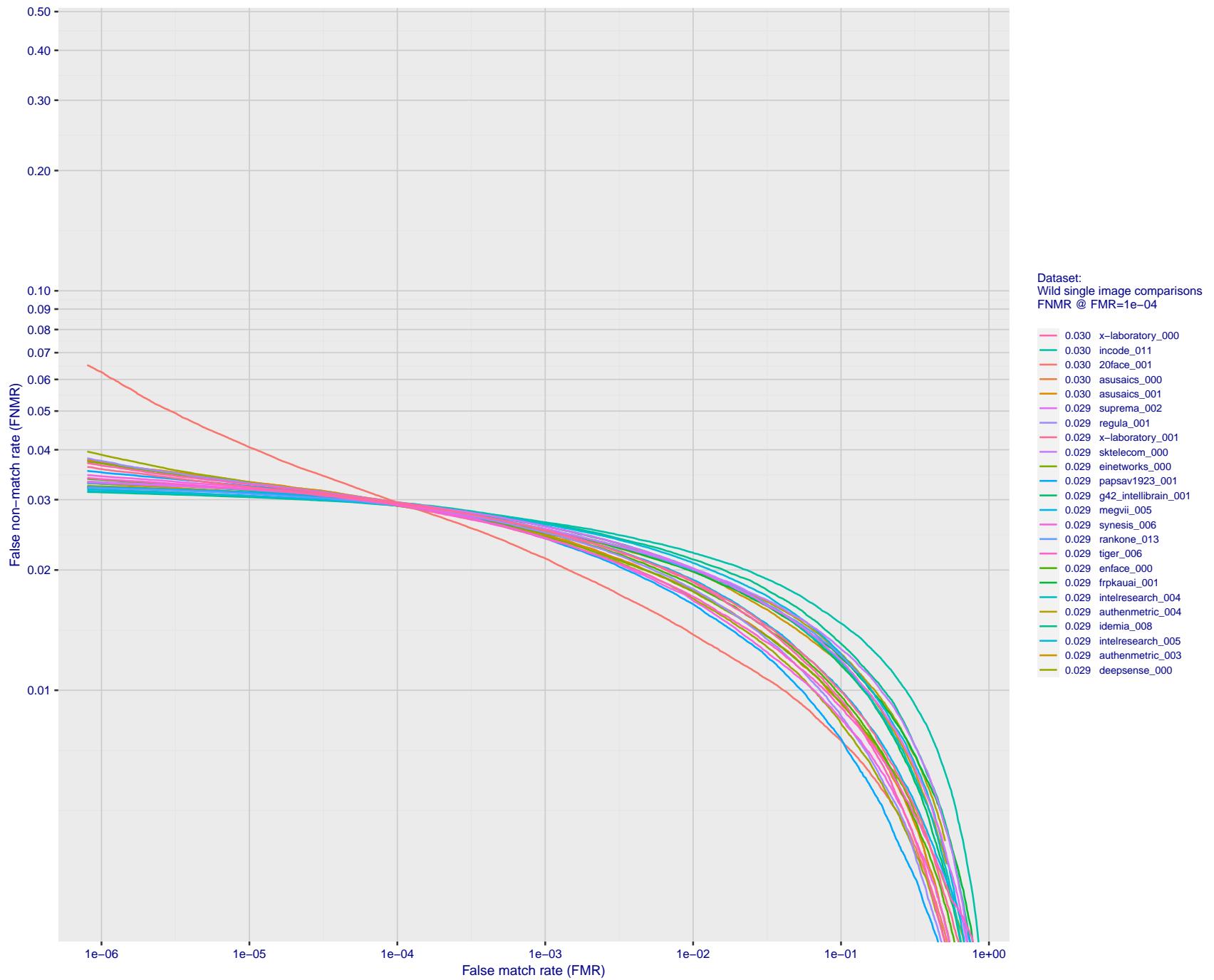


Figure 114: For the 2018 wild image comparisons, detection error tradeoff (DET) characteristics showing false non-match rate vs. false match rate plotted parametrically on threshold, T . The scales are logarithmic in order to show several decades of FMR.

2022/08/30 09:26:06

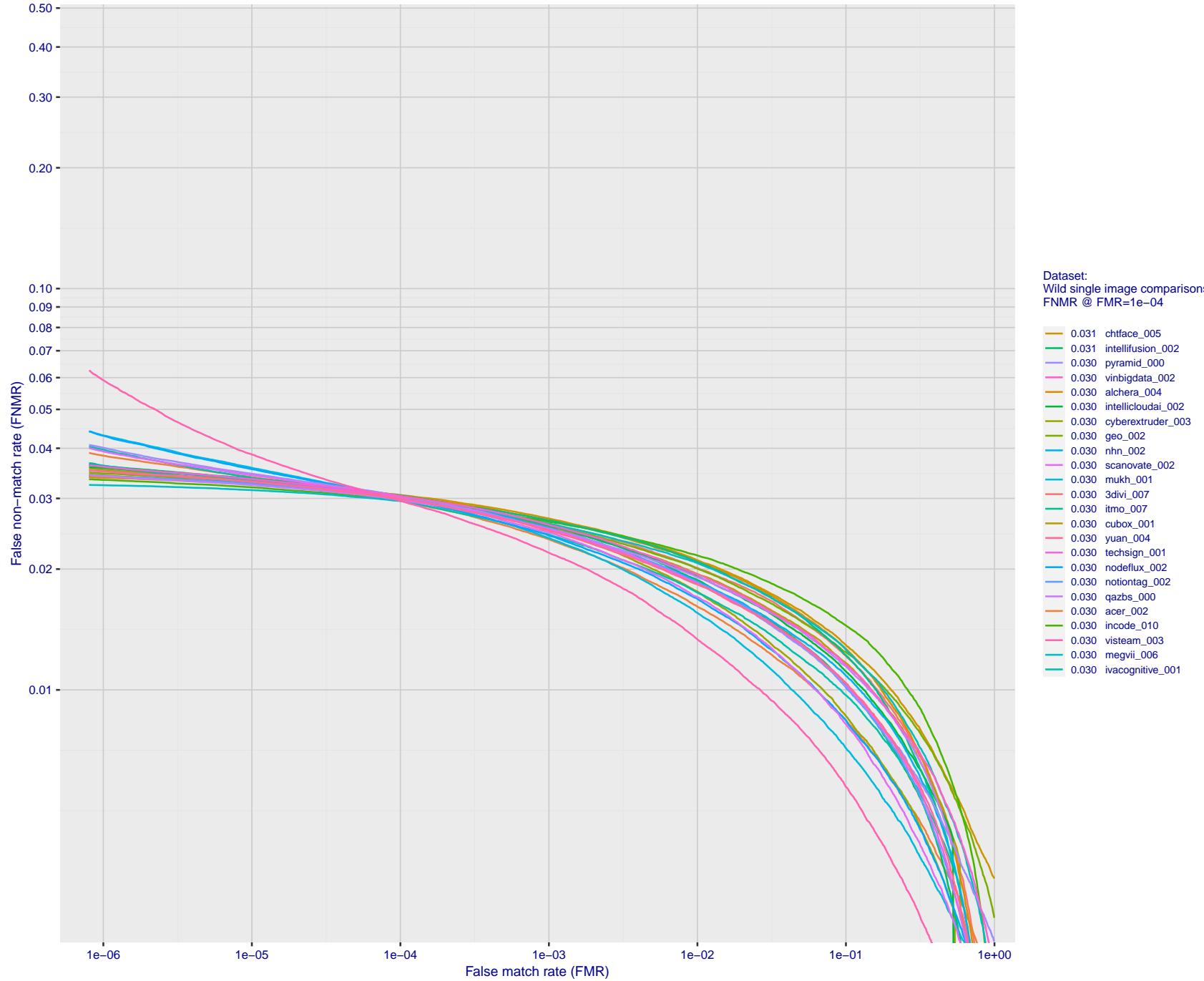


Figure 115: For the 2018 wild image comparisons, detection error tradeoff (DET) characteristics showing false non-match rate vs. false match rate plotted parametrically on threshold, T . The scales are logarithmic in order to show several decades of FMR.

2022/08/30 09:26:06

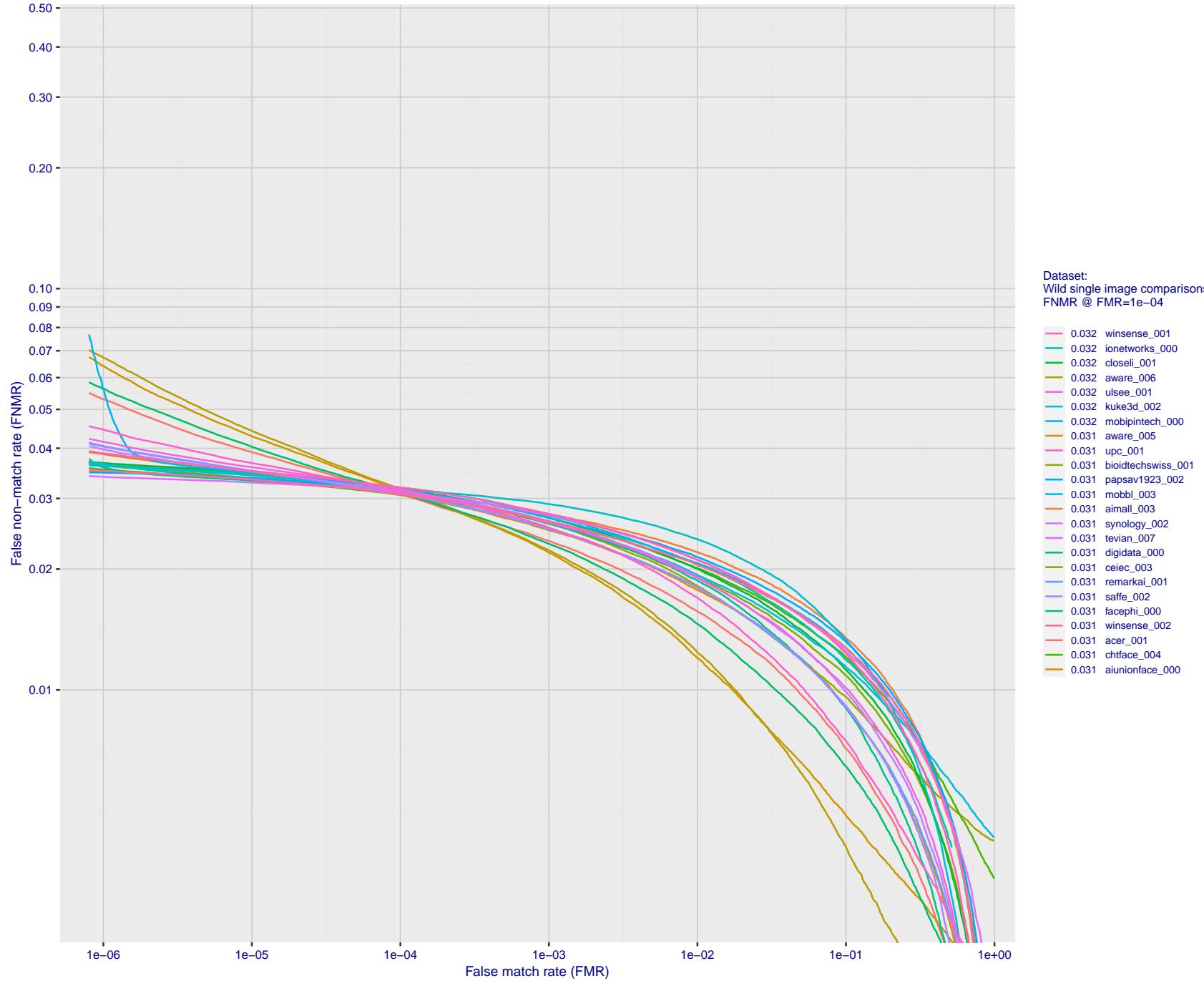


Figure 116: For the 2018 wild image comparisons, detection error tradeoff (DET) characteristics showing false non-match rate vs. false match rate plotted parametrically on threshold, T . The scales are logarithmic in order to show several decades of FMR.

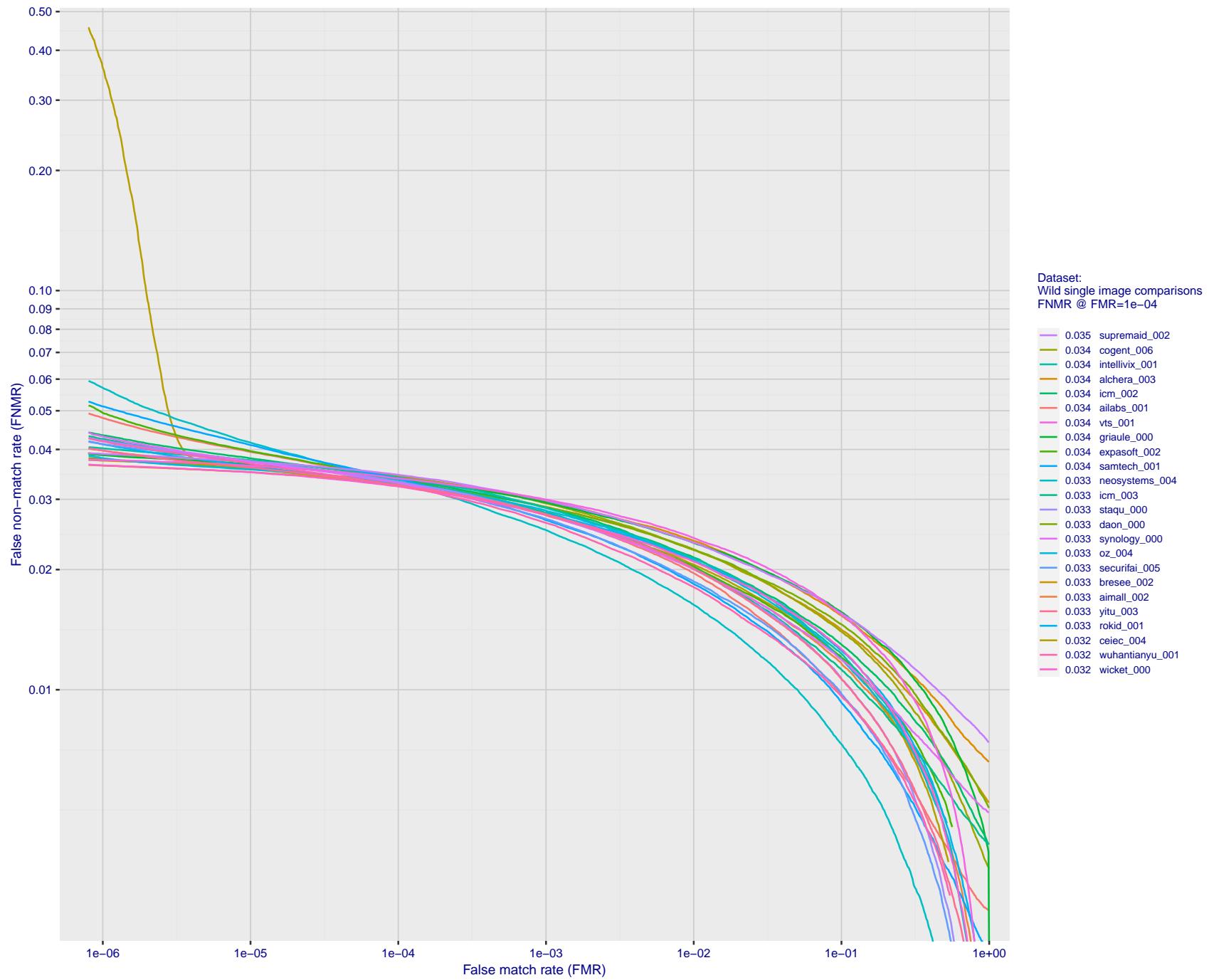


Figure 117: For the 2018 wild image comparisons, detection error tradeoff (DET) characteristics showing false non-match rate vs. false match rate plotted parametrically on threshold, T. The scales are logarithmic in order to show several decades of FMR.

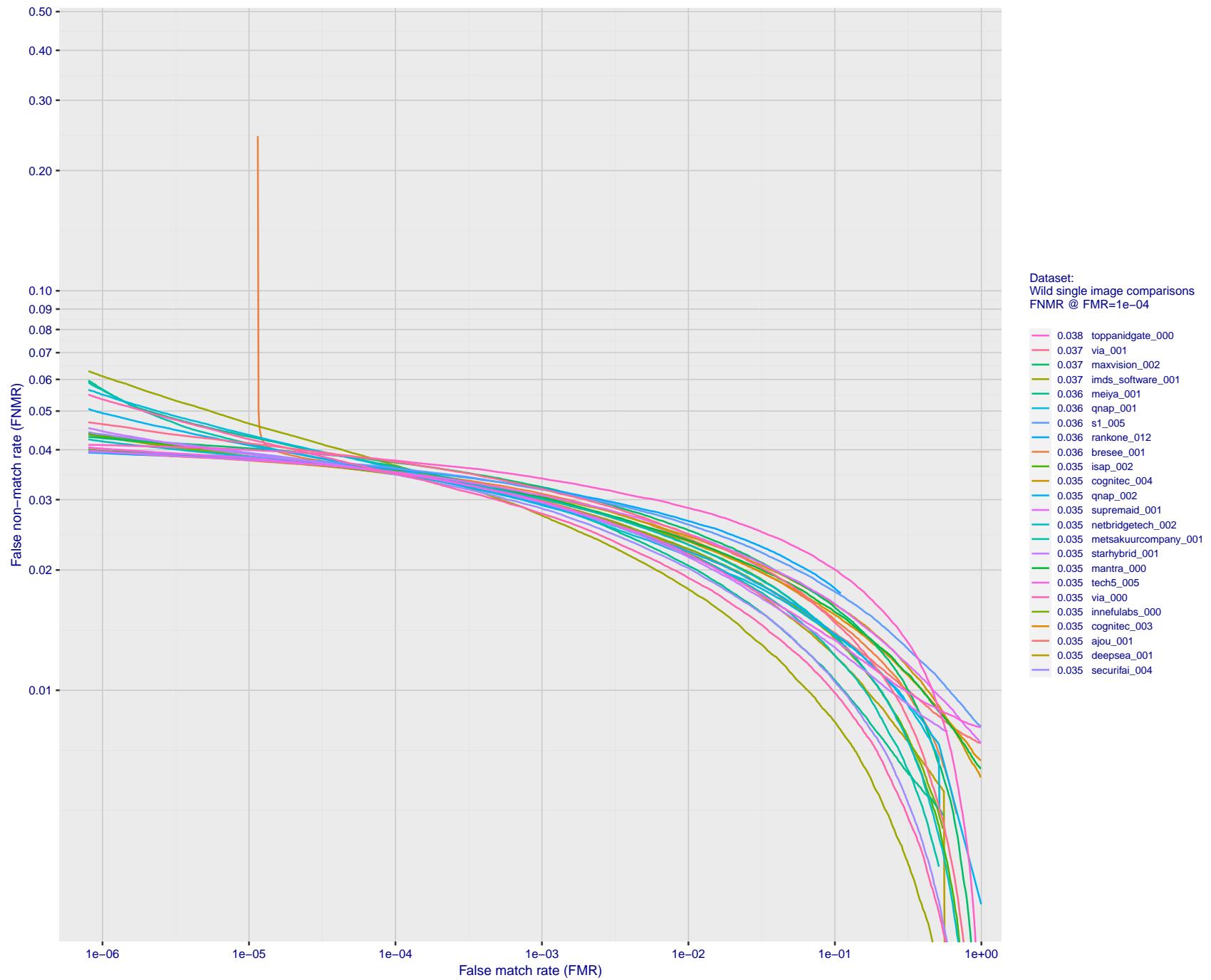


Figure 118: For the 2018 wild image comparisons, detection error tradeoff (DET) characteristics showing false non-match rate vs. false match rate plotted parametrically on threshold, T . The scales are logarithmic in order to show several decades of FMR.

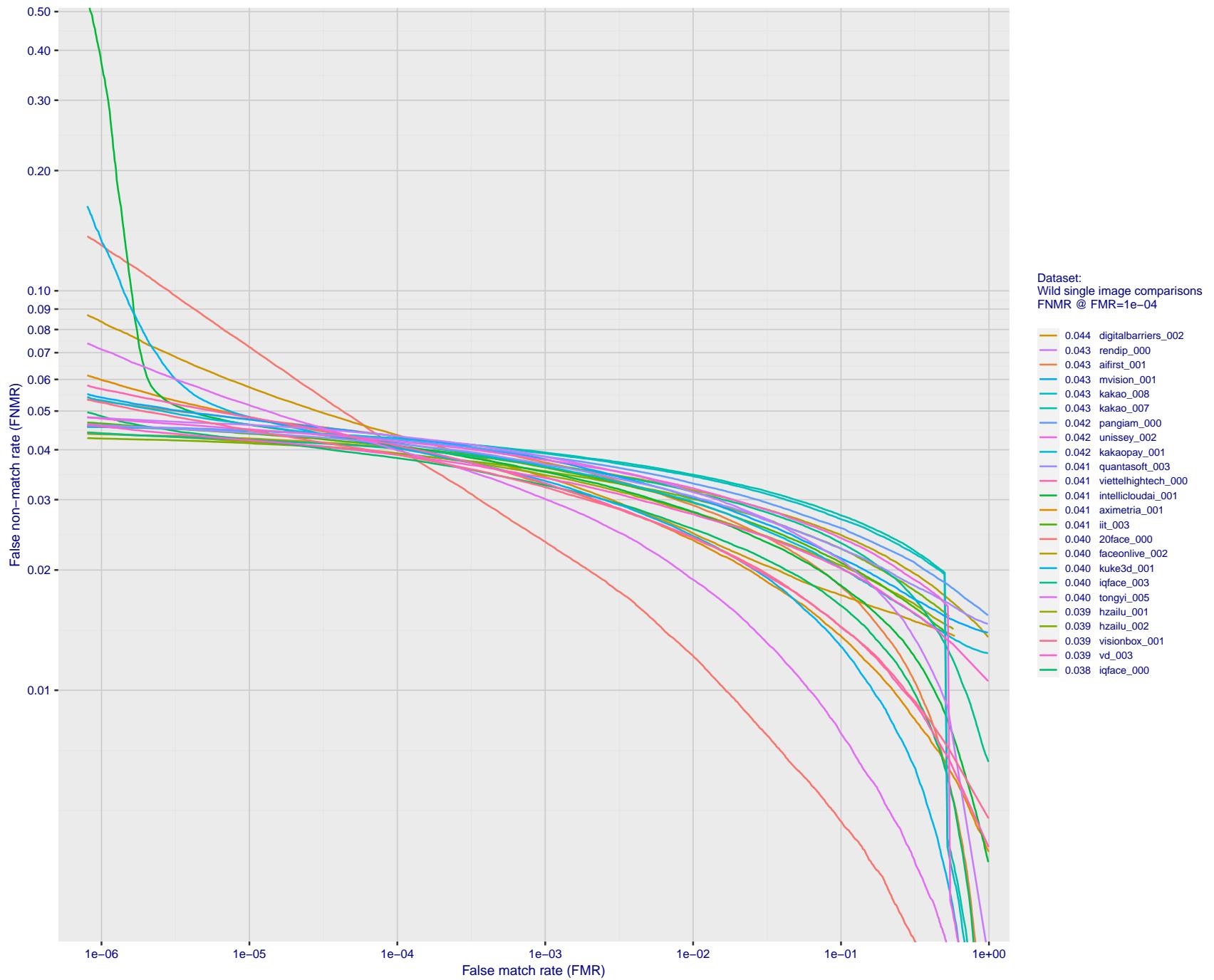


Figure 119: For the 2018 wild image comparisons, detection error tradeoff (DET) characteristics showing false non-match rate vs. false match rate plotted parametrically on threshold, T . The scales are logarithmic in order to show several decades of FMR.

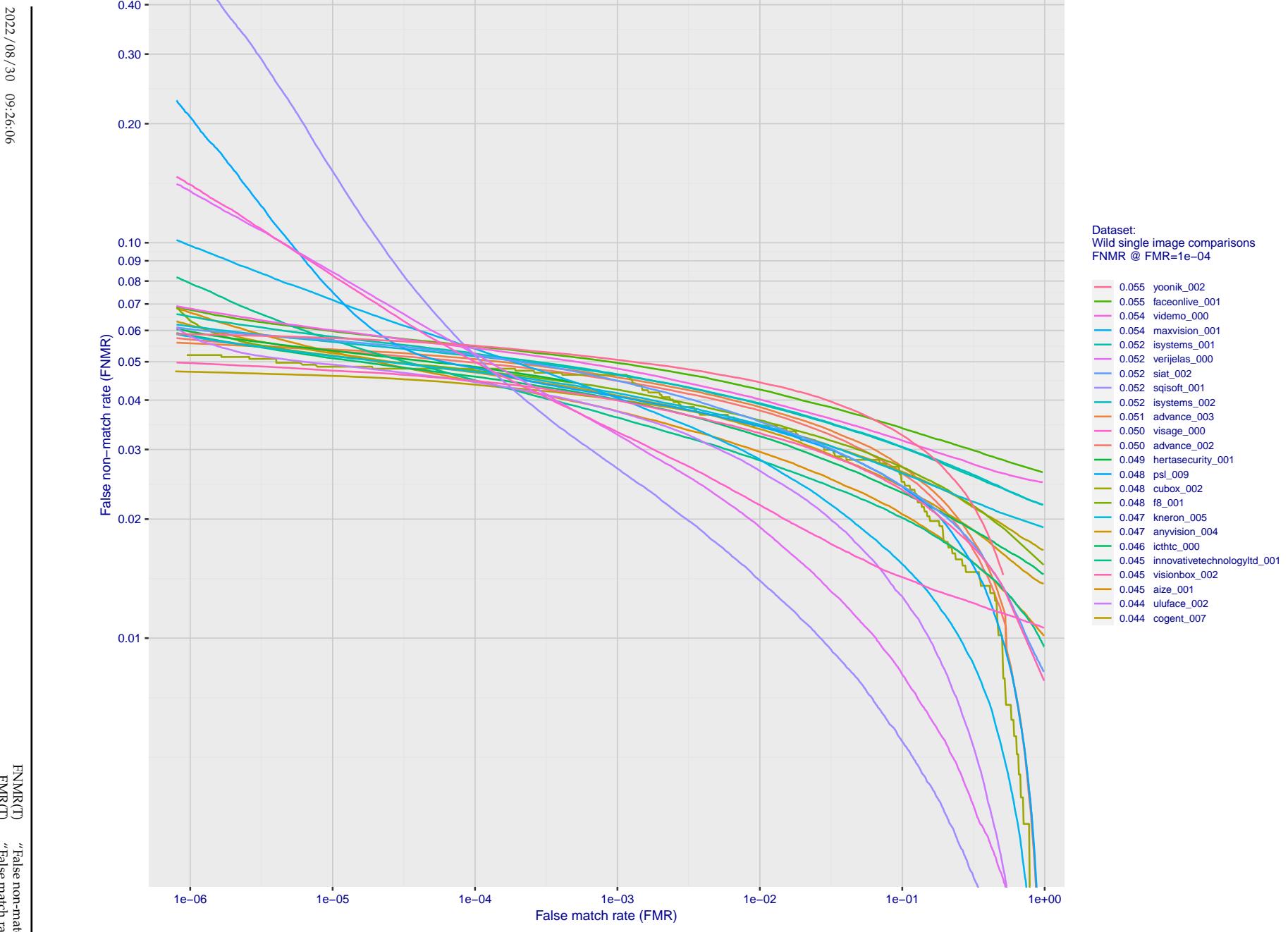


Figure 120: For the 2018 wild image comparisons, detection error tradeoff (DET) characteristics showing false non-match rate vs. false match rate plotted parametrically on threshold, T . The scales are logarithmic in order to show several decades of FMR.

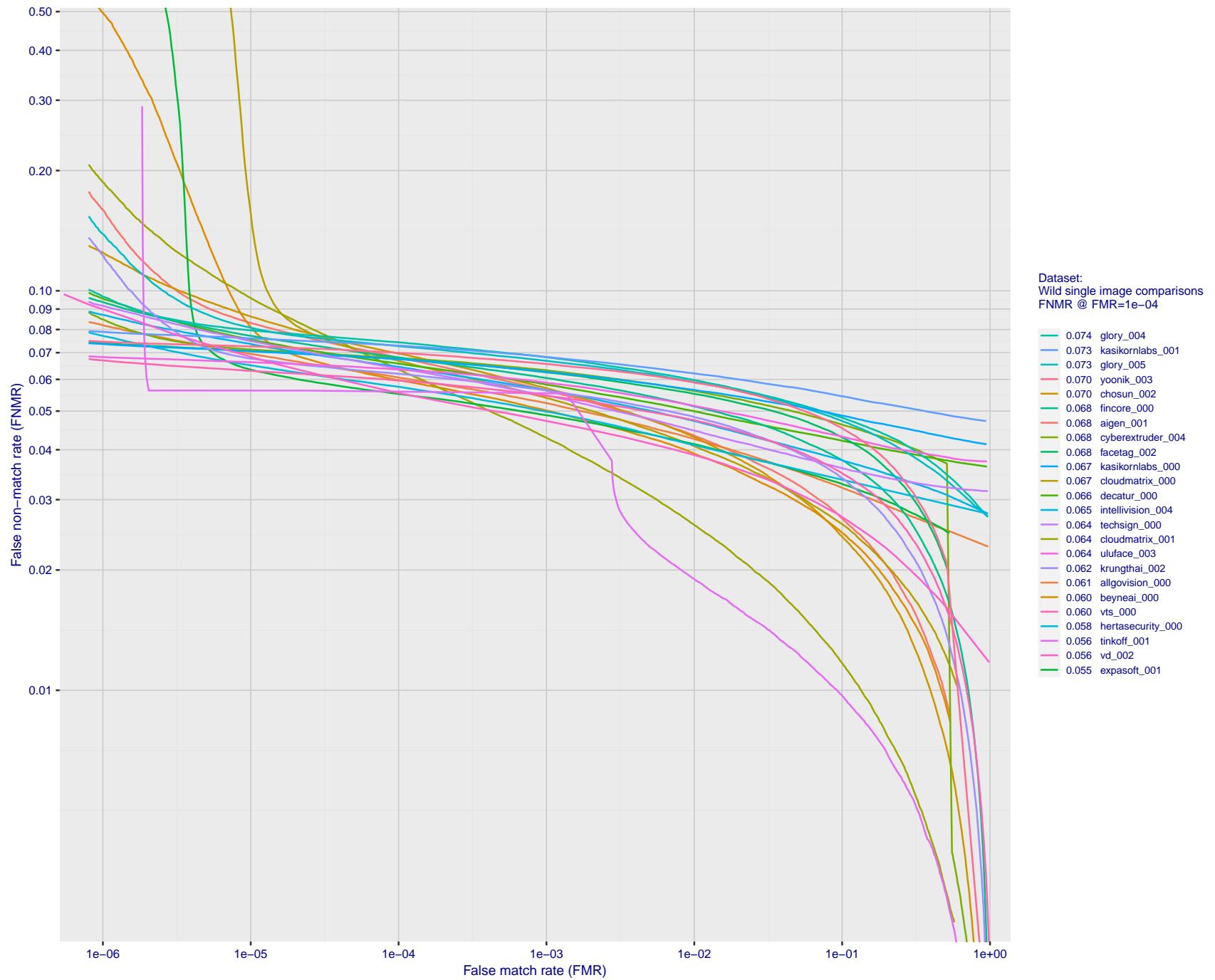


Figure 121: For the 2018 wild image comparisons, detection error tradeoff (DET) characteristics showing false non-match rate vs. false match rate plotted parametrically on threshold, T. The scales are logarithmic in order to show several decades of FMR.

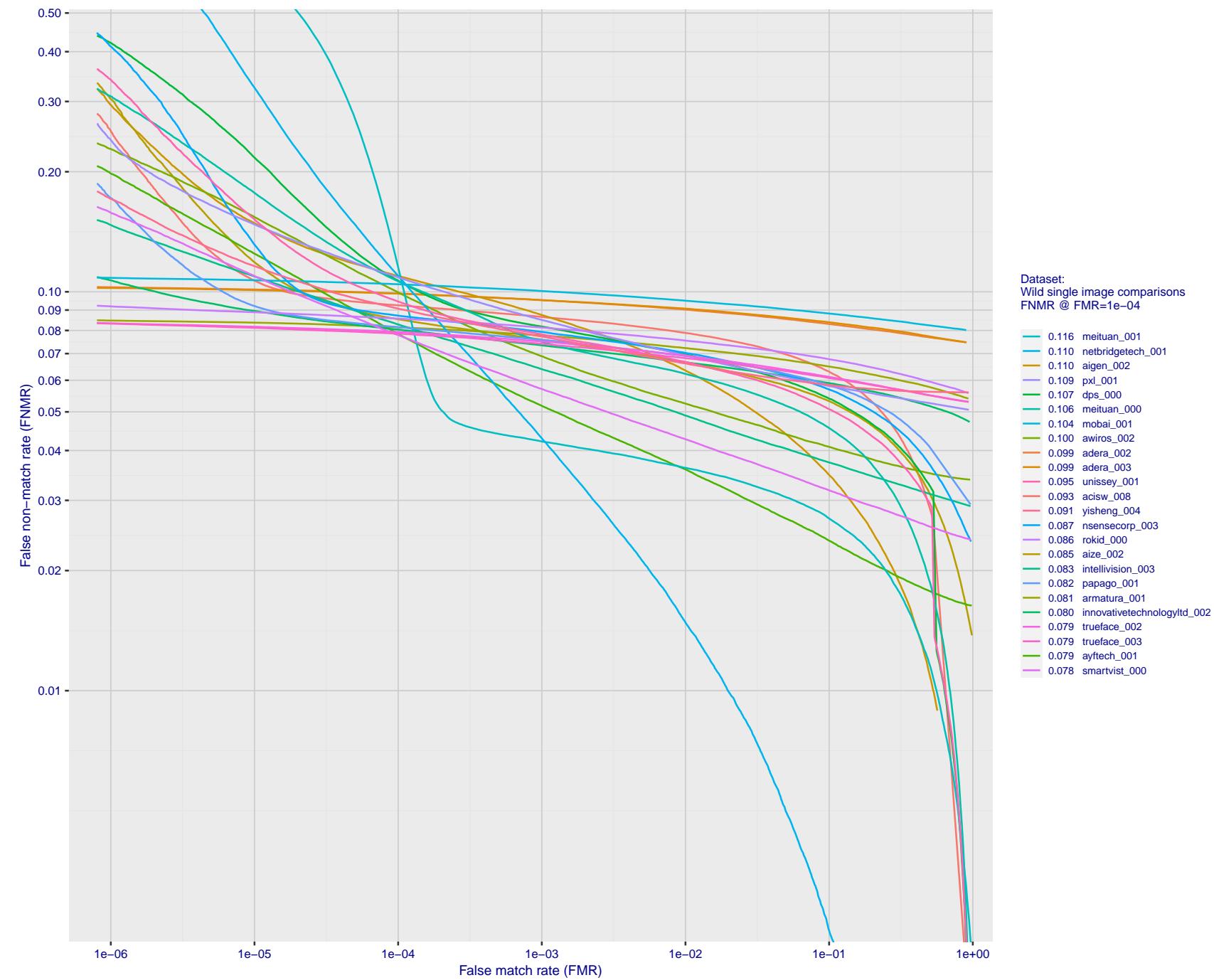


Figure 122: For the 2018 wild image comparisons, detection error tradeoff (DET) characteristics showing false non-match rate vs. false match rate plotted parametrically on threshold, T. The scales are logarithmic in order to show several decades of FMR.

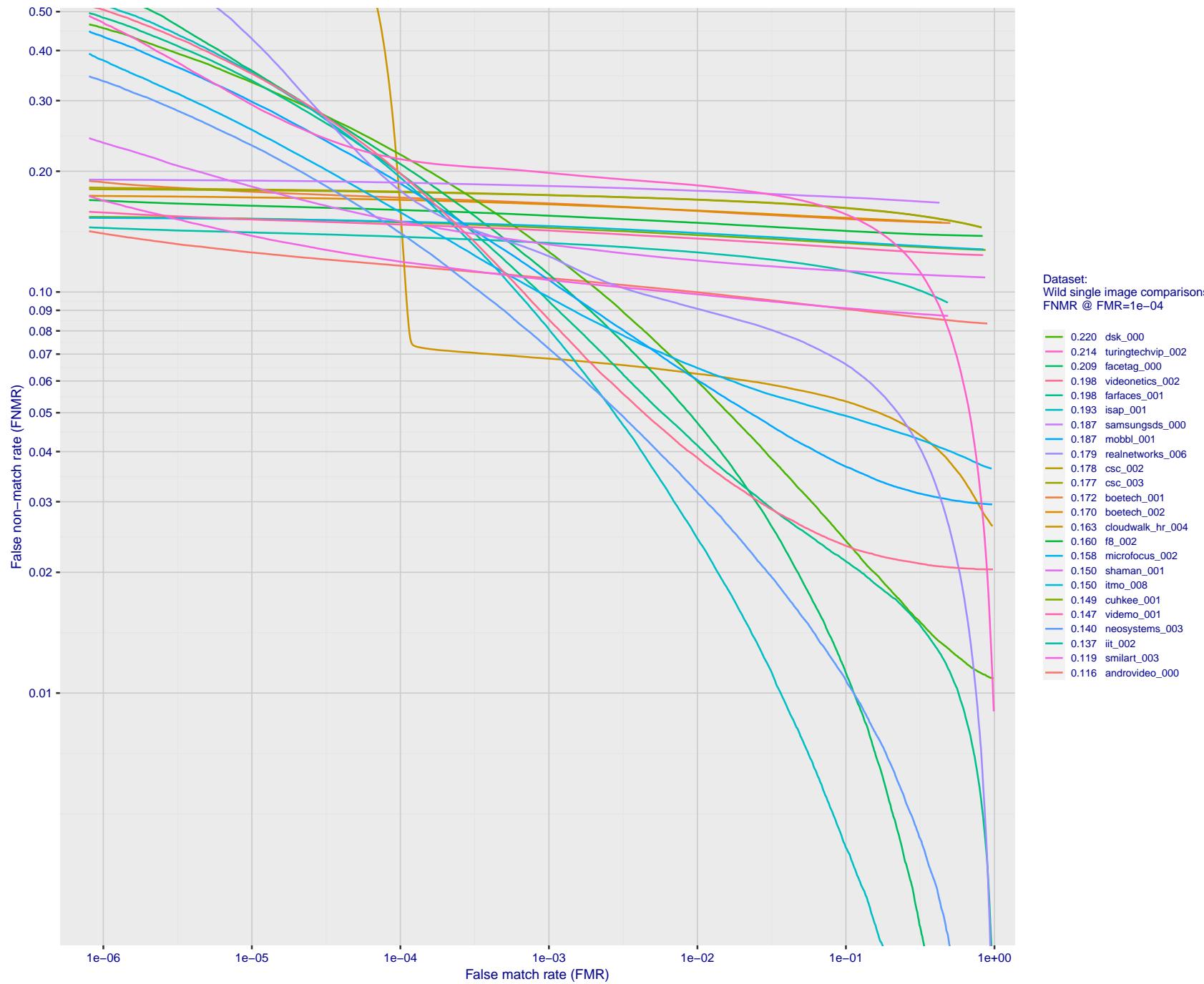


Figure 123: For the 2018 wild image comparisons, detection error tradeoff (DET) characteristics showing false non-match rate vs. false match rate plotted parametrically on threshold, T. The scales are logarithmic in order to show several decades of FMR.

2022/08/30 09:26:06

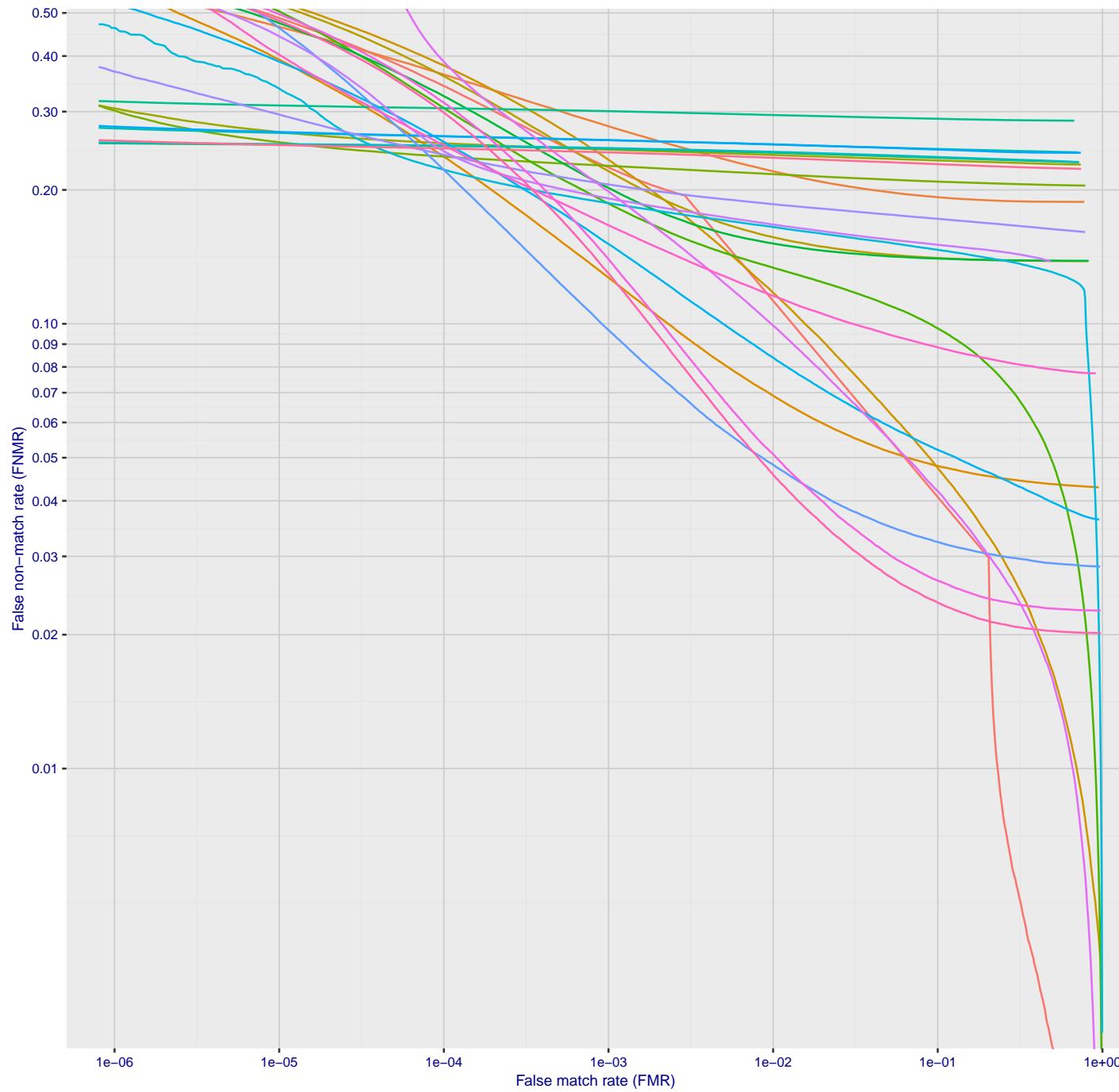


Figure 124: For the 2018 wild image comparisons, detection error tradeoff (DET) characteristics showing false non-match rate vs. false match rate plotted parametrically on threshold, T . The scales are logarithmic in order to show several decades of FMR.

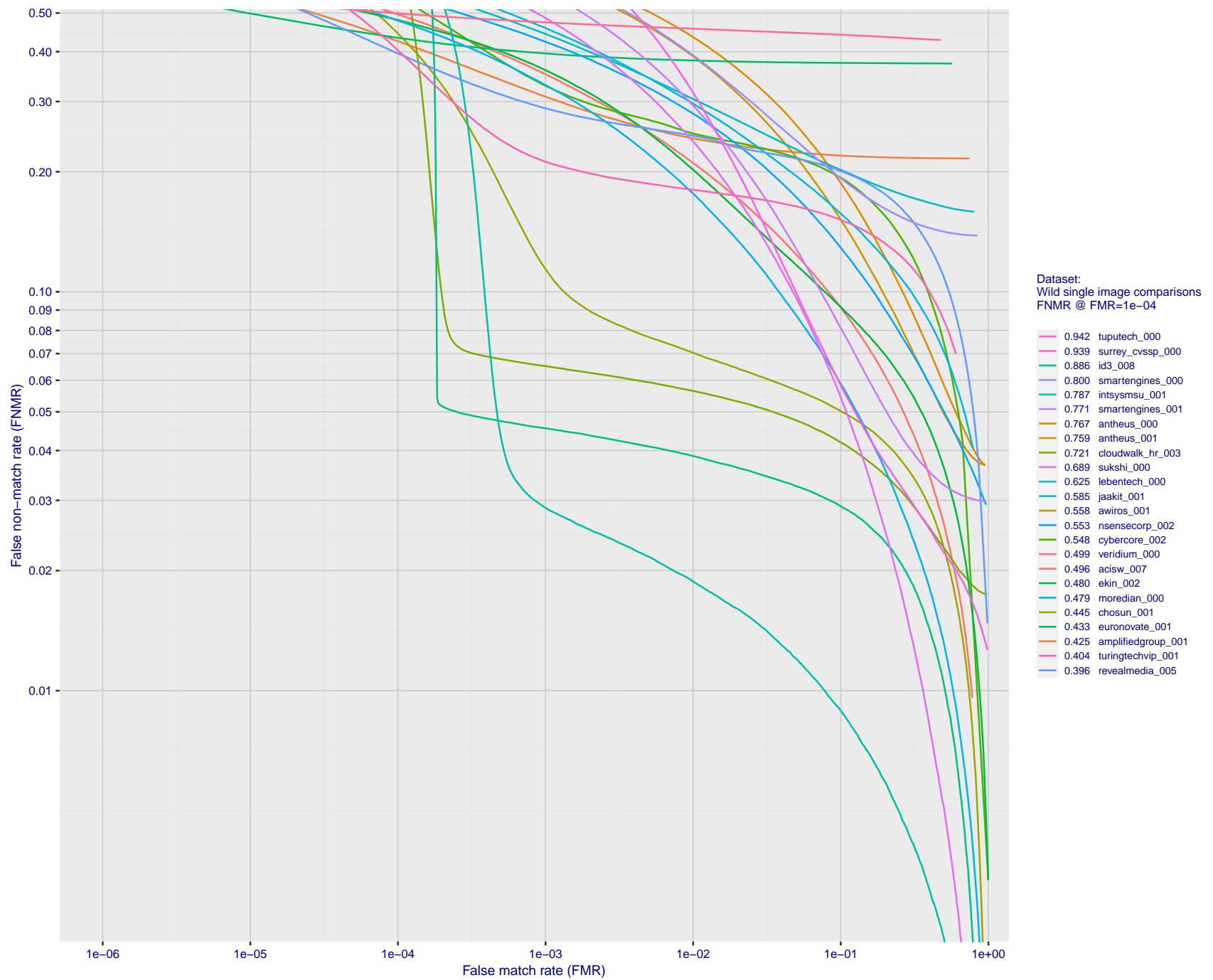


Figure 125: For the 2018 wild image comparisons, detection error tradeoff (DET) characteristics showing false non-match rate vs. false match rate plotted parametrically on threshold, T. The scales are logarithmic in order to show several decades of FMR.

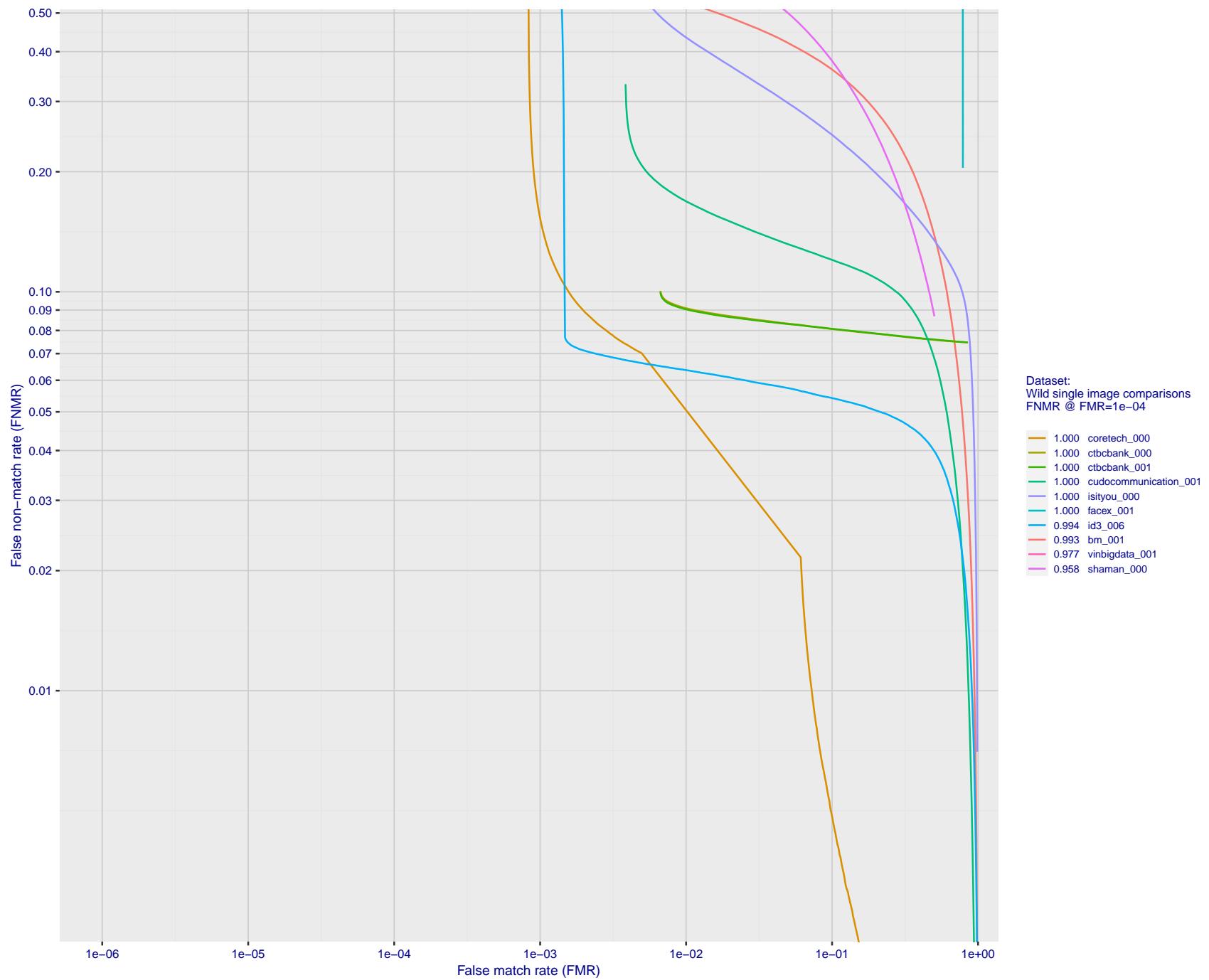


Figure 126: For the 2018 wild image comparisons, detection error tradeoff (DET) characteristics showing false non-match rate vs. false match rate plotted parametrically on threshold, T . The scales are logarithmic in order to show several decades of FMR.

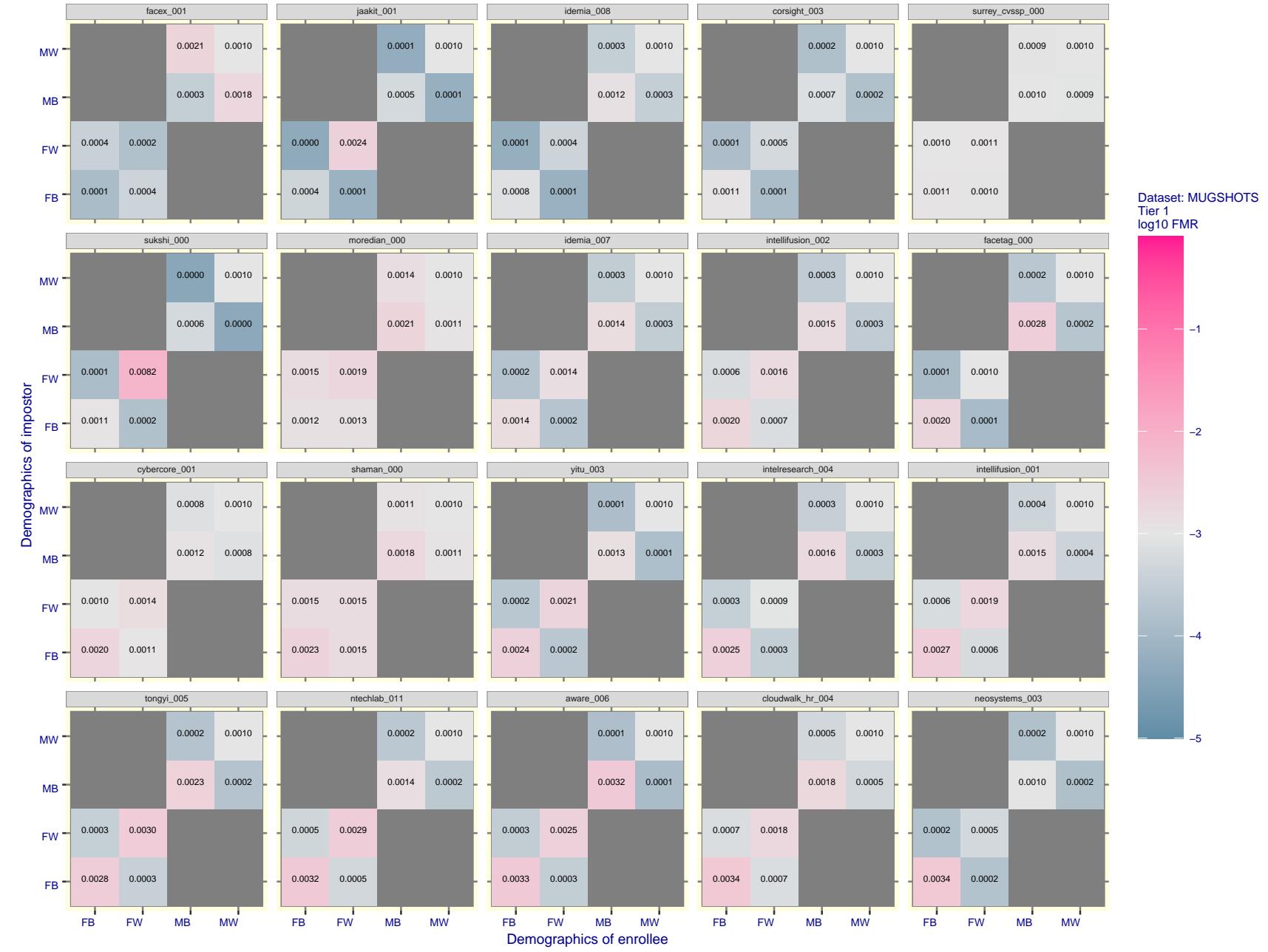


Figure 127: For the mugshot images, FMR for same-sex impostor pairs of images annotated with codes for black female, black male, white female, white male. The threshold is set for each algorithm to give FMR = 0.001 for white males which is the demographic that usually gives the lowest FMR. This means the top right box is the same color in all panels. The panels are sorted over multiple pages in order of FMR on black females, which is the demographic that usually gives the highest FMR.

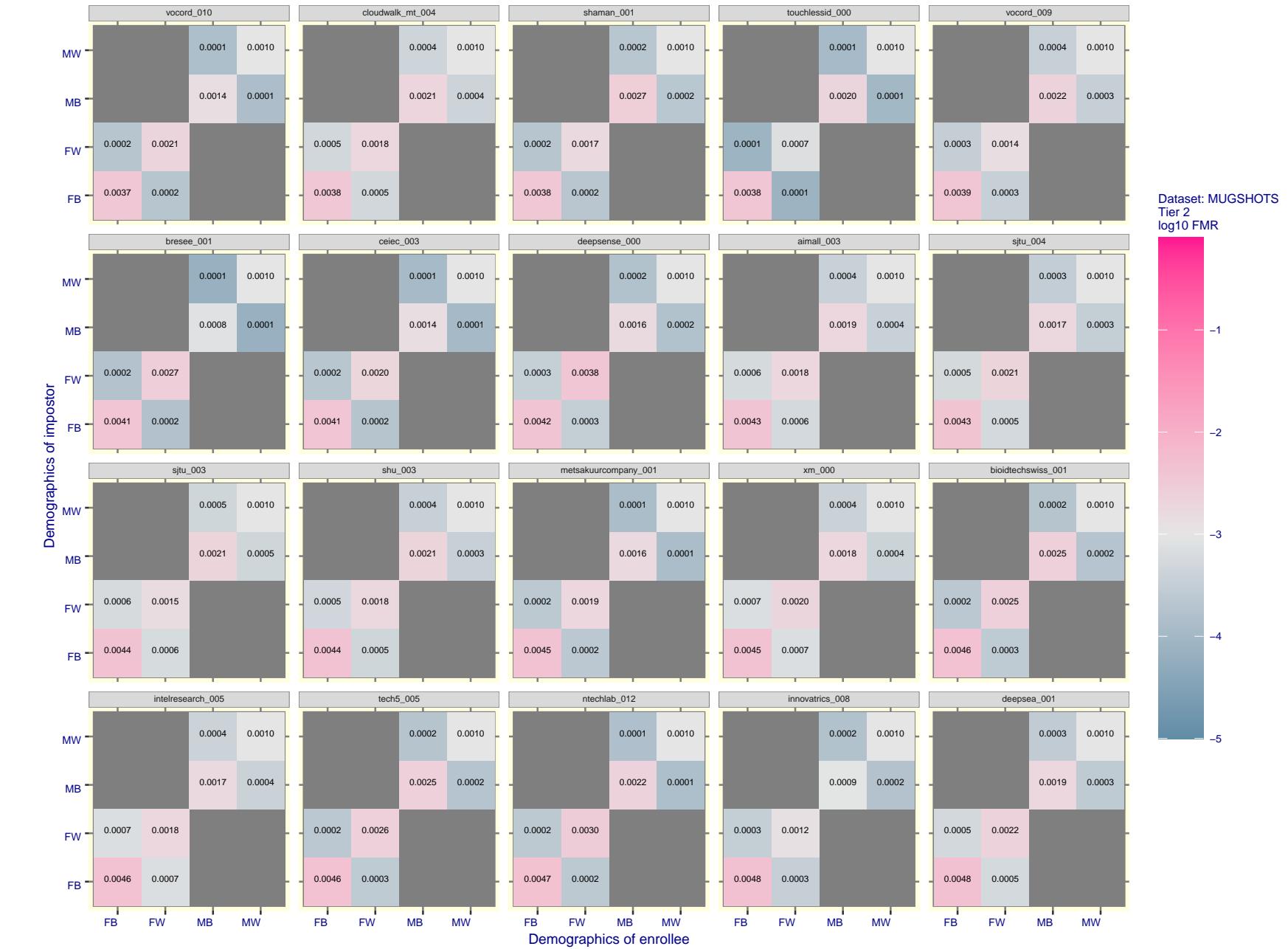


Figure 128: For the mugshot images, FMR for same-sex impostor pairs of images annotated with codes for black female, black male, white female, white male. The threshold is set for each algorithm to give $FMR = 0.001$ for white males which is the demographic that usually gives the lowest FMR. This means the top right box is the same color in all panels. The panels are sorted over multiple pages in order of FMR on black females, which is the demographic that usually gives the highest FMR.

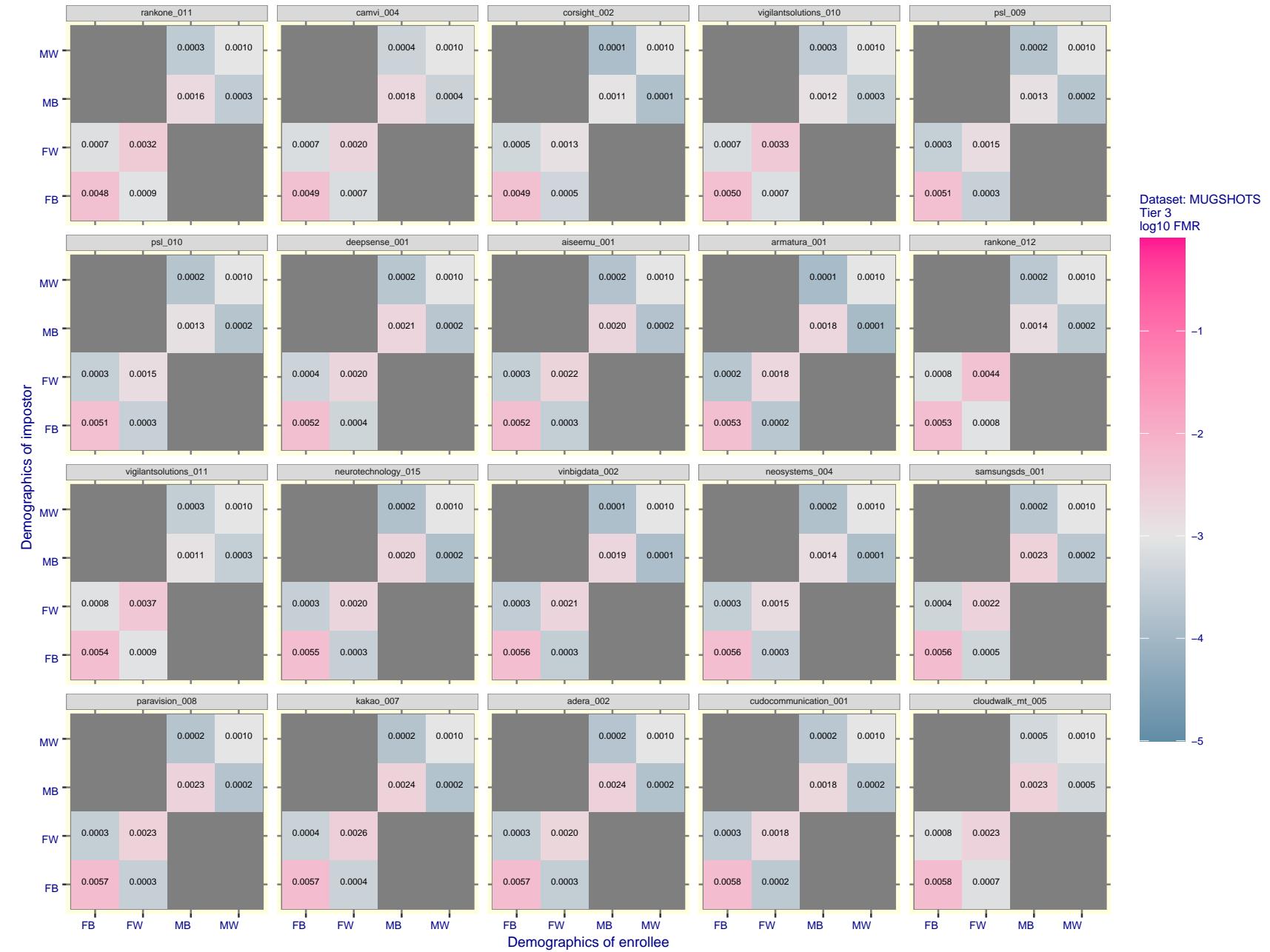


Figure 129: For the mugshot images, FMR for same-sex impostor pairs of images annotated with codes for black female, black male, white female, white male. The threshold is set for each algorithm to give $FMR = 0.001$ for white males which is the demographic that usually gives the lowest FMR. This means the top right box is the same color in all panels. The panels are sorted over multiple pages in order of FMR on black females, which is the demographic that usually gives the highest FMR.

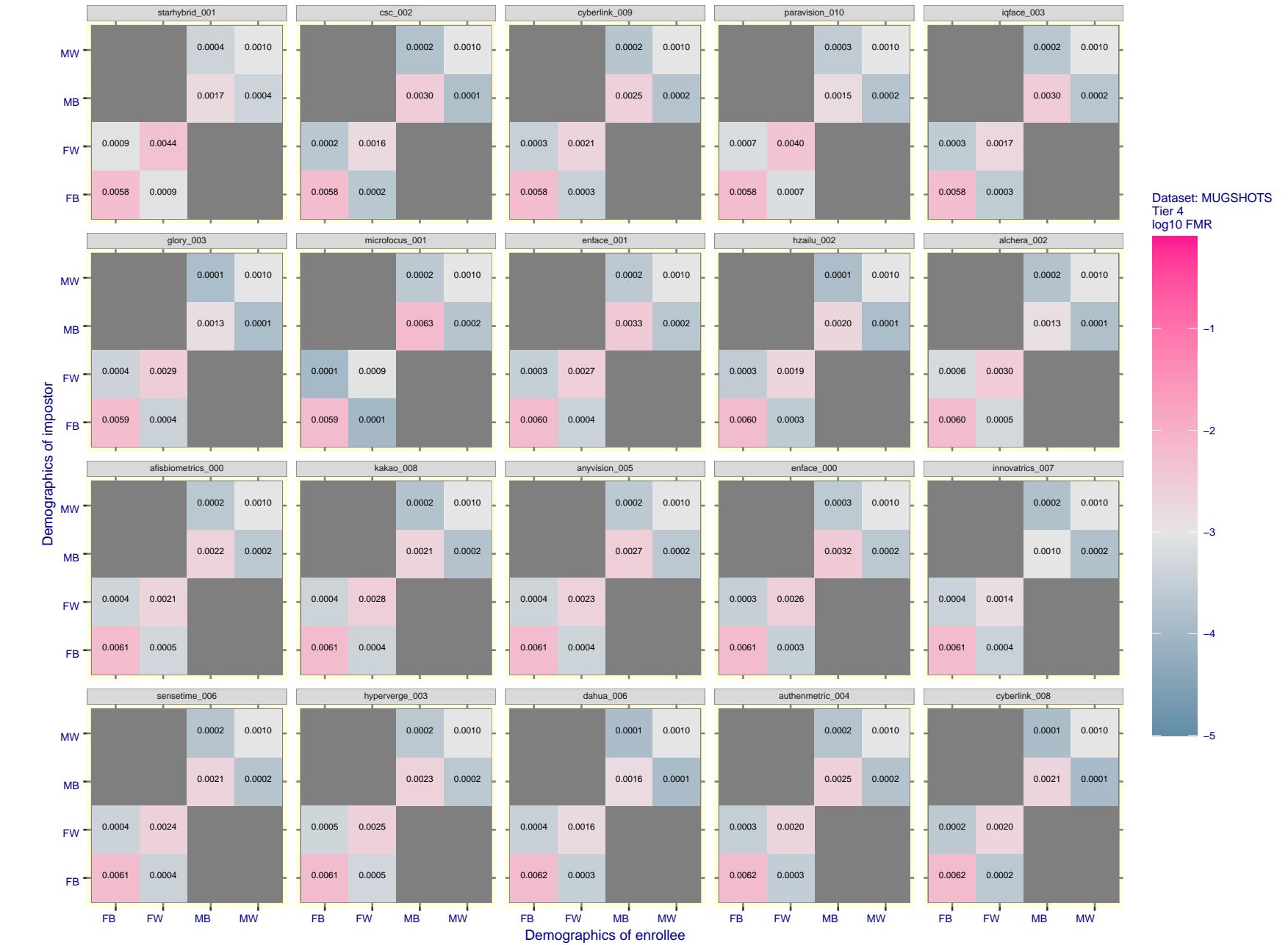


Figure 130: For the mugshot images, FMR for same-sex impostor pairs of images annotated with codes for black female, black male, white female, white male. The threshold is set for each algorithm to give FMR = 0.001 for white males which is the demographic that usually gives the lowest FMR. This means the top right box is the same color in all panels. The panels are sorted over multiple pages in order of FMR on black females, which is the demographic that usually gives the highest FMR.

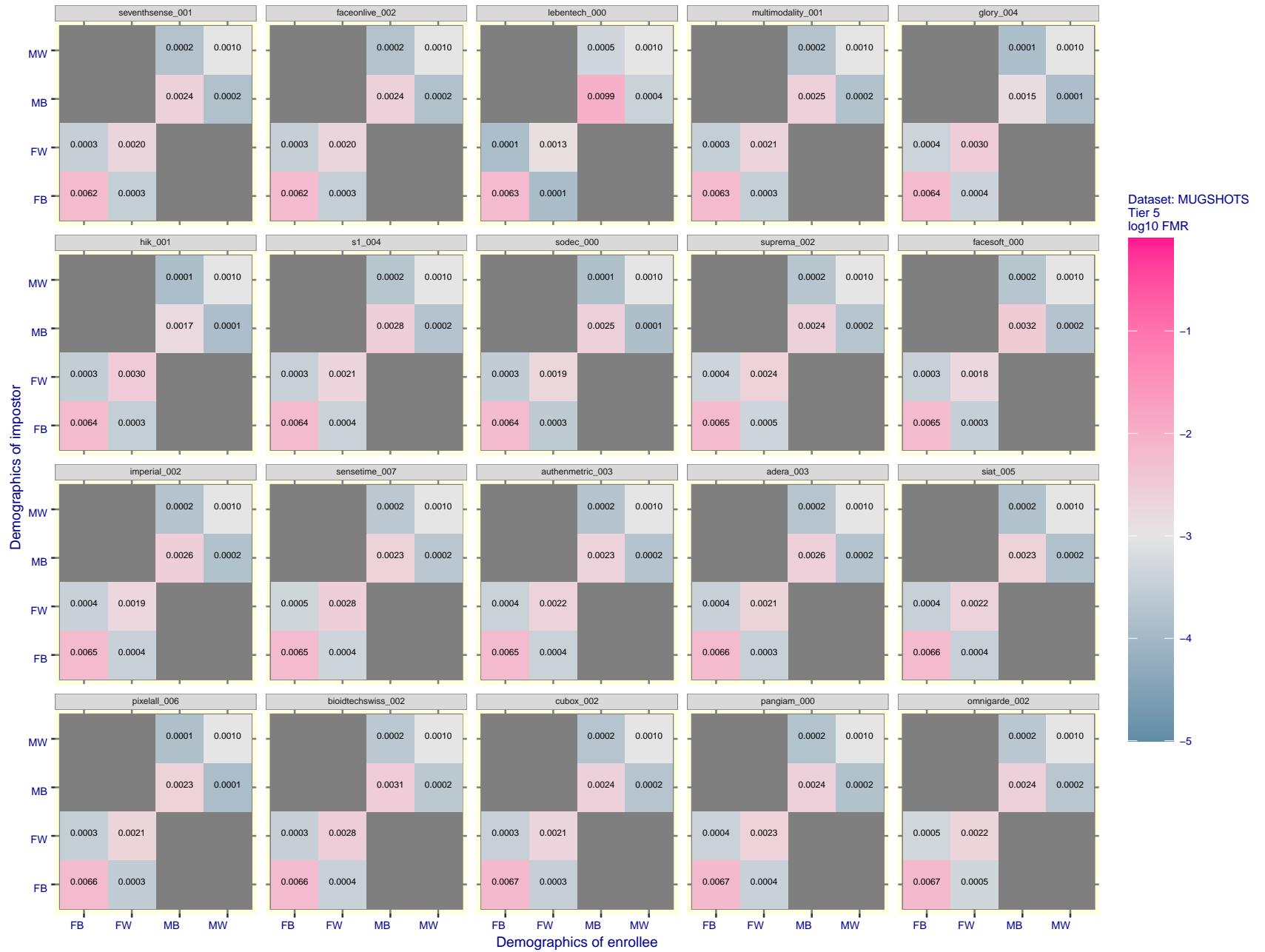


Figure 131: For the mugshot images, FMR for same-sex impostor pairs of images annotated with codes for black female, black male, white female, white male. The threshold is set for each algorithm to give FMR = 0.001 for white males which is the demographic that usually gives the lowest FMR. This means the top right box is the same color in all panels. The panels are sorted over multiple pages in order of FMR on black females, which is the demographic that usually gives the highest FMR.

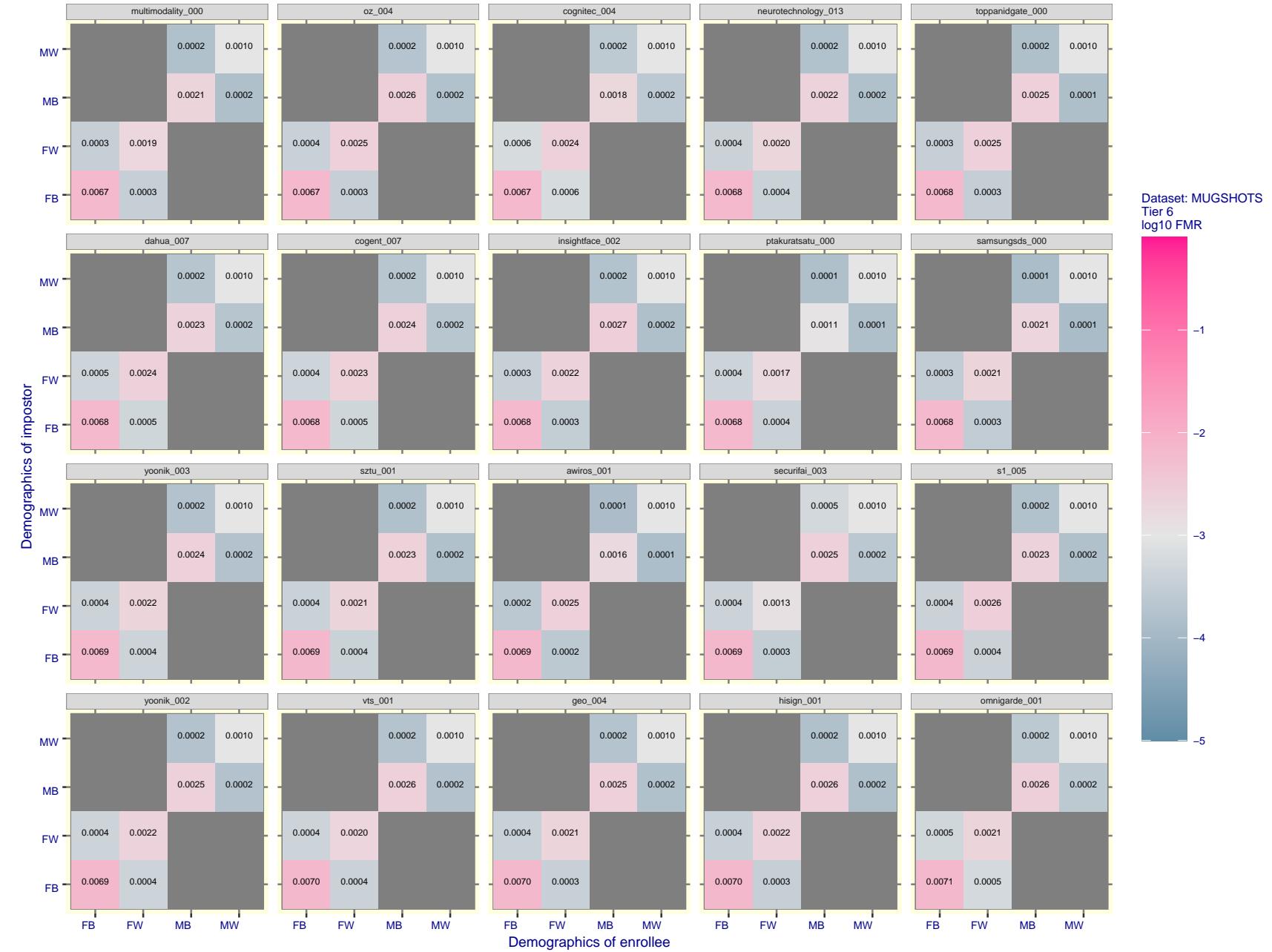


Figure 132: For the mugshot images, FMR for same-sex impostor pairs of images annotated with codes for black female, black male, white female, white male. The threshold is set for each algorithm to give $\text{FMR} = 0.001$ for white males which is the demographic that usually gives the lowest FMR. This means the top right box is the same color in all panels. The panels are sorted over multiple pages in order of FMR on black females, which is the demographic that usually gives the highest FMR.

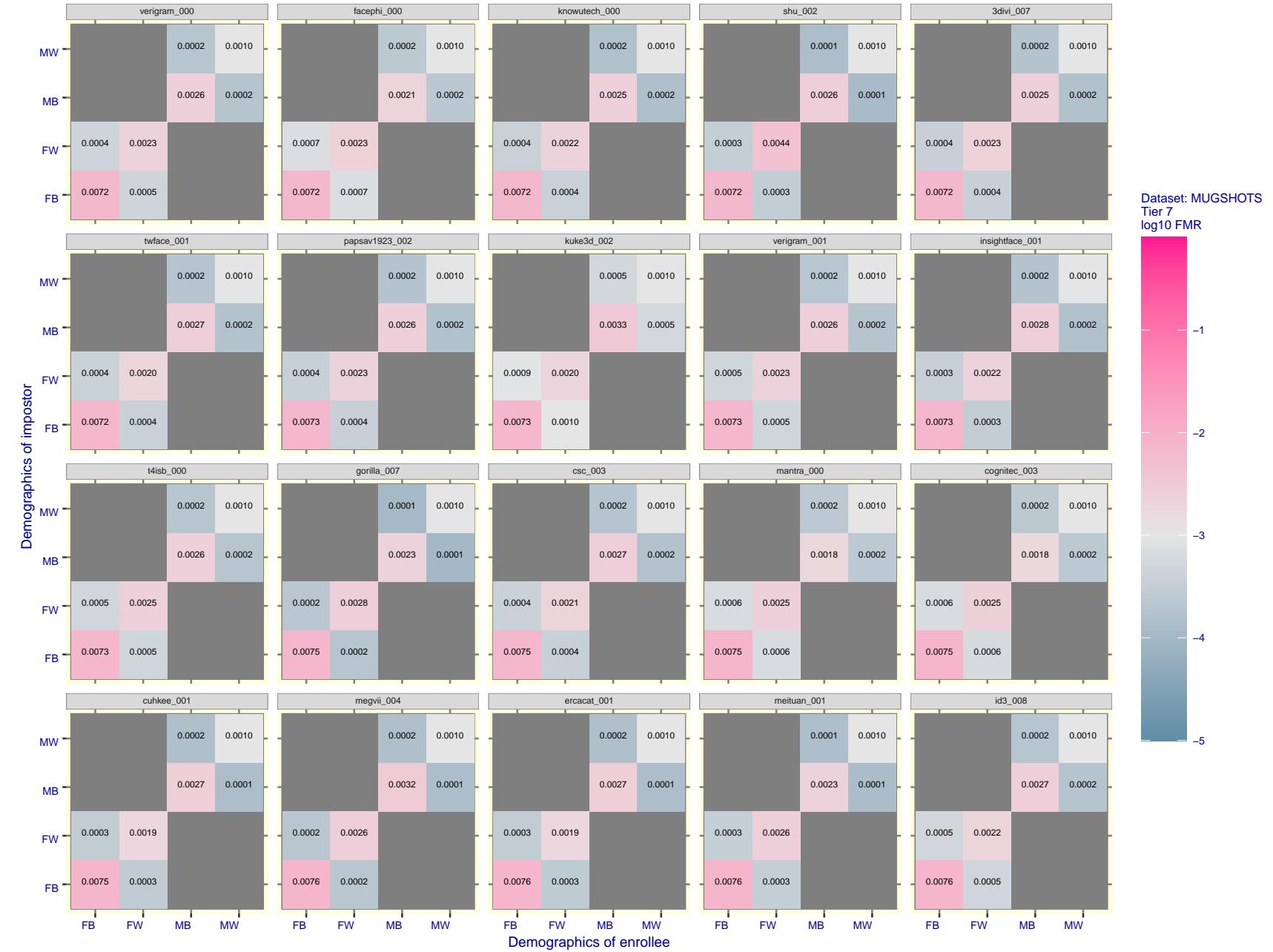


Figure 133: For the mugshot images, FMR for same-sex impostor pairs of images annotated with codes for black female, black male, white female, white male. The threshold is set for each algorithm to give FMR = 0.001 for white males which is the demographic that usually gives the lowest FMR. This means the top right box is the same color in all panels. The panels are sorted over multiple pages in order of FMR on black females, which is the demographic that usually gives the highest FMR.

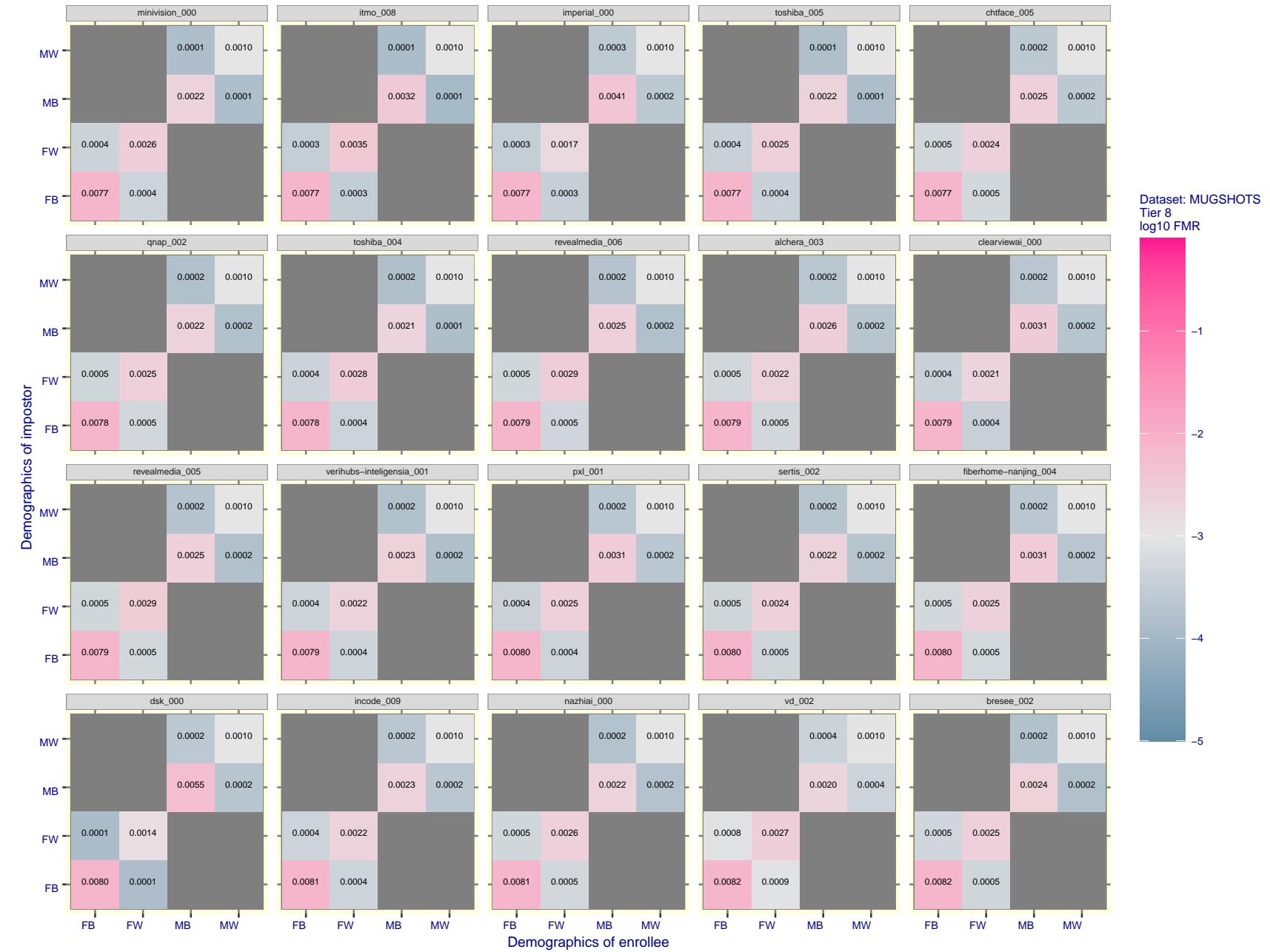


Figure 134: For the mugshot images, FMR for same-sex impostor pairs of images annotated with codes for black female, black male, white female, white male. The threshold is set for each algorithm to give $FMR = 0.001$ for white males which is the demographic that usually gives the lowest FMR. This means the top right box is the same color in all panels. The panels are sorted over multiple pages in order of FMR on black females, which is the demographic that usually gives the highest FMR.

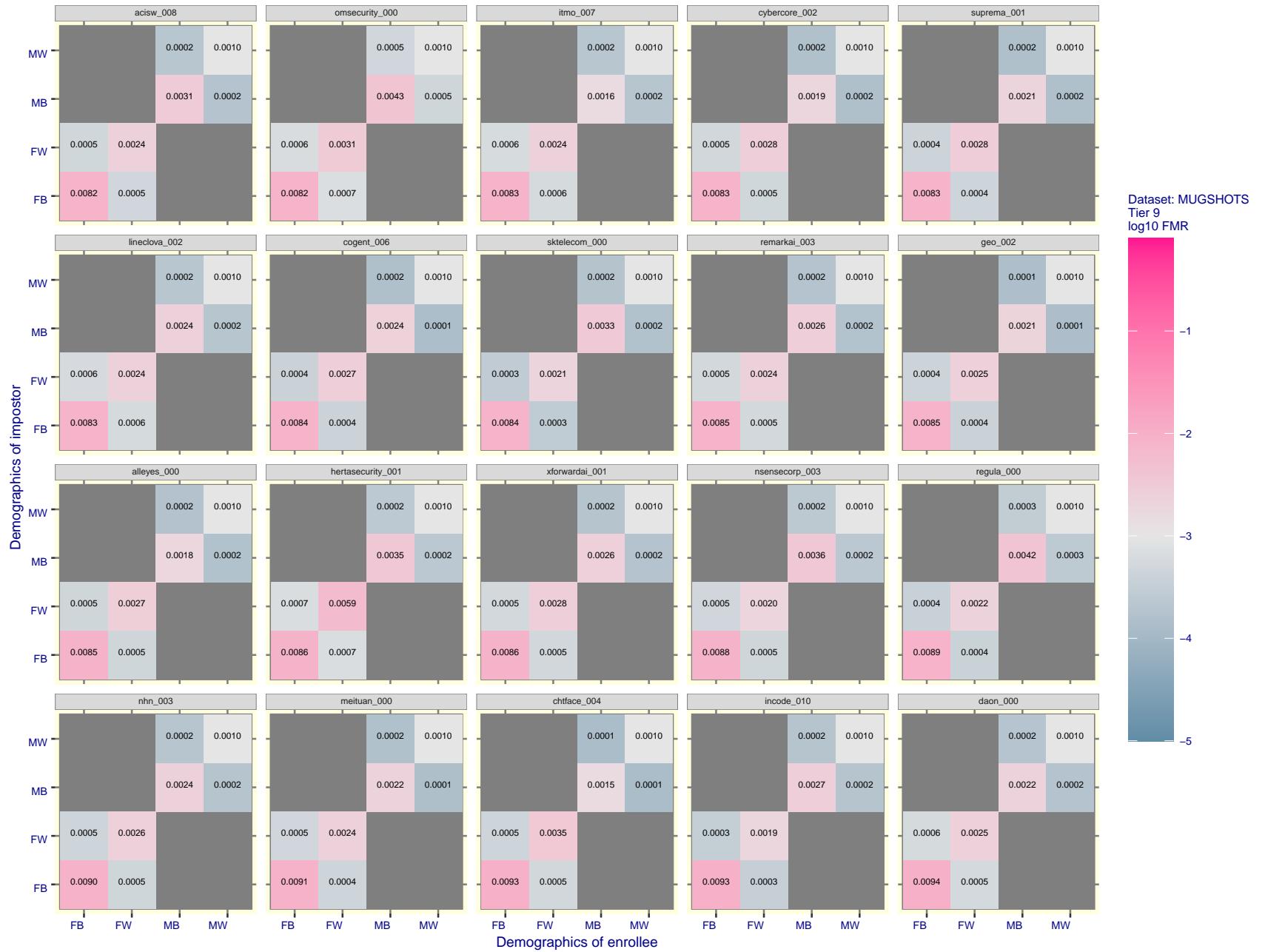


Figure 135: For the mugshot images, FMR for same-sex impostor pairs of images annotated with codes for black female, black male, white female, white male. The threshold is set for each algorithm to give $FMR = 0.001$ for white males which is the demographic that usually gives the lowest FMR. This means the top right box is the same color in all panels. The panels are sorted over multiple pages in order of FMR on black females, which is the demographic that usually gives the highest FMR.

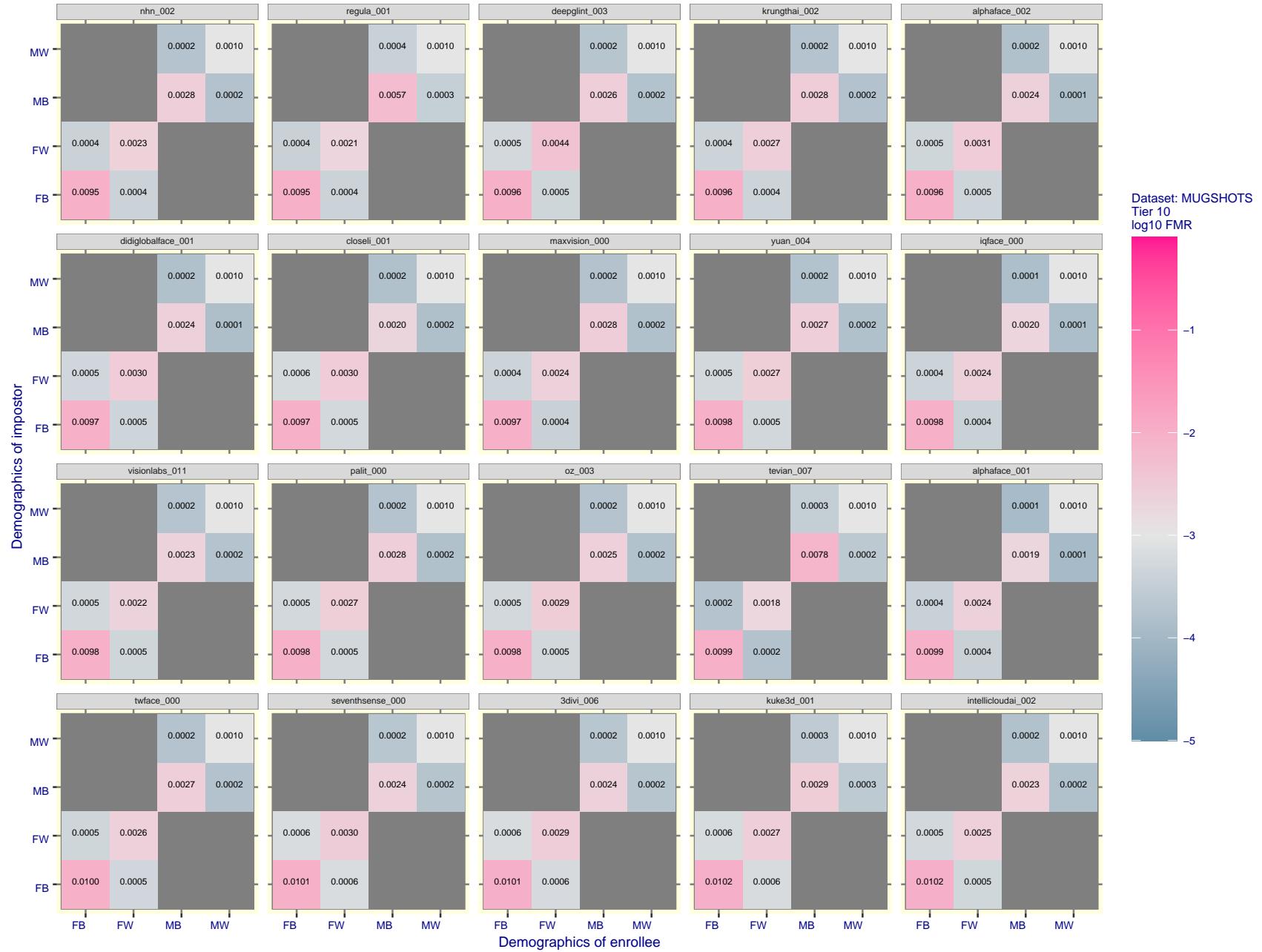


Figure 136: For the mugshot images, FMR for same-sex impostor pairs of images annotated with codes for black female, black male, white female, white male. The threshold is set for each algorithm to give FMR = 0.001 for white males which is the demographic that usually gives the lowest FMR. This means the top right box is the same color in all panels. The panels are sorted over multiple pages in order of FMR on black females, which is the demographic that usually gives the highest FMR.

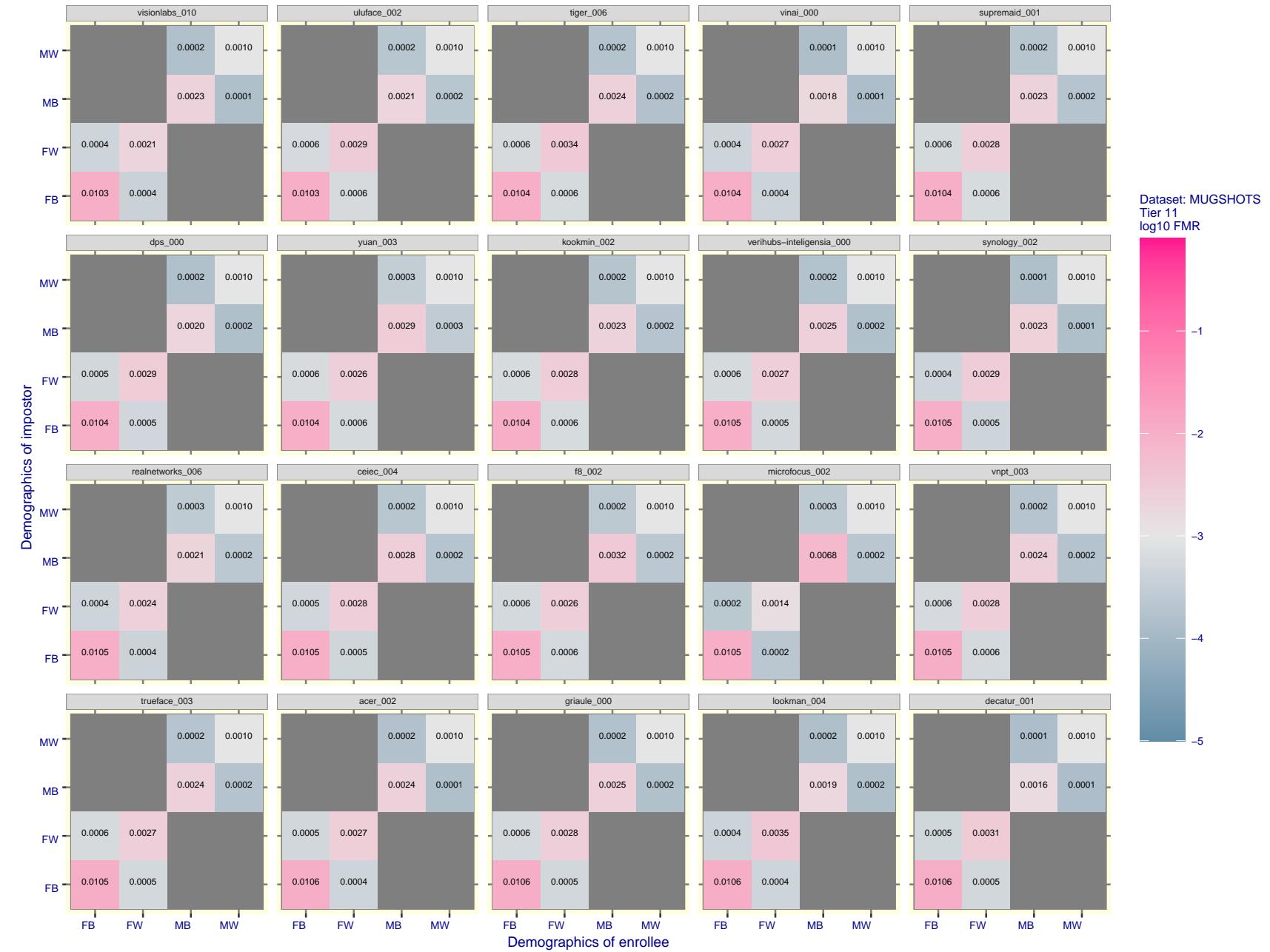


Figure 137: For the mugshot images, FMR for same-sex impostor pairs of images annotated with codes for black female, black male, white female, white male. The threshold is set for each algorithm to give $FMR = 0.001$ for white males which is the demographic that usually gives the lowest FMR. This means the top right box is the same color in all panels. The panels are sorted over multiple pages in order of FMR on black females, which is the demographic that usually gives the highest FMR.

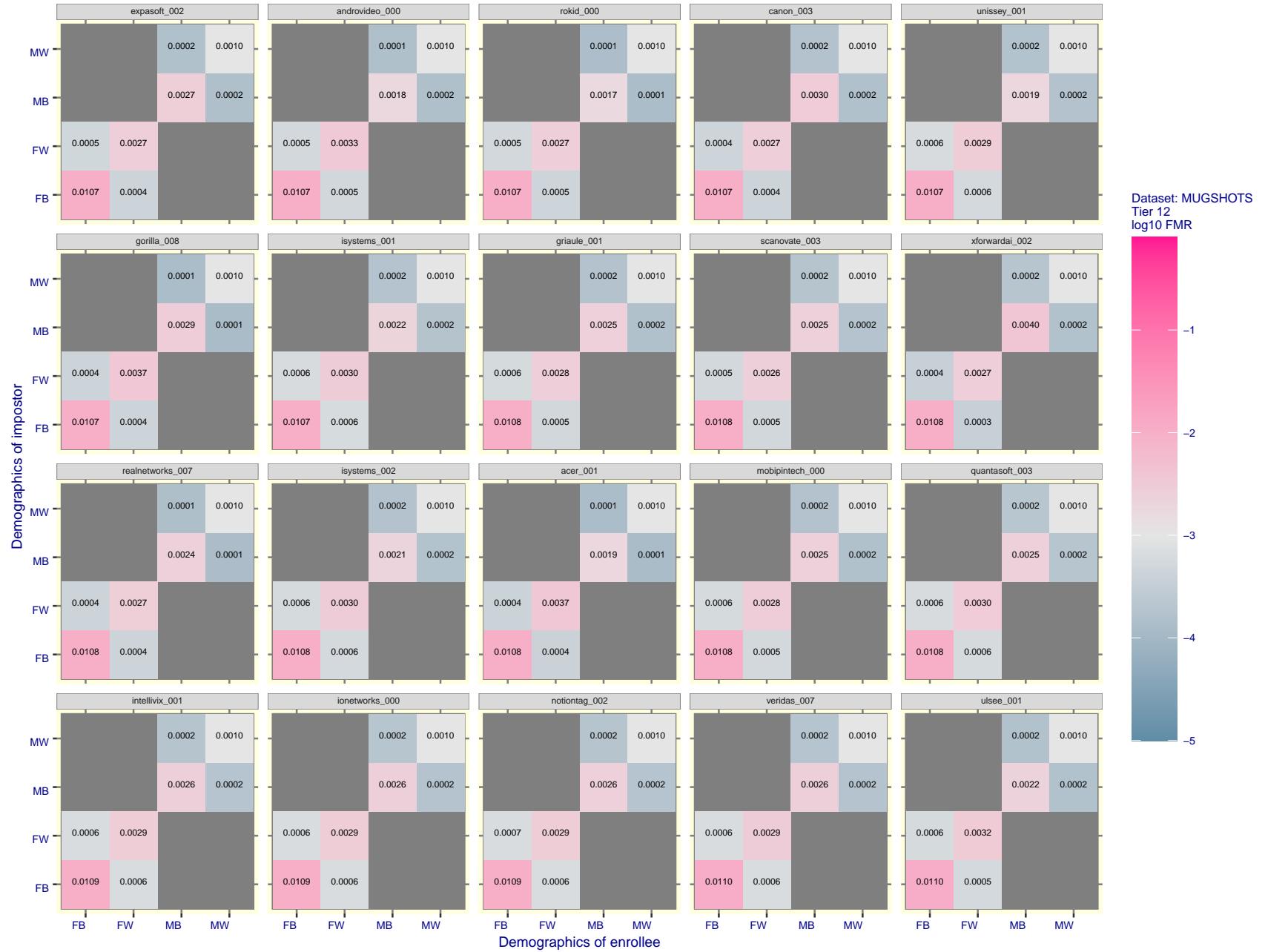


Figure 138: For the mugshot images, FMR for same-sex impostor pairs of images annotated with codes for black female, black male, white female, white male. The threshold is set for each algorithm to give FMR = 0.001 for white males which is the demographic that usually gives the lowest FMR. This means the top right box is the same color in all panels. The panels are sorted over multiple pages in order of FMR on black females, which is the demographic that usually gives the highest FMR.

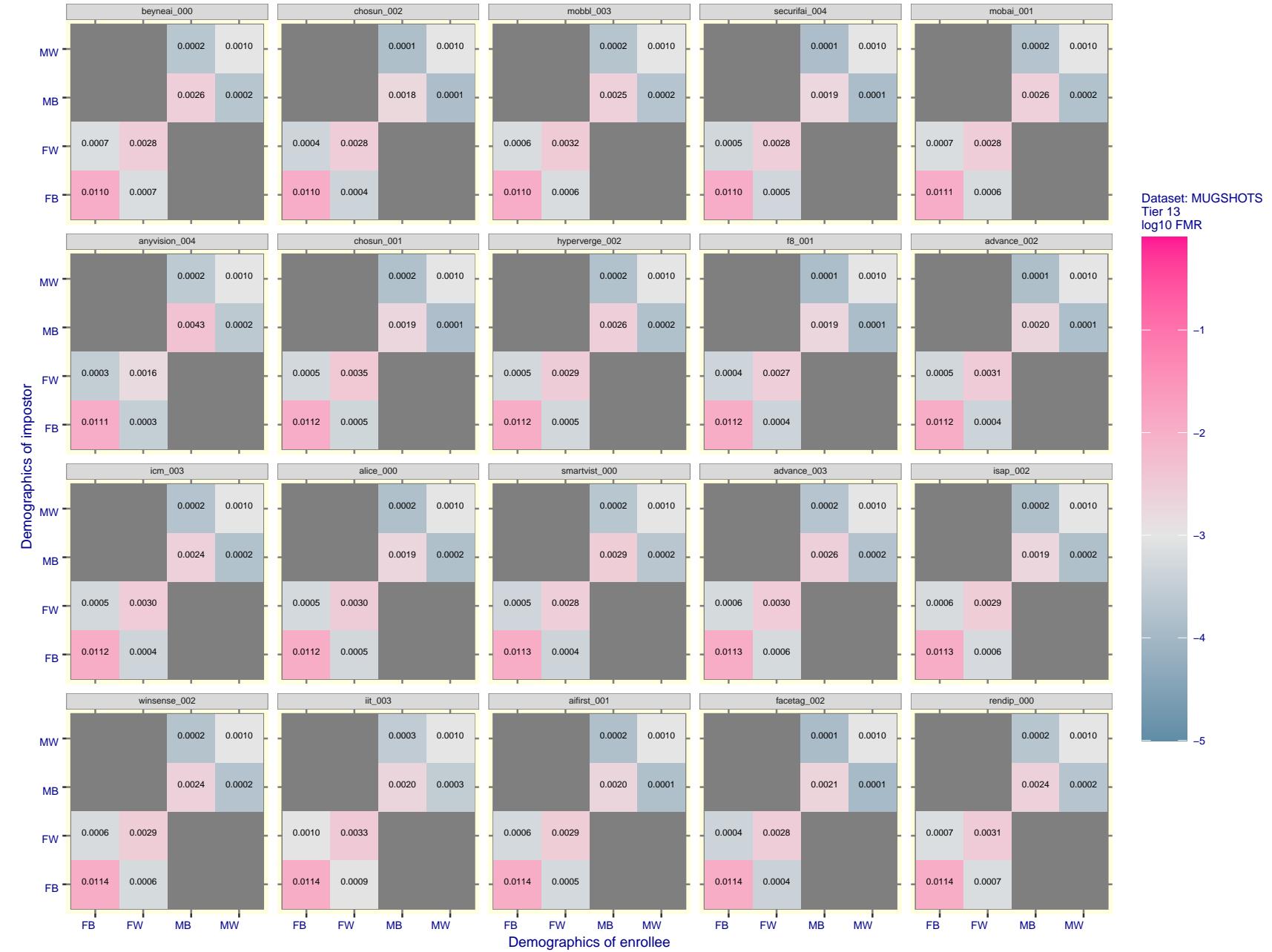


Figure 139: For the mugshot images, FMR for same-sex impostor pairs of images annotated with codes for black female, black male, white female, white male. The threshold is set for each algorithm to give FMR = 0.001 for white males which is the demographic that usually gives the lowest FMR. This means the top right box is the same color in all panels. The panels are sorted over multiple pages in order of FMR on black females, which is the demographic that usually gives the highest FMR.

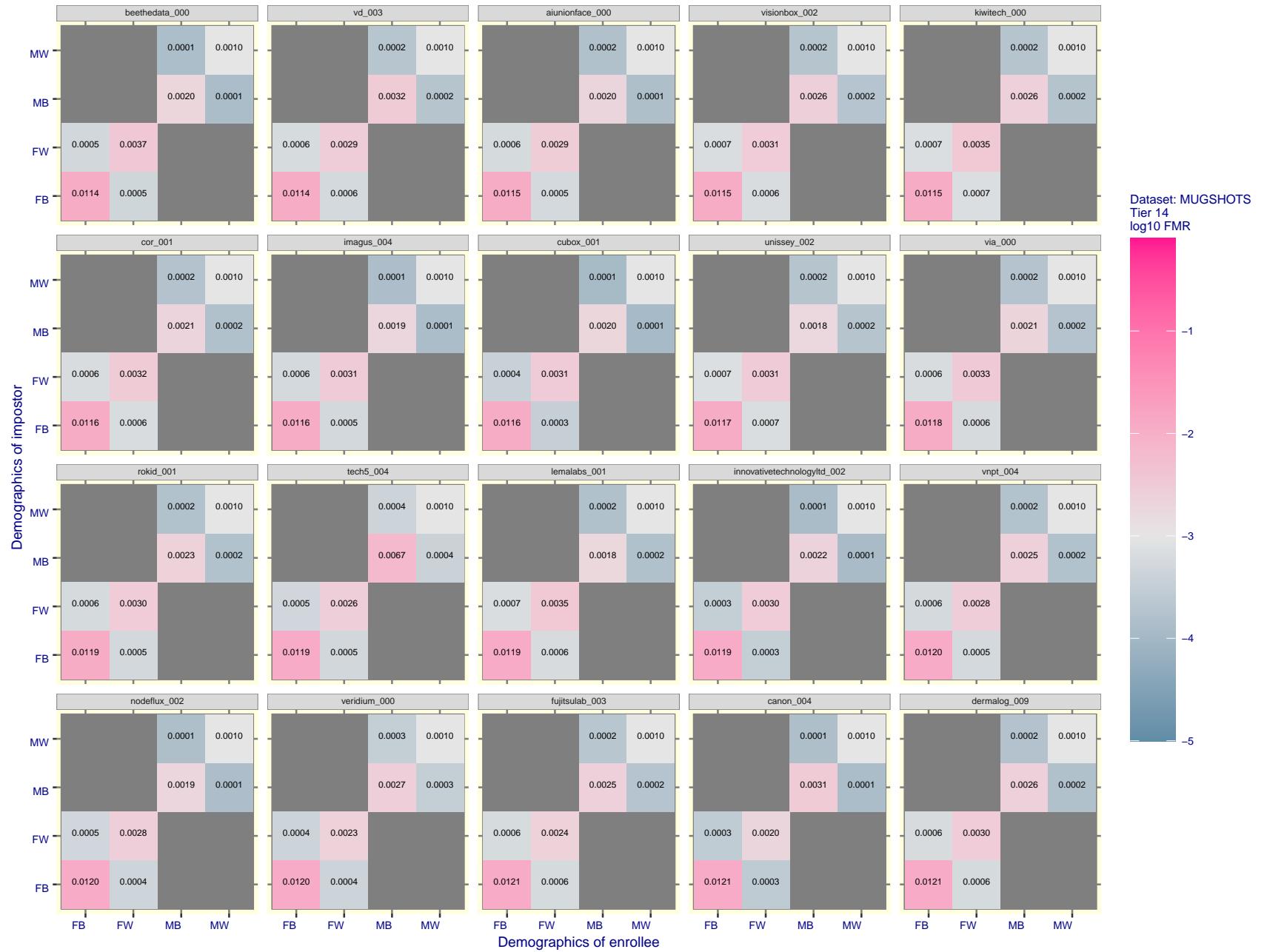


Figure 140: For the mugshot images, FMR for same-sex impostor pairs of images annotated with codes for black female, black male, white female, white male. The threshold is set for each algorithm to give $FMR = 0.001$ for white males which is the demographic that usually gives the lowest FMR. This means the top right box is the same color in all panels. The panels are sorted over multiple pages in order of FMR on black females, which is the demographic that usually gives the highest FMR.

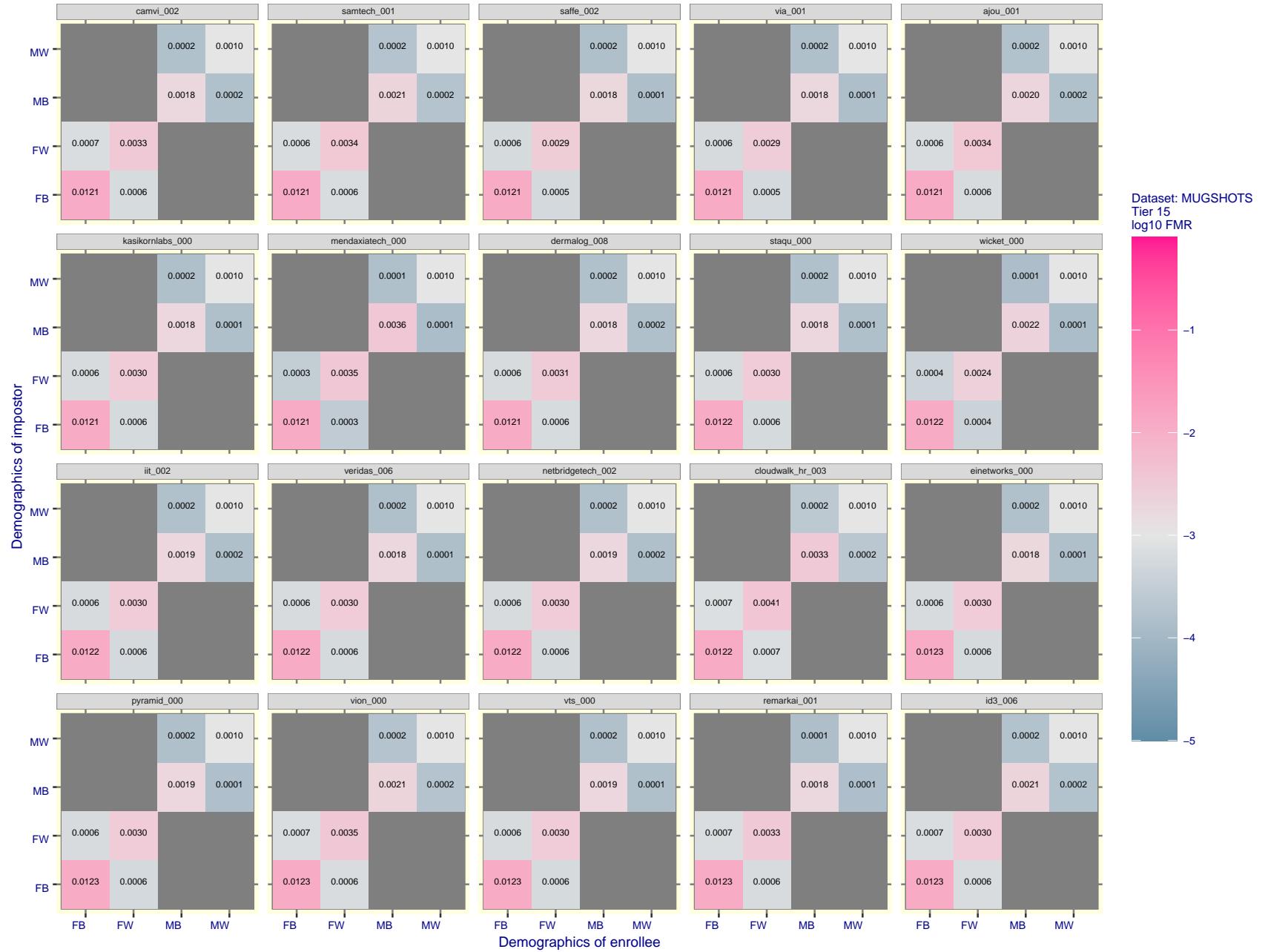


Figure 141: For the mugshot images, FMR for same-sex impostor pairs of images annotated with codes for black female, black male, white female, white male. The threshold is set for each algorithm to give $FMR = 0.001$ for white males which is the demographic that usually gives the lowest FMR. This means the top right box is the same color in all panels. The panels are sorted over multiple pages in order of FMR on black females, which is the demographic that usually gives the highest FMR.

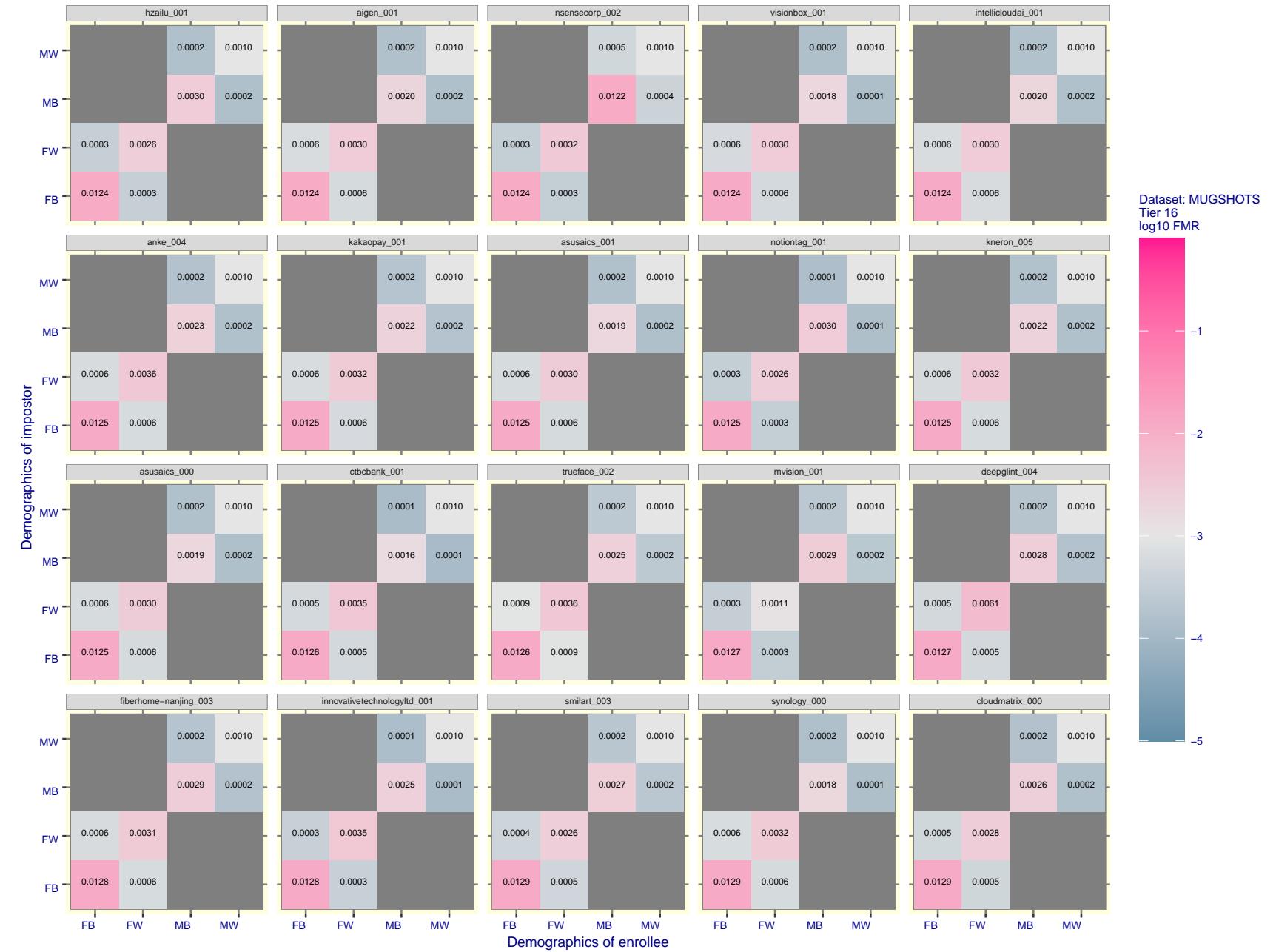


Figure 142: For the mugshot images, FMR for same-sex impostor pairs of images annotated with codes for black female, black male, white female, white male. The threshold is set for each algorithm to give $FMR = 0.001$ for white males which is the demographic that usually gives the lowest FMR. This means the top right box is the same color in all panels. The panels are sorted over multiple pages in order of FMR on black females, which is the demographic that usually gives the highest FMR.

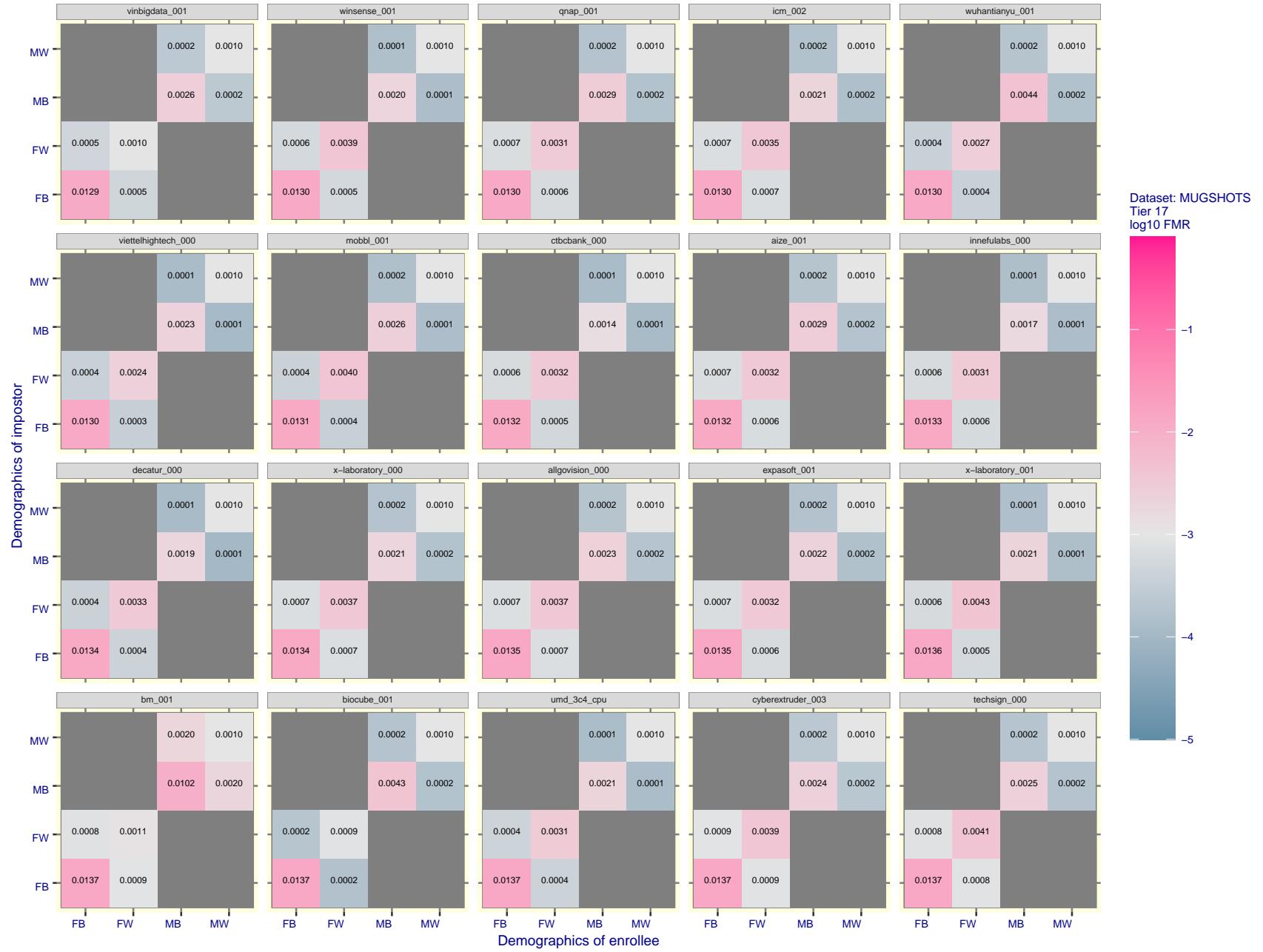


Figure 143: For the mugshot images, FMR for same-sex impostor pairs of images annotated with codes for black female, black male, white female, white male. The threshold is set for each algorithm to give FMR = 0.001 for white males which is the demographic that usually gives the lowest FMR. This means the top right box is the same color in all panels. The panels are sorted over multiple pages in order of FMR on black females, which is the demographic that usually gives the highest FMR.

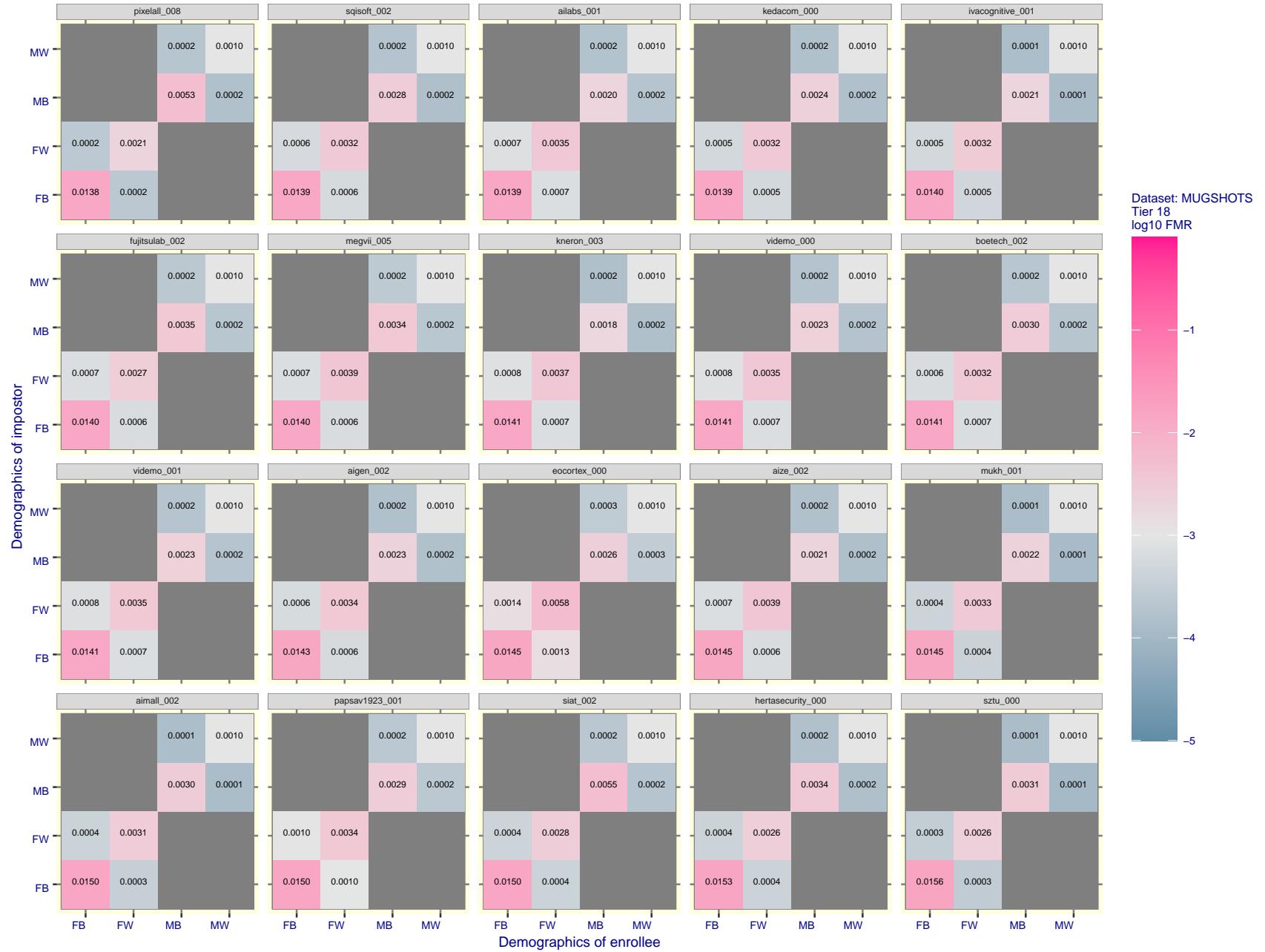


Figure 144: For the mugshot images, FMR for same-sex impostor pairs of images annotated with codes for black female, black male, white female, white male. The threshold is set for each algorithm to give FMR = 0.001 for white males which is the demographic that usually gives the lowest FMR. This means the top right box is the same color in all panels. The panels are sorted over multiple pages in order of FMR on black females, which is the demographic that usually gives the highest FMR.

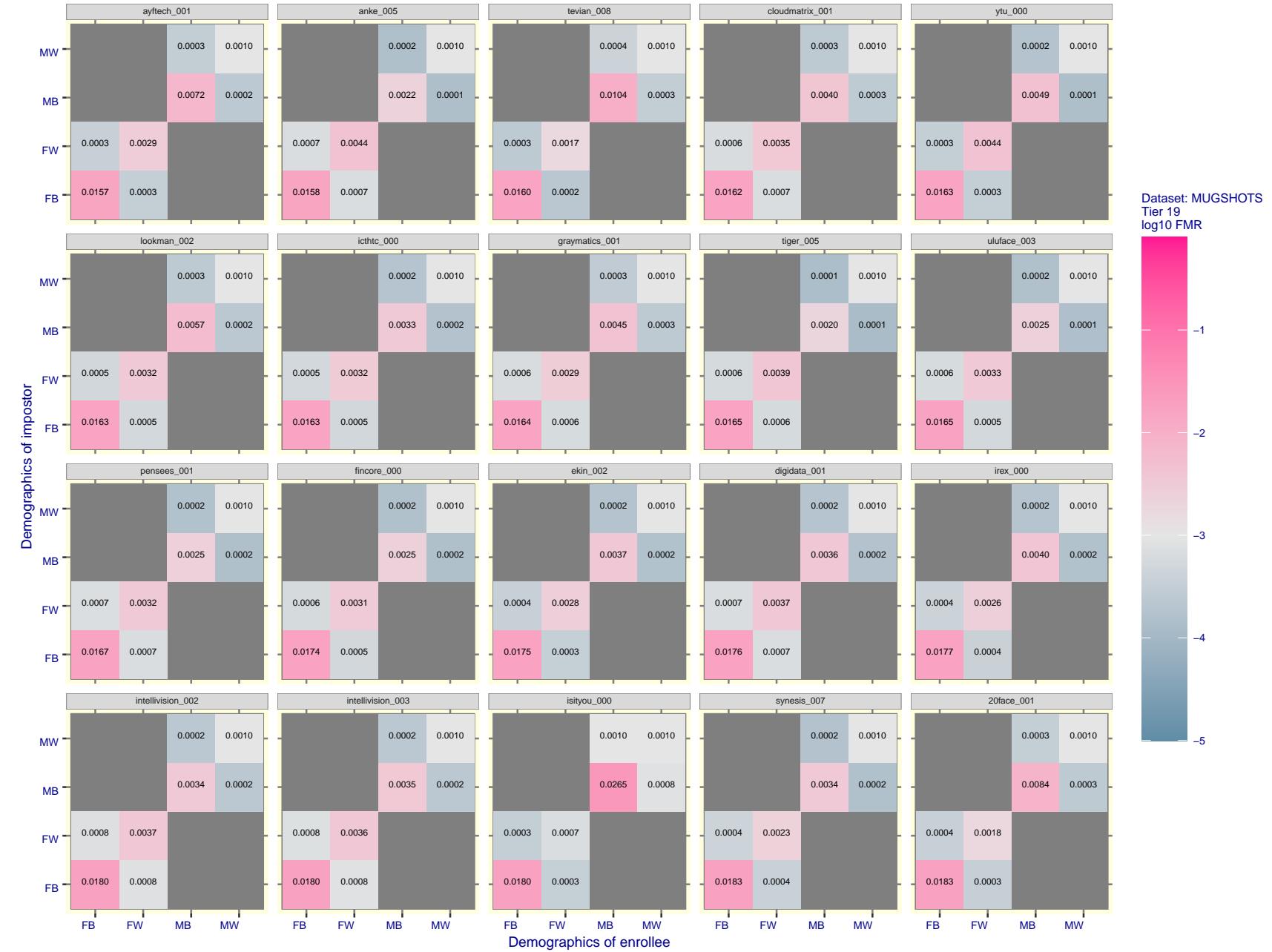


Figure 145: For the mugshot images, FMR for same-sex impostor pairs of images annotated with codes for black female, black male, white female, white male. The threshold is set for each algorithm to give FMR = 0.001 for white males which is the demographic that usually gives the lowest FMR. This means the top right box is the same color in all panels. The panels are sorted over multiple pages in order of FMR on black females, which is the demographic that usually gives the highest FMR.



Figure 146: For the mugshot images, FMR for same-sex impostor pairs of images annotated with codes for black female, black male, white female, white male. The threshold is set for each algorithm to give FMR = 0.001 for white males which is the demographic that usually gives the lowest FMR. This means the top right box is the same color in all panels. The panels are sorted over multiple pages in order of FMR on black females, which is the demographic that usually gives the highest FMR.

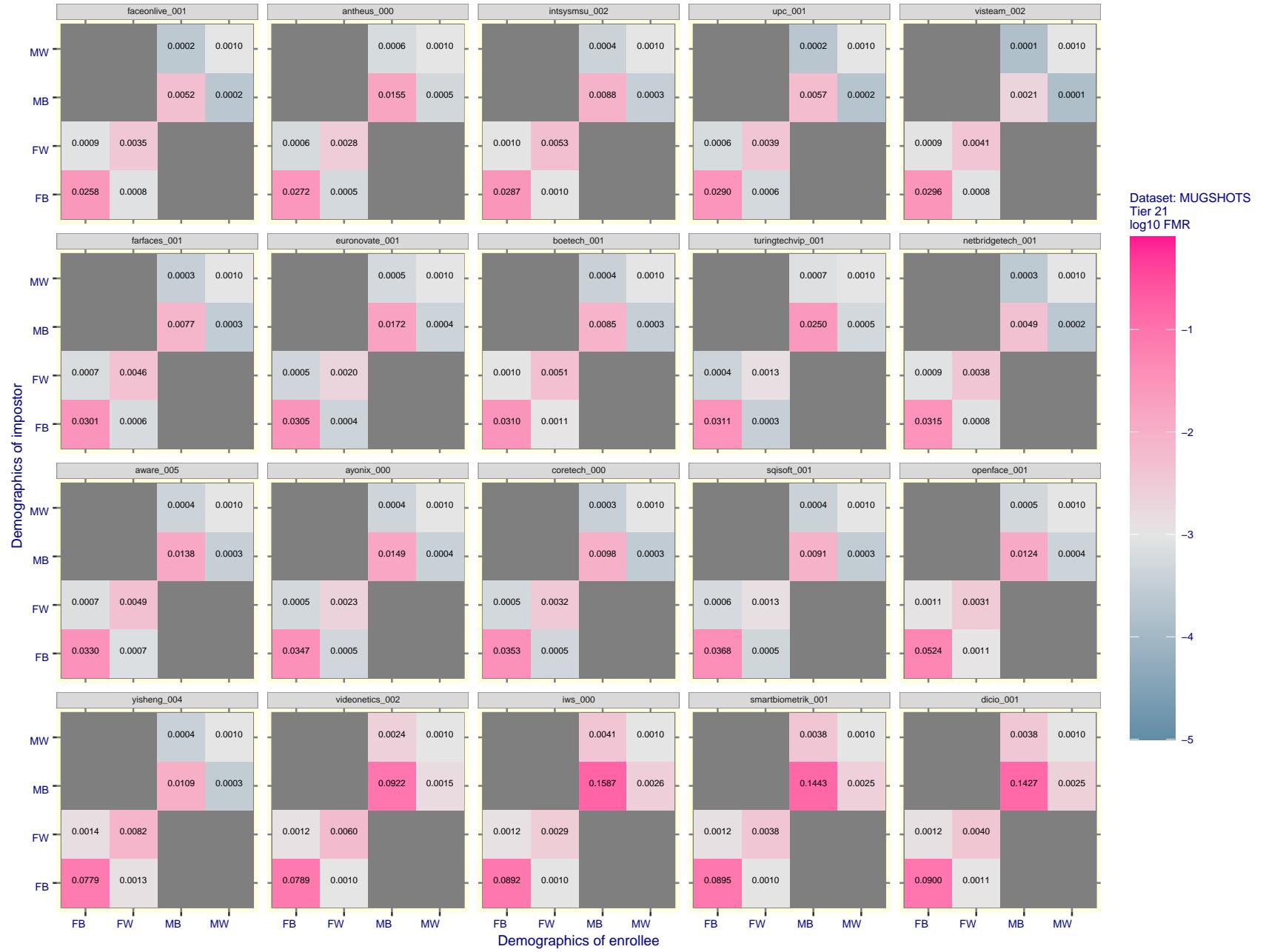


Figure 147: For the mugshot images, FMR for same-sex impostor pairs of images annotated with codes for black female, black male, white female, white male. The threshold is set for each algorithm to give FMR = 0.001 for white males which is the demographic that usually gives the lowest FMR. This means the top right box is the same color in all panels. The panels are sorted over multiple pages in order of FMR on black females, which is the demographic that usually gives the highest FMR.

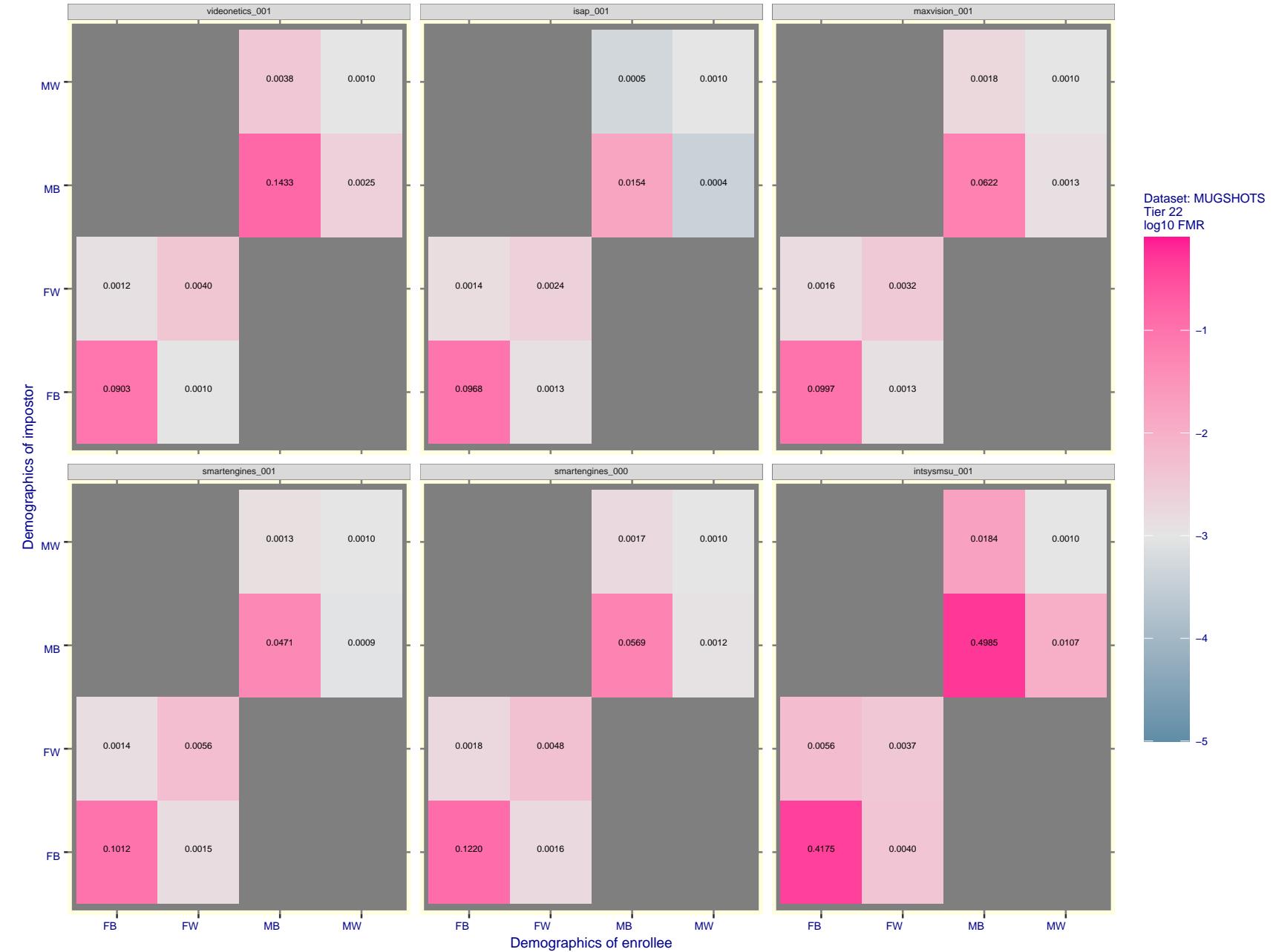


Figure 148: For the mugshot images, FMR for same-sex impostor pairs of images annotated with codes for black female, black male, white female, white male. The threshold is set for each algorithm to give $FMR = 0.001$ for white males which is the demographic that usually gives the lowest FMR. This means the top right box is the same color in all panels. The panels are sorted over multiple pages in order of FMR on black females, which is the demographic that usually gives the highest FMR.

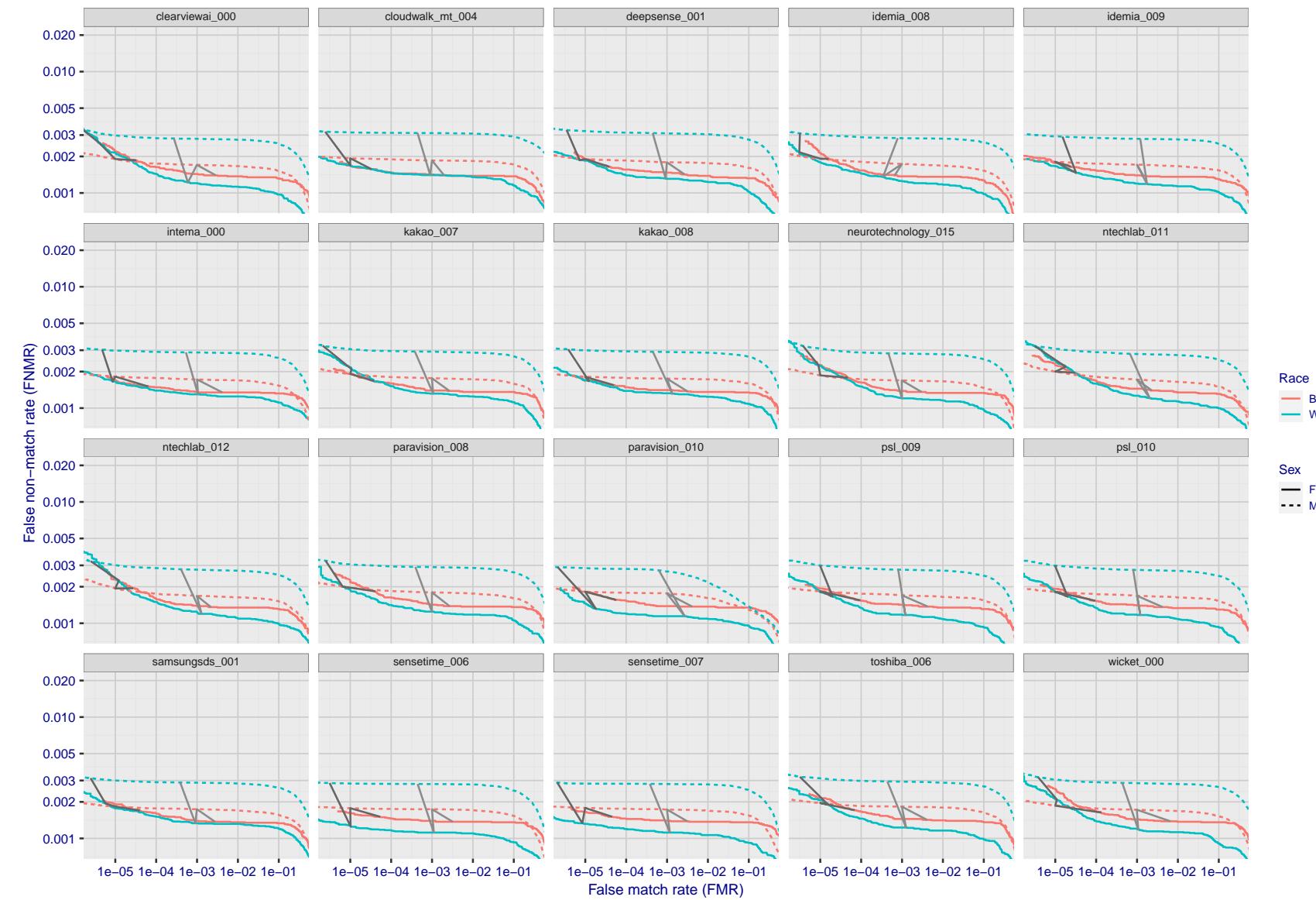


Figure 149: For the mugshot images, error tradeoff characteristics for white females, black females, black males and white males. The Z-shaped grey lines correspond to fixed thresholds, showing both FNMR and FMR vary at one T value. Note: Many of the plots will naively be read as saying women gives worse error rates than men because the solid traces lie above the dotted ones. However, this is misleading and incomplete: The grey lines show the traces reveal horizontal shifts. Thus for the cogent-003 algorithm FNMR for men is higher than for women at a fixed threshold but, at the same time, FMR is higher for women - see Figure 232. As access control systems almost always operate at a fixed threshold, the naive interpretation is incorrect.

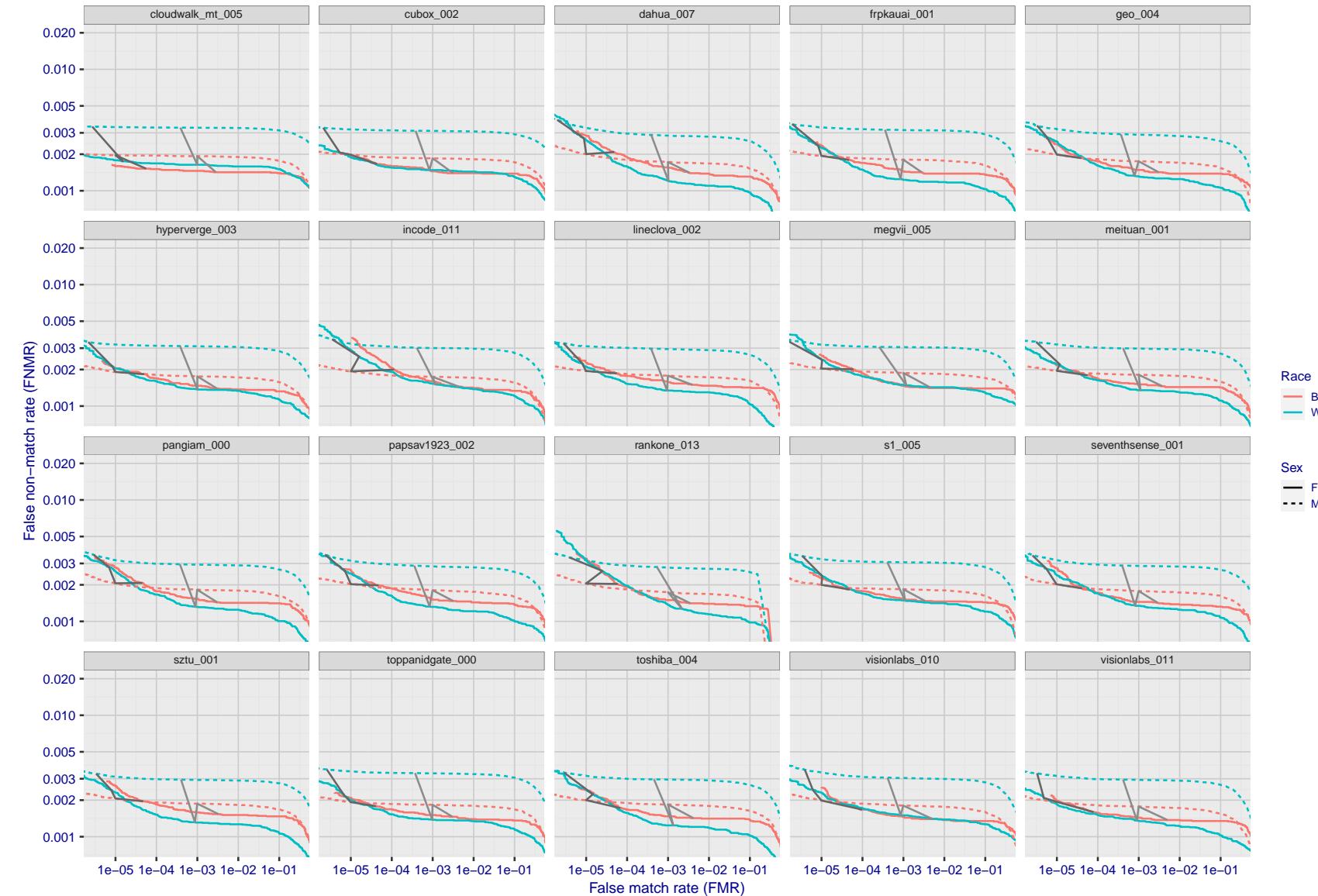


Figure 150: For the mugshot images, error tradeoff characteristics for white females, black females, black males and white males. The Z-shaped grey lines correspond to fixed thresholds, showing both FNMR and FMR vary at one T value. Note: Many of the plots will naively be read as saying women gives worse error rates than men because the solid traces lie above the dotted ones. However, this is misleading and incomplete: The grey lines show the traces reveal horizontal shifts. Thus for the cogent-003 algorithm FNMR for men is higher than for women at a fixed threshold but, at the same time, FMR is higher for women - see Figure 232. As access control systems almost always operate at a fixed threshold, the naive interpretation is incorrect.

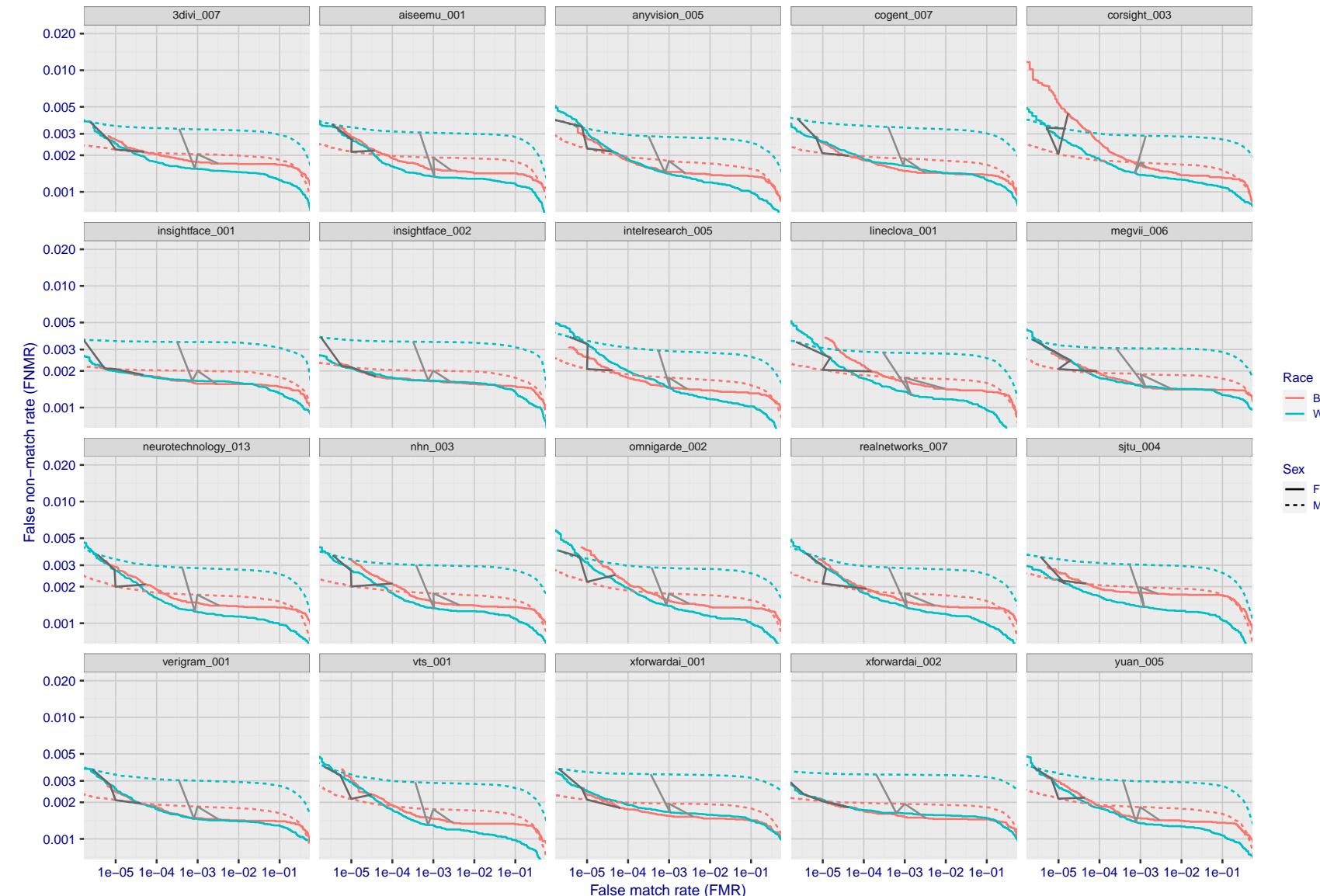


Figure 151: For the mugshot images, error tradeoff characteristics for white females, black females, black males and white males. The Z-shaped grey lines correspond to fixed thresholds, showing both FNMR and FMR vary at one T value. Note: Many of the plots will naively be read as saying women gives worse error rates than men because the solid traces lie above the dotted ones. However, this is misleading and incomplete: The grey lines show the traces reveal horizontal shifts. Thus for the cogent-003 algorithm FNMR for men is higher than for women at a fixed threshold but, at the same time, FMR is higher for women - see Figure 232. As access control systems almost always operate at a fixed threshold, the naive interpretation is incorrect.

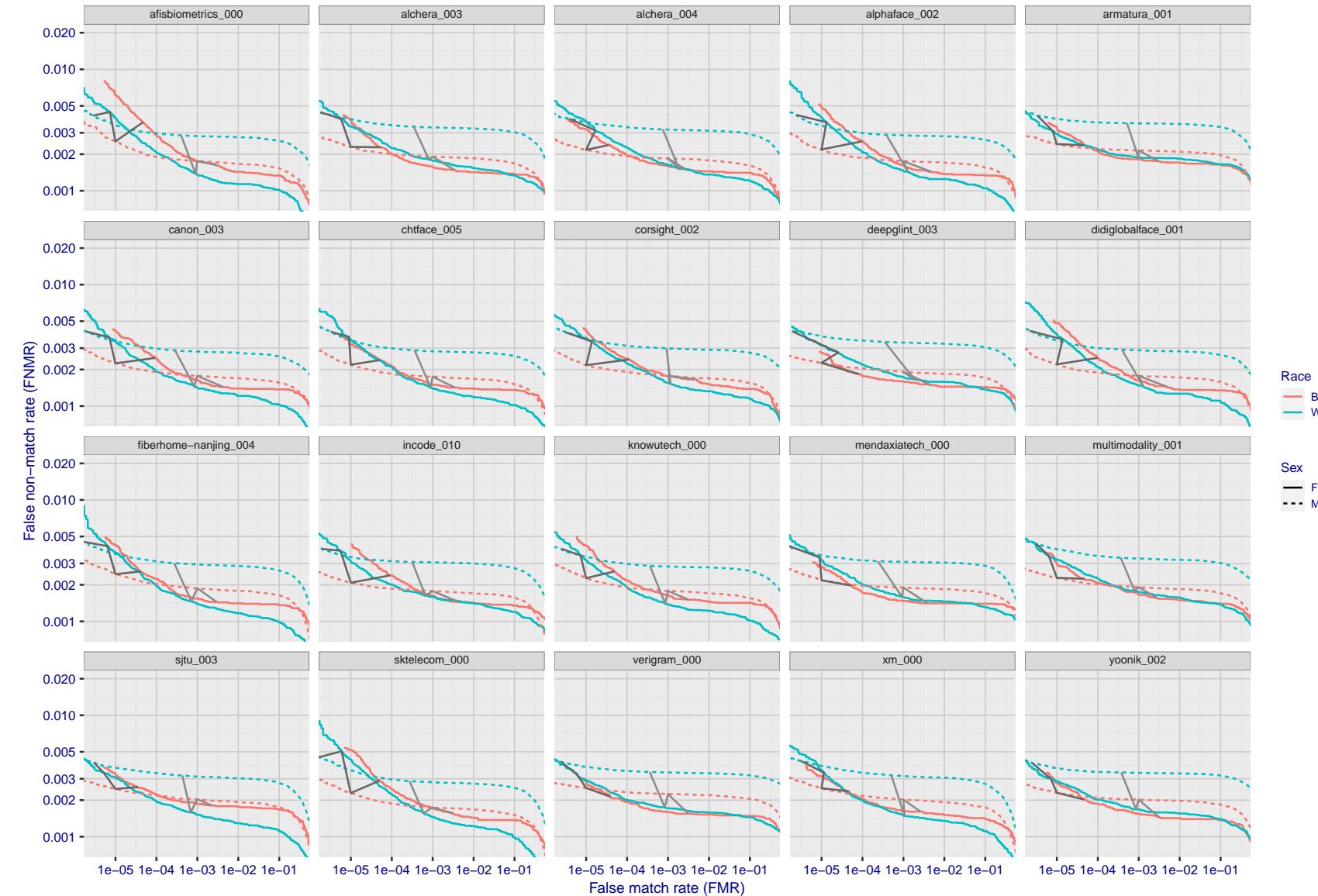


Figure 152: For the mugshot images, error tradeoff characteristics for white females, black females, black males and white males. The Z-shaped grey lines correspond to fixed thresholds, showing both FNMR and FMR vary at one T value. Note: Many of the plots will naively be read as saying women gives worse error rates than men because the solid traces lie above the dotted ones. However, this is misleading and incomplete: The grey lines show the traces reveal horizontal shifts. Thus for the cogent-003 algorithm FNMR for men is higher than for women at a fixed threshold but, at the same time, FMR is higher for women - see Figure 232. As access control systems almost always operate at a fixed threshold, the naive interpretation is incorrect.

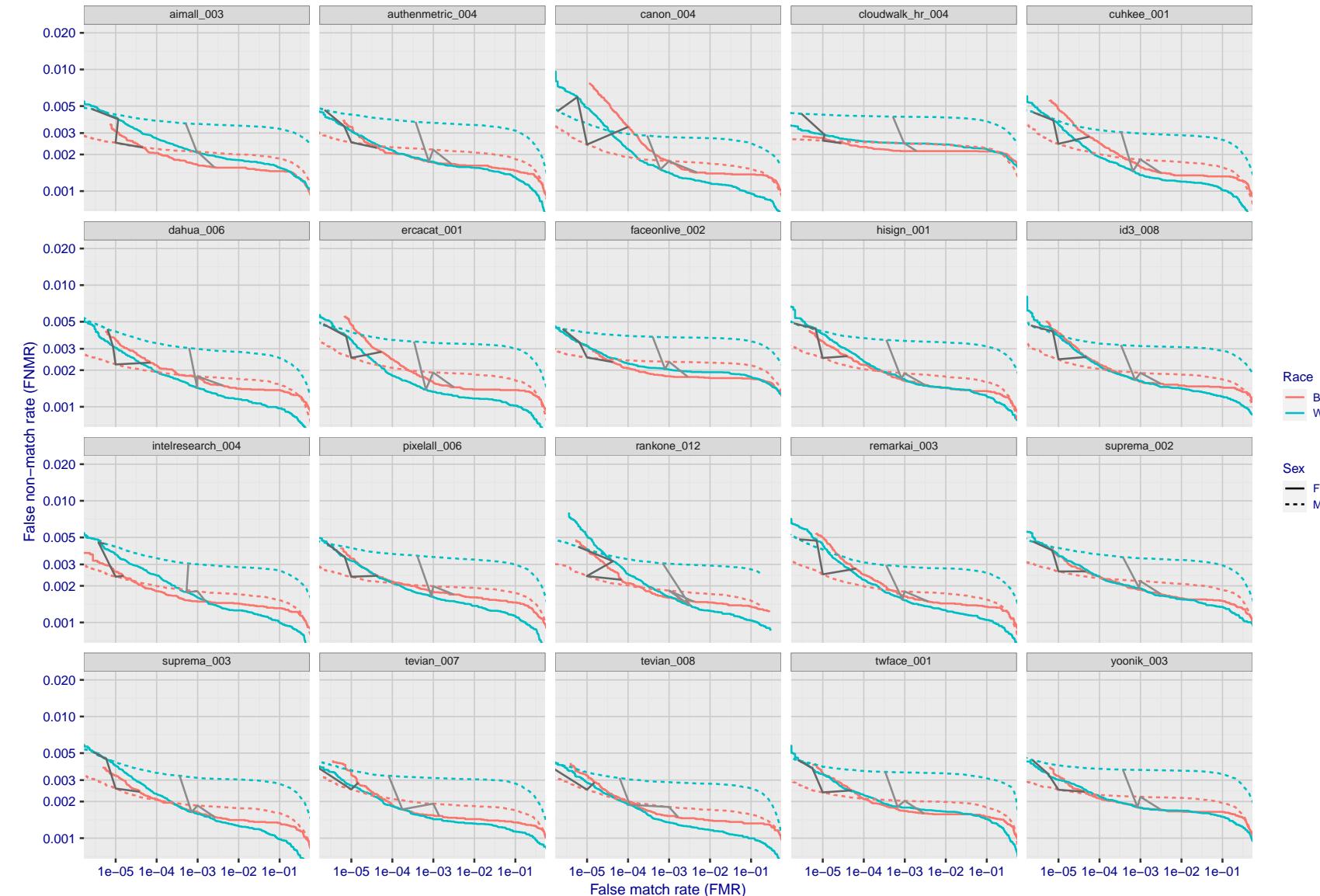


Figure 153: For the mugshot images, error tradeoff characteristics for white females, black females, black males and white males. The Z-shaped grey lines correspond to fixed thresholds, showing both FNMR and FMR vary at one T value. Note: Many of the plots will naively be read as saying women gives worse error rates than men because the solid traces lie above the dotted ones. However, this is misleading and incomplete: The grey lines show the traces reveal horizontal shifts. Thus for the cogent-003 algorithm FNMR for men is higher than for women at a fixed threshold but, at the same time, FMR is higher for women - see Figure 232. As access control systems almost always operate at a fixed threshold, the naive interpretation is incorrect.

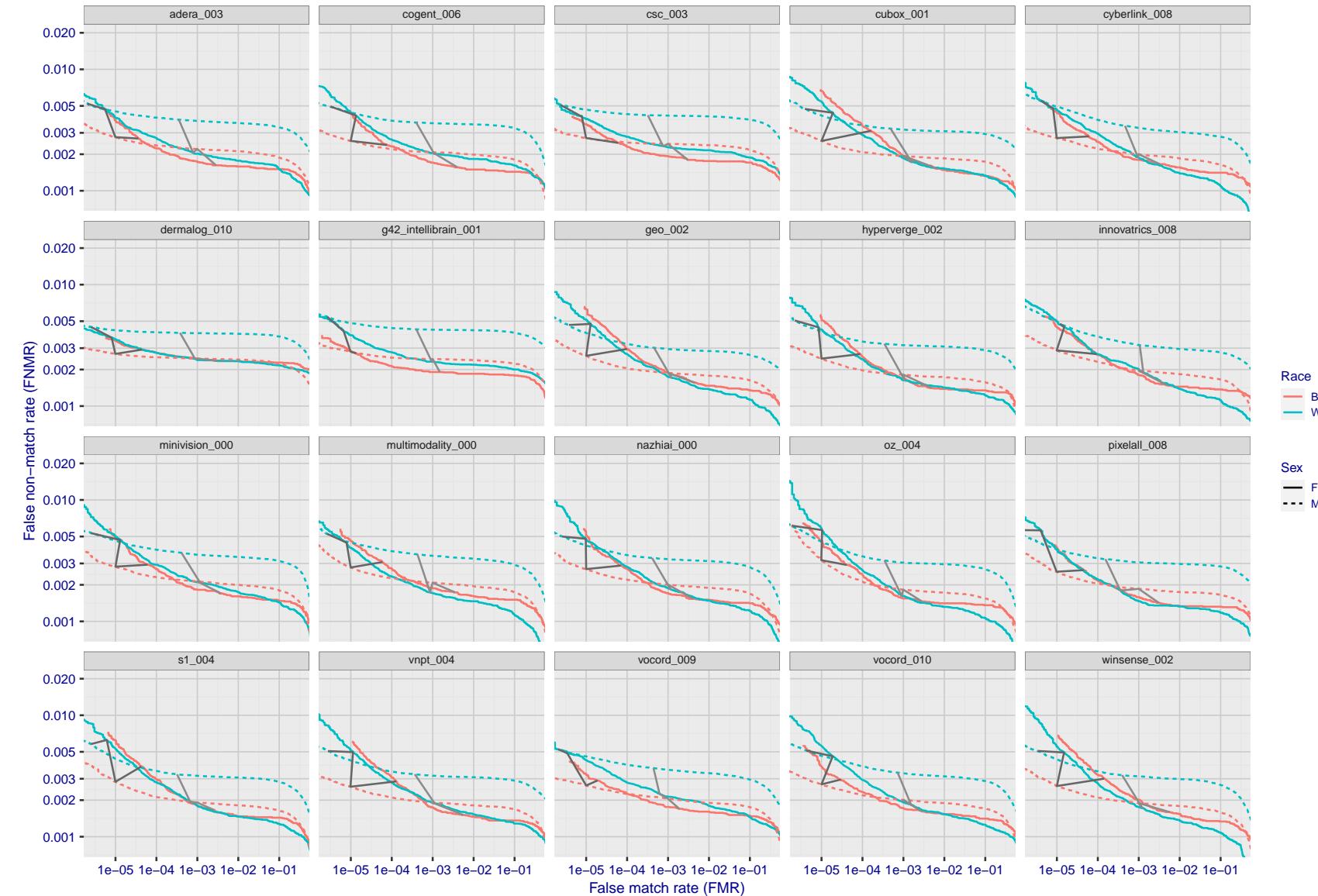


Figure 154: For the mugshot images, error tradeoff characteristics for white females, black females, black males and white males. The Z-shaped grey lines correspond to fixed thresholds, showing both FNMR and FMR vary at one T value. Note: Many of the plots will naively be read as saying women gives worse error rates than men because the solid traces lie above the dotted ones. However, this is misleading and incomplete: The grey lines show the traces reveal horizontal shifts. Thus for the cogent-003 algorithm FNMR for men is higher than for women at a fixed threshold but, at the same time, FMR is higher for women - see Figure 232. As access control systems almost always operate at a fixed threshold, the naive interpretation is incorrect.

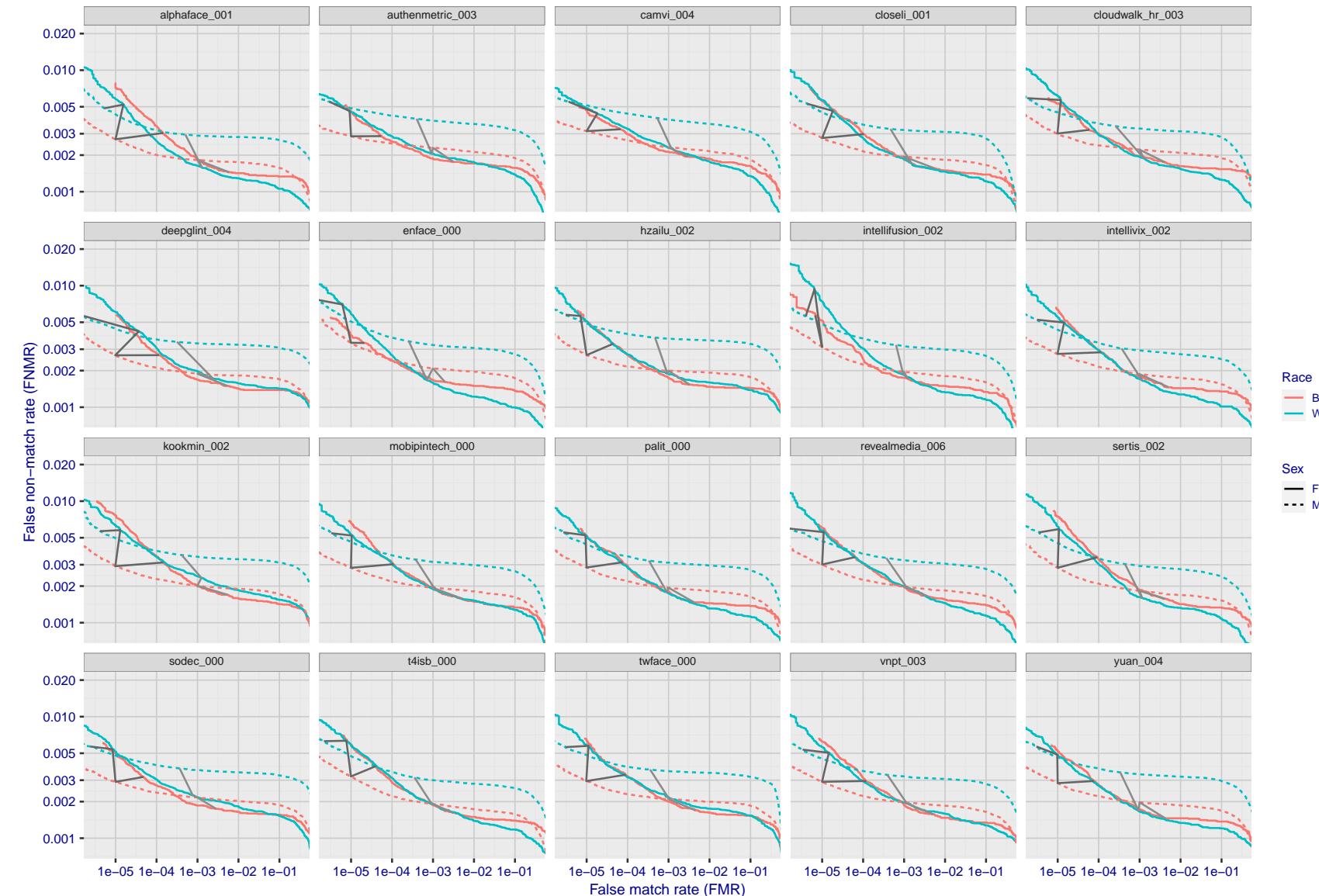


Figure 155: For the mugshot images, error tradeoff characteristics for white females, black females, black males and white males. The Z-shaped grey lines correspond to fixed thresholds, showing both FNMR and FMR vary at one T value. Note: Many of the plots will naively be read as saying women gives worse error rates than men because the solid traces lie above the dotted ones. However, this is misleading and incomplete: The grey lines show the traces reveal horizontal shifts. Thus for the cogent-003 algorithm FNMR for men is higher than for women at a fixed threshold but, at the same time, FMR is higher for women - see Figure 232. As access control systems almost always operate at a fixed threshold, the naive interpretation is incorrect.

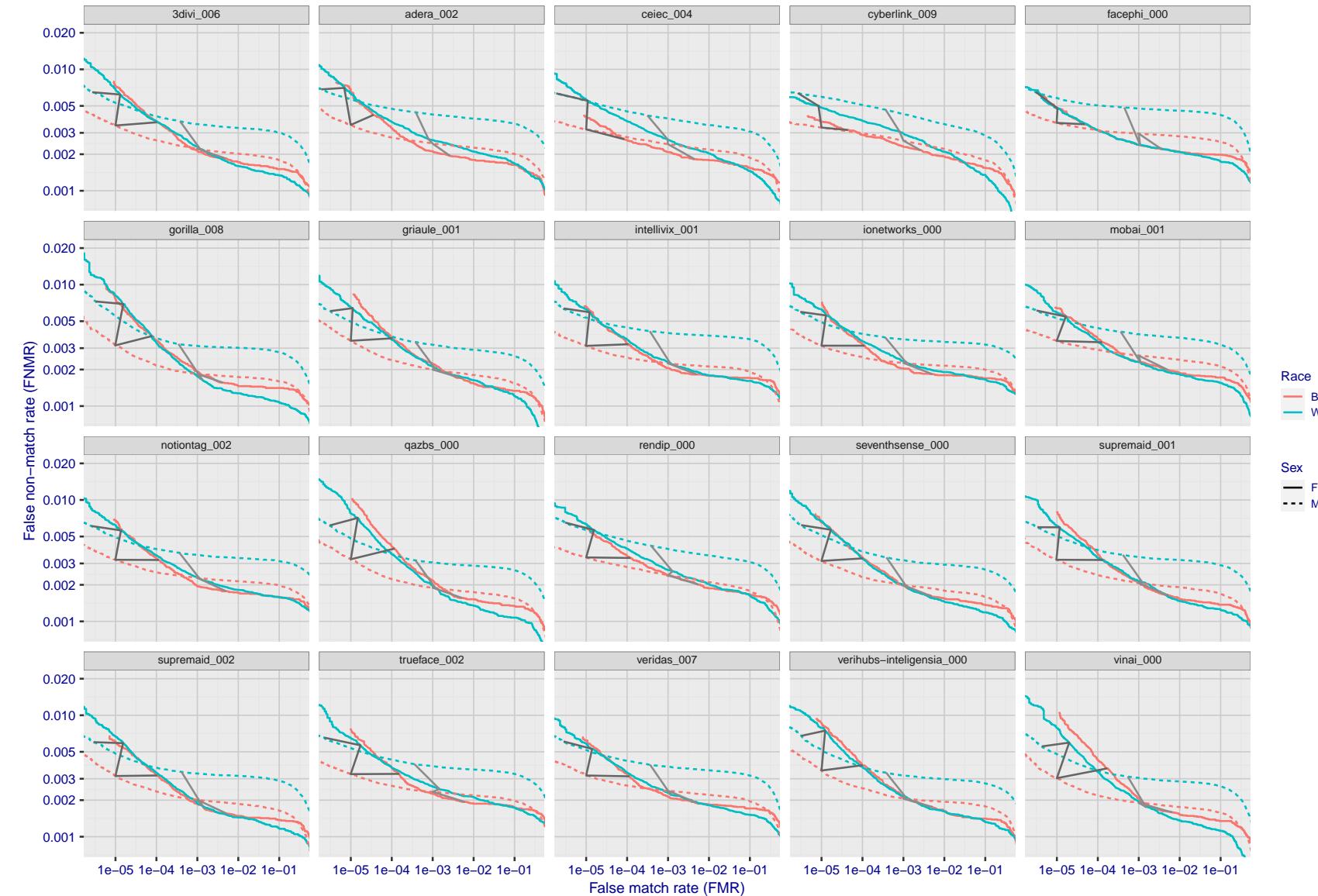


Figure 156: For the mugshot images, error tradeoff characteristics for white females, black females, black males and white males. The Z-shaped grey lines correspond to fixed thresholds, showing both FNMR and FMR vary at one T value. Note: Many of the plots will naively be read as saying women gives worse error rates than men because the solid traces lie above the dotted ones. However, this is misleading and incomplete: The grey lines show the traces reveal horizontal shifts. Thus for the cogent-003 algorithm FNMR for men is higher than for women at a fixed threshold but, at the same time, FMR is higher for women - see Figure 232. As access control systems almost always operate at a fixed threshold, the naive interpretation is incorrect.

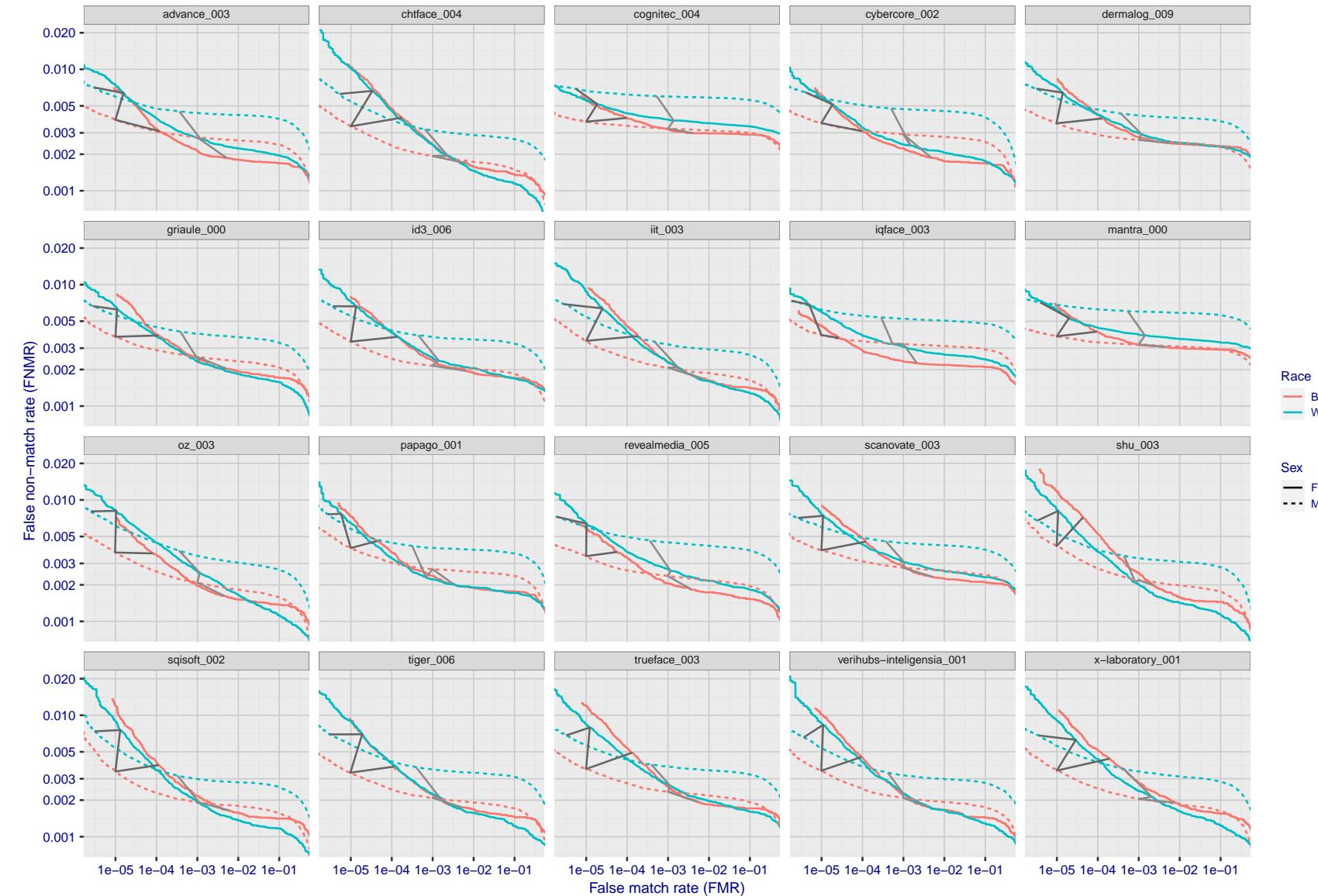


Figure 157: For the mugshot images, error tradeoff characteristics for white females, black females, black males and white males. The Z-shaped grey lines correspond to fixed thresholds, showing both FNMR and FMR vary at one T value. Note: Many of the plots will naively be read as saying women gives worse error rates than men because the solid traces lie above the dotted ones. However, this is misleading and incomplete: The grey lines show the traces reveal horizontal shifts. Thus for the cogent-003 algorithm FNMR for men is higher than for women at a fixed threshold but, at the same time, FMR is higher for women - see Figure 232. As access control systems almost always operate at a fixed threshold, the naive interpretation is incorrect.

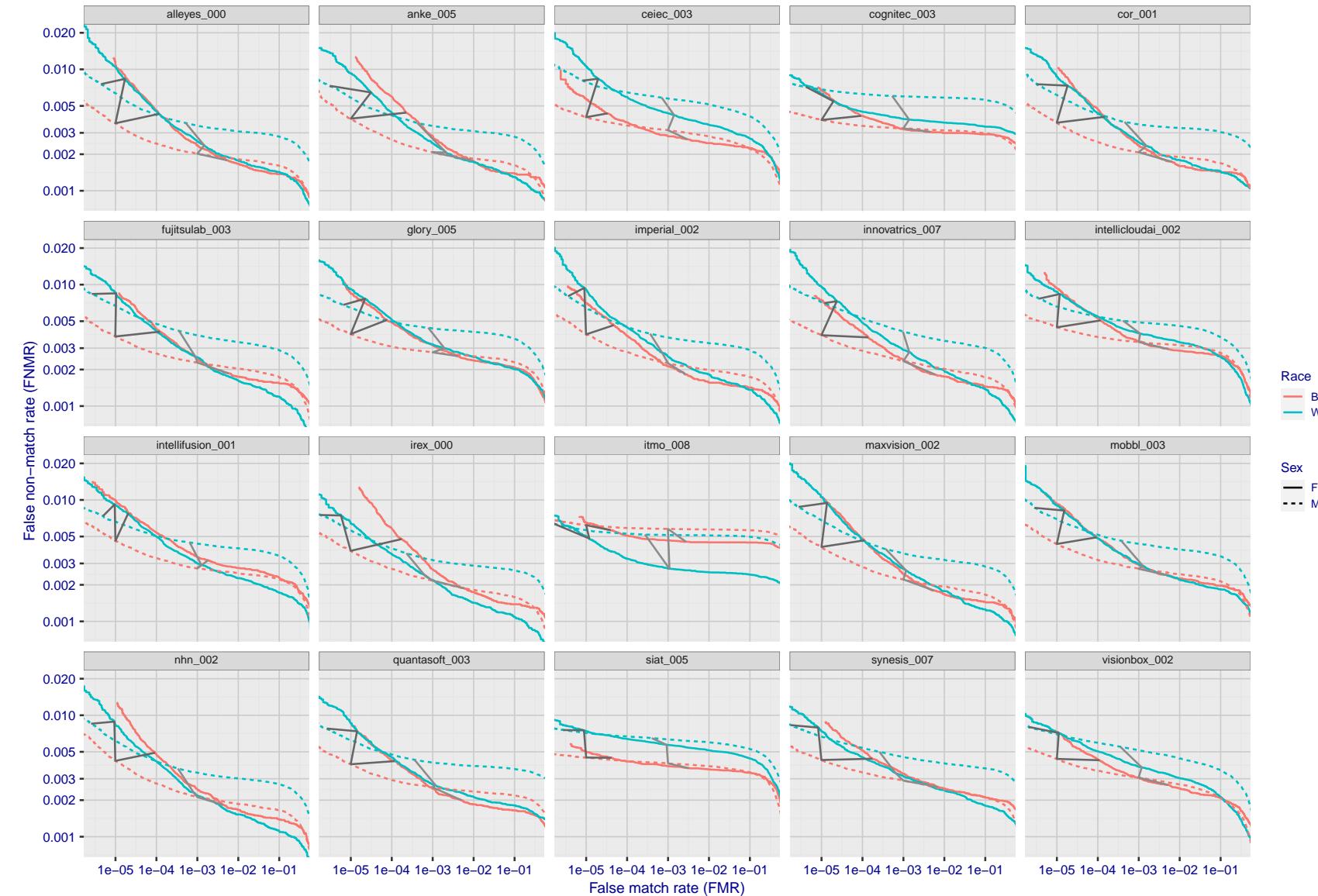


Figure 158: For the mugshot images, error tradeoff characteristics for white females, black females, black males and white males. The Z-shaped grey lines correspond to fixed thresholds, showing both FNMR and FMR vary at one T value. Note: Many of the plots will naively be read as saying women gives worse error rates than men because the solid traces lie above the dotted ones. However, this is misleading and incomplete: The grey lines show the traces reveal horizontal shifts. Thus for the cogent-003 algorithm FNMR for men is higher than for women at a fixed threshold but, at the same time, FMR is higher for women - see Figure 232. As access control systems almost always operate at a fixed threshold, the naive interpretation is incorrect.

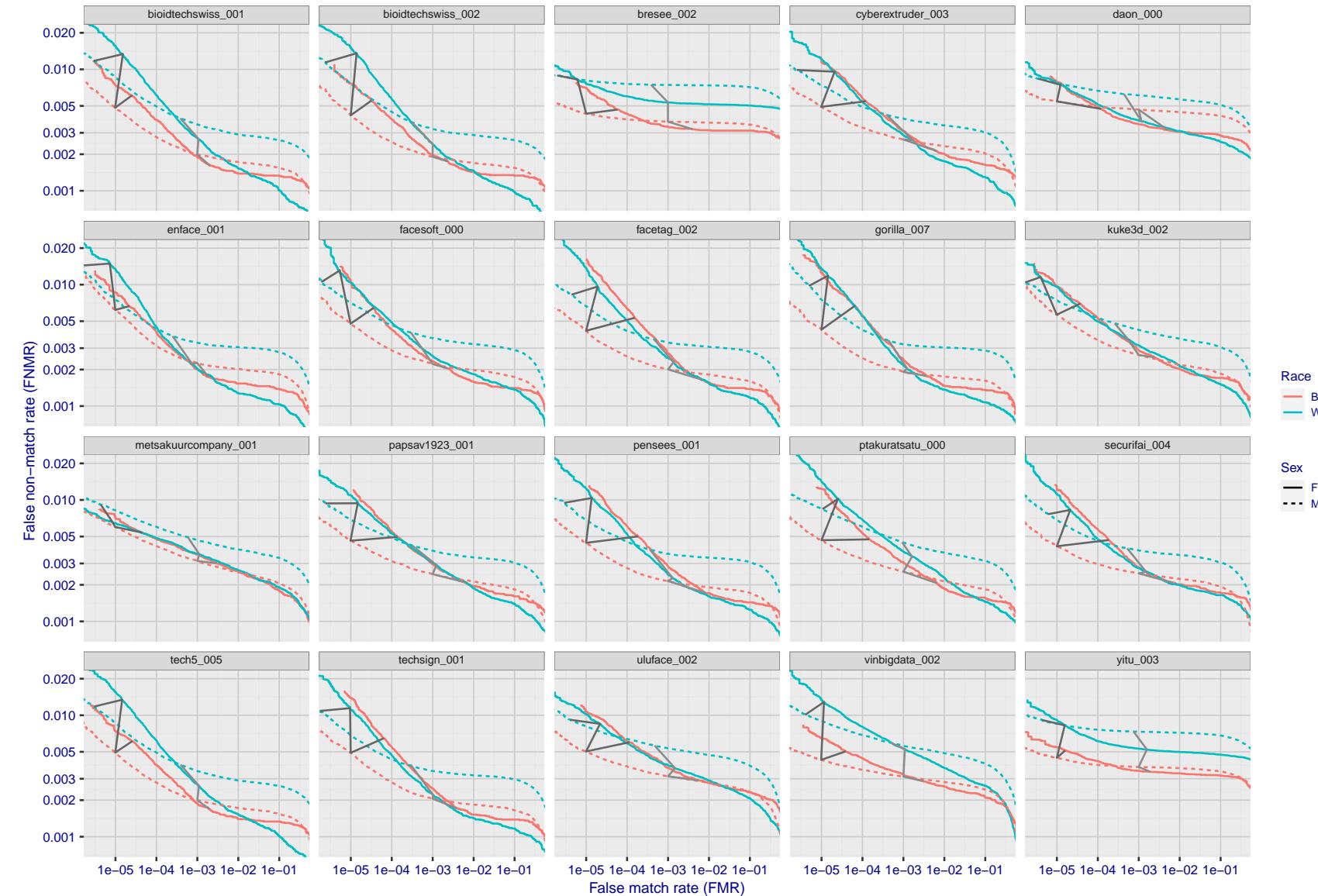


Figure 159: For the mugshot images, error tradeoff characteristics for white females, black females, black males and white males. The Z-shaped grey lines correspond to fixed thresholds, showing both FNMR and FMR vary at one T value. Note: Many of the plots will naively be read as saying women gives worse error rates than men because the solid traces lie above the dotted ones. However, this is misleading and incomplete: The grey lines show the traces reveal horizontal shifts. Thus for the cogent-003 algorithm FNMR for men is higher than for women at a fixed threshold but, at the same time, FMR is higher for women - see Figure 232. As access control systems almost always operate at a fixed threshold, the naive interpretation is incorrect.

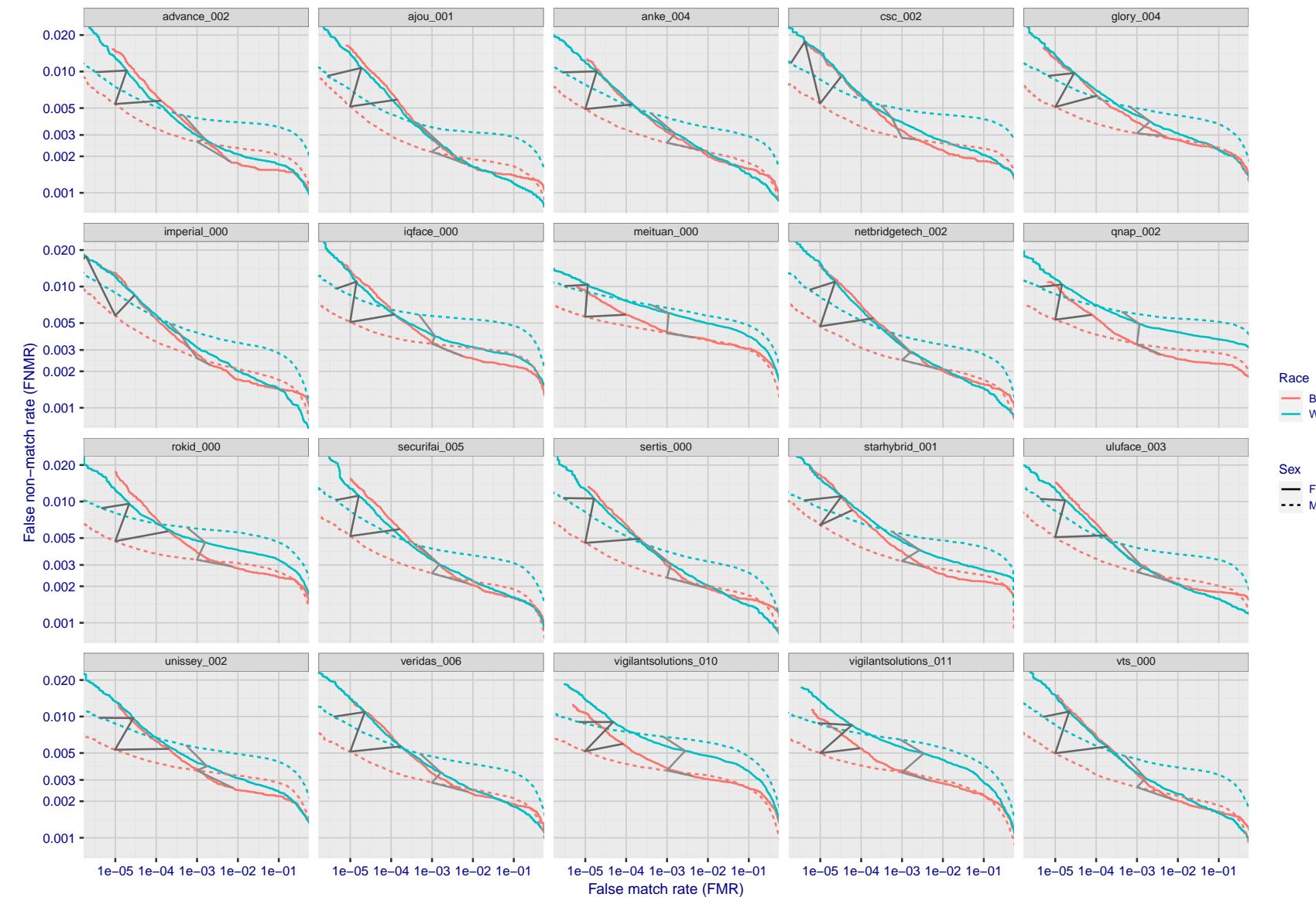


Figure 160: For the mugshot images, error tradeoff characteristics for white females, black females, black males and white males. The Z-shaped grey lines correspond to fixed thresholds, showing both FNMR and FMR vary at one T value. Note: Many of the plots will naively be read as saying women gives worse error rates than men because the solid traces lie above the dotted ones. However, this is misleading and incomplete: The grey lines show the traces reveal horizontal shifts. Thus for the cogent-003 algorithm FNMR for men is higher than for women at a fixed threshold but, at the same time, FMR is higher for women - see Figure 232. As access control systems almost always operate at a fixed threshold, the naive interpretation is incorrect.

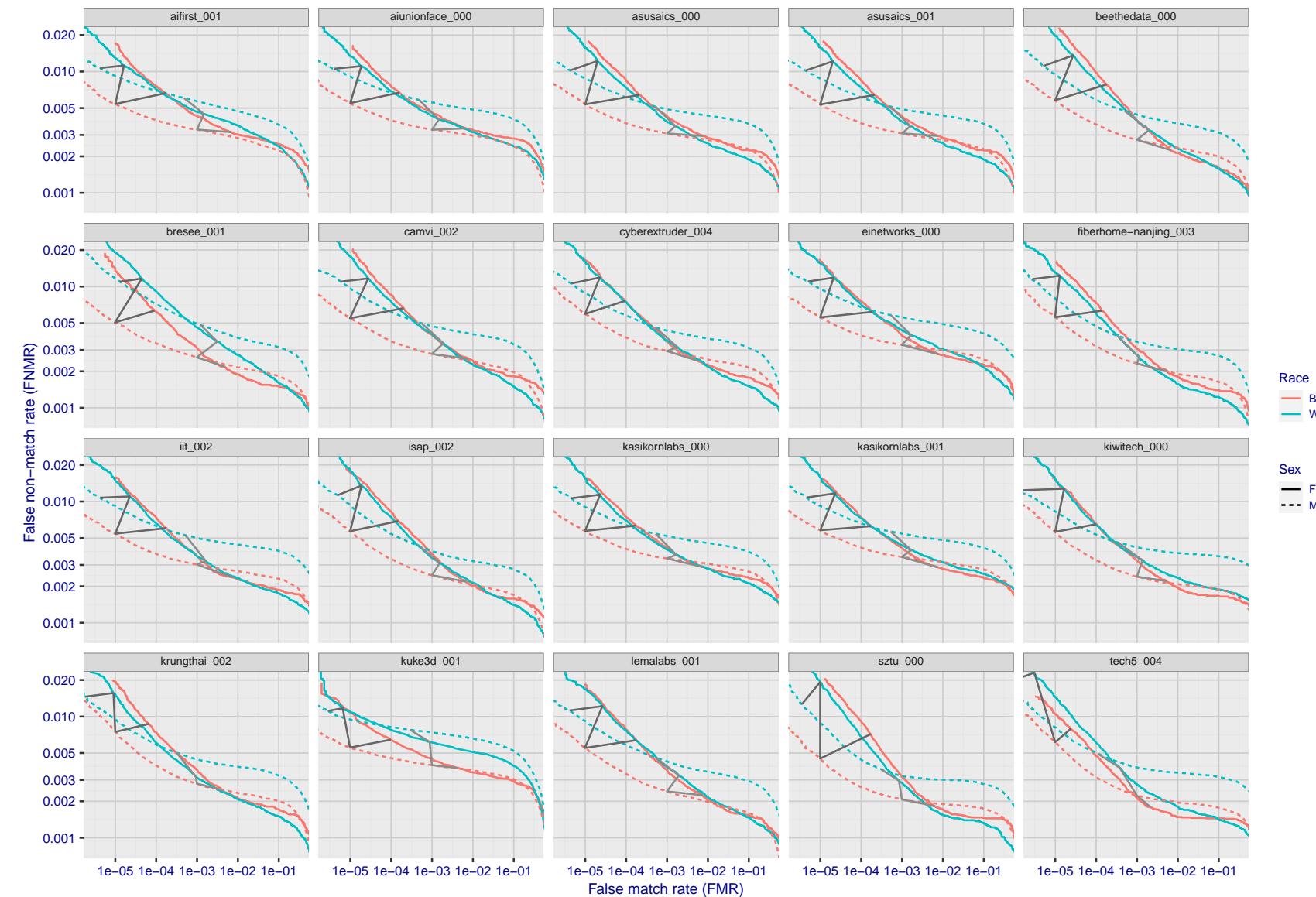


Figure 161: For the mugshot images, error tradeoff characteristics for white females, black females, black males and white males. The Z-shaped grey lines correspond to fixed thresholds, showing both FNMR and FMR vary at one T value. Note: Many of the plots will naively be read as saying women gives worse error rates than men because the solid traces lie above the dotted ones. However, this is misleading and incomplete: The grey lines show the traces reveal horizontal shifts. Thus for the cogent-003 algorithm FNMR for men is higher than for women at a fixed threshold but, at the same time, FMR is higher for women - see Figure 232. As access control systems almost always operate at a fixed threshold, the naive interpretation is incorrect.

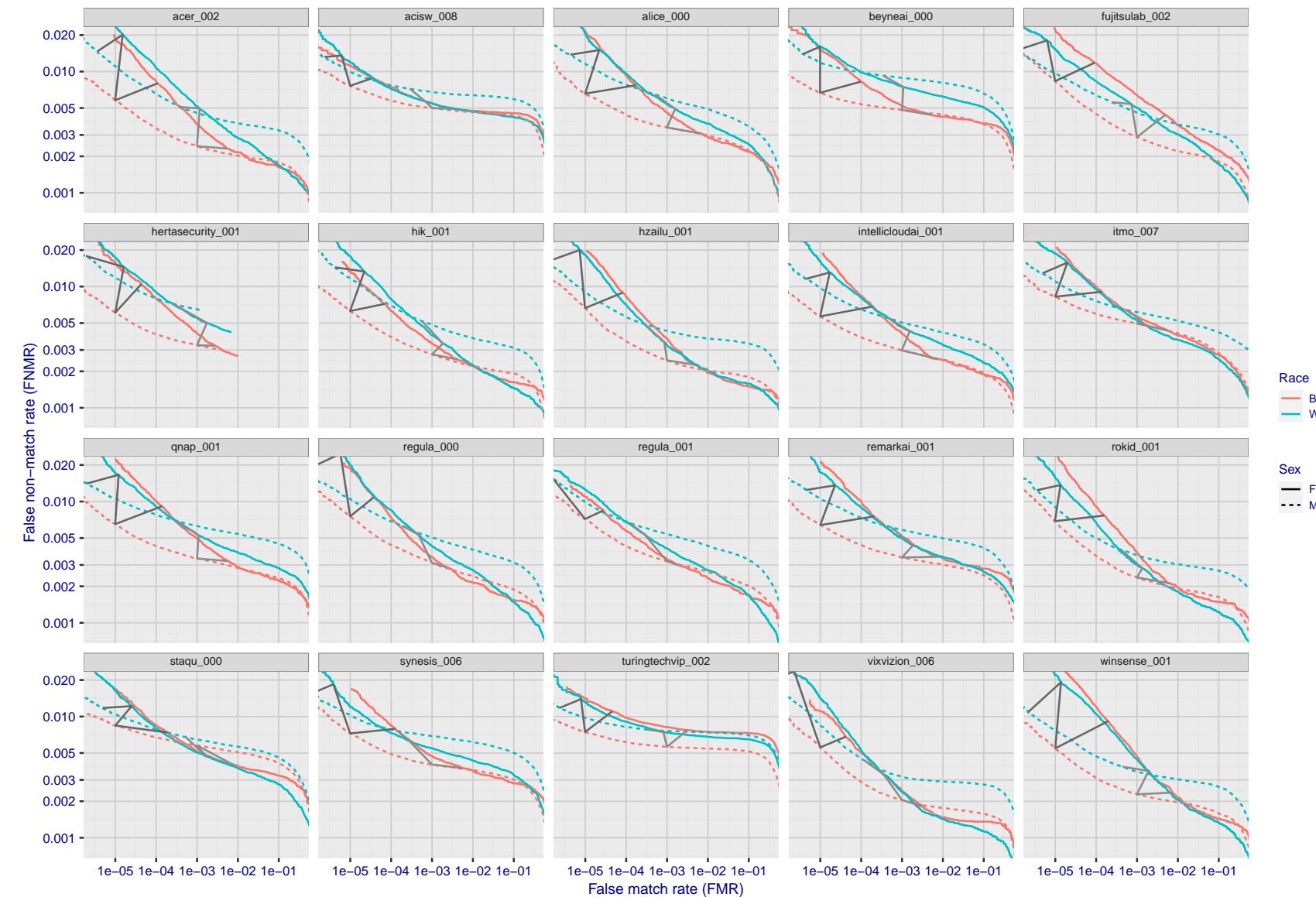


Figure 162: For the mugshot images, error tradeoff characteristics for white females, black females, black males and white males. The Z-shaped grey lines correspond to fixed thresholds, showing both FNMR and FMR vary at one T value. Note: Many of the plots will naively be read as saying women gives worse error rates than men because the solid traces lie above the dotted ones. However, this is misleading and incomplete: The grey lines show the traces reveal horizontal shifts. Thus for the cogent-003 algorithm FNMR for men is higher than for women at a fixed threshold but, at the same time, FMR is higher for women - see Figure 232. As access control systems almost always operate at a fixed threshold, the naive interpretation is incorrect.

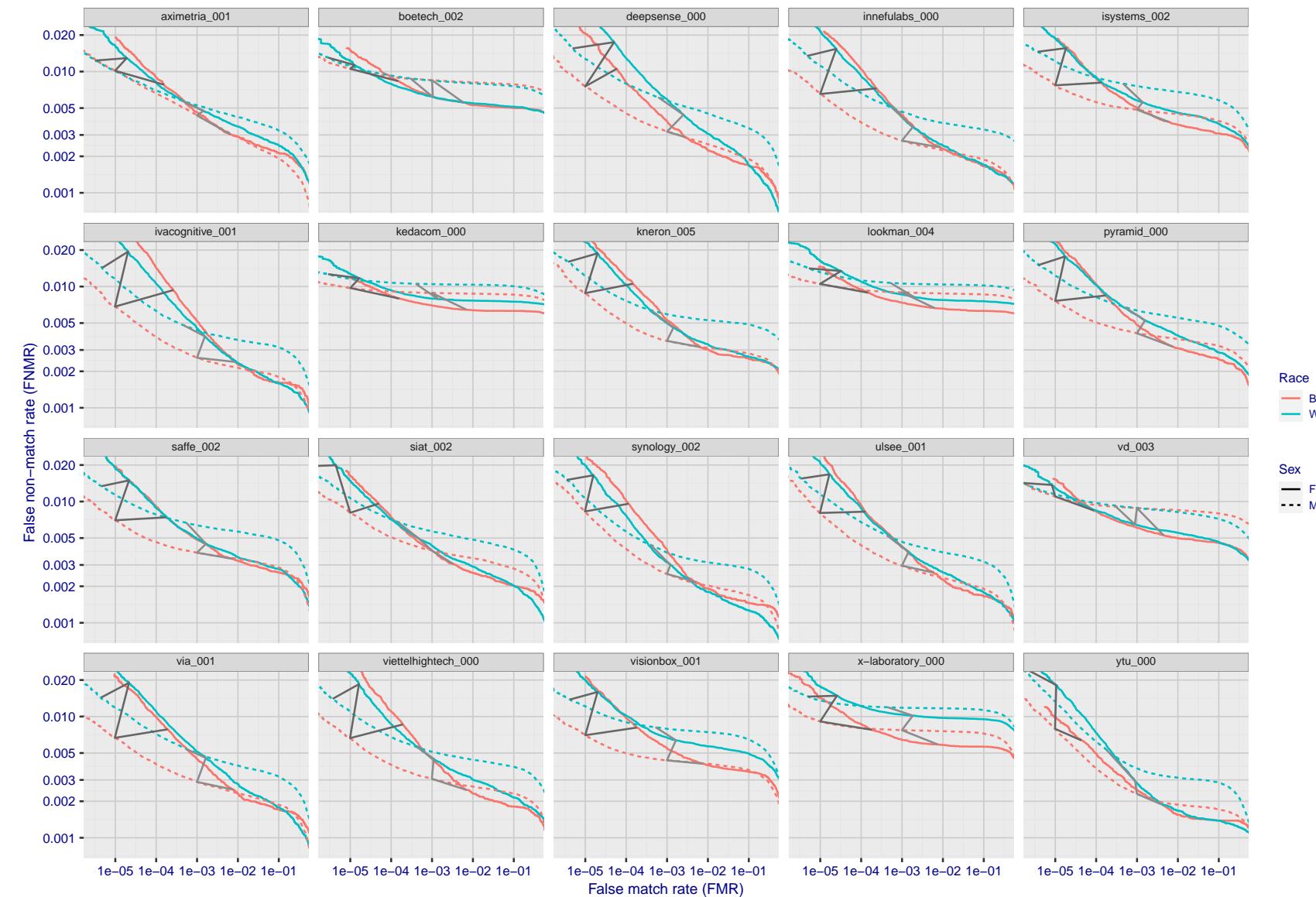


Figure 163: For the mugshot images, error tradeoff characteristics for white females, black females, black males and white males. The Z-shaped grey lines correspond to fixed thresholds, showing both FNMR and FMR vary at one T value. Note: Many of the plots will naively be read as saying women gives worse error rates than men because the solid traces lie above the dotted ones. However, this is misleading and incomplete: The grey lines show the traces reveal horizontal shifts. Thus for the cogent-003 algorithm FNMR for men is higher than for women at a fixed threshold but, at the same time, FMR is higher for women - see Figure 232. As access control systems almost always operate at a fixed threshold, the naive interpretation is incorrect.

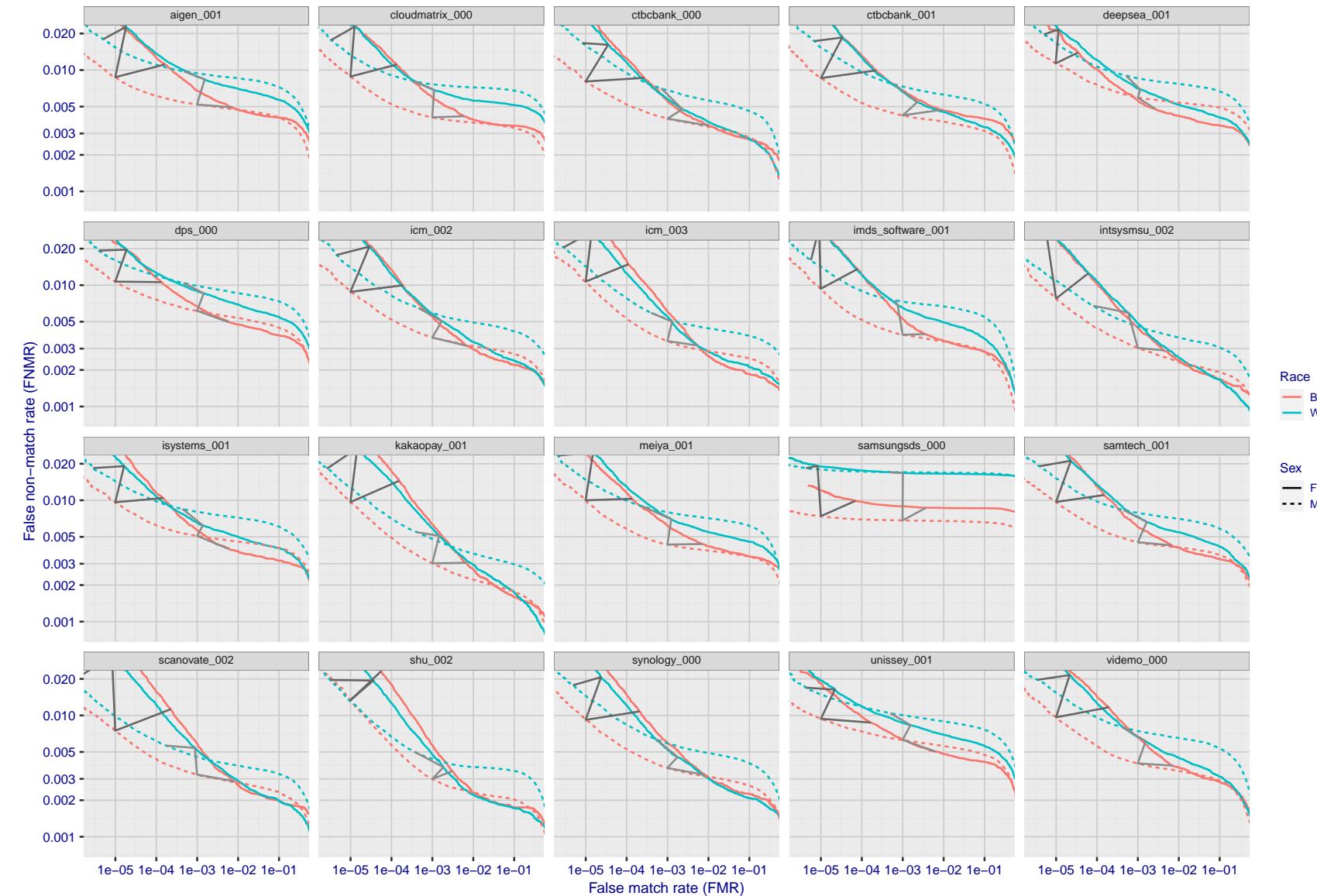


Figure 164: For the mugshot images, error tradeoff characteristics for white females, black females, black males and white males. The Z-shaped grey lines correspond to fixed thresholds, showing both FNMR and FMR vary at one T value. Note: Many of the plots will naively be read as saying women gives worse error rates than men because the solid traces lie above the dotted ones. However, this is misleading and incomplete: The grey lines show the traces reveal horizontal shifts. Thus for the cogent-003 algorithm FNMR for men is higher than for women at a fixed threshold but, at the same time, FMR is higher for women - see Figure 232. As access control systems almost always operate at a fixed threshold, the naive interpretation is incorrect.

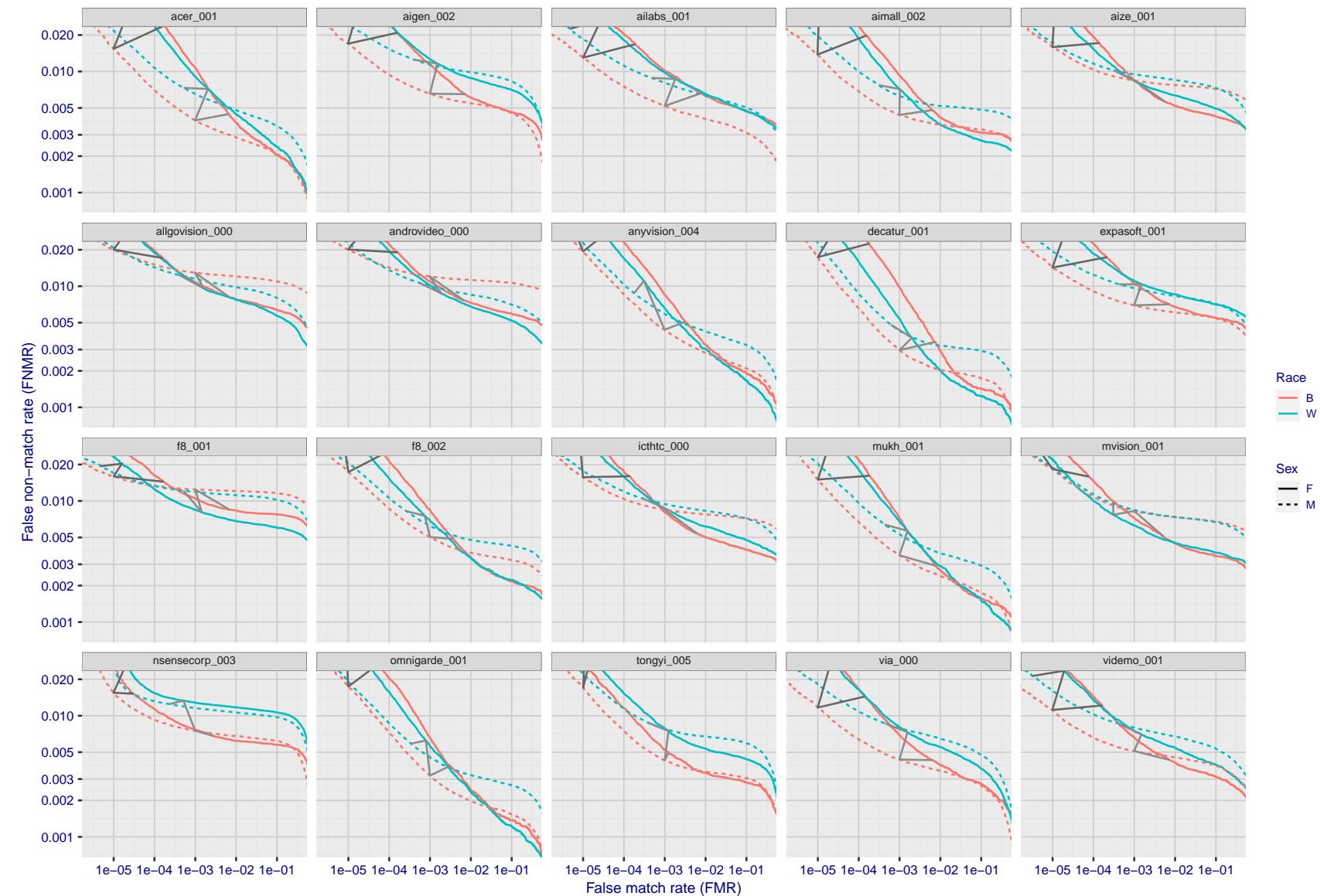


Figure 165: For the mugshot images, error tradeoff characteristics for white females, black females, black males and white males. The Z-shaped grey lines correspond to fixed thresholds, showing both FNMR and FMR vary at one T value. Note: Many of the plots will naively be read as saying women gives worse error rates than men because the solid traces lie above the dotted ones. However, this is misleading and incomplete: The grey lines show the traces reveal horizontal shifts. Thus for the cogent-003 algorithm FNMR for men is higher than for women at a fixed threshold but, at the same time, FMR is higher for women - see Figure 232. As access control systems almost always operate at a fixed threshold, the naive interpretation is incorrect.

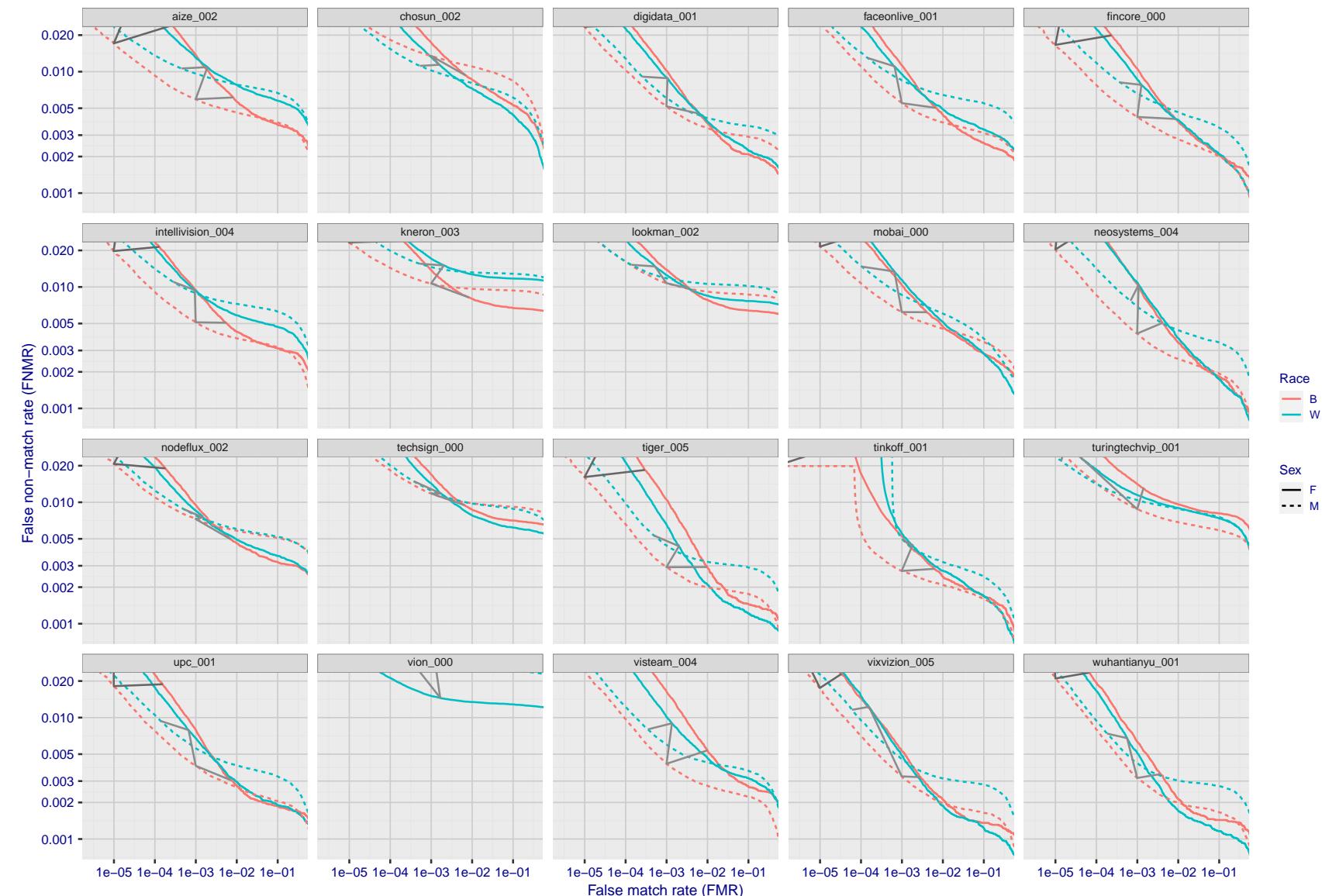


Figure 166: For the mugshot images, error tradeoff characteristics for white females, black females, black males and white males. The Z-shaped grey lines correspond to fixed thresholds, showing both FNMR and FMR vary at one T value. Note: Many of the plots will naively be read as saying women gives worse error rates than men because the solid traces lie above the dotted ones. However, this is misleading and incomplete: The grey lines show the traces reveal horizontal shifts. Thus for the cogent-003 algorithm FNMR for men is higher than for women at a fixed threshold but, at the same time, FMR is higher for women - see Figure 232. As access control systems almost always operate at a fixed threshold, the naive interpretation is incorrect.

2022/08/30 09:26:06

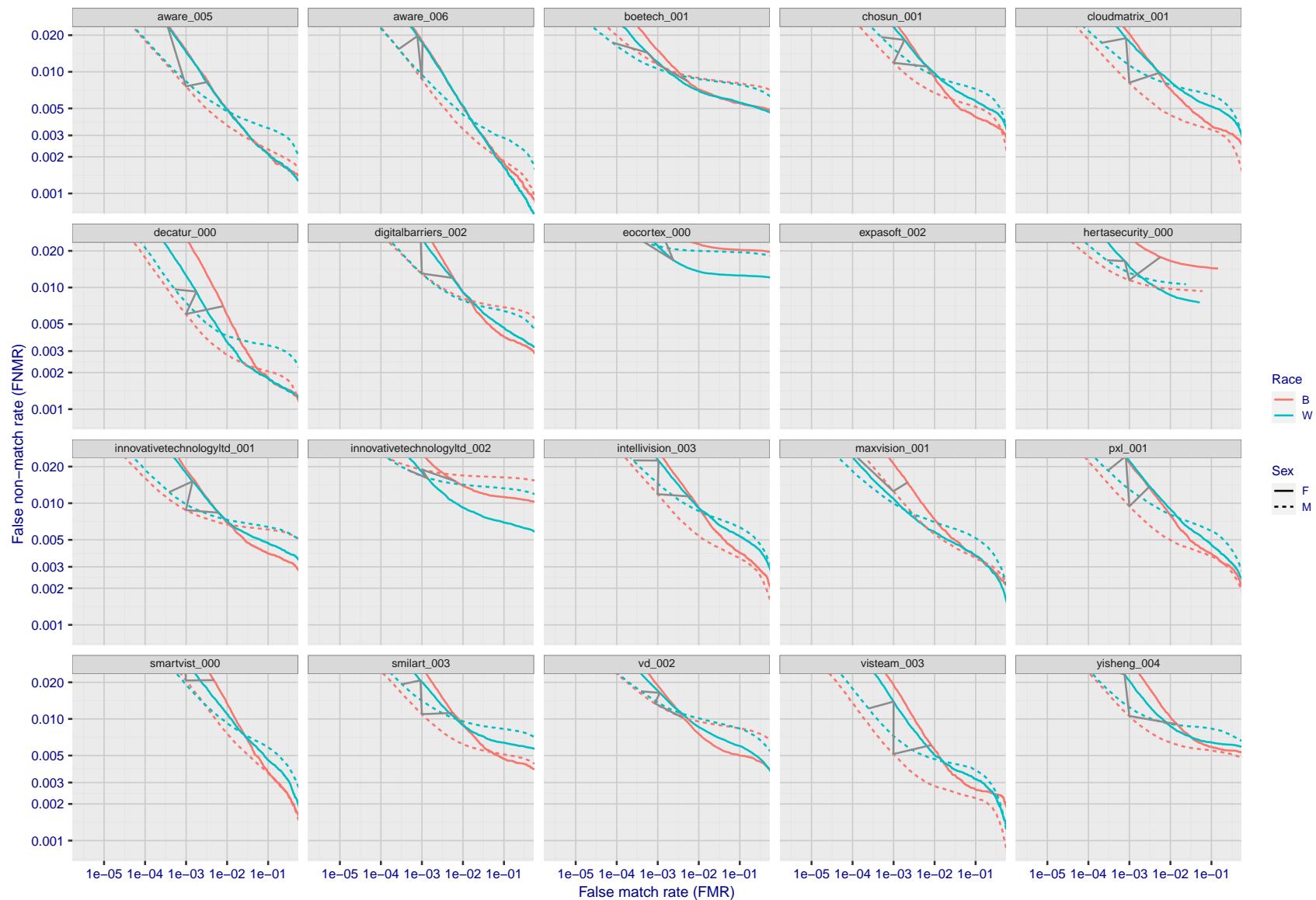


Figure 167: For the mugshot images, error tradeoff characteristics for white females, black females, black males and white males. The Z-shaped grey lines correspond to fixed thresholds, showing both FNMR and FMR vary at one T value. Note: Many of the plots will naively be read as saying women gives worse error rates than men because the solid traces lie above the dotted ones. However, this is misleading and incomplete: The grey lines show the traces reveal horizontal shifts. Thus for the cogent-003 algorithm FNMR for men is higher than for women at a fixed threshold but, at the same time, FMR is higher for women - see Figure 232. As access control systems almost always operate at a fixed threshold, the naive interpretation is incorrect.

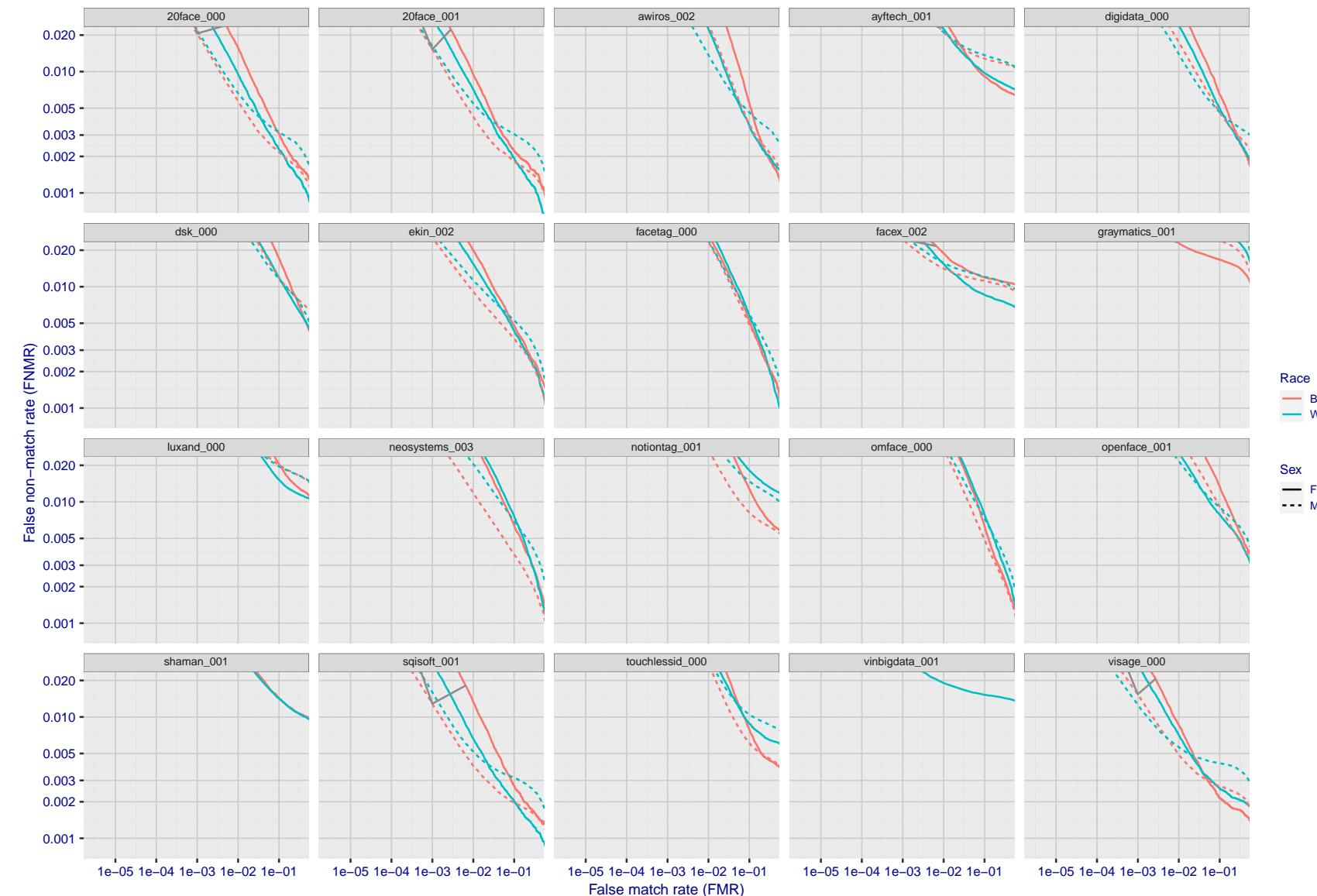


Figure 168: For the mugshot images, error tradeoff characteristics for white females, black females, black males and white males. The Z-shaped grey lines correspond to fixed thresholds, showing both FNMR and FMR vary at one T value. Note: Many of the plots will naively be read as saying women gives worse error rates than men because the solid traces lie above the dotted ones. However, this is misleading and incomplete: The grey lines show the traces reveal horizontal shifts. Thus for the cogent-003 algorithm FNMR for men is higher than for women at a fixed threshold but, at the same time, FMR is higher for women - see Figure 232. As access control systems almost always operate at a fixed threshold, the naive interpretation is incorrect.

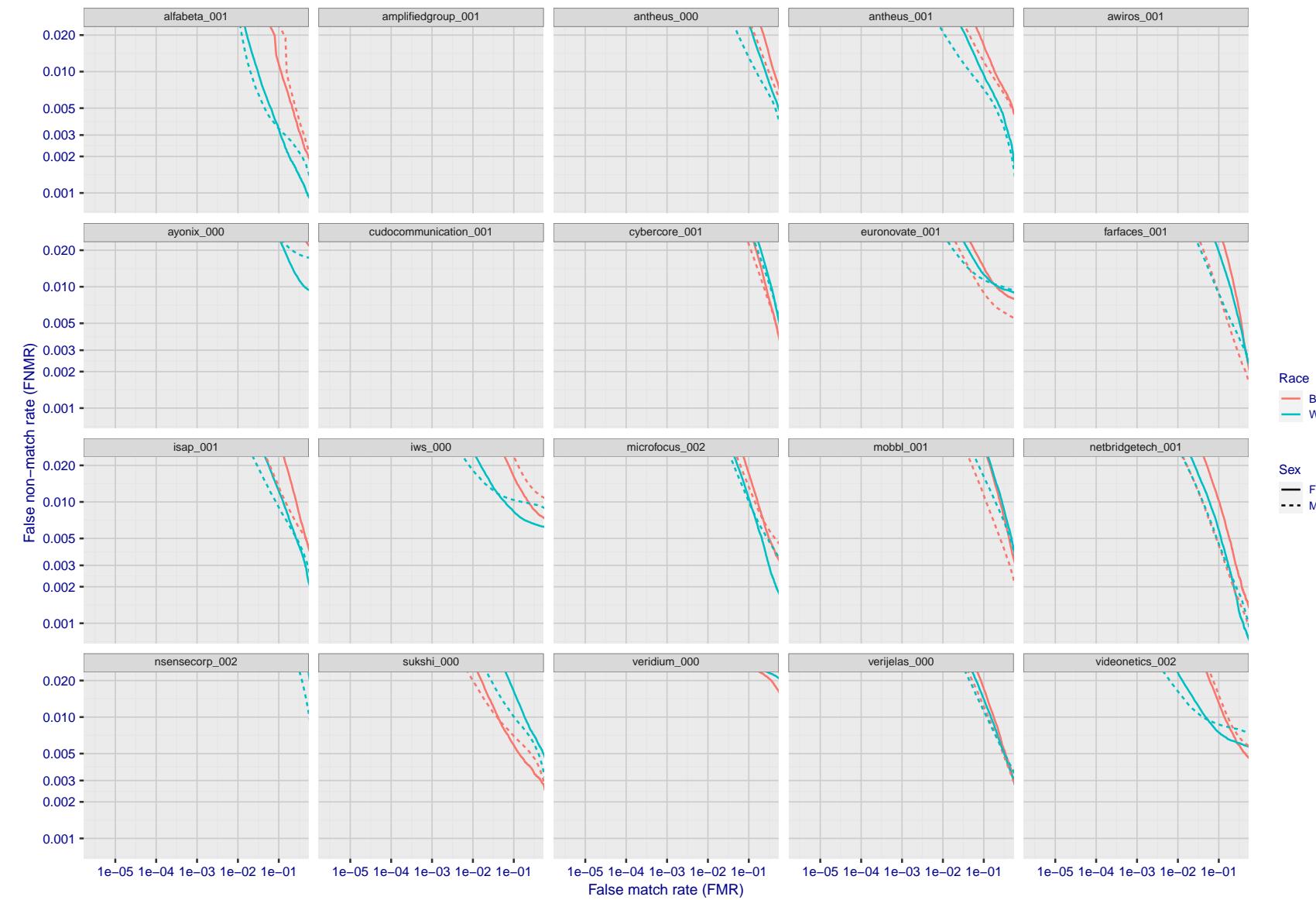


Figure 169: For the mugshot images, error tradeoff characteristics for white females, black females, black males and white males. The Z-shaped grey lines correspond to fixed thresholds, showing both FNMR and FMR vary at one T value. Note: Many of the plots will naively be read as saying women gives worse error rates than men because the solid traces lie above the dotted ones. However, this is misleading and incomplete: The grey lines show the traces reveal horizontal shifts. Thus for the cogent-003 algorithm FNMR for men is higher than for women at a fixed threshold but, at the same time, FMR is higher for women - see Figure 232. As access control systems almost always operate at a fixed threshold, the naive interpretation is incorrect.

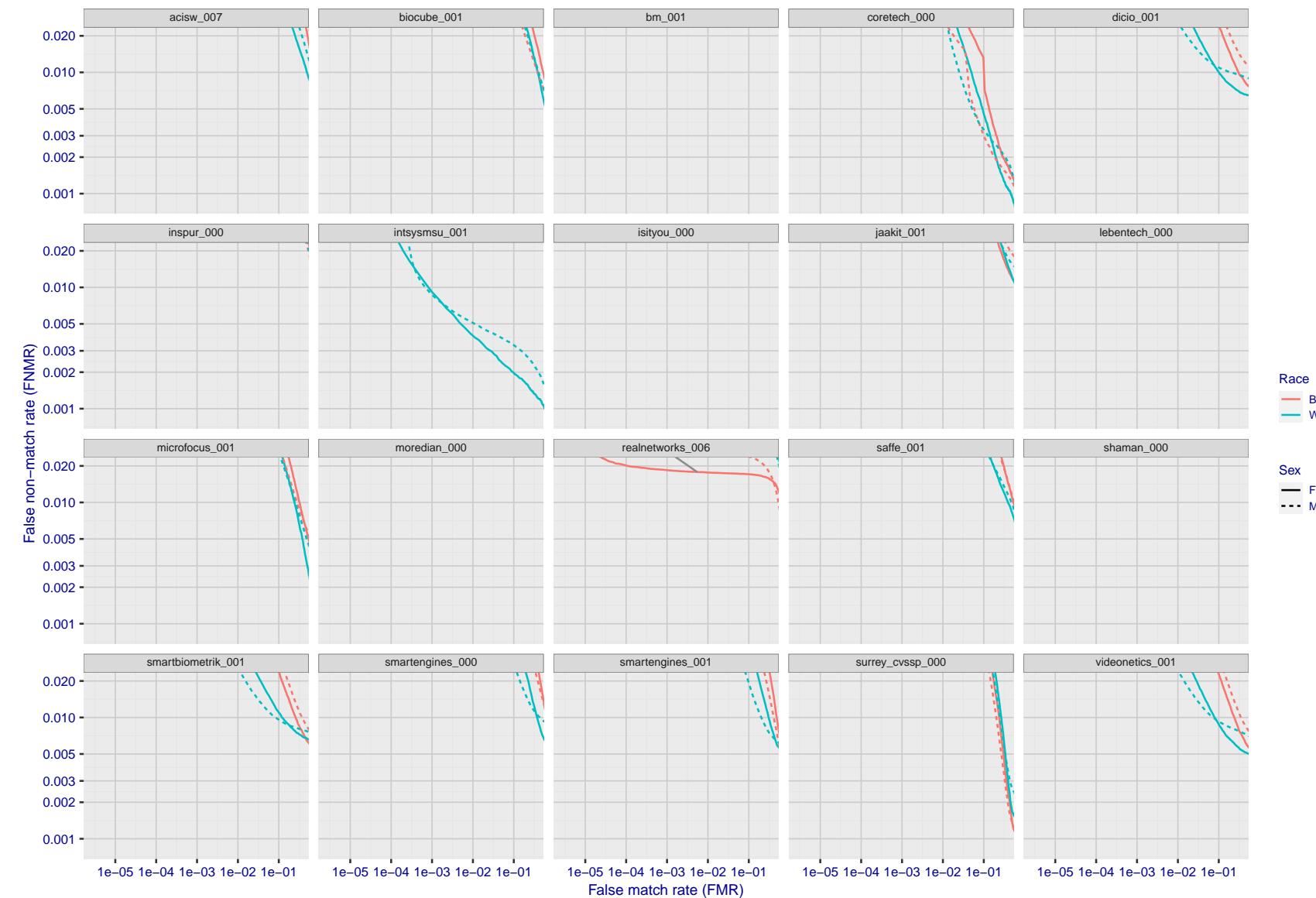


Figure 170: For the mugshot images, error tradeoff characteristics for white females, black females, black males and white males. The Z-shaped grey lines correspond to fixed thresholds, showing both FNMR and FMR vary at one T value. Note: Many of the plots will naively be read as saying women gives worse error rates than men because the solid traces lie above the dotted ones. However, this is misleading and incomplete: The grey lines show the traces reveal horizontal shifts. Thus for the cogent-003 algorithm FNMR for men is higher than for women at a fixed threshold but, at the same time, FMR is higher for women - see Figure 232. As access control systems almost always operate at a fixed threshold, the naive interpretation is incorrect.

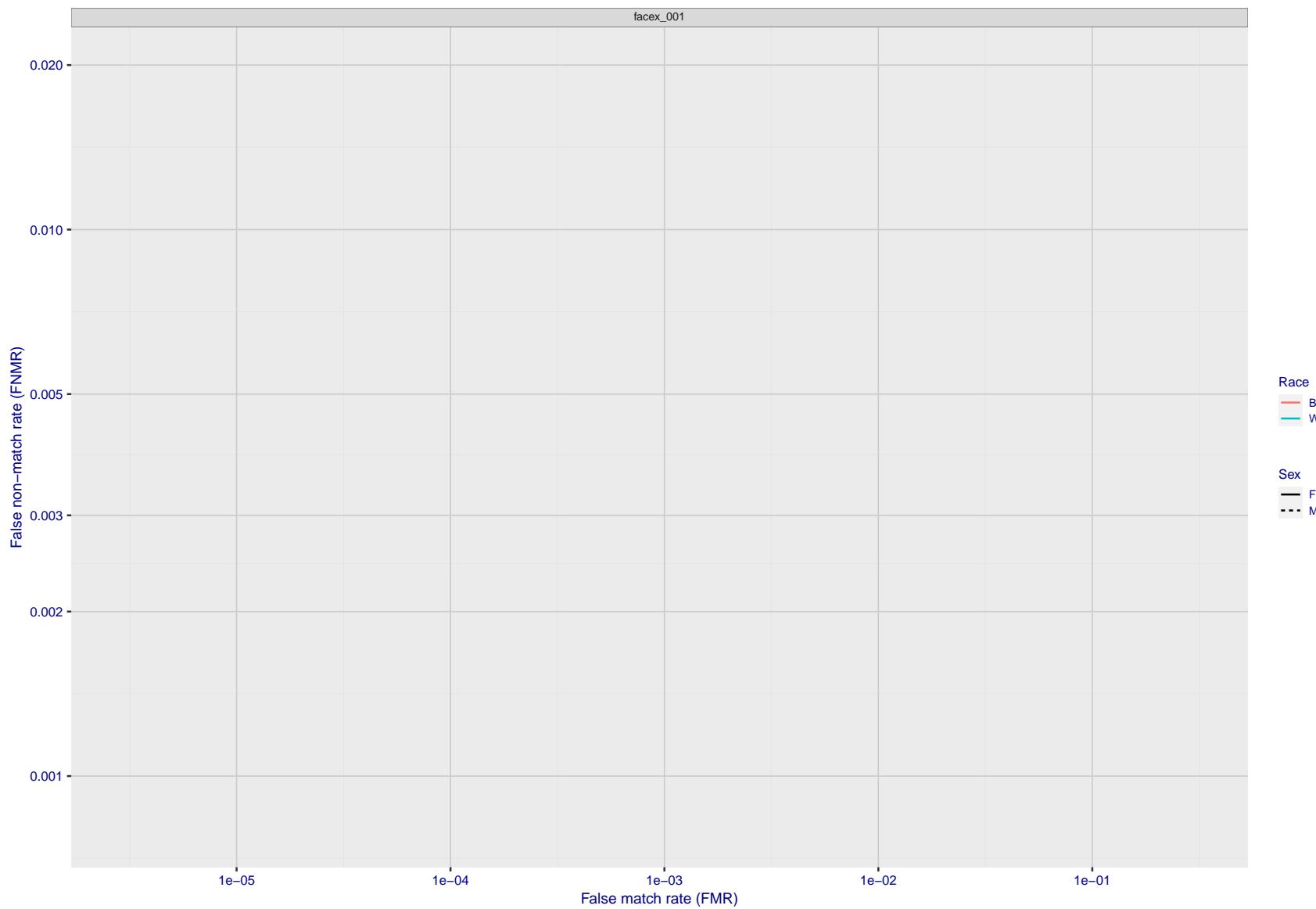


Figure 171: For the mugshot images, error tradeoff characteristics for white females, black females, black males and white males. The Z-shaped grey lines correspond to fixed thresholds, showing both FNMR and FMR vary at one T value. Note: Many of the plots will naively be read as saying women gives worse error rates than men because the solid traces lie above the dotted ones. However, this is misleading and incomplete: The grey lines show the traces reveal horizontal shifts. Thus for the cogent-003 algorithm FNMR for men is higher than for women at a fixed threshold but, at the same time, FMR is higher for women - see Figure 232. As access control systems almost always operate at a fixed threshold, the naive interpretation is incorrect.

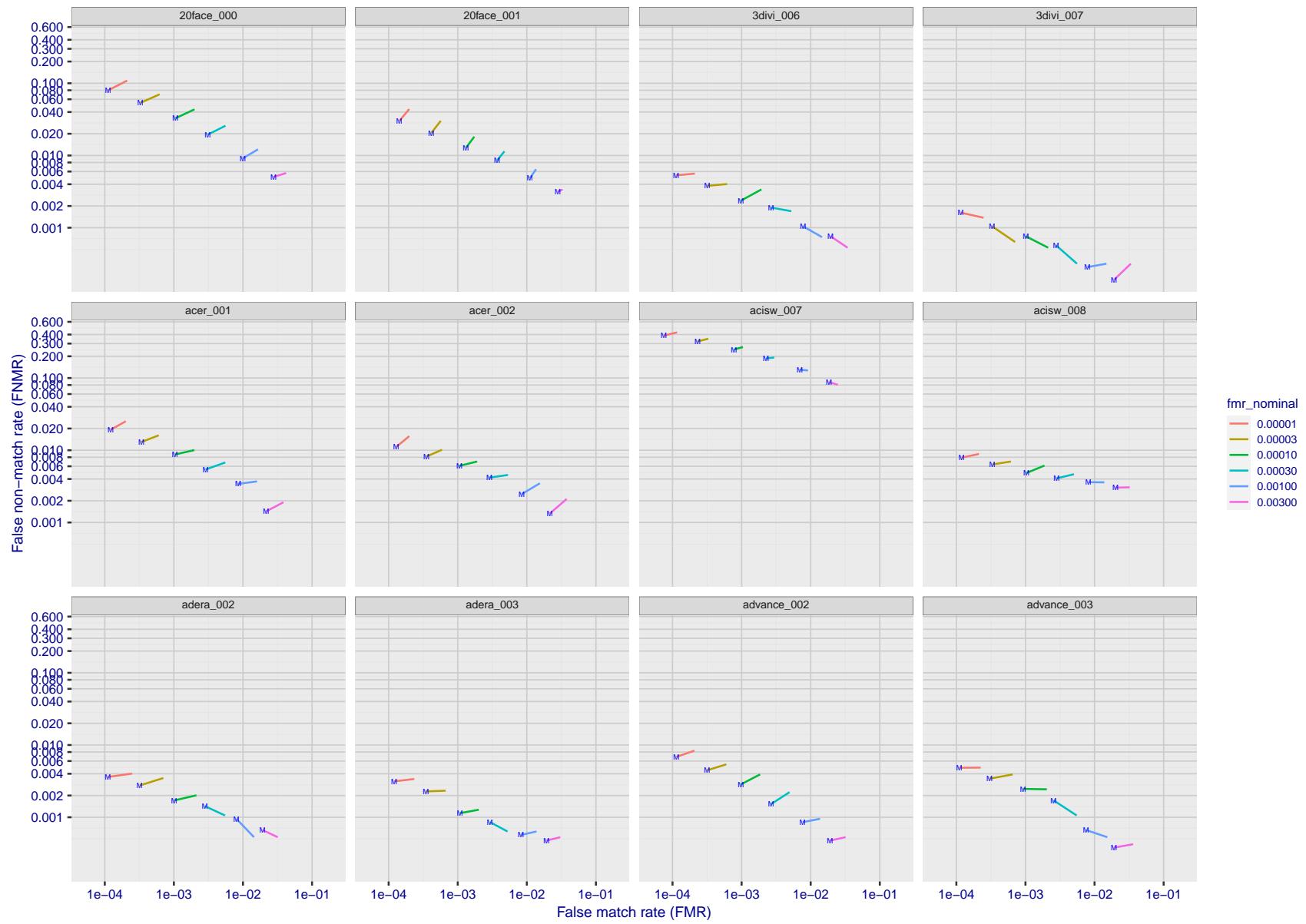


Figure 172: For the visa images, FNMR and FMR at six operating points along the DET characteristic. At each point a line is drawn between $(FMR, FNMR)_{MALE}$ and $(FMR, FNMR)_{FEMALE}$ showing how which sex has lower FMR and/or FNMR. The "M" label denotes male, the other end of the line corresponds to female. The six operating thresholds are selected to give the nominal false match rates given in the legend, and are computed over all impostor pairs regardless of age, sex, and place of birth. The plotted FMR values are broadly an order of magnitude larger than the nominal rates because FMR is computed over demographically-matched impostor pairs i.e individuals of the same sex, from the same geographic region (see section 3.6.1), and the same age group (see section 3.6.2).

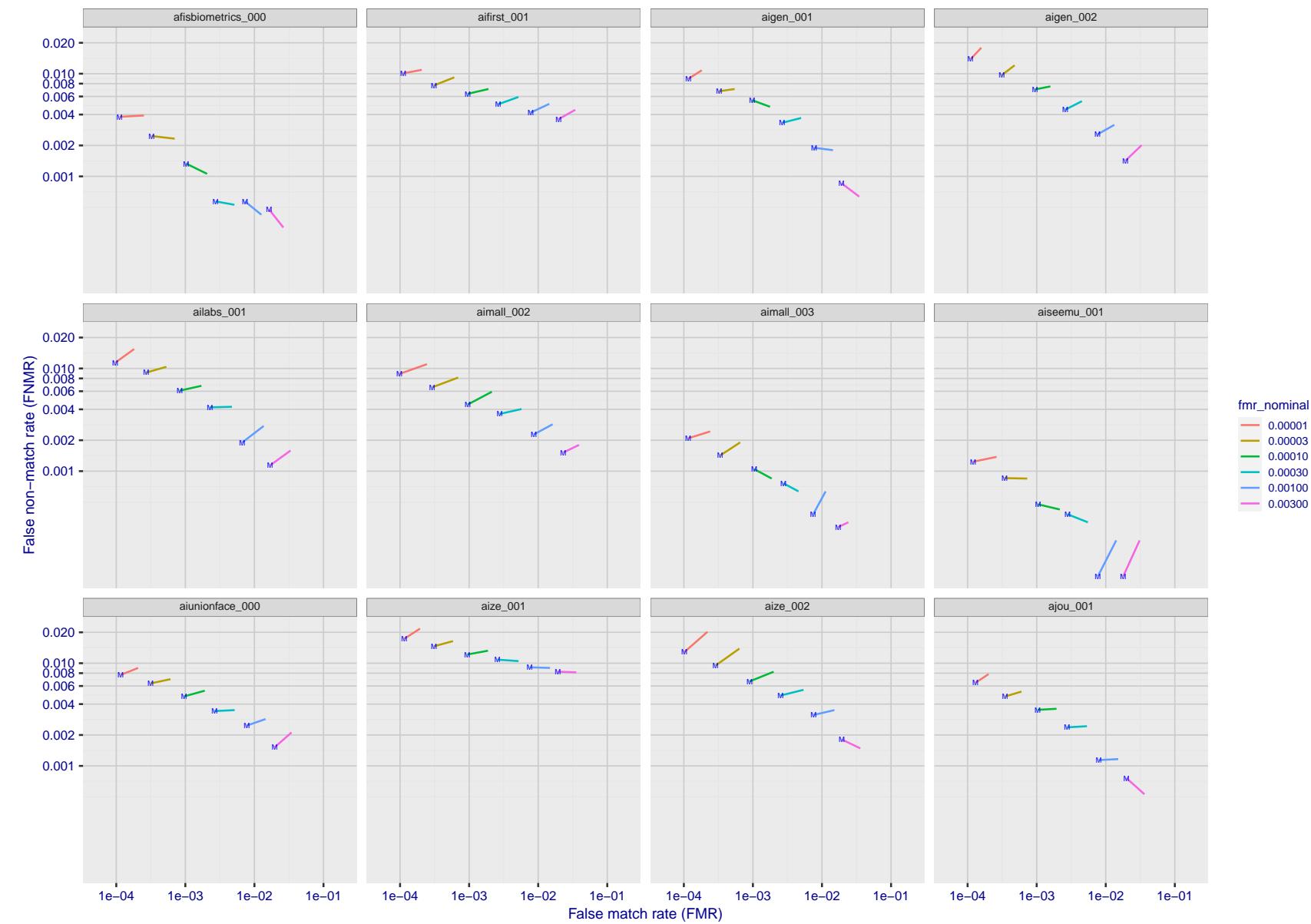


Figure 173: For the visa images, FNMR and FMR at six operating points along the DET characteristic. At each point a line is drawn between $(FMR, FNMR)_{MALE}$ and $(FMR, FNMR)_{FEMALE}$ showing how which sex has lower FMR and/or FNMR. The "M" label denotes male, the other end of the line corresponds to female. The six operating thresholds are selected to give the nominal false match rates given in the legend, and are computed over all impostor pairs regardless of age, sex, and place of birth. The plotted FMR values are broadly an order of magnitude larger than the nominal rates because FMR is computed over demographically-matched impostor pairs i.e individuals of the same sex, from the same geographic region (see section 3.6.1), and the same age group (see section 3.6.2).

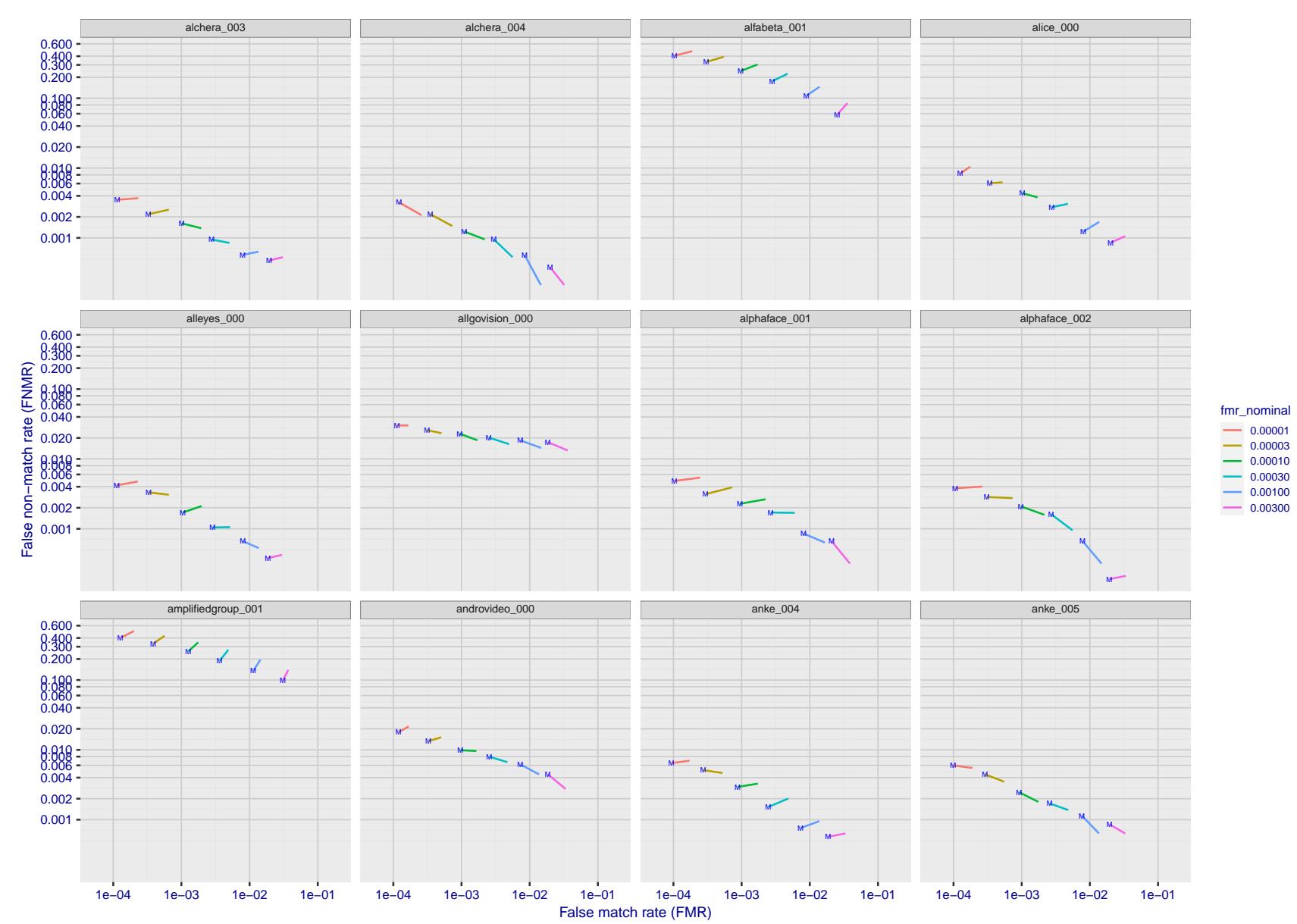


Figure 174: For the visa images, FNMR and FMR at six operating points along the DET characteristic. At each point a line is drawn between $(FMR, FNMR)_{MALE}$ and $(FMR, FNMR)_{FEMALE}$ showing how which sex has lower FMR and/or FNMR. The "M" label denotes male, the other end of the line corresponds to female. The six operating thresholds are selected to give the nominal false match rates given in the legend, and are computed over all impostor pairs regardless of age, sex, and place of birth. The plotted FMR values are broadly an order of magnitude larger than the nominal rates because FMR is computed over demographically-matched impostor pairs i.e individuals of the same sex, from the same geographic region (see section 3.6.1), and the same age group (see section 3.6.2).

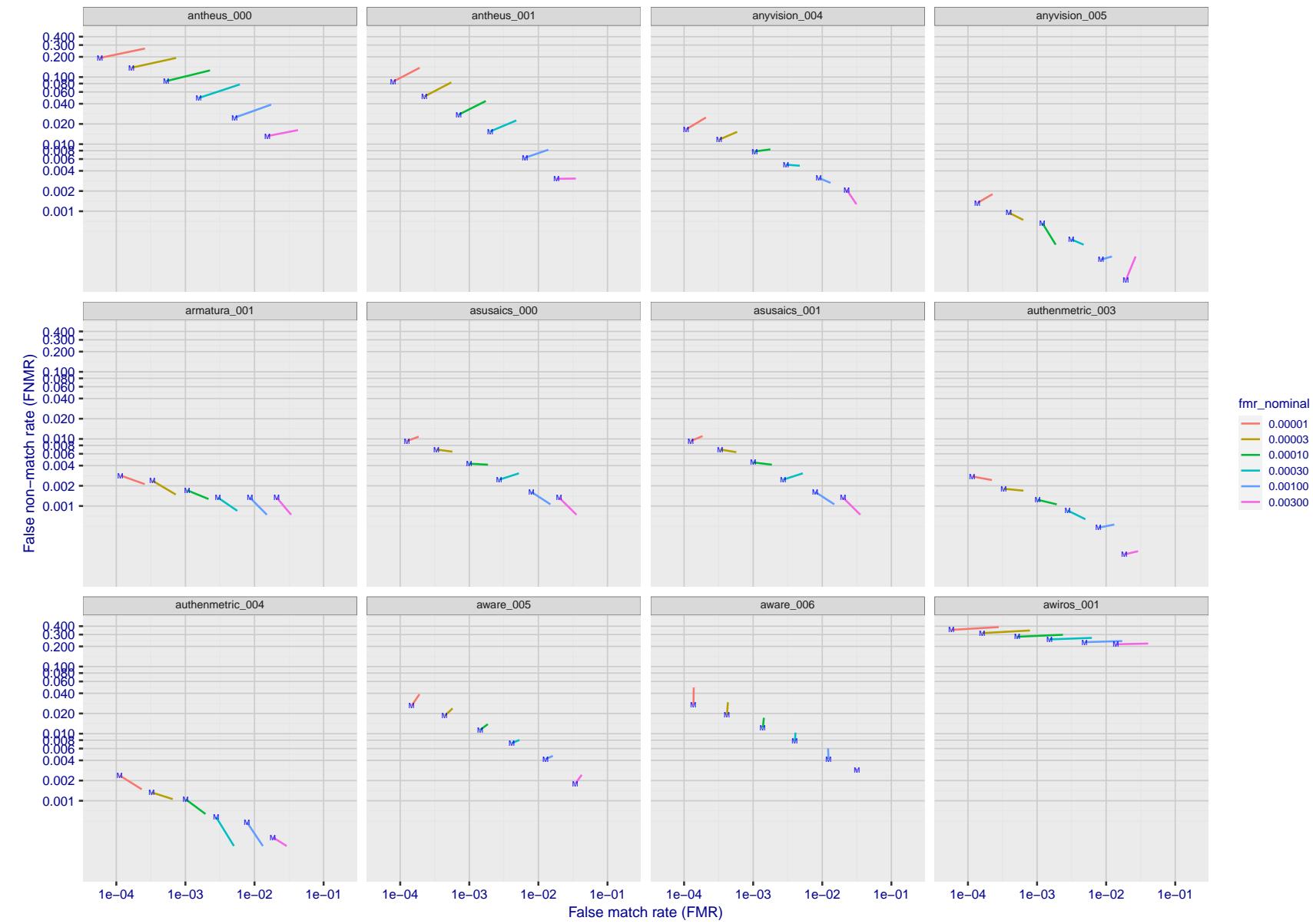


Figure 175: For the visa images, FNMR and FMR at six operating points along the DET characteristic. At each point a line is drawn between $(FMR, FNMR)_{MALE}$ and $(FMR, FNMR)_{FEMALE}$ showing how which sex has lower FMR and/or FNMR. The "M" label denotes male, the other end of the line corresponds to female. The six operating thresholds are selected to give the nominal false match rates given in the legend, and are computed over all impostor pairs regardless of age, sex, and place of birth. The plotted FMR values are broadly an order of magnitude larger than the nominal rates because FMR is computed over demographically-matched impostor pairs i.e individuals of the same sex, from the same geographic region (see section 3.6.1), and the same age group (see section 3.6.2).

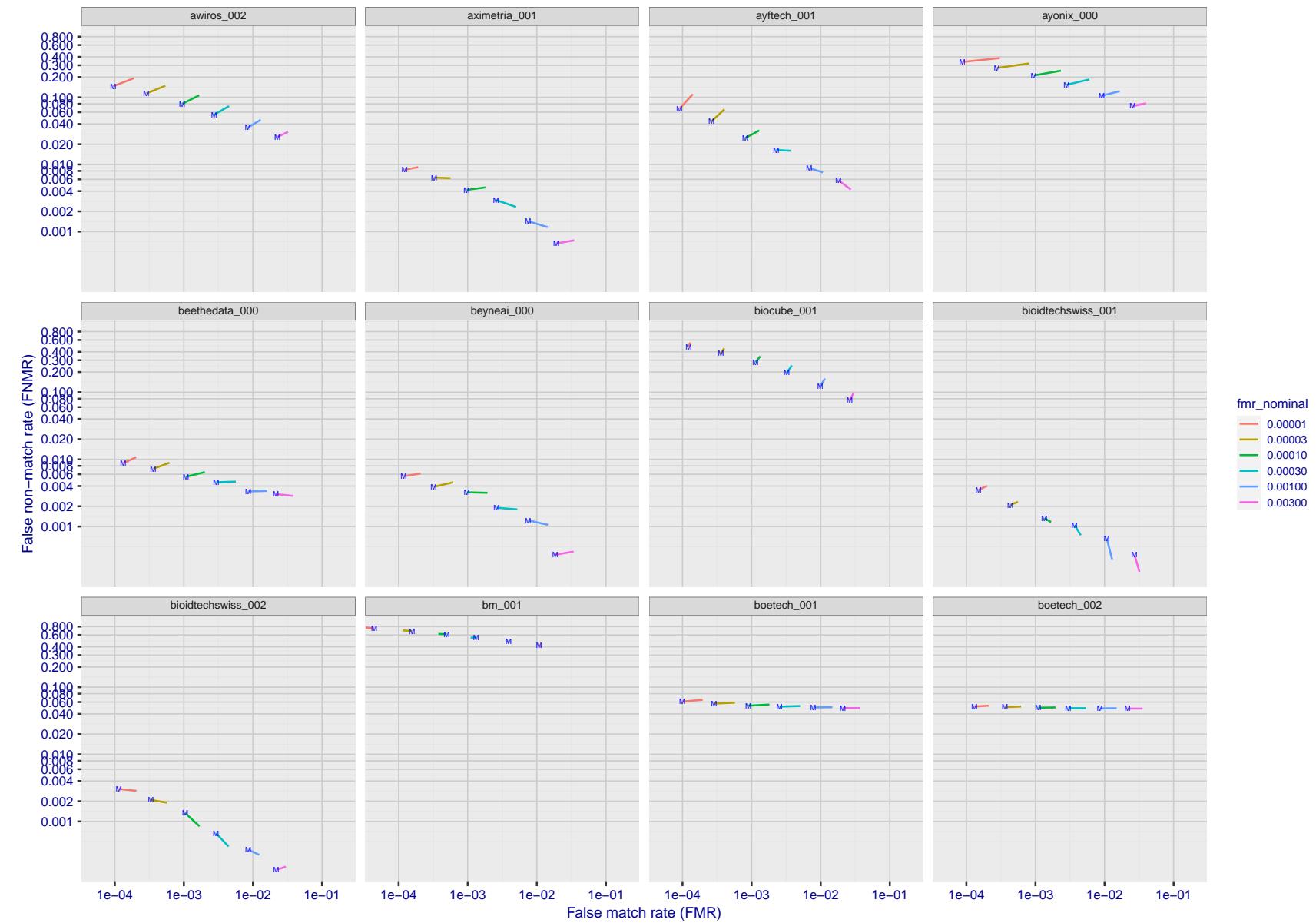


Figure 176: For the visa images, FNMR and FMR at six operating points along the DET characteristic. At each point a line is drawn between $(FMR, FNMR)_{MALE}$ and $(FMR, FNMR)_{FEMALE}$ showing how which sex has lower FMR and/or FNMR. The "M" label denotes male, the other end of the line corresponds to female. The six operating thresholds are selected to give the nominal false match rates given in the legend, and are computed over all impostor pairs regardless of age, sex, and place of birth. The plotted FMR values are broadly an order of magnitude larger than the nominal rates because FMR is computed over demographically-matched impostor pairs i.e individuals of the same sex, from the same geographic region (see section 3.6.1), and the same age group (see section 3.6.2).

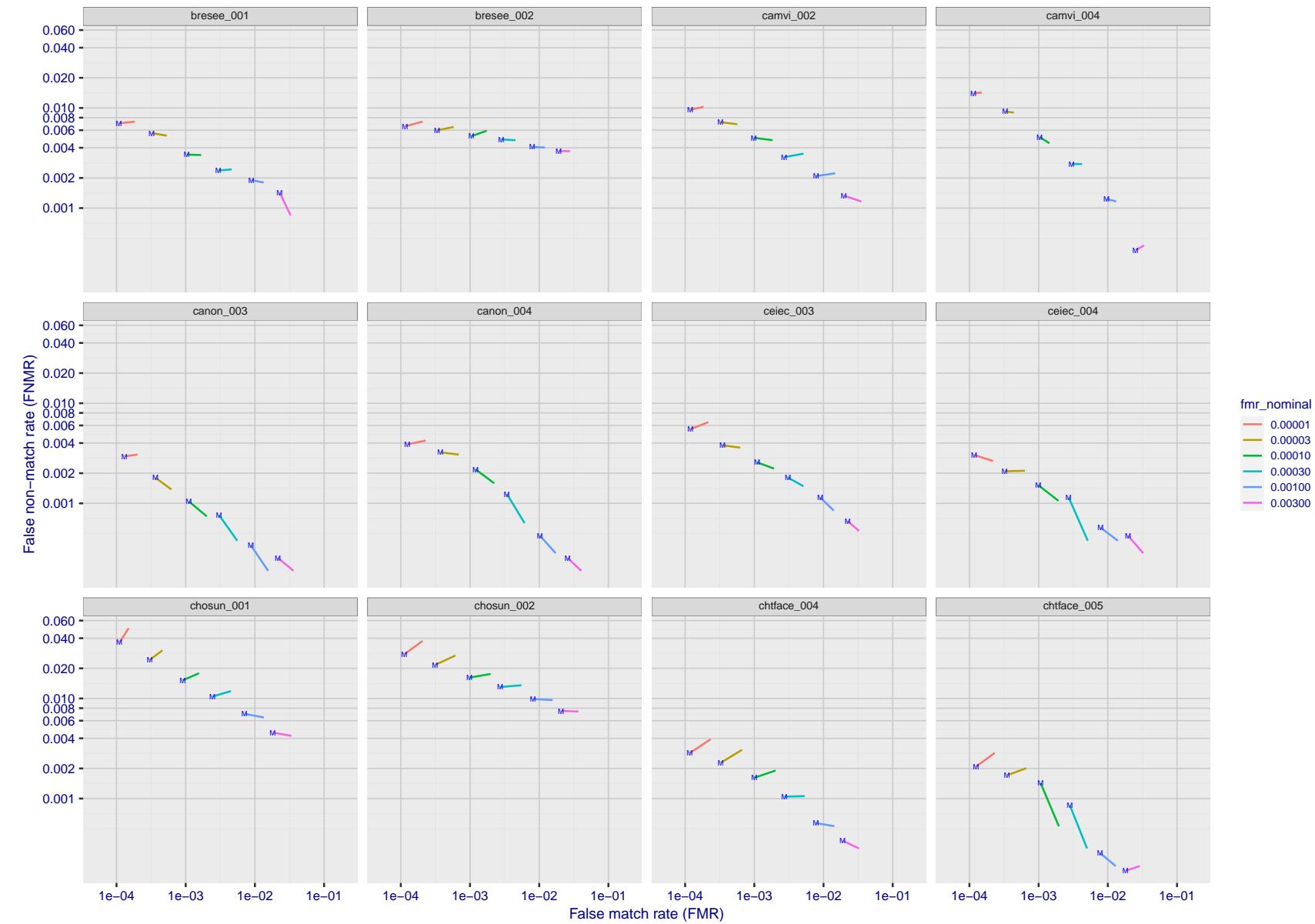


Figure 177: For the visa images, FNMR and FMR at six operating points along the DET characteristic. At each point a line is drawn between $(FMR, FNMR)_{MALE}$ and $(FMR, FNMR)_{FEMALE}$ showing how which sex has lower FMR and/or FNMR. The "M" label denotes male, the other end of the line corresponds to female. The six operating thresholds are selected to give the nominal false match rates given in the legend, and are computed over all impostor pairs regardless of age, sex, and place of birth. The plotted FMR values are broadly an order of magnitude larger than the nominal rates because FMR is computed over demographically-matched impostor pairs i.e individuals of the same sex, from the same geographic region (see section 3.6.1), and the same age group (see section 3.6.2).

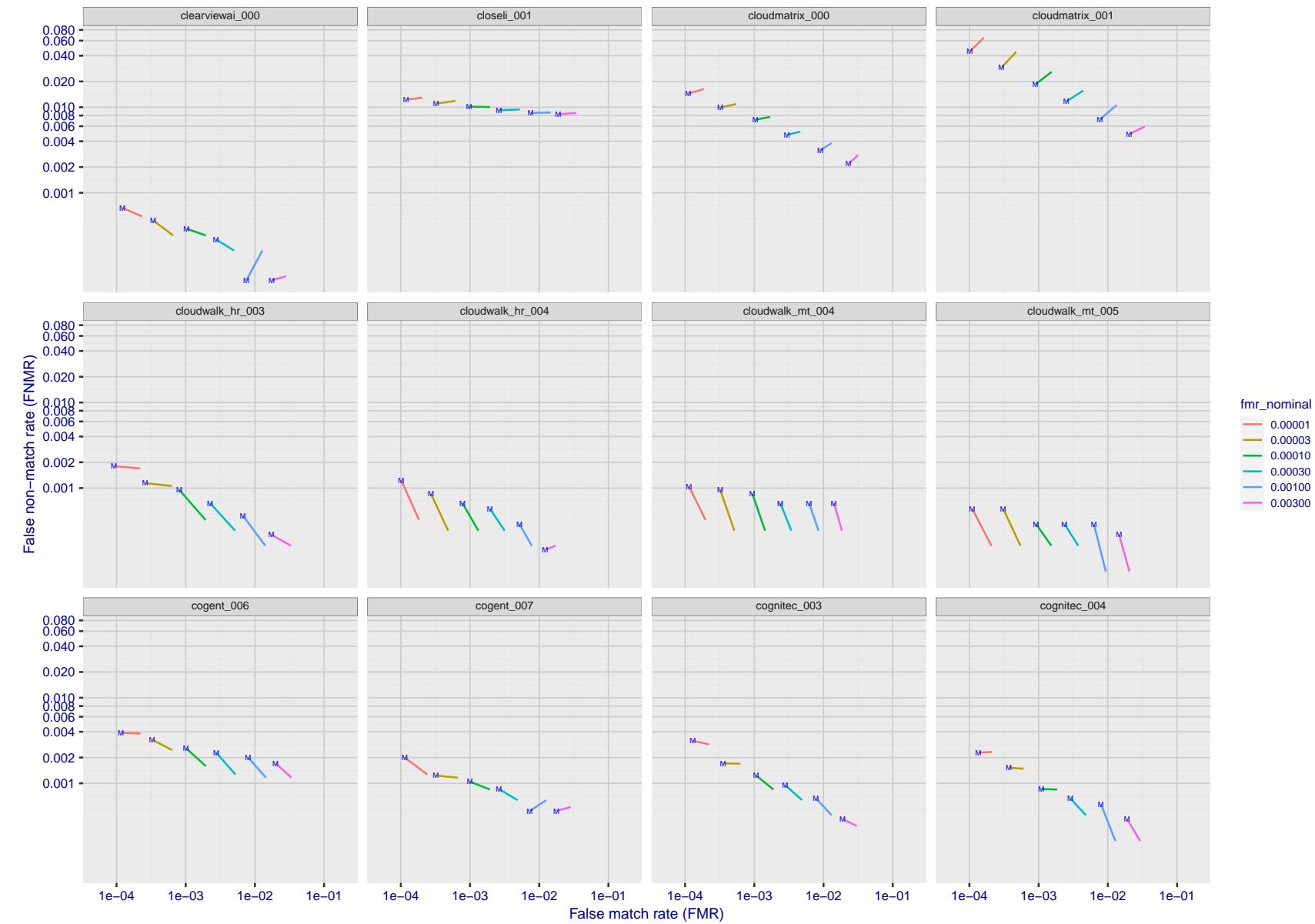


Figure 178: For the visa images, FNMR and FMR at six operating points along the DET characteristic. At each point a line is drawn between $(FMR, FNMR)_{MALE}$ and $(FMR, FNMR)_{FEMALE}$ showing how which sex has lower FMR and/or FNMR. The "M" label denotes male, the other end of the line corresponds to female. The six operating thresholds are selected to give the nominal false match rates given in the legend, and are computed over all impostor pairs regardless of age, sex, and place of birth. The plotted FMR values are broadly an order of magnitude larger than the nominal rates because FMR is computed over demographically-matched impostor pairs i.e individuals of the same sex, from the same geographic region (see section 3.6.1), and the same age group (see section 3.6.2).

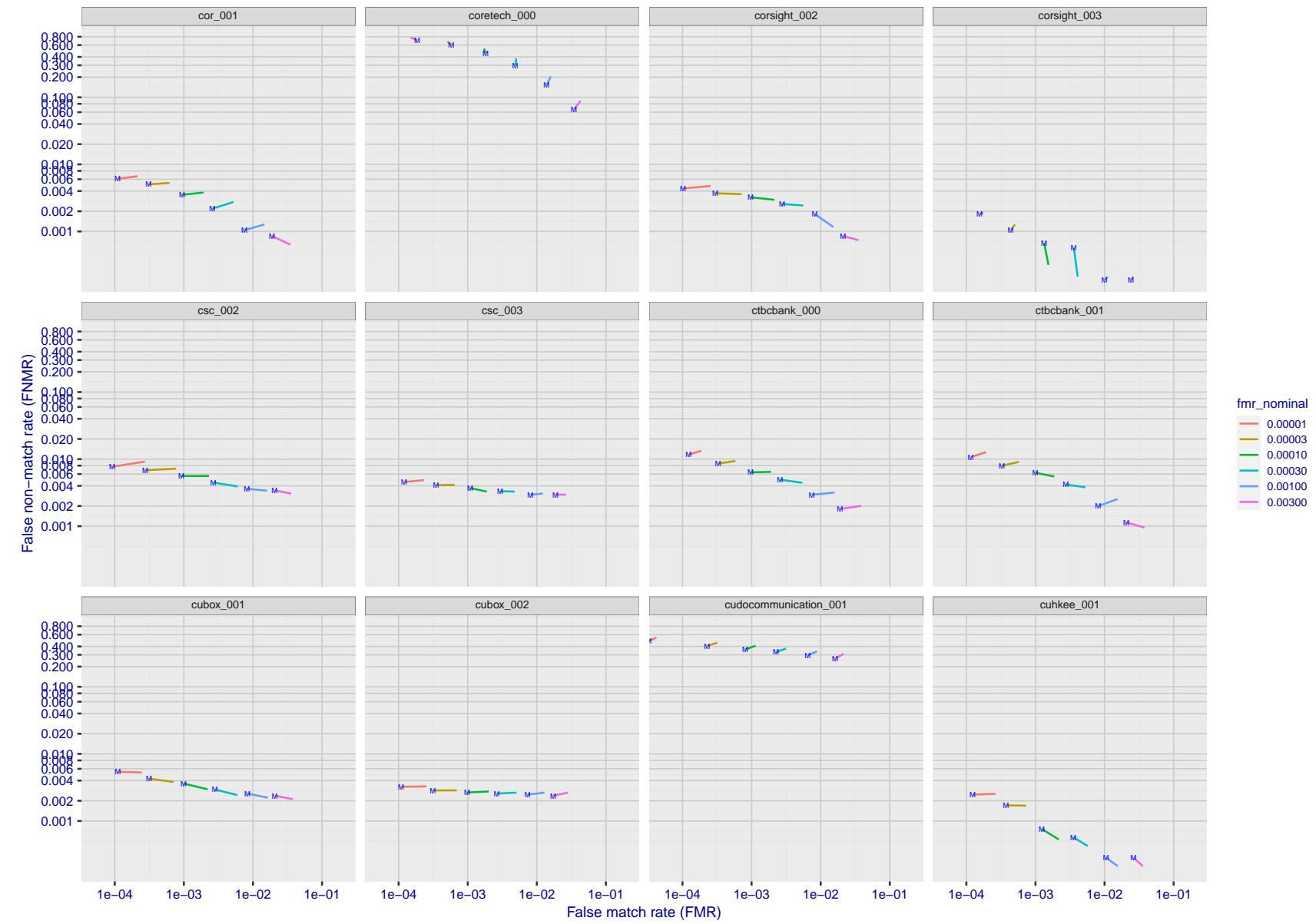


Figure 179: For the visa images, FNMR and FMR at six operating points along the DET characteristic. At each point a line is drawn between $(FMR, FNMR)_{MALE}$ and $(FMR, FNMR)_{FEMALE}$ showing how which sex has lower FMR and/or FNMR. The "M" label denotes male, the other end of the line corresponds to female. The six operating thresholds are selected to give the nominal false match rates given in the legend, and are computed over all impostor pairs regardless of age, sex, and place of birth. The plotted FMR values are broadly an order of magnitude larger than the nominal rates because FMR is computed over demographically-matched impostor pairs i.e individuals of the same sex, from the same geographic region (see section 3.6.1), and the same age group (see section 3.6.2).

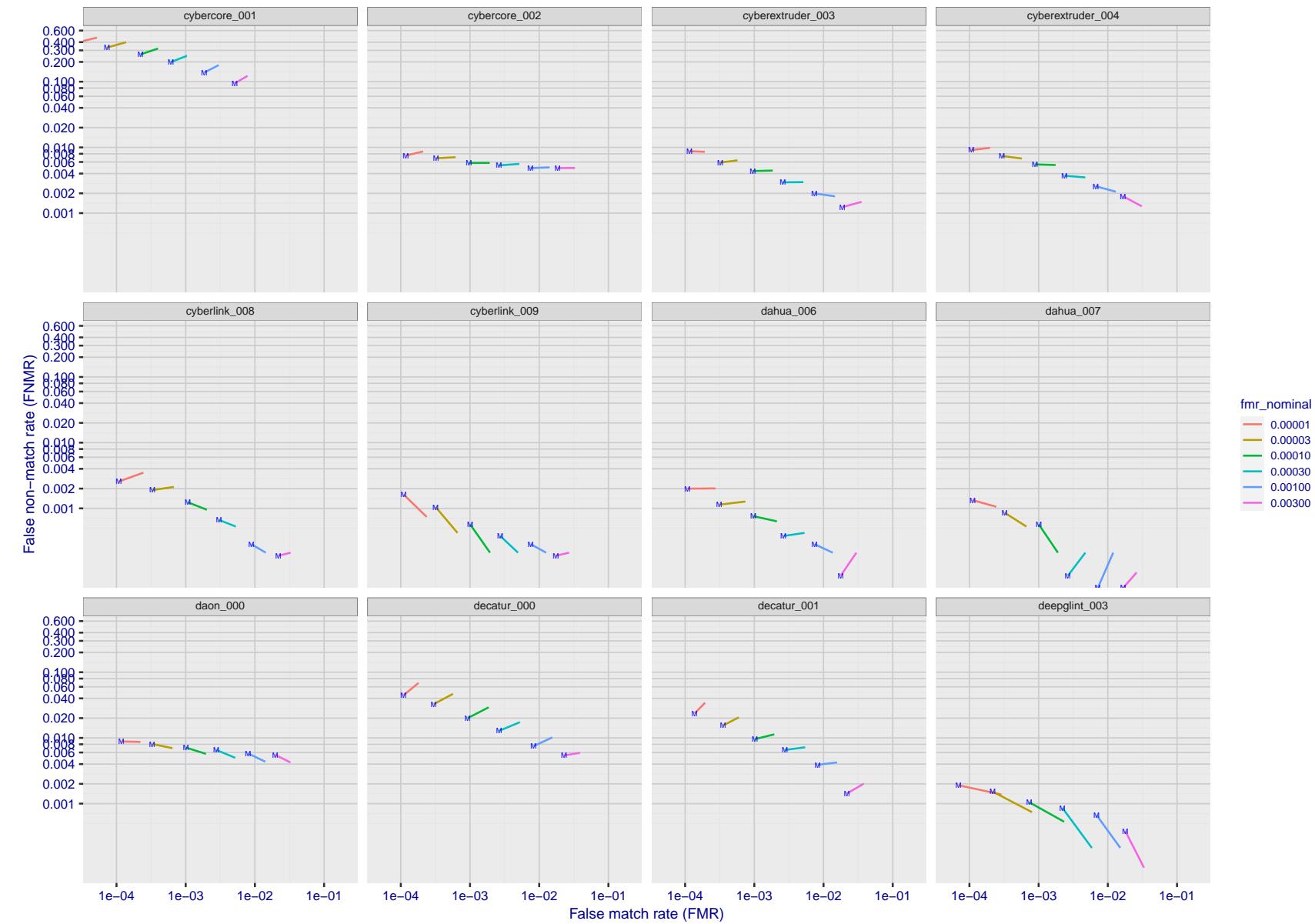


Figure 180: For the visa images, FNMR and FMR at six operating points along the DET characteristic. At each point a line is drawn between $(FMR, FNMR)_{MALE}$ and $(FMR, FNMR)_{FEMALE}$ showing how which sex has lower FMR and/or FNMR. The "M" label denotes male, the other end of the line corresponds to female. The six operating thresholds are selected to give the nominal false match rates given in the legend, and are computed over all impostor pairs regardless of age, sex, and place of birth. The plotted FMR values are broadly an order of magnitude larger than the nominal rates because FMR is computed over demographically-matched impostor pairs i.e individuals of the same sex, from the same geographic region (see section 3.6.1), and the same age group (see section 3.6.2).

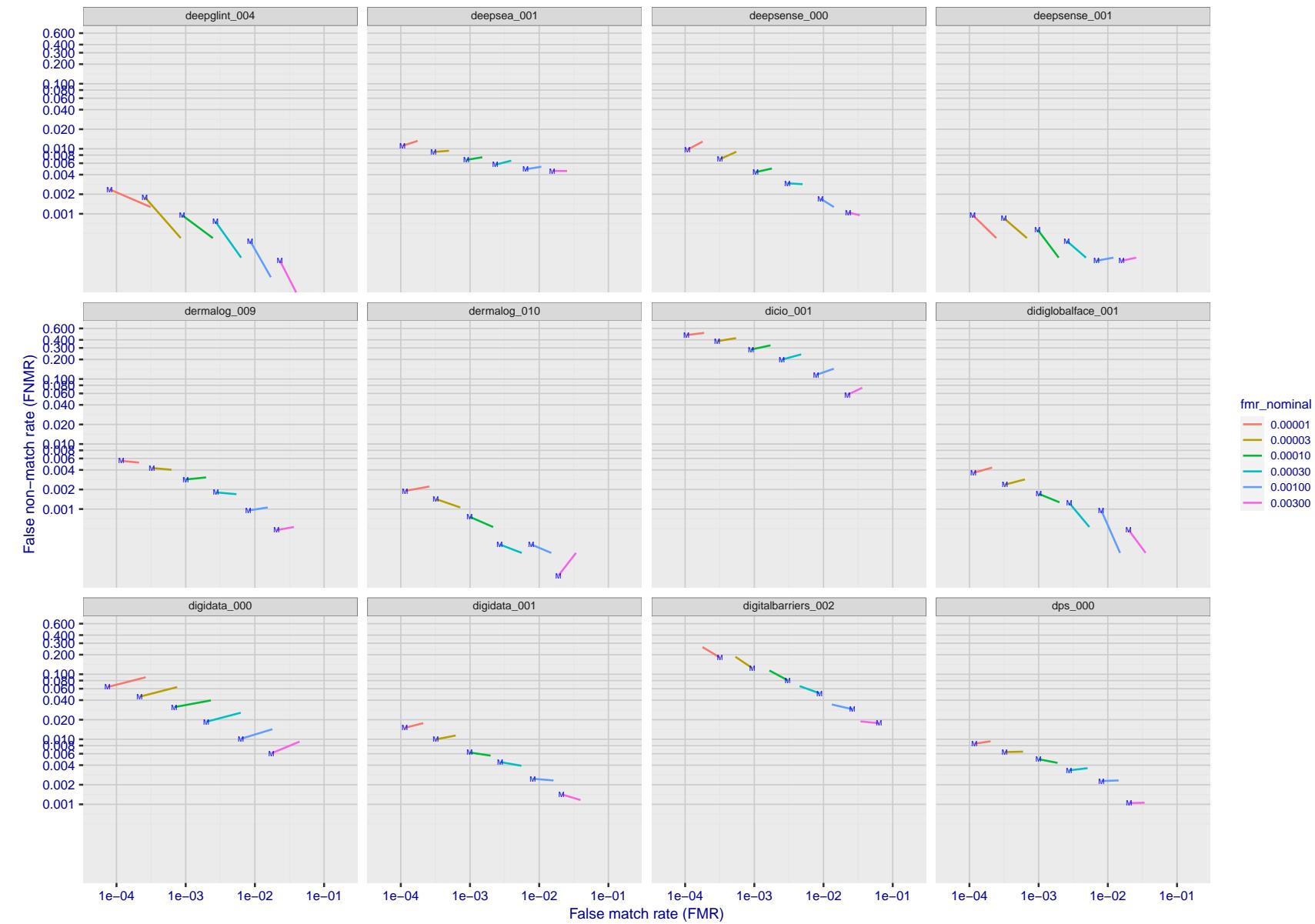


Figure 181: For the visa images, FNMR and FMR at six operating points along the DET characteristic. At each point a line is drawn between $(FMR, FNMR)_{MALE}$ and $(FMR, FNMR)_{FEMALE}$ showing how which sex has lower FMR and/or FNMR. The "M" label denotes male, the other end of the line corresponds to female. The six operating thresholds are selected to give the nominal false match rates given in the legend, and are computed over all impostor pairs regardless of age, sex, and place of birth. The plotted FMR values are broadly an order of magnitude larger than the nominal rates because FMR is computed over demographically-matched impostor pairs i.e individuals of the same sex, from the same geographic region (see section 3.6.1), and the same age group (see section 3.6.2).

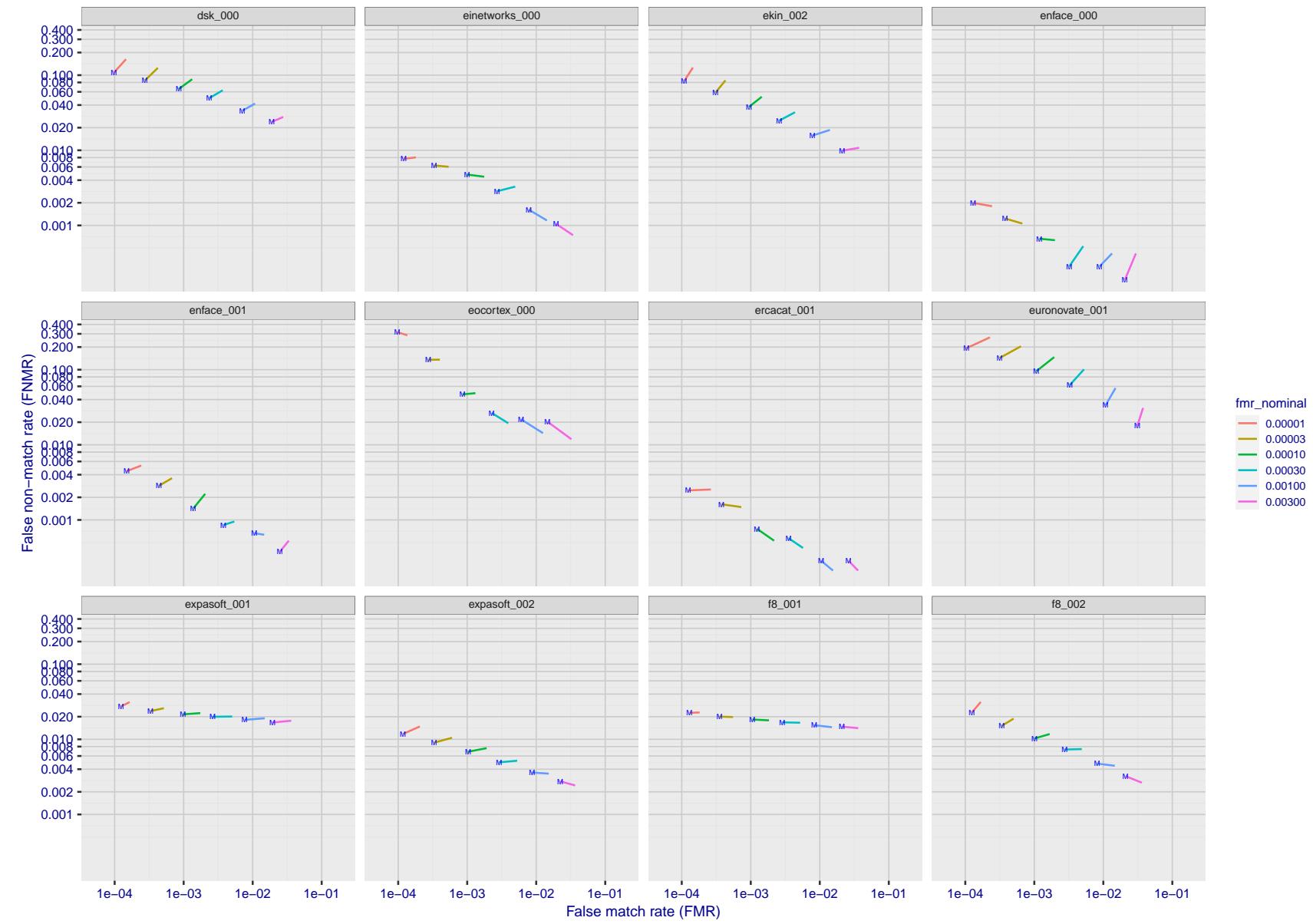


Figure 182: For the visa images, FNMR and FMR at six operating points along the DET characteristic. At each point a line is drawn between $(FMR, FNMR)_{MALE}$ and $(FMR, FNMR)_{FEMALE}$ showing how which sex has lower FMR and/or FNMR. The "M" label denotes male, the other end of the line corresponds to female. The six operating thresholds are selected to give the nominal false match rates given in the legend, and are computed over all impostor pairs regardless of age, sex, and place of birth. The plotted FMR values are broadly an order of magnitude larger than the nominal rates because FMR is computed over demographically-matched impostor pairs i.e individuals of the same sex, from the same geographic region (see section 3.6.1), and the same age group (see section 3.6.2).

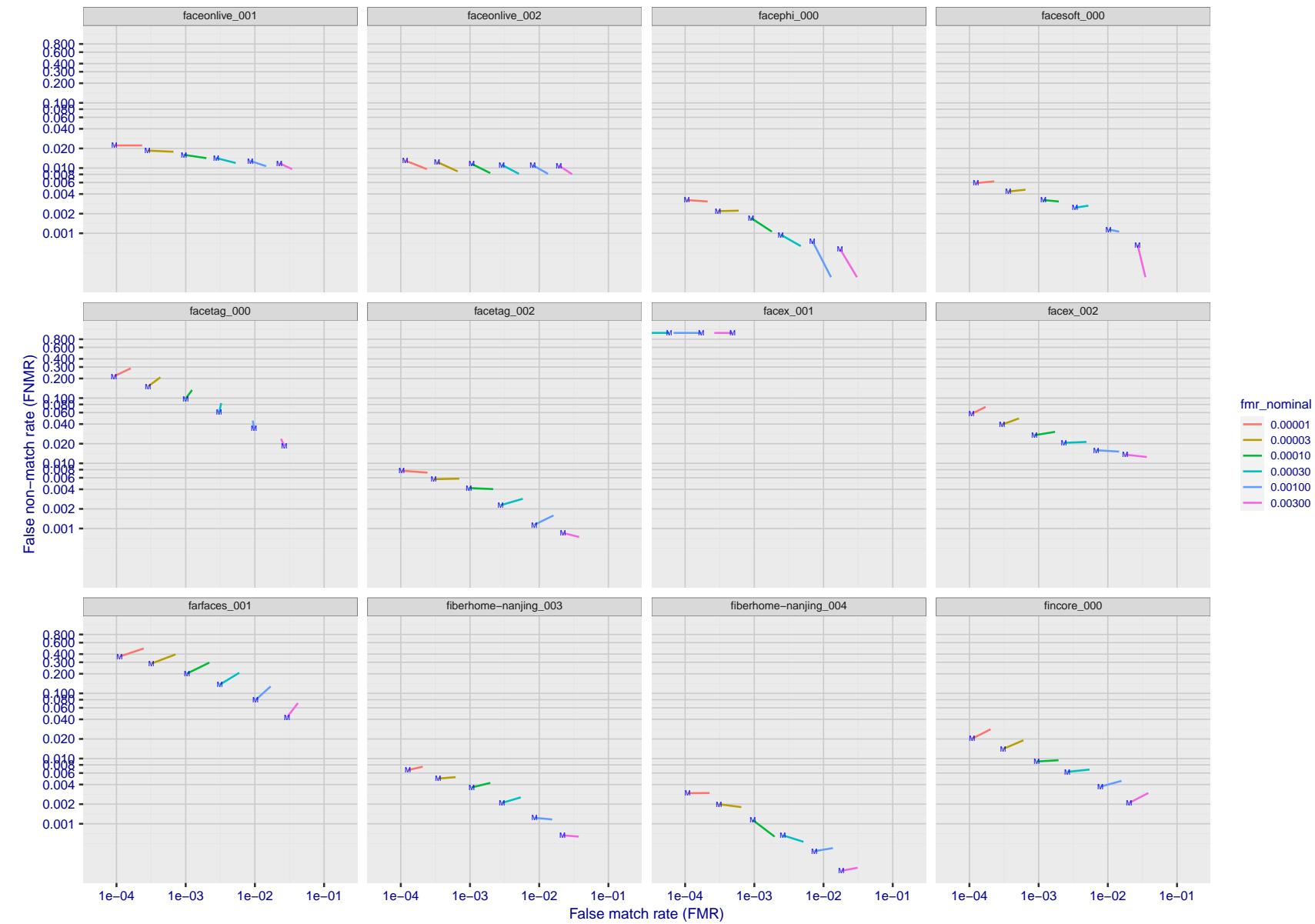


Figure 183: For the visa images, FNMR and FMR at six operating points along the DET characteristic. At each point a line is drawn between $(FMR, FNMR)_{MALE}$ and $(FMR, FNMR)_{FEMALE}$ showing how which sex has lower FMR and/or FNMR. The "M" label denotes male, the other end of the line corresponds to female. The six operating thresholds are selected to give the nominal false match rates given in the legend, and are computed over all impostor pairs regardless of age, sex, and place of birth. The plotted FMR values are broadly an order of magnitude larger than the nominal rates because FMR is computed over demographically-matched impostor pairs i.e individuals of the same sex, from the same geographic region (see section 3.6.1), and the same age group (see section 3.6.2).

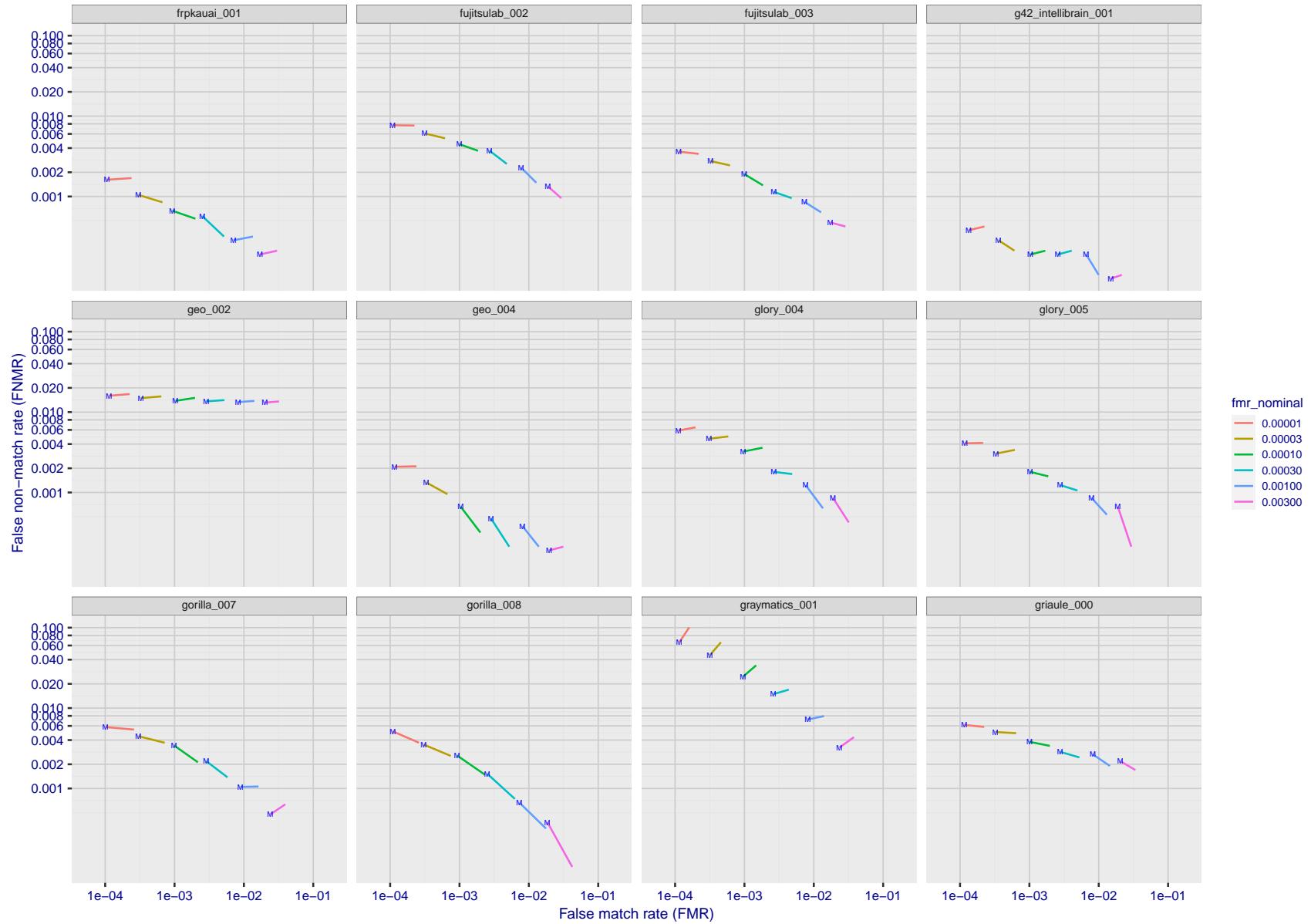


Figure 184: For the visa images, FNMR and FMR at six operating points along the DET characteristic. At each point a line is drawn between $(FMR, FNMR)_{MALE}$ and $(FMR, FNMR)_{FEMALE}$ showing how which sex has lower FMR and/or FNMR. The "M" label denotes male, the other end of the line corresponds to female. The six operating thresholds are selected to give the nominal false match rates given in the legend, and are computed over all impostor pairs regardless of age, sex, and place of birth. The plotted FMR values are broadly an order of magnitude larger than the nominal rates because FMR is computed over demographically-matched impostor pairs i.e individuals of the same sex, from the same geographic region (see section 3.6.1), and the same age group (see section 3.6.2).

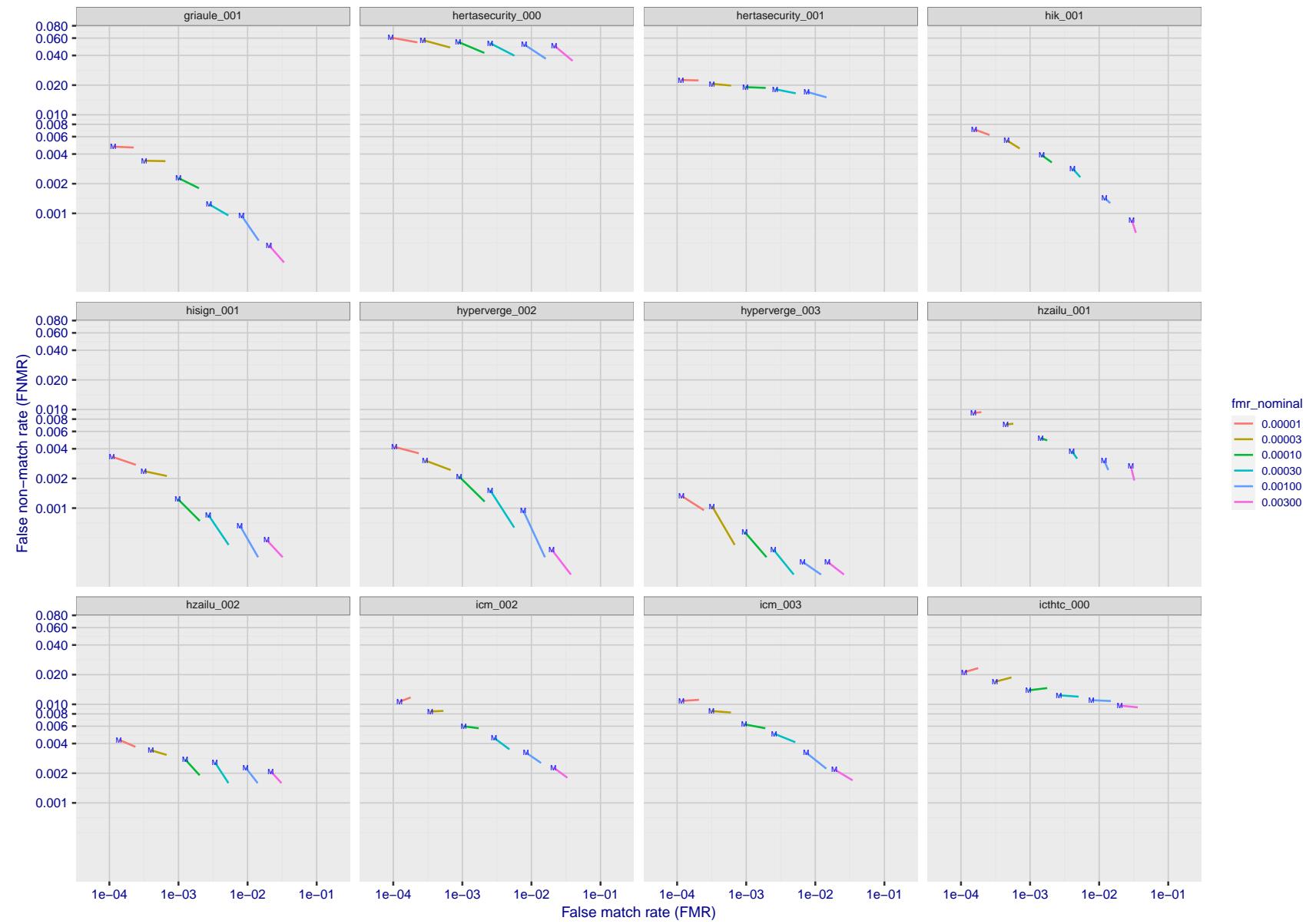


Figure 185: For the visa images, FNMR and FMR at six operating points along the DET characteristic. At each point a line is drawn between $(FMR, FNMR)_{MALE}$ and $(FMR, FNMR)_{FEMALE}$ showing how which sex has lower FMR and/or FNMR. The "M" label denotes male, the other end of the line corresponds to female. The six operating thresholds are selected to give the nominal false match rates given in the legend, and are computed over all impostor pairs regardless of age, sex, and place of birth. The plotted FMR values are broadly an order of magnitude larger than the nominal rates because FMR is computed over demographically-matched impostor pairs i.e individuals of the same sex, from the same geographic region (see section 3.6.1), and the same age group (see section 3.6.2).

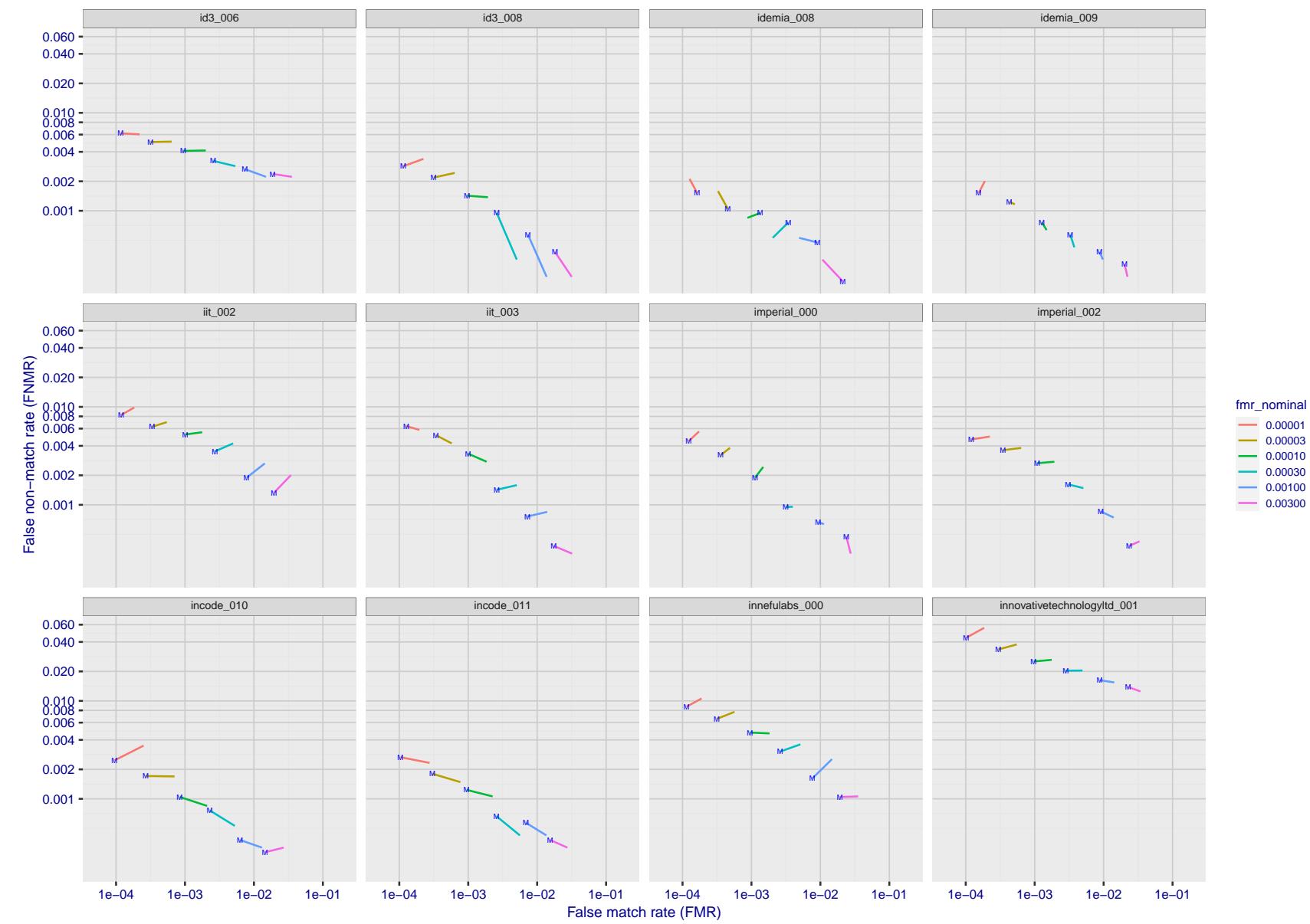


Figure 186: For the visa images, FNMR and FMR at six operating points along the DET characteristic. At each point a line is drawn between $(FMR, FNMR)_{MALE}$ and $(FMR, FNMR)_{FEMALE}$ showing how which sex has lower FMR and/or FNMR. The "M" label denotes male, the other end of the line corresponds to female. The six operating thresholds are selected to give the nominal false match rates given in the legend, and are computed over all impostor pairs regardless of age, sex, and place of birth. The plotted FMR values are broadly an order of magnitude larger than the nominal rates because FMR is computed over demographically-matched impostor pairs i.e individuals of the same sex, from the same geographic region (see section 3.6.1), and the same age group (see section 3.6.2).

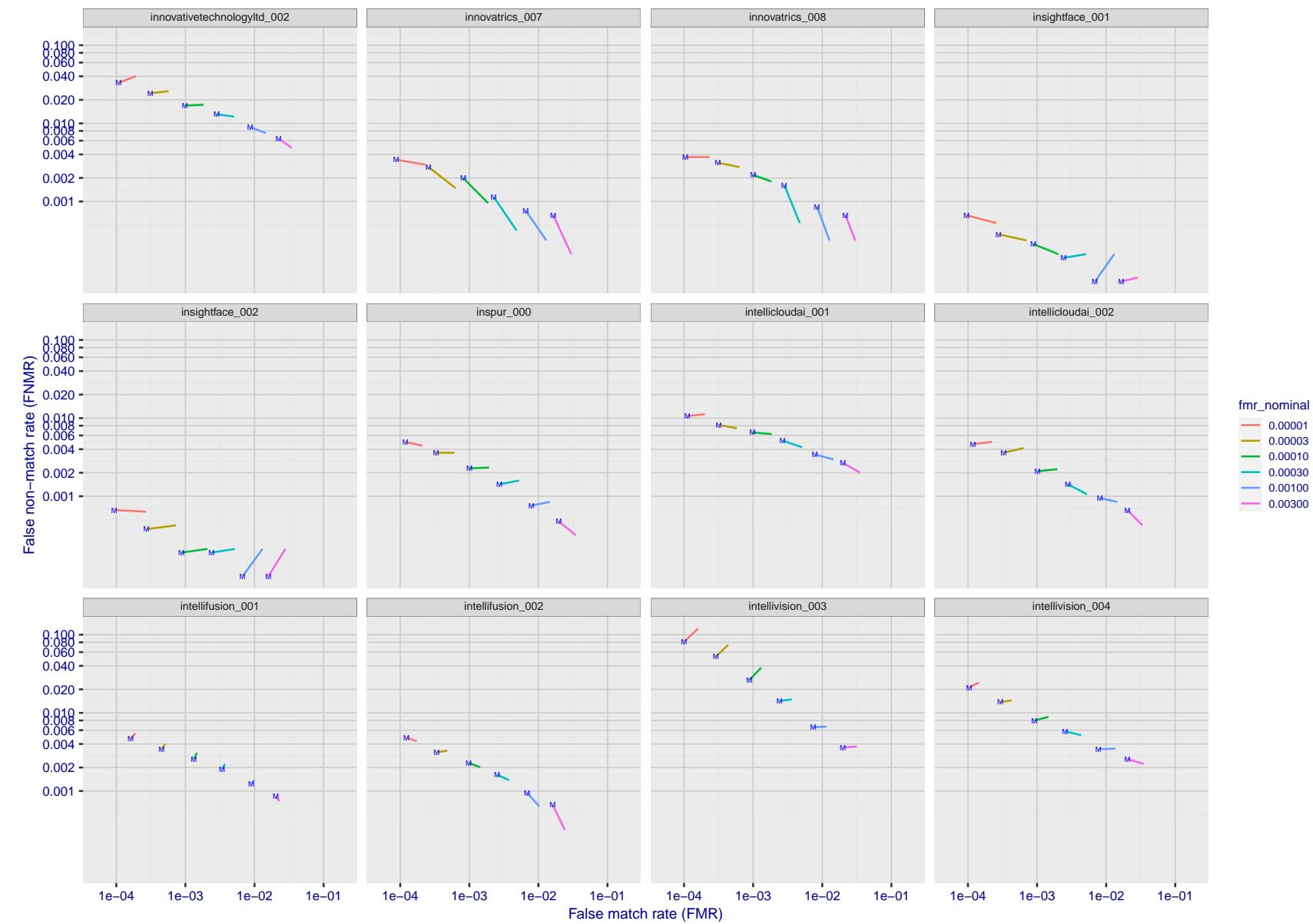


Figure 187: For the visa images, FNMR and FMR at six operating points along the DET characteristic. At each point a line is drawn between $(FMR, FNMR)_{MALE}$ and $(FMR, FNMR)_{FEMALE}$ showing how which sex has lower FMR and/or FNMR. The "M" label denotes male, the other end of the line corresponds to female. The six operating thresholds are selected to give the nominal false match rates given in the legend, and are computed over all impostor pairs regardless of age, sex, and place of birth. The plotted FMR values are broadly an order of magnitude larger than the nominal rates because FMR is computed over demographically-matched impostor pairs i.e individuals of the same sex, from the same geographic region (see section 3.6.1), and the same age group (see section 3.6.2).

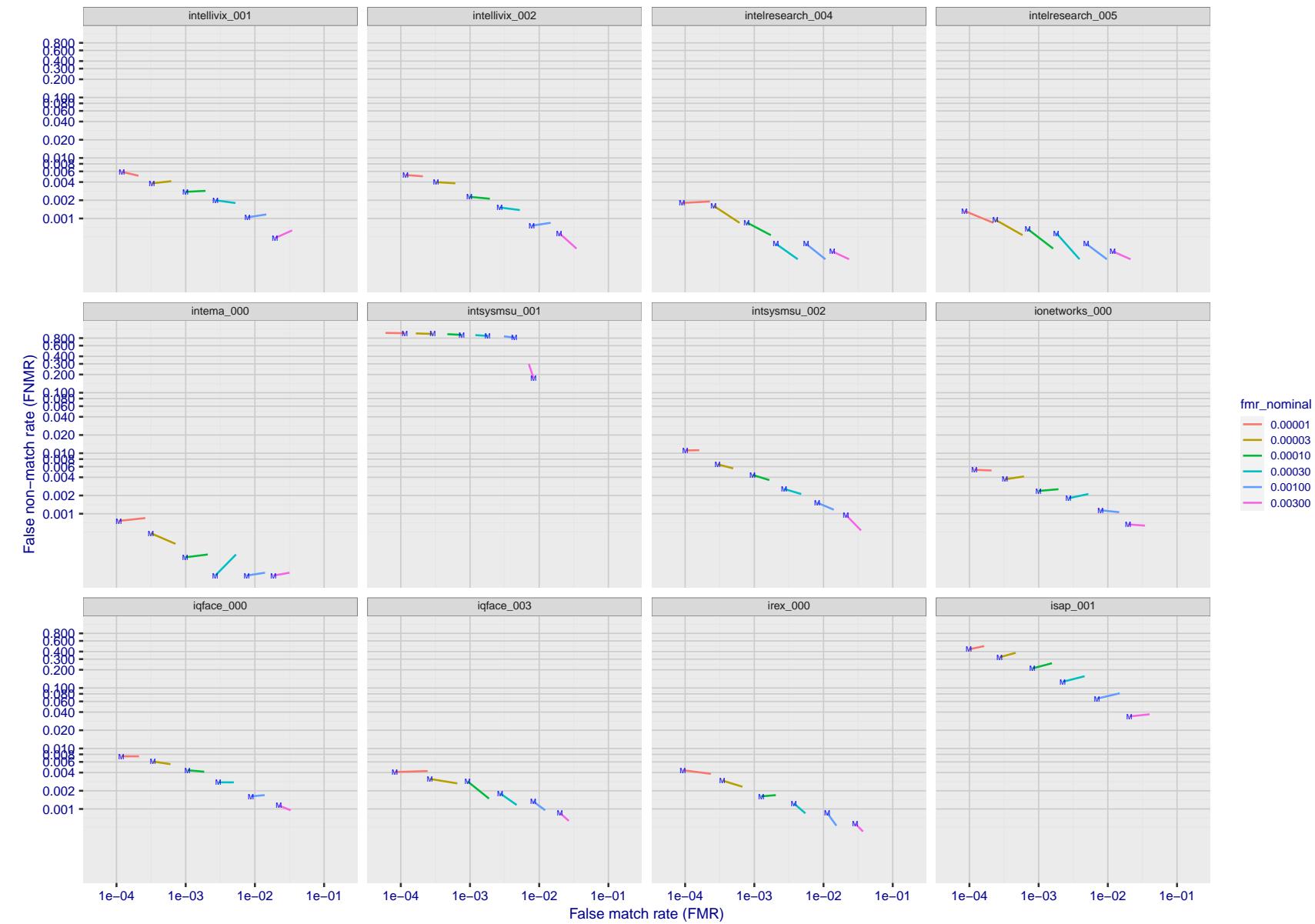


Figure 188: For the visa images, FNMR and FMR at six operating points along the DET characteristic. At each point a line is drawn between $(FMR, FNMR)_{MALE}$ and $(FMR, FNMR)_{FEMALE}$ showing how which sex has lower FMR and/or FNMR. The "M" label denotes male, the other end of the line corresponds to female. The six operating thresholds are selected to give the nominal false match rates given in the legend, and are computed over all impostor pairs regardless of age, sex, and place of birth. The plotted FMR values are broadly an order of magnitude larger than the nominal rates because FMR is computed over demographically-matched impostor pairs i.e individuals of the same sex, from the same geographic region (see section 3.6.1), and the same age group (see section 3.6.2).

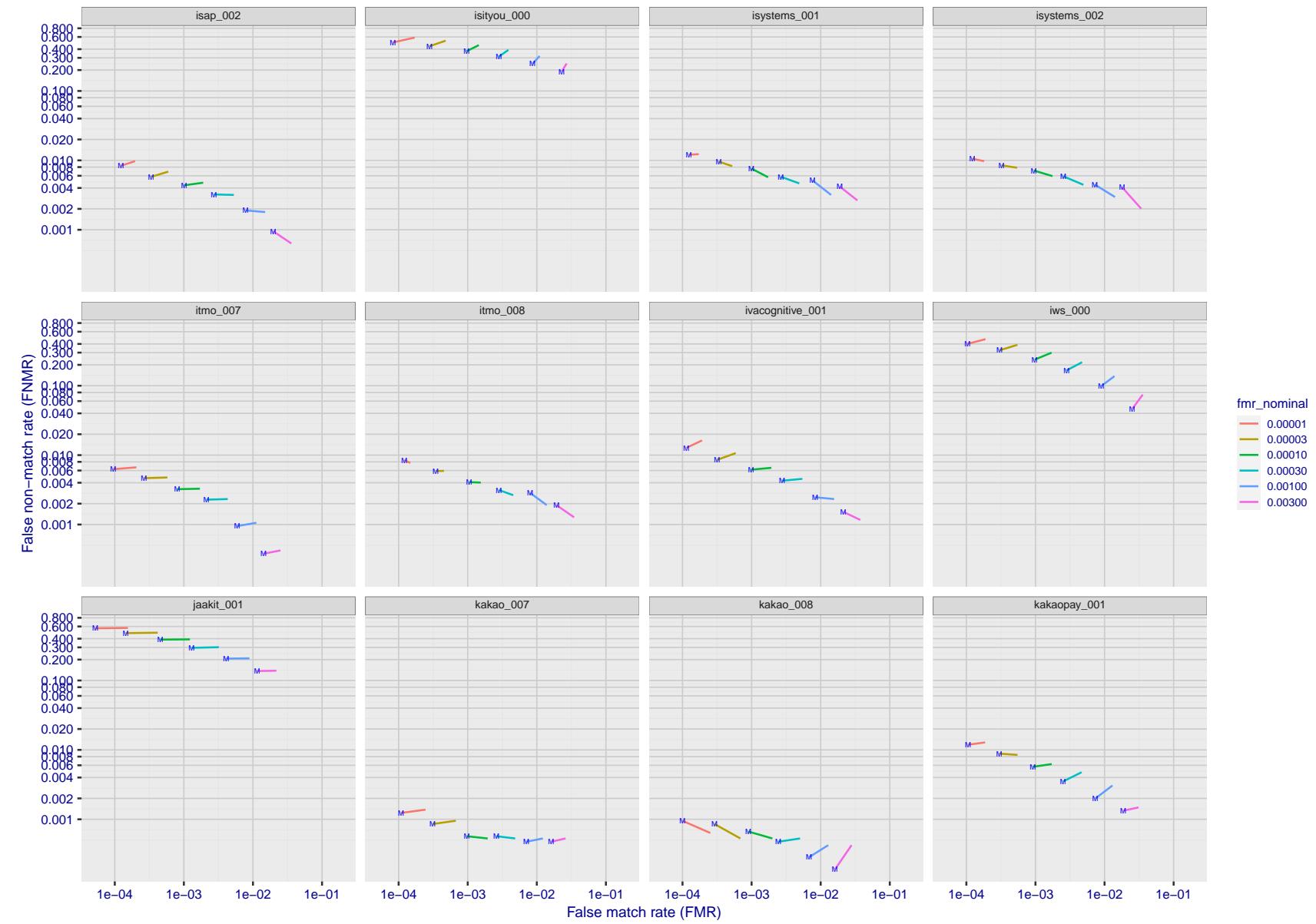


Figure 189: For the visa images, FNMR and FMR at six operating points along the DET characteristic. At each point a line is drawn between $(FMR, FNMR)_{MALE}$ and $(FMR, FNMR)_{FEMALE}$ showing how which sex has lower FMR and/or FNMR. The "M" label denotes male, the other end of the line corresponds to female. The six operating thresholds are selected to give the nominal false match rates given in the legend, and are computed over all impostor pairs regardless of age, sex, and place of birth. The plotted FMR values are broadly an order of magnitude larger than the nominal rates because FMR is computed over demographically-matched impostor pairs i.e individuals of the same sex, from the same geographic region (see section 3.6.1), and the same age group (see section 3.6.2).

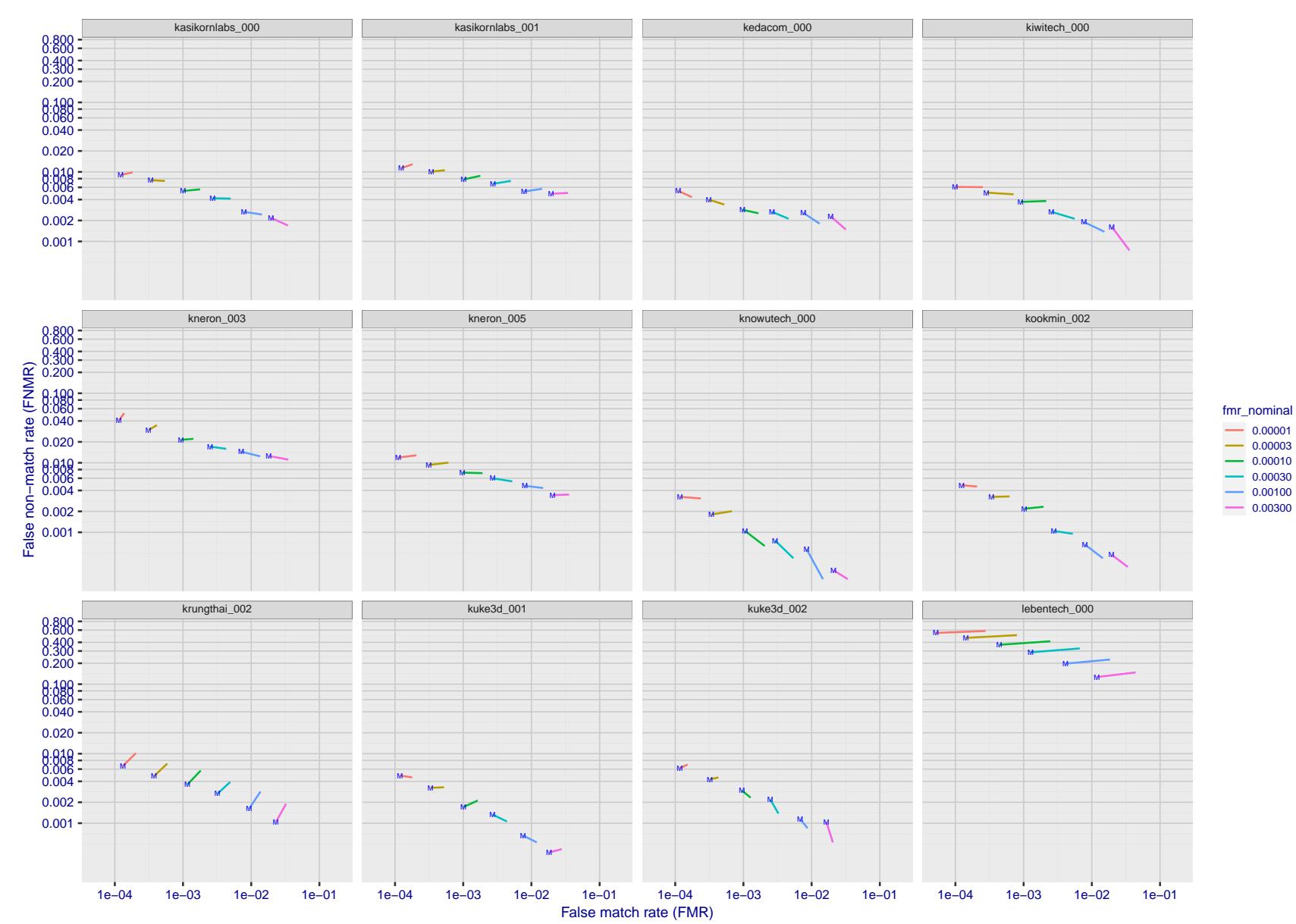


Figure 190: For the visa images, FNMR and FMR at six operating points along the DET characteristic. At each point a line is drawn between $(FMR, FNMR)_{MALE}$ and $(FMR, FNMR)_{FEMALE}$ showing how which sex has lower FMR and/or FNMR. The "M" label denotes male, the other end of the line corresponds to female. The six operating thresholds are selected to give the nominal false match rates given in the legend, and are computed over all impostor pairs regardless of age, sex, and place of birth. The plotted FMR values are broadly an order of magnitude larger than the nominal rates because FMR is computed over demographically-matched impostor pairs i.e individuals of the same sex, from the same geographic region (see section 3.6.1), and the same age group (see section 3.6.2).

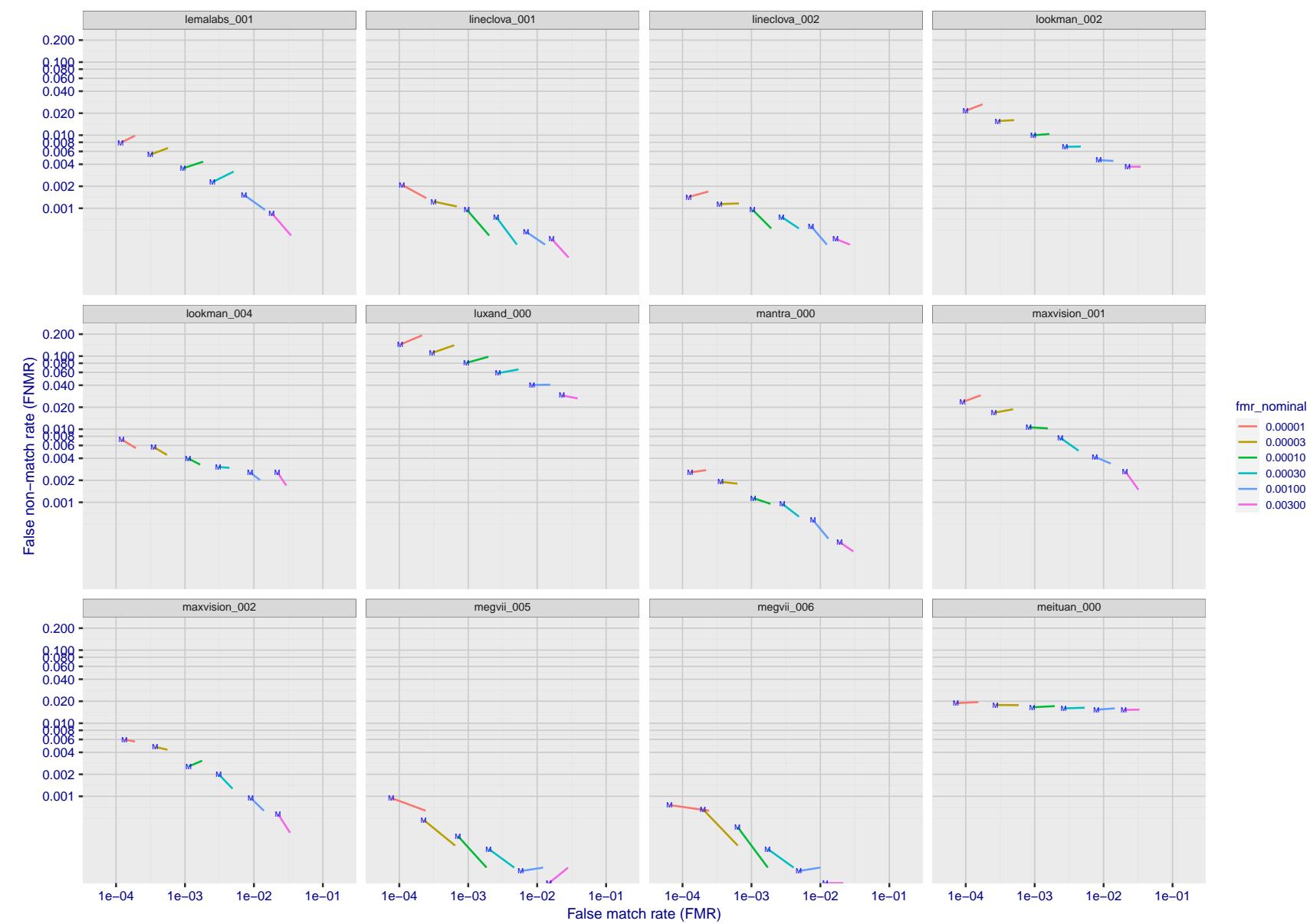


Figure 191: For the visa images, FNMR and FMR at six operating points along the DET characteristic. At each point a line is drawn between $(FMR, FNMR)_{MALE}$ and $(FMR, FNMR)_{FEMALE}$ showing how which sex has lower FMR and/or FNMR. The "M" label denotes male, the other end of the line corresponds to female. The six operating thresholds are selected to give the nominal false match rates given in the legend, and are computed over all impostor pairs regardless of age, sex, and place of birth. The plotted FMR values are broadly an order of magnitude larger than the nominal rates because FMR is computed over demographically-matched impostor pairs i.e individuals of the same sex, from the same geographic region (see section 3.6.1), and the same age group (see section 3.6.2).

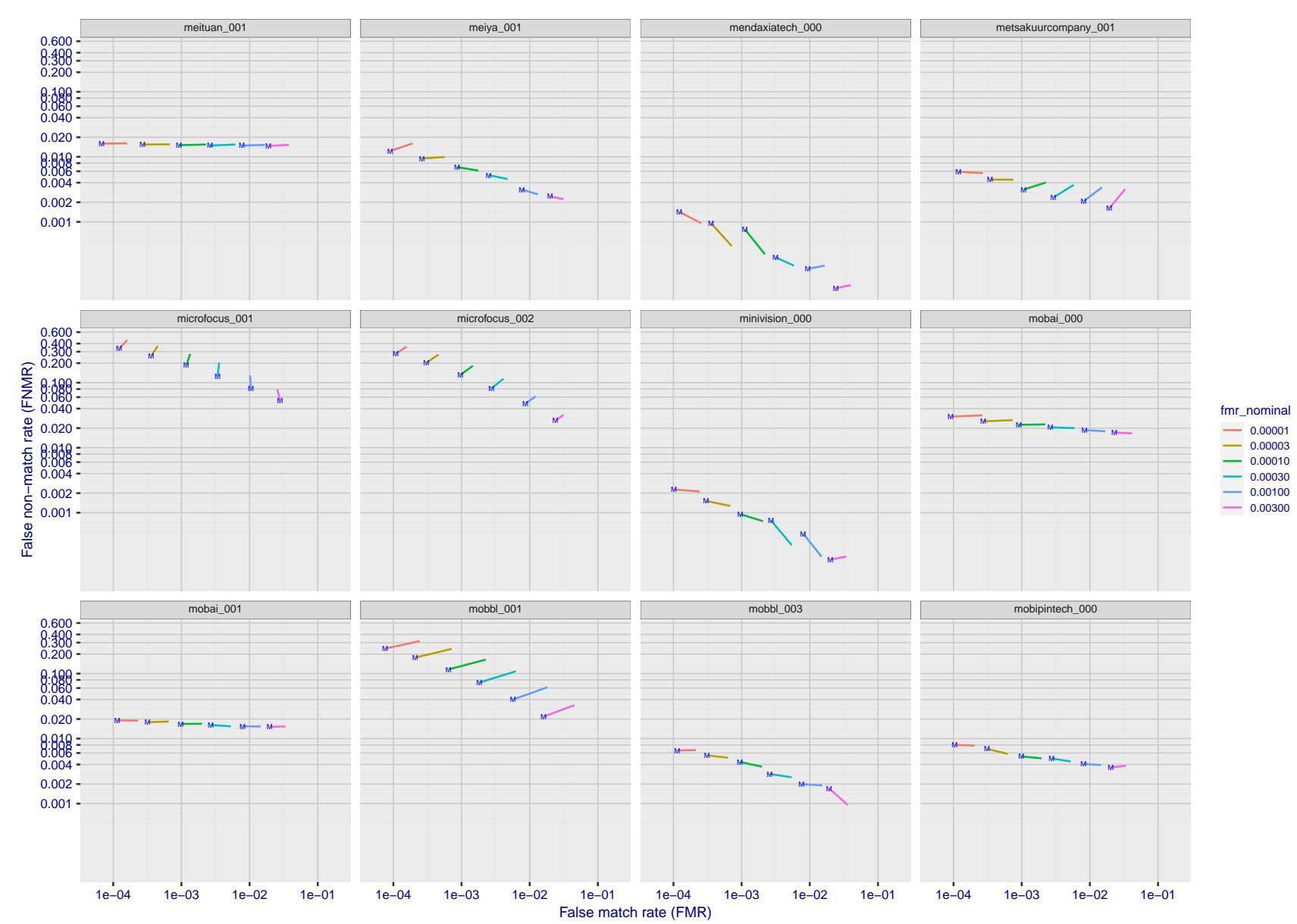


Figure 192: For the visa images, FNMR and FMR at six operating points along the DET characteristic. At each point a line is drawn between $(FMR, FNMR)_{MALE}$ and $(FMR, FNMR)_{FEMALE}$ showing how which sex has lower FMR and/or FNMR. The "M" label denotes male, the other end of the line corresponds to female. The six operating thresholds are selected to give the nominal false match rates given in the legend, and are computed over all impostor pairs regardless of age, sex, and place of birth. The plotted FMR values are broadly an order of magnitude larger than the nominal rates because FMR is computed over demographically-matched impostor pairs i.e individuals of the same sex, from the same geographic region (see section 3.6.1), and the same age group (see section 3.6.2).

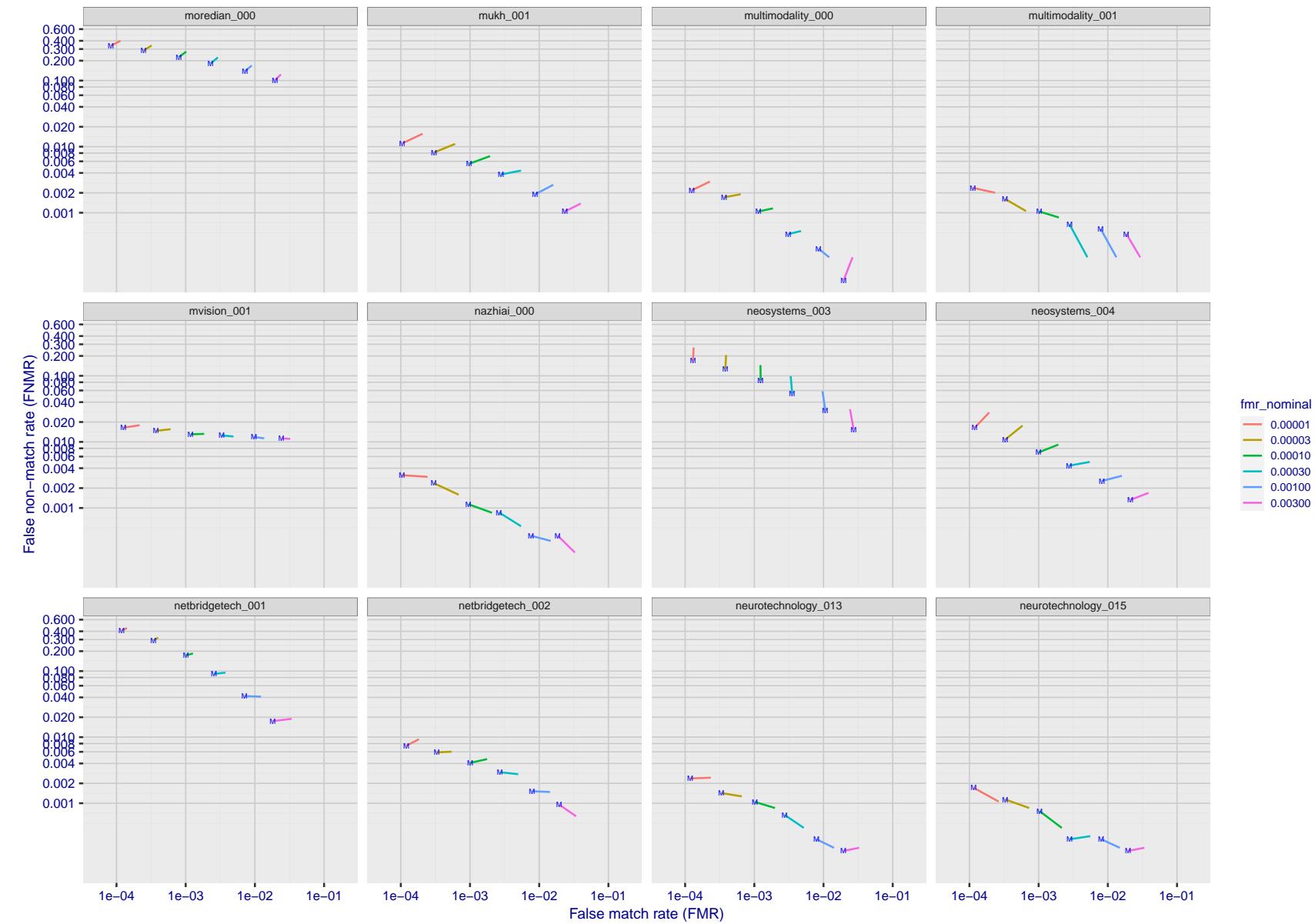


Figure 193: For the visa images, FNMR and FMR at six operating points along the DET characteristic. At each point a line is drawn between $(FMR, FNMR)_{MALE}$ and $(FMR, FNMR)_{FEMALE}$ showing how which sex has lower FMR and/or FNMR. The "M" label denotes male, the other end of the line corresponds to female. The six operating thresholds are selected to give the nominal false match rates given in the legend, and are computed over all impostor pairs regardless of age, sex, and place of birth. The plotted FMR values are broadly an order of magnitude larger than the nominal rates because FMR is computed over demographically-matched impostor pairs i.e individuals of the same sex, from the same geographic region (see section 3.6.1), and the same age group (see section 3.6.2).

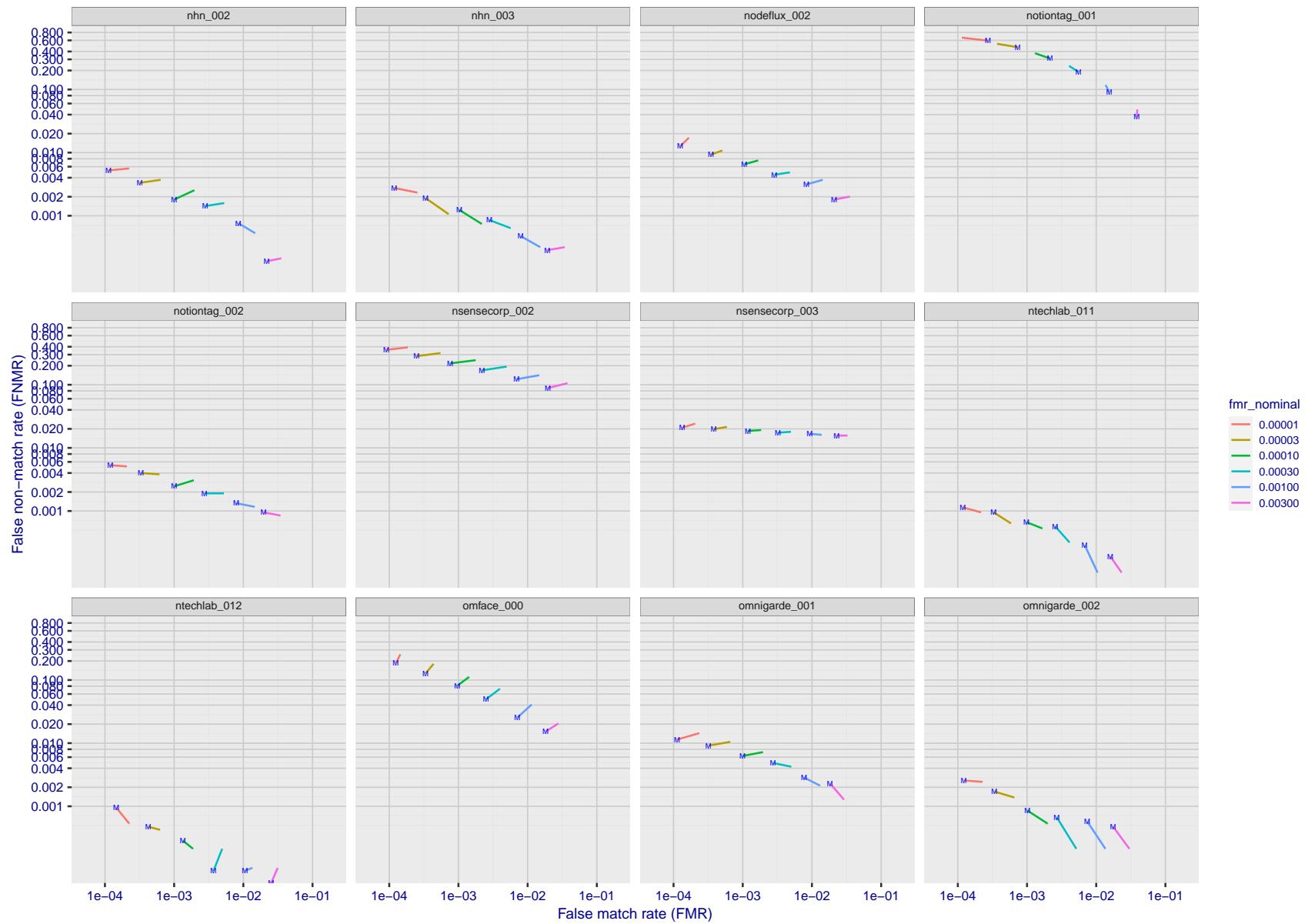


Figure 194: For the visa images, FNMR and FMR at six operating points along the DET characteristic. At each point a line is drawn between $(FMR, FNMR)_{MALE}$ and $(FMR, FNMR)_{FEMALE}$ showing how which sex has lower FMR and/or FNMR. The "M" label denotes male, the other end of the line corresponds to female. The six operating thresholds are selected to give the nominal false match rates given in the legend, and are computed over all impostor pairs regardless of age, sex, and place of birth. The plotted FMR values are broadly an order of magnitude larger than the nominal rates because FMR is computed over demographically-matched impostor pairs i.e individuals of the same sex, from the same geographic region (see section 3.6.1), and the same age group (see section 3.6.2).

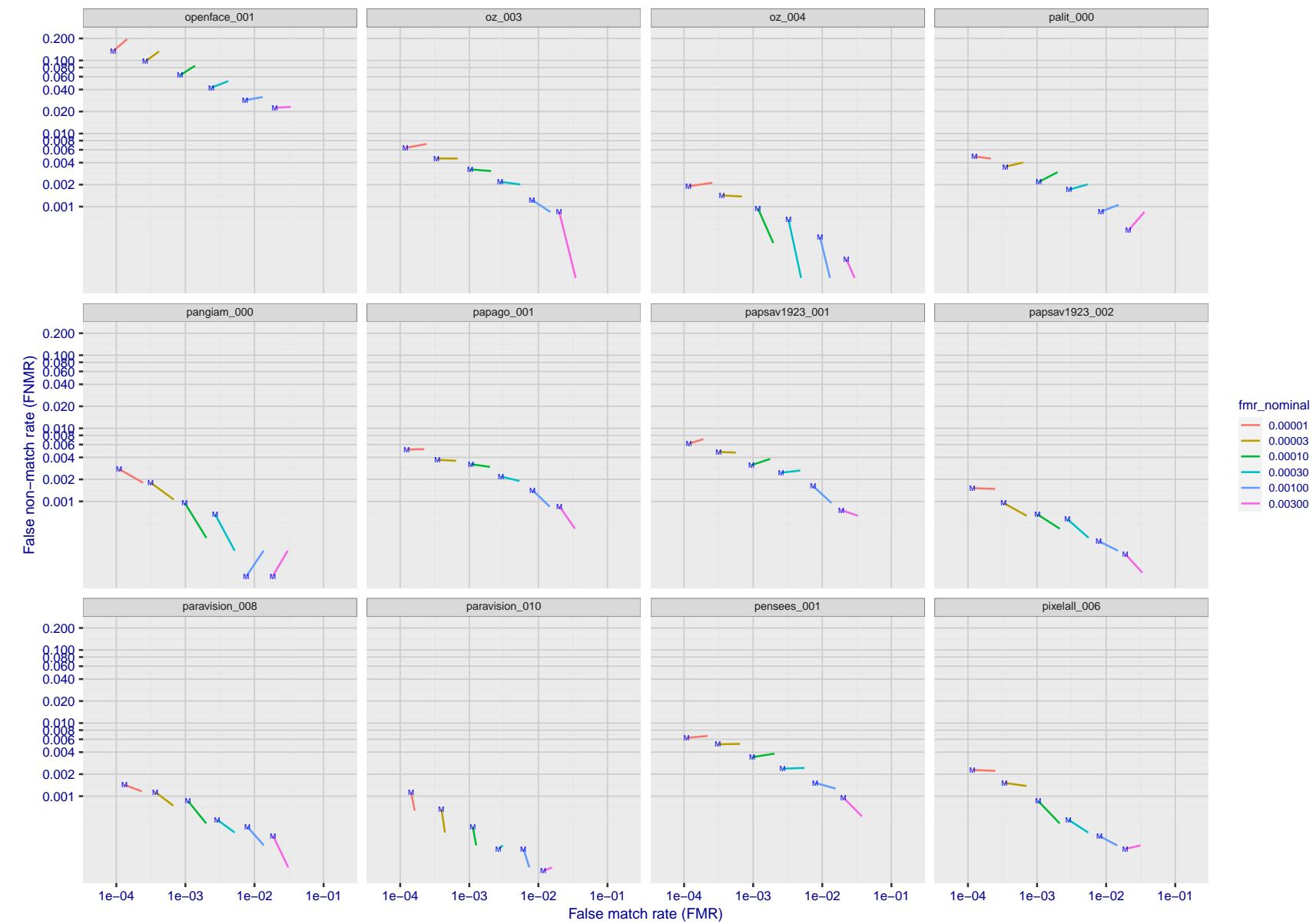


Figure 195: For the visa images, FNMR and FMR at six operating points along the DET characteristic. At each point a line is drawn between $(FMR, FNMR)_{MALE}$ and $(FMR, FNMR)_{FEMALE}$ showing how which sex has lower FMR and/or FNMR. The "M" label denotes male, the other end of the line corresponds to female. The six operating thresholds are selected to give the nominal false match rates given in the legend, and are computed over all impostor pairs regardless of age, sex, and place of birth. The plotted FMR values are broadly an order of magnitude larger than the nominal rates because FMR is computed over demographically-matched impostor pairs i.e individuals of the same sex, from the same geographic region (see section 3.6.1), and the same age group (see section 3.6.2).

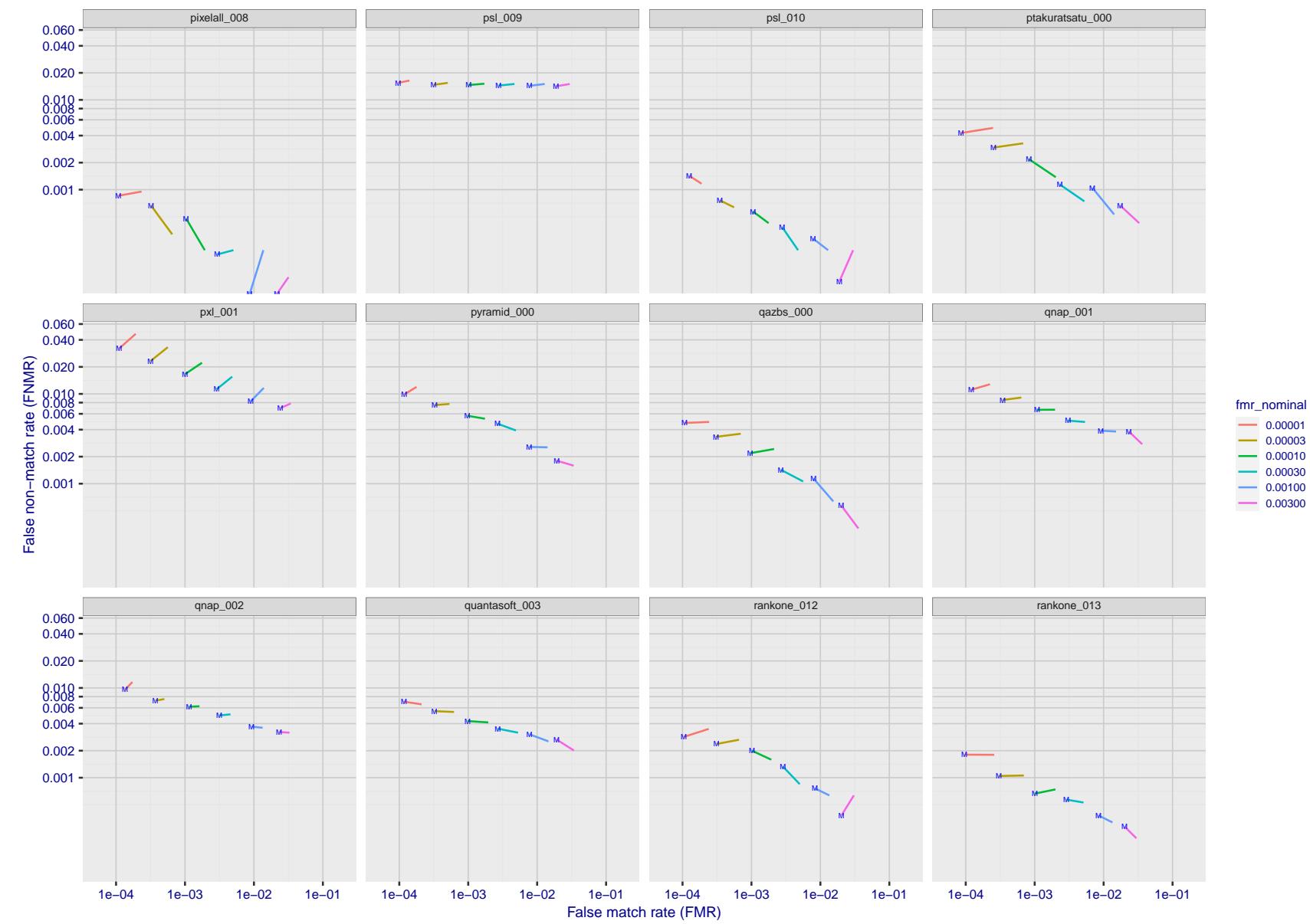


Figure 196: For the visa images, FNMR and FMR at six operating points along the DET characteristic. At each point a line is drawn between $(FMR, FNMR)_{MALE}$ and $(FMR, FNMR)_{FEMALE}$ showing how which sex has lower FMR and/or FNMR. The "M" label denotes male, the other end of the line corresponds to female. The six operating thresholds are selected to give the nominal false match rates given in the legend, and are computed over all impostor pairs regardless of age, sex, and place of birth. The plotted FMR values are broadly an order of magnitude larger than the nominal rates because FMR is computed over demographically-matched impostor pairs i.e individuals of the same sex, from the same geographic region (see section 3.6.1), and the same age group (see section 3.6.2).

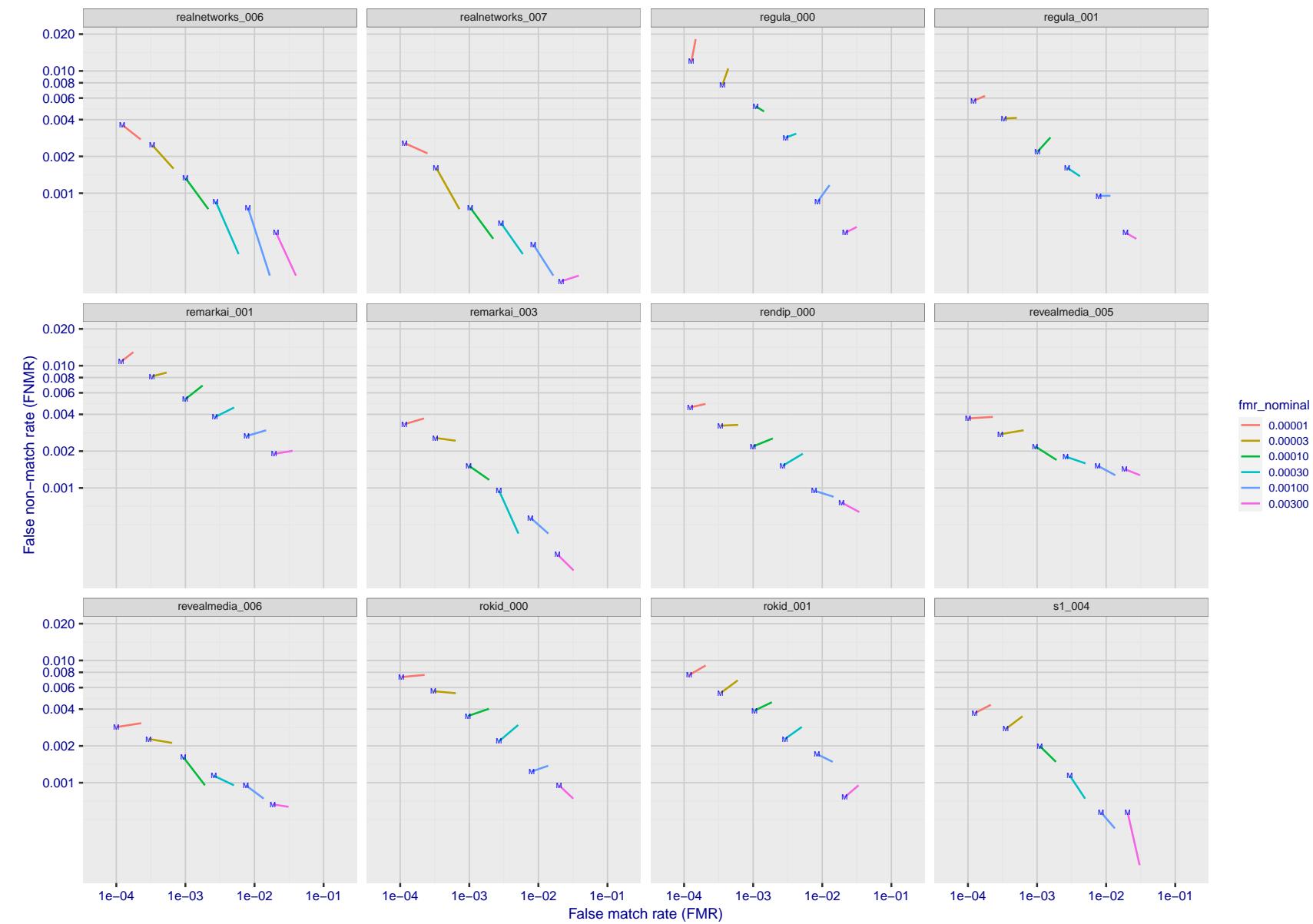


Figure 197: For the visa images, FNMR and FMR at six operating points along the DET characteristic. At each point a line is drawn between $(FMR, FNMR)_{MALE}$ and $(FMR, FNMR)_{FEMALE}$ showing how which sex has lower FMR and/or FNMR. The "M" label denotes male, the other end of the line corresponds to female. The six operating thresholds are selected to give the nominal false match rates given in the legend, and are computed over all impostor pairs regardless of age, sex, and place of birth. The plotted FMR values are broadly an order of magnitude larger than the nominal rates because FMR is computed over demographically-matched impostor pairs i.e individuals of the same sex, from the same geographic region (see section 3.6.1), and the same age group (see section 3.6.2).

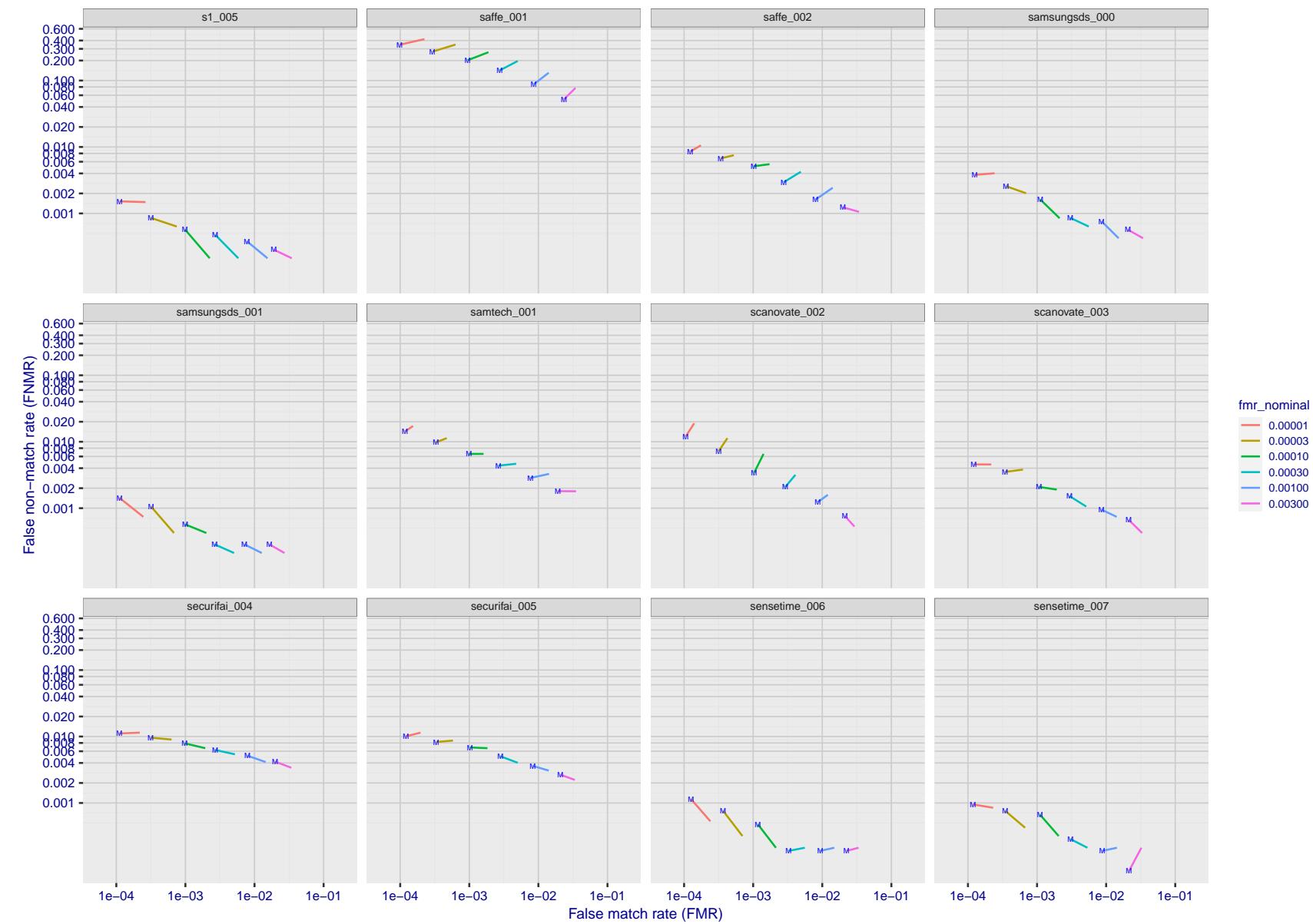


Figure 198: For the visa images, FNMR and FMR at six operating points along the DET characteristic. At each point a line is drawn between $(FMR, FNMR)_{MALE}$ and $(FMR, FNMR)_{FEMALE}$ showing how which sex has lower FMR and/or FNMR. The "M" label denotes male, the other end of the line corresponds to female. The six operating thresholds are selected to give the nominal false match rates given in the legend, and are computed over all impostor pairs regardless of age, sex, and place of birth. The plotted FMR values are broadly an order of magnitude larger than the nominal rates because FMR is computed over demographically-matched impostor pairs i.e individuals of the same sex, from the same geographic region (see section 3.6.1), and the same age group (see section 3.6.2).

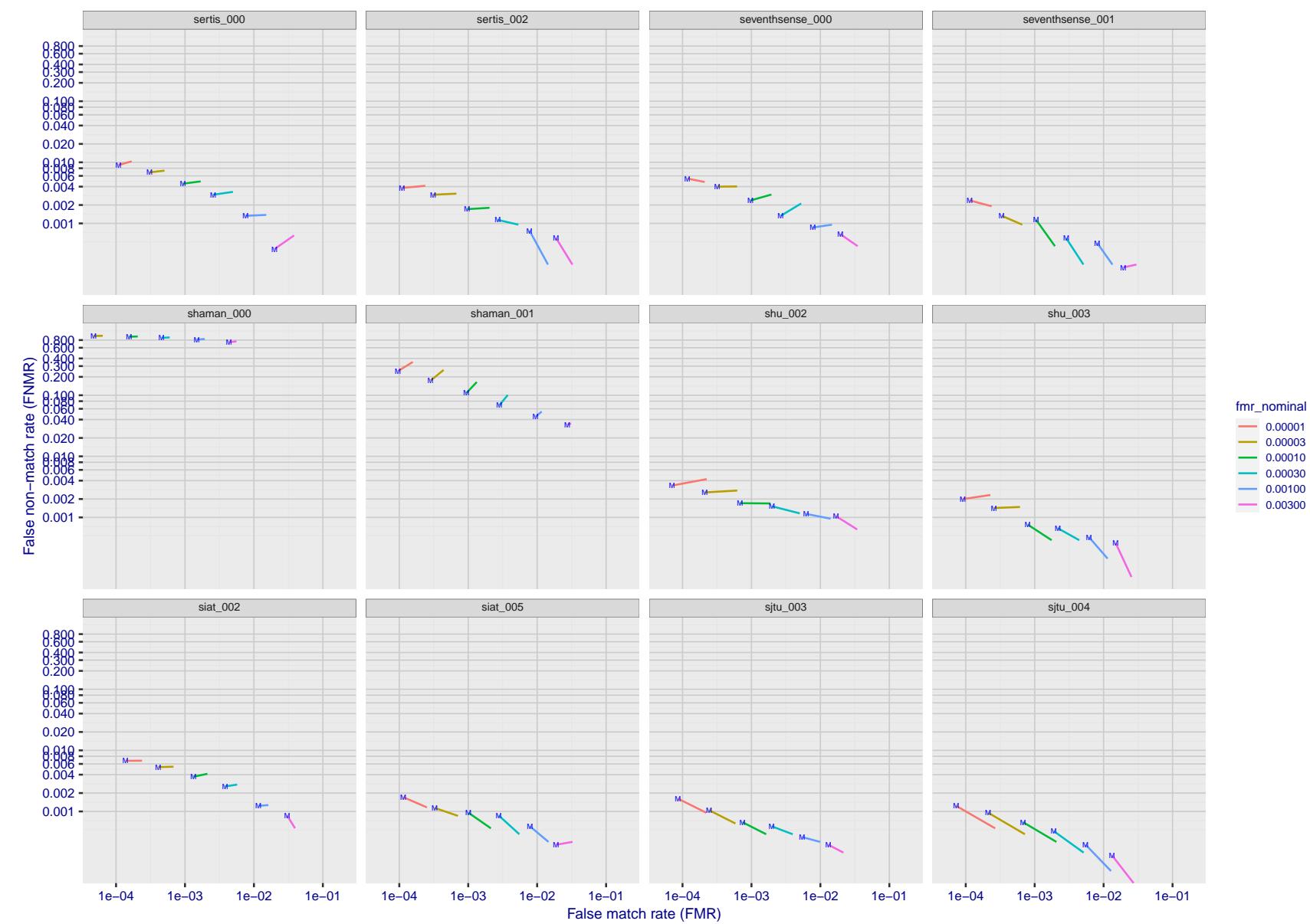


Figure 199: For the visa images, FNMR and FMR at six operating points along the DET characteristic. At each point a line is drawn between $(FMR, FNMR)_{MALE}$ and $(FMR, FNMR)_{FEMALE}$ showing how which sex has lower FMR and/or FNMR. The "M" label denotes male, the other end of the line corresponds to female. The six operating thresholds are selected to give the nominal false match rates given in the legend, and are computed over all impostor pairs regardless of age, sex, and place of birth. The plotted FMR values are broadly an order of magnitude larger than the nominal rates because FMR is computed over demographically-matched impostor pairs i.e individuals of the same sex, from the same geographic region (see section 3.6.1), and the same age group (see section 3.6.2).

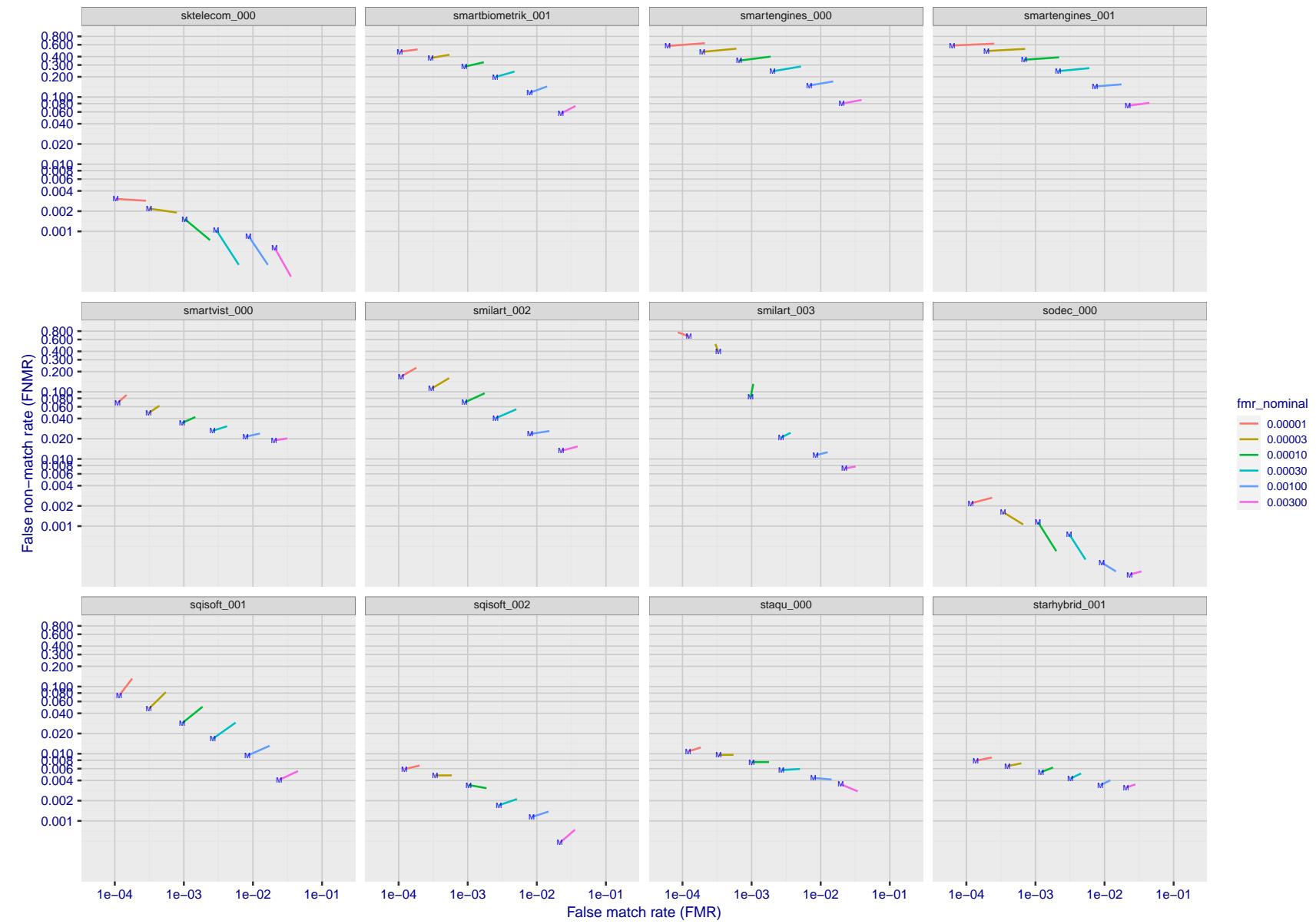


Figure 200: For the visa images, FNMR and FMR at six operating points along the DET characteristic. At each point a line is drawn between $(FMR, FNMR)_{MALE}$ and $(FMR, FNMR)_{FEMALE}$ showing how which sex has lower FMR and/or FNMR. The "M" label denotes male, the other end of the line corresponds to female. The six operating thresholds are selected to give the nominal false match rates given in the legend, and are computed over all impostor pairs regardless of age, sex, and place of birth. The plotted FMR values are broadly an order of magnitude larger than the nominal rates because FMR is computed over demographically-matched impostor pairs i.e individuals of the same sex, from the same geographic region (see section 3.6.1), and the same age group (see section 3.6.2).

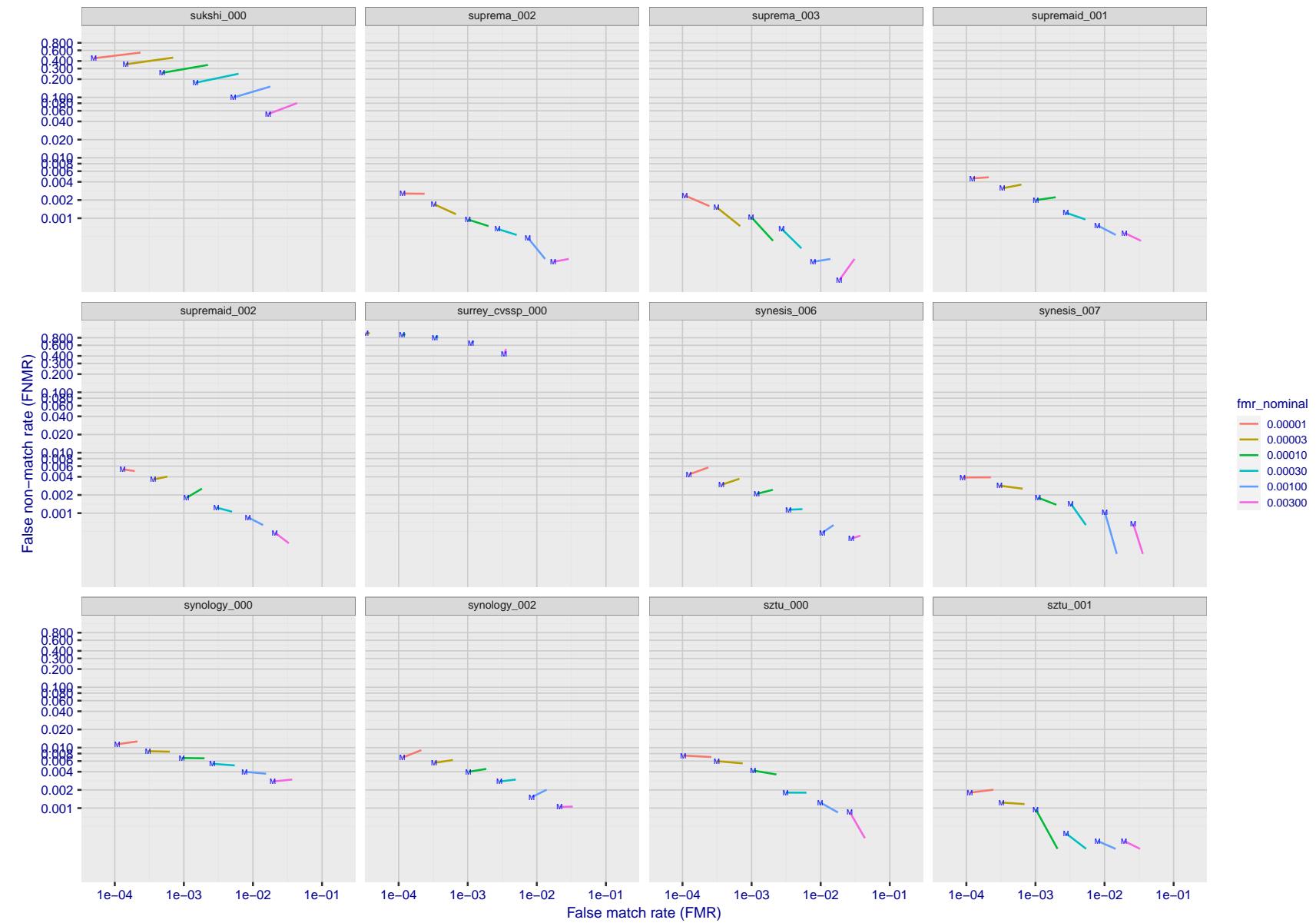


Figure 201: For the visa images, FNMR and FMR at six operating points along the DET characteristic. At each point a line is drawn between $(FMR, FNMR)_{MALE}$ and $(FMR, FNMR)_{FEMALE}$ showing how which sex has lower FMR and/or FNMR. The "M" label denotes male, the other end of the line corresponds to female. The six operating thresholds are selected to give the nominal false match rates given in the legend, and are computed over all impostor pairs regardless of age, sex, and place of birth. The plotted FMR values are broadly an order of magnitude larger than the nominal rates because FMR is computed over demographically-matched impostor pairs i.e individuals of the same sex, from the same geographic region (see section 3.6.1), and the same age group (see section 3.6.2).

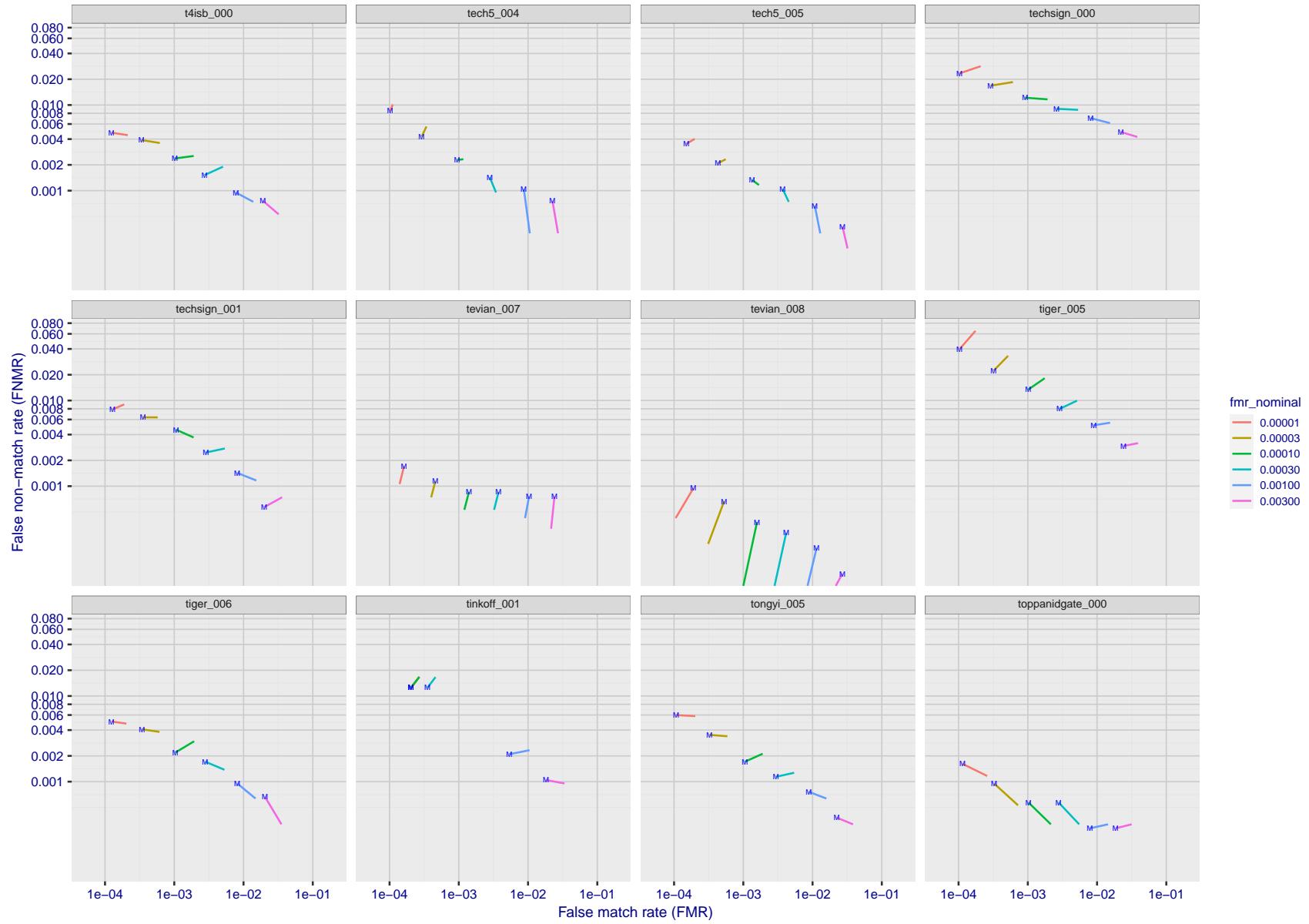


Figure 202: For the visa images, FNMR and FMR at six operating points along the DET characteristic. At each point a line is drawn between $(FMR, FNMR)_{MALE}$ and $(FMR, FNMR)_{FEMALE}$ showing how which sex has lower FMR and/or FNMR. The "M" label denotes male, the other end of the line corresponds to female. The six operating thresholds are selected to give the nominal false match rates given in the legend, and are computed over all impostor pairs regardless of age, sex, and place of birth. The plotted FMR values are broadly an order of magnitude larger than the nominal rates because FMR is computed over demographically-matched impostor pairs i.e individuals of the same sex, from the same geographic region (see section 3.6.1), and the same age group (see section 3.6.2).

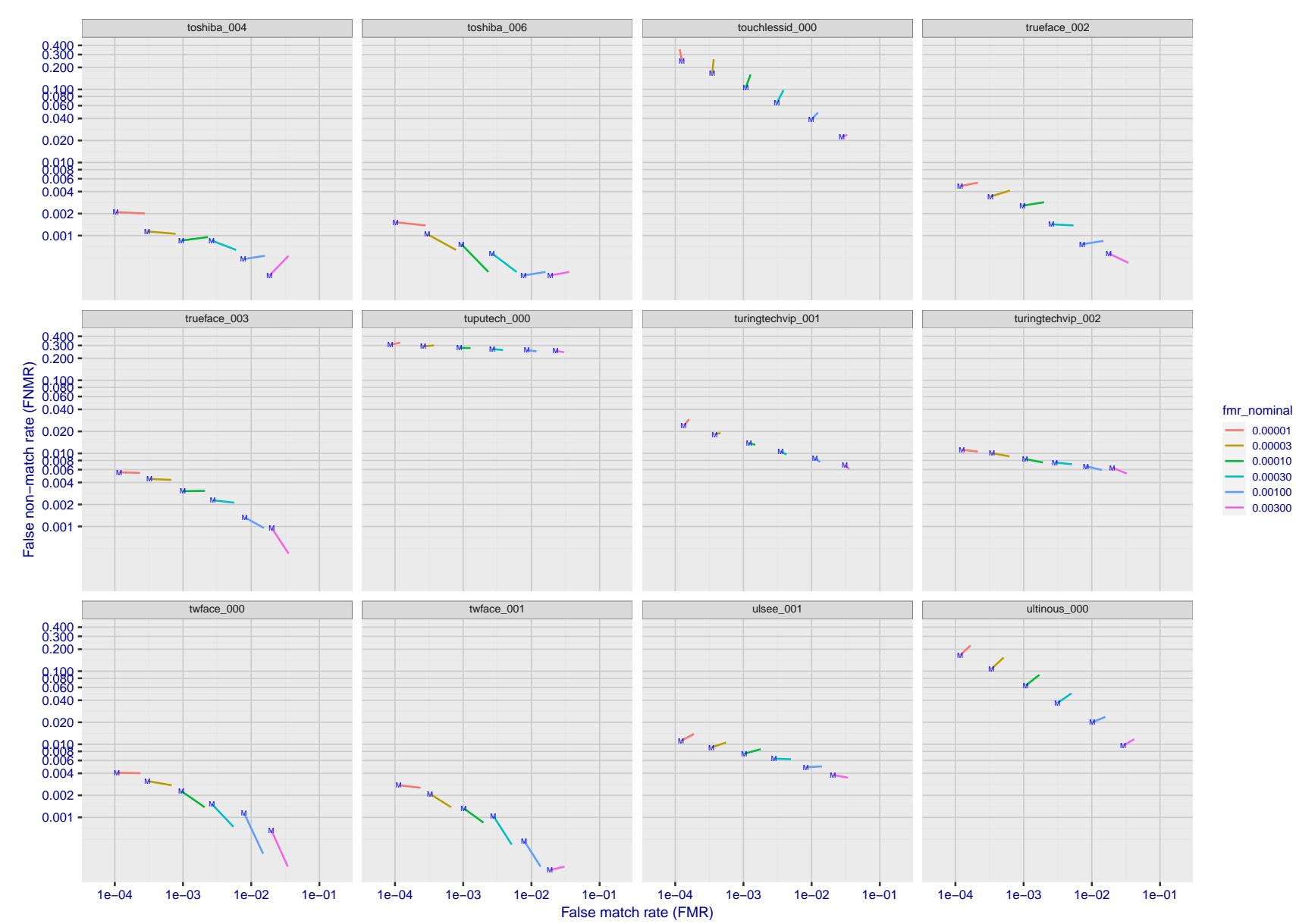


Figure 203: For the visa images, FNMR and FMR at six operating points along the DET characteristic. At each point a line is drawn between $(FMR, FNMR)_{MALE}$ and $(FMR, FNMR)_{FEMALE}$ showing how which sex has lower FMR and/or FNMR. The "M" label denotes male, the other end of the line corresponds to female. The six operating thresholds are selected to give the nominal false match rates given in the legend, and are computed over all impostor pairs regardless of age, sex, and place of birth. The plotted FMR values are broadly an order of magnitude larger than the nominal rates because FMR is computed over demographically-matched impostor pairs i.e individuals of the same sex, from the same geographic region (see section 3.6.1), and the same age group (see section 3.6.2).

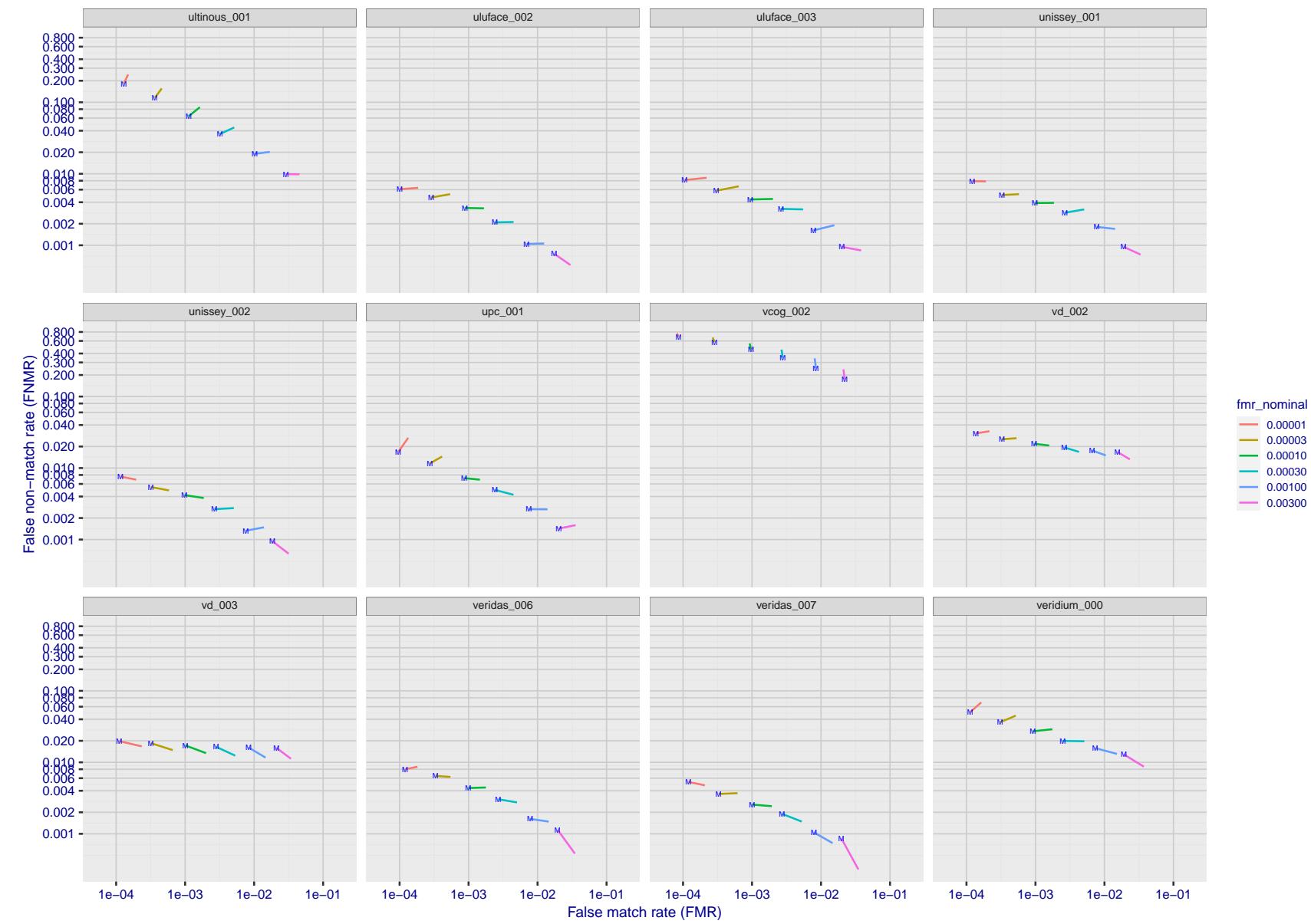


Figure 204: For the visa images, FNMR and FMR at six operating points along the DET characteristic. At each point a line is drawn between $(FMR, FNMR)_{MALE}$ and $(FMR, FNMR)_{FEMALE}$ showing how which sex has lower FMR and/or FNMR. The "M" label denotes male, the other end of the line corresponds to female. The six operating thresholds are selected to give the nominal false match rates given in the legend, and are computed over all impostor pairs regardless of age, sex, and place of birth. The plotted FMR values are broadly an order of magnitude larger than the nominal rates because FMR is computed over demographically-matched impostor pairs i.e individuals of the same sex, from the same geographic region (see section 3.6.1), and the same age group (see section 3.6.2).

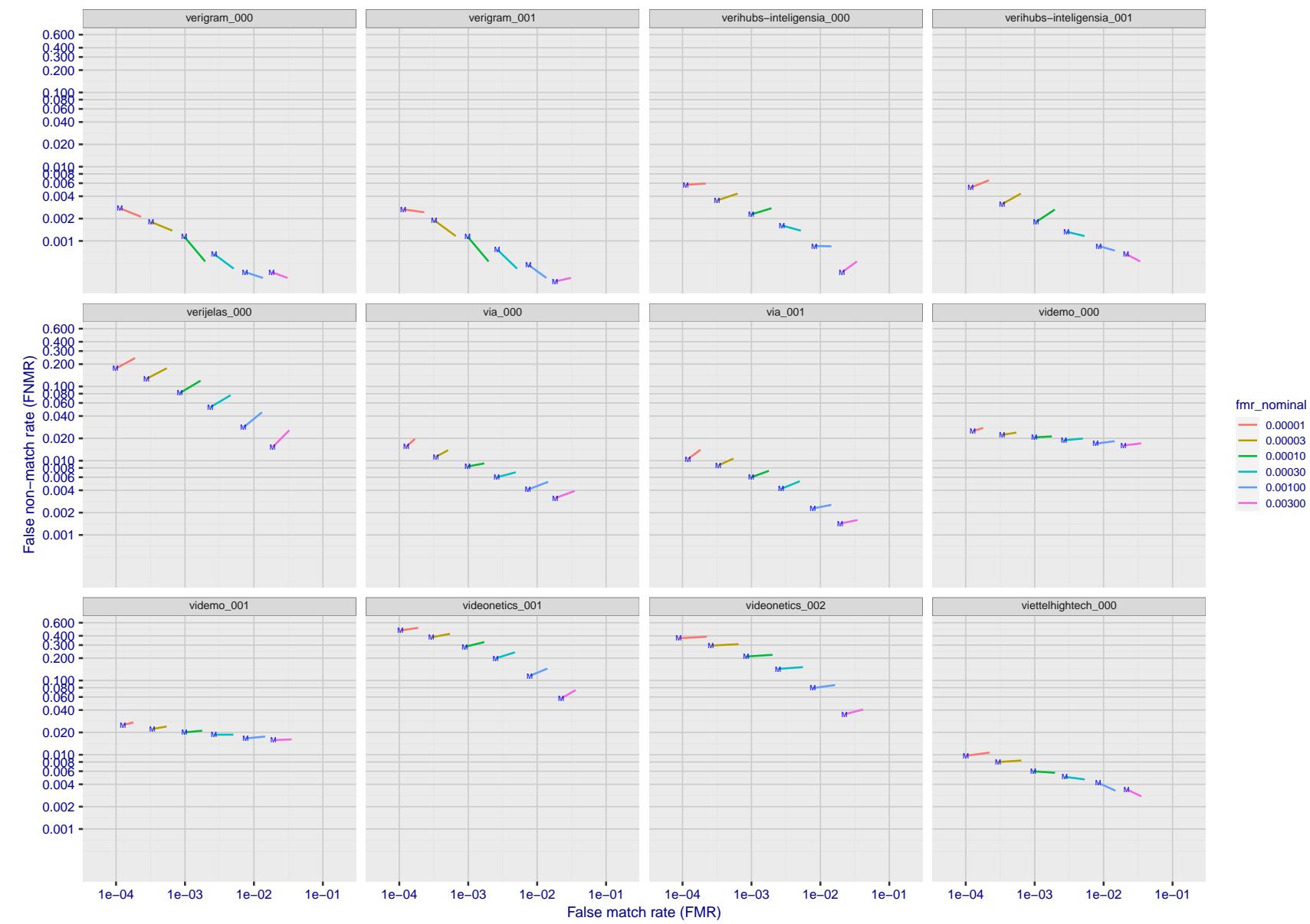


Figure 205: For the visa images, FNMR and FMR at six operating points along the DET characteristic. At each point a line is drawn between $(FMR, FNMR)_{MALE}$ and $(FMR, FNMR)_{FEMALE}$ showing how which sex has lower FMR and/or FNMR. The "M" label denotes male, the other end of the line corresponds to female. The six operating thresholds are selected to give the nominal false match rates given in the legend, and are computed over all impostor pairs regardless of age, sex, and place of birth. The plotted FMR values are broadly an order of magnitude larger than the nominal rates because FMR is computed over demographically-matched impostor pairs i.e individuals of the same sex, from the same geographic region (see section 3.6.1), and the same age group (see section 3.6.2).

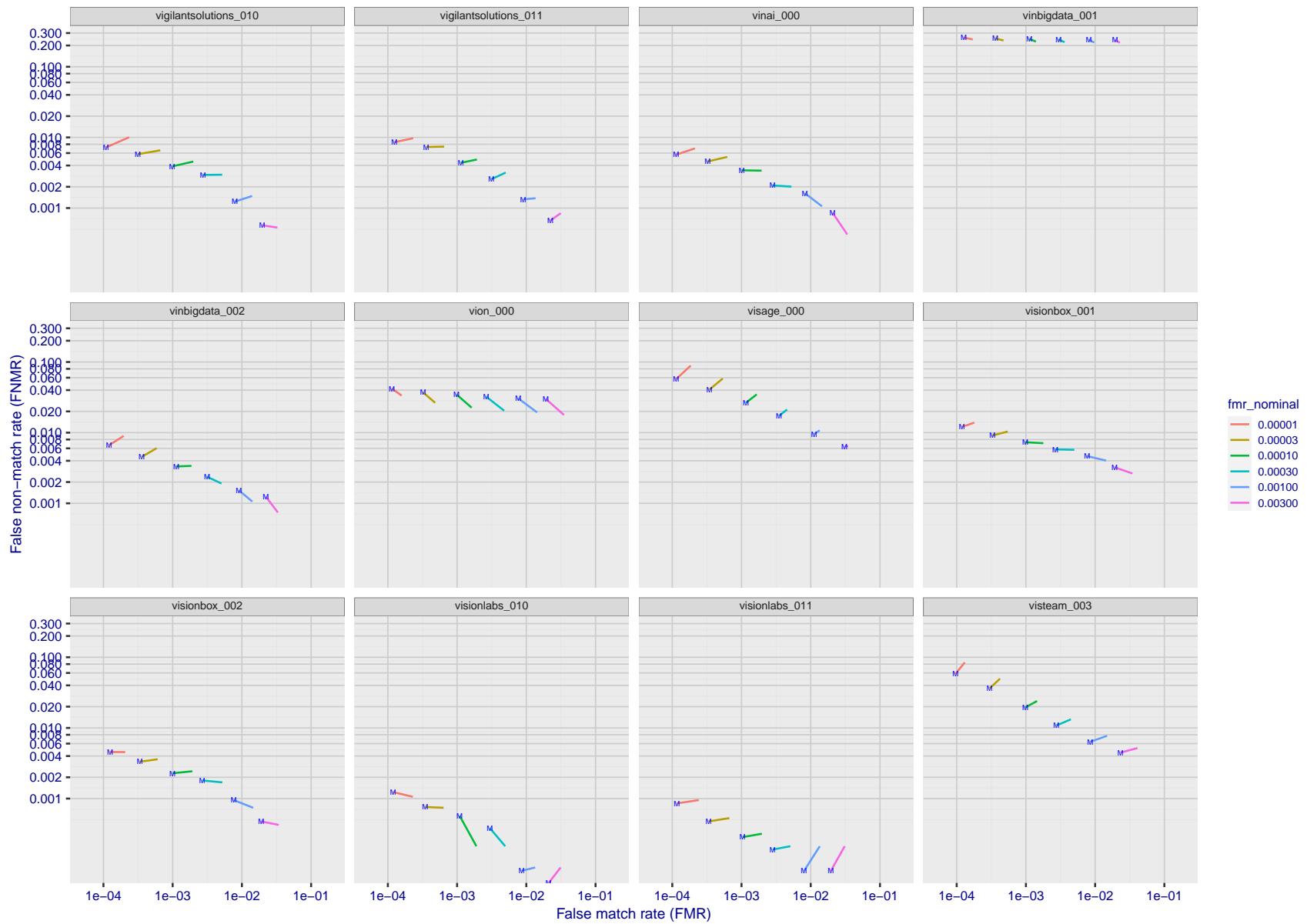


Figure 206: For the visa images, FNMR and FMR at six operating points along the DET characteristic. At each point a line is drawn between $(FMR, FNMR)_{MALE}$ and $(FMR, FNMR)_{FEMALE}$ showing how which sex has lower FMR and/or FNMR. The "M" label denotes male, the other end of the line corresponds to female. The six operating thresholds are selected to give the nominal false match rates given in the legend, and are computed over all impostor pairs regardless of age, sex, and place of birth. The plotted FMR values are broadly an order of magnitude larger than the nominal rates because FMR is computed over demographically-matched impostor pairs i.e individuals of the same sex, from the same geographic region (see section 3.6.1), and the same age group (see section 3.6.2).

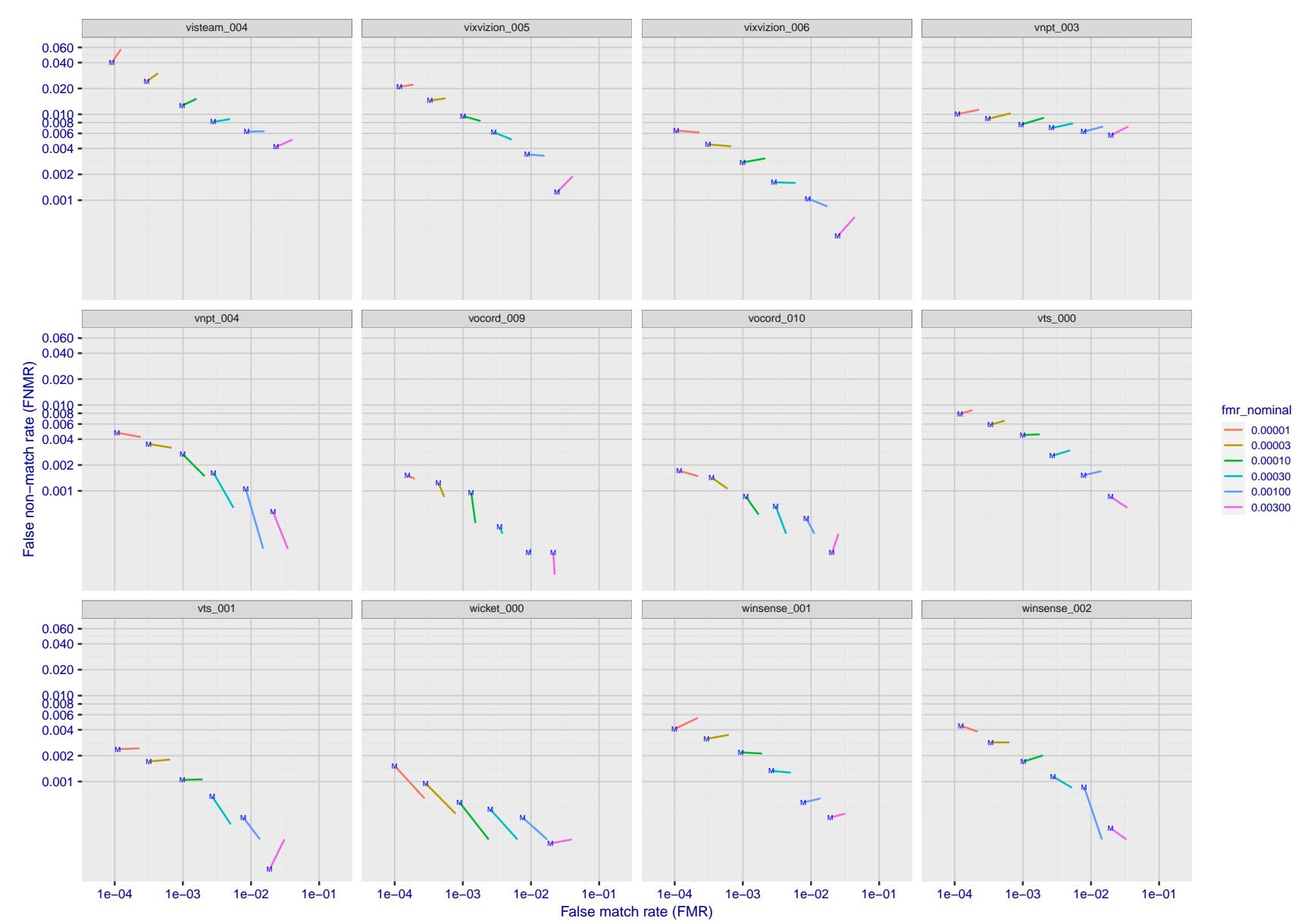


Figure 207: For the visa images, FNMR and FMR at six operating points along the DET characteristic. At each point a line is drawn between $(FMR, FNMR)_{MALE}$ and $(FMR, FNMR)_{FEMALE}$ showing how which sex has lower FMR and/or FNMR. The "M" label denotes male, the other end of the line corresponds to female. The six operating thresholds are selected to give the nominal false match rates given in the legend, and are computed over all impostor pairs regardless of age, sex, and place of birth. The plotted FMR values are broadly an order of magnitude larger than the nominal rates because FMR is computed over demographically-matched impostor pairs i.e individuals of the same sex, from the same geographic region (see section 3.6.1), and the same age group (see section 3.6.2).

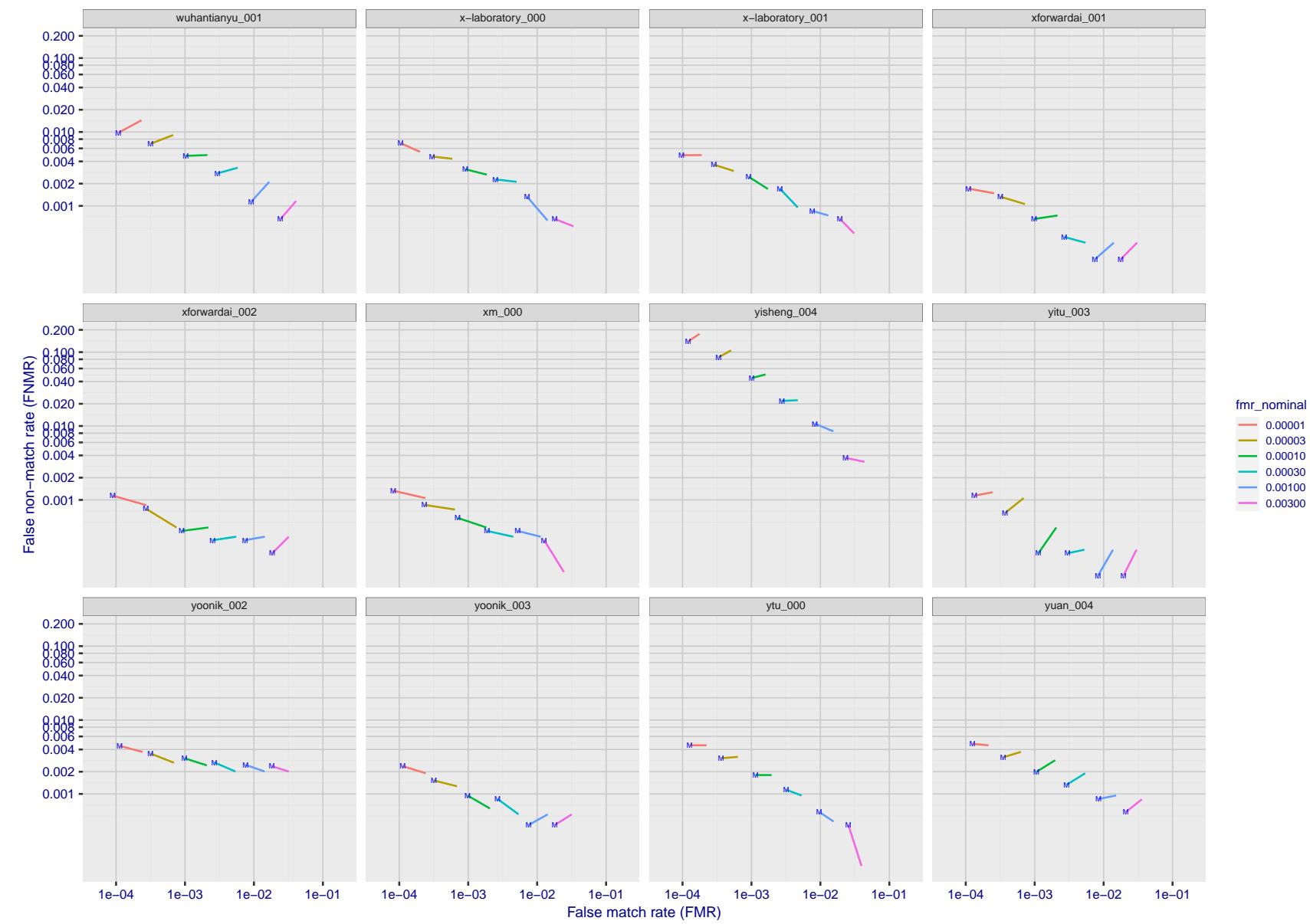


Figure 208: For the visa images, FNMR and FMR at six operating points along the DET characteristic. At each point a line is drawn between $(FMR, FNMR)_{MALE}$ and $(FMR, FNMR)_{FEMALE}$ showing how which sex has lower FMR and/or FNMR. The "M" label denotes male, the other end of the line corresponds to female. The six operating thresholds are selected to give the nominal false match rates given in the legend, and are computed over all impostor pairs regardless of age, sex, and place of birth. The plotted FMR values are broadly an order of magnitude larger than the nominal rates because FMR is computed over demographically-matched impostor pairs i.e individuals of the same sex, from the same geographic region (see section 3.6.1), and the same age group (see section 3.6.2).

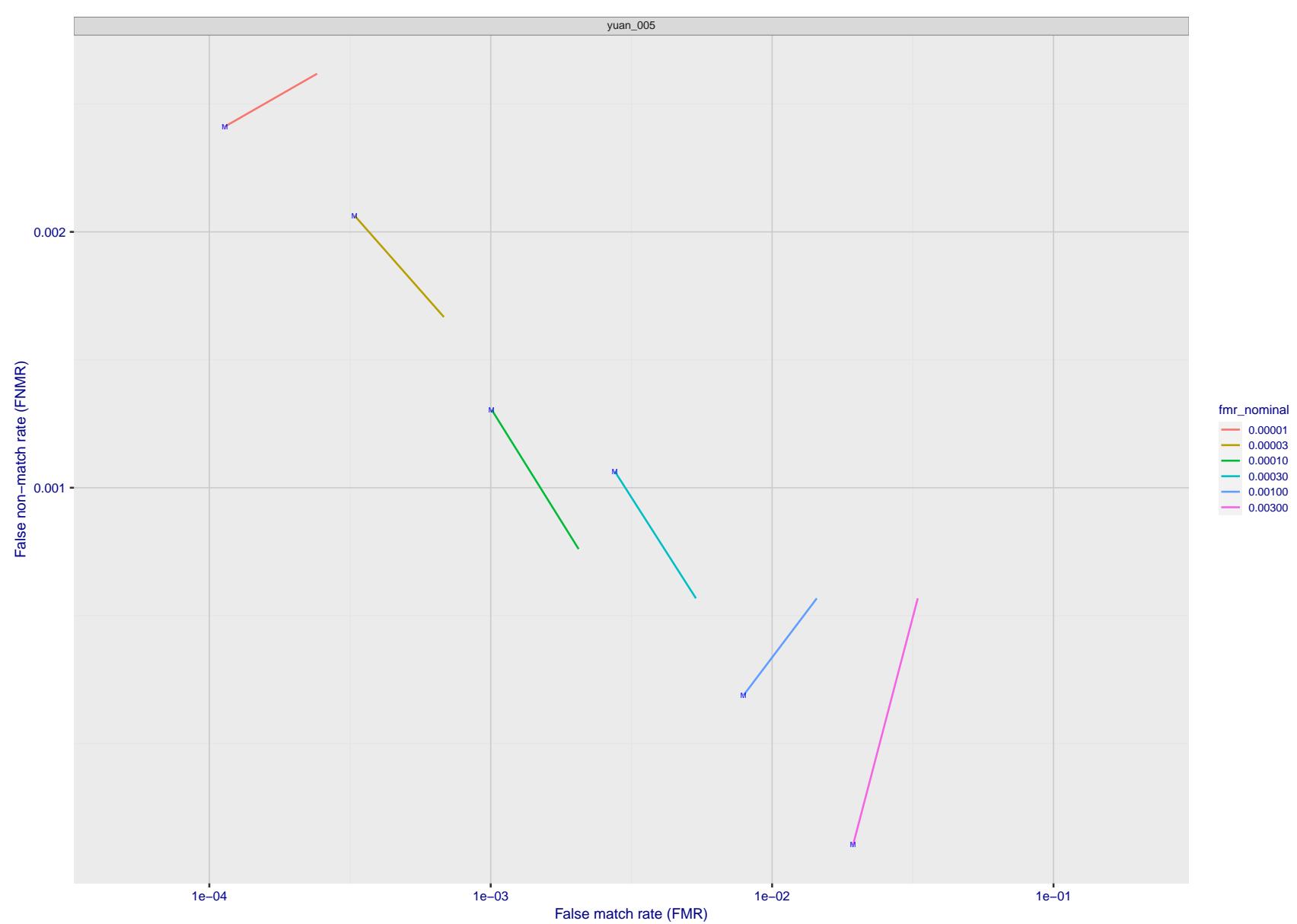


Figure 209: For the visa images, FNMR and FMR at six operating points along the DET characteristic. At each point a line is drawn between $(FMR, FNMR)_{MALE}$ and $(FMR, FNMR)_{FEMALE}$ showing how which sex has lower FMR and/or FNMR. The "M" label denotes male, the other end of the line corresponds to female. The six operating thresholds are selected to give the nominal false match rates given in the legend, and are computed over all impostor pairs regardless of age, sex, and place of birth. The plotted FMR values are broadly an order of magnitude larger than the nominal rates because FMR is computed over demographically-matched impostor pairs i.e individuals of the same sex, from the same geographic region (see section 3.6.1), and the same age group (see section 3.6.2).

2022/08/30 09:26:06

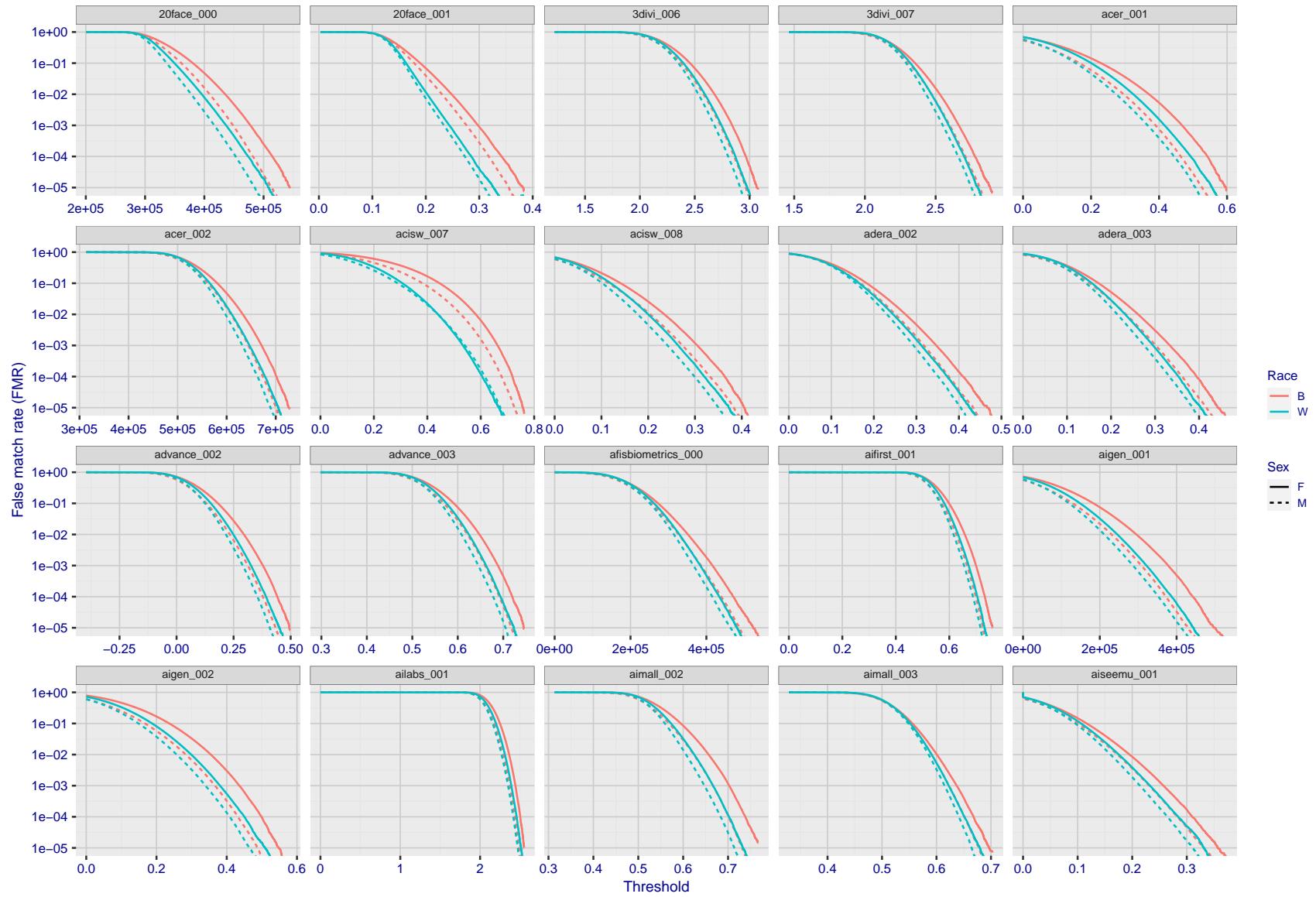


Figure 210: For the mugshot images, the false match calibration curves show false match rate vs. threshold. Separate curves appear for white females, black females, black males and white males.

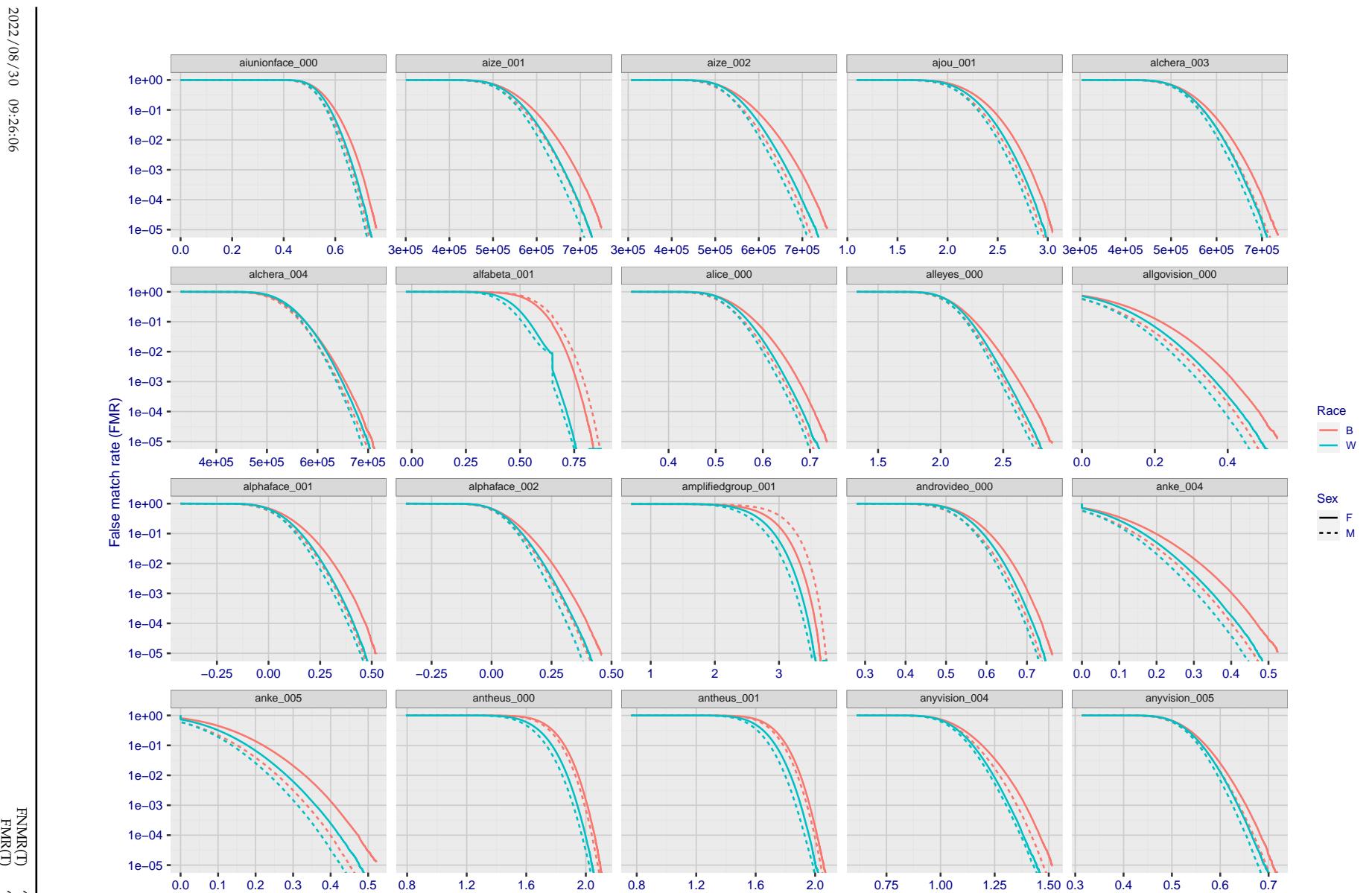


Figure 211: For the mugshot images, the false match calibration curves show false match rate vs. threshold. Separate curves appear for white females, black females, black males and white males.

2022/08/30 09:26:06

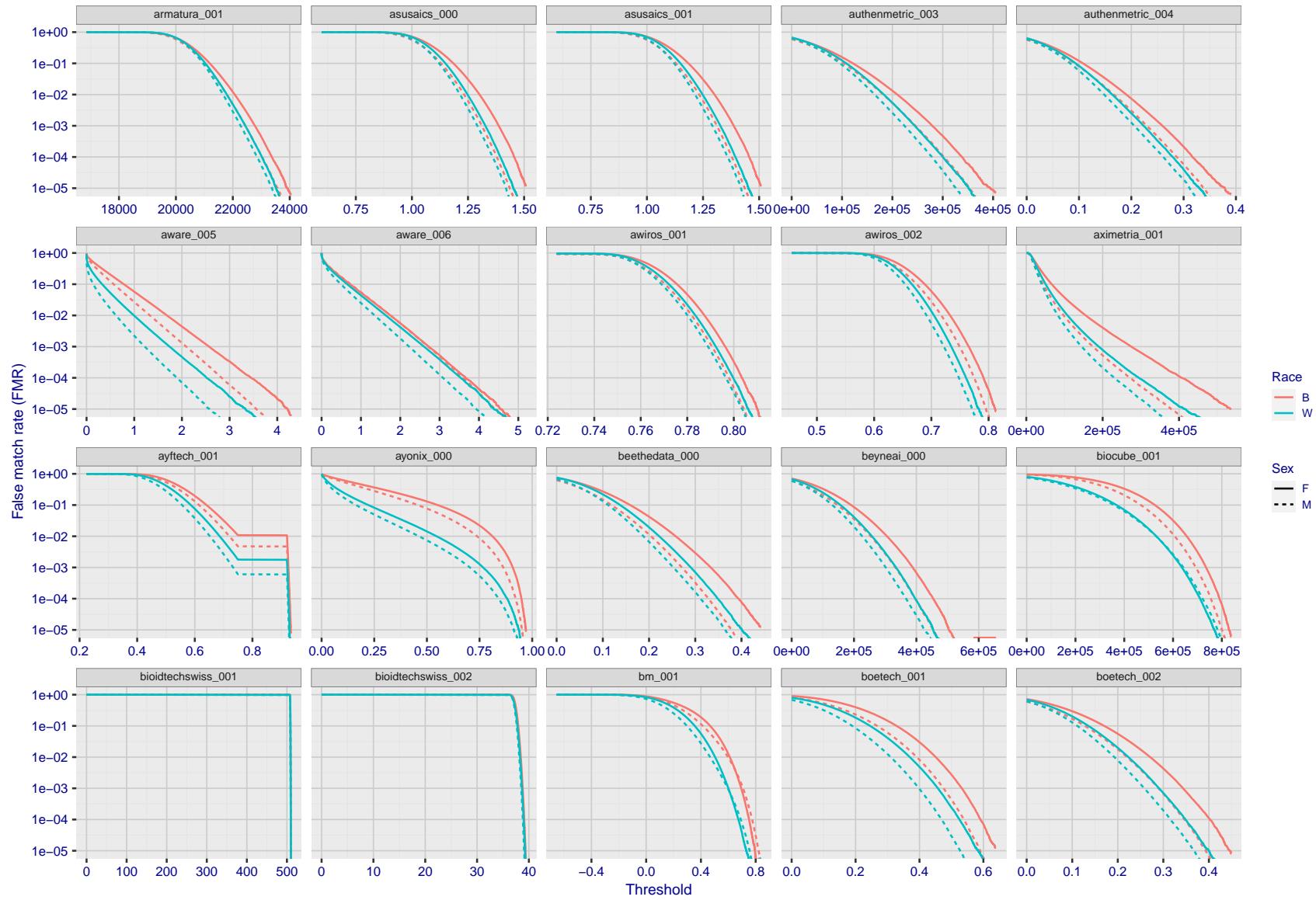


Figure 212: For the mugshot images, the false match calibration curves show false match rate vs. threshold. Separate curves appear for white females, black females, black males and white males.

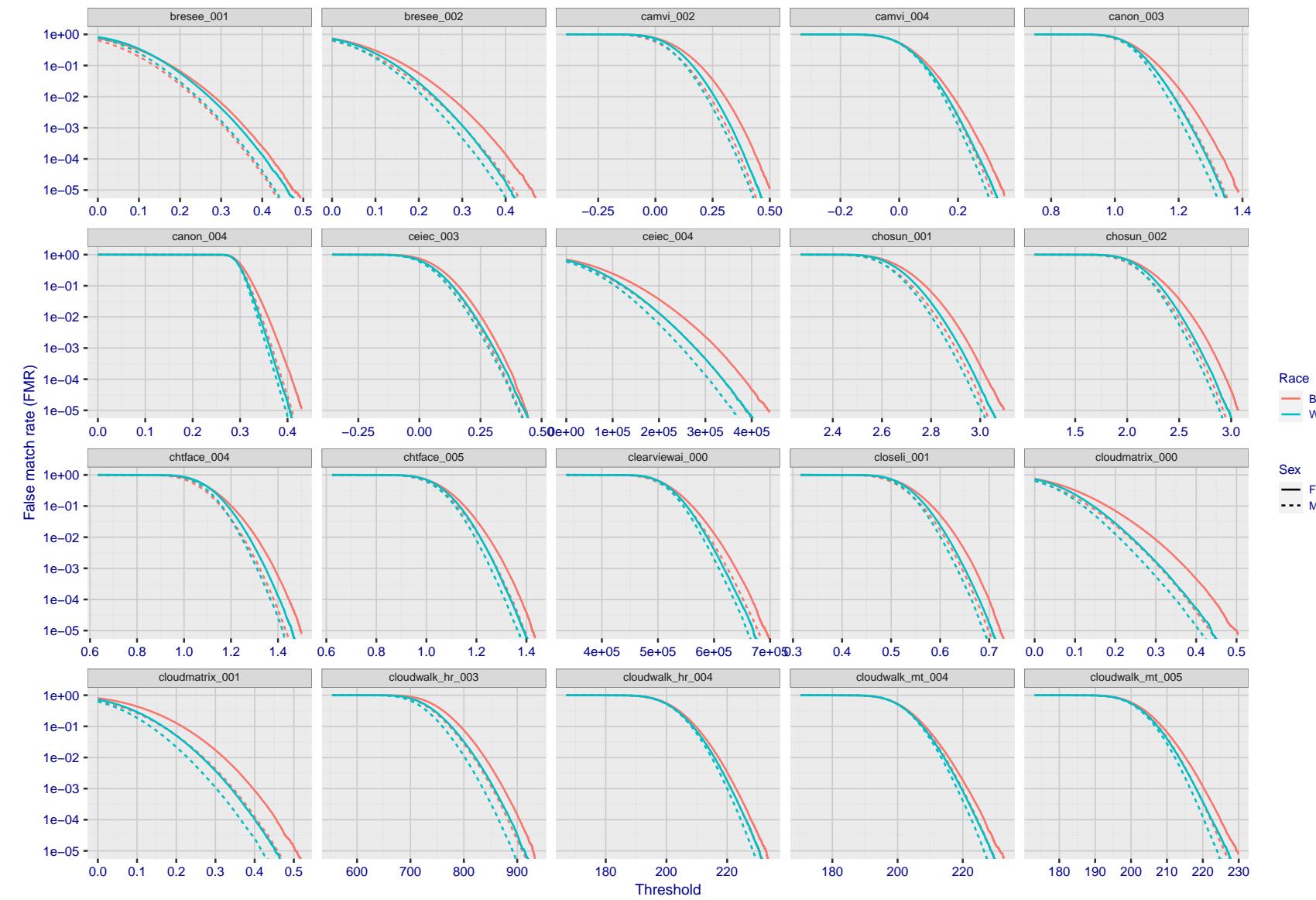


Figure 213: For the mugshot images, the false match calibration curves show false match rate vs. threshold. Separate curves appear for white females, black females, black males and white males.

2022/08/30 09:26:06

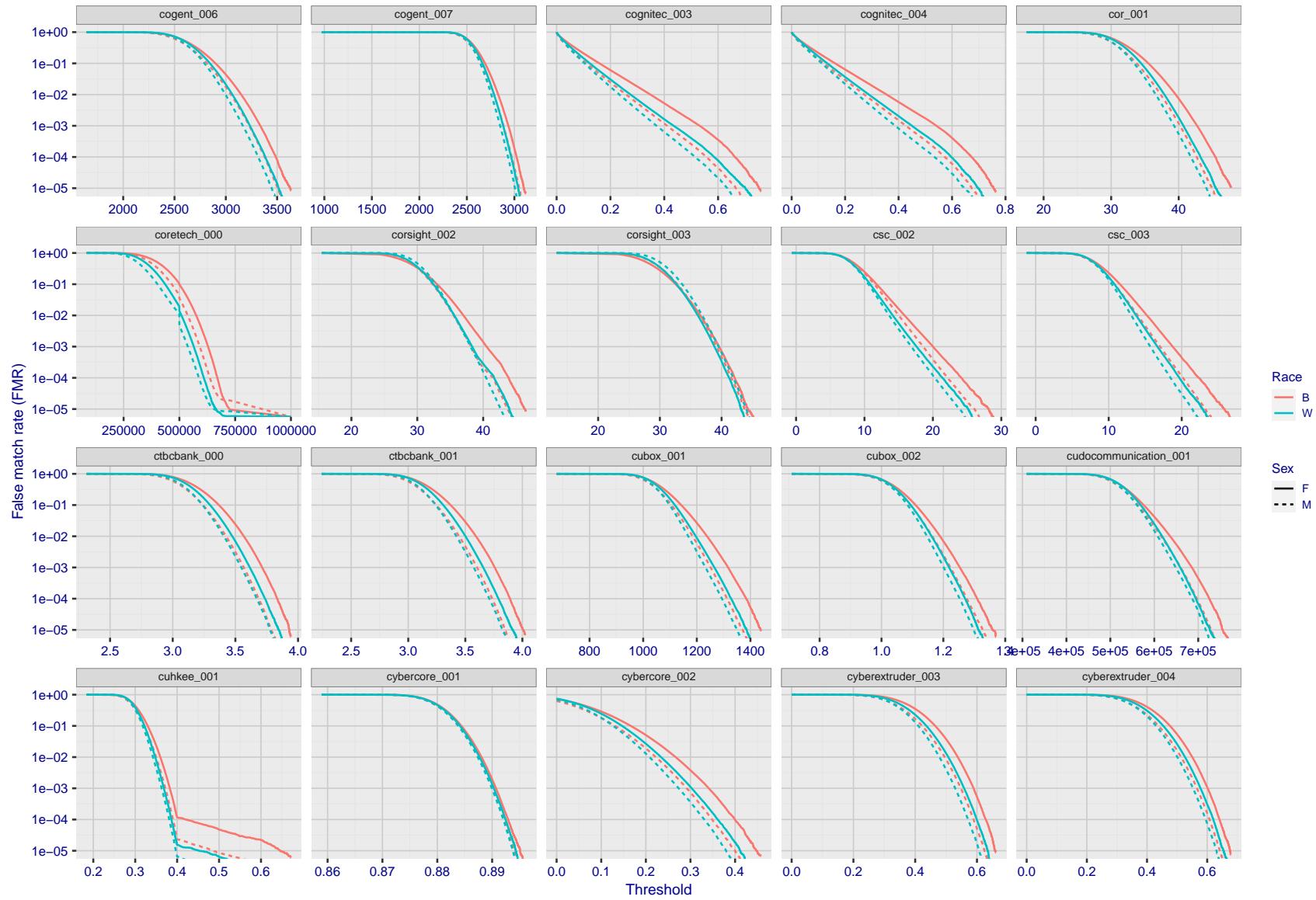


Figure 214: For the mugshot images, the false match calibration curves show false match rate vs. threshold. Separate curves appear for white females, black females, black males and white males.

2022/08/30 09:26:06

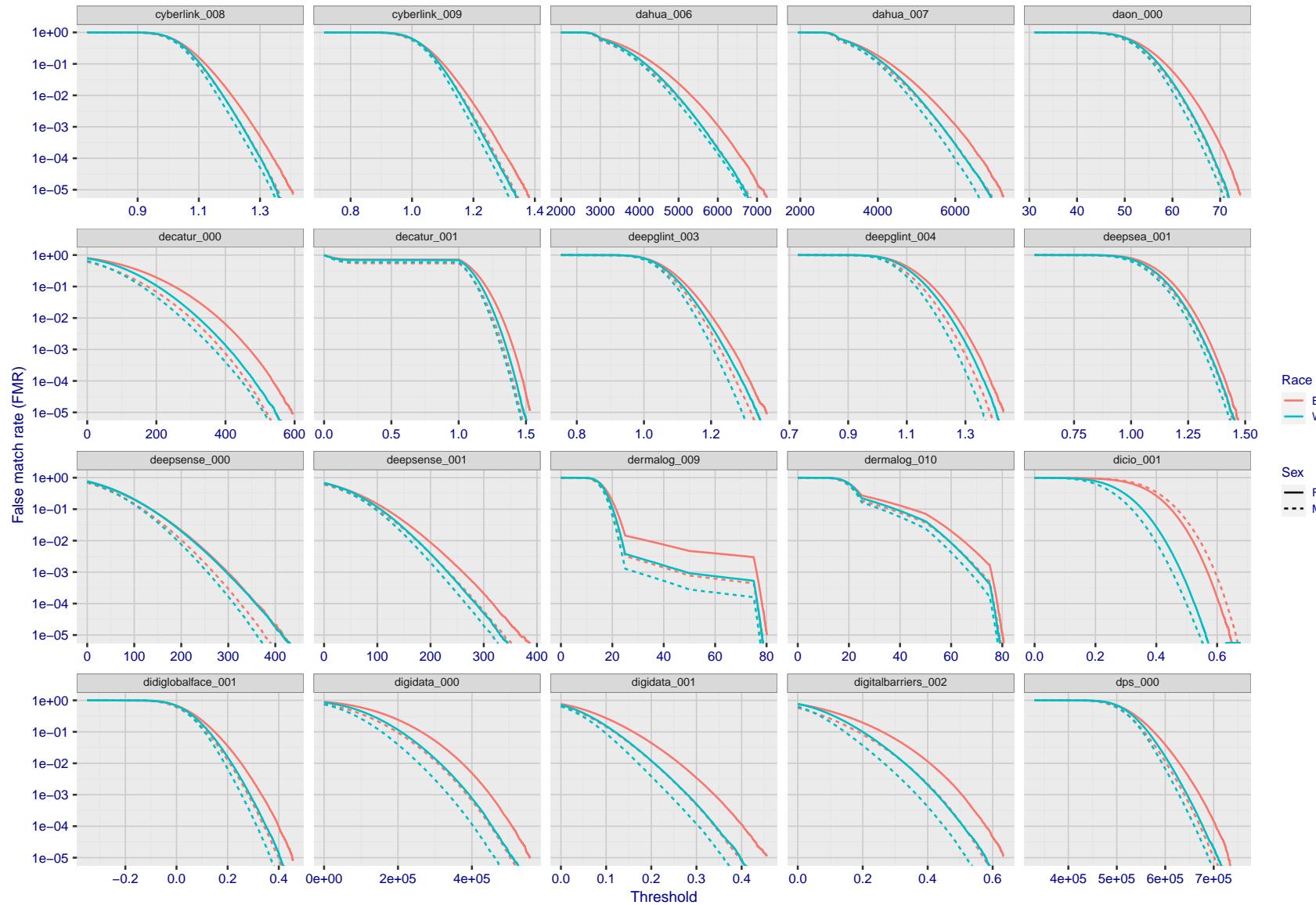


Figure 215: For the mugshot images, the false match calibration curves show false match rate vs. threshold. Separate curves appear for white females, black females, black males and white males.

2022/08/30 09:26:06

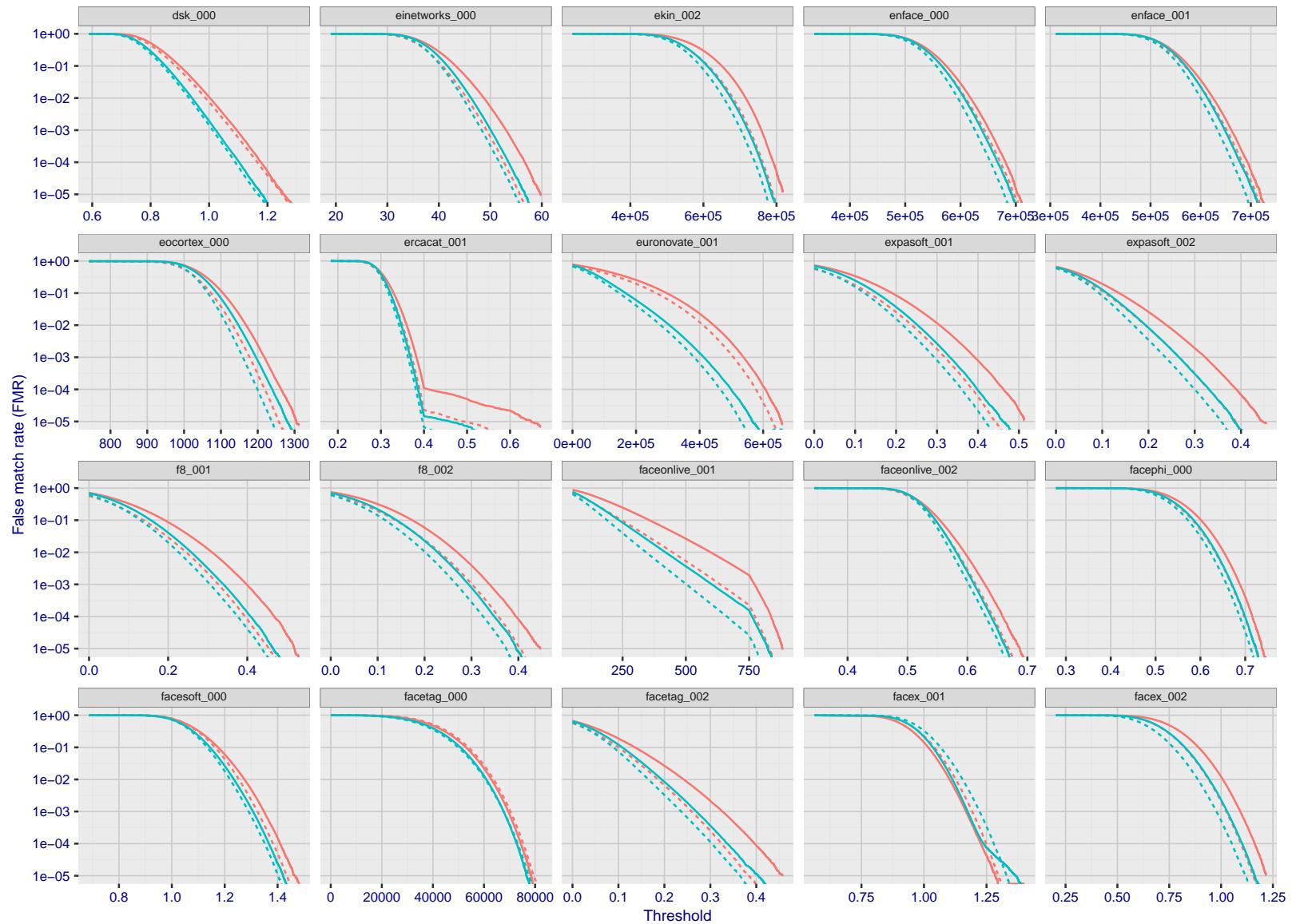


Figure 216: For the mugshot images, the false match calibration curves show false match rate vs. threshold. Separate curves appear for white females, black females, black males and white males.

2022/08/30 09:26:06

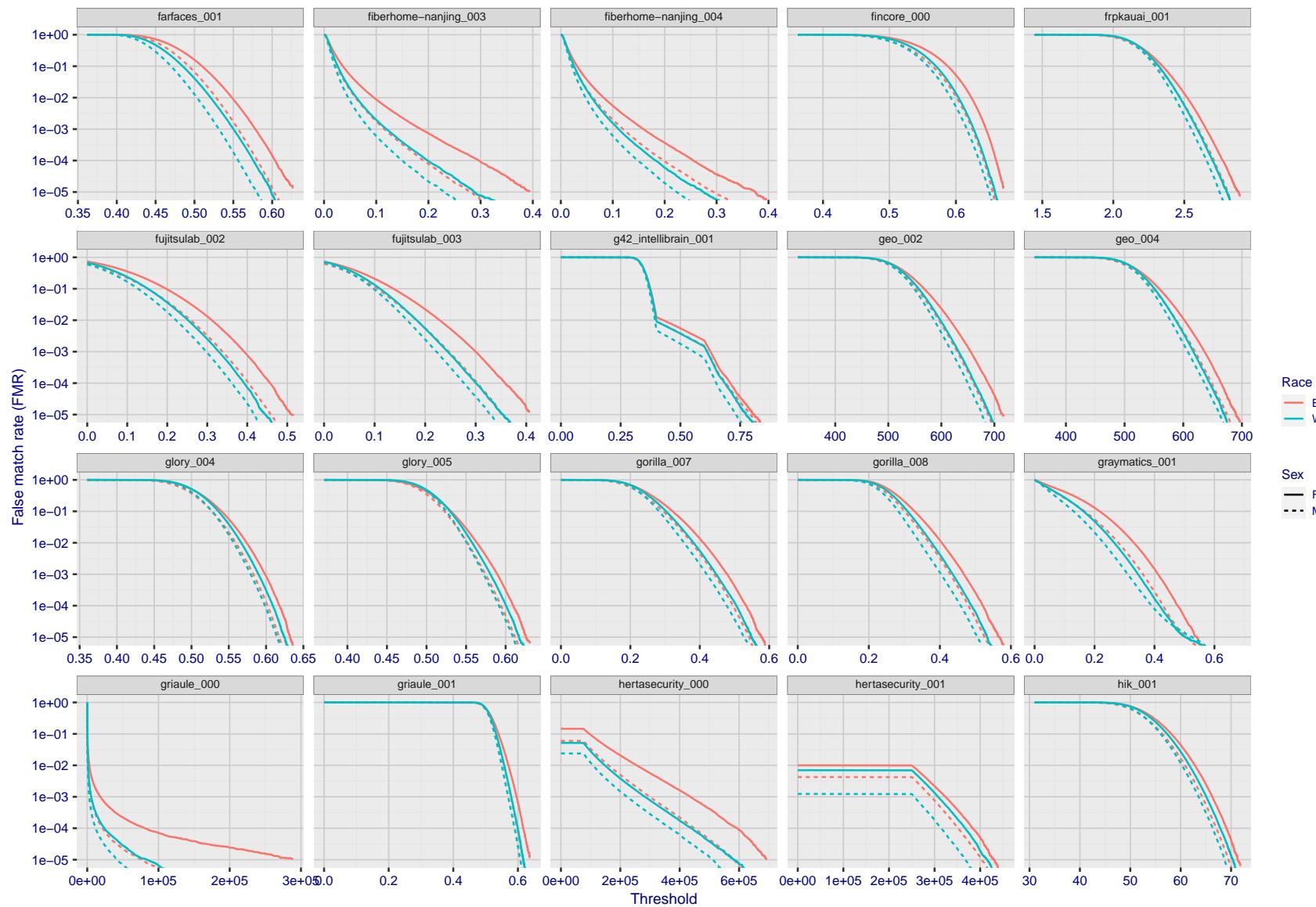


Figure 217: For the mugshot images, the false match calibration curves show false match rate vs. threshold. Separate curves appear for white females, black females, black males and white males.

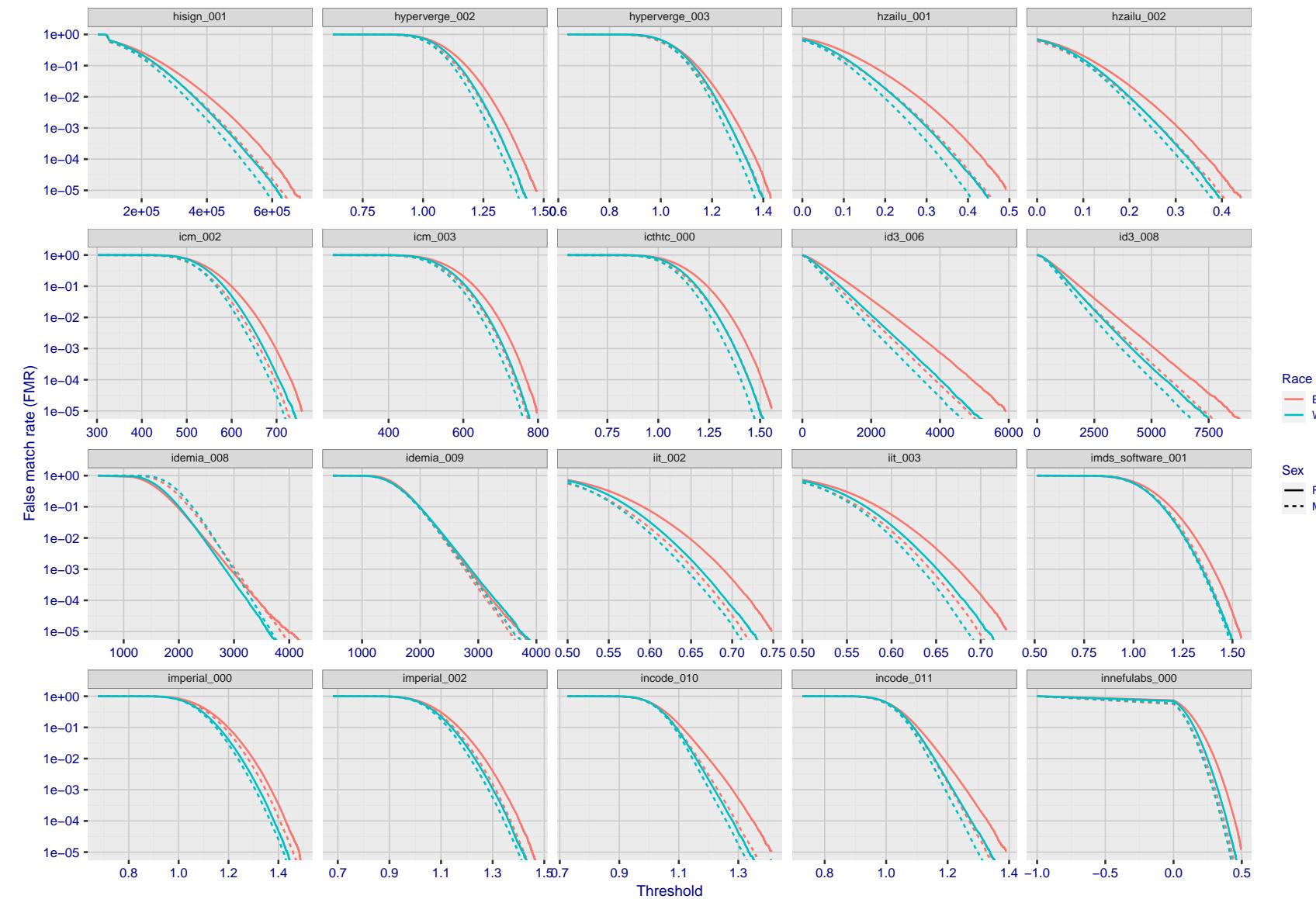


Figure 218: For the mugshot images, the false match calibration curves show false match rate vs. threshold. Separate curves appear for white females, black females, black males and white males.

2022/08/30 09:26:06

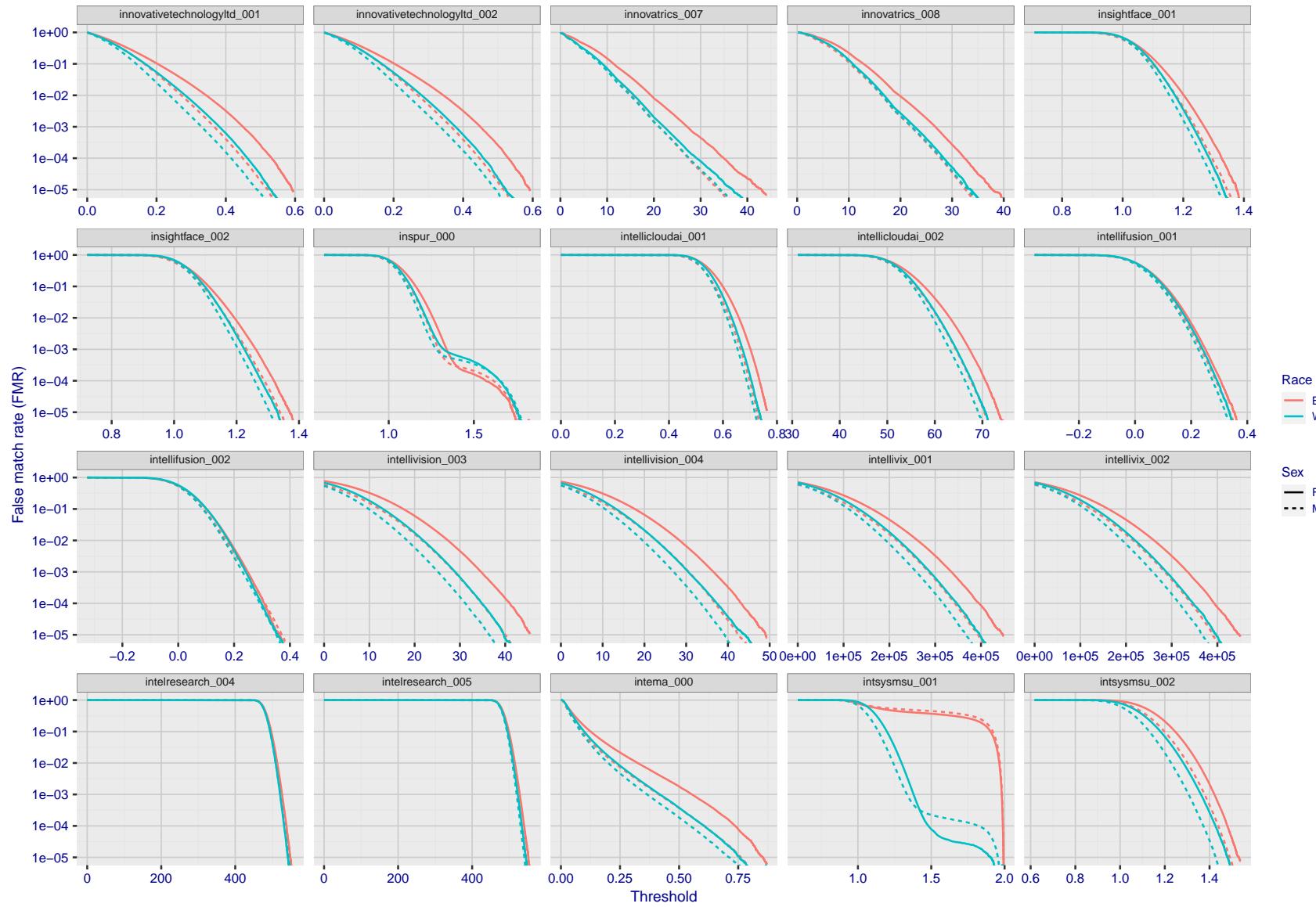


Figure 219: For the mugshot images, the false match calibration curves show false match rate vs. threshold. Separate curves appear for white females, black females, black males and white males.

2022/08/30 09:26:06

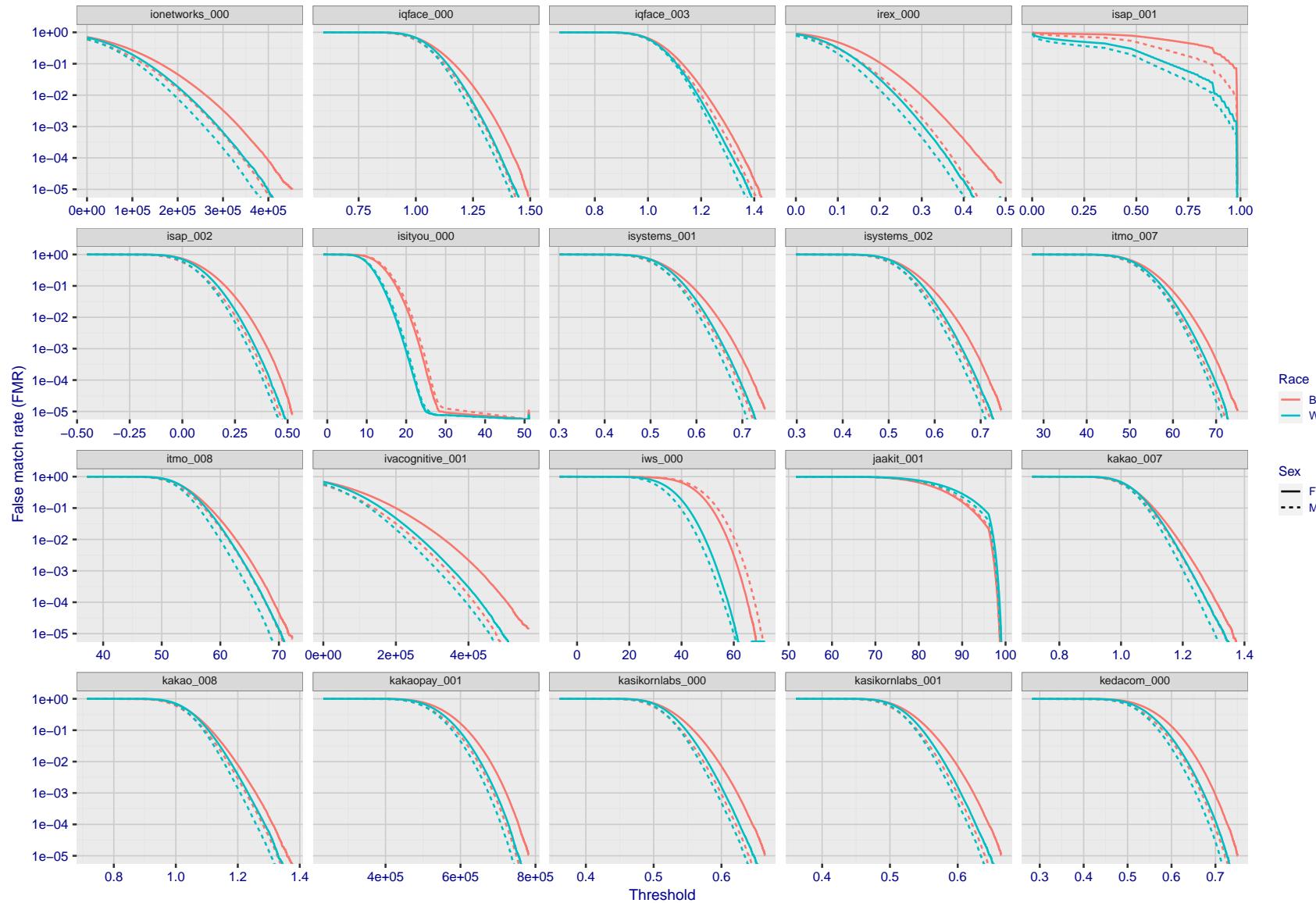


Figure 220: For the mugshot images, the false match calibration curves show false match rate vs. threshold. Separate curves appear for white females, black females, black males and white males.

2022/08/30 09:26:06

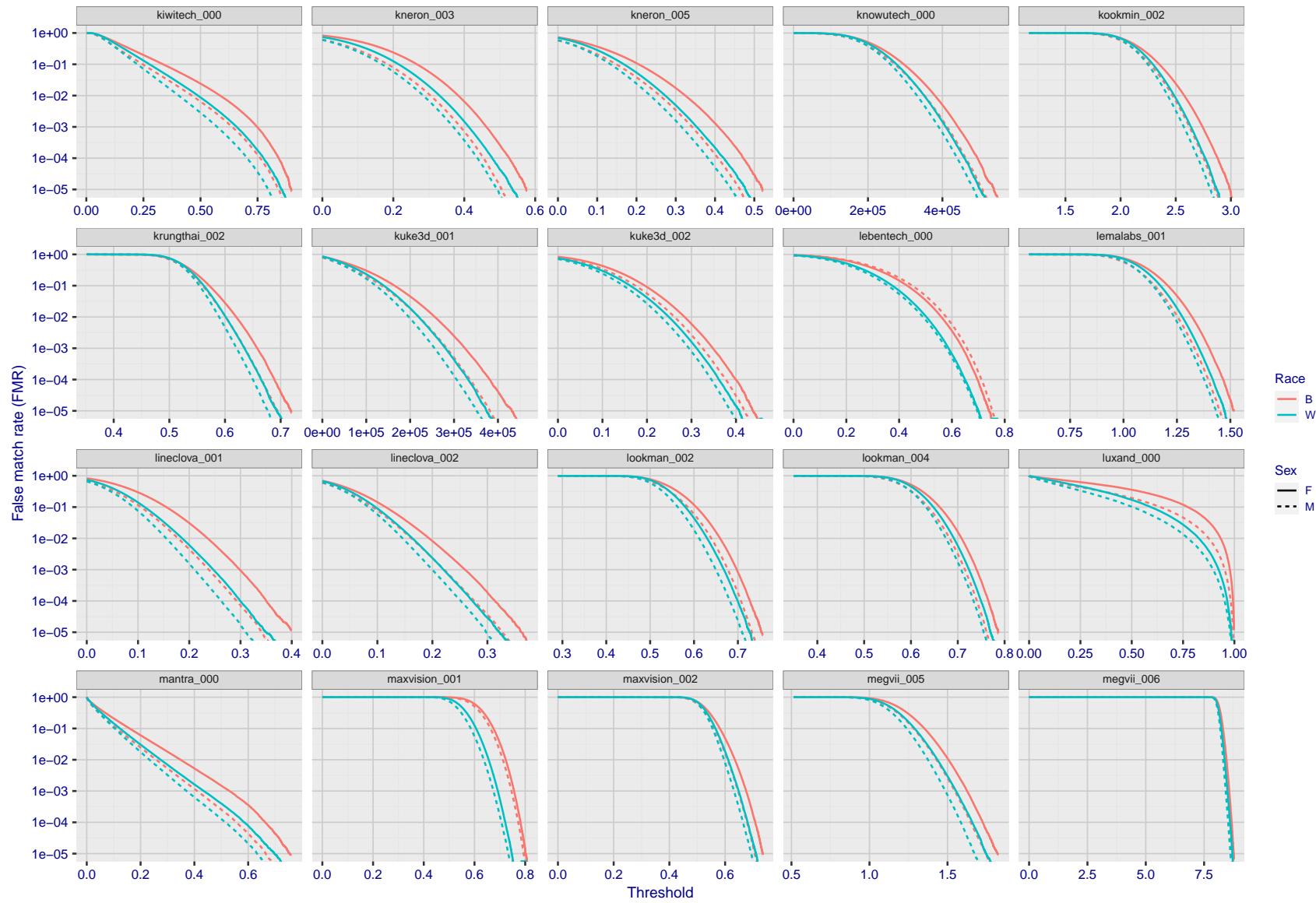


Figure 221: For the mugshot images, the false match calibration curves show false match rate vs. threshold. Separate curves appear for white females, black females, black males and white males.

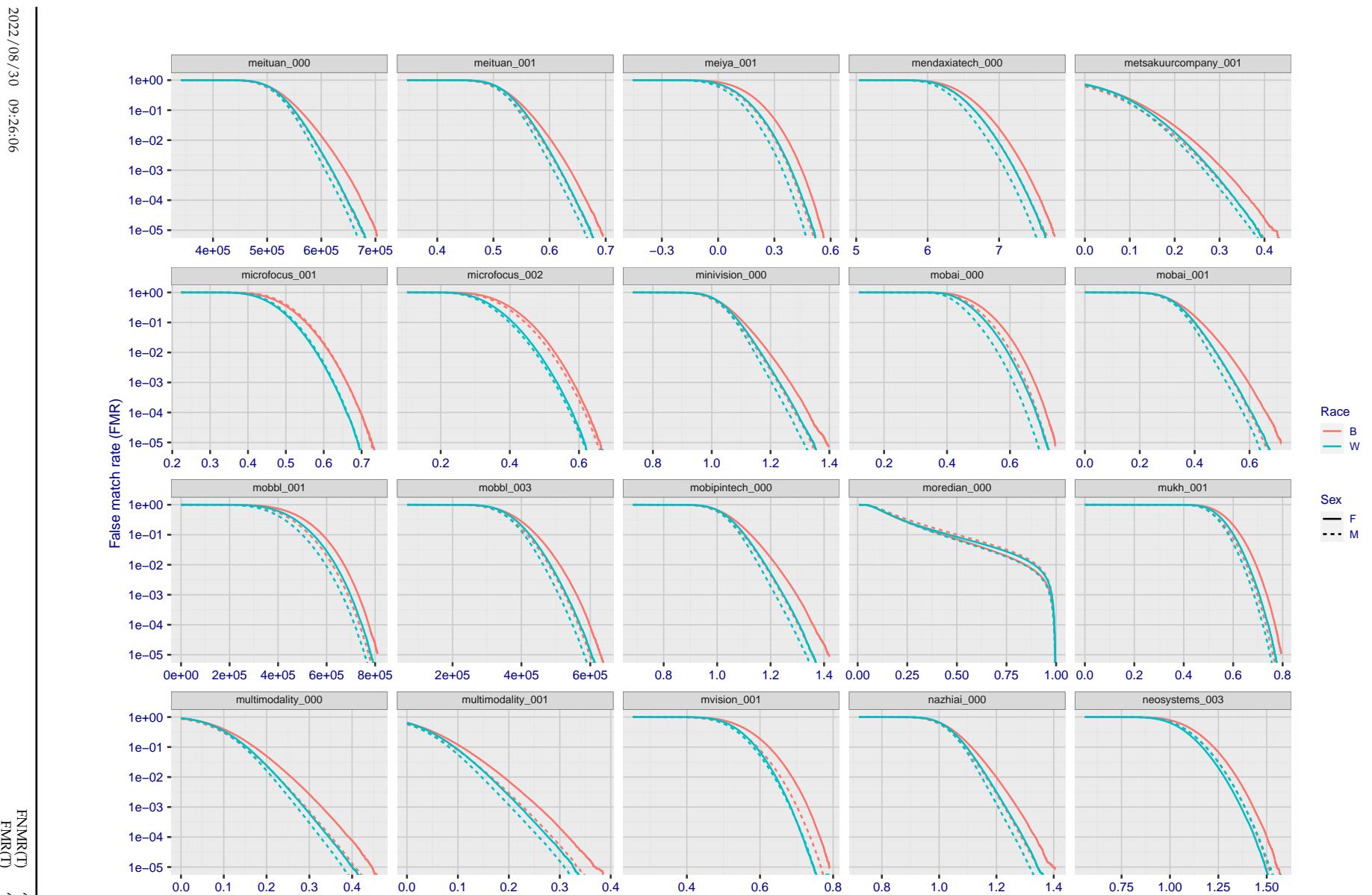


Figure 222: For the mugshot images, the false match calibration curves show false match rate vs. threshold. Separate curves appear for white females, black females, black males and white males.

2022/08/30 09:26:06

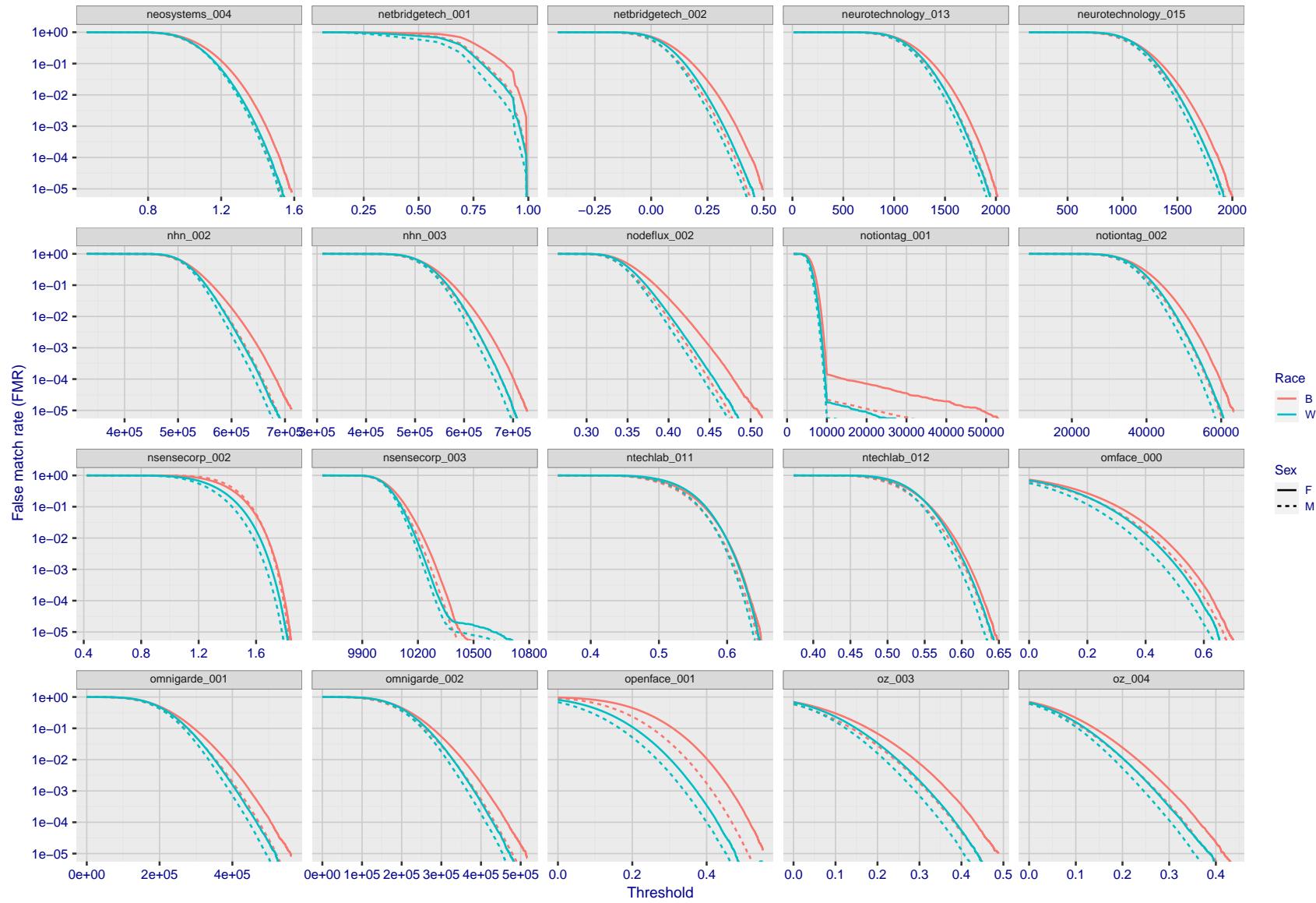


Figure 223: For the mugshot images, the false match calibration curves show false match rate vs. threshold. Separate curves appear for white females, black females, black males and white males.

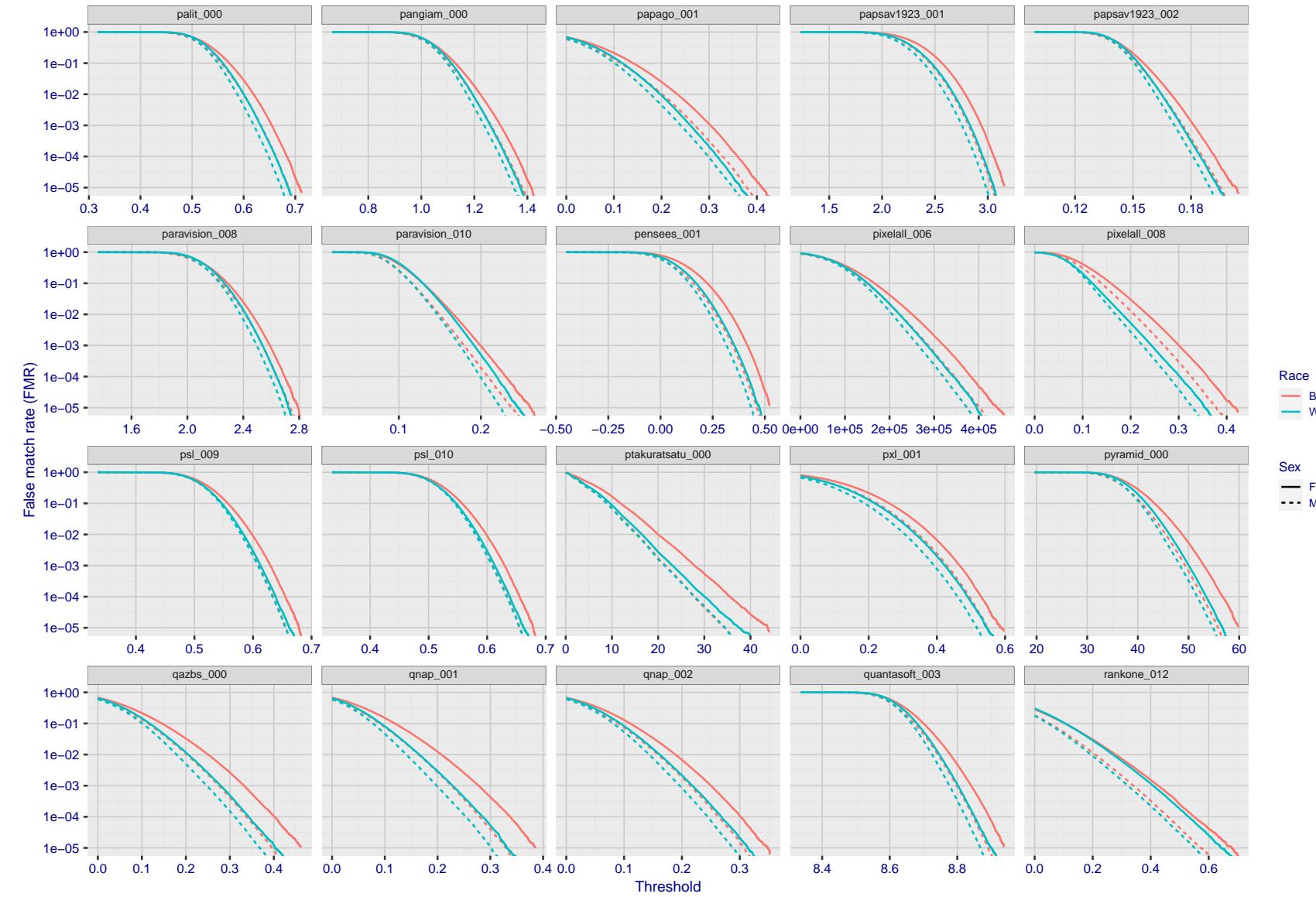


Figure 224: For the mugshot images, the false match calibration curves show false match rate vs. threshold. Separate curves appear for white females, black females, black males and white males.

2022/08/30 09:26:06

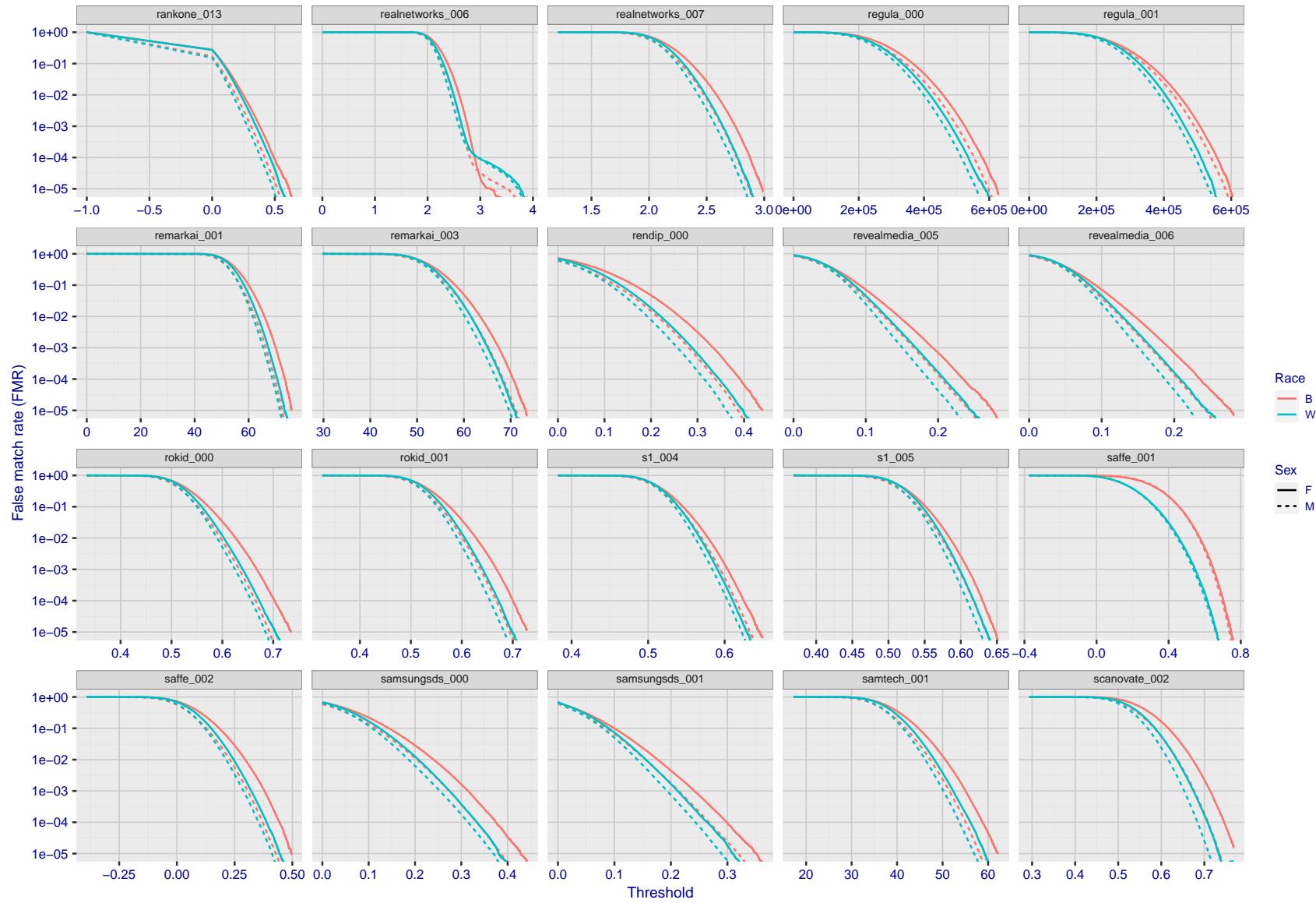


Figure 225: For the mugshot images, the false match calibration curves show false match rate vs. threshold. Separate curves appear for white females, black females, black males and white males.

2022/08/30 09:26:06

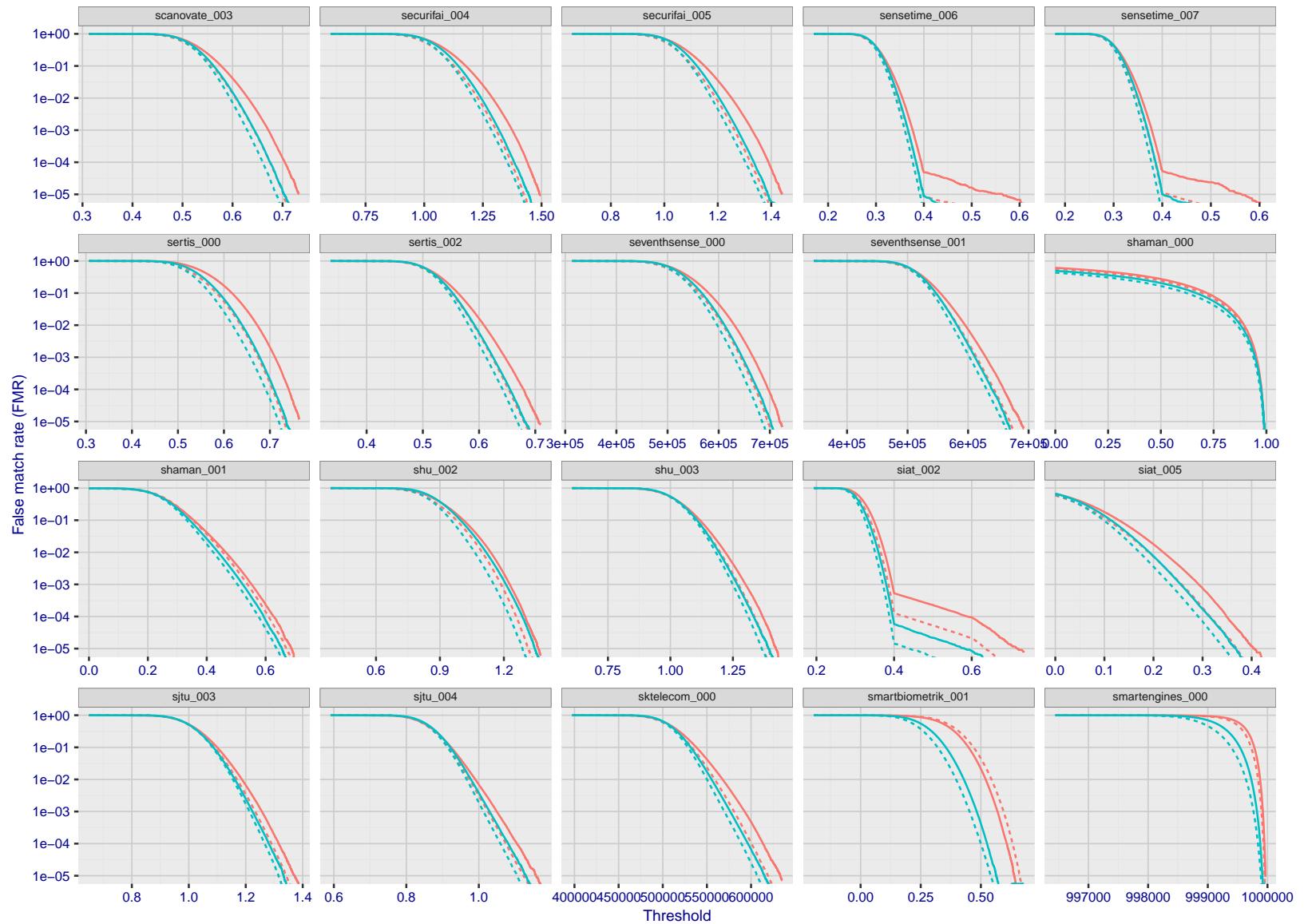


Figure 226: For the mugshot images, the false match calibration curves show false match rate vs. threshold. Separate curves appear for white females, black females, black males and white males.

2022/08/30 09:26:06

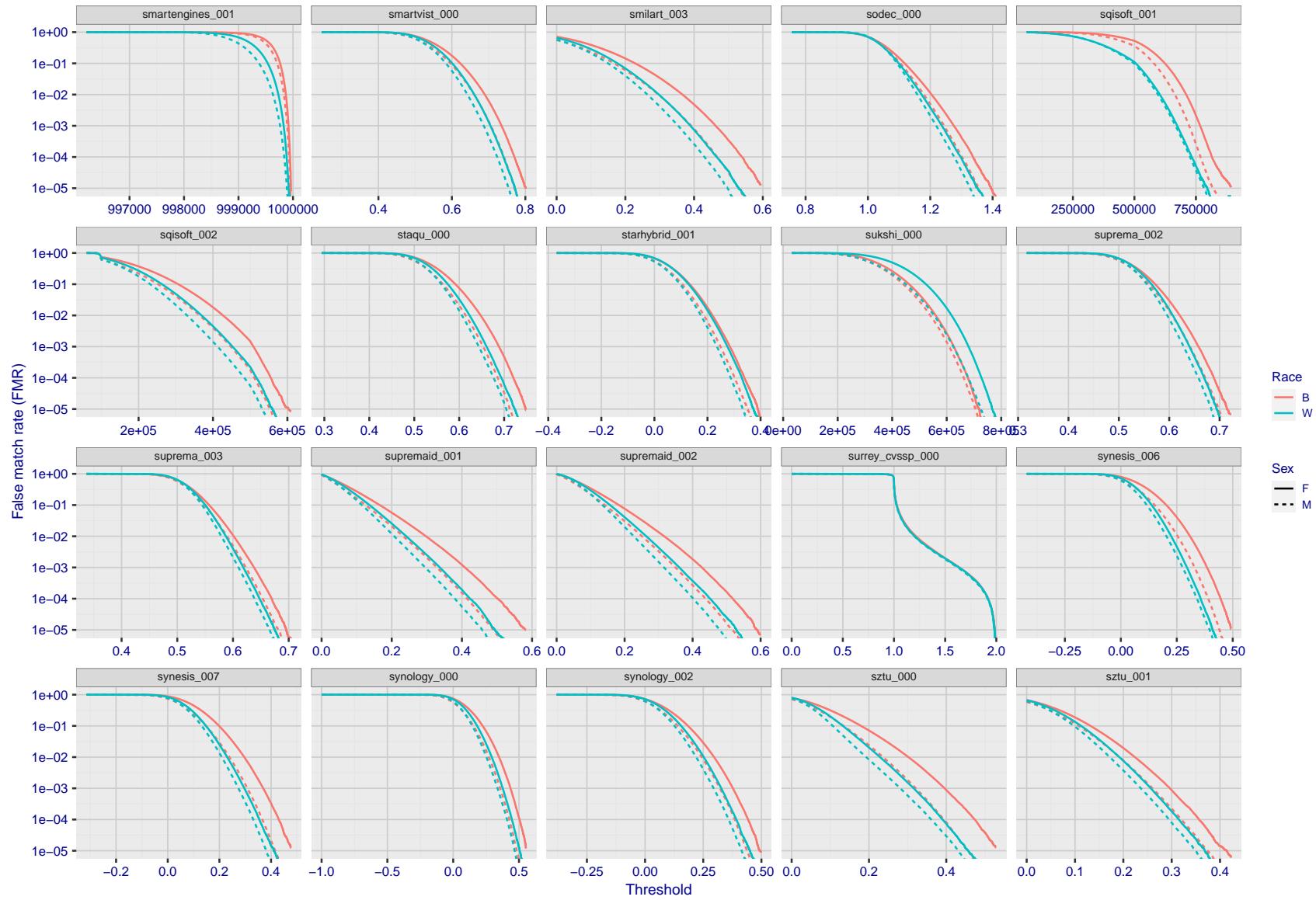


Figure 227: For the mugshot images, the false match calibration curves show false match rate vs. threshold. Separate curves appear for white females, black females, black males and white males.

2022/08/30 09:26:06

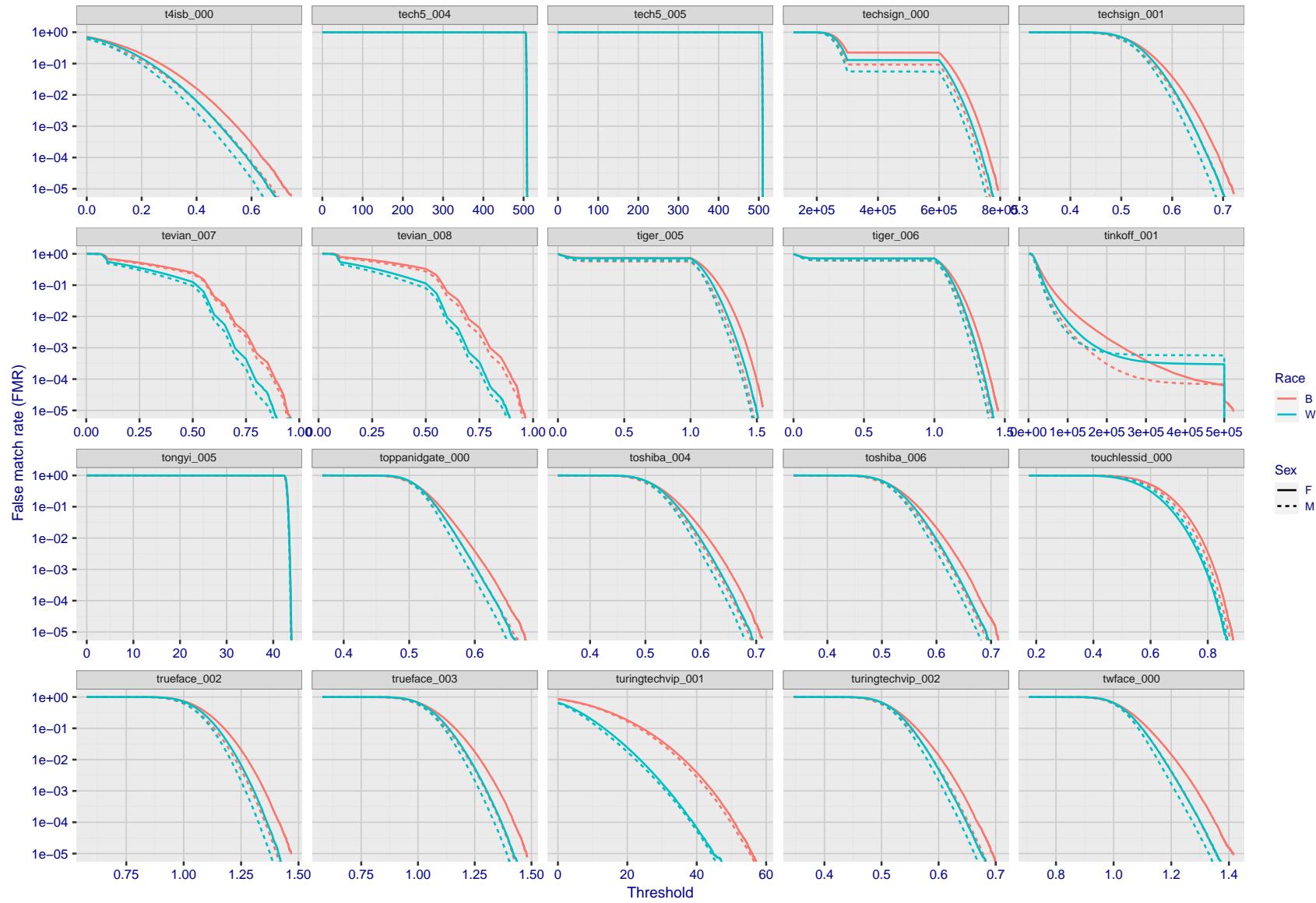


Figure 228: For the mugshot images, the false match calibration curves show false match rate vs. threshold. Separate curves appear for white females, black females, black males and white males.

2022/08/30 09:26:06

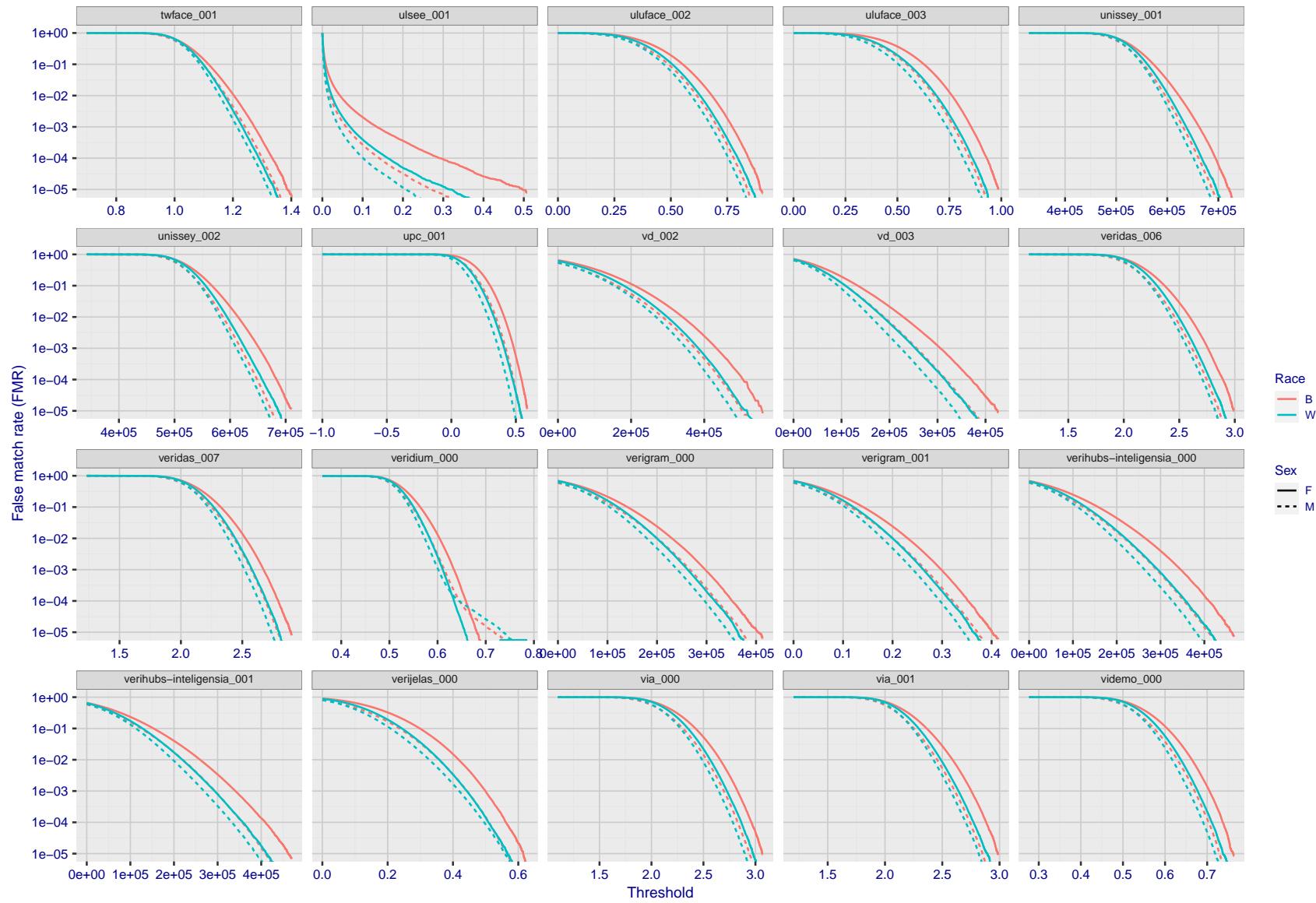


Figure 229: For the mugshot images, the false match calibration curves show false match rate vs. threshold. Separate curves appear for white females, black females, black males and white males.

2022/08/30 09:26:06

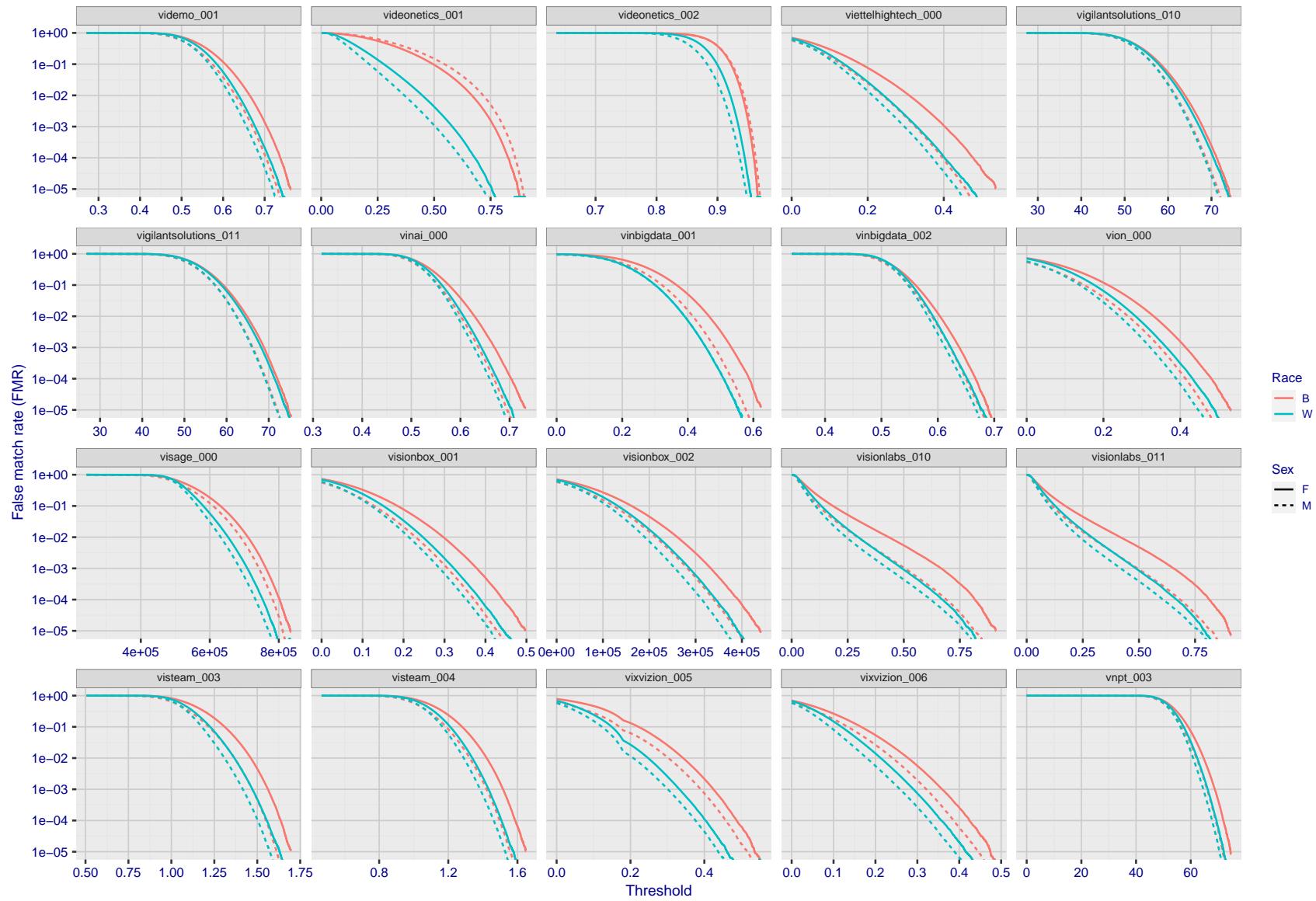


Figure 230: For the mugshot images, the false match calibration curves show false match rate vs. threshold. Separate curves appear for white females, black females, black males and white males.

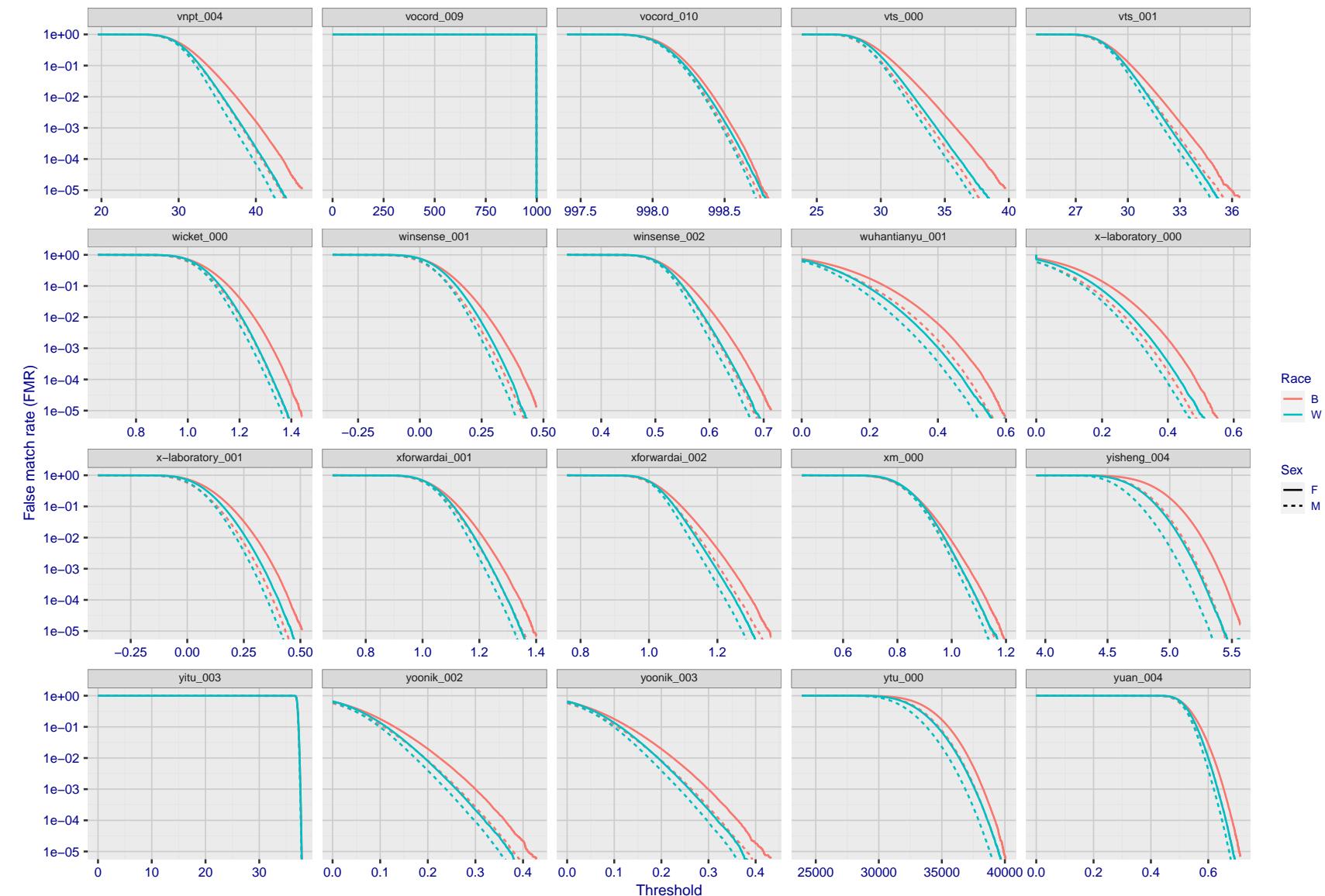


Figure 231: For the mugshot images, the false match calibration curves show false match rate vs. threshold. Separate curves appear for white females, black females, black males and white males.

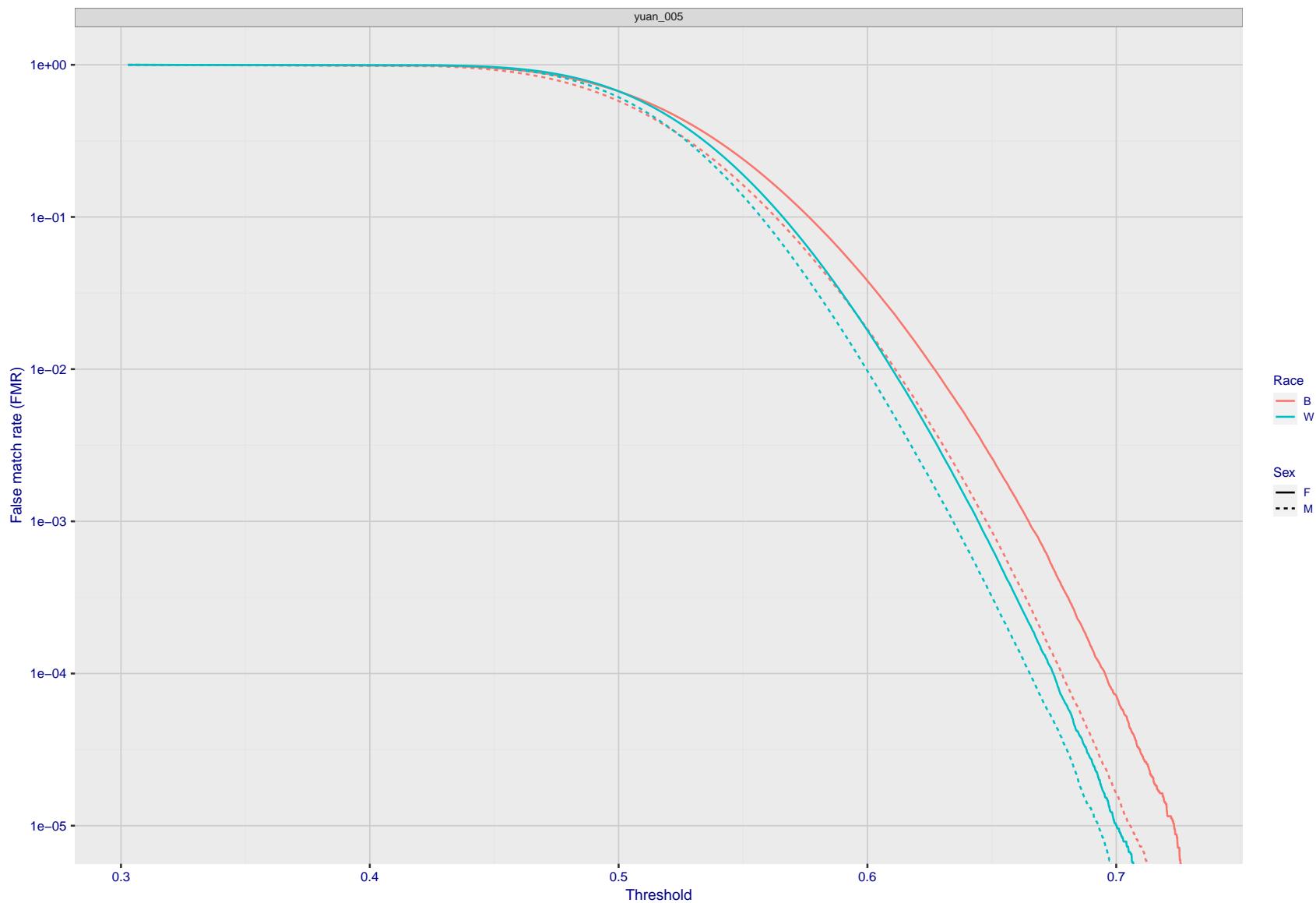


Figure 232: For the mugshot images, the false match calibration curves show false match rate vs. threshold. Separate curves appear for white females, black females, black males and white males.

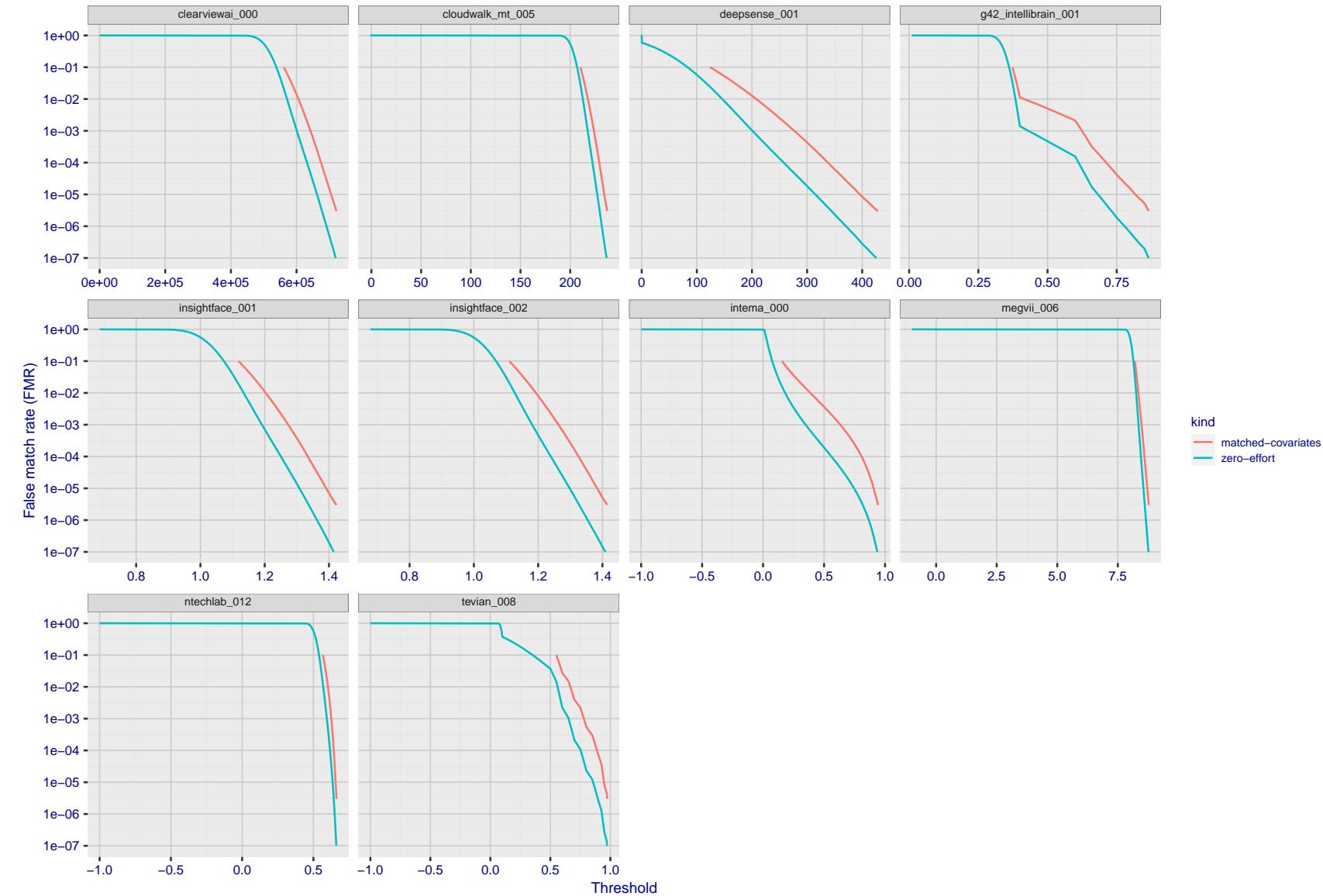


Figure 233: For the visa images, the false match calibration curves show FMR vs. threshold, T . The blue (lower) curves are for zero-effort impostors (i.e. comparing all images against all). The red (upper) curves are for persons of the same-sex, same-age, and same national-origin. This shows that FMR is underestimated (by a factor of 10 or more) by using a zero-effort impostor calculation to calibrate T . As shown later (sec. 3.6), FMR is higher for demographic-matched impostors.

2022/08/30 09:26:06

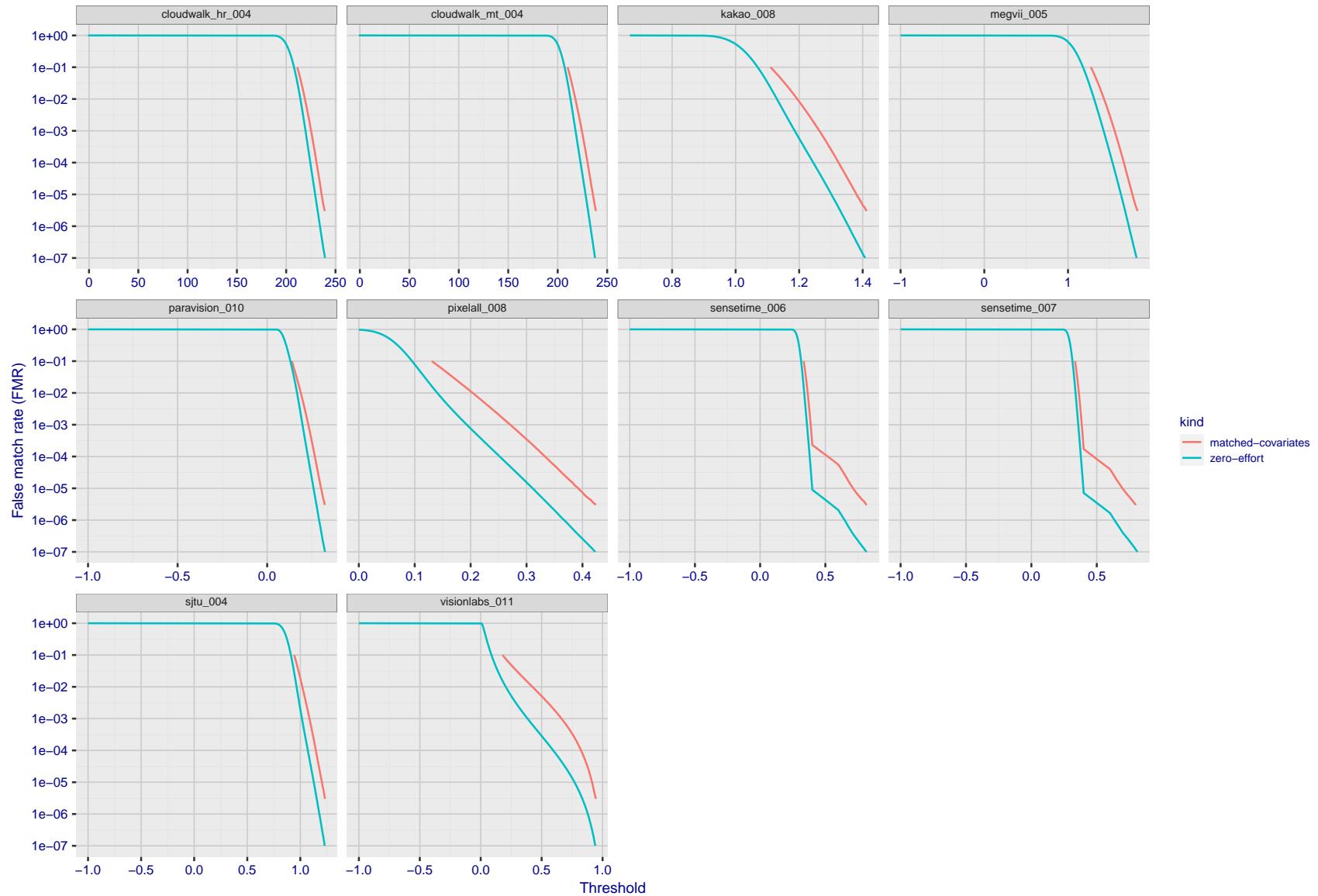


Figure 234: For the visa images, the false match calibration curves show FMR vs. threshold, T . The blue (lower) curves are for zero-effort impostors (i.e. comparing all images against all). The red (upper) curves are for persons of the same-sex, same-age, and same national-origin. This shows that FMR is underestimated (by a factor of 10 or more) by using a zero-effort impostor calculation to calibrate T . As shown later (sec. 3.6), FMR is higher for demographic-matched impostors.

FNMR(T)
"False non-match rate"
"False match rate"

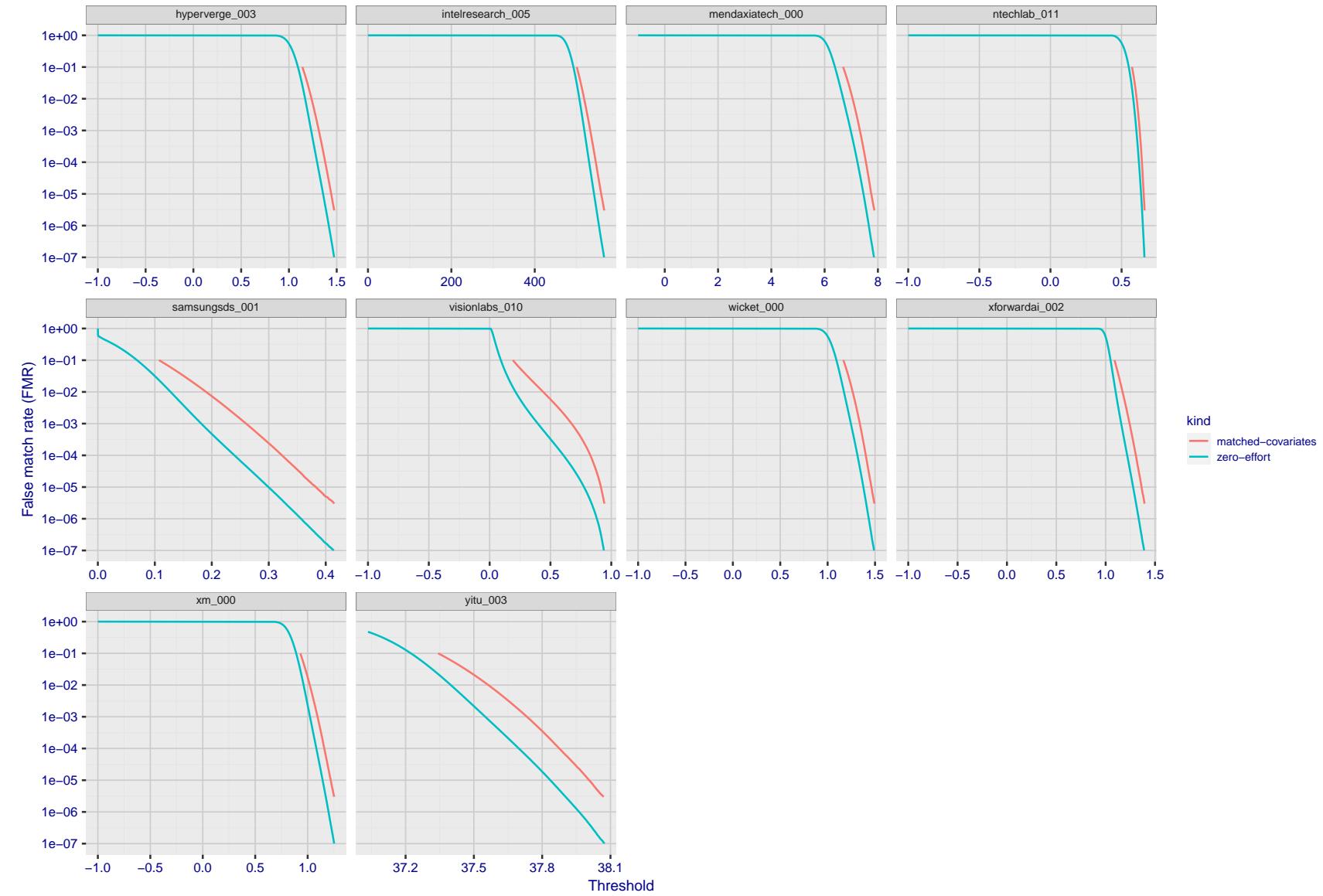


Figure 235: For the visa images, the false match calibration curves show FMR vs. threshold, T . The blue (lower) curves are for zero-effort impostors (i.e. comparing all images against all). The red (upper) curves are for persons of the same-sex, same-age, and same national-origin. This shows that FMR is underestimated (by a factor of 10 or more) by using a zero-effort impostor calculation to calibrate T . As shown later (sec. 3.6), FMR is higher for demographic-matched impostors.

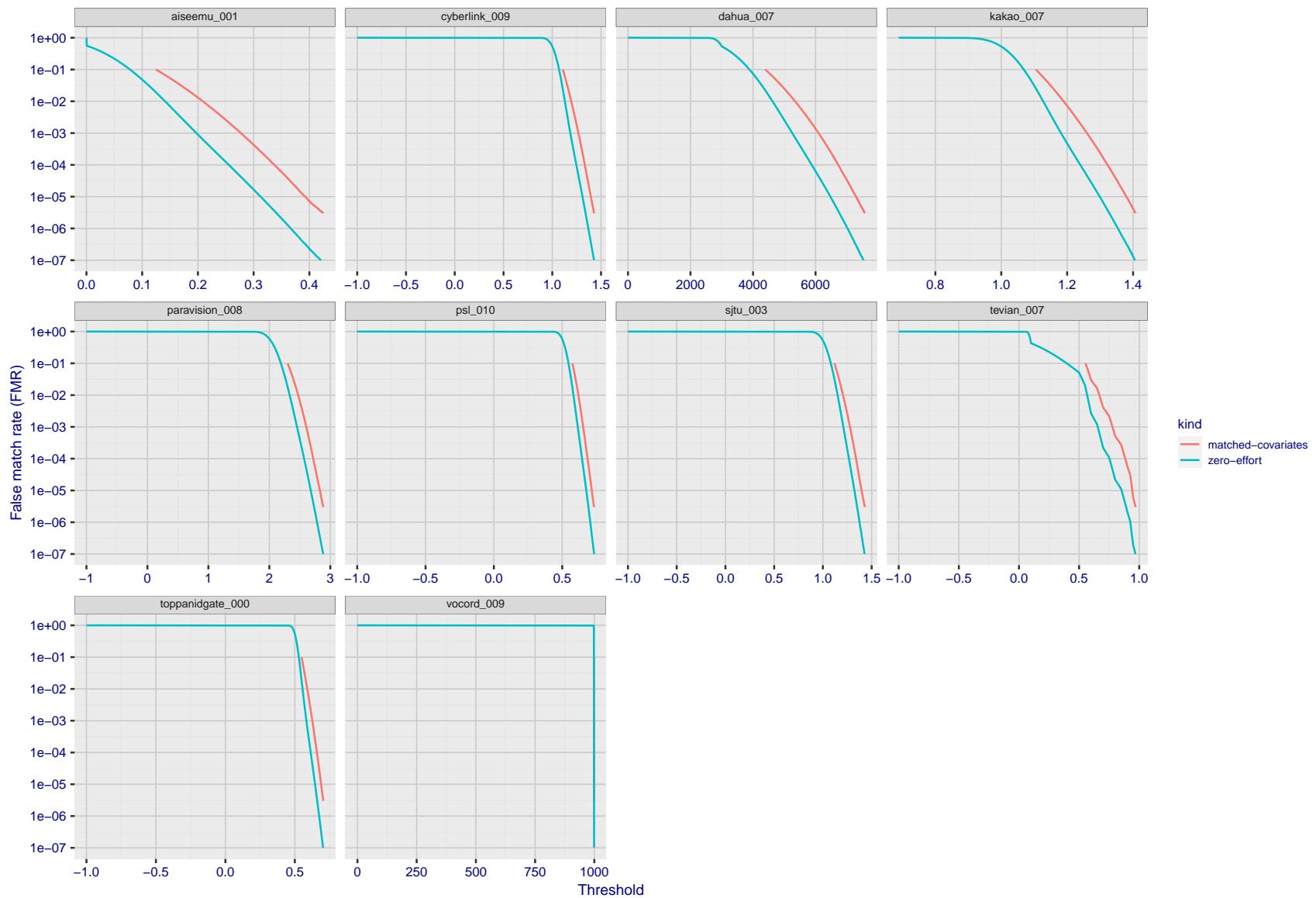


Figure 236: For the visa images, the false match calibration curves show FMR vs. threshold, T . The blue (lower) curves are for zero-effort impostors (i.e. comparing all images against all). The red (upper) curves are for persons of the same-sex, same-age, and same national-origin. This shows that FMR is underestimated (by a factor of 10 or more) by using a zero-effort impostor calculation to calibrate T . As shown later (sec. 3.6), FMR is higher for demographic-matched impostors.

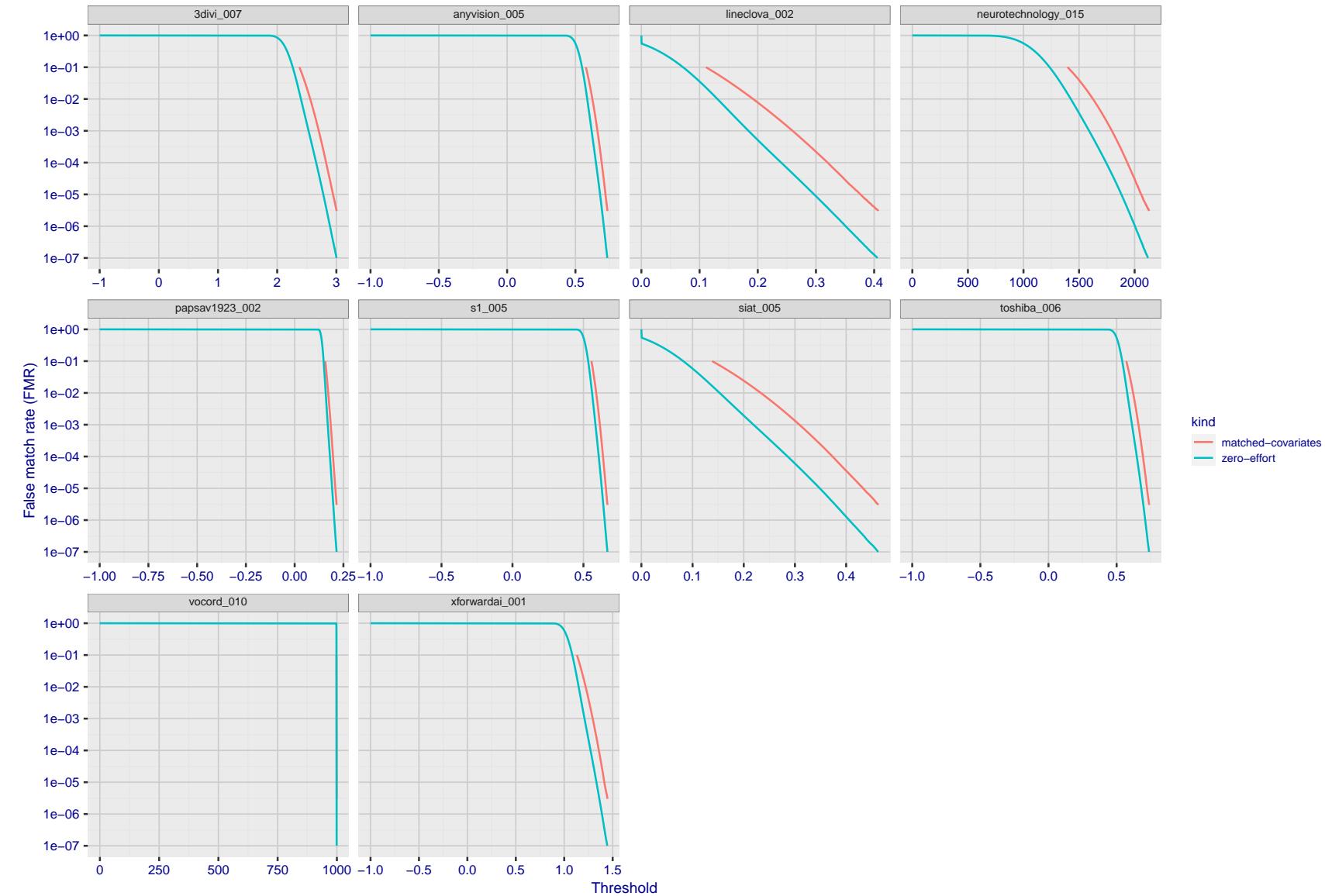


Figure 237: For the visa images, the false match calibration curves show FMR vs. threshold, T . The blue (lower) curves are for zero-effort impostors (i.e. comparing all images against all). The red (upper) curves are for persons of the same-sex, same-age, and same national-origin. This shows that FMR is underestimated (by a factor of 10 or more) by using a zero-effort impostor calculation to calibrate T . As shown later (sec. 3.6), FMR is higher for demographic-matched impostors.

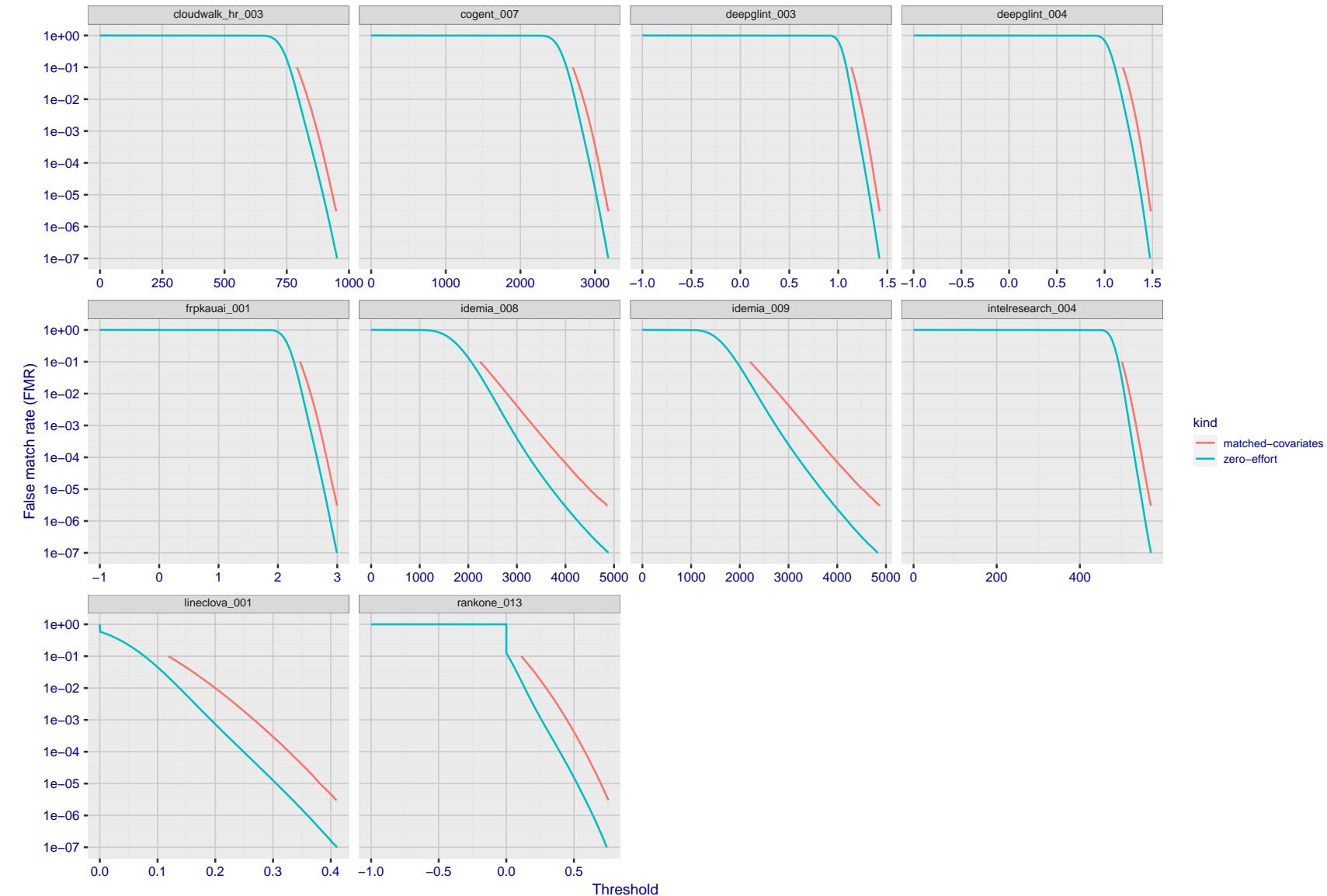


Figure 238: For the visa images, the false match calibration curves show FMR vs. threshold, T . The blue (lower) curves are for zero-effort impostors (i.e. comparing all images against all). The red (upper) curves are for persons of the same-sex, same-age, and same national-origin. This shows that FMR is underestimated (by a factor of 10 or more) by using a zero-effort impostor calculation to calibrate T . As shown later (sec. 3.6), FMR is higher for demographic-matched impostors.

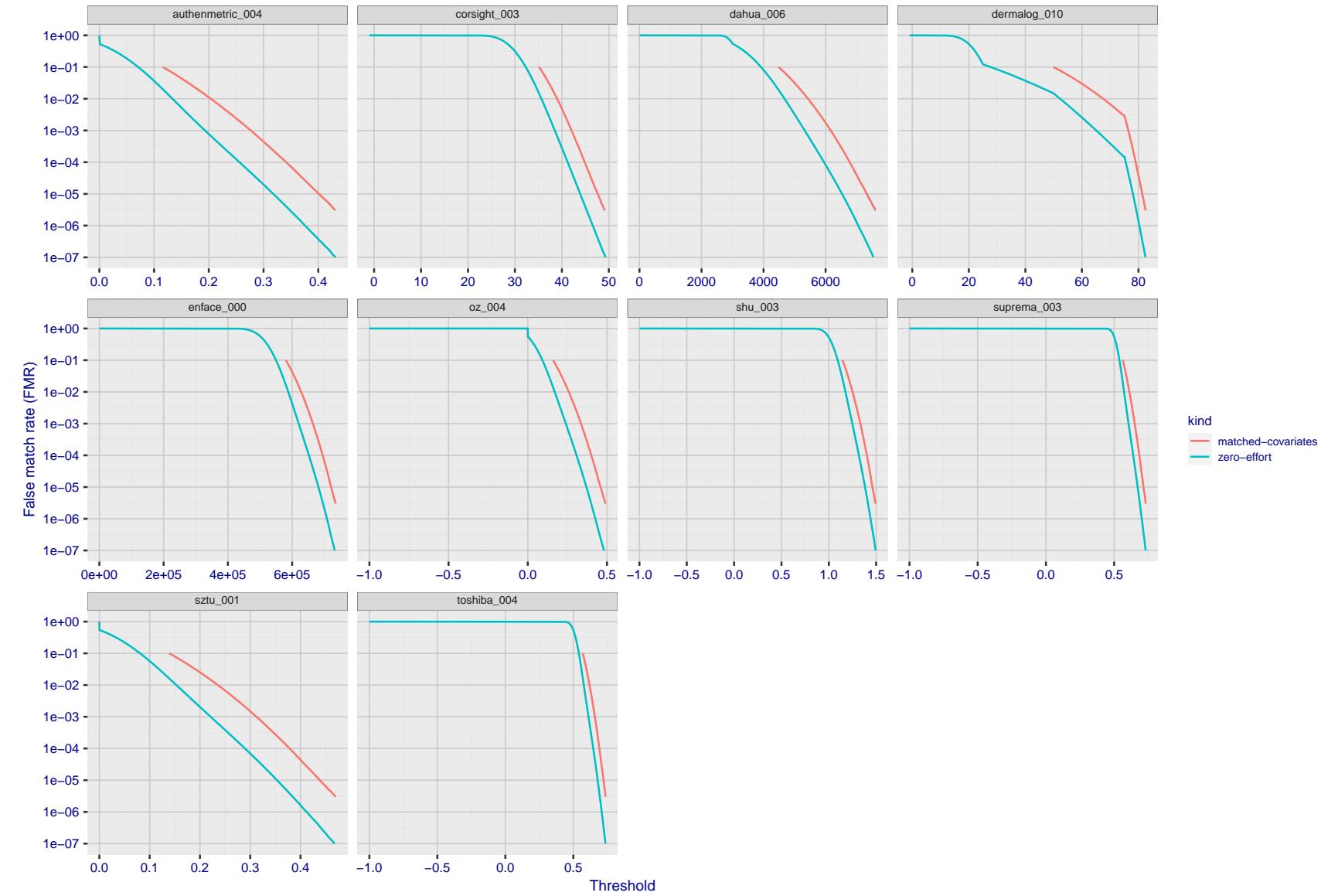


Figure 239: For the visa images, the false match calibration curves show FMR vs. threshold, T . The blue (lower) curves are for zero-effort impostors (i.e. comparing all images against all). The red (upper) curves are for persons of the same-sex, same-age, and same national-origin. This shows that FMR is underestimated (by a factor of 10 or more) by using a zero-effort impostor calculation to calibrate T . As shown later (sec. 3.6), FMR is higher for demographic-matched impostors.

2022/08/30 09:26:06

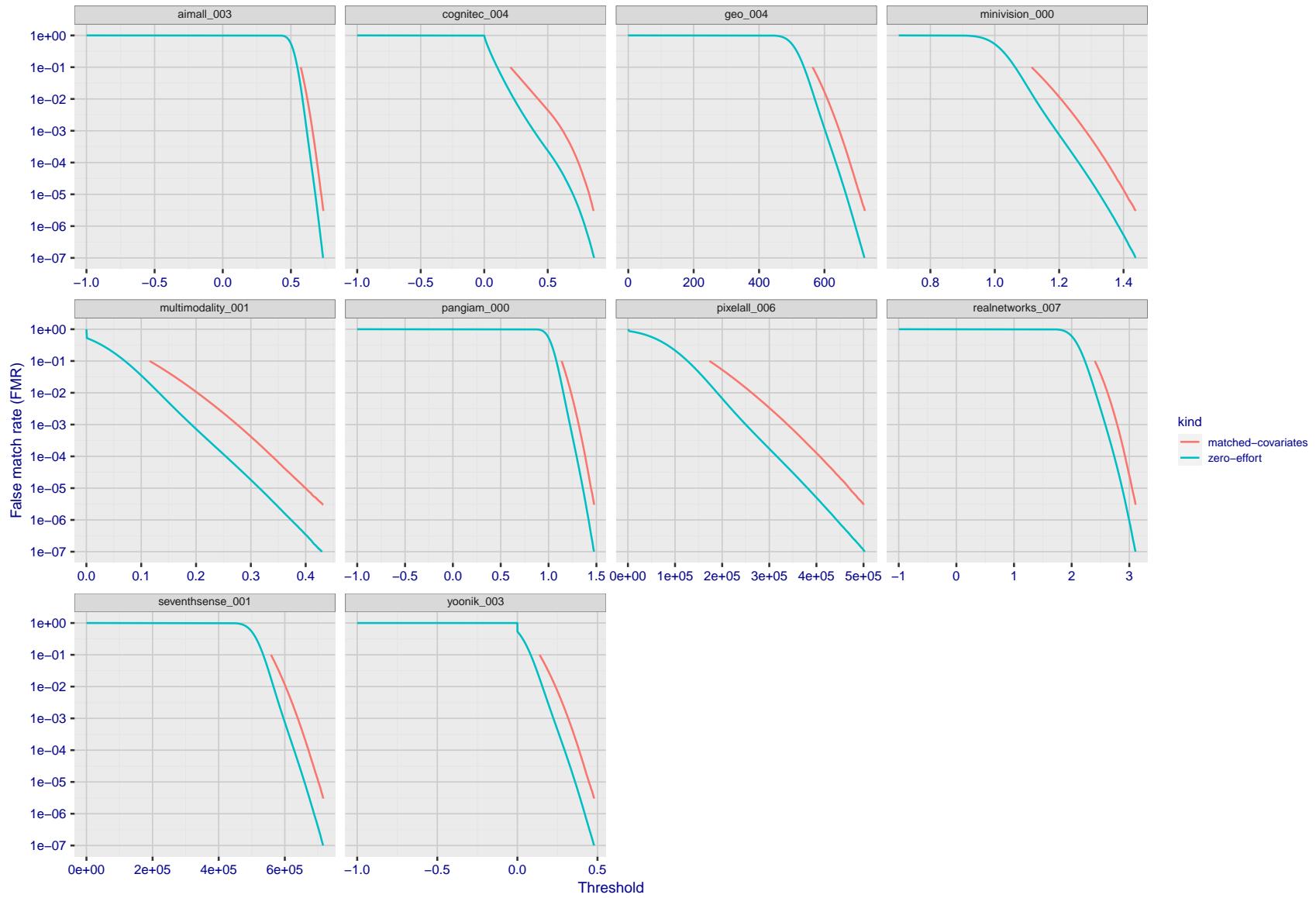


Figure 240: For the visa images, the false match calibration curves show FMR vs. threshold, T . The blue (lower) curves are for zero-effort impostors (i.e. comparing all images against all). The red (upper) curves are for persons of the same-sex, same-age, and same national-origin. This shows that FMR is underestimated (by a factor of 10 or more) by using a zero-effort impostor calculation to calibrate T . As shown later (sec. 3.6), FMR is higher for demographic-matched impostors.

FNMR(T)
"False non-match rate"
"False match rate"

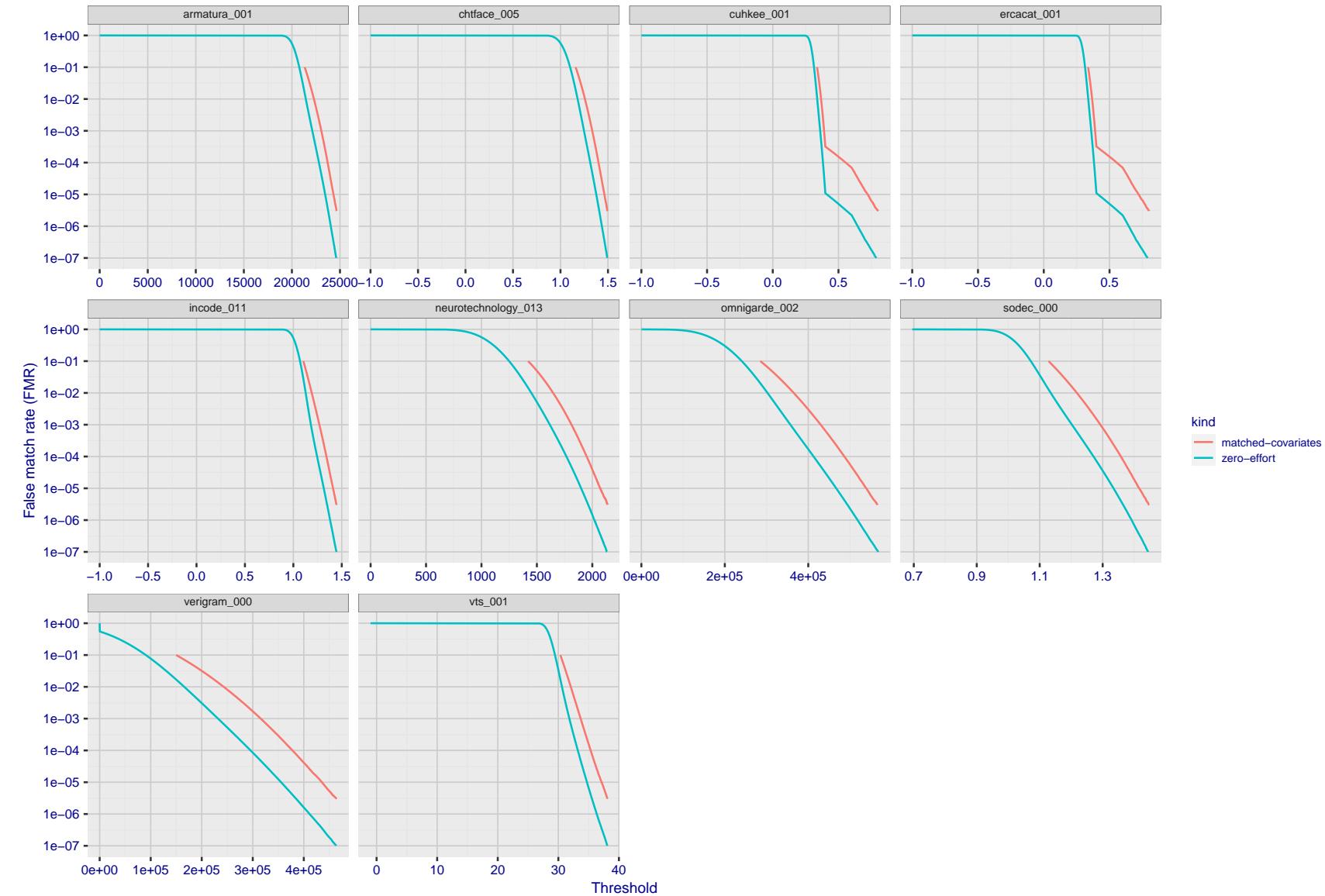


Figure 241: For the visa images, the false match calibration curves show FMR vs. threshold, T . The blue (lower) curves are for zero-effort impostors (i.e. comparing all images against all). The red (upper) curves are for persons of the same-sex, same-age, and same national-origin. This shows that FMR is underestimated (by a factor of 10 or more) by using a zero-effort impostor calculation to calibrate T . As shown later (sec. 3.6), FMR is higher for demographic-matched impostors.

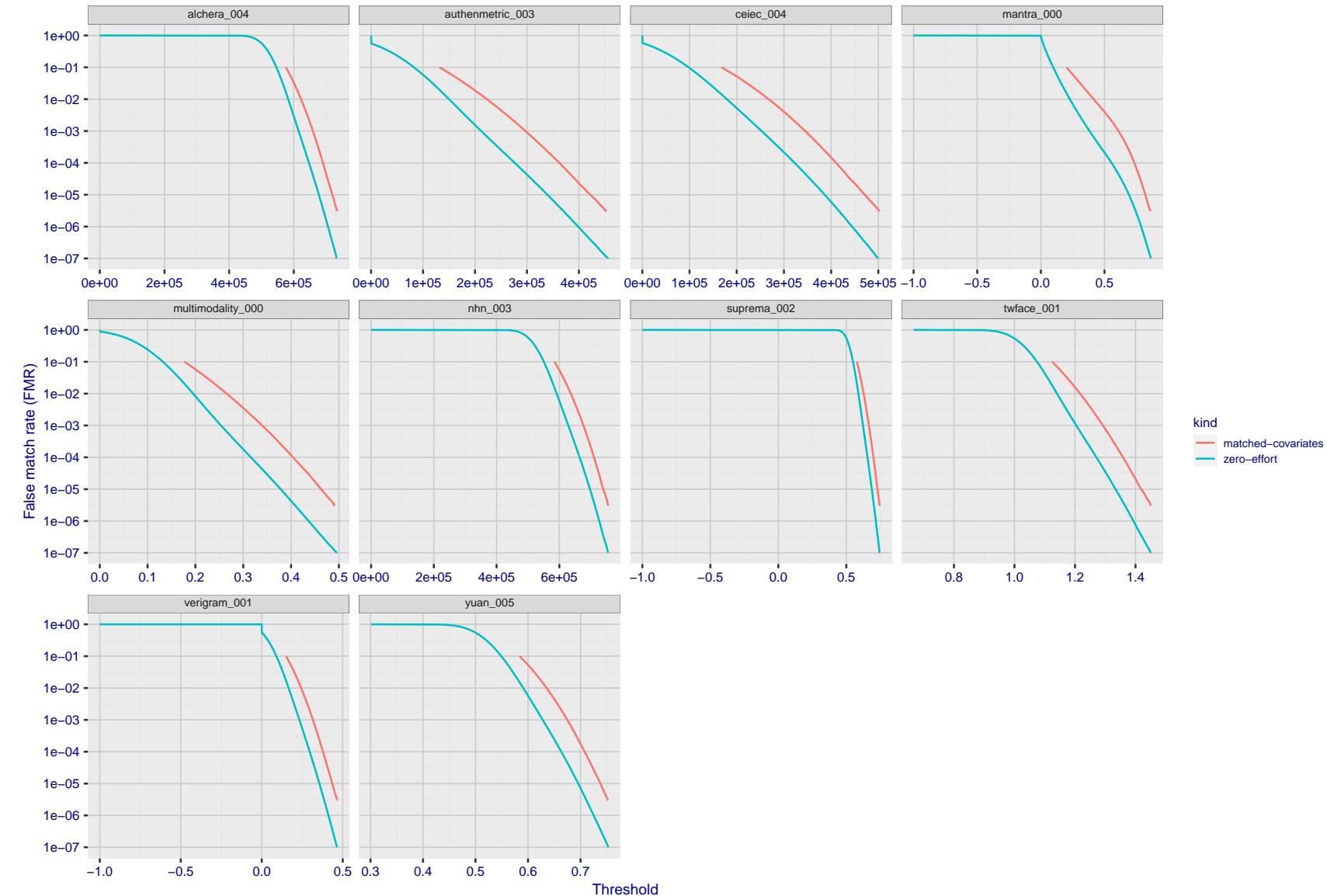


Figure 242: For the visa images, the false match calibration curves show FMR vs. threshold, T . The blue (lower) curves are for zero-effort impostors (i.e. comparing all images against all). The red (upper) curves are for persons of the same-sex, same-age, and same national-origin. This shows that FMR is underestimated (by a factor of 10 or more) by using a zero-effort impostor calculation to calibrate T . As shown later (sec. 3.6), FMR is higher for demographic-matched impostors.

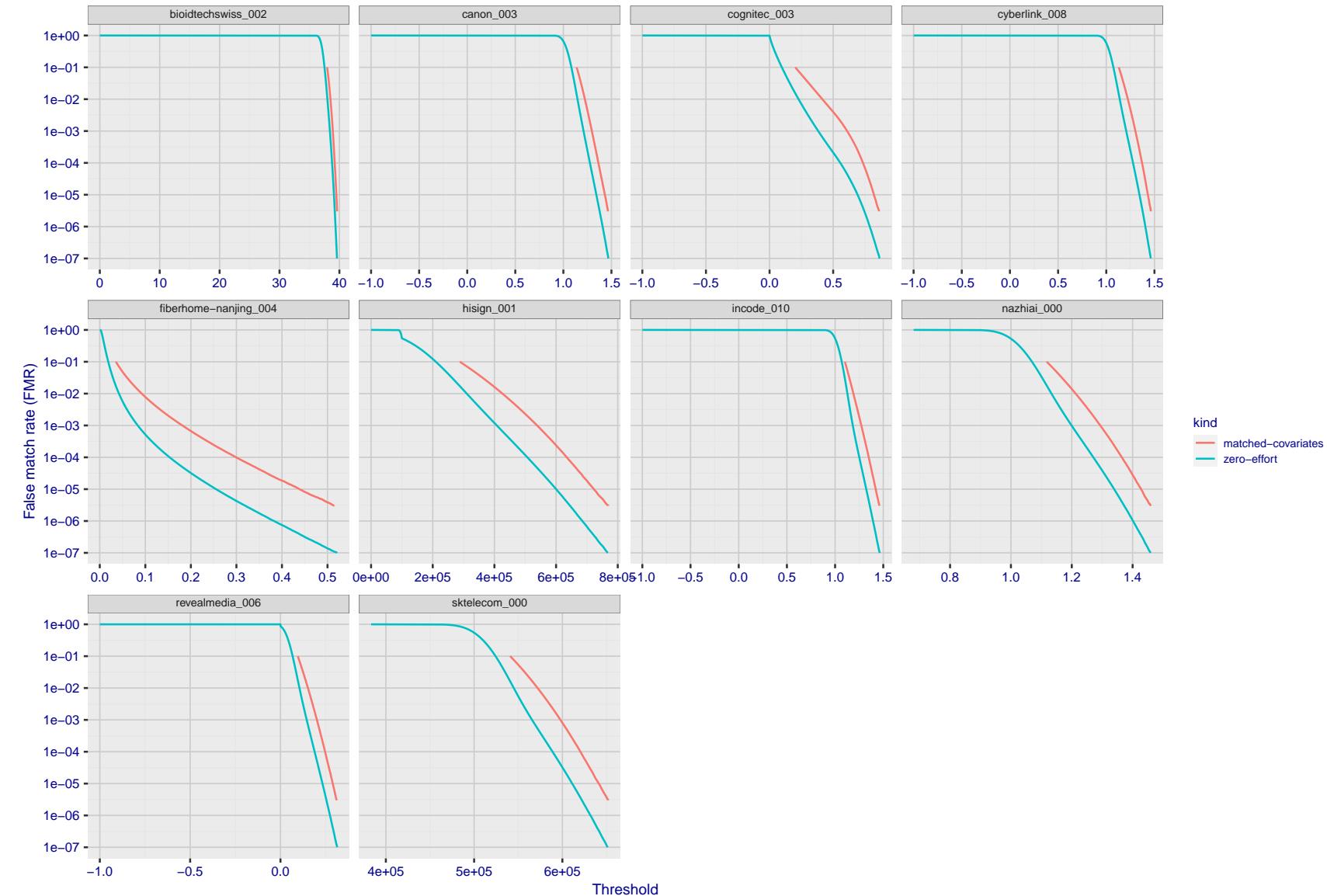


Figure 243: For the visa images, the false match calibration curves show FMR vs. threshold, T . The blue (lower) curves are for zero-effort impostors (i.e. comparing all images against all). The red (upper) curves are for persons of the same-sex, same-age, and same national-origin. This shows that FMR is underestimated (by a factor of 10 or more) by using a zero-effort impostor calculation to calibrate T . As shown later (sec. 3.6), FMR is higher for demographic-matched impostors.

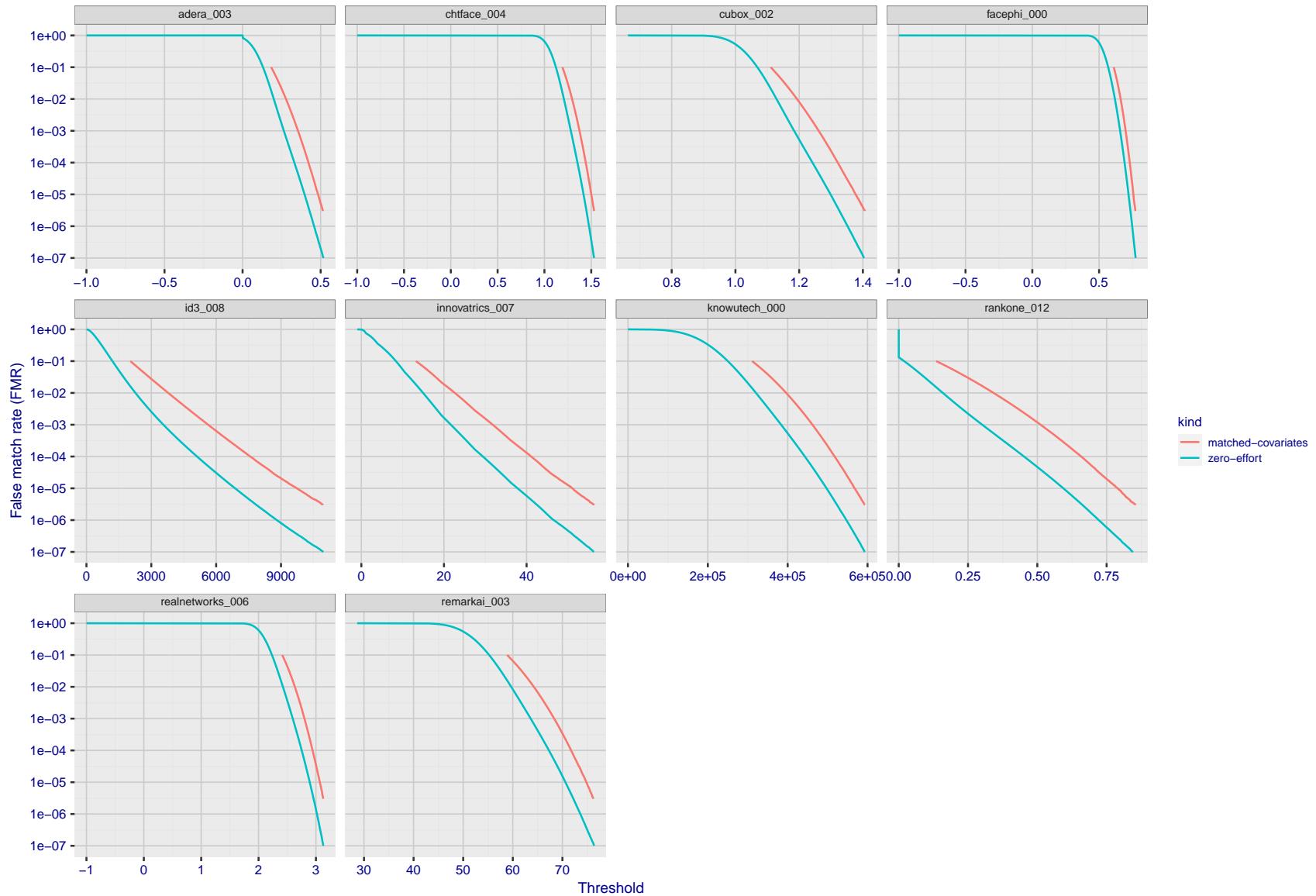


Figure 244: For the visa images, the false match calibration curves show FMR vs. threshold, T . The blue (lower) curves are for zero-effort impostors (i.e. comparing all images against all). The red (upper) curves are for persons of the same-sex, same-age, and same national-origin. This shows that FMR is underestimated (by a factor of 10 or more) by using a zero-effort impostor calculation to calibrate T . As shown later (sec. 3.6), FMR is higher for demographic-matched impostors.

2022/08/30 09:26:06

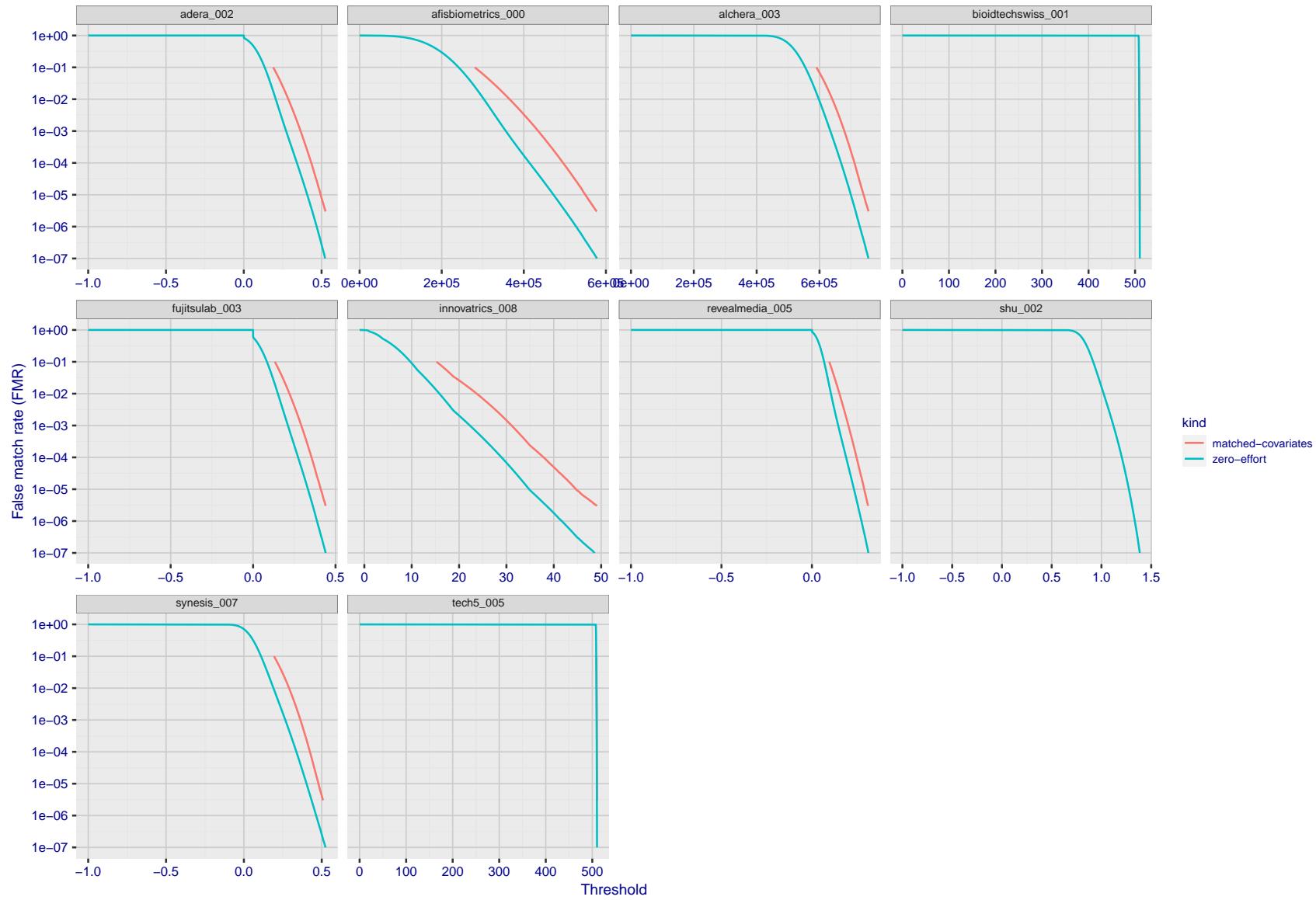


Figure 245: For the visa images, the false match calibration curves show FMR vs. threshold, T . The blue (lower) curves are for zero-effort impostors (i.e. comparing all images against all). The red (upper) curves are for persons of the same-sex, same-age, and same national-origin. This shows that FMR is underestimated (by a factor of 10 or more) by using a zero-effort impostor calculation to calibrate T . As shown later (sec. 3.6), FMR is higher for demographic-matched impostors.

FNMR(T)
"False non-match rate"
"False match rate"

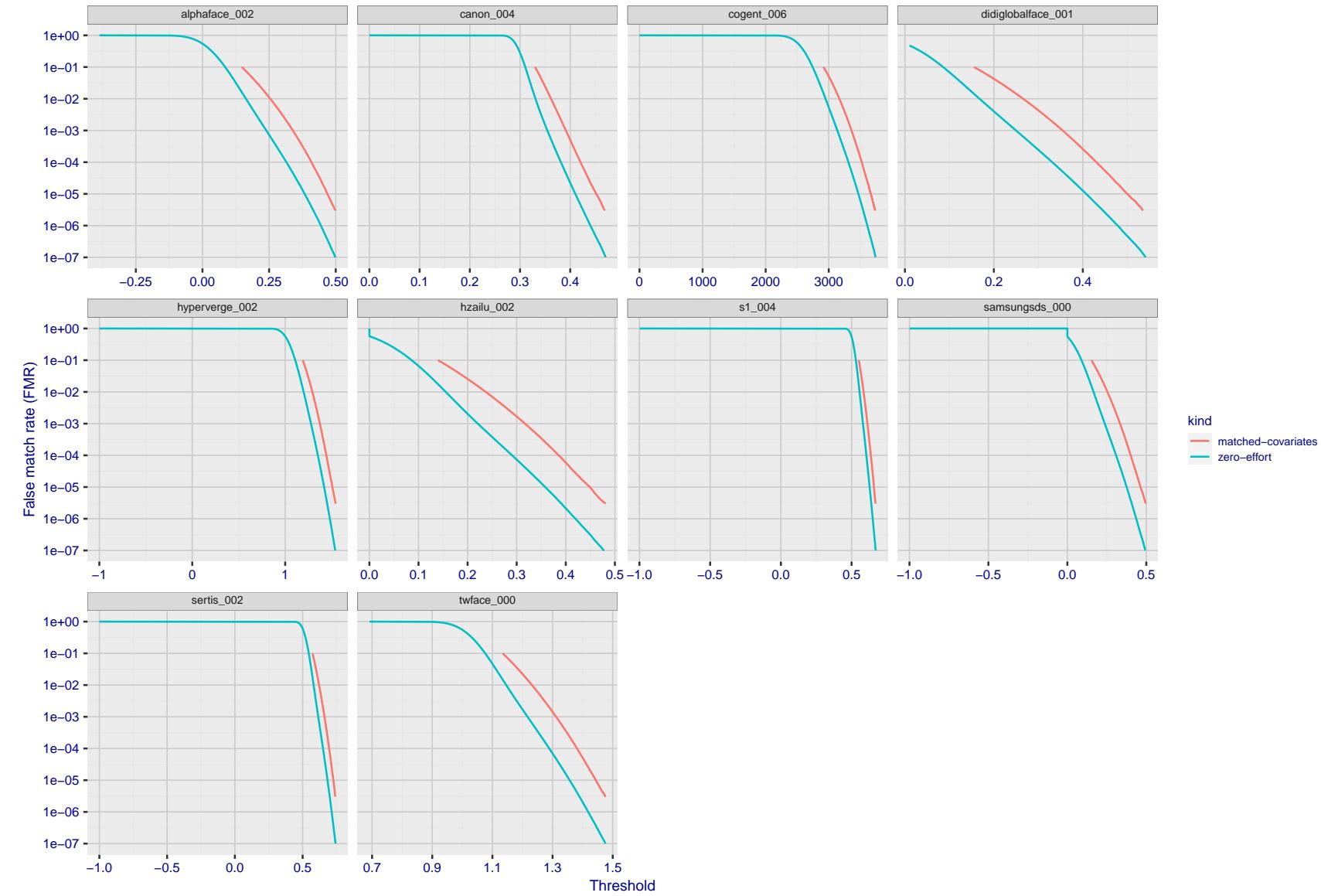


Figure 246: For the visa images, the false match calibration curves show FMR vs. threshold, T . The blue (lower) curves are for zero-effort impostors (i.e. comparing all images against all). The red (upper) curves are for persons of the same-sex, same-age, and same national-origin. This shows that FMR is underestimated (by a factor of 10 or more) by using a zero-effort impostor calculation to calibrate T . As shown later (sec. 3.6), FMR is higher for demographic-matched impostors.

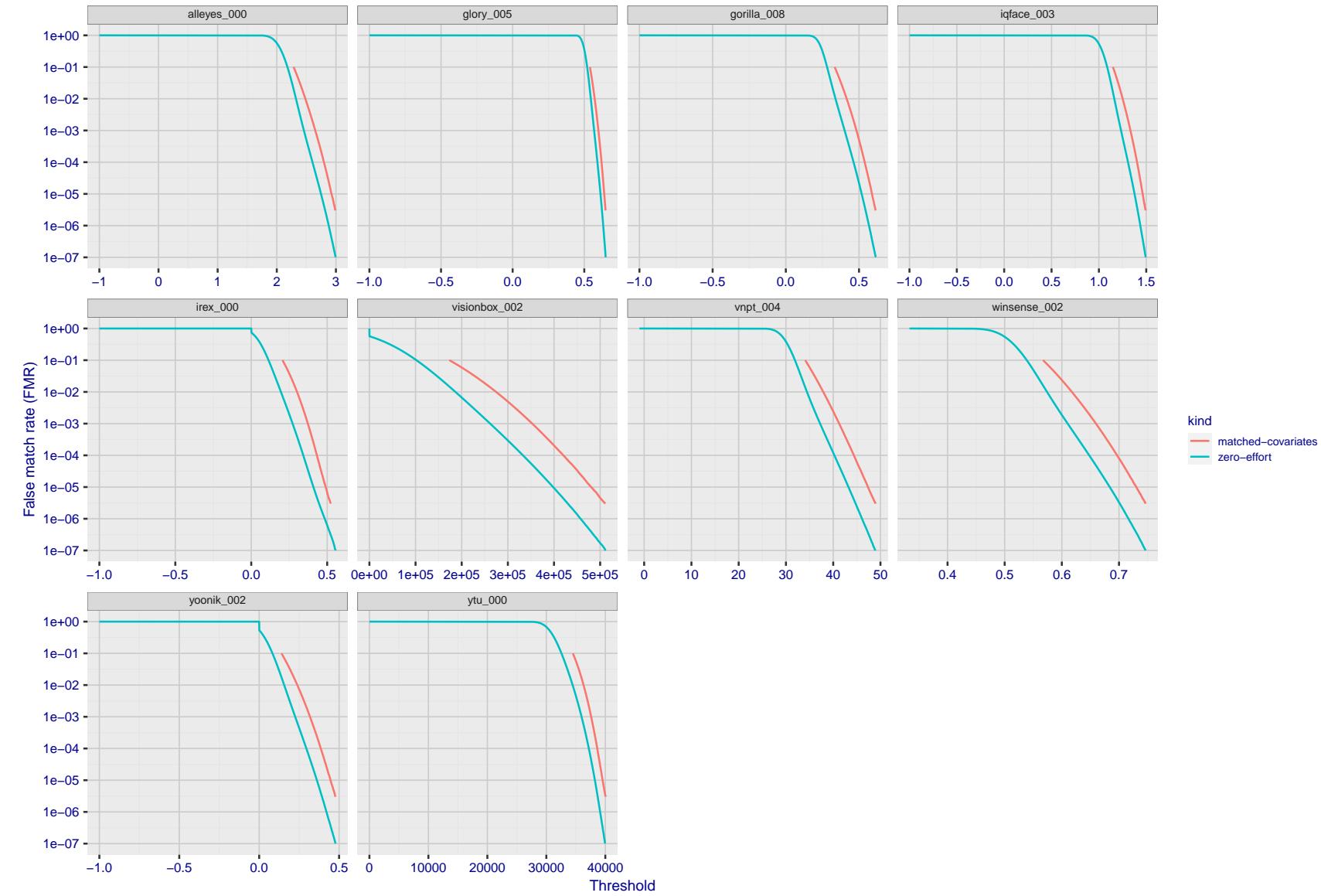


Figure 247: For the visa images, the false match calibration curves show FMR vs. threshold, T . The blue (lower) curves are for zero-effort impostors (i.e. comparing all images against all). The red (upper) curves are for persons of the same-sex, same-age, and same national-origin. This shows that FMR is underestimated (by a factor of 10 or more) by using a zero-effort impostor calculation to calibrate T . As shown later (sec. 3.6), FMR is higher for demographic-matched impostors.

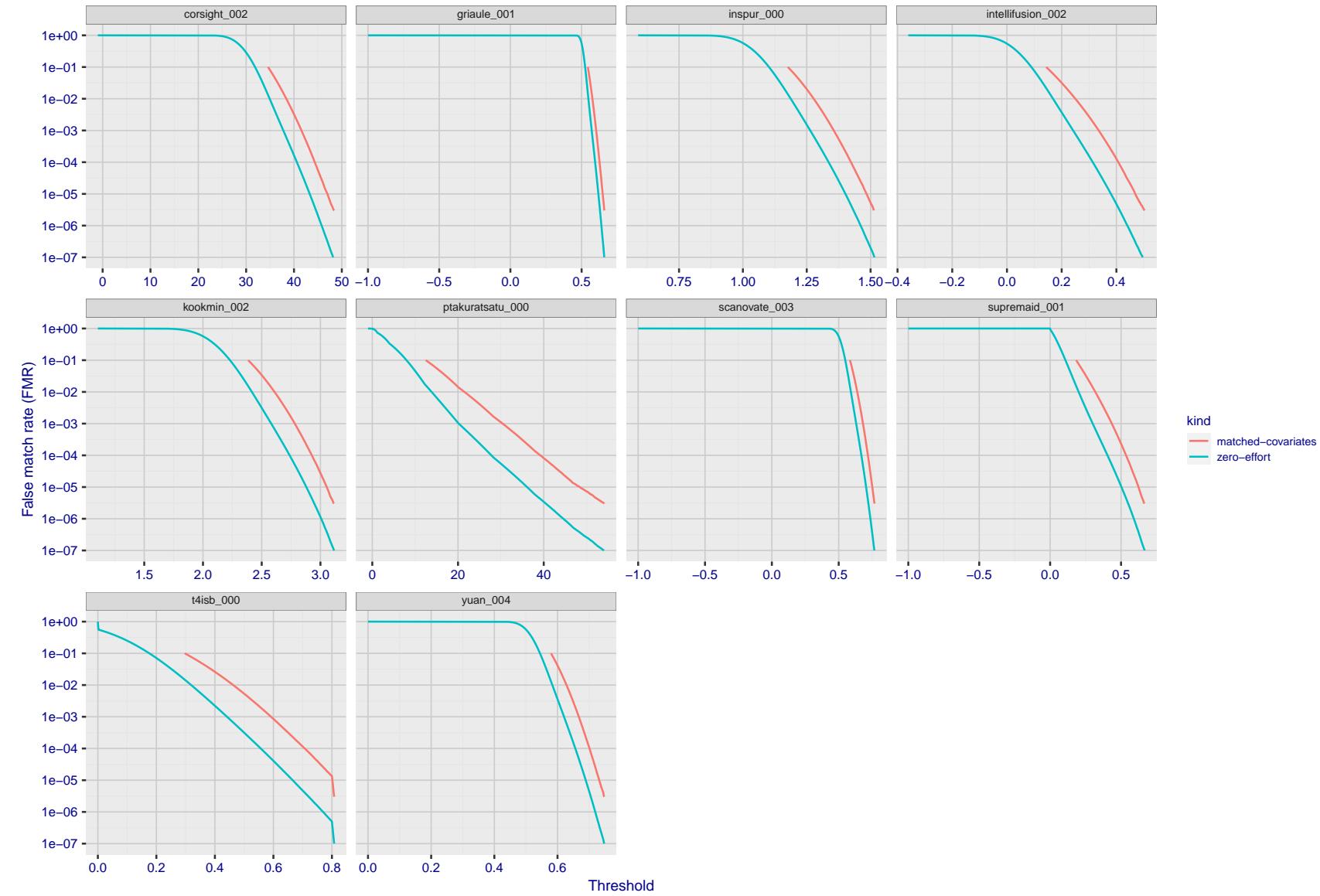


Figure 248: For the visa images, the false match calibration curves show FMR vs. threshold, T . The blue (lower) curves are for zero-effort impostors (i.e. comparing all images against all). The red (upper) curves are for persons of the same-sex, same-age, and same national-origin. This shows that FMR is underestimated (by a factor of 10 or more) by using a zero-effort impostor calculation to calibrate T . As shown later (sec. 3.6), FMR is higher for demographic-matched impostors.

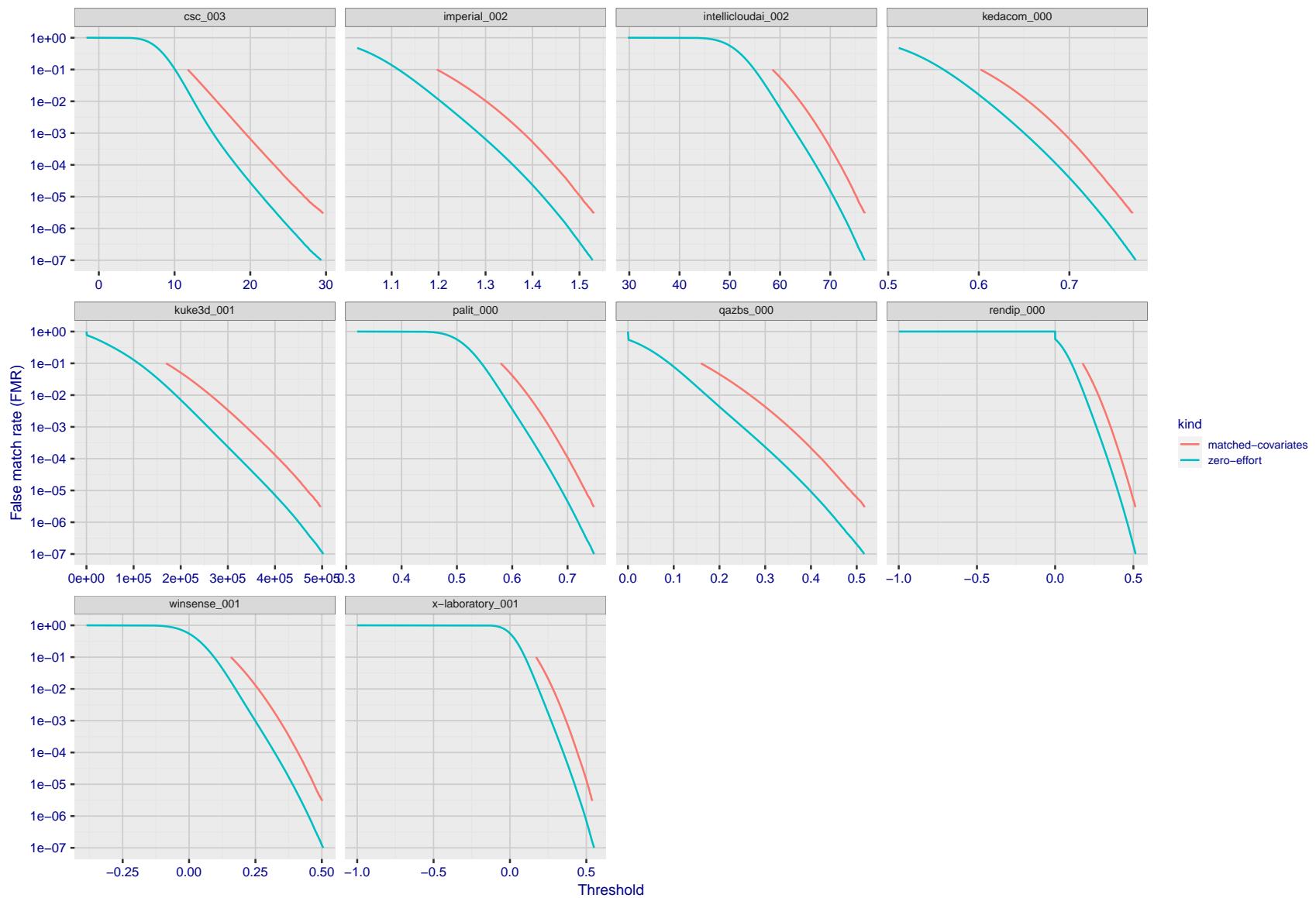


Figure 249: For the visa images, the false match calibration curves show FMR vs. threshold, T . The blue (lower) curves are for zero-effort impostors (i.e. comparing all images against all). The red (upper) curves are for persons of the same-sex, same-age, and same national-origin. This shows that FMR is underestimated (by a factor of 10 or more) by using a zero-effort impostor calculation to calibrate T . As shown later (sec. 3.6), FMR is higher for demographic-matched impostors.

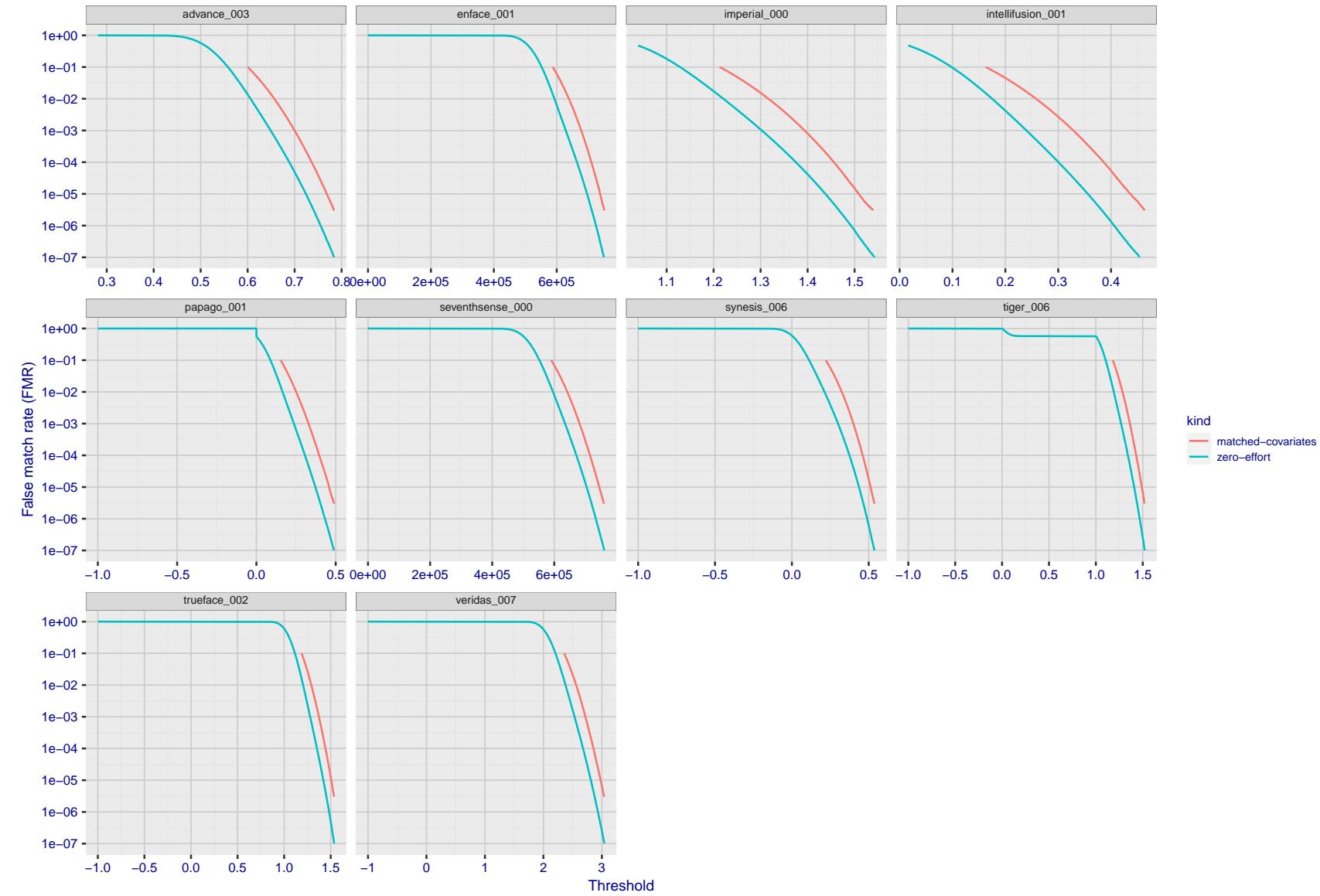


Figure 250: For the visa images, the false match calibration curves show FMR vs. threshold, T . The blue (lower) curves are for zero-effort impostors (i.e. comparing all images against all). The red (upper) curves are for persons of the same-sex, same-age, and same national-origin. This shows that FMR is underestimated (by a factor of 10 or more) by using a zero-effort impostor calculation to calibrate T . As shown later (sec. 3.6), FMR is higher for demographic-matched impostors.

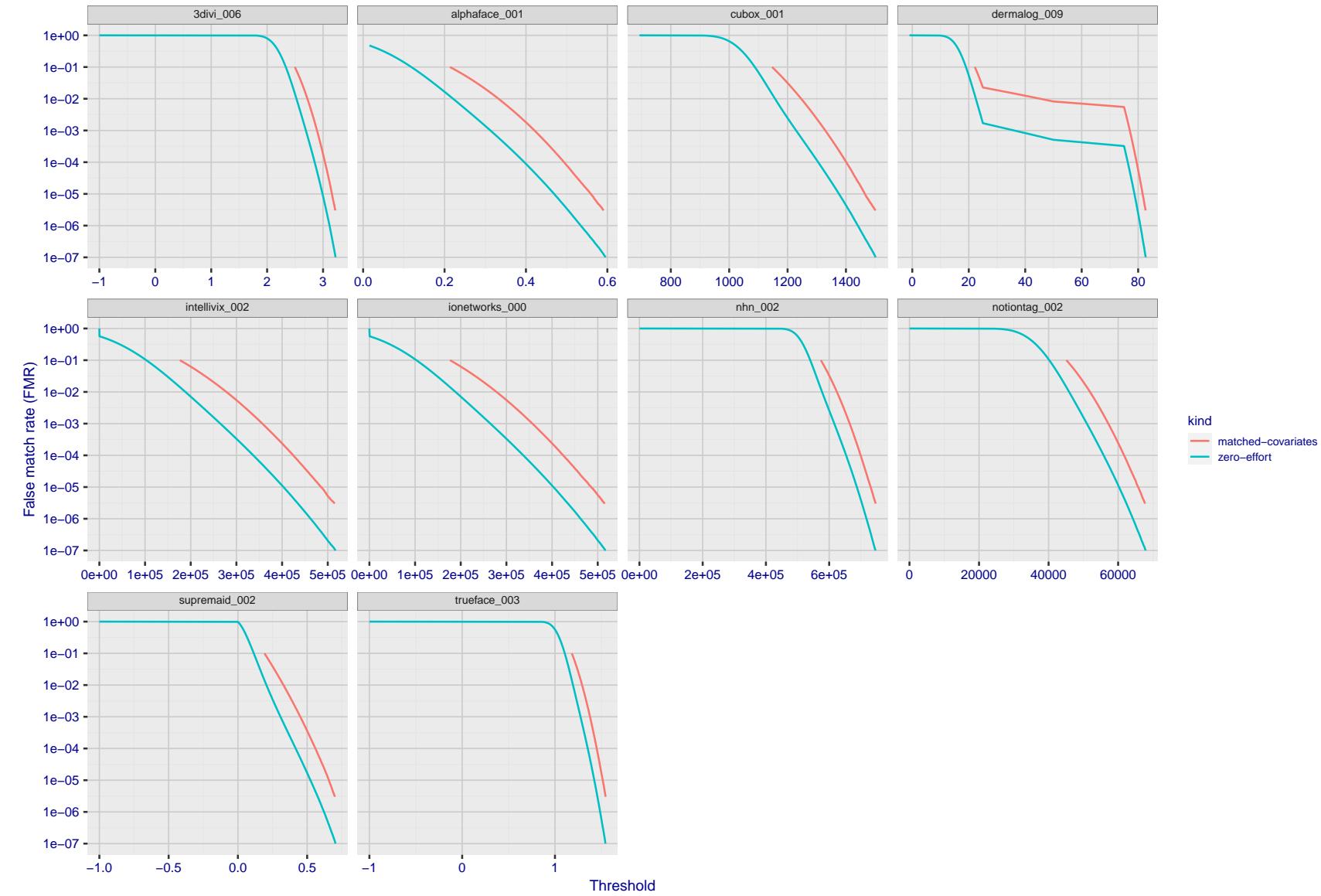


Figure 251: For the visa images, the false match calibration curves show FMR vs. threshold, T . The blue (lower) curves are for zero-effort impostors (i.e. comparing all images against all). The red (upper) curves are for persons of the same-sex, same-age, and same national-origin. This shows that FMR is underestimated (by a factor of 10 or more) by using a zero-effort impostor calculation to calibrate T . As shown later (sec. 3.6), FMR is higher for demographic-matched impostors.

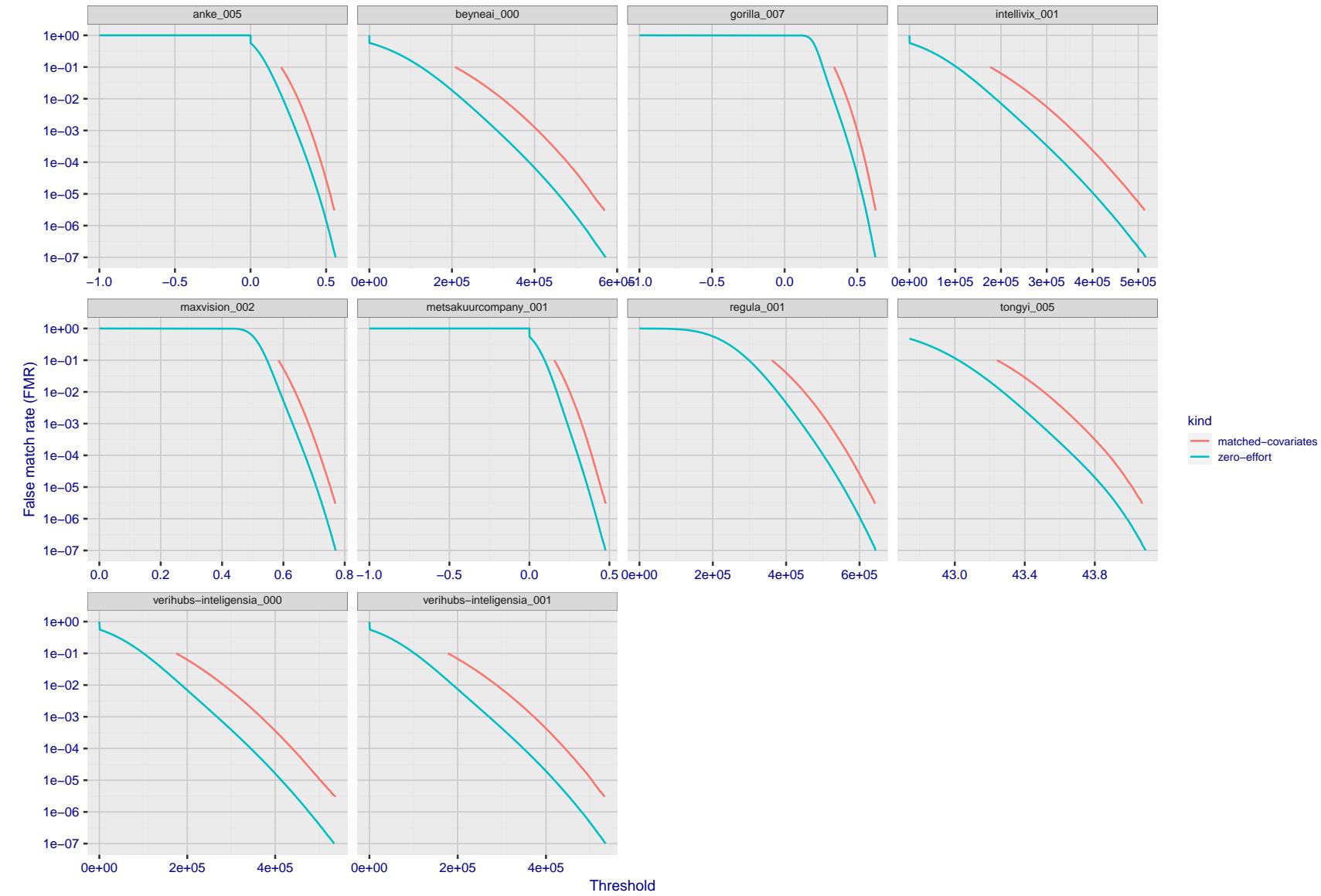


Figure 252: For the visa images, the false match calibration curves show FMR vs. threshold, T . The blue (lower) curves are for zero-effort impostors (i.e. comparing all images against all). The red (upper) curves are for persons of the same-sex, same-age, and same national-origin. This shows that FMR is underestimated (by a factor of 10 or more) by using a zero-effort impostor calculation to calibrate T . As shown later (sec. 3.6), FMR is higher for demographic-matched impostors.

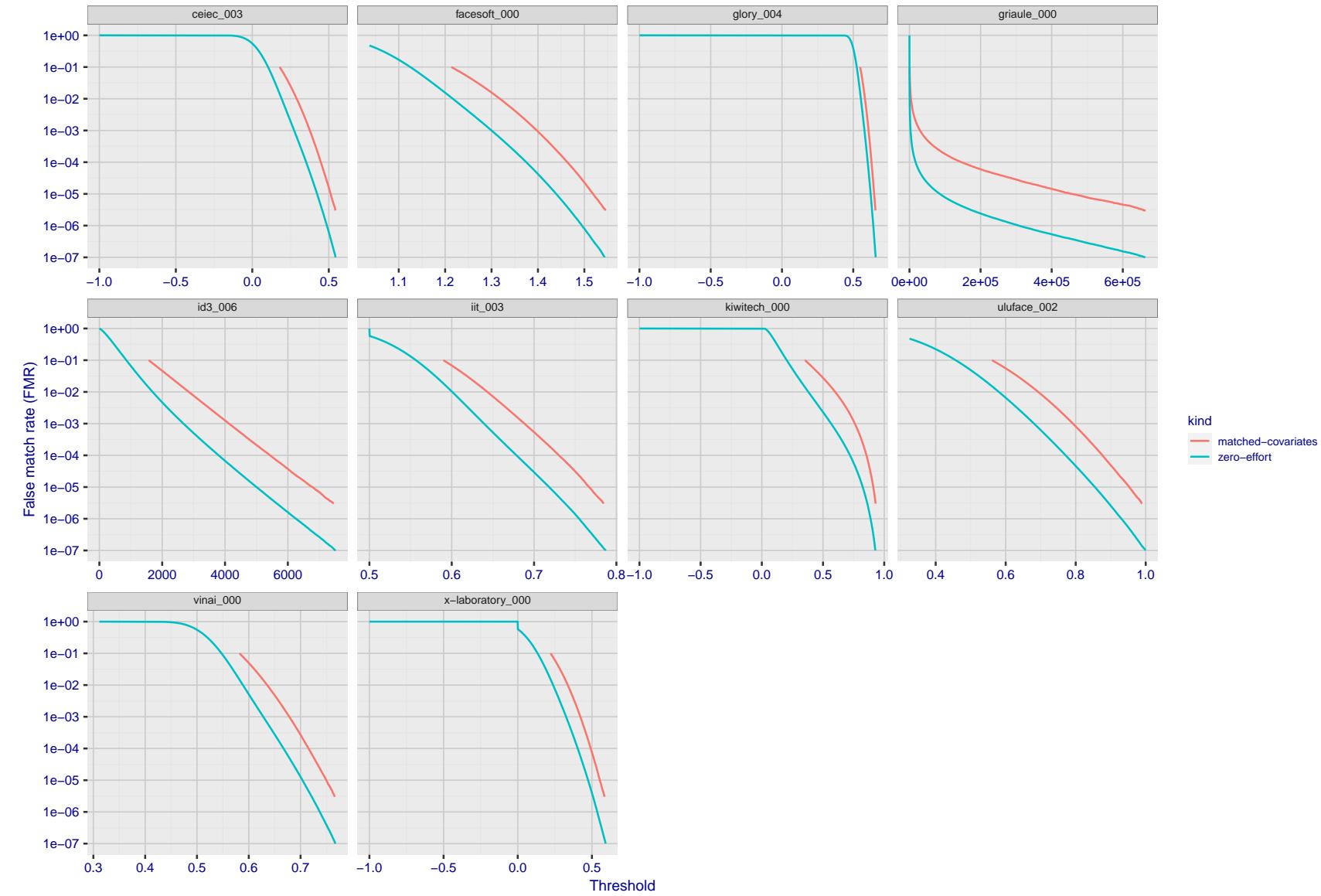


Figure 253: For the visa images, the false match calibration curves show FMR vs. threshold, T . The blue (lower) curves are for zero-effort impostors (i.e. comparing all images against all). The red (upper) curves are for persons of the same-sex, same-age, and same national-origin. This shows that FMR is underestimated (by a factor of 10 or more) by using a zero-effort impostor calculation to calibrate T . As shown later (sec. 3.6), FMR is higher for demographic-matched impostors.

2022/08/30 09:26:06

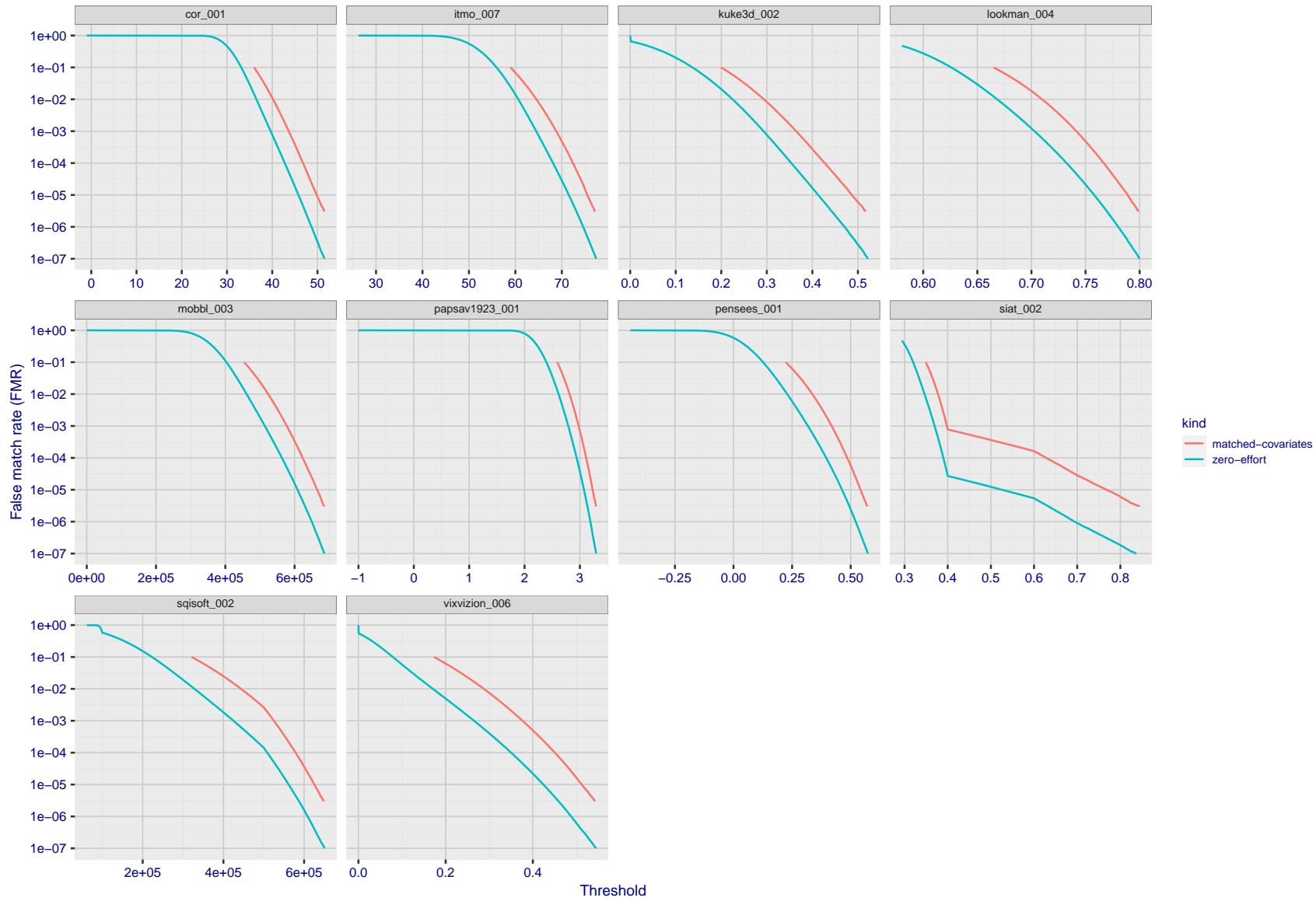


Figure 254: For the visa images, the false match calibration curves show FMR vs. threshold, T . The blue (lower) curves are for zero-effort impostors (i.e. comparing all images against all). The red (upper) curves are for persons of the same-sex, same-age, and same national-origin. This shows that FMR is underestimated (by a factor of 10 or more) by using a zero-effort impostor calculation to calibrate T . As shown later (sec. 3.6), FMR is higher for demographic-matched impostors.

FNMR(T)
"False non-match rate"
"False match rate"

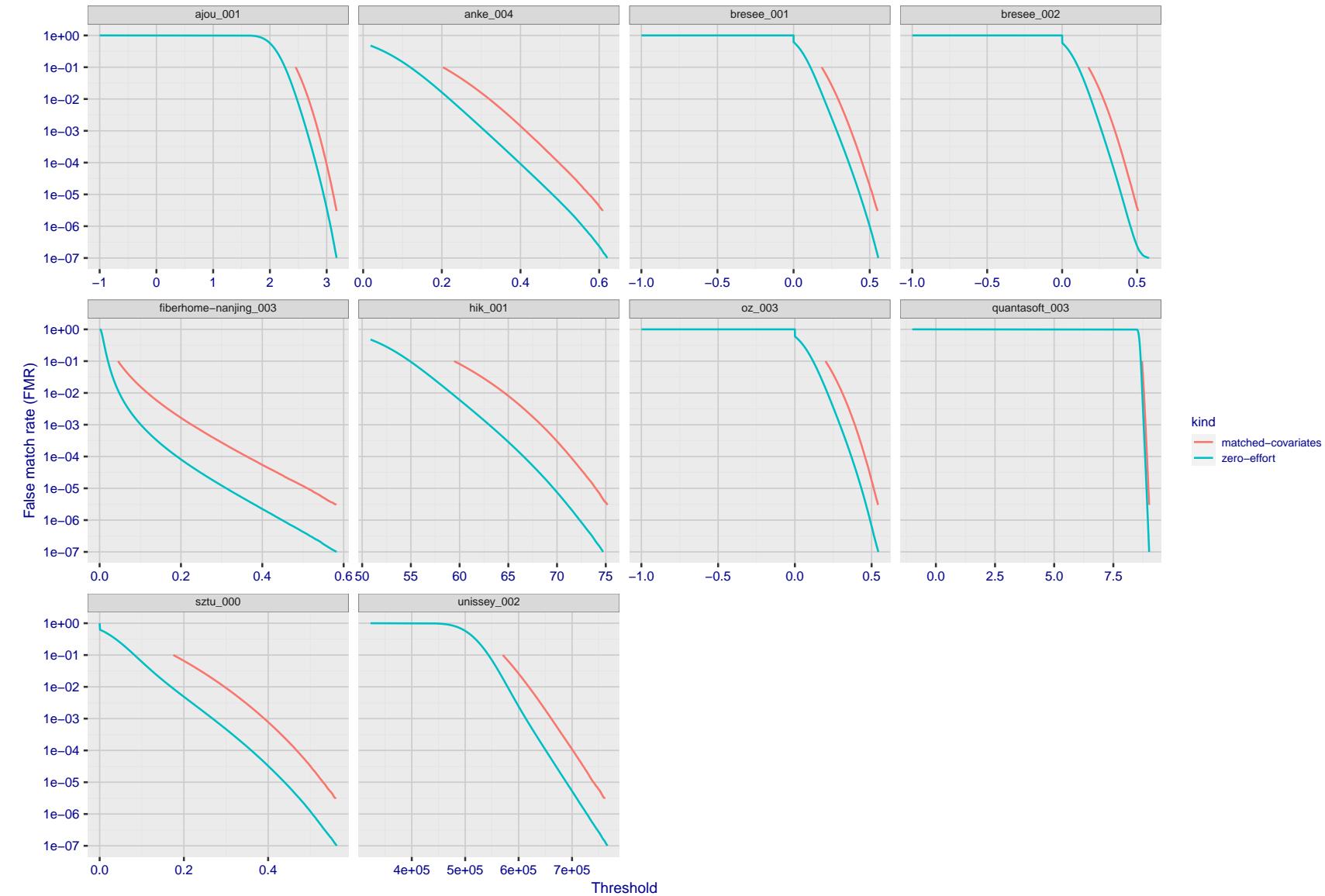


Figure 255: For the visa images, the false match calibration curves show FMR vs. threshold, T . The blue (lower) curves are for zero-effort impostors (i.e. comparing all images against all). The red (upper) curves are for persons of the same-sex, same-age, and same national-origin. This shows that FMR is underestimated (by a factor of 10 or more) by using a zero-effort impostor calculation to calibrate T . As shown later (sec. 3.6), FMR is higher for demographic-matched impostors.

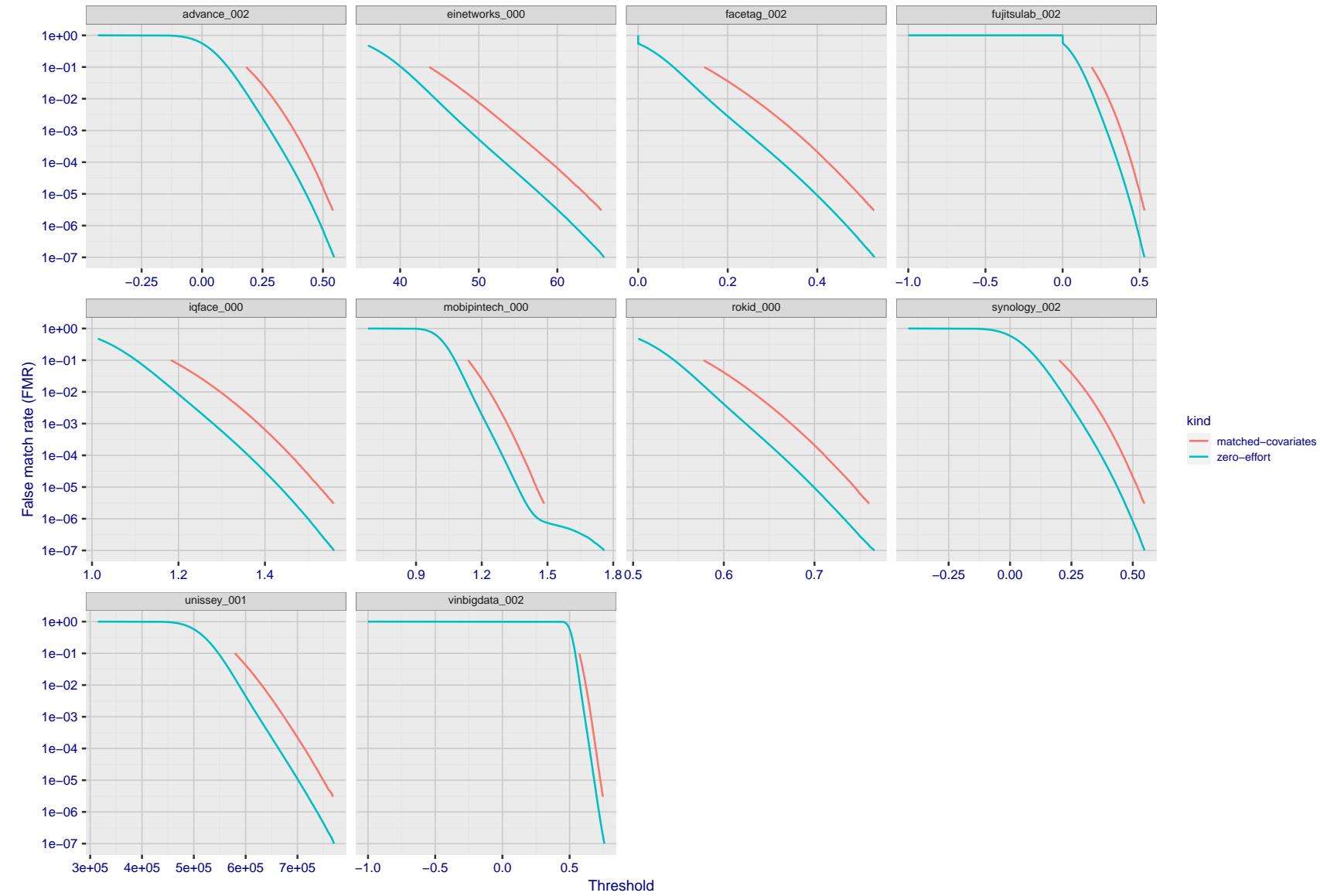


Figure 256: For the visa images, the false match calibration curves show FMR vs. threshold, T . The blue (lower) curves are for zero-effort impostors (i.e. comparing all images against all). The red (upper) curves are for persons of the same-sex, same-age, and same national-origin. This shows that FMR is underestimated (by a factor of 10 or more) by using a zero-effort impostor calculation to calibrate T . As shown later (sec. 3.6), FMR is higher for demographic-matched impostors.

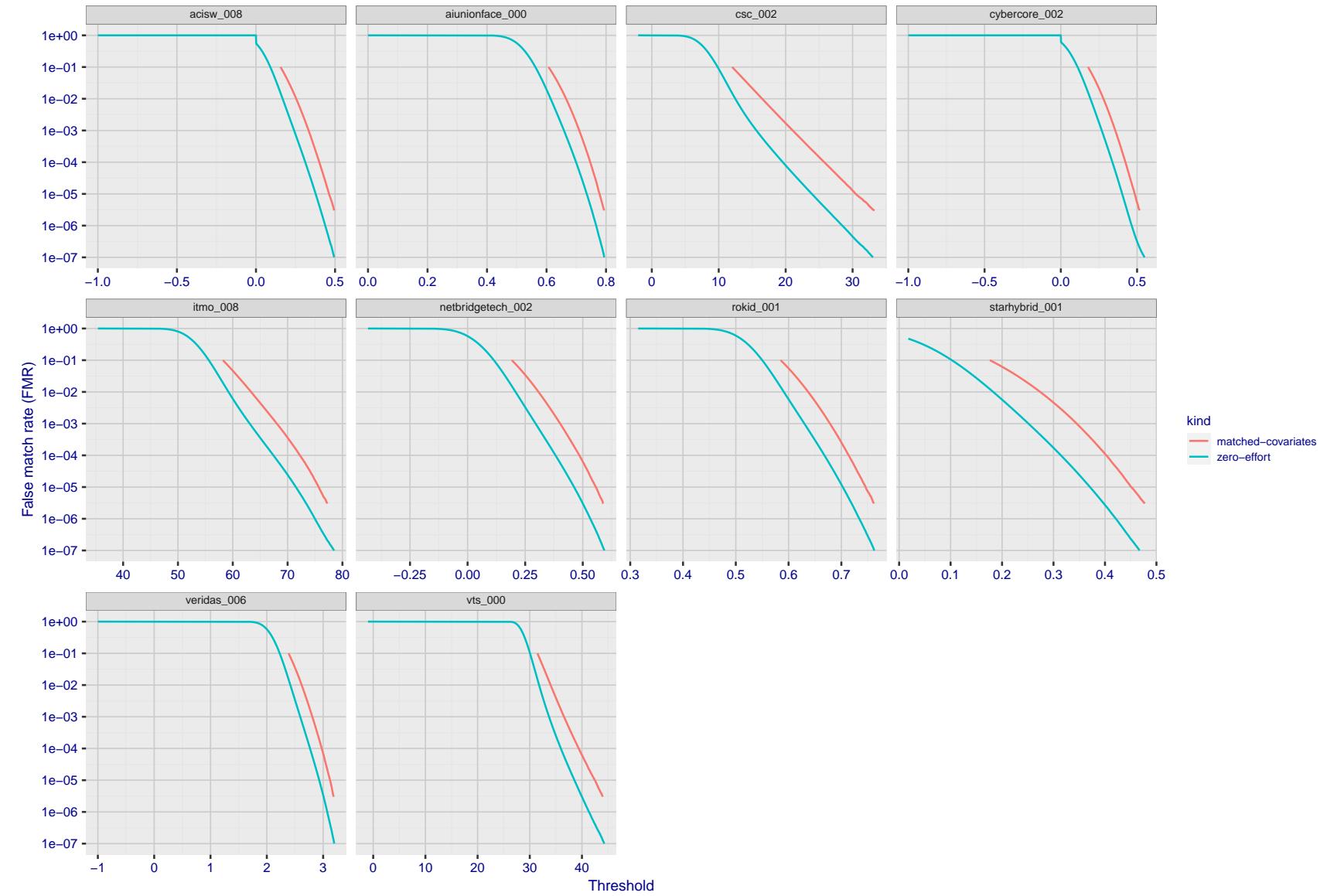


Figure 257: For the visa images, the false match calibration curves show FMR vs. threshold, T . The blue (lower) curves are for zero-effort impostors (i.e. comparing all images against all). The red (upper) curves are for persons of the same-sex, same-age, and same national-origin. This shows that FMR is underestimated (by a factor of 10 or more) by using a zero-effort impostor calculation to calibrate T . As shown later (sec. 3.6), FMR is higher for demographic-matched impostors.

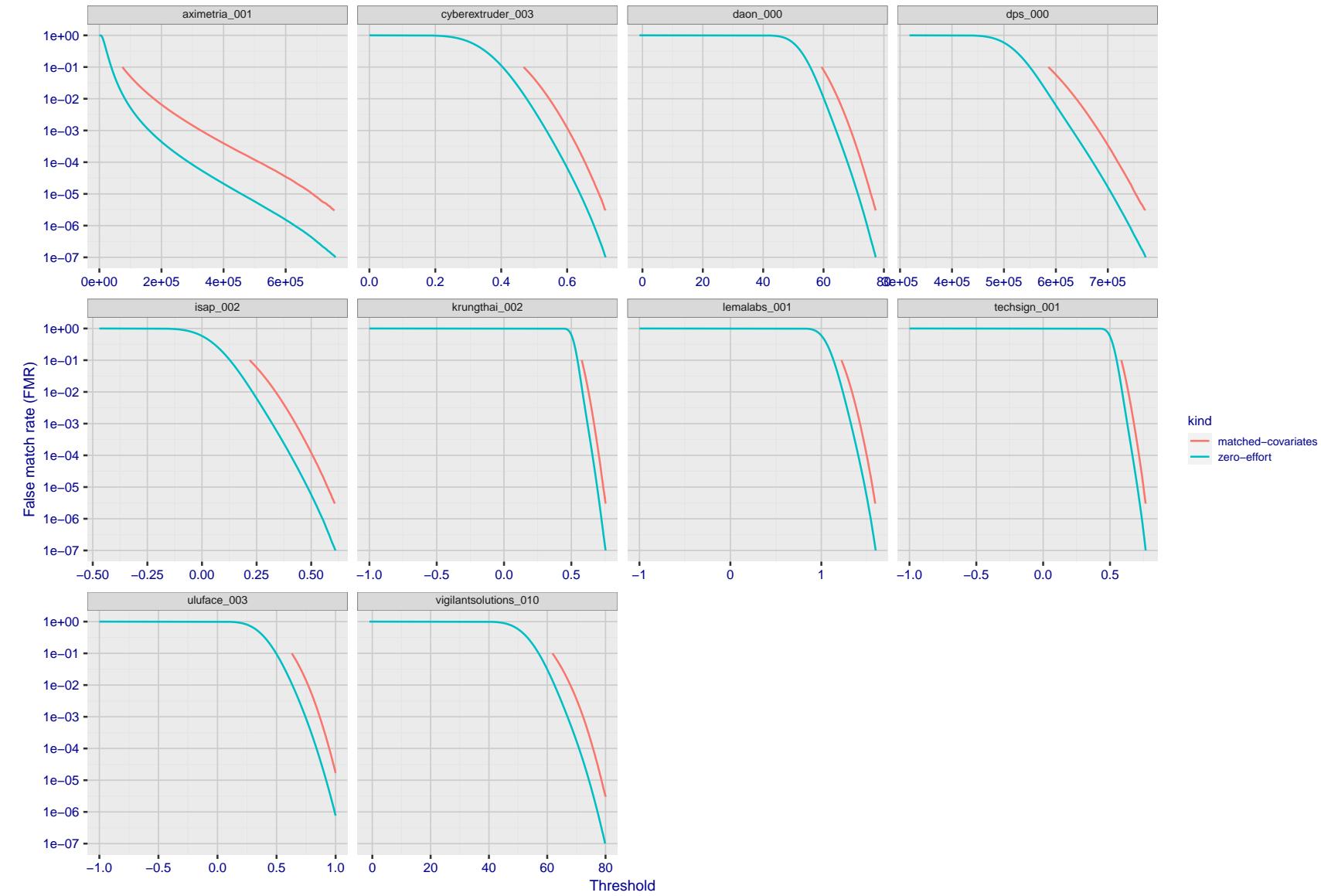


Figure 258: For the visa images, the false match calibration curves show FMR vs. threshold, T . The blue (lower) curves are for zero-effort impostors (i.e. comparing all images against all). The red (upper) curves are for persons of the same-sex, same-age, and same national-origin. This shows that FMR is underestimated (by a factor of 10 or more) by using a zero-effort impostor calculation to calibrate T . As shown later (sec. 3.6), FMR is higher for demographic-matched impostors.

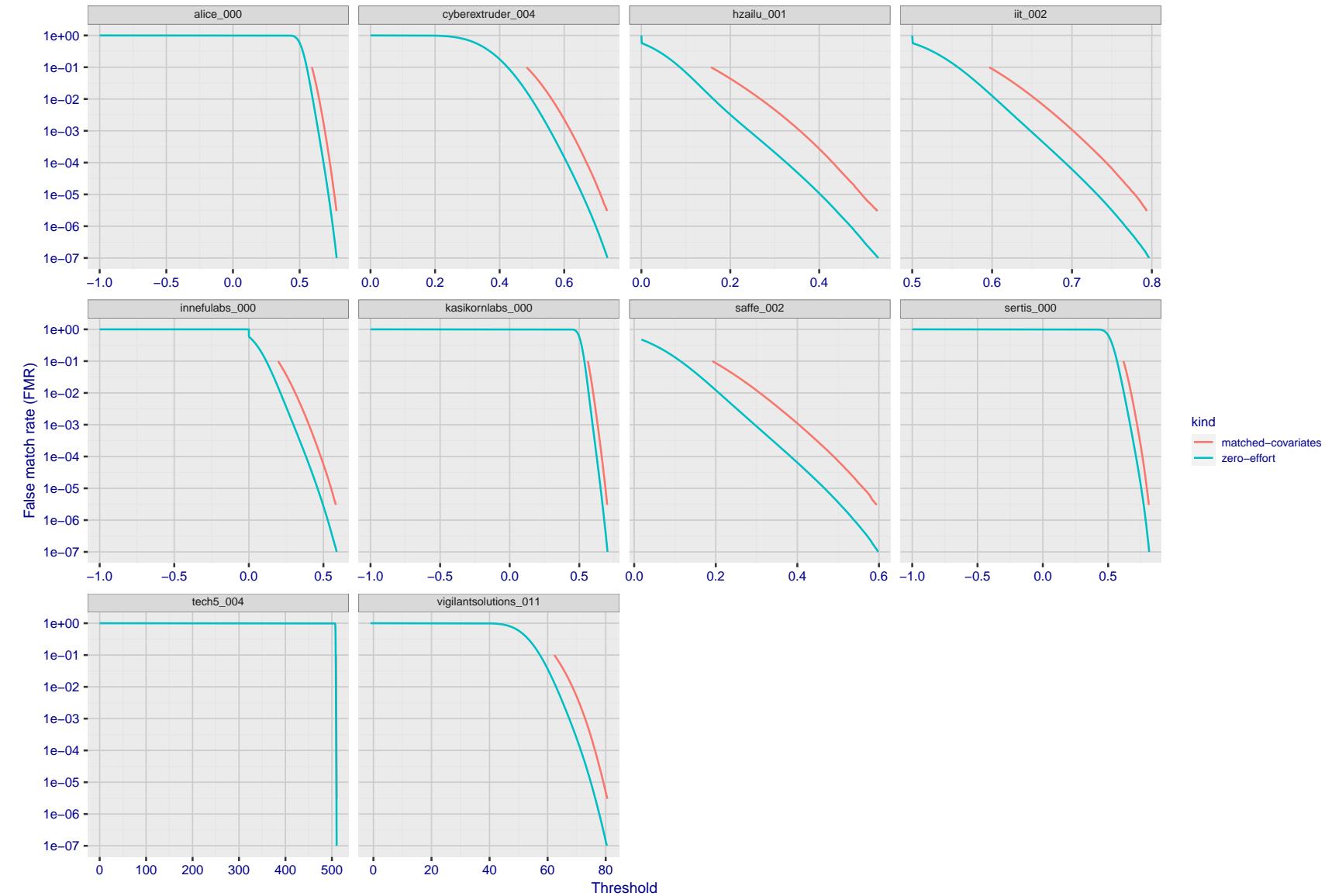


Figure 259: For the visa images, the false match calibration curves show FMR vs. threshold, T . The blue (lower) curves are for zero-effort impostors (i.e. comparing all images against all). The red (upper) curves are for persons of the same-sex, same-age, and same national-origin. This shows that FMR is underestimated (by a factor of 10 or more) by using a zero-effort impostor calculation to calibrate T . As shown later (sec. 3.6), FMR is higher for demographic-matched impostors.

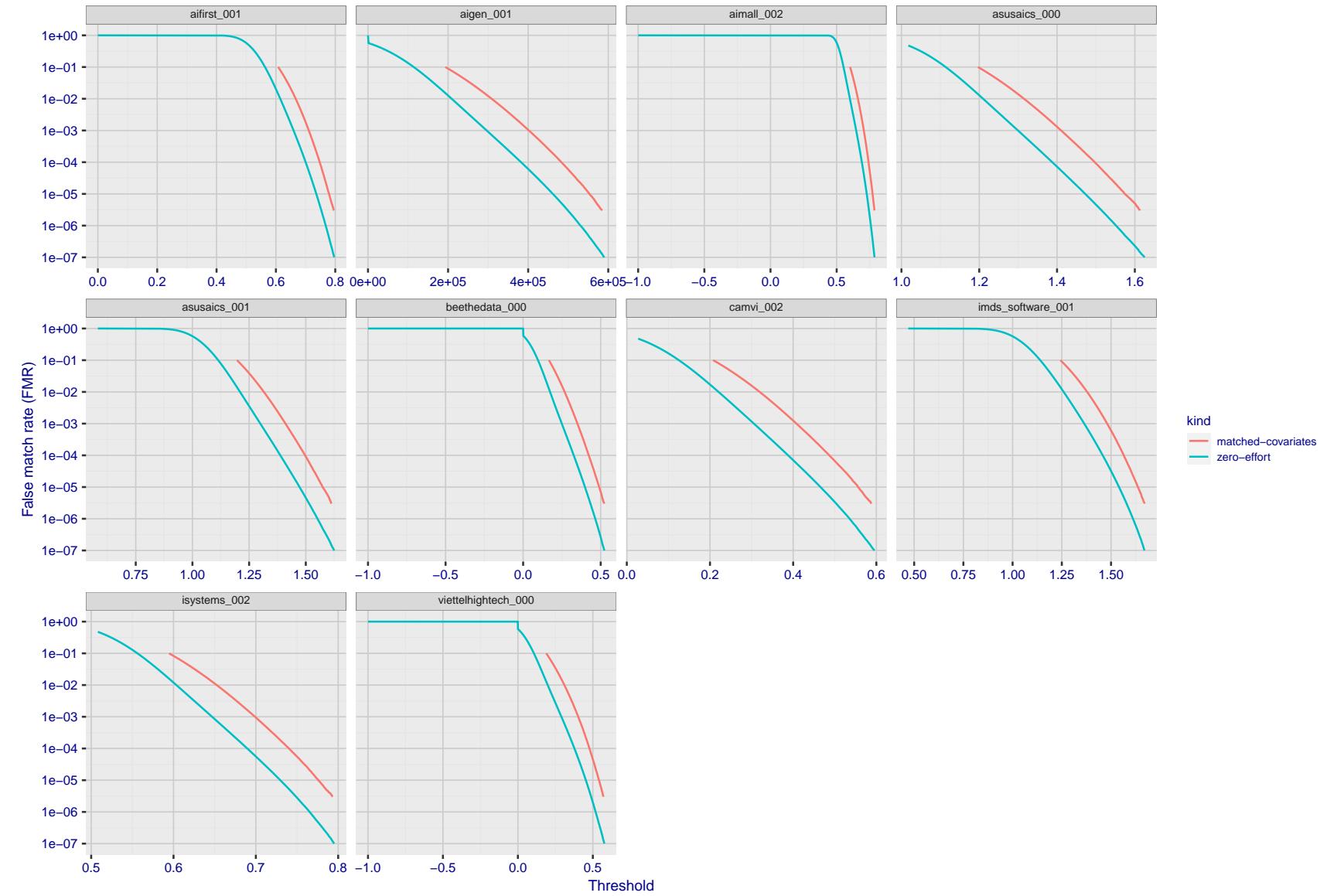


Figure 260: For the visa images, the false match calibration curves show FMR vs. threshold, T . The blue (lower) curves are for zero-effort impostors (i.e. comparing all images against all). The red (upper) curves are for persons of the same-sex, same-age, and same national-origin. This shows that FMR is underestimated (by a factor of 10 or more) by using a zero-effort impostor calculation to calibrate T . As shown later (sec. 3.6), FMR is higher for demographic-matched impostors.

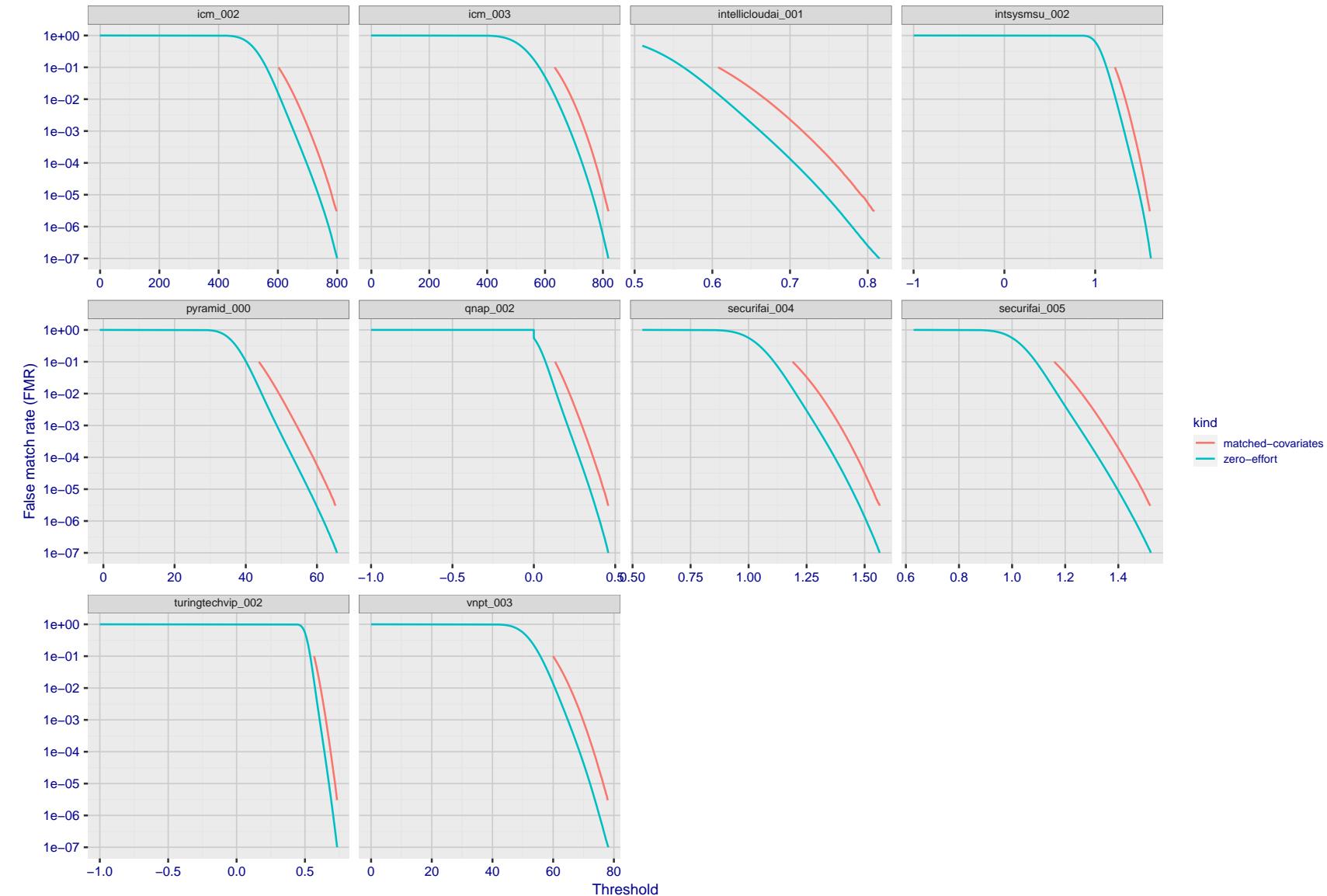


Figure 261: For the visa images, the false match calibration curves show FMR vs. threshold, T . The blue (lower) curves are for zero-effort impostors (i.e. comparing all images against all). The red (upper) curves are for persons of the same-sex, same-age, and same national-origin. This shows that FMR is underestimated (by a factor of 10 or more) by using a zero-effort impostor calculation to calibrate T . As shown later (sec. 3.6), FMR is higher for demographic-matched impostors.

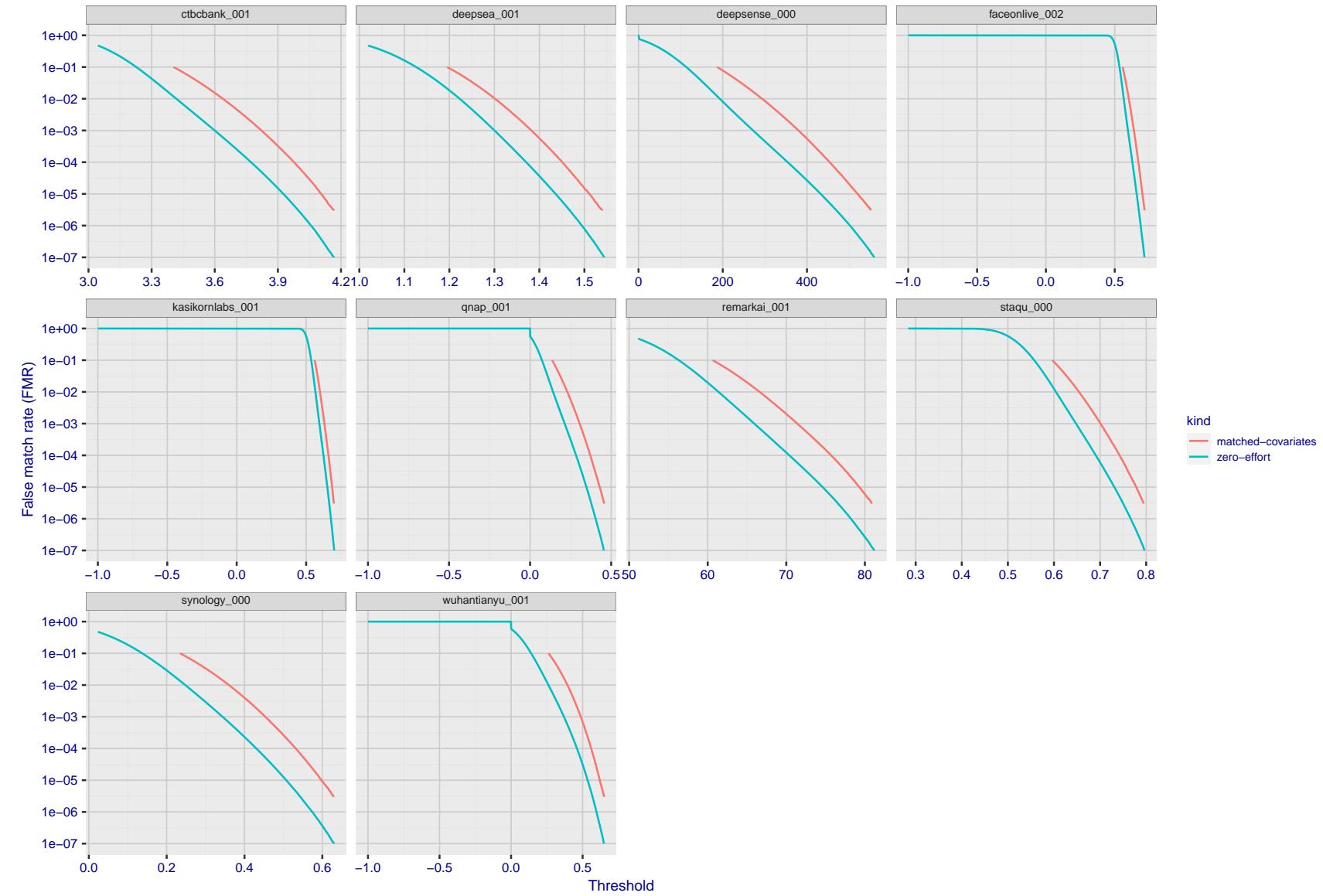


Figure 262: For the visa images, the false match calibration curves show FMR vs. threshold, T . The blue (lower) curves are for zero-effort impostors (i.e. comparing all images against all). The red (upper) curves are for persons of the same-sex, same-age, and same national-origin. This shows that FMR is underestimated (by a factor of 10 or more) by using a zero-effort impostor calculation to calibrate T . As shown later (sec. 3.6), FMR is higher for demographic-matched impostors.

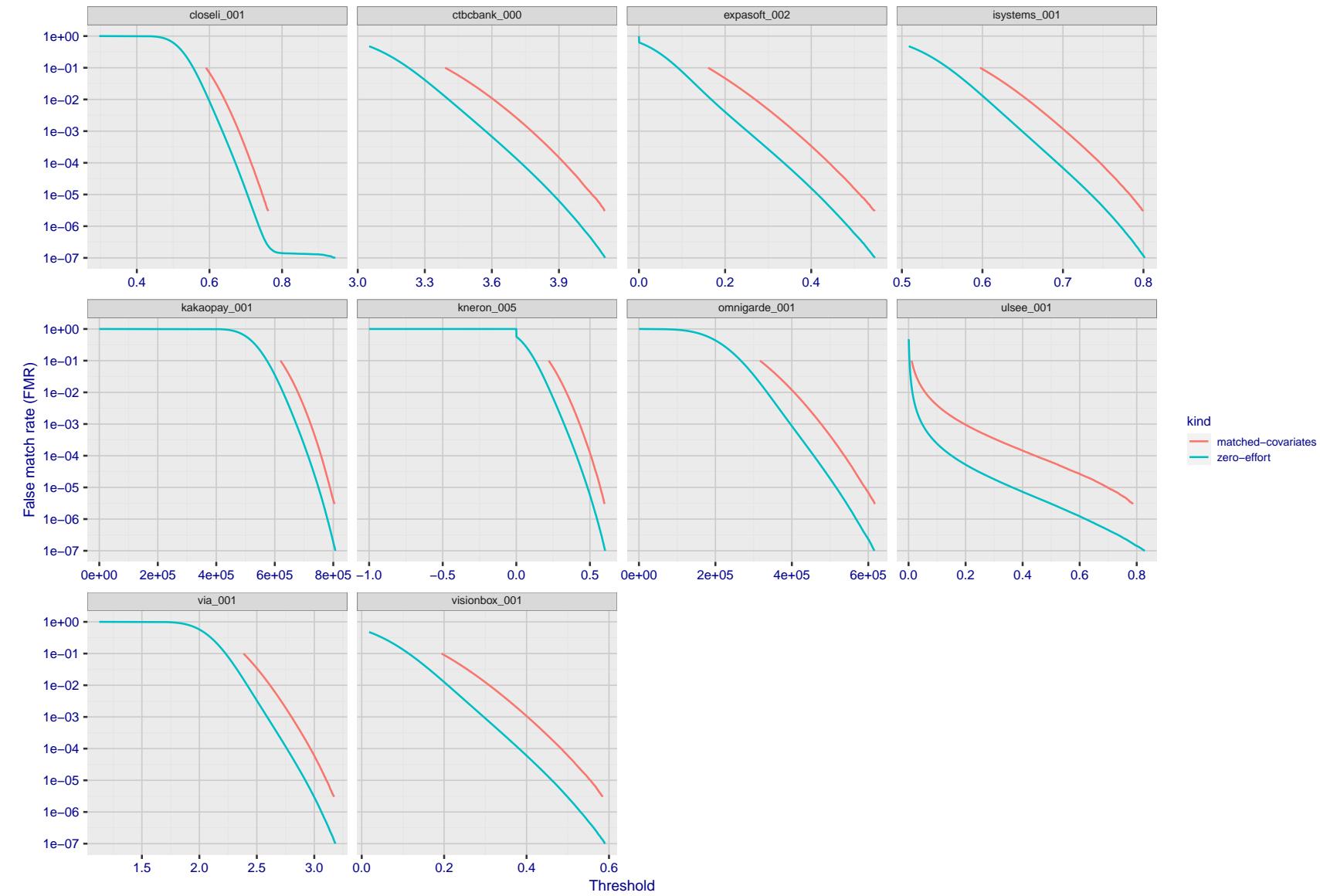


Figure 263: For the visa images, the false match calibration curves show FMR vs. threshold, T . The blue (lower) curves are for zero-effort impostors (i.e. comparing all images against all). The red (upper) curves are for persons of the same-sex, same-age, and same national-origin. This shows that FMR is underestimated (by a factor of 10 or more) by using a zero-effort impostor calculation to calibrate T . As shown later (sec. 3.6), FMR is higher for demographic-matched impostors.

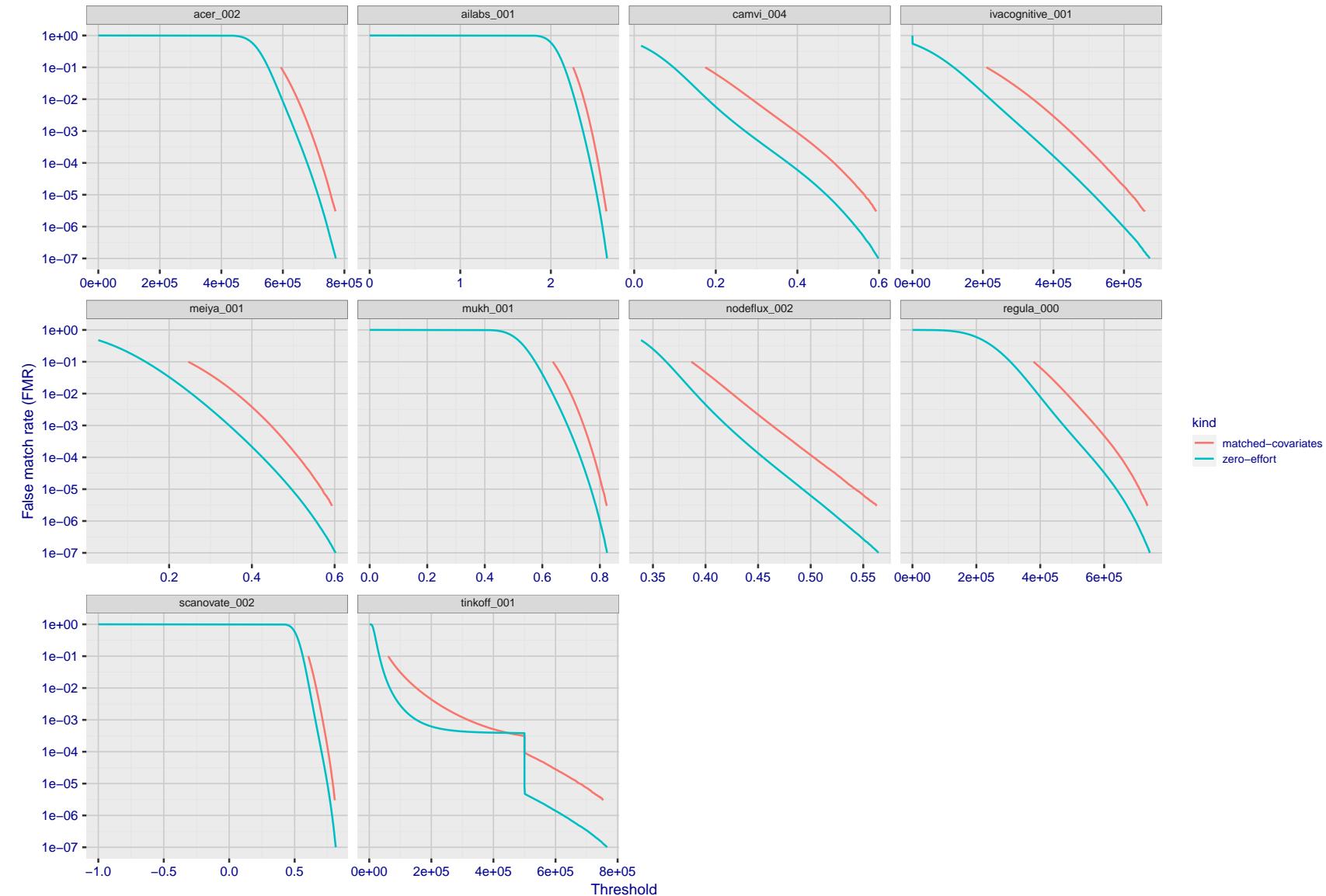


Figure 264: For the visa images, the false match calibration curves show FMR vs. threshold, T . The blue (lower) curves are for zero-effort impostors (i.e. comparing all images against all). The red (upper) curves are for persons of the same-sex, same-age, and same national-origin. This shows that FMR is underestimated (by a factor of 10 or more) by using a zero-effort impostor calculation to calibrate T . As shown later (sec. 3.6), FMR is higher for demographic-matched impostors.

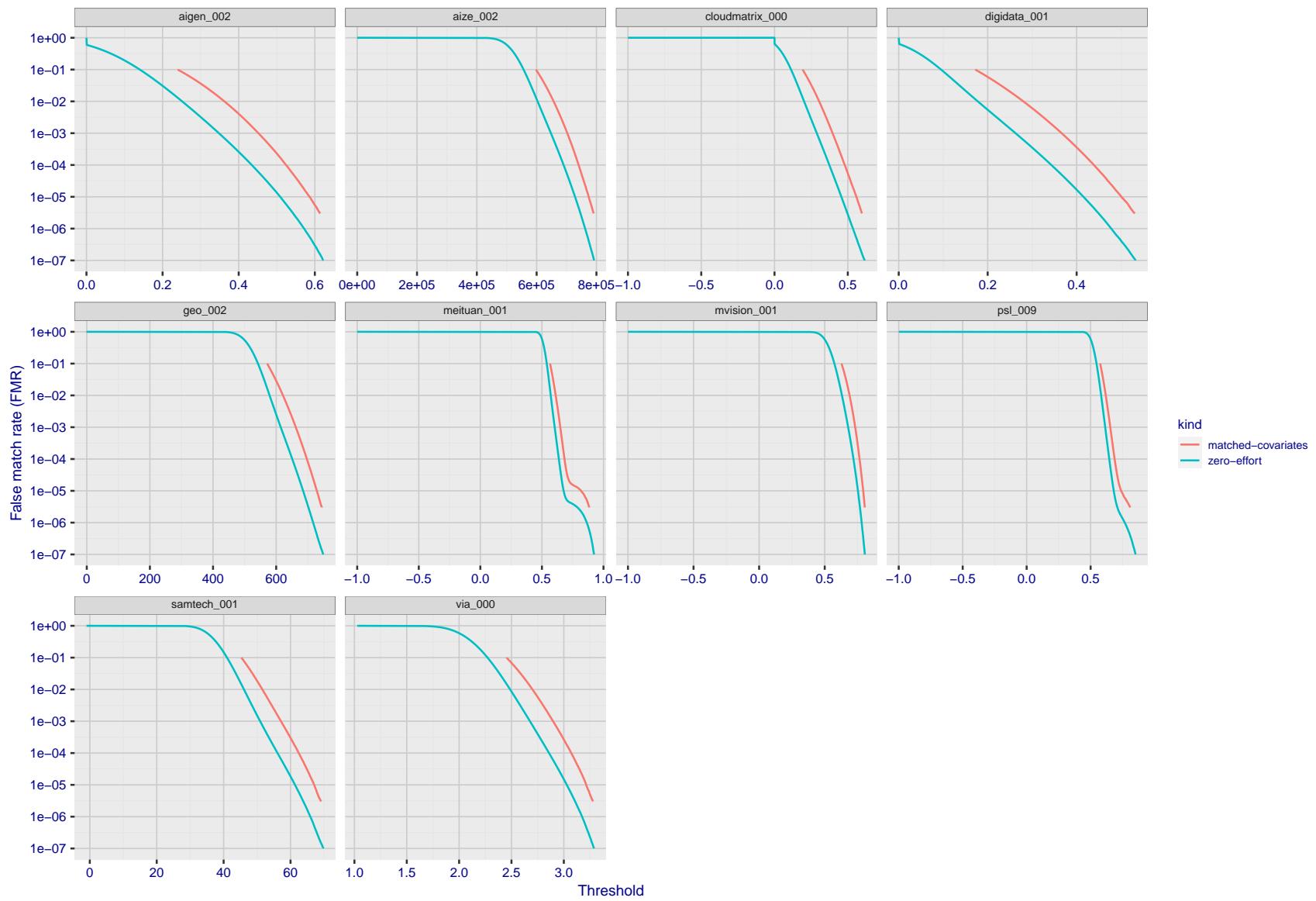


Figure 265: For the visa images, the false match calibration curves show FMR vs. threshold, T . The blue (lower) curves are for zero-effort impostors (i.e. comparing all images against all). The red (upper) curves are for persons of the same-sex, same-age, and same national-origin. This shows that FMR is underestimated (by a factor of 10 or more) by using a zero-effort impostor calculation to calibrate T . As shown later (sec. 3.6), FMR is higher for demographic-matched impostors.

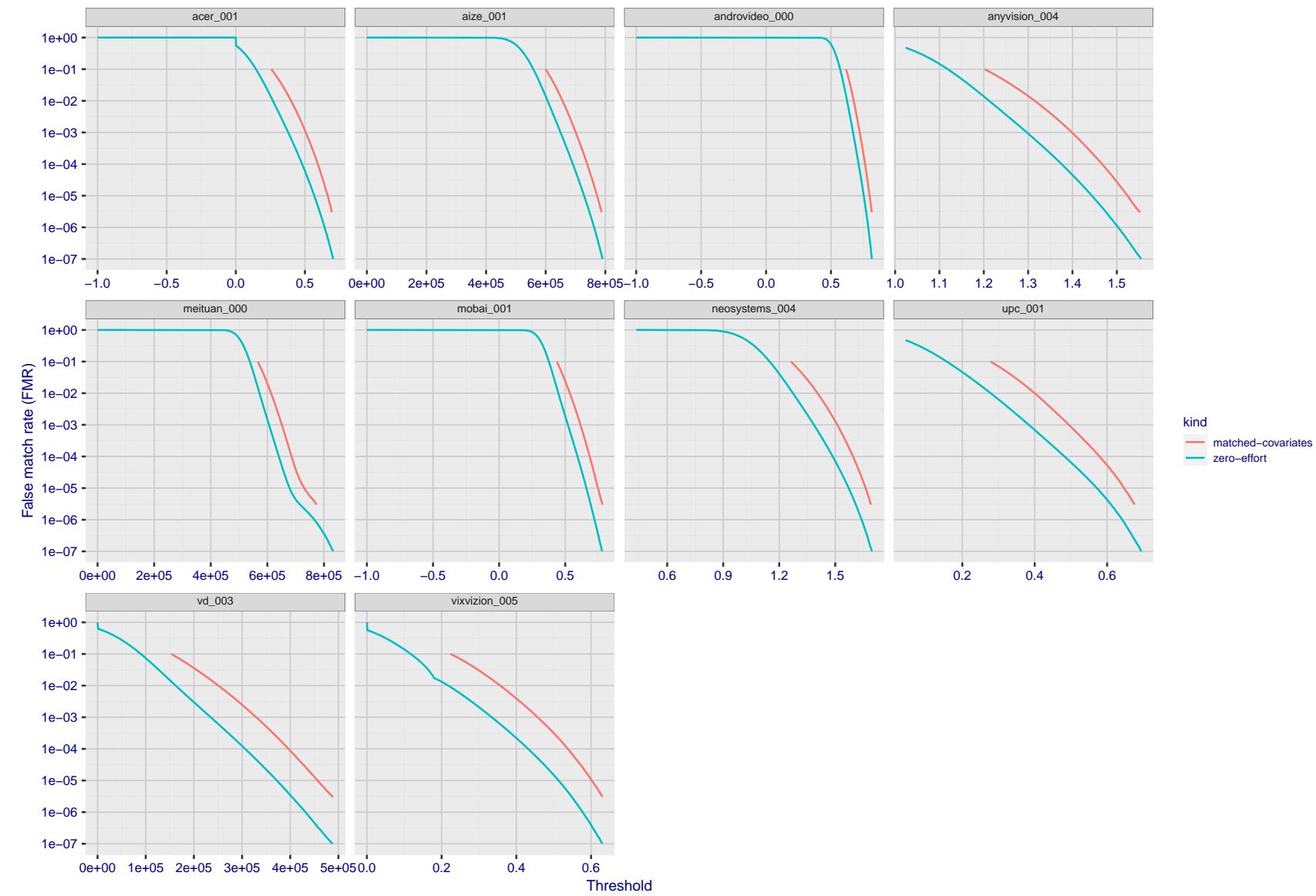


Figure 266: For the visa images, the false match calibration curves show FMR vs. threshold, T . The blue (lower) curves are for zero-effort impostors (i.e. comparing all images against all). The red (upper) curves are for persons of the same-sex, same-age, and same national-origin. This shows that FMR is underestimated (by a factor of 10 or more) by using a zero-effort impostor calculation to calibrate T . As shown later (sec. 3.6), FMR is higher for demographic-matched impostors.

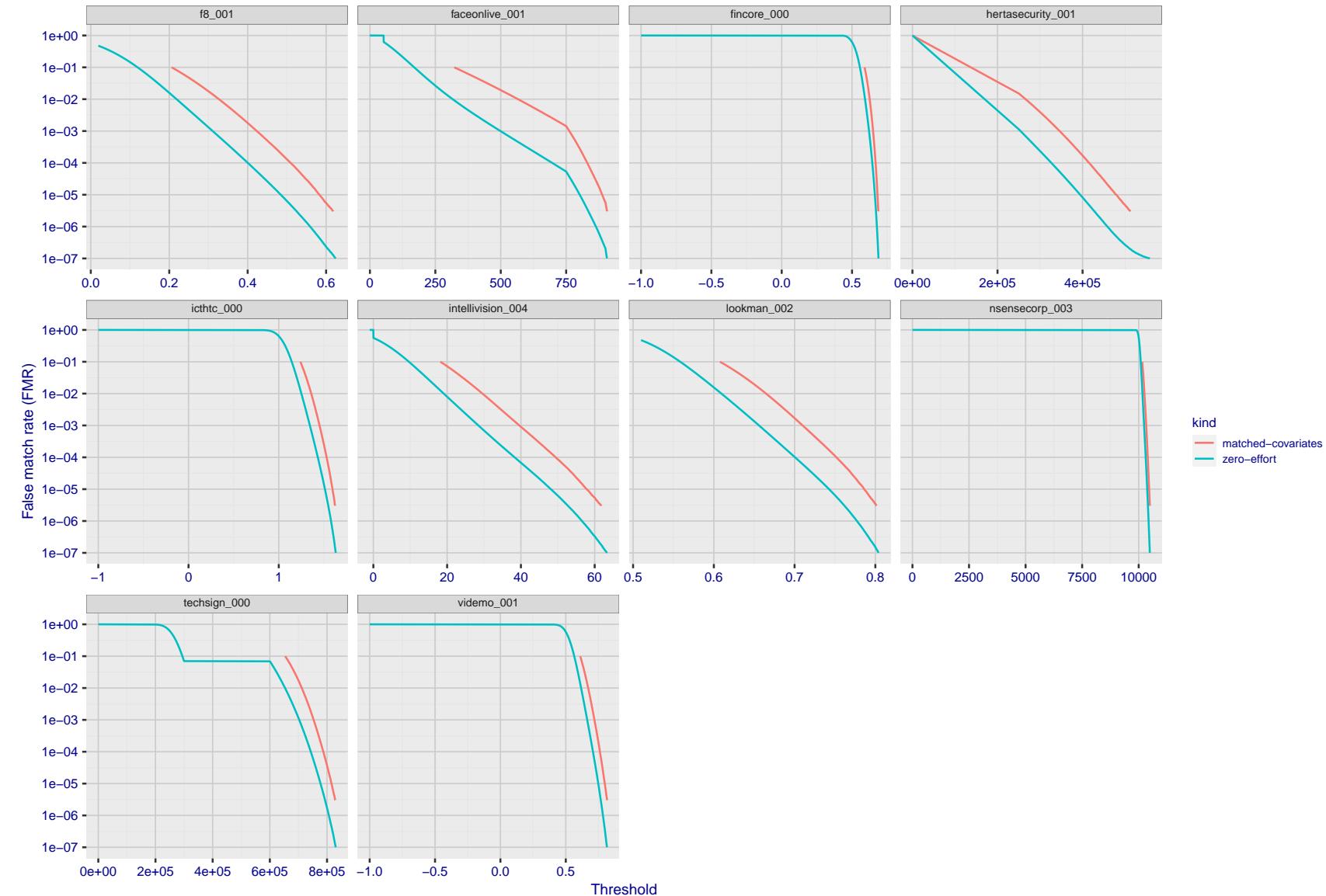


Figure 267: For the visa images, the false match calibration curves show FMR vs. threshold, T . The blue (lower) curves are for zero-effort impostors (i.e. comparing all images against all). The red (upper) curves are for persons of the same-sex, same-age, and same national-origin. This shows that FMR is underestimated (by a factor of 10 or more) by using a zero-effort impostor calculation to calibrate T . As shown later (sec. 3.6), FMR is higher for demographic-matched impostors.

2022/08/30 09:26:06

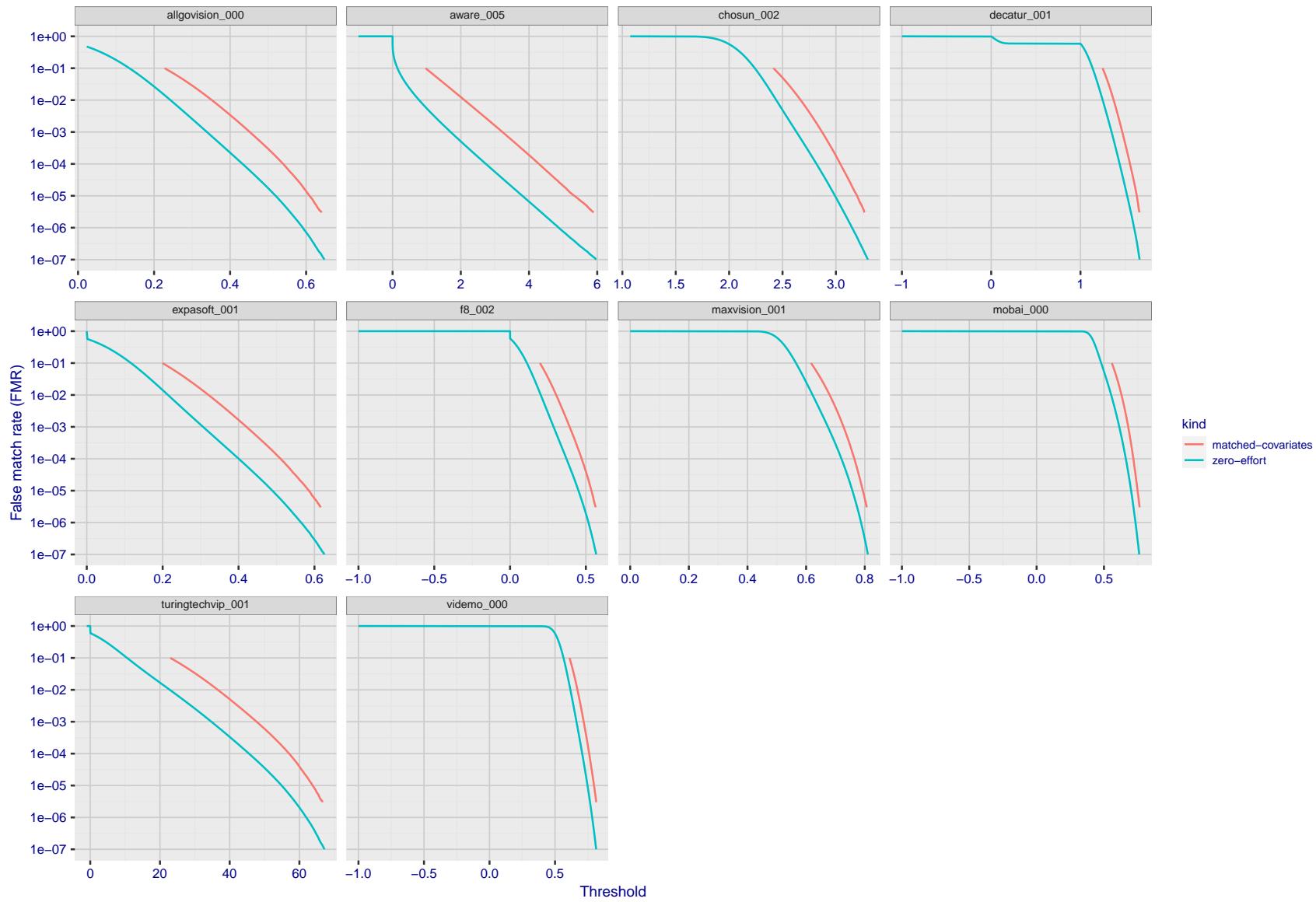


Figure 268: For the visa images, the false match calibration curves show FMR vs. threshold, T . The blue (lower) curves are for zero-effort impostors (i.e. comparing all images against all). The red (upper) curves are for persons of the same-sex, same-age, and same national-origin. This shows that FMR is underestimated (by a factor of 10 or more) by using a zero-effort impostor calculation to calibrate T . As shown later (sec. 3.6), FMR is higher for demographic-matched impostors.

FNMR(T)
"False non-match rate"
"False match rate"

2022/08/30 09:26:06

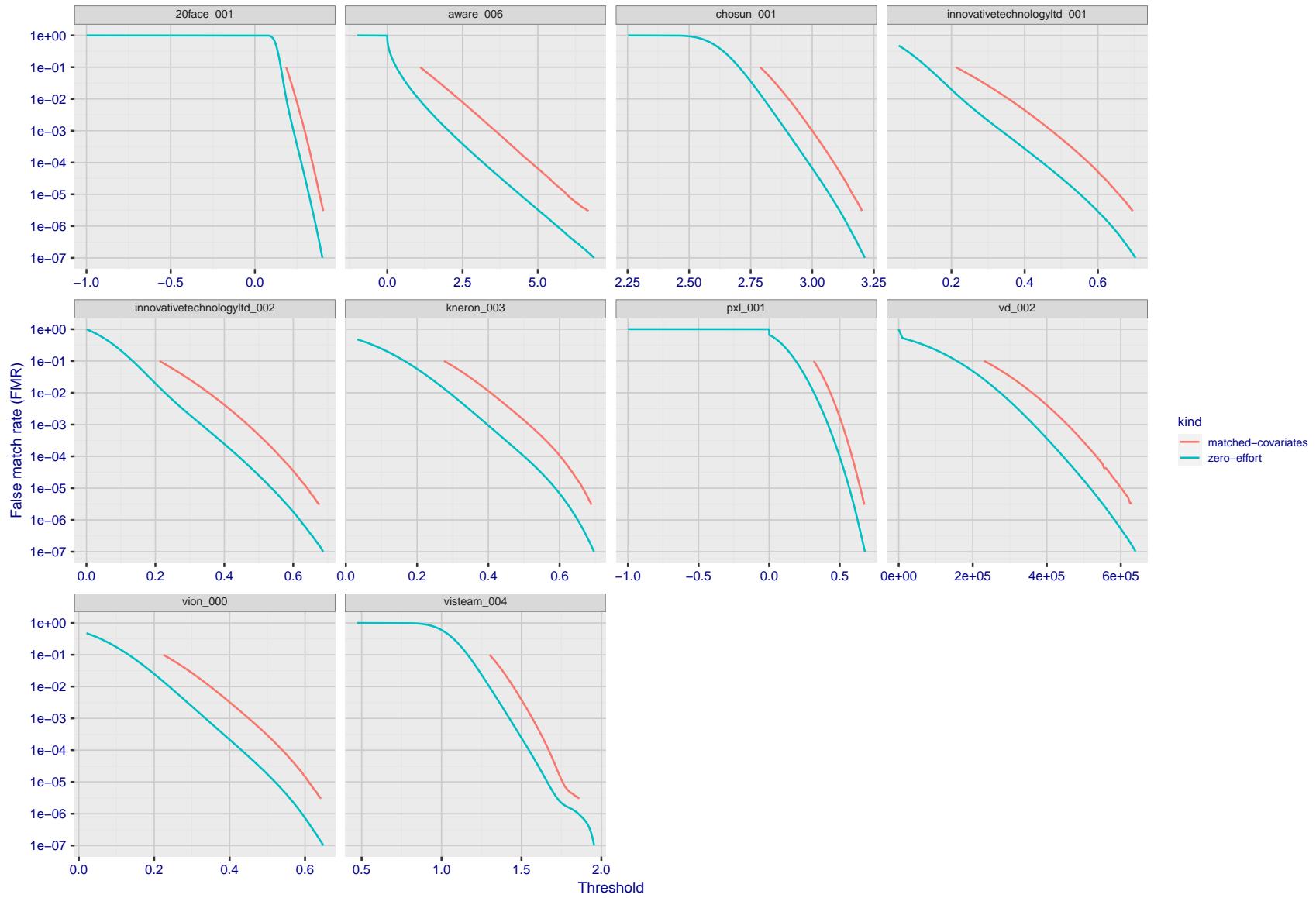


Figure 269: For the visa images, the false match calibration curves show FMR vs. threshold, T . The blue (lower) curves are for zero-effort impostors (i.e. comparing all images against all). The red (upper) curves are for persons of the same-sex, same-age, and same national-origin. This shows that FMR is underestimated (by a factor of 10 or more) by using a zero-effort impostor calculation to calibrate T . As shown later (sec. 3.6), FMR is higher for demographic-matched impostors.

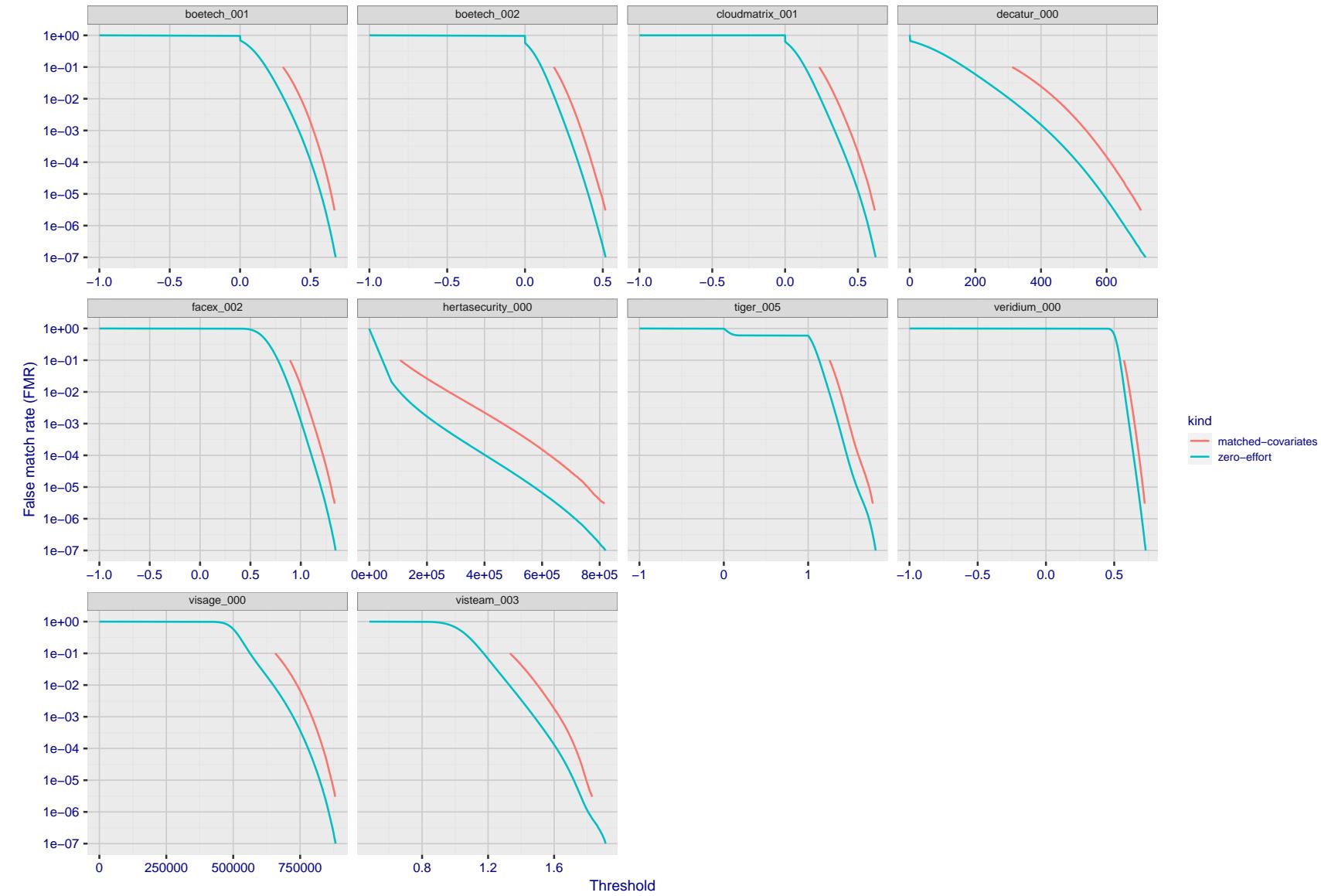


Figure 270: For the visa images, the false match calibration curves show FMR vs. threshold, T . The blue (lower) curves are for zero-effort impostors (i.e. comparing all images against all). The red (upper) curves are for persons of the same-sex, same-age, and same national-origin. This shows that FMR is underestimated (by a factor of 10 or more) by using a zero-effort impostor calculation to calibrate T . As shown later (sec. 3.6), FMR is higher for demographic-matched impostors.

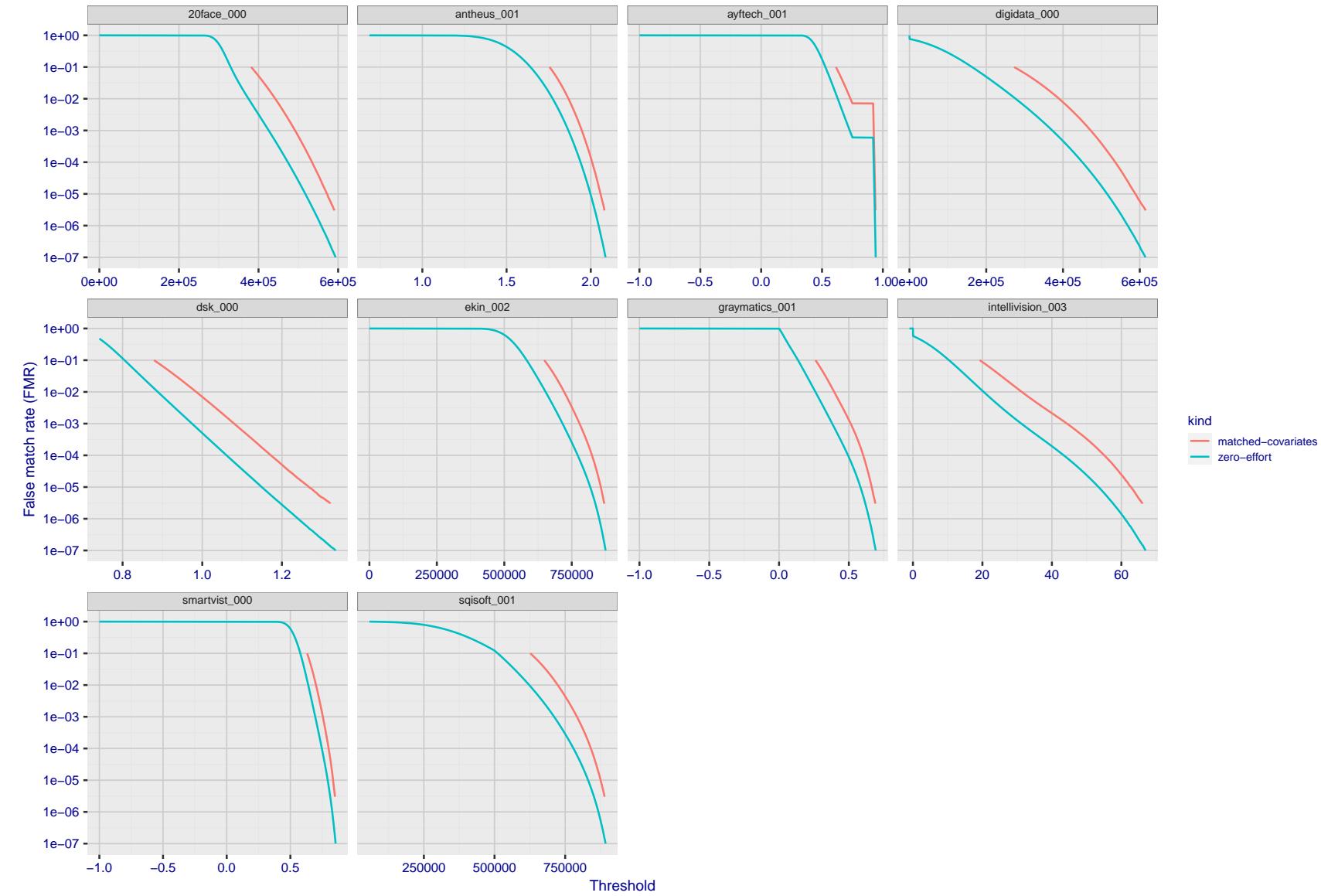


Figure 271: For the visa images, the false match calibration curves show FMR vs. threshold, T . The blue (lower) curves are for zero-effort impostors (i.e. comparing all images against all). The red (upper) curves are for persons of the same-sex, same-age, and same national-origin. This shows that FMR is underestimated (by a factor of 10 or more) by using a zero-effort impostor calculation to calibrate T . As shown later (sec. 3.6), FMR is higher for demographic-matched impostors.

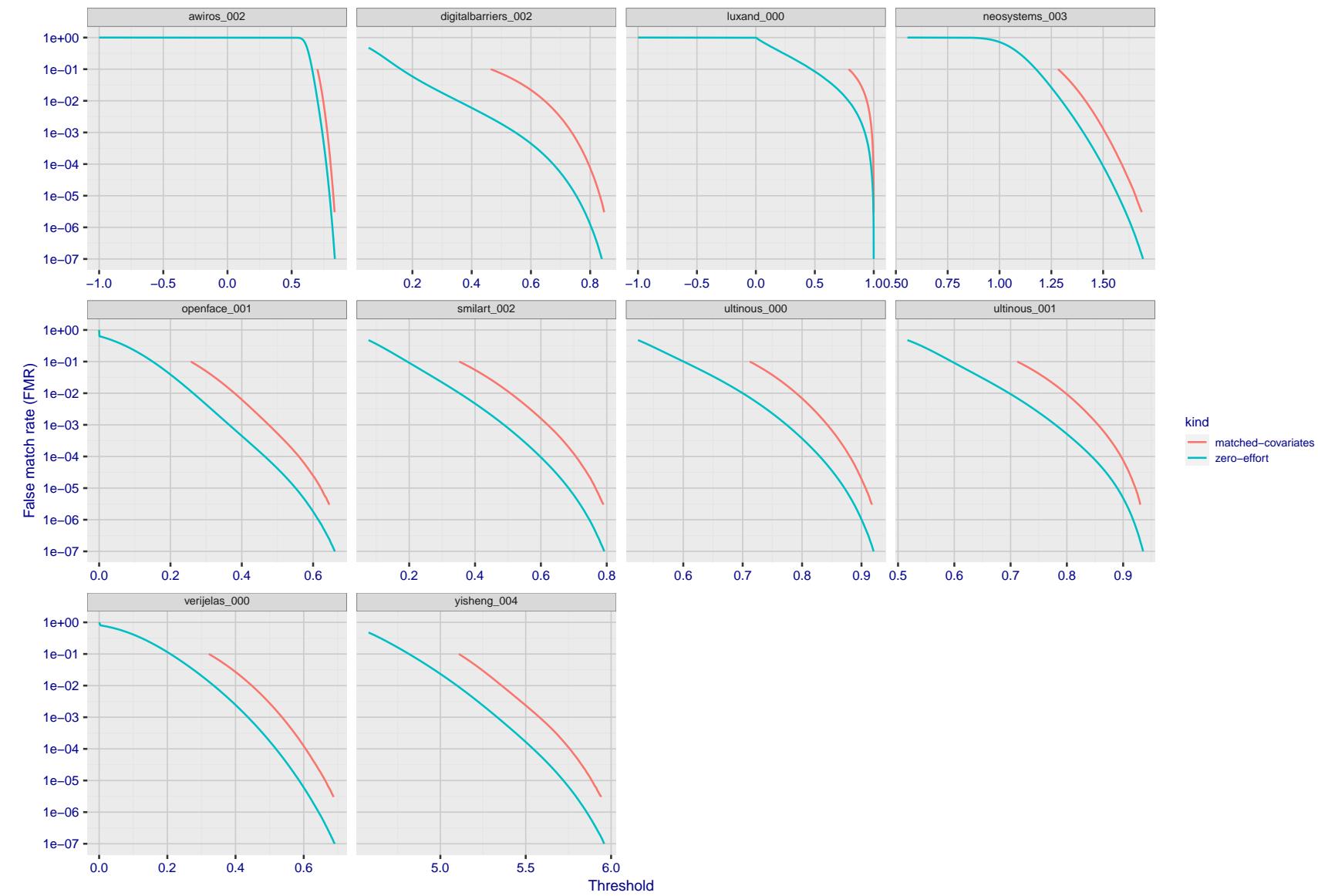


Figure 272: For the visa images, the false match calibration curves show FMR vs. threshold, T . The blue (lower) curves are for zero-effort impostors (i.e. comparing all images against all). The red (upper) curves are for persons of the same-sex, same-age, and same national-origin. This shows that FMR is underestimated (by a factor of 10 or more) by using a zero-effort impostor calculation to calibrate T . As shown later (sec. 3.6), FMR is higher for demographic-matched impostors.

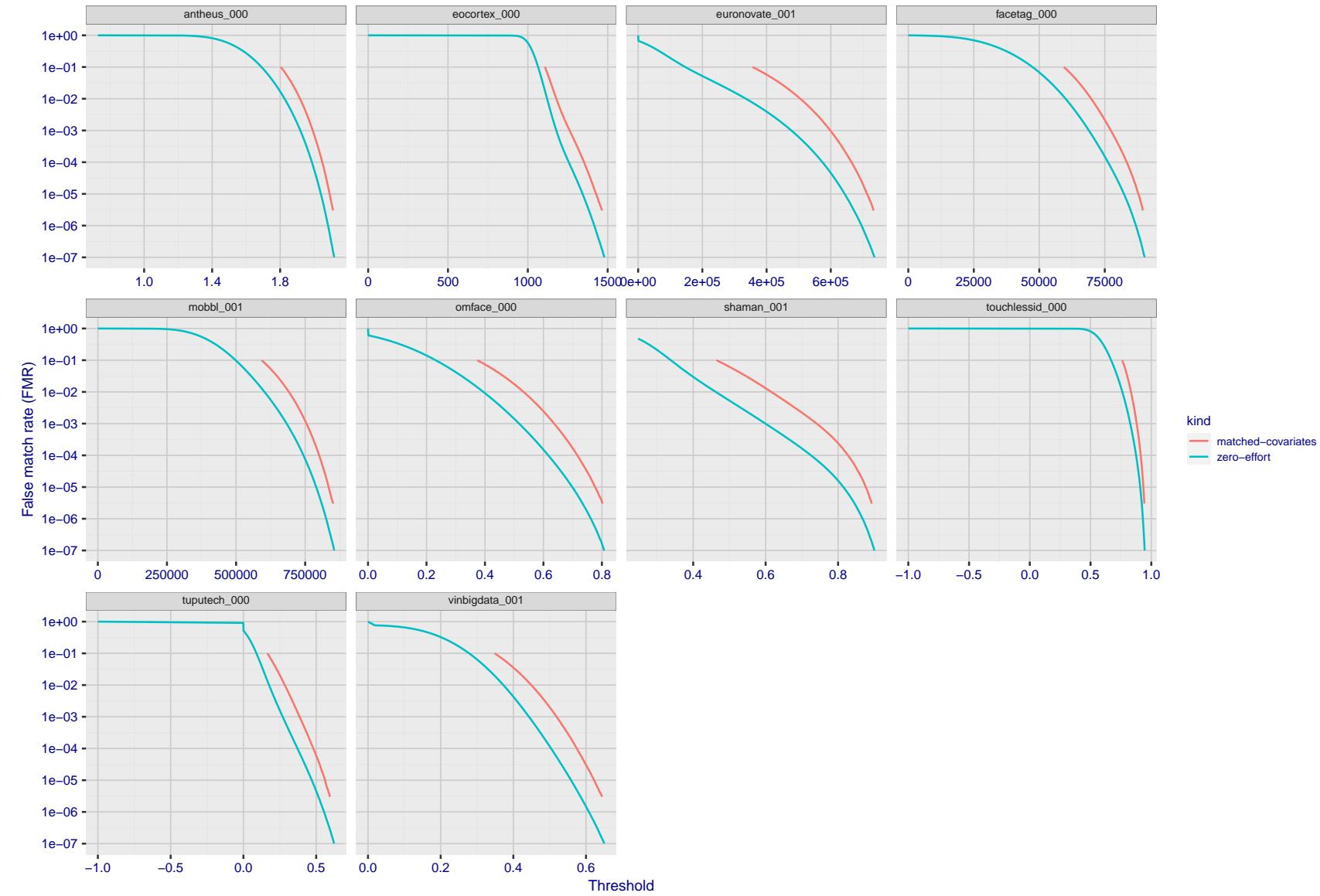


Figure 273: For the visa images, the false match calibration curves show FMR vs. threshold, T . The blue (lower) curves are for zero-effort impostors (i.e. comparing all images against all). The red (upper) curves are for persons of the same-sex, same-age, and same national-origin. This shows that FMR is underestimated (by a factor of 10 or more) by using a zero-effort impostor calculation to calibrate T . As shown later (sec. 3.6), FMR is higher for demographic-matched impostors.

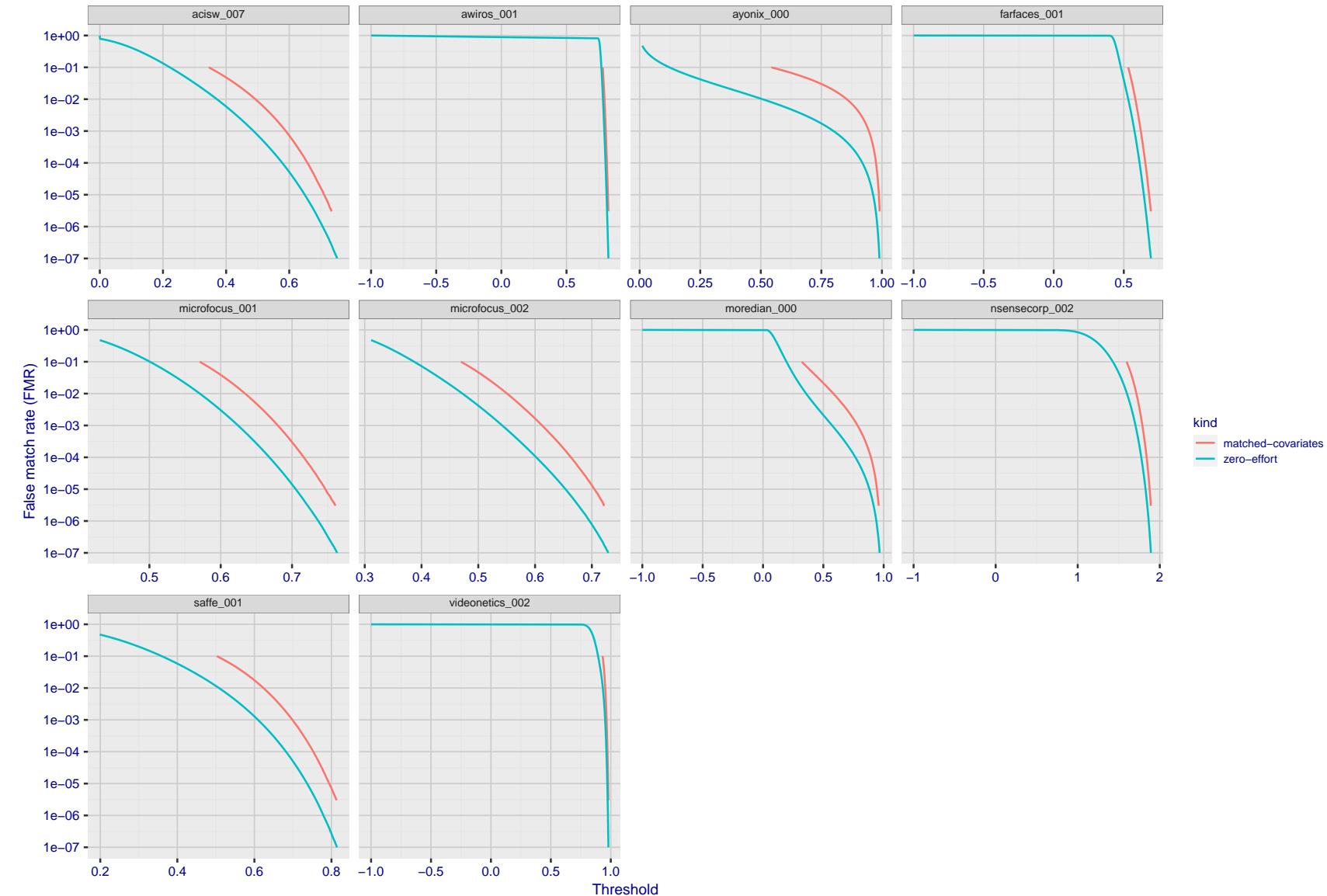


Figure 274: For the visa images, the false match calibration curves show FMR vs. threshold, T . The blue (lower) curves are for zero-effort impostors (i.e. comparing all images against all). The red (upper) curves are for persons of the same-sex, same-age, and same national-origin. This shows that FMR is underestimated (by a factor of 10 or more) by using a zero-effort impostor calculation to calibrate T . As shown later (sec. 3.6), FMR is higher for demographic-matched impostors.

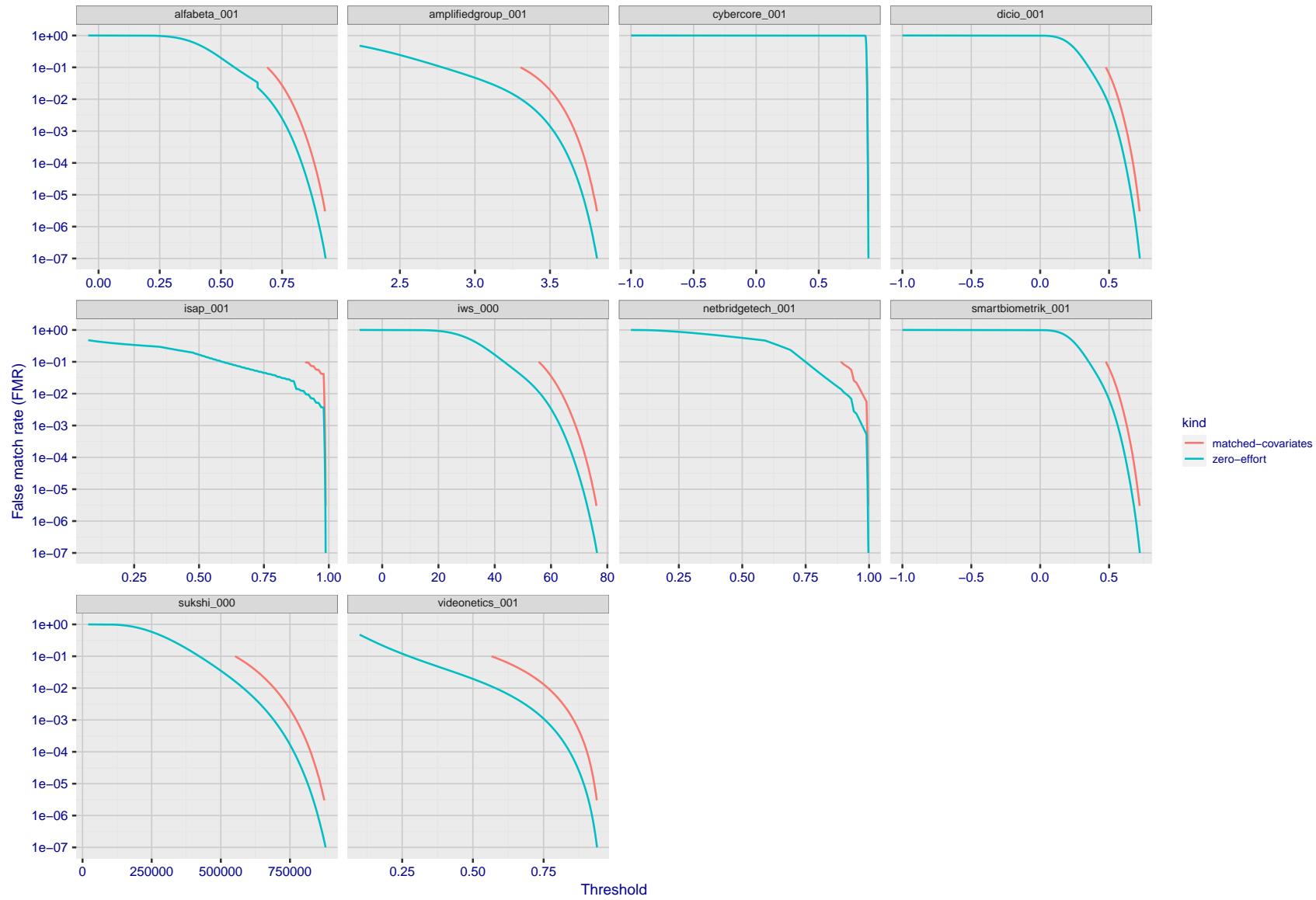


Figure 275: For the visa images, the false match calibration curves show FMR vs. threshold, T . The blue (lower) curves are for zero-effort impostors (i.e. comparing all images against all). The red (upper) curves are for persons of the same-sex, same-age, and same national-origin. This shows that FMR is underestimated (by a factor of 10 or more) by using a zero-effort impostor calculation to calibrate T . As shown later (sec. 3.6), FMR is higher for demographic-matched impostors.

2022/08/30 09:26:06

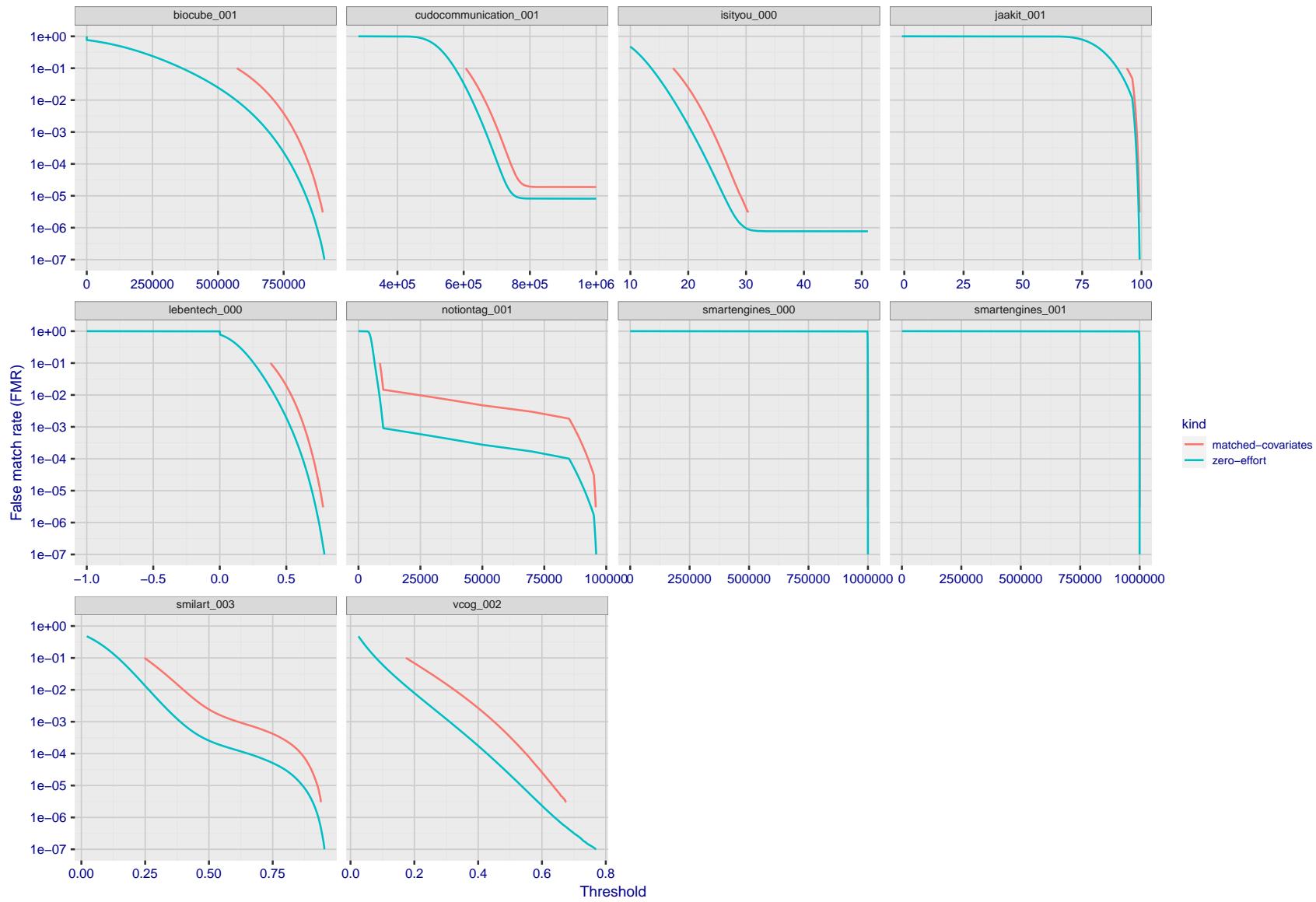


Figure 276: For the visa images, the false match calibration curves show FMR vs. threshold, T . The blue (lower) curves are for zero-effort impostors (i.e. comparing all images against all). The red (upper) curves are for persons of the same-sex, same-age, and same national-origin. This shows that FMR is underestimated (by a factor of 10 or more) by using a zero-effort impostor calculation to calibrate T . As shown later (sec. 3.6), FMR is higher for demographic-matched impostors.

FNMR(T)

"False non-match rate"

"False match rate"

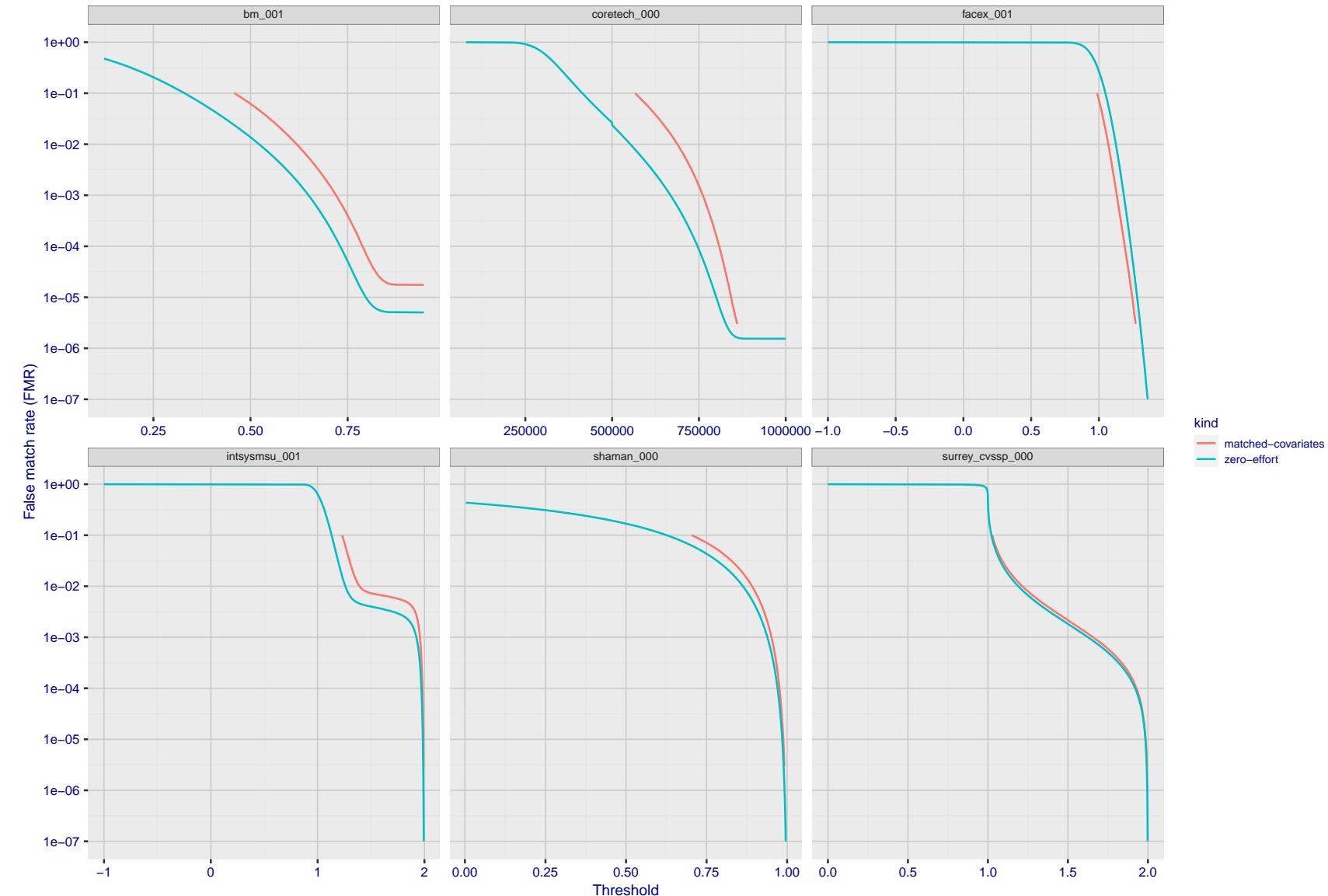


Figure 277: For the visa images, the false match calibration curves show FMR vs. threshold, T . The blue (lower) curves are for zero-effort impostors (i.e. comparing all images against all). The red (upper) curves are for persons of the same-sex, same-age, and same national-origin. This shows that FMR is underestimated (by a factor of 10 or more) by using a zero-effort impostor calculation to calibrate T . As shown later (sec. 3.6), FMR is higher for demographic-matched impostors.

3.5 Genuine distribution stability

3.5.1 Effect of birth place on the genuine distribution

Background: Both skin tone and bone structure vary geographically. Prior studies have reported variations in FNMR and FMR.

Goal: To measure false non-match rate (FNMR) variation with country of birth.

Methods: Thresholds are determined that give $FMR = \{0.001, 0.0001\}$ over the entire impostor set. Then FNMR is measured over 1000 bootstrap replications of the genuine scores. Only those countries with at least 140 individuals are included in the analysis.

Results: Figure 314 shows FNMR by country of birth for the two thresholds.

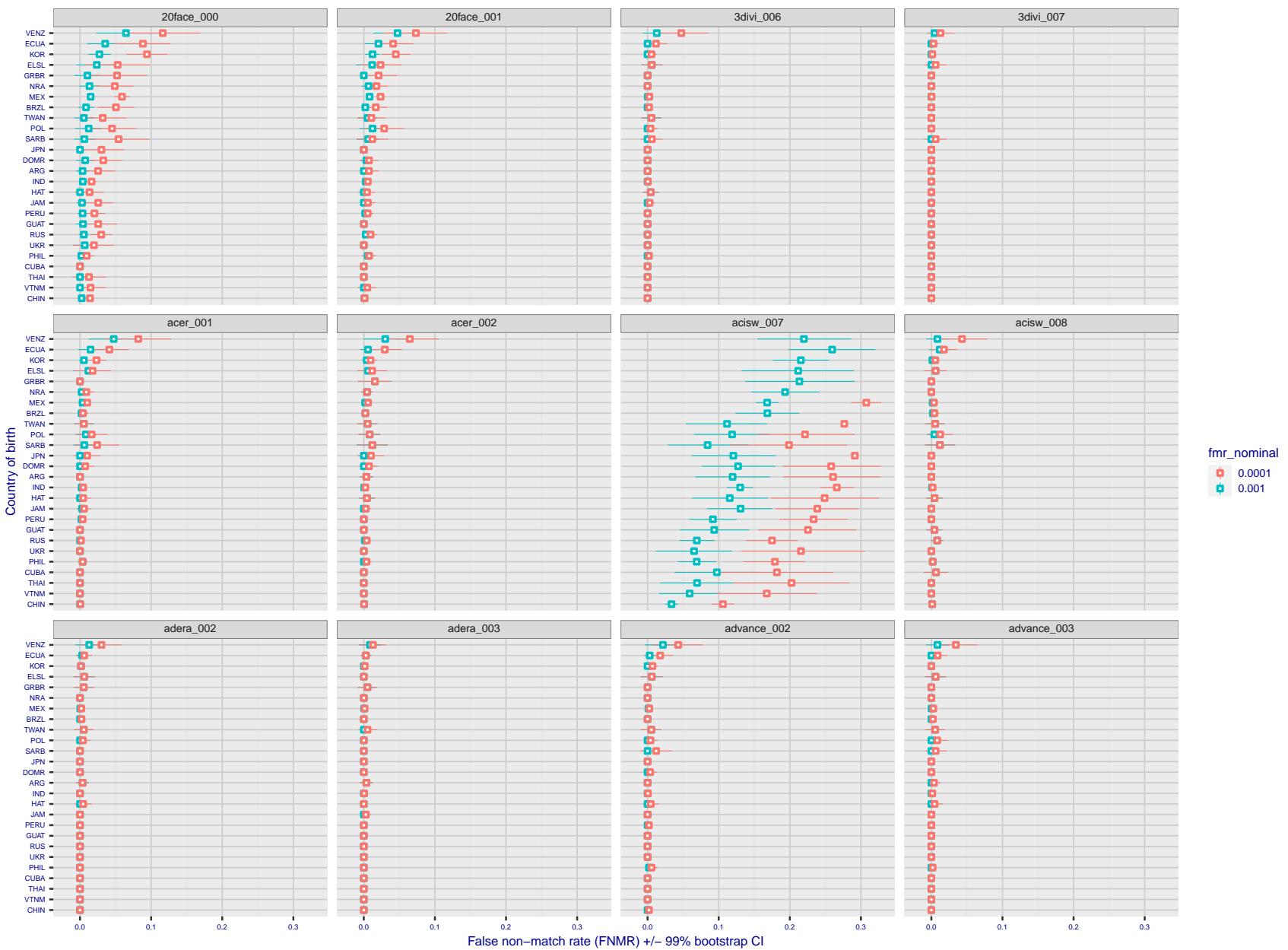


Figure 278: For the visa images, the dots show FNMR by country of birth for two globally set operating thresholds corresponding to $FMR = \{0.001, 0.0001\}$ computed over all on the order of 10^{10} impostor scores. The FMR in each bin will vary also - see subsequent impostor heatmaps in sec. 3.6.1. The figures shows an order of magnitude variation in FNMR across country of birth; these effects are likely due quality variations, then demographics like age and race. The error rates in some cases are zero, and in others the DET is flat so the error rates at the two thresholds are identical. The lines span 1% and 99% of bootstrap replicated FNMR estimates.

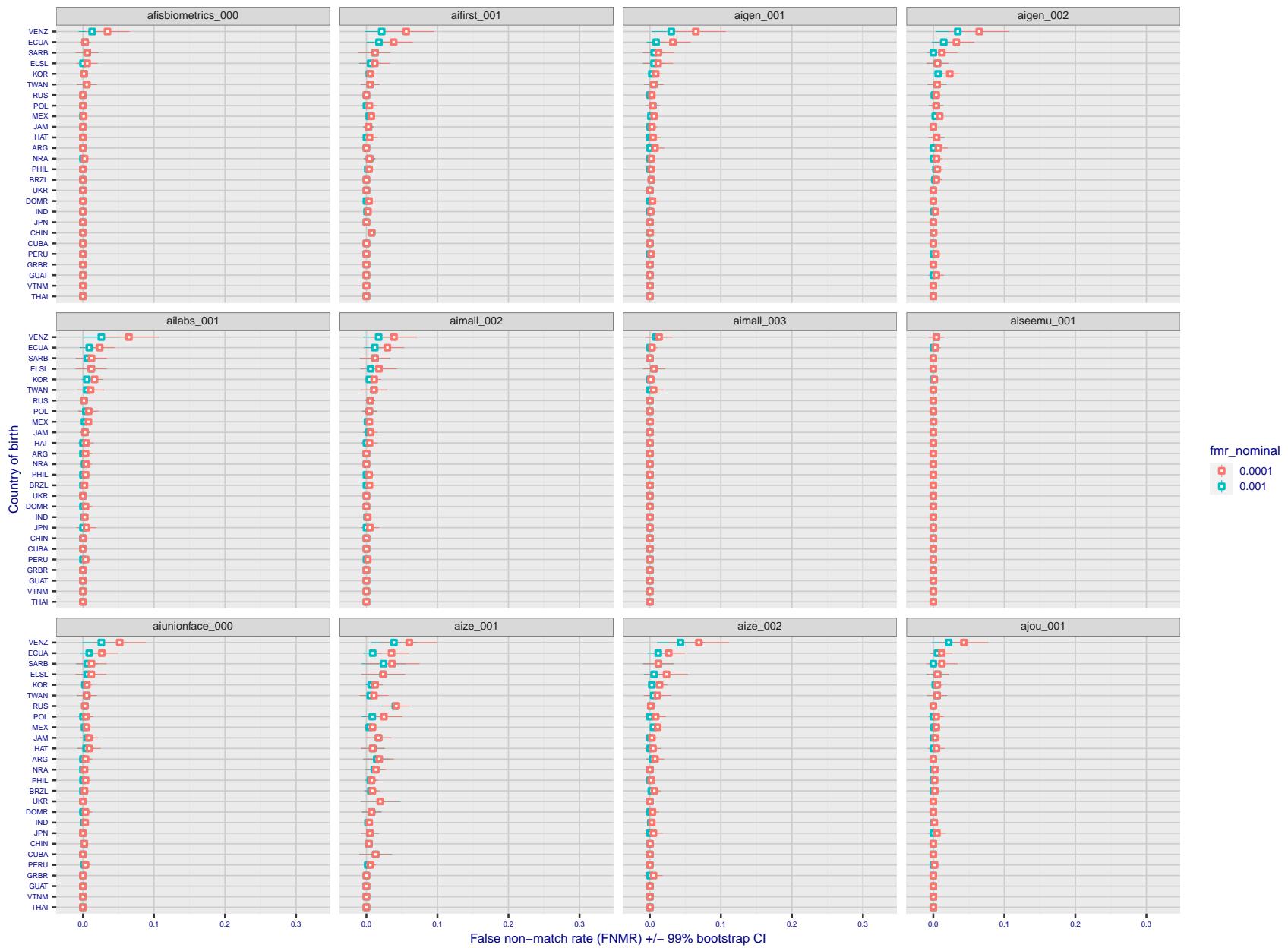


Figure 279: For the visa images, the dots show FNMR by country of birth for two globally set operating thresholds corresponding to $FMR = \{0.001, 0.0001\}$ computed over all on the order of 10^{10} impostor scores. The FMR in each bin will vary also - see subsequent impostor heatmaps in sec. 3.6.1. The figures shows an order of magnitude variation in FNMR across country of birth; these effects are likely due quality variations, then demographics like age and race. The error rates in some cases are zero, and in others the DET is flat so the error rates at the two thresholds are identical. The lines span 1% and 99% of bootstrap replicated FNMR estimates.

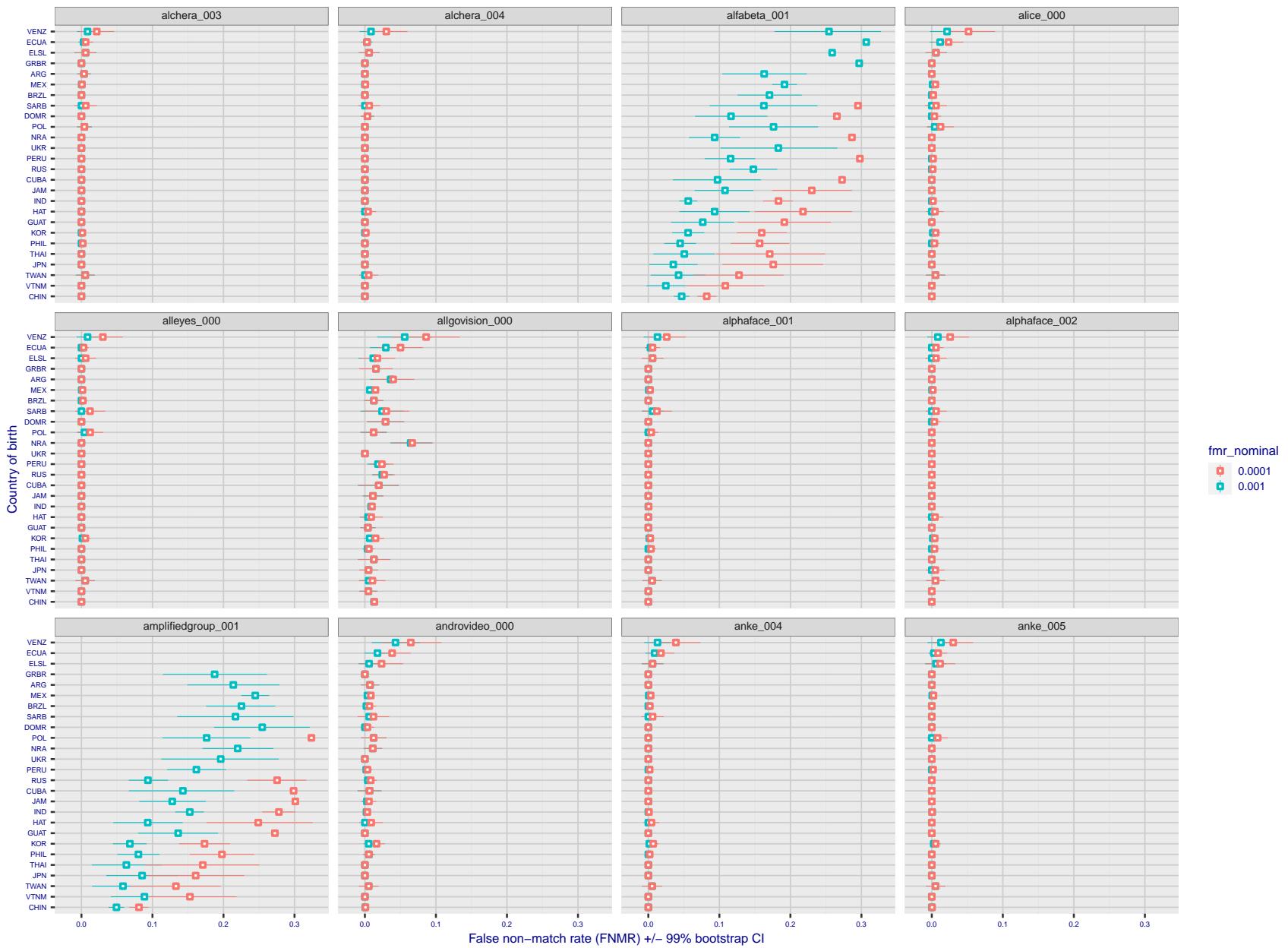


Figure 280: For the visa images, the dots show FNMR by country of birth for two globally set operating thresholds corresponding to $FMR = \{0.001, 0.0001\}$ computed over all on the order of 10^{10} impostor scores. The FMR in each bin will vary also - see subsequent impostor heatmaps in sec. 3.6.1. The figures shows an order of magnitude variation in FNMR across country of birth; these effects are likely due quality variations, then demographics like age and race. The error rates in some cases are zero, and in others the DET is flat so the error rates at the two thresholds are identical. The lines span 1% and 99% of bootstrap replicated FNMR estimates.

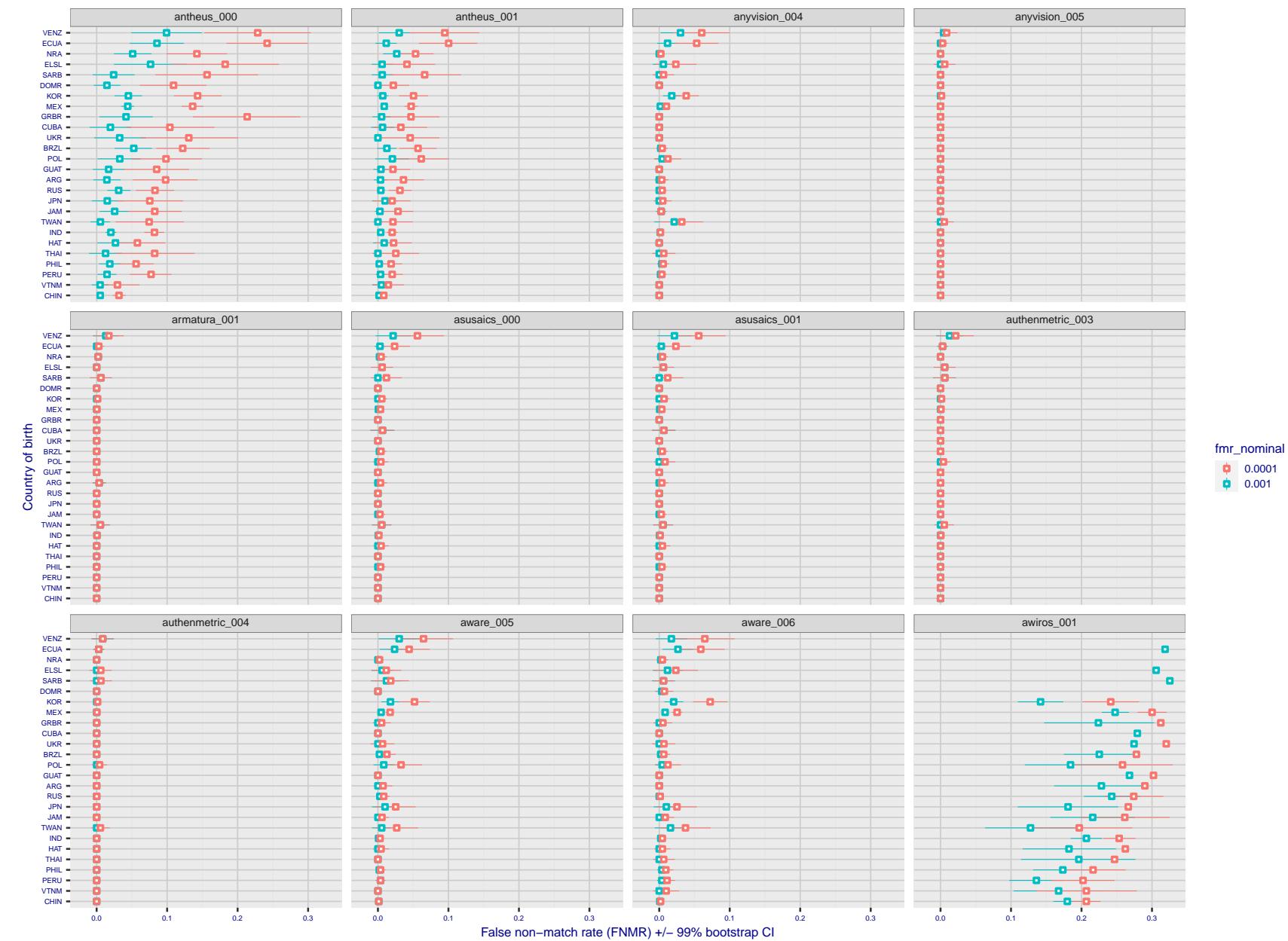


Figure 281: For the visa images, the dots show FNMR by country of birth for two globally set operating thresholds corresponding to $FMR = \{0.001, 0.0001\}$ computed over all on the order of 10^{10} impostor scores. The FMR in each bin will vary also - see subsequent impostor heatmaps in sec. 3.6.1. The figures shows an order of magnitude variation in FNMR across country of birth; these effects are likely due quality variations, then demographics like age and race. The error rates in some cases are zero, and in others the DET is flat so the error rates at the two thresholds are identical. The lines span 1% and 99% of bootstrap replicated FNMR estimates.

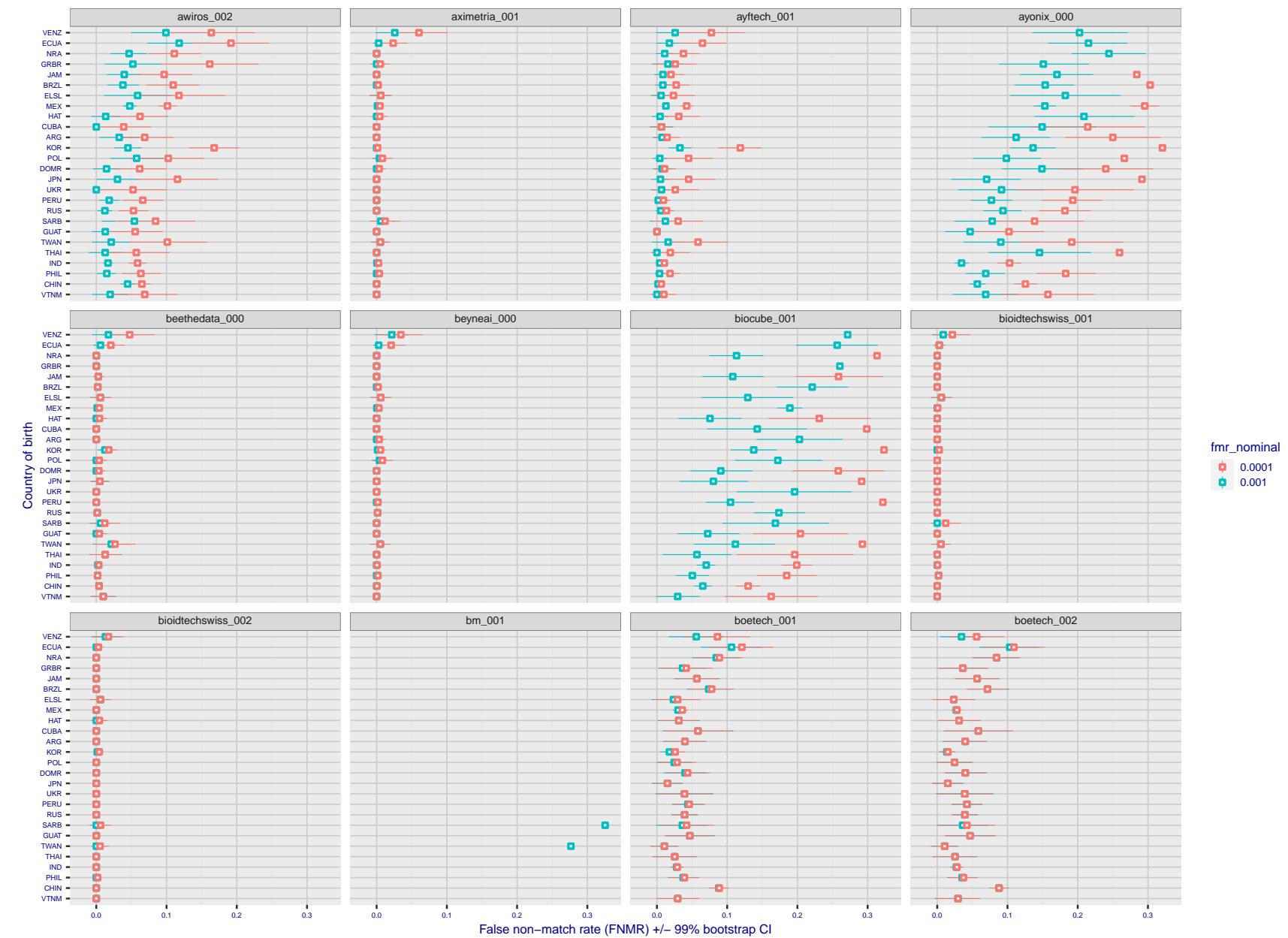


Figure 282: For the visa images, the dots show FNMR by country of birth for two globally set operating thresholds corresponding to $FMR = \{0.001, 0.0001\}$ computed over all on the order of 10^{10} impostor scores. The FMR in each bin will vary also - see subsequent impostor heatmaps in sec. 3.6.1. The figures shows an order of magnitude variation in FNMR across country of birth; these effects are likely due quality variations, then demographics like age and race. The error rates in some cases are zero, and in others the DET is flat so the error rates at the two thresholds are identical. The lines span 1% and 99% of bootstrap replicated FNMR estimates.

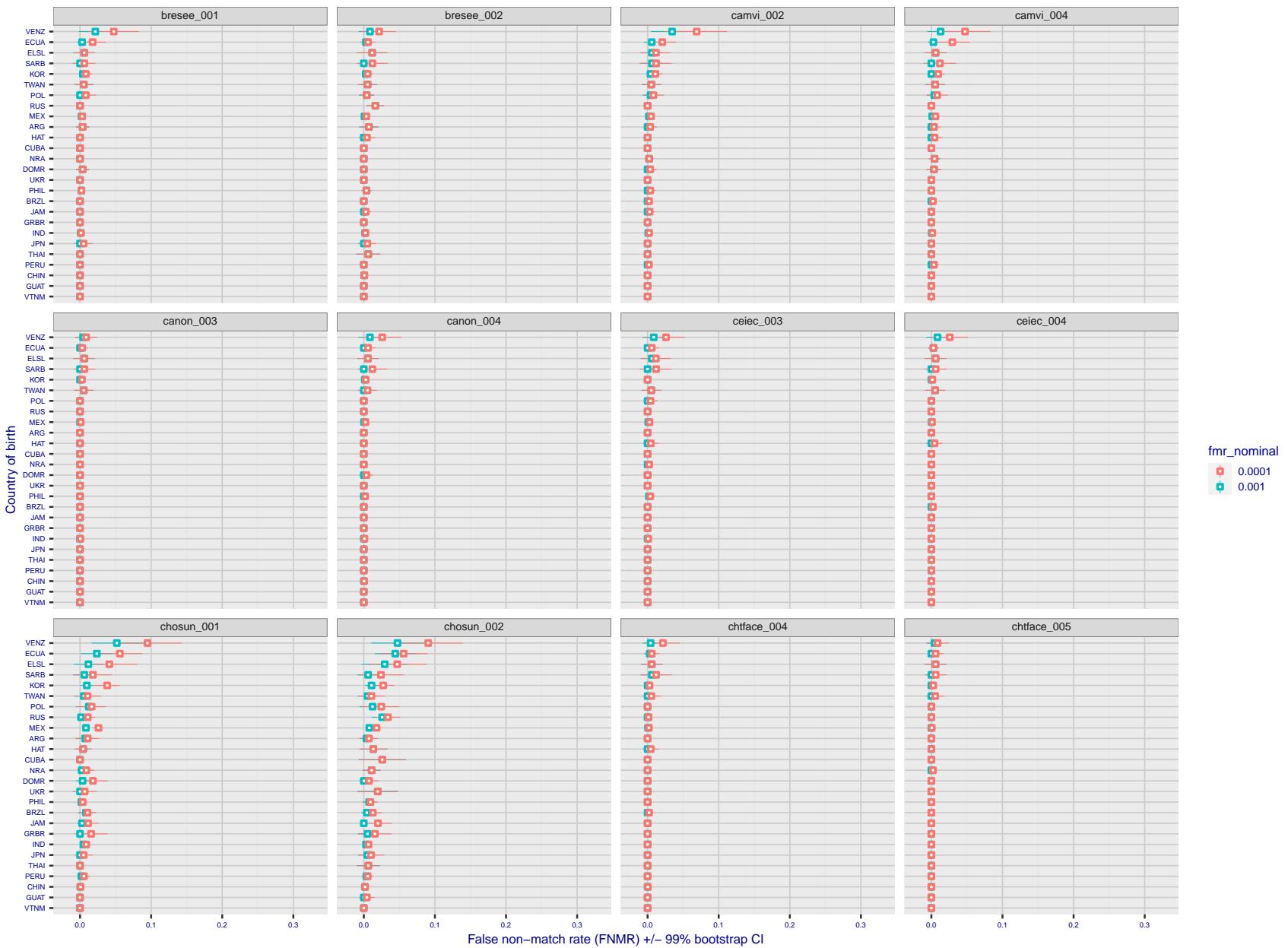


Figure 283: For the visa images, the dots show FNMR by country of birth for two globally set operating thresholds corresponding to $FMR = \{0.001, 0.0001\}$ computed over all on the order of 10^{10} impostor scores. The FMR in each bin will vary also - see subsequent impostor heatmaps in sec. 3.6.1. The figures shows an order of magnitude variation in FNMR across country of birth; these effects are likely due quality variations, then demographics like age and race. The error rates in some cases are zero, and in others the DET is flat so the error rates at the two thresholds are identical. The lines span 1% and 99% of bootstrap replicated FNMR estimates.

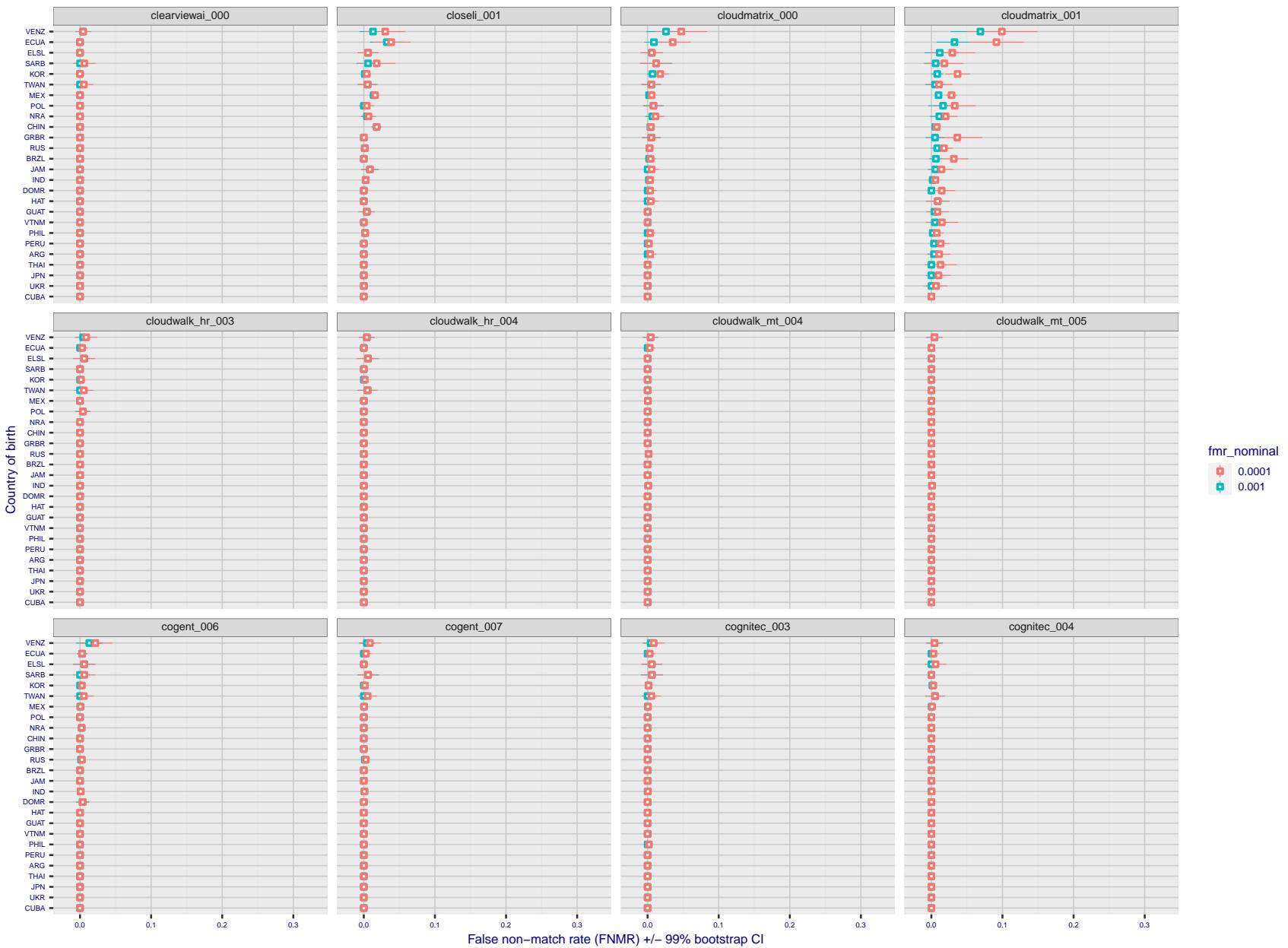


Figure 284: For the visa images, the dots show FNMR by country of birth for two globally set operating thresholds corresponding to $FMR = \{0.001, 0.0001\}$ computed over all on the order of 10^{10} impostor scores. The FMR in each bin will vary also - see subsequent impostor heatmaps in sec. 3.6.1. The figures shows an order of magnitude variation in FNMR across country of birth; these effects are likely due quality variations, then demographics like age and race. The error rates in some cases are zero, and in others the DET is flat so the error rates at the two thresholds are identical. The lines span 1% and 99% of bootstrap replicated FNMR estimates.

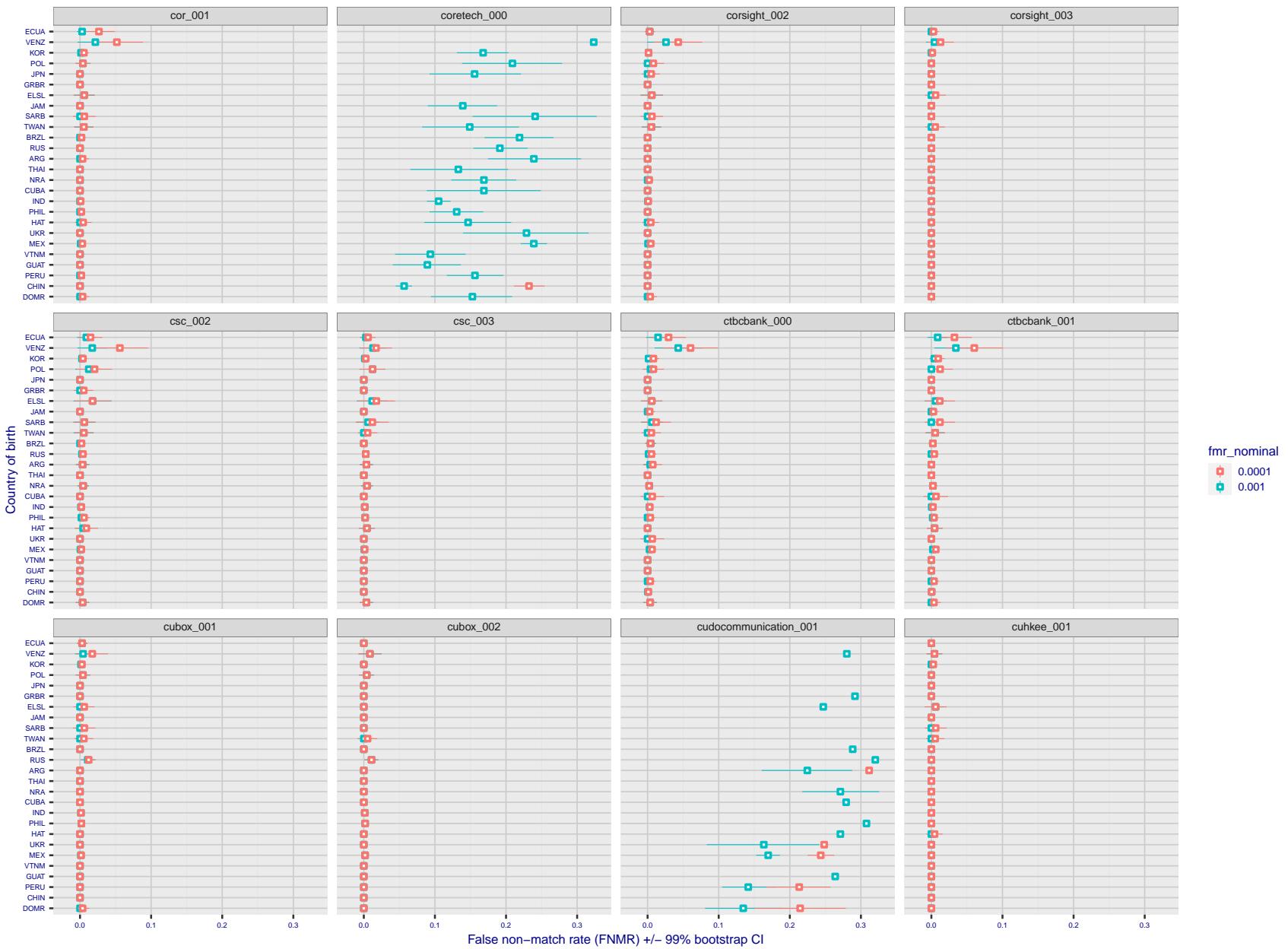


Figure 285: For the visa images, the dots show FNMR by country of birth for two globally set operating thresholds corresponding to $FMR = \{0.001, 0.0001\}$ computed over all on the order of 10^{10} impostor scores. The FMR in each bin will vary also - see subsequent impostor heatmaps in sec. 3.6.1. The figures shows an order of magnitude variation in FNMR across country of birth; these effects are likely due quality variations, then demographics like age and race. The error rates in some cases are zero, and in others the DET is flat so the error rates at the two thresholds are identical. The lines span 1% and 99% of bootstrap replicated FNMR estimates.

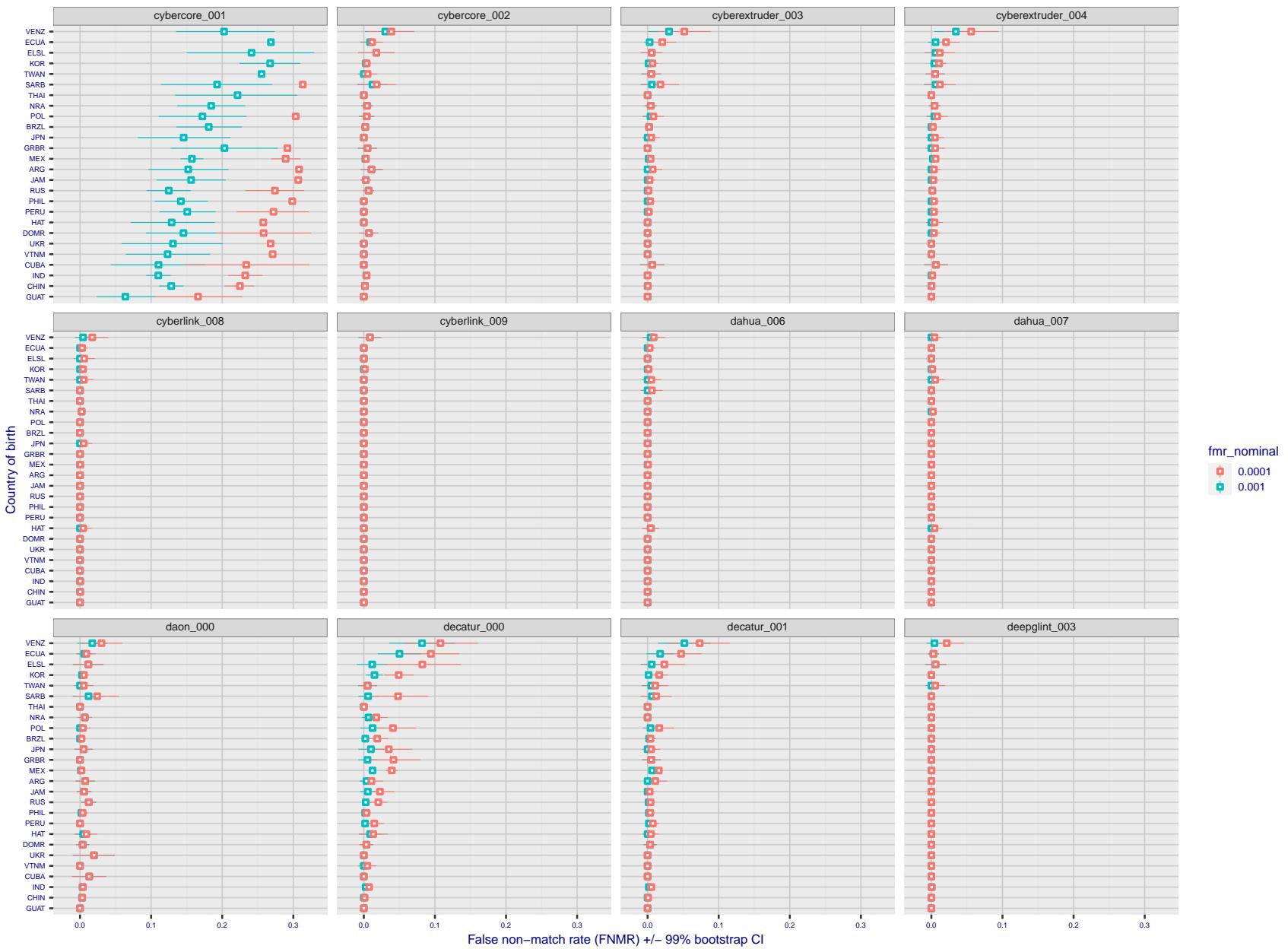


Figure 286: For the visa images, the dots show FNMR by country of birth for two globally set operating thresholds corresponding to $FMR = \{0.001, 0.0001\}$ computed over all on the order of 10^{10} impostor scores. The FMR in each bin will vary also - see subsequent impostor heatmaps in sec. 3.6.1. The figures shows an order of magnitude variation in FNMR across country of birth; these effects are likely due quality variations, then demographics like age and race. The error rates in some cases are zero, and in others the DET is flat so the error rates at the two thresholds are identical. The lines span 1% and 99% of bootstrap replicated FNMR estimates.

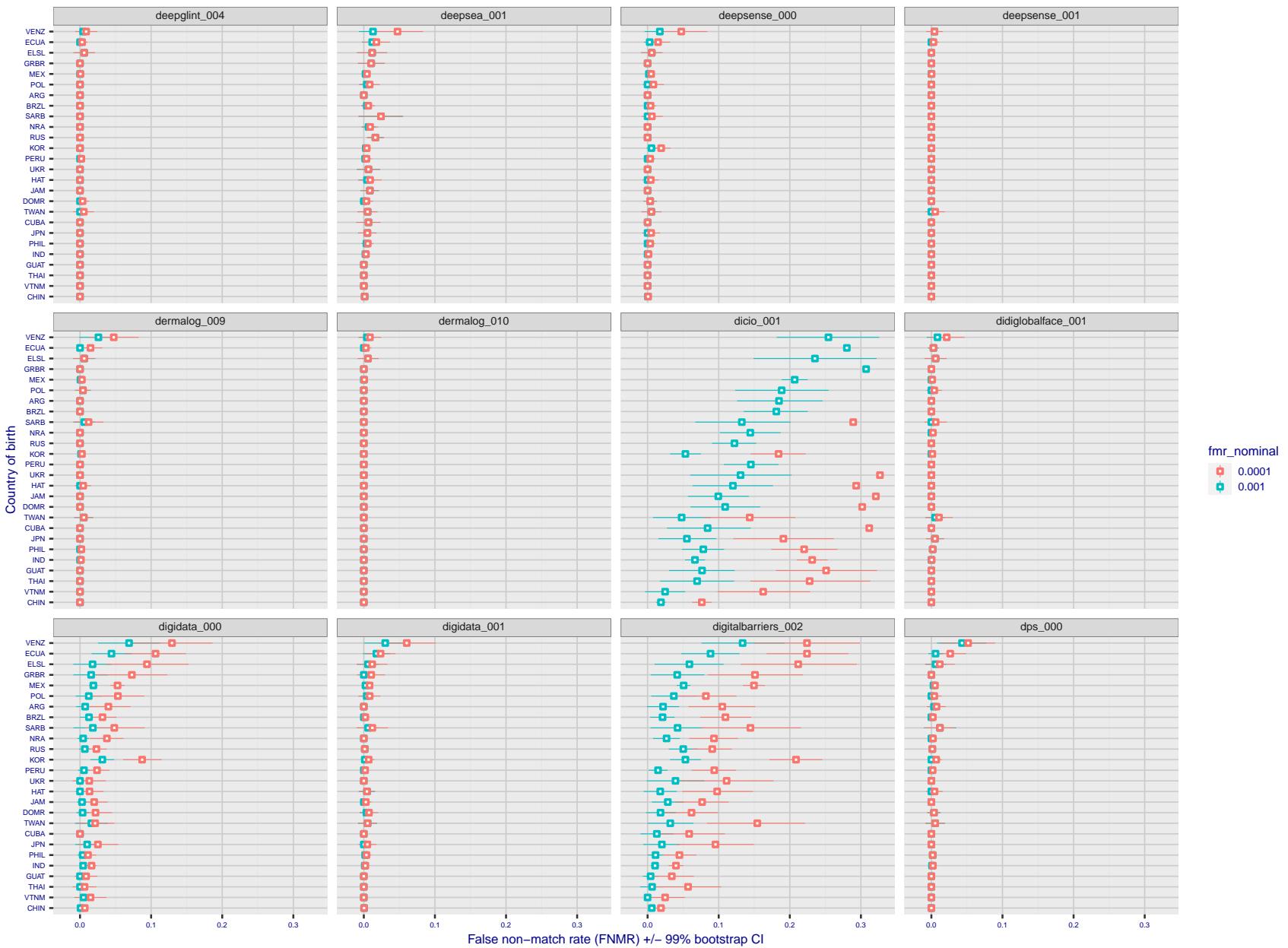


Figure 287: For the visa images, the dots show FNMR by country of birth for two globally set operating thresholds corresponding to $FMR = \{0.001, 0.0001\}$ computed over all on the order of 10^{10} impostor scores. The FMR in each bin will vary also - see subsequent impostor heatmaps in sec. 3.6.1. The figures shows an order of magnitude variation in FNMR across country of birth; these effects are likely due quality variations, then demographics like age and race. The error rates in some cases are zero, and in others the DET is flat so the error rates at the two thresholds are identical. The lines span 1% and 99% of bootstrap replicated FNMR estimates.

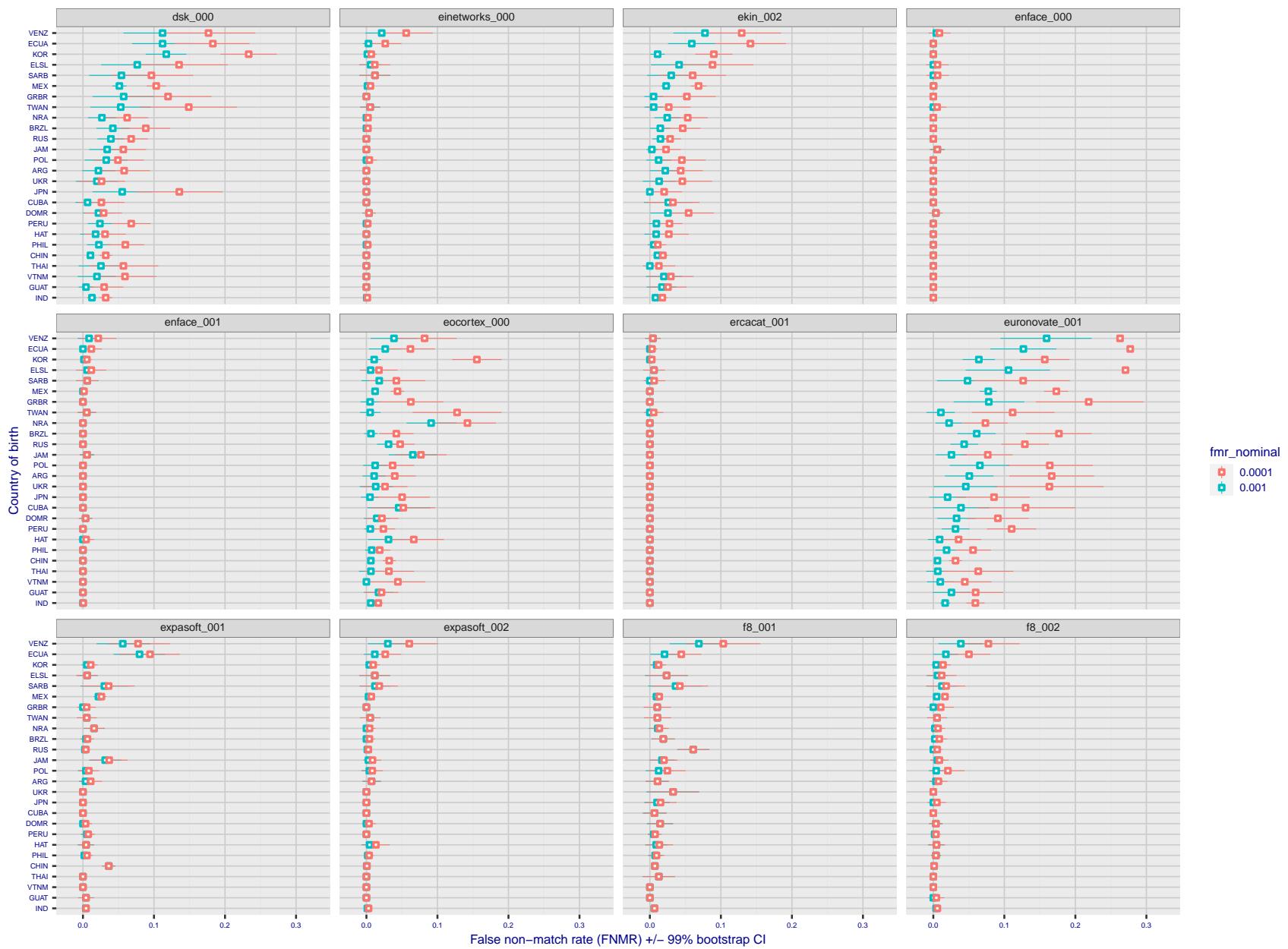


Figure 288: For the visa images, the dots show FNMR by country of birth for two globally set operating thresholds corresponding to $FMR = \{0.001, 0.0001\}$ computed over all on the order of 10^{10} impostor scores. The FMR in each bin will vary also - see subsequent impostor heatmaps in sec. 3.6.1. The figures shows an order of magnitude variation in FNMR across country of birth; these effects are likely due quality variations, then demographics like age and race. The error rates in some cases are zero, and in others the DET is flat so the error rates at the two thresholds are identical. The lines span 1% and 99% of bootstrap replicated FNMR estimates.

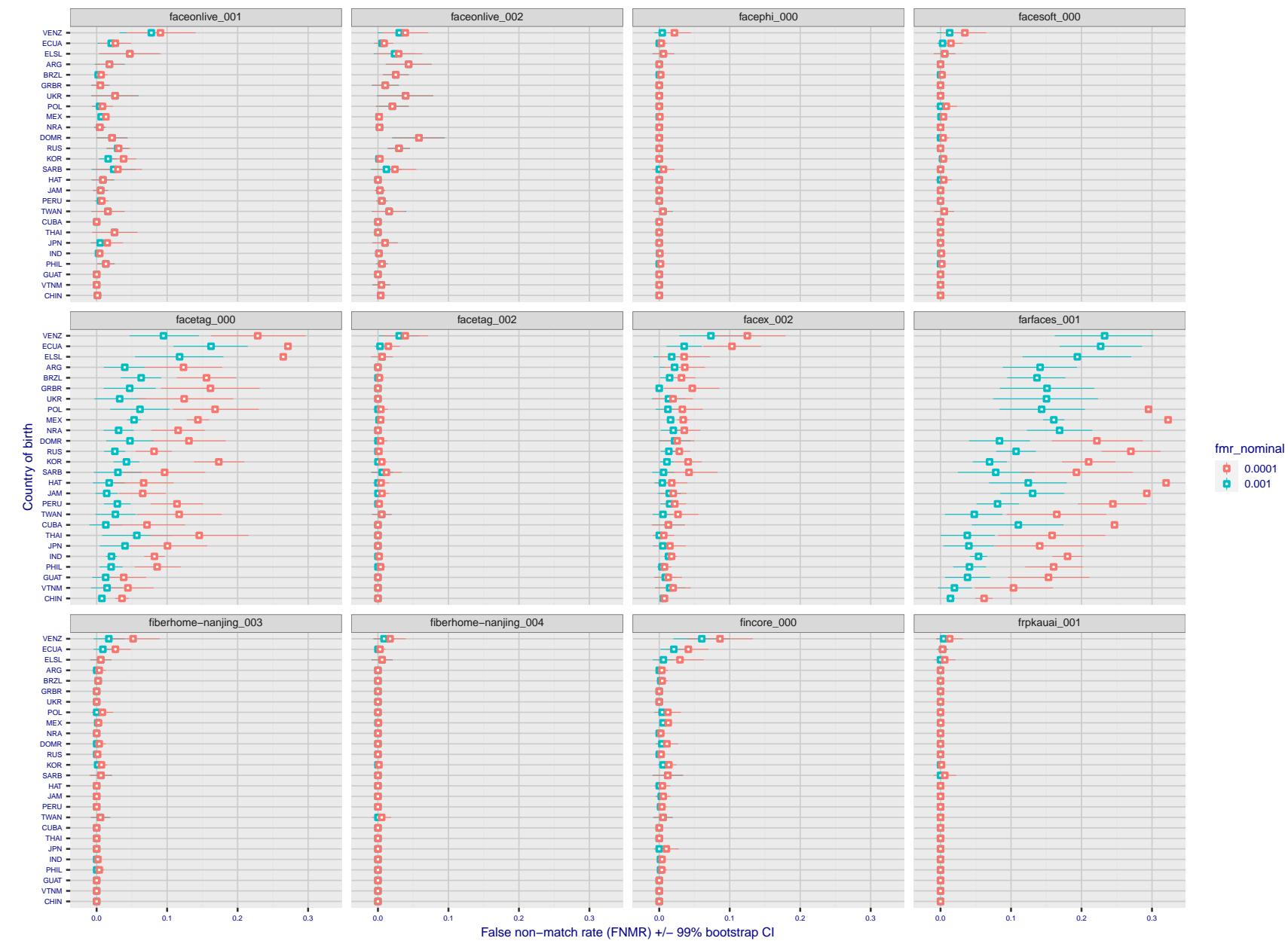


Figure 289: For the visa images, the dots show FNMR by country of birth for two globally set operating thresholds corresponding to $FMR = \{0.001, 0.0001\}$ computed over all on the order of 10^{10} impostor scores. The FMR in each bin will vary also - see subsequent impostor heatmaps in sec. 3.6.1. The figures shows an order of magnitude variation in FNMR across country of birth; these effects are likely due quality variations, then demographics like age and race. The error rates in some cases are zero, and in others the DET is flat so the error rates at the two thresholds are identical. The lines span 1% and 99% of bootstrap replicated FNMR estimates.

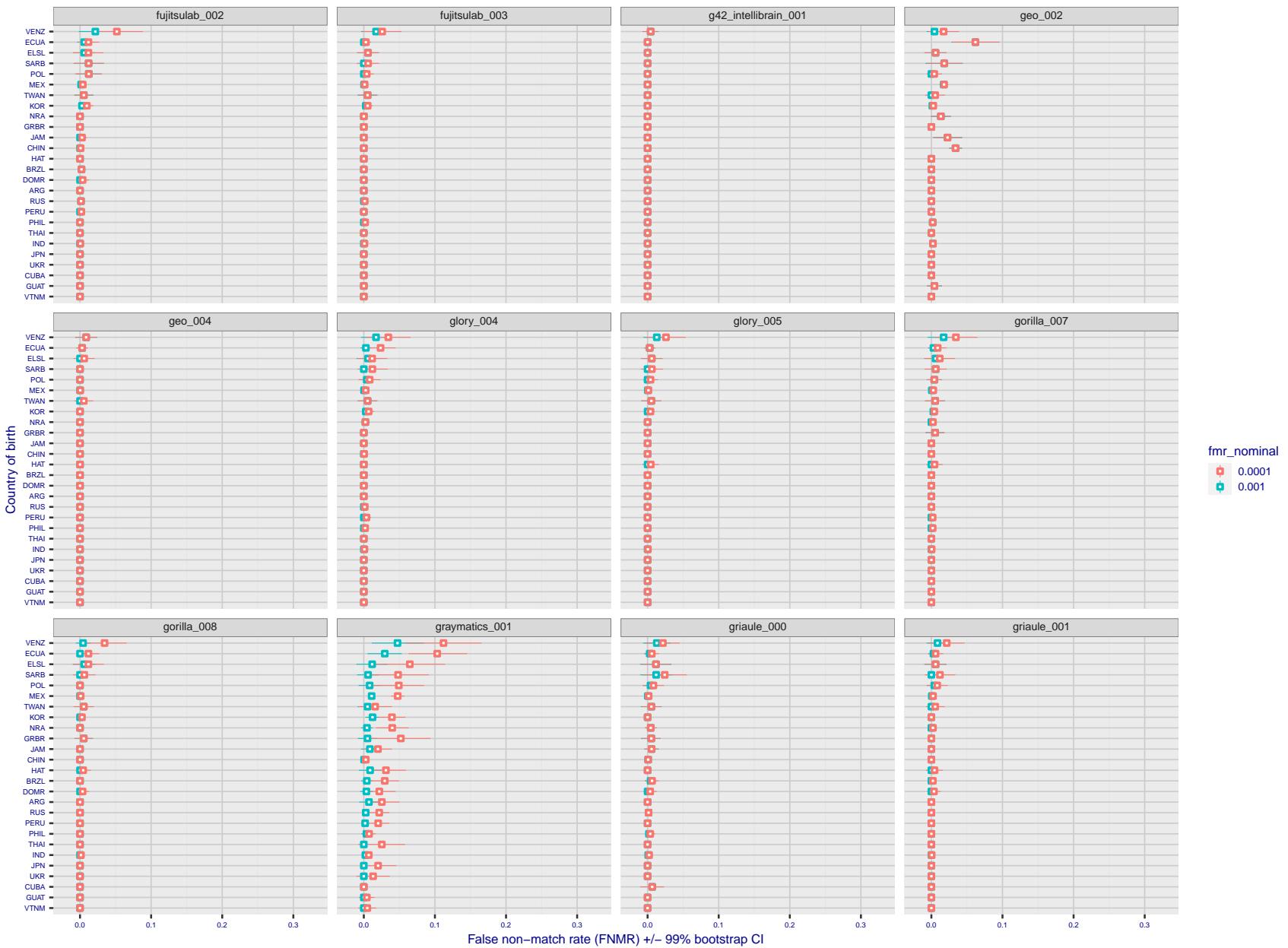


Figure 290: For the visa images, the dots show FNMR by country of birth for two globally set operating thresholds corresponding to $FMR = \{0.001, 0.0001\}$ computed over all on the order of 10^{10} impostor scores. The FMR in each bin will vary also - see subsequent impostor heatmaps in sec. 3.6.1. The figures shows an order of magnitude variation in FNMR across country of birth; these effects are likely due quality variations, then demographics like age and race. The error rates in some cases are zero, and in others the DET is flat so the error rates at the two thresholds are identical. The lines span 1% and 99% of bootstrap replicated FNMR estimates.

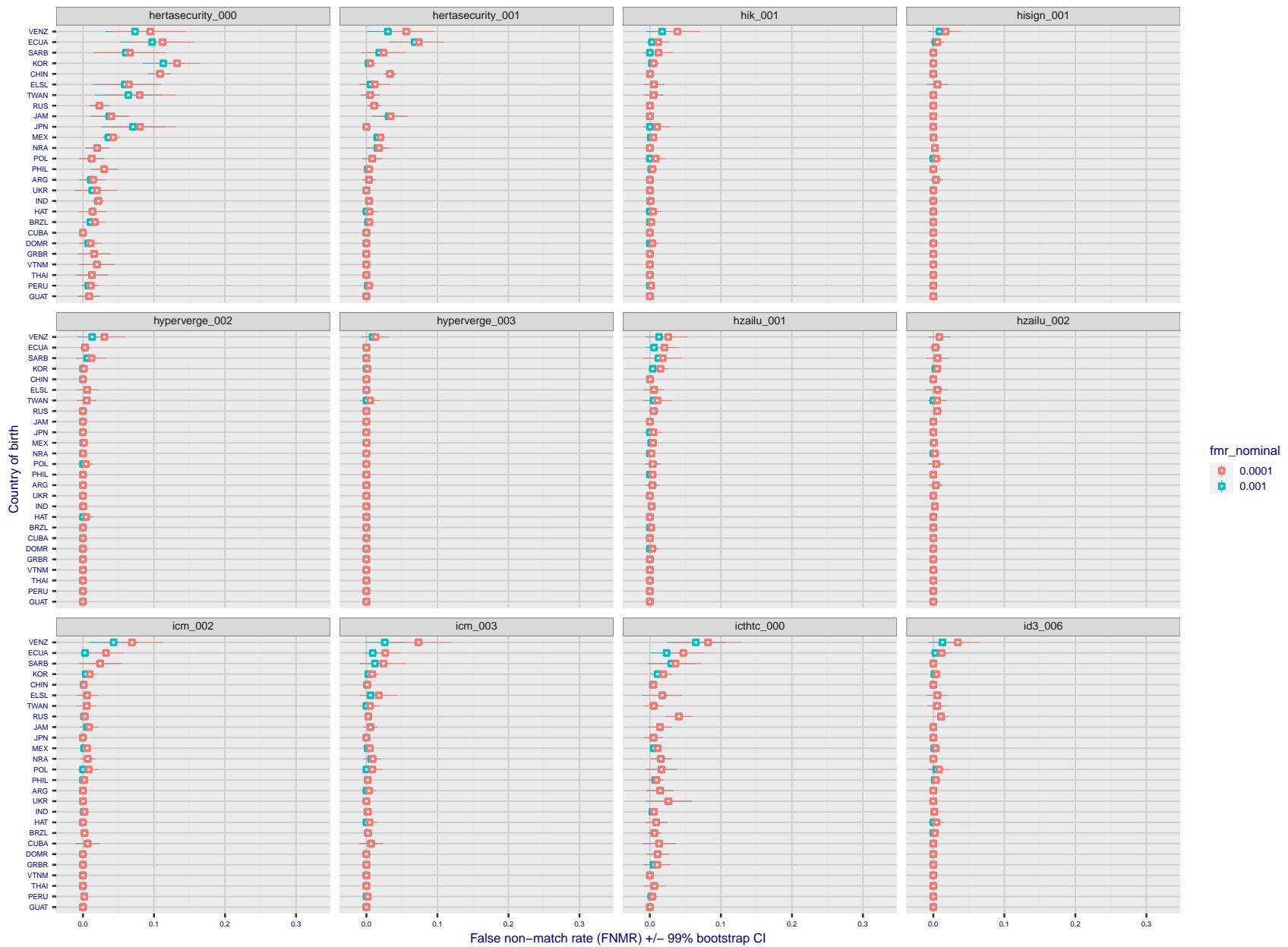


Figure 291: For the visa images, the dots show FNMR by country of birth for two globally set operating thresholds corresponding to $FMR = \{0.001, 0.0001\}$ computed over all on the order of 10^{10} impostor scores. The FMR in each bin will vary also - see subsequent impostor heatmaps in sec. 3.6.1. The figures shows an order of magnitude variation in FNMR across country of birth; these effects are likely due quality variations, then demographics like age and race. The error rates in some cases are zero, and in others the DET is flat so the error rates at the two thresholds are identical. The lines span 1% and 99% of bootstrap replicated FNMR estimates.

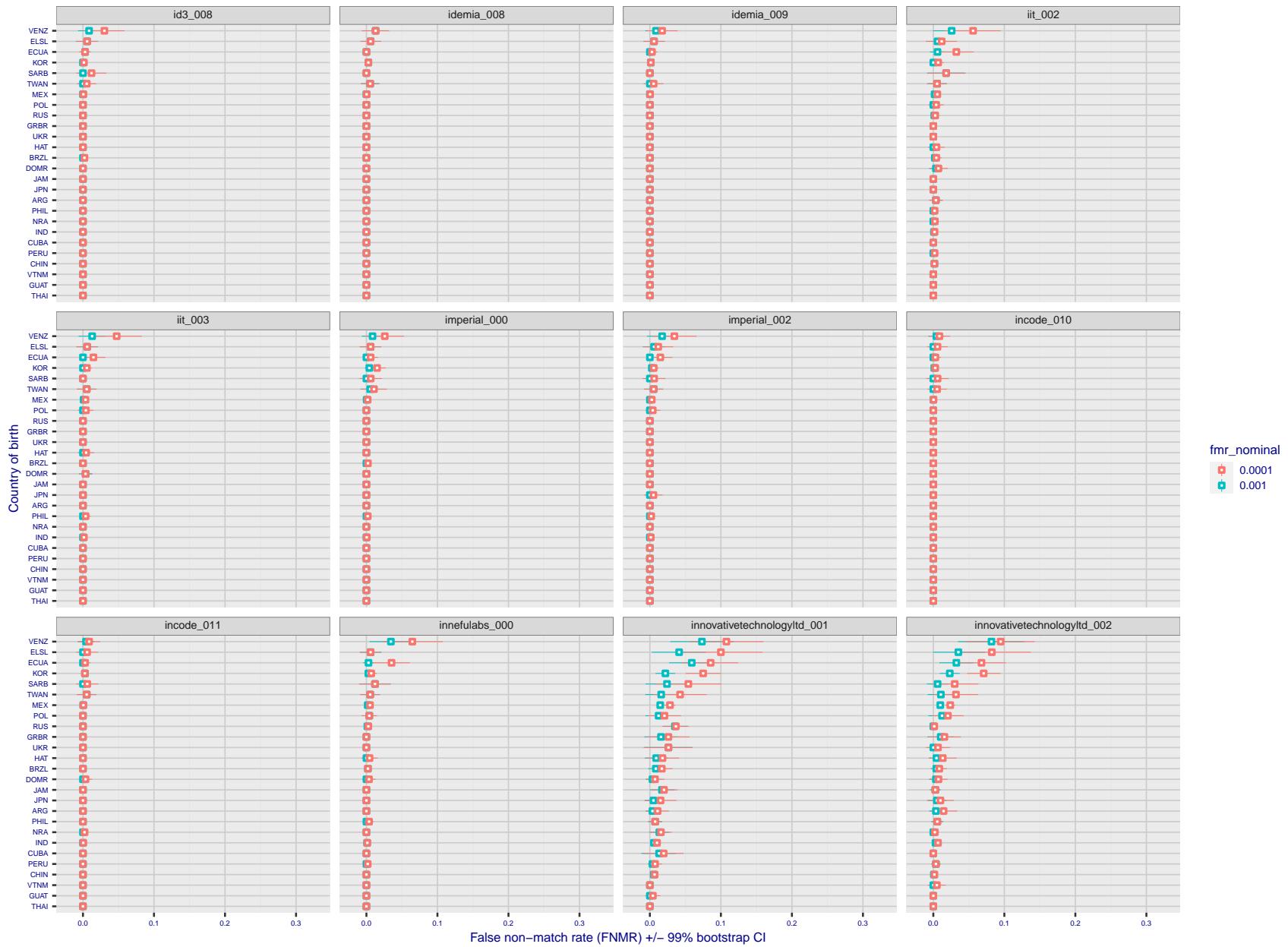


Figure 292: For the visa images, the dots show FNMR by country of birth for two globally set operating thresholds corresponding to $FMR = \{0.001, 0.0001\}$ computed over all on the order of 10^{10} impostor scores. The FMR in each bin will vary also - see subsequent impostor heatmaps in sec. 3.6.1. The figures shows an order of magnitude variation in FNMR across country of birth; these effects are likely due quality variations, then demographics like age and race. The error rates in some cases are zero, and in others the DET is flat so the error rates at the two thresholds are identical. The lines span 1% and 99% of bootstrap replicated FNMR estimates.

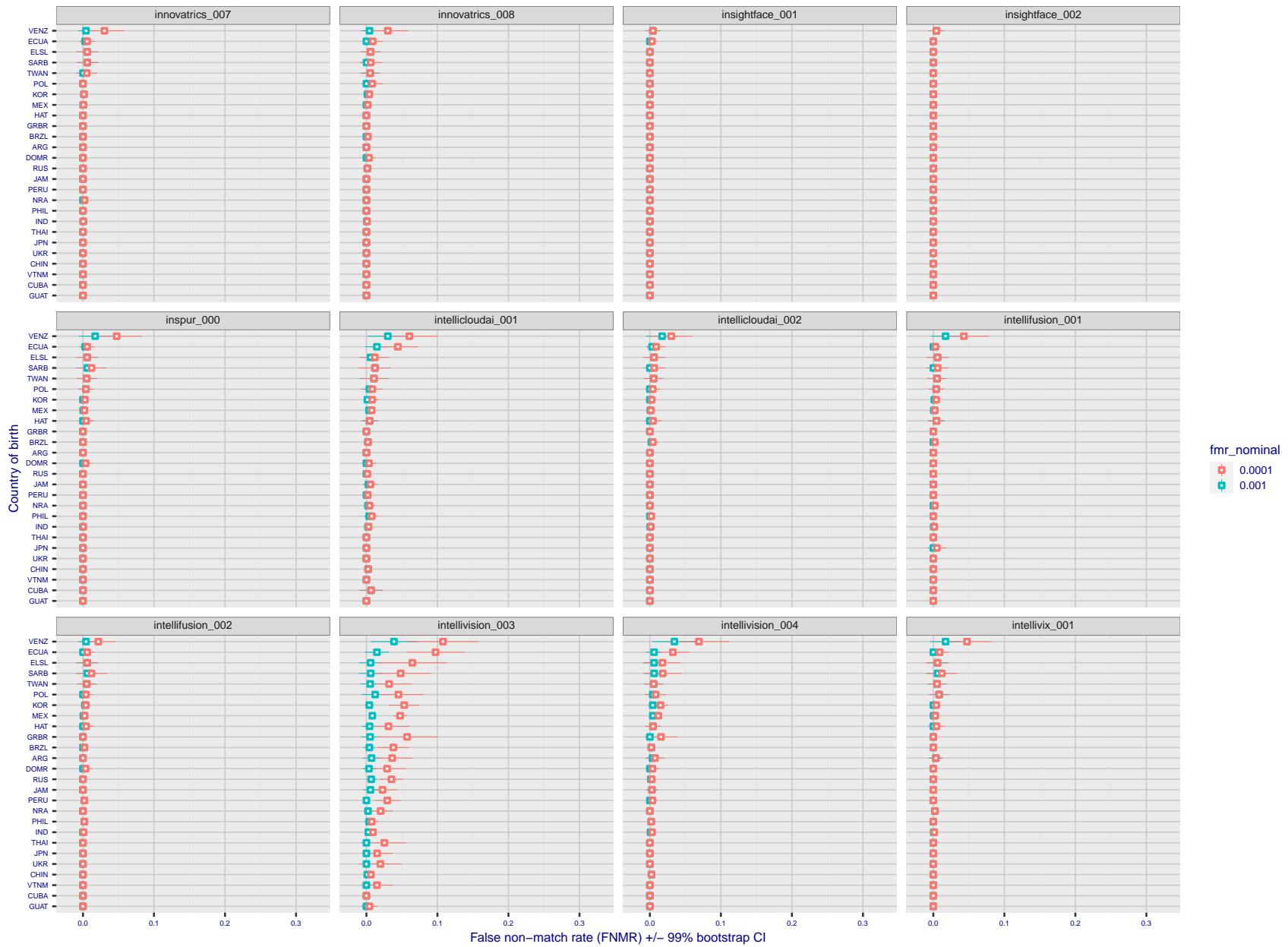


Figure 293: For the visa images, the dots show FNMR by country of birth for two globally set operating thresholds corresponding to $FMR = \{0.001, 0.0001\}$ computed over all on the order of 10^{10} impostor scores. The FMR in each bin will vary also - see subsequent impostor heatmaps in sec. 3.6.1. The figures shows an order of magnitude variation in FNMR across country of birth; these effects are likely due quality variations, then demographics like age and race. The error rates in some cases are zero, and in others the DET is flat so the error rates at the two thresholds are identical. The lines span 1% and 99% of bootstrap replicated FNMR estimates.

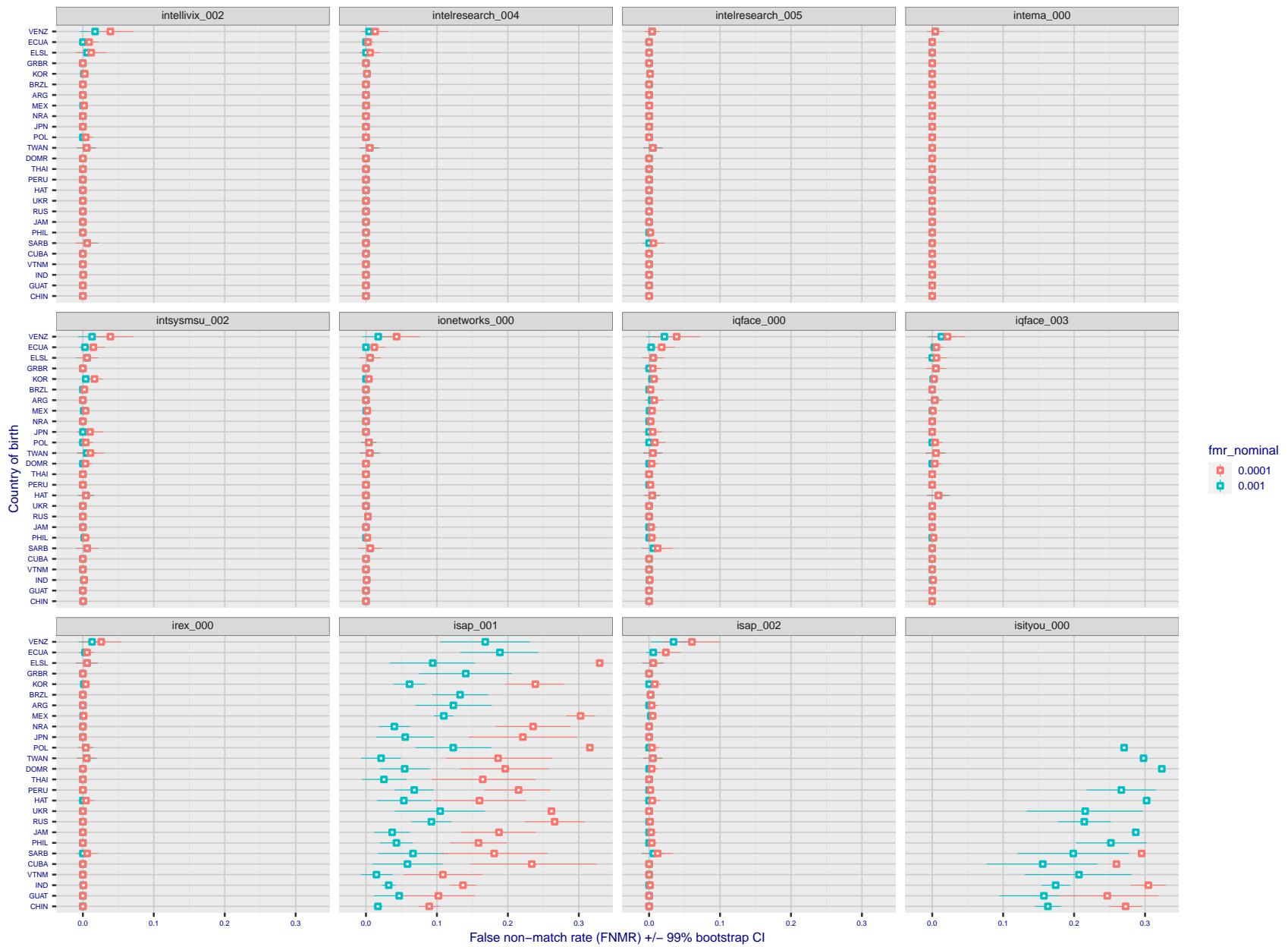


Figure 294: For the visa images, the dots show FNMR by country of birth for two globally set operating thresholds corresponding to $FMR = \{0.001, 0.0001\}$ computed over all on the order of 10^{10} impostor scores. The FMR in each bin will vary also - see subsequent impostor heatmaps in sec. 3.6.1. The figures shows an order of magnitude variation in FNMR across country of birth; these effects are likely due quality variations, then demographics like age and race. The error rates in some cases are zero, and in others the DET is flat so the error rates at the two thresholds are identical. The lines span 1% and 99% of bootstrap replicated FNMR estimates.

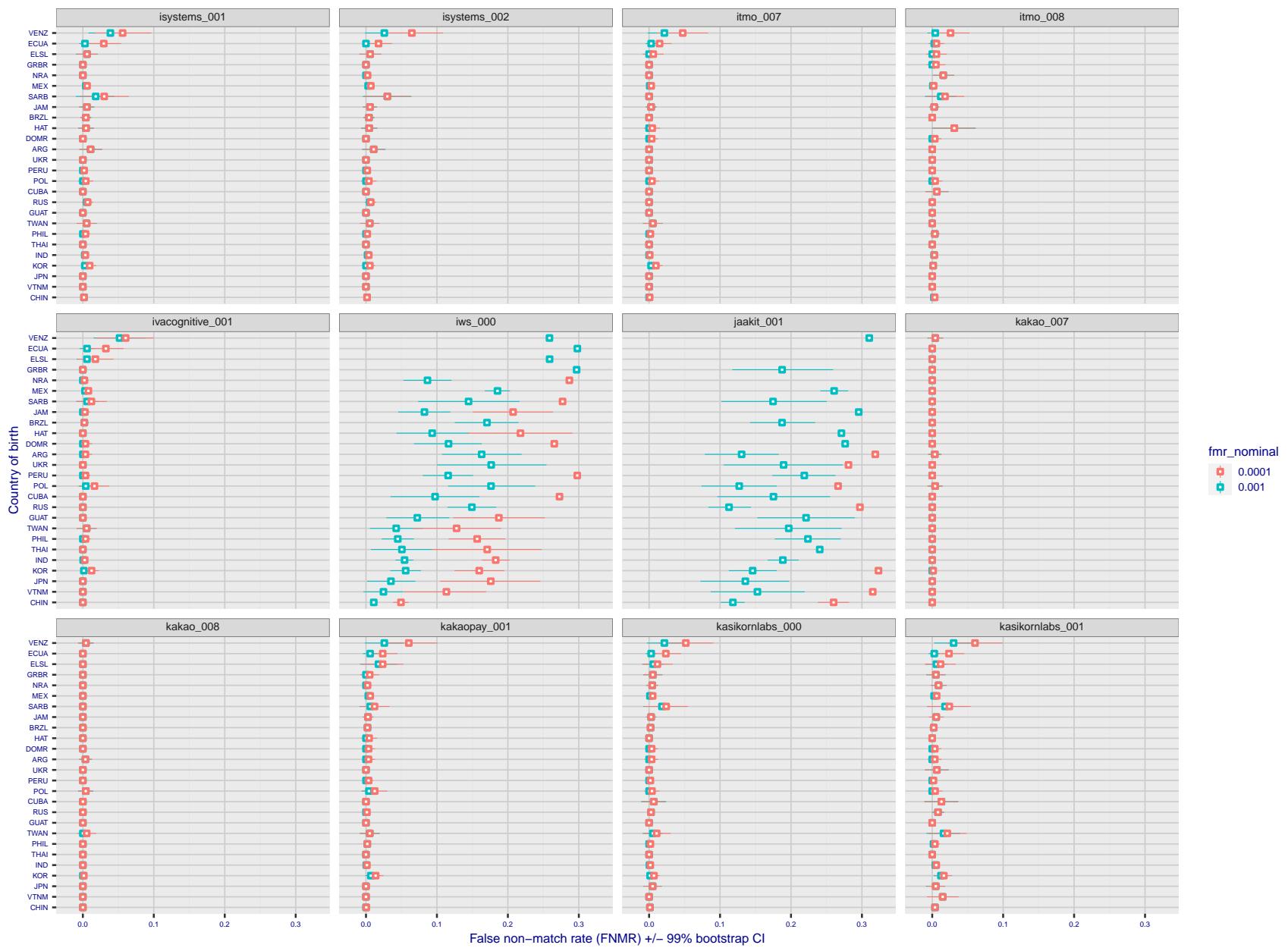


Figure 295: For the visa images, the dots show FNMR by country of birth for two globally set operating thresholds corresponding to $FMR = \{0.001, 0.0001\}$ computed over all on the order of 10^{10} impostor scores. The FMR in each bin will vary also - see subsequent impostor heatmaps in sec. 3.6.1. The figures shows an order of magnitude variation in FNMR across country of birth; these effects are likely due quality variations, then demographics like age and race. The error rates in some cases are zero, and in others the DET is flat so the error rates at the two thresholds are identical. The lines span 1% and 99% of bootstrap replicated FNMR estimates.

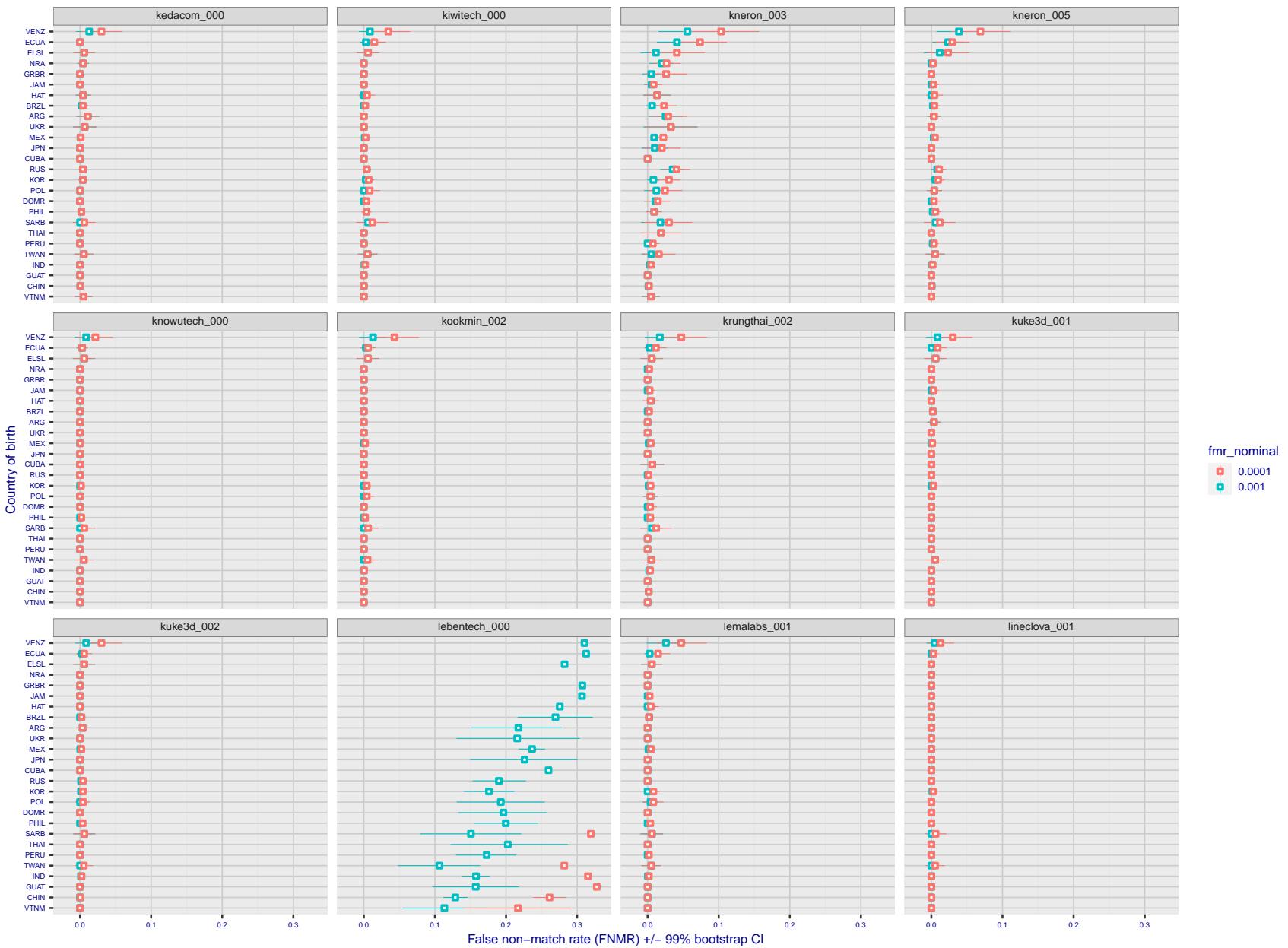


Figure 296: For the visa images, the dots show FNMR by country of birth for two globally set operating thresholds corresponding to $FMR = \{0.001, 0.0001\}$ computed over all on the order of 10^{10} impostor scores. The FMR in each bin will vary also - see subsequent impostor heatmaps in sec. 3.6.1. The figures shows an order of magnitude variation in FNMR across country of birth; these effects are likely due quality variations, then demographics like age and race. The error rates in some cases are zero, and in others the DET is flat so the error rates at the two thresholds are identical. The lines span 1% and 99% of bootstrap replicated FNMR estimates.

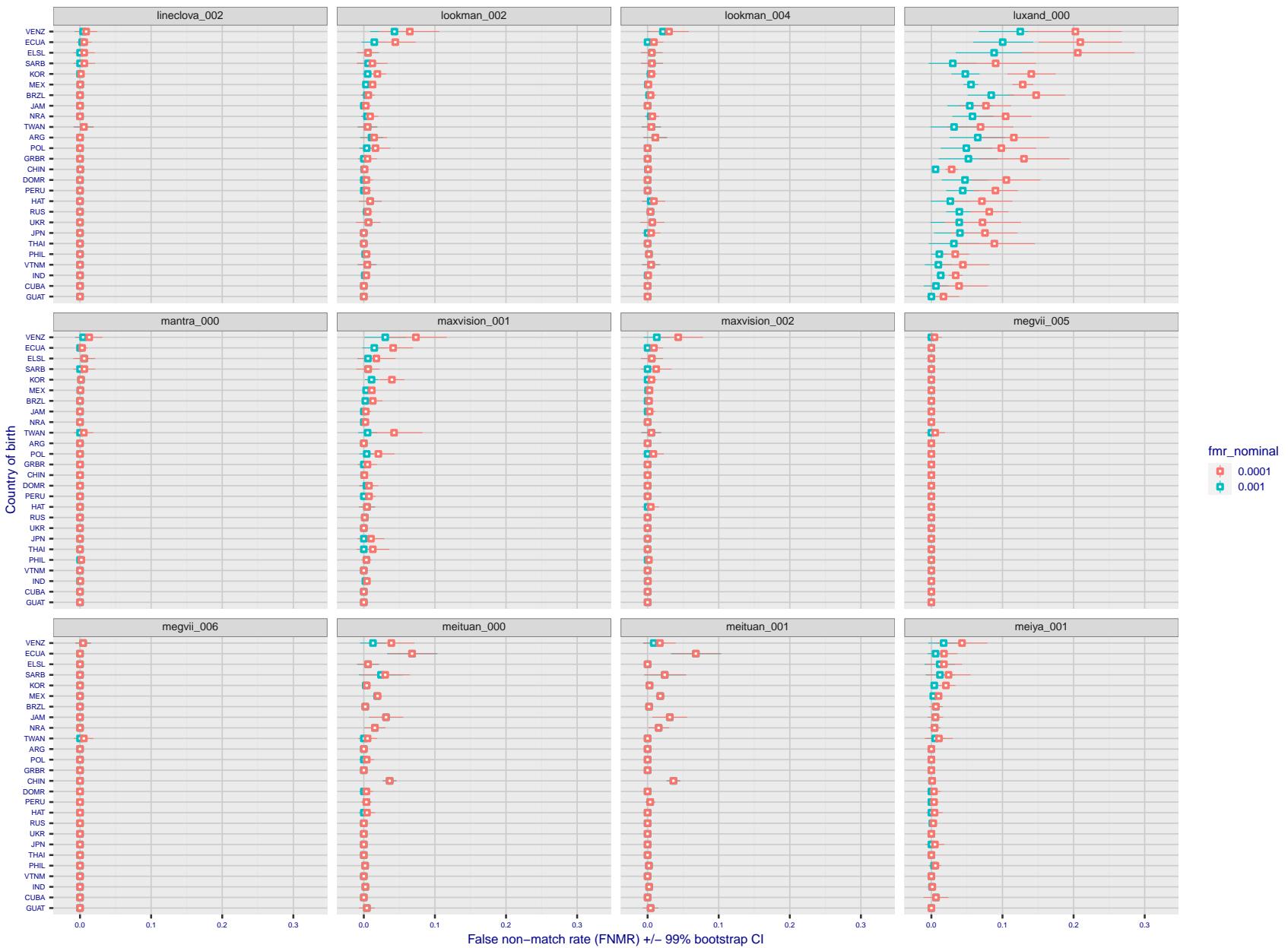


Figure 297: For the visa images, the dots show FNMR by country of birth for two globally set operating thresholds corresponding to $FMR = \{0.001, 0.0001\}$ computed over all on the order of 10^{10} impostor scores. The FMR in each bin will vary also - see subsequent impostor heatmaps in sec. 3.6.1. The figures shows an order of magnitude variation in FNMR across country of birth; these effects are likely due quality variations, then demographics like age and race. The error rates in some cases are zero, and in others the DET is flat so the error rates at the two thresholds are identical. The lines span 1% and 99% of bootstrap replicated FNMR estimates.

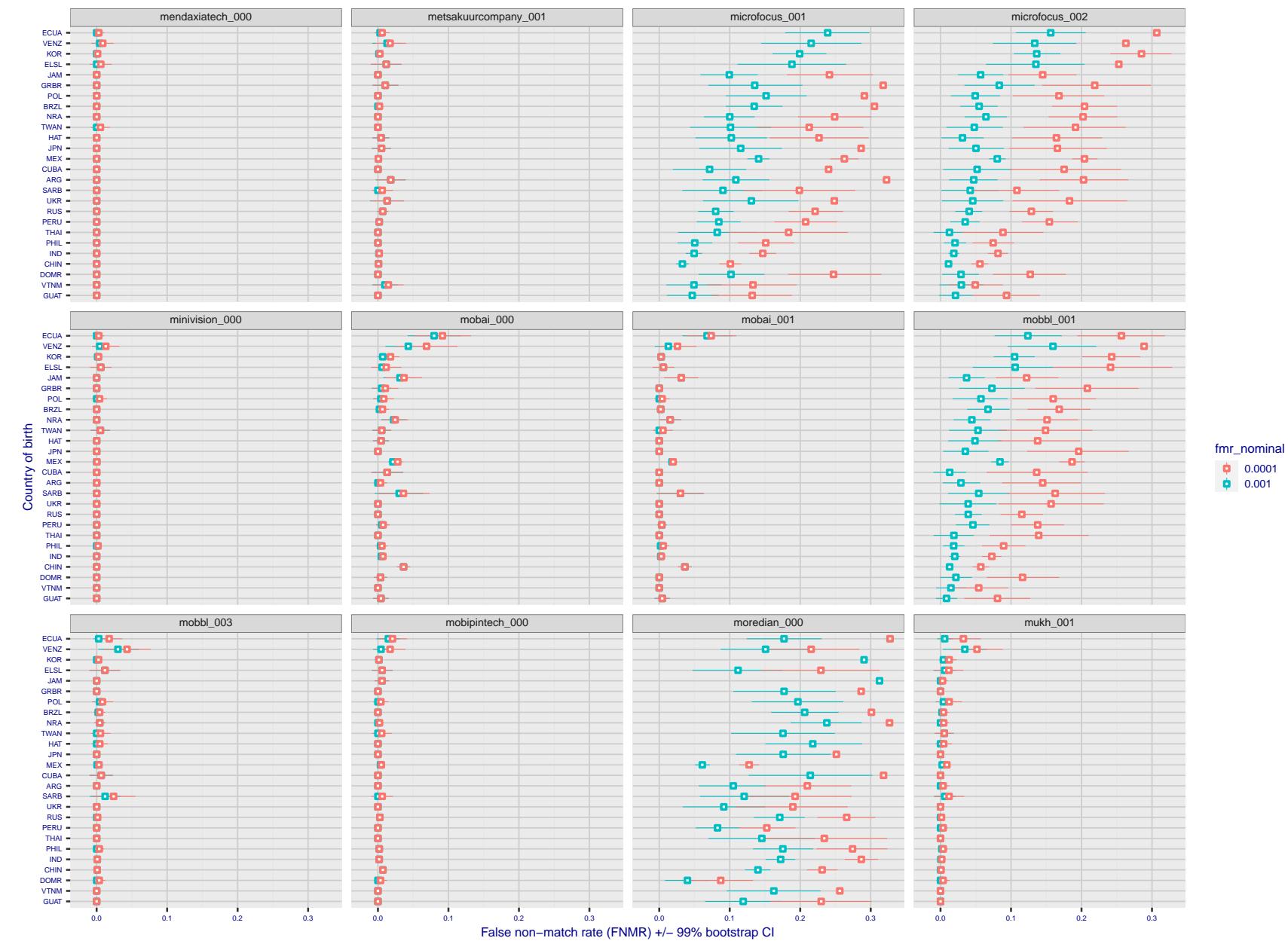


Figure 298: For the visa images, the dots show FNMR by country of birth for two globally set operating thresholds corresponding to $FMR = \{0.001, 0.0001\}$ computed over all on the order of 10^{10} impostor scores. The FMR in each bin will vary also - see subsequent impostor heatmaps in sec. 3.6.1. The figures shows an order of magnitude variation in FNMR across country of birth; these effects are likely due quality variations, then demographics like age and race. The error rates in some cases are zero, and in others the DET is flat so the error rates at the two thresholds are identical. The lines span 1% and 99% of bootstrap replicated FNMR estimates.

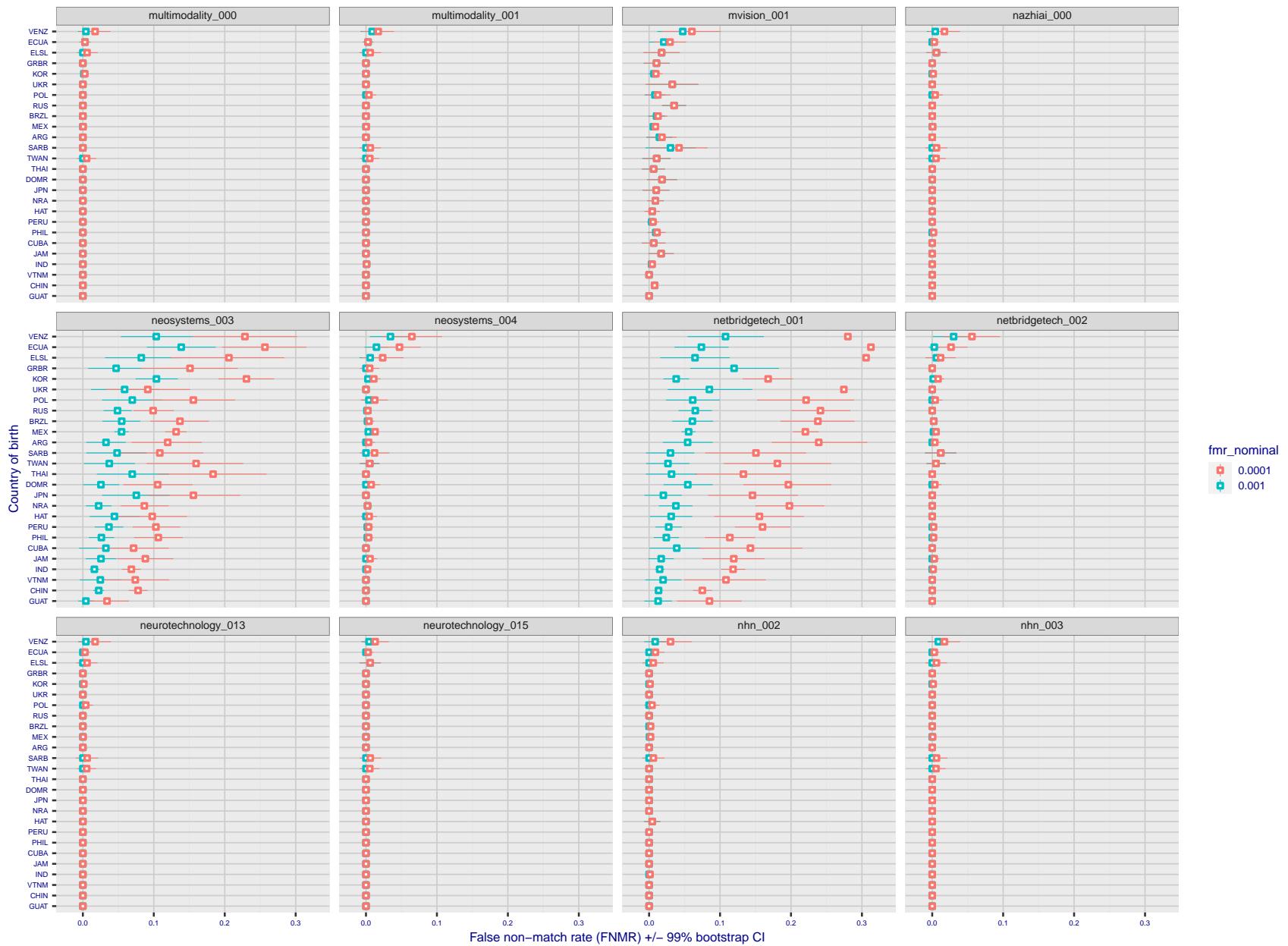


Figure 299: For the visa images, the dots show FNMR by country of birth for two globally set operating thresholds corresponding to $FMR = \{0.001, 0.0001\}$ computed over all on the order of 10^{10} impostor scores. The FMR in each bin will vary also - see subsequent impostor heatmaps in sec. 3.6.1. The figures shows an order of magnitude variation in FNMR across country of birth; these effects are likely due quality variations, then demographics like age and race. The error rates in some cases are zero, and in others the DET is flat so the error rates at the two thresholds are identical. The lines span 1% and 99% of bootstrap replicated FNMR estimates.

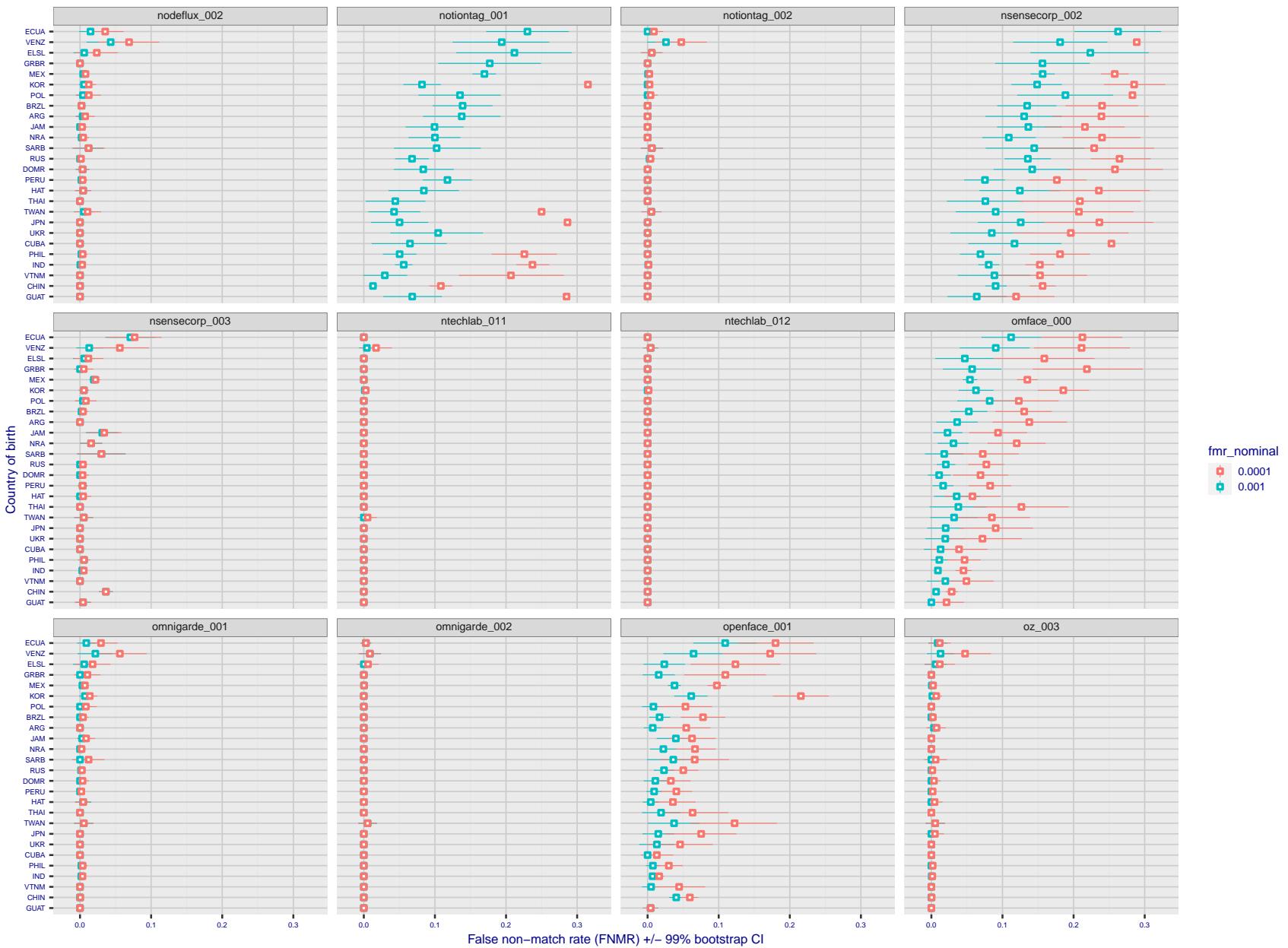


Figure 300: For the visa images, the dots show FNMR by country of birth for two globally set operating thresholds corresponding to $FMR = \{0.001, 0.0001\}$ computed over all on the order of 10^{10} impostor scores. The FMR in each bin will vary also - see subsequent impostor heatmaps in sec. 3.6.1. The figures shows an order of magnitude variation in FNMR across country of birth; these effects are likely due quality variations, then demographics like age and race. The error rates in some cases are zero, and in others the DET is flat so the error rates at the two thresholds are identical. The lines span 1% and 99% of bootstrap replicated FNMR estimates.

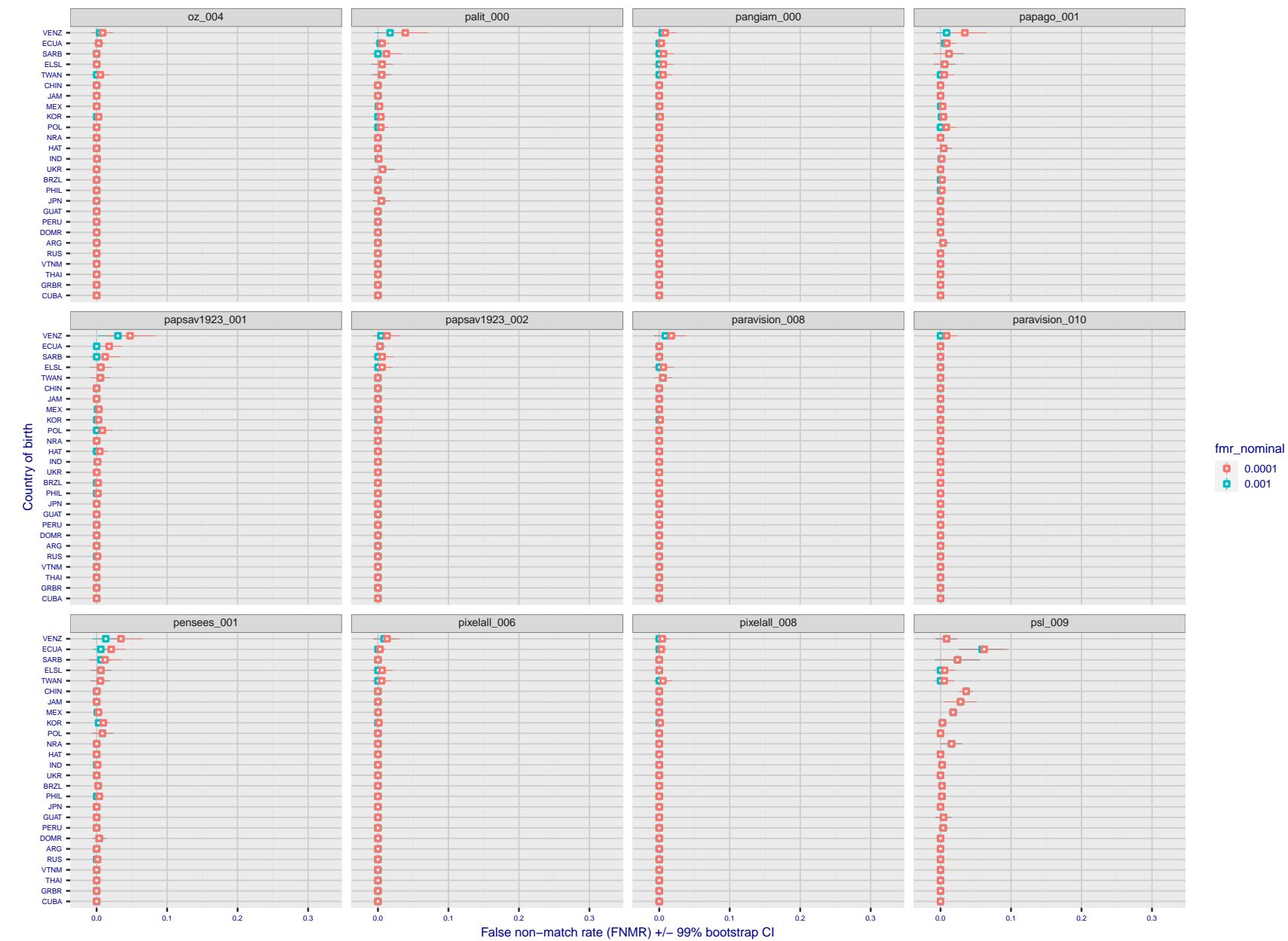


Figure 301: For the visa images, the dots show FNMR by country of birth for two globally set operating thresholds corresponding to $FMR = \{0.001, 0.0001\}$ computed over all on the order of 10^{10} impostor scores. The FMR in each bin will vary also - see subsequent impostor heatmaps in sec. 3.6.1. The figures shows an order of magnitude variation in FNMR across country of birth; these effects are likely due quality variations, then demographics like age and race. The error rates in some cases are zero, and in others the DET is flat so the error rates at the two thresholds are identical. The lines span 1% and 99% of bootstrap replicated FNMR estimates.

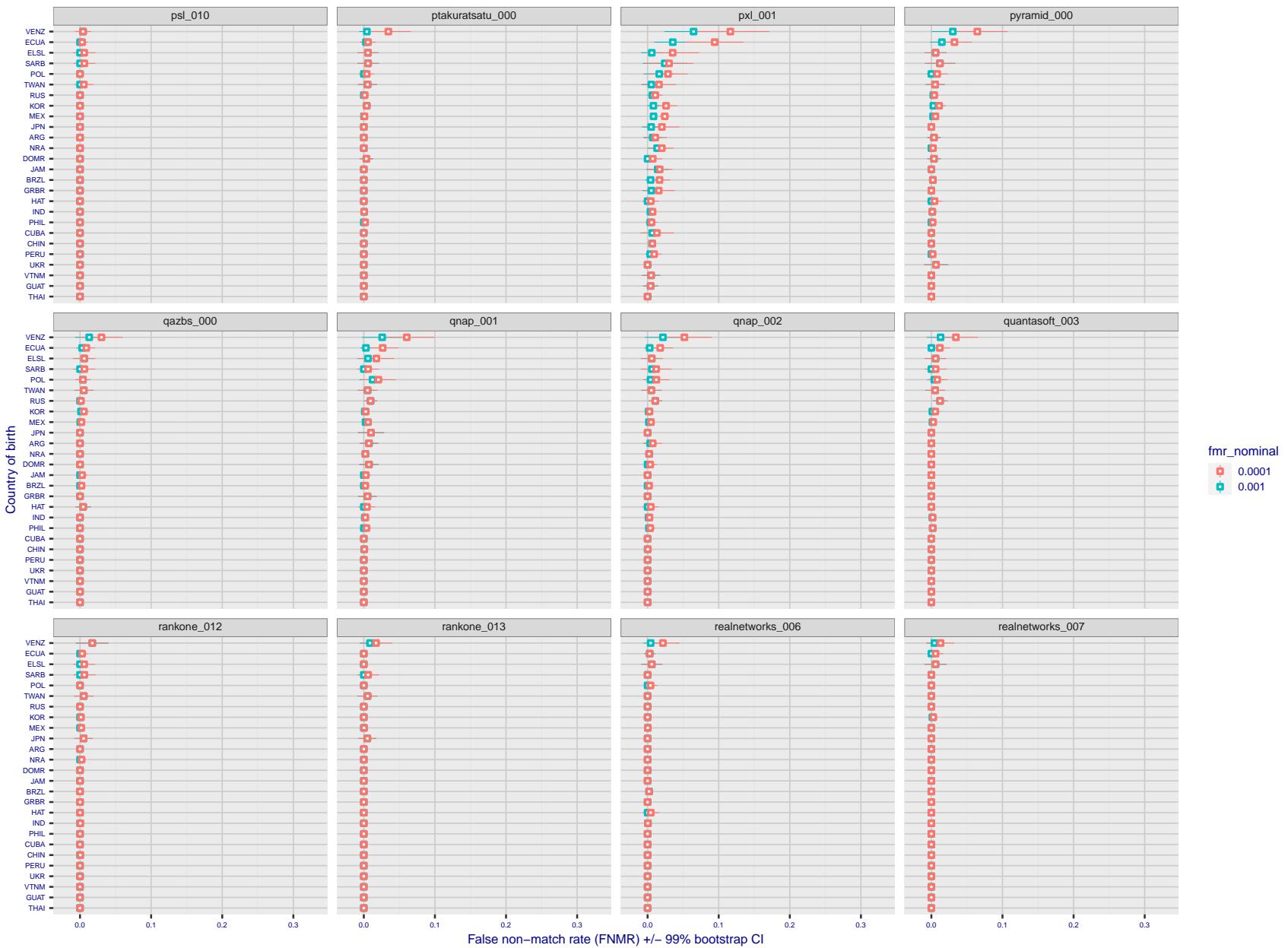


Figure 302: For the visa images, the dots show FNMR by country of birth for two globally set operating thresholds corresponding to $FMR = \{0.001, 0.0001\}$ computed over all on the order of 10^{10} impostor scores. The FMR in each bin will vary also - see subsequent impostor heatmaps in sec. 3.6.1. The figures shows an order of magnitude variation in FNMR across country of birth; these effects are likely due quality variations, then demographics like age and race. The error rates in some cases are zero, and in others the DET is flat so the error rates at the two thresholds are identical. The lines span 1% and 99% of bootstrap replicated FNMR estimates.

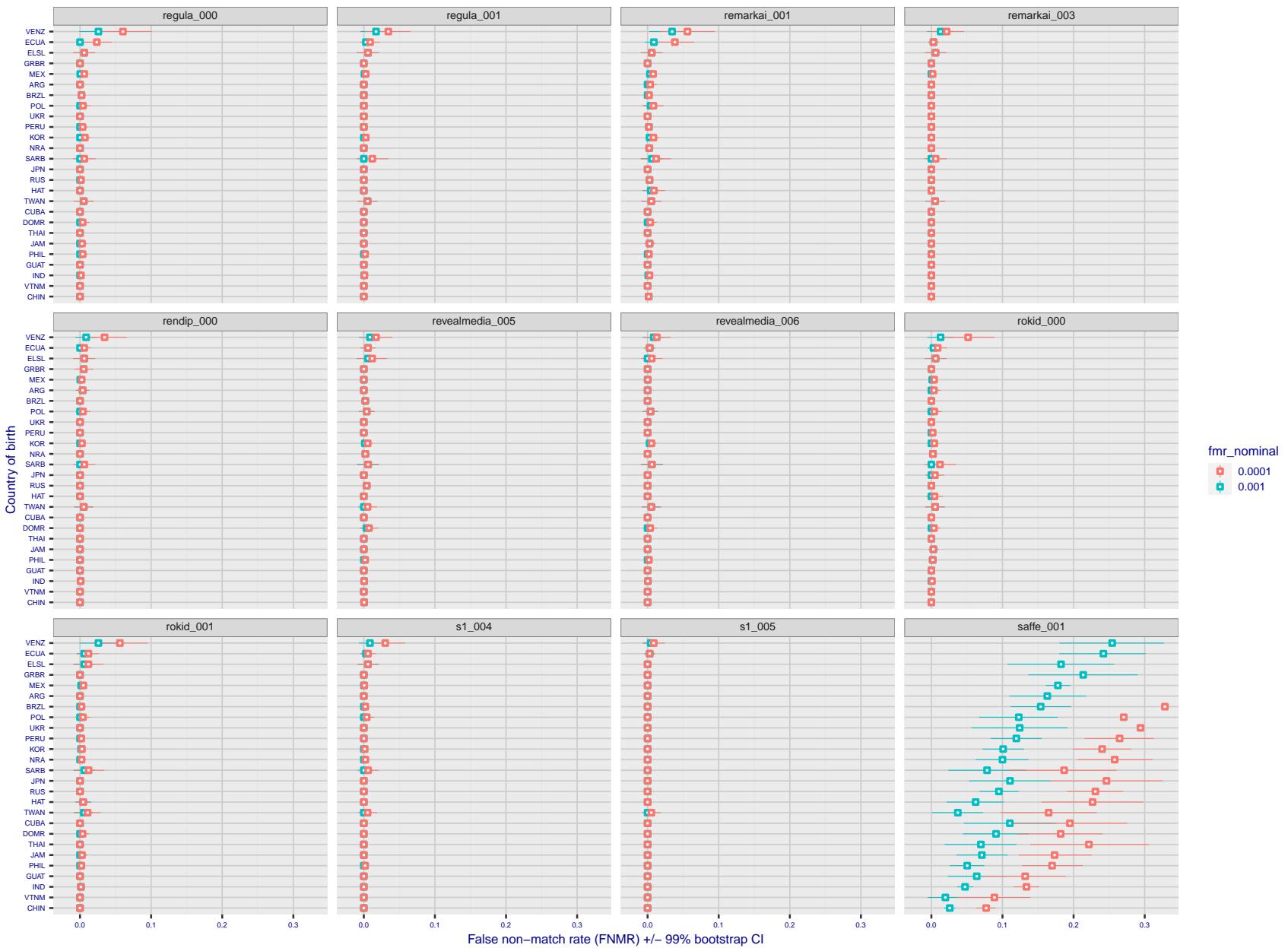


Figure 303: For the visa images, the dots show FNMR by country of birth for two globally set operating thresholds corresponding to $FMR = \{0.001, 0.0001\}$ computed over all on the order of 10^{10} impostor scores. The FMR in each bin will vary also - see subsequent impostor heatmaps in sec. 3.6.1. The figures shows an order of magnitude variation in FNMR across country of birth; these effects are likely due quality variations, then demographics like age and race. The error rates in some cases are zero, and in others the DET is flat so the error rates at the two thresholds are identical. The lines span 1% and 99% of bootstrap replicated FNMR estimates.

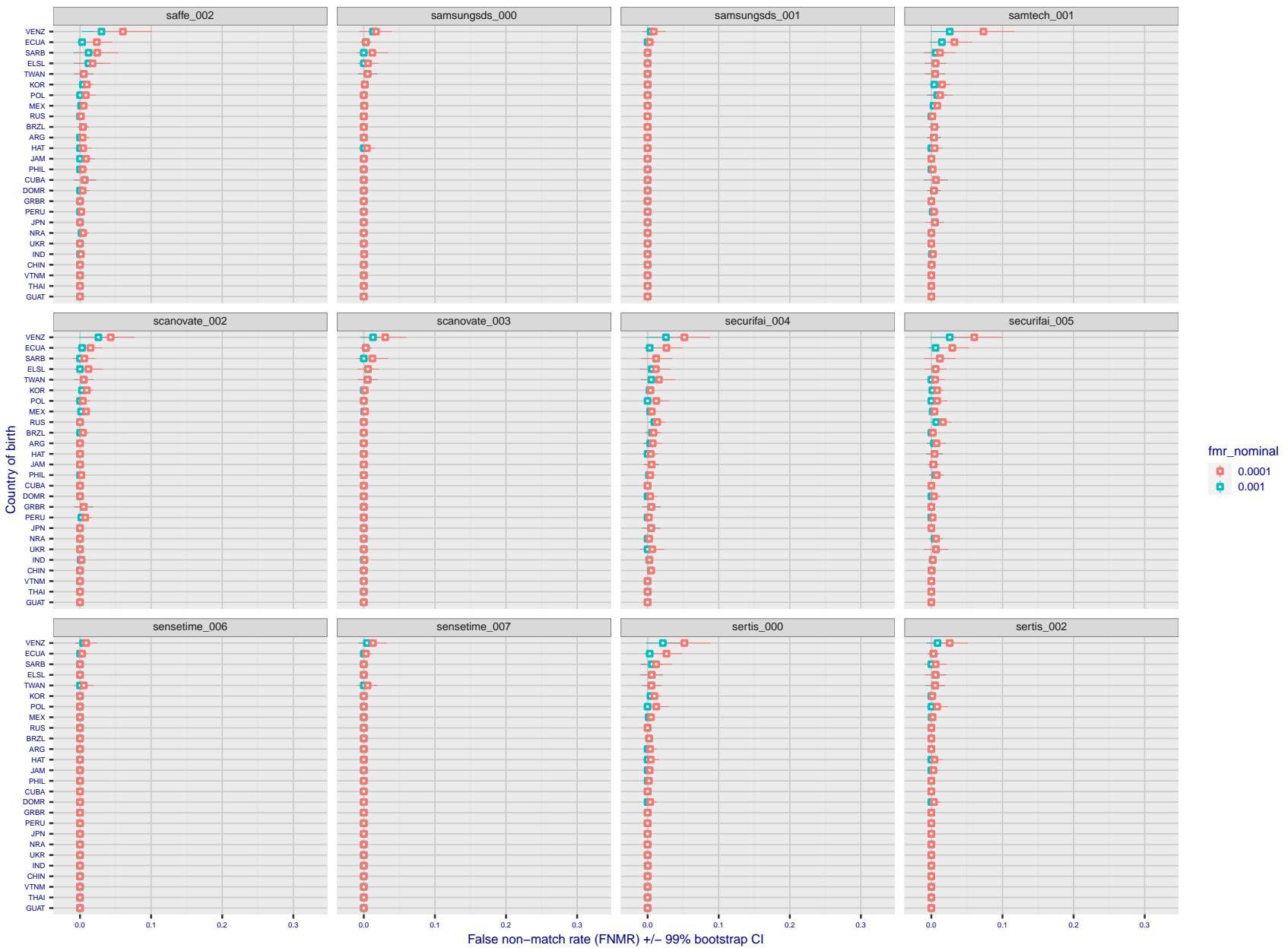


Figure 304: For the visa images, the dots show FNMR by country of birth for two globally set operating thresholds corresponding to $FMR = \{0.001, 0.0001\}$ computed over all on the order of 10^{10} impostor scores. The FMR in each bin will vary also - see subsequent impostor heatmaps in sec. 3.6.1. The figures shows an order of magnitude variation in FNMR across country of birth; these effects are likely due quality variations, then demographics like age and race. The error rates in some cases are zero, and in others the DET is flat so the error rates at the two thresholds are identical. The lines span 1% and 99% of bootstrap replicated FNMR estimates.

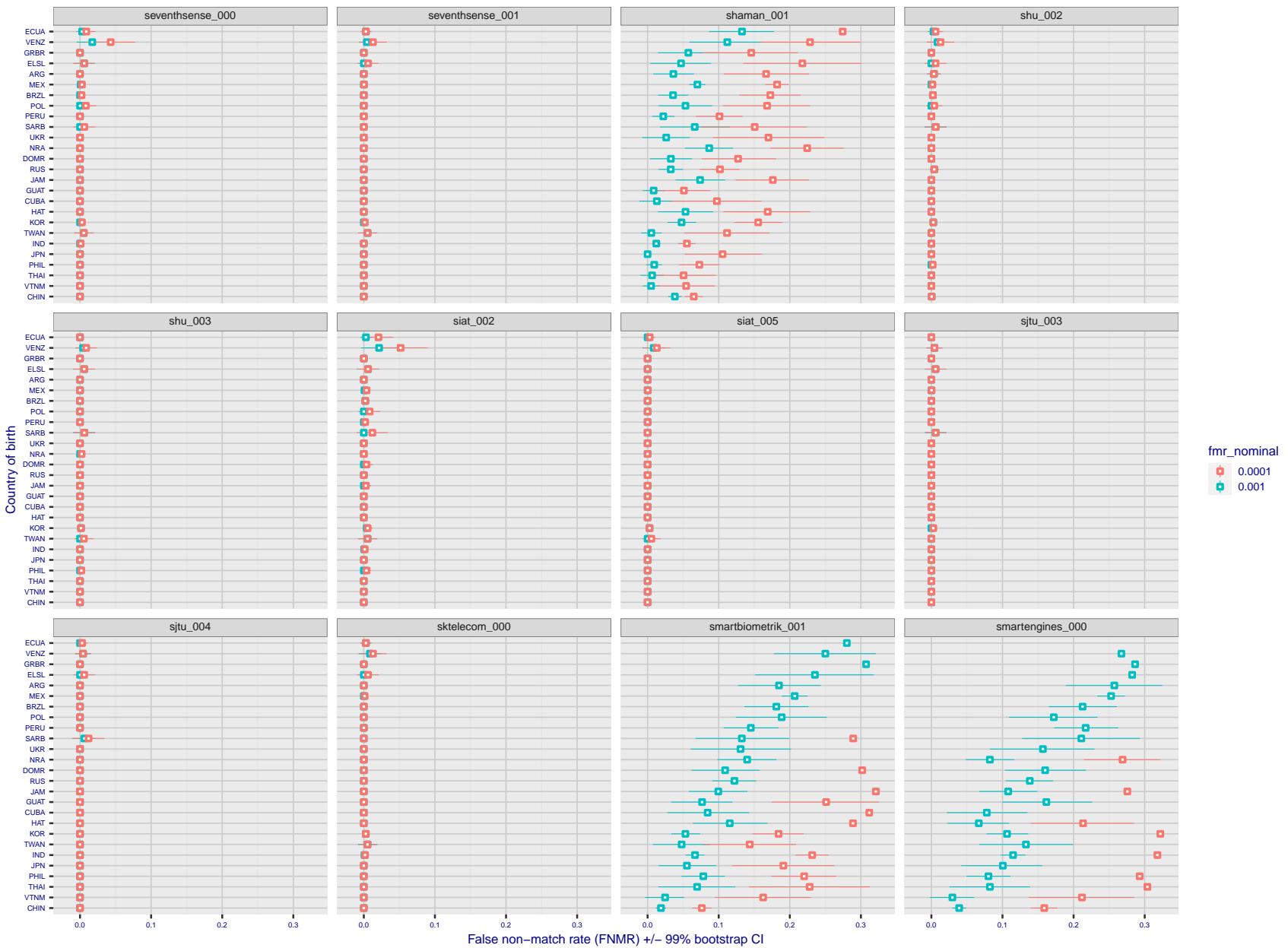


Figure 305: For the visa images, the dots show FNMR by country of birth for two globally set operating thresholds corresponding to $FMR = \{0.001, 0.0001\}$ computed over all on the order of 10^{10} impostor scores. The FMR in each bin will vary also - see subsequent impostor heatmaps in sec. 3.6.1. The figures shows an order of magnitude variation in FNMR across country of birth; these effects are likely due quality variations, then demographics like age and race. The error rates in some cases are zero, and in others the DET is flat so the error rates at the two thresholds are identical. The lines span 1% and 99% of bootstrap replicated FNMR estimates.

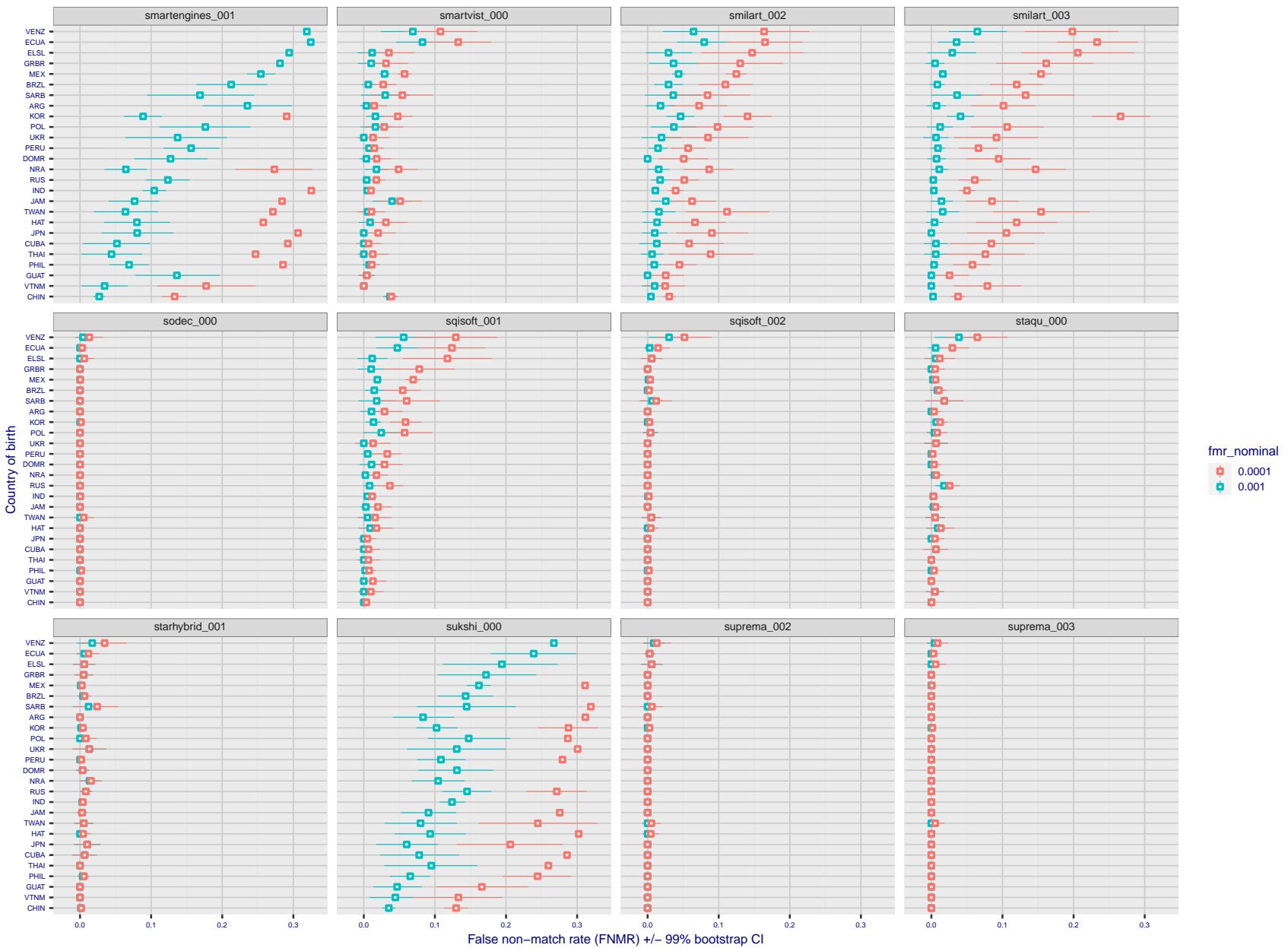


Figure 306: For the visa images, the dots show FNMR by country of birth for two globally set operating thresholds corresponding to $FMR = \{0.001, 0.0001\}$ computed over all on the order of 10^{10} impostor scores. The FMR in each bin will vary also - see subsequent impostor heatmaps in sec. 3.6.1. The figures shows an order of magnitude variation in FNMR across country of birth; these effects are likely due quality variations, then demographics like age and race. The error rates in some cases are zero, and in others the DET is flat so the error rates at the two thresholds are identical. The lines span 1% and 99% of bootstrap replicated FNMR estimates.

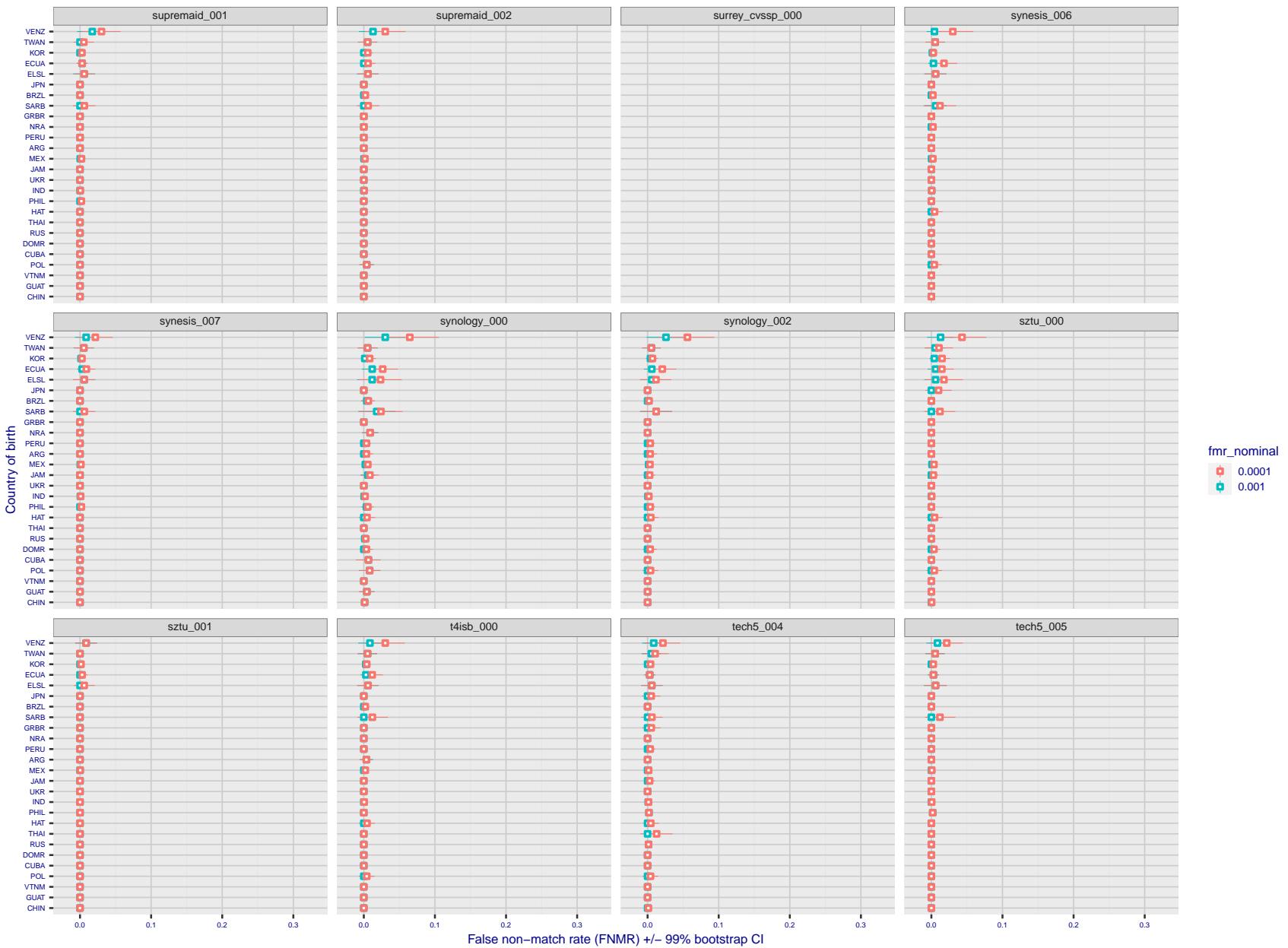


Figure 307: For the visa images, the dots show FNMR by country of birth for two globally set operating thresholds corresponding to $FMR = \{0.001, 0.0001\}$ computed over all on the order of 10^{10} impostor scores. The FMR in each bin will vary also - see subsequent impostor heatmaps in sec. 3.6.1. The figures shows an order of magnitude variation in FNMR across country of birth; these effects are likely due quality variations, then demographics like age and race. The error rates in some cases are zero, and in others the DET is flat so the error rates at the two thresholds are identical. The lines span 1% and 99% of bootstrap replicated FNMR estimates.

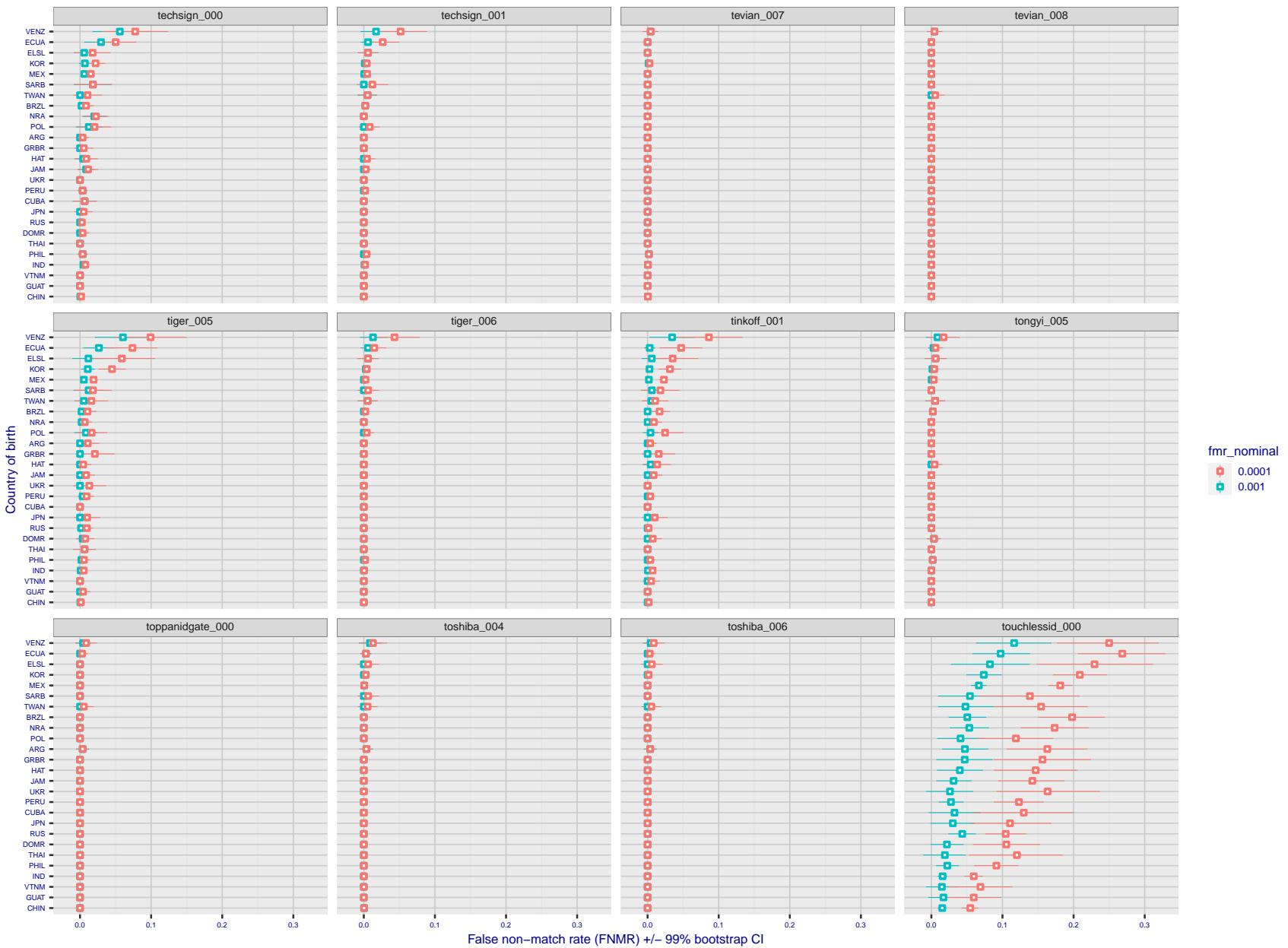


Figure 308: For the visa images, the dots show FNMR by country of birth for two globally set operating thresholds corresponding to $FMR = \{0.001, 0.0001\}$ computed over all on the order of 10^{10} impostor scores. The FMR in each bin will vary also - see subsequent impostor heatmaps in sec. 3.6.1. The figures shows an order of magnitude variation in FNMR across country of birth; these effects are likely due quality variations, then demographics like age and race. The error rates in some cases are zero, and in others the DET is flat so the error rates at the two thresholds are identical. The lines span 1% and 99% of bootstrap replicated FNMR estimates.

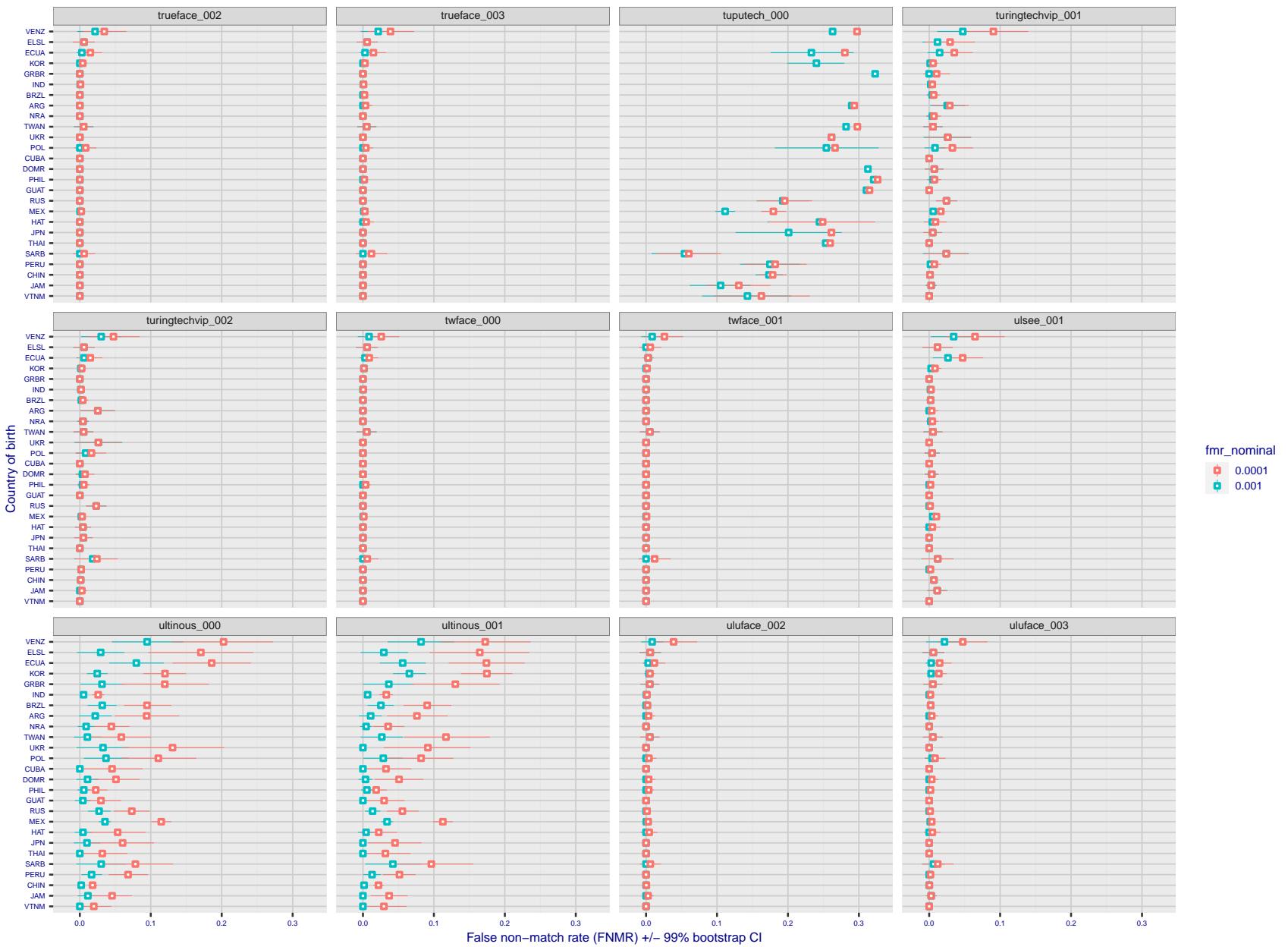


Figure 309: For the visa images, the dots show FNMR by country of birth for two globally set operating thresholds corresponding to $FMR = \{0.001, 0.0001\}$ computed over all on the order of 10^{10} impostor scores. The FMR in each bin will vary also - see subsequent impostor heatmaps in sec. 3.6.1. The figures shows an order of magnitude variation in FNMR across country of birth; these effects are likely due quality variations, then demographics like age and race. The error rates in some cases are zero, and in others the DET is flat so the error rates at the two thresholds are identical. The lines span 1% and 99% of bootstrap replicated FNMR estimates.

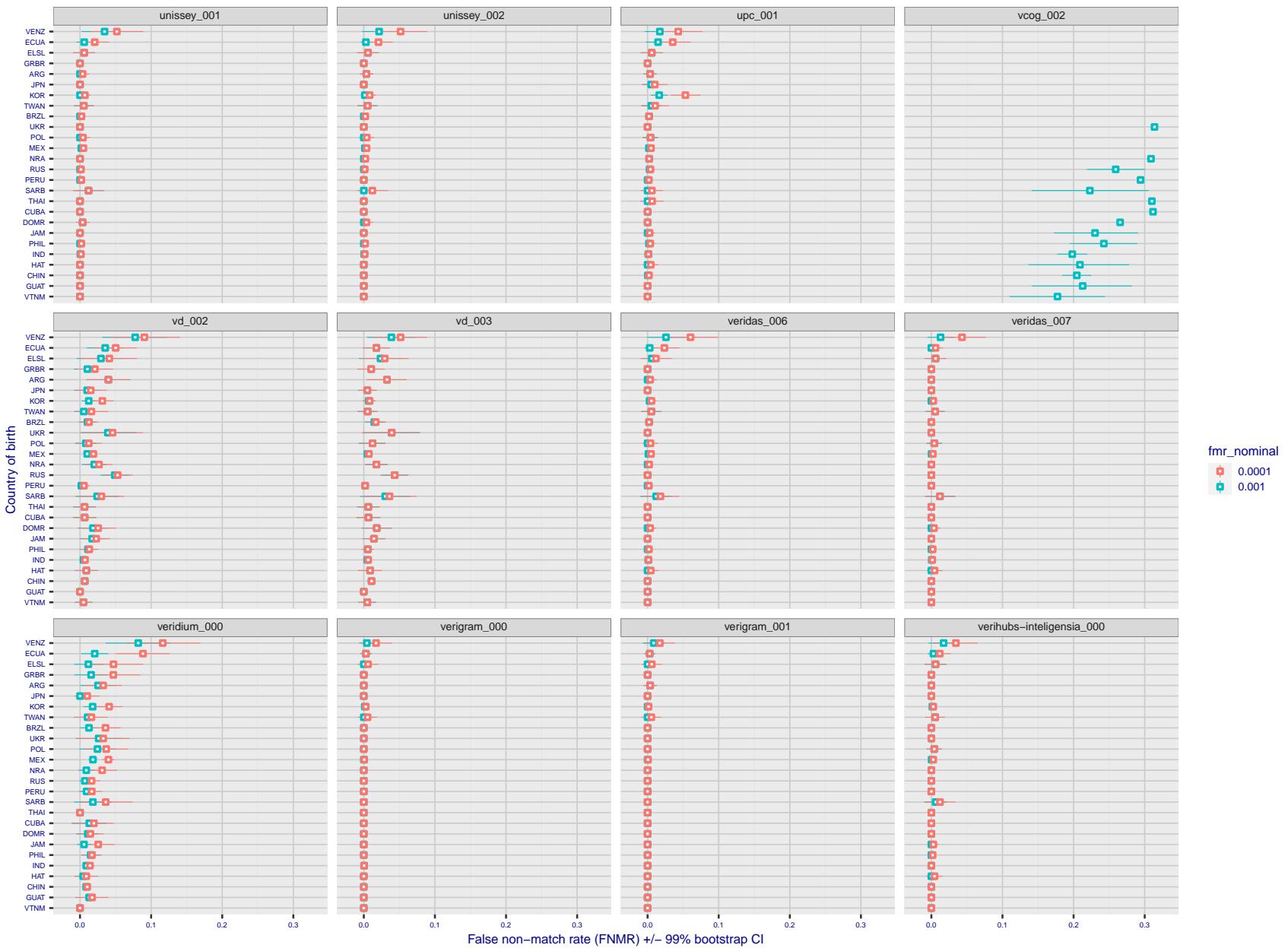


Figure 310: For the visa images, the dots show FNMR by country of birth for two globally set operating thresholds corresponding to $FMR = \{0.001, 0.0001\}$ computed over all on the order of 10^{10} impostor scores. The FMR in each bin will vary also - see subsequent impostor heatmaps in sec. 3.6.1. The figures shows an order of magnitude variation in FNMR across country of birth; these effects are likely due quality variations, then demographics like age and race. The error rates in some cases are zero, and in others the DET is flat so the error rates at the two thresholds are identical. The lines span 1% and 99% of bootstrap replicated FNMR estimates.

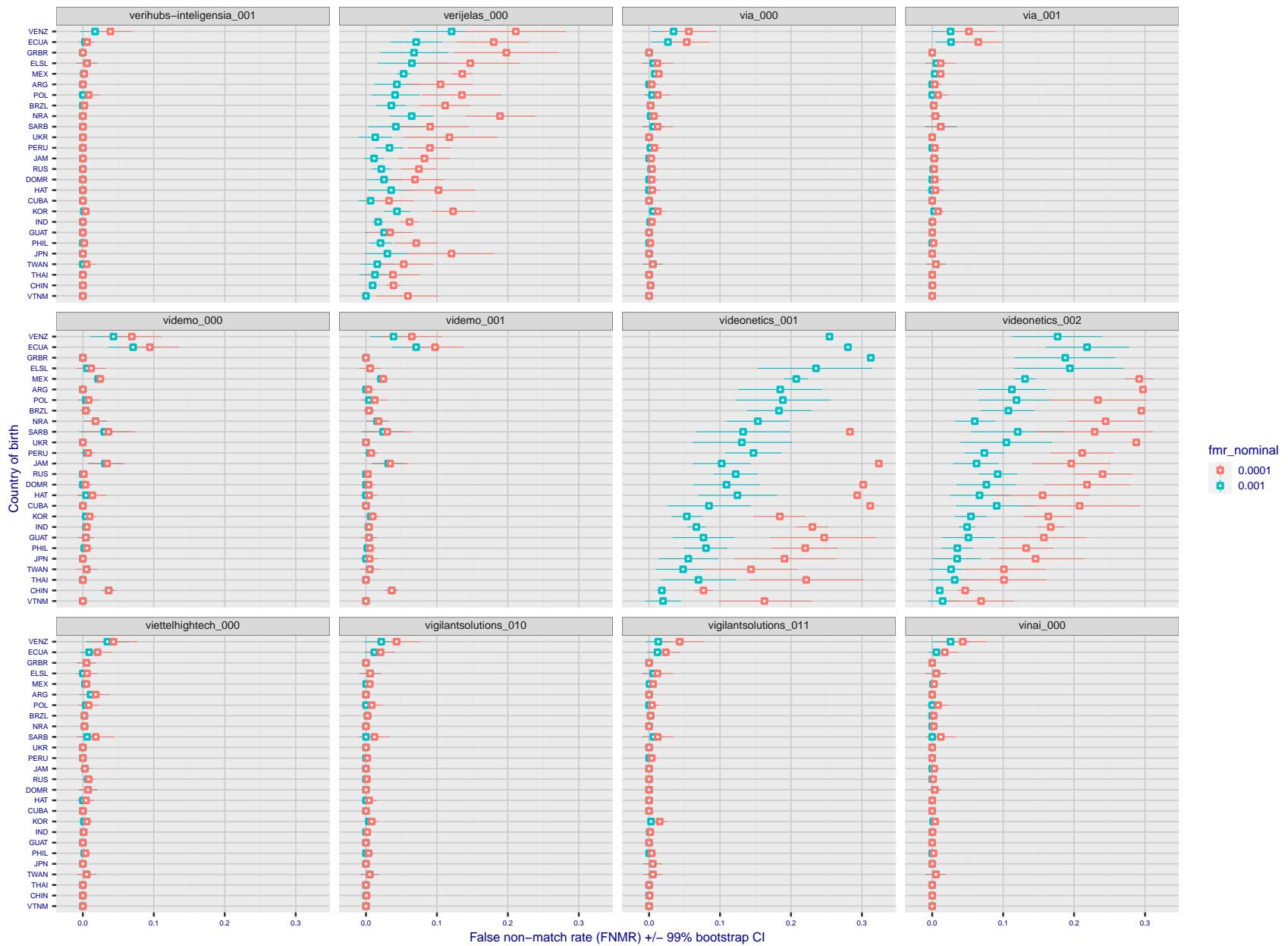


Figure 311: For the visa images, the dots show FNMR by country of birth for two globally set operating thresholds corresponding to $FMR = \{0.001, 0.0001\}$ computed over all on the order of 10^{10} impostor scores. The FMR in each bin will vary also - see subsequent impostor heatmaps in sec. 3.6.1. The figures shows an order of magnitude variation in FNMR across country of birth; these effects are likely due quality variations, then demographics like age and race. The error rates in some cases are zero, and in others the DET is flat so the error rates at the two thresholds are identical. The lines span 1% and 99% of bootstrap replicated FNMR estimates.

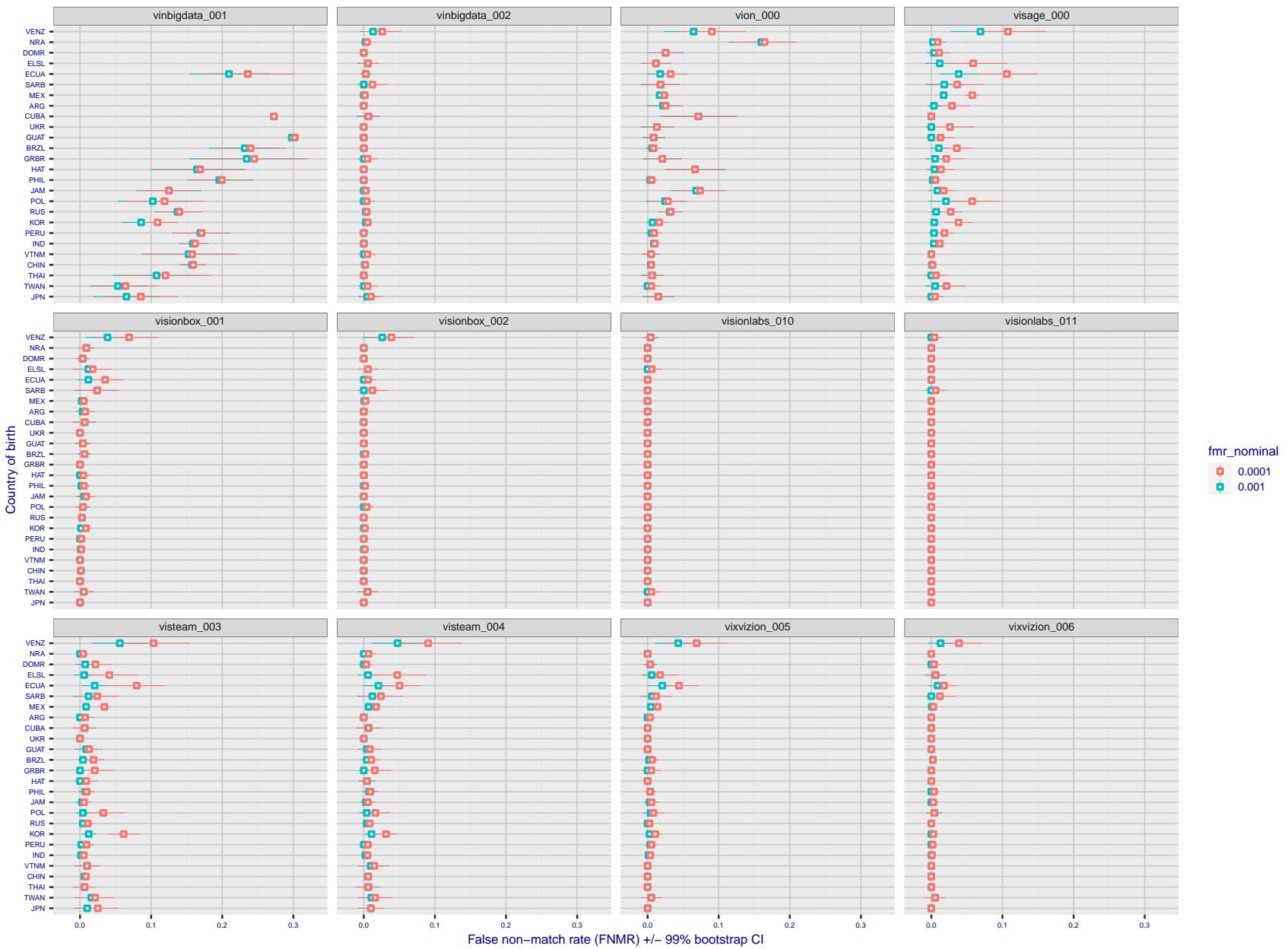


Figure 312: For the visa images, the dots show FNMR by country of birth for two globally set operating thresholds corresponding to $FMR = \{0.001, 0.0001\}$ computed over all on the order of 10^{10} impostor scores. The FMR in each bin will vary also - see subsequent impostor heatmaps in sec. 3.6.1. The figures shows an order of magnitude variation in FNMR across country of birth; these effects are likely due quality variations, then demographics like age and race. The error rates in some cases are zero, and in others the DET is flat so the error rates at the two thresholds are identical. The lines span 1% and 99% of bootstrap replicated FNMR estimates.

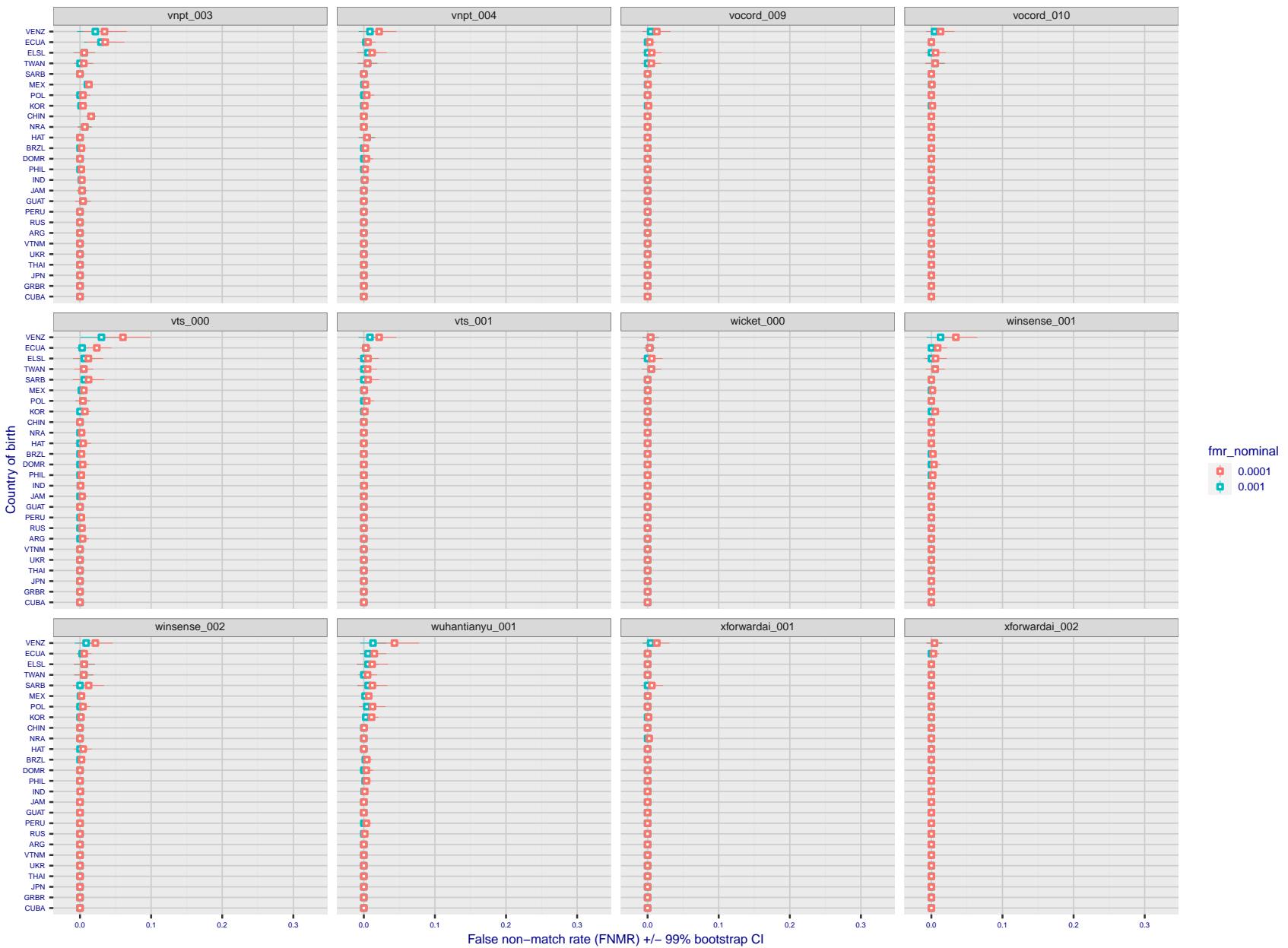


Figure 313: For the visa images, the dots show FNMR by country of birth for two globally set operating thresholds corresponding to $FMR = \{0.001, 0.0001\}$ computed over all on the order of 10^{10} impostor scores. The FMR in each bin will vary also - see subsequent impostor heatmaps in sec. 3.6.1. The figures shows an order of magnitude variation in FNMR across country of birth; these effects are likely due quality variations, then demographics like age and race. The error rates in some cases are zero, and in others the DET is flat so the error rates at the two thresholds are identical. The lines span 1% and 99% of bootstrap replicated FNMR estimates.

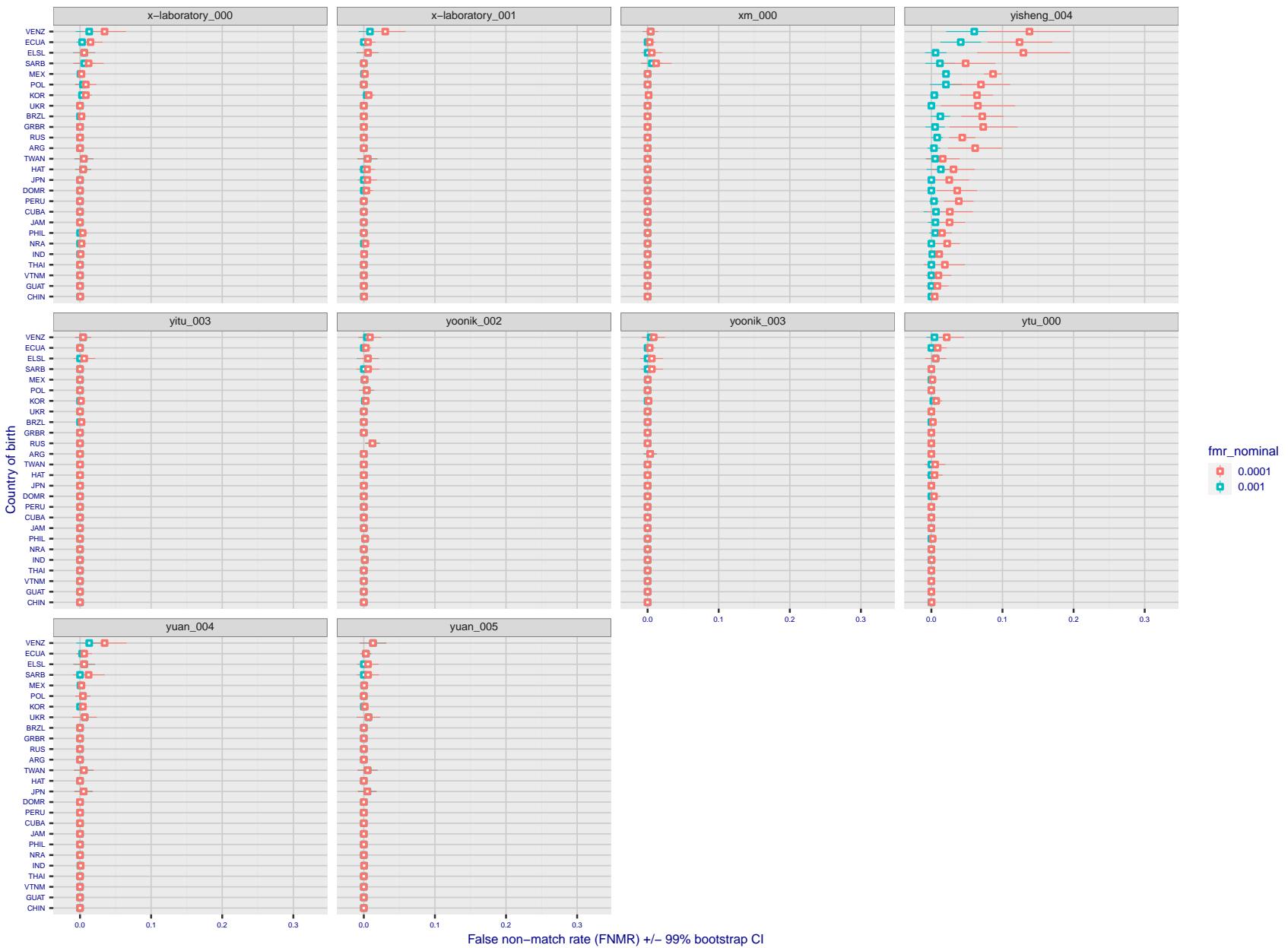


Figure 314: For the visa images, the dots show FNMR by country of birth for two globally set operating thresholds corresponding to $FMR = \{0.001, 0.0001\}$ computed over all on the order of 10^{10} impostor scores. The FMR in each bin will vary also - see subsequent impostor heatmaps in sec. 3.6.1. The figures shows an order of magnitude variation in FNMR across country of birth; these effects are likely due quality variations, then demographics like age and race. The error rates in some cases are zero, and in others the DET is flat so the error rates at the two thresholds are identical. The lines span 1% and 99% of bootstrap replicated FNMR estimates.

Caveats: The results may not relate to subject-specific properties. Instead they could reflect image-specific quality differences, which could occur due to collection protocol or software processing variations.

3.5.2 Effect of ageing

Background: Faces change appearance throughout life. This change gradually reduces similarity of a new image to an earlier image. Face recognition algorithms give reduced similarity scores and more frequent false rejections.

Goal: To quantify false non-match rates (FNMR) as a function of elapsed time in an adult population.

Methods: Using the mugshot images, a threshold is set to give FMR = 0.00001 over the entire impostor set. Then FNMR is measured over 1000 bootstrap replications of the genuine scores.

Results: For the visa images, Figure 342 shows how false non-match rates for genuine users, as a function of age group.

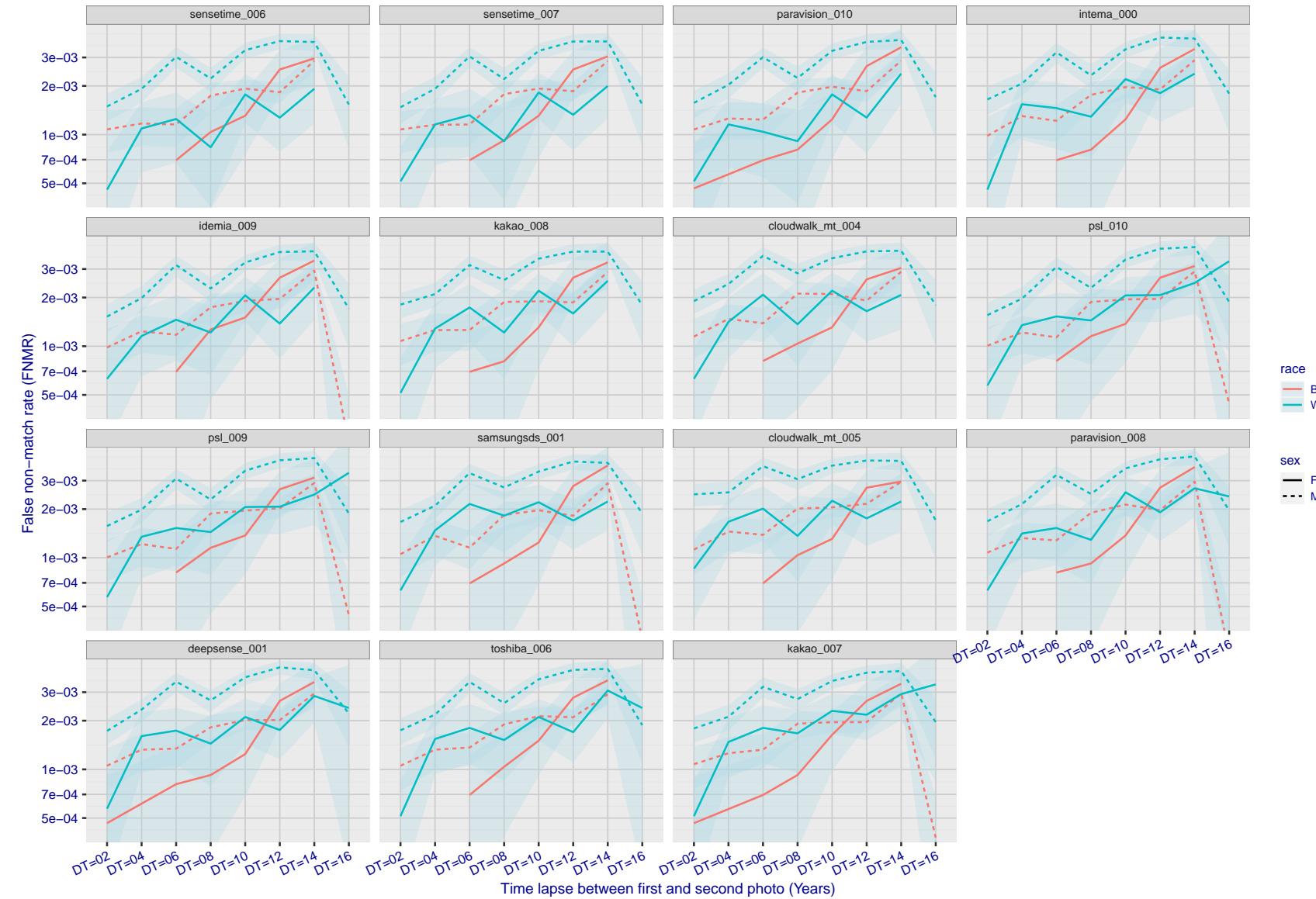


Figure 315: For the mugshot images, FNMR as a function of elapsed time between initial enrollment and second verification images. The panels appear most accurate first, and vertical scale changes on each page. The four traces correspond to images annotated with codes for black female, black male, white female, white male. The threshold is fixed for each algorithm to give FMR = 0.00001 over all (10^8) impostor comparisons. For short time-lapses, the most accurate algorithms give very few errors (FNMR < 0.001) so that the uncertainty estimates are high.

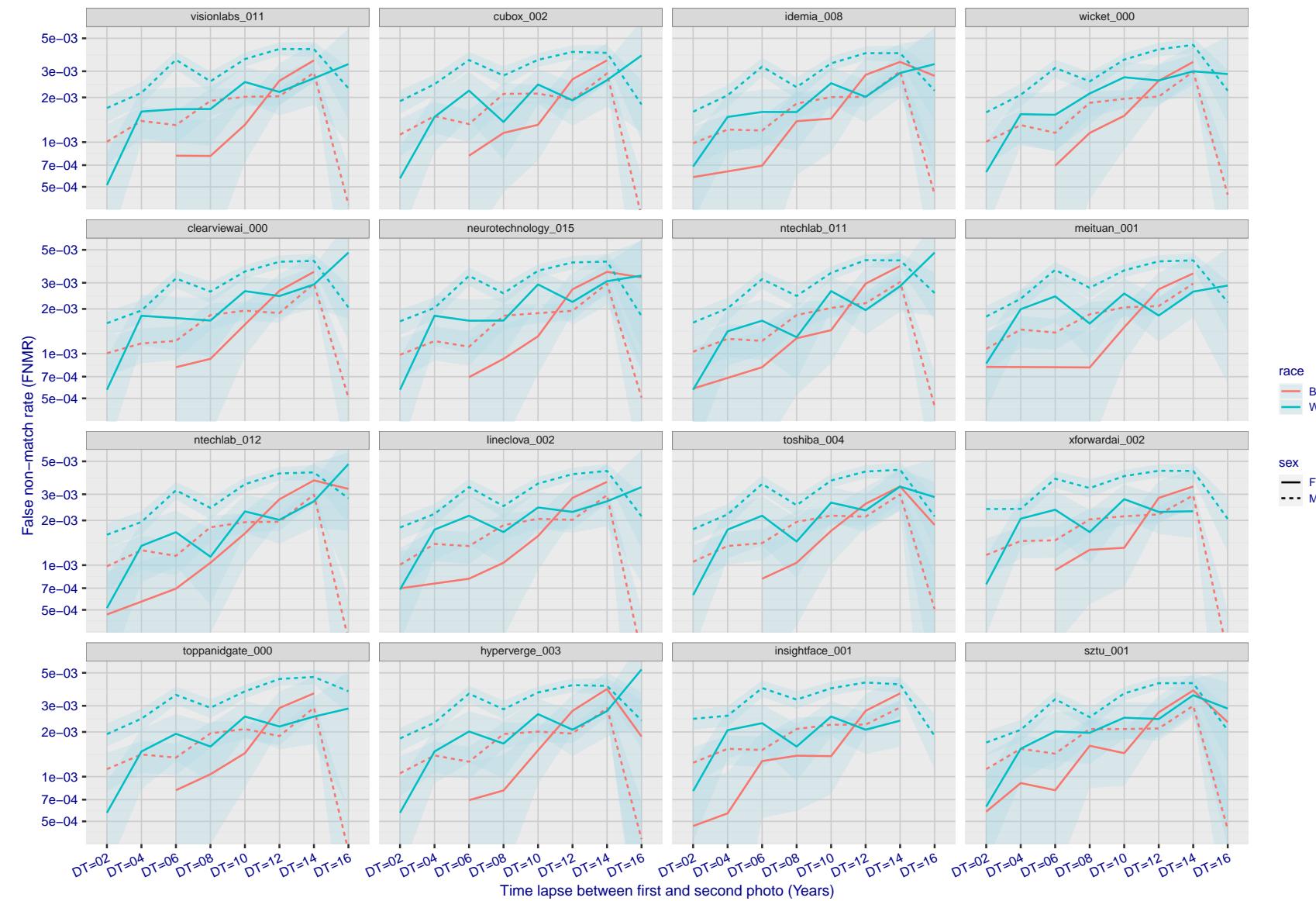


Figure 316: For the mugshot images, FNMR as a function of elapsed time between initial enrollment and second verification images. The panels appear most accurate first, and vertical scale changes on each page. The four traces correspond to images annotated with codes for black female, black male, white female, white male. The threshold is fixed for each algorithm to give $FMR = 0.00001$ over all (10^8) impostor comparisons. For short time-lapses, the most accurate algorithms give very few errors ($FNMR < 0.001$) so that the uncertainty estimates are high.

2022/08/30 09:26:06

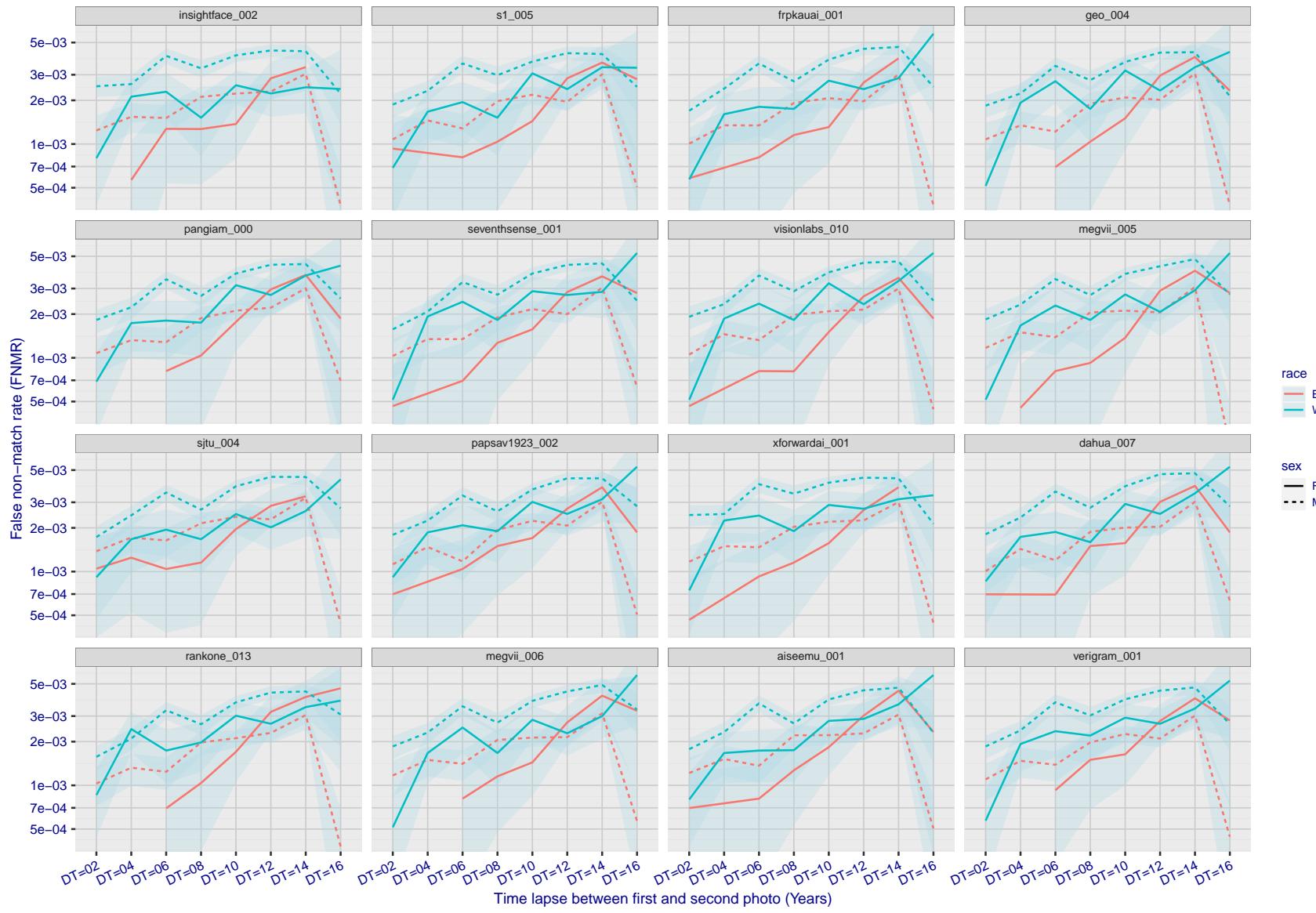


Figure 317: For the mugshot images, FNMR as a function of elapsed time between initial enrollment and second verification images. The panels appear most accurate first, and vertical scale changes on each page. The four traces correspond to images annotated with codes for black female, black male, white female, white male. The threshold is fixed for each algorithm to give $FMR = 0.00001$ over all (10^8) impostor comparisons. For short time-lapses, the most accurate algorithms give very few errors ($FNMR < 0.001$) so that the uncertainty estimates are high.

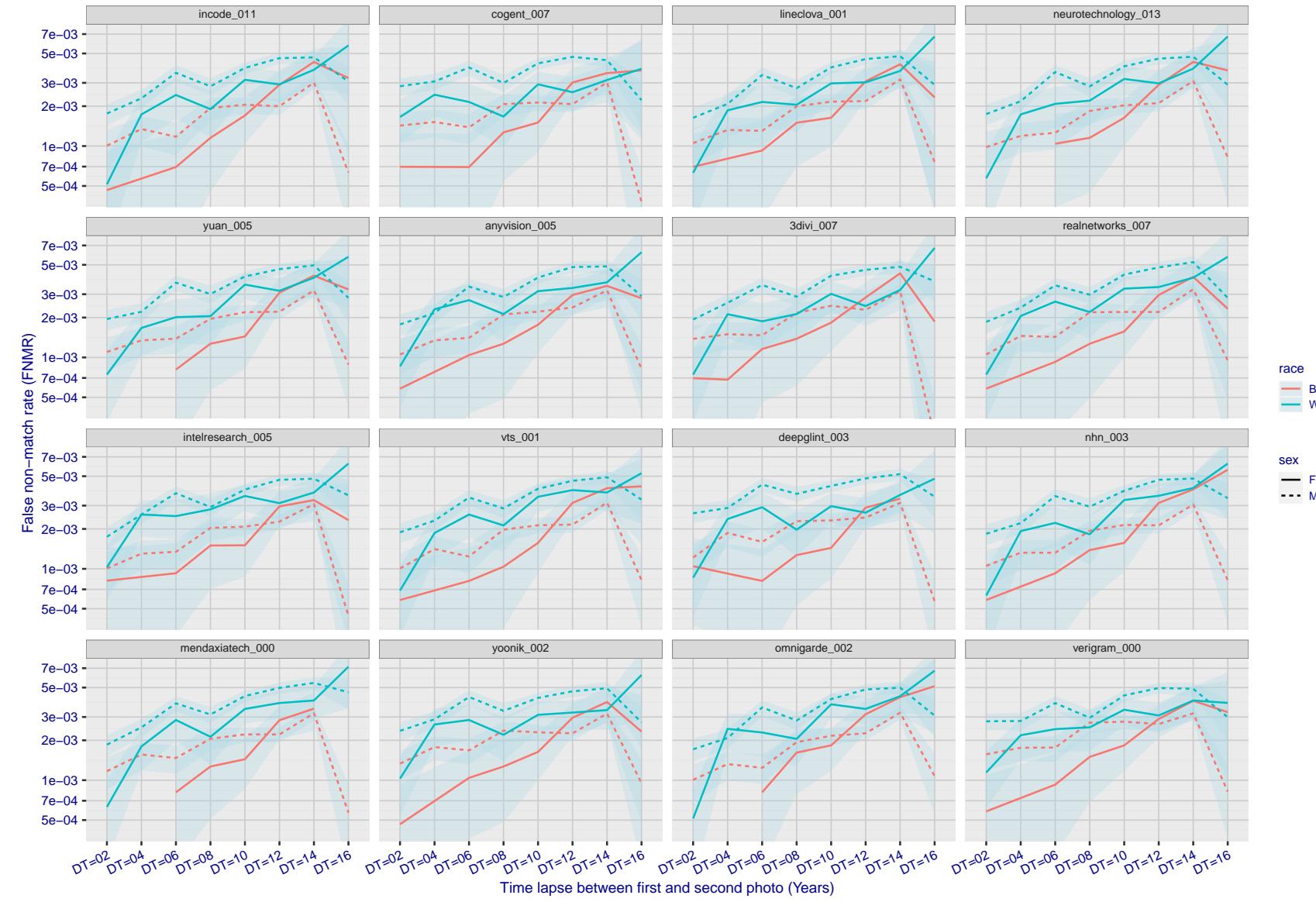


Figure 318: For the mugshot images, FNMR as a function of elapsed time between initial enrollment and second verification images. The panels appear most accurate first, and vertical scale changes on each page. The four traces correspond to images annotated with codes for black female, black male, white female, white male. The threshold is fixed for each algorithm to give $FMR = 0.00001$ over all (10^8) impostor comparisons. For short time-lapses, the most accurate algorithms give very few errors ($FNMR < 0.001$) so that the uncertainty estimates are high.

2022/08/30 09:26:06

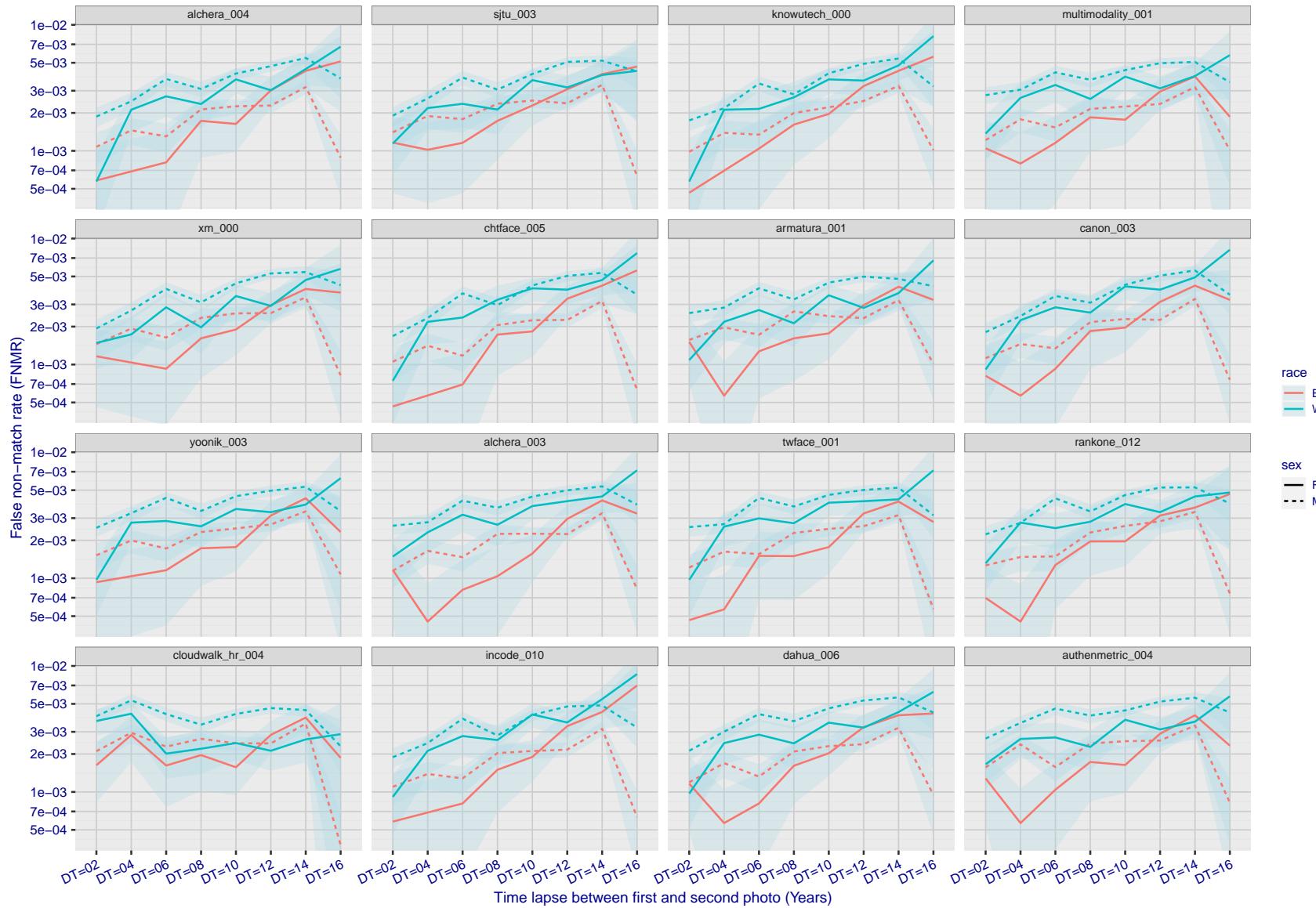


Figure 319: For the mugshot images, FNMR as a function of elapsed time between initial enrollment and second verification images. The panels appear most accurate first, and vertical scale changes on each page. The four traces correspond to images annotated with codes for black female, black male, white female, white male. The threshold is fixed for each algorithm to give $FMR = 0.00001$ over all (10^8) impostor comparisons. For short time-lapses, the most accurate algorithms give very few errors ($FNMR < 0.001$) so that the uncertainty estimates are high.

FNMR(T)
FMR(T)
"False non-match rate"
"False match rate"

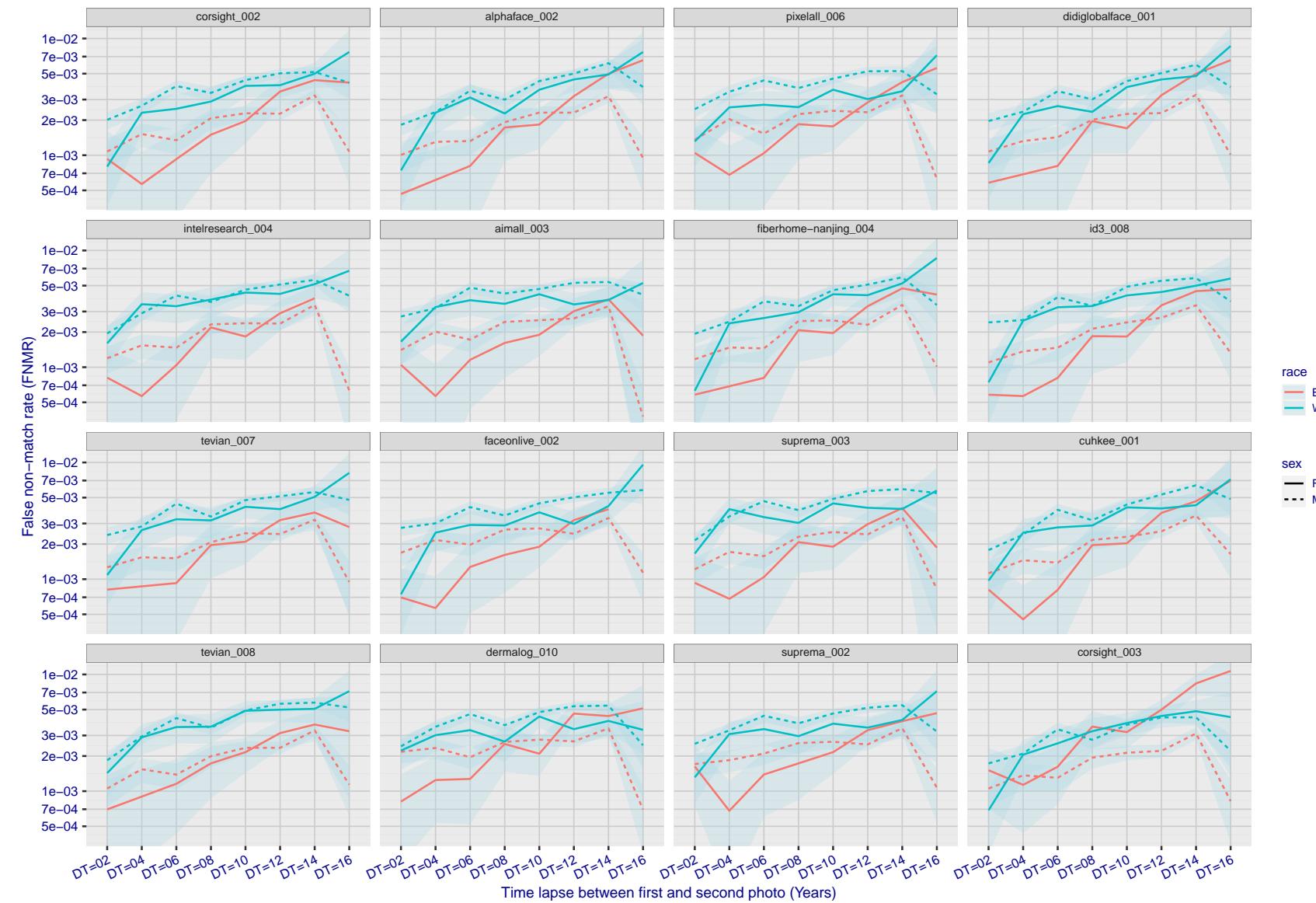


Figure 320: For the mugshot images, FNMR as a function of elapsed time between initial enrollment and second verification images. The panels appear most accurate first, and vertical scale changes on each page. The four traces correspond to images annotated with codes for black female, black male, white female, white male. The threshold is fixed for each algorithm to give FMR = 0.00001 over all (10^8) impostor comparisons. For short time-lapses, the most accurate algorithms give very few errors (FNMR < 0.001) so that the uncertainty estimates are high.

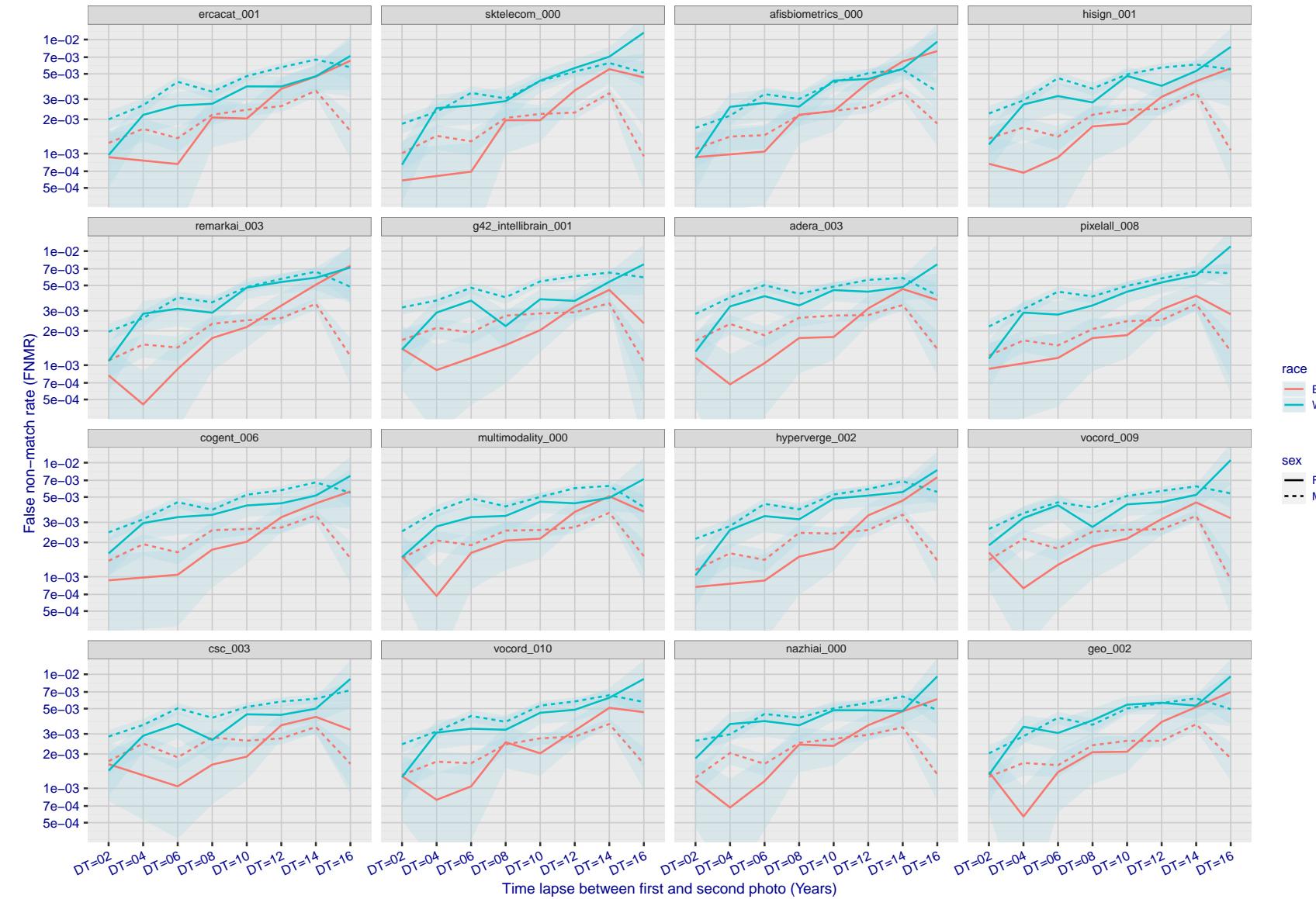


Figure 321: For the mugshot images, FNMR as a function of elapsed time between initial enrollment and second verification images. The panels appear most accurate first, and vertical scale changes on each page. The four traces correspond to images annotated with codes for black female, black male, white female, white male. The threshold is fixed for each algorithm to give $FMR = 0.00001$ over all (10^8) impostor comparisons. For short time-lapses, the most accurate algorithms give very few errors ($FNMR < 0.001$) so that the uncertainty estimates are high.

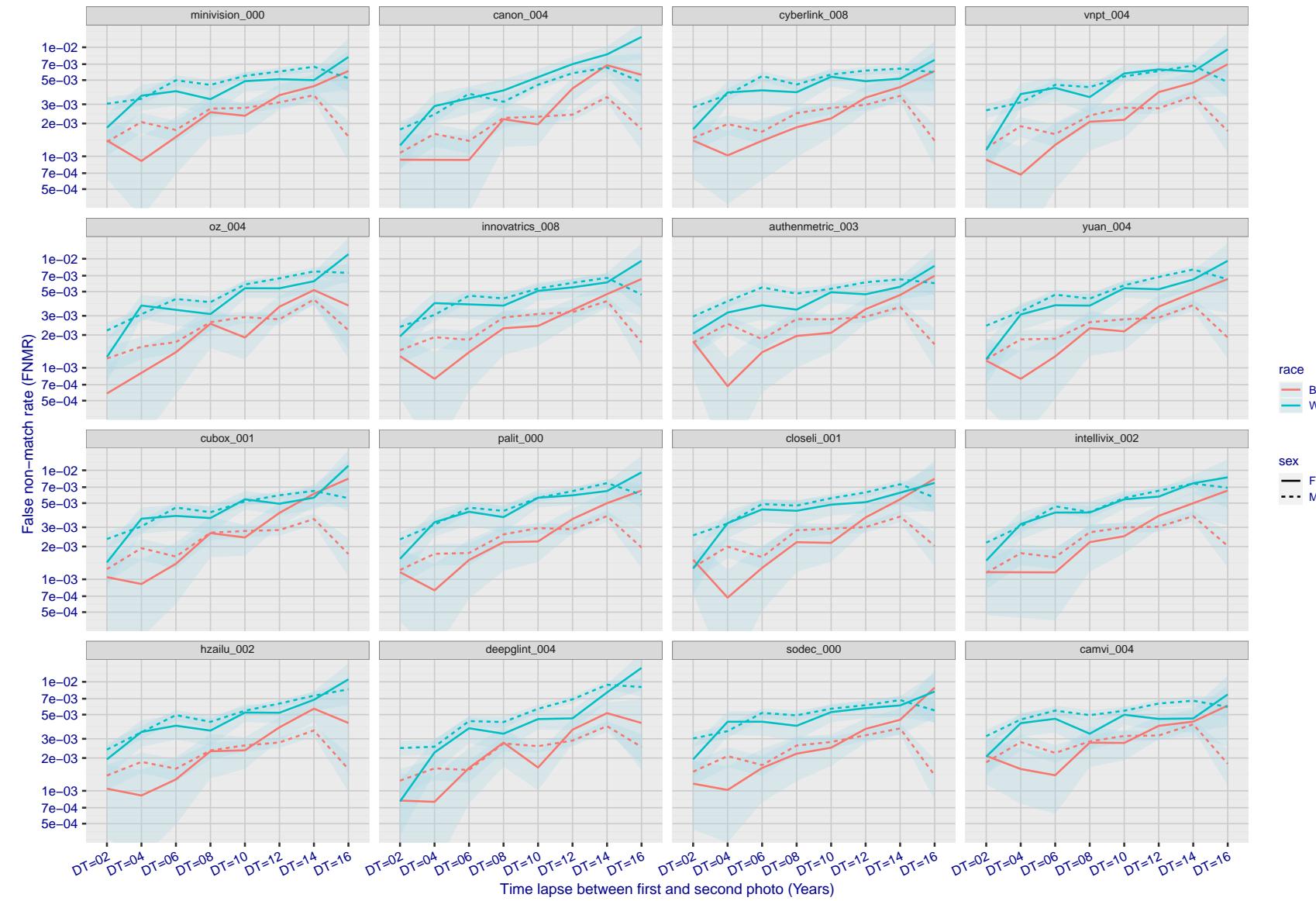


Figure 322: For the mugshot images, FNMR as a function of elapsed time between initial enrollment and second verification images. The panels appear most accurate first, and vertical scale changes on each page. The four traces correspond to images annotated with codes for black female, black male, white female, white male. The threshold is fixed for each algorithm to give $FMR = 0.00001$ over all (10^8) impostor comparisons. For short time-lapses, the most accurate algorithms give very few errors ($FNMR < 0.001$) so that the uncertainty estimates are high.

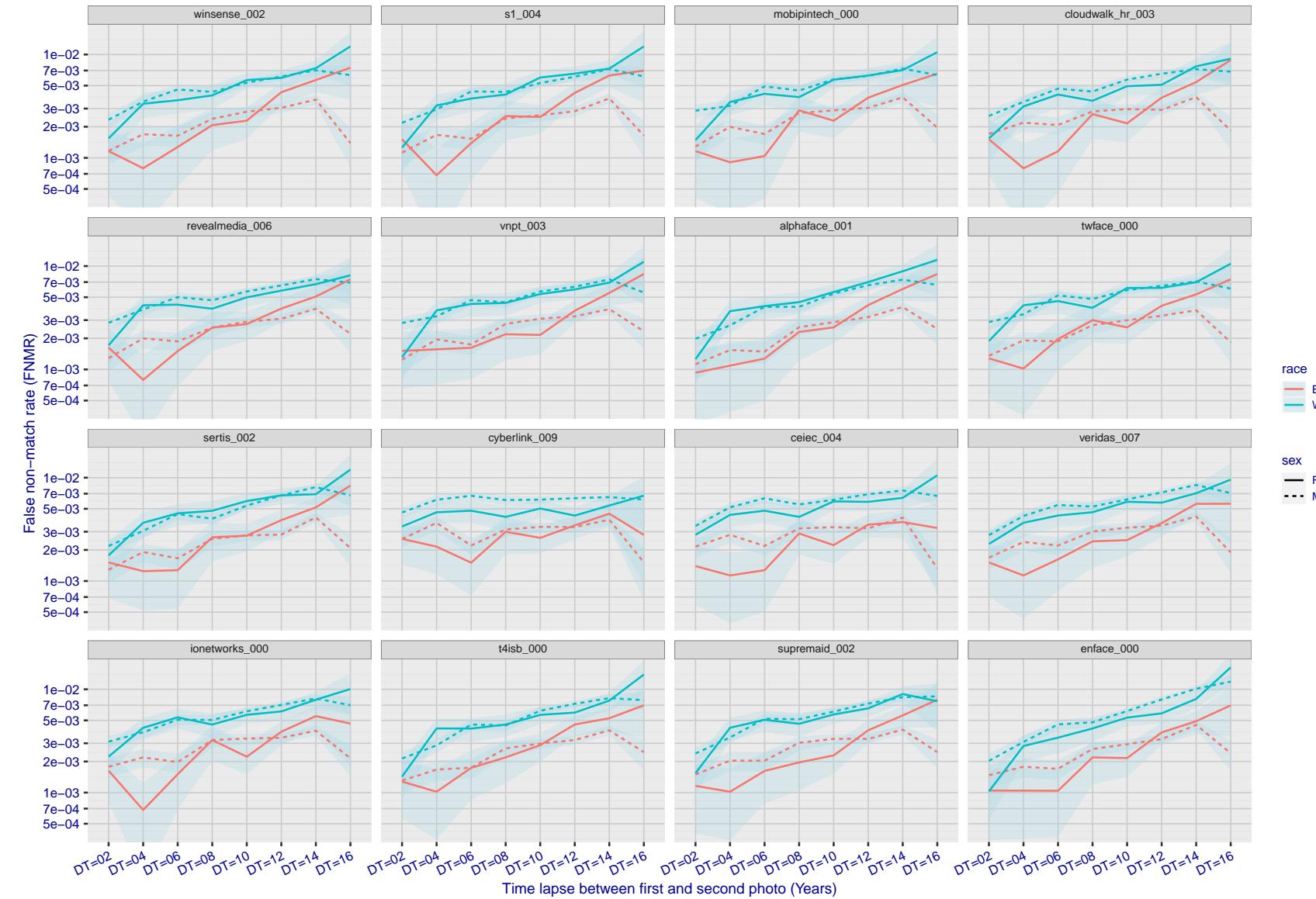


Figure 323: For the mugshot images, FNMR as a function of elapsed time between initial enrollment and second verification images. The panels appear most accurate first, and vertical scale changes on each page. The four traces correspond to images annotated with codes for black female, black male, white female, white male. The threshold is fixed for each algorithm to give $FMR = 0.00001$ over all (10^8) impostor comparisons. For short time-lapses, the most accurate algorithms give very few errors ($FNMR < 0.001$) so that the uncertainty estimates are high.

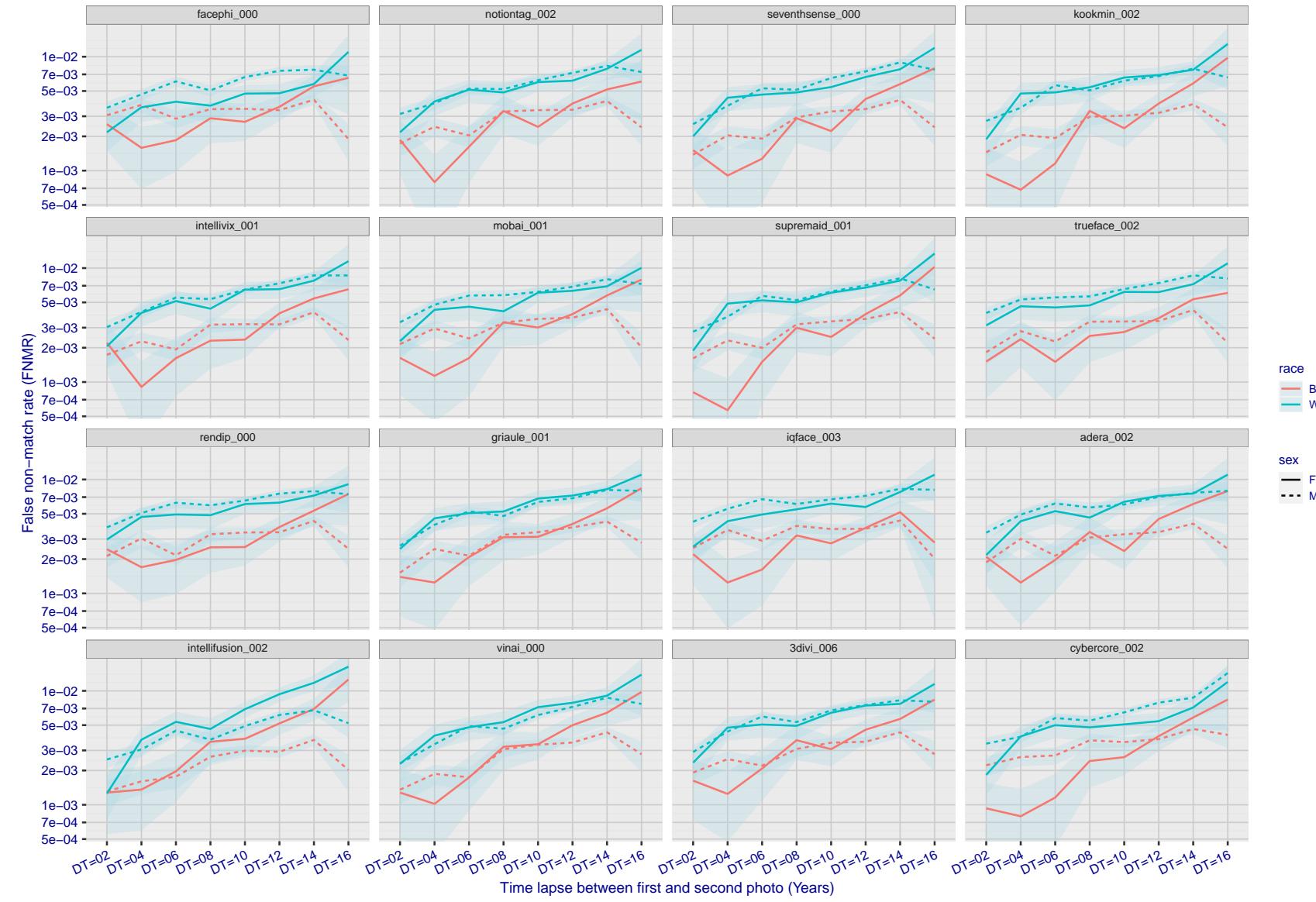


Figure 324: For the mugshot images, FNMR as a function of elapsed time between initial enrollment and second verification images. The panels appear most accurate first, and vertical scale changes on each page. The four traces correspond to images annotated with codes for black female, black male, white female, white male. The threshold is fixed for each algorithm to give $FMR = 0.00001$ over all (10^8) impostor comparisons. For short time-lapses, the most accurate algorithms give very few errors ($FNMR < 0.001$) so that the uncertainty estimates are high.

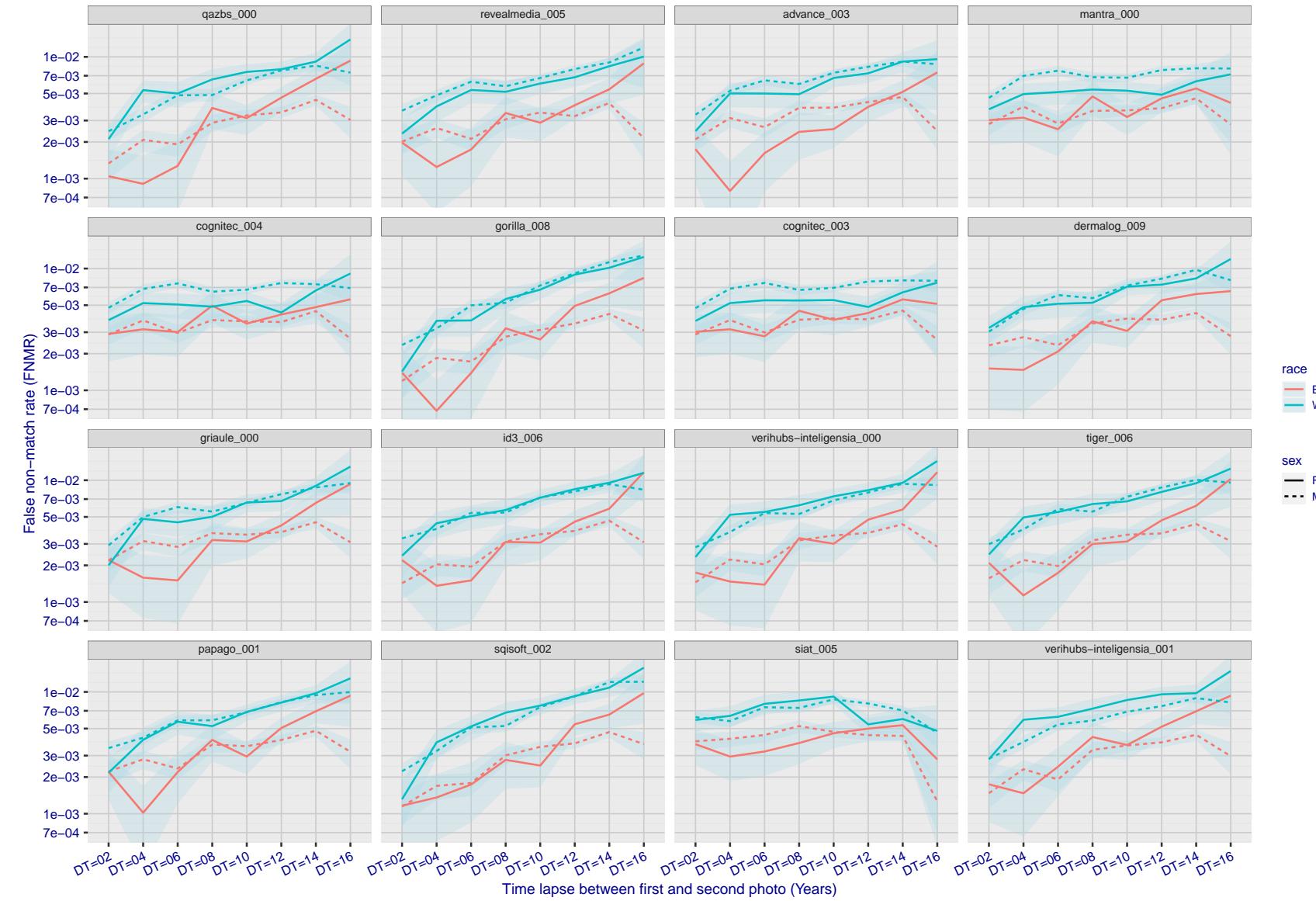


Figure 325: For the mugshot images, FNMR as a function of elapsed time between initial enrollment and second verification images. The panels appear most accurate first, and vertical scale changes on each page. The four traces correspond to images annotated with codes for black female, black male, white female, white male. The threshold is fixed for each algorithm to give $FMR = 0.00001$ over all (10^8) impostor comparisons. For short time-lapses, the most accurate algorithms give very few errors ($FNMR < 0.001$) so that the uncertainty estimates are high.

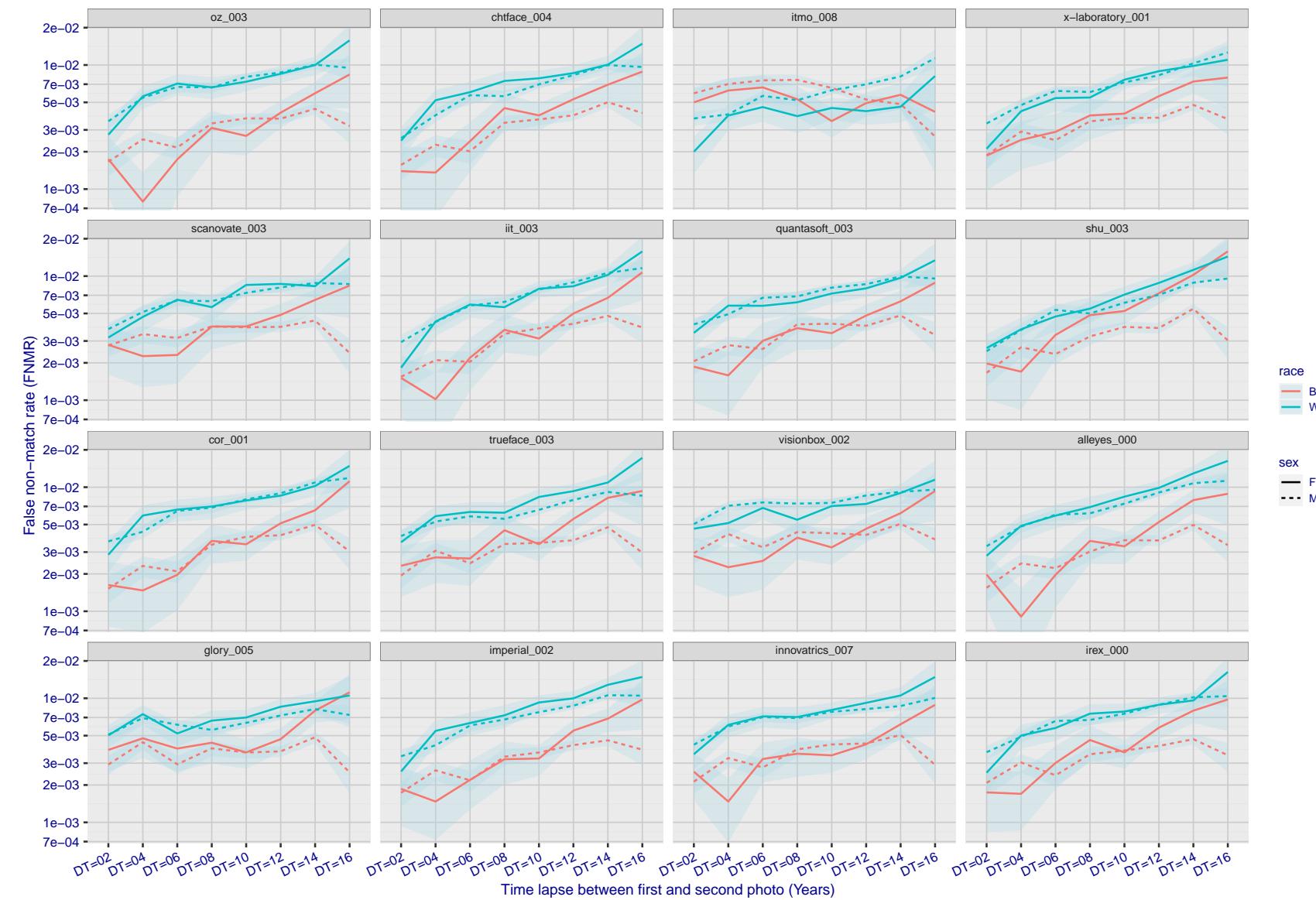


Figure 326: For the mugshot images, FNMR as a function of elapsed time between initial enrollment and second verification images. The panels appear most accurate first, and vertical scale changes on each page. The four traces correspond to images annotated with codes for black female, black male, white female, white male. The threshold is fixed for each algorithm to give $FMR = 0.00001$ over all (10^8) impostor comparisons. For short time-lapses, the most accurate algorithms give very few errors ($FNMR < 0.001$) so that the uncertainty estimates are high.

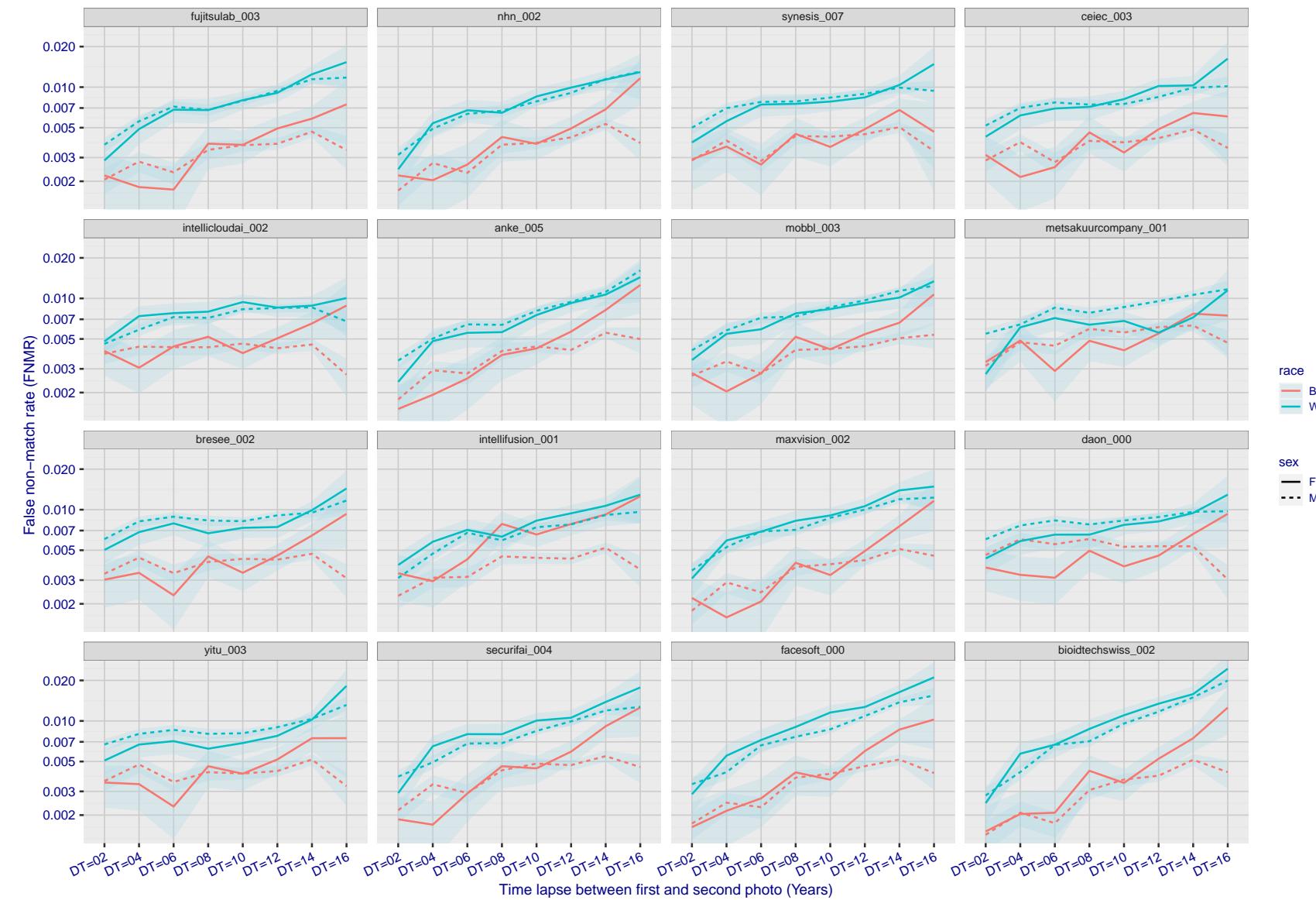


Figure 327: For the mugshot images, FNMR as a function of elapsed time between initial enrollment and second verification images. The panels appear most accurate first, and vertical scale changes on each page. The four traces correspond to images annotated with codes for black female, black male, white female, white male. The threshold is fixed for each algorithm to give FMR = 0.00001 over all (10^8) impostor comparisons. For short time-lapses, the most accurate algorithms give very few errors (FNMR < 0.001) so that the uncertainty estimates are high.

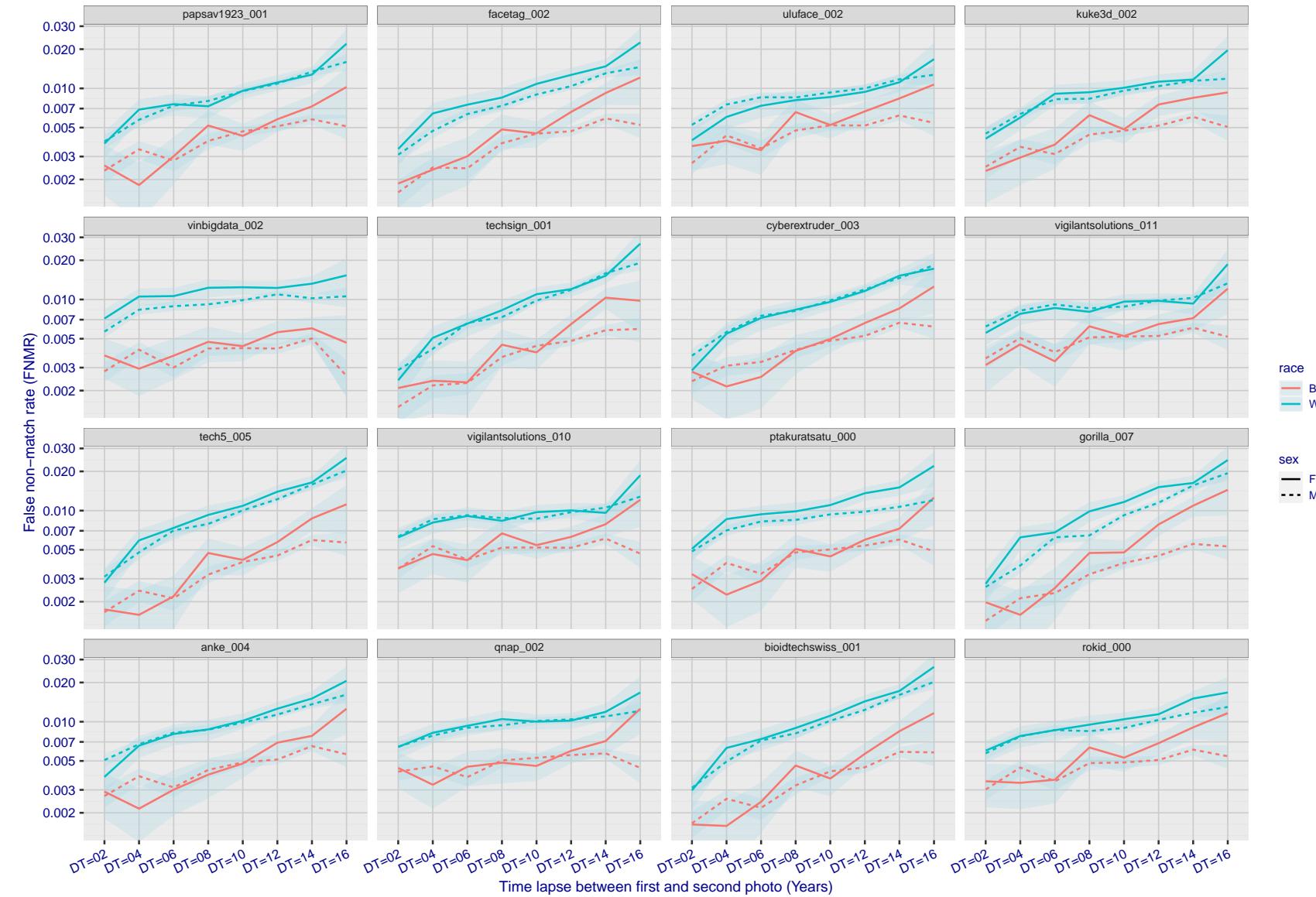


Figure 328: For the mugshot images, FNMR as a function of elapsed time between initial enrollment and second verification images. The panels appear most accurate first, and vertical scale changes on each page. The four traces correspond to images annotated with codes for black female, black male, white female, white male. The threshold is fixed for each algorithm to give $FMR = 0.00001$ over all (10^8) impostor comparisons. For short time-lapses, the most accurate algorithms give very few errors ($FNMR < 0.001$) so that the uncertainty estimates are high.

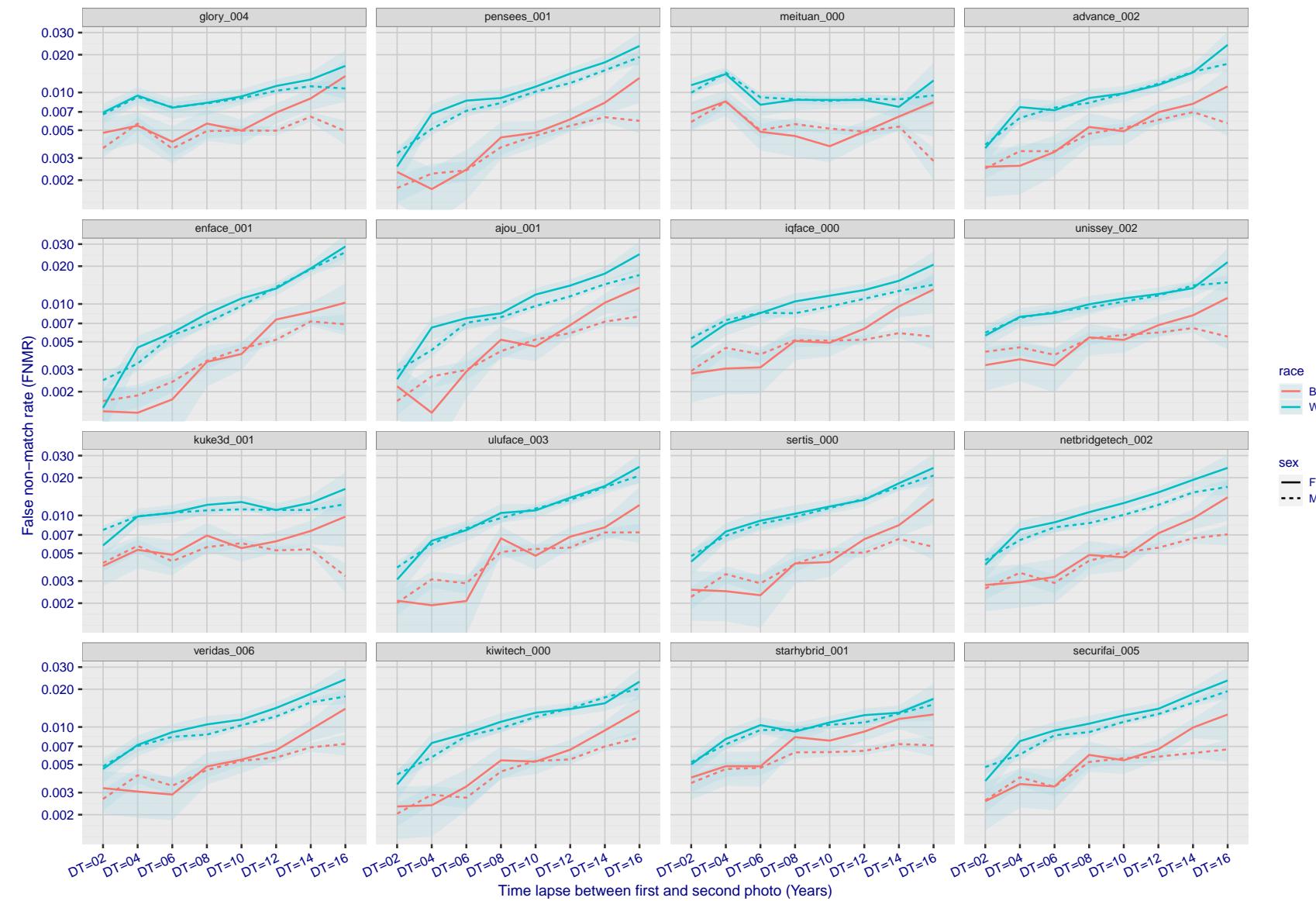


Figure 329: For the mugshot images, FNMR as a function of elapsed time between initial enrollment and second verification images. The panels appear most accurate first, and vertical scale changes on each page. The four traces correspond to images annotated with codes for black female, black male, white female, white male. The threshold is fixed for each algorithm to give $FMR = 0.00001$ over all (10^8) impostor comparisons. For short time-lapses, the most accurate algorithms give very few errors ($FNMR < 0.001$) so that the uncertainty estimates are high.

2022/08/30 09:26:06

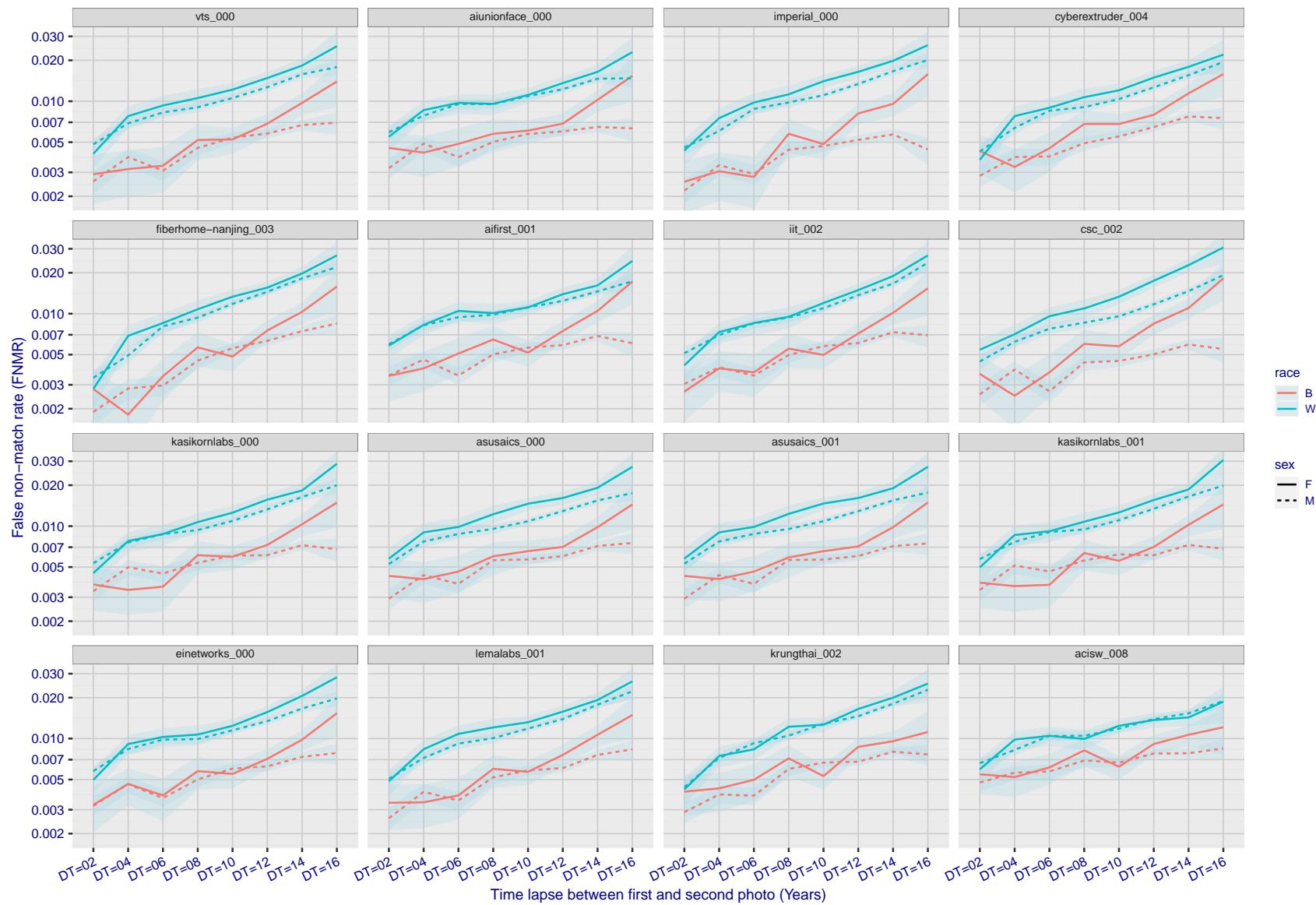


Figure 330: For the mugshot images, FNMR as a function of elapsed time between initial enrollment and second verification images. The panels appear most accurate first, and vertical scale changes on each page. The four traces correspond to images annotated with codes for black female, black male, white female, white male. The threshold is fixed for each algorithm to give FMR = 0.00001 over all (10^8) impostor comparisons. For short time-lapses, the most accurate algorithms give very few errors (FNMR < 0.001) so that the uncertainty estimates are high.

FNMR(T)
FMR(T)
"False match rate"

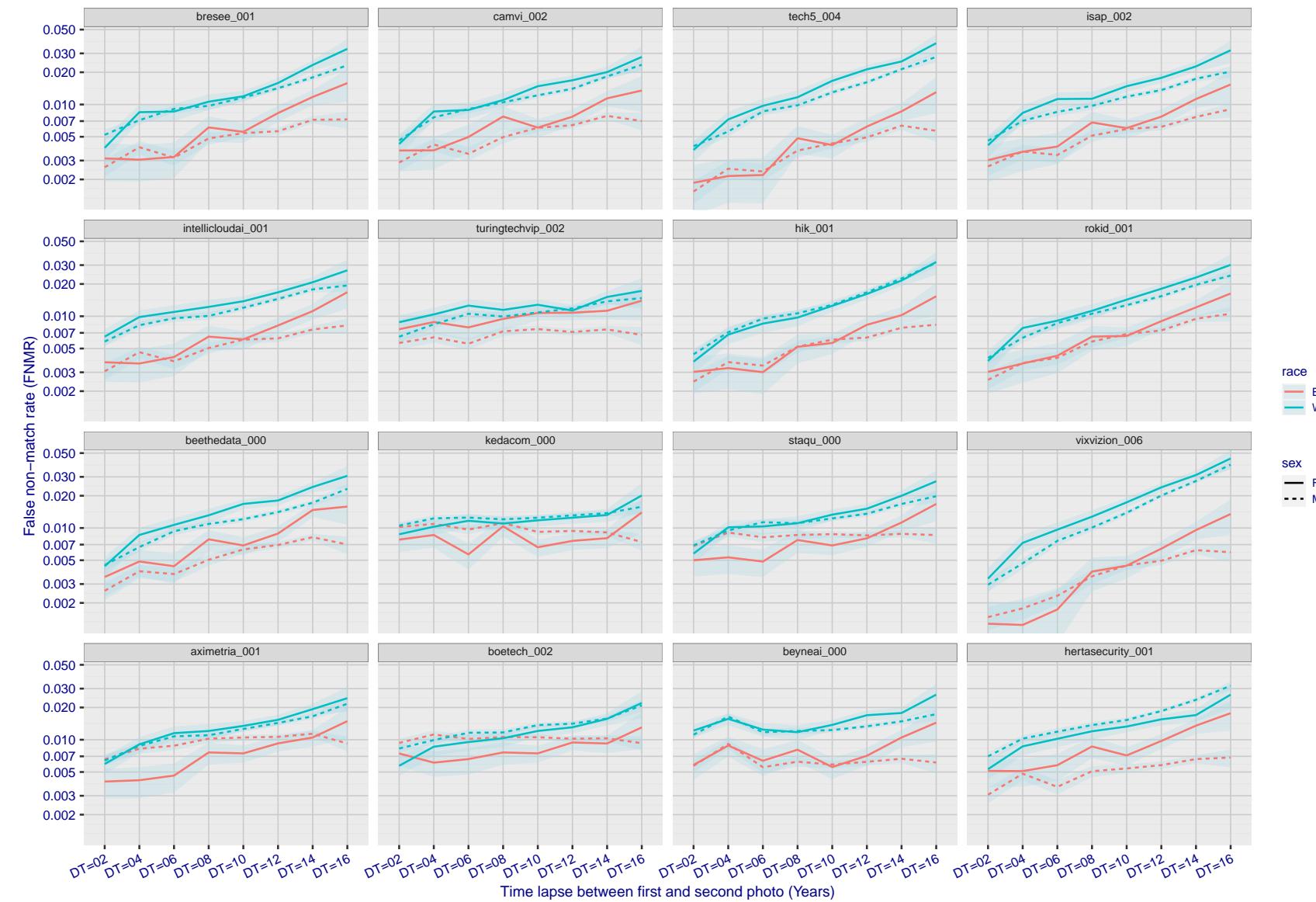


Figure 331: For the mugshot images, FNMR as a function of elapsed time between initial enrollment and second verification images. The panels appear most accurate first, and vertical scale changes on each page. The four traces correspond to images annotated with codes for black female, black male, white female, white male. The threshold is fixed for each algorithm to give FMR = 0.00001 over all (10^8) impostor comparisons. For short time-lapses, the most accurate algorithms give very few errors (FNMR < 0.001) so that the uncertainty estimates are high.

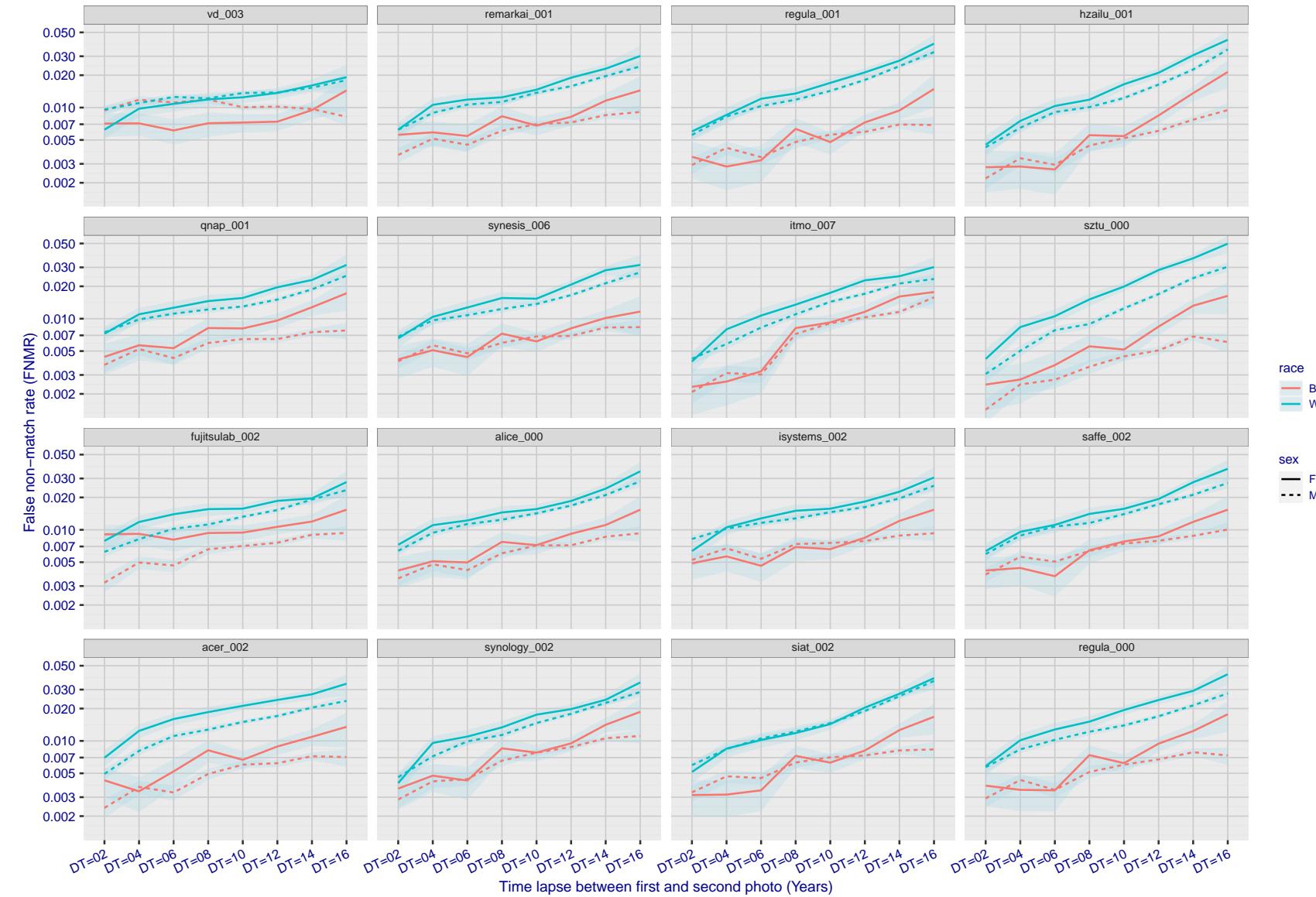


Figure 332: For the mugshot images, FNMR as a function of elapsed time between initial enrollment and second verification images. The panels appear most accurate first, and vertical scale changes on each page. The four traces correspond to images annotated with codes for black female, black male, white female, white male. The threshold is fixed for each algorithm to give FMR = 0.00001 over all (10^8) impostor comparisons. For short time-lapses, the most accurate algorithms give very few errors (FNMR < 0.001) so that the uncertainty estimates are high.

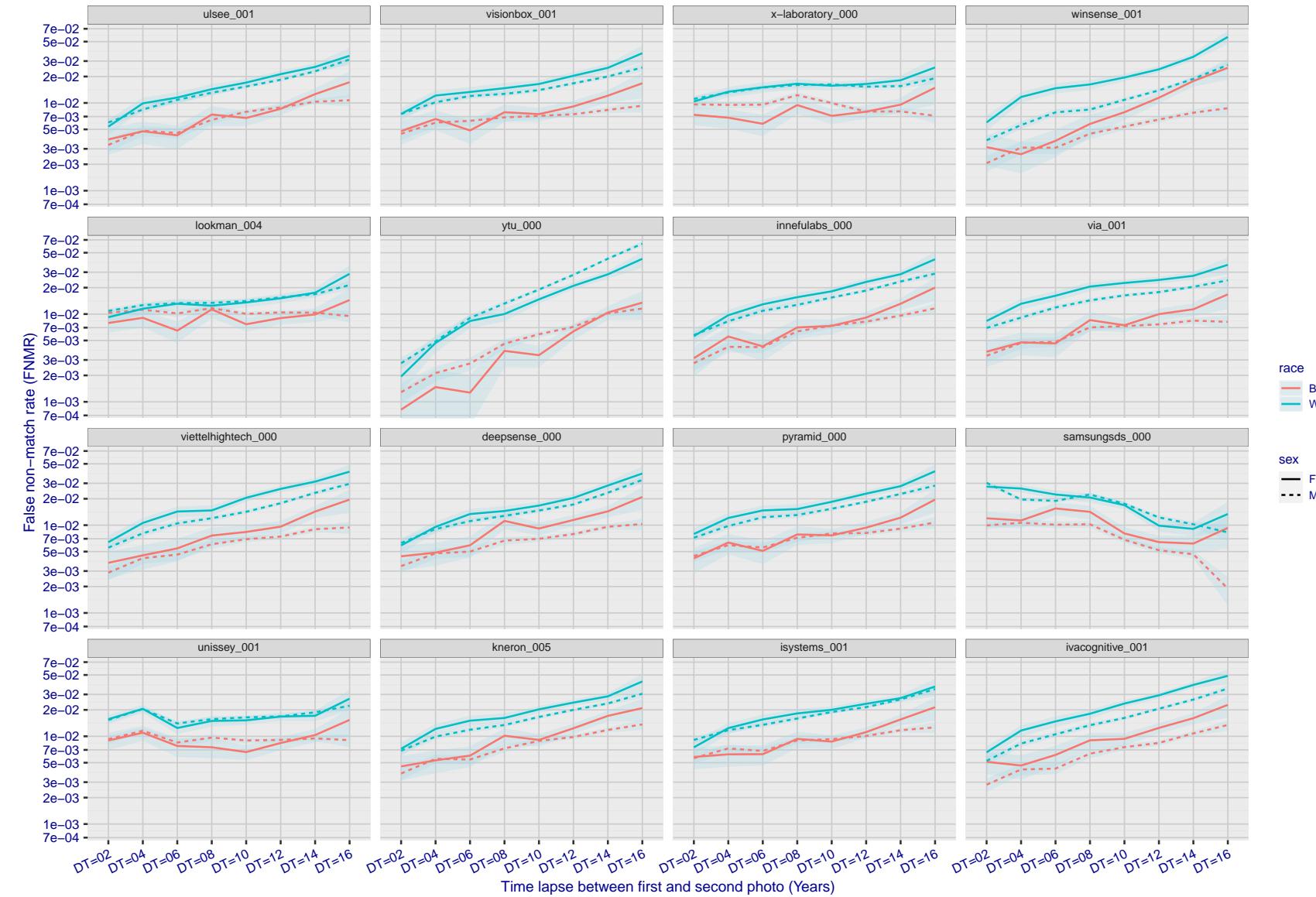


Figure 333: For the mugshot images, FNMR as a function of elapsed time between initial enrollment and second verification images. The panels appear most accurate first, and vertical scale changes on each page. The four traces correspond to images annotated with codes for black female, black male, white female, white male. The threshold is fixed for each algorithm to give $FMR = 0.00001$ over all (10^8) impostor comparisons. For short time-lapses, the most accurate algorithms give very few errors ($FNMR < 0.001$) so that the uncertainty estimates are high.

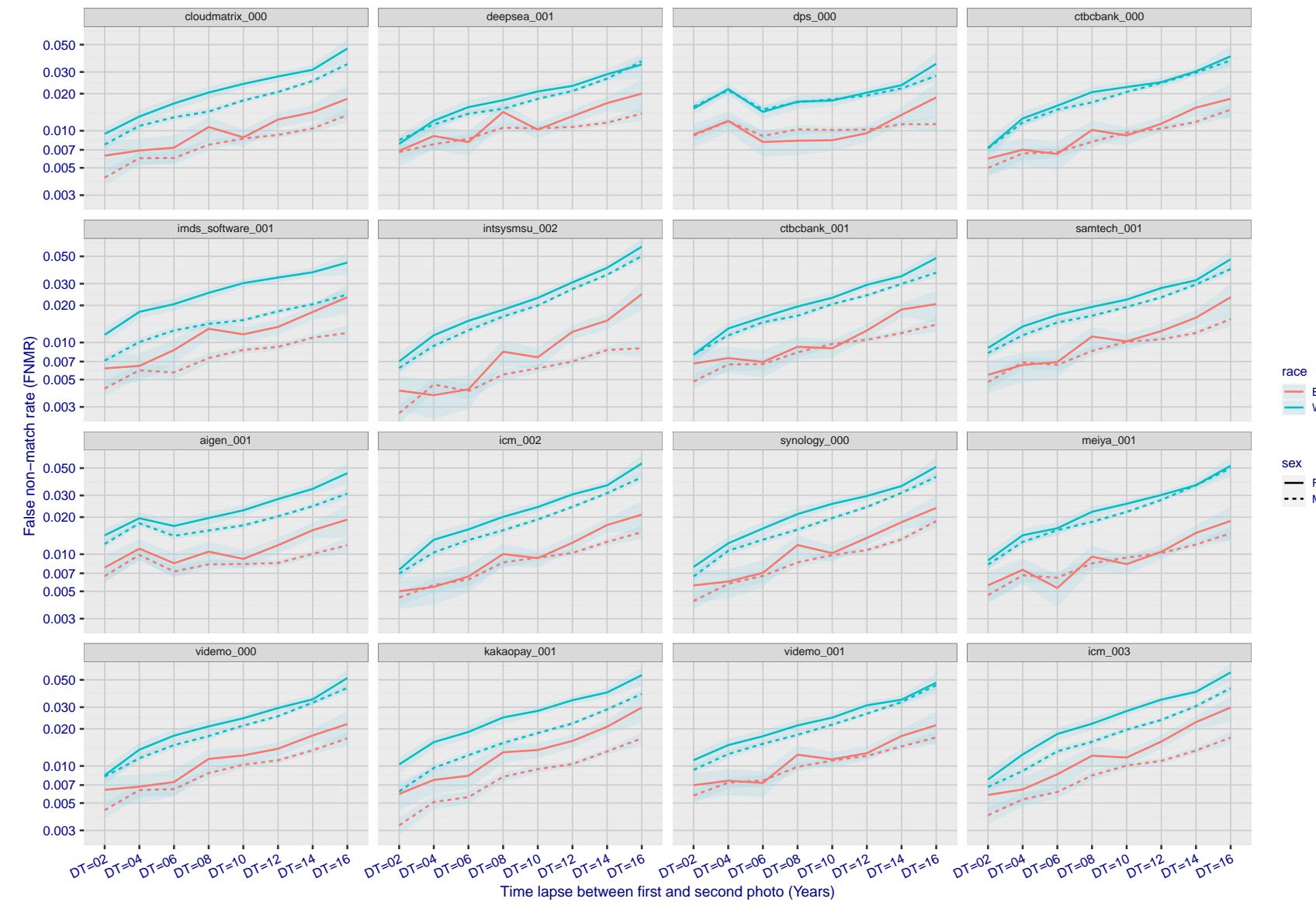


Figure 334: For the mugshot images, FNMR as a function of elapsed time between initial enrollment and second verification images. The panels appear most accurate first, and vertical scale changes on each page. The four traces correspond to images annotated with codes for black female, black male, white female, white male. The threshold is fixed for each algorithm to give FMR = 0.00001 over all (10^8) impostor comparisons. For short time-lapses, the most accurate algorithms give very few errors (FNMR < 0.001) so that the uncertainty estimates are high.

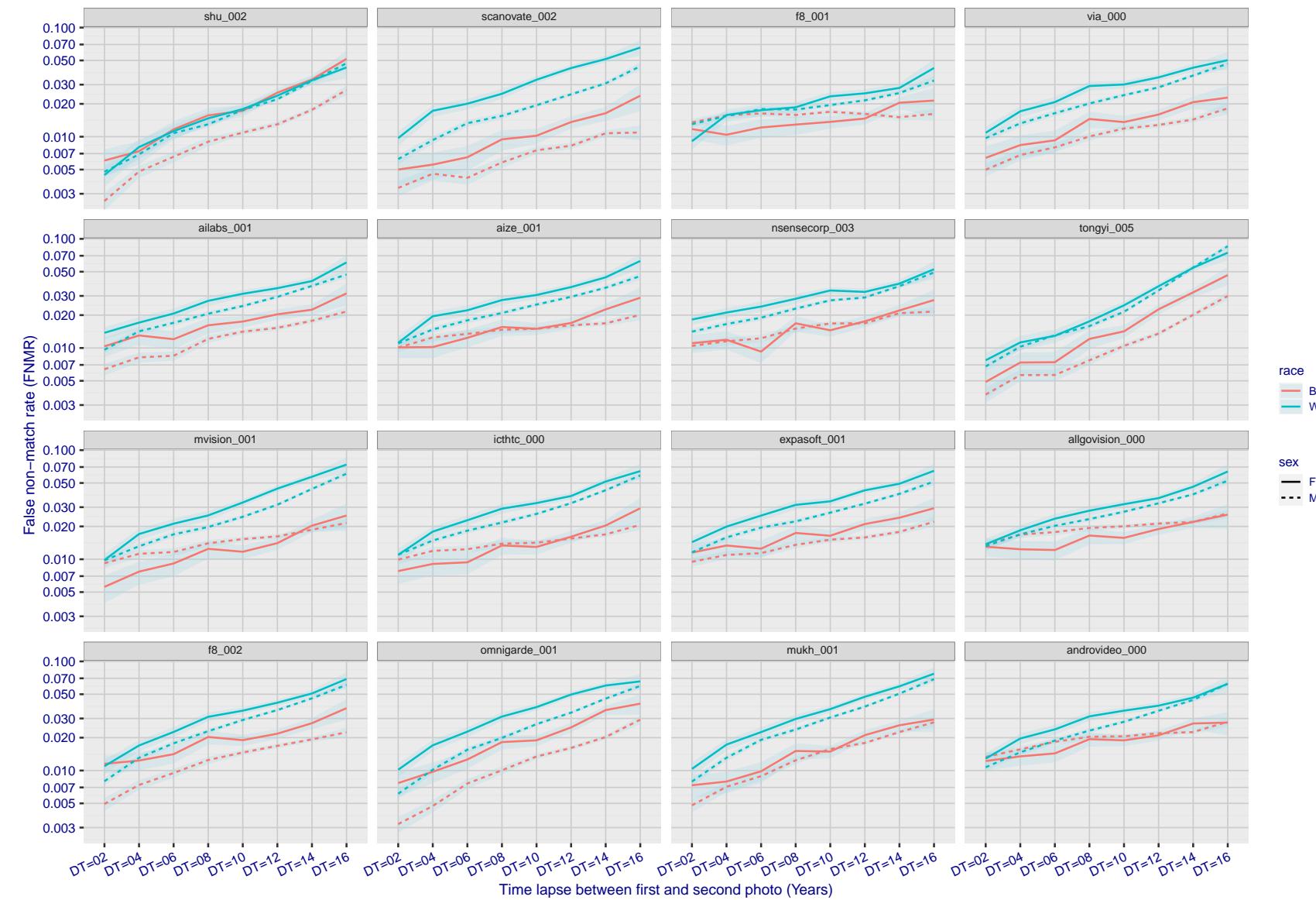


Figure 335: For the mugshot images, FNMR as a function of elapsed time between initial enrollment and second verification images. The panels appear most accurate first, and vertical scale changes on each page. The four traces correspond to images annotated with codes for black female, black male, white female, white male. The threshold is fixed for each algorithm to give FMR = 0.00001 over all (10^8) impostor comparisons. For short time-lapses, the most accurate algorithms give very few errors (FNMR < 0.001) so that the uncertainty estimates are high.

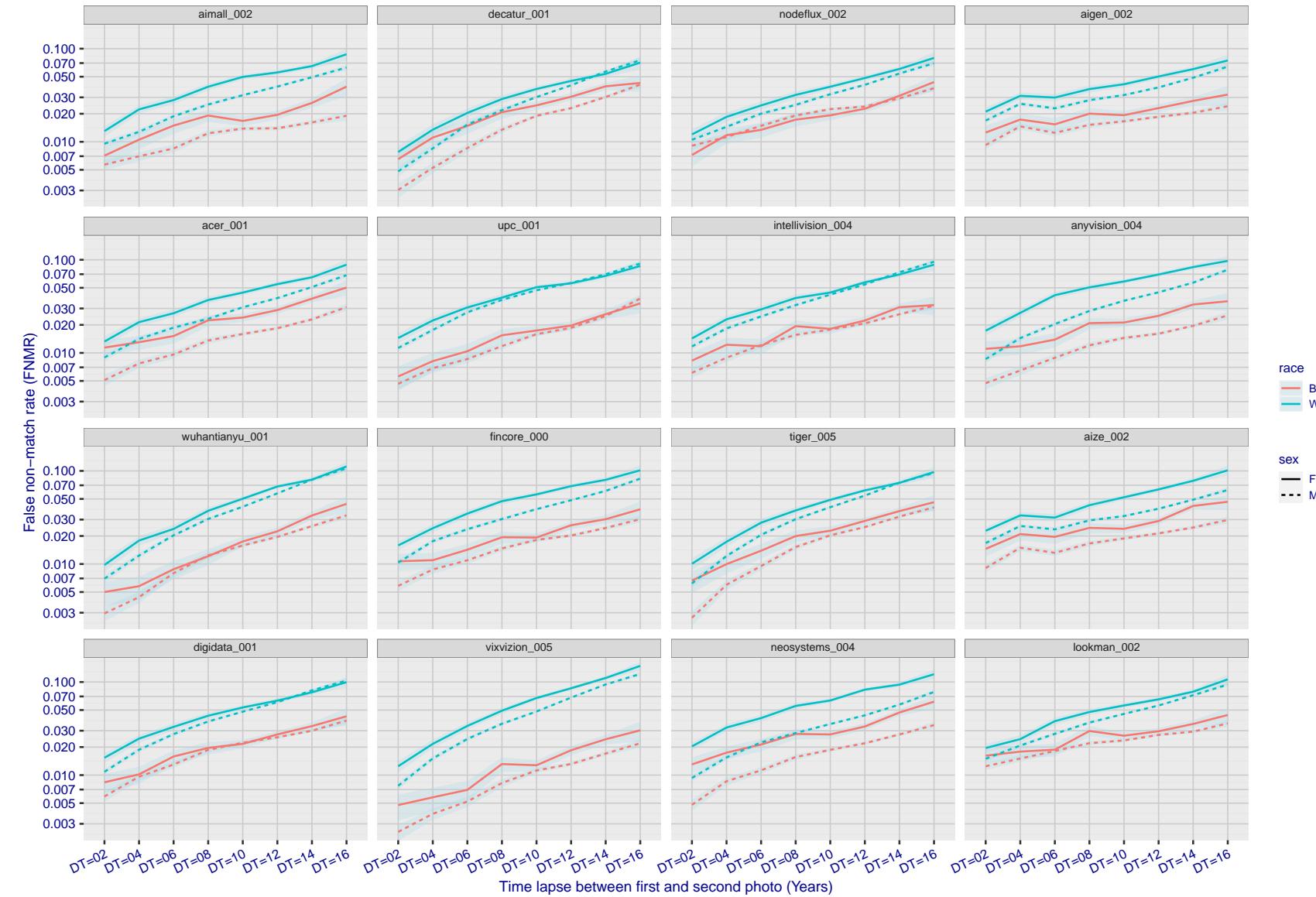


Figure 336: For the mugshot images, FNMR as a function of elapsed time between initial enrollment and second verification images. The panels appear most accurate first, and vertical scale changes on each page. The four traces correspond to images annotated with codes for black female, black male, white female, white male. The threshold is fixed for each algorithm to give FMR = 0.00001 over all (10^8) impostor comparisons. For short time-lapses, the most accurate algorithms give very few errors (FNMR < 0.001) so that the uncertainty estimates are high.

2022/08/30 09:26:06

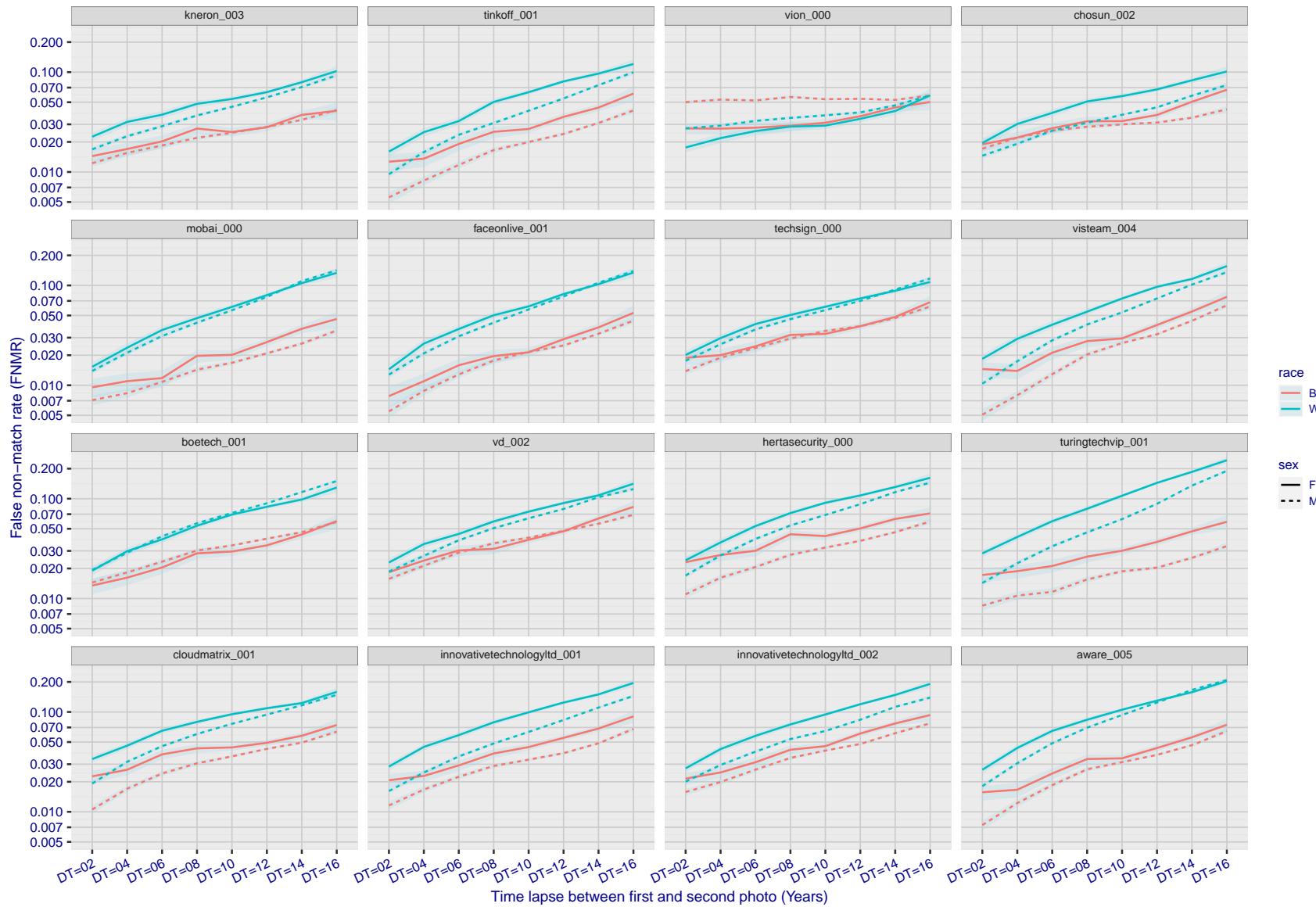


Figure 337: For the mugshot images, FNMR as a function of elapsed time between initial enrollment and second verification images. The panels appear most accurate first, and vertical scale changes on each page. The four traces correspond to images annotated with codes for black female, black male, white female, white male. The threshold is fixed for each algorithm to give FMR = 0.00001 over all (10^8) impostor comparisons. For short time-lapses, the most accurate algorithms give very few errors (FNMR < 0.001) so that the uncertainty estimates are high.

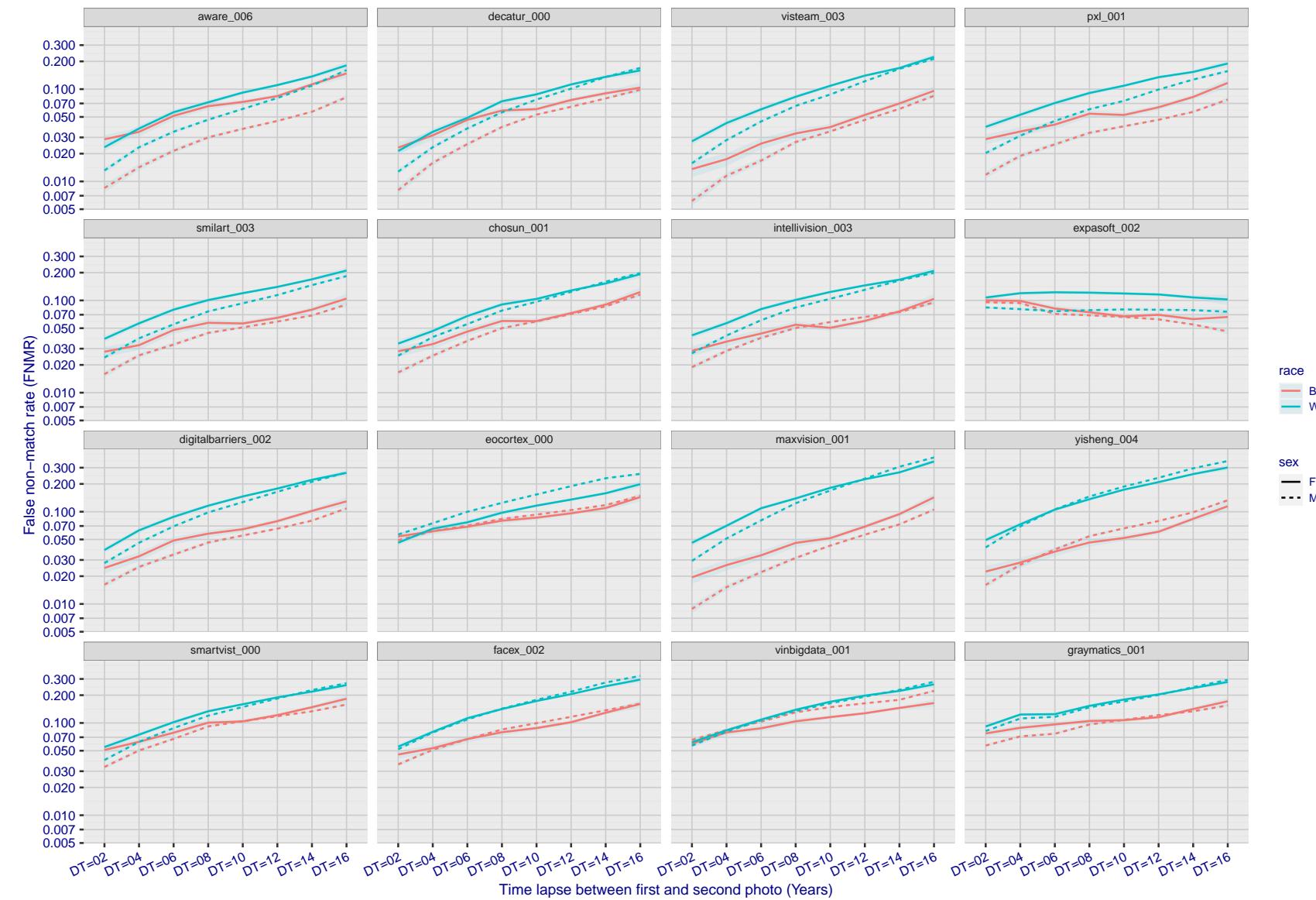
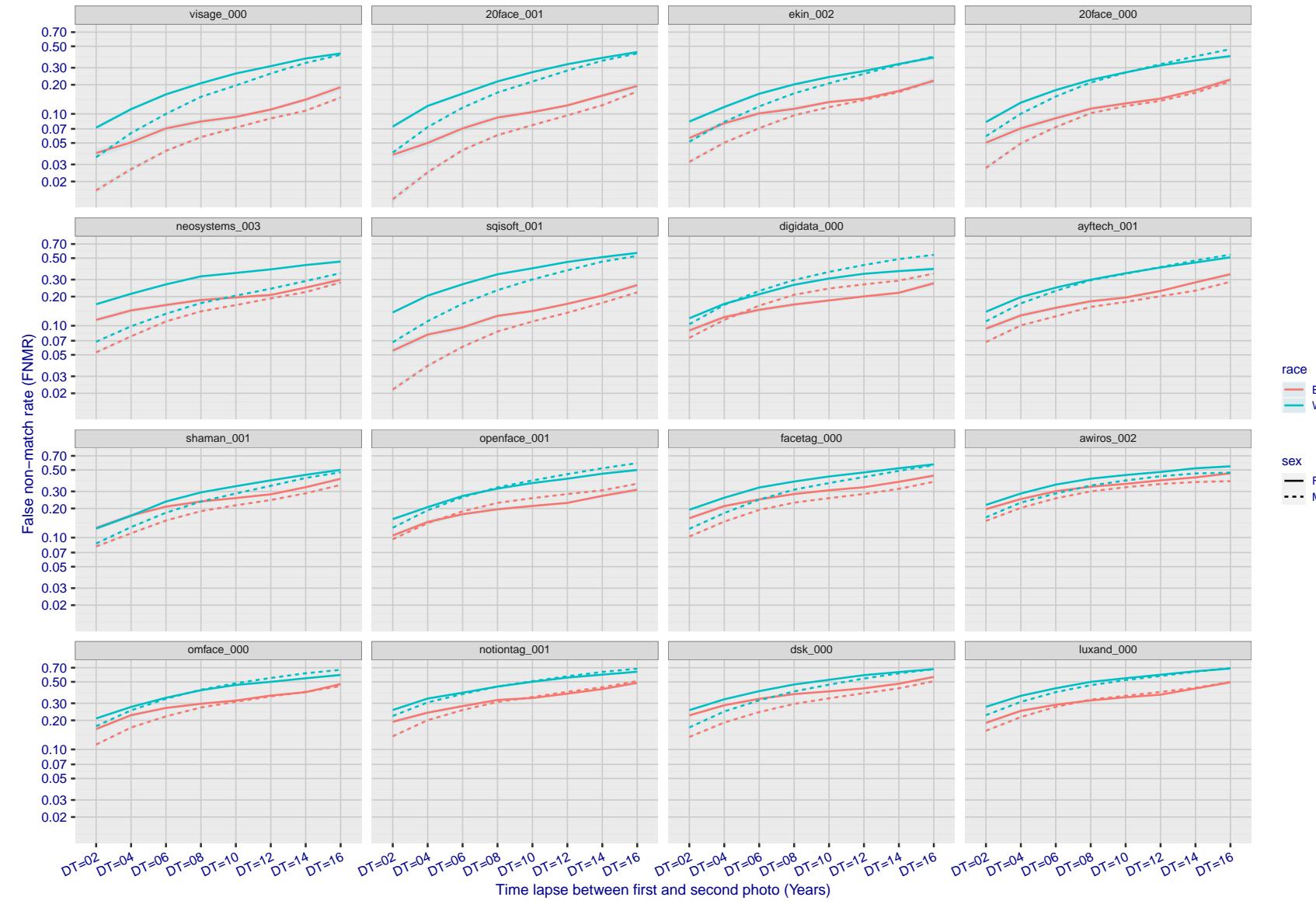


Figure 338: For the mugshot images, FNMR as a function of elapsed time between initial enrollment and second verification images. The panels appear most accurate first, and vertical scale changes on each page. The four traces correspond to images annotated with codes for black female, black male, white female, white male. The threshold is fixed for each algorithm to give FMR = 0.00001 over all (10^8) impostor comparisons. For short time-lapses, the most accurate algorithms give very few errors (FNMR < 0.001) so that the uncertainty estimates are high.



race
B
W

sex
F
M

Figure 339: For the mugshot images, FNMR as a function of elapsed time between initial enrollment and second verification images. The panels appear most accurate first, and vertical scale changes on each page. The four traces correspond to images annotated with codes for black female, black male, white female, white male. The threshold is fixed for each algorithm to give FMR = 0.00001 over all (10^8) impostor comparisons. For short time-lapses, the most accurate algorithms give very few errors (FNMR < 0.001) so that the uncertainty estimates are high.

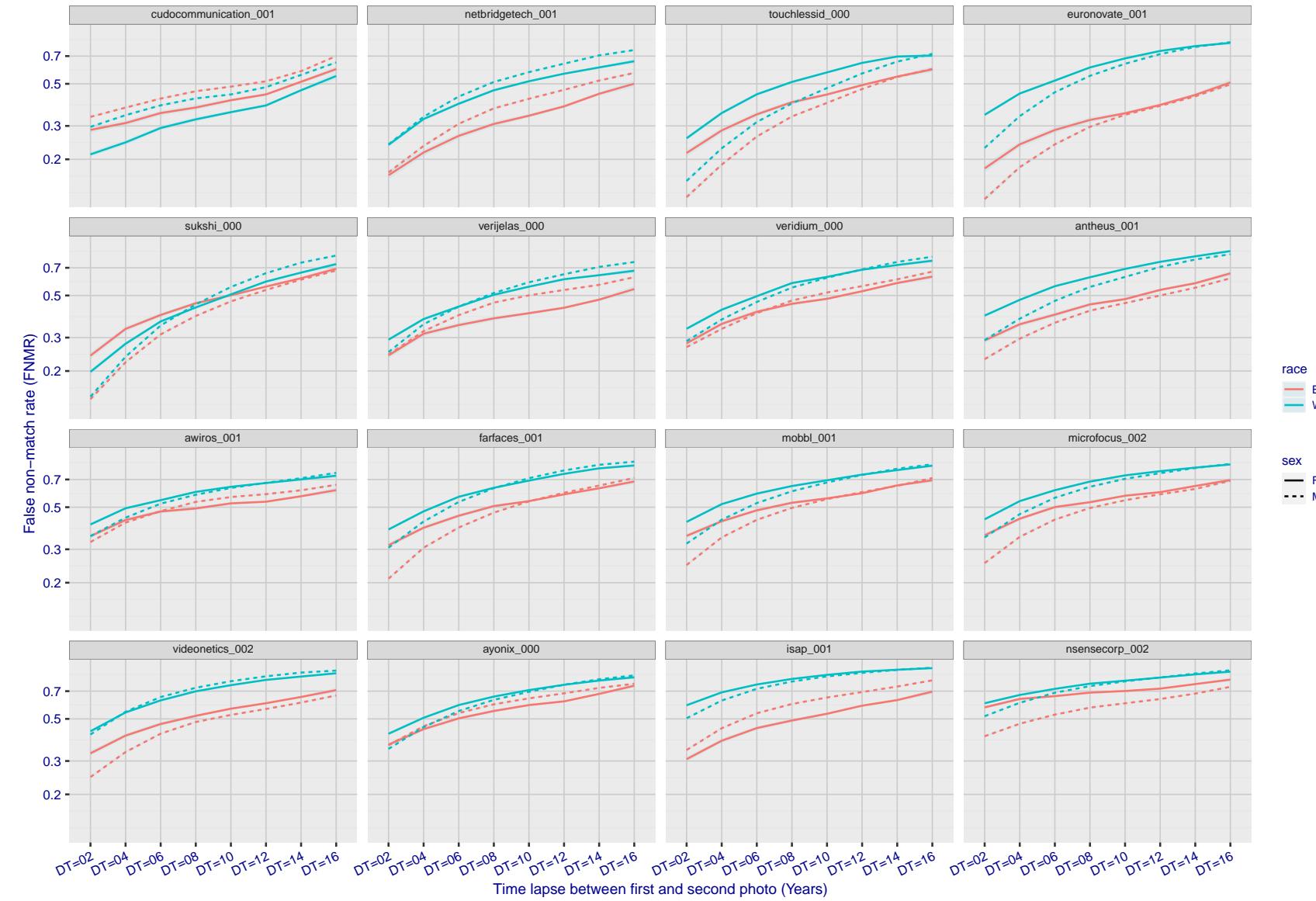


Figure 340: For the mugshot images, FNMR as a function of elapsed time between initial enrollment and second verification images. The panels appear most accurate first, and vertical scale changes on each page. The four traces correspond to images annotated with codes for black female, black male, white female, white male. The threshold is fixed for each algorithm to give FMR = 0.00001 over all (10^8) impostor comparisons. For short time-lapses, the most accurate algorithms give very few errors (FNMR < 0.001) so that the uncertainty estimates are high.

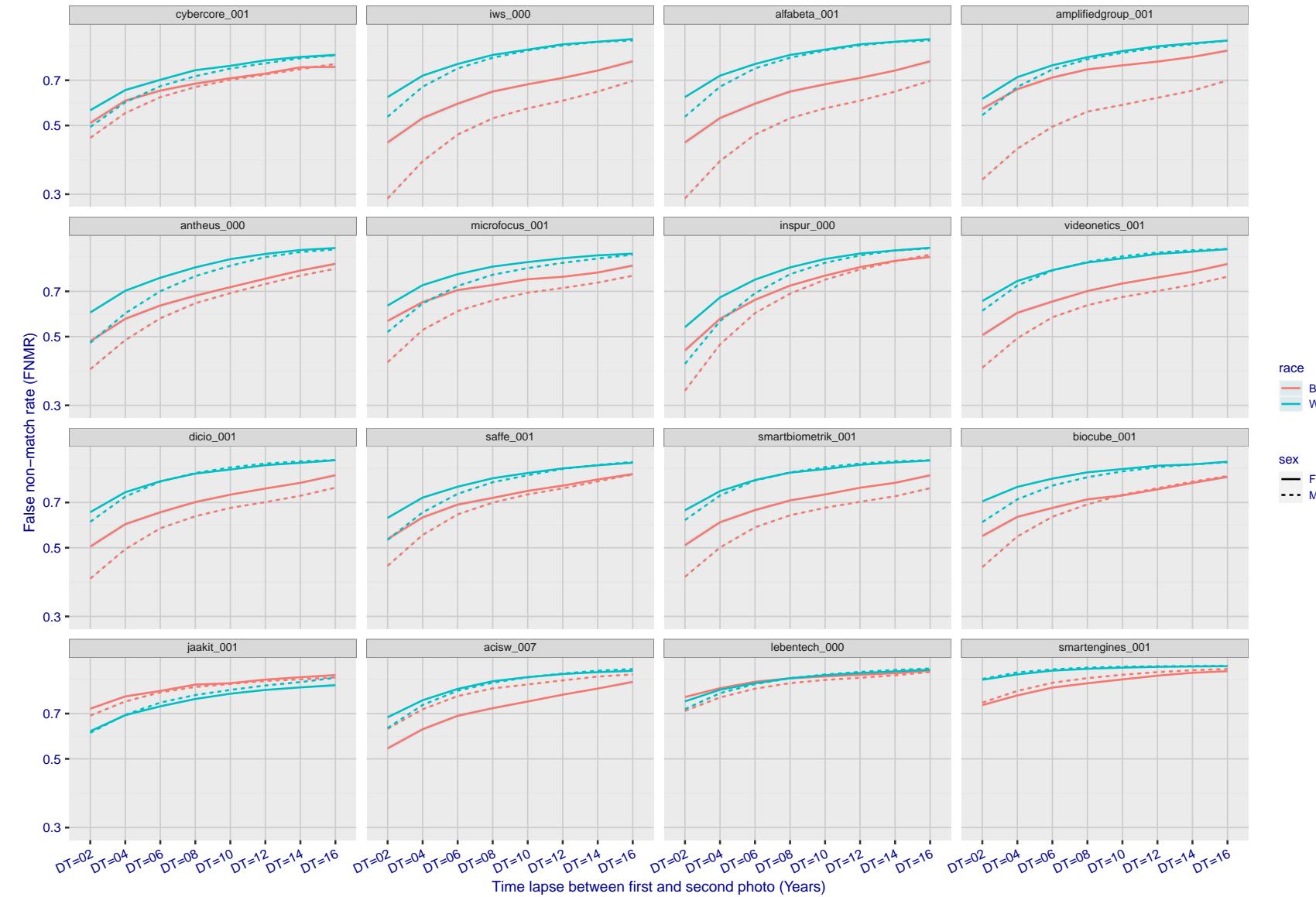


Figure 341: For the mugshot images, FNMR as a function of elapsed time between initial enrollment and second verification images. The panels appear most accurate first, and vertical scale changes on each page. The four traces correspond to images annotated with codes for black female, black male, white female, white male. The threshold is fixed for each algorithm to give $FMR = 0.00001$ over all (10^8) impostor comparisons. For short time-lapses, the most accurate algorithms give very few errors ($FNMR < 0.001$) so that the uncertainty estimates are high.

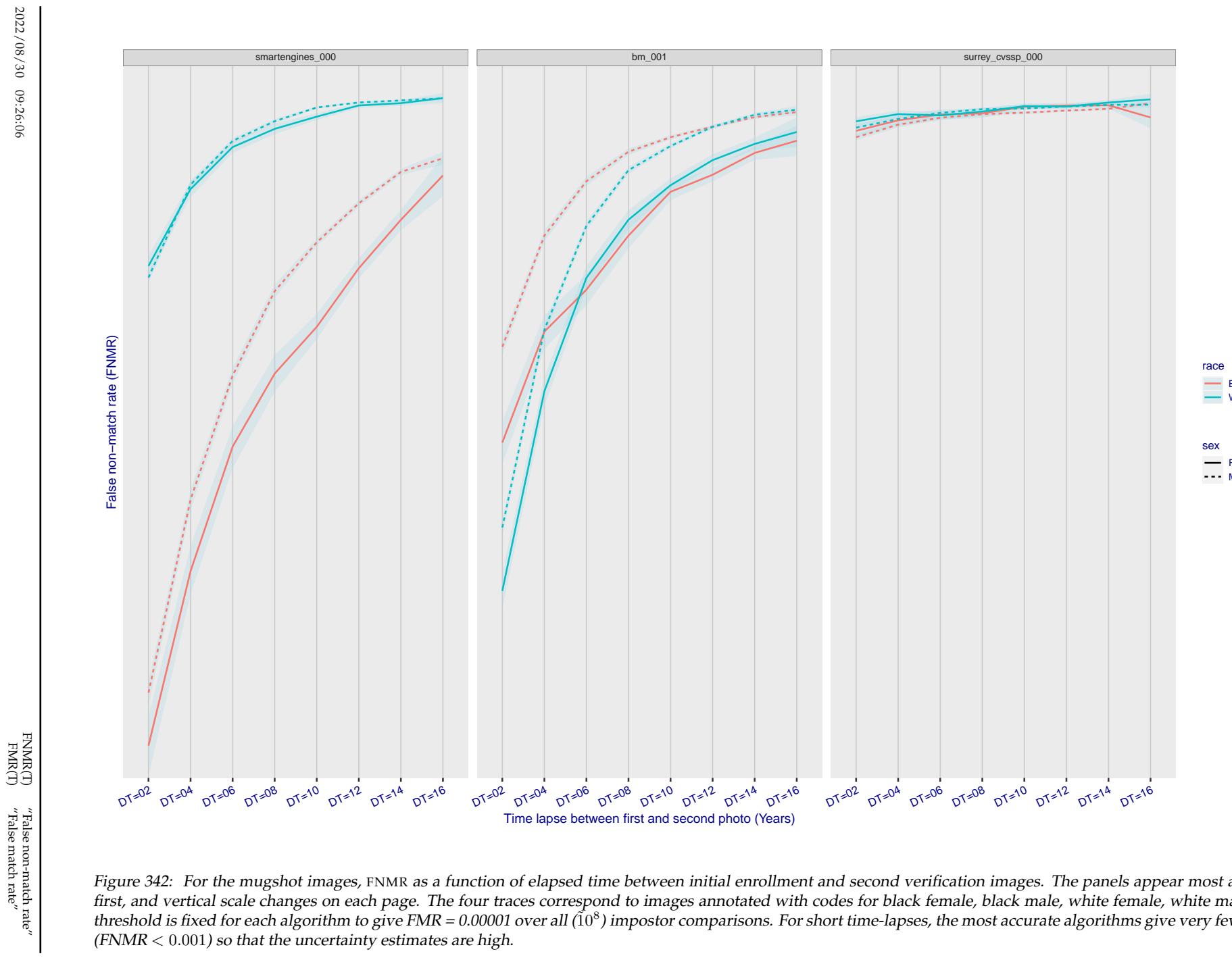


Figure 342: For the mugshot images, FNMR as a function of elapsed time between initial enrollment and second verification images. The panels appear most accurate first, and vertical scale changes on each page. The four traces correspond to images annotated with codes for black female, black male, white female, white male. The threshold is fixed for each algorithm to give $FMR = 0.00001$ over all (10^8) impostor comparisons. For short time-lapses, the most accurate algorithms give very few errors ($FNMR < 0.001$) so that the uncertainty estimates are high.

3.5.3 Effect of age on genuine subjects

Background: Faces change appearance throughout life. Face recognition algorithms have previously been reported to give better accuracy on older individuals (See NIST IR 8009).

Goal: To quantify false non-match rates (FNMR) as a function of age, without an ageing component.

Methods: Using the visa images, which span fewer than five years, thresholds are determined that give FMR = 0.001 and 0.0001 over the entire impostor set. Then FNMR is measured over 1000 bootstrap replications of the genuine scores.

Results: For the visa images, Figure 379 shows how false non-match rates for genuine users, as a function of age group.

The notable aspects are:

- ▷ Younger subjects give considerably higher FNMR. This is likely due to rapid growth and change in facial appearance.
- ▷ FNMR trends down throughout life. The last bin, AGE > 72, contains fewer than 140 mated pairs, and may be affected by small sample size.

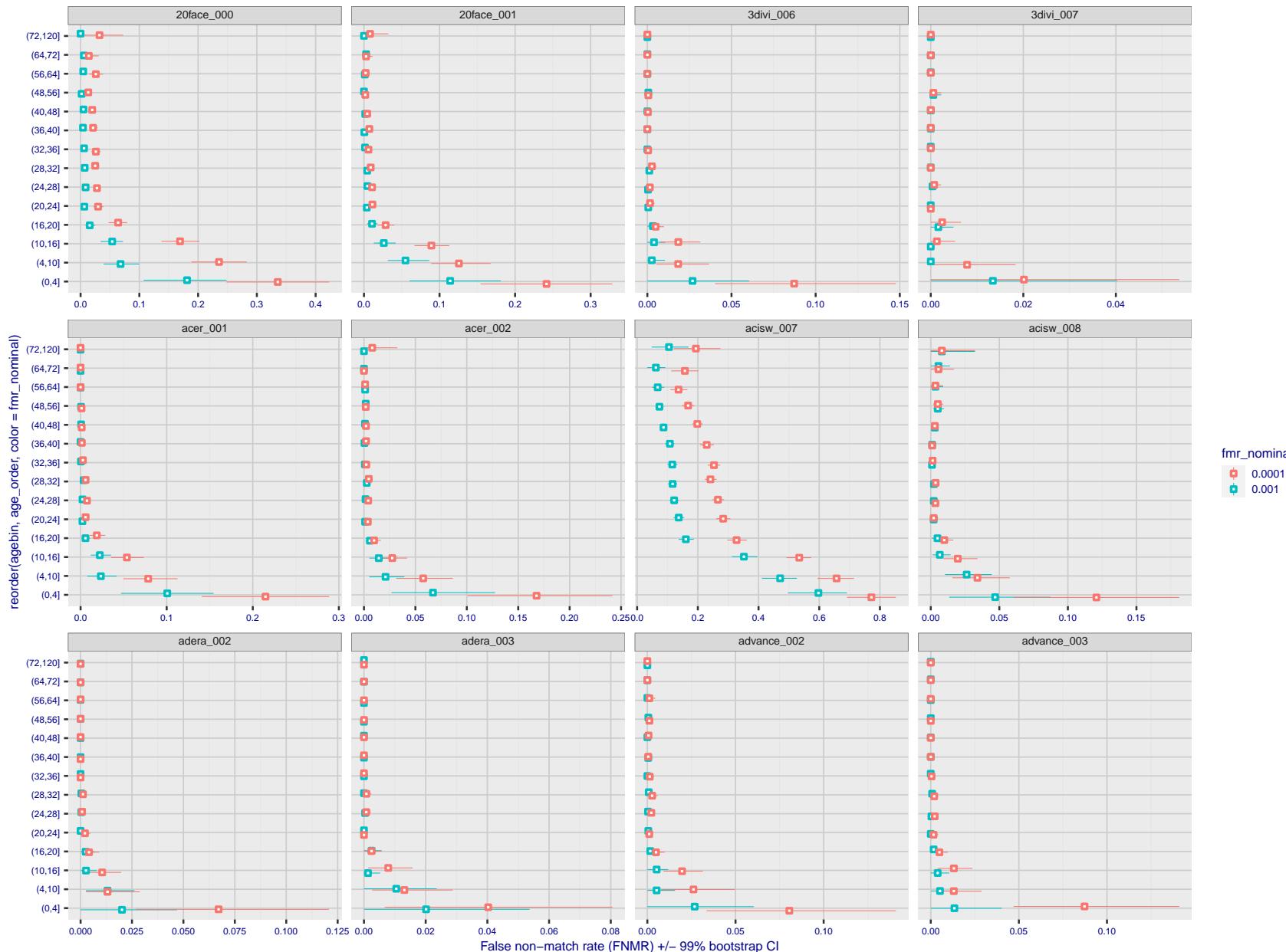


Figure 343: For the visa images, the dots show FNMR by age group for two operating thresholds corresponding to $FMR = \{0.001, 0.0001\}$ computed over all on the order of 10^{10} impostor scores. The FMR in each bin will vary also - see subsequent impostor heatmaps in sec. 3.6.2. Given a pair of face images taken at different times, we assign the comparison to the bin that is the arithmetic average of the subject's ages. This plot shows only the effect of age, not ageing. The number of comparisons in each bin is generally in the thousands, however the first and last bins are computed over 149 and 124 respectively. The error rates in some (adult) cases are zero, and in others the DET is flat so the error rates at the two thresholds are identical. The lines span 1% and 99% of bootstrap replicated FNMR estimates.

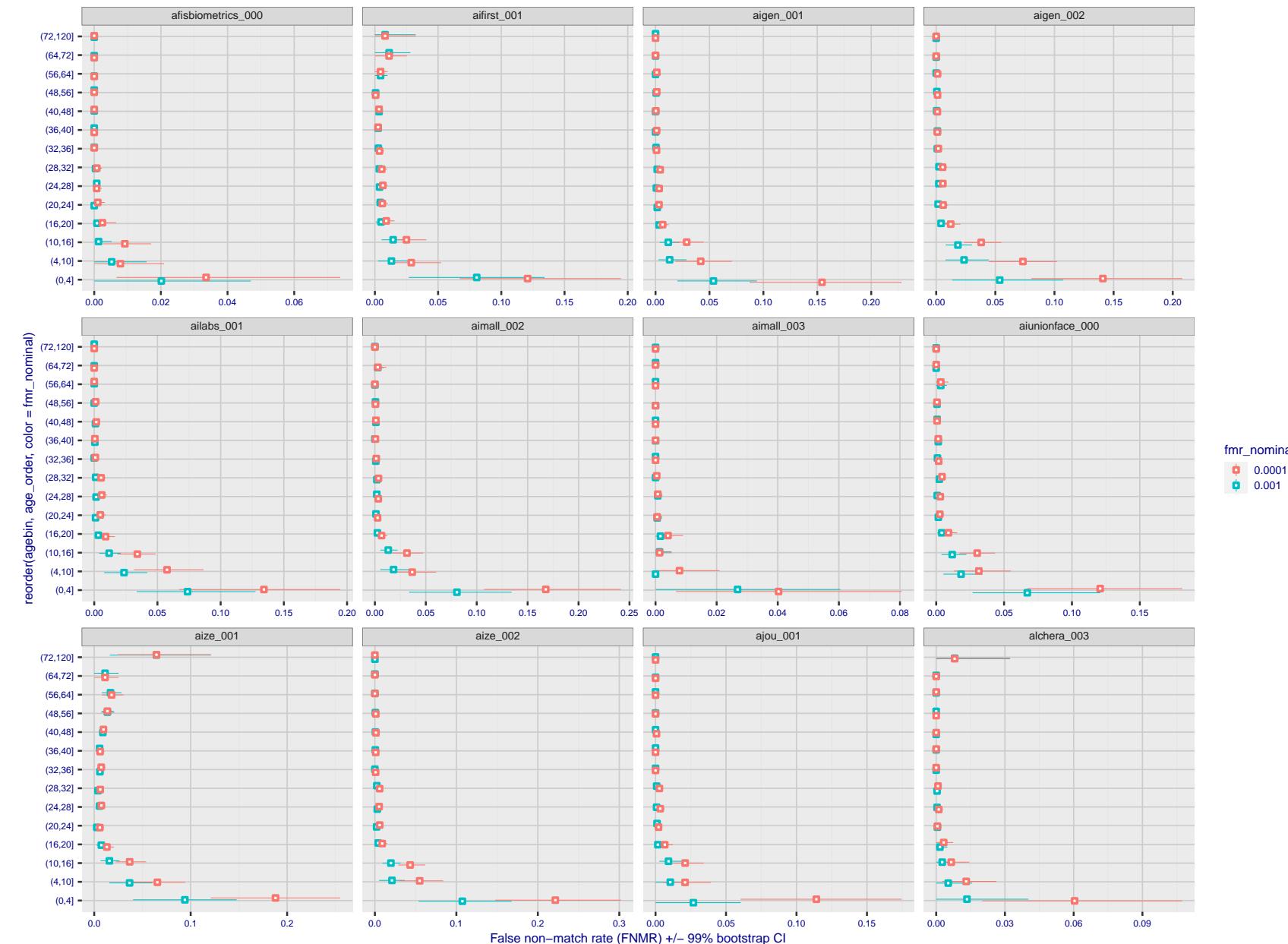


Figure 344: For the visa images, the dots show FNMR by age group for two operating thresholds corresponding to $FMR = \{0.001, 0.0001\}$ computed over all on the order of 10^{10} impostor scores. The FMR in each bin will vary also - see subsequent impostor heatmaps in sec. 3.6.2. Given a pair of face images taken at different times, we assign the comparison to the bin that is the arithmetic average of the subject's ages. This plot shows only the effect of age, not ageing. The number of comparisons in each bin is generally in the thousands, however the first and last bins are computed over 149 and 124 respectively. The error rates in some (adult) cases are zero, and in others the DET is flat so the error rates at the two thresholds are identical. The lines span 1% and 99% of bootstrap replicated FNMR estimates.

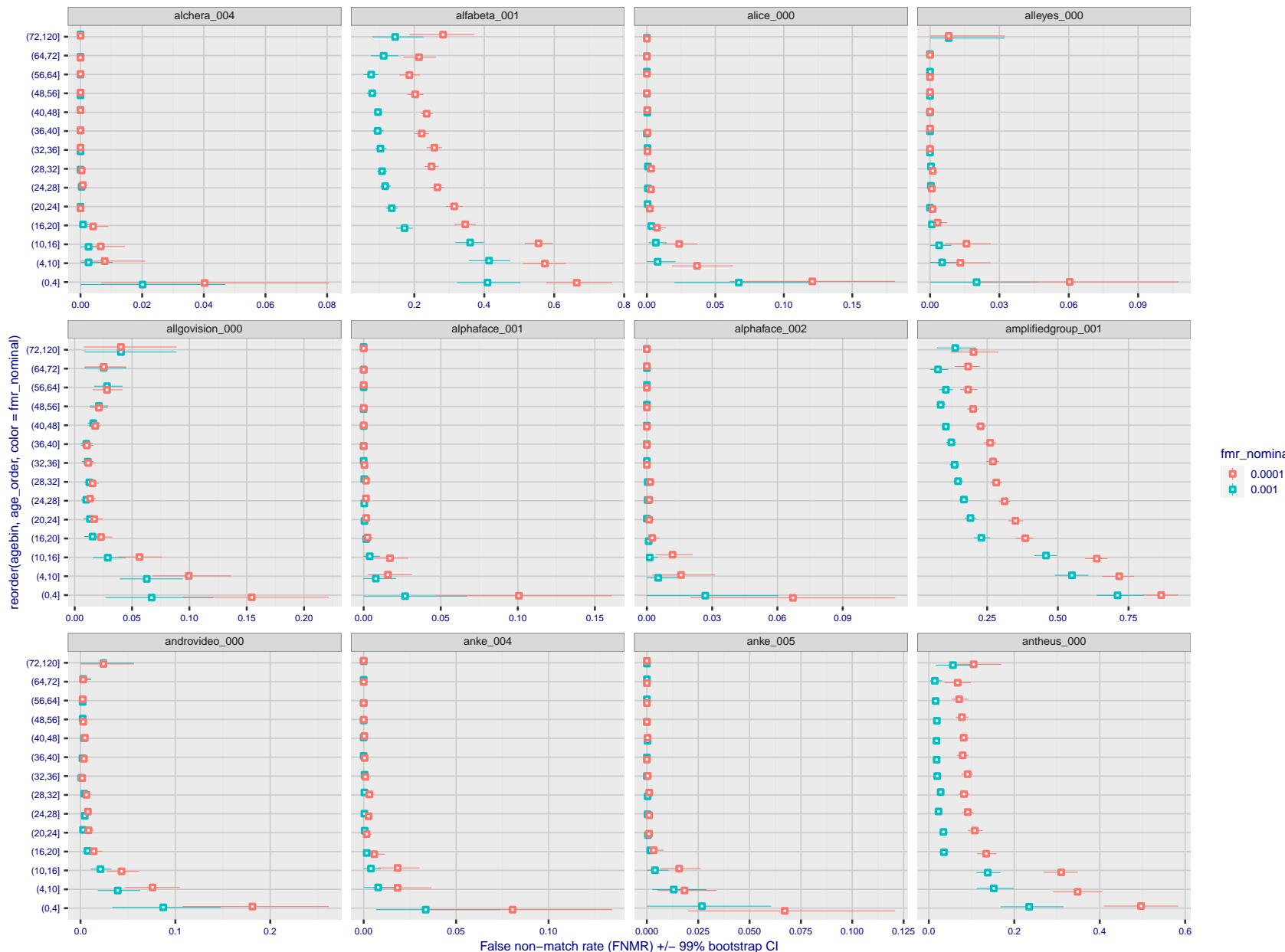


Figure 345: For the visa images, the dots show FNMR by age group for two operating thresholds corresponding to $FMR = \{0.001, 0.0001\}$ computed over all on the order of 10^{10} impostor scores. The FMR in each bin will vary also - see subsequent impostor heatmaps in sec. 3.6.2. Given a pair of face images taken at different times, we assign the comparison to the bin that is the arithmetic average of the subject's ages. This plot shows only the effect of age, not ageing. The number of comparisons in each bin is generally in the thousands, however the first and last bins are computed over 149 and 124 respectively. The error rates in some (adult) cases are zero, and in others the DET is flat so the error rates at the two thresholds are identical. The lines span 1% and 99% of bootstrap replicated FNMR estimates.



Figure 346: For the visa images, the dots show FNMR by age group for two operating thresholds corresponding to $FMR = \{0.001, 0.0001\}$ computed over all on the order of 10^{10} impostor scores. The FMR in each bin will vary also - see subsequent impostor heatmaps in sec. 3.6.2. Given a pair of face images taken at different times, we assign the comparison to the bin that is the arithmetic average of the subject's ages. This plot shows only the effect of age, not ageing. The number of comparisons in each bin is generally in the thousands, however the first and last bins are computed over 149 and 124 respectively. The error rates in some (adult) cases are zero, and in others the DET is flat so the error rates at the two thresholds are identical. The lines span 1% and 99% of bootstrap replicated FNMR estimates.

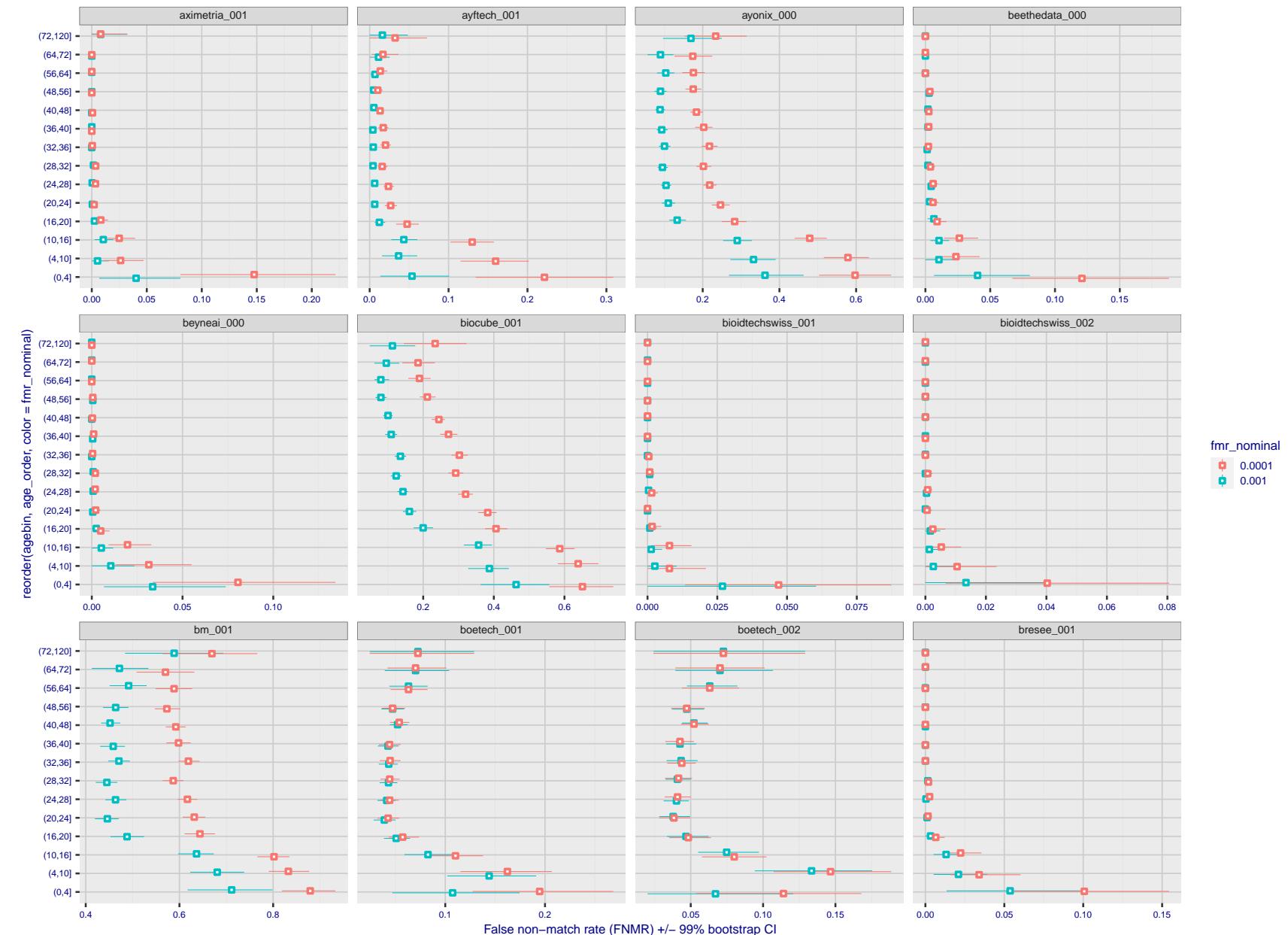


Figure 347: For the visa images, the dots show FNMR by age group for two operating thresholds corresponding to $FMR = \{0.001, 0.0001\}$ computed over all on the order of 10^{10} impostor scores. The FMR in each bin will vary also - see subsequent impostor heatmaps in sec. 3.6.2. Given a pair of face images taken at different times, we assign the comparison to the bin that is the arithmetic average of the subject's ages. This plot shows only the effect of age, not ageing. The number of comparisons in each bin is generally in the thousands, however the first and last bins are computed over 149 and 124 respectively. The error rates in some (adult) cases are zero, and in others the DET is flat so the error rates at the two thresholds are identical. The lines span 1% and 99% of bootstrap replicated FNMR estimates.



Figure 348: For the visa images, the dots show FNMR by age group for two operating thresholds corresponding to $FMR = \{0.001, 0.0001\}$ computed over all on the order of 10^{10} impostor scores. The FMR in each bin will vary also - see subsequent impostor heatmaps in sec. 3.6.2. Given a pair of face images taken at different times, we assign the comparison to the bin that is the arithmetic average of the subject's ages. This plot shows only the effect of age, not ageing. The number of comparisons in each bin is generally in the thousands, however the first and last bins are computed over 149 and 124 respectively. The error rates in some (adult) cases are zero, and in others the DET is flat so the error rates at the two thresholds are identical. The lines span 1% and 99% of bootstrap replicated FNMR estimates.

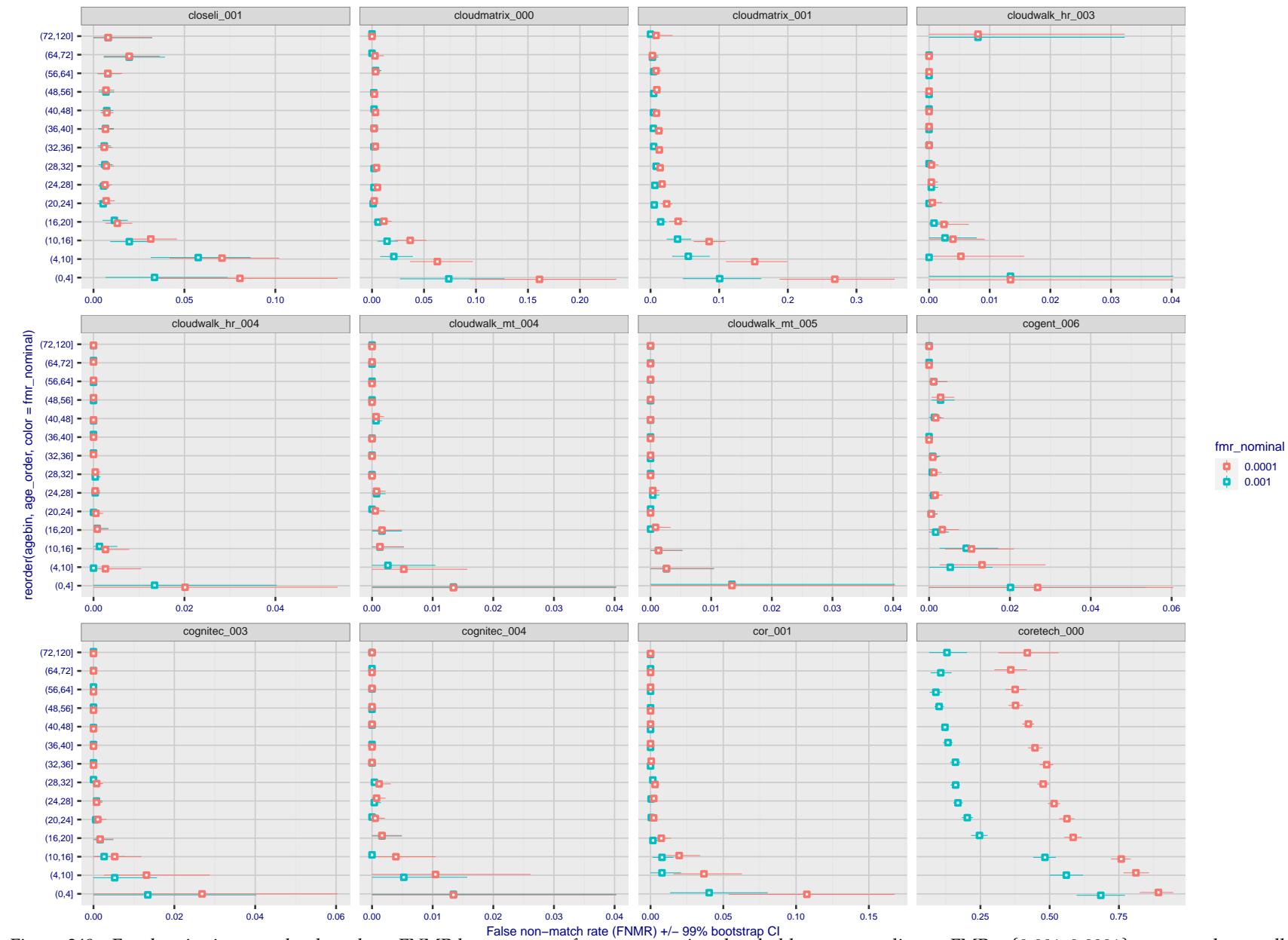


Figure 349: For the visa images, the dots show FNMR by age group for two operating thresholds corresponding to $FMR = \{0.001, 0.0001\}$ computed over all on the order of 10^{10} impostor scores. The FMR in each bin will vary also - see subsequent impostor heatmaps in sec. 3.6.2. Given a pair of face images taken at different times, we assign the comparison to the bin that is the arithmetic average of the subject's ages. This plot shows only the effect of age, not ageing. The number of comparisons in each bin is generally in the thousands, however the first and last bins are computed over 149 and 124 respectively. The error rates in some (adult) cases are zero, and in others the DET is flat so the error rates at the two thresholds are identical. The lines span 1% and 99% of bootstrap replicated FNMR estimates.

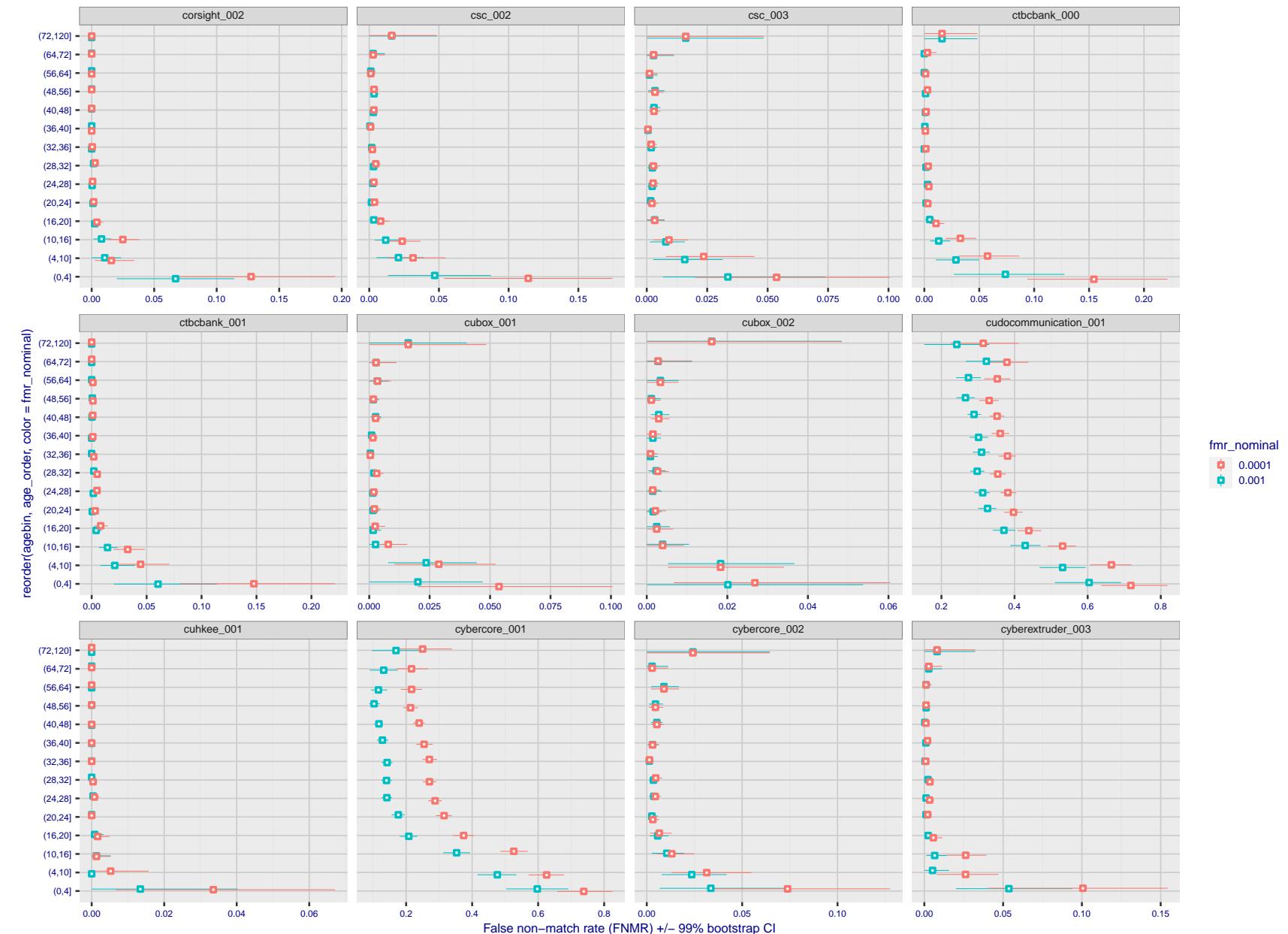


Figure 350: For the visa images, the dots show FNMR by age group for two operating thresholds corresponding to $FMR = \{0.001, 0.0001\}$ computed over all on the order of 10^{10} impostor scores. The FMR in each bin will vary also - see subsequent impostor heatmaps in sec. 3.6.2. Given a pair of face images taken at different times, we assign the comparison to the bin that is the arithmetic average of the subject's ages. This plot shows only the effect of age, not ageing. The number of comparisons in each bin is generally in the thousands, however the first and last bins are computed over 149 and 124 respectively. The error rates in some (adult) cases are zero, and in others the DET is flat so the error rates at the two thresholds are identical. The lines span 1% and 99% of bootstrap replicated FNMR estimates.



Figure 351: For the visa images, the dots show FNMR by age group for two operating thresholds corresponding to $FMR = \{0.001, 0.0001\}$ computed over all on the order of 10^{10} impostor scores. The FMR in each bin will vary also - see subsequent impostor heatmaps in sec. 3.6.2. Given a pair of face images taken at different times, we assign the comparison to the bin that is the arithmetic average of the subject's ages. This plot shows only the effect of age, not ageing. The number of comparisons in each bin is generally in the thousands, however the first and last bins are computed over 149 and 124 respectively. The error rates in some (adult) cases are zero, and in others the DET is flat so the error rates at the two thresholds are identical. The lines span 1% and 99% of bootstrap replicated FNMR estimates.

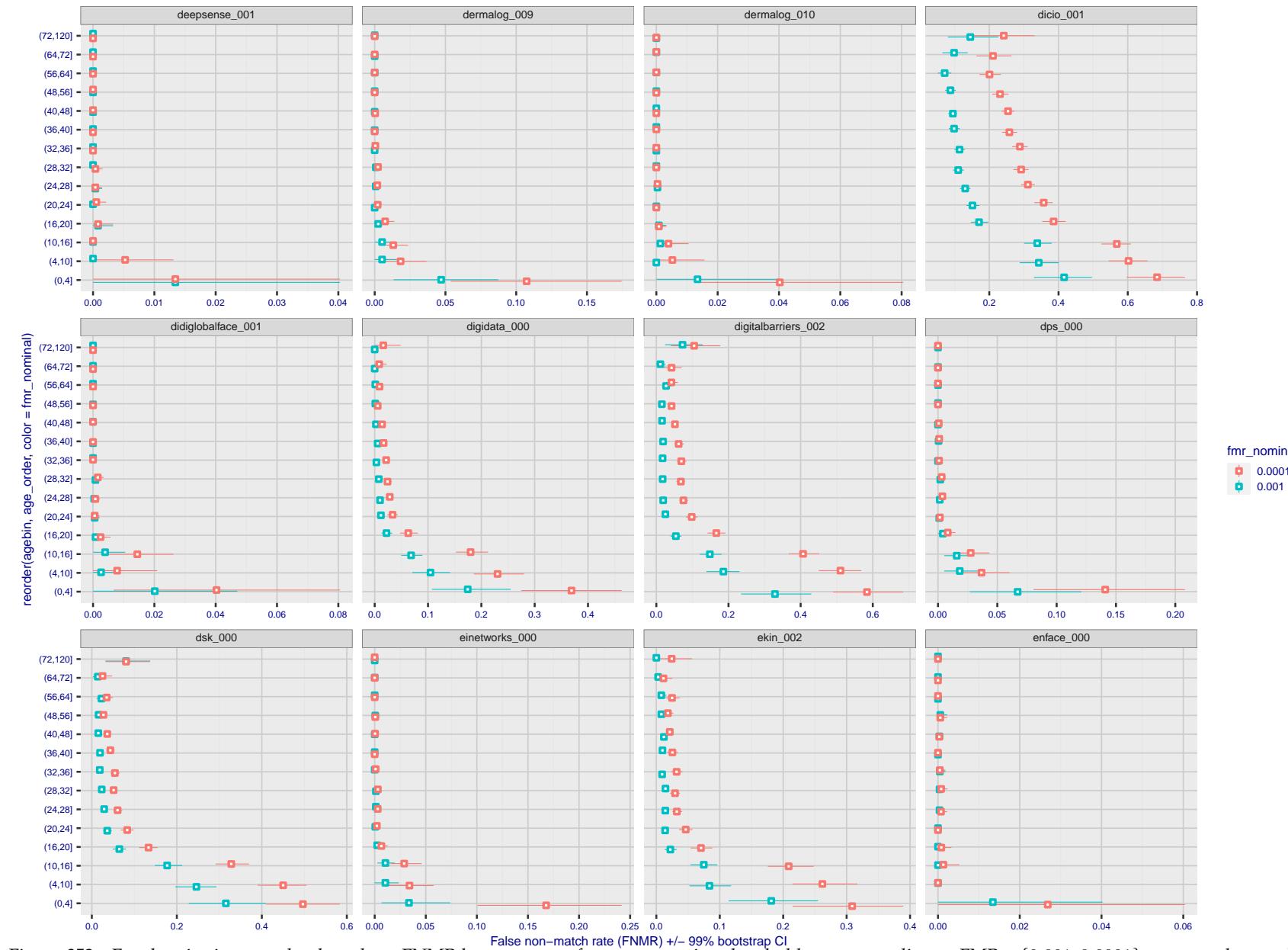


Figure 352: For the visa images, the dots show FNMR by age group for two operating thresholds corresponding to $FMR = \{0.001, 0.0001\}$ computed over all on the order of 10^{10} impostor scores. The FMR in each bin will vary also - see subsequent impostor heatmaps in sec. 3.6.2. Given a pair of face images taken at different times, we assign the comparison to the bin that is the arithmetic average of the subject's ages. This plot shows only the effect of age, not ageing. The number of comparisons in each bin is generally in the thousands, however the first and last bins are computed over 149 and 124 respectively. The error rates in some (adult) cases are zero, and in others the DET is flat so the error rates at the two thresholds are identical. The lines span 1% and 99% of bootstrap replicated FNMR estimates.

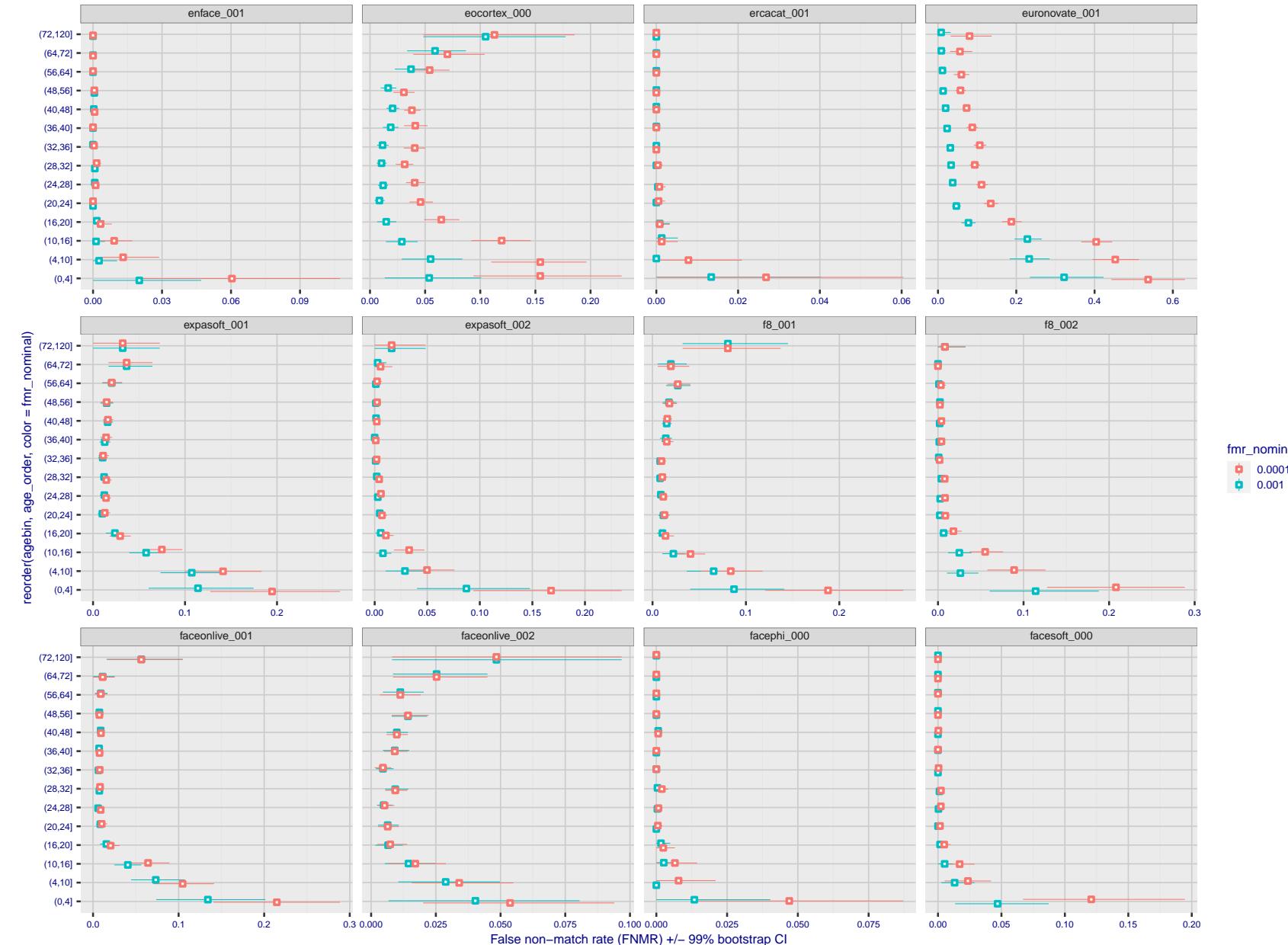


Figure 353: For the visa images, the dots show FNMR by age group for two operating thresholds corresponding to $FMR = \{0.001, 0.0001\}$ computed over all on the order of 10^{10} impostor scores. The FMR in each bin will vary also - see subsequent impostor heatmaps in sec. 3.6.2. Given a pair of face images taken at different times, we assign the comparison to the bin that is the arithmetic average of the subject's ages. This plot shows only the effect of age, not ageing. The number of comparisons in each bin is generally in the thousands, however the first and last bins are computed over 149 and 124 respectively. The error rates in some (adult) cases are zero, and in others the DET is flat so the error rates at the two thresholds are identical. The lines span 1% and 99% of bootstrap replicated FNMR estimates.

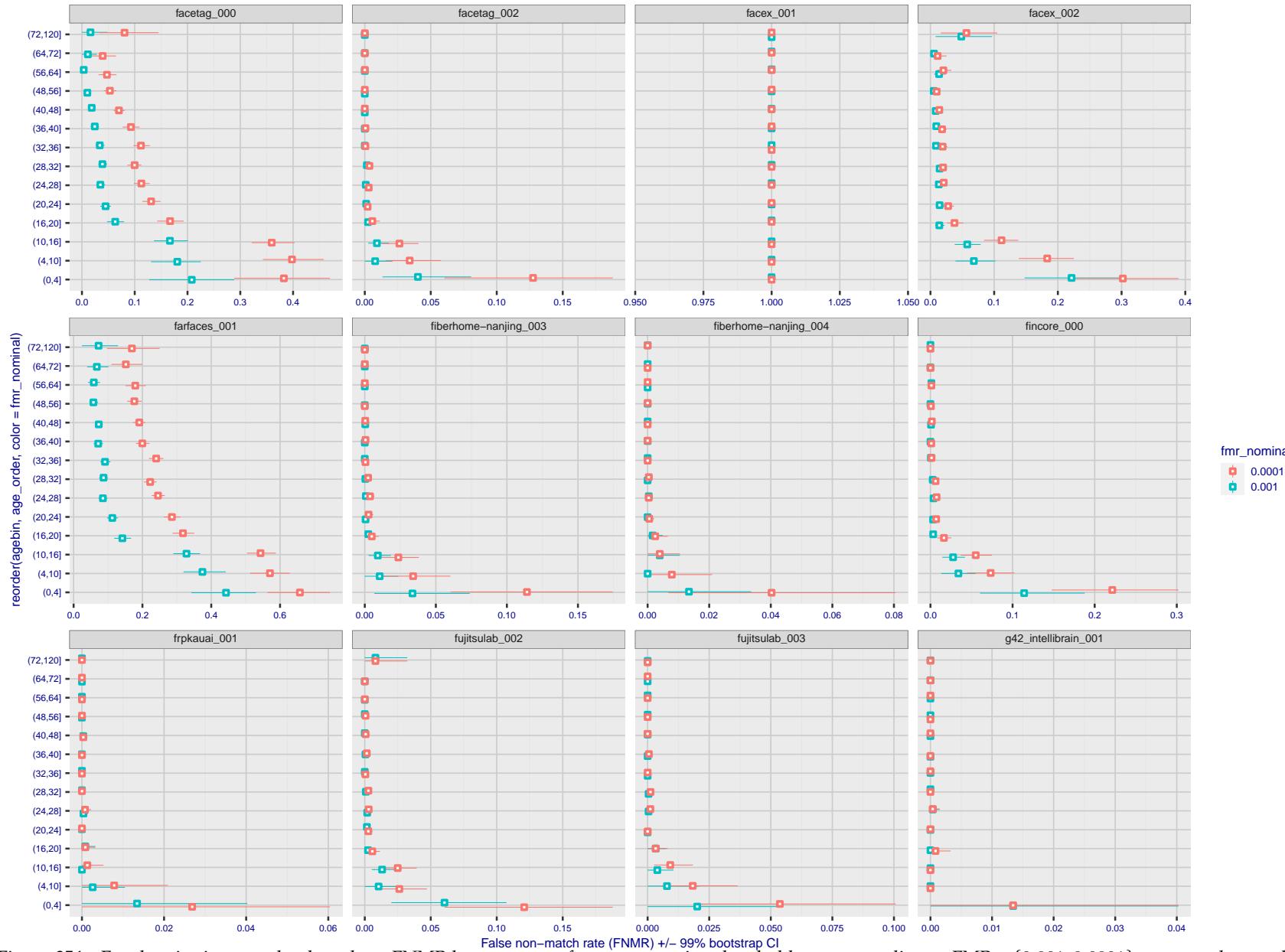


Figure 354: For the visa images, the dots show FNMR by age group for two operating thresholds corresponding to $FMR = \{0.001, 0.0001\}$ computed over all on the order of 10^{10} impostor scores. The FMR in each bin will vary also - see subsequent impostor heatmaps in sec. 3.6.2. Given a pair of face images taken at different times, we assign the comparison to the bin that is the arithmetic average of the subject's ages. This plot shows only the effect of age, not ageing. The number of comparisons in each bin is generally in the thousands, however the first and last bins are computed over 149 and 124 respectively. The error rates in some (adult) cases are zero, and in others the DET is flat so the error rates at the two thresholds are identical. The lines span 1% and 99% of bootstrap replicated FNMR estimates.



Figure 355: For the visa images, the dots show FNMR by age group for two operating thresholds corresponding to $FMR = \{0.001, 0.0001\}$ computed over all on the order of 10^{10} impostor scores. The FMR in each bin will vary also - see subsequent impostor heatmaps in sec. 3.6.2. Given a pair of face images taken at different times, we assign the comparison to the bin that is the arithmetic average of the subject's ages. This plot shows only the effect of age, not ageing. The number of comparisons in each bin is generally in the thousands, however the first and last bins are computed over 149 and 124 respectively. The error rates in some (adult) cases are zero, and in others the DET is flat so the error rates at the two thresholds are identical. The lines span 1% and 99% of bootstrap replicated FNMR estimates.



Figure 356: For the visa images, the dots show FNMR by age group for two operating thresholds corresponding to $FMR = \{0.001, 0.0001\}$ computed over all on the order of 10^{10} impostor scores. The FMR in each bin will vary also - see subsequent impostor heatmaps in sec. 3.6.2. Given a pair of face images taken at different times, we assign the comparison to the bin that is the arithmetic average of the subject's ages. This plot shows only the effect of age, not ageing. The number of comparisons in each bin is generally in the thousands, however the first and last bins are computed over 149 and 124 respectively. The error rates in some (adult) cases are zero, and in others the DET is flat so the error rates at the two thresholds are identical. The lines span 1% and 99% of bootstrap replicated FNMR estimates.

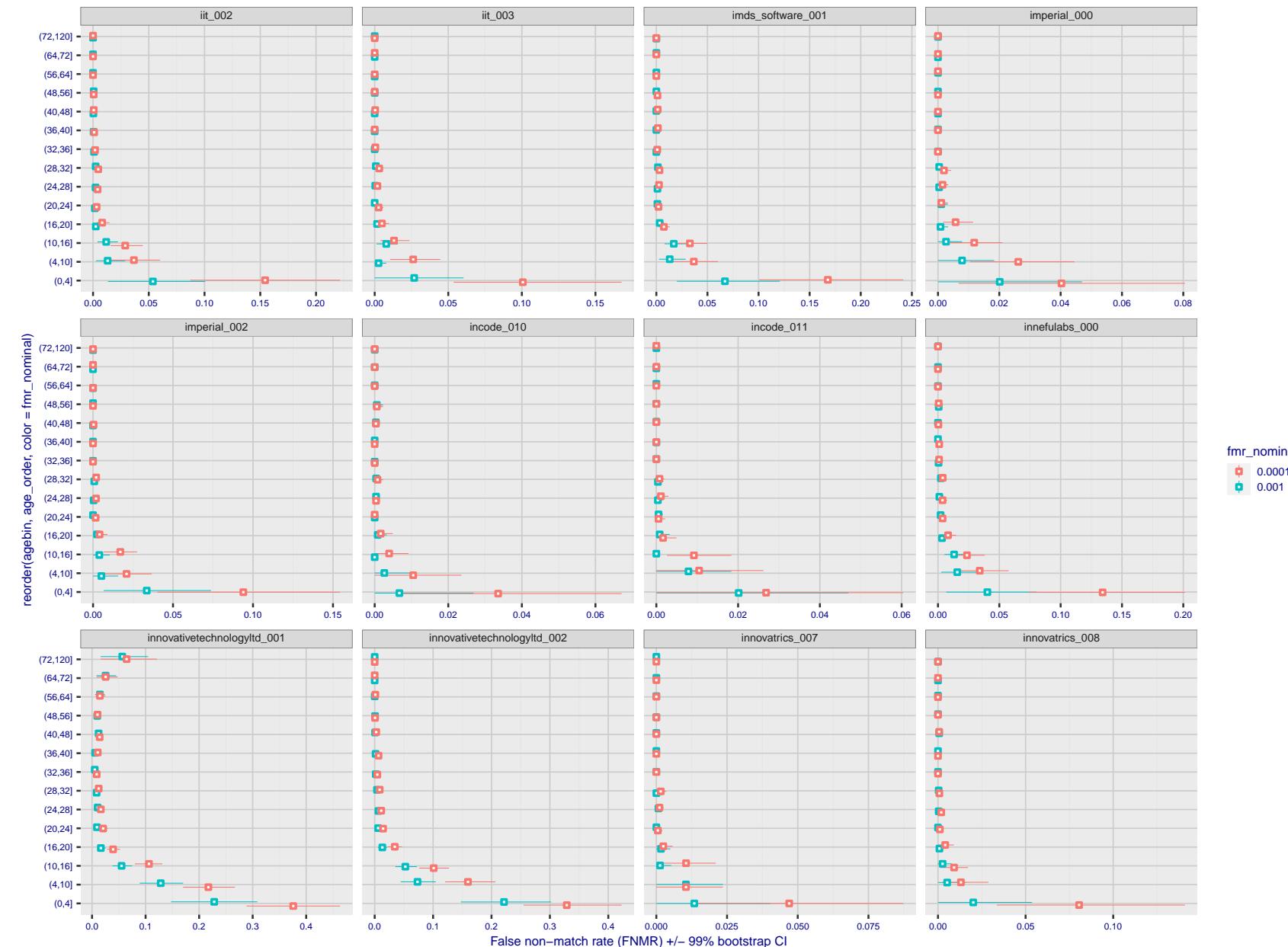


Figure 357: For the visa images, the dots show FNMR by age group for two operating thresholds corresponding to $FMR = \{0.001, 0.0001\}$ computed over all on the order of 10^{10} impostor scores. The FMR in each bin will vary also - see subsequent impostor heatmaps in sec. 3.6.2. Given a pair of face images taken at different times, we assign the comparison to the bin that is the arithmetic average of the subject's ages. This plot shows only the effect of age, not ageing. The number of comparisons in each bin is generally in the thousands, however the first and last bins are computed over 149 and 124 respectively. The error rates in some (adult) cases are zero, and in others the DET is flat so the error rates at the two thresholds are identical. The lines span 1% and 99% of bootstrap replicated FNMR estimates.



Figure 358: For the visa images, the dots show FNMR by age group for two operating thresholds corresponding to $FMR = \{0.001, 0.0001\}$ computed over all on the order of 10^{10} impostor scores. The FMR in each bin will vary also - see subsequent impostor heatmaps in sec. 3.6.2. Given a pair of face images taken at different times, we assign the comparison to the bin that is the arithmetic average of the subject's ages. This plot shows only the effect of age, not ageing. The number of comparisons in each bin is generally in the thousands, however the first and last bins are computed over 149 and 124 respectively. The error rates in some (adult) cases are zero, and in others the DET is flat so the error rates at the two thresholds are identical. The lines span 1% and 99% of bootstrap replicated FNMR estimates.

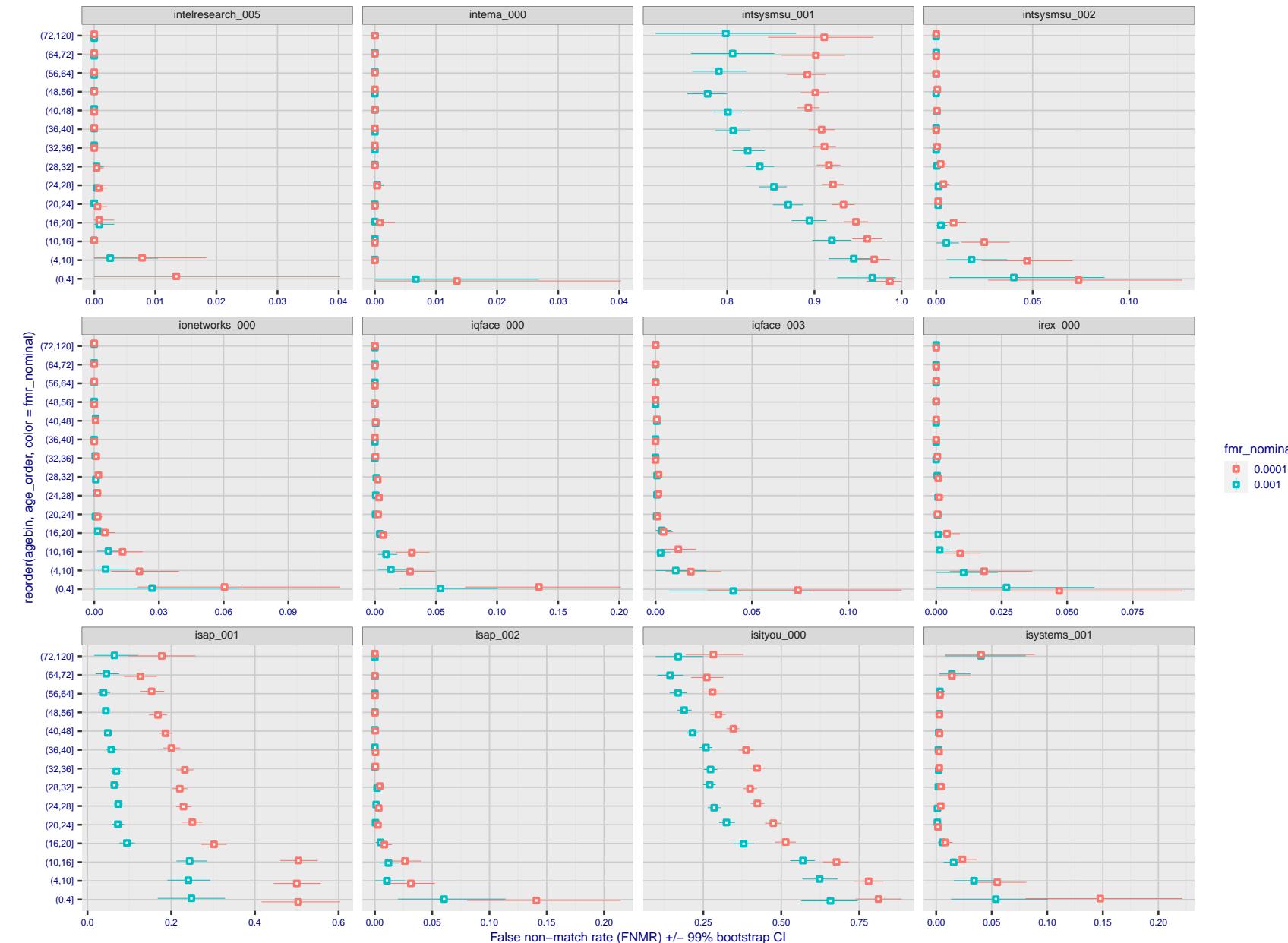


Figure 359: For the visa images, the dots show FNMR by age group for two operating thresholds corresponding to $FMR = \{0.001, 0.0001\}$ computed over all on the order of 10^{10} impostor scores. The FMR in each bin will vary also - see subsequent impostor heatmaps in sec. 3.6.2. Given a pair of face images taken at different times, we assign the comparison to the bin that is the arithmetic average of the subject's ages. This plot shows only the effect of age, not ageing. The number of comparisons in each bin is generally in the thousands, however the first and last bins are computed over 149 and 124 respectively. The error rates in some (adult) cases are zero, and in others the DET is flat so the error rates at the two thresholds are identical. The lines span 1% and 99% of bootstrap replicated FNMR estimates.

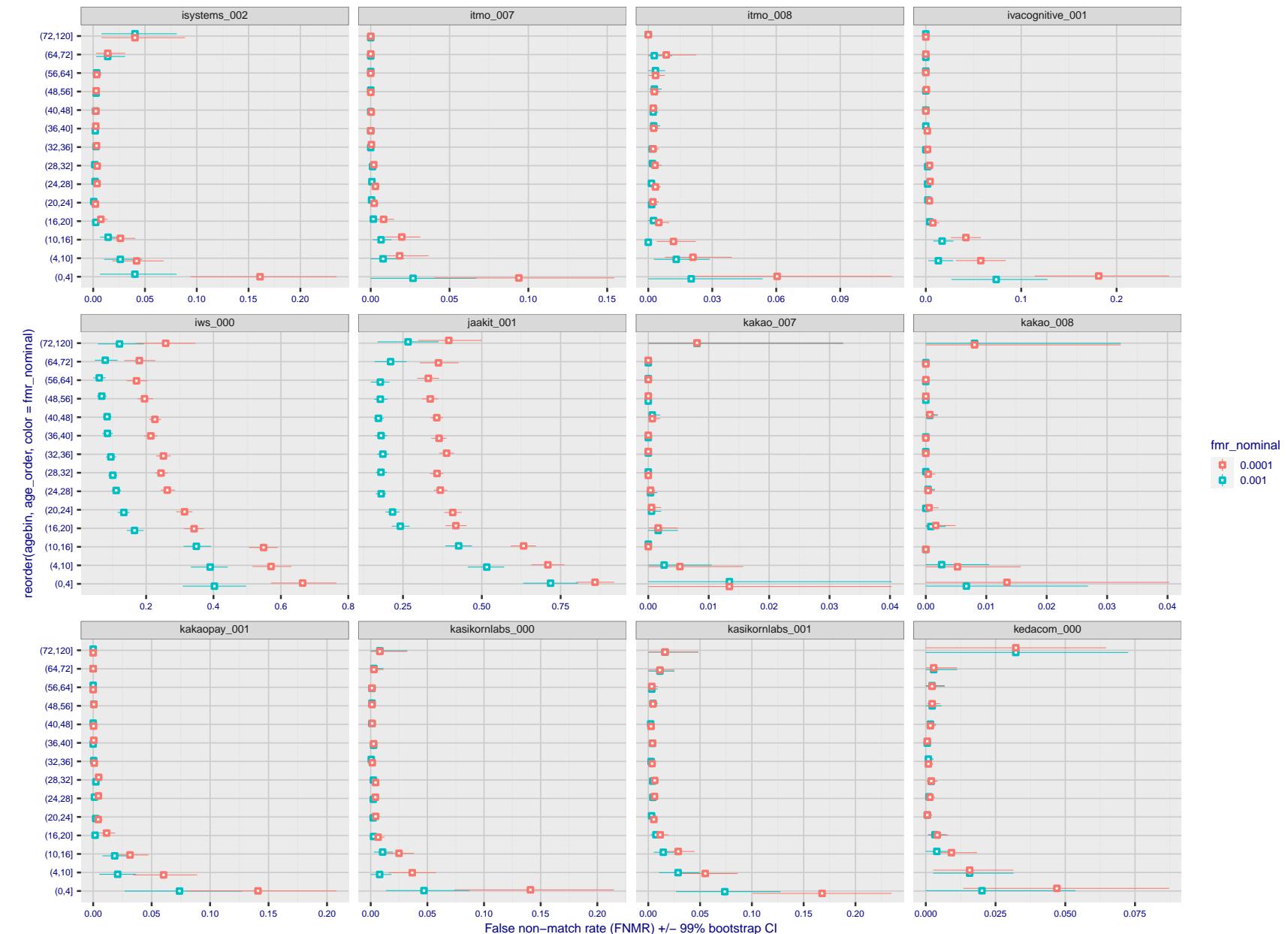


Figure 360: For the visa images, the dots show FNMR by age group for two operating thresholds corresponding to $FMR = \{0.001, 0.0001\}$ computed over all on the order of 10^{10} impostor scores. The FMR in each bin will vary also - see subsequent impostor heatmaps in sec. 3.6.2. Given a pair of face images taken at different times, we assign the comparison to the bin that is the arithmetic average of the subject's ages. This plot shows only the effect of age, not ageing. The number of comparisons in each bin is generally in the thousands, however the first and last bins are computed over 149 and 124 respectively. The error rates in some (adult) cases are zero, and in others the DET is flat so the error rates at the two thresholds are identical. The lines span 1% and 99% of bootstrap replicated FNMR estimates.

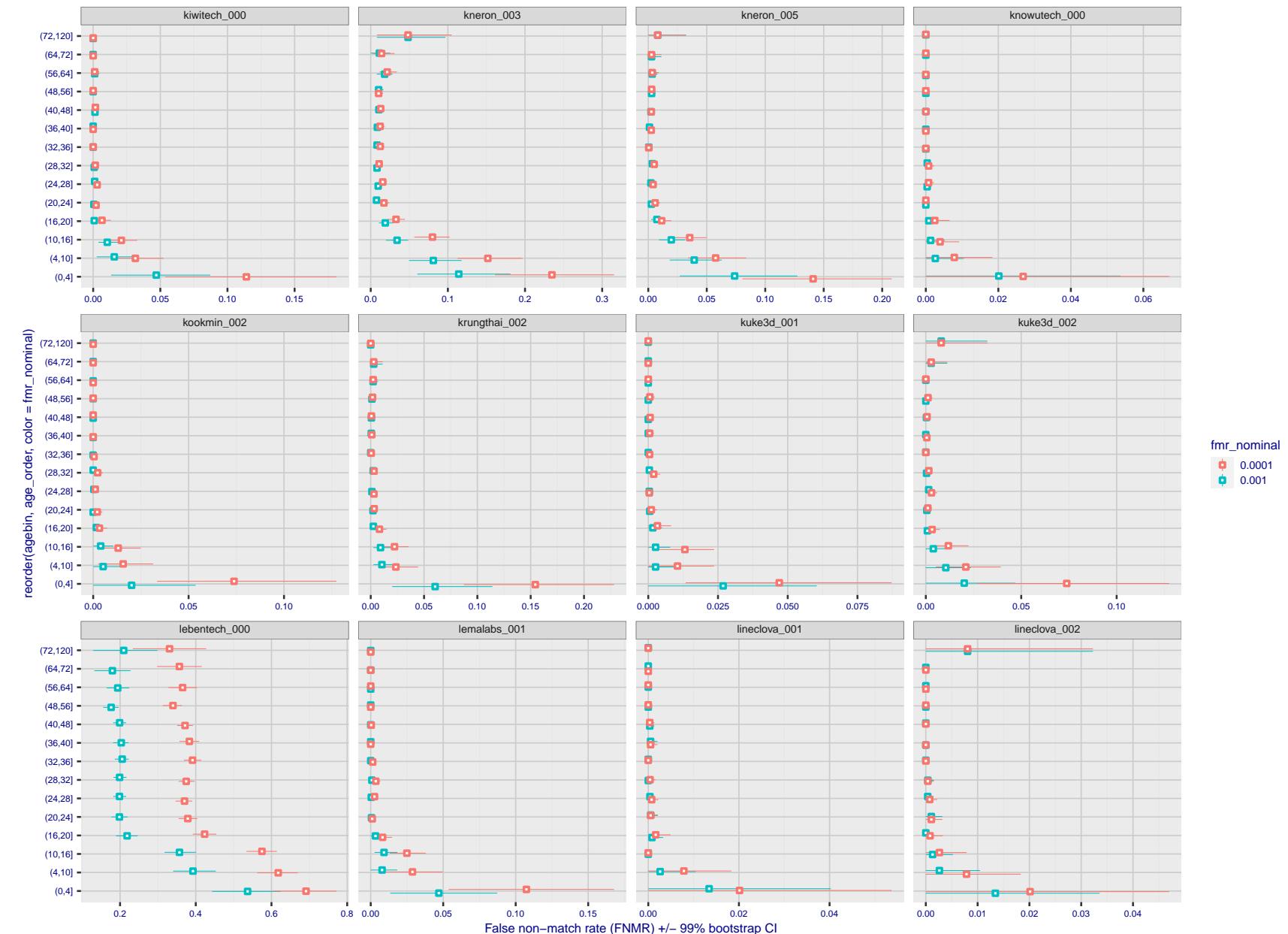


Figure 361: For the visa images, the dots show FNMR by age group for two operating thresholds corresponding to $FMR = \{0.001, 0.0001\}$ computed over all on the order of 10^{10} impostor scores. The FMR in each bin will vary also - see subsequent impostor heatmaps in sec. 3.6.2. Given a pair of face images taken at different times, we assign the comparison to the bin that is the arithmetic average of the subject's ages. This plot shows only the effect of age, not ageing. The number of comparisons in each bin is generally in the thousands, however the first and last bins are computed over 149 and 124 respectively. The error rates in some (adult) cases are zero, and in others the DET is flat so the error rates at the two thresholds are identical. The lines span 1% and 99% of bootstrap replicated FNMR estimates.

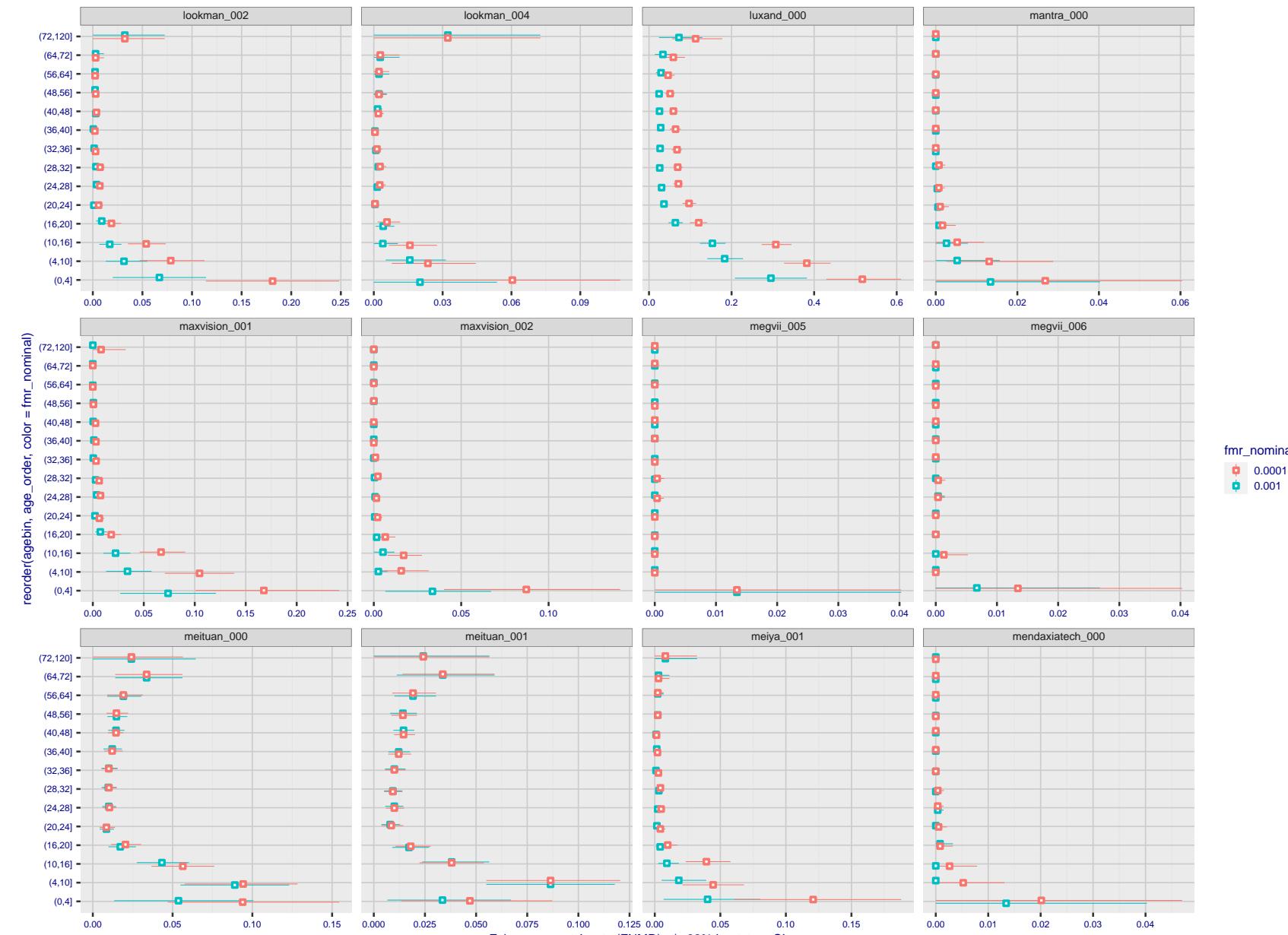


Figure 362: For the visa images, the dots show FNMR by age group for two operating thresholds corresponding to $FMR = \{0.001, 0.0001\}$ computed over all on the order of 10^{10} impostor scores. The FMR in each bin will vary also - see subsequent impostor heatmaps in sec. 3.6.2. Given a pair of face images taken at different times, we assign the comparison to the bin that is the arithmetic average of the subject's ages. This plot shows only the effect of age, not ageing. The number of comparisons in each bin is generally in the thousands, however the first and last bins are computed over 149 and 124 respectively. The error rates in some (adult) cases are zero, and in others the DET is flat so the error rates at the two thresholds are identical. The lines span 1% and 99% of bootstrap replicated FNMR estimates.

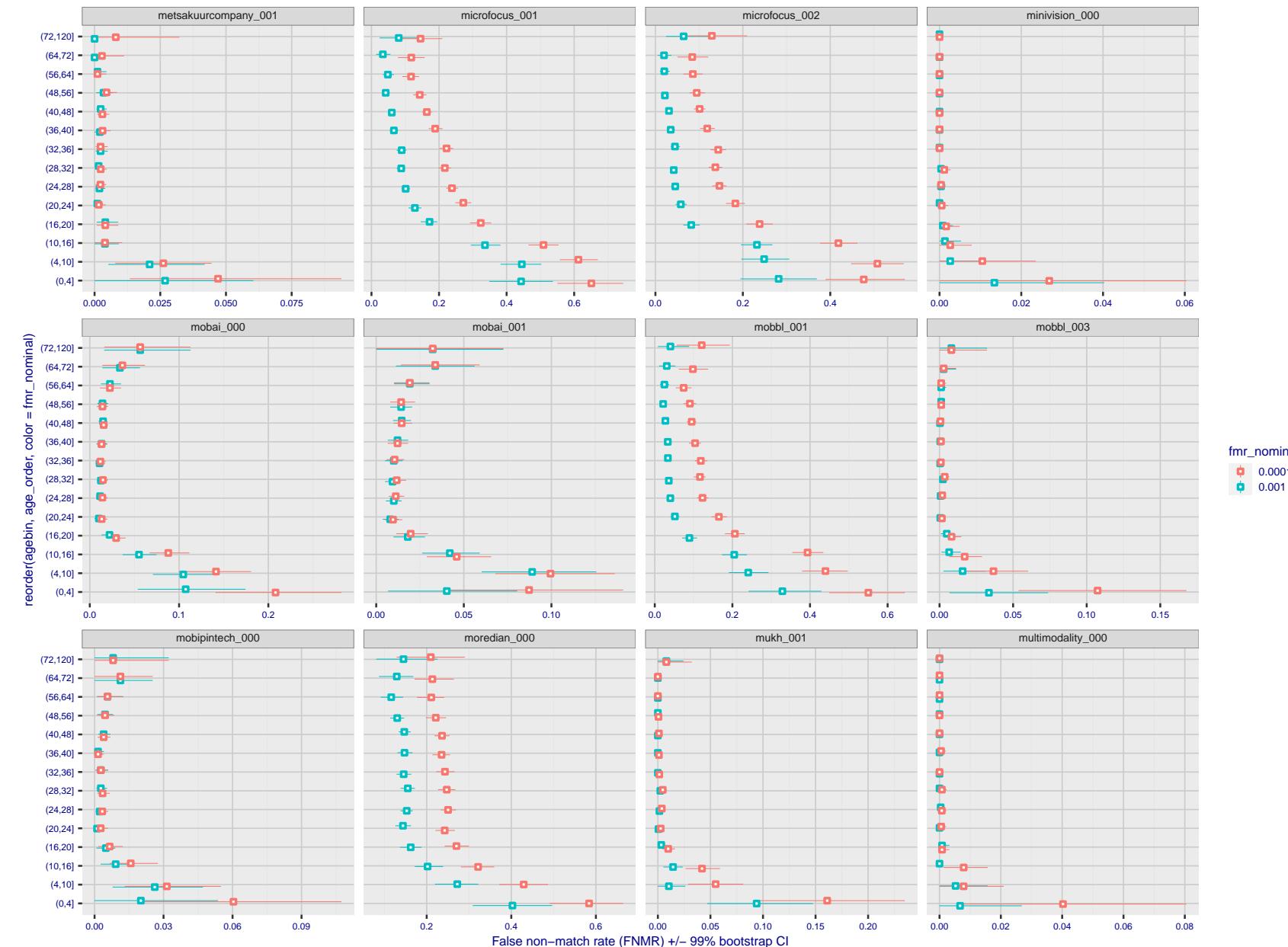


Figure 363: For the visa images, the dots show FNMR by age group for two operating thresholds corresponding to $FMR = \{0.001, 0.0001\}$ computed over all on the order of 10^{10} impostor scores. The FMR in each bin will vary also - see subsequent impostor heatmaps in sec. 3.6.2. Given a pair of face images taken at different times, we assign the comparison to the bin that is the arithmetic average of the subject's ages. This plot shows only the effect of age, not ageing. The number of comparisons in each bin is generally in the thousands, however the first and last bins are computed over 149 and 124 respectively. The error rates in some (adult) cases are zero, and in others the DET is flat so the error rates at the two thresholds are identical. The lines span 1% and 99% of bootstrap replicated FNMR estimates.



Figure 364: For the visa images, the dots show FNMR by age group for two operating thresholds corresponding to $FMR = \{0.001, 0.0001\}$ computed over all on the order of 10^{10} impostor scores. The FMR in each bin will vary also - see subsequent impostor heatmaps in sec. 3.6.2. Given a pair of face images taken at different times, we assign the comparison to the bin that is the arithmetic average of the subject's ages. This plot shows only the effect of age, not ageing. The number of comparisons in each bin is generally in the thousands, however the first and last bins are computed over 149 and 124 respectively. The error rates in some (adult) cases are zero, and in others the DET is flat so the error rates at the two thresholds are identical. The lines span 1% and 99% of bootstrap replicated FNMR estimates.

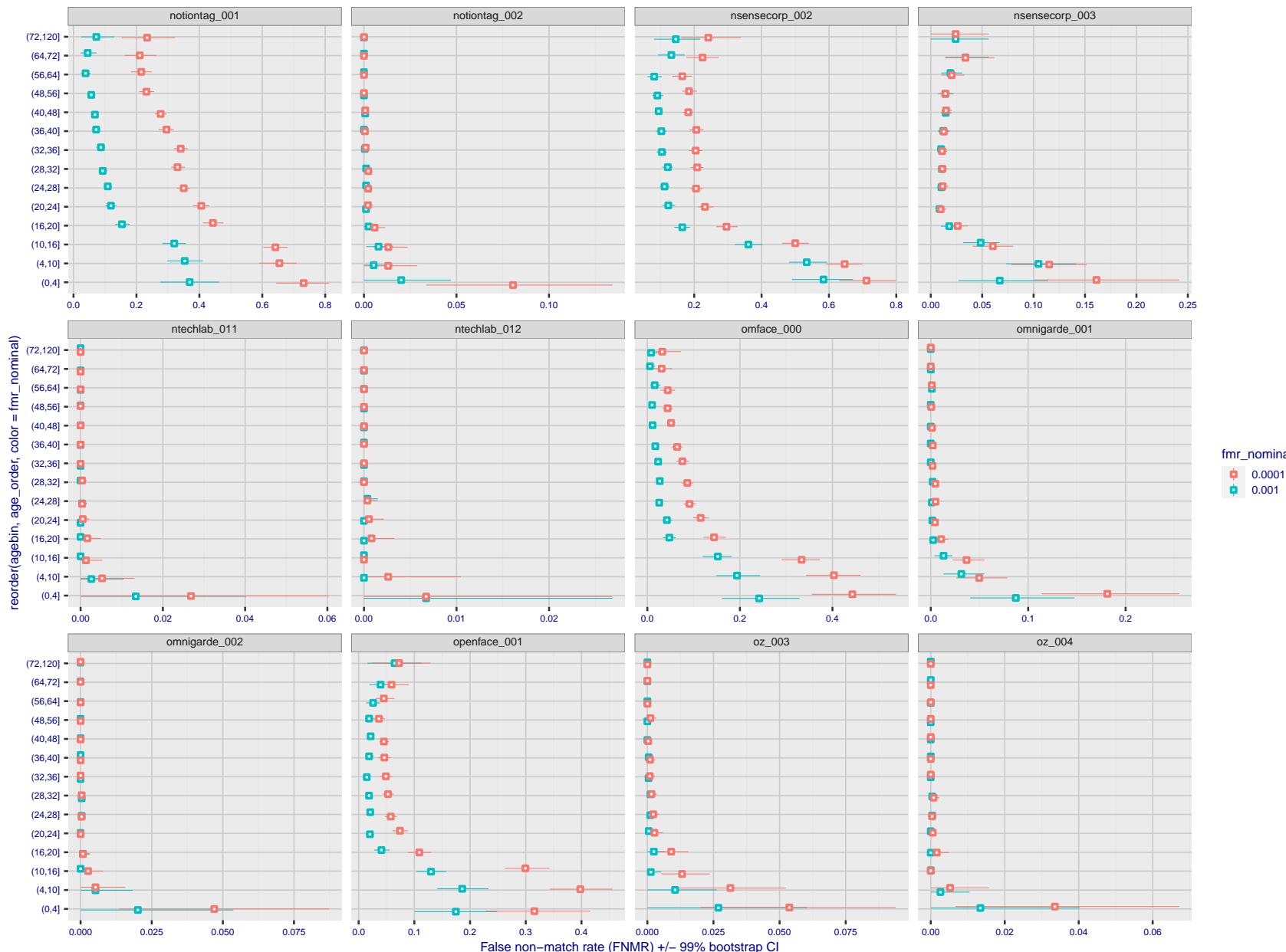


Figure 365: For the visa images, the dots show FNMR by age group for two operating thresholds corresponding to $FMR = \{0.001, 0.0001\}$ computed over all on the order of 10^{10} impostor scores. The FMR in each bin will vary also - see subsequent impostor heatmaps in sec. 3.6.2. Given a pair of face images taken at different times, we assign the comparison to the bin that is the arithmetic average of the subject's ages. This plot shows only the effect of age, not ageing. The number of comparisons in each bin is generally in the thousands, however the first and last bins are computed over 149 and 124 respectively. The error rates in some (adult) cases are zero, and in others the DET is flat so the error rates at the two thresholds are identical. The lines span 1% and 99% of bootstrap replicated FNMR estimates.

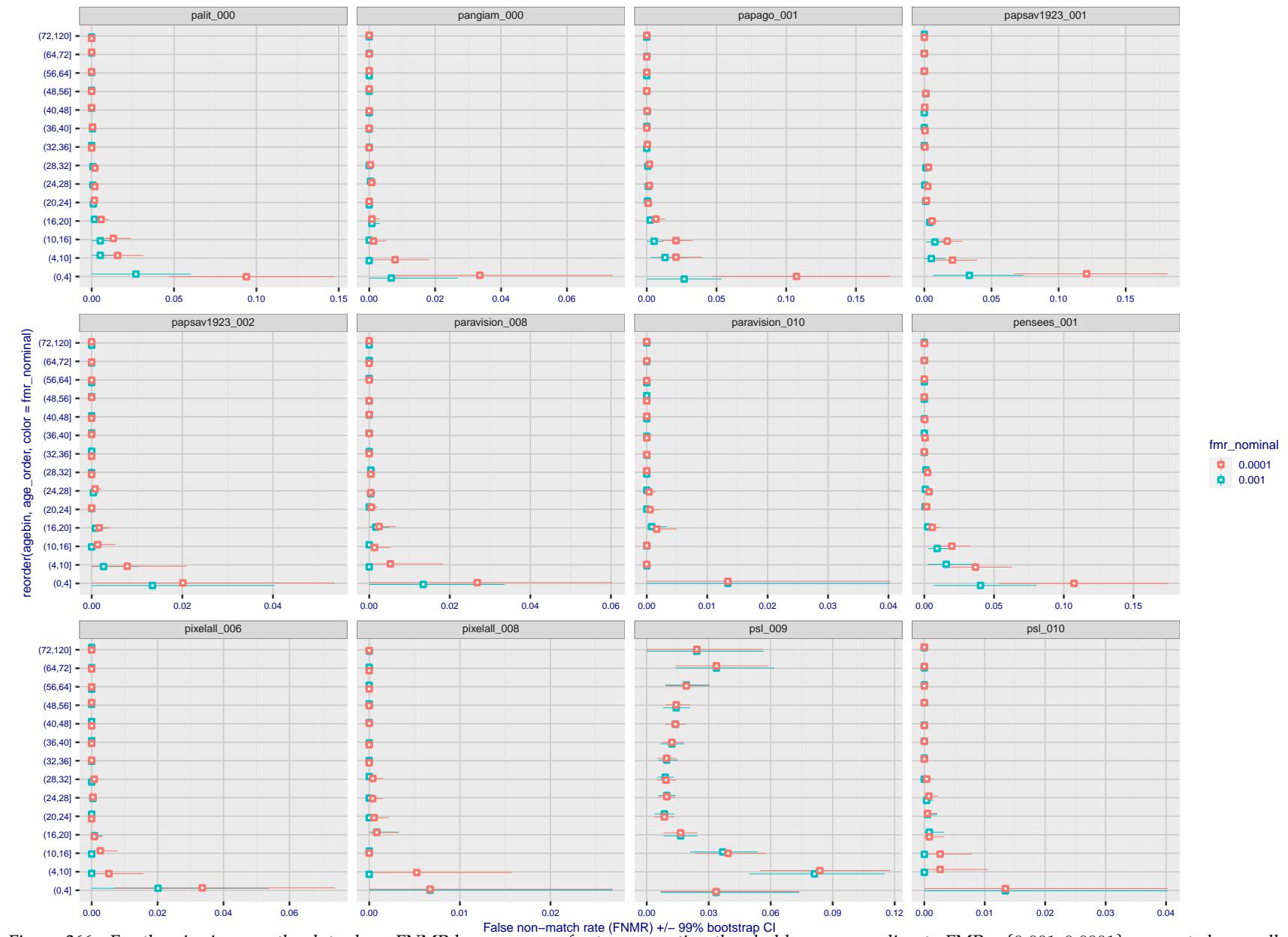


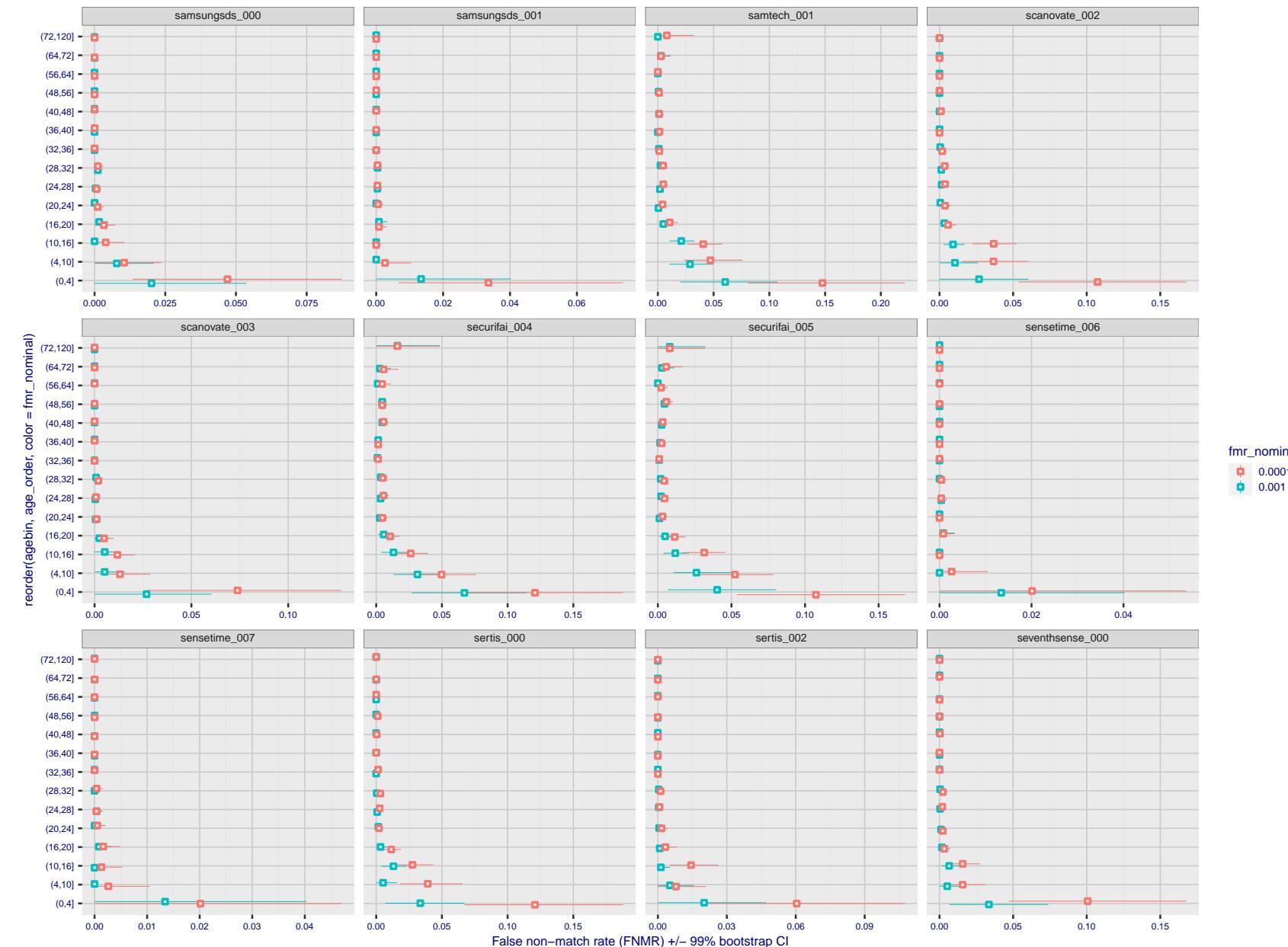
Figure 366: For the visa images, the dots show FNMR by age group for two operating thresholds corresponding to $FMR = \{0.001, 0.0001\}$ computed over all on the order of 10^{10} impostor scores. The FMR in each bin will vary also - see subsequent impostor heatmaps in sec. 3.6.2. Given a pair of face images taken at different times, we assign the comparison to the bin that is the arithmetic average of the subject's ages. This plot shows only the effect of age, not ageing. The number of comparisons in each bin is generally in the thousands, however the first and last bins are computed over 149 and 124 respectively. The error rates in some (adult) cases are zero, and in others the DET is flat so the error rates at the two thresholds are identical. The lines span 1% and 99% of bootstrap replicated FNMR estimates.



Figure 367: For the visa images, the dots show FNMR by age group for two operating thresholds corresponding to $FMR = \{0.001, 0.0001\}$ computed over all on the order of 10^{10} impostor scores. The FMR in each bin will vary also - see subsequent impostor heatmaps in sec. 3.6.2. Given a pair of face images taken at different times, we assign the comparison to the bin that is the arithmetic average of the subject's ages. This plot shows only the effect of age, not ageing. The number of comparisons in each bin is generally in the thousands, however the first and last bins are computed over 149 and 124 respectively. The error rates in some (adult) cases are zero, and in others the DET is flat so the error rates at the two thresholds are identical. The lines span 1% and 99% of bootstrap replicated FNMR estimates.

Figure 368: For the visa images, the dots show FNMR by age group for two operating thresholds corresponding to FMR = {0.001, 0.0001} computed over all on the order of 10^{10} impostor scores.

The FMR in each bin will vary also - see subsequent impostor heatmaps in sec. 3.6.2. Given a pair of face images taken at different times, we assign the comparison to the bin that is the arithmetic average of the subject's ages. This plot shows only the effect of age, not ageing. The number of comparisons in each bin is generally in the thousands, however the first and last bins are computed over 149 and 124 respectively. The error rates in some (adult) cases are zero, and in others the DET is flat so the error rates at the two thresholds are identical. The lines span 1% and 99% of bootstrap replicated FNMR estimates.



fmr_nominal
0.0001
0.001

Figure 369: For the visa images, the dots show FNMR by age group for two operating thresholds corresponding to $FMR = \{0.001, 0.0001\}$ computed over all on the order of 10^{10} impostor scores. The FMR in each bin will vary also - see subsequent impostor heatmaps in sec. 3.6.2. Given a pair of face images taken at different times, we assign the comparison to the bin that is the arithmetic average of the subject's ages. This plot shows only the effect of age, not ageing. The number of comparisons in each bin is generally in the thousands, however the first and last bins are computed over 149 and 124 respectively. The error rates in some (adult) cases are zero, and in others the DET is flat so the error rates at the two thresholds are identical. The lines span 1% and 99% of bootstrap replicated FNMR estimates.

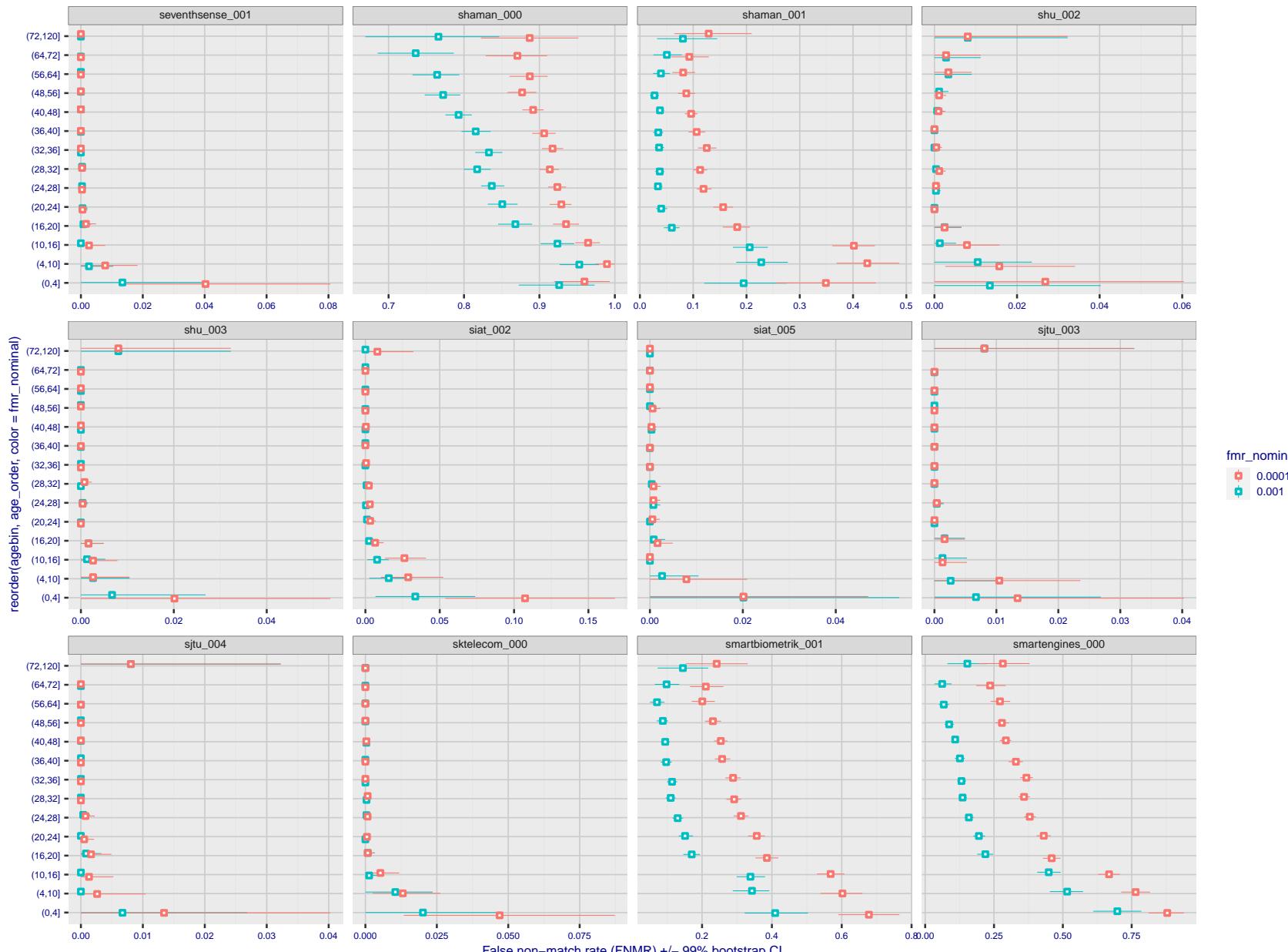


Figure 370: For the visa images, the dots show FNMR by age group for two operating thresholds corresponding to $FMR = \{0.001, 0.0001\}$ computed over all on the order of 10^{10} impostor scores. The FMR in each bin will vary also - see subsequent impostor heatmaps in sec. 3.6.2. Given a pair of face images taken at different times, we assign the comparison to the bin that is the arithmetic average of the subject's ages. This plot shows only the effect of age, not ageing. The number of comparisons in each bin is generally in the thousands, however the first and last bins are computed over 149 and 124 respectively. The error rates in some (adult) cases are zero, and in others the DET is flat so the error rates at the two thresholds are identical. The lines span 1% and 99% of bootstrap replicated FNMR estimates.

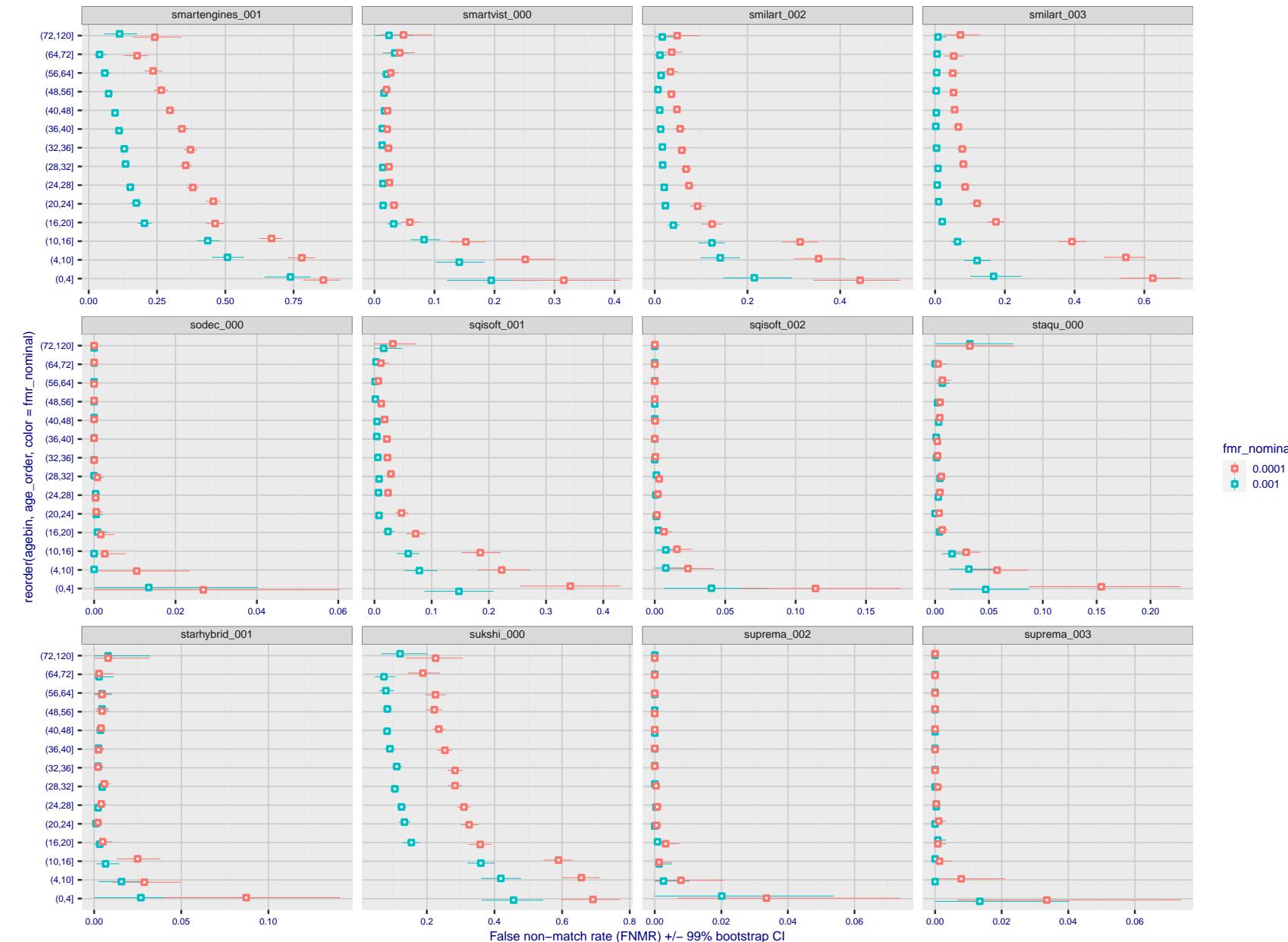


Figure 371: For the visa images, the dots show FNMR by age group for two operating thresholds corresponding to $FMR = \{0.001, 0.0001\}$ computed over all on the order of 10^{10} impostor scores. The FMR in each bin will vary also - see subsequent impostor heatmaps in sec. 3.6.2. Given a pair of face images taken at different times, we assign the comparison to the bin that is the arithmetic average of the subject's ages. This plot shows only the effect of age, not ageing. The number of comparisons in each bin is generally in the thousands, however the first and last bins are computed over 149 and 124 respectively. The error rates in some (adult) cases are zero, and in others the DET is flat so the error rates at the two thresholds are identical. The lines span 1% and 99% of bootstrap replicated FNMR estimates.

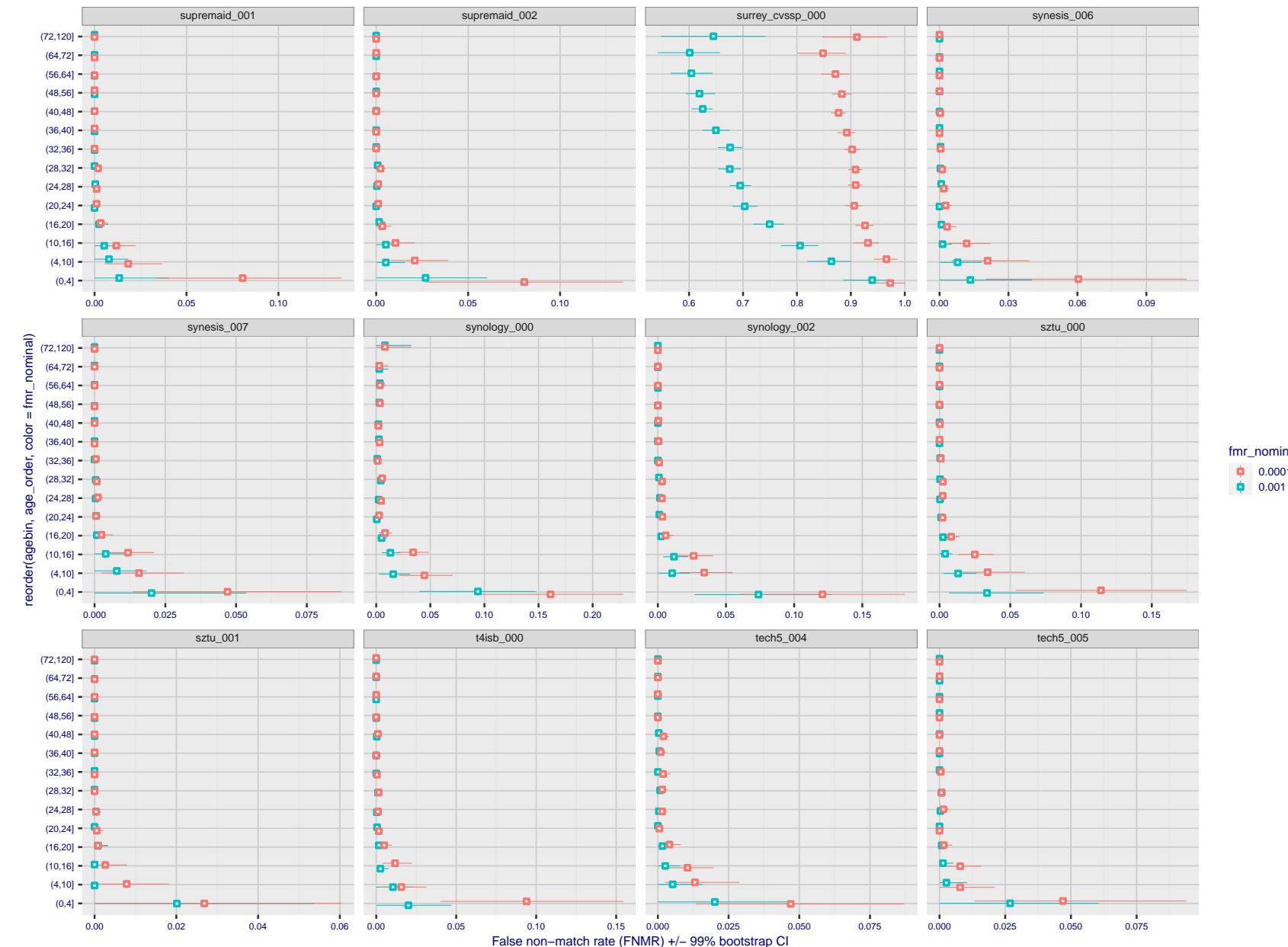


Figure 372: For the visa images, the dots show FNMR by age group for two operating thresholds corresponding to $FMR = \{0.001, 0.0001\}$ computed over all on the order of 10^{10} impostor scores. The FMR in each bin will vary also - see subsequent impostor heatmaps in sec. 3.6.2. Given a pair of face images taken at different times, we assign the comparison to the bin that is the arithmetic average of the subject's ages. This plot shows only the effect of age, not ageing. The number of comparisons in each bin is generally in the thousands, however the first and last bins are computed over 149 and 124 respectively. The error rates in some (adult) cases are zero, and in others the DET is flat so the error rates at the two thresholds are identical. The lines span 1% and 99% of bootstrap replicated FNMR estimates.



Figure 373: For the visa images, the dots show FNMR by age group for two operating thresholds corresponding to $FMR = \{0.001, 0.0001\}$ computed over all on the order of 10^{10} impostor scores. The FMR in each bin will vary also - see subsequent impostor heatmaps in sec. 3.6.2. Given a pair of face images taken at different times, we assign the comparison to the bin that is the arithmetic average of the subject's ages. This plot shows only the effect of age, not ageing. The number of comparisons in each bin is generally in the thousands, however the first and last bins are computed over 149 and 124 respectively. The error rates in some (adult) cases are zero, and in others the DET is flat so the error rates at the two thresholds are identical. The lines span 1% and 99% of bootstrap replicated FNMR estimates.



Figure 374: For the visa images, the dots show FNMR by age group for two operating thresholds corresponding to $FMR = \{0.001, 0.0001\}$ computed over all on the order of 10^{10} impostor scores. The FMR in each bin will vary also - see subsequent impostor heatmaps in sec. 3.6.2. Given a pair of face images taken at different times, we assign the comparison to the bin that is the arithmetic average of the subject's ages. This plot shows only the effect of age, not ageing. The number of comparisons in each bin is generally in the thousands, however the first and last bins are computed over 149 and 124 respectively. The error rates in some (adult) cases are zero, and in others the DET is flat so the error rates at the two thresholds are identical. The lines span 1% and 99% of bootstrap replicated FNMR estimates.

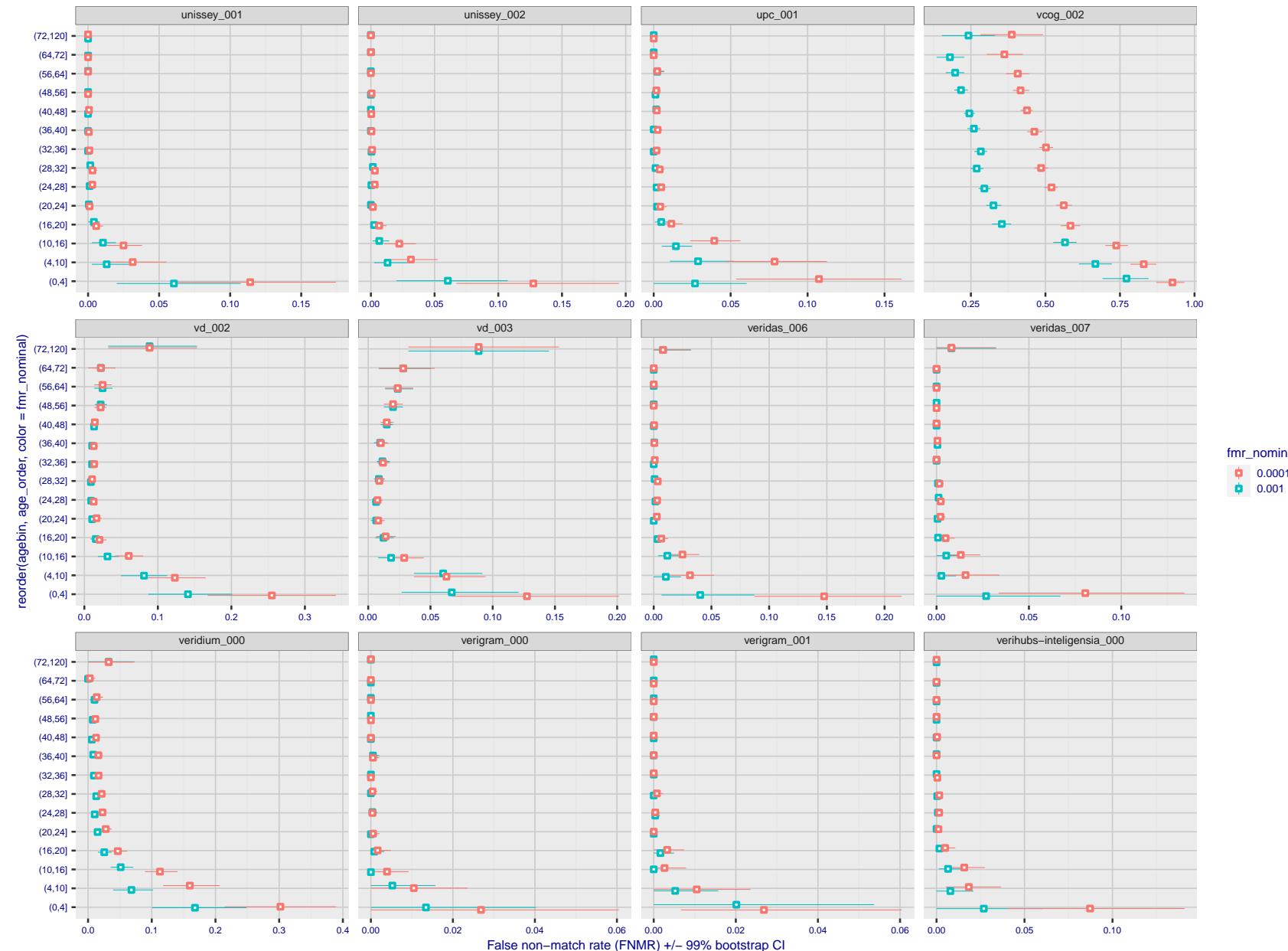


Figure 375: For the visa images, the dots show FNMR by age group for two operating thresholds corresponding to $FMR = \{0.001, 0.0001\}$ computed over all on the order of 10^{10} impostor scores. The FMR in each bin will vary also - see subsequent impostor heatmaps in sec. 3.6.2. Given a pair of face images taken at different times, we assign the comparison to the bin that is the arithmetic average of the subject's ages. This plot shows only the effect of age, not ageing. The number of comparisons in each bin is generally in the thousands, however the first and last bins are computed over 149 and 124 respectively. The error rates in some (adult) cases are zero, and in others the DET is flat so the error rates at the two thresholds are identical. The lines span 1% and 99% of bootstrap replicated FNMR estimates.

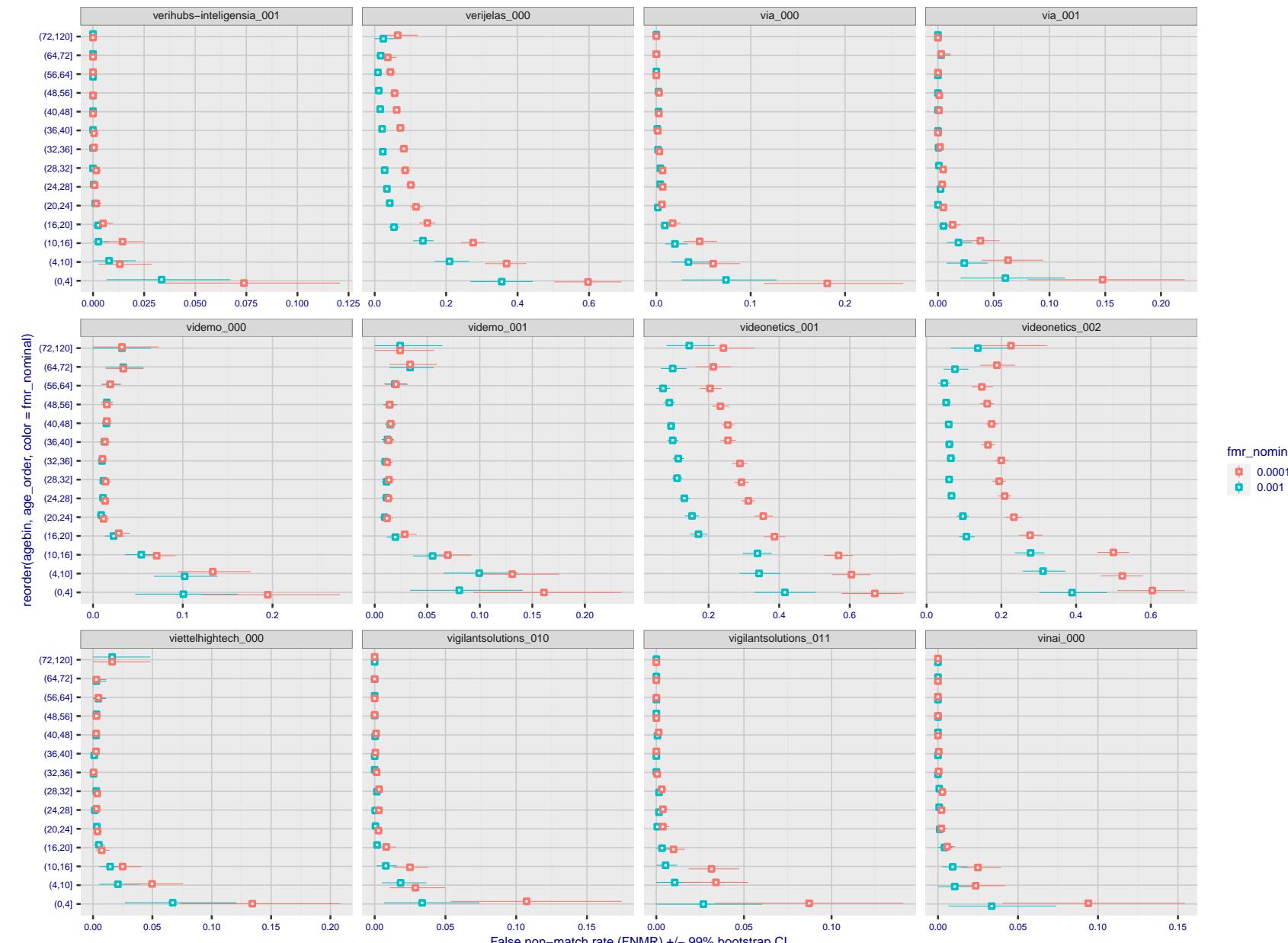


Figure 376: For the visa images, the dots show FNMR by age group for two operating thresholds corresponding to $FMR = \{0.001, 0.0001\}$ computed over all on the order of 10^{10} impostor scores. The FMR in each bin will vary also - see subsequent impostor heatmaps in sec. 3.6.2. Given a pair of face images taken at different times, we assign the comparison to the bin that is the arithmetic average of the subject's ages. This plot shows only the effect of age, not ageing. The number of comparisons in each bin is generally in the thousands, however the first and last bins are computed over 149 and 124 respectively. The error rates in some (adult) cases are zero, and in others the DET is flat so the error rates at the two thresholds are identical. The lines span 1% and 99% of bootstrap replicated FNMR estimates.

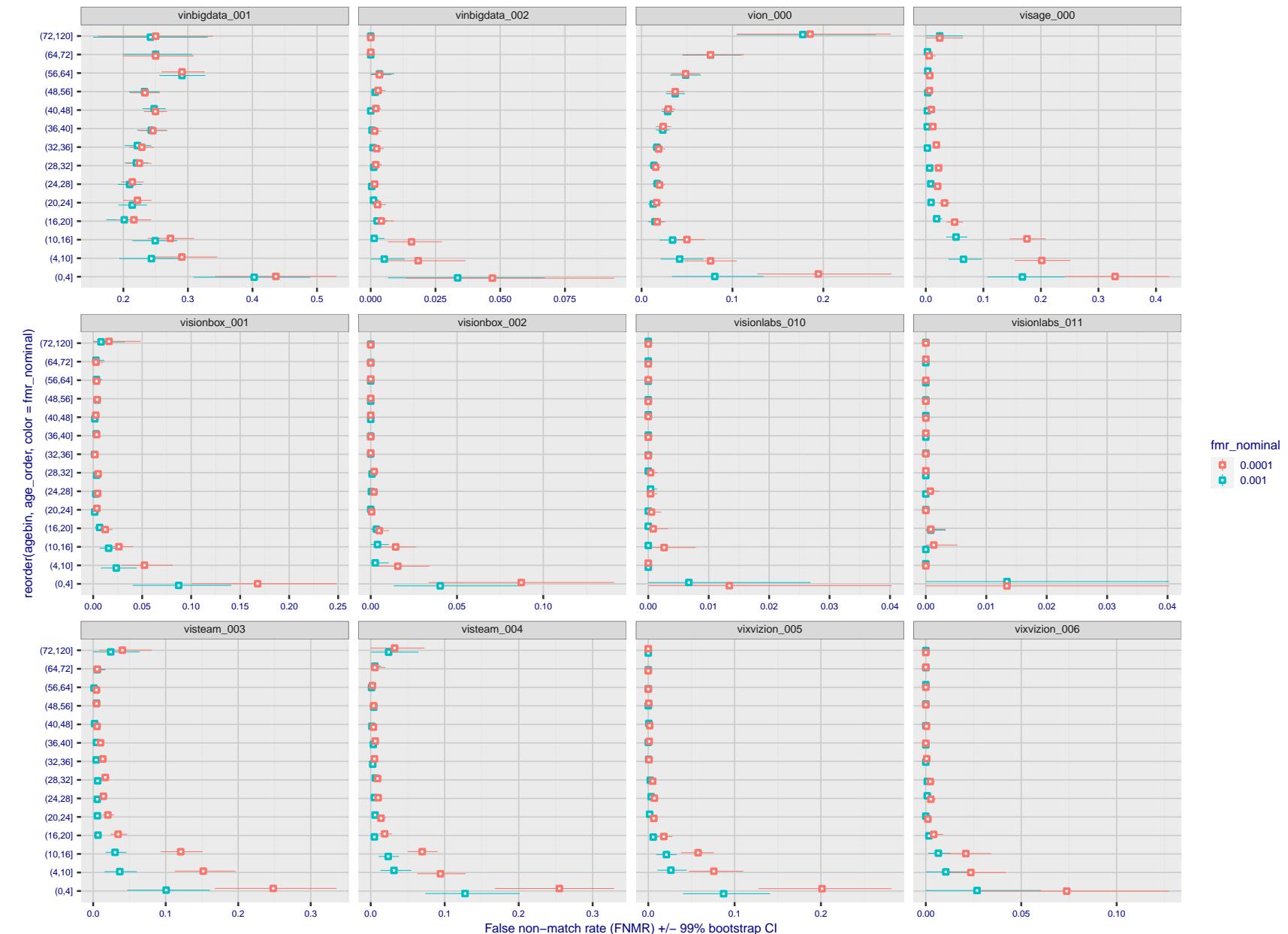


Figure 377: For the visa images, the dots show FNMR by age group for two operating thresholds corresponding to $FMR = \{0.001, 0.0001\}$ computed over all on the order of 10^{10} impostor scores. The FMR in each bin will vary also - see subsequent impostor heatmaps in sec. 3.6.2. Given a pair of face images taken at different times, we assign the comparison to the bin that is the arithmetic average of the subject's ages. This plot shows only the effect of age, not ageing. The number of comparisons in each bin is generally in the thousands, however the first and last bins are computed over 149 and 124 respectively. The error rates in some (adult) cases are zero, and in others the DET is flat so the error rates at the two thresholds are identical. The lines span 1% and 99% of bootstrap replicated FNMR estimates.



Figure 378: For the visa images, the dots show FNMR by age group for two operating thresholds corresponding to $FMR = \{0.001, 0.0001\}$ computed over all on the order of 10^{10} impostor scores. The FMR in each bin will vary also - see subsequent impostor heatmaps in sec. 3.6.2. Given a pair of face images taken at different times, we assign the comparison to the bin that is the arithmetic average of the subject's ages. This plot shows only the effect of age, not ageing. The number of comparisons in each bin is generally in the thousands, however the first and last bins are computed over 149 and 124 respectively. The error rates in some (adult) cases are zero, and in others the DET is flat so the error rates at the two thresholds are identical. The lines span 1% and 99% of bootstrap replicated FNMR estimates.



Figure 379: For the visa images, the dots show FNMR by age group for two operating thresholds corresponding to $FMR = \{0.001, 0.0001\}$ computed over all on the order of 10^{10} impostor scores. The FMR in each bin will vary also - see subsequent impostor heatmaps in sec. 3.6.2. Given a pair of face images taken at different times, we assign the comparison to the bin that is the arithmetic average of the subject's ages. This plot shows only the effect of age, not ageing. The number of comparisons in each bin is generally in the thousands, however the first and last bins are computed over 149 and 124 respectively. The error rates in some (adult) cases are zero, and in others the DET is flat so the error rates at the two thresholds are identical. The lines span 1% and 99% of bootstrap replicated FNMR estimates.

Caveats: None.

3.6 Impostor distribution stability

3.6.1 Effect of birth place on the impostor distribution

Background: Facial appearance varies geographically, both in terms of skin tone, cranio-facial structure and size. This section addresses whether false match rates vary intra- and inter-regionally.

Goals:

- ▷ To show the effect of birth region of the impostor and enrollee on false match rates.
- ▷ To determine whether some algorithms give better impostor distribution stability.

Methods:

- ▷ For the visa images, NIST defined 10 regions: Sub-Saharan Africa, South Asia, Polynesia, North Africa, Middle East, Europe, East Asia, Central and South America, Central Asia, and the Caribbean.
- ▷ For the visa images, NIST mapped each country of birth to a region. There is some arbitrariness to this. For example, Egypt could reasonably be assigned to the Middle East instead of North Africa. An alternative methodology could, for example, assign the Philippines to *both* Polynesia and East Asia.
- ▷ FMR is computed for cases where all face images of impostors born in region r_2 are compared with enrolled face images of persons born in region r_1 .

$$\text{FMR}(r_1, r_2, T) = \frac{\sum_{i=1}^{N_{r_1, r_2}} H(s_i - T)}{N_{r_1, r_2}} \quad (5)$$

where the same threshold, T , is used in all cells, and H is the unit step function. The threshold is set to give $\text{FMR}(T) = 0.001$ over the entire set of visa image impostor comparisons.

- ▷ This analysis is then repeated by country-pair, but only for those country pairs where both have at least 1000 images available. The countries¹ appear in the axes of graphs that follow.
- ▷ The mean number of impostor scores in any cross-region bin is 33 million. The smallest number of impostor scores in any bin is 135000, for Central Asia - North Africa. While these counts are large enough to support reasonable significance, the number of individual faces is much smaller, on the order of $N^{0.5}$.
- ▷ The numbers of impostor scores in any cross-country bin is shown in Figure 380.

Results: Subsequent figures show heatmaps that use color to represent the base-10 logarithm of the false match rate. Red colors indicate high (bad) false match rates. Dark colors indicate benign false match rates. There are two series of graphs corresponding to aggregated geographical regions, and to countries. The notable observations are:

- ▷ The on-diagonal elements correspond to within-region impostors. FMR is generally above the nominal value of $\text{FMR} = 0.001$. Particularly there is usually higher FMR in, Sub-Saharan Africa, South Asia, and the Caribbean. Europe and Central Asia, on the other hand, usually give FMR closer to the nominal value.
- ▷ The off-diagonal elements correspond to across-region impostors. The highest FMR is produced between the Caribbean and Sub-Saharan Africa.
- ▷ Algorithms vary.

¹These are Argentina, Australia, Brazil, Chile, China, Costa Rica, Cuba, Czech Republic, Dominican Republic, Ecuador, Egypt, El Salvador, Germany, Ghana, Great Britain, Greece, Guatemala, Haiti, Hong Kong, Honduras, Indonesia, India, Israel, Jamaica, Japan, Kenya, Korea, Lebanon, Mexico, Malaysia, Nepal, Nigeria, Peru, Philippines, Pakistan, Poland, Romania, Russia, South Africa, Saudi Arabia, Thailand, Trinidad, Turkey, Taiwan, Ukraine, Venezuela, and Vietnam.

- ▷ We computed the same quantities for a global FMR = 0.0001. The effects are similar.

Caveats:

- ▷ The effects of variable impostor rates on one-to-many identification systems may well differ from what's implied by these one-to-one verification results. Two reasons for this are a) the enrollment galleries are usually imbalanced across countries of birth, age and sex; b) one-to-many identification algorithms often implement techniques aimed at stabilizing the impostor distribution. Further research is necessary.
- ▷ In principle, the effects seen in this subsection could be due to differences in the image capture process. We consider this unlikely since the effects are maintained across geography - e.g. Caribbean vs. Africa, or Japan vs. China.

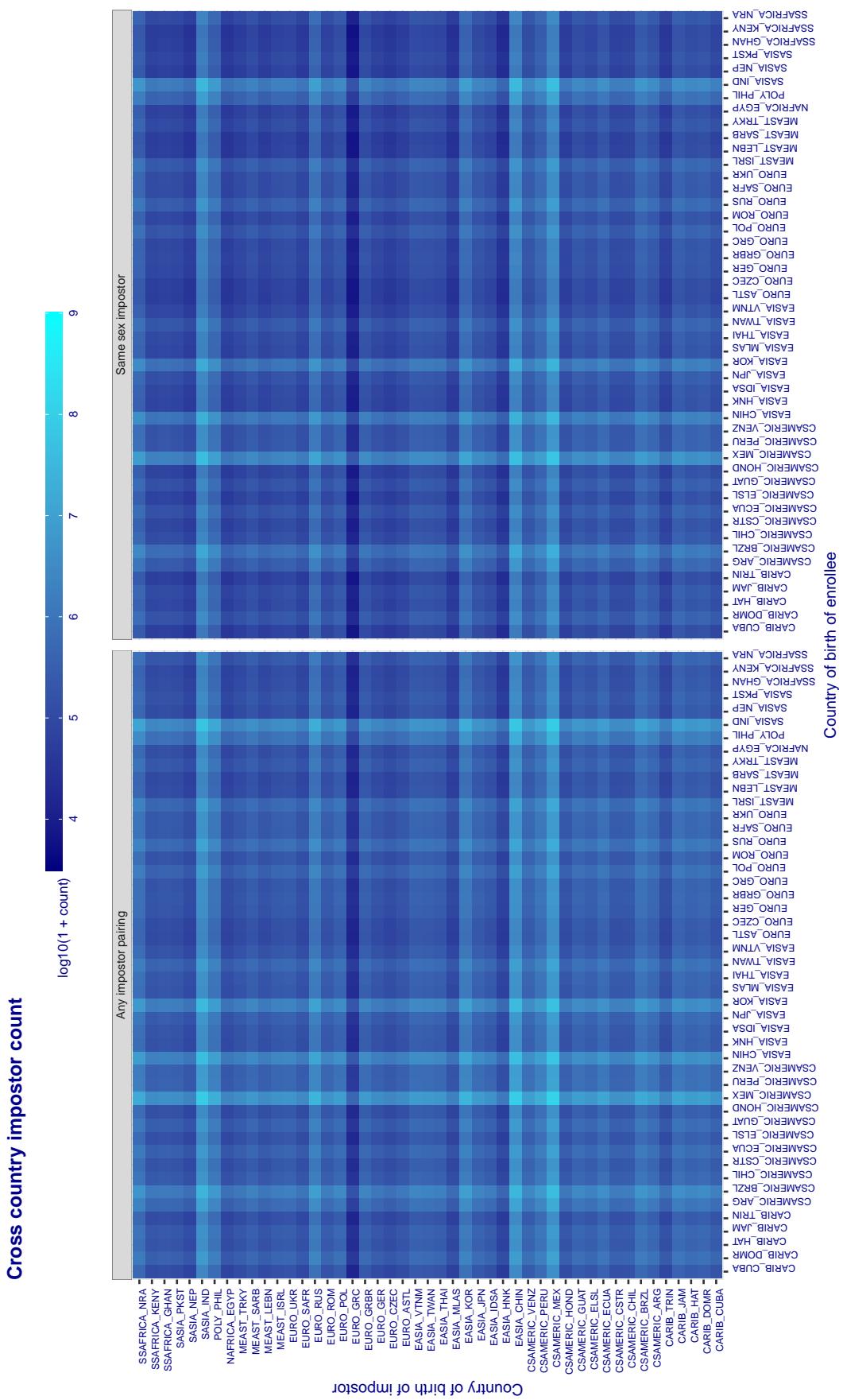


Figure 380: For visa images, the heatmap shows the count of impostor comparisons of faces from different individuals who were born in the given country pair. The FMR heatmaps themselves appear in the 1:1 report cards, for example, [this one](#).

3.6.2 Effect of age on impostors

Background: This section shows the effect of age on the impostor distribution. The ideal behaviour is that the age of the enrollee and the impostor would not affect impostor scores. This would support FMR stability over sub-populations.

Goals:

- ▷ To show the effect of relative ages of the impostor and enrollee on false match rates.
- ▷ To determine whether some algorithms have better impostor distribution stability.

Methods:

- ▷ Define 14 age group bins, spanning 0 to over 100 years old.
- ▷ Compute FMR over all impostor comparisons for which the subjects in the enrollee and impostor images have ages in two bins.
- ▷ Compute FMR over all impostor comparisons for which the subjects are additionally of the same sex, and born in the same geographic region.

Results:

The notable aspects are:

- ▷ Diagonal dominance: Impostors are more likely to be matched against their same age group.
- ▷ Same sex and same region impostors are more successful. On the diagonal, an impostor is more likely to succeed by posing as someone of the same sex. If $\Delta \log_{10} \text{FMR} = 0.2$, then same-sex same-region FMR exceeds the all-pairs FMR by factor of $10^{0.2} = 1.6$.
- ▷ Young children impostors give elevated FMR against young children. Older adult impostor give elevated FMR against older adults. These effects are quite large, for example if $\Delta \log_{10} \text{FMR} = 1.0$ larger than a 32 year old, then these groups have higher FMR by a factor of $10^1 = 10$. This would imply an FMR above 0.01 for a nominal (global) FMR = 0.001.
- ▷ Algorithms vary.
- ▷ We computed the same quantities for a global FMR = 0.0001. The effects are similar.

Note the calculations in this section include impostors paired across all countries of birth.

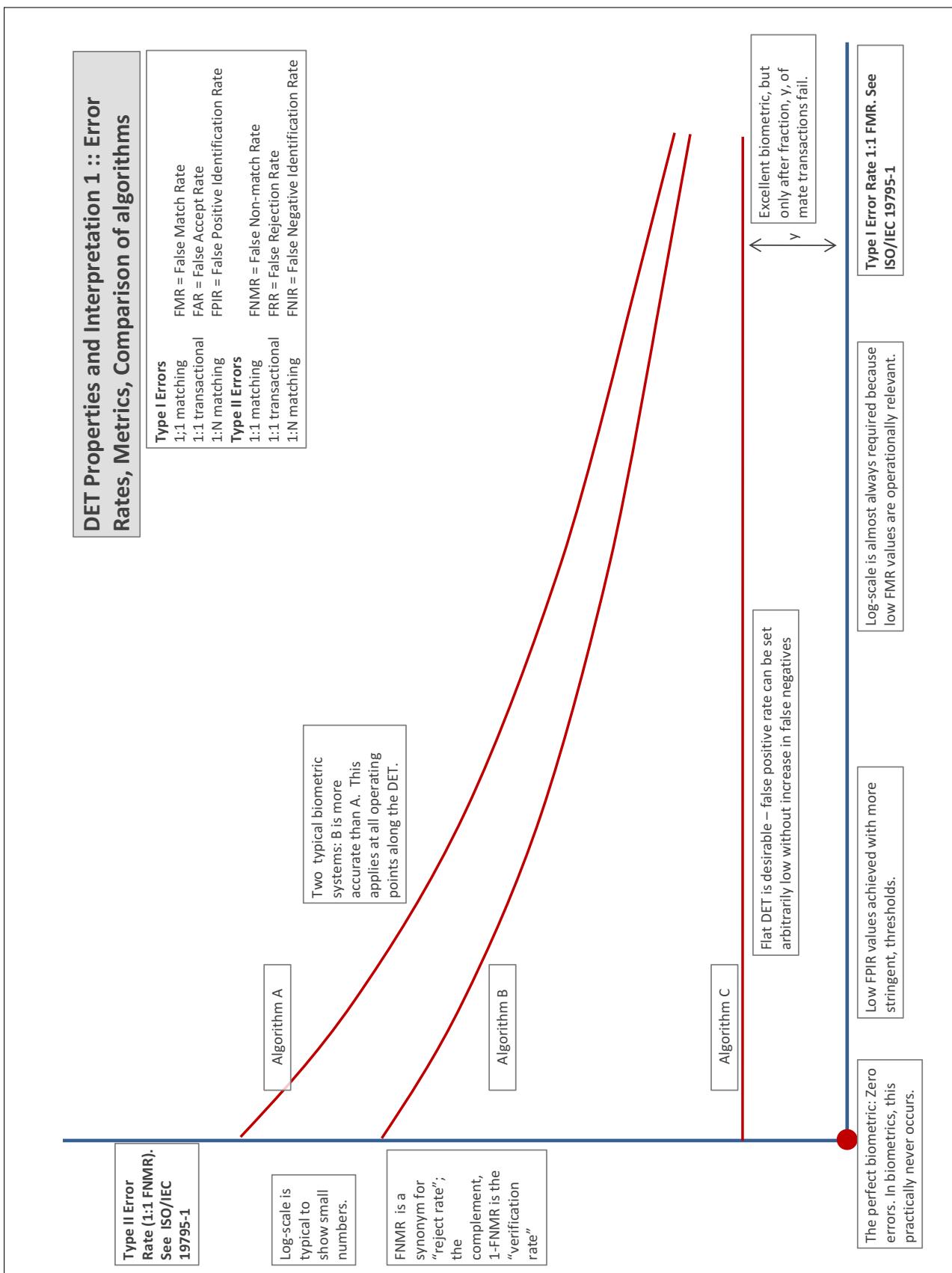
Accuracy Terms + Definitions

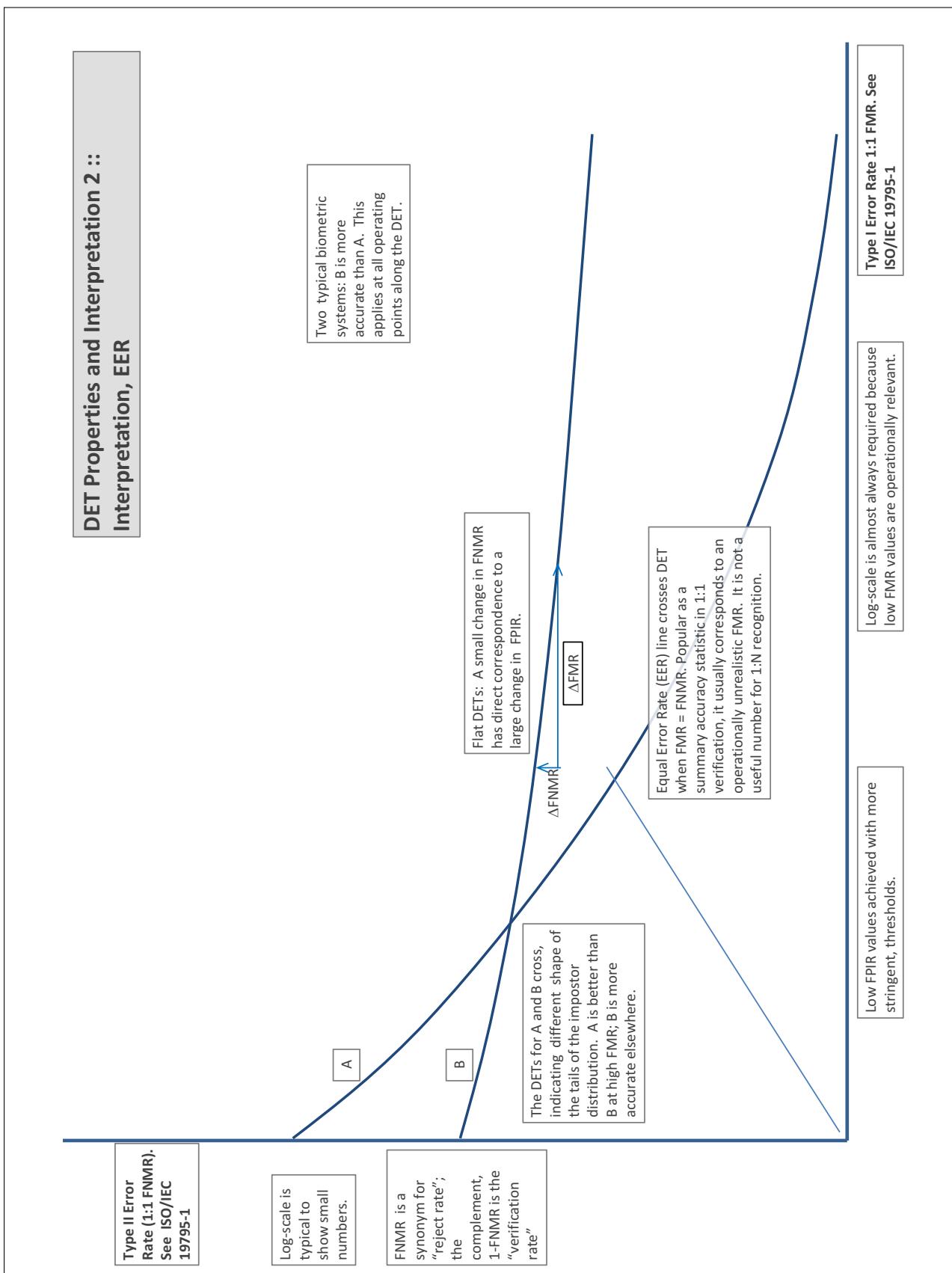
In biometrics, Type II errors occur when two samples of one person do not match – this is called a **false negative**. Correspondingly, Type I errors occur when samples from two persons do match – this is called a **false positive**. Matches are declared by a biometric system when the native comparison score from the recognition algorithm meets some **threshold**. Comparison scores can be either **similarity scores**, in which case higher values indicate that the samples are more likely to come from the same person, or **dissimilarity scores**, in which case higher values indicate different people. Similarity scores are traditionally computed by **fingerprint** and **face** recognition algorithms, while dissimilarities are used in **iris recognition**. In some cases, the dissimilarity score is a distance; this applies only when **metric** properties are obeyed. In any case, scores can be either **mate** scores, coming from a comparison of one person's samples, or **nonmate** scores, coming from comparison of different persons' samples. The words **genuine** or **authentic** are synonyms for mate, and the word **impostor** is used as a synonym for nonmatch. The words mate and nonmatch are traditionally used in identification applications (such as law enforcement search, or background checks) while genuine and impostor are used in verification applications (such as access control).

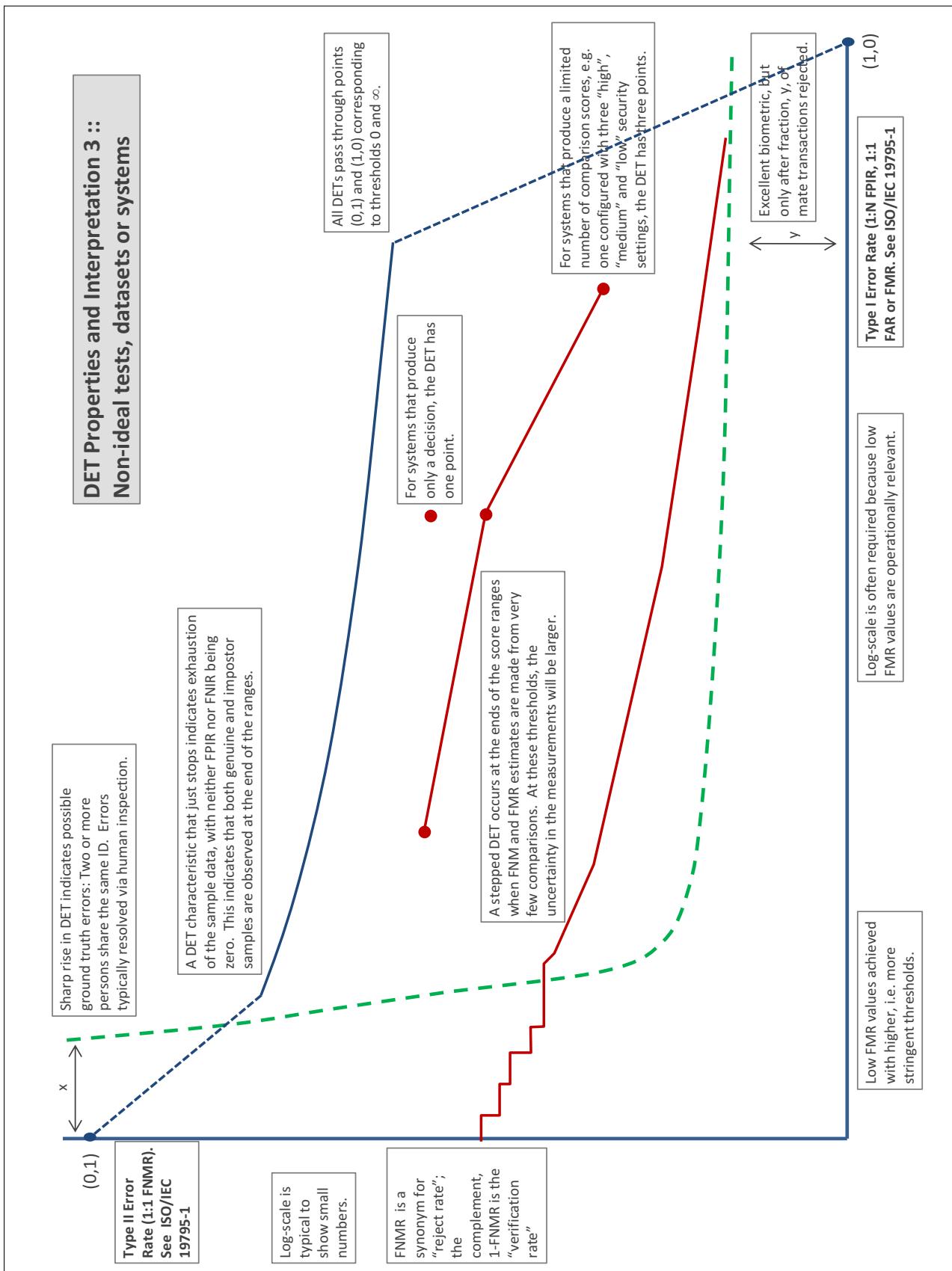
A **error tradeoff** characteristic represents the tradeoff between Type II and Type I classification errors. For verification this plots false non-match rate (FNMR) vs. false match rate (FMR) parametrically with T.

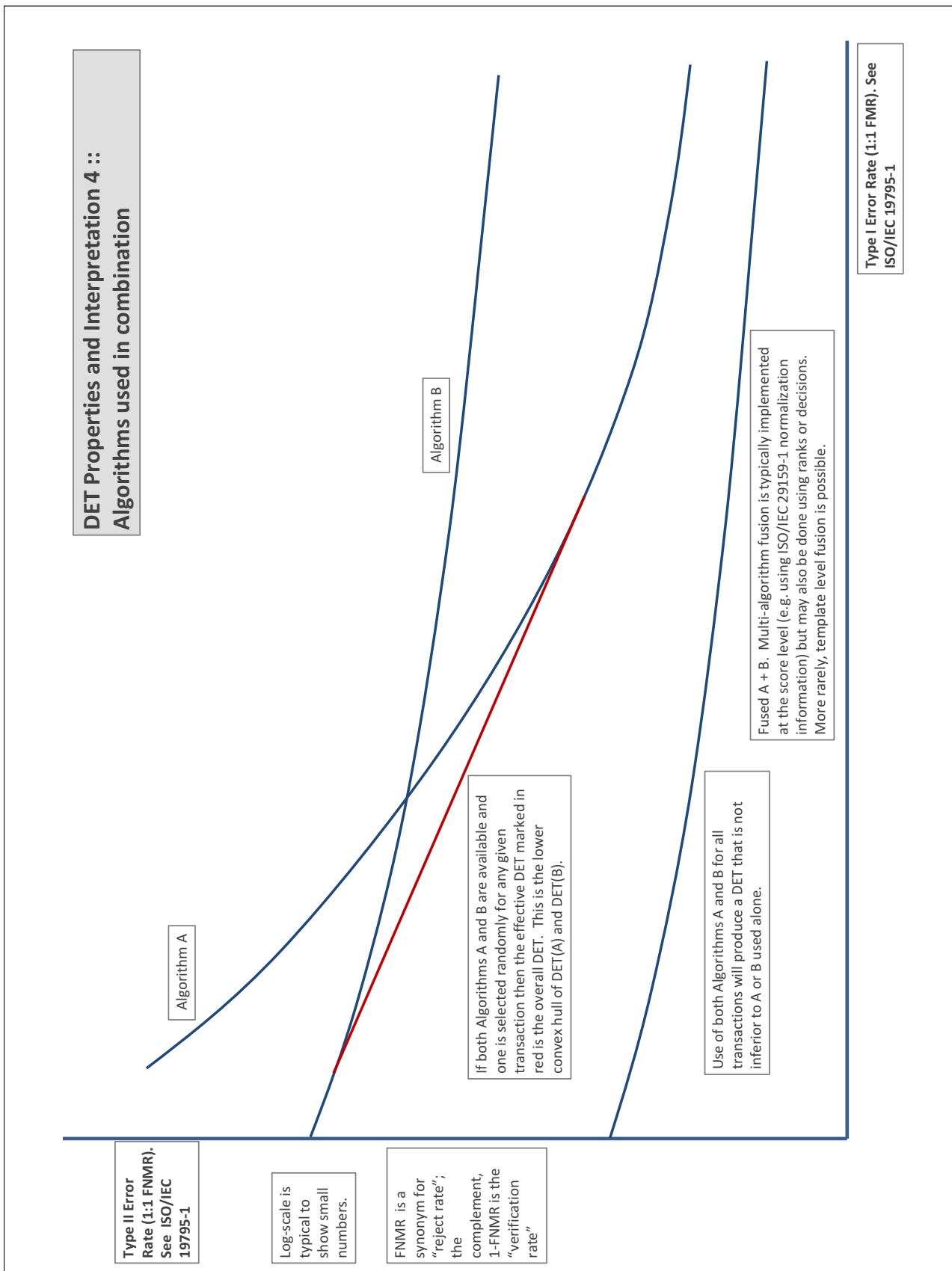
The error tradeoff plots are often called **detection error tradeoff (DET)** characteristics or **receiver operating characteristic (ROC)**. These serve the same function but differ, for example, in plotting the complement of an error rate (e.g., $TMR = 1 - FNMR$) and in transforming the axes most commonly using logarithms, to show multiple decades of FMR. More rarely, the function might be the inverse Gaussian function.

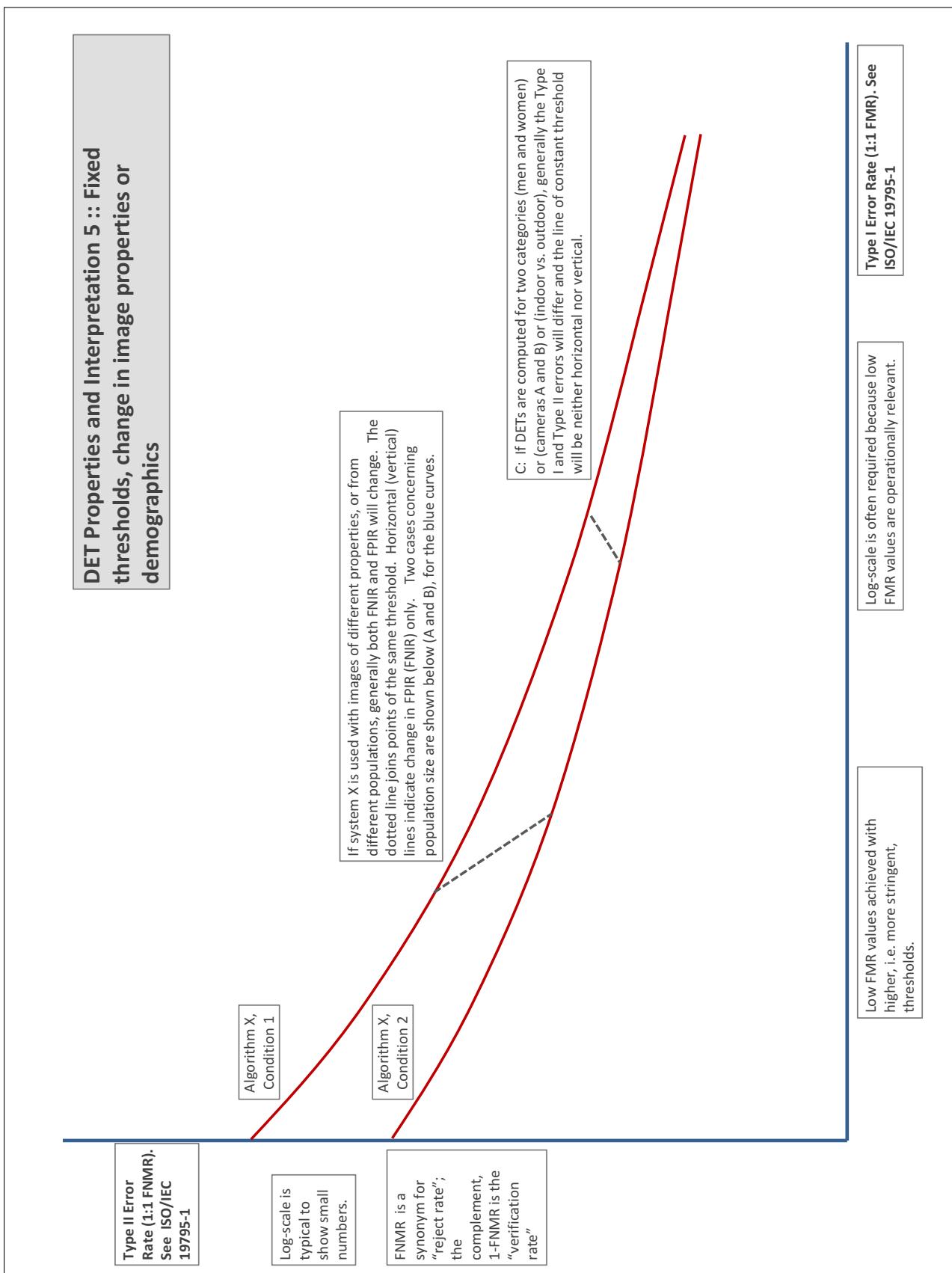
More detail and generality is provided in formal biometrics testing standards, see the various parts of [ISO/IEC 19795 Biometrics Testing and Reporting](#). More terms, including and beyond those to do with accuracy, see [ISO/IEC 2382-37 Information technology -- Vocabulary -- Part 37: Harmonized biometric vocabulary](#)











References

- [1] P. Jonathon Phillips, Amy N. Yates, Ying Hu, Carina A. Hahn, Eilidh Noyes, Kelsey Jackson, Jacqueline G. Cavazos, Géraldine Jeckeln, Rajeev Ranjan, Swami Sankaranarayanan, Jun-Cheng Chen, Carlos D. Castillo, Rama Chellappa, David White, and Alice J. O'Toole. Face recognition accuracy of forensic examiners, superrecognizers, and face recognition algorithms. *Proceedings of the National Academy of Sciences*, 115(24):6171–6176, 2018.